Lecture Notes in Civil Engineering

Ranjith Dissanayake ·
Priyan Mendis · Kolita Weerasekera ·
Sudhira De Silva · Shiromal Fernando ·
Chaminda Konthesingha *Editors*

12th International Conference on Structural Engineering and Construction Management

Proceedings of the ICSECM 2021

Springer

Lecture Notes in Civil Engineering

Volume 266

Lecture Notes in Civil Engineering (LNCE) publishes the latest developments in Civil Engineering - quickly, informally and in top quality. Though original research reported in proceedings and post-proceedings represents the core of LNCE, edited volumes of exceptionally high quality and interest may also be considered for publication. Volumes published in LNCE embrace all aspects and subfields of, as well as new challenges in, Civil Engineering. Topics in the series include:

- Construction and Structural Mechanics
- Building Materials
- Concrete, Steel and Timber Structures
- Geotechnical Engineering
- Earthquake Engineering
- Coastal Engineering
- Ocean and Offshore Engineering; Ships and Floating Structures
- Hydraulics, Hydrology and Water Resources Engineering
- Environmental Engineering and Sustainability
- Structural Health and Monitoring
- Surveying and Geographical Information Systems
- Indoor Environments
- Transportation and Traffic
- Risk Analysis
- Safety and Security

To submit a proposal or request further information, please contact the appropriate Springer Editor:

– Pierpaolo Riva at pierpaolo.riva@springer.com (Europe and Americas);
– Swati Meherishi at swati.meherishi@springer.com (Asia - except China, and Australia, New Zealand);
– Wayne Hu at wayne.hu@springer.com (China).

All books in the series now indexed by Scopus and EI Compendex database!

Ranjith Dissanayake · Priyan Mendis ·
Kolita Weerasekera · Sudhira De Silva ·
Shiromal Fernando · Chaminda Konthesingha
Editors

12th International Conference on Structural Engineering and Construction Management

Proceedings of the ICSECM 2021

Springer

Editors
Ranjith Dissanayake
Department of Civil Engineering
University of Peradeniya
Kandy, Sri Lanka

Kolita Weerasekera
Department of Civil Engineering
The Open University of Sri Lanka
Nugegoda, Sri Lanka

Shiromal Fernando
Civil and Structural Engineering
Consultants (Pvt) Ltd.
Rajagiriya, Colombo, Sri Lanka

Priyan Mendis
Department of Infrastructure Engineering
University of Melbourne
Parkville, VIC, Australia

Sudhira De Silva
Department of Civil and Environmental
Engineering
University of Ruhuna
Galle, Sri Lanka

Chaminda Konthesingha
Department of Civil Engineering
University of Sri Jayawardanepura
Jayawardanepura, Sri Lanka

ISSN 2366-2557 ISSN 2366-2565 (electronic)
Lecture Notes in Civil Engineering
ISBN 978-981-19-2885-7 ISBN 978-981-19-2886-4 (eBook)
https://doi.org/10.1007/978-981-19-2886-4

Preface

It is with great pleasure that we present the proceedings of the 12th International Conference on Structural Engineering and Construction Management (ICSECM) 2021. This is the twelfth consecutively organized conference following a series of international conferences since 2010, keeping its tradition of adhering to engineering excellence.

Taking a step forward from the last eleven events, the coverage of specialty areas in this conference has been diversified. This book contains manuscripts of research work from many different sub-specialties. All the manuscripts were presented at parallel sessions on December 18 and 19, 2021, at the 12th International Conference on Structural Engineering and Construction Management (ICSECM) 2021 held at Earls Regency Hotel, Kandy, Sri Lanka.

We would like to express our appreciation to all keynote speakers and review and scientific committee members for their invaluable contribution to this conference which strives for a sustainable world through driving innovative research. We are also grateful to the authors for contributing research papers of high quality. The manuscripts in this proceeding book have been reviewed by a panel of academic and professional experts who have vast expertise in their respective fields. The enormous work carried out by these reviewers is gratefully appreciated as well. We are also pleased to acknowledge the advice and assistance provided by the members of the international advisory committee and members of the editorial committee along with many others who volunteered to assist to make this very significant event a success. Furthermore, we acknowledge the financial sponsorship provided by many organizations that have been extremely supportive toward the success of this international conference.

It is the earnest wish of the editors that this proceeding book would be used by the research community and practicing engineers who are directly or indirectly involved in studies related to structural engineering and construction management.

Kandy, Sri Lanka
December 2021

Editorial Committee
Prof. Ranjith Dissanayake
Prof. Priyan Mendis
Prof. Kolita Weerasekera
Prof. Sudhira De Silva
Eng. Shiromal Fernando
Dr. Chaminda Konthesingha

Contents

Structural Modeling and Health Monitoring

Application of Virtual Element Method for Plane Stress–Plane Strain Problems 3
Lahiru N. Dissanayake, D. S. T. Costa, and K. K. Wijesundara

Simulation of Reinforced Concrete Beam Shear Behavior: Contact Density Model Approach 17
R. M. A. Buddhika and H. D. Yapa

Comparison of Masonry Wall Modelling Approaches Under In-plane Monotonic Load and Cyclic Load 37
T. Krishanthini, N. Prasanth, and C. S. Bandara

Spherical Indentation Test to Determine Metal Properties Using Representative Strain Concept: A Review 53
S. P. L. Madhumali, J. A. S. C. Jayasinghe, C. S. Bandara, and A. J. Dammika

Influence of Upstream Mature Trees on Wind Loading on the Gable Roof of a Low-Rise Building—A Wind Tunnel Study 69
P. H. Kandamby, C. S. Lewangamage, and A. U. Weerasuriya

Vortex Shedding-Induced Fatigue Analysis for High-Mast Lighting Towers 83
K. Jeyamohan, C. S. Bandara, and J. A. S. C. Jayasinghe

Modeling of Reinforced Concrete Beam–Column Joint Retrofitting 95
Karunakaran Gajanan, Baskaran Pirashangan, and Hiran D. Yapa

Lessons Learnt from Recent Explosions in Storage Facilities with Ammonium Nitrate 113
P. L. N. Fernando, C. Attard, K. Wijesooriya, D. Mohotti, and C. K. Lee

Mitigation of Excessive Vibration in Warehouse Floor Slab—Case Study 125
H. V. W. S. A. Jayawardhane, T. Sasirathan,
D. M. A. G. B. Dissanayake, K. T. S. Karunanayake,
G. R. C. R. Senevirathna, Lahiru N. Dissanayake,
and P. B. R. Dissanayake

Case Study: Investigation of Existing Cracks in the Oxidation Ditches 133
G. R. C. R. Senevirathna, P. B. R. Dissanayake,
D. M. A. G. B. Dissanayake, K. T. S. Karunanayake,
H. V. W. S. A. Jayawardhane, and T. Sasirathan

A Review on the Advances in Distributed Fibre Optic Sensing Technology for Structural Health Monitoring 145
A. Gowshikan, K. Kariyawasam, X. Xu, C. Kechavarzi, N. de Battista,
N. Ferdinando, S. Acikgoz, N. D. Gunawardana, and M. Ranasinghe

Significance of Construction Stage Analysis on the Initial Configuration of Concrete Faced Rockfill Dams 161
T. M. S. Tennekoon, K. K. Wijesundara, P. B. R. Dissanayake,
N. G. P. B. Neluwala, S. De Silva, and S. Venkatesan

Detection of Concrete Surface Crack Depth Using Ultrasonic Pulse Velocity (UPV) Methods 173
B. M. K. L. K. Basnayake, A. R. M. H. B. Amunugama,
and U. B. Attanayake

Load Testing and Rating of a Concrete Arch Bridge 187
C. Hutchinson, A. Peiris, and I. Harik

Lateral Performance of Thin-Walled Steel Box Column with Replaceable Energy Dissipation Mechanism 201
M. Jenothan, J. A. S. C. Jayasinghe, C. S. Bandara, and A. J. Dammika

Geotechnical Engineering

Pavement Degradation Model for Paved and Unpaved Roads in Sri Lanka 217
M. M. N. T. Meghasooriya, K. M. N. M. Jayarathna,
and S. K. Navaratnarajah

Numerical Study on the Shear Behaviour of Railway Ballast Using Discrete Element Method 231
S. Venuja, S. K. Navaratnarajah, W. R. R. Jayawardhana,
P. H. L. Wijewardhana, K. Nirmali, and M. A. M. Sandakelum

Reinforcing of Earth Soil and Cement with Pretreated Cornhusk Fibers in the Development of Building Materials 241
T. N. Fernando and I. P. Batuwita

Stability Analysis of Colombo–Katunayake Expressway Embankment Using Fly Ash-Stabilized Soil as the Embankment Material 255
K. Mathumidah, S. Lavanyan, and M. C. M. Nasvi

Effects of Soil Moisture on Simulated Methane Flow Under Varying Levels of Soil Compaction 271
M. M. T. Lakshani, T. K. K. C. Deepagoda, T. J. Clough, J. R. R. N. Jayarathne, S. Thomas, N. Balaine, B. Elberling, and K. Smits

Numerical Simulation of Energy-Absorbing Rubber Pads Using FEM and DEM Approaches—A Comparative Study 283
H. G. S. Mayuranga, S. K. Navaratnarajah, C. S. Bandara, and J. A. S. C. Jayasinghe

Prediction of Geotechnical Properties of Stabilized Soil Using Fly Ash-Based Stabilizer Systems 297
N. A. N. M. Nissanka, K. M. D. Nimesha, and M. C. M. Nasvi

Elastic and Shear Moduli of Over Consolidated Lime Stabilized Clayey Soil 315
H. S. U. De Silva, D. S. P. Amarasekara, and L. C. Kurukulasuriya

Built Environment Planning and Resilience

Critical Analysis of Tsunami Preparedness at Local Level for Sustainable Urban Planning in Sri Lanka 327
C. J. De Zoysa, A. A. S. E. Abeysinghe, U. T. G. Perera, C. S. A. Siriwardana, P. B. R. Dissanayake, R. Haigh, and D. Amaratunga

An Investigation of Factors Affecting the Marginalized Communities in Disasters from an Intersection Perspective: A Systematic Literature Review 341
R. M. Rinaz and C. S. A. Siriwardana

Ensuring Biological Hazard Preparedness in Health and Safety of Construction Sector: A Framework for a Code of Practice 357
Ravindu Jayasekara, Lahiru Kodithuwakku, Chandana Siriwardana, Sudath Samaraweera, and Nimalka Pannila Hetti

Social Network Analysis-Based Approach to Investigate the Network of Risk and Crisis Communication of Government Agencies During Early Stages of COVID-19 in Sri Lanka 373
K. K. C. L. Kannangara, C. S. A. Siriwardana, and H. A. D. G. S. Jayathilaka

Analysing Facebook Practices for Disaster-Related Communication in Sri Lanka: A Case Study of a Facebook Page Dedicated to Disaster-Related Information 389
H. A. D. G. S. Jayathilaka and C. S. A. Siriwardana

A Systematic Review on Different Approaches Used in the Development of Fragility Curves for Buildings 407
R. A. D. V. Rajapaksha and C. S. A. Siriwardana

Development of a Digital Elevation Model Integrating Different Datasets for an Area of Mahaweli Basin, Sri Lanka 427
P. D. P. O. Peramuna, N. G. P. B. Neluwala, K. K. Wijesundara, P. B. R. Dissanayake, S. De Silva, and S. Venkatesan

Climate Change Impacts on Built Environment: A Systematic Review 443
Bawantha Rathnayaka, Chandana Siriwardana, Dilanthi Amaratunga, Richard Haigh, and Dilan Robert

New Normal Remote Communication for Collaboration 461
P. Vaz-Serra, F. Hui, C. Duffield, P. Mendis, and L. Aye

Advanced Technologies in High-Rise Structures

A Comparison Between Predicted and Actual Thermal Sensation in Non-air-conditioned Residential Buildings in a Tropical Climate: A Case Study 477
M. A. U. R. Maddumaarachchi, V. M. Jayasooriya, and D. M. Senevirathne

A Highly Efficient Numerical Approach Using Fluid–Structure Interaction to Estimate Responses of Super-Tall Structures 489
K. Wijesooriya, D. Mohotti, and P. L. N. Fernando

Challenges in Transport Logistics for Modular Construction: A Case Study 501
P. A. N. Peiris, F. K. P. Hui, T. Ngo, C. Duffield, and M. G. Garcia

Readiness of Sri Lankan Construction Industry Towards Implementing Last Planner System in Lean Construction 511
M. D. L. Priyadarshana, I. W. N. Bandaranayake, and A. K. K. Kulathunga

Life Cycle Assessment for Modular-Constructed Buildings: A Proposed Methodological Framework 519
J. Jayawardana, A. K. Kulatunga, M. Sandanayake, G. Zhang, and J. A. S. C. Jayasinghe

Innovative Building Materials and Concrete Technology

Pre-treated Coir Fibres Reinforced Biocomposite Structures for Green Wall Cultivations 535
K. R. Jayasingha, K. H. G. P. Tharanga, D. G. J. P. Dayarathne, M. M. I. Ahamed, T. N. Fernando, and A. P. Pallewatta

Improving Impact Resistance of Plain-Woven Ultra-High Molecular Weight Polyethylene Fabrics 549
D. Weerasinghe, S. Breen, H. Wang, D. Mohotti, P. J. Hazell, and J. P. Escobedo-Diaz

Investigation of Mechanical Properties of Borax-Treated *Bambusa vulgaris* (Sri Lankan Bamboo) 561
R. Vipushnan, M. T. R. Jayasinghe, S. L. Platt, and H. D. Hidallana-Gamage

Production of Bricks Using Spent Diatomaceous Earth Used in Brewing Industry 577
Rumesh Nanayakkara and Chamila Gunathilaka

Evaluate the Feasibility for Making of Non-load Bearing Blocks Using Plastic Waste as Partial Replacement for Fine Aggregate 589
S. Srisaisoruban, S. Jamesbager, M. Kajalakshi, and M. S. T. Priyadarshana

Assessment of Concrete Durability by Surface Resistivity and Initial Surface Absorption 603
N. H. I. C. Fonseka and S. M. A. Nanayakkara

Investigation of Properties of Ultra-High-Performance Concrete and Development of UHPC Waffle Deck Panels for Pedestrian Bridges 621
R. M. W. Perera, T. S. Dinushika, M. S. Swarnamali, T. Priyadarshana, and K. P. Arandara

Development of Blended Fly Ash-Rice Husk Ash–Based Alkali-Activated Bricks: A Sustainable Alternative to Portland Cement Brick 643
Sarah Fernando, Chamila Gunasekara, David W. Law, M. C. M. Nasvi, Sujeeva Setunge, and Ranjith Dissanayake

Sustainable Construction and Resource Efficiency

Modeling Building Envelop with Vertical Green Living Walls as an Urban Heat Island (UHI) Mitigation Strategy 657
T. A. N. T. Perera, G. Y. Jayasinghe, R. U. Halwatura, and H. T. Rupasinghe

Role of Compatibilization of Phthalic Acid in Cassava Starch/Poly Vinyl Alcohol Thin Films 665
O. H. P. Gunawardene, S. M. Amaraweera, W. M. D. B. Wannikayaka, N. M. L. Fernando, C. A. Gunathilake, W. A. Manamperi, A. K. Kulatunga, and A. Manipura

Adaptation of Scrum and Web-Based Integrated Techniques to Construction Sector of Sri Lanka 691
P. Ashokkumar, I. V. H. Wiratunga, and A. K. Kulatunga

An Integrated Approach for Municipal Buried Infrastructure Asset Management 709
H. T. K. G. Jayawickrama, S. V. Gurupatham, P. Perera, and C. S. A. Siriwardana

Thermal Assessment of Terrace Houses Constructed with Light Weight Eps-Based Panels 719
R. Kathiravelu, N. Athukorala, and M. T. R. Jayasinghe

Key Procurement Selection Factors for Sri Lankan Private-Sector Commercial Building Projects 737
H. A. L. V. Silva and U. Kulatunga

External Stakeholder Management in the Sri Lankan Construction Industry 753
H. G. A. R. Randeniya, K. M. P. Wickramasuriya, and P. B. G. Dissanayake

Evaluation of Risk in Water Supply Projects by Relative Importance Index Method 761
A. W. K. Arif and C. K. Pathirana

Application of GIS to Detect Vulnerability of Water Distribution System 771
H. A. N. S. Kadurugamuwa, G. W. A. S. Dilthara, and H. K. Nandalal

Embodied Energy and Lifecycle Assessment of EPS based Light-weight Panel Apartments in Tropical Uplands 783
R. Shiveswarran, N. Athukorala, and M. T. R. Jayasinghe

Sustainable Water Consumption in Building Industry: A Review Focusing on Building Water Footprint 799
Bhagya Nallaperuma, Zih-Ee Lin, Jithya Wijesinghe, Amila Abeynayaka, Safa Rachid, and Selim Karkour

Structural Modeling and Health Monitoring

Application of Virtual Element Method for Plane Stress–Plane Strain Problems

Lahiru N. Dissanayake, D. S. T. Costa, and K. K. Wijesundara

Abstract Virtual element method (VEM) is an extension of the standard finite element method (FEM), providing a more generalized approach to overcome the drawbacks of the FEM. A comprehensive literature review is carried out to observe the current applications of VEM for two-dimensional structural problems. However, it is observed that the current applications do not focus specifically on the importance of the stability parameter of the VEM. Therefore, this research is focused to study the effects of the stability parameter on the robustness and the stability of the VEM developing a general-purpose VEM code for analysis of the plane stress/plane strain problems. For this purpose, simple shaped polygons are proposed as the discretized element since they fully utilize the importance of VEM. Four case studies are carried out to compare the results obtained from the VEM and the FEM with the exact solution. Analytical results show that the stability parameter of the VEM can be categorized into three regions, and it is very much sensitive to the aspect ratio. This study proposes an equation to estimate the stability parameter as a function of aspect ratio to obtain more accurate results than the standard FEM results. Furthermore, this study concludes that VEM can be effectively used to model the structure using the non-convex element.

Keywords Virtual element method · Stability parameter · Non-convex elements · Finite element method

1 Introduction

Virtual element method (VEM) is a newly implemented method that arises for structural engineering applications. Due to the drawbacks and restrictions in the finite element method (FEM), VEM is introduced which can tackle them more efficiently. The VEM name originated as the local shape functions space defined in this is implicit in each element of VEM [5]

L. N. Dissanayake (✉) · D. S. T. Costa · K. K. Wijesundara
Faculty of Engineering, University of Peradeniya, Peradeniya, Sri Lanka
e-mail: e15085@eng.pdn.ac.lk

R. Dissanayake et al. (eds.), *12th International Conference on Structural Engineering and Construction Management*, Lecture Notes in Civil Engineering 266,
https://doi.org/10.1007/978-981-19-2886-4_1

FEM is developed up to general quadrilaterals elements and does not allow us to use polygonal elements that have more than four nodes. However, in VEM, it allows us to use arbitrary polygonal meshes for discretization. FEM is an acceptable method only for convex elements as the Jacobian matrix used in the transformation to produce the local stiffness matrix leads to inaccurate results in the presence of distorted and non-convex elements. VEM is a numerical technique designed for very general shapes both convex and non-convex. This implemented new technique can easily deal with polygonal and polyhedral meshes without any complex integrations. In FEM, hanging nodes are avoided since they are incompatible when it comes to continuity and assembling. However, in VEM meshes, the presence of hanging nodes can be handled by increasing the number of nodes of a single element.

VEM has developed rapidly in the last decade, and it is able to merge with a vast range of topics. The fundamental theory behind this method is VEM space that is well defined in the boundary of the element and explicitly defined inside the element. It does not require functions inside the element, and VEM does not describe the displacement inside the element. The only consideration of VEM is the nodal coordination of the discretized element. This study aims to study the novel method of the virtual element method to make standard FEM more generalized. Most of the applications are focused on stability parameter $(\tau_h) = 0.5$ and do not corporate the effect of the real importance of the stability parameter [2]. Therefore, our objectives are to compare and analyze the accuracy and robustness of this implemented method and to optimize the variation of convergence with stability parameter. For this, four case studies are developed.

Case 01 is developed to access the effect of stability parameter on the VEM results. Case 02 is developed to investigate the sensitivity of the stability parameter in the aspect ratio. Case 03 is developed to investigate the application of VEM on the non-convex element and its accuracy, and finally, Case 04 is developed to explore the application of VEM on triangular elements and plane strain problems.

2 Formulation of Virtual Element Method

When compared to the newly implemented VEM, standard FEM can only allow elements that are either triangles or quadrilateral since it is computed with iso-parametric formulation, a reference element, where all computations are performed and then transformed to the actual position in space. Because the mapping between reference and actual element involves the Jacobian of the transformation, badly shaped elements result in loss of accuracy and the performance of the method becomes dependent on mesh quality [6]. This results in the limitation of the type of polygons about the number of edged and the shape (i.e., convex, or non-convex polygons).

In addition, in standard FEM, it is incompatible when it comes to hanging nodes, which gives a huge disadvantage for local refinement of meshes.

The formulation is initiated considering the Poisson equation (1) in two dimensions [4],

$$\begin{cases} -\Delta u = f \text{ in } \Omega \\ u = 0 \text{ on } \partial\Omega \end{cases} \tag{1}$$

where Ω is a polygonal domain in $\mathbb{R}^2$. Unlike FEM, the Ω space is discretized into non-overlapping elements that can be either be convex or be non-convex polygons. $\partial\Omega$ denotes the boundary of the polygonal domain of Ω.

The weak formulation, with v being the arbitrary test function, gives the following expression (2) for the bilinear form:

$$a(u, v) = L(v) \forall v \in V \tag{2}$$

The bilinear and linear forms of the above weak formulation are given, respectively, by (3) and (4),

$$a(u, v) = \int_{\Omega} \sigma(u) : \varepsilon(v) d\Omega \tag{3}$$

$$L(v) = \int_{\Omega} v \cdot f \, d\Omega + \int_{\partial\Omega t} v \cdot t \, d\partial\Omega \tag{4}$$

where σ is the Cauchy stress tensor which follows Hooke's law,$\sigma = D\varepsilon$, where $\varepsilon(u) = \frac{1}{2}(\nabla u + \nabla u^{\mathrm{T}})$ is the linearized strain tensor [6].

A VEM discretization for the above problem is constructed by restricting the original weak formulation (2) to the discrete space V_{h} which is a procedure that closely resembles the FEM approach (5) [4],

$$\begin{cases} \text{find } u_h \in V_h \text{ such that} \\ a_h(u_h, v_h) = L_h(v_h) \ \forall v_h \in V_h \end{cases} \tag{5}$$

where $V_h \subset V$ is the virtual continuous space introduced earlier;$a_h(\ldots) : V_h \times V_h \to \mathbb{R}$ is a discrete bilinear form approximating the continuous form $a(\ldots)$;$L_h(v_h)$ is the term approximating the virtual work of the external load.

Taking into account that the unknown vector $v_{\mathrm{h}} \in V_{\mathrm{hlE}}$ has two components, for any $E \in \Omega^h$, the degrees of freedom for V_{hlE} will be; 2 m pointwise values $v_h(v_i)$ at corners v_i of E, i = 1, 2, . . . ,m; 2 m(k − 1) pointwise values $v_h\left(x_j^e\right)$ at edge internal nodes $\left\{x_j^e\right\}$, j = 1, . . . , k − 1, being m the number of edges of a polygon; $2\frac{\mathrm{k(k-1)}}{2}$ scalar moments of the unknown field over the element E.

Since neither the function v_h nor its gradient are explicitly computable in the element interior points, the method proceeds by introducing a projection operator Π. The local projection operator (6) is the most crucial component of VEM. It is designated,

$$\Pi_{E,k} : V_h(E) \rightarrow P_k(E) \tag{6}$$

where $V_h(E) \equiv [V_h(E)]^2$ indicates the local space of VEM shape functions on E and $P_k(E) \equiv [P_k(E)]^2$ denoting the polynomial space of order less than or equal to k defined on element E. The projector is used to obtain the polynomial projection of VEM shape functions onto the standard polynomial function, without losing accuracy in the process [6].

In VEM, using the projection operator, the stiffness matrix (7) is obtained by two contributions, namely consistency and stability, and the formulation was adopted by [6].

$$k_E = k_E^c + k_E^s \tag{7}$$

k_E the local stiffness matrix is of the Laplace operator (8) in the element E.

The matrix representation of the projection $\widetilde{\Pi}$ (8) is given by

$$\widetilde{\Pi} = G^{-1}\overline{B} \tag{8}$$

where matrix G (9) and $\overline{B}$ (10) are represented as follows,

$$G = \begin{bmatrix} a_E(p_1, p_1) & a_E(p_1, p_2) & \cdots & a_E(p_1, p_{nk}) \\ a_E(p_2, p_1) & a_E(p_2, p_2) & \cdots & a_E(p_2, p_{nk}) \\ \vdots & \vdots & \ddots & \vdots \\ a_E(p_{nk}, p_1) & a_E(p_{nk}, p_2) & \cdots & a_E(p_{nk}, p_{nk}) \end{bmatrix} \tag{9}$$

$$\overline{B} = \begin{bmatrix} a_E(p_1, \varphi_1) & a_E(p_1, \varphi_2) & \cdots & a_E(p_1, \varphi_{2nd}) \\ a_E(p_2, \varphi_1) & a_E(p_2, \varphi_2) & \cdots & a_E(p_2, \varphi_{2nd}) \\ \vdots & \vdots & \ddots & \vdots \\ a_E(p_{nk}, \varphi_1) & a_E(p_{nk}, \varphi_2) & \cdots & a_E(p_{nk}, \varphi_{2nd}) \end{bmatrix} \tag{10}$$

Here, it can be seen that both matrices as the internal virtual work produced by element E concerning the virtual strain fields.

Finally, the consistency part (11) is computed as,

$$k_E^c = \widetilde{\Pi}^T \widetilde{G} \widetilde{\Pi} \tag{11}$$

where $\widetilde{G}$ is G but with all zero in the first three rows.

To validate, the G matrix obtained D matrix (12) is defined as follows,

$$D = \begin{bmatrix} dof(p_1) & dof(p_2) & \dots & dof(p_{nk}) \\ dof(p_1) & dof(p_2) & \dots & dof(p_{nk}) \\ \vdots & \vdots & \ddots & \vdots \\ dof(p_1) & dof(p_2) & \cdots & dof(p_{nk}) \end{bmatrix} \tag{12}$$

The matrix representation of the projection operator acting from V_{hlE} can be written as (13),

$$\begin{aligned} \pi_{ij} &= dof_i(\Pi\varphi_i) \\ &= dof_i\left(\sum_{\alpha=1}^{nk} s_{i,\alpha} p_\alpha\right) \\ &= \sum_{\alpha=1}^{nk} D_{i\alpha}\widetilde{\Pi}_{\alpha j} \\ &= (D\widetilde{\Pi})_{ij} \\ \Pi &= D\widetilde{\Pi} \end{aligned} \tag{13}$$

Since $\widetilde{\Pi} = G^{-1}\overline{B}$, therefore, we can obtain (14),

$$G = \overline{B}D \tag{14}$$

Finally, the stability part is computed as (15),

$$k_E^s = \tau^h tr\left(k_E^c\right)(\mathrm{I} - \Pi)^{\mathrm{T}}(\mathrm{I} - \Pi), \tag{15}$$

whereas stated earlier τ^h is a user-defined parameter, $tr\left(k_E^c\right)$ trace of the stability stiffness matrix, and I is the $2nd$ x $2nd$ identity matrix.

Finally, the VEM local stiffness matrix is expressed as shown in (16) [6],

$$k_E = \widetilde{\Pi}^T\widetilde{G}\widetilde{\Pi} + \tau^h tr\left(k_E^c\right)(\mathrm{I} - \Pi)^{\mathrm{T}}(\mathrm{I} - \Pi) \tag{16}$$

2.1 Importance of Stability Parameter

A close inspection of equation (15) reveals that the stability term is a rough approximation of the internal energy associated with the difference between a VEM shape

function and its projection. Namely, the term $(\mathrm{I}-\Pi)^{\intercal}\,(\mathrm{I}-\Pi)$ takes into account this difference, while $tr\left(k_E^c\right)$ scales the term with respect to the consistency part, which is the desired property used for proving convergence of the VEM method. τ^h, a suitable stabilizing term, needed to preserve the coercivity of the system.

The trace term in the definition of k_E^s is added to guarantee the correct scaling of the energy with respect to the element size and material constants. The factor $\tau^h \in \mathrm{R}$, $\tau^h > 0$, can be discarded but is included in order to allow for generalizations. Indeed, a typical choice is simply $\tau^h = 1$, but other choices can be found in the literature such as $\tau^h = 0.5$. A detailed investigation on the region below 0.5 has not been carried out in the literature [6].

3 Methodology

In this study, a general-purpose compute code is developed using MATLAB to carry out a numerical test. A wide numerical investigation is performed to assess the accuracy and robustness of VEM, considering different aspect ratios and the change of stability parameter. Numerical results are also compared with standard FEM results.

The application of VEM has illustrated the simplex case of cantilever beam quadratic element with 0.01 m thickness, modulus of elasticity (E) of 210 GPa, and Poisson's ratio (ν) of 0.3 with a point load of 100 kN at the free end which is considered in the methodology under four cases. Numerical tests are carried out using the general-purpose VEM computer code which is developed.

Case 01: A unit square of 1 m length and height as shown in Fig. 1 is considered to optimize the variation of convergence of VEM results with stability parameters. Here, the stability parameter is varied from 0.1 to 1 with an increment of 0.1, and the vertical displacement at the free end is observed.

Case 02: A rectangle of 1 m length and height of 0.1 m is considered to compare and analyze the accuracy of VEM as shown in Fig. 2. Here, numerical tests are carried out for aspect ratios of 1, 2, 5, and 10, 3 element configuration

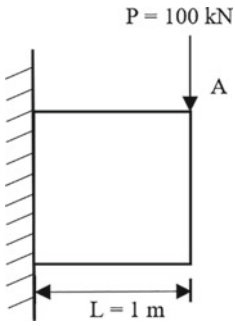

Fig. 1 Unit square element

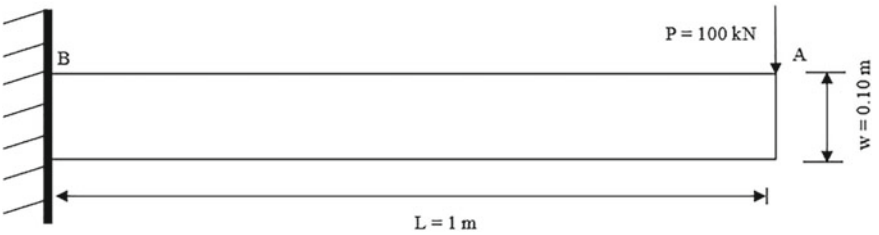

Fig. 2 Cantilever beam problem

cases each. (e.g.,: [Ratio 1 = 10, 40, 160 elements], [Ratio 2 = 5, 20, 80 elements], [Ratio 5 = 2, 8, 32 elements], [Ratio 10 = 4, 16, 64 elements]).

Case 03: Non-convex quadratic elements shown in Fig. 3 are used to investigate the application of VEM and its accuracy.

Case 04: A right-angled triangle element of 1 m by 1 m as shown in Fig. 4 is used to explore the application of VEM on triangular elements and plane strain problems.

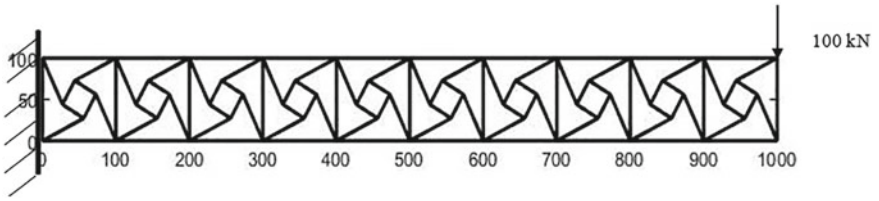

Fig. 3 Non-convex element problem

Fig. 4 Triangular element problem

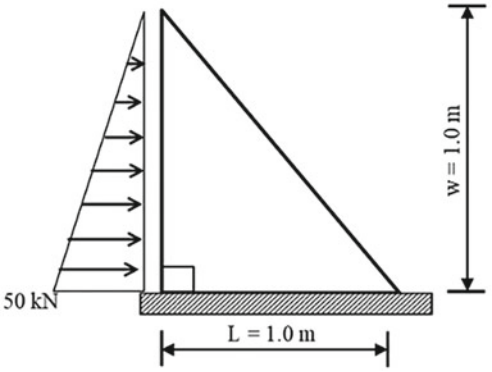

4 Results and Discussion

The accuracy of VEM is studied through a series of patch tests. Unit square element analysis is used to access the effect of stability parameter as mentioned before. The displacement variation of point A with the stability parameter variation is shown in Fig. 5, where the three regions have been identified.

According to the results, with the reduction of the user-defined parameter, the VEM results approach closer to the FEM results. First region is the insensitive region where the stability parameter varies from 0.5 to 1. In this region, VEM results are insensitive to the stability parameter, and there is not much variation in the results. Second region is the effective region where the lower boundary is sensitive to the aspect ratio and the upper boundary of 0.5. In this region, VEM results are highly sensitive to stability parameter, and with a lesser number of elements, results are converged to the exact answer. Most of the previous applications have mainly focused on stability parameter $(\tau_h) = 0.5$ where the convergence is obtained by increasing the number of elements. Third region is the unstable region which is governed by the boundary of the effective region. Elements in this region are unstable and fail the patch test.

Case 01 mainly focuses on the investigation of the variation of results with stability parameter. Hence, Cases 02–04 are conducted for the stability parameter in the effective region to observe the lower boundary of the effective region which is observed to be changing with the aspect ratio.

Under Case 02, the rectangular element is analyzed in different aspect ratios and the displacement variation at point A against the number of elements is obtained as shown in Figs. 6 and 7.

It is observed that the VEM results converge faster than standard FEM with optimizing the stability parameter. The stability parameter values obtained fall under the effective region. It is also observed for aspect ratios of 1, 2, 5, and 10, exact solutions are observed at stability parameter (τ_h) 0.112, 0.045, 0.008, and 0.0017, respectively. With the increment of the aspect ratio, value of the stability parameter

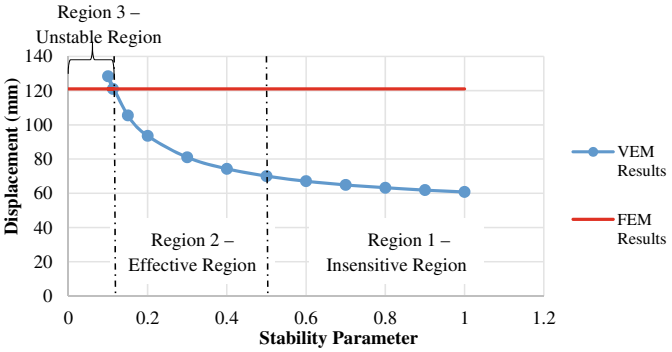

Fig. 5 Displacement variation of point A with the stability parameter

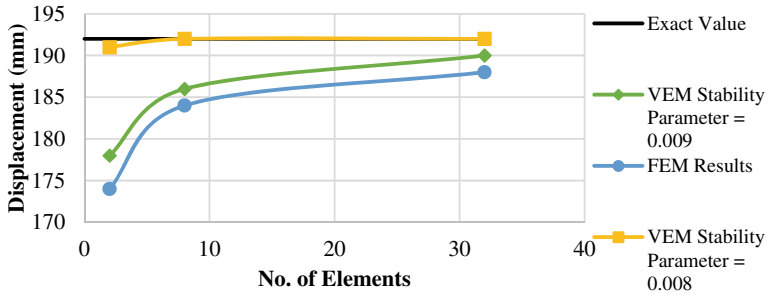

Fig. 6 Displacement variation of aspect ratio 5 with the change of stability parameter

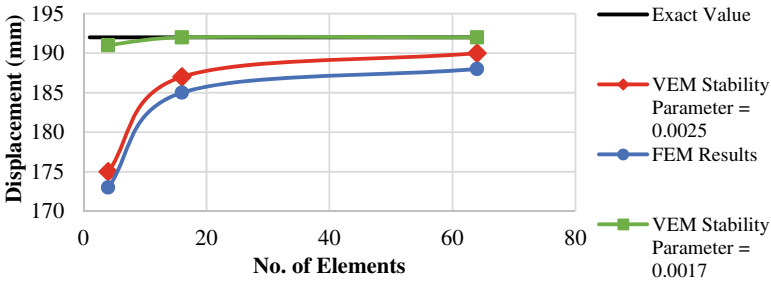

Fig. 7 Displacement variation of aspect ratio 10 with the change of stability parameter

is reduced, which give an almost exact solution. The relationship between the aspect ratio and the stability parameter could be developed from this approach.

Due to the sensitivity of the stability parameter in this effective region, most of the previous applications are conducted for stability parameter in the insensitivity region. It can be observed that VEM shows higher robustness for quadrilateral polygonal discretization. The numerical tests are conducted showed that optimal convergence rates are achieved for $k = 1$ linear polynomial order function. But, accuracy could be more improved by using high-order polynomial functions.

The relationship between the aspect ratio and the stability parameter is plotted in Fig. 8. Stability parameter values for each aspect ratio are obtained where the VEM results give accurate displacement results.

Figure 9 shows the X-direction normal stress variation throughout the cantilever beam element. When the number of elements becomes higher, stress results become converge to the exact results.

Under Case 03 of this study, the application of VEM on the non-convex element and its accuracy is observed. Similar to Case 01, it is observed by optimizing the stability parameter that more accurate answers can be obtained as shown in Fig. 10.

From the above results, it is certain that non-convex elements are constructed with accurate results by optimizing the stability parameter. By analyzing the displacement

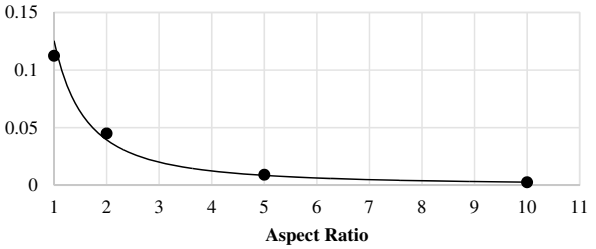

Fig. 8 Variation of the stability parameter with the aspect ratio

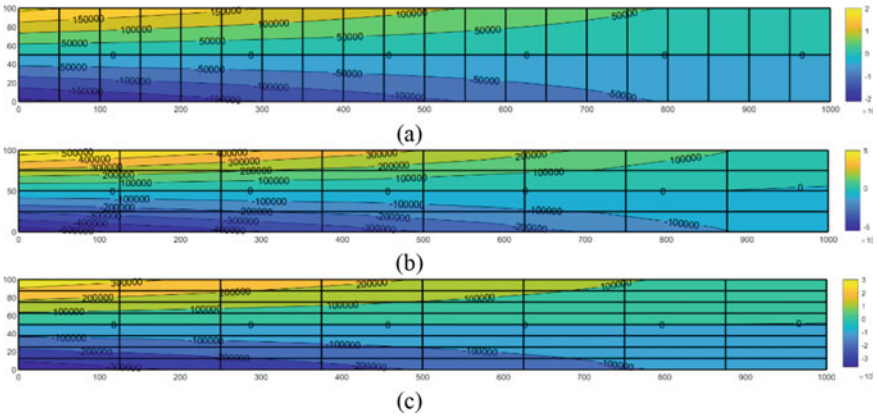

Fig. 9 Stress variation of the cantilever beam **a** 40 element—aspect ratio 1, **b** 32 element—aspect ratio 5, **c** 64 element—aspect ratio 10

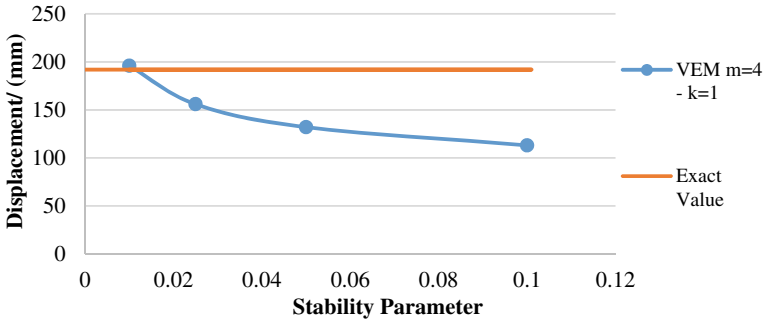

Fig. 10 Variation of the nodal displacement with the stability parameter

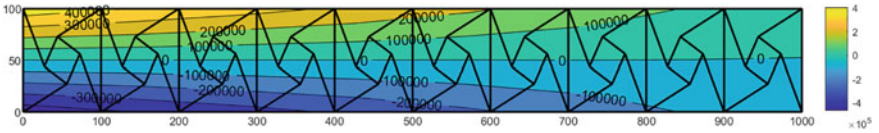

Fig. 11 Stress variation of the cantilever beam with concave elements

field, the stress contour variation could be obtained for the non-convex element cantilever problem as shown in Fig. 11.

For plane strain application problem, triangular dam element is analyzed, and uniformly varying distributed load is applied to the vertical face of the dam section under Case Study 4. Accurate results for triangular elements can be obtained from VEM compared to the FEM. Figure 12 shows the forces at the nodes of the element.

During analysis, the user-defined parameter of the stability part is varied from 0.1 to 1. It is observed that the results are completely insensitive for the stability parameter. Figure 13 shows the shear stress variation within the element.

VEM results show higher values for shear stress variation throughout the element, but it can be optimized by discretizing the element. Since the triangle element is

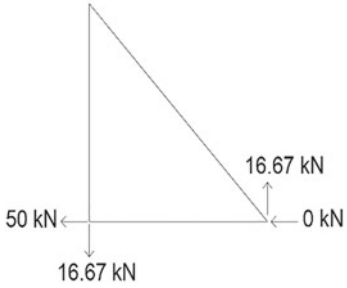

Fig. 12 Forces at the nodes of the element

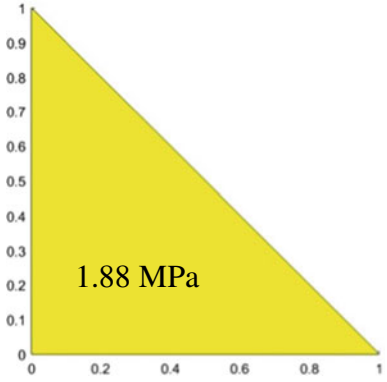

Fig. 13 VEM stress contour variation

insensitive to the stability parameter, optimizing the stability parameter to obtain a more accurate answer is not possible.

5 Conclusions

In this study, the formulation of VEM in the context of 2D linear elastic problems is carried out under four main case studies.

Under Case 01, three regions are identified with the change of the stability parameter. First region is the insensitive region (0.5–1 stability parameter), where VEM results are insensitive to the stability parameter. Second region is the effective region (lower boundary which is sensitive to the aspect ratio), where results are highly sensitive to stability parameter, and with a lesser number of elements, convergence and accurate values are obtained. Finally, third region which is the unstable region beyond the lower limit of the effective region), elements are unstable and fails the patch test.

Considering the effective region in Case 01, compared to standard FEM, more accurate and convergent results are obtained for VEM by optimizing the stability parameter. Hence, optimized stability parameters can be proposed of different ranges of aspect ratio,

- For aspect ratios from 5 and above a constant stability parameter
- For aspect ratios from 1 to 5, optimized stability parameter can be obtained from the stability parameter versus aspect ratio graph.

It can be observed, under Case 03, that VEM can also be applied for non-convex elements which produce accurate results by optimizing the stability parameter.

Under Case 04, it is observed by changing the constitutive matrix, similar to standard FEM, accurate results can be obtained for plane strain problems. VEM shows a higher value for shear stress which can be optimized by discretizing the element. Also, the triangular elements have been identified as completely insensitive for stability parameters.

References

1. Ahmad B, Alsaedi A, Brezzi F, Marini LD, Russo A (2013) Equivalent projectors for virtual element methods. Comput Math Appl 66(3):376–391
2. Artioli E, Beirão da Veiga L, Lovadina C, Sacco E (2017) Arbitrary order 2D virtual elements for polygonal meshes: part I, elastic problem. Comput Mech 60(3):355–377
3. Beirão da Veiga L, Brezzi F, Cangiani A, Manzini G, Marini LD, Russo A (2012) Basic principles of virtual element methods. Math Models Methods Appl Sci 23(01):199–214
4. Beirão da Veiga L, Brezzi F, Marini LD, Russo A (2014) The Hitchhiker's guide to the virtual element method. Math Models Methods Appl Sci 24(08):1541–1573

5. Da Veiga LB, Brezzi F, Marini LD (2013) Virtual elements for linear elasticity problems. SIAM J Numer Anal 51(2):794–812
6. Mengolini M, Benedetto MF, Aragón AM (2019) An engineering perspective to the virtual element method and its interplay with the standard finite element method. Comput Methods Appl Mech Eng 350:995–1023

Simulation of Reinforced Concrete Beam Shear Behavior: Contact Density Model Approach

R. M. A. Buddhika and H. D. Yapa

Abstract Shear failure of reinforced concrete (RC) structures occurs without any warnings, and hence, adequate attention on such failures needs to be paid. However, the shear behavior in concrete structures is not fully comprehended yet, and therefore, the task is a challenge. Original contact density model (OCD), which is based on geometry of aggregate interlock and represent with a simple normal distribution function (NDF), is considered as a potential option to predict the complex nature of shear stress transfer in concrete. The literature shows that the OCD has been subjected to several improvements in the recent past. In this light, this study numerically simulated the global behavior of two shear critical RC beams with the non-linear finite element (FE) method. The simulations were used to test the performance of an OCD-based shear constitutive model and that was compared with the commonly used rotating crack model and constant shear retention crack model. The FE results showed that the performance of the OCD-based shear model was more promising in predicting the global behavior of the beams.

Keywords Shear cracks · Aggregate interlock · Non-linear simulation · Numerical modeling

Abbreviations

RC	Reinforced concrete
ε_{tu}	Crack strain
NSC	Normal strength concrete
OCD	Original contact density
MCD	Modified contact density
NDF	Normal distribution function
CDF	Contact density function

R. M. A. Buddhika (✉) · H. D. Yapa
University of Peraddeniya, Peradeniya, Sri Lanka
e-mail: achinthabuddhika@gmail.com

R. Dissanayake et al. (eds.), *12th International Conference on Structural Engineering and Construction Management*, Lecture Notes in Civil Engineering 266,
https://doi.org/10.1007/978-981-19-2886-4_2

FEM	Finite element modeling
$™_i$	Strain
At	Whole surface area per unit projected crack area
$ς(υ)$	Directional distribution of contact unit
$υ_s$	Resultant contact angle
$υ$	Inclination of deformed unit
$σ_{con}$	Contact stress
$ϖ_υ$	Relative displacement
R_s	Elastic rigidity per unit length
$ϖ_{up}$	Local plasticity
$f_{c,cu}$	Compressive strength of concrete
G_{max}	Maximum aggregate size
$ϖ$	Crack width
$Δ$	Shear displacement
Z	Contact force
T	Shear stress
$σ$	Normal stress
$α$	Crack asperity degradation
$σ_{var}$	Standard deviation
$σ_ς$	Contact density function
m	Mean
A_c	Cross-sectional area
$σ_s$	Axial bar stress
$ρ$	Reinforcement ratio
N	External axial force
T_s	Steel shear stress
$ΔV$	Crack slip
$Δh$	Crack opening
$δ_i$	Shear displacement
Y	Crack strain
L_i	Crack spacing
$σ_t$	Transferred tensile stress
$™_u$	Ultimate tensile strain
E_o	Initial stiffness of concrete
$™_c$	Stress-associated strain
$™_{tot}$	Total strain
$™_{eff\text{-}free}$	Effective stress-free strain of concrete
f_t	Uniaxial tensile strength
C	Tension softening parameter
G_f	Fracture energy
l	Element size

1 Introduction

1.1 Background

Behavior of reinforced concrete (RC) members may considerably be affected by cracked concrete and the stress transfer capabilities of cracks and interfaces. Not like flexural failures, shear failures occur suddenly; hence, assessing shear behavior accurately in a RC structure is more critical Moradi et al. [5].

1.2 Contact Density Model

The diagonal cracking shear force in RC members is transferred in various ways. After the flexural cracks are developed, shear force acting on a cracked section is carried by three main ways. One is the shear resistant of un-cracked concrete in the compression zone, two is the aggregate interlocking action, and third is the dowel action. In a rectangular section, approximately 90% of shear force transferred by aggregate interlocking [7]

A path-dependent shear stress transfer model across concrete cracks known as original contact density (OCD) model was claimed to be impressive to deal with the complex nature of shear stress transfer in concrete where crack surface is divided into infinitely small pieces called contact units [4].

The directional distribution is represented from a simple trigonometric formula used as a contact density function (CDF). The proposed OCD model was just depending on crack unit orientation, θ. Further modifications are proposed to NDF to represent compressive strength of concrete (f_{cu}); maximum aggregate size (G_{max}); initial crack width (w_o); and crack asperity degradation [5]. This function with factors is known as modified contact density function (MCD).

1.3 Finite Element Modeling

Total crack strain constitutive model uses the smeared crack approach in predicting the response of RC elements with three uniaxial material models for tension, compression, and shear. It is widely used in predicting the flexural response of RC elements accurately incorporating moment axial interaction, effects of lateral confinement, etc.

However, it is identified that the accurate prediction of the shear capacity and the overall load deflection response of the RC element dominated by shear is very sensitive to the shear stress–strain curve used in the constitutive relationship, [1].

2 Literature Survey

2.1 Original Contact Density Model

Two proposals on geometry of crack surfaces and contact stress direction and three basic assumptions on contact density function, elasto-plastic model, and effective ratio of contact were considered when developing OCD model. The first proposal was so that complicated asperity of cracked surfaces can be divided into infinitely small pieces defined as contact units with various global inclinations θ. See Fig. 1.

Area of a contact unit was proposed to be, $dA\theta = At \cdot \Omega(\theta)d\theta$ [4] where At is the whole surface area per unit projected crack area and $\Omega(\theta)$ is the directional distribution of contact unit which was proposed as equal to 0.5 cosυ.

Contact reaction is composed of normal reaction (from the unit deformation) and tangential reactions (from friction). See Fig. 1. The resultant contact angle, θ_s, and the inclination of deformed unit, θ, were assumed to be equal under the second proposal. Hence, the direction of contact stress remains constant during loading. θ(s) = θ. The two-dimensional projection of cracked plane was experimentally scanned, and corresponding density distributions were plotted as shown in Fig. 2 [4].

For simplicity, [4] assumed a trigonometry function as the first assumption to represent the directional distribution of contact unit as,

$$\Omega(\theta) = 0.5 \cos\theta \tag{1}$$

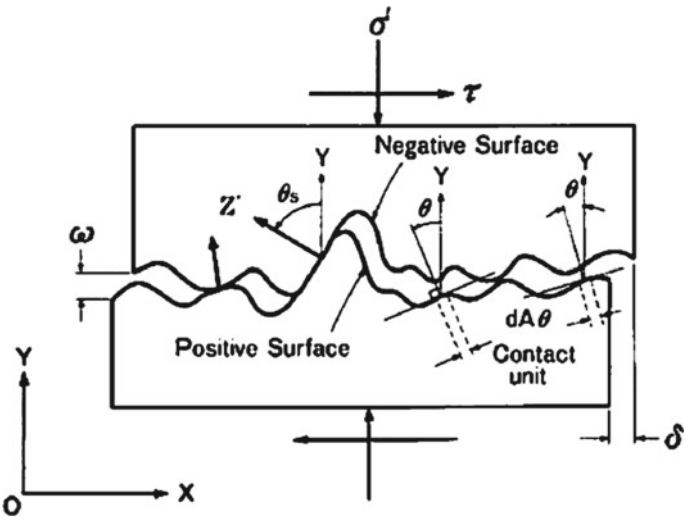

Fig. 1 Contact units [4]

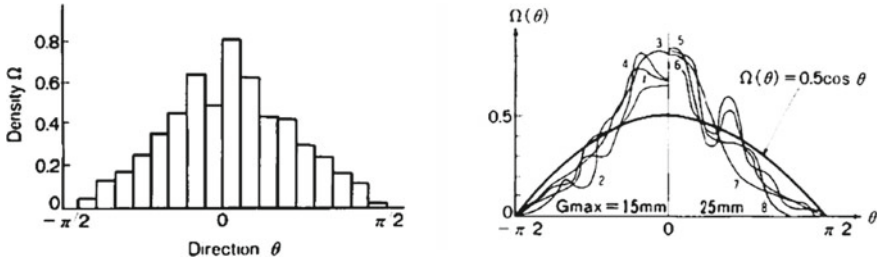

(a) (b)

Fig. 2 **a** Histogram of contact directions θ measured in one specimen and **b** combination of histograms of many specimens [4]

It was assumed that the contact stress σ_{con} in θ direction depends on relative displacement $\omega(\theta)$ as a second assumption. It is mathematically described as,

$$\sigma_{con} = \begin{cases} R_s(\omega_\theta - \omega_{\theta p}), & \omega_\theta \geq \omega_{\theta p} \\ 0, & \omega_\theta < \omega_{\theta p} \end{cases} \tag{2}$$

where Rs is the elastic rigidity per length and $\omega_{\theta p}$ is the local plasticity in θ direction as shown in Fig. 3 and where $f_y^{'} = 13.7 f_c^{1/3}$ and ω_{lim}= 0.04 mm.

Contact between crack surfaces does not occur if the crack width is large enough compared to the roughness. To include crack roughness, the third assumption effective ratio of contact was proposed as,

$$K(\omega) = 1 - e^{\left(\frac{0.5G_{max}}{\omega}\right)} \tag{3}$$

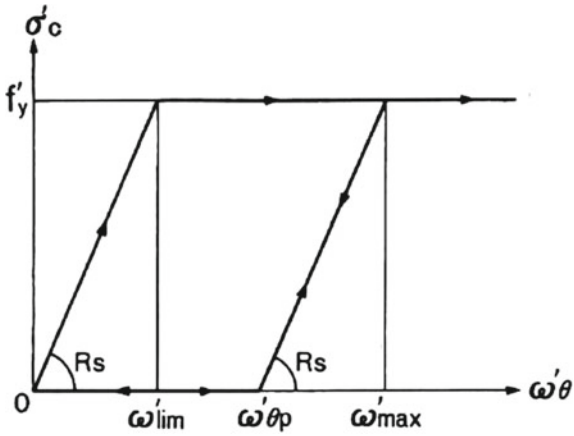

Fig. 3 Elasto-plastic model for contact compression test [4]

2.2 Obtaining Shear Displacement Relationship

By considering the 2D projection of cracked surface, ω_θ can be computed from compatibility of crack deformations.

$$\omega_\theta = \Delta \sin\theta - \omega \cos\theta \tag{4}$$

$$R_s = \frac{f'_y}{\omega_{lim}} \tag{5}$$

$$A_t = \frac{4}{\pi} = 1.27 \tag{6}$$

Contact force Z,

$$\mathrm{Z} = \mathrm{K}(\omega) A_t \Omega(\theta) \sigma_{con} \tag{7}$$

To satisfy the equilibrium condition, the summation of contact forces Z for all contact unit must balance external shear stress.

Shear stress,

$$\tau = \int_{-\frac{\pi}{2}}^{\frac{\pi}{2}} Z \sin\theta d\theta \tag{8}$$

Normal stress,

$$\sigma = \int_{-\frac{\pi}{2}}^{\frac{\pi}{2}} Z \cos\theta d\theta \tag{9}$$

2.3 Modified Contact Density Function

It was observed that the accuracy of the OCD model is reducing with increasing crack width. Hence, as a further modification, parameters of maximum aggregate size (G_{max}), crack width (ω), and crack asperity degradation (α) are included to the formulation [5]. This modified CDF was assumed to be generalized as a normal distribution function (NDF).

Concrete compressive strength and contact unit orientation (F_1)

The general form of a NDF can be written as,

$$F_1(\theta, m, f_c) = \frac{1}{\sigma_{var}\sqrt{2\pi}} \exp\left[-\frac{1}{2}\left(\frac{\theta - m}{\sigma_{var}}\right)^2\right] \tag{10}$$

where m is the mean and σ_{var} is the standard deviation; the CDF is a zero-mean function. Hence, m = 0 [5]

$$E\left[\theta^2\right] = \int_{-\frac{\pi}{2}}^{\frac{\pi}{2}} \Omega(\theta)\theta^2 d\theta\sigma_{var} = \sqrt{E\left[\theta^2\right]} \tag{11}$$

For NSC,

$$(\theta) = 0.5\cos\theta,\ E\left[\theta^2\right] = \frac{\pi^2}{4} - 2,\ \sigma_{var} = \sqrt{\frac{\pi^2}{4} - 2}, \tag{12}$$

Effect of maximum aggregate size , $F_2(\mathrm{G_{max}})$

Decreasing the maximum aggregate size makes crack profile smoother. There was no noticeable difference observed in crack profiles for specimens with aggregate size between 15 and 25 mm. For $G_{max} < 15$mm, the original CDF should be modified [5].

$$\eta = \frac{G_{max}}{15} \tag{13}$$

Effect of crack width, $F_3(\omega)$

Experimental studies show that the amount of shear transfer capacity of cracks directly depends on the crack width. The larger the initial crack width, the lower the shear stress will be transferred. Because for wide crack widths there will be fewer contact units engaged in contact with each other, hence shear capacity will be low.

$$F_3(\omega) = exp\left(\frac{1}{50\omega}\right) \tag{14}$$

Effect of roughness degradation rate, $F_4(\alpha)$

The standard deviation of F1 was observed to be changed with numerous loading steps. Loading causes reduction in initial standard deviation σ_{var0}, and corresponding NDF becomes narrower. The formulation of crack asperity degradation as follows,

$$F_4(\alpha) = \frac{\sigma_{var,i}}{\sigma_{var,0}} \tag{15}$$

The complete and final form of the proposed modified CDF,

$$\sigma_\Omega(\theta, f_c, G_{max}, \omega, \alpha) = \sigma_{var} \times \left\{1 - \left[1 - \frac{\exp(-\alpha_\Omega)\eta}{1 + \left[\exp(-\alpha_\Omega) - 1\right]\eta}\right]\right\} \times exp\left(\frac{1}{50\omega}\right) \times \frac{\sigma_{var}}{\sigma_{var0}} \tag{16}$$

2.4 Dowel Action

Dowel action, which is the effect of reinforcement in shear transfer along crack surfaces, a macroscale model, was proposed to stimulate dowel behavior of crossing bar across crack [5] As shear displacement applied to the cracked plane, roughness of the crack surface tends to widen the crack width. Axial stress of the bar $A_s\overline{\sigma}_s$, as well as shear displacement, causes flexure effect in the bar. The equilibrium of normal stresses at a crack can be written as,

$$\sigma = \frac{N}{A_c} + \rho\overline{\sigma}_s \tag{17}$$

where ρ is the reinforcement ratio, N is the applied force externally and $\overline{\sigma}_s$ is the axial bar stress. Once the displacement satisfies equilibrium, the corresponding mechanism for the constituting model is determined by contributions of concrete shear (τ) steel shear (τ_s)

$$\tau_t = \tau + \rho\tau_s \tag{18}$$

As shown in Fig. 6, the effect from dowel action was found to be very low compared to shear transfer in aggregate interlocking [6] (Figs. 4 and 5).

2.5 Total Crack Strain Model

Analysis models for concrete cracking can be classified into a discrete crack model (discontinues model) and a smeared crack model (continuum model). The discrete crack model uses finite elements at which concrete cracks are separately represented as boundaries. In the smeared crack model, concrete cracks are assumed to be scattered and distributed, such that discrete elements are not used at the crack locations.

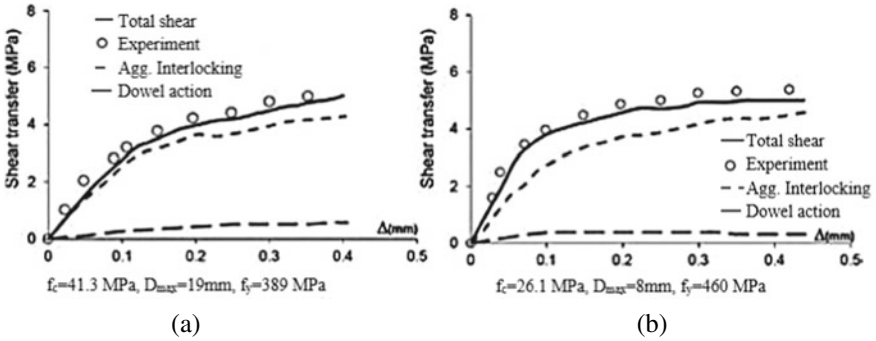

Fig. 4 Predicted and experimental shear stress-associated displacement relationship at interface **a** 41.3 MPa sample and **b** 26.1 MPa sample [5]

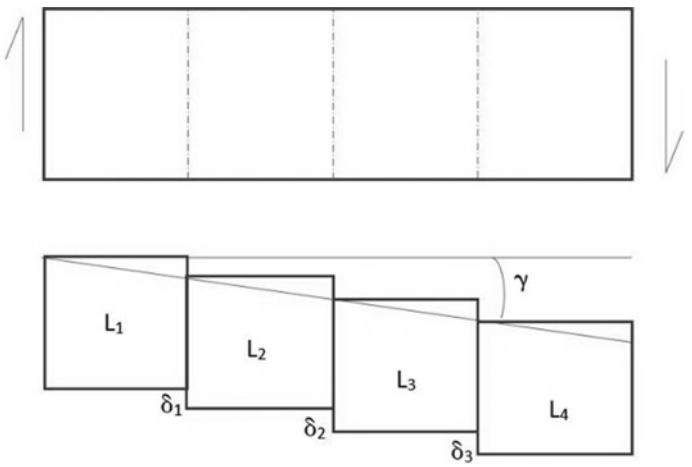

Fig. 5 Element behavior with shear stress

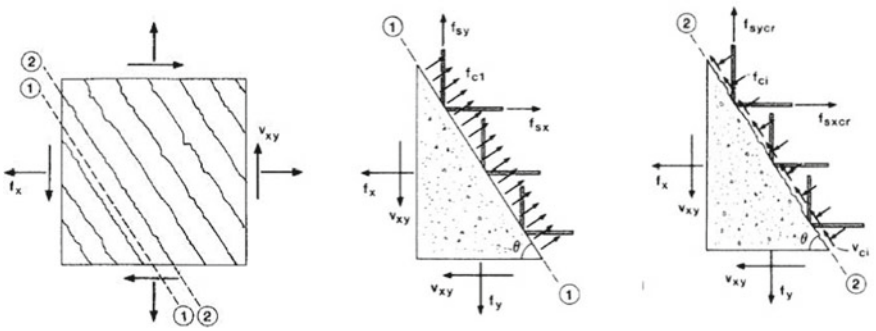

Fig. 6 Comparison of local stresses at a crack with, **a** stresses applied to cracked element, **b** calculated average stresses, **c** local stresses (Vecchio and Collins, 1986)

The smeared crack model assumes that locally generated cracks are evenly scattered over a wide surface. This model is known to be suitable for reinforced concrete structures with reasonable amount of reinforcement, and its finite element modeling is relatively simple [8]. The smeared crack model can be classified into orthogonal and non-orthogonal crack models depending on the assumption of angles of crack development. The orthogonal crack model assumes orthogonal crack directions, whereas non-orthogonal crack model assumes the non-orthogonal directions of cracks. Also, depending on the numerical analysis methods for cracks, the smeared crack model is further classified into various models such as a decomposed strain model and a total strain model [1].

The decomposed strain model in the smeared crack model calculates the total strain in terms of material strain and crack strain. The total strain model in the smeared crack model can be rather simply formulated using total strain without having to decompose it into the strain components. MIDAS uses the total strain crack model classified under the smeared crack model. It provides two methods which are separated into the fixed crack models and the rotating crack model depending on the reference crack axes. The former assumes that the axes of cracks remain unchanged once the crack axes are defined. On the contrary, the latter is a method in which the directions of the crack are assumed to continuously rotate depending on the changes in the axes of principle strains. An iterative scheme needs to be used for concrete crack analysis because of its nonlinearity. In order to satisfy the equilibrium between external and internal force vectors, one of the incremental iterative procedures such as the Newton-Raphson method can be used. To this end, the constitutive model needs to be defined by a proper stiffness matrix. MIDAS uses the secant stiffness and tangent stiffness approaches to determine the stiffness matrix. The secant stiffness approach is especially suitable for finding excellent and stable solutions to analyses of reinforced concrete structures, which widely develop cracks. On the contrary, the tangent stiffness approach is known to be very appropriate for analyses of local cracking or crack propagation.

2.6 Relationship Between Shear Displacement and Shear Strain

In a smeared crack model, an element is assumed to remain continuous even after cracking, and stresses are related to strains rather than the crack width or shear displacement. The ratios of the total crack width and the total shear displacement in an element length are actually the average tensile and shear strains due to cracks developed in an element. Assuming that cracked element is subjected to uniform stresses throughout the whole element, any cracks must carry the same shear and compressive stresses. The total shear displacement and crack opening in an element can be obtained as shown [4].

$$\sum \delta_{\mathrm{i}} = \delta_1 + \delta_2 + \ldots\ldots + \delta_{\mathrm{n}} \tag{19}$$

$$\sum \varpi_{\mathrm{i}} = \varpi_1 + \varpi_2 + \ldots\ldots + \varpi \tag{20}$$

where δ_{i} and ϖ_{i} are the shear displacement and crack width, respectively, in the crack *i*, then the crack strain will take the form of,

$$\gamma = \frac{\delta \mathrm{i}}{L} \tag{21}$$

$$\mathrm{L} = \sum \mathrm{L_i} = \mathrm{L}_1 + \mathrm{L}_2 + \ldots\ldots + \mathrm{L_n} \tag{22}$$

where $\mathrm{L_i}$ is the *i*th crack spacing.

For the vast majority of concretes, cracking will occur along the interface between the cement paste and the aggregate particles. The resulting rough cracks can transfer shear by aggregate interlock [8].

Relationships between the shear across the crack V_{cr}, the crack width w, and the compressive stress on the crack f_{cr} have been studied by any investigators and following relationship was derived,

$$\mathrm{V}_{cr} = 0.18\ \mathrm{V}_{cr\,max} + 1.64 f_{cr} - 0.82\left(\mathrm{f}_{cr}^2/\mathrm{V}_{crmax}\right) \tag{23}$$

In Eq. 24, average crack width w over the crack surface can be taken as the product of the principle tensile strain and the crack spacing L_{υ} [8].

$$\mathrm{w} = {}_1^{\mathrm{TM}}\ \mathrm{xL}_{\upsilon} \tag{24}$$

$$\mathrm{L}_{\upsilon} = \frac{1}{\frac{sin\theta}{Sx} + \frac{cos\theta}{Sy}} \tag{25}$$

where *Sx* and *Sy* are the indicators of the crack control characteristics of x-reinforcement and y-reinforcement.

3 Finite Element Modeling

3.1 Introduction

A three-dimensional non-linear finite element models were developed using MIDAS FEA package to simulate the shear transfer behavior in RC beams where load

displacement results of two test beams which had a compressive strength of 25 MPa compared with the FE analysis results. One beam was with shear links (beam A1), and other beam was without shear links (beam OA1).

In both models, to represent the concrete, eight-node solid brick elements were deployed, and to represent the wooden loading plates and supports, six-node solid wedge like elements were deployed. These solid elements consist of three degrees of freedom per each node. Based on the recommendations of [2], a mesh size of 50 mm which is the size of two times the maximum aggregate size was used to develop the FE model (Figs. 7 and 8).

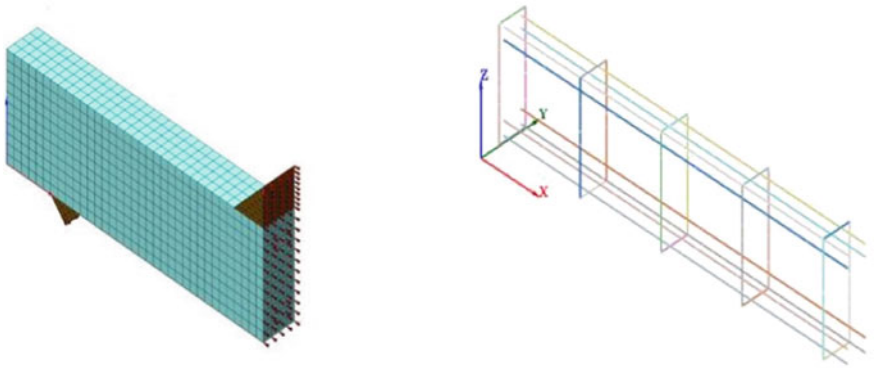

(a) **(b)**

Fig. 7 MIDAS 3D mesh of the finite element model for test specimen, **a** concrete, support, and plates and, **b** reinforcement

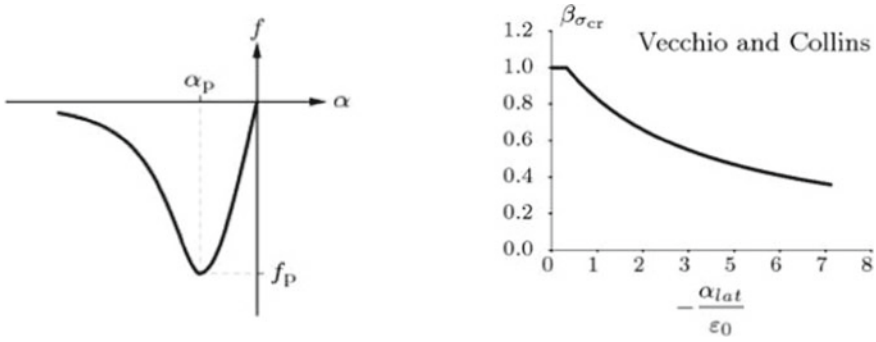

a) b)

Fig. 8 Functions used to model concrete compression behavior, **a** Thorenfeldt compression curve and, **b** Vecchio and Collins' compression softening curve (MIDAS FEA)

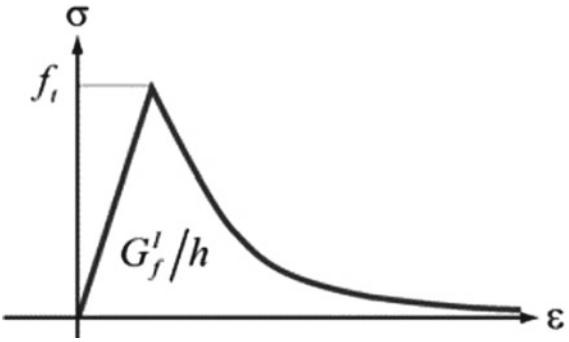

Fig. 9 Function used to model concrete tension behavior; exponential tension softening curve (MIDAS FEA)

3.2 Material Modeling

To model the non-linear material behavior of concrete, smeared crack model was used. Under smeared crack model, total strain model was used in this FE model where concrete is evaluated as the total sum of the normal strain and the crack strain.

Objective of this study was to check whether using the proposed modified shear model would increase the accuracy of predictions compared to the shear models already available; hence, under total strain model, both fixed and rotating models were used separately to compute the predictions.

As the constitutive model needs to be defined by a proper stiffness matrix, secant stiffness matrix was used as it was considered to be more suitable especially for finding excellent and stable solutions to analyze reinforced concrete structures, which widely develop cracks as oppose to local cracking or crack propagation.

The confinement effect of the concrete was incorporated into this material model based on the theory of Selby, whereas the lateral cracking and the compression softening behavior of concrete were incorporated based on the theory of Vecchio and Collins which is an approach based on the fracture energy and crack bandwidth.

3.2.1 Compression Model

The stress–strain behavior of concrete in compression was modeled using the Thorenfeldt compression curve which is based on the compressive cylinder strength of the concrete. The functions used to model compression behavior are depicted in Fig. 9.

3.2.2 Tension Model

The tension stiffening/softening behavior of the concrete was modeled using an exponential tension stress–strain behavior which is an approach based on the fracture energy and the crack bandwidth.

Here, the fracture energy is evaluated using the formula found in [3] (given in the Eq. 28) and the crack bandwidth is assumed as the cube root of the volume of the concrete element as proposed by [3]. The functions used to model the tension behavior of concrete are depicted in Fig. 11.

$$\mathrm{Gf} = 43.2 + 1.13\ \mathrm{fc} \tag{28}$$

3.2.3 Shear Model

Rotating crack model

No shear model was adopted to model the shear behavior of concrete as in the case of rotating crack model the orientation of crack rotates following the direction of the principal stresses where the shear stress acting in that direction is zero. Hence, there is no shear interaction in this rotating crack model. Material and strength parameters of concrete were based on the results of the material tests carried out (Fig. 10)

Fixed crack model

In fixed cracked model, it assumes that the axes of cracks remain unchanged once the crack axes are defined. Under fixed crack model, two main shear models were used to predict the shear stress behavior. One is constant shear retention model. Figure 11 shows the shear stress–strain relationship in constant shear model. The second shear model used was multi-linear stress–strain relationship developed using the MCD model, See Fig. 12.

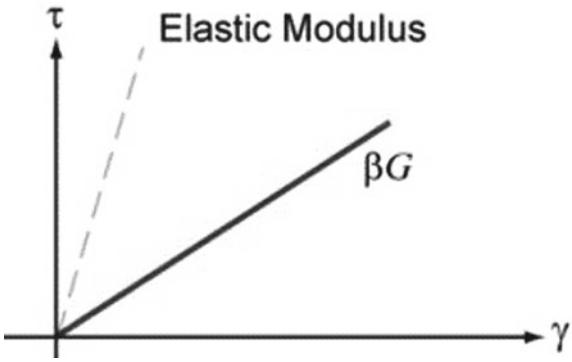

Fig. 10 First function used to model concrete shear behavior; constant shear retention model (MIDAS FEA)

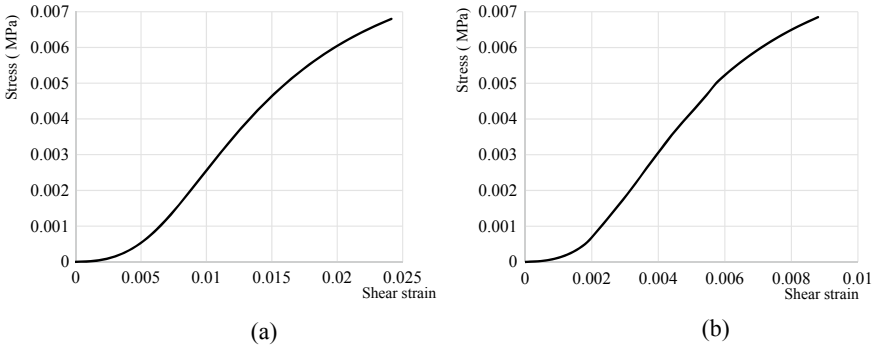

Fig. 11 Second function developed from MCD shear model; multi-linear stress–strain relationship, **a** for beam OA1, **b** for beam A1

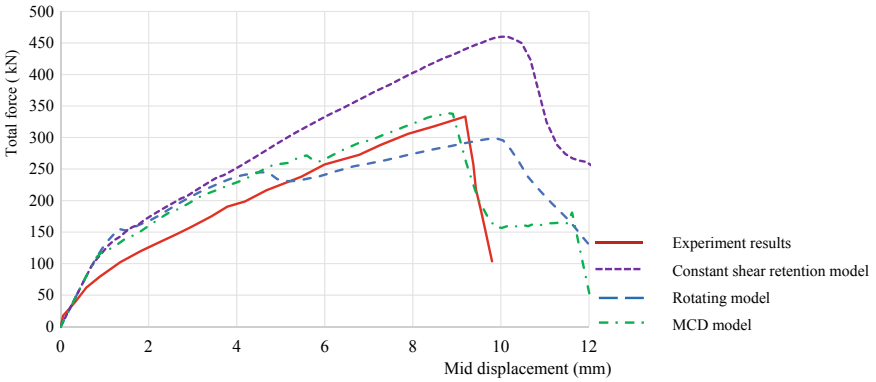

Fig. 12 Load deflection response of experiment and FE model beam OA1

3.3 Results Comparison

3.3.1 Beam OA1 (25 MPa Without Shear Reinforcement)

FE model analysis predictions incorporating MCD shear model, constant shear retention model, and rotating crack models of beam OA1 were compared with the experimental results of beam OA1 where MCD model predictions were found to be more promising compared to the constant shear retention model and rotating shear model predictions.

As depicted in Table 1, MCD model predictions are superior in contrast to all the other models in both total load and mid-displacement predictions. Hence, correlation of MCD model with the experimental behavior can be deemed more satisfactory.

In order to facilitate comparison of overall load predictions in different shear models, the ratio of the FE analysis predictions and the experimental values at any

Table 1 Peak load displacement data in beam OA1

Description	Total load/kN (% of error)	Mid-displacement/mm (% of error)
Experiment results	333	9
Constant shear model predictions	460 (38.1)	10.1 (12.2)
Rotating model predictions	298 (10.5)	10 (11.1)
MCD model predictions	337 (1.2)	8.9 (1.1)

Table 2 Overall load prediction in beam OA1, $\mu(\sigma)$

Description	Mean (standard deviation)			
Displacement	< 2.5 mm	2.5–5 mm	5–7.5 mm	> 7.5 mm
Constant shear model	1.063 (0.498)	1.317 (0.027)	1.31 (0.011)	1.315 (0.070)
Rotating model	1.076 (0.510)	1.243 (0.065)	0.922 (0.026)	0.884 (0.072)
MCD model	1.029 (0.479)	1.209 (0.039)	1.071 (0.039)	0.964 (0.112)

displacement point had been taken as a measurement of the relative accuracy of the prediction models for each of the shear models. The values of mean (μ) and standard deviation (σ) of (Total force_FE)/(Total force_exp) related to four displacement segments are listed in Table 2 for comparison.

As given in Table 2, in all four segments, MCD model predicts the shear behavior with the highest relative accuracy, whereas constant shear models over predict the results and rotating model under predicts the experimental results.

3.3.2 Beam A1 (25 MPa with Shear Reinforcement)

Similar to beam OA1, FE model analysis incorporating MCD shear model, constant shear retention model, and rotating crack model compared with the experimental results for beam A1. In this case also, MCD predictions were found to be more promising compared to the other models. While constant shear retention model

Table 3 Peak load displacement data in beam A1

Description	Total load/kN (% of error)	Mid-displacement/mm (% of error)
Experiment results	473	14
Constant shear model predictions	505 (6.8)	11.7 (16.4)
Rotating model predictions	406 (14.2)	12.3 (12.1)
MCD model predictions	460 (2.7)	11.5 (17.9)

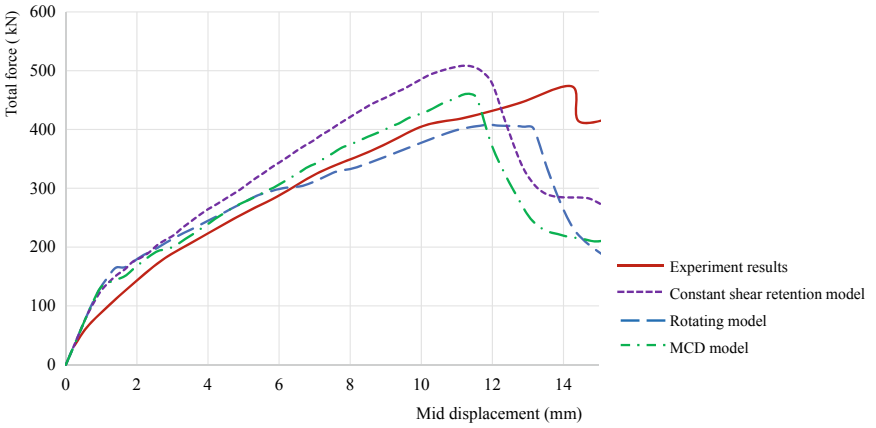

Fig. 13 Load deflection response of experiment and FE model beam A1

over predicts the results, under predictions observed in rotating shear model results (Table 3) (Fig. 13).

As given in Table 1, MCD model shows an error level of 17.9% in mid-displacement predictions whereas the associated other models are lower than that. However, the accuracy in total load prediction is superior in contrast to all the other models. Hence, when the two levels of accuracy are considered together, the correlation of MCD model with the experimental behavior can be deemed more satisfactory (Table 4).

Overall, similar to beam OA1, MCD model predicts the shear behavior with the highest relative accuracy for beam A1 also, whereas constant shear model and rotating model predictions deviate from the actual results.

Table 4 Overall load prediction in beam A1, μ (σ)

Description	Mean (standard deviation)			
Displacement	< 3 mm	3–6 mm	6–9 mm	> 9 mm
MCD model	0.796 (0.572)	1.227 (0.131)	1.071 (0.005)	1.051(0.007)
Rotating model	0.796 (0.572)	1.307 (0.148)	1.075 (0.026)	0.948 (0.013)
Constant shear model	0.794 (0.570)	1.283 (0.093)	1.184 (0.009)	1.202 (0.012)

4 Conclusions

This study explored into prediction potential of shear behavior of concrete via a modified version of a contact density model (MCD) and its applicability in non-linear numerical analysis of shear critical RC beams. Based on the results, the following conclusions and recommendations can be drawn,

1. The contact density-based shear function could be formulated into a form of a constitutive model for concrete shear behavior so that it can be used in non-linear simulation of RC beams with the total strain crack model in the FE approach.
2. The FE prediction with the proposed shear constitutive model was identified to be more accurate than both constant shear retention model in fixed crack model and rotating crack models at a non-linear FE simulation of two 25 MPa (cube strength) RC beams. Here, one beam was with shear reinforcement and the other beam was without shear reinforcement. For both beams, the fixed crack model considerably over predicted the shear behavior whereas the rotating model showed under predictions.
3. The contact density-based shear constitutive model (i.e., MCD model) was identified to be a better option than the commonly used rotating crack model and constant shear retention model in fixed crack model to be used in FE analysis of RC beams. However, application of the model for a range of concrete strengths and over a wide spectrum of beam parameters is necessary to make a solid conclusion upon this finding. Such investigation is identified as a matter for future work.

References

1. Bandara NMSH, Bandara IMLR, Wijesundara KK (2016) Numerical simulation of prediction of shear strength of reinforced concrete beam using total crack strain model. In: Proceeding of 7th international conference on sustainable built environment, ICSBE2016-250
2. Bazant ZP, Oh BH (1983) Crack band theory for fracture of concrete, materials and structures, RILEM, pp 155–177
3. Dirar S, Lees JM, Morley C (2013) Phased nonlinear finite element analysis of pre-cracked RC t-beams repaired in shear with CFRP sheets. J Compos Constr ASCE, pp 476-487
4. Li B, Maekawa K, Okamura H (1989) Contact density model for stress transfer across cracks in concrete. J Fac Eng, Univ Tokyo 40(1):9–52
5. Moradi AR, Soltani MM, Tasnimi AA (2015) Stress-transfer behavior of reinforced concrete cracks and interfaces. ACI Struct J 112(1):69–80
6. Moradi AR, Soltani MM, Tasnimi AA (2012) Simplified constitutive model for dowel action across rc cracks. J Adv Concr Technol 10(8):264–277

7. Perera SVTJ and Matsuyoshi H (2016) Numerical simulation of shear behavior of reinforced high strength concrete members, J Saitama Univ, Japan
8. Vecchio FJ, Collins MP (1986) The modified compression field theory for reinforced concrete elements subjected to shear. ACI J Proc 83(2):219–231

Comparison of Masonry Wall Modelling Approaches Under In-plane Monotonic Load and Cyclic Load

T. Krishanthini, N. Prasanth, and C. S. Bandara

Abstract Masonry structures are widespread around the world due to their relative low cost, availability of raw materials and ease of construction. The prediction of structural masonry behaviour is complex, especially under extreme loading conditions such as earthquake excitation. Nowadays, numerical simulations are used in many engineering applications including masonry. In this study, a numerical 3 dimensional model of a masonry wall was developed for monotonic and cyclic loading. The cyclic load was applied continuously and repeatedly on the masonry wall model to observe the failure. For modelling, first, different numerical modelling approaches and failure modes of unreinforced masonry walls were studied. Two techniques were mainly considered for modelling: (a) micro modelling and (b) macro modelling. Micro modelling further studied as simplified micro modelling and detailed micro modelling. ABAQUS software was chosen for the numerical modelling due to its powerful engineering simulation ability of analysing the masonry wall in both the linear and the nonlinear regions. The validity of the model was demonstrated by simulating the linear and nonlinear response and failure mechanism of a cyclically loaded masonry wall tested experimentally in previous studies. Finally, the validated numerical model was used to investigate the much-needed behaviour of masonry walls under different extreme loading conditions.

Keywords Finite element modelling · Nonlinear response · Cyclic load · Monotonic load

1 Introduction

Masonry is one of the most commonly used building materials around the world and is abundant in both modern and historical construction. Most of the residential buildings and religious places built several decades ago are masonry structures.

T. Krishanthini (✉) · N. Prasanth · C. S. Bandara
Department of Civil Engineering, University of Peradeniya, Peradeniya, Sri Lanka
e-mail: e15352@pdn.ac.lk

R. Dissanayake et al. (eds.), *12th International Conference on Structural Engineering and Construction Management*, Lecture Notes in Civil Engineering 266,
https://doi.org/10.1007/978-981-19-2886-4_3

Masonry is a homogenous anisotropic material that is composed of individual units like bricks, stones, cement blocks, etc., that are bonded together with mortar.

Major reasons for failures of the structure are ground movements, faulty construction, temperature, foundation settlements, external loads, material quality, seismic events, bad design, and moisture variation [10]. The ideal cause for failure of a structure can be a collaboration of the above. Detailed understanding of the response and structural behaviour of masonry under cyclic loads is vital in order to improve resilience.

Experiment analysis of masonry behaviour is not always possible due to the practical constraints and complexity of the material. On the contrary, finite element (FE) analysis can be used to simulate the complex behaviour of masonry under various loading conditions. Nowadays, FE modelling is constantly developing in precision and complication.

A large number of influence factors such as anisotropy of units, dimensions of units, joint widths, material properties of the units and mortar, workmanship, and bond type make modelling and analysis of buildings an extremely complicated work. However, with time, approaches for the numerical modelling of masonry structures have been developed. There are mainly two approaches to model anisotropic behaviour as macro modelling and micro modelling as shown in Fig. 1. The macro model presume that the masonry form is a homogenous continuum to be discretized by a FE mesh that does not use the brick assemblage. Even though this supposition bypasses the physical quality of masonry, it grasps the worldwide manners and reduces the numerical consequence [10].

In the micro model, discretization uses the real configuration of units and mortar, while adopting various essential models for the mortar and brick. Micro modelling can be categorized into two as simplified micro modelling and detailed micro modelling. In the simplified method, each unit is modelled as an expanded block, to keep the geometry unchanged. Each joint is made up of mortar and two unit–mortar interfaces and produced an average interface between blocks. In detailed micro modelling, the real situation is modelled. Unit–mortar interface is represented by discontinuous elements; in fact, the mortar and units are represented by continuum elements.

In the scientific community, there is not yet the same level of understanding of fatigue effects and the prediction of the remaining life of masonry components

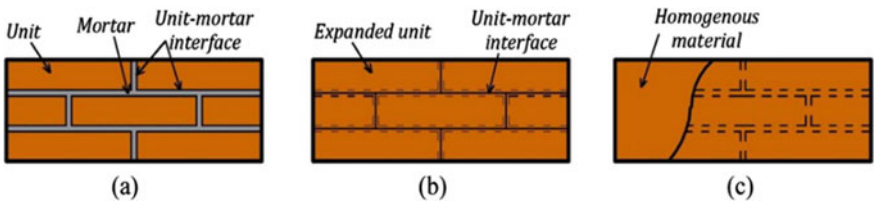

Fig. 1 Modelling strategies for masonry structures: **a** detailed micro modelling; **b** simplified micro modelling; **c** macro modelling [3]

under cyclic compressive loads. In historic masonry buildings, through the study it is found that generally arch bridges are impacted by fatigue problems. This is due to the fact that they currently acquire higher and more frequent cyclic loads due to increased travelling frequency of vehicles, resulting in premature cracking and collapse. As such, the available fatigue strength, that is the maximum stress acting in cyclic conditions, is significantly lower than the one obtained under quasi-static loading conditions. Therefore, rather than the ultimate carrying capacity, it is important to know the actual fatigue strength, starting from which useful indications on the remaining service life with a possible traffic load limitation may be established.

In this present study, for all 3 modelling approaches, FE models were developed, a monotonic load was applied, and the best modelling strategic was selected considering accuracy and time. Thereafter, cyclic load was applied for that selected model subjected to the validation of the model. The validated model was then accustomed to investigate the much-needed behaviour of masonry walls under different loading conditions.

2 Modelling Approach

In this paper, constitutive models and their related failure modes are presented below.

2.1 Surface-Based Cohesive Behaviour Model

Cohesive interaction is defined as a function of displacement separation between the edges of potential cracks (Lee and Fenves 1998). A method that defines the mechanical behaviour of cohesive interaction for brittle materials is called the traction separation model. The failure modes of masonry joints which can be declared using the traction separation model are tensile cracking of joints and shear sliding of joints as exposed in Fig. 2 [3].

Masonry is a mix of two brittle materials: stone, brick, or cement block and mortar, which split in tension at very poor stresses. The initial response of joint interfaces is

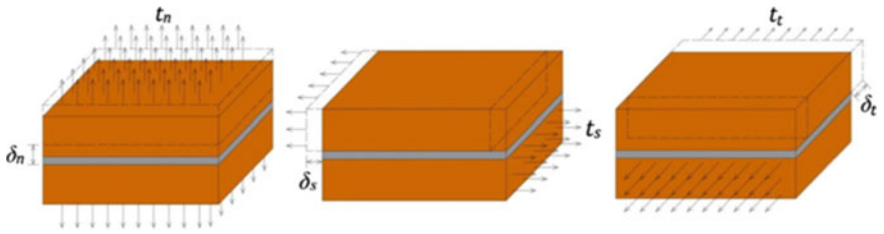

Fig. 2 Failure modes of the joints: **a** tensile cracking; **b** and **c** shear sliding [3]

based on a linear traction separation conduct before the collapse. It can be written in the form of an elastic stiffness matrix given in Eq. (1).

$$t = \begin{Bmatrix} t_n \\ t_s \\ t_t \end{Bmatrix} = \begin{bmatrix} K_{\mathrm{nn}} & 0 & 0 \\ 0 & K_{\mathrm{ss}} & 0 \\ 0 & 0 & 0 \end{bmatrix} \begin{Bmatrix} \delta_n \\ \delta_s \\ \delta_t \end{Bmatrix} = K\delta \tag{1}$$

where t is the nominal traction vector, K is an elastic stiffness matrix, and δ is the separation vector [10]. The stiffness matrix K, for joint interfaces in a masonry micro model, can be given in terms of elastic moduli of unit, elastic moduli of mortar, shear moduli of unit, shear moduli of mortar and thickness of mortar as in Eqs. (2) and (3).

$$K_{nn} = \frac{E_u E_m}{h_m(E_u - E_m)} \tag{2}$$

$$K_{ss} = K_{tt} = \frac{G_u G_m}{h_m(G_u - G_m)} \tag{3}$$

2.2 Elastic Behaviour of Expanded Units

The elastic response of the expanded brick units of the simplified micro model has been proposed based on the assumption of a stack bond between masonry units and uniform stress distribution between masonry elements. In Eq. (4), H is the new depth of the expanded brick unit and n is accustomed to tune Young's modulus of the wall.

$$E = \frac{H E_u E_m}{n h_u E_m + (n-1) h_m E_u} \tag{4}$$

Stiffness of the dry joint in the simplified model is calculated using Eq. (5), and out of plane, stiffness of the dry joint is calculated from Eq. (6), where ν is Poisson's ratio.

$$\mathrm{K}_{n,joint} = \frac{E_u E_{wall}}{h_u(E_u - E_{wall})} \tag{5}$$

$$\mathrm{K}_{s,joint} = \mathrm{K}_{t,joint} = \frac{\mathrm{K}_{n,joint}}{2(1+\upsilon)} \tag{6}$$

2.3 Homogenization Approach

Masonry is a composite. To ease the modelling procedure for masonry walls, homogenization approach can be used. Young's modulus for the wall (E) can be calculated using Eq. (7) where the properties of Young's modulus of brick, Young's modulus of mortar, and thickness of mortar and brick are related. A parameter ρ is defined to relate the bond between the brick and mortar (Nohutcu 2015).

$$E_{wall} = \frac{t_m + t_u}{\frac{t_m}{E_m} + \frac{t_u}{E_u}} \rho \tag{7}$$

2.4 Plastic Response of the Joint Interfaces

The initial linear response of the joints is followed by crack propagation. When the damage initiation criterion is formed on the user-defined tractions between the masonry interfaces, cracking propagates in the masonry joints. The quadratic stress criterion is used to define damage initiation; this criterion is met when the quadratic stress ratios of masonry interfaces are equal to one. This criterion is acquired as it effectively forecasts the damage initiation of joints obtained to mixed-mode loadings, which is the case in masonry joint interfaces (the masonry joint interfaces are subjected to tensile stress in the normal direction and shear stress in the two shear directions). The criterion is expressed as in Eq. (8).

$$\left(\frac{< t_n >}{t_n^{max}}\right)^2 + \left(\frac{< t_s >}{t_s^{max}}\right)^2 + \left(\frac{< t_t >}{t_t^{max}}\right)^2 = 1 \tag{8}$$

This criterion is met when the stress ratios of masonry interfaces are equal to one (Campilho 2008). Here, interfaces are subjected to tensile stress in a normal direction and shear stress in two shear directions. Tensile cracking of masonry joints is ruled by the tensile strength of masonry joints, while critical shear stress of joints is evaluated through Mohr Coulomb failure as given in Eq. (9). The critical sliding shear stress ($\tau_{sliding}$) is calculated from Eq. (10).

$$\tau_{crit} = c + \mu\sigma_n \tag{9}$$

$$\tau_{sliding} = \mu\sigma_n \tag{10}$$

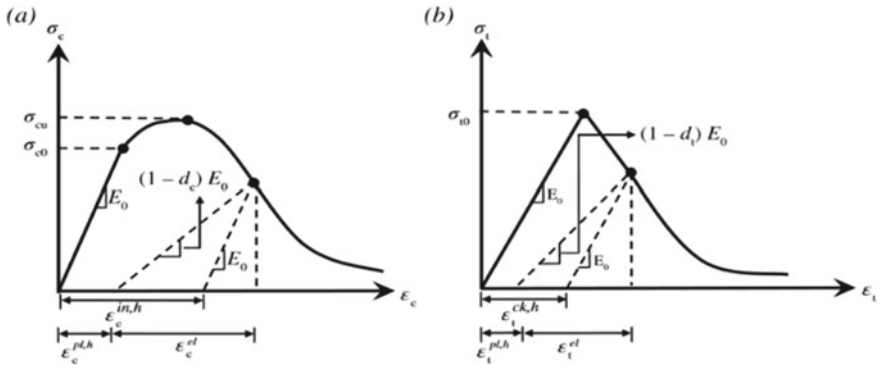

Fig. 3 Reaction of concrete to uniaxial loading in: **a** tension; **b** compression

2.5 Concrete Damage Plasticity

The concrete damage plasticity (CDP) model can generate nonlinear properties of brittle materials such as concrete, brick, and stone. The failure modes of this model are cracking in tension or crushing in compression. The uniaxial tensile and compressive properties of concrete are described by damage plasticity as in Fig. 3. The degradation of the elastic stiffness is identified by two damage variables d_t and d_c as exposed in Eqs. (11) and (12),

$$\sigma_t = (1 - d_t)E_0\left(\xi_t - \xi_t^{pl}\right) \tag{11}$$

$$\sigma_c = (1 - d_c)E_0\left(\xi_c - \xi_c^{pl}\right) \tag{12}$$

where E_0 is the initial (undamaged) elastic stiffness of the material, ξ_t, and ξ_c are strain in tension and compression, and $\xi_c{}^{pl}$ and $\xi_t{}^{pl}$ are equivalent plastic strain in compression and tension.

3 Finite Element Modelling for Monotonic Loading

FE modelling is a tool used for modelling a structure with very complicated arrangements and materials. In this paper, bricks are modelled using 3D hexahedral-shaped eight-node linear brick elements with reduced integration (C3D8R). This element has the capability of representing large deformation, crushing in compression, and cracking in tension. It is explained by 8 nodes, each node has three translational degrees of freedom X, Y, and Z directions. Hard contact behaviour is defined between adjacent surfaces of masonry units by the contact pressure—overclosure relationship.

This feature allows transmitting pressure when they are in contact but prevents penetration and transfer of tensile stress between contact surfaces [1]. The actions can be imposed on the model controlling either the load or the displacement.

In this present study, the model was initially run in the linear region, and then, a nonlinear analysis was done. For automatic stabilization default, dissipated energy fraction was applied. Towards the nonlinear region, stiffness degradation created the numerical stability. Therefore, a viscous regularization was applied in the models.

3.1 Experimental Model Validation for Monotonic Loading

Experiments done by Raijmakers and Vermelfoort (1992) for shear walls have been adopted as an in-plane test. The analysed shear wall is built with dimensions 990 × 1000 mm^2 and 18 courses. The wall is modelled with wire cut solid clay bricks with dimensions 210 × 52 × 100 mm^3 and a 10-mm-thick mortar layer. Mortar is made up of cement: lime: sand with a volumetric ratio of 1:2:9, respectively.

The steel clamp on the wall was initially given a uniformly distributed vertical load of 0.3 N/mm^2, and then, an incremental horizontal load is given to monitor the displacement. The vertical displacements of the top beam were restrained after applying the vertical compressive load. The wall is modelled using all three modelling approaches and compared. The test set-up of the experiment is shown in Fig. 4. The elastic properties used in three models of masonry walls are shown in Table 1. The material properties required for mortar is taken from the comprehensive experimental study conducted by Kaushik et al. (2007).

Tables 2 and 3 give a summary of the nonlinear material properties and interaction properties of the joint interface used in all three models. The fracture energy is specified as a function of the mix mode utilizing the Benzeggagh-Kenane mixed-mode fracture criterion. It is the most appropriate criterion to use for masonry as

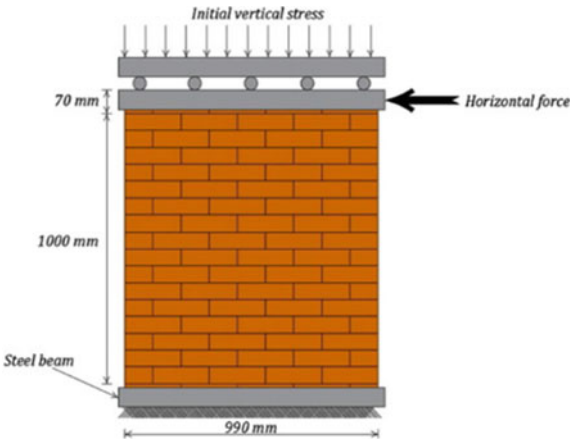

Fig. 4 Experimental set-up of masonry walls for monotonic loading [3]

Table 1 Elastic properties for brick and joints

Material	E (N/mm^2)	ν	K_n (N/mm^2)	K_s, K_t (N/mm^2)
Detailed micro model				
Brick	16700	0.15	82	37
Mortar	780	0.15		
Simplified micro model				
Expanded	4050	0.15	80	37
Macro model				
Brick wall	3450	0.15	–	–

Table 2 Interaction properties for joint interface

Damage criterion	Quadratic traction						
Friction coefficient	Initiation			Evolution			Stabilization
0.75	Normal (MPa)	Shear—I (MPa)	Shear—II (MPa)	G_I (N/mm)	G_{II} (N/mm)	G_{III} (N/mm)	Viscosity coefficient
	0.25	0.5375	0.5375	0.018	0.125	0.125	0.05

Table 3 Nonlinear material properties for brick and joint

Properties	Macro model	Simplified micro model	Detailed micro model	
		Expanded brick	Brick	Mortar
Compressive strength (MPa)	1.56	10.5	10.5	3
Tensile strength (MPa)	0.15	1.05	1.05	0.4
Dilatancy angle	11.3	11.3	11.3	11.3
Eccentricity	0.1	0.1	0.1	0.1
Viscosity parameter	0.05	0.05	0.05	0.05

critical fracture energy since it is the same in both shear directions (mode II and mode III). A linear softening is defined and the exponent in the Benzeggagh-Kenane model, η, is set as 2 assuming a brittle behaviour. Figure 5 shows the model set-up for all 3 models.

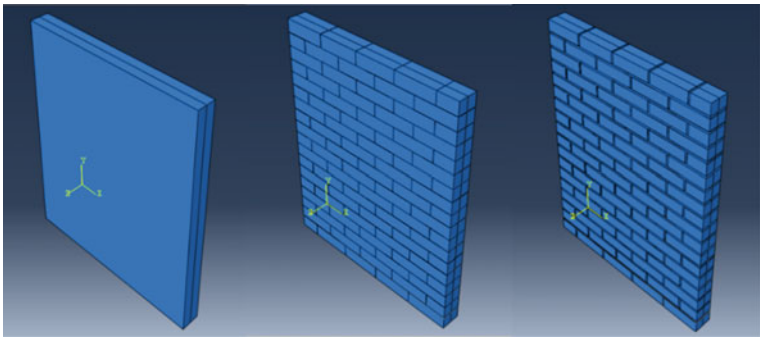

(a) (b) (c)

Fig. 5 Modelling set-up: **a** macro modelling; **b** simplified micro modelling; **c** detailed micro modelling

3.2 Mesh Sensitivity Analysis

The mesh size is generated by the mesh sensitivity study. Variation of the vertical displacement with mesh density was analysed in the mesh sensitivity analysis. A fixed load of 20 kN was tried to each model for the analysis. The base of the model is fixed, and a rigid steel plate is placed on the top for loading actions. A tie constraint is applied for the interaction between the rigid plate and masonry. The mesh density, where the results are shown to be converging, was selected as the converged mesh density. Obtained converged mesh size is 0.03 m.

3.3 Results

The results of all three models were contrasted with the experimental curve as represented in Fig. 6. The linear behaviour and nonlinear behaviour up to ultimate compressive stress were well grasped in all three models. Despite the specific limitations applied in both the simplified micro model and the macro model, a good agreement of results was observed when comparing with the detailed micro model. So, it can be stated that all three modelling approaches provide very reliable solutions. To grasp the complex masonry properties, solid element is the most effective element type. In addition, as time permits and accuracy required, the modelling approach can be chosen. Mean absolute error calculation method was followed to calculate error percentage for all three models. The calculated error percentage and time required run that model is given in Table 4.

Analysis time depends on the performance of the computer. This analysis was done using one computer. Therefore, the analysis time can be compared. According to the error calculation, macro model is the low accuracy model. Simplified micro

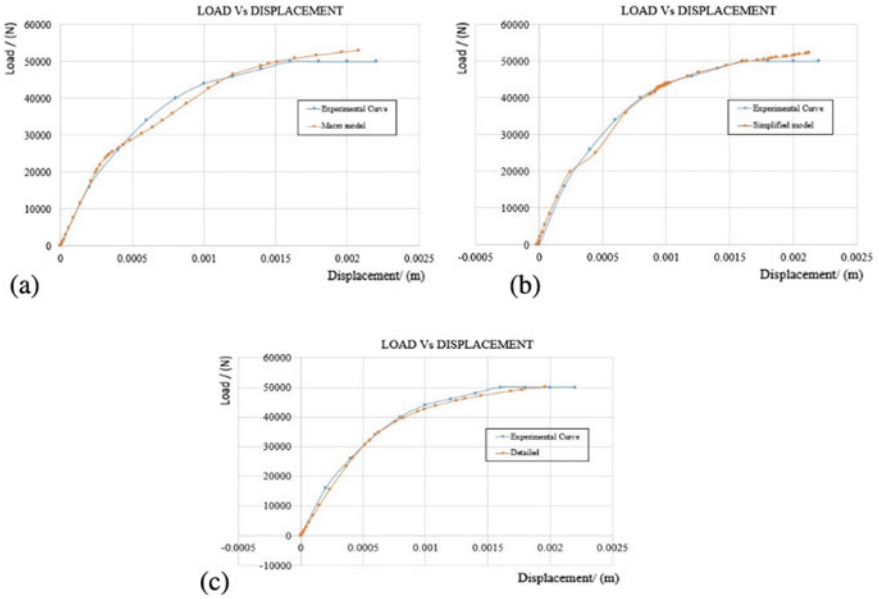

Fig. 6 Comparison of numerical and experimental results: **a** macro model; **b** simplified micro model; **c** detailed micro model

Table 4 Error percentage

Model	Error (%)	Time (min)
Macro model	4.88	10
Simplified micro model	3.92	50
Detailed micro model	1.65	120

model is the medium accuracy model and the detailed micro model has highest accuracy as expected. If we consider the time for analysis, macro model needs less time, simplified micro model needs medium time and the detailed micro model needs the highest time. Considering both the accuracy and the analysis time, the simplified micro model is proposed as a better solution for fatigue load modelling.

4 Finite Element Modelling for Cyclic Loading

4.1 Experimental Model Validation for Cyclic Loading

The experimental results reported in literature (Abdulla et al. 2017) are used to validate the suggested model against the masonry behaviour under static in-plane cyclic loads. The nominal dimensions of the tested walls described in were 1200 mm

long× 1200 mm high × 110 mm thick. The wall was built using clay bricks with dimensions of 230 mm long × 76 mm high ×110 mm thick with a mortar joint thickness of 10 mm (1:1:6 cement: lime: sand). Each wall had five bricks in a row and 14 courses of brick, which were put in a running bond. A series of walls were trailed to look over the behaviour of masonry when a damp-proof course (DPC) is set either in the first bed joint or between its supporting base and the bottom of the wall. The wall was set on a concrete beam that was fixed to a steel spreader beam, which was in turn fixed to the floor; the vertical and horizontal loads were forced to the top of the walls via a spreader beam as shown in Fig. 7. The loads were applied in two steps, initially a pre-compression vertical stress was applied which was kept constant during the tests, and then, the walls were subjected to horizontal in-plane cyclic loads under displacement control. The wall considered for this study was subjected to 19 number of cycles. Figure 8 shows the load protocols applied to the top of the wall. For this paper, a wall, which has been subjected to an initial vertical stress of 0.7 MPa, is considered.

C3D8R elements were used to model the masonry wall. The analysis was managed in two steps. First, vertical stress was applied to the top of the walls via a rigid body in the first step under load control. The rigid body was defined to simulate the top steel beam used in the experiments to distribute the stresses. Then, the cyclic in-plane load was subjected to the wall under displacement control via the rigid body, while the displacement and rotation were restrained. Moreover, the initial vertical stress applied in the first step was kept constant. All mechanical properties are summarized in Tables 5–7. Figure 9 shows the model set-up of the simplified micro model.

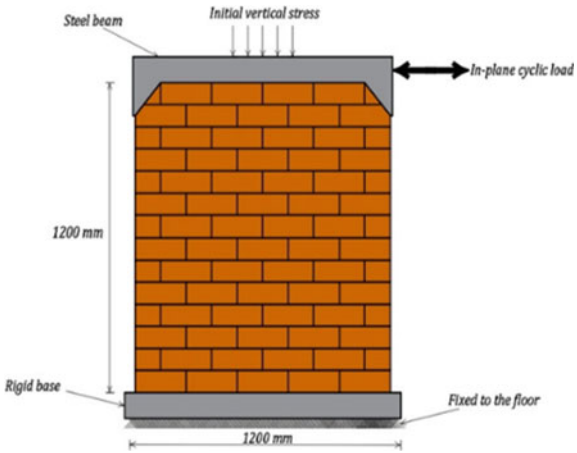

Fig. 7 Experimental set-up of masonry walls for cyclic loading [3]

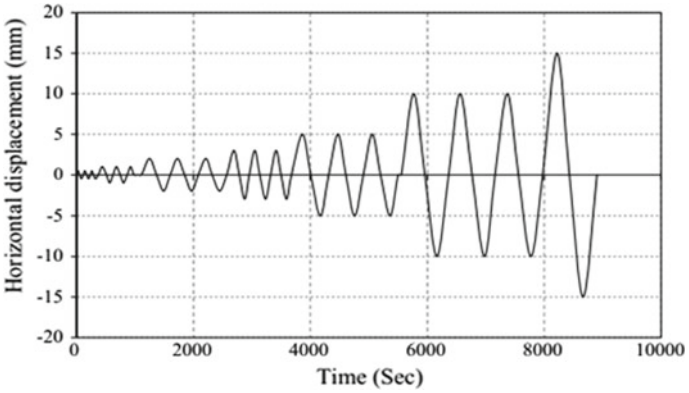

Fig. 8 In-plane horizontal displacement-time history [2]

Table 5 Nonlinear material properties for the joint interface under cyclic load

Damage criterion	Quadratic traction						
Friction coefficient	Initiation			Evolution			Stabilization
0.75	Normal (MPa)	Shear—I (MPa)	Shear—II (MPa)	G_I (N/mm)	G_{II} (N/mm)	G_{III} (N/mm)	Viscosity coefficient
	0.2	0.43	0.43	0.012	0.040	0.040	0.05

Table 6 Nonlinear material properties for the joint interface where the DPC layer presents in the bed joint between the first and second courses

Damage criterion	Quadratic traction						
Friction coefficient	Initiation			Evolution			Stabilization
0.425	Normal (MPa)	Shear—I (MPa)	Shear—II (MPa)	G_I (N/mm)	G_{II} (N/mm)	G_{III} (N/mm)	Viscosity coefficient
	0.028	0.060	0.060	0.001	0.0038	0.0038	0.05

Table 7 Interaction properties for joint interface under cyclic load

Properties	Expanded brick
Compressive strength (MPa)	14.18
Tensile strength (MPa)	0.1
Dilatancy angle	11.3
Eccentricity	0.1
Viscosity parameter	0.002

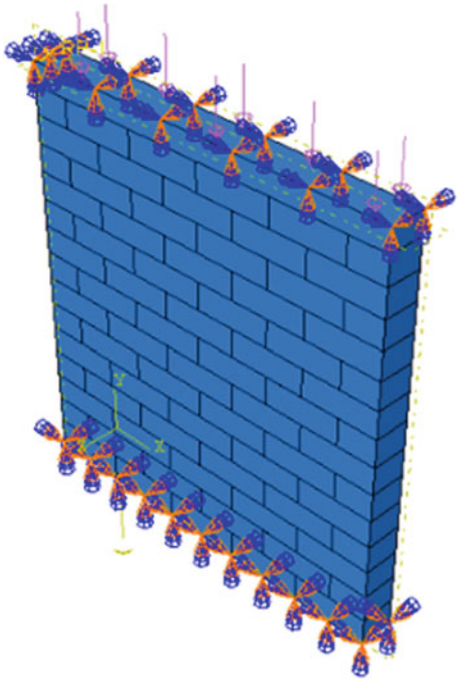

Fig. 9 Model set-up for cyclic load

4.2 Results for Cyclic Load

The numerical results show a good agreement with the experimental results for both horizontal force–displacement relationship and failure modes. The numerical and experimental force–displacement patterns sufficiently match in terms of initial stiffness and nonlinear behaviour. The nonlinear behaviour of the wall was quasi-ductile due the energy dissipated by the bed joint containing the DPC layer. Although it can be noted that the maximum horizontal load attained in the experiment is relatively higher than the maximum load in the numerical model, which indicates that the horizontal crack which propagated in the first bed joint occurred earlier in the numerical model than the experiment. After the propagation of the horizontal crack, the reaction of the model was governed by the proportional relationship of the coefficient of friction to the normal compressive stresses in the first bed joint.

The experimental results showed that the failure mode was due to formation of horizontal cracking along the first bed joint containing the DPC layer and subsequent sliding of the upper part of the wall over the first bed joint. Furthermore, vertical cracks occurred in the first course of the wall because of the cyclic sliding movements of the upper part of the wall over the first bed joint. Figure 10 shows the FE model of the wall and its displacement behaviour. The FE model shows the same behaviour as the experiment. Figure 11 shows the comparison between the numerical and experimental responses that highlights the accuracy of the prediction.

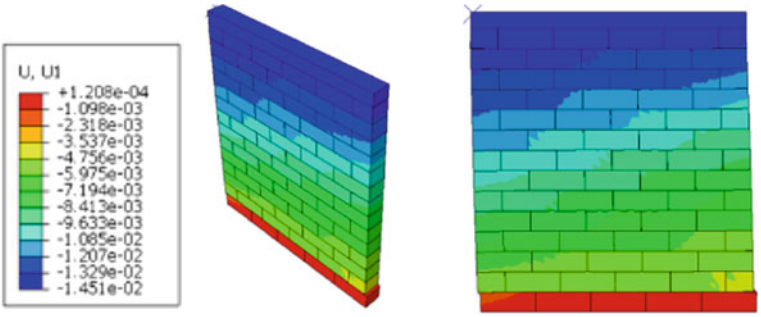

Fig. 10 Finite element modelling for masonry wall with optimum mesh under cyclic load

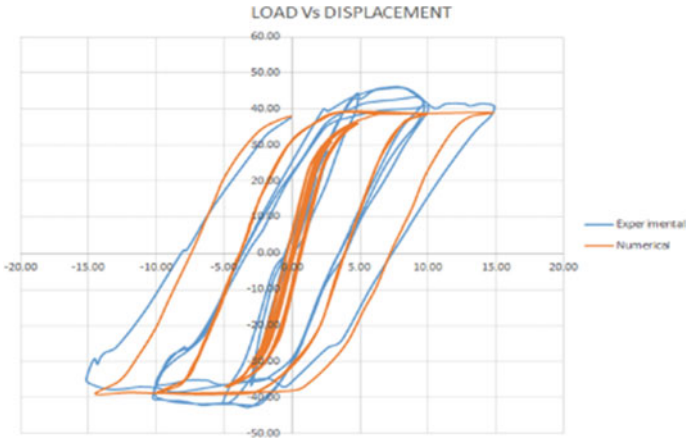

Fig. 11 Comparison of experimental and numerical results under cyclic load

5 Conclusion

This research paper presents results of monotonic and cyclic loading tests carried out using FE models for investigating the in-plan behaviour of partially confined masonry walls. FE models were developed using three modelling approaches. First, monotonic loading was applied for all three models. The FE models showed a good relationship and very close results, and even, the simplified model gave reasonably accurate predictions up to the failure.

Thereafter, cyclic load was applied for the reasonably accurate FE model developed using the simplified micro modelling approach. The numerical results showed a good agreement with the experimental results for both horizontal force–displacement relationship and failure behaviour. The nonlinear behaviour of the wall was quasi-ductile due the energy dissipated by the bed joint containing the DPC layer. In

addition, the experimental results showed that the failure mode was due to formation of horizontal cracking along the first bed joint containing the DPC layer and subsequent sliding of the upper part of the wall over the first bed joint. Furthermore, vertical cracks occurred in the first course of the wall as a result of the cyclic sliding movements of the upper part of the wall over the first bed joint. Similar failure modes were observed in the numerical results. It is also worth mentioning that the numerical compressive stresses obtained were below the compressive strength of the wall during all the cycles, similarly in the experiment no crushing under compression was observed.

References

1. ABAQUS 6.14, Dassault Systèmes Simulia Corp., Providence, RI, USA, 2014.
2. Abdulla K, Cunningham L, Gillie M (2017) Non-linear simulation of masonry behavior under cyclic loads. PGR Conference, University of Manchester, pp 20–22
3. Abdulla KF, Cunningham LS, Gillie M (2017) Simulating masonry wall behavior using a simplified micro-model approach. Eng Struct 151:349–365
4. Allen C, Masia MJ, Page AW (2015) Cyclic in-plane shear testing of unreinforced masonry walls with openings. In: Proceedings of the tenth pacific conference on earthquake engineering building an earthquake-resilient Pacific, Sydney, Australia
5. Asteris PG, Sarhosis V, Mohebkhah A, Plevris V (2015) Numerical modeling of historic masonry structures
6. Bandara CS, Jayasinghe JA, Samarasekara MA, Sathya SU (2020) Numerical approaches for modeling nonlinear behavior of masonry structures. Society of structural engineers, Annual sessions, Sri Lanka
7. Bandara CS, Jayasinghe JA, Samarasekara MA, Sathya SU (2019) Comparison of load bearing masonry wall modelling approaches using in plane loads. In: 2019 Proceedings of 10th international conference on structural engineering and construction management (ICSECM), Earl's Regency Hotel, Kandy, Sri Lanka
8. Bui TT, Limam A, Sarhosis V (2019) Failure analysis of masonry wall panels subjected to in-plane and out-of-plane loading using the discrete element method. Eur J Environ Civil Eng
9. Krawinkler H (1995) New trends in seismic design methodology. In: Proceedings of European conference on earthquake engineering, pp 821–830
10. Lourenço PB (1996) Computational strategies for masonry structures. Delft University of Technology, TU Delft
11. Schwegler G, Kelterborn P (1996) Earthquake resistance masonry structures strengthened with fiber composites. In: 1996 Proceedings of eleventh world conference on earthquake engineering, Switzerland

Spherical Indentation Test to Determine Metal Properties Using Representative Strain Concept: A Review

S. P. L. Madhumali, J. A. S. C. Jayasinghe, C. S. Bandara, and A. J. Dammika

Abstract Depth-sensing instrumented indentation test or hardness test is a very easy, quick and inexpensive, semi-destructive technique that can be used to determine the mechanical properties of materials on small scales (on nano or micrometer scales). During the past two decades, inverse analysis methods were developed to determine the true stress–strain behaviors of materials from the load–displacement curve of indentation. Among those methods, many researchers have widely used the representative (ε_r) strain approach with dimensional analysis to get the relationships between indentation responses and material properties since it reduces the number of apparent unknown variables in the π functions. However, the methods proposed in those studies are valid only for the power-law engineering materials without a plastic plateau in their true stress–strain behavior like most engineering metals. This paper has reviewed the usage of the representative strain approach with spherical indentation to determine the metal properties. In order to develop an inverse analysis method based on spherical indentation in determining the material properties of unknown steel material, the latter part of the paper has focused on exploring the feasibility of using the representative strain approach for power-law engineering materials with a plastic plateau.

Keywords Material properties · Power law · Representative strain · Spherical indentation

1 Introduction

The first widely used and standardized indentation hardness test in engineering and metallurgy was proposed by J. A. Brinell, in 1900. Since then, indentation tests have been used to obtain the hardness of materials for nearly a century. With the advancement of technology, at present, it is possible to obtain indentation load–displacement curves with high accuracy in both the nano and micro-ranges. The

S. P. L. Madhumali (✉) · J. A. S. C. Jayasinghe · C. S. Bandara · A. J. Dammika
Faculty of Engineering, University of Peradeniya, Peradeniya, Sri Lanka
e-mail: madhumalil1995@eng.pdn.ac.lk

R. Dissanayake et al. (eds.), *12th International Conference on Structural Engineering and Construction Management*, Lecture Notes in Civil Engineering 266,
https://doi.org/10.1007/978-981-19-2886-4_4

Table 1 Hardness testing scales defined by ISO 14577-1 [2]

Scale	Load range (L)/(N)	Penetration range (h)/(μm)
Macro-indentation	$2 < L < 30{,}000$	Not-specified
Micro-indentation	$L < 2$	$h > 0.2$
Nano-indentation	Not-specified	$h = <0.2$

characteristics exhibited in the indentation load–displacement curve can be correlated with the properties of the indented material. Hence, it has been used by many researchers to determine the mechanical properties of materials on small scales (on nano or micrometer scales).

Based on the applied load and penetration depth, indentation hardness tests can be categorized as macro, micro, and nano. Table 1 gives the ranges of applied loads (L) and penetration depths (h) specified by ISO 14577-1 norm for determining the above three categories.

Brinell, Meyer, Vickers, Rockwell, Shore durometer, and IRHD (International Rubber Hardness Degree) are the main macro-indentation tests used by the industry and the research community. There are four tests with respect to micro-indentation; Vickers, Knoop, Micro-IHRD and Buchholz, from which micro-Vickers and Knoop are considered as the main micro-indentation tests. When compared with the macro or micro-indentation tests with nano-indentation, it can be said that the nano-indentation load–displacement curve has higher precision [1].

These macro, micro, and nano-indentation tests can be further categorized according to the shape of the indenter used as sharp and spherical indentation. During the last two decades, researchers have used these sharp and spherical indentation responses in numerous ways to determine metal properties such as hardness (H), Young's modulus (E), yield strength $\left(\sigma_y\right)$, strain hardening exponent (n), ratio (α) between the strain at beginning point of strain hardening (ε_{st}) and the yield strain $\left(\varepsilon_y\right)$, Poisson's ratio ($\nu$), fracture toughness, strength coefficient (R), residual stress, etc., and they have identified that the loading–unloading curve of spherical indentation contains more information on the material properties than those from a sharp indentation test [3]. Further, in the determination of materials' elastoplastic properties, spherical indentation has many advantages over a sharp indentation [4]. Figure 1 illustrates the spherical indentation.

To correlate the spherical indentation responses to material elastic–plastic properties, researchers have used many approaches such as dimensional analysis, representative strain, regression analysis, optimization algorithms and stress–strain constraint factors[5–8]. When considering these approaches, the representative strain approach has been widely used since it offers an effective way of obtaining mechanical properties, especially work hardening behavior of metals, from inverse analysis of indentation load–displacement data, and also it does not require measuring the projected contact area [9].

The present paper is a brief review of the usage of the representative strain concept to determine the metal properties using spherical indentation responses.

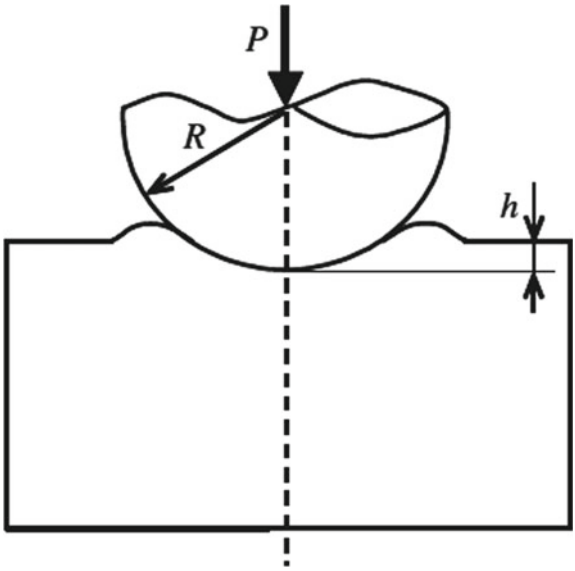

Fig. 1 Illustration of spherical indentation

The summary of the paper is as follows. The first part of the paper gives the existing metal properties detection approaches using indentation. The second part of the paper describes various representative strains which were used by the previous researchers to correlate the indentation response to the material properties. The third part reviews the usage of the representative strain concept with the spherical indentation to determine the material properties of power-law engineering materials without a plastic plateau using dimensional analysis. The final section explores the viability of utilizing representative strain concept with the power-law engineering materials with a plastic plateau using spherical indentation.

2 Existing Metal Properties Detection Approaches Using Indentation

To determine the material properties of metals (i.e.,H, E, σ_y, n, α, ν, R), responses from the indentation tests have been used in a variety of approaches by the researchers for over two decades. Most of those approaches are based on finite element modeling. A brief summary of the existing metal properties detection approaches is shown in Fig. 2.

When considering the approaches listed in Fig. 2, it is evident that the representative stress–strain approach with the dimensional analysis and FE modeling was the popular approach among researchers to determine the elastic–plastic properties of power-law engineering materials like metals.

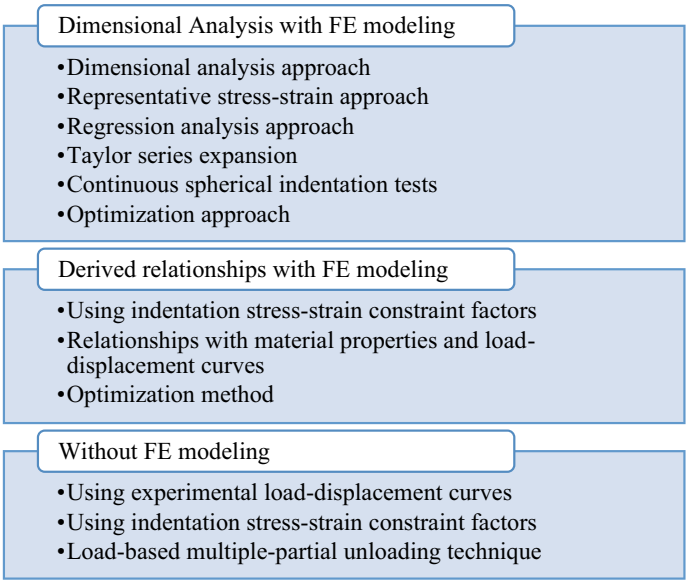

Fig. 2 Summary of the existing metal properties detection approaches using indentation

3 Representative Strain

The representative stress–strain concept was first proposed by Tabor in 1951. He defined the representative strain (ε_r) as Eq. (1) and related its corresponding representative stress to the hardness value.

$$\varepsilon_r = K\frac{a}{R} = K\sin\gamma \tag{1}$$

where K is about 0.2 and γ is the contact angle between the indenter and the specimen. Tabor defined the representative plastic strain as 8–10%, based on his experimental observations [11].

Henceforth, many researchers used this representative strain concept with both sharp and spherical indentation responses to determine the materials' elastoplastic properties. Zhao et al. [4] define the representative strain as a mathematical trick that can be used to reduce the number of apparent unknown variables in the dimensionless functions (π) which relates the indentation responses to material properties. Lee et al. [10] defined the representative strain as a certain plastic strain characterized by a deformed material below a sharp indenter. Indentation load–displacement data can be significantly simplified by using the representative strain. Hence, it is widely used to determine the stress–strain curve of power-law engineering materials from the inverse analysis of indentation load–displacement curve. The definition and value of

Table 2 Representative strains used by the researchers

Paper	Representative strain (ε_r)
Giannakopoulos and Suresh [12]	Used a fixed value of the characteristic strain of 0.29, which has been identified through finite element analyses of a wide range of ductile metals subjected to sharp indentation, and it is independent of the indenter size or indentation load (For $h > \frac{R}{40}$. Here, h is the indentation depth and R is the indenter radius) and weakly influenced by the tip angle of the sharp indenter. Spherical or other blunt indenters do not lead to such a characteristic strain
Dao et al. [13]	Identified a representative plastic strain as a strain level which allows for the construction of a dimensionless description of indentation loading response, independent of strain hardening exponent (n). By minimizing the relative errors using a least-squares algorithm, they confirmed that this representative strain value is 0.033 for a Berkovich indenter
Chollacoop et al. [14]	The representative plastic strain defined in Dao et al. [13] was constructed as a function of tip geometry in the range of 50° and 80°
Cao et al. [5]	The representative strain defined in Dao et al. [13] for sharp indentation has been extended to spherical indentation and identified as the function of the indentation depth (h) with respect to the indenter radius (R)
Cao et al. [15]	Proposed an energy-based representative strain for conical indentation in elastoplastic materials to establish an explicitly one-to-one relationship between the representative stress (σ_r), the indentation loading curvature $\left(C = \frac{P}{h^2}\right)$ and the ratio of reversible work (w_e) to total work (w_t) performed by the indenter
Ogasawara et al. [16]	Representative strain is defined as the plastic strain during axisymmetric deformation, $\left(\varepsilon_r = \varepsilon_a^p = \varepsilon_a + \varepsilon_a^e\right)$. Here, ($\varepsilon_a$) is the equi-biaxial strain. By varying the apex angle of the conical indenter, the representative strain is identified from extensive numerical analyses and fitted by $\varepsilon_r = 0.0319\cot(\alpha)$. Here, it only focuses on Berkovich indenter, and it gives $\varepsilon_r = 0.0115$
Zhao et al. [4]	Identified that the representative strain defined in Cao et al. [5] bears a weak physical meaning and presented the representative strain as plastic strain for uniaxial loading

(continued)

representative strain are not unique. Table 2 gives the various representative strain definitions and values used by the researchers to determine the metal properties.

When considering sharp indentation, most of the existing methods for determining the plastic properties $\left(\sigma_y, n\right)$ of power-law engineering materials using representative strain require two independent indentation tests with different apex angles. Although

Table 2 (continued)

Paper	Representative strain (ε_r)
Cao et al. [17]	Proposed four indentation response-based definitions of the representative strains ($\varepsilon_{r1}, \varepsilon_{r2}, \varepsilon_{r3}, \varepsilon_{r4}$) using finite element analysis based on the incremental plasticity theory and large deformation formulations ε_{r1}—Total effective strain accumulated beyond the yield strain and is dependent on the ratio of the reversible work (w_e) to total work (w_t) done by the indenter ε_{r2}—Plastic strain on the uniaxial stress–strain curve and is dependent on the ratio between the reversible work (w_e) and the total work (w_t) done by the indenter ε_{r3}—Presented ε_{r3} based on their previous researches Cao et al. [15] and Cao et al. [18] and a much wider property range was considered. The definition is the same as Cao et al. [5], but here it is dependent on the parameter loading curvature over reduced modulus $\left(\frac{C}{E^*}\right)$ ε_{r4}—Plastic strain on the uniaxial stress–strain curve (but this is different from Zhao et al. [4] and ε_{r2} dependent on the parameter loading curvature over reduced modulus $\left(\frac{C}{E^*}\right)$
Ogasawara et al. [9]	Defined the representative strain similar to Zhao et al [4]
Lee et al. [20]	Selected a representative strain that follows the conditions, ε_r should be a function of material properties also (not only a function of indenter angle for sharp indenter and indentation depth for spherical indenter), should be much smaller than 0.3 for cone (70.3^0), and the average plastic strain should decrease with increasing hardening
Chang et al. [8]	Used Tabor's representative strain

dual sharp indenter methods give accurate results for plastic properties, they have several disadvantages in practical application [4]. These disadvantages can be overcome by using a single spherical indentation test since it is possible to use only one spherical indentation to determine the plastic properties of a specimen from the indentation data obtained at different depths.

4 Representative Stress–Strain Approach with Spherical Indentation

4.1 Power-Law Engineering Material Model Without a Plastic Plateau

The plastic behavior of many pure and alloyed engineering metals is normally described by the power-law equation shown in Eq. (2) which was suggested by

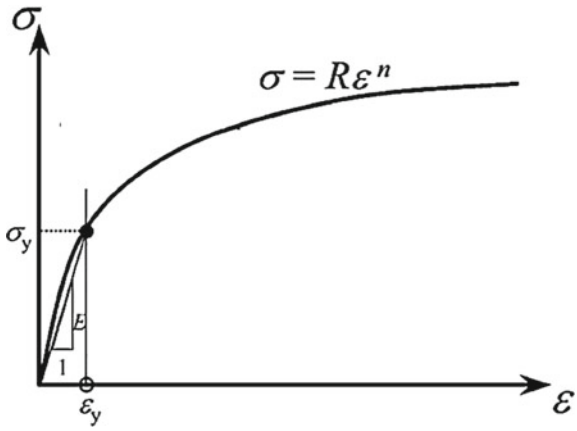

Fig. 3 Schematic illustration of typical stress–strain behavior of power-law work hardening materials

Holloman et al. (1945). It is in good agreement with tensile tests.

$$\sigma = R\varepsilon^n \tag{2}$$

Here, R and n are the strength coefficient and strain hardening exponent, respectively. Nevertheless, steel materials behave a little differently since their true stress–strain consists of a plastic plateau. Therefore, constitutive models for mechanical behavior of metals can be categorized as power-law work hardening and power-law work hardening with a plastic plateau. However, the concept of representative strain was always considered with the power-law work hardening material model without a plastic plateau.

For the materials that their true stress–strain behavior can be accurately modeled by a power-law description (Fig. 3) can be expressed in Eq. (3). Here, Hook's law is followed by elasticity, whereas plasticity follows von Mises yield criterion and power-law hardening.

$$\sigma = \begin{cases} E\varepsilon & ;\left(\varepsilon \le \varepsilon_y\right) \\ R\varepsilon^n & ;\left(\varepsilon \le \varepsilon_y\right) \end{cases} \tag{3}$$

In addition, true strain in the plastic region can be expressed as the addition of the strain at yield and true plastic strain as shown in Eq. (4).

$$\varepsilon = \varepsilon_y + \varepsilon_p \tag{4}$$

Further, the condition shown in Eq. (5) should be held for continuity at yielding.

$$\sigma_y = E\varepsilon_y = R\varepsilon_y^n \tag{5}$$

Then, for $\varepsilon > \varepsilon_y$, Eq. (6) can be obtained by combining Eqs. (3) and (5).

$$\sigma = \sigma_y \left[1 + \frac{E}{\sigma_y} \varepsilon_P \right]^n \tag{6}$$

4.2 Spherical Indentation to Develop the Dimensionless Functions

Spherical indentation is one of the earliest methods used to determine material properties [22, 23]. Dimensional analysis can be used as a tool to analyze the shape of the indentation load–displacement curve [24, 25]. To develop the dimensionless functions to identify the unknown material properties, the representative strain concept was first used by Dao and his co-researchers in 2001. Their method was based on sharp indentation. In 2004, Cao and his co-researcher proposed a new method to extract the plastic properties of metal materials from the spherical indentation loading curve by using Dao's representative strain concept. They have identified a representative strain that makes the dimensionless function independent of the strain hardening exponent as a function of the indentation depth (h) with respect to indenter radius (R). However, their dimensionless fitting function was only valid for a small material range which makes its application fairly limited.

Hence, Zhao and his co-researchers developed a new numerical algorithm for spherical indentation that fits a wide range of materials to measure the elastic–plastic properties of bulk materials by spherical indentation based on a new definition of representative strain. According to their analysis, they argued that the concept of the representative strain does not work well with the spherical indentation since the indentation load (P) does not scale exactly with the square of the indentation depth $\left(h^2\right)$. Therefore, the dimensionless functions proposed in their work are dependent on both the ratio between reduced modulus and representative stress $\left(\frac{E^*}{\sigma_r}\right)$ and strain hardening exponent (n). Further, they argued that friction is a minor factor for indentation. Based on the arguments of Zhao et al. [4], two important issues the effect of friction on the indentation loading curve and the applicability of the representative strain in spherical indentation were further addressed by Cao and his co-researchers in 2007. They established four novel approaches to identify the mechanical properties of elastoplastic materials using spherical indentation. The results reported in their research have provided useful information for selecting the proper $\frac{h}{R}$ ratios in the development of new methods to characterize the mechanical properties of elastoplastic materials using spherical indentation tests. However, the main issue with their approaches is that formulation included many fitting parameters and required advanced numerical analysis.

Ogaswara et al. [9] presented a relatively simple framework for determining the material elastoplastic properties from spherical indentation by reducing the number of fitting parameters involved based on a new formulation of representative strain.

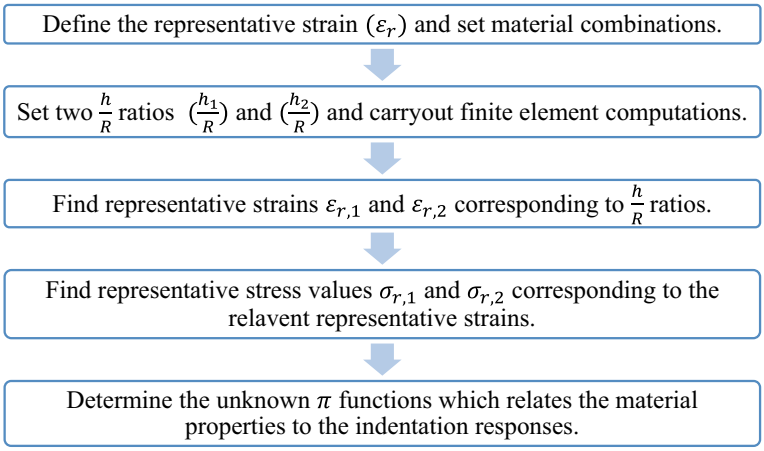

Fig. 4 Main steps involving in developing the forward analysis method

Further, they argued that the main disadvantage of previous shallow spherical indentation studies [4, 5, 17] was due to significant error in practice, and they may not lead to a unique solution. Even though Lee et al, [20], Budiarsa et al. [21] and Chang et al. [8] also used the representative strain concept with the spherical indentation to determine material elastic–plastic properties, their methods were not based on the dimensional analysis.

When analyzing the above-mentioned material property detection methods, which were based on spherical indentation and dimensional analysis as a whole, the main steps involving their studies to develop the forward analysis method can be summarized as shown in Fig. 4.

According to the definition of representative strain, Eq. (6) can be further modified, and it can be used in the reverse analysis to determine the unknown material properties $\left(E^*, \sigma_y, n\right)$. Equations (7), (8) and (9) provide the modifications of Eq. (6) which were used by Cao and Lu [5] and (Cao et al. [17], Zhao et al. [4], Ogaswara et al. [19] for their studies according to their representative strain definitions.

$$\sigma_r = \sigma_y \left[1 + \frac{E}{\sigma_y}\varepsilon_r\right]^n \tag{7}$$

$$\sigma_r = \sigma_y \left[\frac{E}{\sigma_y}\left(\frac{\sigma_r}{E} + \varepsilon_r\right)\right]^n \tag{8}$$

$$\sigma_r = R\left[\frac{\sigma_r}{E} + \varepsilon_r\right]^n \tag{9}$$

Here, σ_r is the representative stress which is defined as the flow stress at ε_r.

5 Applicability of Representative Stress–Strain Approach for Power-Law Engineering Materials with a Plastic Plateau

5.1 *Power-Law Engineering Material Model with a Plastic Plateau*

Structural steel which is a commonly used material in civil engineering exhibits a plastic plateau (Luders behavior) in its true stress–strain behavior as shown in Fig. 5. For the material model of structural steel, the power-law description can be modified and expressed as Eq. (10) by assuming this plastic plateau (solid line from *B* to *D* in Fig. 5) as a perfectly plastic plateau (dotted line in Fig. 5) [26].

$$\sigma = \begin{cases} E\varepsilon & ;\left(\varepsilon \le \varepsilon_y\right) \\ \sigma_y & ;\left(\varepsilon_y \le \varepsilon \le \varepsilon_{st}\right) \\ \sigma_y\left[1 + \dfrac{E(\varepsilon - \varepsilon_{st})}{\alpha\sigma_y}\right]^n & ;(\varepsilon > \varepsilon_{st}) \end{cases} \tag{10}$$

where

$$\alpha = \frac{\varepsilon_{\mathrm{st}}}{\varepsilon_y} = \frac{\text{strain at begining point of strain hardening}}{\text{yield strain}}$$

Then, for $\varepsilon > \varepsilon_{\mathrm{st}}$, Eq. (10) can be expressed as follows.

$$\sigma = \sigma_y^{(1-n)}\left[\frac{E\varepsilon}{\alpha}\right]^n \tag{11}$$

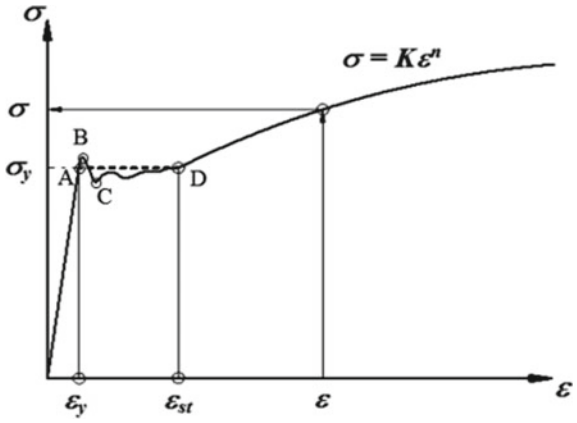

Fig. 5 Schematic illustration of typical true stress–strain behavior of power-law work hardening material with a plastic plateau

5.2 *Ability to Use Representative Strain Approach for Determining Material Properties of Power-Law Engineering Materials with a Plastic Plateau*

To check the ability to use the representative strain concept with the power-law work hardening material with a plastic plateau-like structural steel using spherical indentation responses, we have considered the material model presented in Sect. 5.1. Here, we have defined the representative strain (ε_r) as the total effective strain accumulated beyond the strain at the strain hardening (ε_{st}) of the structural steel material model, as shown in Fig. 5. According to this definition of representative strain, Eq. (11) can be expressed as follows when $\varepsilon > \varepsilon_{st}$.

$$\sigma_r = \sigma_y^{(1-n)} \left[\frac{E\varepsilon_r}{\alpha} \right]^n \tag{12}$$

For the spherical indentation of structural steel, the indentation force (P) during loading can be described as a function of the reduced Young's modulus (E^*), yield strength (σ_y), ratio (α) between the strain at beginning0020point of strain hardening (ε_{st}) and the yield strain (ε_y), the strain hardening exponent (n), the indentation depth (h), and the indenter radius (R) [6]. For fixed indentation depth and indenter radius, using π theorem in dimensional analysis, indentation force (P) can be expressed as Eq. (13).

$$P = \sigma_y h^2 \pi_1 \left(\frac{E^*}{\sigma_y}, n, \alpha \right) \tag{13}$$

Alternatively, Eq. (13) can be expressed as Eq. (14) using the representative stress (σ_r) which is the flow stress at the representative strain according to Eq. (12).

$$P = \sigma_r h^2 \pi_1 \left(\frac{E^*}{\sigma_r}, n, \alpha \right) \tag{14}$$

Identify a representative strain such that dimensionless function (π_1) is independent of the strain hardening exponent, finite element computations were carried out for 35 sets of different material combinations by fixing $\frac{h}{R}$ value to 0.1, and α value to 16 since the popular range of α lies between 7 and 23 [18]. Then, functions were plotted between $\frac{P}{h^2\sigma_r}$ and $\frac{E^*}{\sigma_r}$ as shown in Fig. 6. The figure shows the effect of the selection of ε_r on the form of π_1, for $\frac{h}{R} = 0.1$. The parameters used for defining the material combinations are given in Table 3.

When considering Fig. 6, it can be stated that it is difficult to identify a representative stain that makes the dimensionless function (π_1) independent of the strain hardening exponent (n) within the selected material property range with the used definition of the representative strain for power-law engineering materials with a plastic

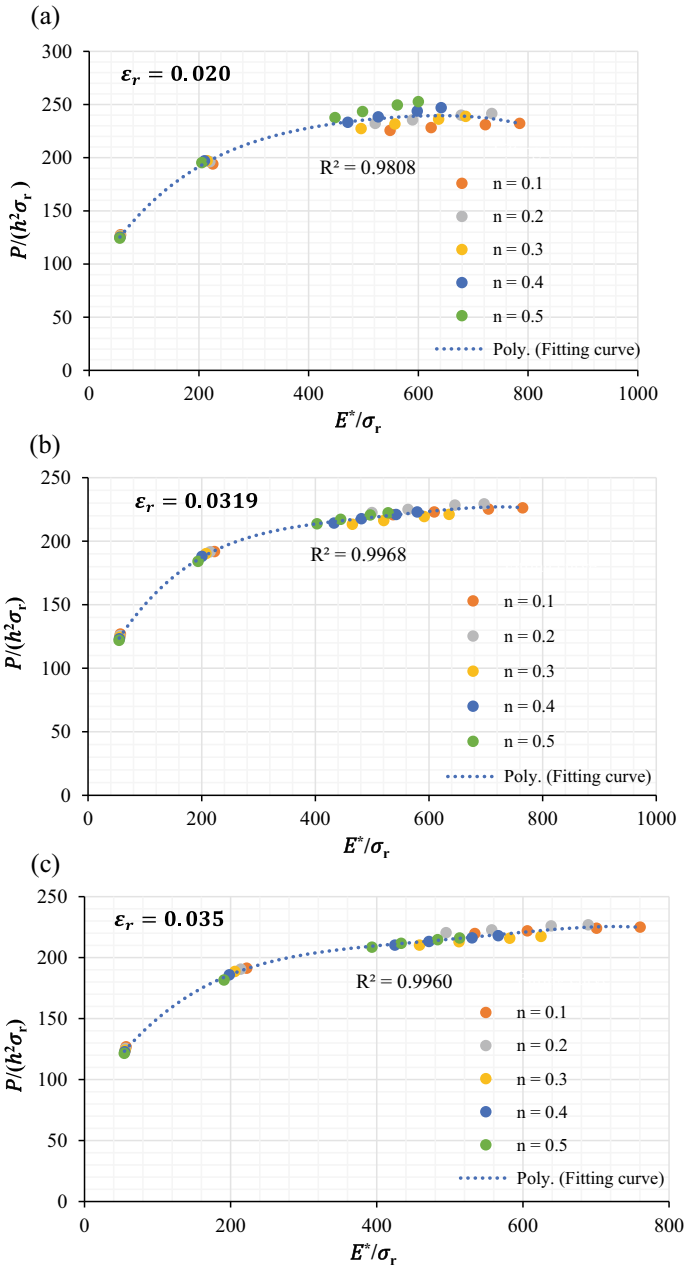

Fig. 6 Dimensionless function π_1 in Eq. (13) constructed for $\frac{h}{R} = 0.1$ by applying three different values of representative strain. **a** $\varepsilon_r = 0.020$, **b** $\varepsilon_r = 0.0319$, and **c** $\varepsilon_r = 0.035$. *Note* For one n value, points from left to right in the graphs represent σ_y values in descending order

Table 3 Parameters used for defining combinations of material properties

$\frac{h}{R} = 0.1$ 35 combinations of material properties Poisson's ratio ν=0.3	$E(GPa)$	α	$\sigma_y(MPa)$	n
	210	16	275 300 350 400 1000 4000	0.1 0.2 0.3 0.4 0.5

Note Material combinations were defined for $E = 210\ GPa$ and α=16, considering one n value and σ_y varied as 275 MPa, 300 MPa, 350 MPa, 400 MPa, 1000 MPa and 4000 MPa. There is no connection between columns

plateau. The fitting curves shown in Fig. 6 give the fourth-order polynomial functions, and by checking the R^2 values, it can be identified that when $\varepsilon_r = 0.0319$, the dimensionless function (π_1) becomes less dependent on strain hardening exponent (n).

Summary

A review on using the representative strain approach with spherical indentation test to determine the metal properties has been conducted in this paper. The ability to use the representative stain approach to develop an inverse analysis method to determine the material properties of power-law engineering materials with a plastic plateau-like structural steel is explored in the latter part of the paper. Based on this review, following important conclusions can be made.

1. There is no specific definition for representative strain, and it depends on the indentation type, indenter geometry, selected material property range, etc.
2. The concept of representative strain has been widely used by many researchers with the indentation tests to identify the plastic properties of power-law engineering materials since it reduces the number of apparent unknown variables in the π functions.
3. When using the representative strain to correlate material plastic properties with indentation responses, instead of dual sharp indentation, it is possible to use a single spherical indentation test to determine the plastic properties of a specimen from the indentation data obtained at different depths.
4. It is important to select proper $\frac{h}{R}$ ratios for spherical indentation such that deformation of the material is plastic and friction effect is negligible.
5. The accuracy of the fitting function (π) and selected material property range is strongly influenced to the results obtained from the inverse analysis method that is based on the representative strain.
6. For the power-law engineering materials with a plastic plateau, we have defined a representative strain (ε_r) as the total effective strain accumulated beyond the strain at the strain hardening (ε_{st}) point. It can be identified that the defined representative strain does not give a strain level that makes the dimensionless function

(π_1) independent of the strain hardening exponent (n) within the selected material property range. Hence, that cannot be used to develop an inverse analysis method to determine the structural steel plastic properties (α, σ_y, n).

References

1. ISO 14577 (2022) Metallic materials—instrumented indentation test for hardness and materials parameters. International organization for standardization, Geneva
2. Broitman E (2017) Indentation hardness measurements at macro-, micro-, and nanoscale: a critical overview. Tribol Lett 65:23
3. Mesarovic SD, Fleck NA (1999) Spherical indentation of elastic-plastic solids. Proc R Soc Lond A 455:2707–2728
4. Zhao M et al (2006) A new approach to meassure the elastic-plastic properties of bulk materials using spherical indentation. Acta Materialia 54(1):23–32
5. Cao YP, Lu J (2004) A new method to extract the plastic properties of metal materials from an instrumented spherical indentation loading curve. Acta Materialia 52(13):4023–4032
6. Pham TH et al. (2018) Identification of the plastic properties of structural steel using spherical indentation. Materials Science and Engineering A. Elsevier B.V.
7. Beghini M et al (2006) Evaluation of the stress-strain curve of metallic materials by spherical indentation. Int J Solids Struct 43(7):2441–2459
8. Chang C et al. (2018) Representative stress-strain curve by spherical indentation on elastic-plastic materials. Adv Mater Sci Eng, vol 2018, Article ID 8316384, 9 pages
9. Ogaswara et al (2005) Representative strain of indentation analysis. J Mater Res 20(8):2225–2234
10. Lee J, Lee C, Kim B (2009) Reverse analysis of nano-indentation using different representative strains and residual indentation profiles. Mater Design 30(9):3395–3404
11. Tabor D (1951) Hardness of metals. Clarendon Press, Oxford
12. Giannakopoulos AE, Suresh S (1999) Determination of elastoplastic properties by instrumented sharp indentation. Scripta Mater 40(10):1191–1198
13. Dao M et al (2001) Computational modeling of the forward and reverse problems in instrumented sharp indentation. Acta Mater 49(19):3899–3918
14. Chollacoop et al (2003) Depth-sensing instrumented indentation with dual sharp indenters. Acta Mater 51:3713–3729
15. Cao YP et al (2005) An energy-based method to extract plastic properties of metal materials from conical indentation tests. J Mater Res 20(5):1194–1206
16. Ogaswara et al (2006) Measuring the plastic properties of bulk materials by single indentation test. Scripta Mater 54:65–70
17. Cao Y, Qian X, Huber N (2007) Spherical indentation into elastoplastic materials: Indentation-response based definitions of the representative strain. Mater Sci Eng A 454–455:1–13
18. Cao, Y. and Huber, N. (2006) Further investigation on the definition of the representative strain in conical indentation. J Mater Res, 21(7):1810-1821
19. Ogaswara et al (2009) A simple framework of spherical indentation for measuring elastoplastic properties. Mech Mater 41:1025–1033
20. Lee et al (2010) A study on robust indentation techniques to evaluate elastic-plastic properties of metals. Int J Solids Struct 47:647–664
21. Budiarsa et al (2015) Characterization of material parameters by reverse finite element modeling based on dual indenters Vickers and spherical indentation. Procedia Manufact 2:124–129
22. Oliver WC, Pharr GM (2004) Measurement of hardness and elastic modulus by instrumented indentation: advances in understanding and refinements to methodology. J Mater Res 19(1):3–20

23. Fischer-Cripps AC (2001) Use of combined elastic modulus in the analysis of depth-sensing indentation data. J Mater Res 16(11):3050–3052
24. Cheng YT, Cheng CM (1999) Scaling relationships in conical indentation of elastic-perfectly plastic solids. Int J Solids Struct 36(8):1231–1243
25. Pham TH (2015) Estimating constitutive equation of structural steel using indentation. Int J Mech Sci 90:151–161
26. Kato B et al (1990) Standardized mathematical expression for stress-strain relations of structural steel under monotonic and uniaxial tensile loading. Mater Struct 23:47–58

Influence of Upstream Mature Trees on Wind Loading on the Gable Roof of a Low-Rise Building—A Wind Tunnel Study

P. H. Kandamby, C. S. Lewangamage, and A. U. Weerasuriya

Abstract Trees planted in rows have been used as shelterbelts to protect crops from strong winds. Similarly, trees can be used as windbreaks to reduce wind loading on buildings to protect them from wind damages. This hypothesis was tested in this study by conducting a series of wind tunnel tests using scaled-down models of a gable-roofed, low-rise building, and a mature tree, which is taller than the building. The tree was fabricated using steel wires and wool at a length scale of 1:50, similar to the building model, and resulted in a drag coefficient (C_d) of 0.75. Several model trees were installed at various distances upstream with side-by-side, staggered, and V-shaped configurations. Wind loads acting on the building roof were estimated by measuring external wind pressure using a synchronized pressure measurement system (SPMS). The results revealed significant variations in wind pressure with the number of trees, their configurations, and distance to the building. With upstream trees, some areas of the windward roof slope, such as the windward eave, lateral edges, and the area just upstream of the ridge, were subjected to increased negative wind pressure, but its magnitude decreased on the leeward roof slope. Negative wind pressure of the roof became smaller with the increase of separation distance between the building and trees except for densely arranged trees in a row. The results also suggested mature trees increased the roof uplift force by 10–30% compared to the treeless case. Among the tested tree configurations, staggered and linearly arranged sparse trees within a 2D distance should be avoided to alleviate the adverse negative pressure of the roof. Furthermore, this study recommended planting trees in rows at a 3D upstream distance (D = building width) or in a V-shaped configuration if the separation distance is less than 3D to reduce wind loading on the gable roof of a low-rise building.

Keywords Low-rise building · Gable roof · Wind tunnel testing · Surrounding trees · External wind pressure

P. H. Kandamby (✉) · C. S. Lewangamage
Department of Civil Engineering, University of Moratuwa, Moratuwa, Sri Lanka
e-mail: pasanhkandamby@gmail.com

A. U. Weerasuriya
Department of Civil and Environmental Engineering, The Hong Kong University of Science and Technology, Kowloon, Hong Kong, China

R. Dissanayake et al. (eds.), *12th International Conference on Structural Engineering and Construction Management*, Lecture Notes in Civil Engineering 266,
https://doi.org/10.1007/978-981-19-2886-4_5

1 Introduction

Accurate estimation of wind loads of low-rise buildings is imperative for preventing wind damages and ensuring the structural safety of the buildings. Such accurate estimation is often evasive in the early design stage due to the difficulties in predicting the complex interactions between the incoming wind, low-rise buildings, and their surrounding [11]. Although modelling efforts and painstaking field measurement campaigns shed light on the understanding of the interaction between wind and low-rise buildings, the current knowledge of how the surrounding modifies wind loading of low-rise buildings is still in an infant stage. Especially in the presence of other objects in the surrounding such as buildings, trees, fences, and boundary walls, the wind effects of low-rise buildings can be highly complex and unpredictable [1, 7]. One such object in the surrounding is trees, which greatly influence the wind loading of low-rise buildings.

Trees are often seen as green oases in built-up areas due to their natural cooling ability resulted from evapotranspiration and shading. Moreover, trees are useful in mitigating the Urban Heat Island (UHI) effect as they reduce ambient and surface temperature [2]. Roadside trees act as noise barriers to attenuate traffic noise [9] and regulate air quality by absorbing pollutants and increasing pollutant disposition [10]. Despite these environmental benefits, the effects of trees on structures are difficult to quantify in part because of the pronounced fluid–structure interaction produced by flexible trees and turbulent winds. Tree branches, leaves, and sometimes trunks are flexible and allow to adjust their shape differently at various wind speeds [3]. As a result, trees impose various degrees of resistance to incoming wind and modify differently the surrounding wind field in strong and calm winds. From the fluid mechanical point of view, trees can be classified as a highly complex porous media that limits the applicability of classic principles of bluff body aerodynamics [4]. For instance, the flow field around and in the wake of trees is distinctly different from that found near bluff bodies such as buildings. One such flow feature is the wake of trees, which extends far downstream compared to the wake of buildings. Moreover, sometimes the downstream flow recirculation zone is detached from the upstream tree rather than found next to bluff bodies. Another distinct feature is the considerable contribution of skin friction (i.e. form drag) of trees to the total drag compared to negligible skin friction of counterpart bluff bodies. Larger surface areas of 'porous' trees result in greater skin friction, which presents itself as the dominant form of drag for trees.

Despite these distinct structural and aerodynamics features, the effects of trees on wind effects of low-rise buildings were scantly investigated in previous studies. One such rare study was conducted by Stathopoulos et al. [12] in a boundary layer wind tunnel by modelling trees in two sizes in the surrounding of a low-rise building. Trees were arranged side-by-side and staggered in single and double rows with high (more trees) and low (fewer trees) densities. The tree rows had three different lengths: 0.6, 1, and 1.4L (L is the width of the building) and were at various distances: 1–10H (H is the tree height) from the building. The wind tunnel experiment has indicated

the advantage of the dense tree arrangement to minimize suction pressure on the roof. Furthermore, mean and minimum pressure at eaves have decreased with the increase of upstream distance to trees up to 6*H* but a further increase of the separation distance has diminished this positive effect. In contrast, the peak suction on the ridge was higher for the presence of trees than that of no tree in the surrounding. Most importantly, Stathopoulos et al. [12] pointed out that despite trees generally decreased wind loading, certain tree arrangements could increase wind loading causing adverse wind effects of low-rise buildings. Surprisingly, since their work, no other study has investigated the effect of trees on wind effects of low-rise buildings.

The current study aims to bridge this knowledge gap by investigating how differently arranged trees modify the wind loading of a gable-roofed, low-rise building. Different from the study of Stathopoulos et al. [12], this study modelled mature trees, which were taller than the low-rise building. Because the two tree models used by Stathopoulos et al. [12] were 3.8 (small trees) and 7.6 m (large tree) in height and were shorter than the eave height (5.85 m) and ridge height (9.1 m), respectively, they imposed greater shielding effect and resulted in a significant reduction in wind loads of the low-rise building. However, in the real world, trees are usually taller than the nearby buildings (Fig. 1), thus imposing a limited shielding effect. Moreover, trees are often planted closer to buildings in suburban than the distances assumed by the previous study due to the limited size of land plots in cities. This study considered these factors when designing the wind tunnel test (Sect. 2) to investigate the wind loads on the gable roof of a low-rise building surrounded by mature trees (Sect. 3). This study mainly focussed on wind loads on the roof because the roof is the most vulnerable building component to wind effects. The findings and conclusions of this

Fig. 1 Mature trees in the surrounding of low-rise buildings (Photos from google images)

study were presented as the recommendations for planting trees to minimize wind effects on the low-rise, gable-roofed buildings (Sect. 4).

2 Wind Tunnel Experiment

2.1 Building Model

The wind tunnel test of this study was conducted in the boundary layer wind tunnel (BLWT) at the Cyclone Testing Station at the James Cook University, Townsville, Australia. The BLWT is 22 m long and has a test section with dimensions 2 × 2.5 m. A low-rise, gable-roofed building was fabricated using plexiglass on a length scale of 1/50. The building model is a representation of the most common type of contemporary houses in Australia with the full-scale dimensions of 19.8 (Length) × 10 (Width) × 2.7 m (Eave height) with a 0.6 m roof overhang and a 22.5° roof pitch angle (Fig. 2a) [6]. The model was installed in the test section by facing the building's longwall face to the incoming wind (i.e. wind incidence angle (θ) = 0). The pressure measurements were recorded by using 248 pressure taps installed on the roof and the building's walls (Fig. 2b). An atmospheric boundary layer wind flow was simulated with a logarithmic type mean wind speed profile, which was characterized by the roughness length (z_o) of 0.00077 m (in model scale), the friction velocity (u_*) of 0.66 m/s and a reference mean velocity (U_{ref}) of 9 m/s at the 0.2 m height (Fig. 2c). The turbulence intensity profile showed a proper decay with height with

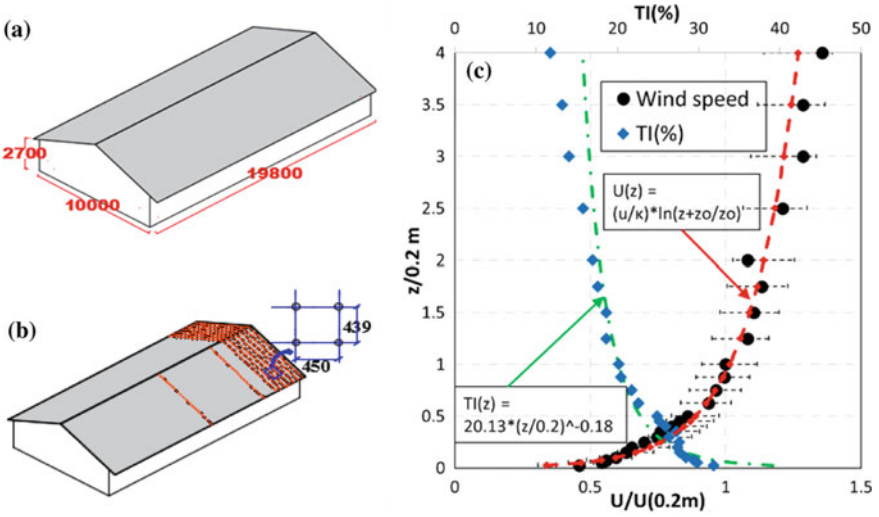

Fig. 2 **a** Dimensions of the full-scale building, **b** the scale-down model with the pressure taps (all dimensions are mm), and **c** the profiles of mean wind speed and turbulence intensity

20% turbulence intensity at 0.2 m height (Fig. 2c). The pressure measurements were recorded four times for 30 s at a frequency of 1000 Hz. All pressure measurements were low pass filtered at 500 HZ and subsequently used for calculating normalized mean pressure coefficient ($C_{p,\,mean}$) as in Eq. (1).

$$C_{p,mean} = \frac{1}{n}\sum_{i=1}^{n}\frac{\overline{P}_i}{1/2\rho\overline{v}_h^2} \tag{1}$$

In Eq. (1), $\overline{P}_i$ is the time-averaged pressure at ith measurement cycle, ρ is the air density, $\overline{v}_i$ is the mean wind speed at the eave height, h, and n is the number of measurement cycles equal to four.

2.2 Tree Model

Trees modelled for the current study were mature trees but they were not representative of any specific tree species. The tree model represents full-scale trees with an average height of 11–13 m with the trunk and foliage heights of 5–6 m and 6–7 m, respectively (Fig. 3a). The tree model was fabricated using steel wires and wools on a length scale of 1/50 similar to the length scale of the building model (Fig. 3b). The aerodynamics properties of the tree model were determined by analysing the photo images of the tree [8]. First, the optical porosity (β) was estimated as 0.15 using the image analysis, and then, the aerodynamic porosity (α) was calculated as 0.468 using the relationship $\alpha = \beta^{0.4}$. The corresponding drag coefficient (C_T) was estimated as 0.75 using the method proposed by Guan et al. [5].

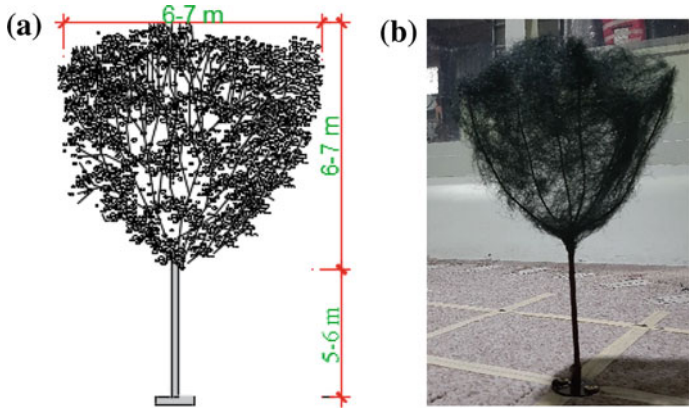

Fig. 3 **a** Schematic diagram of the full-scale tree **b** scaled-down tree model used for the wind tunnel test

The tree models were arranged in three different configurations: linear (L), staggered (ST), and V-shaped. The linear arrangement had either two or five trees in a row upstream of the building, and three upstream trees and two trees on the lateral sides. Trees were at 1, 2, and 3 D distance upstream, downstream, and/or lateral sides of the building, where *D* is the depth of the building, resulting in 13 different tree configurations. For the current study, four tree configurations: linear configuration (L) without trees on the lateral sides, staggered (ST) and reversed-staggered (SR), and V-shaped (V) were selected for the analysis (Fig. 4). Although 37 wind incidence angles in a range of 0°–360° at 10° intervals were tested in the wind tunnel test, only the 0° wind incidence angle, where the wind blew perpendicular to the long side of the building was selected for the analysis. In the analysis, external wind pressure on the roof of the building surrounded by trees was compared with that of the treeless case, hereafter referred to as the base case. In addition, uplift and drag forces on the roof were calculated to quantify the influence of different tree configurations on the wind effects of a gable roof of a low-rise building.

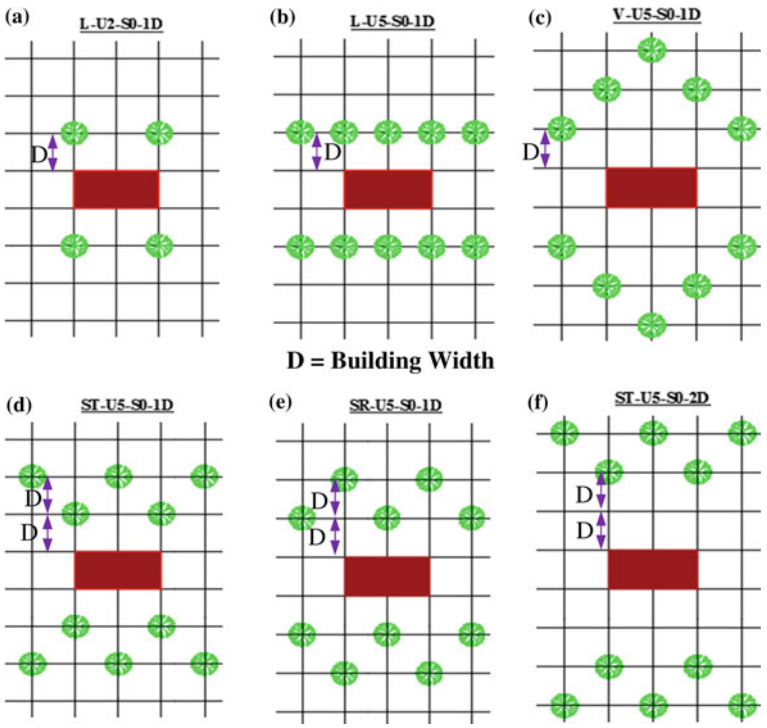

Fig. 4 Some tree configurations of the current study **a** linear arrangement of two trees at 1D, **b** linear arrangement of five trees at 1D; **c** V-shaped; **d** staggered arrangement at 1D; **e** reversed-staggered arrangement at 1D; **f** staggered arrangement at 2D

3 Results and Discussion

3.1 Mean Pressure Distribution on the Roof

Figure 5 shows the distribution of $C_{p,mean}$ on the gable roof of the building at $\theta = 0°$ with and without surrounding trees. Without any trees in the surrounding, a major portion of the upwind roof slope had negative pressure and two areas with positive pressure near the windward roof corners (Fig. 5a). The downwind roof slope had negative pressure, whose magnitude increased from the ridge (marked by the white dashed line) to the downwind eave. After adding two trees in a row at a 1D distance upstream and downstream of the building (i.e. L-U2-S0-1D = linear configuration-two upstream trees—zero trees on lateral sides—1D distance to the nearest tree), the two areas with positive pressure on the upwind roof slope became negative, and the magnitude of negative pressure further increased compared to the base case (Fig. 5b). The negative pressure near the ridge on the downwind roof slope also increased but the magnitude decreased near the downwind eave. The staggered tree configuration (ST-U5-S0-1D) further escalated the suction pressure on the upwind slope with a noticeable increase of negative pressure at the windward eave (Fig. 5c). In contrast, the maximum negative pressure on the downwind roof slope ($C_{p,mean} = -0.5$) was smaller than that of the base model and the tree configuration: L-U2-S0-1D ($C_{p,mean} = -0.6$). The pressure distribution on the roof for the V-shaped tree configuration (V-U5-S0-1D) was very similar to that of ST-U5-S0-1D except for slightly smaller

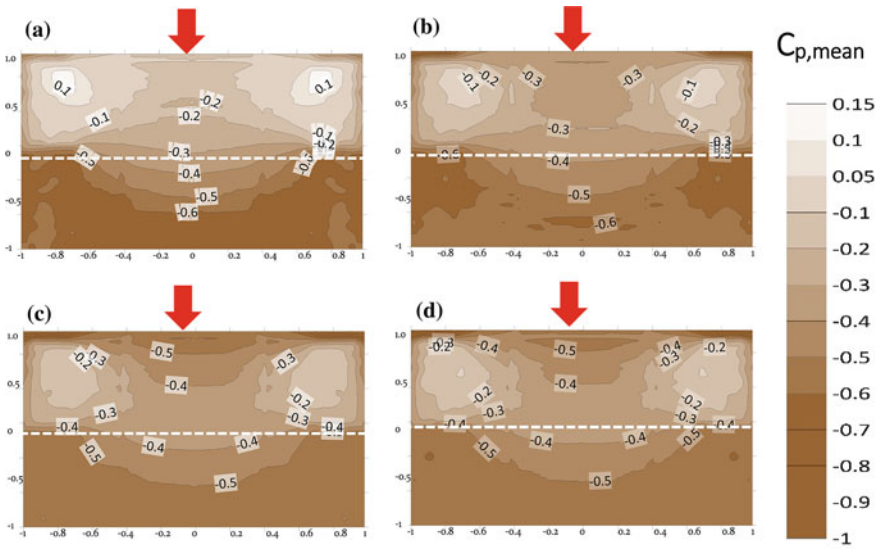

Fig. 5 The distribution of $C_{p,mean}$ on the gable roof of **a** base model, **b** L-U2-S0-1D, **c** ST-U5-S0-1D, and **d** V-U5-S0-1D

negative pressure found at the windward eave, and the windward roof corners for the former tree configuration (Fig. 5d). Overall, Fig. 5 depicts intensified suction pressure on the upwind roof slope with a noticeable rise in negative pressure at the windward eave, near windward roof corners, and the ridge with the presence of trees in the surrounding. Therefore, the rest of the analysis of this study particularly focuses on how wind pressure on these three areas varies with tree configurations in the surrounding.

3.2 *Effect of Number of Upstream Trees*

Figure 6 shows how the number of upstream trees affects wind pressure on the upwind roof slope. The analysis is based on the variation in $C_{p,mean}$ along the windward eave (Fig. 6a–b) and the centre line (Fig. 6c–d) on the windward roof slope. With two trees at a 1D upstream distance, L-U2-S0-1D caused 85 and 107% reductions in $C_{p,mean}$ at the edge and the centre of the windward eave compared to the base case. Having five trees at a 1D upstream distance (i.e. L-U5-S0-1D), $C_{p,mean}$ further decreased by 133% at the edge and 285% at the centre of the windward eave. It can be postulated that the decrease in $C_{p,mean}$ at the edge of the windward eave is attributed to the strong flow separation at the eave caused by the upstream trees. At the centre, $C_{p,mean}$ decreased less than at the edges due to the influence of the two trees were smaller compared to their direct influence at the edges of the eave. As the separation distance between trees and the building grew, the influence of trees gradually diminished as indicated by a steady increase in $C_{p,mean}$ (smaller negative $C_{p,mean}$) at the windward eave. For example, $C_{p,mean}$ decreased by only 33% at the edge and 66% at the centre of the

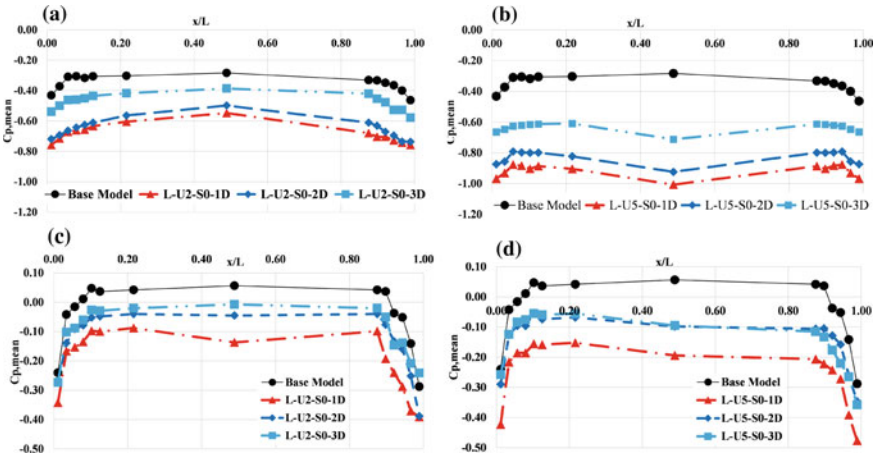

Fig. 6 Variation in $C_{p,mean}$ along the windward eave for **a** two trees in a row, **b** five trees in a row, and on the centre line on the windward roof slope for **c** two trees in a row, **d** five trees in a row

windward eave for L-U2-S0-3D compared to the base case. However, even at a great upstream distance, dense tree configurations can impose considerable influence on the wind pressure at the windward eave as indicated by $C_{p,mean}$ of L-U5-S0-3D. This tree configuration reduced $C_{p,mean}$ by 48% at the edge and 191% at the centre of the windward eave compared to the base case showing a greater adverse effect of densely packed upstream trees on wind effects of the gable roof.

Compared to the windward eave, wind pressure in the middle part of the upwind roof slope was differently modified by the surrounding trees. For instance, $C_{p,mean}$ at the edge of the centreline of the upwind roof slope decreased by 42% and 75%, respectively, for the two linear tree configurations: L-U2-S0-1D and L-U5-S0-1D. In contrast, dramatic $C_{p,mean}$ modifications occurred at the centre of the upwind roof slope, where positive wind pressure observed for the base case transformed into negative wind pressure for the buildings surrounded by trees. Compared to $C_{p,mean} = 0.06$ in the middle of the upwind roof slope of the base case, L-U2-S0-1D and L-U5-S0-1D had $C_{p,mean}$ values of -0.15 and -0.20, respectively, at the same location. Although negative wind pressure in the middle of the windward roof slope decreased with the increase of the distance to trees, it remained as suction pressure for both L-U2-S0-3D and L-U5-S0-3D configurations. Negative pressure in the middle of the upwind roof slope was a result of the absence of flow reattachment for the cases with the surrounding tree. A plausible explanation is flow acceleration by upstream trees that strengthened the flow separation at the windward eave and prevented the flow reattachment in the middle of the windward roof slope.

3.3 Effect of Trees Configuration

Figure 7 compares $C_{p,mean}$ at the windward and leeward eaves, and areas just upstream and downstream of the ridge for four tree configurations: L-U5-S0-1D, ST-U5-S0-1D, SR-U5-S0-1D, and V-U5-S0-1D. For an unbiased comparison, tree configurations that were with five trees at a 1D distance from the building were selected for the analysis. Evidently, the surrounding trees had the strongest influence on wind pressure at the windward eave. On average, the surrounding trees escalated negative pressure by 126% at the edge and 246% in the middle of the windward eave (Fig. 7a). In particular, SR-U5-S0-1D caused the largest increase in negative pressure at the windward eave, while reverse staggered tree configuration—V-U5-S0-1D least increased negative pressure. While these two configurations yielded the smallest negative $C_{p,mean}$ on the windward side of the ridge, L-U5-S0-1D resulted in the largest suction pressure at the same location. It resulted in 23 and 7% smaller $C_{p,mean}$ at the edge and in the middle of the windward side of the ridge than that of the base model (Fig. 7b). In contrast, V-U5-S0-1D caused about 5% and less than 1% reductions at these two locations compared to the base model. The other configuration: ST-U5-S0-1D had similar $C_{p,mean}$ at the edge of the windward side of the ridge to that of the base case. However, some noticeable deviations in $C_{p,mean}$ from the base case were observed in the middle portion of the windward side of the ridge for ST-U5-S0-1D.

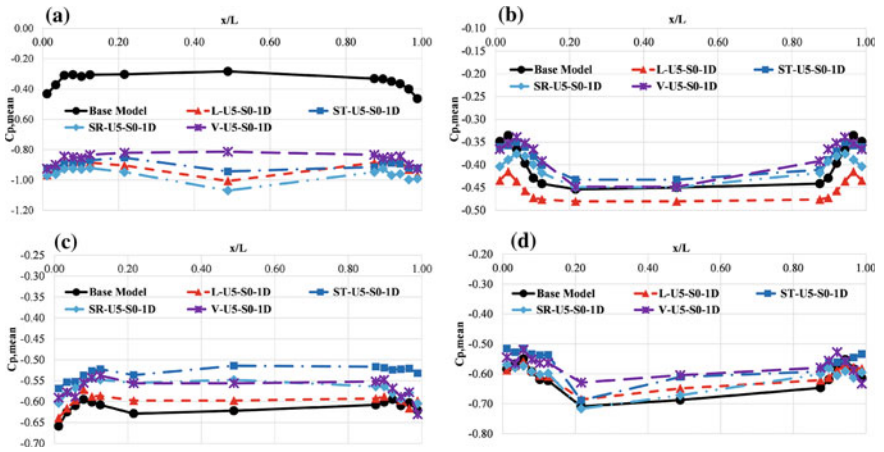

Fig. 7 Variation in $C_{p,mean}$ **a** at the windward eave, **b** windward side of the ridge, **c** leeward side of the ridge, **d** at the leeward eave with four tree configurations at a 1D distance

On the leeward side of the roof, $C_{p,mean}$ was smaller for the buildings surrounded by trees than that of the base case (Fig. 7c and d). In particular, the staggered tree configurations were effective in reducing suction pressure on the downwind slope. For instance, $C_{p,mean}$ at the downwind eave and on the downwind side of the ridge were about 21 and 17% smaller than that of the base case. In contrast, the linear tree configuration least modified wind pressure on the downwind slope as only visible differences in $C_{p,mean}$ with respect to the base case can be seen in the middle part of the roof slope.

Since some tree configurations significantly modified wind pressure on the upwind roof slope but slightly influenced wind pressure on the downwind roof slope, it was ambiguous to estimate the overall effect of tree configurations on the wind loading of the gable roof. Therefore, this study calculated total drag and lift forces acting on the roof to elucidate how each tree configuration modified the wind loads on the gable roof of a low-rise building.

3.4 Overall Effect on Wind Loading of the Roof

The drag and uplift forces of the gable roof were calculated as follows: first, pressure measurements of each pressure tap were multiplied by the corresponding tributary area to estimate the force acting perpendicular to the roof slopes. Then, these forces were decomposed into two orthogonal forces—one parallel (i.e. drag force) and another perpendicular (i.e. uplift force) to the wind flow. The summations of forces parallel and perpendicular to undisturbed wind flow are overall drag and uplift forces, respectively (Fig. 8).

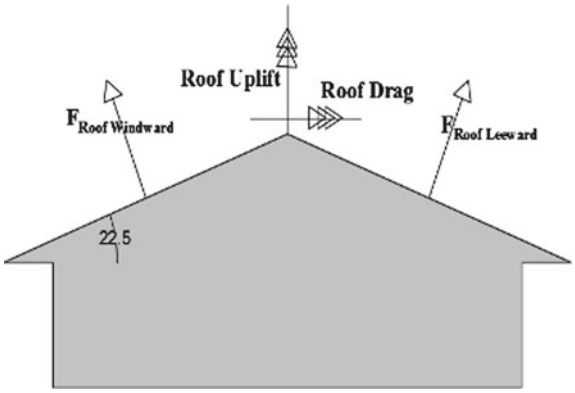

Fig. 8 Vector presentation of forces acting on the roof

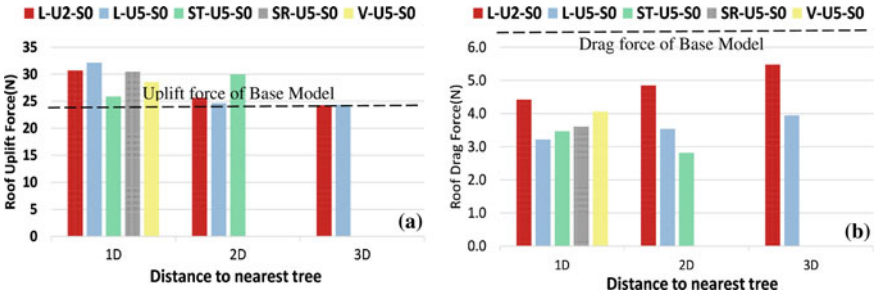

Fig. 9 **a** Roof uplift and **b** roof drag force for the buildings surrounded by various tree configurations

Figure 9 compares drag and uplift forces on the gable roof of the low-rise building surrounded by trees with the treeless base case. All tree configurations caused higher uplift forces than the base case where trees were at a 1D distance from the building. At a 1D distance, linear tree arrangements and the reverse staggered tree configuration resulted in 30% greater uplift forces than that of the base case. ST-U5-S0-1D increased least the uplift force by 10% at a 1D distance but the same staggered tree configuration at a 2D distance aggravated the uplift force by 20%, which was the highest increment observed for any tree configuration at a 2D distance. Interestingly, five trees in a row at 2D (L-U5-S0-2D) did not modify the uplift force compared to the base case while two trees in a row caused a 10% increase. However, the linear configuration of two trees at a 3D distance away from the building did not affect the uplift force. Therefore, it can be concluded that the tendency of the linear tree configurations to escalating the uplift force of the roof diminishes with the increase of the separation distance between trees and the building.

On the contrary, all tree configurations considerably decreased the roof's drag force (Fig. 9b). The drag force was 50–60% of that of the base case for the cases with trees at a 1D away from the building. However, the drag force increased from 60

to 70 to 80% for L-U2-S0 as the separation distance between trees and the building increased from 1D to 2D to 3D. Similarly, the linear configuration with five trees showed a mild increase in the drag force from 50 to 60% as the separation distance increased from 1D to 3D. In contrast, drag force decreased by 10% for ST-U5-S0 as the separation distance increased from 1D to 2D.

4 Conclusion

In contrast to the findings of Stathopoulos et al. [12], this study found a noticeable increase in negative wind pressure (suction pressure) on a gable roof of a low-rise building surrounded by mature trees (i.e. trees taller than the building). In the presence of mature trees in the surrounding, the windward eave, roof's lateral edges, and near upstream of the ridge were vulnerable to high suction pressure. However, having mature trees in the surrounding is advantageous for reducing suction pressure on the downwind slope of the gable roof. It is recommended to avoid linear tree configurations, in particular with dense tree arrangements, to minimize high suction pressure at these vulnerable locations. Instead, it is also recommended to plant trees in a V-shaped configuration to minimize suction pressure on the gable roof.

In the presence of mature trees close to the building, the roof uplift force increased by 10–30% compared to that of the building without trees in the surrounding. It is advised to avoid planting trees in staggered configurations and sparse trees in a row within a 2D distance from the building. Although mature trees caused smaller roof drag force, the increasing trend in the roof uplift force caused by linearly arranged sparse trees suggests this tree configuration should be avoided having near gable-roofed, low-rise buildings.

Acknowledgements The authors are thankful to Prof. John Ginger, Dr. Korah Parakkal, and the staff of the Cyclone Testing Centre at the James Cook University, Townsville, Australia, for their support given for conducting the wind tunnel tests of this study.

References

1. Ahmad S, Kumar K (2001) Interference effects on wind loads on low-rise hip roof buildings. Eng Struct 23(12):1577–1589
2. Buccolieri R, Santiago JL, Rivas E, Sanchez B (2018) Review on urban tree modelling in CFD simulations: aerodynamic, deposition and thermal effects. Urban Urban Green 31:212–220
3. de Langre E (2008) Effects of wind on plants. Annu Rev Fluid Mech 40:141–168
4. Gromke C, Ruck B (2008) Aerodynamic modelling of trees for small-scale wind tunnel studies. Forestry 81(3):243–258
5. Guan D, Zhang Y, Zhu T (2003) A wind-tunnel study of windbreak drag. Agric Meteorol 118(1–2):75–84
6. Jayasinghe NC (2012) The distribution of wind loads and vulnerability of metal clad roofing structures in contemporary Australian houses (Doctoral dissertation, James Cook University)

7. John AD, Gairola A, Krishna P (2008) Wind load on overhangs in a low gable building in presence of free standing wall. J Wind Eng 5(1):39–46
8. Kenney WA (1987) A method for estimating windbreak porosity using digitized photographic silhouettes. Agric Meteorol 39(2–3):91–94
9. Ow LF, Ghosh S (2017) Urban cities and road traffic noise: reduction through vegetation. Appl Acoust 120:15–20
10. Ozdemir H (2019) Mitigation impact of roadside trees on fine particle pollution. Sci Total Environ 659:1176–1185
11. Stathopoulos T (1984) Wind loads on low-rise buildings: a review of the state of the art. Eng Struct 6(2):119–135
12. Stathopoulos T, Chiovitti D, Dodaro L (1994) Wind shielding effects of trees on low buildings. Build Environ 29(2):141–150

Vortex Shedding-Induced Fatigue Analysis for High-Mast Lighting Towers

K. Jeyamohan, C. S. Bandara, and J. A. S. C. Jayasinghe

Abstract The high-mast lighting towers that are subjected to cyclic wind loadings (due to vortex shedding action) tend to fail due fatigue failure. From past studies, based on the testing and finite element analysis, it was found that geometry of the mast arm and base connection are highly influencing on the fatigue performance of the high-mast lighting towers, and also, the design of this wind sensitive structures is mainly governed by wind-induced fatigue. This study investigates the wind-induced fatigue behavior of high-mast lighting towers under the effect of mast arm wall thicknesses and base connection geometry with unstiffened base connection. The thicknesses of the base plate and the mast arm wall are used as variable parameters, because these are highly influencing on the fatigue performances of the system. Generally, finite element analysis is performed for the selected geometry of the high-mast lighting tower system with various thicknesses of the mast arm wall and base plate to obtain the hot spot stress and SCF with considering along and vortex shedding wind action. Finally, the procedure for a detailed fatigue analysis based on Palmgren–Miner theory of cumulative damage method with S–N curves based on EN 1993-1-9 is discussed.

Keywords S–N curve · Stress concentration factor (SCF) · Damage · Fatigue

1 Introduction

The high-mast lighting towers are normally used to provide the light for the airport, sports complex, highway interchange and some industrial yards. The base connection

K. Jeyamohan (✉)
Department of Engineering Technology, Faculty of Technology, University of Jaffna, Jaffna, Sri Lanka
e-mail: Jeya@tech.jfn.ac.lk

C. S. Bandara · J. A. S. C. Jayasinghe
Department of Civil Engineering, Faculty of Engineering, University of Peradeniya, Peradeniya, Sri Lanka

R. Dissanayake et al. (eds.), *12th International Conference on Structural Engineering and Construction Management*, Lecture Notes in Civil Engineering 266,
https://doi.org/10.1007/978-981-19-2886-4_6

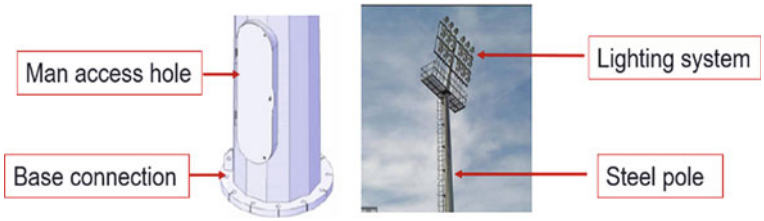

Fig. 1 Features of high-mast lighting towers

geometry, man access hole and mast arm geometry are the important features of the high-mast lighting towers for their structural performances (Fig. 1).

The wind forces acting on the high-mast lighting towers depend on the basic wind speed of the particular location, terrain type, altitude and dynamic and cross-wind effects. In Sri Lanka, less amount of wind occurs due to thunderstorm and large amount wind occurs due to monsoons. The wind-induced fatigue occurs as a result of the along-wind and cross-wind response of the structures [1]. Along-wind response is mainly due to buffeting by atmospheric turbulence and cross-wind response is mainly due to vortex shedding action on the tower. These two wind actions have the potential to produce the vibration that cause the fatigue failure.

Vortex shedding wind action is a complex physical phenomenon, especially when it degenerates into lock-in condition. Due to this phenomenon, structures may undergo a high numbers of load cycles that leads to damage accumulation and may determine the structural failure without exceeding the ultimate loads [2]. When the wind blows across the high-mast steel arm, vortices are shed alternatively from one side and then to the other. Large amplitude vibrations in the plane normal to the wind may develop when the vortex shedding is in resonance with one of the natural frequencies of the vibration, so that, vortex shedding-induced forces on the structures are perpendicular to along-wind direction as shown in Fig. 2.

Geometry of the high-mast steel arm and the base connection, especially thicknesses of the mast arm wall and base plate, are important parameters, because these are highly influencing on the fatigue performance of the high-mast lighting tower system under the along- and cross-wind action. Addition to thicknesses of the mast

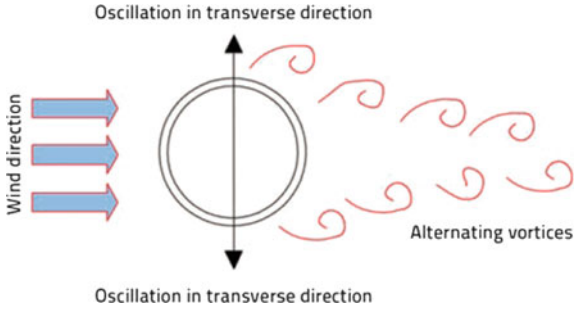

Fig. 2 Von Karman's vortices [2]

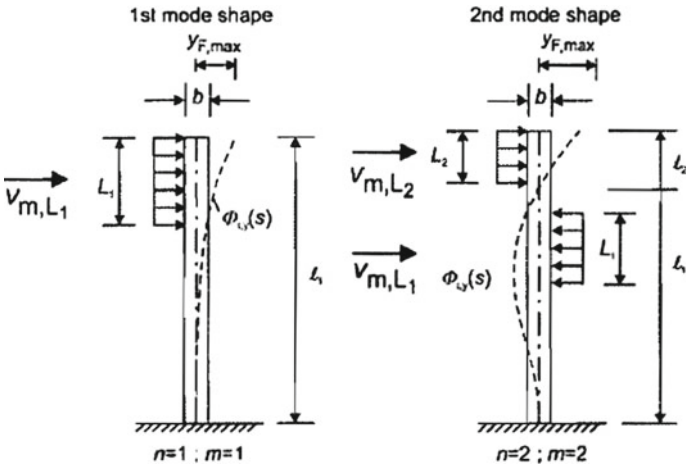

Fig. 3 Location of correlation length and mode shapes for first two modes

arm wall and base plate, diameter of the base plate, free-standing pole length, number of anchor bolts, welding thickness, diameter and slope of the mast arm wall and mesh refinement also contribute in the fatigue performance of the structure [3]. Also, vortex shedding excitation-induced forces on the high-mast lighting tower system are mainly depends on the natural frequency, mean wind velocity, Reynolds number, Scruton number and effective correlation length factor of the system. These parameters are mainly interconnected with geometry of the high-mast steel arm. Effective correlation length and mode shapes for the first two modes are shown in Fig. 3.

Fatigue assessment of the high-mast steel arm is performed by estimating the hotspot stress due to along- and cross-wind action using finite element analysis, along-wind and vortex shedding-induced forces and its impact to be applied statically. Generally, shell and solid elements are used for the mast arm wall and base plate, respectively, with finer mesh arrangement to obtain the high accuracy results. In the code-based fatigue assessment, S (direct stress range)–N (number of cycles) curve is used for the estimation of load cycles with consideration of detail category for each structural part of high-mast steel arm as shown in Fig. 4 [4].

In the S–N curves, reference value of fatigue strength is obtained at 2 million load cycles as provision given in the EN1993-1-9-2005. Palmgren–Miner theory of cumulative damage method is commonly used to estimate the total fatigue damage. For the selected detail category, the resistance of fatigue is estimated by means of accumulation of individual damage caused by individual stress block of each stress set. The number of stress sets depends on the number of analyzed frequency modes and the number of critical positions in which the vortex excitation occurs. So, in order to avoid the fatigue failures on the high-mast steel arm due to cyclic wind loads, total damage accumulation during the design life should be less than one. Under different amplitude conditions, all stress ranges should be less than the constant amplitude fatigue limit to avoid the fatigue failures on the structures. Size

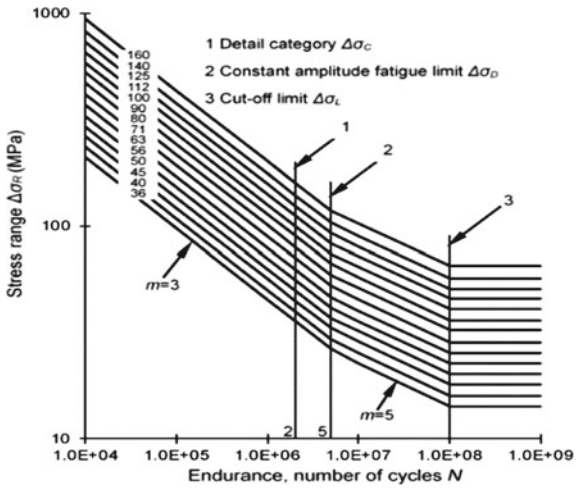

Fig. 4 S–N curves with different detail category [4]

effect due to thickness also should be taken into account. Stress concentration factor (SCF) also is an important parameter in the fatigue performance of the high-mast steel arm. SCF is the ratio of the hot spot stress and the nominal stress.

2 Influence of Geometry in the Fatigue Performance of the System

Geometry of the high-mast steel arm and the base connection are highly influencing on the fatigue performance of the high-mast lighting tower system. There are many geometric variables are influencing on the fatigue performance of the system, which are;

- Base plate thickness
- Mast arm wall thickness
- Number of anchor rods (number of holes in the base plate)
- Base plate size and welding thickness
- Slope and size of the mast arm wall.

From the literatures, it was found that the thicknesses of the base plate and the mast arm wall are highly influencing on the fatigue performance of the system [5]. Figure 5 summarized the variation of stress concentration factor (SCF) with base plate thicknesses from three different research studies.

SCF is decreased with increasing of the base plate thickness of the mast arm structure. It can be concluded that the base plate thickness of the high-mast lighting tower system is an important parameter, and special concerns should be given at the time of the fatigue design of high-mast lighting tower systems. Further, increasing

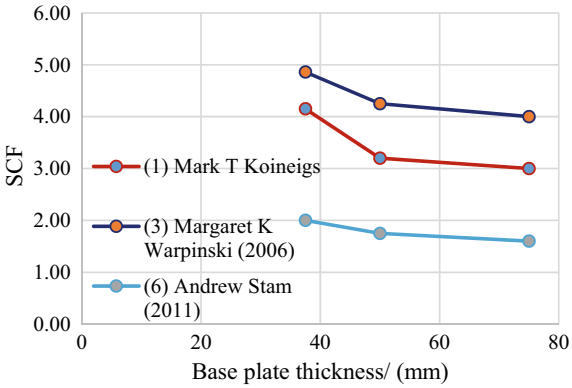

Fig. 5 Variation of SCF with thickness of the base plate

the base plate thickness provides significant improvement to the fatigue life of the tower by reducing the maximum stress at the base plate to tube wall connection as shown Fig. 6. So, base plate flexibility has a considerable influence on the stress behavior in the tube wall adjacent to the unstiffened connection of the high-mast lighting tower system.

Also, from literature [5], it was found that the variation of the hot spot stress is highly influencing on the tube wall thickness of the mast arm wall of the structure. So, increasing the tube wall thickness provides significant improvement to the fatigue life of the tower by reducing the maximum hotspot stress at the mast arm wall adjacent to the base connection.

Addition to these two parameters, number of anchor bolts, welding thickness, base plate geometry, mast arm geometry and free-standing length of the pole also influencing the fatigue performance of the mast arm structures. Based on these results, it can be concluded that the thicknesses of the base plate and the mast arm wall are highly influencing on the fatigue performance of the high-mast lighting tower

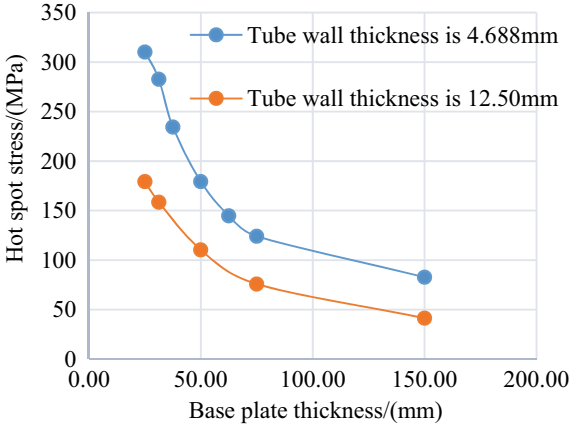

Fig. 6 Variation of hot spot stress with thickness of base plate

structure under unstiffened base connection. In the design stage, the proposed base plate thickness and the mast arm wall thickness for a particular high-mast lighting tower structure should satisfy all these fatigue design requirements to avoid the damages on the mast arm wall and the base connection.

3 Vortex Shedding-Induced Forces

The vortices create across-wind deflections due to an increase in static pressure on one side of the structure and decrease on the other, such that an across-wind forces acts on the structure. Alternating vortices produces alternating forces. The vortices have a primary frequency of N_s, according to the Strouhal relation which is given in Eq. (1) below.

$$S = N_s D/U \tag{1}$$

where S is the Strouhal number, D is the diameter of the mast and U is the wind velocity. Also, Strouhal number is dimensionless and depends on the cross section of the particular structure and Reynolds number of the air flow [6]. Vortex shedding tends to be organized at sub-critical and trans-critical Reynolds numbers. In the critical range, vortex shedding tends to be irregular unless the structural motion is sufficiently large to organize the fluctuating flow around the body. This phenomenon referred to as "locking in" which becomes important for the lightly damped members [2].

The accurate prediction of maximum displacement and induced load on the structures due to vortex shedding is very difficult due to the many variables involved. The important variables are mean velocity profile, turbulence characteristics of approach flow, Reynolds number, Scruton number, mode shape, natural frequency, damping and mass distribution. Based on the Ruscheweyh modification, vortex shedding-induced forces can be applied over a height range less than the total height of the structure [7]. This particular length is known as "effective correlation length." The assumed vortex shedding-induced forces on the high-mast lighting tower system (F_w) can be calculated using Eq. (2), which is given in EN 1991-1-4:2005.

$$F_w(S) = m(s).(2\pi n_{i,y})2\Phi_{i,y}(s)y_{F,\max} \tag{2}$$

where $m(s)$ is the vibrating mass of the structure per unit length (kg/m), $\Phi_{i,y}$ is the mode shape of the structures normalized to 1, $y_{\max}$ is the maximum displacement over time of the point with $\varphi_{i,y}$ (s) equal to 1 and $n_{i,y}$ is the natural frequency of the system. In order to further study the influence of the thicknesses of the mast arm wall and the base plate on fatigue behavior, study was continued with FE models [8]. The geometric details used in the study are given in Table 1.

Table 1 Geometry of the high-mast lighting tower

Constant parameters	
Free-standing length of pole	25.0 m
Base plate size	850 mm diameter
Size of the man access hole	250 * 750 mm opening
Cross section of the mast arm wall	Tapered tubular section (diameter varies from 600 to 250 mm from bottom to top)
Total weight of the lights and accessories	500 kg
Slope of the mast arm wall	14 mm/m
Base connection and mesh refinement are kept as a constant	

Table 2 Natural frequency with mast arm wall thicknesses

Thickness of the mast arm wall/(arm)	Natural frequency/(Hz)	
	First mode ($n_{1,x}$)	Second mode ($n_{2,x}$)
8.0	0.700	3.663
10.0	0.823	3.866
12.0	0.944	4.146
16.0	0.973	4.268
20.0	0.991	4.354

Here except the thicknesses, all the other parameters were kept as constants. The FE model was developed using shell elements in SAP2000. Basic wind velocity of 22 m/s from zone 3 of the wind zonation map of Sri Lanka used [9]. From the modal analysis, the natural frequency was obtained, and first, two natural frequencies at a particular direction and the critical locations are presented in Table 2 and Fig. 7, respectively.

Sinusoidal or harmonic excitation model is generally used for the calculation of vortex shedding-induced forces on the high-mast towers perpendicular to the wind direction. In this study, vortex shedding-induced forces on the high-mast tower were estimated based on EN1991-1-4:2005. As shown in Fig. 8, critical wind velocity ratio is increased with the increasing of the mast arm wall thicknesses, because the critical wind velocity of the mast arm wall is proportional to the natural frequency of the system.

Addition to the critical wind velocity ratio, the lateral force coefficient (C_{lat}), effective correlation length (L_j), mode shape factor (K), effective correlation length factor (K_{w}) and the maximum displacement ($Y_{\text{F,max}}$) were estimated based on the procedures described in the EN1991-1-4:2005 and given in Eq. (3);

$$Y_{\text{F, max}}/b = (1/S_{\text{t}^2}).(1/Sc).K.K_{\text{w}}.c_{\text{lat}} \tag{3}$$

It is observed that the maximum displacement of the high-mast steel arm is decreased with the increasing of the mast arm wall thickness as shown in Fig. 9.

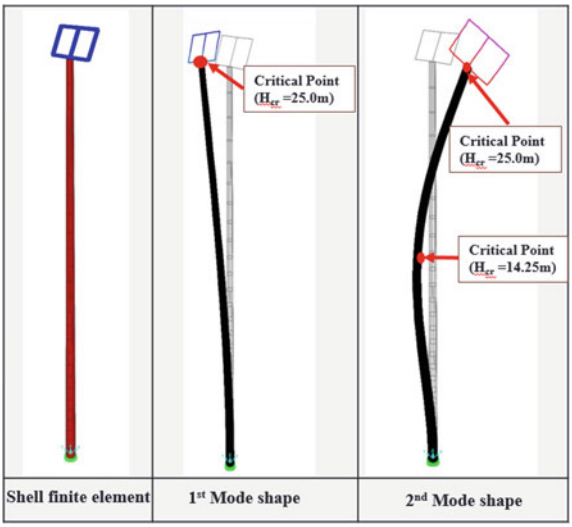

Fig. 7 First and second mode shape with critical location

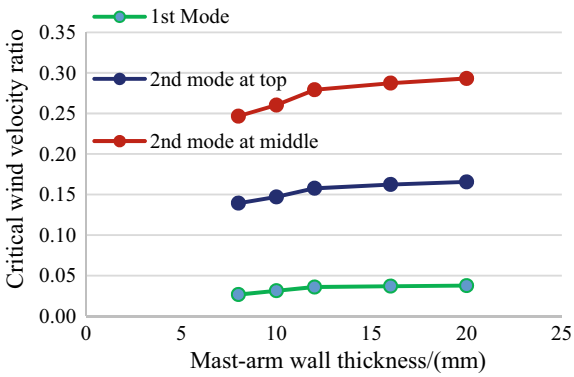

Fig. 8 Variation of critical wind velocity ratio with mast arm wall thicknesses

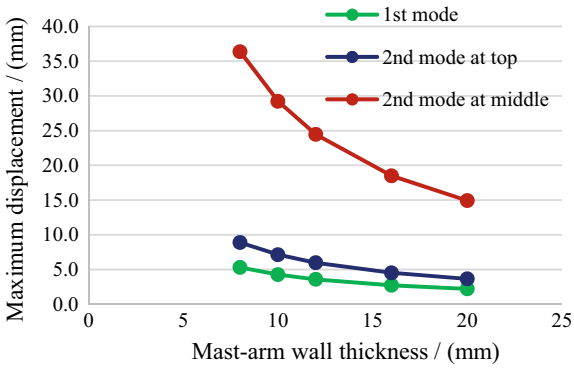

Fig. 9 Variation of maximum displacement with wall thicknesses of the mast arm wall

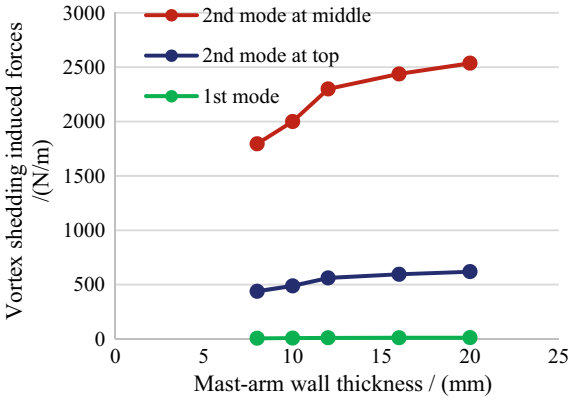

Fig. 10 Variation of vortex shedding-induced forces with mast arm wall thicknesses

The equivalent mass per unit length is increased with the increasing of the mast arm wall thickness. So, the maximum displacement is decreased due to the increasing of Scruton number of the high-mast tower system (Fig. 10).

Also, vortex shedding-induced forces on the high-mast steel arm are increased with the increasing of the mast arm wall thickness. Because, the natural frequency and the vibrating mass are increased with the increasing of the mast arm wall thickness, but maximum displacement is decreased with the increasing of the mast arm wall thickness, so resultantly, vortex shedding-induced forces are increased with the increasing of the mast arm wall thickness.

Vortex shedding-induced forces at the first mode are relatively low compared to the second mode due to less frequency and frontal width or diameter of the mast arm. However, it contributes in the estimation of the cumulative total fatigue damage (D) of the high-mast tower.

4 Fatigue Assessment

FEA analysis is performed for the selected geometry of the high-mast lighting tower system with various thicknesses of the mast arm wall and the base plate to obtain the hot spot stress and SCF considering the estimated vortex shedding wind action. High-mast lighting towers can oscillate at various frequencies and additionally vortex shedding excitation can occur at different heights of the mast arm for a particular frequency mode. In order to satisfy the fatigue design criteria, total cumulative damage (D) should be less than 1. Assessment of fatigue behavior is carried out using Palmgren–Miner theory of cumulative damage method. Total damage can be estimated using Eq. (4), [10].

$$D = \Sigma\{n_i(\Delta\sigma)/N_i(\Delta\sigma)\} \tag{4}$$

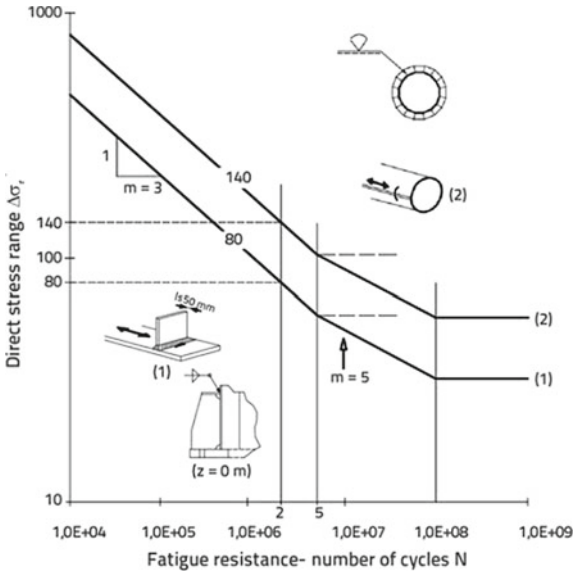

Fig. 11 S–N curves for the detail category of 140 and 80

where $n_i(\Delta\sigma)$ is the number of cycles of stress load for a specified stress range for which N_i $(\Delta\sigma)$ is the cycles of load which is expected before the structure suffers damage [11]. Number of cycles for the particular stress is obtained using S–N curves with consideration of suitable detail category for each structural element. Generally, detail category 140 is used for the mast arm wall and detail category 80 is used for the connection as shown in Fig. 11 [12]. Number of load cycles caused by vortex excitation can be calculated using mean and critical wind velocity profile and natural frequency of cross-wind mode as given in EN1991-1-4:2005 (E10).

5 Conclusion

In order to study the fatigue performance of the high-mast lighting tower with different thicknesses of the base plate and mast arm wall, it is required to compute the along- and cross-wind-induced forces along the free-standing length of the structures. The following conclusions that can be drawn from this investigation are as follows;

- Natural frequency of the high-mast lighting tower is increased with increasing of mast arm wall thicknesses, because the period of the structural system is depending on the mass of the mast arm structures.
- Critical height for the first and second mode was identified at 25 m and 14.25 m height, respectively, with assumption of critical location occurs at antinode points.

- The critical wind velocity ratio is increased with increasing of mast arm wall thicknesses, because critical wind velocity of the mast arm wall is proportional to the natural frequency of the system.
- Maximum displacement of the high-mast steel arm is decreased with increasing of mast arm wall thicknesses, because equivalent mass per unit length is increased with increasing of mast arm wall thicknesses. So, maximum displacement is decreased due to increasing of Scruton number of the high-mast lighting tower system.
- Natural frequency and vibrating mass are increased with increasing of mast arm wall thicknesses, but maximum displacement is decreased with increasing of mast arm wall thicknesses, so resultantly, vortex shedding-induced forces are increased with increasing of mast arm wall thicknesses.
- Vortex shedding-induced forces at first mode is relatively low compare to second mode of the high-mast lighting tower system.
- Thicknesses of the base plate and mast arm wall are highly influencing on the fatigue performance of the high-mast lighting tower structures under unstiffened base connection.

In order to obtain the high accuracy on the vortex shedding action, wind tunnel test or CFD simulation should be performed. Further study on the damage behavior of the high-mast steel arm should be performed.

References

1. Mendis P, Fernando S, Holmes J, Gunawardena T, AbuZidan Y, Dias P (2018) Wind induced analysis of lotus tower mast. In: Nineteenth Australasian wind engineering society workshop. Fatigue
2. Giosan I, Eng P (2005) Vortex shedding induced loads on free standing structures
3. Foley CM, Wan B, Weglarz M, Hellenthal M, Komp J, Smith A, Schmidt JP (2008) Fatigue risks in the connections of sign support structures—phase 1. Marquette University, Department of Civil & Environmental Engineering
4. EN 1991-1-4:2005. Action on structures (Part 1–4: General Actions–Wind actions)
5. Warpinski MK (2006) The effect of base connection geometry on the fatigue performance of welded socket connections in multi-sided high mast lighting towers. Theses and Dissertations, paper 940
6. Halse KH (1997) On vortex shedding and prediction of vortex—induced vibrations of circular cylinders. Norweign University of Science and Technology, Department of Marine structures
7. Holmes JD (1998) Response of cylindrical structures to vortex shedding in the natural wind. In: 13th Australian fluid mechanics conference
8. Aygul M (2012) Fatigue analysis for the welded structures using the finite element method. Chalmers University of Technology, Department of Civil and Environmental Engineering
9. Lewangamage CS, Jayasinghe MTR (2012) Recent development of wind code in Sri Lanka
10. EN 1993-1-9:2009. Design of steel structures (Part 1–9: Fatigue)
11. Maljaars J, Lukic M, Soetens F (2013) Comparisons between the Eurocode for fatigue of steel structures, EN 1993-1-9, and the Eurocode for fatigue of Aluminium structures EN1993-1-3. In: 5th Fatigue design conference

12. Rakocevic M, Popovic S (2018) Calculation procedure for determining wind action from vortex-induced vibration with verification of fatigue strength of steel structures. GRADEVINAR 70:793–809
13. Koenigs MT, TA Botros, Freytag D, Frank KH (2003) Fatigue strength of signal mast arm connections. Research report (9/99–8/01)
14. Stam A, Richman N, Pool C, Rios C, Anderson T, Frank K (2011) Fatigue life steel base plate to Pole connection for traffic structures. Technical report—9-1526
15. Puckett J, Johnson R, Barker M (2011) Study of the effects of wind power and vortex induced vibrations to establish the fatigue design criteria for high-mast poles. University of Wyoming, Civil and Architectural Engineering
16. Datta TK, Jain AK (1986) An analytical study of the across-wind response of cylinders due to vortex shedding. Civil Engineering department, Indian Institute of Technology, New Delhi
17. Basu RI, Vickery BJ (1982) Across wind vibrations of structures of circular cross section. Faculty of Engineering Science, University of western Ontario, London, Part II. Development of a mathematical model for full-scale application

Modeling of Reinforced Concrete Beam–Column Joint Retrofitting

Karunakaran Gajanan, Baskaran Pirashangan, and Hiran D. Yapa

Abstract Failure of reinforced concrete (RC) beam–column joints (BCJs) is sudden especially when they are subjected to high shear demands caused by seismic actions. One novel advantageous method is shear retrofitting of BCJs with carbon fiber-reinforced polymer (CFRP) using an externally bonding technique. CFRP is a lightweight, high strength, flexible, and corrosion-resistant material, and the proposed system is highly efficient and exhibits high shear capacities compared to other retrofitting methods such as concrete and steel jacketing. A recent experimental study on retrofitting of reinforced concrete BCJs using composites shows that the CFRP retrofitting configurations significantly improved the behavior of deficient joints. Strengthened specimens exhibited significant increases in strength and energy dissipation capacities as compared to the unstrengthened control specimen. The lateral load capacities of strengthened specimens increased by 50–100% when compared to the control specimen. Cracks propagated diagonally from one corner to the other corner of the joint. Therefore, CFRP fibers were oriented diagonally closer to principal stresses to prevent shear cracks in the joint core. The anchorages were applied to the beam, preventing the debonding of the CFRP sheets which gave a superior retrofitting effect. However, in the context of RC, shear behavior is still a riddle, exploring shear strengthening optimization as a challenge. The current study verifies the nonlinear numerical simulation potential of beam–column joint retrofitting using the experimental database. CFRP thickness is identified as a governing strengthening parameter via the FE analyses. The failure load increases with the increase of CFRP thickness, but the change in the ultimate load is not proportional to the increment of the thickness of the CFRP material.

Keywords Carbon fiber-reinforced polymer · Finite element · Reinforced concrete · Beam–column joints

K. Gajanan (✉) · B. Pirashangan · H. D. Yapa
Faculty of Engineering, University of Peradeniya, Peradeniya, Kandy, Sri Lanka

R. Dissanayake et al. (eds.), *12th International Conference on Structural Engineering and Construction Management*, Lecture Notes in Civil Engineering 266,
https://doi.org/10.1007/978-981-19-2886-4_7

1 Introduction

Beam–column joint regions in reinforced concrete structural systems are one of the most critical parts, especially under seismic actions where shear demands are very high due to lateral inertia forces, resulting in brittle failures. Hence, the behavior of the joint region directly affects the capacity of the overall structure. Brittle shear failures occur usually with the effects of inadequate design detailing, lack of transverse reinforcement, and low compressive strength concrete.

Many of the heavily damaged or collapsed structures were designed for gravity loads only, with no regard to any significant lateral forces. Furthermore, concrete strength and reinforcement ratios were often below the minimum values specified by the respective design codes. Thus, the lateral load resistance of these structures was naturally very low even to resist small earthquakes.

Several strengthening techniques have been developed in the past, including RC and steel jacketing. Fiber-reinforced polymers are new materials used in the strengthening using externally bonded reinforcement in the critical regions of RC elements.

FRP materials, which are available today in the form of strips or in-place resin-impregnated sheets, are being used to strengthen a variety of RC elements, including beams, slabs, columns, and shear walls, to enhance the flexural, shear, and axial capacities of the elements. FRP materials offer advantages over other conventional methods such as steel and concrete for retrofitting.

The advantages are ease of installation, immunity to corrosion, high stiffness-to-weight ratio, and the ability to control the material's behavior by selecting the proper orientation of the fibers. Even though the cost of CFRP is higher than conventional construction materials, all of these features make the CFRP sheet suitable for infrastructure applications and increase the shear and flexural capacities and ductility of structures including the BCJ of the unstrengthened specimens.

CFRP is a term used to describe a fiber-reinforced composite material that uses carbon fiber as the primary structural component. The binding polymer is usually epoxy. A method of wrapping and bonding FRP sheets along the sides of the beam, column, and surrounding its joints externally with epoxy as a binder to transfer stress between fibers provides high bond strength. The possible strengthening application methods are diagonal wrapping, L-shaped wrapping, longitudinal wrapping, and complete wrapping.

The numerical model analyzes different types of BCJ deficiencies and retrofitting methods. This is more cost and time effective than doing an experimental study. Design guidelines for retrofitting with CFRP wrap in BCJ are compiled using the developed simulation model.

1.1 Objectives and Scope

In this research, the main objective is to develop the simulation tool for validating the experimental results via the nonlinear finite element modeling approach and do a parametric analysis for retrofitting system.

The scope of the project is that to verify the potential of the FE model, the experimental database and parametric analysis will be done for the CFRP thickness.

2 Literature Review

Beam–column joint is one of the most critical parts in reinforced concrete structures under seismic actions. BCJ is subjected to high lateral inertia forces during seismic actions. It is still an unanswered question that how BCJ behaves under shear.

2.1 Experimental Study

Kaya et al. [3] investigated some BCJ behaviors for shear failure. A survey was conducted on existing buildings that were designed during the 1950s to 1990s to find the deficiencies of Turkish design during seismic actions. Plain reinforcement, low-quality concrete, insufficient transverse reinforcement, short beam anchorages, and lack of lap splices in the column were the deficiencies which were contributed to the shear failure of BCJ. TR-1 control specimen as shown in Fig. 1 was designed and detailed according to the Turkish Earthquake Code 1975, and it was experimentally tested through the test setup as shown in Fig. 2 by applying reversed cyclic lateral load (Fig. 3) at the top of the column with the constant axial load applied vertically from the top of the column.

The displacement-controlled loading was applied from the top of the column laterally with a dynamic actuator mounted on a steel reaction wall. Three cycles of the same amplitude in every story drift were repeated before displacement amplitude increased. The specimen was tested in a setup where the beam was placed parallel to the strong floor and attached by a rigid steel link element at its free end, simulating roller support. The column was placed in a vertical position and supported by a universal pin at the bottom end.

The constant axial load was applied vertically from the top of the column by the hydraulic ram. The amount of the constant axial force applied was 40% of the axial load capacity of the column. A steel frame was constructed surrounding the test setup to prevent any possible out-of-plane deformations, where the rollers mounted on both sides of the frame touched the specimen and forced it to move in the direction of loading.

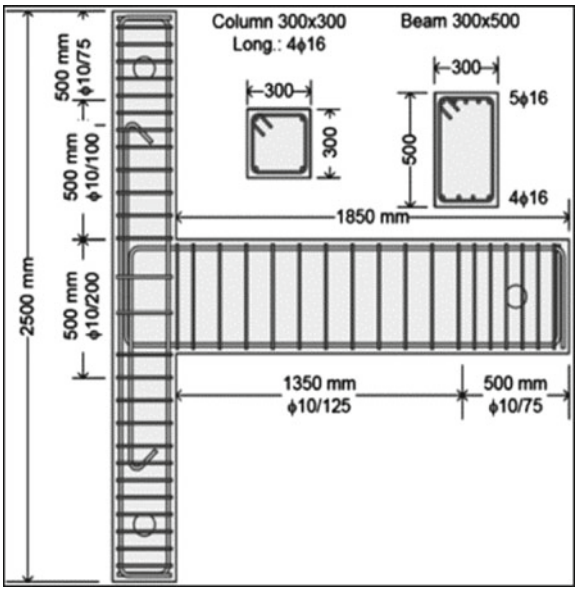

Fig. 1 TR-1 control specimen

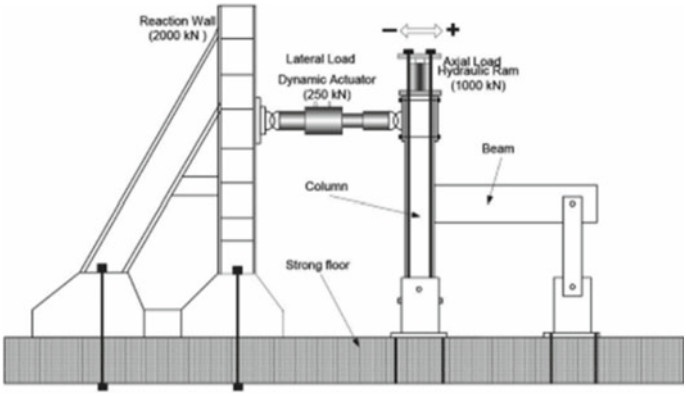

Fig. 2 Test setup for the experimental study

The cylinder strength of the TR-1 control specimen was 15.3 MPa. The yield strength of the steel bars was 280 MPa. The beam and column moment capacities were 98.6 and 122.4 kNm, respectively. Deficiencies were introduced in TR-1 step by step to find the most critical and deficient BCJ specimen. Eventually, TR-5 shown in Fig. 4 was found as the most deficient BCJ with insufficient transverse reinforcement, short beam anchorages, and lack of lap splices in the column.

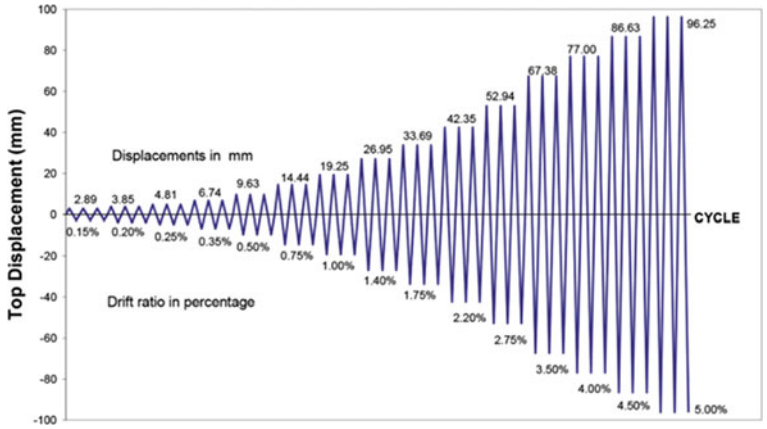

Fig. 3 Lateral cyclic loading pattern in the experimental setup

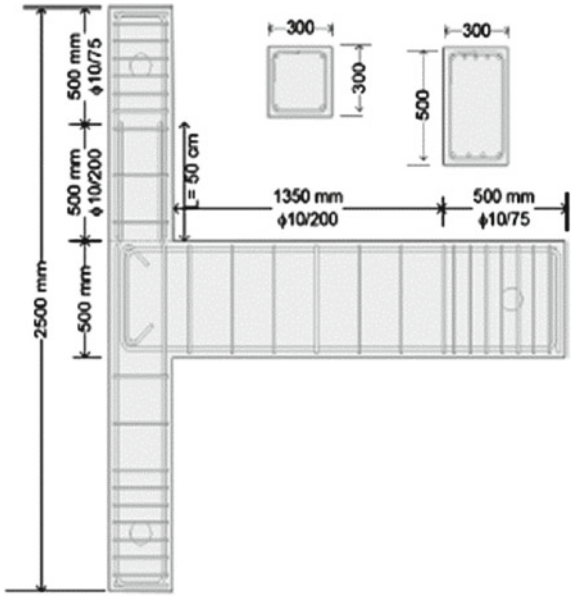

Fig. 4 TR-5 specimen

A total of 11 strain gauges were mounted on the reinforcing steel bars to gather the strain values during the experiment. Displacement at the tip of the column, the shear deformation in the BCJ region, and the curvature readings on the beam and columns near the maximum moment regions were monitored and measured by the linear variable displacement transducers (LVDTs). All data taken from strain gauges, LVDTs, and load cells were recorded by an electronic data acquisition system.

2.2 FRP Retrofitting

Fiber-reinforced polymers are new materials used in the strengthening using externally bonded reinforcement in the critical regions of RC elements. The FRP materials, which are available today in the form of strips or place resin-impregnated sheets, are being used to strengthen a variety of RC elements like beams, slabs, columns, and shear walls, to enhance the flexural, shear, and axial capacities [3]. FRP materials offer advantages over other conventional materials such as steel and concrete jacketing for retrofitting. They are ease of installation, immunity to corrosion, high stiffness-to-weight ratio, and the ability to control the material's behavior by selecting the proper orientation of the fibers. CFRP is a highly engineered material suitable for infrastructure applications and increasing the shear and flexural capacities and ductility of BCJ subassemblies. In Parvin and Wu [5] study on the ply angle effect, it was found that the wrap ply angle stacking sequence of −45°/ +45°/−45°/+45° appeared to offer superior resistance for brittle shear failure when subjected to constant axial and cyclic lateral load. In the second part of the experimental study by Kaya et al. [3], three new strengthened specimens were used to determine the proper CFRP wrapping configuration for strengthening. The first one was strengthened with CFRP while considering the crack patterns, damage, and failure mechanisms that occurred in the TR-5 control specimen. For the next two identical specimens, the strengthening technique was modified step by step by observing the test results, damage, and failure patterns of the previous tests. Finally, an effective strengthening method was obtained for deficient BCJs.

The CFRP wrap was placed perpendicular to the crack propagation direction to give resistance against the tension as shown in Fig. 5. The same application was done in the opposite direction. Hence, X-shaped CFRP orientation was created.

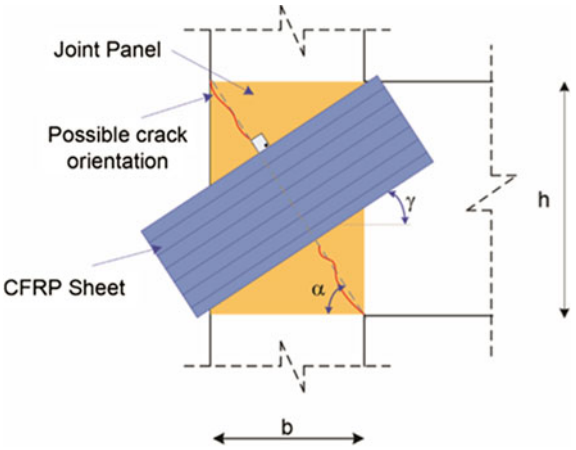

Fig. 5 CFRP wrap

3 Numerical Modeling

The optimum strengthening configuration for the CFRP shear retrofitting system was explored along with the following methodology. First, the parameters that should be included in the FE model were identified through the experimental database [3] and literature review. The properties of steel bars used in the experimental BCJ specimens are listed in Table 1. The properties of CFRP are listed in Table 2.

Then the unstrengthened specimen TR-1 was modeled in 2D using MIDAS FEA. After modeling of TR-1 control specimen in MIDAS FEA, the obtained results were verified with the experimental database. At first, the failure load and the failure mode did not match with the experimental results.

Filets were introduced in the corner regions to avoid local stress concentrations. After trials, the expected failure load and the failure mode were achieved. Similarly, TR-2 and TR-3 were modeled incorporating the deficiencies of insufficient transverse reinforcement and strong beam–weak column configurations, respectively. The cross section of the beam and column in the BCJ, cylinder strength, column reinforcement arrangement, and beam reinforcement arrangement are given in Table 3 to facilitate comparisons in configuration. TR-4 with short beam anchorages and TR-5 the most

Table 1 Properties of steel bars

Bar diameter (mm)	Yield strength f_y (MPa)
16	280
10	280

Table 2 Properties of CFRP

Nominal thickness	0.176 mm/ply
Ultimate tensile strength (0 degrees)	3800 MPa
Tensile modulus (0 degrees)	240 GPa
Ultimate rupture strain (0 degrees)	1.55%
Weight density	330 g/m^2

Table 3 Properties of test specimens

Specimen ID	Beam (mm)	Column (mm)	F'c (MPa)	Column reinforcements		Beam reinforcements	
				Long	Transverse	Long	Transverse
TR-1	300 * 500	300 * 300	15.3	4Φ16	Φ10/100	9Φ16	Φ10/125
TR-2	300 * 500	300 * 300	12.8	4Φ16	Φ10/200	9Φ16	Φ10/200
TR-3	250 * 500	250 * 250	13.5	4Φ16	Φ8/200	7Φ16	Φ8/200
TR-4	300 * 500	300 * 300	14.8	4Φ16	Φ10/200	9Φ16	Φ10/200

critical and deficient specimen with lap splices in the column need incorporating bond properties in the FE analysis which is currently being simulated.

Next, the suitable element for CFRP wrap was explored. After passing these stages, strengthened specimens were modeled in 2D by using the plate element for CFRP. The diagonal wrap was applied in the BCJ region of the TR-2 specimen in both directions. After obtaining the results from FE analysis, they were compared with the unstrengthened TR-2 specimen. Failure loads and displacements were obtained from load–displacement curves. Beam longitudinal reinforcement yielding loads were identified by analyzing the reinforcement stresses. Concrete stresses were studied to ensure that the BCJ failed in shear before the beam or column was able to reach their ultimate flexural strength for the unstrengthened specimens.

4 Numerical Simulation

A commercially available software package MIDAS FEA was used to perform nonlinear modeling of the CFRP retrofitting system (Analysis and Algorithm Manual, MIDAS FEA). The software facilitates the use of the total strain crack model classified under the smeared crack model to simulate concrete shear behavior. Two crack models are available: the fixed crack model and the rotating crack model. As will be discussed later, the validation process showed that the latter considerably underestimates the failure loads.

The rotating crack model was used throughout the modeling procedure. Thorenfeldt stress–strain relationship and linear–exponential softening curve were selected as concrete compression and tension models, respectively. The concrete fracture energy (G_f) was calculated using Eq. (1). The crack bandwidth (h) was taken as the square root of the mesh dimensions as recommended in the (Analysis and Algorithm Manual, MIDAS FEA).

$$G_f = 43.2 + 1.13 \times f_{cu} \tag{1}$$

The element size was selected, that it should be between 2–3 times the maximum aggregate size (ag), and assuming ag = 10 mm. Concrete was modeled using four-node, 25 mm square isotropic plane-stress elements as shown in Fig. 6. A sensitivity check for the FE parameters was done. For example, the mesh size was changed and checked with the results obtained.

The steel bearing plates (load and support bearings of 100 × 105 mm) were modeled to be triangular shape using triangular plane-stress elements to avoid stress singularities. All the reinforcement bars were modeled as embedded 1D elements defined by two-node line sections, and the von Mises yield criterion was used with a yield stress of 280 MPa. The perfect bond assumption can be used successfully to predict the behavior of CFRP strengthened RC structures when bond failure between the two components is not the governing failure mode. The CFRP wrap was modeled as 2D isotropic plate elements.

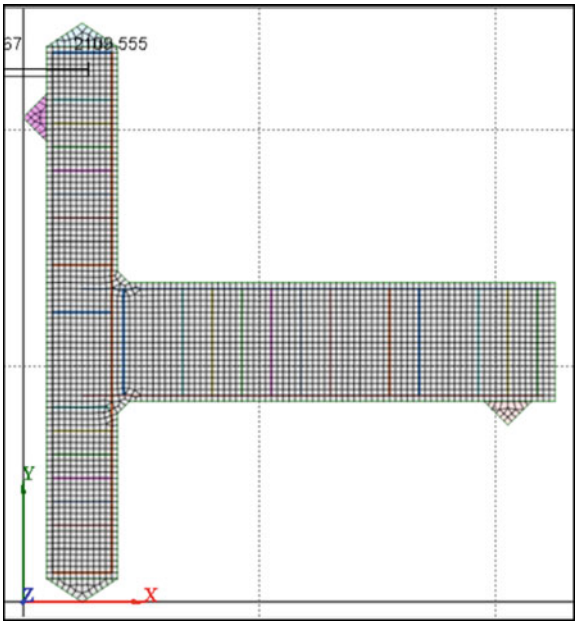

Fig. 6 2D finite element mesh

The two stages of analysis were adopted: the first stage was used to apply the constant axial load vertically from the top of the column, and the second stage was used to apply the load with 1 kN load increments. Two approaches of displacement-based and force-based loading were applied. The Newton–Rapshon method was used for iterations with an energy norm of 0.001 and a maximum number of iterations of 200 as the convergence criterion specified in Kurukulasuriya et al. [4].

5 Numerical Modeling

Obtaining reliable results through any FE modeling is a challenge because the entire modeling is influenced by the implemented material models, meshing, convergence criterion, etc. Hence to validate the FE model, some specimens were selected from the experimental study of Kaya et al. [3] which comprised of unstrengthened and strengthened beam–column joints.

The selected specimens are; control specimen TR-1, specimen TR-2 with Insufficient Transverse Reinforcements (ITR), and TR-3 with ITR and strong beam–weak column configuration. All were designed and detailed according to the Turkish Earthquake Code 1975. The specimens were applied with a force-based load of 75 kN and a displacement-based load of 30 mm in both directions.

Using numerous trials on material models, meshing, iteration method, type of loading, convergence criterion, etc., and considering appropriate recommendations found in the experimental study by Kaya et al. [3], a fairly reasonable validation was achieved. The smeared crack approach implemented in modeling provided the crack distribution as an output under the 2D element stresses. Figures 7, 8, and 9 show that those crack distributions were in a reasonable agreement with the experimental observations for BCJs.

After that, all the above three specimens were subjected to reversed cyclic lateral loading by defining the construction stages for each displacement in both directions. The axial load was defined in the first construction stage with one increment and maintained constant throughout the FE analysis. Three cycles of the same amplitude were repeated before displacement amplitude increased. Depending on the behavior of the specimen, approximately 30 reversed cycles were applied throughout the test. The reversed cyclic lateral load was tried with two different compression models. They are the proposed compression model for loading–unloading (Carreira et al., cited in Aslani et al. [2]) shown in Fig. 10 and the Thorenfeldt curve which is inbuilt in MIDAS FEA.

Figures 11, 12, and 13 show the hysteresis loops of the three specimens TR-1, TR-2, and TR-3 subjected to the reversed cyclic lateral loading with two compression models. The ultimate failure load was approximately similar to the experimental values, but even with the application of cyclic loading, the displacement at the failure

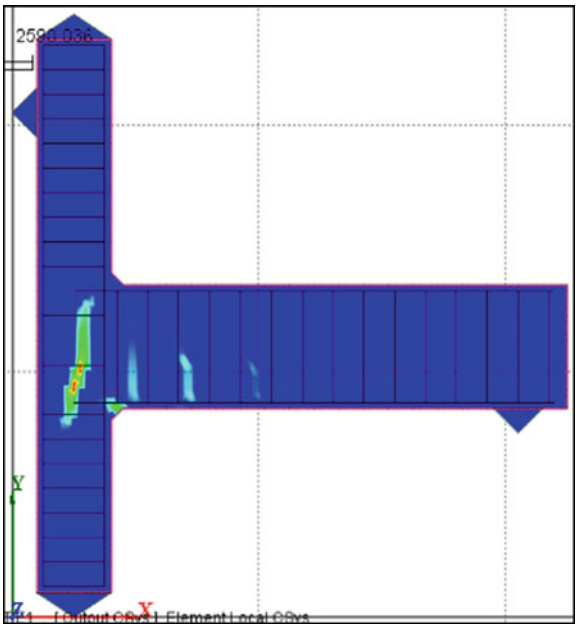

Fig. 7 Crack formation in TR-1

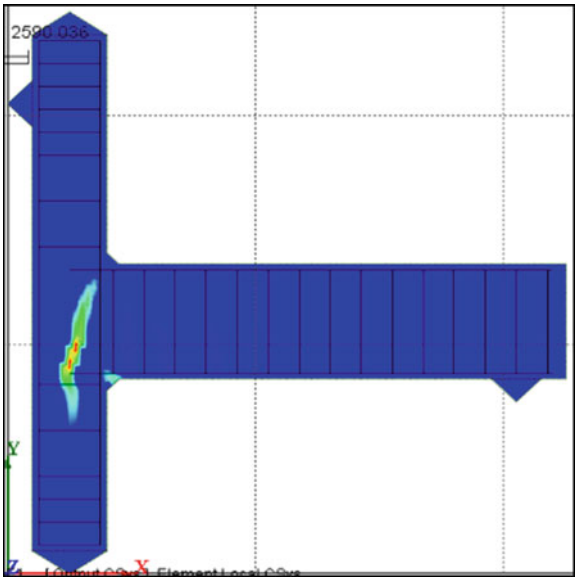

Fig. 8 Crack formation in TR-2

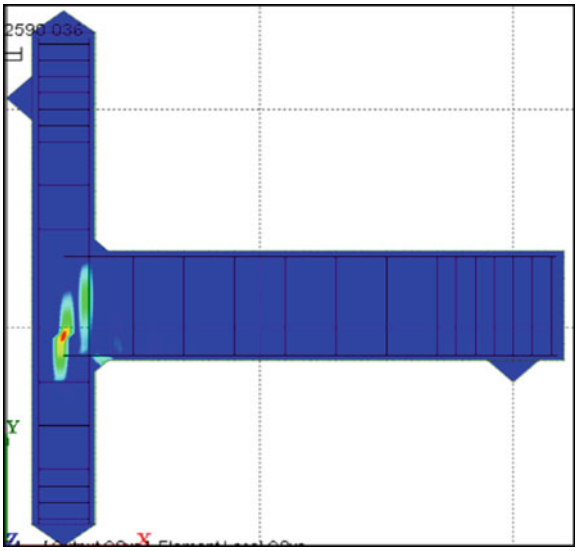

Fig. 9 Crack formation in TR-3

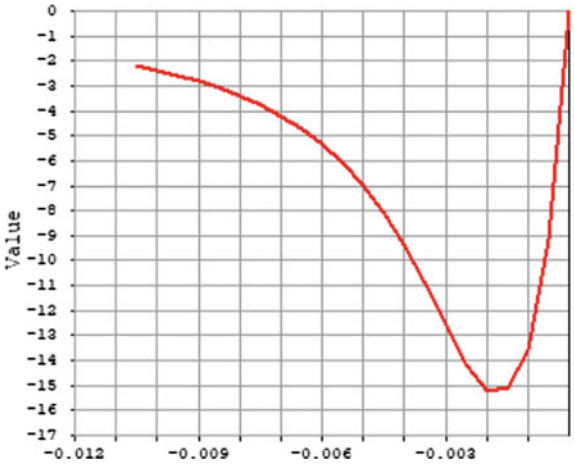

Fig. 10 Compression model for loading–unloading (Carreira et al., cited in Aslani et al. [2])

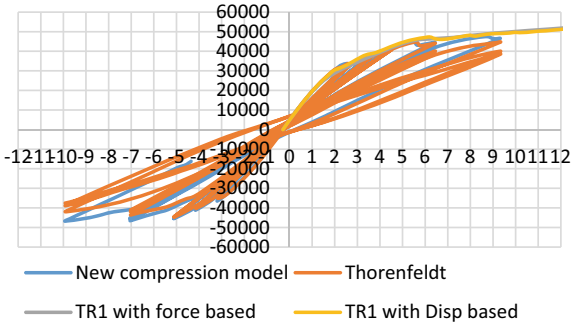

Fig. 11 Hysteresis loops for TR-1 under cyclic loading

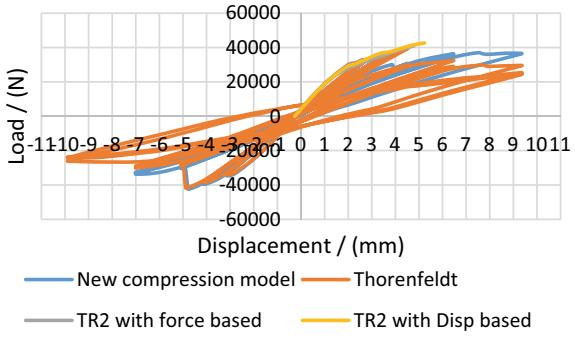

Fig. 12 Hysteresis loops for TR-2 under cyclic loading

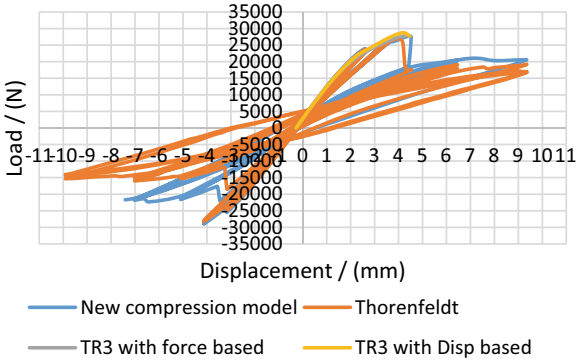

Fig. 13 Hysteresis loops for TR-3 under cyclic loading

load had a significant variation with the experimental data. The crack closure mechanism is governed by the crack closure stress which is the stress at which the crack is supposed to be completely closed. Once the crack is closed completely, the stiffness of the concrete is not affected by accumulated damage in tension. The crack closure mechanism had not been considered in the FE analysis while applying reversed cyclic lateral loading to the unstrengthened specimens. Next, the most deficient specimen TR-2 was selected for the strengthening applications with CFRP. The BCJ of the TR-2 specimen was strengthened with the diagonal wrap of thickness 0.176 mm. This orientation scheme was associated with the cracks observed in the TR-2 specimen that was caused due to the lack of transverse reinforcement in the BCJ region.

First, the CFRP was modeled as a single element with four nodes. There were not enough nodes to transfer the stresses from BCJ to the CFRP plate. Hence, the element size was reduced to 25 mm, and the CFRP plate was modeled as multi-element with many nodes. But still, there were connectivity issues since the nodes of BCJ were not connected to CFRP nodes. As solution, two surfaces were created with the same dimension of CFRP plate, one above the other. BCJ surface and one the CFRP surface were fused and the fused shape meshed with the concrete property. Then the other CFRP surface meshed exactly above that with CFRP property. This procedure eliminated the connectivity issue between BCJ and CFRP.

As a result, there was a significant increment in shear enhancement with the introduction of the CFRP plate into the FEM of TR-2. Figure 14 shows the finite element mesh of the CFRP plate element on the BCJ region of the TR-2 specimen in both directions. The formation of the crack on the BCJ region with CFRP plate in both directions under monotonic loading is illustrated in Fig. 15. Figure 16 shows the load–displacement curves for TR-2 with the application of CFRP diagonal wrap in both directions and without the application of CFRP under the reversed cyclic lateral loading.

After that, CFRP thickness was analyzed through the simulation tool developed for the most vulnerable BCJ TR-2 specimen in the FE analysis. The effects of changing the thickness of the CFRP element were analyzed from 0.704 to 3 mm. Figure 17

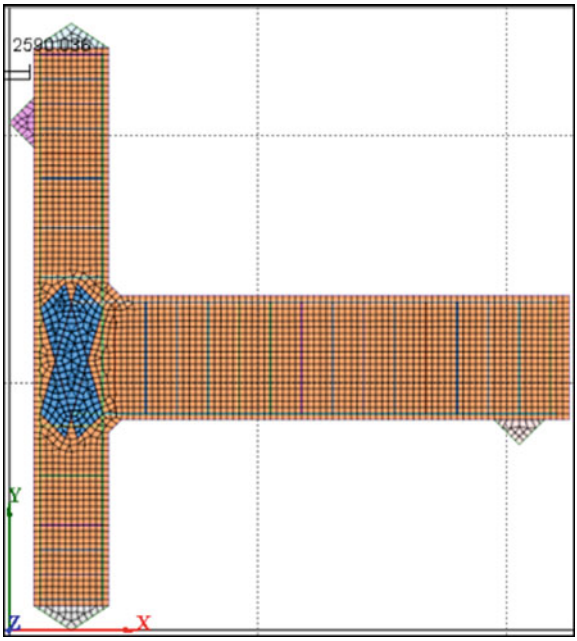

Fig. 14 FE mesh of the CFRP plate element on the BCJ

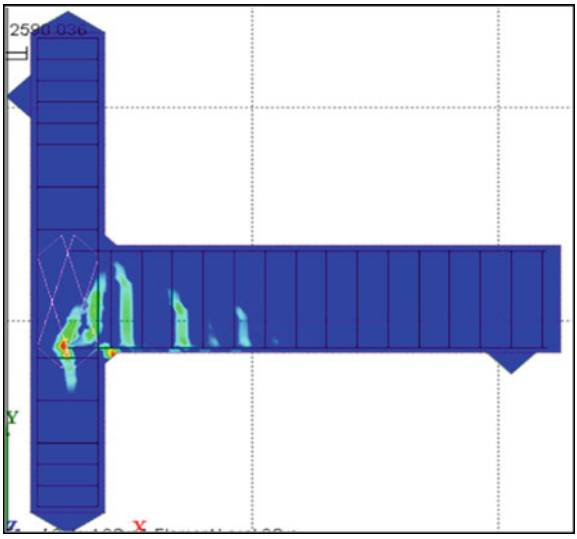

Fig. 15 Formation of crack on the BCJ

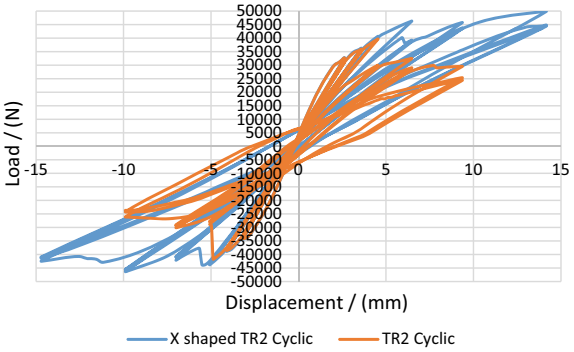

Fig. 16 Load–displacement curves for TR-2 with the application of CFRP in both directions under reversed cyclic lateral loading

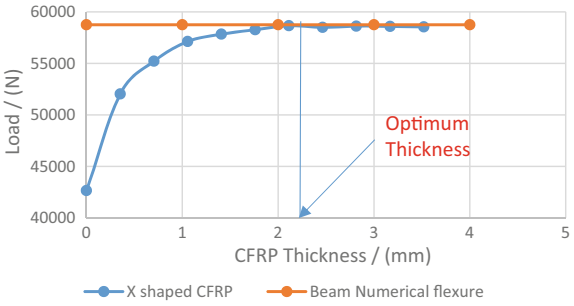

Fig. 17 Variation of failure load with different thicknesses of X CFRP

shows the variation of the failure load with different thicknesses of X CFRP applied on the BCJ.

6 Results

Table 4 summarizes the results for TR-1, TR-2, and TR-3 obtained from FEM in monotonic loading and the results stated in the experimental database. The compressive strength of the concrete used in each specimen and maximum loads obtained in both push and pull monotonic loading are listed below. All results are matched with maximum loading obtained experimentally in both push and pull directions.

Table 5 summarizes the results for TR-1, TR-2, and TR-3 obtained from FEM which is modeled incorporating the inbuilt Thorenfeldt compression curve and new compression model curve (Carreira et al., cited in Aslani et al. [2]) to improve the ductility of the specimen.

Table 4 Experimental verification

Specimen ID	F′c (MPa)	F experimental		F numerical (force based)		F numerical (displacement based)	
		Push (kN)	Pull (kN)	Push (kN)	Pull (kN)	Push (kN)	Pull (kN)
TR-1	15.3	49.2	53.8	52	51	51.4	49.8
TR-2	12.8	39.6	41.5	41	43	42.6	43.9
TR-3	13.5	24.5	27.2	28	33	27.7	33

Table 5 Failure load of specimens under reversed cyclic lateral loading

Specimen ID	F′c (MPa)	F experimental		F numerical (Thorenfeldt)		F numerical (new comp model)	
		Push (kN)	Pull (kN)	Push (kN)	Pull (kN)	Push (kN)	Pull (kN)
TR-1	15.3	49.2	53.8	44.8	44.7	47.5	46.8
TR-2	12.8	39.6	41.5	39.7	41.6	40.3	42.2
TR-3	13.5	24.5	27.2	26.9	28.2	27.7	29

Table 6 Failure load of the strengthened specimen under reversed cyclic lateral loading

Reversed cyclic lateral loading							
Unstrengthened TR-2				Strengthened TR-2			
F experimental		F numerical (Thorenfeldt)		CFRP in one direction (push)		CFRP in both directions	
Push (kN)	Pull (kN)	Push (kN)	Pull (kN)	Push (kN)	Pull (kN)	Push (kN)	Pull (kN)
39.6	41.5	39.7	41.6	42.7	44.3	49.9	46.4

Table 6 summarizes the results of strengthened TR-2 with CFRP plate element in one direction and both directions for displacement-based cyclic loading.

7 Discussion

The FE software has been able to capture the sensitivity of various beam–column joint configurations, both strengthened and unstrengthened specimens. It has also captured the effect of the difference in thickness of CFRP plate elements. All the strengthened beam–column joints have shown significant joint shear enhancement. The validation revealed that the FEM estimates the maximum loadings acceptably but overestimates the stiffness of the beam–column joint in monotonic loading and consequently the displacement obtained is less than the experimental displacement values. Although cyclic loading was expected to deteriorate the stiffness of the beam–column joint, it did not improve the ductility significantly. Hence, material modeling has to be done

to incorporate the loading and unloading curve in the compression model and the pinching effect. The material model has to be programmed in FORTRAN in MIDAS FEA.

The orientation of the joint shear cracks observed in the control specimens depended on the width-to-height ratio of the joint panel cross section. Cracks were propagated diagonally from one corner to the other corner of the joint. From this observation, CFRP fibers were oriented diagonally to prevent the formation of shear cracks in the joint core in the strengthening process. TR-2 was selected for parametric analysis since it is the weakest beam–column Joint in the validated one which has the same size of the beam and column which was retrofitted in the experimental database.

8 Conclusion

The nonlinear FE modeling is promising in predicting the behavior of the beam–column joint for TR-1, TR-2, and TR-3 specimens. The FE model responded well enough for the lack of shear reinforcements and strong beam–weak column configuration as well. Predicted failure loads of the TR-1, TR-2, and TR-3 by the FE model are complying with the experimental failure loads. The projected cracks by the FE model in BCJ are similar to the crack patterns in the experimental database.

The shear strength of the joint is enhanced with the introduction of the CFRP element which is modeled as a plate element. Failure load increases in strengthened TR-2 with the increase of CFRP thickness. It increases with decreasing gradient. Applying CFRP in both directions (X-shaped CFRP) enhanced the shear strength of the BCJ more, instead of applying CFRP in one direction. The optimum thickness of CFRP was found as 2.1 mm, where the beam started to fail in flexure.

The study could be extended in validating TR-4 and TR-5 by introducing short beam anchorages and lap splices in column reinforcement bars. The bond element should be introduced between concrete and reinforcement elements for anchorages. The bond element should be introduced between reinforcement elements for lap splices in the column. The method to include this bond element into the FE model should be studied.

To improve the ductility of the FE model under reversed cyclic lateral loading, the material should be modeled in FORTRAN incorporating loading and unloading curve in both compression and tension models. Hence, the study on the techniques for modeling material in FORTRAN language should be done to achieve the failure displacement of the specimens.

In this study effect of unidirectional fiber, orientation is not taken into account. However, it may influence the optimum CFRP slope. Hence, the material properties of the CFRP element should be refined by considering the unidirectional fibers.

References

1. Analysis and Algorithm Manual, Midas FEA, Chapter 13, pp 301–307
2. Aslani F, Jowkarmeimandi R (2012) Stress-strain model for concrete under cyclic loading. Mag Concr Res 64(8):673–685
3. Kaya O, Yalçın C, Parvin A, Altay S (2019) Retrofitting of reinforced concrete beam-column joints by composites. Part I: Exp Study ACI Struc J 116(1):17–29
4. Kurukulasuriya M, Rathnayake H, Yapa HD (2017) Optimum shear strengthening of reinforced concrete beams using an un-bonded CFRP strap shear retrofitting system. Adv Compos Constr 107–113
5. Parvin A, Wu S (2008) Ply angle effect on fiber composite wrapped reinforced concrete beam-column connections under combined axial and cyclic loads. Compos Struct 82(4):532–538
6. Yalçın C, Kaya O, Biçer E, Parvin A (2019) Retrofitting of reinforced concrete beam-column joints by composites. Part II: Analy Study ACI Struct J 116(1):31–40

Lessons Learnt from Recent Explosions in Storage Facilities with Ammonium Nitrate

P. L. N. Fernando, C. Attard, K. Wijesooriya, D. Mohotti, and C. K. Lee

Abstract Recent events around the world pertaining to explosions due to mishandling and improper storage of hazardous materials such as ammonium nitrate have highlighted the vitality of understanding how to handle explosive material appropriately. One major drawback in order to better understand such explosions is either the contradicting reports that emerge regarding its technical details or in some cases the absence of reliable information. An accurate definition of the source and quantity of explosions is critical towards using such incidents to be better prepared for future events. Hence, firstly, this project aims to study three explosion events of ammonium nitrate storage facilities, namely Beirut-Lebanon in 2020, Tianjin-China in 2015 and Oppau-Germany in 1921, where the incidents are listed in the reducing order of the availability of technical information. Each case was analysed by calculating the upper and lower limit for the quantity of explosives by considering the available information. Moreover, heat maps were developed to illustrate the variation of pressure in the areas surrounding the storage facilities. The second aim of this study is to provide a preliminary analysis related to separation distances between storage facilities and populated areas, where the ammonium nitrate storage facility in Newcastle, Australia, is used a case study. To this end, a major knowledge gap is the absence of regulations regarding appropriate separation distances between stores of ammonium nitrate over 500 tonnes and populated areas. This aspect is studied using the aforementioned incidents, where the pressure estimation developed under the first aim was used to determine separation distances. It was identified that the existing separation distances between the Newcastle storage facility and its surrounding residencies are inadequate to prevent damage in the event of an explosion. Overall, the present study provides a reasonable preliminary approach to analyse possible threats due to the explosion of storage facilities.

P. L. N. Fernando
Department of Civil Engineering, University of Moratuwa, Moratuwa, Sri Lanka

C. Attard · K. Wijesooriya · D. Mohotti (✉) · C. K. Lee
School of Engineering and Information Technology, The University of New South Wales, Canberra ACT 2600, Australia
e-mail: d.mohotti@unsw.edu.au

R. Dissanayake et al. (eds.), *12th International Conference on Structural Engineering and Construction Management*, Lecture Notes in Civil Engineering 266,
https://doi.org/10.1007/978-981-19-2886-4_8

Keywords Blast overpressure · Separation distance · Explosive storage facilities · Heat map · Ammonium nitrate

1 Introduction and Background

The explosion incident in a storage facility containing 2750 tonnes of ammonium nitrate (AN), in Beirut, Lebanon, was a major talking point in 2020. This explosion caused serious damages to structures and recorded a high number of casualties. Although AN is considered a relatively stable and reliable chemical if stored and handled correctly, improper storage of such a chemical can result in catastrophic devastation as was seen in Lebanon. AN is commonly used in agriculture as a high-nitrogen fertiliser, and it has also been used as an oxidising agent in explosives. AN is widely known for its explosive properties and is often used in the creation of improvised explosive devices (IEDs) in the form of fertiliser [16].

An accurate quantification of the mass of AN contributing towards an explosion in a storage facility is important to study the effects of such explosions. With respect to previous incidents, at times, several conflicting magnitudes have got reported, and hence, an accurate quantification of the charge size becomes problematic. Hence, in this study, the reliability of the charge sizes is assessed based on the blast overpressure and the nature of damages to structures at known distances from the source of the explosion.

An explosion causes a shock wave to propagate outwards from the source, which is accompanied by a sudden rise in the air pressure, often significantly greater than the original atmospheric pressure. This rise in pressure is referred to as the blast overpressure, and it is well established that the blast overpressure decreases with the distance. Several empirical formulas have been developed to express the relationship between the overpressure and distance. Moreover, the blast overpressure can cause various types of damages to structures and harmful effects to humans [12]. Generally, in the event of an explosion, the information related to such damages gets reported. Therefore, such recorded incidents can be correlated with the blast overpressure values at known distances, so that a reliable approach can be developed to determine the TNT equivalence of the charge size. This approach will be further explored in the present study.

Historically, as accidental explosions have occurred, regulations related to such events have become more stringent. However, there still lacks universal regulations for the storage of AN and especially for storing AN in quantities exceeding 500 tonnes. As evident by the recent incidents, the explosion of such storage facilities can cause severe damages and casualties if situated within densely populated areas. Hence, there needs to be recommendations with regards to “separation distance” for storage complexes in excess of 500 tonnes.

2 Methodology

As stated in the previous section, the two main objectives of the present study related to the explosion of AN storage facilities are to develop a reliable approach to determine the quantity of AN contributing towards an explosion and providing recommendations for separation distance for storage facilities in excess of 500 tonnes.

For the first objective, three major incidents caused by the explosion of large stores of AN were studied. These are namely, Beirut-Lebanon in 2020, Tianjin-China in 2015 and Oppau-Germany in 1921, where the incidents are listed in the reducing order of the availability of technical information. All three were accidental explosion incidents of over 500 tonnes of AN. Each of these blasts have had a devastating effect on their surroundings and high number of human casualties. The pressure results of these incidents are available in published literature and are compared against the well-established empirical equation developed by Kingery-Bulmash [10]. Calculations were conducted to find the blast overpressure values at different distances from the blast source using different TNT equivalency values for the explosion. The calculated pressure values were then plotted against, and compared to, values found in literature for each case study. Moreover, identifiable forms of damages in structures at known distances from the source of the explosion were compared with the pressure required for such damages to occur. The results were then analysed to identify an upper and lower limit for the TNT equivalency of the explosion, by taking into account pressure values and the level of damage.

As for the second objective, this study aims to provide the groundwork for possible future updates to the regulations by suggesting separation distances between stores of AN over 500 tonnes and populated areas. To this end, an AN storage facility in Newcastle, NSW Australia, is used as an example. This facility has been estimated to store a quantity of AN between 6000 and 12,000 tonnes (ABC [1] and is located within 1000 m of a residential area. This store is approximately between 2 and 4 times the size of the store in Beirut, and hence, if detonated, the consequences could be catastrophic. The approach identified through the three case studies was then applied to the Newcastle case to estimate the potential pressure at different distances from a hypothetical explosion. The pressure estimation data for the Newcastle case and separation distance formulas from safe storage of solid ammonium nitrate [6] were used to calculate the appropriate separation distances for quantities of AN exceeding 500 tonnes.

3 Results and Discussion

3.1 Beirut, 2020

The explosion of the AN storage facility at Beirut's port occurred on the 4th of August 2020. Due to this explosion being a recent event, there is a significant amount of information related to it. Figure 1 shows a comparison of the blast overpressure variation with distance, found in these sources, as well as theoretical values computed using the Kingery-Bulmash empirical formula. Chernogor [4] provided pressure values relative to the distance from the centre of the blast and the corresponding damage observed at that distance. The TNT equivalence of the explosion was estimated to be between 0.5 and 2 kt TNT. Valsamos et al. [17] were another source of information regarding the pressure at specified distances from the blast.

Based on Fig. 1, it can be seen that these pressure values predicted by Valsamos et al. are significantly lower than the other predictions. In Valsamos' curve, the pressure reaches 1 kPa (the pressure required for glass to shatter) at approximately 4.2 km. This is contrary to the data found in literature that stated broken glass was identified only at 10 km from the blast site [2]. If Valsamos' curve was correct, then the pressure at 10 km from the blast would not be enough to break windows or crack glass. For this reason, this curve was discounted when calculating the upper and lower limit of the pressure from the blast. This highlights the possibility of inaccurate technical details being circulated, which can lead to erroneous interpretations of the event. Therefore, 0.5 and 2 kt TNT were identified as the lower and upper limit for the quantity of explosives. This range of pressure is in good agreement with several other studies related to the Beirut explosion [7, 14]. Since AN's TNT equivalency has been suggested as 0.56 [13], based on the Beirut facility's storage quantity of 2750 tonnes

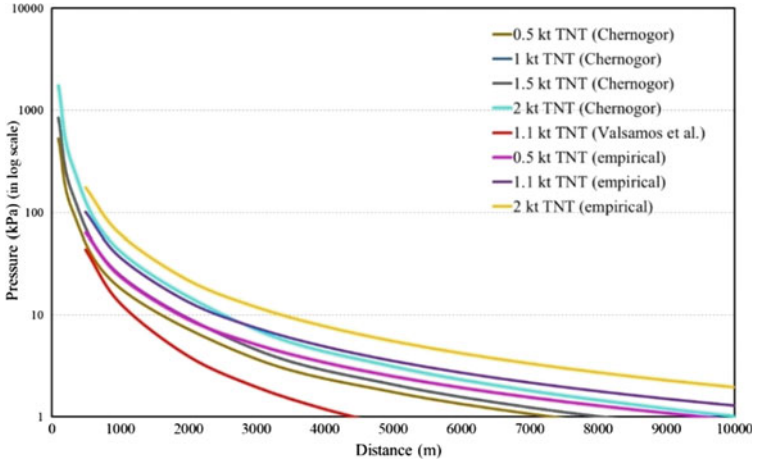

Fig. 1 Comparison of blast overpressure versus distance variation results of the Beirut explosion

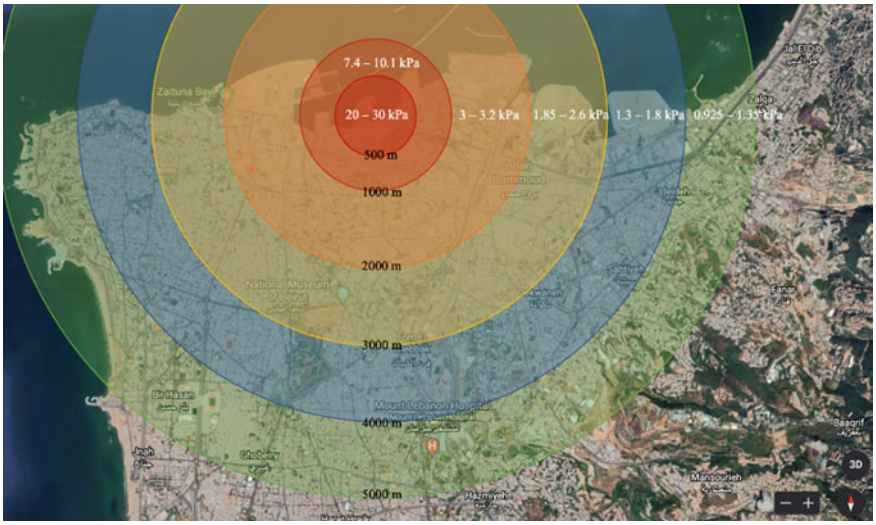

Fig. 2 Heat map for the Beirut explosion for a range of 0.5–2 kt TNT

of AN, its TNT equivalency can be considered as 1.54 kt. Hence, the aforementioned range of 0.5 and 2 kt TNT is approximately 30–130% of the storage facility's TNT equivalency. Hence, it can be seen that the proposed approach of quantifying the size of the explosion can provide a reasonable range, which is particularly important as not all explosives in a storage facility would contribute towards an explosion. Figure 2 illustrates the upper and lower pressure values visually in the form of a heat map.

The heat map is a useful presentation of the explosion event where the areas surrounding the source of explosion are categorised into several regions based on the expected pressure values. For example, even 5 km away from the source of explosion shows a pressure range of 1.5–4 kPa, which can cause damages to glass windows, roof, etc. Therefore, it can provide valuable insights to city planners, for cities with explosive storage facilities.

3.2 Tianjin, 2015

A series of explosions occurred at the Port of Tianjin in China on the 12th of August 2015, where the approximate quantity of AN was recorded as 800 tonnes. Compared to the Beirut explosion, there is limited data available for the Tianjin blast in literature. One such study was conducted by Li and Ma [11], where the TNT equivalency of this blast was taken as 21 tonnes (=0.021 kt). In a study by Chen et al. [3], the TNT equivalency was taken as 0.45 kt TNT. According to Fig. 3—where the pressure values from the previous studies are compared with the empirical calculations—it

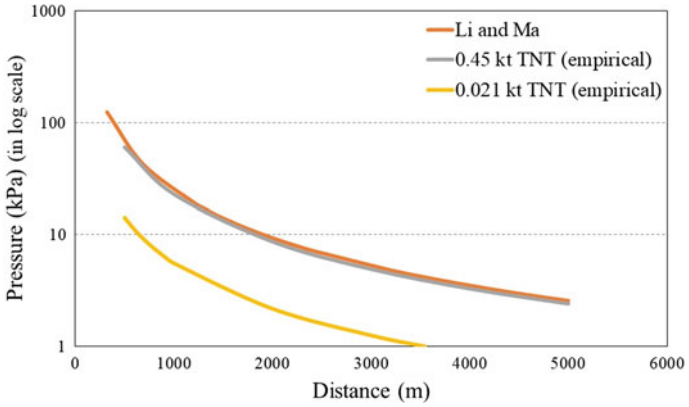

Fig. 3 Comparison of blast overpressure versus distance variation results of the Tianjin explosion

can be seen that the study by Li and Ma in fact follows closely with the pressure calculations for 0.45 kt of TNT. Therefore, 0.45 kt TNT was considered as a reasonable estimation of the quantity of AN and is also confirmed by other studies [18]. Figure 4 displays the heat map for the Tianjin explosion.

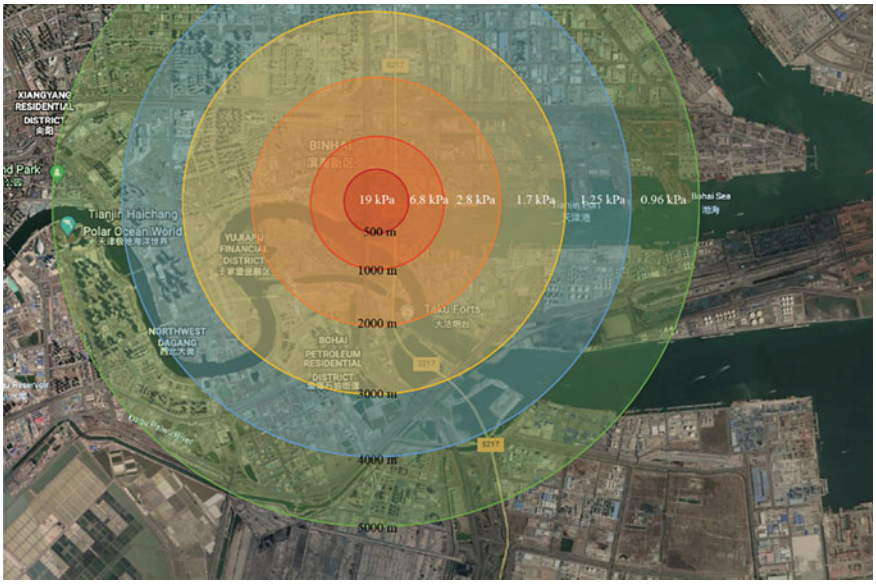

Fig. 4 Heat map for the Tianjin explosion for 0.45 kt TNT

3.3 Oppau, 1921

Literature regarding the Oppau explosion in Germany is even more limited than Tianjin due to the age of the incident. It is difficult to know the complete extent of the damage from the blast which occurred a little over 100 years ago. According to Hernandez and Scarr [9], it was identified that the TNT equivalency of the Oppau explosion was approximately 30–40% greater than that of the Beirut explosion. Hence, based on the lower and upper limits selected for the Beirut explosion, the range for the TNT equivalency of the Oppau event was taken as 0.7–2.8 kt TNT. According to Merrifield and Roberts [13], the storage facility was reported to have contained 4500 tonnes of AN, which was reported equivalent to 2.52 kt TNT, based on a TNT equivalence factor of 0.56. Hence, the aforementioned chosen range for TNT equivalence is justifiable. Several sources have mentioned damages to buildings as far as 30 km from the centre of the explosion (Khomendra et al. 2019) [8]. However, even for the upper limit of the quantity of explosions (2.8 kt TNT), the pressure at 30 km would be approximately 0.36 kPa, which would not result in any kind of structural or cosmetic damage to a structure [15]. In fact, the quantity of explosives required to generate at least 1 kPa at 30 km is unrealistic in magnitude. Therefore, these reports of the events are questionable. It is near impossible to verify these claims since it is too distant an incident. Figure 5 presents a comparison of the pressure versus distance variations calculated using empirical equations. Similar to the previous incidents, Fig. 6 illustrates the heat map for this explosion event.

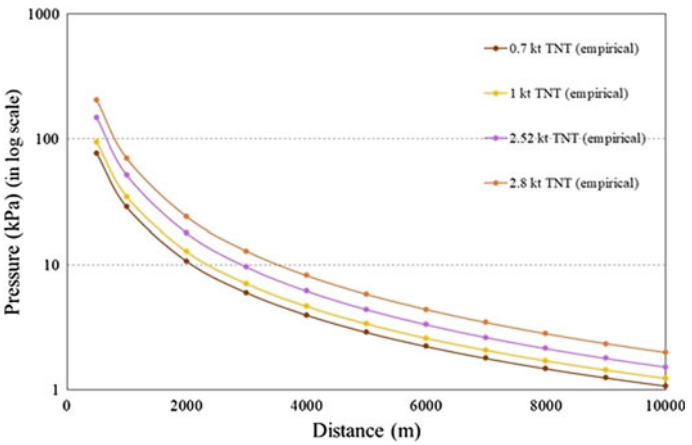

Fig. 5 Comparison of blast overpressure versus distance variation results of the Oppau explosion

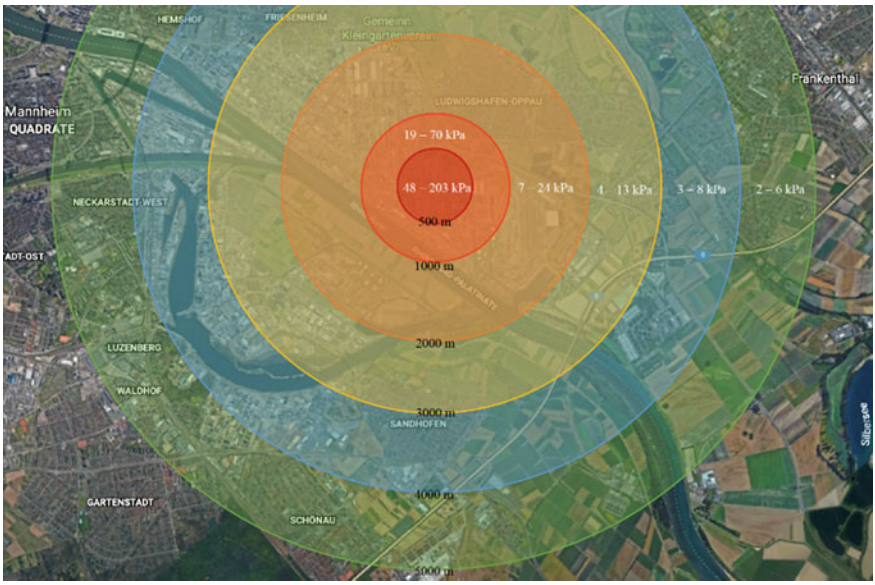

Fig. 6 Heat map for the Oppau explosion for a range of 0.7–2.8 kt TNT

3.4 Newcastle Store

In order to achieve the second objective of the present study, the AN storage facility in Newcastle, in the state of New South Wales, Australia, was chosen as a case study to identify improvements to the existing standards pertaining to separation distances. This storage facility is expected to contain between 6000 and 12,000 tonnes of AN, which translates to 3.36–6.72 kt TNT, when considering a TNT equivalence of 0.56. As identified through the study of the Beirut incident in Sect. 3.1, by considering an approximate range of 30–130%, a lower and upper limit for the explosion was calculated. As such, the corresponding range for 3.36 kt TNT was 1 and 4.2 kt TNT, whereas for 6.72 kt TNT, it was 2 and 8.4 kt TNT. Based on this range, a potential heat map (Fig. 7) similar to the previous cases was developed, by incorporating the pressure values computed using the empirical formula. As seen in this heat map, there is a residential area within the area of 500–1000 m from the storage facility and has a potential pressure ranging from 22 to 119 kPa. Pressures this high can result in reinforced concrete structures being severely damaged or even demolished. Hence, this case study highlights the necessity of revisiting guidelines related to safe separation distances, especially in the case of facilities in excess of 500 tonnes of AN and develop international guidelines based on more rigorous analysis techniques than what was used in this work.

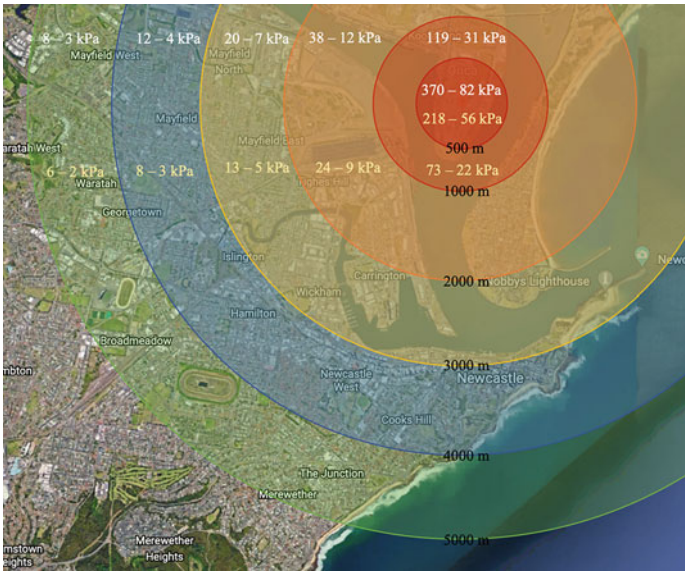

Fig. 7 Hypothetical heat map for an explosion of the Newcastle storage facility for a range of 1–8.4 kt TNT

3.5 Separation Distances and Current Standards

Safe Storage of Ammonium Nitrate: Code of Practice from the Government of Western Australia [6] is one of the several standards that provide guidelines and recommendations on storing large quantities of AN. Structures are categorised based on their functions, and separation distances are recommended based on the expected quantity of explosives. However, a shortcoming of these guidelines is that the maximum quantity of explosives is limited to 500 tonnes of AN, which is inadequate for present day storage facilities. Therefore, separation distances were calculated for amounts exceeding 500 tonnes of AN, based on threshold values for blast overpressure provided in the aforementioned code. This was carried out by considering the empirical relationships between the blast overpressure and distances, as already discussed in relation to previous incidents. The calculated recommended separation distances are given in Table 1.

Hence, this highlights the importance of enhancing the level of knowledge, as well as practical implementation of it, especially for storage facilities with high capacities. The use of these new separation distances as a guideline can help to provide an extra level of safety when dealing with the mass storage of AN so that the events of Beirut, Tianjin, Oppau, or other deadly blasts are not repeated.

Table 1 Calculated minimum separation distances from stores of AN over 500 tonnes

Amount of AN (tonnes)	TNT equivalence (tonnes)	Minimum separation distance (m)			
		Vulnerable facilities	Residential buildings	Commercial buildings	Industrial plant and factories
1000	560	1830	1510	940	730
2000	1120	2310	1910	1190	910
3000	1680	2640	2180	1360	1050
4000	2240	2910	2400	1500	1150
5000	2800	3130	2580	1610	1240
6000	3360	3330	2750	1710	1320
7000	3920	3510	2890	1800	1380
8000	4480	3660	3020	1880	1450
9000	5040	3810	3140	1960	1510
10,000	5600	3950	3250	2030	1560
11,000	6160	4070	3360	2090	1610
12,000	6720	4190	3460	2160	1660
13,000	7280	4310	3550	2210	1700
14,000	7840	4420	3640	2270	1740
15,000	8400	4520	3730	2320	1780

4 Conclusions and Recommendations

In summary, three case studies related to the explosion of AN storage facilities were analysed to propose a method of accurately quantifying the actual size of the explosion, by considering both pressure and reported damages. As such, the TNT equivalence for the Beiruit, Tianjin, and Oppau facilities were calculated as 0.5–2 kt, 0.45 kt and 0.7–2.8 kt, respectively. This approach helped to formulate an accurate prediction of the effects of the Newcastle store for a hypothetical explosion. Based on these predictions, improvements to the existing guidelines on the separation distances between storage facilitates and commonly encountered types of buildings were proposed, especially for quantities in excess of 500 tonnes of AN.

Overall, the present study serves as a preliminary investigation towards better understanding of the explosion of storage facilities, especially in the light of the recent interest in this area. It is recommended that further studies be conducted, especially using advanced finite element software to validate and compliment the empirical approach proposed in this study. Such an approach will enable to incorporate other contributory factors such as the effects of fragmentation, falling debris, variations in ground terrain, and the effect of surrounding structures.

References

1. ABC News (2020) Available at: https://www.abc.net.au/news/2020-08-05/beirut-blast-raises-concern-about-newcastle-ammonium-nitrate/12527546. Accessed 15 Oct 2021
2. Al-Hajj S, Dhaini HR, Mondello S, Kaafarani H, Kobeissy F, DePalma RG (2021) Beirut ammonium nitrate blast: analysis, review, and recommendations. Public Health Front 9:657996
3. Chen Q, Wood M, Zhao J (2019) Case study of the Tianjin accident: application of barrier and systems analysis to understand challenges to industry loss prevention in emerging economies. Process Saf Environ Prot 131:178–188
4. Chernogor LF (2021) Physical effects in the atmosphere and geospace due to ground-based events as exemplified by the explosion in the city of Beirut on August 4, 2020. Theoretical modeling results. Kinemat Phys 37:121–134
5. Clark J, Spencer D (2020) Ammonium nitrate explosions—learning and applying lessons from the past. Marsh JLT Spec, London
6. Department of Mines and Petroleum (2013) Safe storage of solid ammonium nitrate—code of practice, 3rd edn. Resource Safety, Department of Mines and Petroleum, Perth, Western Asutralia
7. Dewey JM (2021) The TNT and ANFO equivalences of the Beirut explosion. Shock Waves 31:95–99
8. French Ministry of Environment (2008) Explosion of nitrogenous fertiliser plant. ARIA Database. Retrieved from French Ministry of Environment, Paris
9. Hernandez M, Scarr S (2020) How powerful was the Beirut blast? Retrieved from Reuters Graphics: https://graphics.reuters.com/LEBANON-SECURITY/BLAST/yzdpxnmqbpx/
10. Kingery CN, Bulmash G (1984) Airblast parameters from TNT spherical air burst and hemispherical surface burst. Technical report ARBL-TR-02555
11. Li J, Ma D (2017) The studies for building failure characteristics of the extraordinarily fire explosion accident in Tianjin port. KSCE J Civ Eng 22:718–724
12. Malhotra A, Carson D, McFadden S (2017) Blast pressure leakage into buildings and effects on humans. Procedia Eng 210:389–392
13. Merrifield R, Roberts TA (1991) A comparison of the explosion hazards associated with the transport of explosives and industrial chemicals with explosive properties. ICHEME Symp Ser No 124
14. Pilger C, Gaebler P, Hupe P et al (2021) Yield estimation of the 2020 Beirut explosion using open access waveform and remote sensing data. Sci Rep 11:14144
15. Shirbhate PA, Goel MD (2019) A critical review of blast wave parameters and approaches for blast load mitigation. Arch Computat Methods Eng 28:1713–1730
16. The Washington Post (2012) Available at: https://www.washingtonpost.com/world/national-security/in-afghanistan-ied-key-component-ammonium-nitrate-fertilizer-is-being-imported-from-pakistan/2012/08/18/60edeb16-e92e-11e1-936ab801f1abab19_story.html. Accessed 15 Oct 2021
17. Valsamos G, Larcher M, Casadei F (2020) Beirut explosion 2020: a case study for a large-scale urban blast simulation. Saf Sci 137:105190
18. Zhao B (2016) Facts and lessons related to the explosion accident in Tianjin Port, China. Nat Hazards 84:707–713

Mitigation of Excessive Vibration in Warehouse Floor Slab—Case Study

H. V. W. S. A. Jayawardhane, T. Sasirathan, D. M. A. G. B. Dissanayake, K. T. S. Karunanayake, G. R. C. R. Senevirathna, Lahiru N. Dissanayake, and P. B. R. Dissanayake

Abstract Composite slab structures are usually designed by static methods which will not cater for the potential dynamic loading on the structures, and hence, the designs do not reveal the true anticipated behavior when subjected to dynamic conditions. The slab deflection may not be in the desired limit conditions when the load frequency gets different to the fundamental natural frequency of the floor structure and thus produces floor vibrations which is disruptive for the building operation and compromising the user comfort. This phenomenon is initiated with the inevitable human movements and thus needs restrictive measures to diminish the impacts. This paper presents experimental data obtained through a detailed visual inspection and a series of onsite testing for complex vibration patterns observed in a composite steel deck frame and uses a numerical model verified through experimental data to carry out a detailed dynamic analysis. The results of the analysis are used to provide vibration mitigation retrofitting methods for floor structures subjected to excessive vibration.

Keywords Composite slabs · Vibration mitigation · Retrofitting methods · Human movements

1 Introduction

Use of concrete-steel composite floor structures has become a reliable advancement in building construction due to carrying economic benefits and sound physical characteristics such as low weight. Especially, the flexibility resulted from the application of larger spans produces a lower inherent damping in the structural system [1]. While having these desirable properties, these structures arise critical problems when subjected to excessive and complex vibration, solutions to which are still

H. V. W. S. A. Jayawardhane (✉) · T. Sasirathan · D. M. A. G. B. Dissanayake · K. T. S. Karunanayake · G. R. C. R. Senevirathna · L. N. Dissanayake · P. B. R. Dissanayake
International Center for Sustainable Built Environment (Pvt) Ltd., 120/10A, Vidya Mawatha, Colombo 07, Sri Lanka
e-mail: supun@icbpvt.com

R. Dissanayake et al. (eds.), *12th International Conference on Structural Engineering and Construction Management*, Lecture Notes in Civil Engineering 266,
https://doi.org/10.1007/978-981-19-2886-4_9

under research [2]. When these composite structures undergo rhythmic dynamical load actions generally caused by human activities and due to supporting electrical engines or other machineries subjected to impact load actions [3], they tend to develop undesirable vibratory patterns that compromise the human comfort. Existing design codes and practice guides provide generic advices, but this guidance is not adequate to control the complex vibration in these low frequency structures.

The major threat to the serviceability of lightweight floors is the low frequency vibrations induced by normal human activities such as primary walking, running, and jumping. e.g., It was realized that walking has a pace frequency of about 1.6–2.4 Hz, and its harmonics might well excite a floor at its fundamental frequency leading to severe response amplification [4]. Regarding the transient dynamic loads, they are caused by a single movement represented by impulsive loadings over a certain structural element [3]. Among the methods used to analyze structural behavior of composite floors, the finite element model analysis has predominated since the early days, and according to Allahavri et al., the errors of the frequencies derived through FEMs are averagely acceptable [5].

However, in the Sri Lankan context, the integration of dynamic analysis is rarely in practice, and the traditional static loading approach is followed by the designs. Designing of these composite slabs with static methods will not reveal the true behavior. When it comes to dynamic condition, allowable deflection ratio must be higher than the static deflection ratio. In Sri Lanka, these composite slab structures are common in warehouse buildings. The present paper exemplified the excessive vibration analysis and vibration mitigation methods for two-storied steel framed warehouse structure consist of composite concrete slab deck.

2 Aim

The purpose of the study is to find possible solutions to mitigate the vibration of a composite steel deck to human comfort level by experimental and numerical methods.

3 Methodology

Assessment must be conducted mainly through a detailed visual inspection and NDT tests to identify the existing condition of the structure. Vibration and deflection measurements must be taken at several selected locations. After that, numerical model must be developed according to the existing drawings and data collected from the investigation. Model can be verified with the measured vibration and deflection data. After the verification, modifications can be done in the model to identify the reduction of vibration [6] (see Figs. 1 and 2).

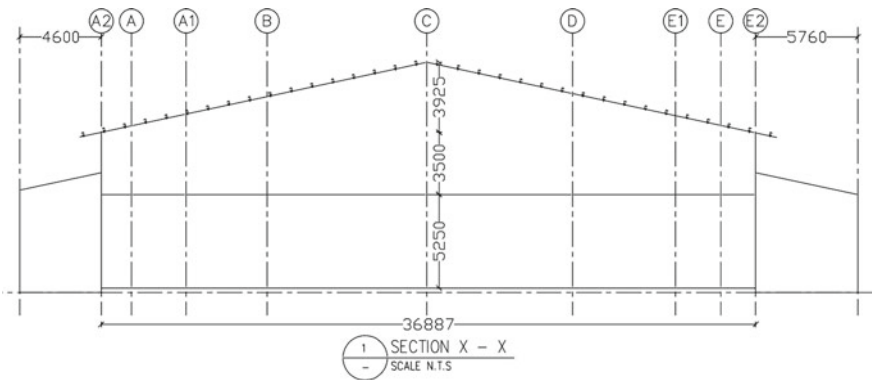

Fig. 1 Sectional view of the building

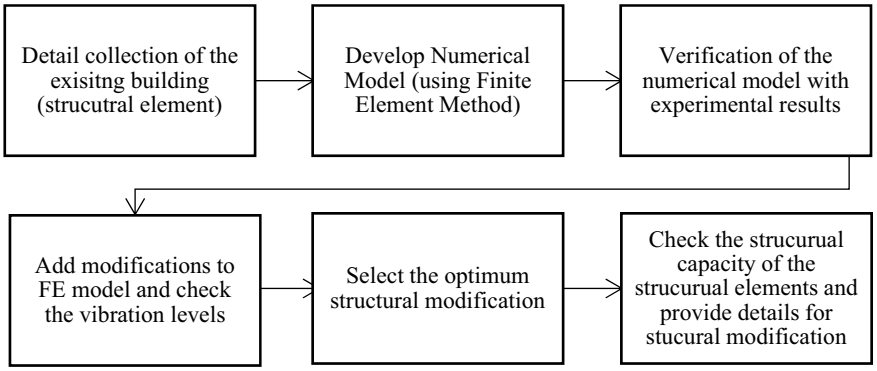

Fig. 2 Process diagram for the vibration assessment and mitigation

Experimental Procedure

Initially, a detailed visual investigation must be conducted to identify major defects in structural component of the building. Non-destructive tests must be conducted to identify the condition of the concrete slab. Rebound hammer test and ultrasonic pulse velocity test can be used to identify the condition on the existing slab.

After that, locations with higher vibrations must identified. Acceleration response (ambient vibration measurements) must be monitored on at least in three locations, and the accelerometers must keep on top of the floor and should be levelled. Two loading patterns must be considered for the test. 1. Impact loading and 2. walking loading. Deflection gauges should mount under the floor on a mid-span of the beam where the loading going to perform. In this study, measurements were obtained using linear variable displacement transducers (LVDT's) and "GURALP FORTIS" accelerometers.

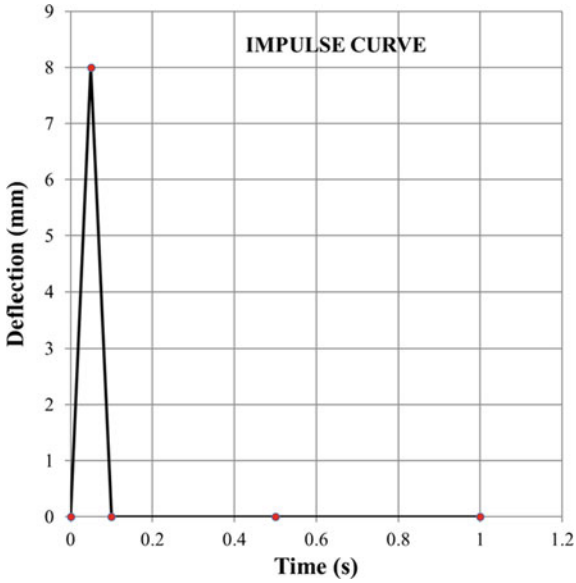

Fig. 3 Developed impulsive curve for dynamic loading

Development of the Numerical Model and Validation

The numerical model was developed using commercial FEM program. Material properties loads and the structural element sizes were applied to the model based on the data collected conservatively based on investigation details. 0.5 kN/m^2 finish load, 5 kN/m^2 storage dead load, and 1.5 kN/m^2 live load were applied to the developed model considering the site.

For dynamic loading, an impulse curve was developed by the deflection data collected from the site as shown in Fig. 3.

Numerical model was verified using experimental ambient vibration measurement and deflection measurement data sets. The developed FEM is shown in Fig. 4, and the results obtained from the experiments and the FEM are listed in Table 1.

4 Results and Discussion

The detailed investigation was able to find out the structural/non-structural defects on the building which could have been caused due to excessive vibration. The upper floor slab, slab supporting beams, and columns were considered as major structural components.

According to the experimental and numerical model analysis results, it was confirmed that the floor vibration of the building has exceeded the acceptable value

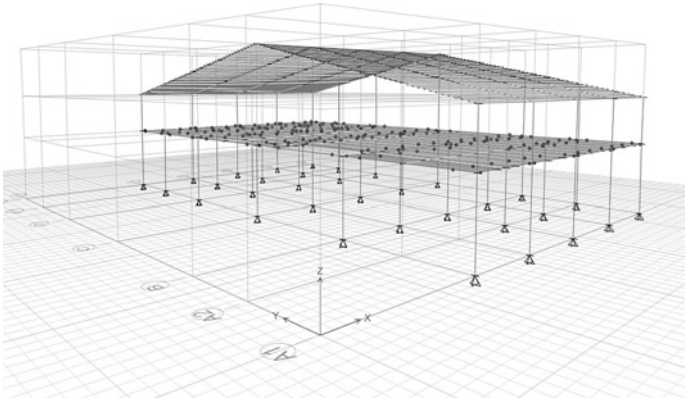

Fig. 4 3D view of develop FEM

Table 1 Comparison of results

Parameter	Experimental results	FE model (connection as Pin)	Results deviation (%)
Deflection (mm)	−0.13	−0.175	35
Acceleration (mm/s^2)	2188	2129.5	−4

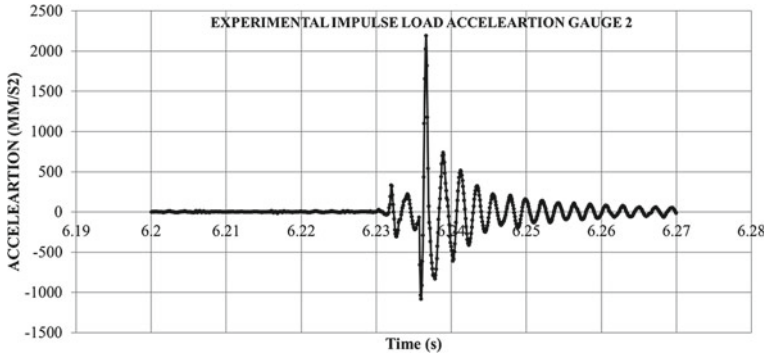

Fig. 5 Experimental impulse load acceleration

of human exposure to continuous and impulsive vibration. After the FEM verification, several FE models were developed with several options to minimize the floor vibration of the building.

- Option 1: Add additional one beam perpendicular to the secondary beam
- Option 2: Add additional two beams perpendicular to the secondary beam

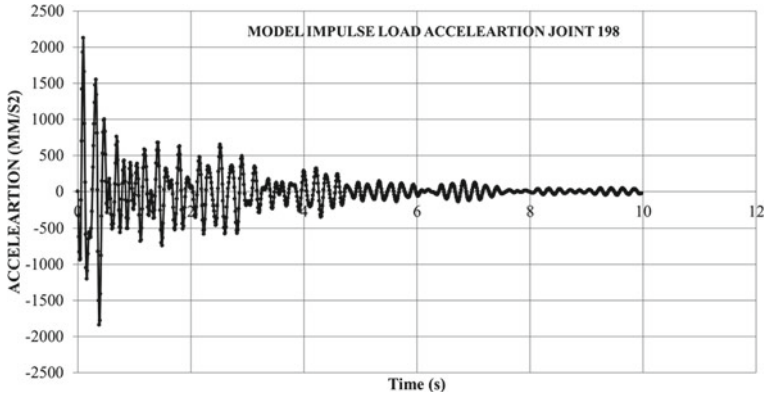

Fig. 6 Model impulse load acceleration before retrofitting

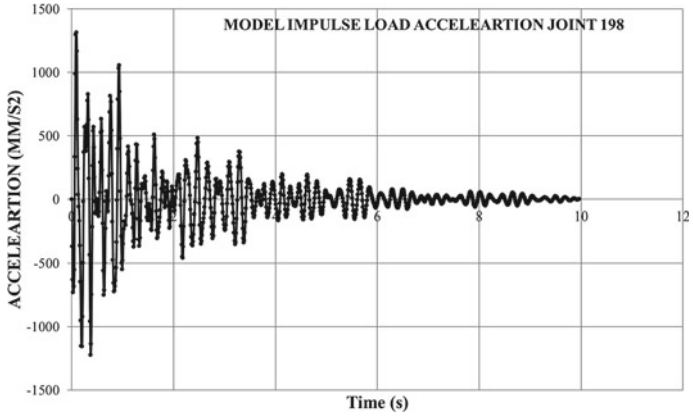

Fig. 7 Model impulse load acceleration after retrofitting (option 4)

- Option 3: Add additional three beams perpendicular to the secondary beam
- Option 4: Add additional three beams perpendicular to the secondary beam and convert connections as moment connections (between beam to beam and beam to columns)
- Option 5: Doubled the existing secondary beams.

These options were selected concerning the limitations of the extra dead load, acceptable value of the human comfortability due to impulsive vibration and constructability and construction cost. The analyzed options and results are shown in Table 2.

Option number four was selected based on the vibration levels for each testing to minimize the existing floor vibration up to comfortable level (Figs. 5, 6, and 7).

Table 2 Summary of the FE vibration analysis

	FEM	Option 1	Option 2	Option 3	Option 4	Option 5
Static deflection (mm)	−0.175	−0.165	−0.179	−0.158	−0.134	−0.065
Acceleration (mm/s^2) due impulse load	2574.46	1650.8	1416.4	1387	1314.2	1383.7
r.m.s Acceleration (mm/s^2) due impulse load	1820.4	1167.3	1001.5	980.8	929.3	978.4
Acceleration (mm/s^2) due to moving pallets	238.14	185.07	129.65	111.9	107.5	67.32
r.m.s Acceleration (mm/s^2) due impulse load	168.4	130.9	91.7	79.1	76.0	47.6
Reduction of the vibration due to impulse load (%)	–	22%	33%	35%	38%	35%
Reduction of the vibration due to moving pallets (%)	–	2%	31%	41%	43%	64%

5 Conclusions and Recommendations

Investigation was able to identify several options to reduce the excessive vibration of the structure and the vibration was significantly reduced for the structure with moment resistance connections and additional cross beams. In this study for selected building, the proposed option 4 has the most optimum solution. Based on the study, following conclusions were made generally.

- Checking the dynamic effect of the structure at the design stage for new buildings with composite slab decks will be able to prevent the excessive vibration and additional cost for repairing.
- Increasing the stiffness of floor slab by introduction of cross beams perpendicular to the existing beams and using moment resistance connections on the structure will reduce the dynamic effect on an existing building floor.

References

1. Gaspar CMR, da Silva JS, Costa-Neves LF (2016) Multimode vibration control of building steel–concrete composite floors submitted to human rhythmic activities. Comput Struct 165:107–122
2. De Silva S, Thambiratnam D (2011) Vibration characteristics of concrete-steel composite floor structures. ACI Struct J 108(6):706–714
3. Da Silva JS, da S Vellasco PCG, De Andrade SAL, da CP Soeiro FJ, Werneck RN (2003) An evaluation of the dynamical performance of composite slabs. Comput Struct 81(18–19):1905–1913
4. Ljunggren F (2006) Floor vibration-dynamic properties and subjective perception, 2006:19. issn:1402–1544, isrn: ltu-dt-06/19–se

5. Allahyari H, Nikbin IM, Rahimi S, Allahyari A (2018) Experimental measurement of dynamic properties of composite slabs from frequency response. Measurement 114:150–161
6. ICB (Pvt. Ltd) (2020) Building condition assessment report, Dart global logistics (Pvt.) Ltd., two storied warehouse at 260 Sri Ramanathan mawatha, Colombo 00015

Case Study: Investigation of Existing Cracks in the Oxidation Ditches

G. R. C. R. Senevirathna, P. B. R. Dissanayake, D. M. A. G. B. Dissanayake, K. T. S. Karunanayake, H. V. W. S. A. Jayawardhane, and T. Sasirathan

Abstract Cracking of concrete is a general phenomenon in majority of concrete structures, while the acceptable magnitude of the cracks varies with the construction purposes. This paper presents the detailed investigation on the cracks appeared on the peripheral walls of four oxidation ditches at a wastewater treatment plant and its structural health monitoring process. According to literature, cracking may be occurred due to different causes such as loading behaviour, chemical reactions, shrinkage, and thermal variations. Initially, the study focuses on identifying the magnitude of the issue and the rate of development. Furthermore, finite element analysis has been carried out to observe the behaviour of the structure under actual loading conditions in addition to the crack width calculations conforming BS 8007. The results of the study have been used to identify the root cause of the problem and determine the most feasible solution for restoration. Since the construction is already completed, preventive measures are being recommended rather than a corrective solution to ensure the serviceability requirements.

Keywords Concrete cracking · Structural health monitoring · Thermal variations · Preventive approach

1 Introduction

Appearance of cracks in reinforced concrete structures is a usual situation in construction even though its severity depends on the application, exposure condition, requirement and so many other features.

Crack width calculations is one major serviceability requirement in the structural concrete elements. Generally, the concrete structures are designed to the maximum

G. R. C. R. Senevirathna (✉) · P. B. R. Dissanayake · D. M. A. G. B. Dissanayake · K. T. S. Karunanayake · H. V. W. S. A. Jayawardhane · T. Sasirathan
International Center for Sustainable Built Environment (Pvt) Ltd., 120/10A, Vidya Mawatha, Colombo 07, Sri Lanka
e-mail: chamath.eng@gmail.com

R. Dissanayake et al. (eds.), *12th International Conference on Structural Engineering and Construction Management*, Lecture Notes in Civil Engineering 266,
https://doi.org/10.1007/978-981-19-2886-4_10

crack width of 0.3 mm, while maximum crack width is limited to 0.2 mm in water retaining structures and to 0.1 mm if the aesthetic value is a matter of concern.

This paper is focused on a case study for an investigation on the appeared cracks at external and internal faces of the 600-mm-thick peripheral walls of the oxidation ditches in a wastewater treatment plant.

The wastewater treatment system at the plant consists of four oxidation ditches, each approximately 77 m long as seen in Fig. 1. Each oxidation unit is semi-buried-type liquid retaining elongated, rectangular reinforced concrete structures. The structures are placed on a raft foundation placed on improved soil. The peripheral liquid retaining walls of the structure are 600 mm in thickness, and the foundation raft is 800 mm in thickness. Each unit comprises two oxidation ditches and separated by compartment wall of 600 mm thickness. The depth of structure is about 4.95 m, and maximum wastewater depth is 4.28 m at operation. The backfill height to the structure is 3.35 m to top level of raft foundation.

The scope of this study was to identify the possible root cause for the visible cracks and provide the necessary recommendations based on the findings. The objectives of the investigation were to review the possible causes for cracking, review the design details, identify the cause behind the visible cracks and propose the possible measures to mitigate the effect of the existing cracks.

Fig. 1 Planar view of the oxidation ditches

2 Methodology

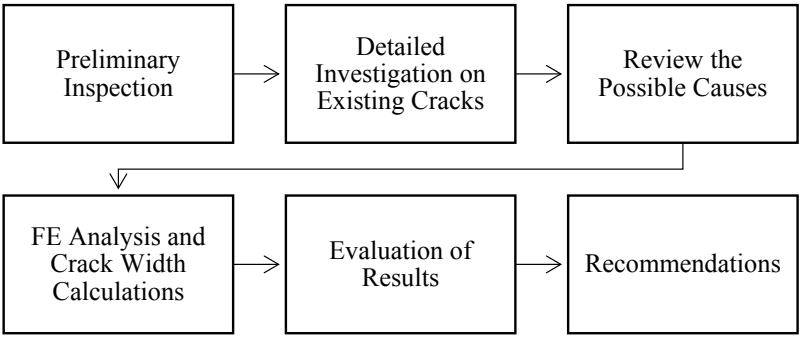

3 Preliminary Inspection

The main purpose of preliminary inspection was to plan the procedure of the study.

4 Detailed Investigation on Existing Cracks

To monitor the growth of the available cracks and have an overall idea on the spread of cracks, it was decided to monitor the growth of the cracks periodically. For that purpose, two crack surveys have been conducted up to now, within an interval of about 20 weeks, which provide a clear indication on the growth of the cracks and the propagation of new cracks. Figures 2 and 3 are images taken during the crack surveys, and the summary of findings of cracks surveys is tabulated below.

When the results in Tables 1 and 2 are compared, the number of higher size cracks has been increased, suggesting that the smaller size cracks have been developed further. Table 3 is the summary of the increased number of cracks and their details during the period between the two crack surveys.

5 Review the Possible Causes

For the identification of the cause for the existing cracks, it was essential to review the possible causes for cracks on concrete walls.

Fig. 2 One appeared crack

Fig. 3 Crack measurement

In this scenario, different types of chemical reactions in concrete mixes result in cracking. Alkali silica reaction (ASR), where active silica in aggregates and alkaline hydroxide in cement reacts with each other, forms alkali silicate gel, which results in water absorption, expansion, and cracking. In alkali carbonate reaction (ACR), dolomitic limestone in aggregates reacts with alkalis in cement to form Mg(OH)2, which results in expansion and cracking. Both alkali aggregate reactions (AARs) could be ignored in this study, since the crack pattern in these types of reactions has found to be map cracking pattern. Thaumasite sulphate attack (TSA) is a chemical reaction occurs in the presence of sulphate, carbonate and water, at temperatures below 150C to form a non-binder called thaumasite, which causes cracking in concrete elements, but this temperature value is rarely predictable, where the treatment plant is located. In the presence of gypsum in cement, delayed ettringite formation (DEF) occurs at temperatures higher than 650C during the hardening stage of concrete, forming high volume ettringite and monosulphate hydrate, which results

Table 1 Summary of cracks measured in the first crack survey

OD No.	No. of cracks	Top surface—crack widths				Vertical wall—external surface crack widths			
		<0.1 mm	>= 0.1 mm <0.2 mm	>= 0.2 mm	Max. crack (mm)	<0.1 mm	>= 0.1 mm <0.2 mm	>= 0.2 mm	Max. crack (mm)
1	71	3	10	29	0.8	49	21	1	0.2
2	143	8	19	78	1	114	26	3	0.2
3	121	8	22	61	1	98	13	2	0.2
4	158	33	8	85	1	113	30	14	1

Table 2 Summary of the same cracks after 20 weeks

OD No.	No. of cracks	Top surface—crack widths				Vertical wall—external surface crack widths			
		<0.1 mm	>= 0.1 mm <0.2 mm	>= 0.2 mm	Max. crack (mm)	<0.1 mm	>= 0.1 mm <0.2 mm	>= 0.2 mm	Max. crack (mm)
1	71	1	4	39	0.8	47	23	1	0.2
2	143	6	8	90	1	112	28	3	0.2
3	121	7	6	81	1	89	30	2	0.2
4	158	25	11	91	1	110	32	15	1

Table 3 Summary of the new cracks appeared between the first and second surveys

OD No.	No. of cracks	Top surface—crack widths				Vertical wall—external surface crack widths			
		<0.1 mm	>= 0.1 mm <0.2 mm	>= 0.2 mm	Max. crack (mm)	<0.1 mm	>= 0.1 mm <0.2 mm	>= 0.2 mm	Max. crack (mm)
1	76	57	12	7	0.4	76	–	–	< 0.1
2	47	32	7	6	0.3	46	1	–	0.1
3	145	120	7	14	0.5	144	–	1	0.2
4	67	60	3	2	0.2	67	–	–	< 0.1

in expansion and cracking. Since the investigated cracks have been appeared after several months after construction, it was concluded that the cause cannot be DEF.

It was found that the reservoir had been designed so that the concrete would have a mechanical resistance and covering of the rebar suitable for the environmental and service conditions, with regards to the parameter of durability. In fact, it was observed that the structure does not show signs of corrosion of embedded reinforcement.

Cracks can be formed due to shrinkage of concrete as well, which can also be ignored since it has a map cracking type [4].

Therefore, the study was drawn to seek for any issues with structural integrity and serviceability criteria.

6 FE Analysis and Crack Width Calculations

The analysis was carried out based on BS 8007: 1987 using SAP2000 software as shown in Fig. 4. In the analysis process, following factors were taken into consideration.

(a) Direct tension in immature concrete. The crack widths arising from restrained shrinkage and heat of hydration movement should be assessed.
(b) Direct tension in mature concrete. The crack widths for reinforced concrete members.
(c) In externally applied direct tension should be assessed.
(d) Tension resulting from seasonal movement of mature concrete should be assessed.
(e) Flexural and direct tension in mature concrete. The crack widths should be assessed.

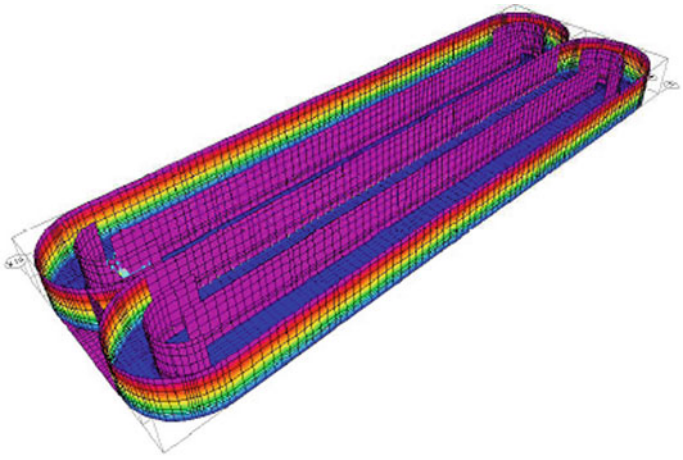

Fig. 4 SAP2000 model created for analysis

To verify the forces on external walls of the oxidation ditch, separate finite element model was developed in SAP 2000. The model facilitated to understand the most critical areas in the structure with the designed loading conditions and evaluate the structural integrity of the structure as well as the deformed shapes with the provided restrained conditions.

Calculation of the crack widths according to BS 8007 facilitated to examine the compliance of serviceability requirements.

7 Evaluation of Results

According to the structural details available on the structure and the finite element analysis results, it was concluded that there is no structural distress affecting the structure under given loading conditions.

Therefore, results of the crack width calculation were reviewed to evaluate the compliance with the serviceability criteria. British Standard BS 8007: 1987, focused on the design of structures for the containment of liquid, determines the maximum value of 0.2 mm for the opening of cracks in elements with severe or very severe exposure. With this value, it is expected that the crack be sealed naturally by the crystallization of the salts of the concrete in a short period, thus preserving the water tightness of the structure.

In calculation of crack width, the fall in temperature between the hydration peak and ambient T1 was taken as 35 °C, and variation in temperature because of seasonal changes T2 was taken as 20 °C. [3] But in the design calculations, these values have been taken as 33 °C and 10 °C, respectively. Therefore, crack width values obtained in design and investigation calculations are 0.197 and 0.25, respectively. Therefore, it can be concluded that major issue is the non-compliance of the serviceability criteria under actual conditions.

There are two other observations to back the fact that there is an impact of temperature variation for the cracking behaviour. It can be obviously seen that the cracking is more severe in the oxidation ditch which is most exposed to sunlight than the least exposed one. In addition to that, to observe the spread of cracks, some extent of the buried section was excavated, where it could be observed that the cracks decrease rapidly and stops just below the fill level under lower temperature variations.

There are several methods for repairing the existing cracks. Before doing any repair the existing surface of the old concrete walls and the floor of the reservoir should thoroughly be cleaned using a wire brush and any laitance on the surface is removed by chipping. Fine dust is removed using a fine bristled brush [1].

Injection of waterproofing material, such as epoxy or polymer modified mortar, to repair cracks is a commonly used method in crack repairing. The properties of the material should be decided according to the aims of repair. In case of patching required for large areas, it is practised to cover the entire surface with sufficient thickness of mortar strengthened with mesh reinforcement, which is not going to be economically feasible in this kind of scenario. If in any case, deteriorated concrete and

highly corroded reinforcement bars are present in the concrete elements, replacement of concrete or bars may be required. If the condition is even worse, the elements may require to be substituted. Stitching is another type of crack repair, where holes are drilled at both sides of a crack and a U bar is inserted before grouting. This method is recommended where tensile strength needed to be restored. Method of drilling and plugging a crack consists of drilling down the length of the crack and grouting it to form a key. The crack repair method is to be decided after carefully evaluating the circumstances (Mishra n.d.).

8 Recommendations

As the continuous crack appearance is observed, it is advised to monitor the propagation of cracks in regular intervals.

To obtain the most accurate results for the crack width, it is recommended to remove the paint, as there might be some misguidance when the crack propagates through the paint.

If the cracks are repaired with a solid material, it will probably recur near the original crack, unless the cause of the cracking has been corrected. But practicability for a corrective solution is very low, since the construction is already completed. Therefore, cracks may propagate until the appeared cracks can allow the effect of temperature. Until then, it is acceptable to repair the crack locations with active leakages with solid material to prevent the leakage and corrosion of reinforcement before the application of final repairing solution.

With the exclusion of a corrective solution, the approach should be a preventive solution which is going to fulfil the serviceability requirements of the structure. Therefore, the solution should ensure the water tightness of the structure as well as the functioning throughout the service life. Hence, it is recommended to seal the cracks with a polymer incorporated non-shrink material that accommodates the movement at the cracks with the effect of temperature variations. If the properties are not complied with the required behaviours, the material might get dry and act as a solid material.

It is recommended to carefully consider the specific temperature variations, at the design stage itself to avoid this kind of issues in future constructions.

Acknowledgements International Center for Sustainable Built Environment (Pvt.) Ltd. is gratefully appreciated for this opportunity to take part in the investigation and perform further studies.

References

1. Anon (2012) Remedial treatment of water retaining structures. s.l.:s.n
2. Mishra G (n.d.) What are the methods of concrete crack repair? [Online] Available at: https://theconstructor.org/concrete/methods-of-crack-repair/886/
3. Nanayakkara S (1999) Design for controlled cracking of water retaining structures based on BS 8007. In: Proceedings of the seminar on design and construction of water retaining structures
4. Sollero M, Bolorino H (2016) Investigation and diagnosis of a reinforced concrete reservoir with intense crack formation from several sources. J Build Rehabil 1(6)

A Review on the Advances in Distributed Fibre Optic Sensing Technology for Structural Health Monitoring

A. Gowshikan, K. Kariyawasam, X. Xu, C. Kechavarzi, N. de Battista, N. Ferdinando, S. Acikgoz, N. D. Gunawardana, and M. Ranasinghe

Abstract Distributed fibre optic sensing (DFOS) technology is being widely exploited in many civil infrastructure monitoring applications due to its inherent advantages over conventional sensing technologies. Over the last decade, research and development have enhanced the performance of DFOS systems in SHM, which led to new applications in civil engineering. This paper presents a brief review of DFOS technology, the latest laboratory experiments utilising DFOS, and the applications of this system in monitoring piles, bridges, tunnels, buildings, and railways. Finally, promising future directions for DFOS technology are discussed. This review demonstrates that DFOS is a versatile monitoring technology with significant capabilities to support the development of smart infrastructure.

Keywords Distributed fibre optic sensing · Brillouin optical time domain analysis · Structural health monitoring · Fibre optics · Civil engineering

A. Gowshikan · K. Kariyawasam (✉) · N. D. Gunawardana · M. Ranasinghe
Department of Civil Engineering, University of Moratuwa, Moratuwa, Sri Lanka
e-mail: kasund@uom.lk

X. Xu · C. Kechavarzi · N. de Battista
Department of Engineering, University of Cambridge, Cambridge, UK

N. Ferdinando
Access Engineering PLC, Colombo, Sri Lanka

S. Acikgoz
Department of Engineering, University of Oxford, Oxford, UK

C. Kechavarzi · N. de Battista
Epsimon Ltd., Hertfordshire, UK

R. Dissanayake et al. (eds.), *12th International Conference on Structural Engineering and Construction Management*, Lecture Notes in Civil Engineering 266,
https://doi.org/10.1007/978-981-19-2886-4_11

1 Introduction

It is vital to monitor the structural health of civil infrastructures such as buildings, roads, tunnels, and bridges, as the failure of these structures poses severe consequences on public welfare and the economy. Innovations in structural health monitoring (SHM) have evolved over many decades. Various monitoring technologies are employed to obtain measurements related to structural health [29]. Fibre optic sensing (FOS) is a promising technology that gained popularity over other conventional sensing technologies in SHM applications due to its durability, small size, stability, and insensitivity to electromagnetic interference [24].

FOS can be mainly categorised into discrete sensing and distributed sensing. Discrete FOS is commonly based on fibre Bragg gratings (FBGs) that allows taking measurements at a specific point, while distributed FOS (DFOS) is based on scattering phenomena that enable simultaneous measurements along the length of the sensing fibre [22]. The main advantage of DFOS over FBG is that it provides continuous profiles of measurements of temperature, strain, pressure, and vibration.

Rayleigh, Raman, and Brillouin scattering are the three types of scattering in optical fibres which can be exploited in distributed sensing. Distributed sensors based on Rayleigh scattering have higher acquisition bandwidth and higher strain sensitivity than the other types of distributed sensors. Rayleigh scattering is predominantly used in distributed acoustic sensing (DAS) systems [12]. Brillouin scattering is the widely used technique for distributed temperature sensing (DTS) and distributed strain sensing (DSS) [24]. Brillouin scattering occurs from stimulated or spontaneous acoustic vibrations in the optical fibre. These vibrations produce Brillouin scattering waves, which eventually incapacitate the forward-moving input pulse. As a result, a shift in the frequency between the Brillouin scattered wave and the input light pulse called the Brillouin frequency shift (BFS) occurs. BFS is intrinsically dependent on Young's modulus and the density of the fibre material, making BFS linearly dependent on temperature and strain. Thus, it is exploited in Brillouin-based DFOS [24]. This linear dependency can be expressed as:

$$v_B(T, \varepsilon) - v_B(T_0, \varepsilon_0) = C_\varepsilon.\delta_\varepsilon + C_T.\delta_T \tag{1}$$

where $v_B(T, \varepsilon)$ is BFS at temperature T and strain ε, C_T and C_ε are the temperature and strain coefficients, respectively.

Brillouin optical time domain analyser (BOTDA) and Brillouin optical time domain reflectometer (BOTDR) are the two popular distributed Brillouin sensing techniques used in engineering applications. BOTDA is based on stimulated Brillouin scattering (SBS), where a laser is pulsed into the fibre cable from both ends, amplifying the reflection within the fibre. BOTDR is based on spontaneous Brillouin scattering (SpBS), where a laser is launched from only one end of the fibre. Thus, the signal received by the interrogator is weaker than in BOTDA. BOTDA can provide a more extensive sensing range than BOTDR with higher resolution, better strain and temperature sensitivity and faster measurement. However, BOTDR is advantageous

for applications where only one end of the fibre is accessible. Another advantage of the BOTDR system is increased resilience: BOTDR still takes readings up to the breaking point if there is any cable break. In contrast, measurements are not possible across the cable length in a BOTDA system after a break.

Spatial resolution and light attenuation are other crucial factors that influence the performance of a DFOS system. In particular, spatial resolution describes the cable length over which strains are averaged while light attenuation properties strongly influence the length over which the measurements can be taken. Studies have been carried out aimed at improving the spatial resolution of several Brillouin-based DFOS systems for specific applications [1]. The review below summarises the studies which focus on improving the DFOS capabilities through laboratory tests and the applications of DFOS systems to various civil infrastructures.

2 Review on Laboratory Experiments on DFOS Technology

DFOS systems are an attractive tool for SHM. It is essential to evaluate the applicability and accuracy of DFOS instruments before applying them in the field, which will help reduce errors in the installation of FO cables and help to minimise the damages caused to the sensors and other DFOS related instruments during installations.

Sun et al. [28] proposed an optical fibre Brillouin sensor in a coil winding setup to measure the expansion deformation of a concrete column with central rebar subjected to accelerated corrosion. The concrete column was moulded with a central steel bar for the experiment. The optical fibre cables were wrapped around the column surface using adhesives in four sections numbered A to D from top to bottom, as shown in Fig. 1a, b. Figure 1c shows the experimental setup where the sample specimens were inserted in 5% NaCl solution, and the rebar was electrified to accelerate the corrosion.

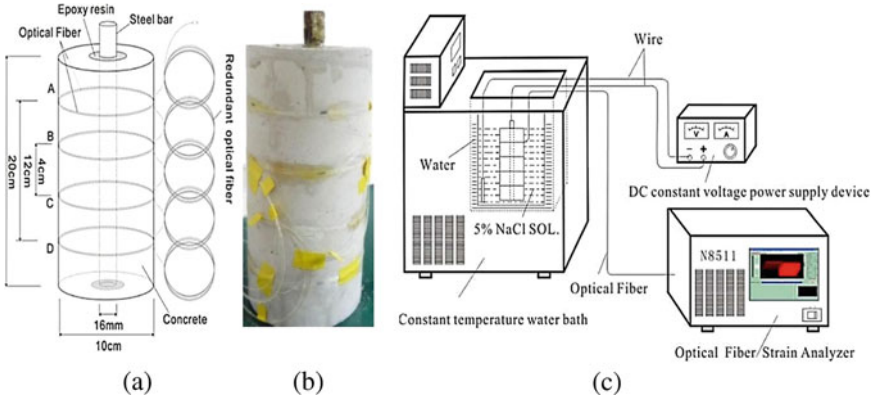

Fig. 1 **a** Schematic diagram of fibre laying, **b** sample specimen, and **c** test setup [28]

A BOTDR analyser was used to obtain the average expansion deformation of the specimen.

Based on the experimental results, the study concluded that the proposed BOTDR-based DFOS technique could accurately identify the location and quantify the strain rate of the concrete expansion caused by the rebar corrosion. The authors also proposed conducting further studies to determine the feasibility of applying the aforementioned technique in field conditions.

Henault et al. [13] conducted an experimental analysis to assess the reliability of strain measurements for surface-mounted and embedded DFOS cables in RC beams. Surface-mounted sensors were in the form of adhesive tape to be attached to the face of the RC beam. A 2 mm—diameter multi-fibre cable was attached to the rebars before concrete placement to allow sensing inside concrete after casting. Four-point bending tests were carried out on the RC specimen. The study concluded that the location of the sensing cable had negligible influence on strain measurements as the strain profiles were comparable for surface-mounted and embedded sensors. The study recommends attaching the sensors to the rebar for a new structure and surface mounting sensors for existing structures.

Hao and Zhishen [11] conducted a study to theoretically investigate the measurement performance of BOTDR for different sensing lengths and strain levels. The theoretical results were validated using experiments. Basic tests were conducted to examine the relationship (1) between sensing length and measured strain values of fibre optics (2) between tested strain distribution and actual strain distribution of a fibre optic cable. The study also proposed standard experiments to calibrate the crack detection performance of the BOTDR-based DFOS approach. The performance of sensors was assessed for three different surface mounting techniques as shown in Fig. 2: (1) Overall bonding, (2) point fixation, and (3) loop installation.

Loop installation was found to be the most effective installation technique for the BOTDR technique to capture the localised damage and deformation. It was also found during the study that the BOTDR equipment with enhanced spatial resolution should be used when the testing strain is minimal.

In a study conducted by Xu and Yin [33] on the performance of GFRP soil anchors using the DFOS technique, a laboratory calibration test was performed to examine the accuracy and installation of BOTDA sensors. It was proposed to use steel clamps with screws to attach the fibre cables along the GFRP bars. This method has been found to save installation time compared to the conventional method of adhesively bonding the fibre cables to the bars.

Broth and Hoult [4] used a dynamic distributed fibre optic sensing (DDFOS) system based on the Rayleigh backscattering principle to understand the dynamic behaviour of RC beams subjected to cyclic loads. Specimens of four slender and four deep beams were fabricated with embedded FO sensors attached to the longitudinal reinforcement. Each beam was exposed to 3600 load cycles at 1 Hz, and four different loading arrangements were used by opting between three-point and four-point bending. Each RC beam specimen was tested in three phases: initial loading, cycling, and loading to failure. The study concluded that the embedded FO cables could withstand cyclic and failure loading tests without breaking. The study also

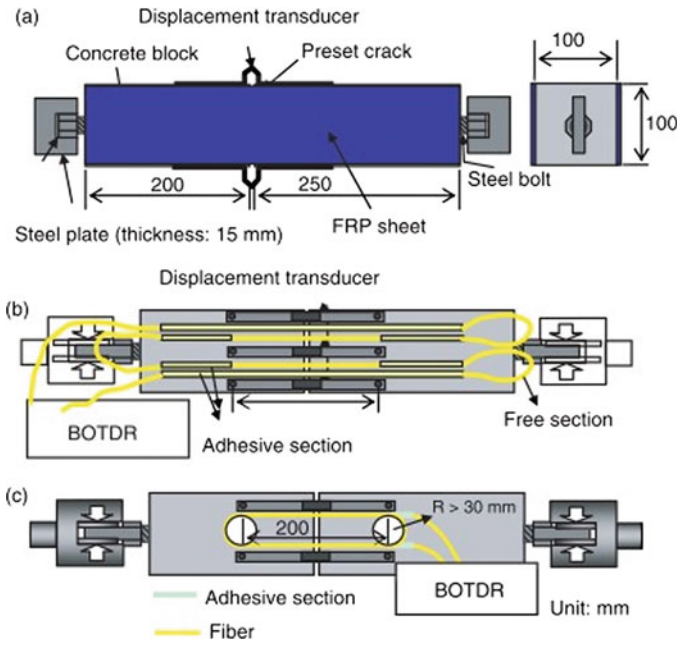

Fig. 2 Experiment specimen **a** side view, **b** plan view (point fixation and overall bonding), **c** plan view (loop installation) [11]

inferred the development of failure mechanisms, such as the growth of arching action and the development of significant cracks using the dynamic DFOS system.

Berrocal et al. [2] conducted several laboratory experiments to evaluate the suitability and accuracy of optical frequency domain reflectometry (OFDR)-based DFOS for crack monitoring in RC structures subjected to superficial loading. The experiments consist of a three-point bending test of concrete beams with an FO cable attached directly to the reinforcement bar. The experiment results concluded that the strain measurement using the DFOS system agreed well with those measured by conventional instruments. It was observed that embedded or surface-bonded FO sensors can detect hairline cracks that are not perceptible to human eyes. The study also identified that bonding FO sensors to the reinforcement would minimise the risk of fibre rupture. Embedded sensors will additionally reduce the risk of idle readings due to the exceedance of the strain range of the sensor, as any significant strain discontinuities are not experienced on the reinforcement surface due to cracking.

3 Application of DFOS in Pile Monitoring

Concrete pile foundations are commonly being used in the construction industry. Instrumented pile tests are vital to establish the performance of a pile and validate the assumptions made during the initial design [23]. Currently, the use of the DFOS system is an advancing technique for pile strain and displacement monitoring.

Pelecanos et al. [23] investigated the performance of concrete bored piles using both conventional vibrating wire strain gauges (VWSG) and BOTDR during maintained pile load tests. The study concluded that BOTDR distributed system offers more confidence than VWSG in determining the developed shaft friction along the pile. The study also concluded that the distributed FO data provided well-grounded information about vertical pile displacements derived from distributed strain data. A similar study conducted by [15] describes the monitoring principles and methodology involved in designing, installing, testing and measuring from the DFOS system in test piles.

Sun et al. [27] conducted a study to measure the strain variation along a precast pile with Pulse Pre-Pump BOTDA (PPP-BOTDA) interrogator. A robust algorithm of random sampling consistency (RANSAC) was engaged to extract and process the DFOS data. Using the RANSAC processed strain data, the authors calculated the axial force and frictional resistance and found that the local anomalies identified in the PPP-BOTDA measured pile strain data shall be effectively eliminated using the RANSAC-based model.

The growing use of larger diameter and longer piles has increased concern over the integrity and quality of cast-in-place foundation piles [36]. Rui et al. [36] carried out a thermal integrity test on a large bored concrete pile of 1.5 m diameter and 51 m long in East London. Rui et al. derived temperature profiles along the pile using BOTDR during the hydration of concrete. The study concluded that the deployed DFOS system could capture the early thermal data precisely. The pile diameter profile evaluated from both the thermal data and the finite element model is in relatively good agreement with the conventional thermal integrity profiling results.

Xu et al. [34] used BOTDA to study the performance of large-diameter bored piles exposed to a slope excavation and proposed a new instrumentation method for the FOS. The lateral deflections calculated from BOTDA sensor data have good accuracy when compared with the traditional inclinometers. The study concluded that the distributed BOTDA sensing system is cost-effective for long-distance distributed sensing or large infrastructures needing many sensors.

Zheng et al. [37] conducted a study for offshore PHC pipe pile performance monitoring using Brillouin optical frequency domain analysis (BOFDA)-based DFOS system. An offshore PHC pipe pile was pre-installed with sensing cables in the study to solve the difficulties in the protection and on-site installation of FO cables. A finite element analysis was conducted with the degradation and hardening hyperbolic model (DHHM) to evaluate the results obtained using the BOFDA-based DFOS system from the static pile load test. The study found that the pre-installation method of FO cables in PHC pipe piles is efficient and reliable. The field study concluded that

the BOFDA-based DFOS system provides reliable offshore PHC pipe pile monitoring measurements.

4 Application of DFOS in Bridge Monitoring

The life cycle of large bridges is generally several decades. Because of the vast investment in bridge construction and the risk of severe disruption to the public in case of bridge failure, it is vital to monitor the structural health of the bridges in real-time [32]. The use of the DFOS system in structural health monitoring of different bridges gained in popularity over the last decade. Experts and scholars worldwide have researched the application of the DFOS system in the real-time monitoring of bridge structures.

Siwowski et al. [25, 26] conducted a study on the application of DFOS technology for the distributed strain and temperature monitoring of the first Polish FRP composite bridge. The study concluded that the smart DFOS could provide reliable strain measurements with acceptable accuracy based on the time-dependent behaviour of the FRP bridge. In 2021, the same research group conducted a study to validate the accuracy and reliability of the DFOS system implemented in the Polish FRP composite bridge monitoring through proof load tests and FEA. The latter study concluded that it is accurate, efficient, and reliable to use the DFOS technique in bridge monitoring and extend to other FRP structures.

Scour of sediments around piers, abutments, and foundations is a common and serious challenge for bridges [18]. Liu et al. [18] proposed a DFOS method based on an ultra-weak fibre Bragg grating (UWFBG) array to monitor and estimate scour. The study suggested that the scour estimation can be achieved by analysing the difference between the signals of the FO cables buried in the sand and those submerged freely in the water. The study concluded that the depth and location of the scour can be determined based on the standard deviation of the signals. This method has many advantages, such as real-time monitoring ability, extensive measurement range, accuracy, and high spatial resolution. The authors added that this method is more favourable than the complex signal processing of the TDR-based method and the complex modelling process of the vibration-based method used for monitoring bridge scour.

Ye et al. [35] used both the discrete and distributed FOS systems to evaluate a pre-stress concrete railway bridge to monitor the pre-stress loss behaviour, including immediate pre-stress losses and time-dependent pre-stress losses. A simplified method based on EC2 and two time-step methods based on EC2 and AASHTO-LRFD were exploited to take measurements. The study concluded that early age pre-stress loss could be better estimated using simplified methods while time-step methods are suitable for long-term pre-stress losses.

A study by Wosniok et al. [31] evaluated the impact of static traffic loading on the slight deflection effects in the concrete structure of the Amsterdam bridge using Tuneable Wavelength Coherent OTDR. The study results concluded that the applied

method and FOS system could identify minimal elastic strain in the range of about 2 μm/m at a spatial resolution of 20 cm.

A study by Li and Sun [16] aimed to improve the damage detection accuracy and efficiency of bridge structures by monitoring the continuous bridge deflection based on DFOS technology and applying a deep-learning algorithm to perform structural damage detection. A 13-layer supervised learning model based on deep convolutional neural networks was proposed in the study. This method reached an accuracy of 96.9% for damage classification, which outperformed the random forest (81.6%), support vector machine (79.9%), k-nearest neighbour (77.7%), and decision tree (74.8%). The study concluded that this proposed model also demonstrated adequate capabilities in automatically extracting damage features and discriminating damage from structurally symmetrical locations.

5 Application of DFOS in Tunnelling

In modern tunnelling, geotechnical deformation monitoring is a crucial component to ensure safe construction and a long lifetime of the tunnel [21]. Although the inner lining surface displacements are traditionally measured using total stations or terrestrial laser scanners, these methods cannot achieve adequate accuracy. Mosberger and Lienhart [21] conducted a study on in situ monitoring of tunnel segments using high-resolution DFOS. A series of load tests of precast tunnel lining segments was conducted at a specifically developed test rig, and it was concluded that the high resolution of 1 με enables crack detection. The results demonstrate the high potential of DFOS in tunnelling applications.

A study was carried out by De Battista et al. [8] for strain monitoring in the Liverpool Street Station tunnel during the excavation of cross passages using a BOTDR-based DFOS system. The FO cables were installed on the 40 cm-thick primary sprayed concrete lining (SCL) surface and covered with an additional 40 cm-thick SCL. The monitoring system provided continuous strain profiles in the SCL during each stage of cross-passage excavation. The study observed a rapid reduction in the increase in strain in the tunnel lining with the increase in distances from the openings. Hence, it was suggested to reduce the extent of thickening the SCL layer. The study concluded that the field data obtained from the DFOS system was instrumental in calibrating the SCL design models.

Minardo et al. [20] applied a distributed fibre optic strain sensor for long-term monitoring of a railway tunnel affected by an active earthflow. The experimental results from the two-year monitoring campaign concluded that the sensors could identify localised strains and their locations along the tunnel walls and follow the development of those identified strains with time.

Gómez et al. [10] conducted a study to monitor a metro tunnel in Barcelona, which could be potentially affected by the construction of a residential building 14 m above the tunnel. A DFOS system was installed with 1 cm spatial resolution by bonding it to the inner surface of the tunnel for monitoring, and strain readings were collected

using optical distributed sensor interrogator (OBR ODiSI-A). An in-depth analysis of the collected strain readings was conducted to assess the reliability of the installed DFOS system. This study concluded that the DFOS measurements very accurately reproduced the tunnel deformation process.

Temporary shoring is provided to ensure the stability of the large cross-section tunnels excavated using the New Austrian Tunnelling Method (NATM). Dismantling temporary shoring for the tunnel's secondary lining construction should be carried out with intensive care as it threatens the tunnel's equilibrium [17]. Li et al. [17] used a BOTDR DFOS system to obtain strain measurements and a numerical model to obtain settlement profiles of the Beijing Rail Transit airport line tunnel during such shoring dismantling process. A metal-based strain-sensing optical cable monitoring that is developed especially for a harsh environment was selected. The embedded method was used to install the fibre cable. During the study, the highest settlement variation value of 5.7 mm was observed, corresponding to the tensile strain variation of 50 με during the continuous removal of the bottom shoring of the tunnel. The axially deployed optical fibres were capable of measuring the horizontal displacement of the tunnel only. Therefore, to calculate the vertical settlement of the tunnel, an inversion model based on the numerical simulation and the strain data from DFOS was extracted. The study concluded that the measurements from the DFOS system are reliable, and the results are applicable to tunnels excavated according to the NATM and have temporary shoring.

6 Application of DFOS in Buildings

Davis et al. [6] investigated the use of distributed fibre optic strain sensors to assess the effect of corrosion on the behaviour of reinforced concrete beams. Six specimens of beams with different levels of corrosion were instrumented with FO sensors and tested in three-point bending. It was found that assessing structures based on crack widths and stiffness may give inaccurate results, whereas distributed strain measurement provides a more quantitative assessment. The FOS could detect the change in strain in the longitudinal reinforcement due to the loss of bond between concrete and reinforcement due to corrosion [6].

In a study conducted by De Battista et al. [7], they used BOTDA technology to measure the progressive axial shortening of a 50-storey reinforced concrete building. The study emphasised utilising a method to measure the floor-to-floor axial shortening of vertical load-bearing elements to install finishes and partitions on lower floors. Measurements were taken regularly during the construction process to observe the change in strain. Thus, the axial shortening at any construction stage has helped verify the predicted differential shortening and adjust the height of column pre-sets if required as the construction progressed [7, 9].

Brault et al. [3] investigated the use of distributed FOS to monitor the beams in a newly constructed RC building during a load test. The authors examined three in situ cast RC elements: a beam, a drop panel, and a larger beam. The FOS data

captured the inflexion points, moment transfer at the supports, crack locations, crack openings, and deflected shapes.

Broth and Hoult [5] assessed the dynamic sensing capabilities of a DDFOS system by performing strain monitoring using ODiSI-B, a Rayleigh-based dynamic distributed analyser on an existing 9.24 m long RC T-beam located within Ellis Hall on the Queen's University campus in Kingston, Ontario, Canada. The dynamic load was applied by aligning 38 students throughout the span of the beam (in uniformly distributed load orientation) and then asked to jump simultaneously for 30 consecutive jumps. A concentrated load test was conducted by gathering the students in a group over the midspan of the beam. The study concluded that both the static and dynamic concrete strains could be successfully measured using a DDFOS system. The DDFOS system was able to capture the actual behaviour of the beam accurately. Also, the DDFOS data provided the dynamic response factor of the instrumented structure, the distributed crack widths, and deflected shapes.

7 Application of DFOS in Railways

The railway is one of the critical infrastructures in civil engineering that has to be monitored precisely over the entire service period. Practical and real-time monitoring technology is required to ensure the safe functioning of the railway operations; otherwise, any abnormalities in railways tend to cause severe fatality and economic loss [14].

Wheeler et al. [30] conducted a lab and field evaluation to measure the distributed dynamic rail strains using Rayleigh backscatter-based fibre optic sensor. The study investigated the ideal fibre cable position and rail surface preparation through laboratory testing by conducting a three-point bending test for static and dynamic loading for a short, instrumented rail section. Two surface preparation methods were used: (1) Optimal rail preparation that involved exposing bare steel along the fibre path, which is labour and time-intensive, and (2) minimal rail preparation that only involved cleaning the rail surface with a damp cloth. The study found out that both surface preparations yielded similar results under static and dynamic loading, hence concluded that minimal rail preparation will be the effective method to affix the fibre optic cables to the rail. Laboratory experiments were also performed to validate the dynamically distributed rail strain measurements obtained using fibre optics. For this purpose, the displacements calculated based on rail strains were compared with the displacements obtained using the digital image correlations (DICs) and linear potentiometers (LPs) and found a good agreement within these measurement systems. During the field evaluation, it was found out that the distributed strain measurement using Rayleigh backscattering cannot measure rail strains under high vibration conditions such as high-speed passenger trains. However, it can be used at a level-crossing to measure the rail strains under low vibrating conditions such as slower-moving vehicles.

Milne et al. [19] conducted a study to evaluate the use of the DAS system to calculate rail deflection and sleeper loading from strain measurements. DAS system with optical fibres based on phase-sensitive OTDR (Φ-OTDR) interrogation is used for obtaining strain measurements. The study concluded that Φ-OTDR-based DAS interrogation is an appropriate technique for monitoring the load–deflection behaviour over long lengths of railway track and can also be used for a range of train speeds. It has the capability for measuring time-varying strain along a rail. However, the spatial resolution and bandwidth of DAS Φ-OTDR are not as satisfactory as Rayleigh-based optical frequency domain reflectometry (OFDR).

In a study conducted by Hsu et al. [14], the authors applied Brillouin frequency shift (BFS) sensing technology in railway strain and temperature measurement. The study concluded that the temperature and strain changes could be measured with the fibre BFS in real-time. It helps identify geometric irregularities and abnormal positions of a rail. The monitoring function was enhanced by automatically displaying warning messages once the critical parameters reached their threshold values.

8 Future Improvements of DFOS Technology

The study by Hsu et al. [14] suggested future improvements to be carried out on the application of BFS sensing for railway monitoring. That includes measuring the accumulation and release of stress in continuously welded rails, especially in curved sections and improving the system accuracy and efficiency in real-time monitoring. A study by Milne et al. [19] mentioned that more research needed to be carried out to enhance the performance of data extraction and interpretation using the DAS Φ-OTDR system. Gómez et al. [10] mentioned using robust and complex algorithms to identify and replace any anomalies present in the raw data set. The study by Gómez et al. [10] also suggested developing standard guidelines regarding fibre bonding to the structure, temperature affections on readings, post-processing of data to minimise or eradicate any anomalies present in the data; thus, a much faster data interpretation could be performed. Future works should also focus on developing systematic approaches for eliminating discrepancies between real-time DFOS measurements and theoretical approaches using various codes.

In the near future, integrity testing of piles can be done more efficiently by improving pile instrumentation with high-resolution DFOS systems. Even when a DFOS system is employed in SHM, the need for conventional measurement technique to acquire a part of the data is not entirely diminished. Future works should include the feasibility study of using the DFOS system as a complete package in SHM. The spatial resolution of the BOTDA and BOTDR is the critical factor in determining the sensing range. A narrower probe pulse is required for a finer spatial resolution to be achieved, which lowers the return backscattered power. Thus, in practical applications, longer measurement lengths cannot be achieved. Also, a finer spatial resolution will degrade the signal to noise ratio (SNR). Hence, future studies should focus on improving the spatial resolution for long-distance measurements.

Although the studies by Henault et al. [13], Hao and Zhishen [11], Xu and Yin [33] evaluated the performance of fibre sensors installation methods, more in-depth evaluation on FO cable installation techniques needed to be performed to ensure that the fibre optic instrumentation serves its purpose. Long-term stability and reliability of DFOS cables in a concrete environment have to be explored in-depth in the future. Attention should be required to eliminate attenuation in FO cables due to external factors such as bending stresses and deterioration of the exterior coatings on optical fibres. Further studies are also needed to be carried out in reducing the measurement time by the DFOS interrogators.

9 Conclusions

The development and application of DFOS in SHM have become steadier and promising in recent years. Due to the gaining popularity of DFOS in real-time monitoring of civil infrastructures, several studies on the applications of DFOS have been undertaken over the past few years. This paper summarised the recent advancements of DFOS and their applications in various civil engineering structures.

Experiments have been conducted to assess the reliability and accuracy of the strain measurements using both surface-mounted and embedded FO cables. It was found that both methods of FO cable installations produce similar results, and it was recommended to surface mount the cables if it is an existing structure and embed the FO cables for a new structure. The capability of the DFOS system based on BOTDR and BOTDA to detect anomalies in RC structures induced by various external factors such as loading and corrosion was analysed through laboratory calibration tests. It was found that measurements obtained using DFOS systems are effective and reliable.

DFOS systems have been applied in civil engineering infrastructures like piles, bridges, tunnels, and buildings. Various studies were conducted on evaluating the performance of pile foundations using DFOS systems, and results were compared with the conventional measurement techniques. These studies have found that the DFOS is a promising measurement technique for real-time and long-term monitoring of piles. The DFOS systems produce reliable results but with far greater spatial coverage than the conventional instrumentation. Scour monitoring is crucial for bridges. The studies found that the DFOS method based on the UWFBG array is effective over the traditional scour monitoring instrumentations due to their ease of installation, ability to take rapid measurements, and reliability and accuracy. The studies also found that the DFOS system can effectively measure pre-stress losses, deflection effects due to traffic loading, and damage detections in bridges.

When it comes to tunnelling applications, studies show that the DFOS system has the potential in detecting tunnel lining displacements. DFOS systems are effective in monitoring RC members of a building. Studies show that the axial shortening of columns, deflection, and crack development in RC beams can be assessed precisely using DFOS systems. The use of DFOS systems in railways was also widely

experimented on over the past few years. Displacements of rails calculated using strain measurements obtained from Rayleigh backscatter-based fibre optic sensors under low vibration conditions are in good agreement with the conventional DIC method and LP method. Using a DAS system based on Φ-OTDR interrogation for strain measurements in railways provided reliable measurements over long lengths of railway tracks.

In addition to the current applications, future improvements suggested by various researchers could possibly extend the applicability of DFOS technology for structural health monitoring.

Acknowledgements The authors would like to thank Access Engineering PLC, Sri Lanka, and its IdeaNest Initiative for the funding provided for this research project. Authors also gratefully acknowledge the research and other facilities provided by the Department of Civil Engineering at University of Moratuwa, the Department of Engineering Science at University of Oxford, and Centre for Smart Infrastructure and Construction at University of Cambridge.

References

1. Barrias A, Casas JR, Villalba S (2016) A review of distributed optical fiber sensors for civil engineering applications. Sensors (Switzerland) 16(5)
2. Berrocal CG, Fernandez I, Rempling R (2021) Crack monitoring in reinforced concrete beams by distributed optical fiber sensors. Struct Infrastruct Eng 17(1):124–139
3. Brault A, Hoult NA, Greenough T, Trudeau I (2019) Monitoring of beams in an RC building during a load test using distributed sensors. J Perform Constr Facil 33(1):04018096
4. Broth ZE, Hoult NA (2020) Field monitoring of RC-structures under dynamic loading using distributed fiber-optic sensors. J Perform Constr Facil 34(4):04020070
5. Broth Z, Hoult NA (2020) Dynamic distributed strain sensing to assess reinforced concrete behaviour. Eng Struct 204:110036
6. Davis M, Hoult NA, Scott A (2017) Distributed strain sensing to assess corroded RC beams. Eng Struct 140:473–482
7. De Battista N, Cheal N, Harvey R, Kechavarzi C (2017) Monitoring the axial displacement of a high-rise building under construction using embedded distributed fibre optic sensors. In: The 8th international conference on structural health monitoring of intelligent infrastructure (SHMII8), pp 1058–1067
8. De Battista N, Elshafie M, Soga K, Williamson M, Hazelden G, Hsu YS (2015) Strain monitoring using embedded distributed fibre optic sensors in a sprayed concrete tunnel lining during the excavation of cross-passages. In: The 7th international conference on structural health monitoring and intelligent infrastructure (SHMII7)
9. De Battista N, Kechavarzi C, Cheal N, Harvey R, Wong S (2019) Monitoring the axial shortening of principal tower using embedded distributed fibre optic sensors. In: International conference on smart infrastructure and construction 2019, ICSIC 2019: driving data-informed decision-making, pp 233–240
10. Gómez J, Casas JR, Villalba S (2020) Structural health monitoring with distributed optical fiber sensors of tunnel lining affected by nearby construction activity. Autom Const 117:103261
11. Hao Z, Zhishen W (2008) Performance evaluation of BOTDR-based distributed fiber optic sensors for crack monitoring. Struct Health Monit 7(2):143–156
12. Hartog AH (2017) An introduction to distributed optical fibre sensors. CRC Press, Boca Raton

13. Henault JM, Quiertant M, Delepine-Lesoille S, Salin J, Moreau G, Taillade F, Benzarti K (2012) Quantitative strain measurement and crack detection in RC structures using a truly distributed fiber optic sensing system. Const Build Mater pp 916–923
14. Hsu WK, Lee YL, Kuan TT (2021) Brillouin frequency shift sensing technology used in railway strain and temperature measurement. Appl Sci (Switzerland) 11(15)
15. Kechavarzi C, Pelecanos L, de Battista N, Soga K (2019) Distributed fibre optic sensing for monitoring reinforced concrete piles. Geotech Eng 50(2):43–51
16. Li S, Sun L (2020) Detectability of bridge-structural damage based on fiber-optic sensing through deep-convolutional neural networks. J Bridg Eng 25(4):04020012
17. Li ZX, Hou GY, Hu T, Zhou TC, Xiao HL (2020) A study on the application of the distributed optical fiber sensing monitoring technology in the process of dismantling temporary tunnel shoring. Arab J Geosci 13(19)
18. Liu W, Zhou W, Li H (2021) Bridge scour estimation using unconstrained distributed fiber optic sensors. J Civ Struct Health Monitor 0123456789
19. Milne D, Masoudi A, Ferro E, Watson G, Le Pen L (2020) 'An analysis of railway track behaviour based on distributed optical fibre acoustic sensing. Mech Syst Sign Process 142:106769
20. Minardo A, Catalano E, Coscetta A, Zeni G, Zhang L, Di Maio C, Vassallo R, Coviello R, Macchia G, Picarelli L, Zeni L (2018) Distributed fiber optic sensors for the monitoring of a tunnel crossing a landslide. Rem Sens 10(8)
21. Monsberger C, Lienhart W (2017) In-situ deformation monitoring of tunnel segments using high-resolution distributed fibre optic sensing. In: SHMII 2017 - 8th international conference on structural health monitoring of intelligent infrastructure, proceedings, (December), pp 149–160
22. Muanenda Y, Oton CJ, Di Pasquale F (2019) Application of Raman and Brillouin scattering phenomena in distributed optical fiber sensing. Front Phys 7(October):1–14
23. Pelecanos L, Soga K, Elshafie MZEB, de Battista N, Kechavarzi C, Gue CY, Ouyang Y, Seo H-J (2018) Distributed fiber optic sensing of axially loaded bored piles. J Geotech Geoenviron Eng 144(3):04017122
24. Rajan G, Prusty BG, Iniewski K (2016) Structural health monitoring of composite structures using fiber optic methods. In: Rajan G, Prusty BG (eds) CRC Press
25. Siwowski T, Rajchel M, Howiacki T, Sieńko R, Bednarski Ł (2021) Distributed fibre optic sensors in FRP composite bridge monitoring: validation through proof load tests. Eng Struct 246(May)
26. Siwowski T, Rajchel M, Sienko R, Bednarski L (2018) Smart monitoring of the FRP composite bridge with distributed fibre optic sensors. In: 9th International conference on fibre-reinforced polymer (FRP) composites in civil engineering, CICE 2018, 2018-July(July), pp 918–925
27. Sun Y, Li X, Ren C, Xu H, Han A (2020) Distributed fiber optic sensing and data processing of axial loaded precast piles. IEEE Access 8:169136–169145
28. Sun Y, Shi B, Chen SE, Zhu H, Zhang D, Lu Y (2014) Feasibility study on corrosion monitoring of a concrete column with central rebar using BOTDR. Smart Struct Syst 13(1):41–53
29. Vardanega PJ, Webb GT, Fidler PRA, Huseynov F, Kariyawasam KKGKD, Middleton CR (2021) Bridge monitoring. In: Innovative bridge design handbook. Butterworth-Heinemann, pp 893–932
30. Wheeler LN, Pannese E, Hoult NA, Take WA, Le H (2018) Measurement of distributed dynamic rail strains using a Rayleigh backscatter based fiber optic sensor: lab and field evaluation. Transp Geotech 14:70–80
31. Wosniok A, Jansen R, Chen L, Toet P, Doppenberg E, De Jong W, Chruscicki S (2019) Static load monitoring of a concrete bridge using a high-precision distributed fiber optic sensor system. In: SMAR 2019 - proceedings, pp 1–8
32. Wu T, Liu G, Fu S, Xing F (2020) Recent progress of fiber-optic sensors for the structural health monitoring of civil infrastructure. Sensors (Switzerland) 20(16):1–25
33. Xu D, Yin J (2016) Analysis of excavation induced stress distributions of GFRP anchors in a soil slope using distributed fiber optic sensors. Eng Geol 213:55–63

34. Xu D, Yin J, Liu H (2018) A new measurement approach for deflection monitoring of large-scale bored piles using distributed fiber sensing technology. Meas: J Int Meas Confederation 117:444–454
35. Ye C, Butler LJ, Elshafie MZEB, Middleton CR (2020) Evaluating prestress losses in a prestressed concrete girder railway bridge using distributed and discrete fibre optic sensors. Constr Build Mater 247:118518
36. Yi R, Kechavarzi CF, O'Leary C, Duncan B, Soga K (2017) Integrity testing of pile cover using distributed fibre optic sensing. Sensors 17(12):2949. https://doi.org/10.3390/s17122949
37. Zheng X, Shi B, Zhu HH, Zhang CC, Wang X, Sun MY (2021) Performance monitoring of offshore PHC pipe pile using BOFDA based distributed fiber optic sensing system. Geomech Eng 24(4):337–348

Significance of Construction Stage Analysis on the Initial Configuration of Concrete Faced Rockfill Dams

T. M. S. Tennekoon, K. K. Wijesundara, P. B. R. Dissanayake, N. G. P. B. Neluwala, S. De Silva, and S. Venkatesan

Abstract Rockfill dams bear large water bodies; therefore, assessment of the stability of these structures is crucial. Different approaches have been followed by previous researchers to numerically analyze concrete faced rockfill dams. A proper guideline to define the initial configuration when developing finite element models for large-scale analysis like seismic analysis is not available. Therefore, in this research a 3-dimensional finite element model of the Kotmale dam has been developed using MIDAS FEA NX software, and the construction sequence has been adopted in the static analysis. In a CFRD dam, a large volume of rockfill material is used; therefore, it is crucial to select the appropriate material model. The Duncan and Chang EB model was selected based on previous research to model the material behavior of the rockfill and the transition layers. Linear elastic model was used for modeling of the concrete face of the dam. The bedrock was modeled using linear elastic material models. The results are compared for two different analysis conducted with construction stage analysis and without construction stage analysis with the actual observed deformations of the dam. The results agree well when the construction sequence is considered; furthermore, the deformation shape is completely different for the two cases.

Keywords Concrete faced rockfill dams · 3D Dam model · Construction stage analysis

T. M. S. Tennekoon (✉) · K. K. Wijesundara · P. B. R. Dissanayake · N. G. P. B. Neluwala
Department of Civil Engineering, University of Peradeniya, Peradeniya, Sri Lanka
e-mail: e14342@eng.pdn.ac.lk

S. De Silva · S. Venkatesan
Department of Civil Engineering, Royal Melbourne Institute of Technology, Melbourne, Australia

R. Dissanayake et al. (eds.), *12th International Conference on Structural Engineering and Construction Management*, Lecture Notes in Civil Engineering 266,
https://doi.org/10.1007/978-981-19-2886-4_12

1 Introduction

A breach in a dam can cause heavy floods leading to many catastrophic results (failure of Edenville and Sanford *dams* in Michigan). Therefore, it is important to assess the stability of these structures for disaster mitigation purposes. Concrete faced rockfill dams are build all around the world due to the less complex construction and the cost effectiveness [1]. The rockfill material bears a major volume of the CFRD, and a concrete slab is used to reduce seepage through the rockfill material.

Different approaches were taken by previous researchers to accurately predict the behavior of rockfill materials. References [3–5] used the Duncan and Chang EB model to model the rockfill. Xu et al. [2] adopted a generalized plasticity model which is often used for material like sand. Clough—Duncan model and the modified ideal model were used by Zhang et al. [4] for the numerical modeling of the rockfill material. Linear elastic models have been commonly used to analyze the concrete face of CFRDs.

Earthquakes and sudden water rise in the reservoir can create large forces on the structure [6]. In order to simulate this behavior, a finite element model is required. Before conducting large-scale analysis, the finite element model should be analyzed for static conditions and the deformed configuration would be used for the next steps of the analysis. Even for static analysis, the prediction of nonlinearity of the rockfill material is important and most importantly the material parameter values should agree well with the actual material properties at the site. For this research, the material parameters are obtained from previous researches.

In reality, dams are constructed in layers. The strain is accumulated according to these construction layers. In dam modeling, this phenomenon should be adopted for the results to agree with the actual readings. Furthermore, in order to conduct large-scale analysis for an instance dynamic analysis, the deformations during the construction stages should be considered and the dynamic analysis should be conducted on the deformed configuration. The importance of construction stage analysis and the deviation of the results obtained with and without construction stage analysis have not been discussed in detail in previous literatures.

Therefore, the objective of the research is to identify the variation of the static deformations obtained through a 3-dimensional model and to identify the significance of nonlinear response of CFRD under static loading incorporating construction stage analysis to predict the right deformed configuration before adding extreme loading conditions. For this purpose, the Kotmale dam in Sri Lanka was selected as a case study.

In this study, initially the Duncan and Chang EB model was selected for the analysis of the Kotmale dam because previous researchers have pointed out the accuracy of this particular model in predicting the material behavior with a small number of material parameters. Three-dimensional finite element model was developed using 8-node hexahedron solid elements and 6-node pentahedron solid elements. Analysis was conducted including the construction sequence and neglecting the construction

sequence. The results were compared with the in situ measurements obtained from the site.

2 Material Models

The main components of the concrete faced rockfill dams are the rockfill and the concrete slab. Linear elastic models were used for modeling of the concrete.

Since the rockfill material is nonlinear and pressure dependent, different material models are used to depict the material behavior as mentioned in the previous chapter. Although the Duncan and Chang EB model is widely used, Cloug–Duncan model, modified ideal model, and generalized plasticity models have also been used for this purpose as well. For this research, the Duncan and Chang EB model is used due to the simplicity and the accuracy to predict the rockfill behavior.

2.1 Duncan and Chang EB Model

The Duncan and Chang model depicts the nonlinear elasticity of the rockfill material. The stress–strain behavior is developed through the Hook's law and the Mohr–Coulomb's law as shown in the Fig. 1.

$$\sigma_1 - \sigma_3 = \frac{\varepsilon_1}{a + b\varepsilon_1} \tag{1}$$

Equation 1 defines the hyperbolic stress–strain curve where $\sigma_1 - \sigma_3$ is the deviator stress, σ_1 is the major principal stress, σ_3 is the minor principal stress, and ε_1 is the

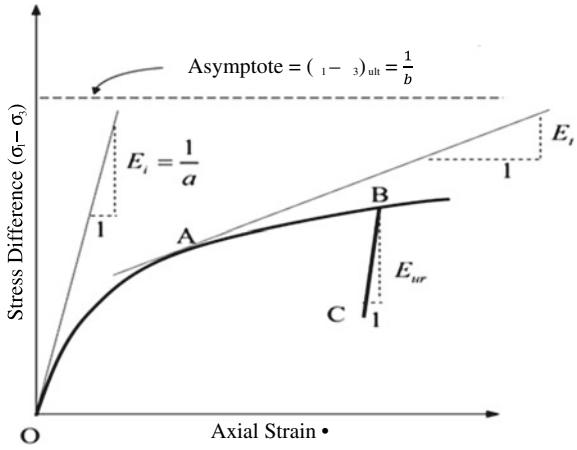

Fig. 1 Duncan and Chang EB model

corresponding strain. Parameters a and b are curve fitting parameters based on the rockfill material property. The tangent modulus is obtained using the expression given in Eq. 2,

$$E_t = \left[1 - \frac{R_f(1-\sin\emptyset)}{2c.\cos\emptyset + 2\sigma_3\sin\emptyset}(\sigma_1 - \sigma_3)\right]^2 .K.P_a\frac{\sigma_3}{P_a}^n \tag{2}$$

Here, K is the modulus number, P_a is the atmospheric pressure, c defines the cohesion, $\emptyset$ is the friction angle, R_f is the failure ratio, and m and n are defined as the exponent related to the confining pressure on the initial modulus.

Bulk modulus (B) depends on the confining stress given in Eq. 3.

$$B = K_b.P_a.\left(\frac{\sigma_3}{P_a}\right)^m \tag{3}$$

The variation of the Bulk modulus with the Poisson's ratio is defined as given in the Eq. 4.

$$B = \frac{E}{3(1-2v)} \tag{4}$$

The material parameters of the Duncan and Chang EB model are $K, \emptyset, c, R_f, n, m$, and K_b. The values for these parameters can be obtained through laboratory tests and optimization methods such as displacement-based back analysis. In this research, the material parameters adopted by References [3, 4] were used for the initial part of the developed finite element model.

3 Developing Finite Element Model

3.1 Geometric Model Development

In order to investigate the significance of defining the initial configuration of concrete faced rockfill dams, the Kotmale CFRD dam is selected for this study. Out of the entire volume of material, rockfill is significant in CFRDs. The dam body is constructed by adding layers of rockfill material and compacting according to the design configuration. In order to reduce the seepage, a concrete face is introduced. In between the rockfill and the concrete layer, there exist two transition layers to provide a good contact. The drainage layers provide a drainage path to the seepage water, thus protecting the rockfill material from getting washed off. Toe weights provide stability to the dam, and the concrete grouting reduces the cavities in the foundation rock. Under the Kotmale dam, there is a gneiss layer, and below that, there is limestone.

Table 1 Material parameters of the Duncan and Chang EB model

Material type	E (MPa)	Kb	C (kPa)	$\emptyset$ (deg)	K	n	R_f	m
Rockfill	50	340	1225	51	600	0.45	0.59	0.18
Transfer 1	55	800	1225	52.5	970	0.36	0.76	0.18
Transfer 2	60	800	1225	50.6	1050	0.35	0.71	0.18
Drainage	30	800	1225	54	720	0.3	0.8	0.18

Table 2 Material parameters for linear elastic material

Name	Elastic modulus (GPa)	Poisson's ratio	Unit weight (kN/m^3)
Concrete	33.4	0.2	25
Gneiss	58.6	0.21	26
Limestone	50.4	0.25	24

Since limestone has larger cavities compared to the gneiss, seepage is a possibility through this layer.

As mentioned in the previous chapter, Duncan and Chang EB material model is used to model the rockfill material. Table 1 gives the material properties selected for this study. It is important to note that these material parameters are consistent with the material parameters available in the literature for rockfill material [3, 5]. Furthermore, material behavior of the concrete and the foundation material are assumed to be linear elastic in the developed finite element model. According to the experimental data obtained during construction of the Kotmale dam, the material parameters of the concrete and the rockfill material are obtained as given in Table 2.

3.2 Three-Dimensional Finite Element Model Development

Three-dimensional finite element model of the Kotmale CFRD dam is developed using MIDAS FEA NX finite element software as shown in Fig. 2. The construction layers of rockfill material were developed using 8-node hexahedron solid elements. Foundation and the embankments were modeled using 8-node hexahedron solid elements and 6-node pentahedron solid elements. Similar to the rockfill layers, the transition layers, concrete layer, and the toe weights were modeled using 8-node hexahedron solid elements. Node-to-node connection was maintained throughout the finite element model. The boundaries of the foundation and the embankments were fixed, and the water pressure was added on the upstream face of the rockfill dam.

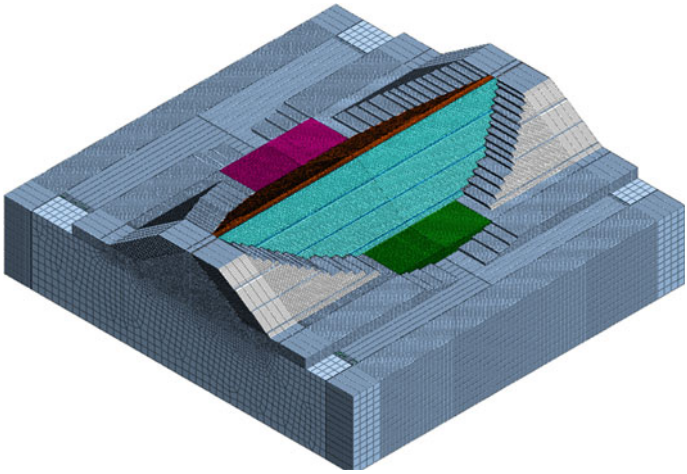

Fig. 2 3D finite element model of the Kotmale dam

3.3 Construction Stage Analysis

The construction of rockfill in concrete faced rockfill dams is done in layers. Kotmale dam has being constructed using 20 layers of rockfill material. When constructing these layers, the rockfill material is added and then compacted in layers according to the design configuration. The strain will be accumulated for each construction layer when the above layer is added. Therefore, it is crucial to correctly depict the actual construction stages in the finite element model. In the 3D model development, the foundation and the embankments were added first and the construction stages of the rockfill were followed by the transition layers and the toe weights. In the final step, the water pressure was added. In Midas FEA NX software, the construction stages can be defined and the analysis can be conducted accordingly for the 3-dimensional model.

4 Results and Discussion

4.1 Introduction

In order to assess the importance of the construction stage analysis of concrete faced rockfill dams, a three-dimensional finite element model of the Kotmale dam was analyzed under static loading conditions with and without the construction sequence.

The in situ measurements of the dam deformations were used in the comparison to validate the finite element model. The dam settlements are measured at the chainage 400 m cross section of the dam in 2 different levels located at 33.5 m from the dam base

and 53.5 m from the dam base. The vertical settlements recorded after the construction of the rockfill layers were used for the comparison with the analysis results obtained with construction stage analysis and without construction stage analysis.

Lateral deformation of the dam is obtained using the installed horizontal gauges. The observed readings indicate the lateral deformation after the construction of the dam. For the comparison, readings after the reservoir impounding are used. Finite element analysis gives the accumulated horizontal deformation. Therefore, from the construction stage analysis, the horizontal deformation before and after adding the water pressure is obtained, and then, the difference is compared with the in situ measurements.

4.2 Comparison of Numerically Predicted Settlement with in Situ Measurements

In this research, the 3-dimensional Kotmale dam model has being analyzed with and without construction stages using the nonlinear static analysis. As mentioned before, the Duncan and Chang material parameters were used to define the rockfill material behavior. Initially, the deformations due to the self-weight of the material were considered. The maximum deformations can be observed in the cross section at the center of the dam axis (at chainage 400 m). As shown in Fig. 3, the maximum vertical deformation of 1823 mm is observed at the top of dam toward the right slope when the construction stages were not considered.

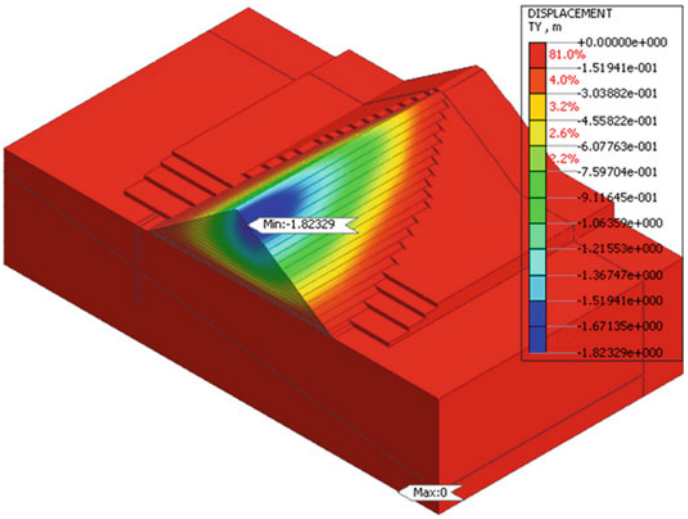

Fig. 3 Vertical displacement without construction stage analysis

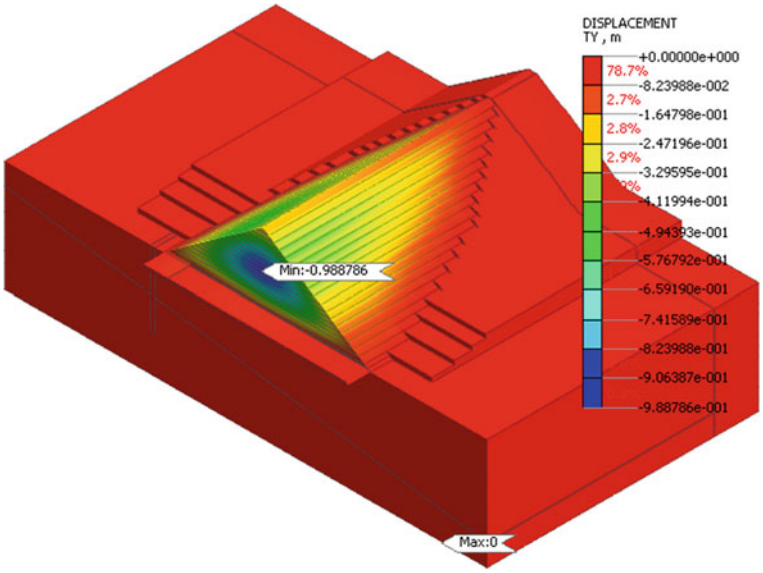

Fig. 4 Vertical displacement with construction stage analysis

Figure 4 depicts the vertical settlement of the dam through construction stage analysis. In contrast to deformed shape without construction stage analysis, the maximum settlement of 989 mm could be observed at the middle of the dam. This phenomenon is due to the accumulation of the strain at the middle sections due to the adding and compaction of the layers above. No deformation can be observed in the foundation and the embankments for both cases.

In situ settlement monitoring stations are located at the section of chainage 400 m. 5 stations are located at 35 m height above the dam base and 3 stations at 55 m above the dam base. The actual deformations after the construction were compared with the numerically obtained deformations at these locations as shown in Figs. 5 and 6.

As shown in Fig. 5, the deformation variation along the dam cross section at level 55 m from the dam base agrees well when the construction sequence is considered where the settlements increase toward the center of the section from both the directions. There is a slight deviation less than 5% to the monitored data at the center and toward the slopes. However, the analysis without incorporating the construction stages results in settlements increasing toward the right slope which is erroneous. A variation of 55% from the actual measurements can be seen at the center and toward the right bank. At the left bank, the deviation is around 10%.

At a height of 35 m above the dam base, the same phenomena can be observed where the in situ measurements agree well with the construction stage analysis and have large deviations without construction stage analysis. As shown in Fig. 6, without incorporating the construction sequence a deviation of 50% with the actual deformations can be observed toward the right slope but moving toward the left slope there

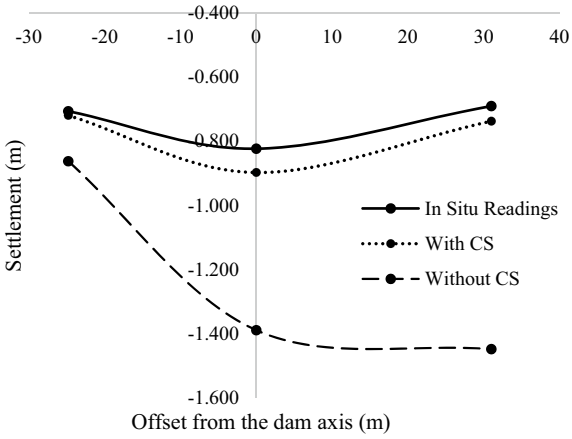

Fig. 5 Settlement at 55 m from the dam base

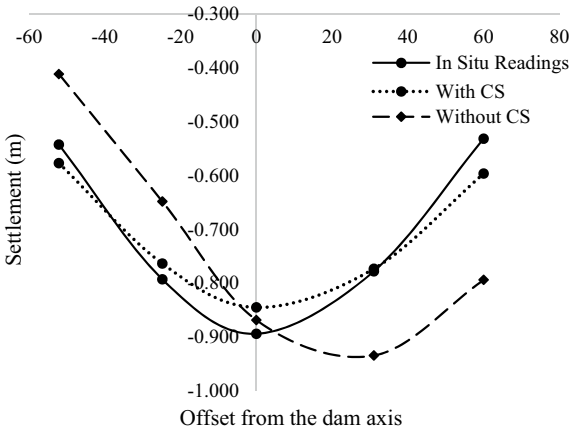

Fig. 6 Settlement at 35 m from the dam base

is an under prediction of 10% with the observed readings. When the construction sequence is considered, the deviation of less than 5% with the actual readings can be observed but toward the left and the right slopes there is an over prediction but at the center a similar under prediction is observed.

Therefore, including the construction stage analysis is crucial to obtain the correct deformation shape of the dam. When conducting analysis with extreme loading conditions like seismic analysis, if the construction stages are not considered for the initial configuration, then the analysis under extreme conditions would give erroneous results.

4.3 *Lateral Displacements Obtained Through Numerical Analysis*

Until the completion of the rockfill layers, a symmetric displacement of 167 mm can be observed in the transverse direction at level 60 m from the dam base as shown in Fig. 7. Once the transition layers, concrete layer, and the water pressure was added, the deformations vary as shown in the Fig. 8. The maximum deformation at the left slope has increased by 108 mm, and at the right slope, the lateral deformation has reduced by 35 mm. The maximum deformation is now visible at 55 m level from the dam base.

The horizontal movement gauges are located at the chainage 400 m similar to the settlement gauges. At the level 55 m (from the dam base), there are 3 monitoring stations, whereas at level 35 m, readings from 4 stations are available. Unlike the settlement cells, during the construction it is not possible to obtain the horizontal deformation. Therefore, the horizontal movement after adding the water pressure is compared with the results obtained through the construction stage analysis as shown in Figs. 9 and 10. At both levels, the deformation shapes agree with the actual readings but there are deviations when the values are compared. At the right slope which is critical for the analysis, the values obtained through the analysis agree well with in situ measurements. However, displacements obtained toward the left bank, there is a deviation with the in situ measurements.

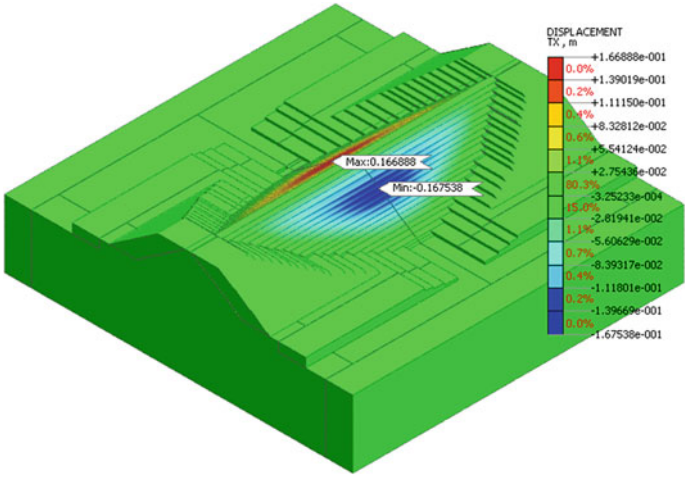

Fig. 7 Horizontal displacement after construction of rockfill layers

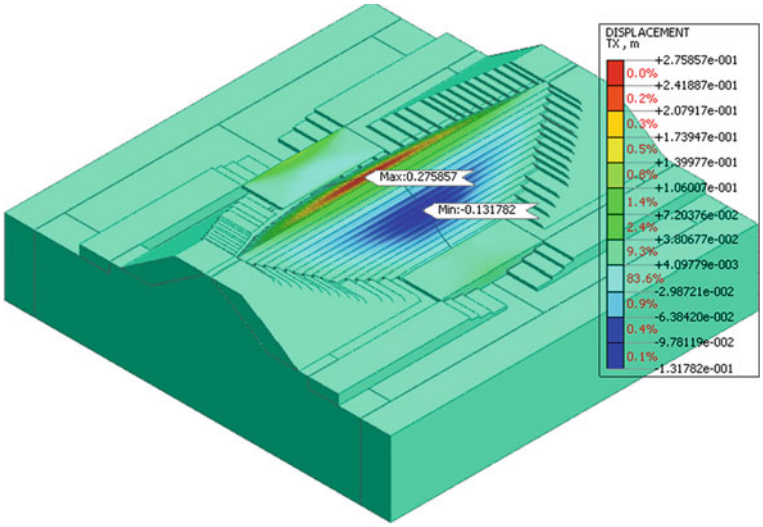

Fig. 8 Horizontal displacement after adding the water pressure

Fig. 9 Horizontal Deformation at 55 m from the dam base

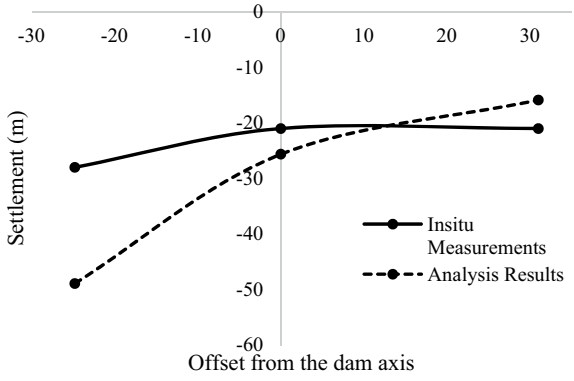

Fig. 10 Horizontal Deformation at 35 m from the dam base

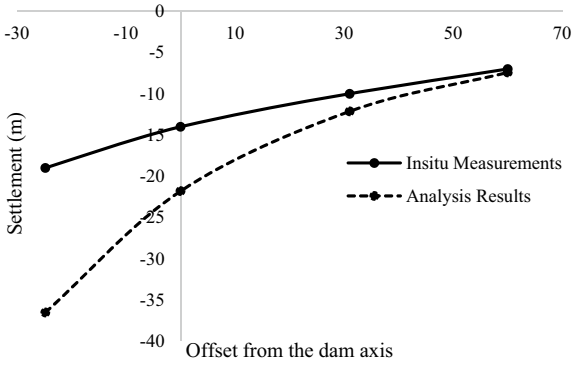

5 Conclusion

It is crucial to develop an accurate finite element model to depict the behavior of the actual dam which would be used to assess the stability under extreme loading conditions. The material behavior pays an important role in the accuracy of the dam response. According to this study, it can be concluded that the Duncan and Chang EB model is able to correctly map the behavior of the rockfill material. Furthermore, it is important to note that a linear elastic material behavior for concrete material would be sufficient to be considered in the analysis.

The results show the importance of adopting the construction sequence when developing finite element models for analysis under extreme loading conditions. As expressed precisely, without construction stages, the results obtained have large errors which is around 55% deviation to the in situ measurements, whereas when the construction sequence is considered, the results agree well with the in situ measurements.

The horizontal deformation variation pattern obtained through the finite element analysis agrees with the in situ measurements. But when the values are compared, there are deviations present. The in situ measurements of the horizontal deformation are obtained through electromagnetic probes. Therefore, small errors could be present when obtaining readings.

Acknowledgements This research was supported by the Mahaweli Authority by providing the required data. The authors would like to express their sincere appreciation to the Director of the Mahaweli Authority Engineer S. R .K. Aruppola and the staff members.

References

1. Seiphoori A, Haeri SM, Karimi M (2011) Three-dimensional nonlinear seismic analysis of concrete faced rockfill dams subjected to scattered P, SV, and SH waves considering the dam–foundation interaction effects. Soil Dyn Earthquake Eng 31:792–804
2. Xu B, Zou D, Liu H (2012) Three-dimensional simulation of the construction process of the Zipingpu concrete face rockfill dam based on a generalized plasticity model. Comput Geotech 43:143–154
3. Yu Y, Zhang B, Yuan H (2007) An intelligent displacement back-analysis method for earth-rockfill dams. Comput Geotech 34:423–434
4. Zhang B, Wang JG, Shi R (2004) Time-dependent deformation in high concrete-faced rockfill dam and separation between concrete face slab and cushion layer. Comput Geotech 31:559–573
5. Zhou W, Hua J, Chang X, Zhou C (2011) Settlement analysis of the Shuibuya concrete-face rockfill dam. Comput Geotech 38:269–280
6. Zou D, Zhou Y, Ling H, Kong X, Xu B (2012) Dislocation of face-slabs of Zipingpu concrete face rockfill dam during Wenchuan earth quake. J Earthquake Tsunami 6(2):1250007

Detection of Concrete Surface Crack Depth Using Ultrasonic Pulse Velocity (UPV) Methods

B. M. K. L. K. Basnayake, A. R. M. H. B. Amunugama, and U. B. Attanayake

Abstract Surface cracks are one of the most commonly observed distresses in concrete structures. Even though the crack depth is an important parameter to evaluate the depth of degradation and section capacity, only crack length and width are commonly documented. The typical ultrasonic pulse velocity (UPV)-based test setup available for crack depth measurement uses compression waves and two transducers, as a transmitter and a receiver. Since the crack depth measurement uses an indirect mode of transmission and requires a good coupling with the concrete surface, the implementation of this system is challenging. In this study, the feasibility of using a commercially available ultrasonic tomography equipment with an array of dry-point-contact shear wave transducers to estimate the depth of concrete surface opening cracks was evaluated under laboratory conditions. UPV data was collected on three concrete slab specimens with known notch depths using different transducer arrangements. The data was processed to identify the impact of notch depth and the transducer combinations on the notch depth calculation. Later, the depth of longitudinal cracks in two prestressed concrete girders was evaluated using the same ultrasonic tomography equipment. The results are promising and require further studies to develop guidelines to effectively use this technique for assessing crack depth in various components.

Keywords Crack depth · Longitudinal waves · Multi-array transducers · Shear waves · Tomography · Ultrasonic pulse velocity

1 Introduction

Typical longitudinal cracks in prestressed concrete (PC) box- and I-beams are shown in Fig. 1. The length and width of cracks are documented during the biennial inspection. Even though the crack depth is an important parameter to determine the depth of degradation and potential impacts on embedded reinforcing steel and prestressing

B. M. K. L. K. Basnayake · A. R. M. H. B. Amunugama · U. B. Attanayake (✉)
Western Michigan University, Kalamazoo, MI, USA
e-mail: upul.attanayake@wmich.edu

R. Dissanayake et al. (eds.), *12th International Conference on Structural Engineering and Construction Management*, Lecture Notes in Civil Engineering 266,
https://doi.org/10.1007/978-981-19-2886-4_13

(a) PC box-beam: Longitudinal cracks at the bottom flange

(b) PC I-beam: Longitudinal cracks along the bottom flange

Fig. 1 Typical crack types observed in prestressed concrete beams

strands, an accurate estimation of crack depth is challenging without extracting cores. Deep surface cracks in PC beams could easily expose prestressing strands and reinforcing steel to chloride-laden moisture and promote corrosion. Due to lack of information and procedures to measure surface crack depths, the typical approach is to disregard the strands adjacent to the crack(s) during beam capacity calculation. Hence, the quantification of crack length and depth is essential for the accurate estimation of beam capacity.

Ultrasonic pulse velocity (UPV)-based nondestructive evaluation (NDE) techniques are commonly used for assessing concrete quality and uniformity [3]. Several studies have been conducted to evaluate the capabilities and limitations of using UPV-based methods to determine the depth of surface cracks or notches that simulate the surface cracks [4–8, 11, 12, 16]. Majority of these studies used commercially available UPV devices with two transducers and compression waves that required using a coupling agent between the concrete surface and the transducers. In this study, the feasibility of calculating crack depth using the data collected from a commercially available tomography equipment with an array of dry-point-contact shear wave transducers was evaluated. This device was developed and commonly used for evaluating concealed anomalies in concrete members and posttension ducts. UPV data was collected on three concrete slab specimens with known notch depths using different transducer arrangements. The data was processed to identify the impact of notch depth and the transducer combinations on the calculated notch depth. This article presents (i) a summary of crack depth evaluation methods, (ii) crack depth evaluation using tomography data collected using laboratory specimens and (iii) the implementation of the procedures on two PC I-beams to calculate the depth of longitudinal cracks.

2 Calculation of Concrete Surface Crack Depth Using UPV Data

Figure 2 shows two commercially available UPV measurement systems, one with only two transducers and the other with an array of transducers. Longitudinal or compression waves, shear waves and surface waves are the three major stress wave

(a) Proceq Pundit Lab - Two-transducer system (b) MIRA A1040 device - Multi-array transducer system [1]

Fig. 2 Commercially available UPV measurement systems

types generated in a solid mass during the application of UPV method. Since the particle motion of a surface wave is restricted to near surfaces, the depth of penetration of the surface waves is smaller compared to the other two types. Longitudinal waves are faster than the shear waves [5]. Even though longitudinal waves are faster, the amplitude and energy of shear waves are comparatively greater [13]. With a two-transducer system, stress waves are generated by a transducer placed on the concrete surface, i.e. transmitter. These stress waves reflected from various boundaries (reflectors within the concrete mass) are captured by a second transducer, i.e. receiver. The wave velocity is calculated using the length of the wave travel path and the travel time of the wave between the transmitter and the receiver (time of flight).

2.1 The Application of Two-Transducer Systems

The two-transducer systems have one acting as the transmitter and the other as the receiver. Figure 2a shows Proceq Pundit Lab, a commercially available two-transducer system. A coupling agent is required to establish a proper contact between the specimen surface and the transducers. Transducers are designed to generate and capture longitudinal waves. Literature presents different transducer arrangements to calculate the depth of cracks that are perpendicular to the surface. Figure 3 shows one-transducer arrangement proposed by Bungey et al. [5] and two-transducer arrangements proposed in BS 1881-Part 203 [4, 11] with relevant equations to calculate crack depth (h). Several other transducer arrangements have been improvised from these basic transducer arrangements to calculate surface crack depth (h) [11].

Surface crack depth measurement with a two-transducer system requires arranging transducers for indirect wave transmission, which is considered less reliable than direct transmission due to poor signal strength, scattering due to discontinuities, near-surface influence and travel path uncertainties [5]. BS 1881-Part 203 states that the wave velocity calculated based on the indirect transmission is about 5 to 20% less

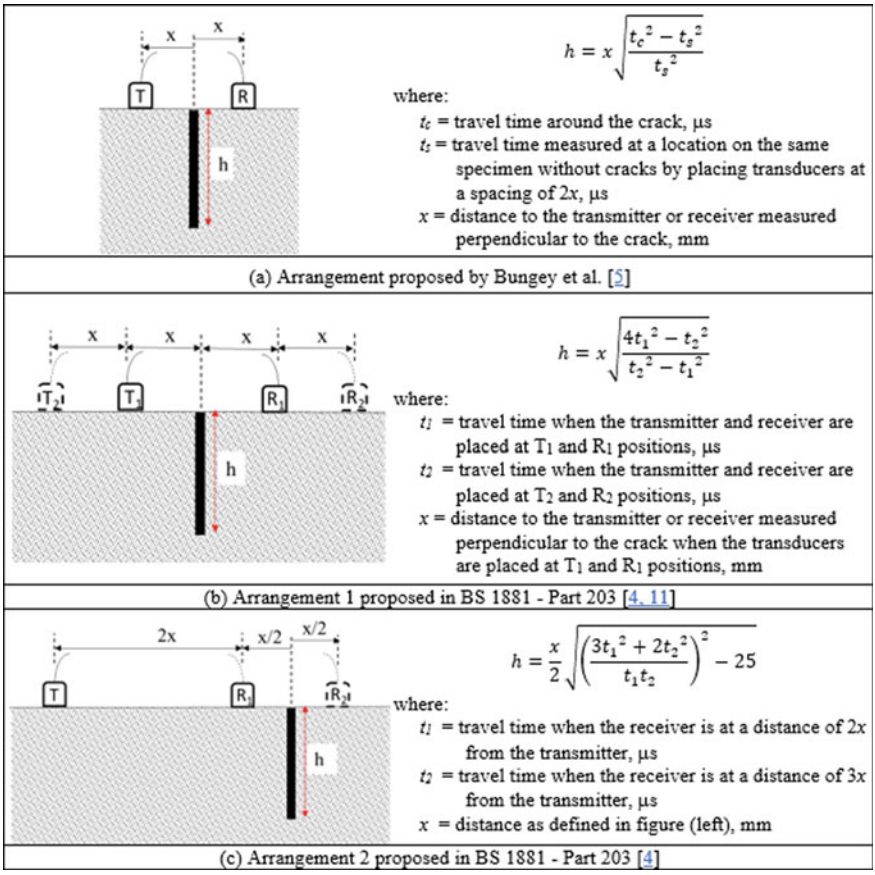

Fig. 3 Transducer arrangements to measure surface crack depth (T: Transmitter and R: Receiver)

than velocity from the direct transmission. Specimen details, maximum aggregate size, transducer spacing and surface condition affect the accuracy of the calculated surface crack depth [8, 18]. Recommendations for transducer spacing are provided in literature to improve the reliability of the UPV readings acquired through indirect transmission. The BS 1881-Part 203 and [14] recommend a minimum distance of 100 mm and 150 mm between the transducers for concrete with a maximum aggregate size of 20 mm or less and for concrete with a maximum aggregate size between 20 and 40 mm, respectively. Yaman et al. [18] recommended recording the travel time using a minimum of four measurement points on uncracked concrete with the first receiver location being at least two times the wavelength (λ) and the subsequent distances increased by at least one-half of the wavelength (i.e. 2λ, 2.5λ, 3λ and 3.5λ) to maintain the maximum error at or below 2%. Although the basic two-transducer UPV testing systems are successful in providing data for the calculation of surface

crack depths in concrete under laboratory settings, the application in the field with limited space to maintain the required transducer spacing is challenging.

2.2 The Application of Multi-array Transducer Systems

In contrast to the basic two-transducer system, a multi-array transducer system or the so-called tomography device includes an array of dry-point-contact shear wave transducers that can transmit and receive shear waves in a sequential mode to provide a wide aperture. Shear waves result in lower signal attenuation and backscattering compared to longitudinal waves. Also, because of having an array of transducers (with 24 or 48 transducers), multiple measurements made at a single location using shear waves improve the measurement accuracy compared to a single measurement with a typical compression wave two-transducer system. Figure 2b shows MIRA A1040 with 48 transducers, a commercially available ultrasonic shear wave tomography equipment [1]. The data collected on a grid can be used to generate B-, C- and D-scans. The fundamentals of data analysis and post-processing procedures for MIRA are discussed in References [2, 9, 10].

In comparison to the two-transducer system, limited studies have been conducted using multi-array transducer systems to estimate the depth of surface cracks. Helmerich et al. [6] evaluated the feasibility of using MIRA A1040 to detect surface notch and crack depths. The data was collected on a slab with a surface notch by placing the excitation direction parallel to the notch (i.e. placing the device perpendicular to the notch), as shown in Fig. 4a. The presence of the notch reduced the strength of backwall reflections compared to the backwall reflection observed on a specimen without a notch, as shown in Fig. 4b, c. Although signal disturbances were observed around the notch tip in the B-scans, significant reflections were absent to accurately estimate a depth. With the experience gained by scanning the notched

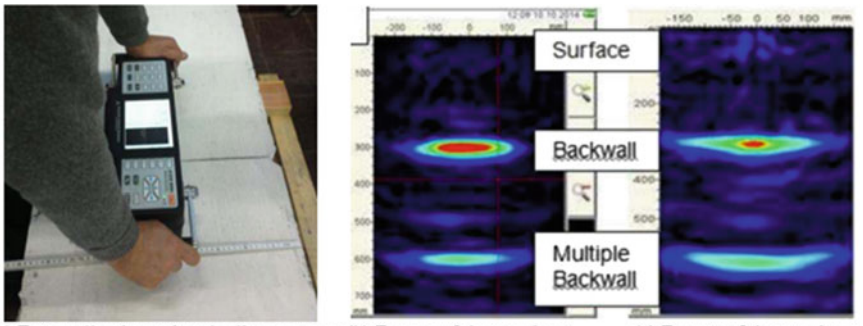

(a) Data collection using the linear array device on the specimen with notch (b) B-scan of the specimen without notch (c) B-scan of the specimen with notch

Fig. 4 Evaluation of the surface notch using MIRA [6]

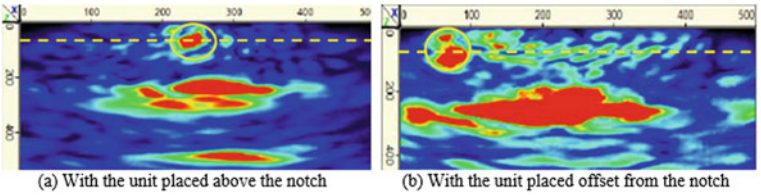

Fig. 5 B-scans recorded on a slab specimen with a 75 mm deep notch [12]

specimen, Helmerich et al. [6] used the same device to scan a slab specimen with a longitudinal crack on the top surface. This longitudinal crack was a result of a corroded rebar embedded within the specimen. An array of measurements with the excitation direction parallel to the longitudinal crack was recorded to reconstruct a B-scan. The surface wave transmission was disturbed when the crack was located directly below the array. However, Helmerich et al. [6] could not estimate the depth of the longitudinal crack.

Popovics et al. [12] used MIRA A1040 to scan a 250 mm thick concrete slab with a surface notch located at the centre of the top surface. MIRA B-scans were recorded at three notch depths: 10, 75 and 155 mm. For each notch depth, two MIRA scanning configurations were evaluated—scanning position directly above the notch and scanning position with the MIRA device offset from the notch. All the B-scans displayed signal disturbance at the notch tips. Both 10 and 75 mm deep notches showed better reflections compared to the 155 mm deep notch. Figure 5 shows the reflections observed at the notch tip for the specimen with a 75 mm deep notch. In addition, Popovics et al. [12] evaluated the performance of the MIRA device under field conditions using 8 concrete pavement panels with visible cracks. Strong backwall reflections were observed from 7 panels. However, the detection of surface cracking on these panels was challenging.

3 Evaluation of the Data Collected Using a Multi-array Tomography System for Crack Depth Detection

3.1 Device Description

The Pundit 250 Array (shown in Fig. 6a) is a commercially available multi-array transducer device that is not standardized to measure surface crack depths. This device has 3 rows and 8 columns of dry-point-contact shear wave transducers. When a single column of transducers triggers shear waves, the echoes are received by the remaining columns. This process starts from the left-most column, as shown in Fig. 6b, and continues sequentially up to the 7th column during a single measurement. Since the columns on the left to the trigger column do not record data, the first column works only as a transmitter while the 8th column works only as a receiver. Therefore,

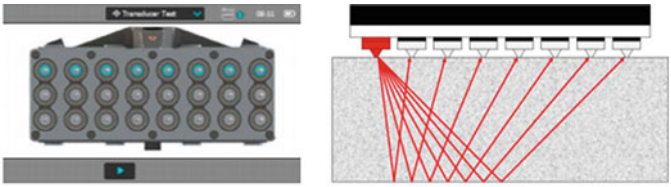

(a) 3 rows and 8 columns of transducers (b) Schematic of shear wave travel path

Fig. 6 Proceq Pundit 250 Array unit [15]

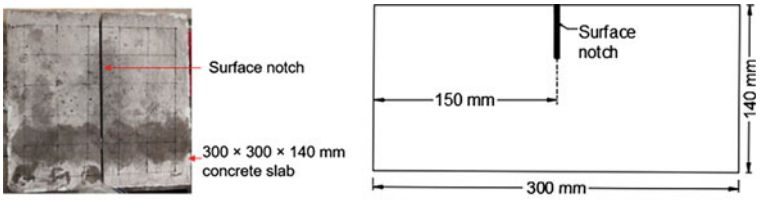

(a) Slab specimen with a surface notch (b) Elevation view of the slab with the notch

Fig. 7 Concrete slab specimen details

each measurement produces a total of 28 A-scans that are mapped to produce B-scans for real-time display. The nominal shear wave frequency is 50 kHz [15].

3.2 Laboratory Specimen Details

Three 300 × 300 × 140 mm concrete slab specimens were fabricated. A 300 mm long and 3.94 mm wide saw cuts (notches) were made along the top surface centerline of each specimen to simulate surface cracks, as shown in Fig. 7. The depth of notches was 12.70, 31.75 and 44.45 mm.

3.3 Data Collection and Analysis Procedure

Data was collected by placing the array in three distinct arrangements:

1. *Arrangement 1*: Excitation direction is parallel to the notch, and the unit is placed symmetrically over the notch (Fig. 8a).
2. *Arrangement 2*: Excitation direction is parallel to the notch with the unit placed offset from the notch (Fig. 8b).
3. *Arrangement 3*: Excitation direction is perpendicular to the notch, and the unit is placed symmetrically over the notch (Fig. 8c).

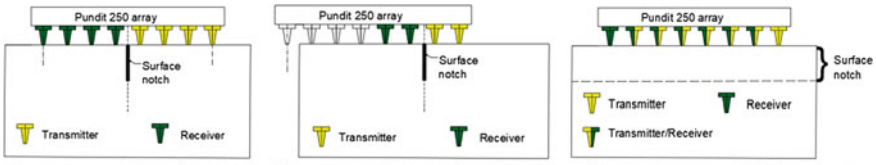

(a) *Arrangement 1*: Transmitters: T_1 to T_4, Receivers: T_5 to T_8 (b) *Arrangement 2*: Transmitters: T_5 to T_6, Receivers: T_7 to T_8 (c) *Arrangement 3*: Transmitters: T_1 to T_7, Receivers: T_2 to T_8

Fig. 8 Transducer arrangements on slab specimens and transducer selection for data analysis

The objective of all three scanning arrangements was to evaluate the impact of each arrangement on the evaluation of notch depth. *Arrangement 2* is used to evaluate the feasibility of estimating the notch depth with an instrument offset from the notch and with the absence of data from a set of transducers. The data was analysed using a propriety software, *InterSAFT*, which is commercially available as Pundit Vision [17]. The data was processed to reconstruct B-scans, and the notch depths were estimated. When processing the scans, columns of transducers in the array were selected as transmitters or receivers to obtain a selected set of data to construct reliable B-scans. Figure 8 shows the selection of transducers for the analysis of data collected using the three-transducer arrangements. For *Arrangement 1*, T_1 to T_4 columns and T_5 to T_8 columns were selected as transmitters and receivers, respectively. For *Arrangement 2*, T_5 to T_6 columns and T_7 to T_8 columns were selected as transmitters and receivers, respectively. For *Arrangement 3*, T_1 to T_7 columns and T_2 to T_8 columns were selected as transmitters and receivers, respectively.

3.4 Results and Discussion

3.4.1 Reconstructed B-Scans

Figure 9 shows the reconstructed B-scans using the data collected with three transducer arrangements. The physical location of the notch tip in each slab is indicated by a red dashed line.

Figure 9a shows the processed B-scans for the three slabs using *Arrangement 1* data. As shown in Fig. 9a, the backwall reflection is observed at the 140 mm depth in all the slabs. Significant reflections are observed around the tips of 12.70 and 31.75 mm deep notches. In the slab with 44.45 mm deep notch, a low-intensity reflection is observed at the notch tip. These reflections are observed at the vertical centrelines of the B-scans (about $x = 0.1$ m). The reflection around the notch tip locations is centred about their corresponding notch tip locations in the slabs with 31.75 and 44.45 mm deep notches, except in slab with 12.70 mm deep notch. Figure 9b shows the processed B-scans for the three slabs using *Arrangement 2* data. In all the slabs, the backwall reflection is observed at the 140 mm depth. Significant reflections are observed around the notch tips in all the slabs. These reflections are observed at

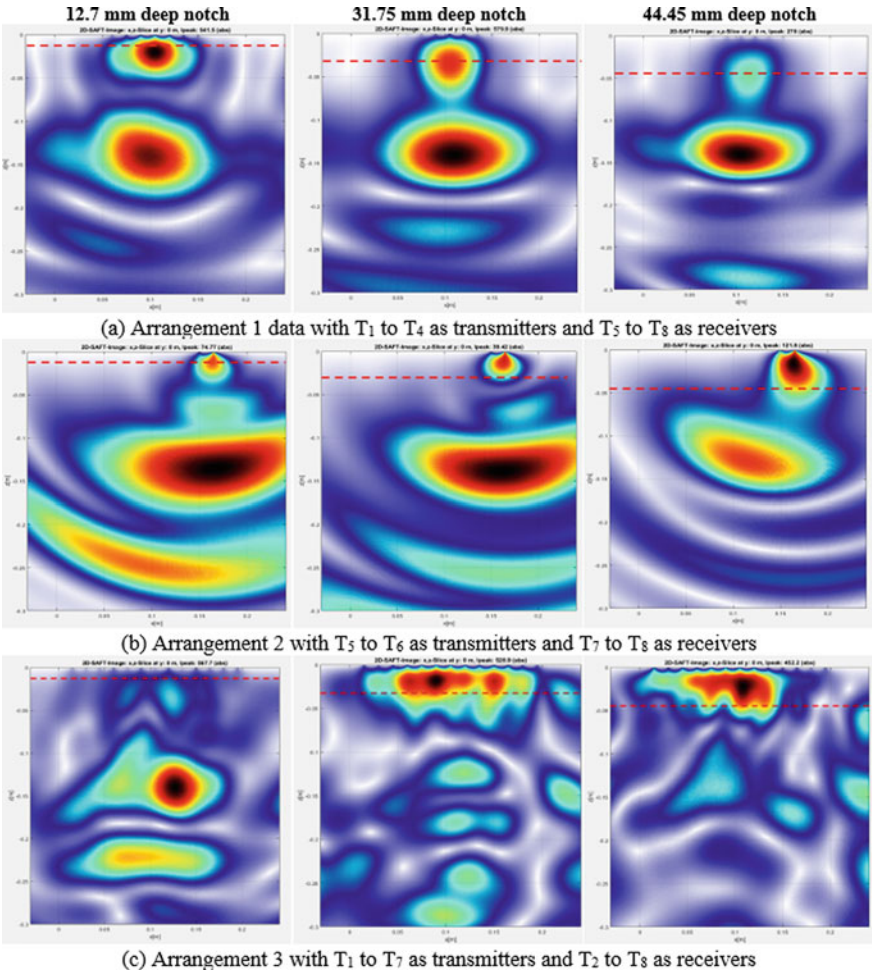

Fig. 9 B-scans of slabs reconstructed using the transducer arrangements

an offset from the vertical centreline of the B-scans (between $x = 0.15$ m and $x = 0.2$ m), as expected from the offset scanning configuration used in *Arrangement 2*. The bottom of the reflections corresponds to their physical notch tip locations in the slabs with 31.75 and 44.45 mm deep notches, except in the slab with 12.70 mm deep notch. Figure 9c shows the processed B-scans for all three slabs using *Arrangement 3* data. The backwall reflection is only observed in the slab with 12.70 mm deep notch. Distinct reflections are observed at the notch tip in the slabs with 31.75 and 44.45 mm deep notches, except in the slab with 12.70 mm deep notch. The bottom of these reflections lies at the notch tip locations in the slabs.

Table 1 Estimated notch depths from B-scans

Transducer arrangement	Estimated notch depth		
	12.70 mm	31.75 mm	44.45 mm
Arrangement 1	19.28 mm	33.83 mm	44.10 mm
Arrangement 2	22.70 mm	23.99 mm	41.96 mm
Arrangement 3	–	33.00 mm	44.95 mm

3.4.2 Notch Depth Estimation

Based on the processed B-scans in Fig. 9, notch depths were estimated and are summarized in Table 1. The notch depth is estimated to the centre of the reflections in the B-scans developed from transducer *Arrangement 1* data. The notch depth is estimated to the bottom of the reflections in the B-scans developed using transducer *Arrangement 2* and *Arrangement 3* data. For deeper notches (31.75 and 44.45 mm), all three-transducer arrangements produced approximate results to the actual notch depth.

3.4.3 Impact of Notch Depth on Shear Waves at the Surface

The presence of a surface crack disturbs the surface wave propagation. This can be evaluated by analysing surface wave profile around a crack. The surface wave module in *InterSAFT* provides a graphical output indicating the presence of disturbances to the surface waves as shown in Fig. 10. Figure 10a shows a contour plot with straight, horizontal colour bands indicating the presence of undisturbed shear waves at the surface. Figure 10 b and c show the impact of notch depth and transducer arrangement on surface wave propagation. As indicated by the discontinued colour bands in Fig. 10b, deeper notches (31.75 and 44.45 mm) significantly impacted the propagation of shear waves at the surface when the transducer array is placed symmetrically over the notch with the excitation direction parallel to the notch. The influence of the shallower notch (12.70 mm) is minimal and clarifies the reasons for observing greater inaccuracies in estimating the depth of shallower cracks. As shown in Fig. 10c, irrespective of the notch depth, undisturbed shear waves are present at the surface when the unit is placed symmetrically over the notch with the excitation direction perpendicular to the notch. The results show that the transducer array needs to be placed symmetrically over the notch with the excitation direction parallel to the notch for the detection of notches.

4 Field Implementation

The Pundit 250 Array was used to scan a longitudinal crack on the inclined face of the bottom flange of two PC I-beams: (1) southern exterior beam of the bridge (SN 424)

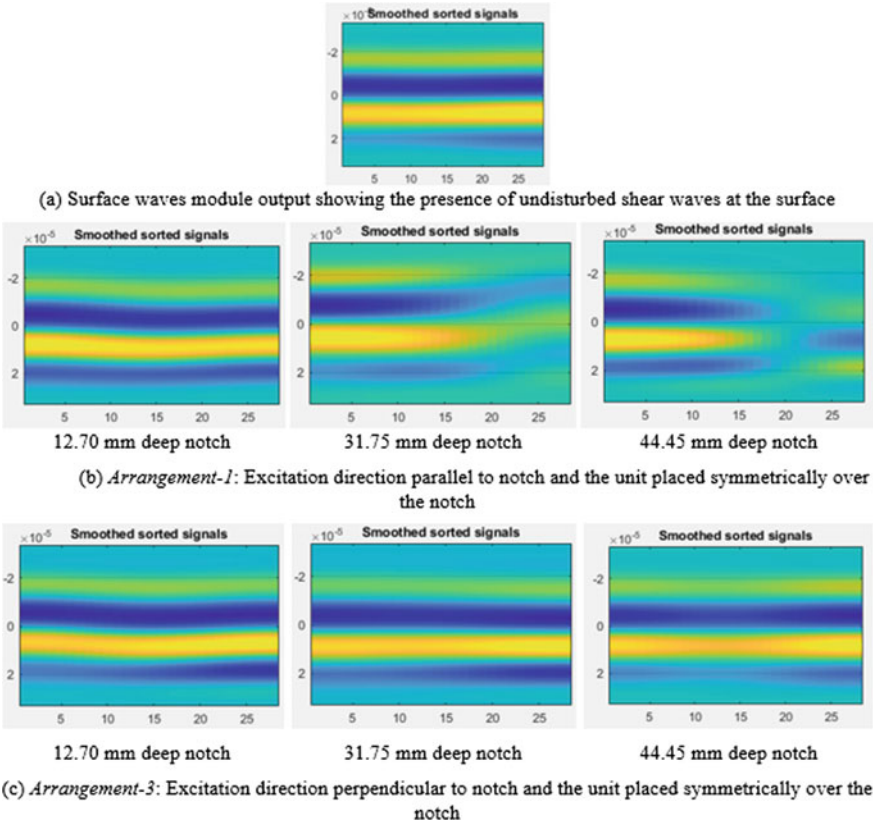

(a) Surface waves module output showing the presence of undisturbed shear waves at the surface

12.70 mm deep notch 31.75 mm deep notch 44.45 mm deep notch

(b) *Arrangement-1*: Excitation direction parallel to notch and the unit placed symmetrically over the notch

12.70 mm deep notch 31.75 mm deep notch 44.45 mm deep notch

(c) *Arrangement-3*: Excitation direction perpendicular to notch and the unit placed symmetrically over the notch

Fig. 10 The impact of notch depth and transducer arrangement on surface wave propagation

that carries the Lincoln Road over I-75 southbound and (2) southern exterior beam of the bridge (SN 2618) that carries M-57 Road over Flint River. Figure 11 shows the measurement grid used to collect the UPV data and the position of the longitudinal crack with respect to the measurement grid. The unit was placed symmetrically over the crack with the excitation direction parallel to the crack (*Arrangement 1*). The data was processed to reconstruct the B-scans, and the crack depth was estimated at each measurement location. For fascia beam of SN 424, the longitudinal crack depth varied between 25.06 and 56.85 mm. For fascia beam of SN 2618, the longitudinal crack depth varied between 17.89 and 58.85 mm. Field verification of the crack depth was not possible because the coring of in-service bridge beams is not allowed.

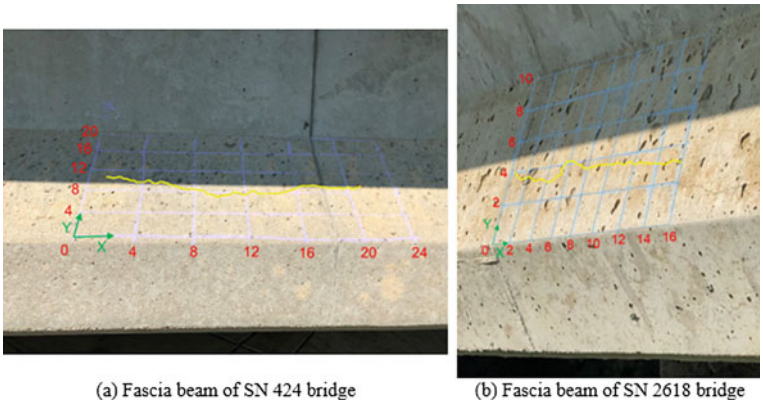

(a) Fascia beam of SN 424 bridge (b) Fascia beam of SN 2618 bridge

Fig. 11 Data collection on two prestressed concrete I-beams with a longitudinal crack (yellow line shows the longitudinal crack.)

5 Summary, Conclusions and Recommendations

Multi-array shear transducer devices are being evaluated to measure the depth of surface cracks. Multi-array devices provide a large aperture and an array of dry-point-contact transducers to overcome the shortcomings in the indirect transmission of longitudinal waves used in two-transducer UPV devices. This study demonstrated the impact of various arrangements of a multi-array transducer device (Proceq Pundit 250 Array) to collect data and the selection of transducer groups as transmitters and receivers to reconstruct B-scans and identify the indications of the presence of surface cracks in concrete specimens. Three concrete slab specimens with known notch depths (12.70, 31.75 and 44.45 mm) that simulated surface cracks were used for this purpose. The UPV data was collected on the slab specimens and processed to reconstruct the B-scans. The following are the findings of this study:

- Reflections with varying intensity were observed in the B-scans at locations corresponding to the actual notch tip locations. However, reflections produced at the actual notch tip locations were distributed over a region. Hence, the prediction of a crack depth would be approximate and subjective.
- Comparable notch depth estimations were made based on the reconstructed B-scans for deeper notches (31.75 and 44.75 mm). Notches with depths less than 31.75 mm were detected, but the degree of accuracy needs to be further evaluated.
- The impact of notch width on notch depth measurements is unknown since a constant notch width of 3.94 mm was maintained in all three slabs.
- Use of *Arrangement 1* on PC I-beams with longitudinal cracks produced the necessary data to estimate the surface crack depth. However, the accuracy of estimated crack depth was not verified since extracting cores from PC beams of in-service bridges was not allowed. Even though not verified through coring, the estimated crack depth can be conservatively used to evaluate the beam capacity.

The findings of this study are based on a set of data collected from a limited number of specimens. This study needs to be extended to develop implementation guidelines for various applications, generate a large data set to enhance confidence and identify potential implementation challenges.

References

1. ACS (2021) MIRA A1040 operation manual. A1040 MIRA. https://acs-international.com/product/a1040-mira/. Accessed on 7 Apr 2021
2. Attanayake U, Dissanayake A, Mayer K, Wiggenhauser H (2018) SAFT analysis and phase evaluation procedures using ultrasonic shear wave imaging device (MIRA) data. In: 97th TRB annual meeting, Washington, DC, January 07–11, 2018
3. ASTM International (2016) C597-16: standard test method for pulse velocity through concrete. ASTM International, West Conshohocken, PA, USA
4. Baehaki Andi M, Yohannes GR (2019) Experimental study of crack depth measurement of concrete with ultrasonic pulse velocity (UPV). In: IOP conference series: materials science and engineering, p 673
5. Bungey JH, Millard SG, Grantham MG (2006) Ultrasonic pulse velocity methods (Chap. 3). In: Testing of concrete, 4 th ed. Taylor and Francis, Abingdon, pp 51–81
6. Helmerich R, Mielentz F, Milmann B, Adam L, Villalobos S, Guimaraes M, Wiggenhauser H (2015) Detection of cracks perpendicular to the surface using acoustic methods. In: Proceedings in international symposium non-destructive testing in civil engineering (NDT-CE), Berlin, Germany, September 15–17, 2015
7. In CW, Arne K, Jin-Yeon K, Kurtis KE, Jacobs LJ (2017) Estimation of crack depth in concrete using diffuse ultrasound: validation in cracked concrete beams. J Nondestruct Eval 36(4)
8. Kalyan T, Kishen CJM (2014) Experimental evaluation of cracks in concrete by ultrasonic pulse velocity. In: Asia pacific conference on non-destructive testing (14th APCNDT), Mumbai, India, November 18–22, 2013
9. Mayer K, Langenberg KJ, Krause M, Milmann B, Mielentz F (2008) Characterization of reflector types by phase-sensitive ultrasonic data processing and imaging. J Nondestr Eval 27:35–45
10. Mayer K, Chinta PK, Langenberg KJ, Krause M (2012) Ultrasonic imaging of defects in known anisotropic and inhomogeneous structures with fast synthetic aperture methods. In: Proceedings of 18th world conference on nondestructive testing, Durban, South Africa, April 16–20, 2010
11. Pinto R, Medeiros A, Padaratz IJ, Andradfe PB (2010) Use of ultrasound to estimate depth of surface opening cracks in concrete structures. e-J Nondestruct Test (NDT) ISSN 1435-4934
12. Popovics JS, Roesler JR, Bittner J, Amirkhanian AN, Brand AS, Gupta P, Flowers K (2017) Ultrasonic imaging for concrete infrastructure condition assessment and quality assurance. Illinois Department of Transportation (SPR), Urbana, IL
13. Popovics JS, Abraham O (2010) Surface wave techniques for evaluation of concrete structures (Chap. 20). In: Non-destructive evaluation of reinforced concrete structures, vol 2. Woodhead Publishing Series in Civil and Structural Engineering, pp 441–465
14. Proceq (2014) Pundit Lab PL-200 ultrasonic pulse velocity and Pundit PL-200PE Ultrasonic Pulse Echo. Schwerzenbach, Switzerland
15. Proceq (2017) Proceq Pundit operating instructions. Schwerzenbach, Switzerland

16. Ramamoorthy SK, Kane Y, Turner JA (2004) Ultrasound diffusion for crack depth determination in concrete. J Acoust Soc Am 115(2):523–529
17. Screening Eagle Technologies (2021) Screening eagle acquires ultrasound imaging software solution. Screening Eagle. https://www.screeningeagle.com/en/about-us/news/2307. Accessed on 31 July 2021
18. Yaman IO, Inci G, Yeseiller N, Aktan HM (2001) Ultrasonic pulse velocity in concrete using direct and indirect transmission. ACI Mater J 98(6):450–457

Load Testing and Rating of a Concrete Arch Bridge

C. Hutchinson, A. Peiris, and I. Harik

Abstract The bridge carrying 19th Street over Yellow Creek in Middlesboro, Kentucky, is a 16.8 m (55′) long and 14.8 m (48′–6″) wide concrete arch bridge constructed in 1943. Structural plans for the bridge are unavailable. This paper details the methods used to determine the safe live load carrying capacity of the bridge based on diagnostic load testing. Load Factor Ratings were determined for legal truck loads in accordance with the AASHTO Manual for Bridge Evaluation utilizing a 2D Finite Element model and then adjusted based on field measured strain data. Despite substandard theoretical load ratings, load testing revealed that the bridge has sufficient capacity to carry legal traffic without restriction.

Keywords Concrete arch · Load testing · Load rating · Bridge test

1 Introduction

Irrespective of how carefully designed and constructed, the load carrying capacity of a bridge cannot be assumed constant throughout its life. Because of this, the Federal Highway Administration (FHWA) requires that bridges be inspected at least every 24 months and possess a load rating quantifying their safe live load capacity [5] determined in accordance with the American Association of Highway and Transportation Officials' (AASHTO) Manual for Bridge Evaluation (MBE).

The MBE [2] provides detailed guidance on analytically assessing the capacity of bridges based on available design information as well as any changes to the structure found during field inspection. Generally, the result of this analysis is a quantification of the safe load carrying capacity of the bridge in the form of a Rating Factor (RF). The RF is essentially the ratio of the analytically determined capacity (less permanent load effects) to the live load effect of the truck being rated. For routine load rating purposes, RFs may be divided into two categories: Inventory Ratings and Operating Ratings. An Inventory Rating describes the maximum live load which a bridge may

C. Hutchinson (✉) · A. Peiris · I. Harik
University of Kentucky, Lexington, KY, USA
e-mail: Cody.Hutchinson@uky.edu

R. Dissanayake et al. (eds.), *12th International Conference on Structural Engineering and Construction Management*, Lecture Notes in Civil Engineering 266,
https://doi.org/10.1007/978-981-19-2886-4_14

support over an indefinite period of time. Meanwhile, the Operating Rating describes the maximum load a bridge may safely support but this loading may shorten the life of the bridge if allowed for an indefinite period of time [2].

Theoretical RFs determined in accordance with the MBE are, by nature, conservative due to many assumptions that are made in the methods outlined for analysis [2]. These RFs become even more conservative when bridges lack structural plans and/or material properties as engineers are required to make further assumptions taking care not to overestimate any parameter. The compounding effects of these conservative assumptions may lead to exaggerated underestimates of RFs and needless postings for reduced loads. Such load postings are undesirable as re-routing traffic can have consequences (e.g., congestion, overloading nearby structures, etc.).

However, due to advances in instrumentation and data acquisition technology, field testing as a means of load rating has become a viable option in many cases. Field testing can be considered when theoretical load ratings are low, structural plans/details are missing or incomplete, and/or when an analytical model can be developed but confidence in the accuracy is low (2, [1]). Such testing allows for the conservative theoretical load ratings of a bridge to be modified based on measurements of the actual bridge behavior. In the vast majority of cases, field testing allows for the theoretical load ratings to be increased as the response of bridges is oftentimes better than predicted by theory (2, [1]). Because of the usefulness of load testing for load rating, the MBE provides an entire chapter detailing the benefits and methods used for load testing. Additionally, the MBE provides an outline of a general load testing procedure to streamline the process of developing a load testing program.

In this case study, the development of a load testing program and subsequent load rating of a concrete arch bridge without design plans will be discussed. This includes a discussion on the instrumentation layout and load cases used for testing. Details on the reusable, rapidly deployable, and wireless strain measurement and data acquisition system are also provided. Lastly, the development of the Finite Element (FE) model, theoretical load ratings, and field adjusted load ratings are discussed.

2 Theoretical Load Rating

Within the MBE, there are three rating methodologies: Allowable Stress Rating (ASR), Load Factor Rating (LFR), and Load and Resistance Factor Rating (LRFR). Although LRFR is comparable to modern LRFD design practices, many bridges still in service were designed prior to the widespread implementation of LRFD. As a result, it is a common practice to rate such bridges using ASR or LFR methods. The arch bridge being rated herein was rated using LFR as it predates the LRFD methodology. The LFR equation for the Rating Factor (RF) is provided here:

$$\mathrm{RF} = \frac{C - A_1 D}{A_2 L(I + 1)} \tag{1}$$

Within this equation, C represents the capacity of the member being rated determined in accordance with the AASHTO Standard Specifications [3]. Meanwhile, D and L are the dead and live load effects ascribed to the member, respectively. I is the impact factor calculated in accordance with the AASHTO Standard Specifications [3]. The factors A_1 and A_2 are the dead and live load factors, respectively. For LFR, A_1 is 1.3 while A_2 varies depending on the rating level: 2.17 for inventory and 1.3 for operating [2].

The AASHTO standard HS20 truck and four Kentucky Legal Trucks (KY Type 1–4) were used for load rating. These trucks (shown in Fig. 1) were applied to the analytical model to determine the live load effects, L, for calculating the RF.

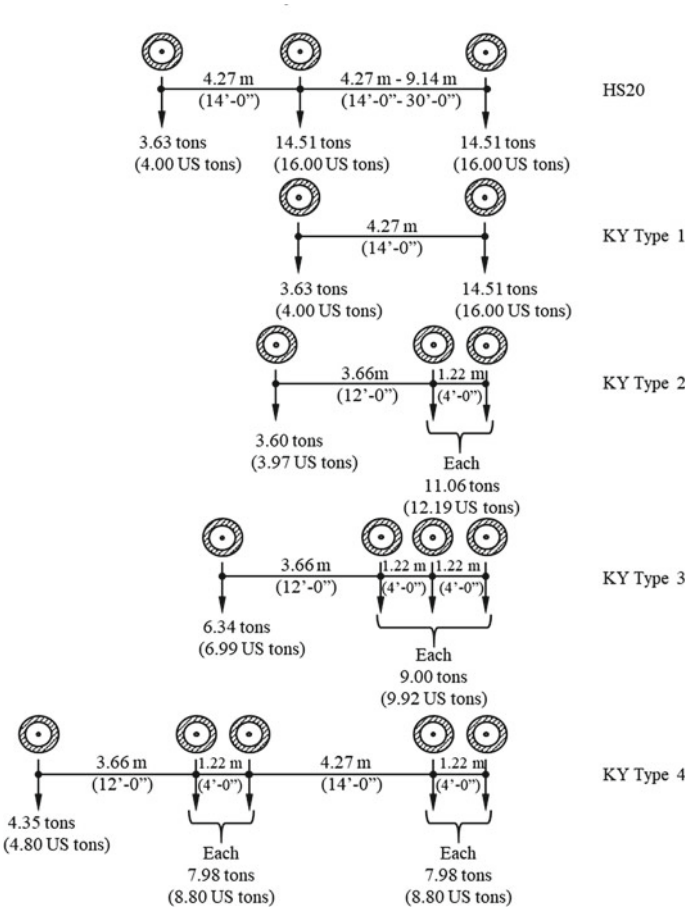

Fig. 1 Truck axle weights and spacings for load rating

3 Load Rating Through Load Testing

When load rating through load testing, the calculated load ratings, RF_C, found in accordance with Eq. 1 (for LFR) are modified using an adjustment factor, K, to arrive at the rating factor based on field tests results, RF_T, as shown in Eq. 2.

$$RF_T = RF_C K \tag{2}$$

The field test adjustment factor, K, is further broken down into two sub factors, K_a and K_b, as shown in Eq. 3.

$$K = 1 + K_a K_b \tag{3}$$

K_a takes into account the results from the load test as well as the relevant cross-sectional properties of the member. As such, K_a can be expressed with the following equation:

$$K_a = \frac{\varepsilon_C}{\varepsilon_T} - 1 \tag{4}$$

where ε_T is the maximum measured strain during the load testing and ε_C is the calculated strain corresponding to the same loading conditions which produced ε_T [2]. It should be noted that K_a can be negative if the bridge reacts undesirably to the testing.

The second subfactor, K_b, considers how well analysis is believed to accurately capture the bridge behavior. This factor takes on a value between 0 and 1 where 0 means that the behavior of the bridge, as seen through testing, is not able to be explained or modeled while a value of 1 means that measured data is easily explained and can be extrapolated to higher loads. The MBE provides guidance on the selection of a K_b factor based on two criteria: (1) if member behavior can be extrapolated to 1.33 times the unfactored rating load and (2) the ratio of calculated test vehicle effect to the calculated rating load effect [2].

4 19th Street Concrete Arch Bridge

The bridge in question is located in Middlesboro, Kentucky, and carries 19th Street over Yellow Creek. The bridge conveys 2 lanes of traffic (one in each direction) with a curb-to-curb width of 14.8 m (48′–6″). The bridge also has cantilevered sidewalk overhangs on either side. With an estimated construction date of 1943, the bridge has no known design nor as-built plans. By inspection, the bridge is a simple concrete arch with a clear span 16.8 m (55′), rise of 4.27 m (14′), and 30° skew. Without structural plans, the arch is estimated to be 0.61 m (2 ft) thick based on field measurements. The bridge is shown in Fig. 2.

Fig. 2 19th Street Bridge in Middlesboro, Kentucky

Fig. 3 Arch joint leaching and spalling

Inspection of the underside of the bridge revealed joints from segmented construction running parallel to the arch. Evidence of leaching and spalling were noted along the joints. Figure 3 shows typical deterioration of the arch.

5 Load Testing

The load testing of the 19th Street Bridge was carried out in accordance with the MBE. As a first step, a thorough inspection of the current in situ condition of the bridge was carried out. Such an inspection becomes vital when structural plans for the bridge are not available. The majority of findings from the pre-testing inspection are shown in Table 1.

In addition to measurements of the geometry of the bridge, rebound hammer testing was performed at 15 distinct locations along the arch. Testing indicated an average compressive strength of 27.6 MPa (4 ksi).

A preliminary finite element model was used to analytically determine safe test load limits for load testing. This 2D frame model approximated the arch as 50 straight line segments of a unit width and 0.61 m (2 ft) depth. Such a model has been

Table 1 Field-measured bridge geometry

Parameter	Value
	m (ft)
Clear span	16.8 (55.0)
Curb-to-curb width	14.8 (48.5)
Rise	4.27 (14.0)
Arch thickness	0.61 (2.0)

shown to be a reliable method of approximating arch behavior without significant computational effort [4, 7].

Diagnostic load testing allows for the load effects for a standard test truck weight/axle configuration to be used to adjust the predicted load effects based on an analytical model for any truck for which a rating is desired.

Reusable strain gages manufactured by Bridge Diagnostics, Inc. (BDI), were used to record the strain due to the test trucks. The Kentucky Transportation Cabinet (KYTC) provided two scale measured loaded tandem rear axle dump trucks as well as the traffic control. To capture as much of the bridge response as possible, 23 strain gages were placed in a grid pattern along the intrados of the arch. Gage placement was symmetric along the longitudinal centerline of the bridge as shown in Fig. 4.

This gage layout was selected to provide the strain profiles along the longitudinal and transverse centerlines of the bridge. These centerlines also contain the crown points at the center of the bridge and at the edge of the arch (see Fig. 4). These points were identified as the critical locations for load rating arch bridges in a research study published by the Delaware Center for Transportation [4].

For load rating, it was decided to use 7 single-truck and 6 two-truck static load cases to assess the bridge. Load case 1 had the truck straddling the longitudinal centerline of the bridge. Load case 2 had the truck offset 0.91 m (3 ft) to the West from the longitudinal centerline placing the tires directly over the centerline gages and the adjacent gage line. Load case 3 had the truck offset 2.74 m (9 ft) to the West from the centerline placing the tires over the two lines of gages adjacent to

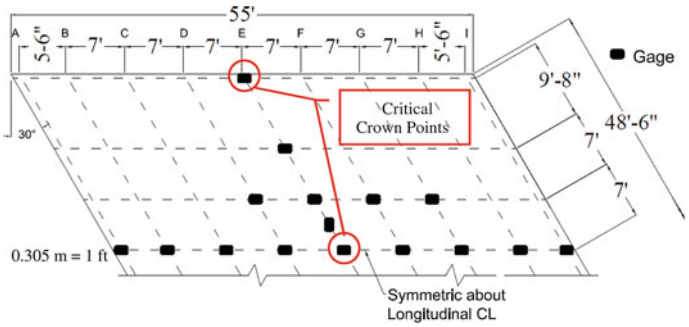

Fig. 4 Strain gage pattern for 19th street Bridge

the longitudinal centerline. Load case 4 had the truck as near the West sidewalk curb as possible such that the exterior tire line passed over the outermost gage. Load cases 5, 6, and 7 mirrored load cases 2, 3, and 4, respectively, about the longitudinal centerline. Three readings for each load case were taken by having the truck advance slowly and stop at lines D, E, and F (labeled in Fig. 4) for measurement. Three two-truck load cases had the trucks back-to-back at the transverse centerline of the bridge and (1) along the longitudinal centerline of the bridge, (2) by one sidewalk curb, and (3) by the opposing sidewalk curb. Two additional two-truck load cases placed the trucks side-by-side on either side of the longitudinal centerline to investigate multiple presence effects. Each of the single truck and side-by-side load cases were also repeated in the opposing direction resulting in a total of 21 tests.

The reusable strain gages are affixed to the bridge by metal tabs which are adhered to the concrete with an epoxy. The strain gages were connected to the BDI wireless nodes under the bridge which, in turn, connected wirelessly to the BDI base station located near the roadway. This base station then connected wirelessly to a laptop which served as the data acquisition system. The mostly wireless connectivity of this setup allowed for greater flexibility in the gage layout.

The axle placement on top of the bridge was marked to align with the gage locations under the bridge. Measurements of the truck dimensions were also taken. Both test trucks were nearly identical in weight with a gross weight of 31.66 tons (34.38 US tons) as shown in Fig. 5.

By using the BDI reusable strain gages and the companion data acquisition software, it was possible to monitor the bridge in real time during testing. Such real-time monitoring is essential when load testing bridges without detailed plans as it allows for behavioral anomalies to be quickly spotted and prevents accidental damage to the structure by the load test. Furthermore, by preparing the gage locations in advance, using reusable strain gages, and having a well-planned testing procedure prepared, testing was completed in only a few hours.

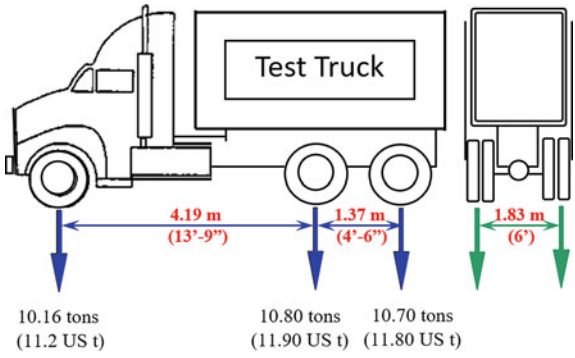

Fig. 5 Tandem rear axle dump truck used for testing

6 Load Test Results

Within this paper, only the evaluation of the controlling load case (that which produced the highest measured strain at the critical location) will be discussed. The controlling load case was identified as Load Case 4 which had a single test truck stopped with the inner rear tandem axle over the crown (Fig. 6) as close to the edge of the arch as possible.

The longitudinal and transverse strain distributions and truck position for the controlling load case are presented in Figs. 7 and 8, respectively.

The highest strain reading of 10.7×10^{-6} occurred at the crown along the edge of the arch (peak in Fig. 8). The low maximum strain value provides evidence that

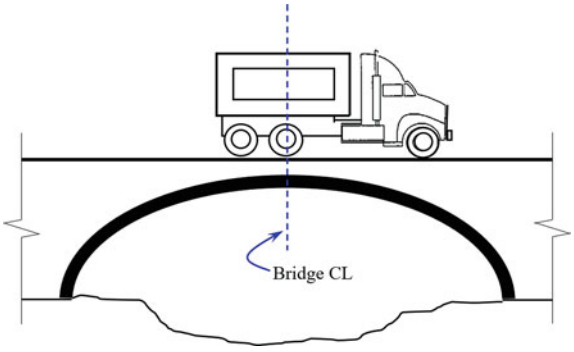

Fig. 6 Controlling load case for load rating

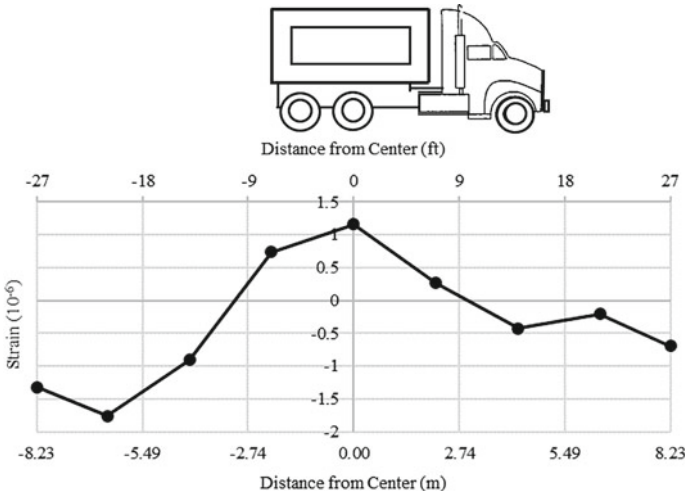

Fig. 7 Controlling load case longitudinal strain profile

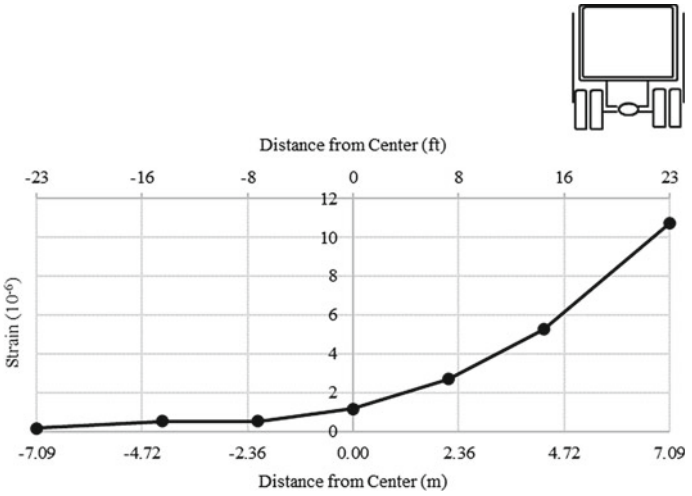

Fig. 8 Controlling load case transverse strain profile

the bridge is under no duress from typical loading. By inspection, the shape of the longitudinal strain distribution is close to what one would expect for a theoretical arch under a series of point loading [7]. Furthermore, the longitudinal strain distribution matches those measured by previous researchers for another arch bridge [4]. Additionally, the transverse strain distribution provides evidence of complete shear transfer between the aforementioned longitudinal construction joints. Such general checks of the shape of strain distributions are important for quantifying the quality of data as well as refining analytical models to accurately represent the in situ bridge response.

7 Load Rating

Conservative values were chosen for the material properties. As mentioned previously, rebound hammer testing suggested a compressive strength around 27.6 MPa (4 ksi). However, the MBE recommends a compressive strength of 17.24 MPa (2.5 ksi) for bridges built prior to 1959 [2]. The use of 17.24 MPa (2.5 ksi) was deemed appropriate as the arch is likely of much higher strength and this is a highly conservative assumption. Reinforcement was assumed to be 227.5 MPa (33 ksi) based on guidance from the MBE [2]. Because the arch bridge is buried, properties for the fill materials needed to be selected as well. The fill material properties were selected based on values used for load rating culverts in Kentucky, and previous buried arch culvert research carried out in Kentucky [6]. A summary of material properties is presented in Table 2.

Table 2 Material properties for finite element modeling

Material	Parameter	Value	
		SI	USCS
Concrete	Strength	17.2 MPa	2.5 ksi
	Modulus of elasticity	19.7 GPa	2850 ksi
	Unit weight	22.8 kN/m^3	145 pcf
	Poisson's ratio	0.15	
Steel reinforcement	Strength	228 MPa	33 ksi
	Modulus of elasticity	200 GPa	29,000 ksi
	Unit weight	77 kN/m^3	490 pcf
Fill	Modulus of elasticity	276 MPa	40,000 psi
	Unit weight	20.4 kN/m^3	130 pcf
	Poisson's ratio	0.35	
Pavement Subgrade	Modulus of elasticity	414 MPa	60,000 psi
	Unit weight	21.2 kN/m^3	135 pcf
	Poisson's ratio	0.35	
Asphalt	Modulus of elasticity	207 MPa	300,000 psi
	Unit weight	22 kN/m^3	140 pcf
	Poisson's ratio	0.30	

With the material properties selected, the Finite Element (FE) model was created using SAP2000. This FE model consisted of a 1 ft wide section of the bridge modeled using a refined mesh of solid elements. The use of a unit width of the bridge was deemed appropriate because evidence of good shear connection was established, as noted previously. The geometry of the concrete arch was defined using the field measurements presented in Table 1. The fill layers above the arch were also modeled using solid elements. The fill layer had a variable depth ranging from 5.18 m (17 ft) at the base of the arch to a 0.30 m (1 ft) minimum above the crown. Above the fill layer was a 20.32 cm (8 in) thick compacted pavement subgrade layer and a 5.08 cm (2 in) thick asphalt layer. The fill, compacted pavement subgrade, and asphalt layers extended laterally 3.05 m (10 ft) on either side of the arch supports. The fill layer depths were based on previous load rating projects and engineering judgment.

Two fixity conditions for the base of the arch were considered: roller and pinned. The roller condition restrained the arch base from vertical displacement only, while the pinned condition restrained the arch base from all displacement. For both arch

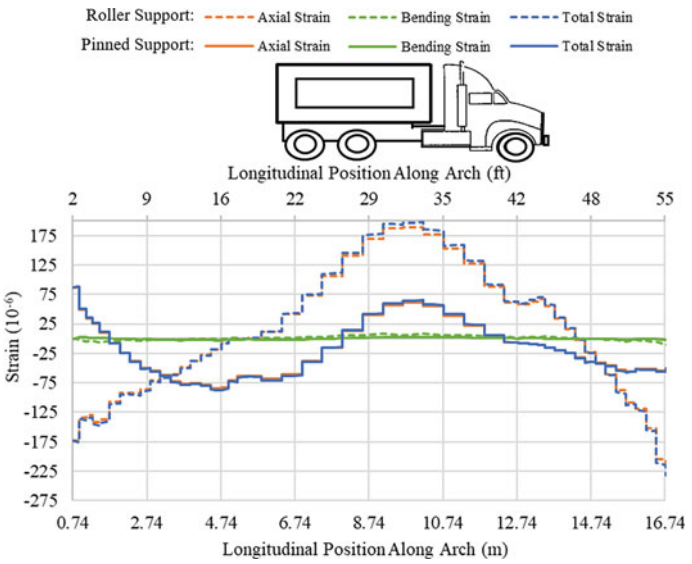

Fig. 9 Strain distributions from preliminary finite element model subjected to controlling load case

base fixity conditions, the horizontal soil mass face was only restrained against vertical displacement while the vertical soil mass faces were restrained from horizontal displacement. To refine this model, it was subjected to the controlling load case with the resultant strains shown in Fig. 9.

As one would expect, allowing the arch to translate laterally with the roller condition increased the maximum strain significantly. This represents the "worst case" behavior of an arch. Thus, to be conservative, the final model had the roller boundary condition for the arch base. It was also decided to modify the arch base by the addition of small 0.91 m × 1.83 m (3 ft × 6 ft) footings on either side. Another key insight from Fig. 9 was that the axial compression strain component comprises most of the resultant total strain, regardless of the base fixity condition. Because of this, it was decided to model the arch as unreinforced due to the minimal amount of bending strain developed. Lastly, because the arch is a buried structure, the modeled lateral soil mass length influences the response. Based on previous research of arch culverts, it was decided to use the bridge span length as the lateral soil mass length [6]. The final FE model used for load rating is shown in Fig. 10.

Loads were applied to the FE model as pressures across a 25.4 cm × 50.8 cm (10 in × 20 in) area which corresponds to the AASHTO tire footprint (LRFD 2014). To be conservative, loads were not reduced to account for transverse distribution. In other words, half the axle weight was applied as a pressure and supported by the modeled unit width of the bridge and only spread longitudinally through the modeled soil elements down to the arch. The dead load effects were taken directly from the model using the unit weights of the materials.

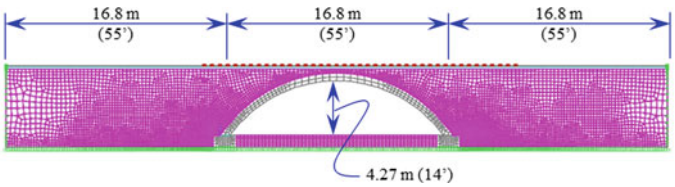

Fig. 10 Finite element model used for load rating

The LFR method outlined previously was used to establish the theoretical load ratings for the bridge. Because the analysis found that the bridge carries virtually all of the load in compression, the capacity of the bridge was taken as the cracking strain of the concrete. Because the compressive strength of the concrete is likely higher than what was assumed, this was seen as a conservative capacity estimate. A 27.8% impact allowance was also applied to the live loads in accordance with the MBE and AASHTO Standard Specifications [3]. Because the dead and live load effects varied along the arch, load ratings were determined for multiple points along the arch. The overall rating for each truck was selected as the lowest rating factor found along the arch which coincided with the crown for every truck considered. A summary of the load ratings is presented in Table 3.

Because the model was highly conservative and predicted high strains, the K_a factor was relatively large at 8.2. The K_b factor varies for each truck being load rated because it accounts for the ratio of the test truck effect to the rated truck effect determined in the FE model. This ratio was found to be greater than 0.7 for all trucks being load rated. Additionally, the K_b factor accounts for whether or not there is confidence that the member has at least a 33% reserve capacity beyond the rated effect. As a conservative assumption, it was not assumed that such a reserve capacity existed for any of the rated trucks. Based on these assumptions and the highly conservative nature of the FE model, the K_b factor was taken as 0.5 for every truck based on guidance within the MBE [2]. As a result, the benefit from the field

Table 3 AASHTO theoretical load ratings versus field-adjusted load ratings for 19th street Bridge

Truck type and weight		Theoretical LFR		Field adjusted rating	
Truck	Gross weight	Inventory	Operating	Inventory	Operating
HS20	32.66 tons (36.00 US tons)	0.68	1.13	3.45	5.77
KY Type 1	18.14 tons (20.00 US tons)	0.68	1.14	3.48	5.82
KY Type 2	25.72 tons (28.35 US tons)	0.51	0.85	2.60	4.34
KY Type 3	33.34 tons (36.75 US tons)	0.49	0.82	2.49	4.16
KY Type 4	36.29 tons (40.00 US tons)	0.74	1.24	3.78	6.30

testing was a 5.1 times increase in the theoretical load ratings. The field adjusted load ratings are presented in Table 3.

8 Summary and Conclusions

This paper presents the load rating and testing of a reinforced concrete arch bridge using Finite Element (FE) modeling and field load testing. The development of a 2D FE model using field measurements, conservative material properties, and idealized boundary conditions resulted in substandard theoretical Rating Factors (RF < 1.0) using the Manual for Bridge Evaluation's (MBE) Load Factor Rating (LFR) methodology. This would require the bridge to be load posted. However, the bridge was load tested to capture the benefit of load testing for the purpose of load rating.

The testing program involved the use of 23 reusable strain gages strategically placed to capture the longitudinal and transverse strain distributions. The controlling load case proved to be the placement of a tandem rear axle dump truck's inner rear axle over the crown, as close to the edge of the arch as possible. The strain data generated from the field test was used to adjust the theoretical RFs which raised to serviceable levels (RF $\geq$ 1.0) for all trucks. This proved that the bridge has sufficient capacity to carry legal traffic without restriction and load posting was avoided.

References

1. Alampalli S, Frangopol DM, Grimson J, Halling MW, Kosnik DE, Lantsoght EO, Yang D, Zhou YE (2021) Bridge load testing: state-of-the-practice. J Bridge Eng 26(3):03120002. https://doi.org/10.1061/(ASCE)BE.1943-5592.0001678
2. American Association of State Highway and Transportation Officials (AASHTO) (2018) The manual for bridge evaluation, 3rd ed. Washington, DC
3. American Association of State Highway and Transportation Officials (AASHTO) (2002) Standard specifications for highway bridges, 17th ed. Washington, DC
4. Chajes M (2002) Load rating of arch bridges. Delaware Center for Transportation, Newark, Delaware
5. Federal Highway Administration (FHWA) (2004) National bridge inspection standards. Washington, DC
6. Jawdhari A, Peiris A, Harik I (2020) Load rating of bridge-size reinforced concrete arch culverts. Struct Infrastruct Eng. https://doi.org/10.1080/15732479.2020.1850803
7. Karnovsky IA (2011) Theory of arched structures: strength, stability, vibration. Springer Science & Business Media, New York, NY

Lateral Performance of Thin-Walled Steel Box Column with Replaceable Energy Dissipation Mechanism

M. Jenothan, J. A. S. C. Jayasinghe, C. S. Bandara, and A. J. Dammika

Abstract A numerical investigation on the effective use of low yield point (LYP) steel as a replaceable energy dissipation mechanism in a thin-walled steel box column is presented in this paper. Three column sections with modified cross-section using four L angles and replaceable LYP steel plates were tested under constant axial and lateral cyclic loading, so that after a severe lateral loading, the LYP steel plate could be replaced while the L angle supports the column. A standard column with SM490 grade component plates was also analysed to compare the performance of a similar column with an energy dissipation mechanism made out of stiffened LYP steel plate welded to the L angles. The results show that, with the proper corner stiffening technique, the buckling was initiated and developed at the LYP steel plate, which can be easily recovered by replacing the LYP steel plate. In contrast, the columns without the corner stiffening arrangement showed excessive overall buckling in L angles and LYP steel plates. Also, the largest ductility and strength were observed in the column with both plate and L plate stiffeners, while the column with corner plate stiffeners only showed good ductility improvement without a significant strength gain.

Keywords Cyclic lateral loading · Ductility · Low yield point steel · Nonlinear finite element simulation · Strength · Thin-walled steel box column

1 Introduction

Thin-walled stiffened columns are becoming more popular, especially in constructing bridges, overpasses, transmission towers, viaducts, and turbines in urban areas due to their aesthetic appearance, structural rigidity, post-buckling behaviours, and possible easy rectification techniques. These steel piers have the advantages of high strength to weight ratio, less construction time, easy production, and transportation compared to reinforced concrete piers. In most cases, thin-walled box sections are preferred over

M. Jenothan (✉) · J. A. S. C. Jayasinghe · C. S. Bandara · A. J. Dammika
Faculty of Engineering, University of Peradeniya, Peradeniya, Sri Lanka
e-mail: makeswaranjenothan@eng.pdn.ac.lk

R. Dissanayake et al. (eds.), *12th International Conference on Structural Engineering and Construction Management*, Lecture Notes in Civil Engineering 266,
https://doi.org/10.1007/978-981-19-2886-4_15

the thin-walled circular sections due to the easy manufacturing process of component plates and cost-effective connection between the box section and crossbeam.

However, due to their very high width to thickness ratio, these types of structures are vulnerable to local buckling and overall interaction buckling or both when subjected to cyclic lateral loads such as earthquake loading, which leads to a significant loss in strength and ductility. Past earthquakes, such as those reported by Hyogoken-Nanbu (1995), resulted in bridge pier failures such as local buckling of plates, brittle cracks, and low cycle fatigue. As a result of the above earthquakes, many investigations were carried out to enhance the sufficient strength and ductility of steel box piers to withstand severe earthquakes [18]. Stiffening arrangements, concrete infilling, double tube arrangement, higher material strength plates and stiffeners are some techniques used to enhance the strength and ductility of steel box piers.

Qian and Astaneh-Asl [9] numerically investigated the effect of stiffener cross-sections and width to thickness ratio of plates on the ductility of the steel piers. Results showed that using both pipe section or angle section stiffeners instead of conventional plate stiffeners improves the ductility and post-buckling capacity of the steel column. Terayama et al. [14] investigated steel piers by adding corner plates and discussed the ductility improvement of the column and the effect of axial load ratio and slenderness ratio. Nishikawa et al. [8] experimented with steel piers by adding corner stiffeners and longitudinal stiffeners. Results showed that the corner stiffening method delayed the local buckling of the corners of the pier. Hsu and Juang [6] discussed how the internal strengthening braces enhance the post-buckling behaviour of steel columns. Usami et al. [16] investigated the cyclic performance of steel piers by replacing the stiffeners with high-strength material. Results showed an increase in strength and superior post-buckling behaviour than the conventional steel piers.

Concrete filling is also a popular technique worldwide due to its strength and ductility performance with better post-buckling characteristics. Usami [15] and Usami et al. [17] experimentally investigated the ductility performance of partially concrete-filled steel columns and revealed that concrete-filled columns significantly increase both ductility and energy absorption capacity. In addition to that, Hanbin [5] investigated the cyclic performance of partially concrete-filled steel columns and found that providing a diaphragm on the concrete fill effectively increases both strength and ductility.

Furthermore, several experimental and numerical studies revealed that the critical local buckling of thin-walled steel structures occurred in the compressive flange near the base [19, 20]. The accumulation of plastic strain at the bottom is the main cause of the local buckling of these plates. To address this shortcoming, increasing the yield spread area or using an appropriate material to handle large accumulated plastic strain at the lower panel may be a good solution. Studies have shown that ductility and strength can be improved by using a graded thickness plate [1]. To avoid stress concentration at the connection between two different thickness plates and avoid filler plates at the junction, Susantha et al. [13] investigated the applicability of steel box columns with thickness tapered steel panels at the lower section. They found that

the outer tapered section, which has the highest bending rigidity, shows enhanced ductility performance over the centre and inner tapered section regardless of its large $P - \Delta$ effect. Furthermore, both the graded thickness section and tapered section should be handled very carefully. Excessive increase in stiffness at the lower area may induce easy local buckling at the intersection between tapered or graded thickness and constant thickness plates.

On the contrary, Susantha et al. [11] investigated the steel piers by replacing low yield strength steel (LYS) at the lower panel and discussed how the strain-hardening property of LYS can be utilized to gain strength and ductility of the steel piers. Li et al. [7] used this idea and tested steel piers by installing specific energy dissipation components (consists of LYP steel plates attached to the constraining steel plate) at the bottom. Results showed an increase in ductility of the column and in most of the cases column failed at the corners, which are away from the energy dissipation zone. Several studies have been undertaken to enhance the strength and ductility of steel piers. However, many techniques still exhibit issues related to recovering seismic resistance after a large earthquake load.

Highway bridges are the most common and critical civil infrastructure of the transportation network. They play an important role in evacuation and emergency routes for rescues, first-aid, firefighting, medical services, transporting disaster commodities, etc. However, damaged bridges should be closed while repairing takes place. It is important that after a severe earthquake, the bridge piers should be capable of carrying at least the dead weight of the bridge (axial load) until the repairing work complete and this is where the past studies lack to offer clear techniques.

This study proposes a steel column by replacing its bottom part with an energy dissipation mechanism made out of LYP steel plates welded to the steel L angles (Fig. 1) to enhance the performance. In addition to that, the LYP steel plate can be easily replaced after a large earthquake where the L angle can support the dead weight (axial force) until the repair work is done. To achieve this goal, thin-walled steel square column is numerically analysed under a constant axial load with a cyclic lateral load using commercial finite element software *ABAQUS*. The numerical results were verified with the experimental result from the literature. Finally, the performance of the conventional column and newly introduced columns were compared. The results showed that the column with the energy dissipation component showed better seismic performance than the conventional steel column. Furthermore, deformed shapes of

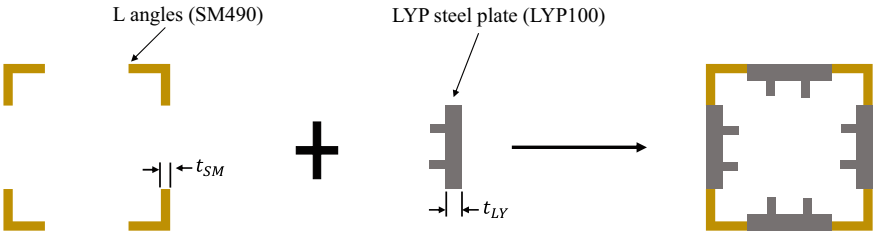

Fig. 1 Energy dissipation mechanism with LYP steel plate

the columns were analysed to verify that the introduced stiffening methods delayed the buckling of the corners. At the same time, it was found that the energy dissipation zone (LYP steel plate) buckled at the end of the loading.

2 Numerical Analysis

2.1 Material Model

During cyclic analysis, steel piers go through repeated large deformations that involves material and geometrical nonlinearities. Modelling of the cyclic response of the steel plays a vital role in the accurate prediction of the behaviour of the structure. Some important factors to be considered to assign a material model for structural steel include yield criteria, flow rule, and hardening rule. The standard column was analysed using isotropic, kinematic, and combined hardening models. Then, hysteretic and envelop curves obtained from analysis using all three hardening model were compared with the experimental results. After that, the most appropriate hardening model is used for the further analysis. In the material model, residual stress due to the welding and initial deflection are neglected due to their very small effect on the cyclic behaviour of the pier [2].

2.2 Material Properties

In this study, both LYP steel (LYP100) and normal strength steel (SM490) (Japanese Industrial Standard) grades are used. The yield strength of SM490 steel is 420 MPa, the tensile strength is 550 MPa and Young's modulus is 206 GPa [10]. LYP100 steel has a very low yield strength of 100 MPa but nearly three times higher ultimate strength of 296 MPa with Young's modulus of 200 GPa [4]. This study used the combined hardening material model with the bi-linear material stress–strain curve, as shown in Fig. 2.

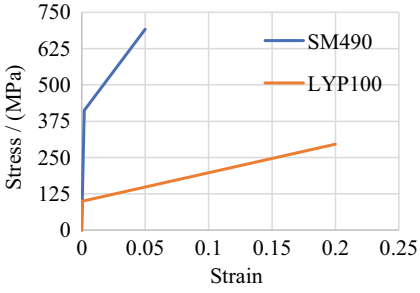

Fig. 2 Stress–strain behaviour of steel

2.3 Equivalent Thickness of LYP Steel Plate

Under lateral cyclic loading, piers demand large strain levels after the elastic limit, whereas the strain-hardening characteristic of the LYP steel expands in the plastic limit along with the cyclic loading [11]. To determine the thickness of the LYP plate, ultimate strength of the LYP steel was considered and the equivalent thickness of LYP plate (t_{LY}) was calculated using Eq. (1), where $\sigma_{y\mathrm{SM}}$ is the yield strength of SM490 steel, $\sigma_{u\mathrm{LY}}$ is the ultimate strength of LYP steel and t_{SM} is the plate thickness of SM490 steel (Fig. 1).

$$t_{\mathrm{LY}} = \frac{\sigma_{y\mathrm{SM}}}{\sigma_{u\mathrm{LY}}} \times t_{\mathrm{SM}} \tag{1}$$

2.4 Test Specimen

The lateral cyclic analysis was done for four different columns using commercially available *ABAQUS* software. All four columns have the same height of 2420 mm with the 450 mm × 450 mm square cross-section (Figs. 3 and 4). Three of the columns were modelled with the energy dissipation component of the replaceable stiffened LYP steel plates, which are welded to the L angles between the bottom diaphragm and base plate (Fig. 4).

The first column, namely SM-B, was made out of SM490 steel, which is used as a standard column for the comparison (Fig. 3). FE model was validated using experimental results available in the literature [12]. The second column LY-PL consists of four L angles at the corners between the bottom diaphragm and the base plate (height of 450 mm) and LYP steel plates welded between L angles (Fig. 4a). The third column LY-PL-CO was modelled as same as the LY-PL specimen and corner plates

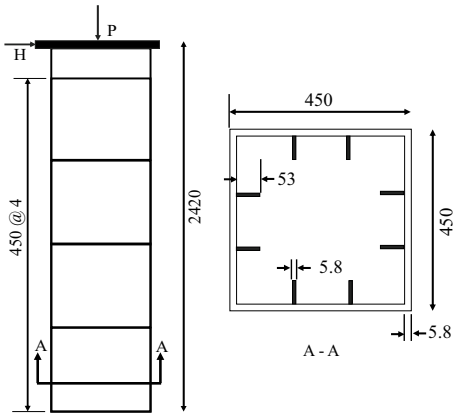

Fig. 3 Longitudinal and cross-sections of standard column SM-B (Dimensions in mm)

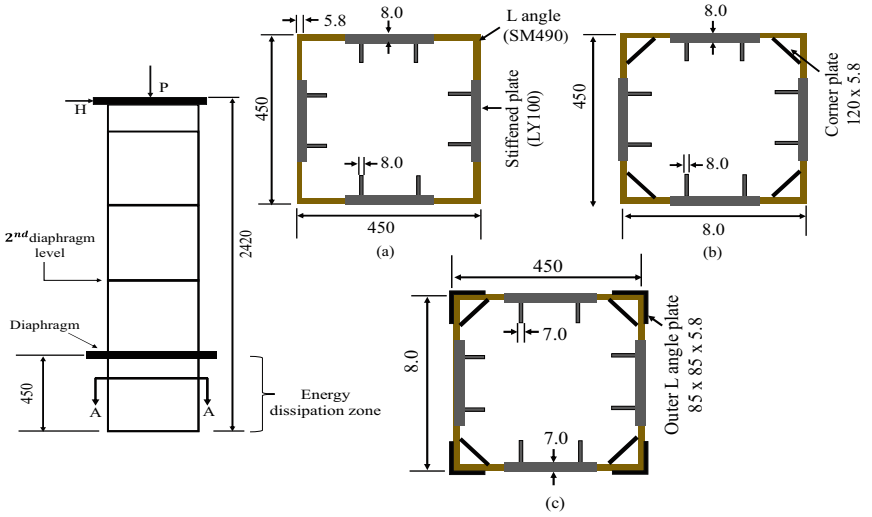

Fig. 4 Cross sections (A-A) of column arrangement: **a** LY-PL, **b** LY-PL-CO, and **c** LY-PL-CO-LCO (Dimensions in mm)

Table 1 Geometrical details of the columns

Specimen	SM-B	LY-PL	LY-PL-CO	LY-PL-CO-LCO
Plate thickness (mm)	5.8	8	8	7
L angle (mm)	–	100 × 100 × 5.8	100 × 100 × 5.8	100 × 100 × 5.8
Longitudinal stiffener (mm)	53 × 5.8	53 × 8	53 × 8	53 × 7
Corner plate stiffener (mm)	–	–	120 × 5.8	120 × 5.8
L plate stiffener (mm)	–	–	–	80 × 5.8
Cross section (cm^2)	128	159	189	193

were introduced to prevent the buckling of corners of the piers (Fig. 4b). Finally, the last column, LY-PL-CO-LCO, was further stiffened using L corner stiffeners (Fig. 4c) to delay the buckling of corners. The geometrical details of the standard and columns with the energy dissipation components are shown in Figs. 3 and 4 with that important geometrical parameter are listed in Table 1.

2.5 Loading Sequence

All the specimens first loaded with 0.2 times the yield axial load of the standard stiffened column ($P_y = Af_y$) and two-sided cyclic lateral loading were applied in the multiplies of yield displacement δ_y as shown in Fig. 5. The two-sided cyclic load refers that the positive and negative lateral load applied to the column top

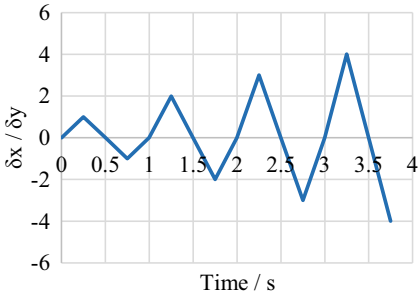

Fig. 5 Lateral cyclic loading applied to the model

alternatively. The application of this load pattern is to obtain the most conservative ductility capacity and very closely represent the earthquake loading condition [16]. This study aims to evaluate the performance of the columns with energy dissipation components concerning to the standard steel column with the same loading condition. So that the corresponding yield displacement ($\delta_y = 13.88$ mm) of the standard column were used for all the columns considered.

2.6 Finite Element Model

The stiffened steel column specimens were modelled using a four-node doubly curved shell element (S4R) available in the commercial finite element software *ABAQUS*. Then, the boundary condition to the base is given as fixed while a rigid plate is connected to the top of the column using tie connection to apply the axial and lateral cyclic load. Finally, mesh sensitivity tests were conducted and appropriate mesh sizes were obtained considering both accuracy of the results and the computational power required. Finer mesh size is used between base and the second diaphragm level (Fig. 4) because the lower part of the pier carries large plastic strain, whereas the upper part of the pier is meshed using coarse mesh size.

3 Results and Discussion

3.1 Validation of the Finite Element Model

Hysteretic and envelop curves obtained from the finite element model were compared with the experimental results available in the literature [12]. The combined hardening model showed very close prediction with the experimental results shown in Fig. 6, whereas the combined hardening model is a combination of isotropic and kinematic hardening where the yield surface expands symmetrically and moves in the stress space [3]. So, the combined hardening model is used in further analysis.

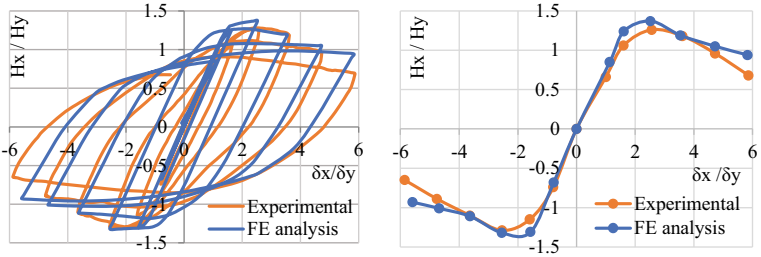

Fig. 6 Hysteretic and envelop curves of experimental results and finite element analysis

3.2 Strength and Ductility

The lateral load versus lateral displacement hysteretic curves and respective envelop curves of all specimens with the standard column (SM-B) were given in Figs. 7. The maximum strength of each specimen $H_{\max}$ and comparison with the standard specimen $H_{\max}/H_{\max-\mathrm{SM}-B}$ are tabulated in Table 2. The ductility parameters used to evaluate the deformation capacity are μ_m, μ_{95} where the μ_m defined as the ratio of displacement at maximum strength (δ_m) and displacement at the yield load (δ_y). Although δ_m is physically clear, it does not represent the cyclic hardening characteristic of the column since component plates do not experience plastic strains. So that the μ_{95} seems a good parameter that can incorporate effects due to cyclic loading [5]. Therefore, the ductility ratio μ_{95} is used to further comparison in this study. For the better understanding, both the δ_m, δ_{95} are given in the Table 2.

$$\mu_{95} = \frac{\delta_{95}}{\delta_y} \tag{2}$$

Here, δ_{95} is the deformation at 95% of $H_{\max}$ beyond the peak. Finally, the ductility was nondimensionalized using the ductility of SM-B column as listed in Table 2.

3.2.1 Column LY-PL (No Corner Stiffeners)

It can be observed from the hysteretic and the envelope curves shown in Fig. 7a that there is no significant deviation in strength and ductility of the LY-PL column compared to the SM-B column. However, both the strength and the ductility decreased by 13% and 6%, respectively, even though the thickness of the LYP plate was 1.4 times higher than the SM-B column's plates. After the maximum strength, the strength degradation rate is quite large, which is unfavourable post-buckling behaviour during the seismic events. In addition to that, buckling of L angles initiated at $2\delta_y$ displacement level and grew transversely with the increasing load (Fig. 8). This indicates that using stiffened LYS plate with the L angles only does not utilize

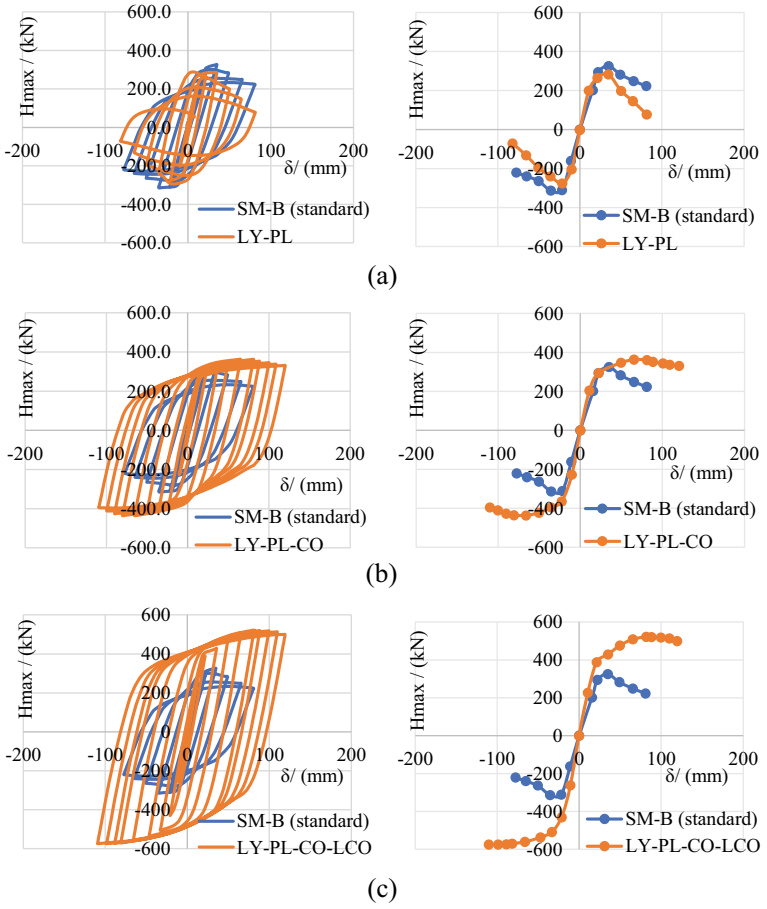

Fig. 7 Comparison of hysteretic and envelop curves of SM-B column with: **a** LY-PL, **b** LY-PL-CO, and **c** LY-PL-CO-LCO

Table 2 Strength and ductility comparison

Specimen	H_{max}	δ_m	δ_{95}	μ_{95}	$\frac{H_{Max}}{H_{max(SM-B)}}$	$\frac{\mu_{95}}{\mu_{95(SM-B)}}$
SM-B	325	35.0	40	2.88	1.00	1.00
LY-PL	283	34.8	37.5	2.70	0.87	0.94
LY-PL-CO	363	65.5	92.5	6.66	1.12	2.31
LY-PL-CO-LCO	521	81.7	115	8.29	1.60	2.88

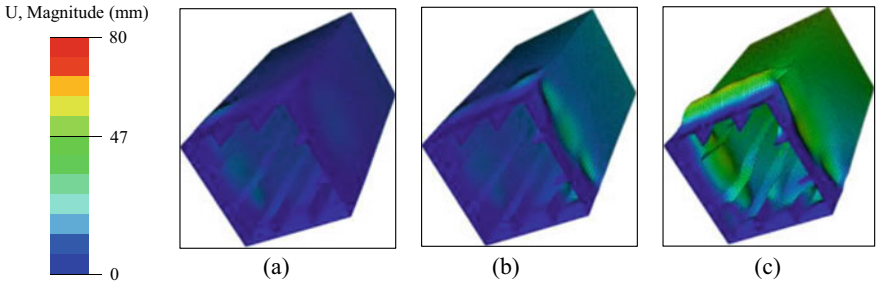

Fig. 8 Deformed shapes of column LY-PL: **a** initiation of buckling, **b** δ_{95}, and **c** end of loading

either ductility or strength as expected. Since the corners of the column buckled first, there is no use of a replaceable energy dissipation component at the bottom.

3.2.2 Column LY-PL-CO (with Corner Plate Stiffeners)

Corner plate stiffener was included in the specimen LY-CO to reduce the width to thickness ratio of the L angles. Concave plate buckling between longitudinal stiffeners was observed first at $5\delta_y$ displacement level (Fig. 9a) and buckling continued up to δ_{95} displacement level with minor strength degradation, but the minor buckling wave was observed at the L angles towards the end of the loading (Fig. 9c). Although the buckling at L angles was initiated at the end, the column showed a huge increment in ductility of about 131% with a small strength gain of 12% compared to the SM-B (Fig. 7b), which is favourable for the rectification of existing columns.

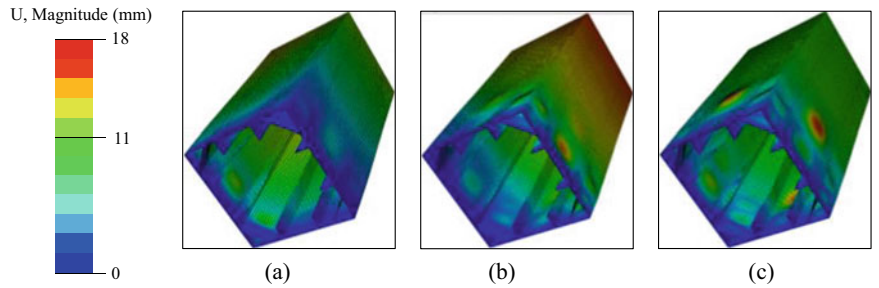

Fig. 9 Deformed shapes of column LY-PL-CO: **a** initiation of buckling, **b** δ_{95}, and **c** end of loading

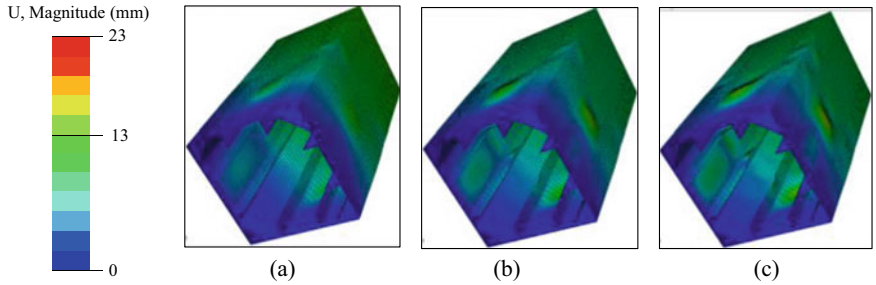

Fig. 10 Deformed shapes of column LY-PL-CO-LCO: **a** initiation of buckling, **b** δ_{95}, and **c** end of loading

3.2.3 Column LY-PL-CO-LCO (with Corner Plate Stiffeners and L Plate Stiffeners)

As the L angle of column LY-CO started to deform at the later stage of the loading, the LY-CO-LCO column was analysed with the L plate stiffener attached to the L angles in addition to the corner plate stiffener. The hysteretic and corresponding envelop curves shown in Fig. 7c indicate that both the strength and ductility increased by 60% and 188% compared to the SM-B column. Local buckling of plates between longitudinal stiffeners initiated at $5\delta_y$ as the same as the LY-CO column, but the progression of the buckling is restricted within the LYP steel plate as shown in Fig. 10, which can be replaced after the severe seismic event while the L angles could carry the axial load during the repairing work. At the end of the loading, some minor buckling waves were observed above the LYP plates, which shows the probability of the buckling in the upper part of the energy dissipation zone, which needs special attention on energy dissipation zone height, dimensions of stiffening arrangements, and LYP plate thickness.

3.3 Failure Modes

The images shown in Figs. 8, 9, and 10 are the deformed shapes of the column at various displacement levels, such as initiation of buckling, δ_{95}, and end of the loading. The column with the stiffened LYP steel plate and four L angles (LY-PL) initiated the local buckling at the corners and the buckling progressively developed transversely (Fig. 8a, b). Due to the overall buckling, the column underwent a rapid strength distortion after the peak (Fig. 8c).

The columns with the corner stiffening arrangement delayed the buckling of the corners until the buckling of the LYP steel plate. Corners of the column LY-PL-CO initiated the buckling at the δ_{95} displacement as shown in Fig. 9b, whereas the column LY-CO-LCO exhibits no corner torsion until the end of the loading as shown

in Fig. 10. Therefore, it can be said that the specimen LY-CO-LCO corners worked as a stable, rigid frame consisting of four L angles at the corners.

4 Conclusions

LYP steel plates can be used to enhance the ductility of the steel column. In this study, the seismic performance of thin-walled steel columns with replaceable energy dissipation component (LYP steel plates) connected with the L angle at the column base was investigated using numerical simulations. Totally, there are four column sections, three with the LYP steel plate and L angles, and one standard column with the SM490 steel plates. The feasibility of the proposed method is discussed in terms of strength, ductility, and maintaining the column's corners to a stable position where the LYP steel plates buckled first. Based on this study, some important conclusions were drawn;

1. Failure of the steel column with the LYP steel plate at the base can be divided into two types. The first one is the local buckling of the LYP steel plate between L angles and the other one is the overall buckling of the L angle together with the LYP steel plate.
2. A large strength distortion rate in the column with the LYP steel plate (LY-PL) was observed due to the overall buckling of the L angle together with the LYP plate, even though the strength and ductility of the column were almost similar to the standard column. Therefore, proper techniques should be incorporated to delay the buckling of the L angles at the corner to use replaceable LYP steel plates effectively.
3. Two different stiffening techniques were used to delay the buckling of L angles in both LY-PL-CO and LY-PL-CO-LCO columns. Both the columns showed very high ductility improvement concerning the standard column. At the same time, the column with the corner plate stiffener showed a very small amount of strength gain, while the other column with both corner plate and L plate stiffener showed significant strength gain.
4. LY-PL-CO column arrangement is suitable for rectification of existing columns. The column showed a very large ductility improvement of 130% concerning the standard column while a very small strength gain of 12%. So, there is no need for rectification in the existing foundation, which is too difficult in urban cities.
5. Among the proposed columns with the energy dissipation zone, the column with the corner plate and L plate stiffeners was found to be the best due to the local buckling of column (LY-PL-CO-LCO) occurred in the LYP steel plate. While the L angles at the corners remain straight, which can support the axial load until the buckled LYP steel plates are replaced. In addition to that, it showed a significant increment in strength and ductility of 60% and 188%, respectively.
6. At the end of the cyclic loading, it was observed in the column LY-PL-CO-LCO very small buckling above the LYP plate, which indicates the possibility of

local buckling in the upper section of the LYP steel plate. Detailed parametric studies should be done in the cases of energy dissipation zone height, optimum thicknesses of both LYS plate and stiffeners for various ranges of column's slenderness ratio, width to thickness ratio and axial load ratio to avoid the buckling above the energy dissipation zone.

References

1. Al-Kaseasbeh Q, Mamaghani IHP (2019) Buckling strength and ductility evaluation of thin-walled steel stiffened square box columns with uniform and graded thickness under cyclic loading. Eng Struct 186:498–507. https://doi.org/10.1016/j.engstruct.2019.02.026
2. Aoki T, Susantha KAS (2005) Seismic performance of rectangular-shaped steel piers under cyclic loading. J Struct Eng 131(2):240–249. https://doi.org/10.1061/(asce)0733-9445(2005)131:2(240)
3. Bäker M, Rösler J, Harders H (2007) Mechanical behaviour of engineering materials. Mech Behav Eng Mater. https://doi.org/10.1007/978-3-540-73448-2
4. Gao Y, Shi G, Wang X (2021) Mechanical properties of low yield point steels subjected to low-cycle structural damage. J Constr Steel Res 183:106733. https://doi.org/10.1016/j.jcsr.2021.106733
5. Ge H, Usami T (1996) Cyclic tests of concrete-filled steel. J Struct Eng 122(October):1169–1177
6. Hsu HL, Juang JL (2000) Performance of thin-walled box columns strengthened with internal braces. Thin-Walled Struct 37(3):241–258. https://doi.org/10.1016/S0263-8231(00)00020-3
7. Li H, Luo W, Luo J (2020) Seismic performance of steel box bridge piers with earthquake-resilient function. Adv Civ Eng 2020(August). https://doi.org/10.1155/2020/8877785
8. Nishikawa K et al (1998) Retrofitting for seismic upgrading of steel bridge columns. Eng Struct 20(4–6):540–551. https://doi.org/10.1016/s0141-0296(97)00025-4
9. Qian X, Astaneh-Asl A (2016) Behaviour and seismic design of stiffeners for steel bridge tower legs and piers. In: World Congress on civil, structural, and environmental engineering (May). https://doi.org/10.11159/icsenm16.117
10. Shen C et al (1992) A two-surface model for steels with yield Plateau. Doboku Gakkai Ronbunshu 441:11–20. https://doi.org/10.2208/jscej.1992.11
11. Susantha KAS et al (2005) Applicability of low-yield-strength steel for ductility improvement of steel bridge piers. Eng Struct 27(7):1064–1073. https://doi.org/10.1016/j.engstruct.2005.02.005
12. Susantha KAS, Aoki T, Jayasinghe MTR (2007) Finite element analysis of steel columns subjected to bi-directional cyclic loads. Eng: J Inst Eng Sri Lanka 40(4):35. https://doi.org/10.4038/engineer.v40i4.7152
13. Susantha KAS, Aoki T, Kumano T (2006) Strength and ductility evaluation of steel bridge piers with linearly tapered plates. J Constr Steel Res 62(9):906–916. https://doi.org/10.1016/j.jcsr.2005.11.006
14. Terayama T et al (1998) Ductility improvement of steel columns with corner plates based on large-scale cyclic loading tests, stability and ductility of steel structures (SDSS'97). Woodhead Publishing Limited. https://doi.org/10.1016/b978-008043320-2/50029-0
15. Usami BT (1994) Experimental program and test specimen. J Struct Eng 120(7):2021–2040
16. Usami T, Gao S, Ge H (2000) Stiffened steel box columns. Part 2: ductility evaluation. Earthquake Eng Struct Dynam 29(11):1707–1722. https://doi.org/10.1002/1096-9845(200011)29:11%3c1707::AID-EQE990%3e3.0.CO;2-7

17. Usami T, Ge HB, Saizuka K (1997) Behavior of partially concrete-filled steel bridge piers under cyclic and dynamic loading. J Constr Steel Res 41(2–3):121–136. https://doi.org/10.1016/S0143-974X(97)00007-2
18. Watanabe E et al (1998) Performances and damages to steel structures during the 1995 Hyogoken-Nanbu earthquake. Eng Struct 20(4–6):282–290. https://doi.org/10.1016/S0141-0296(97)00029-1
19. Yamao T et al (2002) Steel bridge piers with inner cruciform plates under cyclic loading. Thin-Walled Struct 40(2):183–197. https://doi.org/10.1016/S0263-8231(01)00059-3
20. Zheng Y, Usami T (2000) Ductility evaluation procedure for thin-walled steel structures, (November), pp 1312–1319

Geotechnical Engineering

Pavement Degradation Model for Paved and Unpaved Roads in Sri Lanka

M. M. N. T. Meghasooriya, K. M. N. M. Jayarathna, and S. K. Navaratnarajah

Abstract Pavement degradation prediction is essential for road management systems to predict the most effective maintenance time. The existing degradation prediction models are calibrated for different countries; therefore, they cannot be used directly for the local condition to predict the maintenance requirements. In Sri Lanka, this is causing many difficulties during the maintenance activities of road infrastructure and drainage systems running along the roadways. Therefore, in this study, a pavement degradation model for unpaved road infrastructure in Sri Lanka is proposed using Markov analysis. The analysis consists of identifying performance parameters, condition stages of the road sections, Transition Probability Matrix (TPM), and finally prediction of the road lifetime and level of maintenance requirements. Developed Unpaved Condition Index (DUPCI) is proposed for the unpaved roads as the performance parameter which includes all the possible deterioration types of gravel roads such as potholes, corrugations, overexposed aggregates, erosion, roadside drainage, and rutting. Development of the TPM is proposed based on the data collected at three gravel roads in Dambulla Pradeshiya Sabha. Calibrated HDM3 model is proposed for Sri Lankan paved roads based on the data collected at A9 road. Both models were calibrated and validated using the collected data for Sri Lankan unpaved and paved roads.

Keywords Pavement degradation · Maintenance · Markov model · Unpaved condition index · HDM3

1 Introduction

Pavement maintenance is one of the most important tasks after the construction. Every country adopts various pavement management systems (PMS) which consist of many prediction models developed in their state or calibrated models from other states. Model is depending on the road types such as unpaved, paved, and rigid

M. M. N. T. Meghasooriya · K. M. N. M. Jayarathna · S. K. Navaratnarajah (✉)
Faculty of Engineering, University of Peradeniya, Peradeniya, Sri Lanka
e-mail: navask@eng.pdn.ac.lk

R. Dissanayake et al. (eds.), *12th International Conference on Structural Engineering and Construction Management*, Lecture Notes in Civil Engineering 266,
https://doi.org/10.1007/978-981-19-2886-4_16

pavements. Among various models that developed in many countries, the Australian Road Research Board (ARRB) models, Highway Development and Management (HDM) models, and Technical Recommendations for Highway Manual 20 (TRH-20) model are widely used.

Pavement degradation models are widely used in PMSs to predict when maintenance will be required. Models can predict the degradation with time as well as the lifetime economic evaluation. After the construction, long-term funding requirements for pavement maintenance can be estimated with the sense of the lifetime of the road [7]. Also, Saha and Ksaibati [10] concluded that models are used to decide the best maintenance type such as re-graveling, blading, reconstruction, and major drainage repair considering cross-section, roadside drainage, rutting, potholes, loose aggregates, dust, corrugation, and ride quality. The model can be used for any country after it is calibrated to local conditions. Calibration is essential because universal degradation models can vary from country to country with many factors. Better prediction can be obtained by calibrated models for local conditions.

Age of the pavement, traffic volume, and weight, thickness of last overlay, strength, and condition of pavement structure, surface deflection, and construction quality are the affecting factors for pavement degradation [7]. Among them, age was identified as significant in predicting pavement deterioration. Giummarra et al. [8] found that plasticity factors, traffic, rainfall, and material properties can be considered as the affecting factors. Furthermore, Zyl et al. [14] recommend taking pavement material properties, climate, and road geometry as the affecting factors for TRH-20, HDM-4, and ARRB models. HDM-4 and ARRB models incorporate all four major fields of input, but geometry is omitted from the TRH-20 Model. For road geometry, HDM-4 uses the gradient and the curvature whereas ARRB incorporates only the gradient. Wijk et al. [12] compared gravel loss prediction models such as TRRL Model, South African Model, Australian Model, and Highway Design and Maintenance model. The mechanistic-empirical model was developed for paved roads in George et al. [7]. Overall pavement index which consists of ride quality, rutting, and cracking was used in Saha et al. [10]. The difference between those models is George et al. concluded a combination of the empirical base with regard to mechanistic principles and Saha et al. [10] used field distress data for performance parameters. According to the review of literature, a summary of the affecting factors can be identified as traffic volume, age of pavement, the thickness of last overlay, material properties of wearing course (plasticity factor, material type, particle size distribution), climate (rainfall, wet zone, and dry zone, Weinert N-value, wind), and road geometry (average rise and fall, gradient of the road, average curvature).

George et al. [7], Chamorro and Tighe [5], and Abaza [1] used combined performance parameters to predict the lifetime of a road. Giummarra et al. [8], Wijk et al. [12], Aleadelat et al. [2], and Uys [11] reported individual performance parameters to rate the condition of the road. Combined performance parameters are related to the overall condition of the road which is suitable for combined maintenance procedures. Individual performance parameters identify each degradation individually, and distinct maintenance is proposed such as blading and re-graveling.

2 Markov Approach

Prediction of performance is done by two types of models: deterministic and stochastic (probabilistic). Deterministic models include primary response, structural performance, functional performance, and damage models according to George et al. [7]. Stochastic models are based on probability which is applied widely because of the consideration of uncertainty. Markov approach and survivor curves are two main approaches for stochastic models as suggested by Carnahan et al. [4] and Lytton [9]. Markov approach is mainly consisting of four main steps: performance parameter selection, condition stages identification, transition probability matrix development, and finally Markov chain development to predict the lifetime of a road. Markov chains can be identified as homogeneous and non-homogeneous chains based on the transition probability matrix used. According to Abaza [1], the homogeneous Markov model assumes steady-state transition probabilities over the entire analysis period which presents a major drawback for predicting future pavement conditions. The non-homogeneous Markov model deploys different transition probabilities for each transition which can lead to superiority in predicting future pavement conditions. But as concluded by Butt et al. [3], this required more data and time to develop TPM for each transition. In this research, homogenous Markov modeling is used for final analysis.

2.1 Performance Parameter Selection

Individual performance parameters identify each degradation individually. Therefore, separate models are needed to identify specific deterioration types. Maintenance activity might recover many degradations but some other deteriorations might not be recovered. Combined performance parameters are related to the overall condition of the road which is suitable for combined maintenance procedures. Prediction is done considering all the degradation types including all parameters into one model. Both types of performance parameters are presented in Table 1.

Table 1 Performance parameters

Individual performance parameters	Combined performance parameters
Roughness rating	Unpaved Road Condition Index (URCI)
Structural strength rating	Unpaved condition Index (UPCI)
Rutting rating	Unpaved Pavement Condition (UPC)
Cracking rating	
Stone loss rating	

Eaton et al. [6] reported Unpaved Road Condition Index (URCI)-combined performance parameter developed by the U.S. Army Corps of Engineers. This index consists of properties of the cross-section. Roadside drainage, corrugations, dust, potholes, rutting, and loose aggregate into a value between 0 and 100. Common Unpaved Condition Index (UPCI) model for both gravel and earth roads with and without roughness was used in Chamorro and Tighe [5]. But Unpaved Pavement Condition (UPC) was defined only as a function of age by Saha and Ksaibati [10].

a. **Condition Stages**

Condition stages represent the level of road degradation. Each stage has a fixed range of performance parameter ratings useful in identifying the transitions from one stage to another. The number of stages depends on the degradation rate of the road. Five condition stages and seven condition stages are the most ideal number of stages [2].

b. **Transition Probability Matrix**

The transition probability matrix (TPM) consists of the probabilities of transitions from upper stages to the same stage or lower stages after a considerable period. Each probability is computed as a percentage of the total number of sections transferred to the total number of sections considered. TPM which is composed of the diagonal probability in addition to extra probabilities concerning the first raw of the TPM has been used [2]. Entries along the main diagonal represent the probabilities of pavements remaining in the same condition states and entries above the main diagonal denote the probabilities of pavements transmitting to the worse condition states after one condition. Similarly, entries below the main diagonal indicate the probabilities of pavement transiting to the better condition which cannot happen. This is the most common method of developing the transition probability matrix. But cumulative probability matrixes are also defined by calculating the cumulative probability per row in each TPM [5].

c. **Markov Chain**

Markov chain is developed to predict life by calculating the transferring fractions for the considered period in TPM. Homogenous TPM assumes that the transition probabilities for each period are equal. Therefore, the prediction of the condition rating for an equal period can be computed by continuing the multiplication using the same TPM. Equally distributed TPM is required for a better prediction.

d. **Data Collection**

Lion Rock road around Sigiriya (1), Naula Road along the Mahaweli canal (2), and Inamaluwa Road to Kandalama Lake (3) were selected for unpaved road analysis, and A9 road (4) was selected for paved road data collection as shown in Fig. 1. (1) and (2) roads are maintained directly by Naula Pradeshiya Sabha, and (3) is maintained by Mahaweli Authority.

As stated previously, many factors affect gravel road degradation. But if the condition is rated using few or one factor, or one condition parameter, the entire effect

Fig. 1 Map of the selected roads

cannot conclude in the model. Also, the models consist of condition parameters that are recommended to use rather than models with factors because parameters consist of the effect of all factors. Therefore, Unpaved Condition Index (UPCI) was selected as the most appropriate performance parameter to rate the gravel roads in Sri Lanka because it consists of many degradation parameters which give overall condition with less use of measuring instruments.

The index consists of six degradation measurements such as corrugation, potholes, erosion, rutting, exposed over-size aggregate, and crown condition. First, each road was divided into 100-m sections, and three sections among them were selected which represent the condition of the entire road. UPCI values were assigned to subdivided sections with 10 m in length. UPCI needs several in situ measurements to calculate the current condition of each section. Three data sets were collected in three different periods, two for TPM development and the other one for validation. UPCI has performed a technique of reducing the maximum possible rating of 10 by the measured degradations as shown in Eq. (1).

$$\text{UPCI} = 10 - 1.16\text{CR} - 2.25\text{PT} - 1.47\text{ER} - 0.33\text{RT} - 1.56\text{OA} - 1.58\text{CW} \quad (1)$$

UPCI shows a linear variation for each parameter. But the effect of each parameter on the overall condition is different and proportional to the magnitude of parameter coefficient, showing higher coefficients for highly affecting parameters in road degradation. All coefficients should be negative to reduce the rating from 10 to null, but should not be less than 0. Corrugations (CR) are measured as the mean vertical deformation observed in a section in centimeters. But corrugation was not observed in any section of selected three roads during the entire investigation time. Potholes (PT) are calculated as the product of the mean diameter in meters, maximum depth in meters, and the number of potholes in a sample section. Erosion (ER) is a dummy variable, considered as 1 if either erosion depth or width is greater than or equal to 5 cm. Measuring the depth and width of the erosion can be conducted as same as pothole diameter and depth measurements. Rutting (RT) or transverse deformations,

caused by the loose aggregate, are measured as the mean vertical deformation of five readings for each 10-m subsection using a straight bar in centimeters. Exposed oversized aggregate (OA) is another dummy variable, considered as 1 when oversized aggregates with mean diameters greater or equal to 10 cm are observed as a generalized phenomenon within the sample section. Crown condition (CW) is depends on roadside drainage and transverse profile of the road. The combined effect of drainage and transverse profile is averaged and taken as CW. Both defects are rated as 0 when observed in good condition, 0.5 in fair condition, and 1 in poor condition.

HDM 3 model was used to measure the roughness of the paved roads. Due to the unavailability of data on some parameters, the application of several models for the study might not be possible. When a general model is required without knowledge of the surface distress, Paterson and Attoh-Okine (1992) developed an alternative relationship for predicting roughness. The model required the cumulative equal single axle, the modified structural number of the pavement, age, environmental coefficient, and initial roughness to predict the roughness. Hence, all parameters are available at RDA, following developed HDM 3(2) model was used for the study.

$$\mathrm{RI}_t = 1.04e^{mt}(\mathrm{Rio} + 263(1 + \mathrm{SNC})^{-5}\mathrm{NE}_t) \tag{2}$$

RI_0: Initial Roughness

RI_t: Roughness after t years

m: Climate coefficient

t: Time. years

SNC: Modified structural number

NE_t: cumulative ESALs at age t

The environmental coefficient (m) was selected according to the proposed values by Paterson and Attoh-Okine (1992). Hence, the selected roads are in the dry zone of Sri Lanka and the climate is nonfreezing, m is taken as 0.01. Structural numbers (SNC) were calculated using falling weight deflectometer test values. Data were collected from RDA for each 500-m section which was collected just after the relaying of pavement in 2015. All deflection values from the deflectometer were transferred to relevant SNC values using Horak et al. (2015). According to the model, three deflection values were required for one SNC. Cumulative equal single-axle load was calculated using traffic survey data provided by RDA. Axle loads for each vehicle category were assumed, and an equivalent factor was calculated. Multiplying the number of vehicles, the equivalent factor for each vehicle category into 365, equal single-axle load was calculated for the base year. Each vehicle category equal single-axle loads are required to multiply with the growth factor to get the ESA for each year.

3 Data Analysis

UPCI model is calibrated to United States road conditions. Therefore, model calibration is required for Sri Lankan conditions before lifetime prediction in Sri Lankan gravel roads. To find the actual rating of the road, a Visual and Direct Measurement (VDM) method was used as proposed by Woll et al. [13]. UPCI model was calibrated equating VDM values as the dependent variable. But it was observed that the R^2 is only 63% indicates that something remains in the residuals that can be removed by a more appropriate model. Therefore, all variables, their interaction terms, and square terms were subjected to stepwise regression. Concluding the analysis results, the authors have proposed a developed model called Developed Unpaved Condition Index (DUPCI) shown in Eq. (3) with R^2 of 78% for gravel road condition rating in Sri Lanka which was calibrated for the dry zone.

$$\begin{aligned} \text{DUPCI} = {} & 9.009 - 1.169\text{RT} - 0.752\text{ER} - 0.6264\text{RT} \times \text{OA} \\ & + 1.602\text{RT} \times \text{CW} - 0.1232\text{PT} \times \text{ER} - 2.465\text{CW}^2 \end{aligned} \tag{3}$$

DUPCI shows a maximum rating of 9. Therefore, the number of condition stages was reduced to 4 including very good (VG), good (G), poor (P), and fail (F) stages and new ranges of ratings were proposed by the authors as shown in Table 2.

Initially, separate analyses were conducted for each road preparing 3 transition probability matrixes. During the first data collection, it was observed that all sections of the Lion Rock road comprised very good and good stages. After the second data collection, TPM was developed as shown in Table 3. Hence, the initial conditions only belong to higher stages, and TPM consists of probabilities only at the upper triangle of the matrix.

Table 2 Condition stages

Stage	UPCI range
Very good	9–7
Good	7–5
Poor	5–3
Fail	3–1

Table 3 Transition probability matrix for Lion Rock road

	TPM			
	VG	G	P	F
VG	0.421	0.526	0.053	0.000
G	0.000	0.909	0.091	0.000
P	0.000	0.000	0.000	0.000
F	0.000	0.000	0.000	0.000

Table 4 concluded the TPM for Naula Road. Similar to Lion Rock road, only very good and good sections were identified at the first data collection. All very good sections have transferred to each stage, and good sections have remained in the same condition.

Inamaluwa Road was in poor condition during the first visit. According to the TPM, all 30 sections have been distributed within every stage but more sections were related to lower stages as indicated in Table 5.

Figure 2 shows the lifetime predictions of Lion Rock road, Naula Road, and Inamaluwa Road. Lion Rock road shows better variation showing a complete failure after 80 months from the construction.

The lifetime of the Naula Road consists of better prediction during the 1st few and the final rating is converged to rating 4. But Markov chain has the capability of prediction until the complete degradation occurred with accurate TPM. Therefore, it can be concluded that the matrix is not complete enough for a better prediction. Inamaluwa Road also shows the same variation as Naula road.

Individual analysis of Lion Rock, Naula, and Inamaluwa roads do not show complete behavior during the entire life because the number of transitions is not enough. The main reason for this is an inadequate number of sections selected for the analysis. Also, the selected period might be not enough to show each stage's transitions. Therefore, combined analysis was conducted to overcome difficulties and data deficiency faced during the individual road analysis. All data were concluded to develop one TPM which defines the entire selected region as shown in Table 6. The developed Markov chain is shown in Table 7.

The time difference between the first two data collections is 2.5 months. Therefore, chain was developed for 2.5-month time intervals. Figure 3 shows more accept-

Table 4 Transition probability matrix for Naula Road

	TPM			
	VG	G	P	F
VG	0.545	0.318	0.091	0.045
G	0.000	1.000	0.000	0.000
P	0.000	0.000	0.000	0.000
F	0.000	0.000	0.000	0.000

Table 5 Transition probability matrix for Inamaluwa Road

	TPM			
	VG	G	P	F
VG	0.400	0.200	0.000	0.400
G	0.000	0.563	0.438	0.000
P	0.000	0.000	0.750	0.250
F	0.000	0.000	0.000	1.000

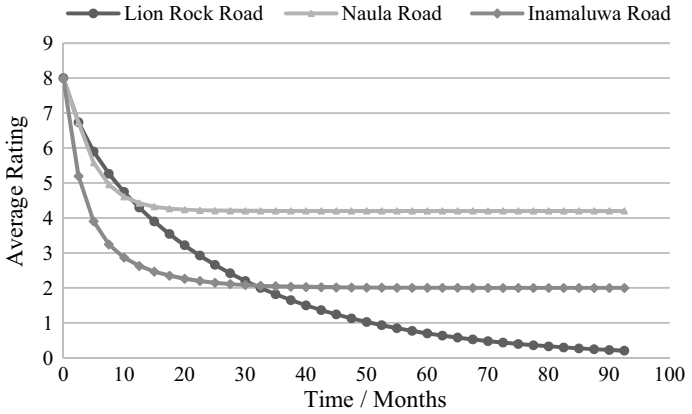

Fig. 2 Pavement lifetime prediction for individual analysis

Table 6 Transition probability matrix for combined analysis

	TPM			
	VG	G	P	F
VG	0.468	0.404	0.064	0.064
G	0.000	0.771	0.229	0.000
P	0.000	0.000	0.750	0.250
F	0.000	0.000	0.000	0.000

Table 7 Markov chain

Stage	Month	*VG*	*G*	*P*	*F*	Average condition
0	0	1.0000	0.0000	0.0000	0.0000	8.00
1	2.5	0.4680	0.4040	0.0640	0.0640	6.55
2	5	0.2190	0.5006	0.1705	0.0460	5.53
3	7.5	0.1025	0.4744	0.2565	0.0566	4.81
4	10	0.0480	0.4072	0.3076	0.0707	4.20
5	12.5	0.0225	0.3333	0.3270	0.0800	3.65
6	15	0.0105	0.2661	0.3230	0.0832	3.14
7	17.5	0.0049	0.2094	0.3039	0.0814	2.67
8	20	0.0023	0.1634	0.2762	0.0763	2.26
9	22.5	0.0011	0.1269	0.2447	0.0692	1.89
10	25	0.0005	0.0983	0.2127	0.0612	1.57
11	27.5	0.0002	0.0760	0.1820	0.0532	1.29
12	30	0.0001	0.0587	0.1539	0.0455	1.06
13	32.5	0.0001	0.0453	0.1289	0.0385	0.86

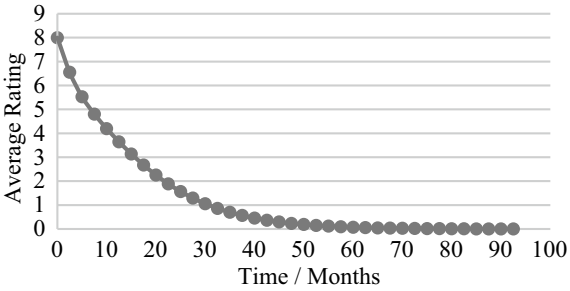

Fig. 3 Pavement lifetime prediction for combined analysis

able lifetime predictions than individual predictions. The final value of the rating is converged to 0 confirmed that the matrix selected for the analysis has enough transitions between every stage.

Two data sets were used to build the Markov chain from 1st data collection until the fail condition. The Markov chain can predict future conditions with time but not backward. Therefore, the predicted lifetime is not included in the time from construction to 1st data collection. According to the data records of Naula Pradeshiya Sabha and Mahaweli Authority, all the roads were graveled in February 2019. The third data set was used to validate the proposed model for Sri Lankan gravel roads. Considering the condition rating of a gravel road just after the construction is 9, all four data sets were plotted in the lifetime prediction graph for validation as shown in Fig. 4.

The actual mean rating trends to go with the predicted lifetime confirming the model is applicable. Hence, all the calibration was done using roads in the dry zone of Sri Lanka, and this model is applicable only for the dry zone roads. According to the results, a gravel road in the dry zone, Sri Lanka, is completely failed within 7 years.

HDM 3 model was used for the roughness prediction of selected paved roads. Measured values for roughness were collected from RDA for 6 consecutive years to compare with the calculated values. 2015 data set was used as the initial roughness

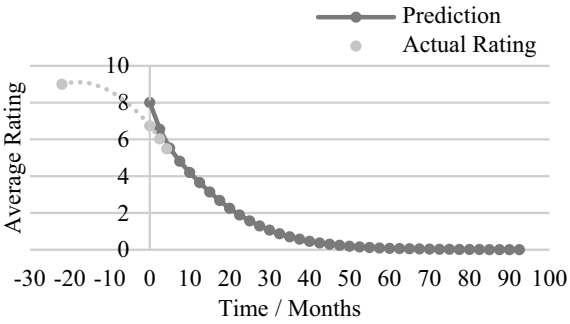

Fig. 4 Pavement lifetime prediction validation

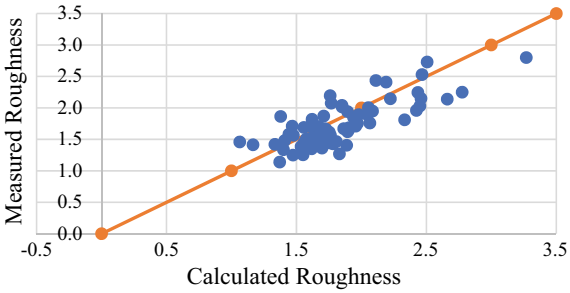

Fig. 5 Calculated versus measured roughness for 2016

value because the selected road was repaved in 2015. Compression for 2016 is shown in Fig. 5.

According to the results, 2016 and 2021 show congested data around the $y = x$ line. But all other years show considerable deviation of data from the $y = x$ axis. The reason might be the use of the non-calibrated model for Sri Lanka. Therefore, HDM3 model was calibrated using regression analysis to get a better prediction.

2016, 2017, and 2018 data were used to calibrate the model. 2020 and 2021 data were taken for validation purposes. Using a total of 68 data for the regression analysis, the model proposed for Sri Lankan paved roads is shown in Eq. (4).

$$\mathrm{RI}_t = 0.949^{0.01t}(\mathrm{RI}_0 + 493.661\mathrm{N}_E(1 + \mathrm{SNC})^{-5} \tag{4}$$

Using the calibrated model, calculated versus measured roughness for the year 2021 is shown in Fig. 6.

According to the above results, 2021 data set shows some improvement than the HDM3 model. Results show an improved R^2 from 59 to 73%.

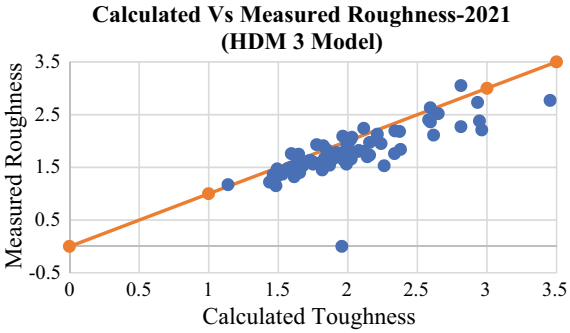

Fig. 6 Calculated versus measured roughness for the year 2021

4 Conclusions

According to the observed results, rehabilitation is required to commence at the rating of 5 for unsealed roads. According to the prediction curve, it is 2.5 years after the construction. Reconstruction is proposed after 3 years from the construction when the road reaches rating 3. Another important conclusion is corrugations were not observed during the entire investigation period on all roads. According to the analysis in this study, Markov analysis can be used for forward prediction but not backward. During the study period, considerable variation was noticed in rutting and potholes making them the most significant factors affecting road degradation. UPCI and DUPCI do not consider the smaller exposed over-size aggregates. This might be caused for errors in calculations of rating. Therefore, it is recommended to consider the factor OA as a function of the area or diameter of exposed aggregates. Rutting is measured as the maximum depth relative to the road centerline and edge. Proper TPM can be defined using data of more sections. The number of transitions from each stage to lower stages contributes to proper distributions in transition probabilities. Also, it is recommended to take a higher number of lengthy sections rather than selecting small sections to observe better degradation. Selected gravel roads had average daily traffic of less than 50. The predicted lifetime is relevant to less ADT, and the same analysis can be conducted to higher ADT ranges, different climate zones, and different terrains.

The increment of the roughness of the roads shows more than 20 years to reach critical range of roughness and extremely minor deviation observed even for one year period of time. Every value of roughness shows the deviation in the second or third decimal. Also, according to the experience of the field experts, roughness does not show a gradual increment or reduction with time for the first few years after construction or reconstruction. The measured values also proved that fluctuation. The initial roughness of the road is a significant factor for the condition of the road. The results show the variation of the traffic is less significant for roughness value. Therefore, calculation of initial roughness should be more precise. All the required data were collected manually using a leveled bar and measuring ruler. Then, the readings might be different from observer to observer. Therefore, a sensor network or echo-sounder system can be developed to take measurements by scanning the road similarly to the bathymetry survey which is done to identify the topography of a river bed.

Acknowledgements The authors would like to appreciate the support of the Road Development Authority (RDA), Provincial Road Development Authority (PRDA), Kundasale, and Naula Pradeshiya Sabha and Miss. Nuwani Jayakody, postgraduate student, Department of Civil Engineering, University of Peradeniya.

References

1. Abaza K (2015) Simplified staged homogenous Markov model for flexible pavement performance prediction. Road Mater Pavement Des 17(2):365–381
2. Aleadelat W, Wulff S, Ksaibati K (2019) Development of performance prediction models for gravel roads using Markov chains. Am J Civ Eng 7(3):73–81
3. Butt A, Shahin M, Feighan K, Carpenter S (2011) Pavement performance prediction m**odel** using the Markov process. Transp Road Res Board 1123:12–19
4. Carnahan JV, Davis WJ, Shahin MY, Keene PL, Wu MI (1987) Optimal maintenance decisions for pavement management. J Transp Eng ASCE 113(5):554–572
5. Chamorro A, Tighe SL (2011) Condition performance models for network-level management of unpaved roads. J Transp Res Board 2204:21–28
6. Eaton RA, Gerard S, Datillo RS (1987) A method for rating unsurfaced roads. J Transp Res Board 1106
7. George KP, Rajagopal AP, Lim LK (1989) Models for predicting pavement deterioration. Department of Civil Engineering, University of Mississippi, MS
8. Giummarra GJ, Martin T, Hoque Z, Roper R (2007) Establishing deterioration models for local roads in Australia. J Transp Res Board 1989(2):270–276
9. Lytton RL (1987) Concepts of pavement performance prediction modeling. In: Proceedings of the North American conference on managing pavements, Toronto, Canada, vol 2
10. Saha P, Ksaibati K (2017) Developing an optimization model to manage unpaved roads. J Adv Transp 2017, Article ID 9474838
11. Uys R (2011) Evaluation of gravel loss deterioration models case study. Transp Res Record 2205:86–94
12. Wijk LV, Williams D, Serati M (2011) Roughness deterioration models for unsealed road pavements and their use in pavement management. Int J Pavement Eng
13. Woll JH, Surdahl R, Marquez R, Everett R, Andresen R (2011) Road stabilizer product performance: Seedskadee National Wildlife Refuge, U.S. Central Federal Lands Highway Division, Lakewood. November 23, 2011
14. Zyl GV, Uys R, Henderson M (2007) Applicability of existing gravel road deterioration models questioned. J Transp Res Board 1989(1):217–225

Numerical Study on the Shear Behaviour of Railway Ballast Using Discrete Element Method

S. Venuja, S. K. Navaratnarajah, W. R. R. Jayawardhana, P. H. L. Wijewardhana, K. Nirmali, and M. A. M. Sandakelum

Abstract Rail transport is the most popular mode of transport where a large number of passengers and a large amount of freights are transported efficiently with economical benefits. Ballasted tracks are the widely used track foundation system around the world. Railway ballast is a coarse granular material with high bearing capacity and shear strength. The ballast layer uniformly transmits the loads from moving trains and sleepers to the underlying layers at a reduced level. When studying the behaviour of ballast under different loading conditions, a huge amount of ballast materials are consumed and it is very labour intensive work for large-scale laboratory tests. Nowadays, numerical studies are adopted by many researchers to reduce the usage of human resources and materials. And also, numerical studies enable extended analysis through conducting a parametric study using the validated model. In this study, a numerical model was developed to study the shear behaviour of ballast and ballast–concrete interface using the discrete element method. Ballast with different shapes and sizes were modelled using multi-sphere clumps. The model was run under 30, 60, and 90 kPa normal stresses with a constant shearing rate of 4 mm/min as same as the laboratory test conditions. The model was validated using previous experimental results, and an acceptable agreement was observed for the ballast–concrete interface. The formation of the shear band in direct shear loading was observed by analysing the contact force distribution and the displacement vectors. The validated model can be used to study the change in shear behaviour of ballast when geogrid is inserted. Further, the model can be improved to incorporate the breakage of ballast particles.

Keywords Discrete element method · Multi-sphere clumps · Railway ballast · Shear band · Shear behaviour

S. Venuja (✉) · S. K. Navaratnarajah · W. R. R. Jayawardhana · P. H. L. Wijewardhana · K. Nirmali · M. A. M. Sandakelum
Department of Civil Engineering, Faculty of Engineering, University of Peradeniya, Peradeniya, Sri Lanka
e-mail: venujas@eng.pdn.ac.lk

R. Dissanayake et al. (eds.), *12th International Conference on Structural Engineering and Construction Management*, Lecture Notes in Civil Engineering 266,
https://doi.org/10.1007/978-981-19-2886-4_17

1 Introduction

Rail transport is one of the most popular modes of land transport all over the world. Ballasted tracks and slab tracks are the two types of track systems on which trains are travelling. Even though the maintenance cost and frequency are higher for ballasted rail tracks than that for slab tracks, the former is highly adopted due to ease of construction, low initial investment, and good noise and vibration absorption [1, 2]. The enormous growth in population and urbanization increases the necessity for heavier and faster trains. Cyclic and impact loads generated by fast-moving heavy haul trains cause breakage, high lateral spread, and settlement of ballast, leading to rail–sleeper misalignment and loss of load-bearing capacity, and hence, compromised safety and frequent track maintenance [6, 8, 13, 15, 16, 19, 23].

Ballast material is placed underneath and around the sleepers and followed by sub-ballast and subgrade layers. The ballast layer is the largest layer by volume and weight in the track foundation system. The primary function of the ballast layer is to transfer the train-exerted loads to the underlying layers more uniformly at a minimal level and provide lateral safety to the rail tracks [14, 25, 27]. The high shear resistance of ballast is due to the rough surface texture and sharp edges of particles which give higher frictional resistance. When loads on the ballast layer increase, ballast undergoes breakage and smoothening of surface and edges, thus leading to a reduction in frictional resistance. Loss of shear resistance of the ballast layer leads to high lateral spreading and loss of track geometry. Ballast breakage depends on the interface types such as concrete–ballast, timber–ballast, ballast–ballast, ballast–rubber, ballast–geogrid, and so on [17, 18]. Therefore, it is necessary to analyse the shear behaviour of ballast with different interfaces. In this study, a numerical model was developed to analyse the shear behaviour of ballast and validated using the results from a previous experiment-based study [17] carried out on a large-scale direct shear apparatus.

2 Numerical Modelling

2.1 Literature Review

Adaptation of numerical modelling is developed over years with the advancements in computational power within a short period of time. The common types of numerical approaches are the Finite Element Method (FEM) and the Discrete Element Method (DEM). FEM is a continuum numerical method that has domains with boundary conditions whereas DEM is a discrete approach that analyses the macroscopic behaviour of the system from individual particle interactions.

Modelling of ballast in FEM purely depends on the material model adopted to mimic the nature of ballast material. Chawla et al. [3], Fattah et al. [7], Indramohan et al. [10], Jiang and Nimbalkar [12], Navaratnarajah et al. [20], Ramos et al. [22],

and Varandas et al. [26] are a few of the numerical studies carried out on ballast using FEM. Indramohan et al. [10] developed a model using FEM to calibrate the triaxial testing on railway ballast. 150 mm diameter and 600 mm high cylindrical model was used to represent the ballast. Since ballast shows elastoplastic failure, elastic and Drucker–Prager yielding properties were assigned as ballast material properties. This developed model produced similar results with the experimental results up to 120 kPa confining pressure and this study suggested that the FEM is useful in analysing the behaviour of ballast and other track components under different loading conditions.

Many other numerical studies have been carried out on ballast under various loading conditions using DEM [4, 5, 9, 11, 21, 24, 28]. Ngo et al. [21] developed a numerical model in DEM to simulate the fouled ballast behaviour with geogrid insertion under shear loading. Ballast aggregates with different shapes were created by connecting several spheres of various sizes and positions, and a library with different particle shapes was generated. Biaxial and triaxial geogrids were created by bonding small spheres (4 mm diameter balls at ribs and 8 mm diameter balls at junctions) using contact and parallel bonds. Coal fouling was adopted by inserting several 1.5 mm spheres into the voids of fresh ballast considering the contamination percentage. Normal stress was applied using a top-loading plate under a numerical servo-control mechanism. DEM models of fresh and coal-fouled ballast were in good agreement with the experimental results and minor deviations resulted from the rigidity of the top-loading plate and inadequate capturing of particle breakage. Coal fines reduced the interlocking of ballast particles into the geogrid apertures; thus, a reduction in the shear strength was observed.

2.2 Significance of Modelling Ballast by DEM

The limitations of FEM in modelling ballast are no exact material model that can exactly reflect the elastoplastic and discrete properties of ballast, difficulty to obtain the displacements and deformations, and not considering ballast breakage. DEM is capable to capture the microscopical and macroscopical behaviour of granular materials. It captures the complete particle information during the numerical simulations, considers the characteristics of individual ballast particles, and understands the effects of ballast particle degradation on the performance and deformation of the entire system. But DEM consumes more computational time when considering complex particle shapes, particle breakage, and a large number of loading cycles together. Therefore, there are only limited studies on railway ballast performance analysis using DEM.

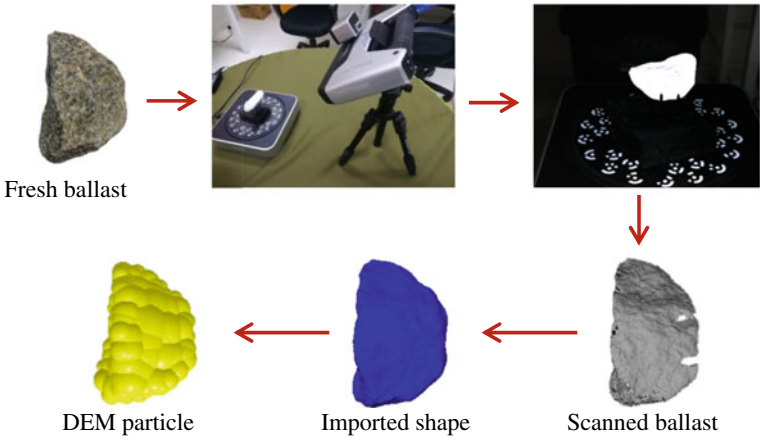

Fig. 1 Particle generation procedure in DEM with actual shapes

2.3 Particles Generation

Computational time primarily depends on the complexity of the particle shape; therefore, particle shape should be simple enough as well as efficiently represent the real shape. When the real shape of a particle is used in numerical simulation, that model can produce more realistic outcomes. Therefore, the 3D scanning method was used to adopt the actual shape of the ballast particle in the numerical model. Three representative ballast aggregates each from four different particle size intervals within the gradation of ballast selected. Initially, the selected ballast aggregates were washed, air-dried, and painted with mat type of white colour paint. A 3D laser scanner (EinScan-Pro) was used to capture the irregular shape of the ballast aggregate in the form of point cloud data. Then, a closed surface was established and sphere balls were randomly generated using the radius expansion method inside it to make DEM particles as elaborated in Fig. 1.

A solid density of 2680 kg/m^3 and Poisson's ratio of 0.35 were used for ballast material. Particle size distribution was defined as the same as used in the laboratory tests. A constant mass loading rate was applied to a virtual injector to fill the apparatus with a predetermined mass of ballast particles.

2.4 Contact Modelling

Particle to particle and particle to geometry are the two interactions considered in DEM. The accuracy of DEM results is highly influenced by the contact model parameters. Unbreakable particles were created using the multi-sphere method where an infinity bond is between spheres inside a particle. DEM commonly uses simplified

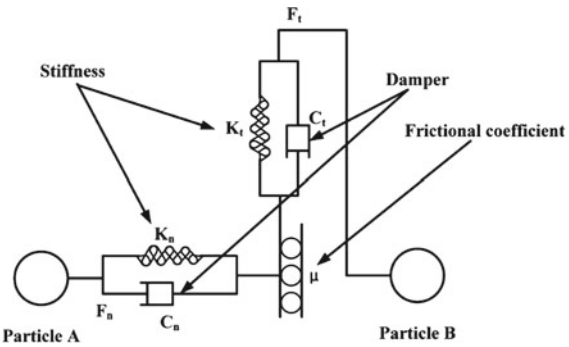

Fig. 2 Hertz-Mindlin contact model

contact models that find the forces acting on a particle due to contact within an efficient computational time. A linear contact model was used to simulate the interaction between ballast particles and particles to geometry. Figure 2 illustrates the Hertz-Mindlin contact model which is used to provide an accurate and deep understanding of granular motion contacts of ballast particles.

2.5 Test Apparatus Modelling

A large-scale direct shear apparatus was modelled numerically in this study. The dimensions and components of the apparatus can be found elsewhere [17]. The main three components are the lower part, upper part, and top-loading plate and are shown in Fig. 3. The thickness of the top and bottom parts of the shear box is kept as 60 mm to keep the ballast sample inside the apparatus while the shear boxes are moving, but it does not affect the real testing procedure. Steel is used as the equipment material of these three parts. The upper part is stationary and the lower part is movable in the shearing direction with a constant velocity of 4 mm/min. Both upper and lower parts are vertically immovable. The top-loading plate is used to apply normal stresses on ballast during the test.

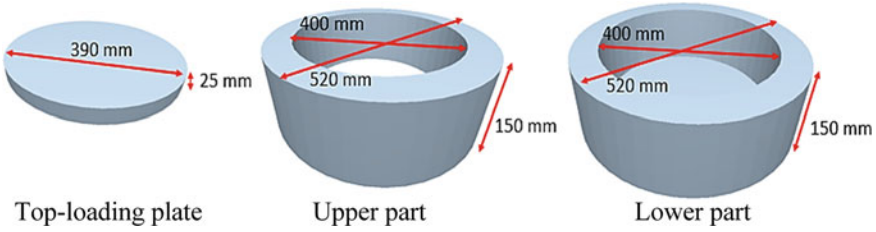

Fig. 3 Major components in the numerical model of the large-scale direct shear apparatus

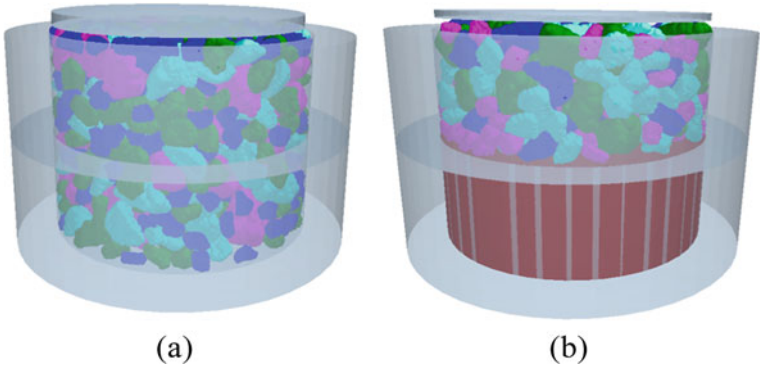

Fig. 4 **a** Model of ballast–ballast interface test; **b** Model of ballast–concrete interface test

Figure 4a shows the particle-filled model used to analyse the ballast shear behaviour. For the concrete–ballast interface test, a concrete cylinder was placed completely in the lower part of the cylinder as shown in Fig. 4b. Thus, in the numerical model also a solid cylinder geometry with concrete properties was used at the lower part. On top of it, ballast particles were filled.

3 Model Validation

A three-dimensional discrete element model is used to predict the shear behaviour of the ballast–ballast interface and ballast–concrete interface. Based on the results, the ballast–ballast interface exhibited higher shear resistance than that of the ballast–concrete interface (see Fig. 5). This was due to the higher interlocking nature of ballast aggregates which produced higher resistance to shear loading.

In numerical results, shear stress increased with the normal stress increment regardless of the type of interface (see Figs. 6 and 7). This is due to the increase in particle rolling and interlocking which results in higher resistance to shear loading. When comparing the numerical results with the experimental results, the ballast–concrete interface gave an acceptable agreement compared with the ballast–ballast interface. In this numerical method, ballast particle breakage was not taken into account and the material properties were used exactly the same as the ballast properties obtained from laboratory tests. These may considerably affect the numerical results in the ballast–ballast interface as shown in Fig. 6. In ballast–concrete interface shear behaviour, after attaining higher shear stress between 0 and 4% of shear strain, a minimal increase in shear stress was observed between 4 and 15% of shear strain in experimental results under all three normal stresses. A similar trend was observed in numerical results as shown in Fig. 7.

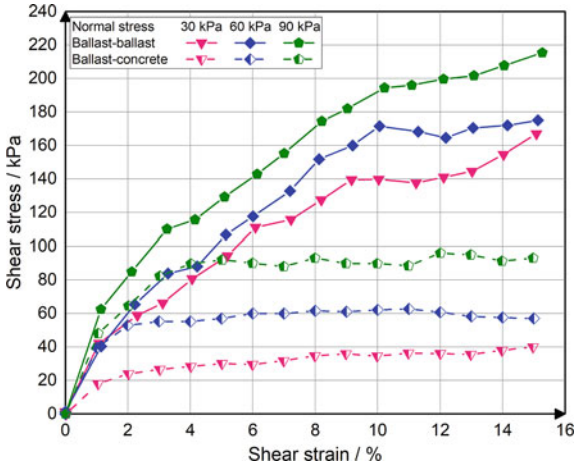

Fig. 5 Shear stress variation of ballast–ballast and ballast–concrete interfaces [17]

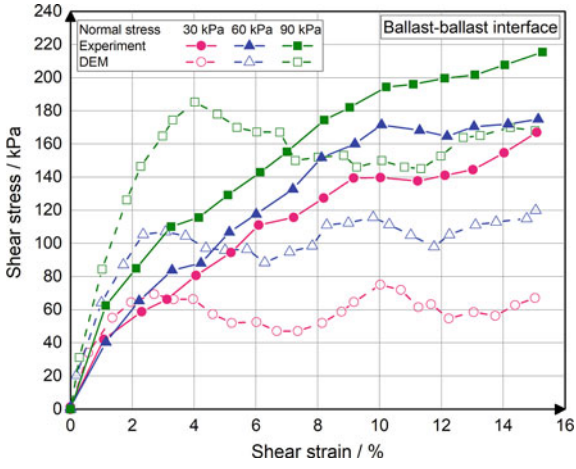

Fig. 6 Comparison of numerical and experimental results of ballast–ballast interface

4 Conclusions

Ballast particles with different shapes were created using the multi-sphere method by bonding several spheres with various diameters together. The shear behaviour of ballast–ballast and ballast–concrete interfaces under three different normal stresses was observed. Shear stress increased with higher normal stresses for both interfaces. Higher shear stress was obtained for the ballast–ballast interface than that of the ballast–concrete interface under the same normal stress. This higher shear resistance results from the increased particle interlocking at the ballast–ballast interface. The numerical model produced results that were acceptably matched with the experimental results. For more agreement with the experimental results, it is essential to use some different properties of ballast for spheres to get the real ballast

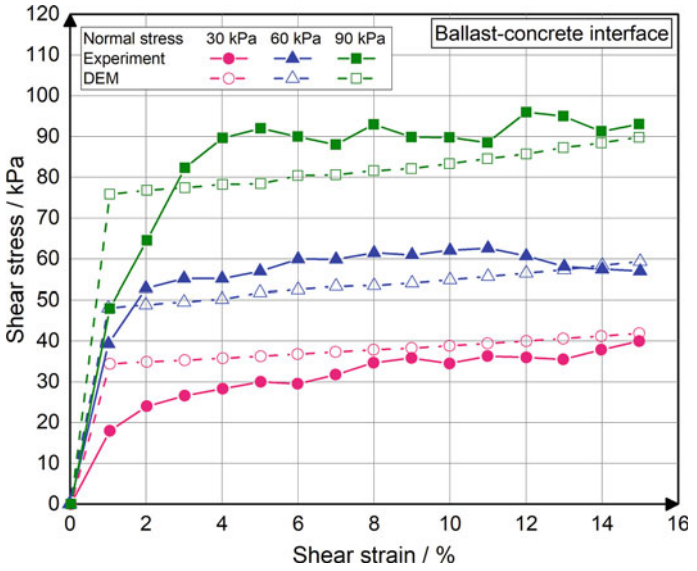

Fig. 7 Comparison of numerical and experimental results of ballast–concrete interface

behaviour in discrete element modelling when using the multi-sphere method to develop ballast particles. And also, ballast particles created in this simulation are unbreakable. Therefore, this model could not exhibit the breakage behaviour of ballast.

Acknowledgements The financial support provided by the Accelerating Higher Education Expansion and Development (AHEAD) Operation of the Ministry of Higher Education funded by the World Bank (Grant No: AHEAD/RA3/DOR/STEM/No.63) is appreciated. The support from the University of Peradeniya Research Grant (Grant No.: URG-2017-29-E) is also acknowledged.

References

1. Al-Douri YK, Tretten P, Karim R (2016) Improvement of railway performance: a study of Swedish railway infrastructure. J Mod Transp 24(1):22–37
2. Alemu AY (2011) Survey of railway ballast selection and aspects of modelling techniques. Master degree. Royal Institute of Technology. Available at:
3. Chawla S, Banerjee L, Dash SK (2018) Three dimensional finite element analyses of geocell reinforced railway tracks. In: Indian geotechnical conference. Bengaluru, India, pp 1–5
4. Chen C, McDowell GR, Thom N (2013) A study of geogrid-reinforced ballast using laboratory pull-out tests and discrete element modelling. Geomech Geoeng 8(4):244–253
5. Dahal B, Mahmud SN, Mishra D (2018) Simulating ballast breakage under repeated loading using the discrete element method. In: ASME/IEEE joint rail conference. American Society of Mechanical Engineers, p V001T01A003
6. Ebrahimi A, Tinjum JM, Edil TB (2015) Deformational behavior of fouled railway ballast. Can Geotech J. https://doi.org/10.1139/cgj-2013-027152(3),344-355

7. Fattah MY, Mahmood MR, Aswad MF (2017) Experimental and numerical behavior of railway track over geogrid reinforced ballast underlain by soft clay. In: International Congress and exhibition - sustainable civil infrastructures: innovative infrastructure geotechnology. Springer, Berlin, pp 1–26
8. Guo Y, Zhao C, Markine V, Jing G, Zhai W (2020) Calibration for discrete element modelling of railway ballast: a review. Transp Geotech. https://doi.org/10.1016/j.trgeo.2020.100341 23,100341
9. Hossain Z, Indraratna B, Darve F, Thakur P (2007) DEM analysis of angular ballast breakage under cyclic loading. Geomech Geoeng: Int J 2(3):175–181
10. Indramohan SA, Goswami P (2016) Stress strain behavior of railway ballast under static loading using finite element method. Int J Sci Eng Res 7(12):7–10
11. Indraratna B, Thakur PK, Vinod JS (2010) Experimental and numerical study of railway ballast behavior under cyclic loading. Int J Geomech 10(4):136–144
12. Jiang Y, Nimbalkar SS (2019) Finite element modelling of ballasted rail track capturing effects of geosynthetic inclusions. Front Built Environ 5:69 (01–11)
13. Juhasz E, Fischer S (2019). Specific evaluation methodology of railway ballast particles' degradation. Science and transport progress. Bull Dnipropetrovsk Natl Univ Railway Transp 0(3(81)):96–109. https://doi.org/10.15802/stp2019/171778
14. Le Pen LM, Powrie W (2011) Contribution of base, crib, and shoulder ballast to the lateral sliding resistance of railway track: a geotechnical perspective. Proc Inst Mech Eng, Part F: J Rail Rapid Transit. https://doi.org/10.1177/0954409710397094225(2),113-128
15. Mishra A, Goyal S, Muttharam M, Nanthakumar S (2018) Study on the performance of railway ballasted track reinforced with geogrid. Indian J Sci Technol. 11(23):1–4. https://doi.org/10.17485/ijst/2018/v11i23/114374
16. Navaratnarajah S, Indraratna B, Nimbalkar S (2015) Performance of rail ballast stabilized with resilient rubber pads under cyclic and impact loading. In: International conference on geotechnical engineering. Colombo, pp 617–620
17. Navaratnarajah SK, Gunawardhana KRCM, Gunawardhana MASP (2019) Influence of type of interfaces on railway ballast behavior. In: ICSECM 2019, lecture notes in civil engineering. Springer, Berlin, pp 243–251
18. Navaratnarajah SK, Indraratna B (2020) Application of under sleeper pads to enhance the sleeper-ballast interface behaviours. In: Construction in geotechnical engineering. Springer, Singapore, pp 619–636
19. Navaratnarajah SK, Indraratna B (2020) Stabilisation of stiffer rail track substructure using artificial inclusion. Indian Geotech J 50(2):196–203
20. Navaratnarajah SK, Indraratna B, Ngo NT (2018) Influence of under sleeper pads on ballast behavior under cyclic loading: experimental and numerical studies. J Geotech Geoenviron Eng 144(9):1–16
21. Ngo NT, Indraratna B, Rujikiatkamjorn C (2014) DEM simulation of the behaviour of geogrid stabilised ballast fouled with coal. Comput Geotech. https://doi.org/10.1016/j.compgeo.2013.09.00855,224-231
22. Ramos A, Correia AG, Calçada R, Costa PA, Esen A, Woodward P, Connolly D, Laghrouche O (2021) Influence of track foundation on the performance of ballast and concrete slab tracks under cyclic loading: Physical modelling and numerical model calibration. Constr Build Mater 277:122245
23. Shih JY, Thompson DJ, Zervos A (2017) The influence of soil nonlinear properties on the track/ground vibration induced by trains running on soft ground. Transp Geotech. https://doi.org/10.1016/j.trgeo.2017.03.00111,1-16
24. Sluganović V, Lakušić S, Lazarević D (2019) Track ballast modelling by discrete element method. Gradevinar 7:589–600. https://doi.org/10.14256/JCE.2350.2018
25. Sweta K, Hussaini SKK (2018) Effect of shearing rate on the behavior of geogrid-reinforced railroad ballast under direct shear conditions. Geotext Geomembr 46(3):251–256
26. Varandas J, Paixão A, Fortunato E, Coelho BZ, Hölscher P (2020) Long-term deformation of railway tracks considering train-track interaction and non-linear resilient behaviour of aggregates–a 3D FEM implementation. Comput Geotech 126:103712

27. Venuja S, Navaratnarajah SK, Bandara CS, Jayasinghe JASC (2019) Review on geosynthetic inclusions for the enhancement of ballasted rail tracks. In: ICSECM 2019, Lecture notes in civil engineering. Springer, Berlin, pp 459–468
28. Zhao H, Chen J (2020) A numerical study of railway ballast subjected to direct shearing using the discrete element method. Adv Mater Sci Eng. https://doi.org/10.1155/2020/3404208202 0,1-13

Reinforcing of Earth Soil and Cement with Pretreated Cornhusk Fibers in the Development of Building Materials

T. N. Fernando and I. P. Batuwita

Abstract The modern construction industry in Sri Lanka focuses on introducing environment friendly and long durable sustainable materials in constructions. Modern trend is producing different types of earth soil-based building blocks and innovating modified daub mixture-based structures. However, surface cracking and damage due to flood are the major issues that are faced in some soil-based structures. The use of cellulose fiber as a reinforcement material has many advantages such as providing adequate stiffness, strength, and bonding capacity to cement-based matrices for substantial enhancement of their flexural strength. The aim of present study was to find out the possibility of using Alkaline Hydrogen Peroxide (AHP)-pretreated cornhusk fibers as a reinforcement material to prepare soil and cement-based composite mixture for development of roofing sheets, ceiling sheets, and wall panels. The AHP pretreatment is an effective pretreatment that could be performed at room temperature and under atmospheric pressure for extracting cellulose from agro plant residue like cornhusks. Cornhusks is comparatively one of freely available agro plant residues in Sri Lanka and with required chemical composition, from which cellulose could be extracted easily from AHP pretreatment. The selected earth soil was laterite and has dark reddish color. The composite mixture was prepared by mixing of earth soil, cement, and AHP-pretreated cornhusks fibers in the weight ratios of 1:1:0.025 of, respectively, with a certain amount of water. Roofing sheets, ceiling sheets, and wall panels were prepared using the said composite mixture and were analyzed for morphological characteristics, water absorbency, flexural load, and durability. The developed composite samples have reddish to brownish color. The water absorbency, flexural load, and durability were of satisfactory level. These can be used in construction of low cost attractive and environment friendly architectural constructions especially in areas where tourists frequent in Sri Lanka.

Keywords Alkaline hydrogen peroxide pretreatment · Cellulose fibers · Cement · Cornhusks and earth soil

T. N. Fernando (✉) · I. P. Batuwita
National Engineering Research and Development Centre of Sri Lanka, Industrial Estate, Ekala, Ja-Ela, Sri Lanka
e-mail: nilanthifernando45@yahoo.com

R. Dissanayake et al. (eds.), *12th International Conference on Structural Engineering and Construction Management*, Lecture Notes in Civil Engineering 266,
https://doi.org/10.1007/978-981-19-2886-4_18

1 Introduction

These days, worldwide search for sustainable construction materials to overcome effects of global warming and improve the environmental sustainability has increased. Earthen construction materials are the oldest sustainable building materials that have been used throughout the world. Ten thousand years ago, soil is undoubtedly one of the most widely used construction materials in the world to build human homes and other constructions [1]. Also, in ancient Sri Lanka simple dwellings were built using natural clay and thatched roofs and which was referred as "mati geya" (clay house) in Sinhala is built using the wattle and daub method. In this style of building, a framework of poles is sunk into the ground, with reeds or jungle vines woven horizontally between the poles to make mat-like screens (wattle or "warichchi" in Sinhala). The spaces between the exterior and interior walls are then filled with mud. Both sides of these walls are then plastered (daubed) with a wet mud mixture [2]. This style of building (Fig. 1) and the materials used have remained unchanged over the centuries. While natural decay and the development of building materials have left very few ancient wattle and daub houses, the process is being followed faithfully by the few who continue to live in these simple houses. The use of natural clay and thatched roof is ideally suited to the hot tropical climate of Sri Lanka. When the weather is cool and humid, especially at night, the porosity of the clay absorbs moisture, and during the day, when it is warm, the moisture is expelled. Therefore, the walls of these houses literary breath, acting as a natural "air conditioner," which prevents heat from crossing the walls. The traditional rural homes, which were made of clay earth walls and thatched roof, are both eco-friendly and ideally suited to the local climate.

However, surface cracking, low strength, damage after exposure to flooding, and heavy rain are major issues with ancient structures made of daub mixture. Therefore, some researchers in Sri Lanka have been carrying out some research activities to improve the ancient daub mixture method for application in modern constructions. In ancient Sri Lanka, clay, lime, cow dung, and mud were mostly used as stabilizing materials for preparation of daub mixture and researchers have identified some advantages in mixing cement with ancient daub mixture to improve its negative issues [3]. Over the past few decades, construction sector in Sri Lanka has mainly

Fig. 1 A developed ancient sustainable home in Sri Lanka [2]

moved toward the introduction of soil and cement-based constructions, and different types of soil-based blocks were innovated [4]. Then, some construction companies have introduced construction of sustainable houses and shelters (Cabanas) that are similar to ancient clay houses in different parts of Sri Lanka [3]. They have used ancient daub mixture or modified daub mixture for constructing of some structures. Also, some use cement blocks or bricks for constructing of walls and applying sand and clay mixture as a finishing coat to level and smoothen the surface of the walls. Most of these types of construction are built in areas not only where foreign tourists frequent in Sri Lanka, but for locals as well who live in highly urbanized communities where land space is limited and where the inhabitants lead busy lives and would like to spend time in these resorts for recreation and relaxation. These are healthier for humans and for the planet as well as it is an essential part of sustainability. However, damage due to flood and use of low durable roofing materials (paddy straw, coconut, and Palmyra leaf) and surface cracking of plastered walls due to non-application of reinforcement materials are major issues in these types of constructions as shown in Fig. 2a, b. Sometimes, an experienced person is needed for plastering the walls and it is labor intensive.

Since ancient times, cellulosic fiber-reinforced cement-based composites were used to reinforce brittle building materials [6]. The use of cellulose fiber as a reinforce material has more advantages such as providing adequate stiffness, strength, and bonding capacity to cement-based matrices for substantial enhancement of their flexural strength, toughness, and impact resistance [7–9]. Thus, these fibers can reduce the free plastic shrinkage [10], decrease the thermal conductivity [11], and improve the acoustic performance increasing the sound absorption and the specific damping and the density of the composite [12]. According to all clarifications, the use of cellulose fiber as a reinforce material in the modified daub mixture has more advantages.

Cotton is the cellulose available in nature and is not abundantly available in Sri Lanka [13]. Paper pulp is one source where cellulose component is easily found, the major issue is that preparation of paper pulp from inked waste paper requires intensive deinking, and it is a capital intensive. However, some agro plant residues of cornhusks, corn leaves, bagasse, and guinea grass are rich in cellulose and are widely available

Fig. 2 **a** Constructed modern doubt wall **b** Constructed modern Clay house [5]

material in Sri Lanka. The Alkaline Hydrogen Peroxide (AHP) pretreatment is an effective pretreatment that can be performed at room temperature and atmospheric pressure for extracting of cellulose from agro plant residues [14]. The procedure of AHP is an easy technique once introduced will encourage a small-scale industry, not only in rural areas but also in urban areas as well in any developing country from which an income can be earned through self-employment. Thus, introducing AHP pretreatment for extracting of cellulose can be done with all agro plant residues and extracted fibers could be used for processing of cellulose-based bio composites. There are self-employed people selling boiled corncobs in wayside kiosks in areas frequented by tourists and pilgrims and others selling raw corn to industries producing foodstuff. Therefore, a bulk amount of cornhusks and cobs are discarded in different areas in Sri Lanka. To date, no one has done any research or produced any report on how much of a bulk of cornhusks and cobs are discarded or burned after obtaining seeds and kernel. However, researchers are focusing on processing corn and other plant residues which otherwise are wasted, to produce a marketable product to add to the economy of Sri Lanka.

The present study was focused on preparation of a composite mixture by reinforcing of AHP-pretreated cornhusk fibers with earth soil and cement to develop building materials (roofing sheets, ceiling sheets, wall panels, and plasters) for different applications in construction, landscaping, and architectural sectors.

2 Material and Methodology

2.1 Materials

Industrial grade sodium hydroxide (NaOH), hydrogen peroxide (H_2O_2), and hydro chloric (HCl) acid were purchased from Glorchem Enterprise in Sri Lanka. Cornhusk residues for the experiment were collected from corn sellers in surrounding areas of Gampaha District in Sri Lanka. A "Bruker" Fourier Transform Infrared (FTIR) Spectroscopy and Scanning Electronics Microscope (SEM) were used at the Department of Materials Science and Engineering, University of Moratuwa, Sri Lanka. The used soil type was a laterite. It was collected from the Anuradhapura district (North Central Province, Sri Lanka). It has a reddish color and consists of 90% clay, and the pH was 6.2. A collected soil sample was spread on the floor and solar dried. Finally, it was sieved using a sieve (mesh size 4.00 mm/ No: 5). In addition, Ordinary Portland Cement (OPC) was used.

Table 1 Different composition of materials, used for preparation of the composite mixtures

Concentration of pretreatment	Cement (kg)	Earth soil (kg)	Pretreated fiber weight
10 ml of 0.625 mol/L NaOH + 0.5 ml of H_2O_2 to 1 g of dried cornhusk residues	5	5	Pretreated wet fibers from 300 g of dried shaded cornhusks
			Pretreated wet fibers from 400 g of dried shaded cornhusks
			Pretreated wet fibers from 500 g of dried shaded cornhusks
10 ml of 1 mol/L NaOH + 0.5 ml of H_2O_2 to 1 g of dried cornhusk residues	5	5	Pretreated wet fibers from 300 g of dried shaded cornhusks
			Pretreated wet fiber from 400 g of dried shaded cornhusks
			Pretreated wet fiber from 500 g of dried shaded cornhusks

2.2 Methodology

2.2.1 Pretreating of Cornhusks

Solar-dried and shaded cornhusks were pretreated using AHP pretreatment that is described in Fernando et al. [14]. They have prepared one pretreatment solution by mixing 10 ml 1.25 mol/L with 1 ml of H_2O_2 to 1 g of dried plant residues. The concentration they used is not economical for development of composite materials. Therefore, two pretreatment solutions were prepared using low concentrations of NaOH adding half of the amount of H_2O_2 that was used in the above instant, as given in Table 1. Finding the percentages of cellulose and confirmation of extraction of fibers from FTIR spectroscopy were carried out by the methods described by Fernando et al. [14]. In additionally, tensile strength of raw and pretreated fibers were measured using a universal testing machine.

2.2.2 Preparation of Composite Mixtures

The composite mixtures were prepared by mixing of earth soil (laterite), cement, and AHP-pretreated cornhusk fibers in the weights ratios as describe in Table 1. The same portion of cement and earth soil were used for the preliminary studies, and 10 kg of composite mixture could be added to the iron frame (length-1 m × width-1 m × thickness-0.008 m) in the vibration machine, which was used for the spreading of composite mixture.

2.2.3 Preparation and Characterization of Building Materials Using Prepared Composite Mixtures

Roofing sheets were prepared by spreading the composite mixture on the iron frame, which was fixed on the vibrating bed, and it was allowed to vibrate for 2 or 3 min. Then, vibrated mixture was moved to the mold (asbestos sheet was used as a mold) for making a roofing sheet with shape of existing asbestos roofing sheet. The similar procedure was used for making of flat sheets (celling sheets and wall panels), and the required iron frames for the molding of each material was fabricated separately. A day after prepared composite material was removed from the mold, water was sprayed on top of the materials. After three days, the prepared materials were immersed in a water tank and allowed soaking for 24 h. Then, the materials with low handling strength, large surface cracking, and damaged after soaking were rejected. This experiment was used for identification of the best composite mixture to prepare composite materials for the testing of the following characteristics. Thus, all prepared materials were kept 28–30 days in a shady place after curing, prior to its move to testing of characteristics.

(a) Morphological characteristics
Internal structural arrangement of prepared composite materials was identified using a SEM.

(b) Water absorption test
Three pieces were used from the casted composite materials for the testing of water absorbency. First, those were dried at 60 °C until weight became constant in an electric oven. Then, immersed in a water tank for 24 h. The difference in weight was calculated and given as a percentage of water absorbed by the composite material using the Eq. 1.

$$\text{Water absorption} = [(\text{A}-\text{B})/\text{B}] \times 100\% \tag{7}$$

where A = weight of specimen after 24 hours immersion, B = weight of the dry specimen.

(c) The testing of the flexural load on the casted materials
The method used by Eswaramoorthi and Nandhakumar [15] was used for testing of the flexural load using a universal testing machine. Corrugated sheets are subjected to a centerline load over a simply supported span of 400 mm. The load was gradually applied until failure of the specimen.

(d) Assessment of permeability test
The specimen was prepared as shown in Fig. 3. Two small weirs were prepared using cement mortar to allow water to stand in a pool with a maximum depth of 10 mm to 15 mm. Then, the sample was stored at 30 °C and at least 40% relative humidity for 20 h, and stored the casted sheets to be tested at 30 °C and a minimum of 40% relative humidity for 24 h.

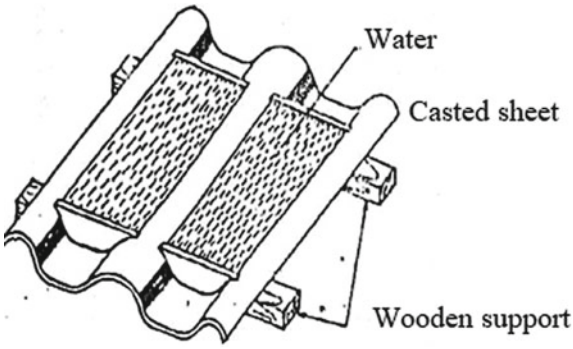

Fig. 3 Procedure of the measuring of water impermeability of roofing sheet

3 Results and Discussions

The composite materials with low handing strength as shown in Fig. 4a, b and materials with surface cracking in Fig. 4c, d were removed for characterizations. It was evident that applying a suitable fiber reinforcement material is a requirement in casting of composites to avoid surface cracking. The results of Table 2 show that the ideal pretreatment concentration was 10 ml of 1 mol/L NaOH with 0.5 ml of H_2O_2 to 1 g of dried cornhusks. Adding this pretreatment to 400 g and 500 g of dried cornhusk with 5 kg of soil, 5 kg of cement-added composite materials shows good appearance (no damages). Further, average flexural loads were highest in materials prepared by adding 400 g, rather than by adding 500 g of pretreated fibers from dried cornhusks to 10 kg of cement and soil mixture and it is evident that the weight of applied pretreated fibers affect the characteristics of the casted materials. Studies by Stevulova and Hospodarova [16] show that the compressive strength decreases with increased amount of cellulose fiber due to the increased number of voids in the specimen. Thus, the result of the present study inclines to agree with their findings.

The comparison of FTIR results of raw cornhusk fibers and pretreated fibers (Fig. 5) from the AHP pretreatment with concentrations of 10 ml of 1 mol/L NaOH and 0.5 ml of H_2O_2 to 1 g of plant residue has confirmed that the extracted fibers were cellulose as comparison the wavenumbers that described in our previous study [14]. Figure 6a–c show pretreated cornhusk solution of selected concentration, neutral-

Fig. 4 Visual observations of rejected materials after the casting

Table 2 Results of the prepared materials using different composite mixture

Concentration of pretreatment	Cement (kg)	Earth soil (kg)	Pretreated fibers weight	Visual observations after absorbing water	Average Flexural load
10 ml of 0.625 mol/L NaOH + 0.5 ml of H_2O_2 to 1 g of dried cornhusk residues	5	5	Pretreated wet fiber from 300 g of dried shaded cornhusks	Low handling strength and damaged after soaking	N/A
			Pretreated wet fiber from 400 g of dried shaded cornhusks	Low handling strength and damaged after soaking	N/A
			Pretreated wet fiber from 500 g of dried shaded cornhusks	Low handling strength and damaged after soaking	N/A
10 ml of 1 mol/L NaOH + 0.5 ml of H_2O_2 to 1 g of dried cornhusk residues	5	5	Pretreated wet fiber from 300 g of dried shaded cornhusks	Good handling strength and damaged occurs after soaking	N/A
			Pretreated wet fiber from 400 g of dried shaded cornhusks (dried cellulose fibers 125 g)	Good handling strength and no damages after soaking	Roofing sheets-0.85 kN
					Ceiling sheet and wall panels (flat sheets)—0.45 kN
			Pretreated wet fibers from 500 g of dried shaded cornhusks (dried cellulose fibers 155 g)	Good handling strength and no damages after soaking	Roofing sheets-0.6 kN
					(Flat sheets)—broken when applying load

ized pretreated solution, and dried pretreated fibers, respectively. The neutralized pretreated fibers have white to off-white color, and average tensile load was 0.076 kN and percentage of cellulose was 79.3%. Figure 7a, b shows the SEM diagrams of the pretreated cornhusk fibers, and rougher surface has occurred due to removing of surface impurities. Ashori et al. [17] indicated that lignocellulose fibers are used

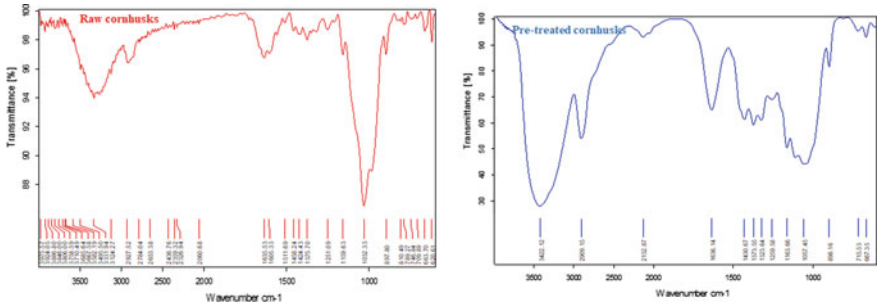

Fig. 5 FTIR analysis of raw and pretreated cornhusk from selected best pretreatment

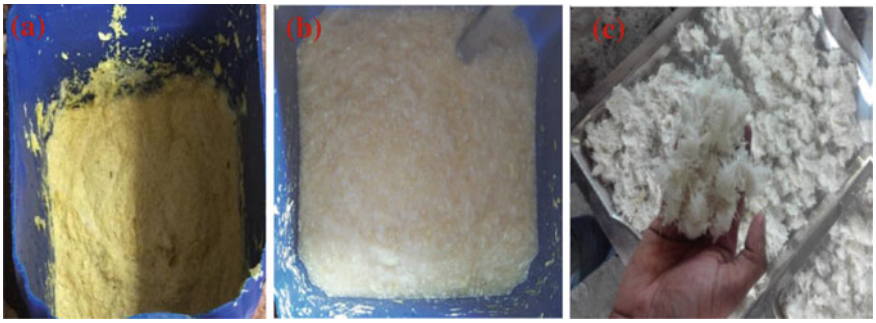

Fig. 6 Pretreated fibers—**a** pretreated cornhusk solution **b** neutralized pretreated solution **c** dried and neutralized pretreated fibers

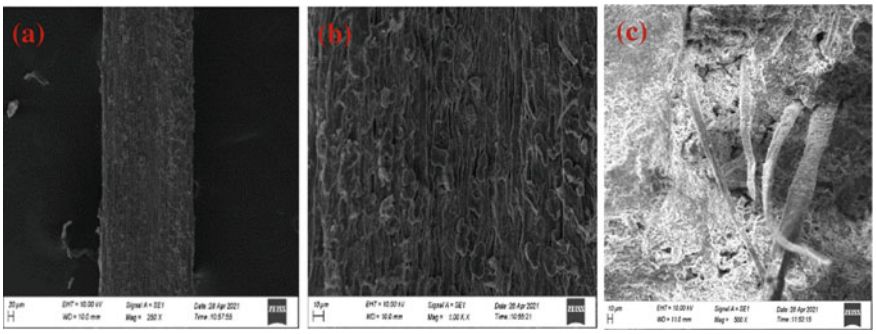

Fig. 7 SEM diagrams—**a**, **b** pretreated cornhusks, **c** casted composite material

as reinforcing fibers in composite materials, and the pretreated surface is needed for the reacting of fiber surface in forming a bridge of chemical bonds between the fibers and matrix. This mechanism is evident on the SEM diagram of the casted composite material as shown in Fig. 7c. Thus, the porous structure was observed in

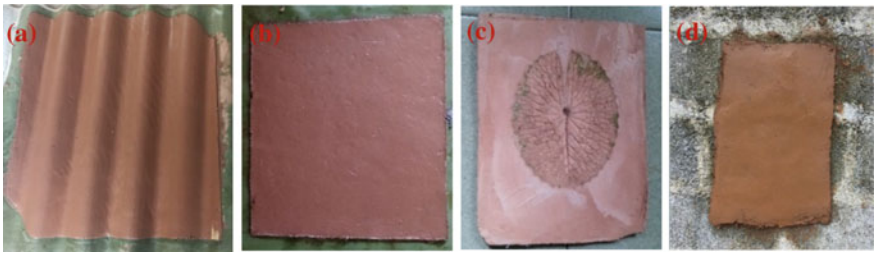

Fig. 8 Casted materials—**a** roofing sheet, **b** ceiling sheet, **c** wall panel, **d** wall plaster

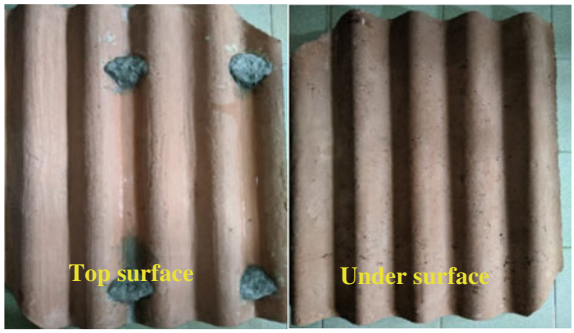

Fig. 9 Visual observation of the water permeability testing after 24 h

SEM diagram. Normally, soil-based materials consist of porous structure that helps warm the environment as describes in Google [2]. However, many larger pores are not good for the composite, and it lowers flexural load and increases water permeability and water absorption rate in the casted materials. Figure 8 shows visual observations of casted cellulose fiber-reinforced materials, and all have reddish to brownish color. The average flexural loads were 0.85 and 0.45 kN respective in roofing sheets and flat sheets (ceiling sheets and wall panels). Figure 9 indicates the visual observation of result of water permeability test and found that water drops have not appeared on the underside of the roofing sheet after 24 h. The results of percentage of water absorption of casted roofing sheets and flat sheets are indicated in Fig. 10. The percentage of water absorption varied between 7 and 14.5%. However, roofing sheets had high water absorption characteristics in comparison with those of flat ones made using same composite mixture. An iron frame (length-0.5 m × width-0.3 m × thickness-0.008 m) was used as a mold for preparing flat sheets, and additionally, compression force was applied manually instead of applying vibration. However, vibration bed was used only for casting of roofing sheets. The additional compression force applied manually may have been effective in decreasing the percentage of water absorption in flat casted materials due to elongation or removal of air bubbles and increasing compression tightens plaits in the composite materials in the frame area. Udagama and Kulathunga [18] has used a hydraulic jack in molding composite materials. Therefore, using of vibration bed and applying compression force on top of the composite

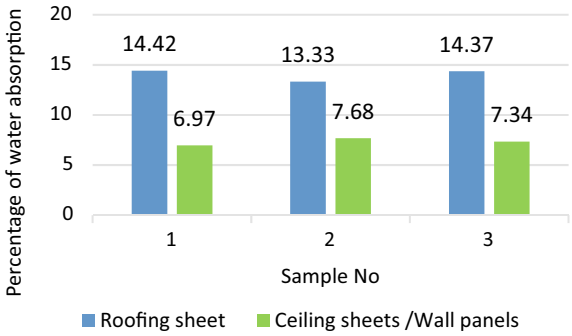

Fig. 10 Percentage of water absorption

mixture in the mold could increase flexural load and decrease porosity of the casted composite materials. Also, this reduces water absorption. However, casted materials in the present study have not shown any degradation after being kept immersed in a water tank for three months.

According to the Sri Lankan standard for concrete roofing semi-sheet [19], the flexural load shall be not less than 0.5 kN and the maximum percentage of water absorption should be less than 28%. The flexural load of roofing sheet and water absorption values of all materials in the present study were compared with the SLS standards for the concrete corrugated semi sheet. Further, there was no standard for material of flat sheet similar to that developed in the present study to compare flexural load results. However, the developed flat sheet are expected to be introduced as wall tiles and ceiling sheets. When compared with those of flexural load of SLSI [19] standard, the flexural load of flat sheet developed in the present study was at a satisfactory level. Thus, the developed composite mixture and wall panels in the present study could be used for plastering or application on the wall surfaces, which are made using cement sand blocks and bricks. Cement sand blocks are most popular in Sri Lanka due to some advantages such as cement is relatively easy to import, most raw materials for cement come from Japan or India. However, use of bulk amount of cement sand blocks has more disadvantages such as poor management of global resources, which increases the already high-embodied energy and carbon emissions involved in cement production and the large amounts of sand required for preparation of cement-based plastering. On the contrary, there are other issues like pressure on river sand resources, resulting price hikes, saltwater intrusion on water-table, and coastal erosion. Further, cement sand block houses are very thermally inefficient and extremely hot in this climate [20]. Further, laterite soils could be easily found in different part of Sri Lanka and cost less compared to that of sand. Therefore, the use of laterite soil-based materials have more advantages in the tropical country of Sri Lanka. Furthermore, the use of composite materials in the ratio of 1:1:0.025 (earth soil, cement, and AHP-pretreated cornhusk fibers in the weight ratio, respectively) is ideal for reinforcing all casted composite materials, and it was revealed in the present study. However, future research will be continued to find some materials to partially replace cement and to develop an earth soil, and cement product with cellulose fiber

reinforcing material for high strength, durability, and other positive characteristics seen in ancient clay houses. Such a product can be introduced for constructing of cabanas, in applications of landscaping and architectural structures in areas highly frequented by tourists in Sri Lanka.

4 Conclusion

The results of the present study indicate the validity of applying reinforce material when preparing roofing sheets and flat sheets to avoid surface cracking. The ideal pretreatment concentration was 10 ml 1.0 mol/LNaOH and 0.5 ml of H_2O_2 to 1 g of dried cornhusk residues. In addition, pretreated fibers from 400 g of raw cornhusks are sufficient for a 10 kg of soil and cement-based composite mixture to cast the materials with good handling strength. The quantity of fiber weight affects the flexural load of the developed material. The increasing fiber weights results in decreased flexural load due to increase in porosity of the materials. The flexural load of roofing sheet and water absorption values of all materials in the present study were compared with the SLS standards for the concrete corrugated semi sheet. The use of composite materials in the ratio of 1: 1: 0.025 (earth soil, cement, and AHP-pretreated cornhusk fibers in the weight ratio, respectively) is ideal for reinforcing all casted composite materials, and it was revealed in the present study. The developed building materials have attractive colors ranging from reddish to brown that may be used for construction and design of structures with ancient appearance.

5 Recommendations

A homogeneous composite mixture, prepared by mixing all ingredients, is needed prior to be used as molding material to avoid surface cracking**.** Further, low-income earners living in areas surrounding tea plantations normally construct line houses, which in effect is a visual pollution. Some laterite soils are widely available in the lands of tea plantations. Therefore, if soil-based materials, which are prepared in the present study are introduced, people living in those areas will benefit more. The reason is they can build attractive houses using laterite soil at a low cost. Furthermore, these can be used in the construction of low cost and environment friendly constructions of attractive architectural design similar to ancient clay houses in areas where tourists frequent in Sri Lanka.

Acknowledgements The authors would like to acknowledge Ms. T. M. N Perera and Ms. K.V.A.T.N Senevirathne, undergraduate training students at the Faculty of Engineering Technology, University of Wayamba, for assistant given to conduct all experiments in the present study. Special thanks to Mr. B. Gunaratne for making this manuscript a success.

References

1. Gisele P, De Pádua L, Maskell D, Heath A, Walker P (2016) Cement with SCBA as a stabilizer in compressed earth blocks. Available at: https://craterre.hypotheses.org/files/2018/05/Terra-2016_Th-4_Art-231_P%C3%ADdua.pdf. Accessed 29 Apr 2021
2. Google.com (2012) Redirect notice. Available at: https://www.google.com/url?sa=i&url=http%3A%2F%2Fexploresrilanka.lk%2F2012%2F07%2Fgreen-homes-of-our-past%2F&psig=AOvVaw13wTVDWhZ-f6XRmxc0ytBn&ust=1619771106381000&source=images&cd=vfe&ved=0CGIQr4kDahcKEwiIxZHqg6PwAhUAAAAAHQAAAAAQAw. Accessed 29 Apr 2021
3. Udawatthe C, Arooz R, Halwatura RU (2016) New earth walling material: integrating modern technology into ancient mud wall. In: Proceedings of the 7th international conference on sustainable built environment, Sri Lanka, vol 8, pp 24–31
4. Jayasinghe C (1999) Stabilized soil block technology for Sri Lanka. Available: https://www.researchgate.net/publication/304242442
5. Google.com (2021) Redirect notice. Available at: https://www.google.com/url?sa=i&url=http%3A%2F%2Fgwisolutions.com%2Fchandulaconstruction%2FClay%2520House.html&psig=AOvVaw13wTVDWhZ-f6XRmxc0ytBn&ust=1619771106381000&source=images&cd=vfe&ved=0CA0QjhxqFwoTCIjFkeqDo_ACFQAAAAAdAAAAABAK. Accessed 29 Apr 2021
6. Tonoli GHD, Santos SF, Savastano H, Delvasto S, de Gutiérrez RM, de Murphy MD (2011) Effects of natural weathering on microstructure and mineral composition of cementitious roofing tiles reinforced with fique fibre. Cem Concr Compos 33:225–232
7. Savastano H, Warden PG, Coutts RSP (2013) Mechanically pulped sisal as reinforcement in cementitious matrices 25:311–319
8. Tolêdo-Filho RD, Ghavami K, England GL, Scrivener K (2003) Development of vegetable fibre-mortar composites of improved durability. Cem Concr Compos 25(2003):185–196
9. Morton JH, Cooke T, Akers SAS (2010) Performance of slash pine fibers in fiber cement products. Constr Build Mater 24:165–170
10. Toledo Filho RD, Ghavami K, Sanjuán MA, England GL (2005) Free, restrained and drying shrinkage of cement mortar composites reinforced with vegetable fibres. Cem Concr Compos 27:537–546
11. Bentchikou M, Guidoum A, Scrivener K, Silhadi K, Hanini S (2012) Effect of recycled cellulose fibres on the properties of lightweight cement composite matrix. Constr Build Mater 34:451–456
12. Neithalath N, Weiss J, Olek J (2004) Acoustic performance and damping behavior of cellulose–cement composites. Cem Concr Compos 26:359–370
13. Fernand TN, Ranathunga YMMK (2020) Processing of carboxymethyl cellulose from bagasse. In: Proceedings of national engineering research symposium (NERS 2020), vol 1, pp 8; 13–12
14. Fernando TN, Aruggoda AGB, Ariyadurai SA, Dissanayaka CK, Kulatunga S (2015) Evaluation of alkaline peroxide pretreatment for extraction of cellulose from selected plant biomasses. J Eng Technol Open 3(2):10
15. Eswaramoorthi P, Nandhakumar S, Karthikeyan P, Magudeaswaran P (2017) Study on improvement in strength properties of corrugated roofing sheets with the addition of various fibres in the Mortar. Int J Civ Eng Technol 8(8):463–471
16. Stevulova N, Hospodarova V (2015) Cellulose fibres used in building materials. In: Proceedings of REHVA annual conference 2015 "Advanced HVAC and Natural Gas Technologies" Riga, Latvia, May 6–9
17. Ashori A, Ornelas M, Sheshmani S, Cordeiro N (2012) Influence of mild alkaline treatment on the cellulosic surfaces activesites. Carbohyd Polym 88(4):1293–1298. https://doi.org/10.1016/j.carbpol
18. Udagama UDGUC, Kulathunga KA (2014) Development of sustainable roofing materials from waste, a research Gate article, www.academia.edu. Available at: https://www.academia.edu/20872422/Development_of_Sustainable_Roofing_material_from_Waste. Accessed 28 Sep 2021

19. SLSI (1999) Specification for concrete roofing semi-sheets, tiles and fittings Test Methods, SLS 1189: Part 2
20. Davis Lara K, Serge M (2017) Feasibility report for compressed stabilised earth block (CSEB) production and use in the North and East of Sri Lanka developmental housing reconstruction support to Sri Lankan internally displaced people (IDPs) A European Commission's Aid to Uprooted People (AUP) 2014 regional facility for Asia programme
21. Ardoğa MK, Şengün E, Alam B, Yaman İÖ (2018) Determination of the tensile strength of different fiber reinforced concrete mixtures. Published research gate paper

Stability Analysis of Colombo–Katunayake Expressway Embankment Using Fly Ash-Stabilized Soil as the Embankment Material

K. Mathumidah, S. Lavanyan, and M. C. M. Nasvi

Abstract There is a huge scarcity in good-quality embankment materials in Sri Lanka with the rapid development of highway construction in the country. On the other hand, huge amount of fly ash (FA) is produced at Lakvijaya coal power plant and bulk of the FA produced ends up in landfills causing adverse environmental impacts. Therefore, this research aims to predict the feasibility of using FA-stabilized marginal soil (the soil that does satisfy the Road Development Authority requirements for embankment material) as an embankment material by analyzing the stability and deformation of the embankment constructed using FA-stabilized marginal soil. For this purpose, two selected embankment sections at Colombo–Katunayake Expressway (CKE) were analyzed numerically using PLAXIS 2D and SLOPE/W software. FA percentages of 0, 10, 20, 30, and 40% (by weight) were considered for the stabilization, and the soil properties of the marginal soil and the FA-stabilized soil were obtained from relevant literature. First, model was validated using PLAXIS by analyzing various material model combinations (Mohr coulomb (MC), soft soil (SS) and soft soil creep (SSC)) for different soil layers, and the model combination providing consistent settlement results with the field observation was selected for further analysis. Based on the selected model, analyses were conducted to predict the optimum FA content and long-term settlement behavior of the FA-stabilized embankment. Results revealed that MC-SS-SSC (SS for soft soil, SSC for peat, and MC for to other soil type) is the most reliable model to predict the field settlement accurately. The optimum FA content is 30% FA (by weight) for better performance in terms of both deformation and stability behavior. Long-term analysis revealed that there is a significant reduction in vertical settlement, lateral deformation, and improvement in factor of safety (FOS) of FA-stabilized embankment compared to nonstabilized embankment.

Keywords Embankment fill · Finite-element method · Fly ash · Marginal soil · Settlement

K. Mathumidah · S. Lavanyan · M. C. M. Nasvi (✉)
Department of Civil Engineering, University of Peradeniya, Peradeniya, Sri Lanka
e-mail: Nasvimcm@eng.pdn.ac.lk

R. Dissanayake et al. (eds.), *12th International Conference on Structural Engineering and Construction Management*, Lecture Notes in Civil Engineering 266,
https://doi.org/10.1007/978-981-19-2886-4_19

1 Introduction

As a developing country, highway construction-related activities are rapidly increasing in Sri Lanka as there have been many highway projects undertaken in the recent past including Central Expressway project, iRoad Program, Badulla–Chenkaladi Road Improvement, Extension of Southern Expressway project, etc [25]. This has created a shortage of suitable embankment materials due to the scarcity of good quality embankment materials meeting the compliance requirements. Colombo–Katunayake Expressway (CKE) is the second major highway in Sri Lanka connecting the International Airport at Katunayake to the capital city of Colombo. The CKE has been constructed over soft soils, of which 53% of the land covers peat, organic soil, clays, and sludge [31]. Even though different types of soft ground treatments were implemented for CKE sections during the construction stage, considerable consolidation settlement was observed with time [19]. As good quality embankment materials cannot be found in the vicinity of the project area, they need to be hauled from longer distances making the process very uneconomical while causing other adverse environmental and social effects. On the other hand, in Sri Lanka, 300,000 metric tons of fly ash (FA) is produced annually [10]. Use of these by-products to stabilize marginal embankment materials offers sustainable solution to the issues related to the scarcity of construction materials and waste management associated with the industrial by-products. Therefore, this project aims to use FA to stabilize marginal embankment material for highway construction.

FA is a nonplastic material and pozzolanic in nature, proven as a best stabilizing material for years due to its self-cementing properties [16, 17, 23, 28]. Some of the engineering properties that make FA as a suitable material in replacement for fill materials in embankment construction include relatively lightweight, high shear strength, low compressibility, permeability, and self-cementitious characteristics. There are many studies [1, 5, 10, 18, 21, 24] focusing on the use of FA to improve the marginal soil for road applications. Prabakar et al. [21] investigated the behavior of three different types of soils mixed with 9 to 46% of FA and they found that FA can be effectively utilized as base materials for the roads and backfilling applications. It was noted that FA stabilization showed improvements in shear strength, California bearing ratio (CBR), and reduction in compressibility and swelling behavior. Bose [5] studied the effect FA addition on the geotechnical behavior of the expansive soil and concluded that the optimum mix for better unconfined compressive strength (UCS) and CBR is 20% FA—80% clay mix. [18] studied the influence of FA addition on compaction and consolidation characteristics of expansive soil, and they found that addition of 30% FA to the local expansive soil decreases the compressibility parameters of the stabilized soil. Gimhan [10] investigated the suitability of class F FA as an embankment material for road construction by analyzing the geotechnical properties of three FA samples obtained from Lakvijaya coal power plant, Sri Lanka, and found that coal ashes do not meet some of the Road Development Authority (RDA) specifications, and therefore, it is not possible to use them as an embankment material for heavily loaded embankments. However, they concluded that it is possible

to use them ash as lightweight embankment material for construction purposes. Rajak [24] conducted numerical analysis to analyze the slope stability of FA-stabilized soil as embankment material using FLAC/Slope software, and it was found that 30% FA (by weight) is the optimum FA mix considering the stability aspects. Ariyarathne [1] analyzed the suitability of FA as a substitutes for material in road construction, and it was recommended that 30% of FA is the preferred percentage to stabilize the road base as it showed decrease of plasticity index and increase in CBR value similar to 1% cement addition.

Although there are many studies on the use of FA to stabilize the marginal soils, to date, there are a very limited number of studies focusing on the stability analysis of the FA-stabilized embankment for highway construction. Therefore, this research aims to analyze the stability of CKE embankment constructed with FA-stabilized marginal soil as the embankment material. Although the FA-stabilized soil was not used in the actual CKE embankment, it is hypothesized in this study to predict the stability of the stabilized embankment to verify the feasibility of FA to stabilize the marginal embankment material. To address the suitability of this stabilized material for CKE, it is important to understand the appropriate proportion of soft soil and FA, embankment stability during construction, and long-term embankment settlement after construction. Two embankment sections of the CKE were considered for the study, and the load-settlement behavior (vertical and lateral deformation) and the slope stability were analyzed using finite-element method (FEM)-based PLAXIS 2D software and limit equilibrium method (LEM)-based SLOPE/W software.

2 Research Methodology

Two critical embankment sections along CKE alignment at chain ages K2 + 600 and K6 + 850 as shown in Fig. 1 have been chosen for this study. The cross-sectional details of the two embankments are shown in Fig. 2.

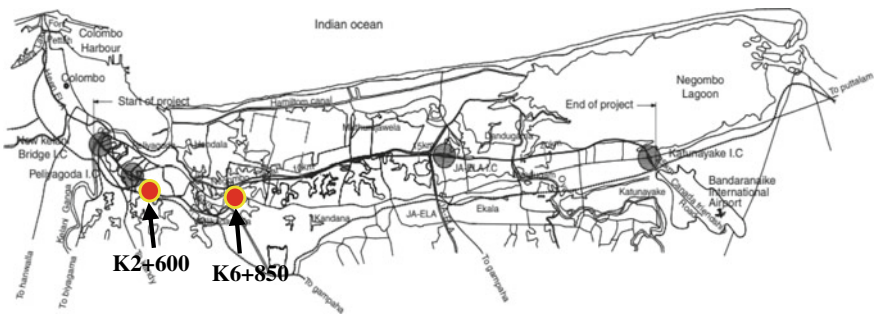

Fig. 1 Location of the two embankment sections selected for the study

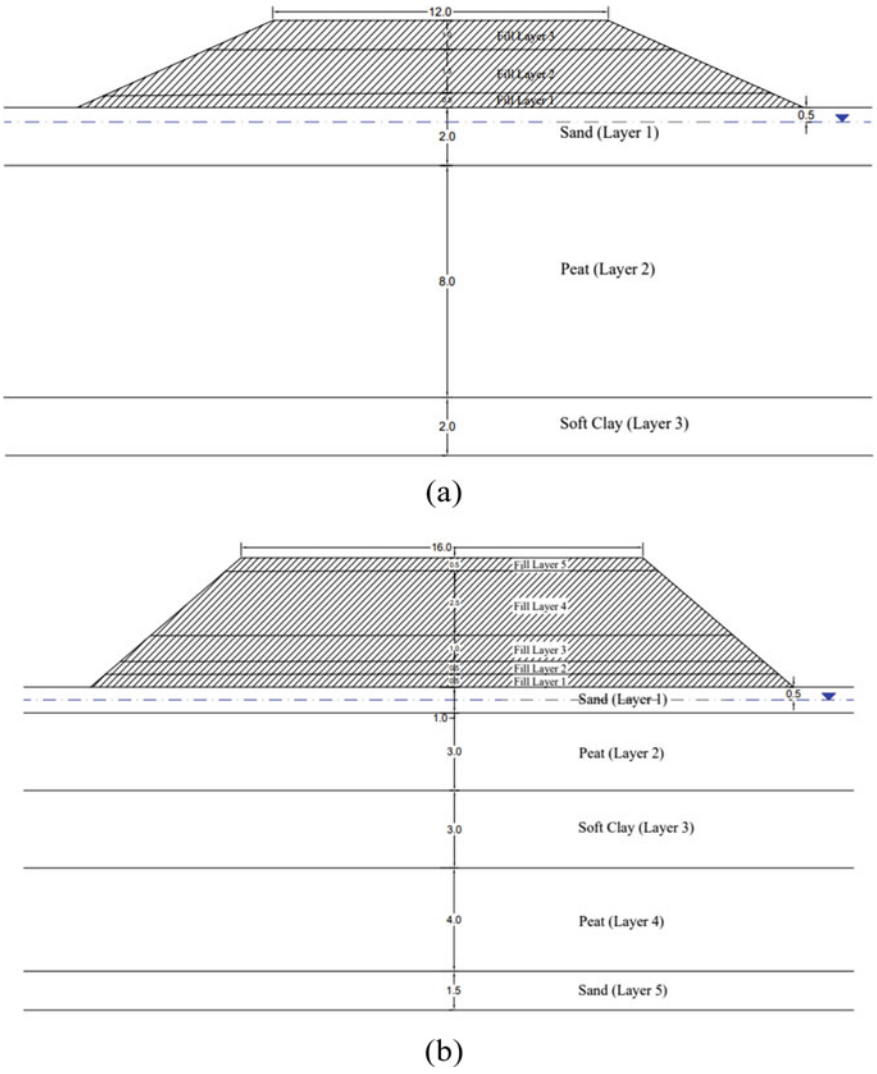

Fig. 2 Embankment section at **a** K2 + 600 and **b** K6 + 850

It is hypothesized in this study to use FA-stabilized marginal soft clayey soil, which does not meet the requirements for type I and type II embankment materials of standard specifications for construction and maintenance of roads and bridges [14]. As it has been found that the optimum FA content to stabilize marginal soils resulting in better geotechnical properties of the stabilized soil varies up to 40% FA (by weight) [1, 18, 24, 30], it was decided to use FA-stabilized soil at FA dosages of 0, 10, 20, 30, and 40% (by weight) to stabilize the marginal embankment material. The marginal soil considered in this study was adopted from Rajak [24] and the

preliminary geotechnical properties of the FA-stabilized soil, including unit weight, cohesion, friction angle, etc., were also adopted from the same study as they have conducted laboratory experiments to determine the geotechnical properties of the stabilize soil by adding 0–40% FA to the soil.

2.1 Deformation and Stability Analysis Using FEM

Stability and deformation analyses were performed using the finite-element program PLAXIS 2D (professional version 8.2). A series of two-dimensional finite-element analyses on selected two cross sections of CKE embankment were performed to understand the effect and feasibility of using FA-stabilized soil embankment fills. Owing to the symmetry of the problem, only one-half needs to be modeled by geometry line in a working space of 20 m × 50 m, and standard fixities were used to define the boundary condition. Figure 3 shows the geometry model used for the embankment K2 + 600 in PLAXIS analysis. The deformation at the base of the foundation layer was assumed to be zero as the base is fixed in x- and y-directions. The two vertical boundaries were assumed to be fixed in the x-direction. Initial stresses were generated using K0 procedures or gravity loading. Staged construction of the embankment was effectively modeled followed by the application of overburden pressure on the embankment. The initial conditions include the existence of the phreatic level at a depth of 0.5 m below the ground level in both embankment sections (Fig. 2).

Three different types of analyses were conducted by adopting the following three types of models for foundation soil based on the findings of [19]: (i) Mohr–Coulomb model (MC)—MC model was used for all the soil layers, (ii) Mohr–Coulomb—Soft soil model (MC-SS)—SS model for peat and soft clay layers, and MC model for remaining soil layers, and (iii) Mohr–Coulomb-Soft soil-soft soil creep model (MC-SS-SSC)—SSC model for peat soil layers, SS model for soft clay and MC model for remaining soil layers (Fig. 3).

The properties of the existing foundation soil (Table 1) and filling sequence of CKE embankment fill layers at chainages K2 + 600 and K6 + 850 were adopted from

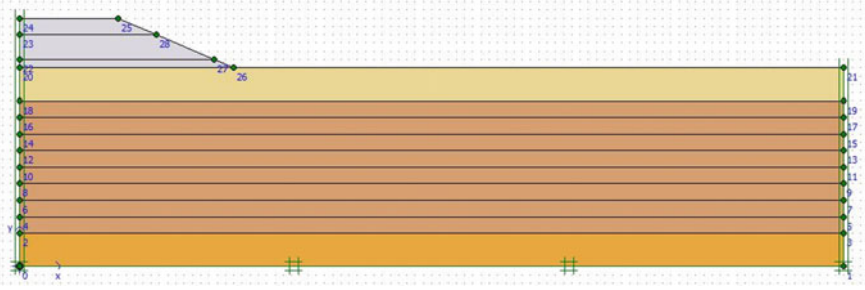

Fig. 3 Geometry model of the embankment at K2 + 600 in PLAXIS

Table 1 Foundation of soil properties used for sections K2 + 600 and K6 + 850

Section		K2 + 600			K6 + 850				
Layer		1	2	3	1	2	3	4	5
Material model		MC	SSC	SS	MC	SSC	SS	SSC	MC
γ_{sat} (kN/m^3)	[12]	18	16.5	17	19	17	16	17	20
ϕ' (°)		20	18	15	28	23	21	23	28
c' (kPa)		1	5	2	1	10	21	10	1
k_x and k_y (m/day)	[15]	86	$k_x = 1 \times 10^{-5}$ $k_y = 2 \times 10^{-5}$	9×10^{-4}	86	$k_x = 1 \times 10^{-5}$ $k_y = 2 \times 10^{-5}$	9×10^{-4}	$k_x = 1 \times 10^{-5}$ $k_y = 2 \times 10^{-5}$	86
E (kPa)		15.600	240	12,600	15,400	250	12,600	250	15,400
v		0.3	0.3	0.3	0.3	0.33	0.33	0.33	0.3
C_c	[20]	–	3.9	0.1	–	3.35	0.1	3.35	–
C_s		–	0.39	0.01	–	0.335	0.01	0.335	–
C_s	[12]	–	0.01	–	–	0.035	–	0.035	–
e_{int}		–	0.65	0.5	–	0.65	0.5	0.65	–

Nasvi and Krishnya [19]. Considering filling sequence for K2 + 600, bottom layer of the fill of the embankment was constructed for 5 days and allowed to consolidate for 7 days before constructing the second layer of the fill. Once the final layer of the fill construction was finished, it was allowed to consolidate for 335 days. For K6 + 850, bottom layer of the fill of the embankment was constructed for 7 days and was allowed to consolidate for 8 days before constructing the second layer of the fill. Once the final layer of the fill construction was finished, it was allowed to consolidate for 338 days. The preliminary soil properties of the marginal embankment soil and FA-stabilized soil, such as unit weight, cohesion, and friction angle, were obtained from Rajak et al. [24]. Other parameters required for FA-stabilized soil, such as horizontal and vertical permeability (k_x and k_y), Poisson's ratio (v), and Young's modulus (E), were obtained from relevant literature [6–8, 22, 26] as these values were not reported in the study conducted by Rajak et al. [24]. It should be noted that the values of horizontal (k_x) and vertical permeability (k_y) values were assumed to be the same for the numerical analysis. Table 2 provides the soil properties used for

Table 2 Soil properties used for FA-stabilized embankment soil

Mix proportions	γ_{sat}(kN/m^3)	φ' (°)	c' (kPa)	k_x and k_y (m/day)	E (kPa)	v
	[24]			[6, 8]	[7, 22]	[26]
100S + 0FA	21.6	29	38.1	7.5×10^{-6}	1616	0.35
90S + 10FA	21.1	32	32.3	3.5×10^{-5}	1656	0.32
80S + 20FA	20.6	35	29.1	8.0×10^{-5}	1693	0.28
70S + 30FA	20.2	37	20.1	1.3×10^{-4}	2461	0.24
60S + 40FA	19.9	39	10.2	1.7×10^{-4}	3051	0.21

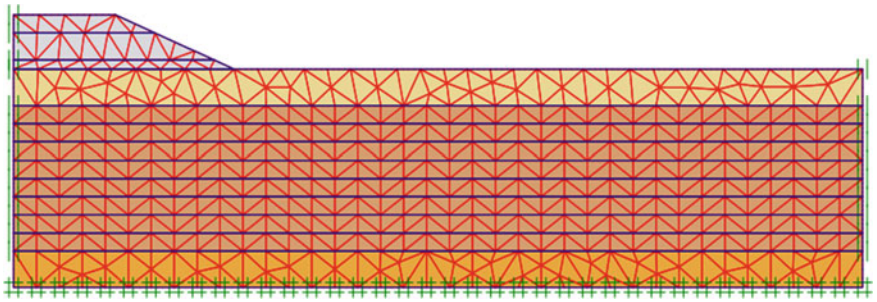

Fig. 4 Adopted finite-element mesh for the analysis

the FA-stabilized embankment soil in the numerical analysis.

A mesh convergence analysis was conducted to eliminate the mesh size dependency of the results by considering variation of vertical and lateral deformation at section K2 + 600 with varying the mesh size from 1.98 m to 0.92 m. Based on the results, vertical and lateral deformation did not show any further variation when the mesh size was very fine (0.92 m), and hence a very fine mesh was adopted for the FEM analysis. The adopted finite-element mesh is shown in Fig. 4.

For the model validation, vertical settlement values obtained at the center of the embankment for different analyses types (MC, MC-SS, MC-SS-SSC) were compared with the measured field settlement values. Based on the comparison of the field results, the best material model combination (analysis type) was selected and it was adopted for any further analysis to predict the effect of stabilization on vertical settlement at the center of the embankment, lateral deformation at the toe of the embankment, pore water pressure, and stress variations.

Stability analysis of the two embankments was also conducted using PLAXIS 2D to obtain minimum FOS at final phase for each embankment section. The calculation of FOS was done using phi/*c* reduction method. The strength parameters tan (φ) and *c* of soil were reduced in the same proportion until failure of the embankment occurs.

2.2 Stability Analysis Using LEM

The FOS of FA-stabilized embankment sections were analyzed with five different LEM analysis types such as ordinary method (OM), Bishop simplified method (BSM), Janbu simplified method (JSM), Spencer method (SM), and Morgenstern–Price method (M-PM) using SLOPE/W 2012 software. The simple nonlinear MC soil model was used as the material model for all the soil layers. Entry and exit method was chosen to define the slip surface. The critical slip surface was searched from thousands of possible slip surfaces by defining the input of 30 slices, 2000 iterations, and four numbers of increments for both entry and exit. In stability analysis,

validation of results was done by comparing the FOS values obtained from PLAXIS 2D and SLOPE/W.

2.3 Long-Term Stability of the FA-Stabilized Embankments

Based on the deformation and stability analysis results, the optimum mix composition for the FA-stabilized soil was selected, and based on the optimum FA content, a long-term analysis (up to 15 years) was conducted to predict the deformation and stability behavior of the two embankments. The long-term settlement analyses were performed with a consolidation-based model, and the analyses were carried out until the ultimate pore-pressure state is reached.

3 Results and Discussion

3.1 Model Validation

Figure 5 shows the vertical settlement with time of the two embankments for various analyses types. According to Fig. 5, of the analyzed models, both MC-SS and MC-SS-SSC models show closer results compared to the observed field settlement values for both the embankments. The MC is a simple nonlinear model which assumes elastic perfectly plastic behavior, and it is not suitable for soil layers such as peat and soft clay. Although both MC-SS and MC-SS-SSC models capture the field behavior reasonably well, MC-SS-SSC model is selected as the best model for further analysis taking into account secondary compression effects such as creep, which is mainly prominent in peat soil. Previous researchers [4, 19] have also recommended SSC model for modeling soft soil embankments.

3.2 Effect of Stabilization on Load-Settlement Behavior

Effect of FA stabilization on the vertical and lateral deformation of the embankment K2 + 600 is shown in Fig. 6. According to Fig. 6, FA stabilization of the marginal embankment material reduces the overall vertical and lateral deformation by 3–10% and 7–25%, respectively, after 374 days of construction. Similar reduction for embankment K6 + 850 was 5–8% and 18–39%, respectively, after 765 days of construction. This reduction is due to the cementitious reaction that takes place between FA and soil in the presence of water resulting in the formation of cementitious gels (CSH and CASH) that create strong binding between particles and reduce the ability of soil-FA matrix to undergo deformation [17, 27, 29].

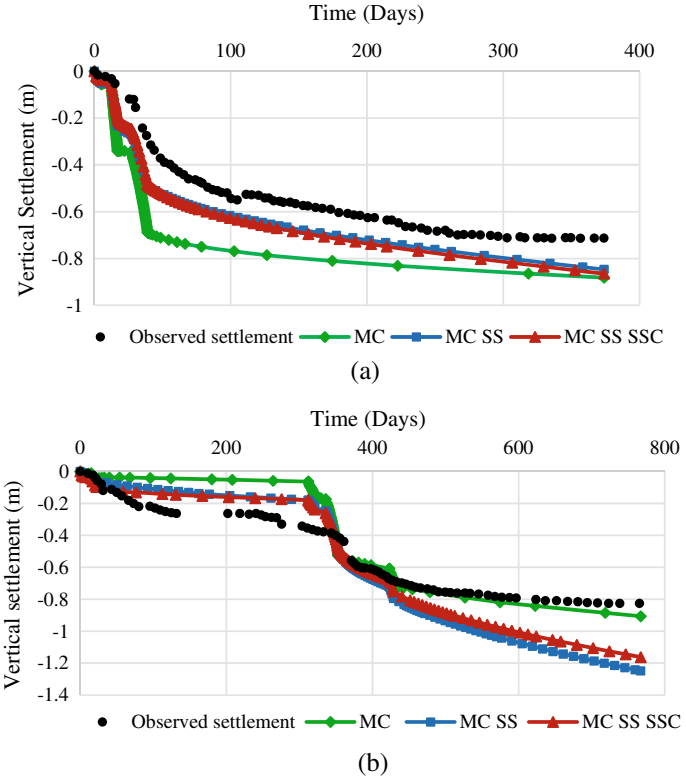

Fig. 5 Variation of vertical settlement with time for embankment section **a** K2 + 600 and **b** K6 + 850

Although 40% FA addition provided the highest reduction in vertical settlement, it was noted that the reduction in settlement is not significant beyond 30% (0.01 m). In addition, it is interesting to note that the maximum reduction in lateral deformation of the two embankment sections is reported for 30% FA addition (24.8% and 38.3% for K2 + 600 and K6 + 850, respectively). Percentage reduction in lateral deformation for 30% addition is higher than that of 40% FA addition, and it is because increase of fines (beyond 30%) tends to separate adjacent soil particles resulting in decrease interlocking between particles, thereby reducing the compaction. Hence, it can be concluded that 30% FA addition is the optimum FA content for the better performance of the FA-stabilized embankment. Moreover, with the increase of FA content, there are possibilities for leaching of some heavy metals and also reduction in PH of the soil. Previous researchers [1, 11, 24] have also recommended 30% as the optimum FA content for soil stabilization works.

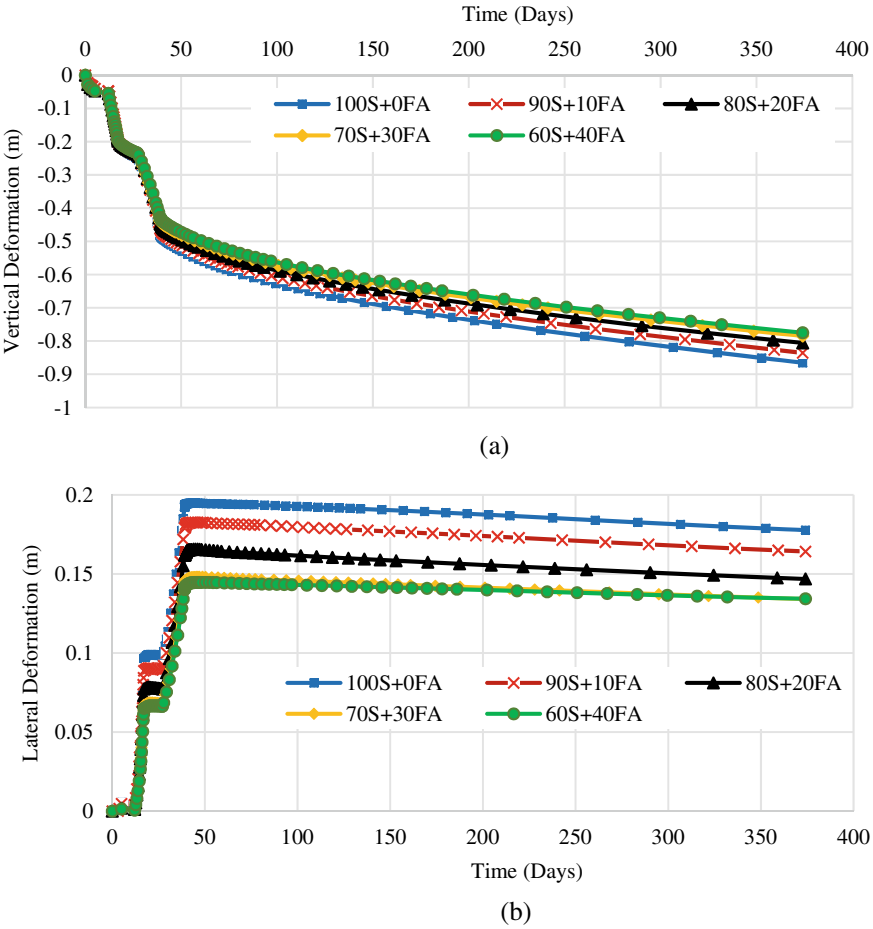

Fig. 6 Variation of **a** vertical settlement and **b** lateral deformation of FA-stabilized embankment with time for section K2 + 600

3.3 Variation of Excess Pore Water Pressure (PWP)

Figure 7 shows the variation of excess PWP for FA-stabilized embankment sections K6 + 850. Considering the effect of stabilization on the dissipation of PWP, the maximum PWP experienced below the embankment is reduced with the stabilization of FA. When the FA content is increased from 0 to 40%, the maximum PWP experienced decreases from 48.8 to 43.8 kPa for K2 + 600 and from 82.9 to 68.1 kPa for K6 + 850. This is because of the reduction in embankment fill surcharge load due to the low unit weight of FA compared to the natural soil. In addition, the reduction in PWP is significant at K6 + 850 compared to the reduction at K2 + 600, and this

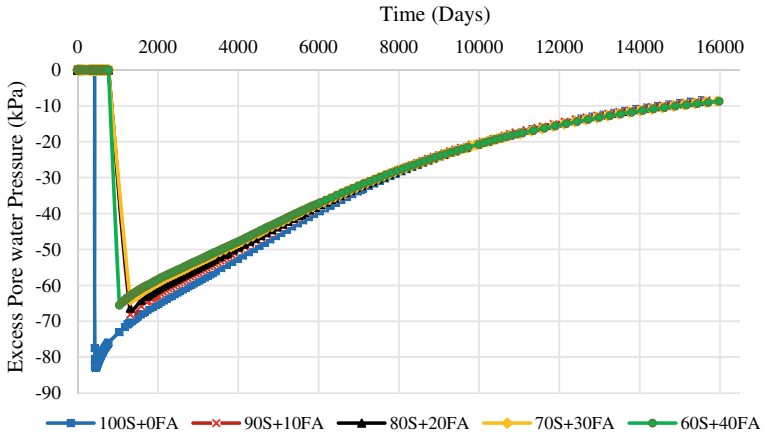

Fig. 7 Variation of excess pore water pressure with time for K6 + 850

is due to the higher embankment height at K6 + 850 compared to K2 + 600 which increases the overburden pressure at the point of calculation.

3.4 Stability Analysis Results from FEM and LEM Techniques

Figure 8 shows the critical slip surface for section K2 + 600 obtained using PLAXIS 2D and SLOPE/W with M-PM method. The FOS values obtained from different analyses methods in SLOPE/W are also given in Fig. 8b. The M-PM is selected as the best method as it considers force and moment equilibrium in FOS calculations [2, 3, 13]. The critical slip surfaces generated by PLAXIS 2D and SLOPE/W are quite similar in all the cases for both embankment sections (Fig. 8). The failure mode is base failure mode in both embankment sections which is generally possible for low slope angles.

Table 3 shows the FOS results of two embankment sections with FA stabilization. The FOS values obtained from PLAXIS 2D and SLOPE/W were not comparable as there is a 10–40% difference in the FOS values obtained from the two methods. It can be to the different numerical techniques (FEM and LEM) and material models (MC-SS-SSC and MC) used for stability analysis in PLAXIS and SLOPE/W. It can be observed that slip surface location cuts the peat clay layers in both embankment sections, and because of this reason, the FOS values obtained from PLAXIS 2D can be accurate as the behavior of the peat is captured in PLAXIS by incorporating SSC model. Previous researchers [2, 3] have also reported that FOS results from PLAXIS 2D are more accurate than SLOPE/W results.

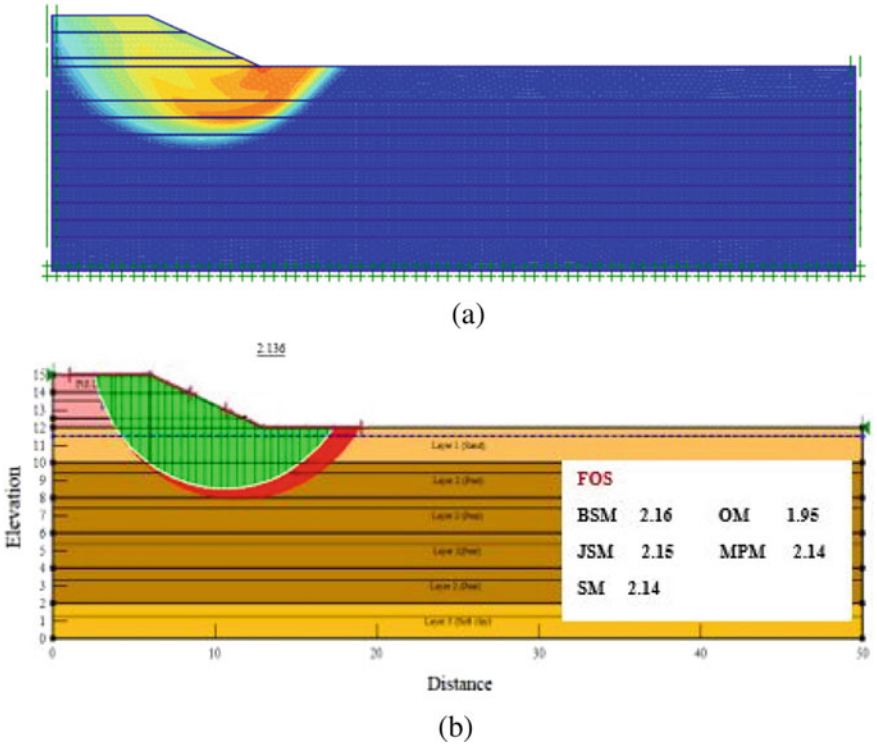

Fig. 8 Location of critical slip surface at section K2 + 600 **a** PLAXIS 2D and **b** SLOPE/W

Table 3 FOS values obtained for FA-stabilized embankment from PLAXIS 2D and SLOPE/W

Mix proportions	FOS values of stabilized soil embankment			
	K2 + 600 section		K6 + 850 section	
	PLAXIS 2D	SLOPE/W (M-PM)	PLAXIS 2D	SLOPE/W (M-PM)
100S + 0FA	1.31	2.14	1.22	2.03
90S + 10FA	1.33	2.12	1.23	2.05
80S + 20FA	1.38	2.10	1.24	2.06
70S + 30FA	1.41	1.94	1.23	1.92
60S + 40FA	1.39	1.80	1.16	1.73

In general, FOS values obtained from SLOPE/W show a decreasing trend with the increase of FA percentage for both the embankments. On the other hand, according to PLAXIS results, it can be seen that FA stabilization generally improves the stability of the embankment up to 30% FA addition for both the embankments. When the FA content in the soil is increased beyond 30%, the fines tends to separate the particles and oppose the shearing resistance provided by increasing angle of friction. This will

reduce the stability of the embankment. Therefore, it can be concluded that 30% FA addition is the optimum FA content for the FA-stabilized embankment considering the stability aspects.

3.5 Long-Term Stability Results for the FA-Stabilized Embankment

Table 4 shows the deformation and stability analysis results obtained after 5, 10, 15 years for both the embankments with and without stabilization (30% FA addition). The FOS values of both embankment sections tend to increase with time. Most of the lateral movements in the embankments occurred in foundation peat soil layers, and significant vertical settlement is observed near the center of the embankment. Vertical settlement at the center increases with the time for both the embankment, and the vertical settlement values after 15 years are 1.759 m for K2 + 600, 2.52 m for K6 + 850 and nearly 2.4 times higher than the vertical settlement after construction for embankments K2 + 600 and K6 + 850, respectively. On the other hand, lateral deformation at the toe showed a reducing trend with time for K2 + 600, whereas it increased with time for K6 + 850. This increasing trend in lateral deformation is related to creep effects of peat layers which is near to toe of the embankment in K6 + 850. Fatahi et al. [9] studied soil creep effects on ground lateral deformation under embankments and reported an increase in lateral deformation with the soil creep for long-term period. FA stabilization significantly reduces both the vertical and lateral deformation values in the long-term. The percentage reductions in the vertical settlement after 15 years are 9% and 8.5% for embankment K2 + 600 and K6 + 850, respectively, compared to nonstabilized embankments. Similar reductions in the lateral deformation values at the toe of the embankment are 7.5% and 11.8% for embankments K2 + 600 and K6 + 850, respectively, compared to nonstabilized embankments.

Table 4 Long-term deformation and stability results of the two embankments

Section	Years	Settlement at the center (m)	Lateral deformation at the toe (m)	FOS (PLAXIS)		
		30% FA stabilization	Non-stabilized	30% FA stabilization	Non-stabilized	For 30% FA stabilization
K2 + 600	5	−1.225	−1.345	0.117	0.145	1.45
	10	−1.538	−1.687	0.106	0.123	1.49
	15	−1.759	−1.933	0.099	0.107	1.53
K6 + 850	5	−1.606	−1.746	0.222	0.322	1.27
	10	−2.159	−2.366	0.256	0.318	1.33
	15	−2.520	−2.754	0.276	0.313	1.39

4 Conclusions

This study was conducted to predict the feasibility of using fly ash (FA)-stabilized marginal soil as embankment material by analyzing the two embankment sections at Colombo–Katunayake Expressway (CKE) constructed with FA-stabilized soil. The following conclusions are drawn based on the outcome of this research study:

- A model combination having soft soil creep model (SSC) for peat soil, soft soil model (SS) for soft clay, and Mohr coulomb (MC) for other soil layers (MC-SS-SSC) is the best material model combination to predict the field settlement behavior accurately.
- Both vertical settlement and lateral deformation of the embankments reduce with the FA stabilization and the percentage reduction in the vertical settlement and lateral deformation were 3 to 10% and 7 to 39% for different embankment sections.
- The optimum FA content considering the deformation behavior (vertical settlement and lateral deformation) and slope stability of the stabilized embankments is 30% FA (by weight).
- There is a significant reduction in the long-term settlement (8 to 9% in vertical settlement and 7 to 31% in lateral deformation) and increase in the FOS for FA-stabilized embankments compared to nonstabilized embankments.

References

1. Ariyarathne BHT (2020) Utilisation of coal ash for road constructions in Sri Lanka
2. Aryal KP (2006) Slope stability evaluations by limit equilibrium and finite element methods. Doctoral thesis. Available at: http://hdl.handle.net/11250/231364. Accessed 20 Oct 2021
3. Ayob M, Kasa A, Sulaiman MS, Devi N (2019) Slope stability evaluations using limit equilibrium and finite element methods. Int J Adv Sci Technol 28(18):27–43
4. Bandyopadhyay K, Bhattacharjee S, Ghosh S (2011) Numerical approach for analysis of highway fly ash embankment. In: Proceedings of Indian geotechnical conference december, pp 15–17
5. Bose B (2012) Geo engineering properties of expansive soil stabilized with fly ash. Electron J Geotech Eng 17(1):1339–1353
6. Boroumand A, Baziar MH (2005) Determination of compacted clay permeability by artificial neural networks. In: Ninth international water technology conference, IWTC9, Sharm El-Sheikh, Egypt, pp 515–526
7. Buwa V, Wayal AS (2016) Use of fly ash and lime for stabilization of soft soil. Electron J Geotech Eng 21(18):6235–6246
8. Deb T, Pal SK (2014) Effect of fly ash on geotechnical properties of local soil fly ash mixed samples. Int J Res Eng Technol 3(5):507–516
9. Fatahi B, Le TM, Le MQ, Khabbaz H (2013) Soil creep effects on ground lateral deformation and pore water pressure under embankments. Geomech Geoeng 8(2):107–124
10. Gimhan PGS, Nasvi MCM, Disanayaka JPB (2018) Geotechnical engineering properties of fly ash and bottom ash: use as civil engineering construction material. J Inst Eng Sri Lanka 51(1):49–57
11. Gruchot A, Zydroń T (2020) Shear strength of industrial wastes and their mixtures and stability of embankments made of these materials. Appl Sci 10(1):250

12. Hsi J, Gunasekara C, Nguyen V (2005) Characteristics of soft peats, organic soils and clays, Colombo-Katunayake expressway, Sri Lanka. Elsevier Geo-Eng Book Series 3:681–722
13. Huang YH (2014, February) Slope stability analysis by the limit equilibrium method: fundamentals and methods. American Society of Civil Engineers
14. Institute for Construction Training and Development (ICTAD) (2009) Standard *specifications* for *Construction* and maintenance of *Roads* and bridges
15. Kazemian S, Bujang BKH, Prasad A, Barghchi M (2011) A state of art review of peat: geotechnical engineering perspective. Int J Phys Sci 6(8):1974–1981
16. Kim B, Prezzi M, Salgado R (2005) Geotechnical properties of fly and bottom ash mixtures for use in highway embankments. J Geotech Geo Environ Eng 131(7):914–924
17. Moghal AAB (2017) State-of-the-art review on the role of fly ashes in geotechnical and geo environmental applications. J Mater Civ Eng 29(8):04017072
18. Mohanty SK, Pradhan PK, Mohanty CR (2016) Consolidation and drainage characteristics of expansive soil stabilized with fly ash and dolochar. Geotech Geol Eng 34(5):1435–1451
19. Nasvi MCM, Krishnya S (2019) Stability analysis of Colombo-Katunayake Expressway (CKE) using finite element and limit equilibrium methods. Indian Geotech J 49(6):620–634
20. Nawarathna THK, De Silva LIN (2014) Applicability of the limit equilibrium method and the finite element methods in predicting the stability of embankment slopes. Annual Session of IESL, pp 11–17
21. Prabakar J, Dendorkar N, Morchhale RK (2004) Influence of fly ash on strength behavior of typical soils. Constr Build Mater 18(4):263–267
22. Putri EE, Rao NSVK, Mannan MA (2012) Evaluation of modulus of elasticity and modulus of subgrade reaction of soils using CBR test. J Civ Eng Res 2(1):34–40
23. Rai AK, Paul B, Singh G (2010) A study on backfill properties and use of fly ash for highway embankments. J Adv Lab Res Biol 1:110–114
24. Rajak TK, Yadu L, Pal SK (2019) Analysis of slope stability of fly ash stabilized soil slope. Geotech Appl pp 119–126
25. Road Development Authority (2021) Available at: https://www.rda.gov.lk/source/project_details.htm/. Accessed 22 Oct 2021
26. Saride S, Dutta TT (2016) Effect of fly-ash stabilization on stiffness modulus degradation of expansive clays. J Mater Civ Eng 28(12):04016166-1-12
27. Simatupang M, Mangalla LK, Edwin RS, Putra AA, Azikin MT, Aswad NH, Mustika W (2020) The mechanical properties of fly-ash-stabilized sands. Geosciences 10:132
28. Singh RR, Goyal N, Kaur N (2015) Fly ash as an embankment material. SSRG Int J Civ Eng (SSRG-IJCE) 3:14–16
29. Tastan EO, Edil TB, Benson CH, Aydilek AH (2011) Stabilization of organic soils with fly ash. J Geotech Geoenviron Eng 137(9):819–833
30. Turan C, Javadi A, Consoli NC, Turan C, Vinai R, Cuisinier O, Russo G (2019) Mechanical properties of calcareous fly ash stabilized soi'. Eurocoalash 1:184–194
31. Zhang Q, Qin X, Dong H, Qu D (2010) Foundation treatments for embankments over highly compressible peat in CKE project. In: 5th Civil engineering conference in the Asian Region and Australasian structural engineering conference 2010, vol 5, pp 1138–1141

Effects of Soil Moisture on Simulated Methane Flow Under Varying Levels of Soil Compaction

M. M. T. Lakshani, T. K. K. C. Deepagoda, T. J. Clough, J. R. R. N. Jayarathne, S. Thomas, N. Balaine, B. Elberling, and K. Smits

Abstract Soil density plays an important role in regulating the migration of greenhouse gases from terrestrial soils to the atmosphere. Soil moisture is one of the main soil physical controls determining the fate and transport of gases in soils. This study investigated the transport of methane (CH_4) originating from a simulated CH_4 source within a variably compacted pasture soil. Simulations were carried out for dry and variably saturated soils. Steady-state methane flow was simulated as a density-dependent, multiphase flow considering a multicomponent mixture of CH_4, water vapor and air, under different soil moisture conditions. We used measured soil–water characteristic (SWC) and gas diffusivity data at five density levels (1.1, 1.2, 1.3, 1.4, and 1.5 Mg m^{-3}) to parameterize predictive models. Permeability was estimated using an existing SWC-based saturated hydraulic conductivity function. Results show a distinct effect of soil density on CH_4 concentration profiles within the soil. Clear effects of soil moisture on CH_4 transport could also be seen in differentially compacted soils. Relatively smaller CH_4 concentrations were observed in dry soils where permeability, gas diffusivity, and air-filled porosity were higher. With increasing density, the profile-accumulated concentrations >0.3% increased up to 200 times under the dry condition. In moist soils, on the other hand, smaller air-filled porosity and higher moisture-controlled tortuosity resulted in reduced permeability

M. M. T. Lakshani (✉) · T. K. K. C. Deepagoda
Department of Civil Engineering, Faculty of Engineering, University of Peradeniya, Peradeniya 20400, Sri Lanka
e-mail: mmtharindilakshani@gmail.com

T. J. Clough · N. Balaine
Department of Soil and Physical Sciences, Lincoln University, P.O. Box 85084, Lincoln 7647, New Zealand

J. R. R. N. Jayarathne · K. Smits
Department of Civil Engineering, University of Texas, Arlington, TX 76019, USA

S. Thomas
Plant and Food Research Ltd., Gerald St., Lincoln 7608, New Zealand

B. Elberling
Department of Geosciences and Natural Resource Management, Center for Permafrost (CENPERM), University of Copenhagen, Øster Voldgade 10, 1350 Copenhagen, Denmark

R. Dissanayake et al. (eds.), *12th International Conference on Structural Engineering and Construction Management*, Lecture Notes in Civil Engineering 266,
https://doi.org/10.1007/978-981-19-2886-4_20

and gas diffusivity, yielding high CH_4 concentrations in the soil profile with only a maximum fivefold increase in the accumulated concentration with increasing density.

Keywords Soil–Gas diffusivity · Soil compaction · Soil moisture · Methane transport · Numerical modeling

1 Introduction

Methane (CH_4) is a potent greenhouse gas with a global warming potential of 28 over a 100-year time horizon and a radiative forcing value, from 1750 to 2011, of 0.48 ± 0.05 W m^{-2} [1]. The atmospheric CH_4 concentration has increased by 150% since 1750 to be 1803 ± 2 ppb in 2011, increasing at ~6 ppb yr^{-1} between 2007 and 2011 [2]. Furthermore, CH_4 is a chemically reactive molecule that plays an important role in atmospheric chemistry. Methane reacts with hydroxyl radicals in the atmosphere, reducing their oxidative potential and hence the atmosphere's ability to counteract anthropogenic pollutants, for example, chlorofluorocarbons [3].

Methane sources may be broadly classified into three categories: biogenic, thermogenic, and pyrogenic. Atmospheric CH_4 is predominantly (70–80%; [4]) of biogenic origin and stems largely from terrestrial ecosystems with environments favoring methanogens. Globally, it has been estimated [5] that between 2000 and 2009, rice paddy agriculture (36 Tg CH_4 yr^{-1}) and landfills (75 Tg CH_4 yr^{-1}) equated to approximately 33% of all anthropogenic CH_4 sources (331 Tg CH_4 yr^{-1}). Potentially, soils acts as a CH_4 sink where aerobic conditions favor methanotrophy, leading to oxidation of atmospheric CH_4 [6]. Therefore, in order to better understand soil emissions of CH_4 and their potential mitigation, a thorough understanding of the soil properties controlling CH_4 emissions under different environmental conditions is required.

Compaction-induced changes in soil structure essentially affect the transport and retention characteristics of both soil–water and soil–gas and thereby affect the soil's potential for uptake and emission of greenhouse gases. Density-controlled effects on soil–water retention, gas diffusivity (D_p/D_o, where D_p and D_o are gas diffusion coefficients in soil and free air, respectively) [7, 8], and hydraulic conductivity/permeability [9] have been highlighted in the literature; however, their impacts on the fate and transport of greenhouse gases (e.g., CH_4) have not been adequately studied.

The main objective of this study was to provide computational insight into the subsurface migration of CH_4 originating from a simulated CH_4 source located in differentially compacted soil systems under varied soil compaction and moisture status. Soil physical measurements included soil bulk density, soil–water characteristic (SWC), and gas diffusivity, to estimate subsurface CH_4 concentrations in the absence of measured concentration data. We test the hypothesis that soil moisture will considerably affect subsurface CH_4 in density-controlled soil systems.

2 Mathematical Modeling

2.1 Soil–Water Characteristic (SWC)

We used the [10] model to characterize soil–water retention and parameterize the capillary suction (ψ)-soil moisture content (θ) relation as follows:

$$\theta(h) = \theta_r + (\theta_s - \theta_r)\left(\frac{1}{1 + |\alpha h|^n}\right)^m \tag{1}$$

where θ_s is the soil water content at saturation ($cm^3\ cm^{-3}$), θ_r is the residual water content ($cm^3\ cm^{-3}$), α is model scaling factor (cm^{-1}), and n and m are model shape factors. Although it is a common practice to constrain the shape factors by linking them together (e.g., $m = 1 - 1/n$; [11]), in this study, we treated both n and m as unconstrained/fitting parameters to obtain a better numerical fit to the measured data.

The maximum slope of the θ (h) function (Eq. 1) at the inflection point (i.e., at $d^2\theta/d\mathrm{h}^2 = 0$) can be expressed by S as follows [12],

$$S_i = -m^{1+m} n\alpha(\theta_s - \theta_r)(1 + m)^{-m-1} \tag{2}$$

2.2 Hydraulic Conductivity and Permeability

In the absence of measured hydraulic conductivity ($m\ s^{-1}$) data, several models are available in the literature to estimate hydraulic conductivity from basic and easy-to-measure soil physical properties. Then, [13] proposed an empirical hydraulic conductivity function based on the parameterized van Genuchten model linking to S (Eq. 2) which can be presented as:

$$K_s = 1632.5|S|(3.9f)^{(-3.9.f)} \tag{3}$$

$$f = \alpha\Phi_e$$

where Φ_e is the effective porosity (i.e., the total porosity minus the volumetric moisture content at a suction of − 33 kPa); [14] representing the pore space where water flow effectively occurs.

Intrinsic permeability, k, (m^2) of a porous medium can be computed from the hydraulic conductivity as follows:

$$K_s = k\frac{\rho g}{\eta} \tag{4}$$

Note that the saturated hydraulic conductivity is a function of the porous medium and the fluid properties which are denoted by the permeability (k, m^2) and fluidity ($\rho g/\eta$, $m^{-1}\ s^{-1}$), respectively.

2.3 Soil–Ggas Diffusivity (D_p/D_o)

Few predictive soil–gas diffusivity models account for the effect of soil density, although some models implicitly take the density effects into account via reduction in total porosity (e.g., [15, 16]). Here, we adopted a recent empirically based soil–gas diffusivity model [17] that was developed, based on a previous predictive model, and calibrated against the same gas diffusivity data that we use in this study.

$$\frac{D_p}{D_o} = 0.4\left(2\left(\frac{\varepsilon}{\Phi}\right)^{5.2} + 0.04\left(\frac{\varepsilon}{\Phi}\right)\right) \tag{5}$$

where the constant scale factors are best-fit values to the measured data.

2.4 Fate and Transport of Methane in Soil

For the governing equations (mass and energy balance, advective mass flux, and diffusive mass flux) relevant to the present study, the reader is referred to [18].

3 Materials and Methods

We considered measured soil water characteristic (SWC) and gas diffusivity data from Balanine et al. [19] to parameterize the models. The soil was sampled from a pasture site at Duncan Block (43°38′0.7″ S, 172°29′40″ N), Lincoln, New Zealand. The soil was identified as a Templeton silt loam, Typic Immature Pallic under the New Zealand Soil Classification System [20]. The soils, sampled at a depth of 15 cm, were air-dried and sieved (< 2 mm) prior to packing at five bulk density (ρ_b) levels: 1.1, 1.2, 1.3, 1.4, and 1.5 Mg m^{-3}. The samples were subsequently drained at 11 levels of matric potential (ψ); −1.0, −1.5, −2.0, −3.0, −4.0, −5.0, −6.0, −7.0, −8.0, −9.0, and −10 kPa. Soil–gas diffusivity (D_p/D_o) was measured at each matric potential using a one-chamber diffusion apparatus [21]. All measurements were performed in triplicate. For detailed information on soil sampling, pre-treatments, and calculation procedures, the reader is referred to [19].

For numerical simulations, we used the multiphase transport simulator TOUGH2 [22] together with the equation of state module EOS7CA [23]. TOUGH2/EOS7CA can potentially simulate subsurface flow and transport of aqueous and gas phases

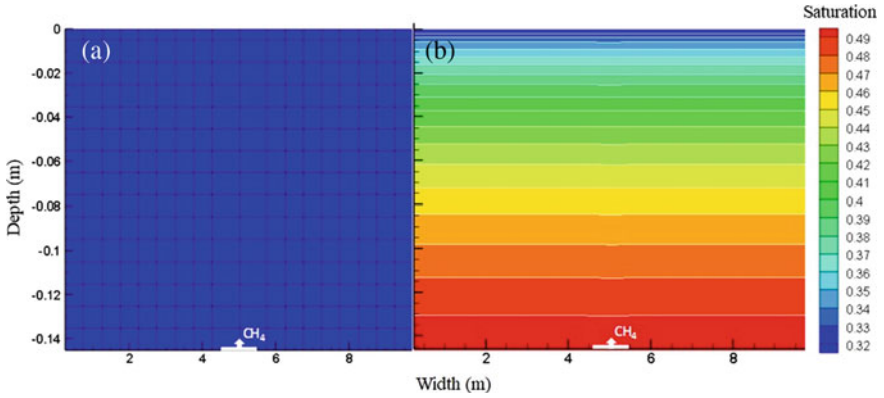

Fig. 1 Discretized 2-D computational domains for methane migration simulations in **a** completely dry soil and **b** partially saturated soil with a known soil moisture gradient. Location of the methane point diffusive source is also shown. Note different scales in *X* and *Y* axes

containing up to five components (i.e., H_2O, brine, non-condensable gas (e.g., CH_4), gas tracer, and air) under isothermal or non-isothermal conditions.

A temperature-corrected Fickian molecular diffusion coefficient was used to model methane gas diffusion. Henry's coefficients were estimated using the method described by [24] to determine dissolution of CH_4 in the aqueous phase. Since the Henry's law approach formulated in the model is accurate for low pressure (< ~ 1 MPa) conditions, the model is essentially applicable to relatively shallow subsurface porous media systems [23] as considered in this study. See [22] and [23] for further information on the TOUGH2/EOS7CA model. In this study, simulations were carried out for both dry ($\theta = \theta_r$) and partially saturated conditions ($\theta = 0.30$–0.50 cm^3 cm^{-3}). We assumed that at each density level, homogeneous and isotropic conditions, with respect to transport parameters, prevailed across the entire domain.

Figure 1 shows the 2-D Cartesian computational domain used in the TOUGH2/EOS7A modeling framework for simulating CH_4 flow in the subsurface. A 10 m (width) × 0.15 m (height) numerical domain was discretized into 270 porous elements for simulations. The width of the domain (10 m) was selected based on the assumption that this width was large enough not to have boundary effects on flow simulations, while the height (0.15 m) represents the sampling depth. The left and right boundaries and the bottom boundary were treated as having no-flow conditions (Neumann-type) for gas flow and adiabatic conditions for heat transport, while the top boundary was considered as an open boundary for both mass and heat flows. A diffusive point CH_4 source was located at the mid-section of the domain 10 cm above the bottom boundary (Fig. 1) with a production rate converted to a flux of 9 μmol m^{-2} h^{-1}, an average value presented in literature [25]. Simulations were performed for both completely dry conditions (Fig. 1a) and for partially saturated

conditions under a predefined soil moisture gradient (Fig. 1b). For partially saturated conditions, a pre-simulation was first performed to obtain the gravity-capillary equilibrium within the domain before applying the CH_4 flux.

4 Results and Discussion

Figure 2 shows the measured soil–water characteristic (SWC) in the pasture soil measured at five density levels. Note the systematic decline in saturated moisture content (θ_s) with increasing density, due to the drop in total porosity upon compaction. Compaction not only decreases the total volume of pores, but also causes a significant shift in dominant pore regions, thereby making an impact on pore size distribution. It is commonly accepted that compaction causes an increase in micropore (pore dia. < 0.02 μm) and mesopore (0.02–30 μm) regions, but decreases macropore (> 30 μm) domains [17, 26]. Increases in the relative number of micro(or capillary)pores essentially increase the air-entry pressure/bubbling pressure (P_b) with increasing density, as also demonstrated in Fig. 2. The van Genuchten model (Eq. 1) provided a very good description of the measured data as shown by the solid

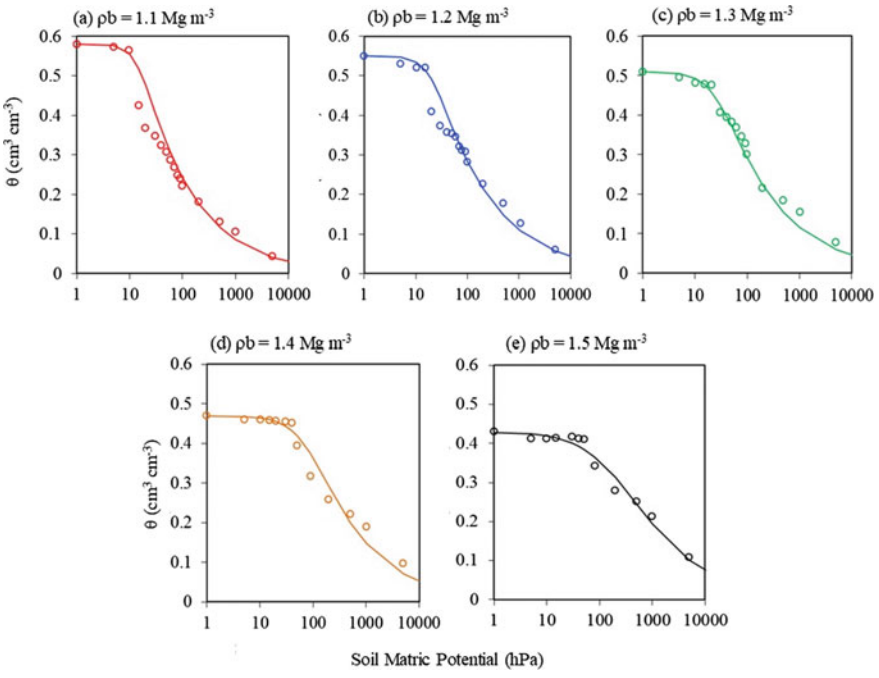

Fig. 2 Measured soil–water characteristic data for pasture soil at different densities (in Mg m^{-3}): **a** 1.1, **b** 1.2, **c** 1.3, **d** 1.4, and **e** 1.5. Predictions from parameterized van Genuchten model (Eq. 1) are also shown (in solid lines). *Note* 10 hPa ≈ 1 kPa

lines. Note the slight disparity between measured and simulated data for 1.1 and 1.2 (Mg m^{-3}) density levels around 10 hPa matric suction, which is likely due to the aggregation of soil under low bulk density.

The best-fit van Genuchten model parameters, together with the basic soil properties, are given in Table 1.

Another notable change in the SWC with the density is the change in slope of the curve at the inflection point, S (Eq. 2). A very good linear relationship ($r^2 = 0.95$) could be observed between the soil density and S (Fig. 3a), implying the applicability of S as a good indicator of the degree of soil densification/compaction, as evidenced also by previous studies (e.g., [12, 27]) also calculated the slope of the SWC at the inflection point (but expressed in a different form), and noted a linear decrease of slope (in non-aggregated soils) with increasing density. Ref. [27] hypothesized the slope as a measure of microstructure that can be used as an index of soil physical quality. Figure 3b illustrates the variation of two dominant gas transport parameters

Table 1 Basic soil physical properties and parameterization

Bulk density Mg m^{-3}	Total porosity m^3 m^{-3}	Soil–gas diffusivity (dry soil)	Permeability ($\times 10^{-12}$ m^2)	Soil–water characteristics Eq. (1)			
				θ_r	α	n	m
1.1	0.58	0.069	19.54	0	0.07	3	0.15
1.2	0.55	0.060	11.68	0	0.05	2.5	0.16
1.3	0.51	0.036	6.84	0	0.038	1.9	0.21
1.4	0.47	0.023	2.81	0	0.012	1.65	0.3
1.5	0.43	0.016	1.30	0	0.005	0.94	0.48

Estimated from K_{sat} assuming a fluidity of 9.81×10^6 m^{-1} s^{-1} at 20 °C

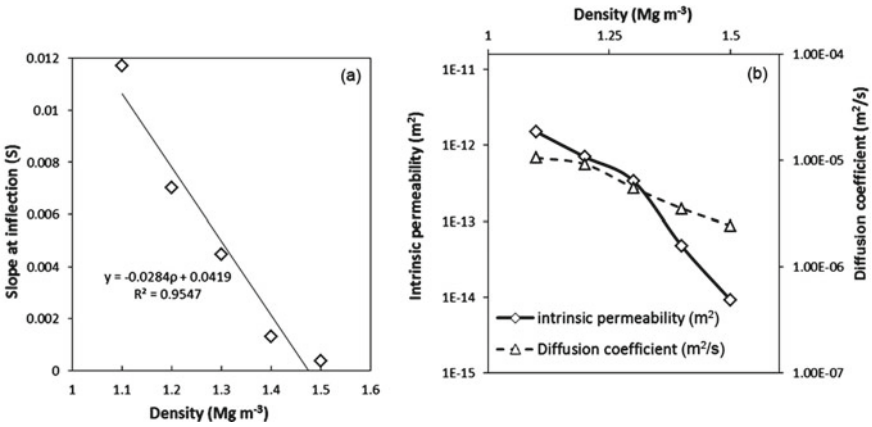

Fig. 3 **a** Derived slope (Eq. 2) at the inflection point of the soil–water characteristic as a function of soil density. The best-fit linear regression line is also shown (in solid line). **b** Intrinsic permeability (k, Eq. 2) and soil–gas diffusion coefficient (D_s, Eq. 5) against soil density

with density: intrinsic permeability, k (m^2) (Eqs. 3 and 4), and the soil–gas diffusion coefficient, D_s (m^2/s) (Eq. 5). Importantly, within the range of measured density, k varied over three orders-of-magnitude, whereas the variation of D_s occurred within a single order-of-magnitude, while both parameters showing a decrease with increasing density. Since compaction causes the rearrangement of particles, and thereby changes the soil structure, the parameters which are predominantly soil structure controlled become mostly affected due to compaction. Also, air permeability, which characterizes the advective flow of gases in porous systems, is highly soil structure controlled, since advective gas flow occurs preferentially in macropore-dominant pore regions. As described earlier, compaction can cause a marked decrease in macropore density, yielding a remarkable drop in air permeability with increasing compaction. The soil–gas diffusion coefficient, on the other hand, is not predominantly controlled by the soil structure particularly under completely dry conditions, since diffusive gas flow occurs in all gas-accessible pore domains. However, due to the compaction-induced decrease in total porosity and increase in (solid-induced) tortuosity, a decrease in D_s can also be observed with increasing compaction.

It is worth mentioning that the soil–gas transport properties need not necessarily be of equal importance across the entire soil system of interest. For example, if a gas is originating from a point source with a high pressure within the subsurface, the gas movement is more advective near the source and hence is controlled primarily by the air permeability. As the gas moves away from the source, the pressure decreases, and therefore, the flow becomes more diffusion controlled, making gas diffusivity the controlling parameter. When the gas reaches the soil-atmosphere interface, the wind-induced near-surface pressure fluctuations may potentially make an advective gradient, thus making again the air permeability the controlling parameter. Further, the characteristics of the gas may also decide whether the dominant flow is advective or diffusive. For example, a low-density gas such as CH_4 may preferentially move upward by advection (buoyancy) which is facilitated predominantly by the air permeability, with diffusion playing a minor role. Lateral CH_4 movement, however, occurs primarily by diffusion and hence is controlled by gas diffusivity. In that respect, the anisotropy of the porous system with respect to the above transport properties is also of key concern in characterizing the gas flow in porous media.

Figure 4 shows the steady-state CH_4 concentration profiles for the five density levels for dry soils. The low density of CH_4 with respect to air causes density-driven advective flow which preferentially occurs upward, leading to an upward-bulging CH_4 profile as can be seen at all density levels. The lateral and downward movements are only diffusion controlled. Note that due to the assumed isotropic conditions of soil regardless of compaction, diffusive movement is virtually the same in all directions at a given density. However, with increasing compaction, due to the marked decrease in total porosity, the diffusion coefficient, and permeability (see Fig. 2b), the outward movement of CH_4 is constrained, increasing the mean residence time of methane in the soil profile, causing an increase in the CH_4 concentration and potential oxidation within the profile.

Simulated steady-state CH_4 concentration profiles for partially saturated conditions are shown in Fig. 5. The saturation contours, after simulations, are also shown

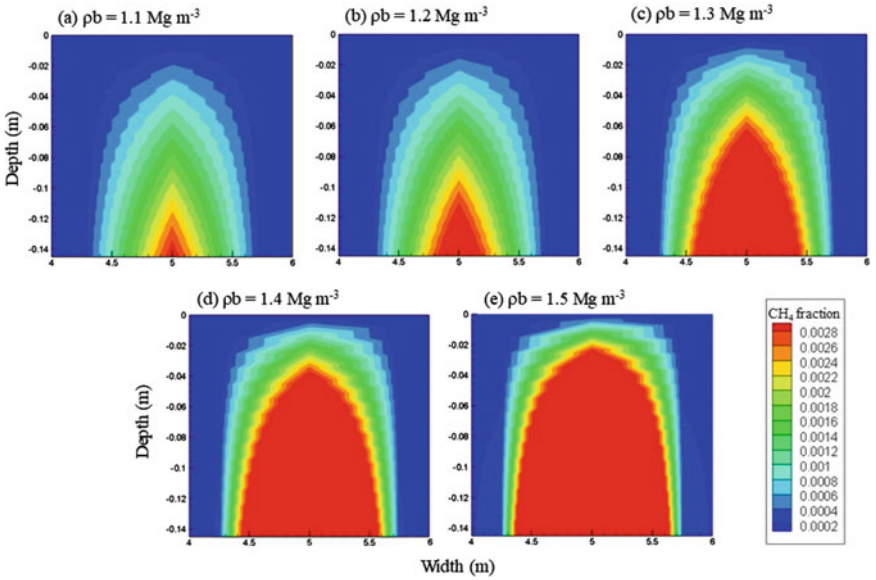

Fig. 4 Simulated steady-state methane concentration maps for five soil density (ρ_b) levels for dry soils. Colors denote the mass fraction of gaseous methane

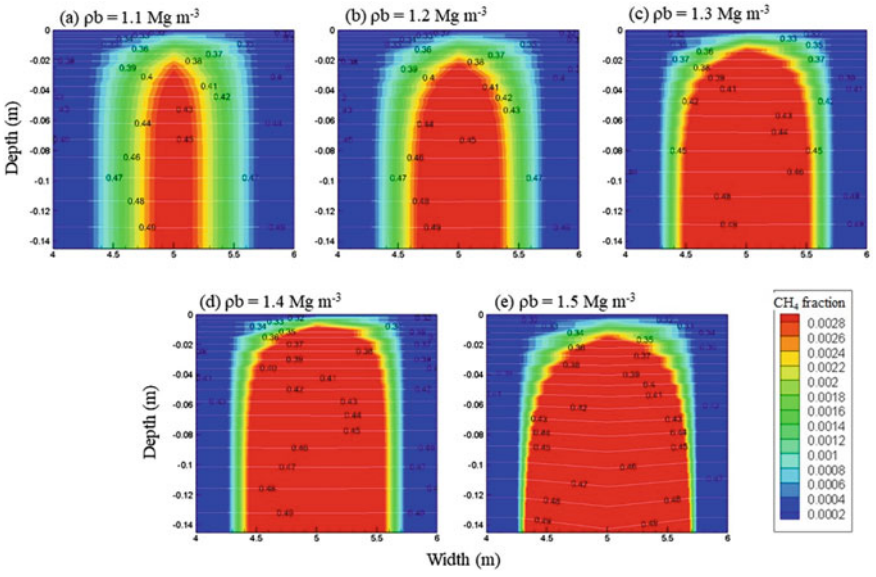

Fig. 5 Simulated steady-state methane concentration maps for five soil density (ρ_b) levels for partially saturated soils with a predefined soil moisture gradient. Colors denote the mass fraction of gaseous methane. Soil moisture contours, after methane flow is applied, are denoted in white color

(white color). Methane concentration contours are distinctly different from those in dry soil systems (Fig. 4), demonstrating the clear effect of soil moisture on subsurface CH_4 dynamics. Note that the effect of soil moisture on CH_4 concentration profiles is more evident at lower soil density (e.g., $\rho_b = 1.1$ Mg m^{-3}) than high-density soil (e.g., $\rho_b = 1.5$ Mg m^{-3}). Although the low-density soil has a larger air-filled pore space than the denser soils under the same moisture gradient, water held dominantly in micropores largely constrains movement of CH_4 through the gaseous phase, yielding a marked change in CH_4 concentration profiles in low-density soil. In fact, the diffusion-controlled lateral movement of CH_4 varies more markedly, across density levels, under partially statured condition (Fig. 5) as compared to buoyancy (advection)-dependent vertical movement, suggesting a clear effect of soil moisture on diffusive movement of CH_4 in the soil subsurface. Notably, the saturation contours are slightly distorted near the source in the higher-density soil ($\rho_b = 1.5$ Mg m^{-3}) due to the inlet velocity allowing for a gaseous phase in otherwise fully saturated soil layers.

Greatest variation of CH_4 accumulation is shown by dry conditions (see Fig. 4) with an approximate 200-fold accumulated area at the highest density (1.5 Mg m^{-3}) as compared to the lowest (1.1 Mg m^{-3}), with a systematic increase with increasing density. Accumulation CH_4 variation of under partially saturated condition, however, showed only a fivefold difference between the highest and the lowest densities. It is, therefore, clear that CH_4 accumulation within the profile is largely soil structure controlled in the absence of soil moisture.

5 Conclusions

Based on measured soil–water characteristic (SWC), measured soil–gas diffusivity, and derived permeability characteristics, we simulated CH_4 transport in five differently compacted soils ($1.1 - 1.5$ Mg m^{-3}) and determined the effects of soil moisture. Results showed a pronounced effect of soil density on subsurface CH_4 concentration profiles with enhanced concentrations in denser soils both for dry and partially saturated conditions. With increasing density (from 1.1 to 1.5 Mg m^{-3}), CH_4 concentration (above 0.3%) increased 200 times for dry soils, but only 5 times for partially saturated soils. The effect of soil moisture was observed to be more pronounced in less dense soils than in highly dense soils. Other environmental effects such as temperature, wind-induced atmospheric dynamics, porous media anisotropy, and CH_4 oxidation need to be considered in the future simulation studies.

Acknowledgements We gratefully acknowledge the funding from the Asia-Pacific Network for Global Change Research (APN) grant (CRRP2020-07MY-Deepagoda). The New Zealand Government and New Zealand Agricultural Greenhouse Gas Research Centre (NZAGRC) under the Livestock Emissions and Abatement Research Network (LEARN) are also acknowledged.

References

1. Myhre G, Shindell D, Bréon F-M, Collins W, Fuglestvedt J, Huang J, Koch D, Lamarque J-F, Lee D, Mendoza B, Nakajima T, Robock A, Stephens G, Takemura T, Zhang H (2013) Anthropogenic and natural radiative forcing. In: Stocker TF, Qin D, Plattner G-K, Tignor M, Allen SK, Boschung J, Nauels A, Xia Y, Bex V, Midgley PM (eds) Climate change 2013: the physical science basis. Contribution of working group I to the Fifth assessment report of the intergovernmental panel on climate change. Cambridge University Press, Cambridge, United Kingdom and New York, NY, USA
2. Hartmann DL, Klein Tank AMG, Rusticucci M, Alexander LV, Brönnimann S, Charabi Y, Dentener FJ, Dlugokencky EJ, Easterling DR, Kaplan A, Soden BJ, Thorne PW, Wild M, Zhai PM (2013) Observations: atmosphere and surface. In: Stocker TF, Qin D, Plattner G-K, Tignor M, Allen SK, Boschung J, Nauels A, Xia Y, Bex V, Midgley PM (eds) Climate change 2013: the physical science basis. Contribution of working group I to the fifth assessment report of the intergovernmental panel on climate change. Cambridge University Press, Cambridge, United Kingdom and New York, NY, USA
3. Montzka SA, Dlugokencky EJ, Butler JH (2011) Non-CO_2 greenhouse gases and climate change. Nature 476:43–50
4. Mer JL, Roger P (2001) Production, oxidation, emission and consumption of methane by soils: a review. Eur J Soil Biol 37:25–50
5. Ciais P, Sabine C, Bala G, Bopp L, Brovkin V, Canadell J, Chhabra A, DeFries R, Galloway J, Heimann M, Jones C, Le Quéré C, Myneni RB, Piao S, Thornton P (2013) Carbon and other biogeochemical cycles. In: Stocker TF, Qin D, Plattner G-K, Tignor M, Allen SK, Boschung J, Nauels A, Xia Y, Bex V, Midgley PM (eds) Climate change 2013: the physical science basis. Contribution of working group I to the fifth assessment report of the intergovernmental panel on climate change. Cambridge University Press, Cambridge, United Kingdom and New York, NY, USA
6. Gebert J, Groengroeft A, Pfeiffer EM (2011) Relevance of soil physical properties for the microbial oxidation of methane in landfill covers. Soil Biol Biochem 43:1759–1767
7. Croney D, Coleman JD (1954) Soil structure in relation to soil suction (pF). J Soil Sci 5:75–84
8. Gupta SC, Sharma PP, Defranchi SA (1989) Compaction effects on soil structure. Adv Agron 42:311–338
9. Gent JA, Ballard R, Hassan AE (1983) The impact of harvesting and site preparation on the physical properties of lower coastal plain forest soils. Soil Sci Soc Am J 47:595–598
10. van Genuchten MT (1980) A closed-form equation for predicting the hydraulic conductivity of unsaturated soils. Soil Sci Soc Am J 44:892–989
11. Mualem Y (1986) Hydraulic conductivity of unsaturated soils: prediction and formulas. In: Klute A (ed) Methods of soil analysis: part 1 physical and mineralogical methods, 2nd edn. America social agronomy, Monograph, vol 9, pp 799–823
12. Aschonitis VG, Kostopoulou SK, Antonopoulos VZ (2012) Methodology to assess the effects of rice cultivation under flooded conditions on van Genuchten's model parameters and pore size distribution. Transp Porous Med 91:861–876
13. Aschonitis VG, Antonopoulos VZ (2013) New equations for the determination of soil saturated hydraulic conductivity using the van Genuchten model parameters and effective porosity. Irrig Drain 62:537–542
14. Ahuja LR, Naney JW, Green RE, Nielsen DR (1984) Macroporosity to characterize spatial variability of hydraulic conductivity and effects of land management. Soil Sci Soc Am J 48:699–702
15. Millington RJ, Quirk JM (1960) Transport in porous media. In: Van Beren FA et al (ed) Transactions international congress soil science, 7th, Madison, WI. 14–21 August 1960. vol 1. Elsevier, Amsterdam pp 97–106
16. Millington RJ, Quirk JM (1961) Permeability of porous solids. Trans Faraday Soc 57:1200–1207

17. Chamindu Deepagoda TKK, Clough TJ, Thomas S, Balaine N, Elberling B (2018) Density effects on soil-water characteristics, soil–gas diffusivity, and emissions of N_2O and N_2 from a re-packed pasture soil. Soil Sci Am J https://doi.org/10.2136/sssaj2018.01.0048
18. Chamindu Deepagoda TKK, Smits KM, Oldenburg CM (2016) Effect of subsurface soil moisture variability and atmospheric conditions on methane gas migration in shallow subsurface. Int J Greenh Gas Control 55:105–117
19. Balaine N, Clough TJ, Beare MH, Thomas SM, Meenken ED (2016) Soil gas diffusivity controls N_2O and N_2 emissions and their ratio. Soil Sci Soc Am J 80:529–540
20. Hewitt AE (1998) Manaaki Whenua-Landcare Research New Zealand Ltd. New Zealand soil classification. Lincoln, N.Z, Manaaki Whenua Press
21. Taylor SA (1949) Oxygen diffusion in porous media as a measure of soil aeration. Soil Sci Soc Am Proc 14:55–56
22. Pruess K, Oldenburg CM, Moridis GJ (1999) TOUGH2 user's guide version 2. E.O. Lawrence Berkeley national laboratory report LBNL-43134
23. Oldenburg CM (2015) EOS7CA version 1.0: TOUGH2 module for gas migration in shallow subsurface porous media systems, Lawrence Berkeley national laboratory report LBNL-175204
24. Cramer SD (1982) Solubility of methane, carbon dioxide, and oxygen in brines from 0/sup 0/ to 300/sup 0/C. United States: N
25. Oertel C, Matschullat J, Zurba K, Zimmermann K, Erasmi S (2016) Greenhouse gas emissions from soils—a review. Soil Sci Soc Am J 76:327–352
26. Yahya Z, Husin A, Talib J, Othman J, Darus SZ, Ahamed OH, Jalloh MB (2011) Pores reconfiguration in compacted Bernam series soil. Am J Appl Sci 8:212–216
27. Dexter AR (2004) Soil physical quality part I. Theory, effects of soil texture, density, and organic matter, and effects on root growth. Elsevier: Geoderma 120:201–214

Numerical Simulation of Energy-Absorbing Rubber Pads Using FEM and DEM Approaches—A Comparative Study

H. G. S. Mayuranga, S. K. Navaratnarajah, C. S. Bandara, and J. A. S. C. Jayasinghe

Abstract To lessen the track deterioration and the life cycle cost of ballasted railway tracks, the application of energy-absorbing rubber pads such as rail pads (RP), under sleeper pads (USP), and under ballast mats (UBM) is becoming popular in many countries. Recent experimental studies explore the ability of these rubber pads to reduce ballast layer stress, ballast degradation, and excessive track settlement through large-scale laboratory investigations. Numerical simulation of these large-scale experiments provides an efficient and cost-effective approach to extend for more investigations. Finite element method (FEM) and discrete element method (DEM) are the main approaches used in many studies to simulate the ballasted rail track behaviour. The selection of an appropriate numerical approach mainly depends on the nature of the materials, simulation type, computational cost, and the expected level of accuracy. However, limited numerical studies have been done so far to simulate the static and cyclic loading behaviour of energy-absorbing rubber pads as a solid element for railway applications using either FEM or DEM approaches. Therefore, in this study, 3D models of a rubber pad were developed using both FEM and DEM approaches and they were validated based on the experimental data from the literature for the quasi-static loading condition. Then, a parametric study was carried out by changing the thickness of the rubber pad using both numerical approaches and the results were compared. The results exhibited that the developed numerical models captured the behaviour of the rubber pad with reasonable accuracy for both FEM and DEM approaches. Therefore, the developed rubber pad models can be effectively used in numerical simulations of large-scale experiments and railway applications using either FEM or DEM approaches based on the requirement.

Keywords Ballast · FEM · DEM · Energy-absorbing rubber pads · Hyper-elastic materials

H. G. S. Mayuranga (✉) · S. K. Navaratnarajah · C. S. Bandara · J. A. S. C. Jayasinghe
Department of Civil Engineering, Faculty of Engineering, University of Peradeniya, Peradeniya, Sri Lanka
e-mail: sushanm@eng.pdn.ac.lk

R. Dissanayake et al. (eds.), *12th International Conference on Structural Engineering and Construction Management*, Lecture Notes in Civil Engineering 266,
https://doi.org/10.1007/978-981-19-2886-4_21

1 Introduction

The demand for railway transportation is being increased worldwide as it provides numerous benefits to society. Ballasted railway corridors play a significant role in railway transportation as it is the most common type of railway corridors adopted in many railway networks worldwide. The presence of faster and heavier trains on existing rail corridors has increased the rate of ballast degradation, ballast fouling, track settlement, damage to track components, and finally the track maintenance cost [1, 2]. To mitigate these issues, energy-absorbing rubber pads known as rail pads (RP), under sleeper pads (USP), and under ballast mats (UBM) are adopted in ballasted corridors as a popular method [3, 4]. The impact of these rubber pads on the rail track performance has been investigated by recent studies through field investigations and large-scale laboratory experiments such as ballast box test, direct shear test, and triaxial test [5–7]. All these laboratory tests are developed to capture the behaviour of the granular ballast layer which is the most important and load-bearing component in ballasted rail tracks. However, only few numerical studies have captured the behaviour of rubber pads in large-scale experimental simulations.

Finite element method (FEM) and discrete element method (DEM) are the major approaches used in many numerical studies for railway applications [8–12]. FEM has been successfully used to capture ballast layer stress, vertical and horizontal deformations of ballast, sleeper stress, and so on. Few numerical studies have adopted rubber pads as a 3D solid element with linear elastic material properties in FEM to simulate large-scale laboratory tests [7, 13]. However, according to the authors knowledge, no studies have been performed in FEM using hyper-elastic material properties to represent the nonlinear behaviour of rubber pads for railway applications considering the energy dissipation. DEM has been successfully used to simulate the granular nature of ballast and captured the particle breakage, ballast layer stress, and deformations. Only few studies have been adopted the rubber pads in DEM as a discrete element to validate the numerical models with laboratory tests [14, 15].

The static bedding modulus is the main characteristic parameter of an energy-absorbing rubber pad which can be evaluated using the static load test at the laboratory. In this study, numerical models were developed to simulate the static load test of a rubber pad using both FEM and DEM approaches. The rubber pad was modelled in FEM using hyper-elastic material properties and in DEM as a discrete element to capture the nonlinear behaviour of rubber. The models were validated using experimental data from [16] for quasi-static loading conditions. Then, a parametric study was done by changing the thickness of the rubber pad to capture the variation of static bedding modulus of rubber pad using both numerical approaches and the results were compared.

2 FEM Simulation of Rubber Pad

Energy-absorbing rubber pads are made of rubber-like material [17]. Rubber is an isotropic, homogenous, and incompressible material. Hyper-elastic materials are commonly used to capture the nonlinear stress–strain behaviour of rubber when subjected to large deformations [18, 19]. Hyper-elastic material models are developed based on the strain energy potential, and there are several forms of strain energy potentials introduced by different researchers. In this study, a hyper-elastic material model was adopted to capture the behaviour of the rubber pad along with viscoelastic properties in *ABAQUS/CAE 6.14* commercial FEM software. *ABAQUS* provides several forms of hyper-elastic material models including Ogden model, Mooney Rivlin model, Arruda-Boyce model, Neo-Hooke model, Yeoh model, and Van Der Waals model [20–23]. It is important to select the best-suit hyper-elastic material model to accurately predict the behaviour of the rubber pad in FEM analysis.

2.1 Selection of Best-Suited Material Model for Rubber Pad

To select the best-suited material model for a particular rubber application, it is required at least one test data from uniaxial test, biaxial test, planar test, and volumetric test. The curve fitting approach in *ABAQUS* facilitates the user to compare these test data with hyper-elastic material models and determines the coefficients corresponding to each material model. In this study, uniaxial compression test data and volumetric test data were obtained from [16] and used as input data in the curve fitting operation. The obtained stable material models from *ABAQUS* were evaluated to fit the test data considering statistical indexes such as mean absolute deviation (MAD), mean absolute percentage error (MAPE), and mean squared deviation. Based on that, the Arruda-Boyce model was selected as the best-suit material model to fit the test data. Equation (1) shows the strain energy potential of Arruda-Boyce model, where U, $\overline{I}_1$, and J_{el} are the strain energy per unit of reference volume, the first deviatoric strain invariant, and the elastic volume ratio, respectively. Also, μ, λ_m, and D are the temperature-dependent material parameters which were obtained from the curve fitting operation as given in Table 1 and used as input parameters for the numerical simulation of the rubber pad.

Table 1 Coefficient values of Arruda-Boyce model

μ	λ_m	D
0.5936	7.0020	3.7541

$$U = \mu \left\{ \begin{array}{l} \frac{1}{2}\left(\overline{I}_1 - 3\right) + \frac{1}{20\lambda_m^2}\left(\overline{I}_1^2 - 9\right) + \frac{11}{1050\lambda_m^4}\left(\overline{I}_1^3 - 27\right) \\ + \frac{19}{7000\lambda_m^6}\left(\overline{I}_1^4 - 81\right) + \frac{519}{673750\lambda_m^8}\left(\overline{I}_1^5 - 243\right) \end{array} \right\} + \frac{1}{D}\left(\frac{J_{el}^2 - 1}{2} - \ln J_{el}\right) \quad (1)$$

2.2 *Validation of FE Model*

A numerical model of static load test on UBM according to DIN 45673–5 specifications was developed in *ABAQUS* which is used to evaluate the static bedding modulus of UBM in the laboratory. The rubber pad was modelled as a 3D deformable solid element having the dimensions of 200 × 200 × 10 mm according to the laboratory test conducted by [16]. The rubber pad was placed on a strong base plate, and the load was applied on top of the rubber pad using the loading plate. The base plate and the loading plate were represented in the model as discrete rigid shell elements having the dimensions of 200 × 200 mm. The experimental setup and the developed numerical model of test assembly are shown in Fig. 1a, b, respectively. The applied load on the top loading plate is shown in Fig. 2.

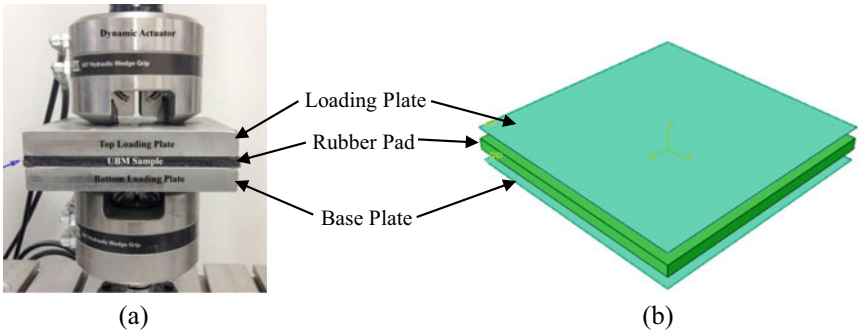

Fig. 1 **a** Experimental setup [16] and **b** FE model of static load test of rubber pad

Fig. 2 Applied load on rubber pad according to DIN 45673–5 specification

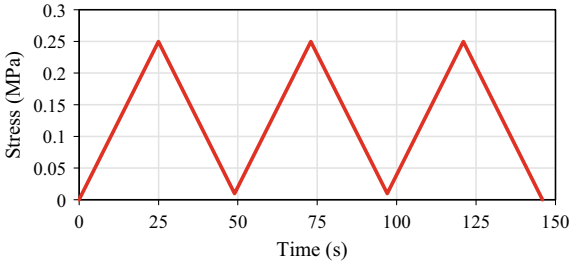

Table 2 Viscoelastic coefficient values used in *ABAQUS*

	$\overline{g}_i^p$	τ_i^G
1	0.225	8.640
2	0.120	330.615

The density of the rubber pad was used as 920 kg/m^3, and the elasticity was defined under the hyper-elastic material models using the coefficients of Arruda-Boyce model given in Table 1. The viscoelastic properties obtained from [24] were modified and adopted to capture the energy dissipation of rubber pad under time domain using Prony series coefficients as shown in Table 2.

The relaxation function $g_R(t)$ in terms of Prony series coefficients is given in Eq. (2), where $\overline{g}_i^p$ and τ_i^G denote the shear relaxation modulus ratio and the relaxation time, respectively.

$$g_R(t) = G_0\left(1 - \sum_{i=1}^{N} \overline{g}_i^p \left(1 - e^{-t/\tau_i^G}\right)\right) \tag{2}$$

The dynamic implicit analysis was adopted in *ABAQUS* to simulate the quasi-static loading on the rubber pad. Surface-to-surface interaction was used to define the interactions at base plate to rubber pad and loading plate to rubber pad interfaces. The rubber pad was meshed using C3D8RH elements, and a mesh sensitivity analysis was carried out to find the optimum mesh size for the simulation. The number of elements used for the optimized mesh size of the rubber pad was 25,600. The base plate was fixed, and the loading plate was only allowed to displace along the load application direction by using displacement/rotation boundary conditions. Then, the load on top loading plate was applied as a uniformly distributed pressure.

Based on the simulation, Fig. 3 depicts the variation of vertical stress of rubber pad with vertical displacement for three loading cycles applied. Also, Fig. 4 compares the stress-displacement variation of simulation results with experimental results reported by [16] for the third load cycle.

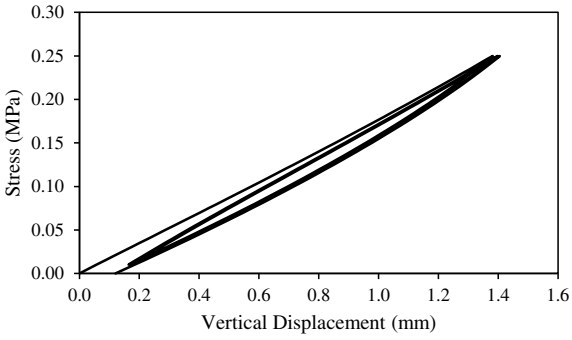

Fig. 3 Variation of vertical stress with vertical displacement

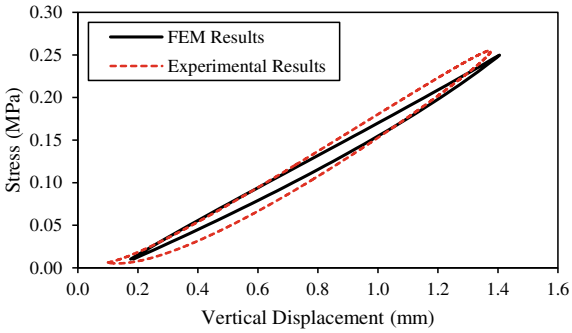

Fig. 4 Comparison of FEM results and experimental results [16] for the third load cycle

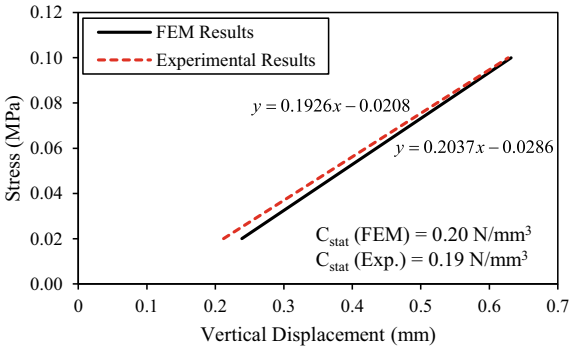

Fig. 5 Gradients of stress-displacement curves and calculated static bedding modulus values

Following the DIN 45673–5 specification, the calculated static bedding modulus (C_{stat}) values based on the gradients of stress-displacement curves are shown in Fig. 5.

The experimental and numerical bedding modulus values are 0.20 N/mm^3 and 0.19 N/mm^3, respectively, and the variation between them is only 5%. Therefore, the developed FE model can be used to accurately predict the static bedding modulus of rubber pads. Hence, the parametric study was conducted by using the developed FE model as described in the next section.

2.3 Parametric Study

The validated numerical model with the 10 mm thick rubber pad was used to investigate the effect of rubber pad thickness on its static bedding modulus value. For that, three different numerical models of static load test were developed with 8 mm, 12 mm, and 14 mm thick rubber pads. Based on the results, the variation of vertical stress with vertical displacement for 8 mm, 10 mm, 12 mm, and 14 mm thick rubber pads under the third load cycle are shown in Fig. 6. The gradients of stress-displacement curves and the calculated static bedding modulus values for each thickness are shown in Fig. 7.

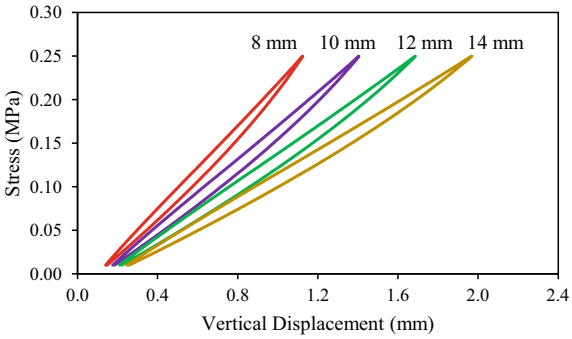

Fig. 6 Variation of vertical stress with vertical displacement of rubber pads for the third load cycle

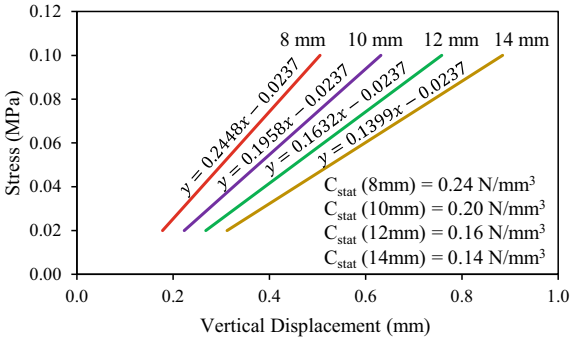

Fig. 7 Gradients of stress-displacement curves and calculated static bedding modulus values

The results clearly show that the static bedding modulus of the rubber pad increases as the thickness decreases. This trend was previously reported by Sol-Sanchez [25] for deconstructed tire rubber pads through a series of experimental investigation. Therefore, the developed numerical models in FEM can be successfully used for the simulation of large-scale laboratory tests where rubber pads are adopted.

3 DEM Simulation of Rubber Pad

The static load test on the rubber pad was simulated again using discrete element method (DEM). DEM generates a number of particles to simulate the test materials, and the interactions between particles are used to calculate the forces between them. Newton's second law of motion is used to determine the translational and rotational accelerations of particles in a simulation. In this study, a numerical simulation of the static load test on the rubber pad was done. The rubber pad was modelled in DEM as a discrete element.

3.1 Validation of DEM Model

The rubber pad with the dimensions of 200 × 200 × 10 mm was formed in DEM by using three layers of closely packed spheres having 4 mm diameter. The total number of spheres in the assembly was 7401. The Hertz-Mindlin contact model with the Bonding V2 model was adopted to define the interactions and bonding between particles. The base plate and the loading plate were modelled as geometries and steel material properties were assigned to them to incorporate the actual laboratory conditions. The load given in Fig. 2 was applied to the rubber pad through the loading plate. Figure 8 represents the developed numerical model, and Table 3 shows the parameters used in the simulation.

Based on the simulation results, the variation of vertical stress with vertical displacement of rubber pad was obtained as shown in Fig. 9. Then, the numerical results were compared with the experimental results of [16] for the third load cycle as shown in Fig. 10.

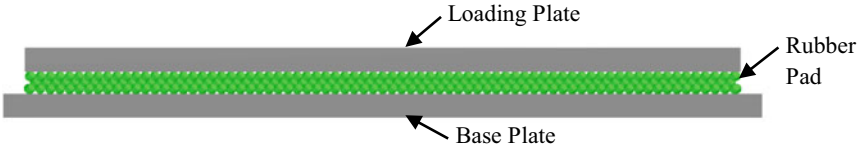

Fig. 8 DEM model of static load test of rubber pad

Table 3 Parameters used for DEM simulation

Parameter	Rubber	Steel
Solid density (kg/m^3)	920	7850
Shear modulus (MPa)	2.87	8
Poisson's ratio	0.48	0.3
Interface	Rubber-Rubber	Steel-rubber
Coefficient of restitution	0.85	0.4
Coefficient of static friction	0.5	0.5
Coefficient of rolling friction	0.01	0.01
Bonding parameters		
Normal stiffness per unit area (N/m^3)	1×10^7	
Shear stiffness per unit area (N/m^3)	1×10^7	
Normal strength (Pa)	1×10^{60}	
Shear strength (Pa)	1×10^{60}	
Bond disc scale	1	

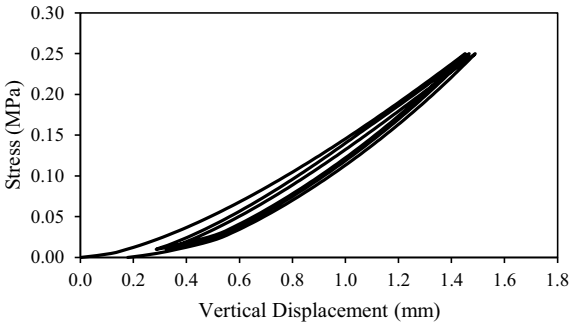

Fig. 9 Variation of vertical stress with vertical displacement

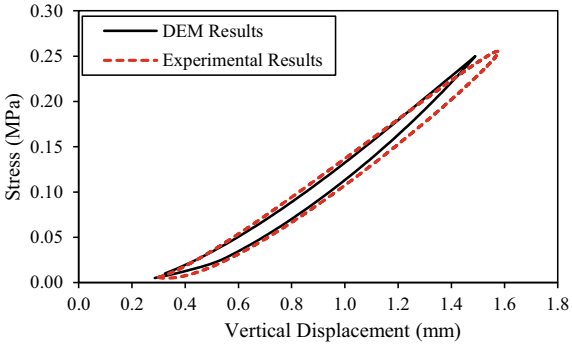

Fig. 10 Comparison of DEM results and experimental results [16] for the third load cycle

Based on that, the gradients of stress-displacement curves were obtained following the DIN 45673–5 specification and the static bedding modulus values were calculated for numerical and experimental results as shown in Fig. 11. The static bedding modulus values calculated from numerical model results and experimental results are 0.18 N/mm^3 and 0.19 N/mm^3, respectively. Since the deviation of numerical value from experimental value is about 5%, the developed model was used for the parametric study.

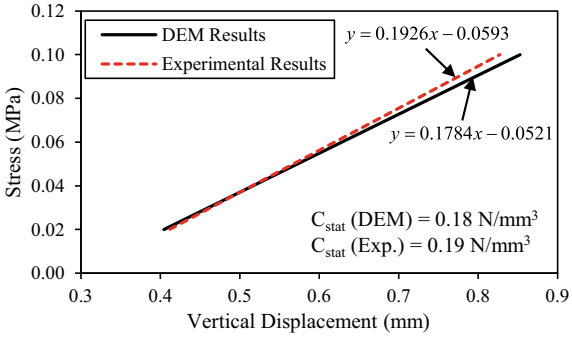

Fig. 11 Gradients of stress-displacement curves and calculated static bedding modulus values

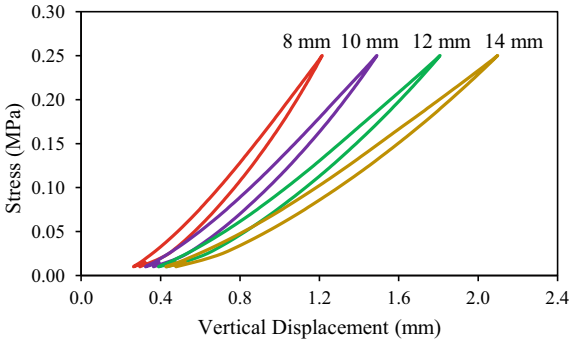

Fig. 12 Variation of vertical stress with vertical displacement of rubber pads for the third load cycle

3.2 Parametric Study

The parametric study explained under Sect. 2.3 was done by using the DEM approach for 8 mm, 10 mm, 12 mm, and 14 mm thick rubber pads. In DEM, the thickness of the rubber pad can be easily changed by changing the diameter of small spheres. Figure 12 explores the stress-displacement variation of each rubber pad for the third load cycle, while Fig. 13 depicts the gradients of each curve and calculated static bedding modulus values.

As expected, the static bedding modulus of the rubber pad increases as the thickness decreases following the similar trend reported in the literature [25]. Therefore, the developed DEM model can be effectively used in DEM simulation of large-scale experiments with rubber pads.

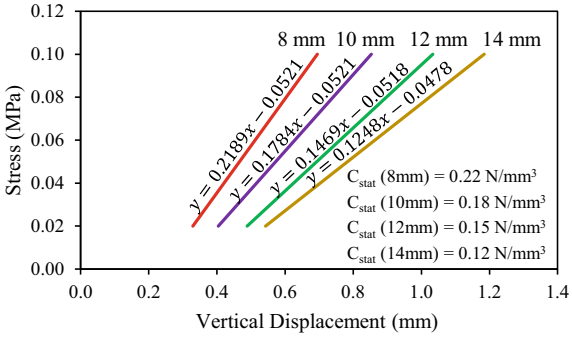

Fig. 13 Gradients of stress-displacement curves and calculated static bedding modulus values

Table 4 Comparison of results of FEM and DEM simulations

Rubber pad thickness (mm)	Static bedding modulus (N/mm^3)		Variation (%)
	FEM results	DEM results	
8	0.24	0.22	8.3
10	0.20	0.18	10.0
12	0.16	0.15	6.3
14	0.14	0.12	14.3

4 Comparison of Results

The static bedding modulus values obtained for different thicknesses of rubber pad using FEM and DEM simulations were compared as shown in Table 4. Based on that, the percentage deviations of results are equal to or less than 10% for all thicknesses except for the 8 mm thickness. Therefore, both FEM and DEM simulations show a good agreement between the results.

The development of the rubber pad geometry in the FEM approach is simple and easy to locate within the global coordinate system. But, in the DEM approach, it is required to provide the coordinates of each small spheres to create the rubber pad geometry. However, it is simple to assign material properties of rubber in the DEM approach as it deals with discrete elements (small spheres) to represent the rubber pad. But, in the FEM approach, the selection of the best-suit hyper-elastic material model for the rubber pad requires accurate and expensive experimental results. When considering the computational cost, to simulate the static load test of a 10 mm thick rubber pad with 25,600 number of elements in the FEM approach, it was required about 30 min to complete the simulation by utilizing 20 CPU cores in a workstation computer having 128 GB RAM. However, by utilizing similar facilities, it was required about 6 h to simulate the static load test of a 10 mm thick rubber pad with 7401 number of spheres in the DEM approach. In addition, the FEM approach cannot be used to capture the particle breakage of granular materials such as railway ballast together with rubber pads. But DEM is capable of capturing the particle breakage of granular materials which can be effectively used for railway applications. Therefore, depending on the requirement, the developed FEM and DEM models of the rubber pad can be adopted to investigate the granular behaviour of railway ballast in large-scale laboratory experiments.

5 Conclusion

The application of energy-absorbing rubber pads in ballasted railway corridors is a common practice in most railway networks. However, only limited numerical studies have been done to capture the behaviour of rubber pads in railway applications. In this

study, numerical models of static load test on rubber pads following DIN 45673–5 specifications were developed using both FEM and DEM approaches. The hyper-elastic material behaviour and discrete elements were adopted in FEM and DEM methods, respectively, to capture the nature of rubber-like materials. The models were validated using the experimental data from [16]. Then, parametric studies were carried out to investigate the effect of rubber pad thickness on its static bedding modulus value.

The results obtained from both FEM and DEM simulations exhibited a good agreement showing the percentage deviations of results equal to or less than 10% for all thicknesses except for the 8 mm thickness which exhibited 14% deviation. Based on the results, the static bedding modulus of the rubber pad increased as the thickness decreased. This relationship was well agreed with previous experimental investigations. When considering the computational time, FEM required a smaller simulation time compared to DEM. However, FEM does not capture the particle breakage of granular materials such as railway ballast but DEM provides that capability. Therefore, the developed numerical models of the rubber pad can be effectively used in the simulation of large-scale laboratory studies of railway ballast depending on the requirement of representing the particle breakage.

Acknowledgements The support provided by the Accelerating Higher Education Expansion and Development (AHEAD) Operation of the Ministry of Higher Education funded by the World Bank (Grant No: AHEAD/RA3/DOR/STEM/No.63) is gratefully appreciated.

References

1. Mayuranga HGS, Navaratnarajah SK, Gimhani MMN, Karunarathne JMMY (2022) The effect of fouling materials on permeability behaviour of large size granular materials. In: Dissanayake R, Mendis P, Weerasekera K, De Silva S, Fernando S (eds) ICSBE 2020, Lecture notes in civil engineering, vol 174. Springer, Singapore, pp 33–46
2. Navaratnarajah S, Indraratna B (2020a) Stabilisation of stiffer rail track substructure using artificial inclusion. Indian Geotech J 1–8
3. Mayuranga HGS, Navaratnarajah SK, Bandara CS, Jayasinghe JASC (2019) A state of the art review of the influence of rubber inclusions in railway tracks. 10th International conference on structural engineering and construction management. Kandy, Sri Lanka, pp 367–377
4. Navaratnarajah SK, Indraratna B (2020b) Application of under sleeper pads to enhance the sleeper-ballast interface behaviors. Construction in geotechnical engineering. Springer, pp 619–636
5. Abadi T, Le Pen L, Zervos A, Powrie W (2015) Measuring the area and number of ballast particle contacts at sleeper/ballast and ballast/subgrade interfaces. Int J Railway Technol 4(2):45–72
6. Kaewunruen S, Aikawa A, Remennikov AM (2017) Vibration attenuation at rail joints through under sleeper pads. Procedia Eng 189:193–198
7. Navaratnarajah SK, Indraratna B, Ngo NT (2018) Influence of under sleeper pads on ballast behavior under cyclic loading: experimental and numerical studies. J Geotech Geoenvironmental Eng 144(9):04018068
8. Ferreira P, López-Pita A (2013) Numerical modeling of high-speed train/track system to assess track vibrations and settlement prediction. J Transp Eng 139(3):330–337

9. Gong H, Song W, Huang B, Shu X, Han B, Wu H, Zou J (2019) Direct shear properties of railway ballast mixed with tire derived aggregates: experimental and numerical investigations. Constr Build Mater 200:465–473
10. Johansson A, Nielsen JCO, Bolmsvik R, Karlström A, Lundén R (2008) Under sleeper pads-Influence on dynamic train-track interaction. Wear 265(9–10): 1479–1487. https://doi.org/10.1016/j.wear.2008.02.032
11. Ngo NT, Indraratna B, Rujikiatkamjorn C (2016) Modelling geogrid-reinforced railway ballast using the discrete element method. Transp Geotech 8:86–102
12. Paixão A, Varandas JN, Fortunato E, Calçada R (2018) Numerical simulations to improve the use of under sleeper pads at transition zones to railway bridges. Eng Struct 164:169–182
13. Ngamkhanong C, Kaewunruen S (2020) Effects of under sleeper pads on dynamic responses of railway prestressed concrete sleepers subjected to high intensity impact loads. Eng Struct 214:110604
14. Li H, McDowell GR (2018) Discrete element modelling of under sleeper pads using a box test. Granular Matter 20(2):1–12
15. Ngo T, Indraratna B (2020) Mitigating ballast degradation with under-sleeper rubber pads: experimental and numerical perspectives. Comput Geotech 122:103540
16. Navaratnarajah SK (2017) Application of rubber inclusions to enhance the stability of ballasted rail track under cyclic loading Ph.D. thesis, school of civil, mining and environmental engineering. University of Wollongong
17. Sol-Sanchez M, Moreno-Navarro F, Rubio-Gámez MC (2015) The use of elastic elements in railway tracks: a state of the art review. Constr Build Mater 75:293–305. https://doi.org/10.1016/j.conbuildmat.2014.11.027
18. Diani J, Brieu M, Gilormini P (2006) Observation and modeling of the anisotropic visco-hyperelastic behavior of a rubberlike material. Int J Solids Struct 43(10):3044–3056
19. Shahzad M, Kamran A, Siddiqui MZ, Farhan M (2015) Mechanical characterization and FE modelling of a hyperelastic material. Mater Res 18:918–924
20. Arruda EM, Boyce MC (1993) A three-dimensional constitutive model for the large stretch behavior of rubber elastic materials. J Mech Phys Solids 41(2):389–412
21. Mooney M (1940) A theory of large elastic deformation. J Appl Phys 11(9):582–592
22. Ogden R (1973) Large deformation isotropic elasticity—on the correlation of theory and experiment for incompressible rubberlike solids. Rubber Chem Technol 46(2):398–416
23. Yeoh OH (1990) Characterization of elastic properties of carbon-black-filled rubber vulcanizates. Rubber Chem Technol 63(5):792–805
24. Wei C, Olatunbosun OA (2016) The effects of tyre material and structure properties on relaxation length using finite element method. Mater Des 102:14–20
25. Sol-Sanchez M, Moreno-Navarro F, Rubio-Gámez MC (2014) Viability of using end-of-life tire pads as under sleeper pads in railway. Constr Build Mater 64:150–156. https://doi.org/10.1016/j.conbuildmat.2014.04.013

Prediction of Geotechnical Properties of Stabilized Soil Using Fly Ash-Based Stabilizer Systems

N. A. N. M. Nissanka, K. M. D. Nimesha, and M. C. M. Nasvi

Abstract Development of predictive models to estimate the geotechnical properties of fly ash (FA)-stabilized soil will enable practicing engineers to obtain the required properties without conducting time-consuming and labor-intensive laboratory experiments. Therefore, this study aimed to develop predictive models to determine the geotechnical properties (optimum moisture content (OMC), maximum dry density (MDD), and unconfined compressive strength (UCS)) of soil stabilized with FA-based stabilizer systems (FA-stabilized soil (FA-S) and FA-based geopolymer-stabilized soil (FA-GP-S)). For this purpose, a large number of data were collected from relevant literature and predictive models were developed using artificial neural network (ANN). Models were developed for OMC, MDD, and UCS of FA-S, whereas only the UCS model was developed for FA-GP-S due to the limited availability of data. The developed models were validated with independent sets of data obtained from the literature. Finally, the developed predictive models were used to predict the geotechnical properties with various input parameters. Results revealed that ANN can successfully be used to develop predictive models for geotechnical engineering properties of the stabilized soils as there was a good correlation between predicted and experimental results for both the training and validation data set for all the models. Therefore, the developed correlations can be used to obtain OMC, MDD, and UCS of the stabilized clayey soil using FA-based stabilizer systems such as FA-S and FA-GP-S. As part of the model extension, the trends predicted for various geotechnical properties with the input parameters were consistent with the trends reported in the literature.

Keywords Artificial neural network · Fly ash · Geopolymer · Soil stabilization · Unconfined compressive strength

N. A. N. M. Nissanka · K. M. D. Nimesha · M. C. M. Nasvi (✉)
Department of Civil Engineering, Faculty of Engineering, University of Peradeniya, Peradeniya, Sri Lanka
e-mail: nasvimcm@eng.pdn.ac.lk

R. Dissanayake et al. (eds.), *12th International Conference on Structural Engineering and Construction Management*, Lecture Notes in Civil Engineering 266,
https://doi.org/10.1007/978-981-19-2886-4_22

1 Introduction

Due to the rapid increase in urbanization, there is a huge demand for the lands for civil engineering constructions, and therefore, land areas with problematic soils, such as expansive soil, collapsible soil, peat, and landfills, need to be utilized for construction purposes. One of the common soil improvement methods is the chemical stabilization method, in which chemical additives like cement and lime are mixed with soil to achieve enhanced strength, durability, and volume stability [1, 2]. However, a major problem with these conventional Portland cement (PC)-based stabilizers is that their production process is highly energy-intensive, involves over-extraction of mineral resources, and releases a large amount of CO_2 to the atmosphere [2]. It has been found that the production of one tonne of PC emits about one tonne of CO_2 to the atmosphere [3]. Hence, the use of mineral additives which are received as industrial by-products, such as fly ash (FA), blast furnace slag, bottom ash, and rice husk ash for chemical stabilization has become a popular research area mainly due to the low CO_2 emission and cost associated with their production [4–9].

FA is one of the abundant and versatile industrial by-products [10] which is produced by coal combustion. The use of FA for chemical stabilization is well documented, and the recommended FA dosage for soil stabilization varies from 9 to 20% by weight [4, 5, 11–14]. In the recent past, FA-based geopolymers have been identified as successful precursors for soil stabilization works [15–19]. All these studies have found that geopolymers can be successfully used to stabilize soft soils. The mechanical and durability properties of soil stabilized with FA-based systems (raw FA and FA-based geopolymer) depend on various parameters including the type of soil, type of FA, dosage of FA, activator type, dosage, mix composition, curing time, curing temperature, etc. [9, 15, 17, 20, 21]. Since the properties of stabilized soil depend on many parameters, a number of labor-intensive trial and error tests have to be conducted to develop relationships between the geotechnical properties of the mix parameters. Hence, the development of predictive models to obtain the geotechnical properties of stabilized soil will be useful and this has been the recent trend in this area.

In the literature, there are several tools and techniques to predict the geotechnical properties of FA-stabilized systems including multi-variable regression (MVR) [22–24], artificial neural network (ANN) [25–26], genetic programming [25, 27, 28], etc. Among these tools, the ANN approach has been emerging in the recent past as one of the versatile techniques due to its ability to learn by examples and handle complex problems where an exact analytical solution does not exist or is difficult to be developed [29]. ANN is a computational model which is developed based on the structure and the functions of biological neural networks in the human brain. It provides the ability to map a set of input parameters into a set of output parameters through a 'training' process, and once trained, it can be used to predict the outcome of a new input data set. The ANN detects patterns and trends between data by learning through a sample set of data, and hence, it allows easy handling of multi-variable problems with non-linear relationships. Due to all the above advantages, ANN was

used as the model development tool in the current study. Few studies [24–26] focus on developing predictive models using ANN for FA-based stabilizer systems. The section below summarizes the findings of those previous studies.

Muzumder and Laskar [26] investigated the feasibility of ANN in predicting the UCS of geopolymer-stabilized clayey soil using ground granulated blast furnace slag (GGBS) and FA as source materials for geopolymerization. Prediction performances of ANN were compared with that of the MVR model, and the results suggested that the ANN model with multilayer perceptron feed-forward network is more flexible and it has more ability to generalize the data compared with the MVR model.

Hanandeh et al. [25] presented the results of using ANN and genetic algorithm for estimating the resilient modulus for subgrade soil stabilized with FA, lime, and cement. Eight input parameters (soil moisture content, clay percentage, silt percentage, optimum moisture content (OMC), plasticity index, FA, cement, and lime) were used for model development, and according to the results, both the model development methods showed satisfactory performances. However, ANN model with one hidden layer and nine hidden neurons exhibited the highest prediction ability.

Leong et al. [27] investigated the effect of significant variables on the compressive strength of soil-FA geopolymer using ANN as the model development tool. Garson's algorithm and the connection weight approach were used comparatively to quantify the importance of input parameters; the results indicate that connection weight approach is superior to the Garson's algorithm in identifying variability importance; and according to connection weight approach, percentages of soil, FA, and water were identified to have the highest significance for compressive strength of FA geopolymer-stabilized soil.

Binal and Binal [24] developed prediction models to evaluate the UCS after 1-day curing (UCS_1) and UCS after 28-day curing (UCS_{28}) of FA-stabilized soil using FA content, liquid limit, plastic limit, clay activity, OMC, and MDD as model input parameters. According to the obtained coefficient of correlation values (R^2), ANN models exhibited better performances compared to MVR models. However, in both the model types, (UCS_{28}) model showed higher performances when (UCS_1) is also considered as one of the model input parameters.

However, to date, there have been no studies focusing on developing generalized predictive models with a large number of literature data. Further, the majority of the existing models lack the validation study. Therefore, this research aims to develop predictive models to estimate geotechnical properties of soil stabilized using FA-based stabilizer systems (FA and FA-based geopolymer) using a large number of literature data from various studies. The following sections explain data collection, model development, model validation, sensitivity analysis, and parametric analysis in detail.

2 Data Collection and Parameter Identification

A database was developed by collecting laboratory experimental data available in the literature. The data were obtained for the FA-based soil stabilization considering the soil classified as inorganic clays of low to medium plasticity (CL) and high plasticity (CH) as per the Unified Soil Classification System (USCS). Experimental studies that used both class F and class C FAs were considered due to the limited data availability under each category. In addition, stabilized soil samples cured only at the ambient temperature were considered for the model development considering the practical applications. In the present study, predictive models were developed for OMC, MDD, and UCS of FA-stabilized soil (hereafter referred to as "FA-S"), whereas the predictive model for FA-based geopolymer-stabilized soil (hereafter referred to as "FA-GP-S") includes only the UCS. As there are not enough data on the OMC and maximum dry density (MDD) of FA-GP-S, they were excluded from the model development.

According to the results of previous studies conducted on evaluating geotechnical properties of FA-stabilized soil, there is clear evidence that all OMC, MDD, and UCS of FA-S directly depend on FA/soil ratio in the stabilized mix. Moreover, OMC, MDD, and UCS of raw soil (OMC_0, MDD_0, UCS_0) were incorporated as input parameters following the study done by Ahmed et al. [23] because soil used to develop models is coming from different sources and their geotechnical properties are different from one another. Therefore, predictive models for OMC of FA-S were developed with FA/soil (w/w) and OMC of raw soil (OMC_0) as input parameters while the FA/soil (w/w) and MDD of raw soil (MDD_0) were considered as input parameters for the MDD model. A summary of the data collected for developing OMC and MDD models for FA-S is given in Table 1. A total of 100 data points extracted from 17 research articles were used for developing the two models, and 12 data points extracted from 3 independent research articles were considered for the model validation.

To develop the predictive model for UCS of FA-S, FA/soil (w/w) and curing time (days) were selected as model input parameters and (UCS-UCS_0) as an output parameter. A total of 121 data points extracted from 9 research articles were used for developing the UCS model for FA-S, and the model was validated using 31 data points extracted from 5 independent research articles, as given in Table 2.

For the UCS model of FA-GP-S, previous studies on geopolymer stabilization, where a combination of NaOH and Na_2SiO_3 was used as alkaline activator, were considered. This is because it is the most commonly used activator yielding better strength values [9]. According to previous studies conducted on evaluating the geotechnical properties of FA-GP-S, FA/soil ratio, NaOH concentration, Na_2SiO_3/NaOH ratio, activator/FA ratio, and curing time are the major parameters affecting UCS of the FA geopolymerized soil [15, 17, 53, 54]. Parameters such as FA/soil (w/w), NaOH molarity, Na_2SiO_3/NaOH (w/w), and curing period (days) were selected as the model input parameters and ($UCS - UCS_0$) was selected as the model output parameter. However, activator/FA was not considered as an input

Table 1 Data used for developing OMC and MDD models for FA-S

Data source	FA/soil (w/w)	OMC_o (%)	OMC range (%)	MDD_o (g/cm^3)	MDD range (g/cm^3)	No. of data
Training data						
[16]	0.05–0.25	21.73	21.73–24.62	1.62	1.50–1.62	4
[6]	0.05–0.25	21.54	21.43–24.2	1.62	1.51–1.62	4
[30]	0.05–0.25	21.64	20.89–24.60	1.62	1.42–1.62	4
[31]	0.1–0.20	16.00	16.53–17.53	1.80	1.75–1.80	4
[32]	0.05–0.33	30.00	30.00–34.84	1.82	1.44–1.82	5
[33]	0.11–1.00	13.30	13.30–20.40	1.98	1.64–1.98	5
[34]	0.11–0.67	15.73	15.73–20.00	1.76	1.60–1.76	4
[35]	0.05–0.43	21.00	21.00–30.00	1.48	0.60–1.48	6
[36]	0.05–0.25	21.40	21.40–26.60	1.602	1.43–1.60	5
[37]	0.05–0.54	17.00	17.00–20.90	1.70	1.59–1.70	7
[38]	0.05–0.30	15.80–17.20	15.80–19.80	1.672–1.764	1.52–1.76	24
[39]	0.17–0.33	12.00	12.00–16.00	1.998	1.92–1.19	4
[5]	0.05–0.25	19.40	19.00–21.20	1.670	1.64–1.72	4
[40]	0.05–0.43	14.00	14.00–15.20	1.850	1.64–1.85	4
[41]	0.05–0.33	10.00	10.00–14.20	1.480	1.40–1.56	5
[42]	0.03–0.11	7.63	7.20–8.34	2.188	2.10–2.18	5
[11]	0.02–0.15	23.00	23.00–28.97	1.570	1.42–1.57	6
Validation data						
[43]	0.11–0.43	18.89	18.89–21.39	1.651	1.51–1.65	5
[44]	0.05–0.33	22.00	22.00–24.00	1.480	1.39–1.48	4
[45]	0.08–0.19	16.00	16.00–16.99	1.489	1.43–1.48	3

parameter in the current study due to the unavailability and the uncertainty of activator/FA in the previous studies used for model development. A total of 139 data points extracted from 6 research articles were used for model development, while 33 data points extracted from 3 research articles were considered for the model validation as shown in Table 3. It should be noted that geopolymer-based soil stabilization is still in its infancy, and hence, there are a limited number of published papers in this area. Therefore, the analysis was conducted using the limited numbers of data set available in the literature although a large number of data will yield an accurate model.

Table 2 Data used for developing UCS models for FA-S

Data source	FA/Soil (w/w)	Curing period (days)	UCS_o (kPa)	UCS range (kPa)	No. of data
Training data					
[11]	0.02–0.15	7–28	202.0	250.0–490.0	18
[46]	0.11 -0.25	7–90	200.0	600.0–850.0	8
[47]	0.60 -1.00	7	185.0	85.0–272.0	3
[36]	0.05 -0.25	7–90	82.0	240.0–688.0	15
[38]	0.05 -0.23	1–28	215.4	172.3–947.8	42
[48]	0.05 – 0.30	1–28	225.0	230.0–600.0	18
[5]	0.05–0.25	1	108.0	112.0–132.0	4
[4]	0.08–0.24	7–45	107.0	323.0–643.0	9
[49]	0.25–1.5	3	170.0	52.0–260.0	3
Validation data					
[50]	0.05–0.20	7–45	200.0	325.6–586.1	12
[51]	0.11–0.43	1	76.0	122.6–182.5	5
[45]	0.08–0.19	7–28	373.4	755.0–1582.0	6
[14]	0.03–0.15	7	450.0	503.0–568.5	5
[52]	0.05–0.17	7	172.0	299.2–451.1	3

Table 3 Data used for developing UCS models for FA-GP-S

References	FA /Soil (w/w)	NaOH (Molarity)	Na_2SiO_3/NaOH (w/w)	Curing period (days)	UCS_o (kPa)	UCS range (kPa)	No. of data
Training data							
[20]	0.11–0.25	10	2.0	7–28	100.0	171.1–1749.1	3
[55]	0.25–0.67	10–15	2.0	7–28	767.0	1643.0–7979.0	28
[6]	0.05–0.25	5	1.5	7–28	172.0	1096.5–1810.1	12
[56]	0.125–0.50	5	1.0	0–28	88.0	113.5–368.7	13
[30]	0.05–0.25	5	0.5–2.0	0–28	172.0	172.5–2214.9	59
[57]	0.15–0.35	6	0.51	0–28	109.1	118.2–480.1	24
Validation data							
[16]	0.05–0.25	5	0	0–28	172.0	138.5–2715.0	18
[58]	0.05–0.43	3	0	3–28	49.0	130.3–672.2	12
[22]	0.25–0.30	6–8	0–0.4	7–28	500.0	1970.0–2180.0	3

3 Model Development

Outliers in databases were identified by checking the Mahalanobis distance of each set of data and comparing them to a chi-square probability distribution. Data sets

having a probability less than 0.001 were then removed from the databases. ANN models were developed using IBM SPSS statistics (version 26) software, and a feed-forward multilayer perceptron ANN architecture having only one hidden layer was adopted in developing the models. The optimum number of neurons in the hidden layer was determined by trial and error procedure. Hyperbolic tangent function and pure linear function were used as activation functions at the hidden layer and output layer, respectively. Input data were standardized as a part of pre-processing. The batch training process together with scaled conjugate gradient optimization algorithm was adopted for training due to the small number of data sets used for each model. The model performances were evaluated based on three criteria: coefficient of determination (R^2), mean squared error (MSE), and mean absolute percentage error (MAPE). These statistical parameters can be expressed mathematically using Eq. (1) to (3);

$$R^2 = \frac{\left(n\sum_i to - \sum_i t \sum_i o\right)^2}{\left[n\sum_i t^2 - \left(\sum_i t\right)^2\right]\left[n\sum_i o^2 - \left(\sum_i o\right)^2\right]} \tag{1}$$

$$\text{RMSE} = \sqrt{\sum_{i=1}^{n} \frac{(t-O)^2}{n}} \tag{2}$$

$$\text{MAPE} = \frac{1}{n}\sum_{t=1}^{n}\left|\frac{t-O}{t}\right| \tag{3}$$

where t is the target value, o is the output value, and n is the number of data sets.

Figure 1 illustrates the schematic view of the ANN architectures resulting from each model with the optimum number of hidden neurons. The associated weights and biases are given in Table 4. Figures 2 and 3 show the plots of predicted versus experimental results of all the developed models. Best fitting lines having R^2 values of 0.973, 0.961, 0.815, and 0.963 were obtained for OMC, MDD, UCS models of FA-S, and UCS model of FA-GP-S, respectively. This shows that there is a good agreement with the line of equity yielding better correlations between experimental and predicted results for all the four developed models.

4 Model Validation

Model validation was carried out to assess the predictive ability of each developed model using an independent set of data from several past studies as detailed in Tables 1, 2, and 3. As the validation data were not used in developing the models, the error associated with validation data provides the predictive ability of the model for a given unfamiliar set of data. Figures 4 and 5 show the validation plots for OMC-FA-S, MDD-FA-S, UCS-FA-S, and UCS-FA-GP-S. According to Figs. 4 and 5, the

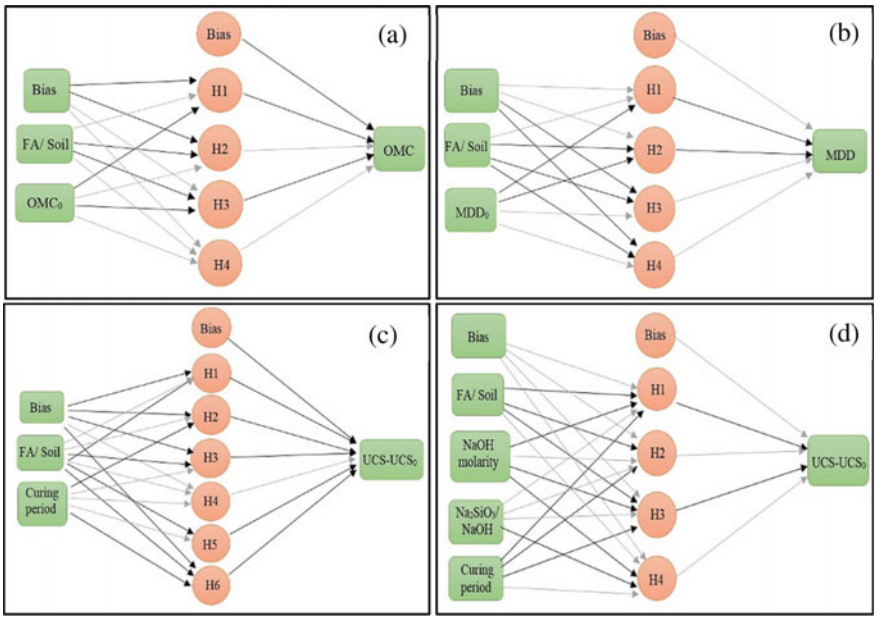

Fig. 1 Schematic views of the ANN model architecture for **a** OMC, **b** MDD, **c** UCS models for FA-S, and **d** UCS model for FA-GP-S

predicted values of all the ANN models exhibit a reasonable correlation with the experimental values for validation data sets. The R^2 values associated with OMC, MDD, and UCS models of FA-S were 0.970, 0.975, and 0.702, while the R^2 value of the UCS model of FA-GP-S was 0.842. Statistical performances of training and validation data for all ANN models exhibit good accuracy as summarized in Table 5.

5 Sensitivity Analysis

The relative influence of input parameters cannot be readily observed in an ANN model. Hence, the connection weight approach was used as suggested by [27] to evaluate the variable contribution to the model. Figure 6 shows the sensitivity analysis conducted for UCS models for FA-S and FA-GP-S. According to Fig. 6, it can be seen that this approach ranks NaOH molarity as the most important parameter followed by Na_2SiO_3/NaOH, curing time, and FA/soil for the UCS model for FA-GP-S. When a sufficient amount of FA is available in the mix, NaOH concentration is directly relative to the amount of alumina and silica in the geopolymer gel [17]. Therefore, this result highlights the critical effect of NaOH concentration on the geopolymerization process. Curing time holds higher importance compared to FA/soil for the UCS

Table 4 Weights and biases of the ANN models

OMC model for FA-S		Hidden layer						
		Bias	H (1)	H (2)	H (3)	H (4)		
Input layer	Bias		−2.056	−1.363	0.852	−0.121		
	FA/soil		0.122	−0.521	−0.511	0.296		
	OMC_0		−1.011	1.336	−1.144	−0.058		
Output layer		−0.458	−1.486	0.816	−0.740	0.343		
MDD model for FA-S		Hidden layer						
		Bias	H (1)	H (2)	H (3)	H (4)		
Input layer	Bias		0.032	0.000	−0.164	−0.817		
	FA/soil		0.241	−0.342	−0.276	−0.477		
	MDD_0		−0.043	−0.473	0.062	0.675		
Output layer		0.563	−1.024	−1.594	0.825	0.714		
UCS model for FA-S		Hidden layer						
		Bias	H (1)	H (2)	H(3)	H(4)	H (5)	H (6)
Input layer	Bias		−0.574	−3.448	−0.568	1.189	0.048	−0.556
	FA/soil		1.556	0.404	−0.283	0.187	−0.249	−1.648
	Curing		−0.286	−4.430	0.001	0.089	0.149	−0.363
Output layer		−1.802	−1.133	−1.106	−0.392	0.105	−0.131	−1.401
UCS model for FA-GP-S		Hidden layer						
		Bias	H (1)	H (2)	H (3)	H (4)		
Input layer	Bias		1.088	0.207	2.591	0.219		
	FA/soil		−0.073	−0.774	−0.336	1.021		

(continued)

Table 4 (continued)

OMC model for FA-S		Hidden layer				
		Bias	H (1)	H (2)	H (3)	H (4)
	NaOH molarity		0.487	0.284	−1.189	−0.208
	Na_2SiO_3/NaOH		0.790	1.273	0.992	−0.950
	Curing		−0.128	−0.054	−0.477	0.231
	Bias	1.673	−0.412	1.213	−1.905	0.916

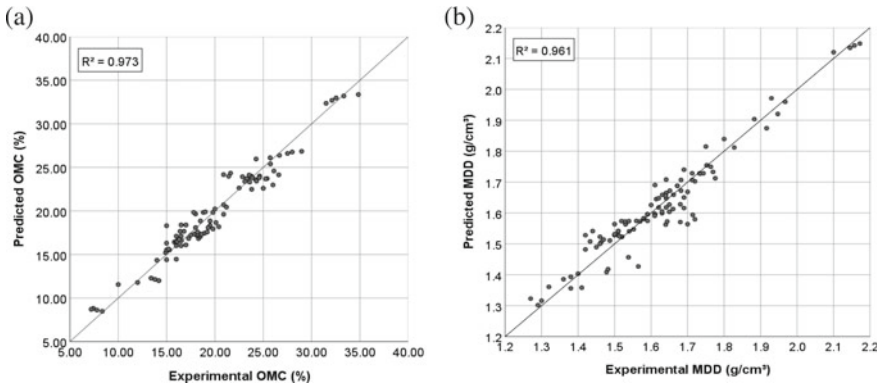

Fig. 2 Plots of predicted versus experimental values for **a** OMC and **b** MDD models for FA-S

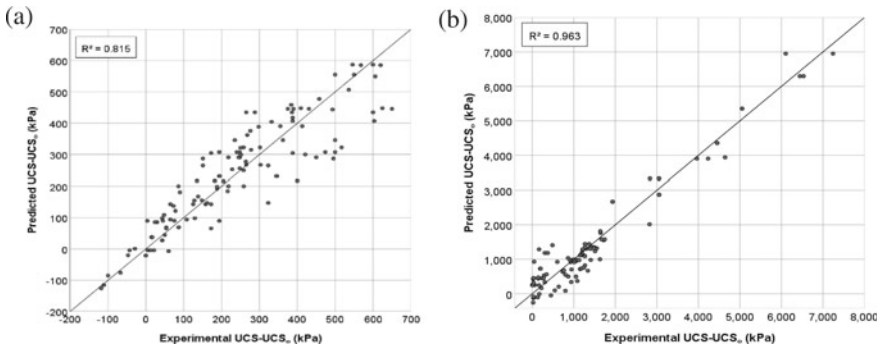

Fig. 3 Plots of predicted versus experimental values for UCS models: **a** FA-S and **b** FA-GP-S

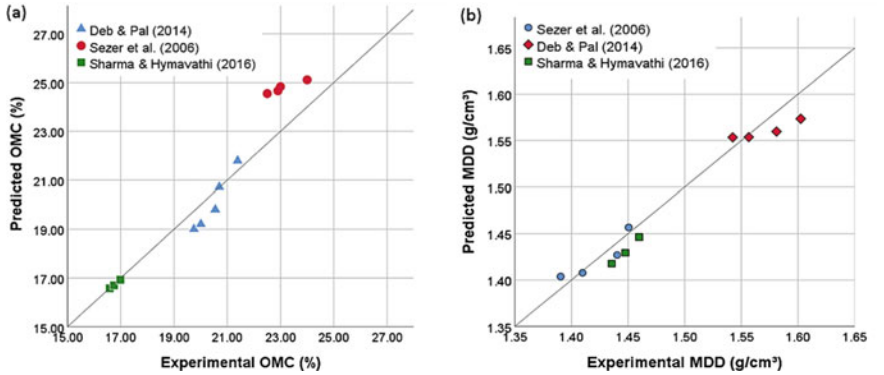

Fig. 4 Model validation plots for **a** OMC and **b** MDD of FA-S

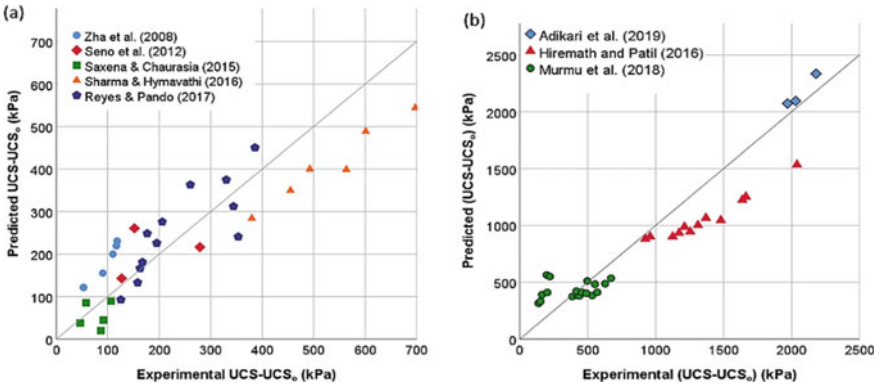

Fig. 5 Model validation plots for UCS of **a** FA-S and **b** FA-GP-S

Table 5 Performances of developed models

Model	Data set	R^2	RMSE	MAPE
OMC-FA-S	Training	0.973	1.254	0.055
	Validation	0.970	1.073	0.036
MDD-FA-S	Training	0.961	0.047	0.022
	Validation	0.975	0.381	0.246
UCS-FA-S	Training	0.815	80.578	0.475
	Validation	0.802	90.896	0.432
UCS-FA-GP-S	Training	0.963	474.136	6.664
	Validation	0.842	231.908	0.378

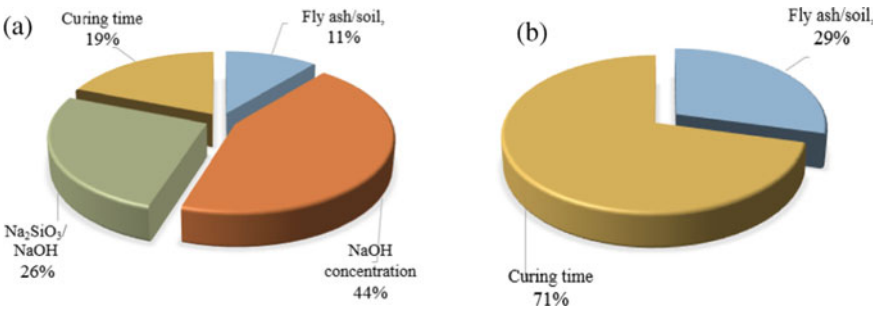

Fig. 6 Sensitivity analysis results of UCS models of **a** FA-S and **b** FA-GP-S

model for FA-S. This highlights that the strength variation in FA-S with the curing time is paramount compared to the strength variation with FA/soil.

6 Parametric Analysis

A parametric analysis was conducted to predict the relevant geotechnical properties (OMC, MDD, and UCS) using independent values of input parameters within the range of the data collection. For the prediction of OMC versus FA/soil of FA-S, the value of OMC_0 was considered as 17.8% (mean value of the collected data) and the developed curve is shown in Fig. 7a. According to Fig. 7a, when the FA/soil ratio is increased from 0.05 to 0.5, there is a 36.4% increase in the OMC of the FA-S. This variation is attributed to the increase in surface area of soil mix with the addition of FA which absorbs more water content [12]. Previous researchers [32, 34, 36, 38] have also found that the OMC of the stabilized soil increases with the increase in FA/soil ratio in the mix.

Figure 7b illustrates the variation of MDD with FA/soil for FA-S with a MDD_0 value of 1.73 g/cm^3 (mean value of the collected data). When the FA/soil ratio in the mix is increased from 0.05 to 0.5, the MDD of FA-S is reduced by 6.22%. Similar findings have been made in the previous studies as well [35, 32, 34]. This is due to the low specific gravity of FA compared with clayey soil and the increased void ratio due to the flocculation of clay particles [43]. However, some other researchers [6, 16, 30, 31, 58] have found contrasting conclusions on the variation of MDD with FA/soil. For an instance, Murmu et al. [6, 16, 30] observed that MDD reduced with an increase in FA/soil up to 0.15, and then, it increases with any further increase in FA/soil. On the other hand, few others [31, 58] concluded that MDD increases with the increase in FA/soil. The findings from this study match with the findings of the majority of the previous studies [32, 37, 33, 43, 34, 35] and therefore can be considered as reliable. However, it is recommended to validate the outcome of these models with experimental results as there are contrasting findings on the variation between MDD and FA/soil.

Figure 8 shows the independent variation of $(UCS - UCS_0)$ with FA/soil and curing time for the FA/soil and curing time values within the data collection range. According to Fig. 8a, maximum strength development of 451.62 kPa is obtained at FA/soil of 0.18 after 28 days of curing. The UCS increase with FA/soil at the initial

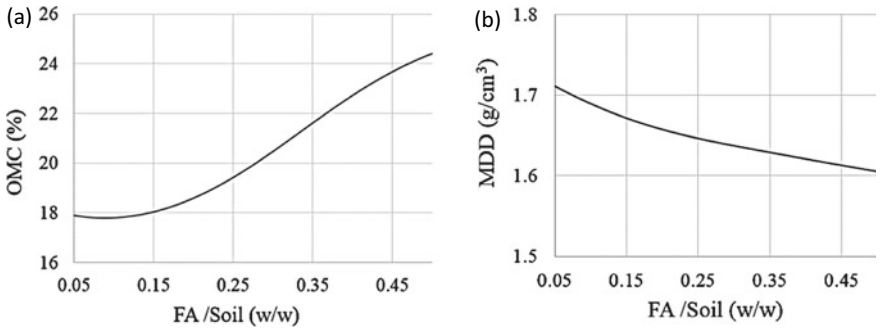

Fig. 7 Independent prediction of the variation **a** OMC and **b** MDD models with FA/soil for FA-S

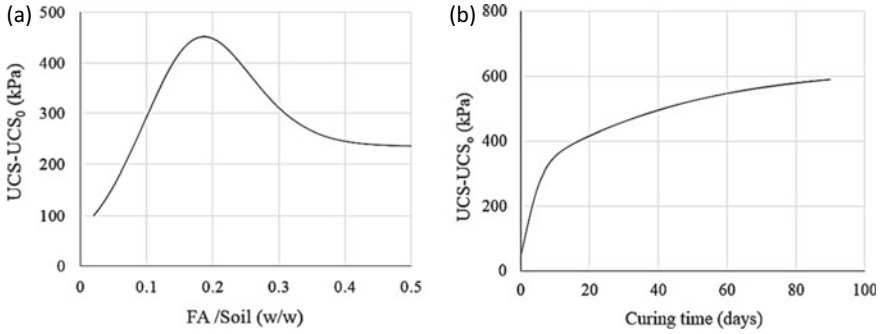

Fig. 8 Independent prediction of the variation of (UCS-UCS$_0$) with **a** FA/soil and **b** curing time of FA-S

stage is attributed to the enhanced pozzolanic reaction that takes place between soil and FA leading to a uniform product. However, a higher amount of FA in the soil mix weakens the bond due to its low frictional and cohesive properties [4]. This can be related to the decrease of UCS beyond the optimum dosage. By the end of 90 days, the cumulative strength development of soil reaches a near-constant value of about 600 kPa as shown in Fig. 8b indicating that by the end of 90 days, most of the pozzolanic reactions are completed. These trends of UCS versus FA/soil and UCS versus curing time are consistent with similar trends reported in the literature [4, 5, 11, 12,13, 14].

The variation of (UCS − UCS$_0$) of FA-GP-S with different input parameters (FA/soil, NaOH molarity, Na_2SiO_3/NaOH, and curing time) as predicted by the developed model is shown in Fig. 9. For each plot, when an input parameter is used as the independent variable, the values of the remaining input parameters were set at a constant value. These constant values used for FA/soil, NaOH molarity, Na_2SiO_3/NaOH, and curing period are 0.3, 12 M, 1.5, and 28 days, respectively. According to the simplified reaction mechanism of geopolymerization [59], the initial step in geopolymerization process is the dissolution of solid aluminosilicates in the source material by the alkaline hydroxide solution to produce aluminate and silicate species in the liquid phase. Hence, the obtained variation in Figs. 9a, b is anticipated because higher FA/soil and higher NaOH concentrations contribute a higher amount of aluminates and silicates to the geopolymer gel. However, with the further addition of FA, the alkaline solution may fail to consume the total amount of solid aluminosilicates. This can be attributed to the plateau shape obtained in Fig. 9a at higher FA/soil.

According to Fig. 9c, strength increases with Na_2SiO_3/NaOH up to an optimum value of 1.5, and then, it reduces with any further increase in the Na_2SiO_3/NaOH ratio. This initial increase is attributed to the presence of more silicates which are supplied from the activator to bind the monomers together and to form a denser geopolymer matrix [9]. However, after an optimum value, UCS tends to decrease with the further increase of Na_2SiO_3/NaOH ratio because of the reduced NaOH content in

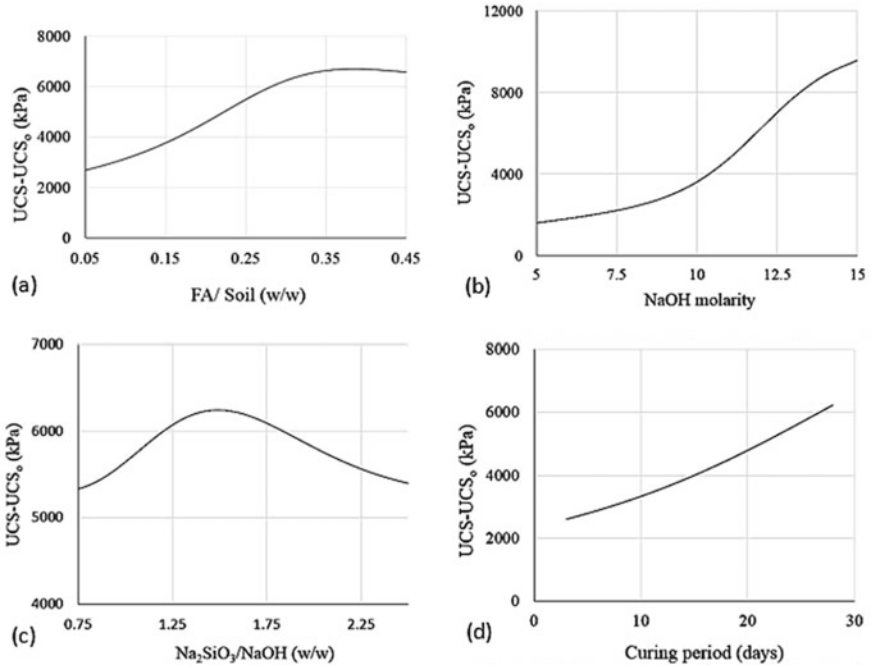

Fig. 9 Model predicted variation of $(UCS - UCS_0)$ with **a** FA/soil, b NaOH molarity, **c** Na_2SiO_3/NaOH, and **d** curing time of FA-GP-S

the activator solution which dissolves less amount of FA. When a prolonged curing period is allowed, it helps to enhance the geopolymerization reaction with the time leading to strength gain (Fig. 9c).

7 Conclusions

This study was conducted to predict the geotechnical properties (optimum moisture content (OMC), maximum dry density (MDD), and unconfined compressive strength (UCS)) of the stabilized clayey soil using fly ash (FA)-based stabilizer systems (FA-stabilized soil (FA-S) and FA-based geopolymer-stabilized soil (FA-GP-S)). Based on the results obtained, the following major conclusions can be drawn.

- Accurate correlations were developed for OMC, MDD, UCS of FA-S, and UCS of FA-GP-S, and ANN can be used to develop the correlation among geotechnical properties of the stabilized soil.
- All the developed models were validated using an independent set of data from the literature, and the validation plots also showed good correlation verifying the reliability of the predicted models.
- A set of independent predictions were made for OMC, MDD, UCS of FA-S, and UCS of FA-GP-S, and the developed trends were consistent with similar trends reported in the literature.

References

1. Bell FG (1996) Lime stabilization of clay minerals and soils. J Eng Geol 42(4):223–237
2. Eidgahee DR, Rafiean AH, Haddad A (2020) A novel formulation for the compressive strength of IBP-based geopolymer stabilized clayey soils using ANN and GMDH-NN approaches. Iran J Sc Technol, Trans Civil Eng 44(1):219–229
3. Khedari J, Watsanasathaporn P, Hirunlabh J (2005) Development of fibre-based soil–cement block with low thermal conductivity. Cem Concr Compos 27(1):111–116
4. Dissanayake TBCH, Senanayake SMCU, Nasvi MCM (2017) Comparison of the stabilization behavior of fly ash and bottom ash treated expansive soil. J Eng 01:11–19
5. Karim MR, Hasan MH, Alim MA (2015) Improvement of clay soil characteristics by using fly ash, bamboo leaf ash and rice husk ash. J Eng Sci 6:81–85
6. Murmu AL, Patel A (2020) Studies on the properties of fly ash-rice husk ash based geopolymer for use in black cotton soils. Int J Geosynthetics Ground Eng 6:38
7. Sharma AK, Sivapullaiah PV (2016) Ground granulated blast furnace slag amended fly ash as an expansive soil stabilizer. Soils Found 56(2):205–212
8. Yadu L, Tripathi RK (2013) Stabilisation of soft soil with granulated blast furnace slag and fly ash. Int J Res Eng Technol 2(2):115–119
9. Yaghoubi MJ, Arulrajah A, Disfani MM, Horpibulsuk S, Bo MW, Darmawan S (2018) Effects of industrial by-product based geopolymers on the strength development of a soft soil. J Soil Found 58:716–728
10. Senol A et al (2006) Soft subgrades' stabilization by using various fly ashes. Resour Conserv Recycl 46(4):365–376
11. Jafer H, Atherton W, Sadique M, Ruddock F, Loffill E (2015) Stabilization of soft soil using binary blending of high calcium fly ash and palm oil fuel ash. Appl Clay Sci 152:323–332
12. Rangaswamy K (2016) Influence of burnt ash additives on stabilisation of soft clay soils. Innovative Infrastruct Solutions 1(1)
13. Somaiya P, Zala Y, Dangar R (2013) Stabilization of expansive soil using fly ash. Available in: https://www.researchgate. net/publication/280153059

14. Zha F, Liu S, Du Y, Cui K (2008) Behavior of expansive soils stabilized with fly ash. Nat Hazards 47(3):50
15. Cristelo N, Glendinning S, Fernandes L, Pinto AT (2013) Effects of alkaline-activated fly ash and Portland cement on soft soil stabilization. Acta Geotech 8(4):395–405
16. Murmu A, Dhole N, Patel A (2018) Stabilization of black cotton soil for subgrade application using fly ash geopolymer. J Road Mater Pavement Des 21:867–885
17. Phetchuay C, Horpibulsuk S, Arulrajah A, Suksiripattanapong C, Udomchai A (2016) Strength development in soft marine clay stabilized by fly ash and calcium carbide residue based geopolymer. Appl Clay Sci 127–128:134–142
18. Phummiphan I, Horpibulsuk S, Sukmak P, Chinkulkijniwat A, Arulrajah A, Shen S (2015) Stabilization of marginal lateritic soil using high calcium fly ash-based geopolymer. J Road Mater Pavement Des 17(4):877–891
19. Teerawattanasuk C, Voottipruex P (2018) Comparison between cement and fly ash geopolymer for stabilized marginal lateritic soil as road material. Int J Pavement Eng 20:1264:1274.25
20. Cristelo N, Glendinning S, Fernandes L, Pinto AT (2012) Effect of calcium content on soil stabilization with alkaline activation. Constr Buil Mater 29:167–174
21. Parhi PS, Garanayak L, Mahamaya M, Das SK (2018) Stabilization of an expansive soil using alkali activated fly ash based geopolymer. In: McCartney J (ed) Advances in characterization and analysis of expansive soils and rocks. Springer, Cham, pp 36–50
22. Adhikari B, Khattak MJ, Adhikari S (2019) Mechanical and durability characteristics of flyash-based soil-geopolymer mixtures for pavement base and subbase layers. Int J Pavement Eng 22(9):1193–1212
23. Ahmed BS, Gadouri H, Ghrici M, Harichane K (2020) Best-fit models for predicting the geotechnical properties of FA–stabilised problematic soils used as materials for earth structures. Int J Pavement Eng 21(7):939–953
24. Binal A, Binal B (2020) Ternary diagrams for predicting strength of soil ameliorated with different types of Fly Ash. Arab J Sci Eng 45:8199–8217
25. Hanandeh S, Ardah A, Abu-Farsakh M (2020) Using artificial neural network and genetics algorithm to estimate the resilient modulus for stabilized subgrade and propose new empirical formula. Transp Geotech 24
26. Mozumder RA, Laskar AI (2015) Prediction of unconfined compressive strength of geopolymer stabilized clayey soil using artificial neural network. Comput Geotech 69:291–300
27. Leong HY, Ong DEL, Sanjayan JG, Nazari A, Kueh SM (2018) Effects of significant variables on compressive strength of soil-fly ash geopolymer: variable analytical approach based on neural networks and genetic programming. J Mater Civ Eng 30(7):04018129
28. Soleimani S, Rajaei S, Jiao P, Sabz A, Soheilinia S (2017) New prediction models for unconfined compressive strength of geopolymer stabilized soil using multi-gen genetic programming, measurement
29. Lee JA, Almond DP (2003) A neural-network approach to fatigue-life prediction, Bryan Harris (eds), Fatigue in composites, Woodhead Publishing, pp 569–589
30. Murmu AL, Jain A, Patel A (2019) Mechanical properties of alkali activated fly ash geopolymer stabilized expansive clay. KSCE J Civ Eng 23(9):3875–3888
31. Pandya RR, Shah AJ (2017) Effect of alkali activated fly ash on the strength of clayey soil. Indian geotechnical conference, GeoNEst
32. Binal A (2016) The effects of high alkaline Fly Ash on strength behaviour of a cohesive soil. Advan Mater Sci Eng 1–11
33. Mishra E, Kumar N (2012) Strength characteristics of clayey sub-grade soil stabilized with fly ash and lime for road works. Indian Geotech J 42(3):206–211 https://doi.org/10.1007/s40098-012-0015-5
34. Ramlakhan B, Kumar SA (2013) Effect of lime and fly ash on engineering properties of black cotton soil. Int J Emerg Technol Adv Eng 3:535–541
35. Takhelmayum G, Savitha AL, Gudi K (2013) Laboratory study on soil stabilization using fly ash mixtures. Int J Eng Sci Innovative Technol 2(1): 477–482

36. Athanasopoulou A, Kollaros G (2016) Improvement of soil engineering characteristics using lime and Fly Ash. J Mater Civ Eng 26(4):773–775
37. Anupam AK, Kumar P, Ransinchung GD (2013) Use of various agricultural and industrial waste materials in road construction. Procedia Soc Behav Sci 104:264–273
38. Seyrek E (2018) Engineering behavior of clay soils stabilized with class C and class F fly ashes. Sci Eng Compos Mater 25(2):273–287
39. Bhat IA, Mohi ud din I, ul Islam N, Garg P (2018) Improvement in properties of clay soil by using calcium carbide residue and Fly-ash. Int J Creative Res Thoughts 6:688–694
40. Ahmad H, Ahmed S (2015) Stabilization of low shear strength soil by using fly ash. IOSR, 12(4):33
41. Narasimha Rao B, Nagaraju A, Lavanya Bai P, Sarath V, Rupla Naik I (2020) Stabilization of black cotton soil by using fly ash and rice husk ash. Int J Advan Sci Technol 29(05):9465–9470
42. Ozdemir MA (2016) Improvement in bearing capacity of a soft soil by addition of fly ash. Procedia Eng 143:498–505
43. Deb T, Pal SK (2014) Effect of fly ash on geotechnical properties of local soil-fly ash mixed samples. IJRET: Int J Res Eng Technol 3(5): 507–516
44. Sezer A, İnan G, Yılmaz HR, Ramyar K (2006) Utilization of a very high lime fly ash for improvement of Izmir clay. Build Environ 41(2):150–155
45. Sharma RK, Hymavathi J (2016) Effect of Fly Ash, construction demolition waste and lime on geotechnical characteristics of a clayey soil: a comparative study. Environ Earth Sci 75(5): 377
46. Mahedi M, Cetin B, White DJ (2021) Closure to "Cement, lime, and fly ashes in stabilizing expansive soils: performance evaluation and comparison" by Masrur Mahedi, Bora Cetin, and David J. White. J Mater Civil Eng 33(9):07021013
47. Geliga EA, Ismail DSA (2010) Geotechnical properties of fly ash and its application on soft soil stabilization. J Civil Eng, Sci Technol 1(2):1–6
48. Turan C, Javadi A, Vinai R, Shariatmadari N, Farmani R (2020) Use of class C fly ash for stabilization of fine-grained soils. E3S web of conferences, vol 195, p 06001
49. Bose B (2012) Geo-engineering properties of expansive soil stabilized with fly ash. Electron J Geotech Eng 17:1339–1353
50. Reyes A, Pando M (2007) Evaluation of CFBC fly ash for improvement of soft clays. World of Coal Ash (WOCA), Covington. Kentucky, USA
51. Saxena G, Chaurasia N (2015) Strengthening black cotton soil with fly ash and moorum: an investigation of the role of subgrade and subbase layers. Coal Combust Gasification Prod 30–32
52. Senol A, Etminan E, Olgun CG (2012) Stabilization of clayey soils using fly ash and homopolymer polypropylene. Geo Congress: State of the Art Pract in Geotechnical Eng 3929–3938
53. Canakci H, Güllü H, Alhashemy A (2019) Performances of using geopolymers made with various stabilizers for deep mixing. Materials 12(16):2542
54. Sukmak P, Horpibulsuk S, Shen S-L (2013) Strength development in clay–fly ash geopolymer. Constr Build Mater 40:566–574
55. Cristelo N, Glendinning S, Teixeira Pinto A (2011) Deep soft soil improvement by alkaline activation. Proc ICE Ground Improv 164(2):73–82
56. Debanath OC, Rahman MA, Farooq SM (2019) Use of fly ash based geopolymer for stabilization of expansive soil. 9th International conference on geotechnique, construction materials and environment, pp 344–347
57. Joshi S, Gupta S, Bhatt BC (2021) Effect of geopolymer on the unconfined compressive strength value of clay soil. Int J Eng Res Technol 10
58. Hiremath P, Patil G (2016) Stabilization of black cotton soil using Alkali activated fly ash. Int J Innovative Res Sci Technol 2349–6010
59. Duxson P, Fernández-JiméneZ A, Provis JL, Lukey GC, Palomo A, van Deventer JS (2007) Geopolymer technology: the current state of the art. J Mater Sci 42(9):2917–2933

Elastic and Shear Moduli of Over Consolidated Lime Stabilized Clayey Soil

H. S. U. De Silva, D. S. P. Amarasekara, and L. C. Kurukulasuriya

Abstract The clay core is an essential element in any Rockfill earth dam. It acts as an impermeable barrier minimizing the seepage and provides the water tightness of the dam. Usually, constructing an impermeable clay core requires a substantial quantity of clayey soil. The material of the clay core in a dam is required to have adequate shear strength as well as low compressibility and hydraulic conductivity values. There may be situations where the required quantity of clayey soil having desired mechanical and hydraulic properties is not readily available in the vicinity and those that are available may not marginally meet such properties. However, there are many methods to improve the engineering properties of a soil which does not meet the desirable properties. This research focuses on investigating on the effects of such improvement on the elastic deformation of dam clay core. For this purpose, hydrated lime was selected as the cementitious material to stabilize a clayey soil obtained from Matale District, Sri Lanka. Laboratory experiments were carried out to determine the optimum lime content of the soil based on reaching a pH value of 12.4, which was found to be 5%. Drained triaxial tests were performed at natural moisture content to obtain the elastic properties on remolded lime stabilized samples compacted to 100% Standard Proctor Density at curing periods of 3 days, 14 days and 56 days and prepared at over consolidation ratios of 2, 4 and 6. It was observed in this study that the Elastic and Shear moduli of lime treated candidate soil increased with the curing period. They are further increased by reducing the over consolidation ratio.

Keywords Lime stabilization · Elastic modulus · Shear modulus · Over consolidation ratio

H. S. U. De Silva · D. S. P. Amarasekara · L. C. Kurukulasuriya (✉)
Department of Civil Engineering, University of Peradeniya, Peradeniya, Sri Lanka
e-mail: chank@eng.pdn.ac.lk

R. Dissanayake et al. (eds.), *12th International Conference on Structural Engineering and Construction Management*, Lecture Notes in Civil Engineering 266,
https://doi.org/10.1007/978-981-19-2886-4_23

1 Introduction

A Rock fill dam is built of rock fragments of various sizes and boulders of large size. The rock fill part of the dam is highly porous. Many techniques can be implemented to prevent or reduce the seepage through the dam, such as,

i. Constructing a clay core in the dam
ii. Placing an impervious membrane made of concrete, asphaltic concrete or steel on the upstream slope of the dam.
iii. Constructing a diaphragm wall made of clay, concrete, asphalt or any other impervious material in the dam.

Constructing a dam clay core is a common method in reducing the seepage through a rock fill dam. There are many types of clay cores in rock fill dams namely: central clay core and inclined clay core. Maduruoya, Randenigala and Moragahakanda dams of Sri Lanka are examples for rock fill dams with an impervious central clay core.

In addition to reducing the seepage through the dam, a clay core also provides stability to the dam. Therefore, the dam clay core material is required to have exceptional strength in addition to good hydraulic properties. Insufficient strength in clay core material may lead to dam failures. Usually in the construction of a rock fill dam, the construction of an impermeable clay core requires a substantial amount of clay soil of good strength. The rock fill dam construction can be quite inexpensive if the required rock material and clay core material are easily available. It would be uneconomical to transport soils with required properties from far away locations. Therefore, attention should be given to improving the properties of the available clay soil.

This research was focused on soil stabilization using hydrated lime. The gaining of strength in the soil after lime stabilization is caused by ion exchange and pozzolanic reactions [1]. When quicklime is used for soil stabilization, the resulting heat may accelerate the reactions [2–5] but considering practicality in field scale applications hydrated lime was used in this research.

The expected outcomes of this research are the determination of the optimum lime content of the selected candidate soil and the observation of the effects of optimum lime content and curing period on the shear modulus and the elastic modulus of the candidate soil. According to [6], there is a corresponding optimum lime content which causes the maximum strength to increase for a particular curing time and soil type. After determining the optimum lime content, samples were prepared with optimum moisture content and cured for 3, 14 and 56 days. Consolidated, drained triaxial tests were conducted on the cured soil samples to determine the elastic modulus and shear modulus. Over consolidation ratios of 2, 4 and 6 were considered. The elastic and shear moduli of a fine grained candidate soil before and after lime stabilization were compared in this research.

2 Literature Review

According to [4], lime stabilization of soil consists of two stages, namely, modification stage and stabilization stage. In the modification stage, clay texture is modified by lime. Reduction of plasticity and improvement of compaction characteristics of clay soil occur during the modification stage. The reason for this improvement is the cation exchange between the clay particles and lime. In the stabilization stage, the long-term strength improvement is effectively developed**.** This strength development is the result of pozzolanic reactions.

According to [6], for a particular soil type, there is a corresponding optimum lime content which produces the maximum strength gain using a minimum lime content. Ref. [7] observed in their research that a minimum pH level of 12.4 is required for the silica in the clay mineral to dissolve in order to react with calcium ions released from $Ca(OH)_2$. According to [1], the minimum lime content required for stabilization varies with the available clay mineral content.

The studies conducted by [1, 8] suggest that the elastic modulus of clayey soils increase significantly after lime stabilization. Ref. [9] observed that the value of elastic modulus of lime stabilized clayey soil increased with the curing period. According to his observations, the elastic modulus increased by approximately 15 times after 3 weeks and 35 times after 16 weeks.

Various studies suggest that the shear modulus of clayey soils increase significantly after lime stabilization [10, 11]. In their research, [11] also observed that the shear modulus is directly dependent on the elastic modulus. According to [12], the shear modulus of lime treated samples also increase significantly with curing time. They also observed that the shear modulus of samples compacted dry of optimum moisture content is higher than the samples compacted wet of optimum moisture content. This behavior is useful when the degree of compaction required is less than 100%. Comparatively higher strength values can be obtained by compacting the samples dry of the optimum moisture content.

3 Materials and Methods

3.1 Materials

In this study, commercially available slaked lime ($Ca(OH)_2$) was used as the stabilizing agent. A fine grained soil collected from Matale district (GPS N 7°36.232′, E 80°49.418′) with properties given in Table 1 was used as the candidate soil. The soil was classified as Sandy Clay of Intermediate Plasticity (CIS) based on British Soil Classification System. The elastic properties given in Table 2 were obtained through a triaxial testing procedure described in Sect. 3.3.

Table 1 Properties of the candidate material

Parameter	Value
Fine particles content	49%
Liquid limit	41%
Plastic limit	22%
Specific gravity	2.75
Optimum moisture content	17.5%
Maximum dry unit weight	17 kN/m^3

Table 2 Elastic properties of the candidate soil

Parameter	OCR = 2	OCR = 4	OCR = 6
Elastic modulus (MPa)	17.82	11.62	3.87
Shear modulus (MPa)	8.800	5.60	1.80
Poisson's ratio	0.015	0.040	0.075

3.2 Optimum Lime Content (OLC)

The method suggested by [7] was used to determine the optimum lime content of the candidate soil. Soil samples of 0, 2, 3, 4, 5 and 6% of lime by weight of the soil were prepared. Each sample was passed through a 425 μm sieve. From one sample, 20 g of soil was mixed with 100 ml of distilled water and shook for 30 s and then for another 30 s every 10 min for a total of 1 h. The pH value of the resultant slurry was measured using a pH meter. The test was repeated for all the samples. The optimum lime content is the minimum lime content required to produce a soil water pH of 12.4. The OLC was identified as 5% lime by mass.

3.3 Triaxial Tests

Soil samples stabilized with 5% lime were compacted to 100% Standard Proctor density in preparation of specimens for triaxial testing. Consolidated drained (CD) triaxial tests were conducted on the samples cured for 3 days, 14 days and 56 days. A cell pressure of 720 kPa was applied on the sample initially as the pre-consolidation pressure. Then the cell pressure was lowered to 120 kPa and then increased to 180 kPa and 360 kPa subsequently to obtain over consolidation ratios (OCR) of 6, 4 and 2, respectively. From the stress–strain curve obtained from the triaxial tests corresponding to each OCR, the Elastic Moduli for the corresponding curing duration and OCR were obtained.

3.4 Shear Modulus

Three-dimensional Hooke's law [13] was used to obtain the Poisson's ratio for the corresponding curing period and OCR from the triaxial test results. The simplified equation used for this purpose is give in Eq. (1) where E is the Young's modulus, ν is the Poisson's ratio, σ_3 is the cell pressure, $\Delta\sigma_1$ is the change in vertical stress and ε_1 is the change in vertical strain in case of the triaxial tests conducted.

$$\varepsilon_1 = \frac{1}{E}(\Delta\sigma_1 - 2\nu\sigma_3) \tag{1}$$

Equation (2) was used to determine the Shear modulus (G) of the corresponding curing period and OCR.

$$G = \frac{E}{2(1+\nu)} \tag{2}$$

4 Results and Discussions

4.1 Elastic Modulus

Stress–strain data were obtained from the triaxial tests. Regression lines were drawn for the corresponding OCR and the Elastic modulus was computed from the gradients of the regression lines. The Elastic modulus values obtained from the triaxial tests are given in Table 3.

It can be observed that the elastic modulus increased as the curing duration increased. For the over consolidation ratio of 6, there is a 60% increase in the Elastic modulus after lime stabilization at 3 days curing. For the same over consolidation ratio, there is a 480% and 1805% increase in elastic modulus after lime stabilization for 14 days and 56 days curing, respectively. For the over consolidation ratio of 4, there is a 32% increase in the Elastic modulus after lime stabilization at 3 days curing. Likewise, there is an increase of 244% and 1403% in the Elastic modulus after lime stabilization for 14 days and 56 days curing, respectively. For over consolidation

Table 3 Elastic modulus values

Curing period (Days)	Elastic modulus (MPa)		
	OCR = 2	OCR = 4	OCR = 6
3	19.95	15.34	6.23
14	61.62	40.05	22.45
56	291.08	174.65	73.74

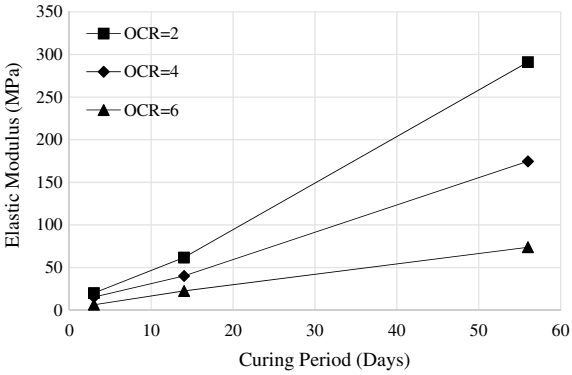

Fig. 1 Variation of elastic modulus with curing period

ratio of 2, there is an increase of 12%, 251% and 1533% in Elastic modulus after lime stabilization for 3 days, 14 days and 56 days curing periods, respectively.

The reason for this behavior is that the amount of binding agents that result from the pozzolanic reactions, which are $3CaO \cdot 2SiO_2 \cdot 3H_2O$, $3CaO \cdot Al_2O_3 \cdot 3H_2O$ and $3CaO \cdot Al_2O_3 \cdot 2SiO_2 \cdot 3H_2O$, increase with the curing duration. The amount of the binding agents is directly related to the strength increase in lime stabilized soils since these hydrates act as the cementitious compounds that bind the soil particles together [14, 15]. They cement the soil particles in a manner similar to the effect produced by the hydration of Portland cement. This behavior is shown in Fig. 1. This observed behavior of the elastic modulus is in harmony with the observations made by [1, 9]. Ref. [9] observed that the elastic modulus of lime stabilized clayey soils increase approximately 15 times after three weeks. In this research, approximately the same increase occurred in 8 weeks. The slow rate of increase in elastic modulus is due to the difference in clay mineral composition. This behavior also confirms [4] findings, which state that Young's modulus of soil–lime mixtures increase with curing duration.

Furthermore, there is a significant increase in the Elastic modulus observed after 14 days. The reason for this behavior can be identified as the beginning of the stabilization stage of lime stabilization process. According to [4], the modification stage lasts for approximately 14 days for soil–lime mixtures. After that the stabilization stage begins. In the stabilization stage, the pozzolanic reaction begin to occur. Therefore, the elastic modulus increases at a higher rate during the stabilization stage than during the modification stage.

It is also observed that the elastic modulus increases when the over consolidation ratio decreases for a given curing period. The reason for this behavior is the increase in the confining pressure when the OCR decreases. This increase in the confining pressure contributes to the increase in the Elastic modulus. The effect of curing period is significant in increasing the Elastic modulus of lime treated soil for a particular OCR. This behavior can also be observed in Fig. 2.

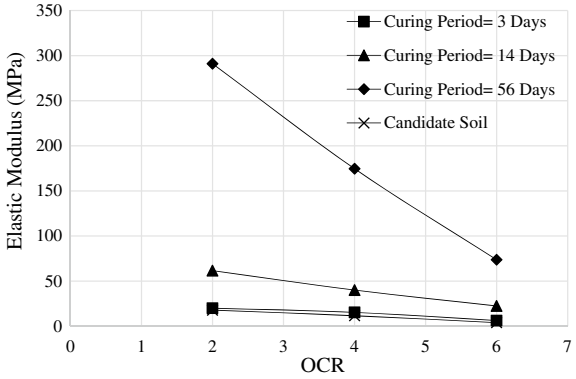

Fig. 2 Variation of elastic modulus with OCR

Table 4 Poisson's ratio values

Curing period (Days)	Poisson's ratio		
	OCR = 2	OCR = 4	OCR = 6
3	0.012	0.036	0.069
14	0.010	0.011	0.015
56	0.001	0.0013	0.004

4.2 Poisson's Ratio

Poisson's ratio values as given in Table 4 were calculated using the three-dimensional Hooke's law.

It was observed that the Poisson's ratio decreases when the curing period increases especially beyond 14 days. The reason for this behavior is the increase in the stiffness of the soil sample which in turn is as a result of the binding of soil particles together by the binding agents $3CaO \cdot SiO_2 \cdot 3H_2O$, $3CaO \cdot Al_2O_3 \cdot 3H_2O$ and $3CaO \cdot Al_2O_3 \cdot 2SiO_2 \cdot 3H_2O$, which are the products of pozzolanic reactions. It is also apparent that the Poisson's ratio decreases when the over consolidation ratio decreases. This is due to the effects of confining pressure which is greater for lower OCR values. This variation of Poisson's ratio with the curing period is shown in Fig. 3.

4.3 Shear Modulus

Using Eq. (2), the Shear Modulus (G) was evaluated for the corresponding curing periods and over consolidation ratios. The obtained Shear modulus values are given in Table 5.

It was observed that the Shear modulus increased when the curing duration increased, which confirms the observations of [12]. The variation of Shear modulus

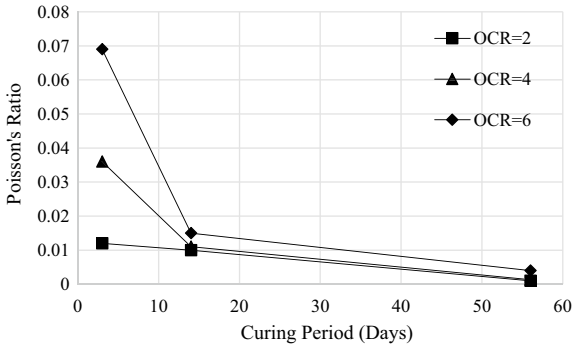

Fig. 3 Variation of poisson's ratio with curing period

Table 5 Shear modulus values

Curing period (Days)	Shear modulus (MPa)		
	OCR = 2	OCR = 4	OCR = 6
3	9.33	7.40	3.08
14	30.35	19.81	11.13
56	145.42	87.21	36.72

is observed to be as same as that of the elastic modulus, which confirms the observations of [11]. For the over consolidation ratio of 6, there is a 71% increase in the Shear modulus after lime stabilization at 3 days curing. For the same over consolidation ratio, there is a 518% and 3088% increase in Shear modulus after lime stabilization for 14 days and 56 days curing, respectively. For the over consolidation ratio of 4, there is a 34% increase in the Shear modulus after lime stabilization at 3 days curing. Likewise, there is an increase of 254% and 1457% in the Shear modulus after lime stabilization for 14 days and 56 days curing, respectively. For over consolidation ratio of 2, there is an increase of 77%, 245% and 1553% in Shear modulus after lime stabilization for 3 days. 14 days and 56 days curing periods, respectively. The reason behind this behavior is as same as that for the behavior of Elastic modulus, which is the increase in produced binding agents. This behavior is shown in Fig. 4.

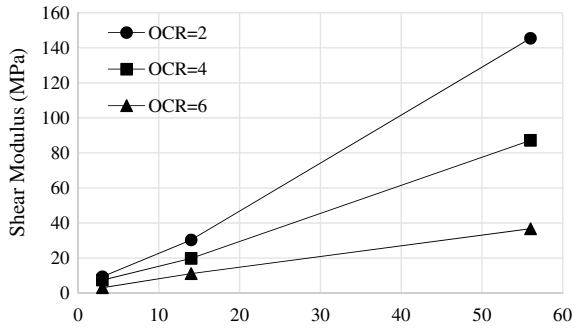

Fig. 4 Variation of shear modulus with curing period

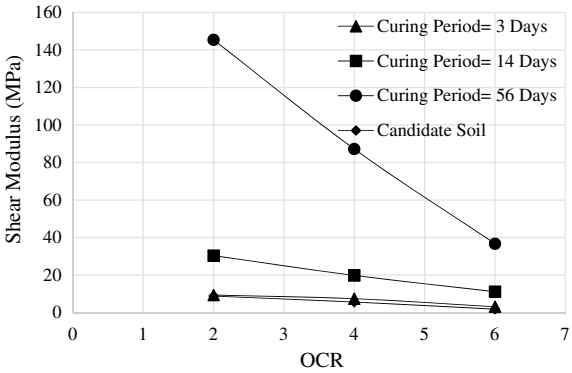

Fig. 5 Variation of shear modulus with OCR

Furthermore, there is a significant increase in the Shear modulus after 14 days. The reason for this behavior can be identified as the beginning of the stabilization stage of lime stabilization process. Ref. [12] observed the same behavior of the Shear modulus in their study.

It was also observed that the Shear modulus increases when the OCR decreased. The reason for this behavior is the increase in the confining pressure when the OCR was decreased. This increase in the confining pressure contributes to the increase in the Shear modulus. However, the curing period has a more significant effect on the Shear modulus of lime treated soil for a particular OCR. This behavior can be observed in Fig. 5.

The above results infer that use of lime stabilized clay as a core material in rockfill earth dams would result in reduced elastic settlement and lateral deformation. This again would reduce the shear stresses developing in the interface between clay core and filter or rockfill material due to reduced differential settlement.

5 Conclusions

Based on the study on Elastic and Shear moduli of lime stabilized fine grained soil, the following conclusions can be made.

1. Elastic Modulus and Shear Modulus of a soil increases significantly after lime stabilization.
2. Elastic Modulus and Shear Modulus of lime stabilized soil are directly proportional to the curing duration and inversely proportional to OCR.
3. Poisson's Ratio of lime stabilized soil is inversely proportional to the curing duration and directly proportional to OCR.
4. Poisson's Ratio of lime stabilized soil is drastically reduced during the early stages of stabilization and reaches a value which is not influenced much by the OCR.

Therefore it can be concluded that, lime stabilization using optimum lime content can be used to increase the Elastic and Shear moduli values of clayey soils, to be used as construction material in rockfill dam clay cores. This method will be useful in maintaining the stability of the rockfill dam when clayey soils with adequate strength are not available for construction.

References

1. Bell FG (1996) Lime stabilization of clay minerals and soils. Eng Geol 42(4):223–237
2. Broms BB (1984) Stabilization of soft clay with lime columns. Seminar on soil improvement and construction techniques in soft ground, pp 120–133
3. Broms BB, Anttikoski U (1983) Soil stabilization, general report, specialty session 9, proceedings of the 8th European conference on soil mechanics and foundation engineering, Helsinki, vol 3, pp 1298–1301
4. Chong SY, Kassim KA (2015) Effect of lime on compaction, strength and consolidation characteristics of Pontian marine clay. J Teknologi 72(3):41–47
5. Kezdi A (1979) Soil physics: selected topics, developments in geotechnical engineering, vol 25. Elsevier Scientific Pub. Co, New York
6. Herrin M, Mitchell H (1961) Lime-soil mixtures. Highway Res Board Bull 304:99–138
7. Eades JL, Grim RE (1966) A quick test to determine lime requirement for lime stabilization. Highway Res Rec 139:62–72
8. Bozbey I, Garaisayev S (2009) Effects of soil pulverization quality on lime stabilization of an expansive clay. Environ Earth Sci 60(6):1137–1151
9. Holm G (1979) Lime column stabilization—experience concerning strength and deformation properties. Vag-och Vottenbyggaren 25(7–8):45–19
10. Consoli NC, Lopes LS, da Prietto PDM, Festugato L, Cruz RC (2011) Variables controlling stiffness and strength of lime-stabilized soils. J Geotech Geoenviron Eng 137(6):628–632
11. Jahandari S, Mojtahedi SF, Zivari F, Jafari M, Mahmoudi MR, Shokrgozar A, Jalalifar H (2020) The impact of long-term curing period on the mechanical features of lime-geogrid treated soils. Geomech Geoengineering 1–13
12. Wang Y, Cui Y-J, Benahmed N, Tang AM, Duc M (2019) Changes of small strain shear modulus and suction for a lime-treated silt during curing. Géotechnique 1–19
13. Bowles JE (1997) Foundation analysis and design, international, 5th edn
14. Ingles OG, Metcalf JB (1972) Soil stabilization-principles and practices. Butterworth's, Sydney, Australia
15. Little DN (1995) Stabilization of pavement subgrades and base courses with lime. Kendall/Hunt Publishing Company, Dubuque, Iowa

Built Environment Planning and Resilience

Critical Analysis of Tsunami Preparedness at Local Level for Sustainable Urban Planning in Sri Lanka

C. J. De Zoysa, A. A. S. E. Abeysinghe, U. T. G. Perera, C. S. A. Siriwardana, P. B. R. Dissanayake, R. Haigh, and D. Amaratunga

Abstract Coastal cities often suffer from extreme natural hazards such as sea level rise, coastal storms, and heavy rains. Amidst them, tsunami being a hazard with a very low frequency still claims to be the most detrimental disaster faced by coastal communities due to its unpredictable nature and the high impact caused by a single hit. The 2004 Indian Ocean tsunami affected 15 countries alarming the nations to revamp their urban planning frameworks to be more inclusive of preparedness for Tsunamis. Sri Lanka being an island greatly devastated by 2004 IOT, with the records for around 35,399 fatalities, 114,069 damaged or destroyed houses and 480,000 human displacements was undeniably compelled to build back better from the lessons learnt. Moreover, tsunami accounts for the greatest percentage, nearly 0.2% from its population of loss of lives and the greatest economic damage from a disaster in Sri Lanka in the recent history. Nevertheless, Sri Lanka's urban planning guidelines lack the preparedness measures that need implementing in tsunami prone cities. This further highlights the necessity of sustainable and resilient urban planning. This study synthesizes and critically analyzes the current level of integration of strategies for tsunami preparedness in Sri Lankan urban planning frameworks and related policies. A comprehensive review was carried out on urban planning policy frameworks and guidelines in Sri Lanka where the inclusion of tsunami preparedness measures under a set of pre-identified parameters was investigated. A critical analysis was then followed by means of comparing the existing local frameworks with globally practiced guidelines under the same categories which enabled identifying the gaps in Sri Lankan coastal city planning. In this context, this paper highlights the current state of the art of existing urban planning policy frameworks and guidelines in Sri

C. J. De Zoysa (✉) · C. S. A. Siriwardana
Department of Civil Engineering, University of Moratuwa, Moratuwa, Sri Lanka
e-mail: chandulajithmi@gmail.com

A. A. S. E. Abeysinghe · P. B. R. Dissanayake
Department of Civil Engineering, University of Peradeniya, Peradeniya, Sri Lanka

U. T. G. Perera · R. Haigh · D. Amaratunga
Global Disaster Resilience Centre, University of Huddersfield, Huddersfield, UK

R. Dissanayake et al. (eds.), *12th International Conference on Structural Engineering and Construction Management*, Lecture Notes in Civil Engineering 266,
https://doi.org/10.1007/978-981-19-2886-4_24

Lanka which highlights that it does not adequately include the tsunami preparedness measures to better prepare the country for similar future hazards.

Keywords Sustainable urban planning · Tsunami preparedness measures · Sri Lankan policy frameworks and guidelines · Resilient cities

1 Introduction

Urban areas in Asia are among the world's fastest growing areas and are expected to house 55% of the estimated 5 billion Asians by 2030 and [1] reveal that the majority of Asian megacities and other urban municipalities are located in hazard prone areas. Also, over the past half century the statistics show that in developing countries extremely high levels of population are concentrated in cities [2]. Meanwhile, natural hazards that result in not only fatalities and property damages but eventually a huge socioeconomic and environmental disruption have been uncovered as a major contributor for death tolls in the past decade accounting for more than 0.4% of annual deaths in some years [3]. Out of them, coastal hazards account for the most severe hazards around the world bringing the most serious impacts [4] and forty-six million people per year are currently at risk from coastal flooding due to storm surges [5].

Sri Lanka being both a developing country with the aforementioned urbanization crisis and an island surrounded by the sea, Sri Lankan communities are highly vulnerable to such coastal hazards. Sri Lanka was considered as the 2nd most affected country from extreme weather events during 2018 by Germanwatch Global climate index [6]. Even though the most common natural hazards in Sri Lanka include localized and seasonal floods and associated landslides, [7] Tsunamis are considered as the event that has caused the highest impact in recent history. The unpredictable nature of its occurrence has highlighted the importance of making the coastal communities Tsunami resilient and Bryant (2014) claims it to be the most underrated natural hazard of all time [8]. Tsunamis in 1998–2017 decade accounts for casualties and damages that are of one hundred times higher than that experienced during the previous decade (1978–1997). Sri Lanka has been ranked the sixth in terms of total estimated damages from Tsunamis during the above period of time [9, 10].

The above-discussed facts and statistics spotlight that as a country unveiled to coastal hazards of which Tsunamis are the most severe in nature with the highest impact, the coastal communities should be well prepared and the cities should be well planned to act resistive to these hazards mitigating the impact. Sri Lanka is a country which undergoes many city center development projects which involve the coast and the sea, and the inclusion of risk reduction measures in building and landscape designs for Tsunamis cannot be overlooked.

Therefore, this paper presents a review of the state of the art of urban planning and development to address tsunami risk in Sri Lanka.

2 Methods

First, a literature survey was carried out in the form of a systematic review using Google Scholar and Science Direct databases. Using the keywords, Sustainable Urban Planning; Tsunami Preparedness Measures; Sri Lankan Policy Frameworks and Guidelines; Resilient Cities. The scholarly articles written in English language during the period 2004–2021 were only selected for the initial search. After removing the duplications, the inclusion and exclusion criteria 1 listed in Table 1 were applied resulting in 35 retrieved articles. Then, 13 more articles were excluded through applying the exclusion criteria 2 and during the data extraction. 22 articles retained for the study from this search. The PRISMA flow diagram followed in the process is shown in Fig. 1.

First, the feasible urban planning techniques and potential strategies to reduce tsunami risk in Sri Lankan coastal cities were identified referring the 22 articles. These articles were based on researches carried out in Sri Lanka, mostly by the local researchers to suggest the strategies for future urban planning in Sri Lanka in regard to tsunami preparedness.

Then, 6 urban planning frameworks were studied to investigate the actual level of inclusion of the suggested strategies in literature. The referred frameworks are,

1. Urban Development Authority (UDA) Frameworks and Guidelines [11]
2. National Building and Research Organization (NBRO) Guidelines [12]
3. Guidelines of Society of Structural Engineers—Sri Lanka [13]
4. Coastal Conservation Act and Coastal Zone Management Plan [14]
5. Guidelines of National Housing Development Authority, Sri Lanka [15]
6. GreenSL Rating Systems [16].

Finally, comparing the suggested strategies and actual context an analysis was carried out to highlight the prevailing gaps in coastal city planning in Sri Lanka.

Table 1 Inclusion and exclusion criteria

	Inclusion	Exclusion
Criterion 1	Original studies and reviews	Not based on Sri Lanka
Criterion 2	Articles and book chapters	General disaster preparedness/not specific for Tsunamis
Criterion 3		Post-tsunami/recovery stage

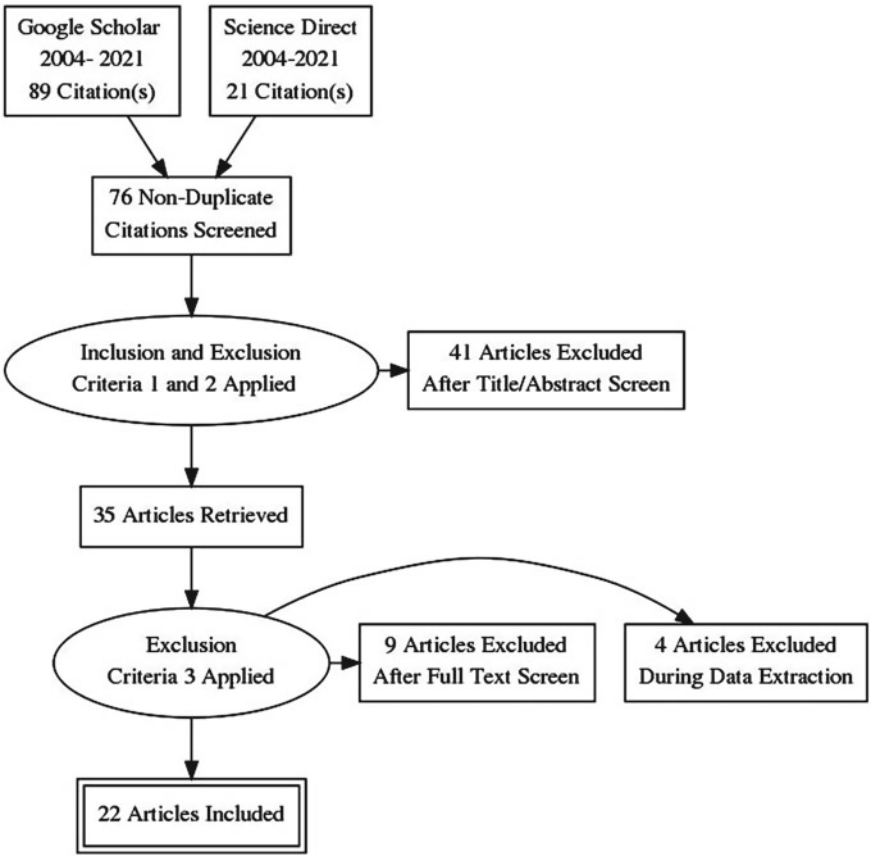

Fig. 1 Prisma flow diagram of the systematic review

3 Results and Discussion

3.1 Review of Scholarly Articles

Key aspects discussed in the reviewed scholarly articles and the recommendations and feasible strategies to Sri Lanka suggested by them are listed in Table 2.

The above aspects were grouped into 6 main parameters/indicators and were selected as the parameters defining tsunami and multihazard preparedness in coastal cities.

1. Spatial Planning
2. Communities and key stakeholder groups
3. Resilience Thinking' approaches
4. Soft engineering structures

Table 2 Recommended strategies in literature to incorporate into urban planning in Sri Lanka

Key aspect	Recommendation	Source
Inundation modeling and vulnerability assessments	Understanding possible vulnerable areas of future Tsunamis to prepare and implement disaster mitigation and management plans Use of dashboard tools for wave propagation modeling Inundation Modeling with primary considerations as inundation depth and recommended story heights	[17] [18]
Bathymetric assessments	Continuous assessment of bathymetric changes that have taken place in near shore areas	[19]
Evacuation	Availability and functionality of the vertical and horizontal tsunami evacuation facilities with safe evacuation routes	[18, 20]
Awareness	Increasing and monitoring continuous awareness of the exposed population	[21]
Design of buildings	Overall design guidelines providing advice on location, layout, orientation, structural configuration, geotechnical, and other considerations Detailed design guidelines leading to hydraulic and structural loads and geotechnical issues	[19]
Public open spaces (POS)	The locations of POS according to risk zonation Terrain quality and the Topographic character-guided allocation Determining the DRR use based on the location and size of POS Multipurpose uses of POS Networking of POS as a DRR passage Network of public open spaces linked with green corridors	[22, 23]
Key stakeholder engagement	Planning regulations should provide a strong institutional basis to clarify the role and requirements of vulnerability and risk information in the planning process A clarification of the roles of various stakeholders Coordination between authorities	[21, 24]
Buffer zones	Buffer zones have to be developed consistently and transparently while considering the needs of different household types as fishermen	[21]

(continued)

Table 2 (continued)

Key aspect	Recommendation	Source
Regulations for coast protection	Legal actions against mining activity	[25]
Flood prevention	Protect the flood-prone areas from land encroachment Keeping flood-prone areas for open space purposes to control the future development	[23]
Sand dunes	Combination of the sand dune followed by vegetation toward landside to retard Tsunamis Sand dunes (with or without vegetation)	[25] [26]
Education strategies	Public education strategy in collaboration with media institutions to enhance public engagement with early warning mechanisms Community mobilization	[27, 28]
Vegetation schemes	Use of a complex aerial-root structured specie in the frontline to dissipate energy when a tsunami hits. (Pandanus odoratissimus) Two layers of vegetation (odoratissimus and equisetifolia) in the vertical direction have a greater ability to lower the damage	[29]
Blue spaces	Water body/lakes (blue spaces)	[25]
Mangroves and plantation	Features such as dense vegetation and sand dune/beach and aquaculture pond/saltpans Sparse vegetation with some paddy fields plantations (e.g., coconut) and multi-species vegetation (e.g., mangrove) mixed with settlement areas When there is limited mangrove cover, vegetation like Casuarina, Cocos, Pandanus, etc., can be propagated in the coastal zone (with a prior knowledge on the consequences, if any, in relation to the local eco-socioeconomic conditions)	[25]
Urban forests	Urban forests and green spaces are resilient to rising heat and the threat of extreme weather hazards of changing climate, improve health and well-being, and promote resilience of urban dwellers	[30]
Marginalized communities and patterns of urbanization	Assess and prioritize vulnerable and marginalized people in the cities in urban land use planning The patterns of urbanization play more important role in the speed of urban land expansion which make more contribution for climate change	[30]

(continued)

Table 2 (continued)

Key aspect	Recommendation	Source
Ecosystem	Invest in ecosystem-based integration of disaster risk reduction (DRR) in urban planning	[31]
Green belt	Multipurpose green belt along the coast	[30]
Network of elements	Green elements including street trees, gardens and parks that support the connectivity creating a network	[32]
Local authorities	Effective utilization of local authority resources (physical/human/capital) in provision of services and good governance which increases planning capacity and responsiveness Establishment of disaster management unit Practice building application approval from national building research organization Climate change adaptation strategies Control the development activities in hazard prone areas through development permits Providing an adequate number of public toilets and urinals Daily sweeping and scavenging of streets Obtaining community participation for maintenance of road and storm water drainage	[33]
Data and technology	Using big data for urban planning	[34]
Key Stakeholders	Increase Institutional capacity and resources and address cognitive and cultural factors	[35]
Human Settlement planning	Planned human settlement through the adoption of new parameters based on population density, land suitability, and environmental sustainability, including adoption of the vertical development approach in high and medium population density areas	[36]
Drainage	Plan, construct, and maintain the city's drainage system to avoid or limit the risk of floods	[36]
Building standards	Development and enforcement of building standards	[37]
Waste management	Solid waste management	[38]
Catchment management	Catchment and integrated water resource management	[38]

(continued)

Table 2 (continued)

Key aspect	Recommendation	Source
DIA and EIA	Disaster impact assessment to be integrated to environmental impact assessment	[38]
Coastal structures	Structures with co-benefits, e.g., revetments and railway embankments	[39]

5. Hard engineering structures
6. Nature-based solutions.

3.2 Review of Urban Planning Frameworks

The Urban Development Authority Law, No. 41 of 1978, of the National State Assembly governs the Regulations made by the Minister of Urban Development and Housing, and it recently underwent a revision and the regulation will be cited as the Urban Development Authority Planning & Development Regulations 2020 henceforth. Even though it has introduced its own Green Rating System to assess buildings for the implementation of sustainable and green measures, neither the rating system nor the general guidelines include measures to reduce tsunami or coastal hazard risks, except for fire hazard.

Tsunami resilient building planning aspects have been demonstrated in NBRO guidelines in terms of site selection, shape and orientation of buildings, design of the structure, and also the external adjoining structures to the buildings.

Guidelines for buildings at risk from natural disasters by Society of Structural Engineers—Sri Lanka came about as a response to the tsunami of 26/12/2004 and as a contribution to the task of reconstruction. It discusses the following aspects shown in Table 5 regarding tsunami resilient housing construction. According to the framework, any building within 500 m of the coastline or 3 m elevation from mean sea level (which we shall call the "Coastal Zone") should be designed according to these guidelines; the above limits should read as "1 km of the coastline or 5 m elevation from mean sea level" for the East Coast. However, the scope is limited to the structural measures for buildings.

Coast Conservation act, 1981, along with the coastal zone management plan only seems to bring out the nature-based solutions for the protection of coast minimizing the erosion and other issues in beaches where most of the measures indirectly contribute to tsunami and coastal hazard prevention.

Guidelines for housing development in coastal Sri Lanka brings out statutory requirements and best practice guides to settlement planning, housing design, and service provision for hazard preparedness in general.

Both the GreenSL rating systems for Built Environment and Transportation Infrastructure lacks measures for prevention and preparedness for any kind of natural

hazard while the GreenSL rating system for Sustainable Cities addresses few aspects for general disaster resilience. However, the integration of tsunami and other multi-hazard (including the pandemics) preparedness into thee rating systems is vital and a separate rating system can be introduced for coastal zones if addition of tsunami prevention measures to the general building and city tool might cause unnecessary point reduction in unaffected areas.

After analyzing the local literature referred under Sect. 3.1 and their considered aspects in regard to tsunami and multihazard preparedness in tsunami prone areas, when moved on to analyze the consideration of above aspects to the actual planning context in Sri Lanka (discussed in Sect. 3.2), the following comparison shown in Table 3 can be reached.

The aspects that should be ideally addressed or the pre-identified main 6 indicators have been listed as column headings in Table 4. A gap analysis of Sri Lankan urban planning frameworks shown in Table 4 confirms that some important aspects have been neglected in most of the local codes while the prominence has been given to the structural aspects of the preparedness measures. The current inclusion of measures is indicated as the darker color shows the deeper integration and the blank cells indicate the absence of any measure under the given aspect.

4 Conclusion

The work intended to study the existing strategies for tsunami and other coastal hazard preparedness in Sri Lankan urban planning frameworks and guidelines. Searching for guidelines under the pre-identified aspects allowed realizing that apart from the guidelines for erecting buildings in tsunami prone areas by National Building and Research Organization (NBRO), Society of Structural Engineers—Sri Lanka, and National Housing Development Authority and other local codes lack the preparedness and planning aspects of a city in regard to tsunami and multihazard resilience. Also lack of proper legal compliance requirements of many of the discussed frameworks creates loopholes and a set of optional manuals which will most likely be violated and not complied in the practical context.

The above local codes can be modified and the integration of tsunami and other coastal hazard preparedness measures can be deepened through mainstreaming the suggested strategies in local literature as well as the globally practiced concepts and guidelines into the local context appropriately. For example, the community engagement in policy and decision-making and other highlighted areas of lack of integration could be improved through the guidelines in global frameworks such as RELi 2.0 (Rating guidelines for Resilient Design and Construction) which bring out certain missing aspects in the local codes. However, relation and impact for fishery and marine products, industry and tourism, financial limitations, and disturbance to the natural environment and resources will be the risk drivers and conflicting factors which need to be handled with care when proposing guidelines.

Table 3 Comparison of measures suggested and measures implemented

Aspects highlighted in research	Actual frameworks/policies
Modeling and assessments	Not recommended
Spatial planning for disaster response	• General spatial planning requirements by UDA and NHDA (not specified for disasters)
Land use planning for risk mitigation	General spatial planning requirements by UDA and NHDA (not specified for disasters)
Public awareness/stakeholders	Participatory (community) approach recommended in NHDA Guidelines Sri Lanka national disaster management plan does not recommend multi stakeholder engagement Coordination between different authorities is lacking • Planning and policy making through DMC and some other organizations—government acts through coastal conservation dept. etc. • Early warning through Meteorological Dept • Enforcing and response mechanisms through local authorities • Non-legally binding guidelines and manuals by several other parties
Design of buildings	Recommended in SSESL guidelines/NBRO guidelines No building code
Design of city infrastructure	Not recommended in any
Vegetation and other soft measures	Specific plantation schemes not recommended in any
Protection of natural buffers	Coast conservation act
Buffer zones and legal compliance/permits	Coast conservation act/UDA general guidelines Clearance from costal conservation department and UDA/local authority (NBRO requirements are not legally binding for coastal districts compliance required only for landslides)
Resilience approaches (Build back better)	Sri Lanka national disaster management policy (governed by disaster management act no 13) has removed build back better aspect in its final version (2014)
Multi-hazard aspect	Only multihazard early warning is highlighted in national disaster management plan (2017)

Table 4 Gap analysis of Sri Lankan urban planning frameworks

Framework	Spatial planning	Communities and key stakeholder groups	Resilience thinking' approaches	Soft engineering structures	Hard engineering structures	Nature-based solutions
Urban development authority (UDA) frameworks and guidelines						
NBRO guidelines						
Guidelines of society of structural engineers Sri Lanka						
Coastal conservation act and coastal zone management plan						
Guidelines of national housing development authority, Sri Lanka						
GreenSL rating system for cities						

Acknowledgements This work was supported by the project Covid 03-Integrating Tsunami and other Multihazard Preparedness into Urban Planning. All partners, University of Huddersfield, UK—Lead, Ministry of Health, Sri Lanka, State Ministry of Rural Roads and other Infrastructure, Sri Lanka, University of Colombo, Sri Lanka, University of Moratuwa, Sri Lanka, University of Peradeniya, Sri Lanka, Bandung Institute of Technology, Indonesia, Federation of Sri Lankan Local Government Authorities, Sri Lanka, Disaster Management Centre, Sri Lanka, Intergovernmental Oceanographic Commission of UNESCO IOTWMS (Indian Ocean Tsunami Early Warning and Mitigation system), The Asian Disaster Preparedness Centre, Thailand, and The Ceylon Chamber of Commerce, Sri Lanka, are greatly acknowledged.

References

1. Hochrainer S, Mechler R (2011) Natural disaster risk in Asian megacities: a case for risk pooling? Cities 28(1):53–61
2. Henderson V (2002) Urbanization in developing countries. The world bank research observer 17(1):89–112. https://ourworldindata.org/natural-disasters [accessed on [14/03/2021]
3. Asian Disaster Reduction Center (2003) Glossary on natural disasters. available at: www.adrc.or.jp/
4. Zou LL, Wei YM (2010) Driving factors for social vulnerability to coastal hazards in Southeast Asia: results from the meta-analysis. Nat Hazards 54(3):901–929
5. IPCC (2001) IPCC third assessment report: climate change 2001 (TAR). IPCC assessment report. Geneva, Switzerland, intergovernmental panel on climate change

6. Eckstein D, Künzel V, Schäfer L, Winges M (2019) Global climate risk index 2020. Bonn: Germanwatch
7. Abeysinghe AASE, Bandara CS, Siriwardana CSA, Haigh R, Amarathunga D, Dissanayake PBR (2021) Incorporation of disaster risk reduction mechanisms for flood hazards into the greensl® rating system for built environment in Sri Lanka. In ICSECM 2019. Springer, Singapore, pp 573–587
8. Bryant E (2014) Tsunami: the underrated hazard. Springer
9. UNISDR W (2012) Disaster risk and resilience. Thematic think piece, UN system task force on the post-2015 UN development agenda
10. Department of Census and Statistics (2017) Population census
11. The urban development authority law, no. 41 of 1978 of the national state assembly
12. Hazard Resilient Housing Construction Manual, Hazard Resilient Construction Series No. 1, 2015, Research & Development Programme of National Building Research Organisation
13. Society of Structural Engineers (Sri Lanka) (2005) Guidelines for buildings at risk from natural disasters: a response to the Tsunami of 26/12/2004 and a contribution to the task of reconstruction. Society of Structural Engineers
14. Lanka S (2013) Coast conservation act no. 57 of 1981. http://www.commonlii.org/lk/legis/num_act/cca57o1981263/Consultado, 5
15. National Housing Development Authority (NHDA) (2005) Guidelnes for housing development in coastal Sri Lanka
16. GreenSL Rating system for sustainable cities, version 1
17. Josiah NR, Laknath DPC, Araki S (2020) Assessment of Tsunami preparedness measures in east coast of Sri Lanka based on 2004 Tsunami event. In: Proceedings of 22nd congress of international association for hydro environment engineering and research and Asia Pacific division. Sapporo, Japan
18. Laknath DPC, Josiah NR, Sewwandi KAHS, Araki S (2020) Simulation of 2004 Tsunami inundation in Galle city in Sri Lanka and revisit the present evacuation measures. Coastal engineering proceedings, vol 36, pp 36–36
19. Hettiarachchi S, Samarawickrama S (2006) The tsunami hazard in Sri Lanka strategic approach for the protection of lives, ecosystems and infrastructure. Coast Eng J 48(03):279–294
20. Suppasri et al (Dec 2015) A decade after the 2004 Indian ocean Tsunami: the progress in disaster preparedness and future challenges in Indonesia, Sri Lanka, Thailand and the Maldives. Pure Appl Geophys 172(12):3313–3341. https://doi.org/10.1007/s00024-015-1134-6
21. Løvholt F, Setiadi NJ, Birkmann J, Harbitz CB, Bach C, Fernando N, Kaiser G, Nadim F (2014) Tsunami risk reduction–are we better prepared today than in 2004? Int J Disaster Risk Reduction 10:127–142
22. Jayakody RC, Amaratunga D (2020) Guiding factors for planning public open spaces to enhance coastal cities' disaster resilience to Tsunamis. Int J Disaster Resilience Built Environ
23. Jayakody RRJC, Amarathunga D, Haigh R (2018) Integration of disaster management strategies with planning and designing public open spaces. Procedia Eng 212:954–961
24. Saja AA, Sahid ML, Sutharshanan M (2020) Implementing Sendai framework priorities through risk-sensitive development planning—a case study from Sri Lanka. Prog Disaster Sci 5:100051
25. Sooriyaarachchi P, Sandika AL, Madawanarachchi N (2018) Coastal community resilience level of Tsunami prone area: a case study in Sri Lanka. Procedia Eng 212:683–690
26. Tanaka N, Sasaki Y, Mowjood MIM (2006) Effects of sand dune and vegetation in the coastal area of Sri Lanka at the Indian ocean Tsunami advances in geosciences. Namsik P et al (eds) Hydrological science, vol 6. World Scientific Publishing Company pp 149–59
27. Haigh R, Sakalasuriya MM, Amaratunga D, Basnayake S, Hettige S, Premalal S, Arachchi AJ (2020) The upstream-downstream interface of Sri Lanka's tsunami early warning system. Int J Disaster Resilience in the Built Environment
28. Rajarathna WNS, Nianthi KR (2019) Special coastal management area concept experience in Sri Lanka. In: Coastal management. Academic Press, pp 5–20

29. Tanaka N, Sasaki Y, Mowjood MIM et al (2007) Coastal vegetation structures and their functions in tsunami protection: experience of the recent Indian Ocean tsunami. Landsc Ecol Eng 3(1):33–45
30. De Zoysa M. Urbanization, climate change and environmental resilience: experiences in Sri Lanka
31. Hettiarachchi SSL, Weeresinghe S (2014) Achieving disaster resilience through the Sri Lankan early warning system: good practises of disaster risk reduction and management. Procedia Econ Fina 18:789–794. https://doi.org/10.1016/S2212-5671(14)01003-X
32. Grădinaru SR, Hersperger AM (2019) Green infrastructure in strategic spatial plans: evidence from European urban regions. Urban For Urban Greening 40:17–28. https://doi.org/10.1016/j.ufug.2018.04.018
33. Bandara D, Jayasinghe AB (2014) Climate responses of local authorities: a case of Sri Lankan coastal urban areas. Int J Res Soc Sci 4(3):2307–3227
34. Samarajiva R, Lokanathan S, Madhawa K, Kreindler G, Maldeniya D (2015) Big data to improve urban planning. Econ Polit Wkly 42–48
35. Mahanama PS, Abenayake CC, Jayasinghe P (2014) Challenge of local responses to climate change; perceptions of urban planning practitioners in Sri Lanka. Asian J Humanit Soc Stud 2(4)
36. Malalgoda C, Amaratunga D, Haigh R (2013) Creating a disaster resilient built environment in urban cities: the role of local governments in Sri Lanka. Int J Disaster Resilience Built Environ
37. De Silva PGJ (2017) Role of international and national standards in improving quality of life in urban environments in Sri Lanka. Cities People Places: Int J Urban Environ 2(1)
38. Dissanayake P, Hettiarachchi S, Siriwardana C (2018) Increase in disaster risk due to inefficient environmental management, land use policies and relocation policies. Case studies from Sri Lanka. Procedia Eng 212:1326–1333
39. Samarasekara RSM, Sasaki J, Esteban M, Matsuda H (2017) Assessment of the co-benefits of structures in coastal areas for tsunami mitigation and improving community resilience in Sri Lanka. Int J Disaster Risk Reduction 23:80–92

An Investigation of Factors Affecting the Marginalized Communities in Disasters from an Intersection Perspective: A Systematic Literature Review

R. M. Rinaz and C. S. A. Siriwardana

Abstract Disasters have different effects on different people. Natural and man-made calamities have ravaged Sri Lanka on several occasions, disproportionately affecting the socially excluded and marginalized people. When it comes to the treatment of marginalized people in disasters, the primary rule is that everyone, regardless of their differences, should have the same privileges and rights. However, there has been fewer study of the literature on the extent of social exclusion experienced by Sri Lanka's excluded population during disasters. Building disaster-resilient communities has become a top priority for crisis management organizations around the world in recent years, as resilient communities are more likely to incur less losses and recover more swiftly in the case of a disaster. To improve a society's resilience, however, one must first create a baseline, or a starting point from which to compare communities. This research uses a Systematic Literature Review to synthesize the context of marginalization during disasters in Sri Lanka, drawing on examples and models from other countries. Data was acquired utilizing two databases, as well as scanning the gray literature. The PRISMA model was used for the screening process of the literature. Studies conducted on marginalization in disasters, published in English, were selected by the reviewer. Furthermore, the VOS viewer data mining tool was used for developing a network map of keywords of the selected literatures to identify the most investigated areas. Out of 2072 of total articles published between 2016 and 2021, 37 articles have been included and reviewed in this study. In order to define a socially excluded marginalized community during disasters, six significant parameters of marginalization were eventually identified. The problem describes how marginalization accelerates as a result of various overlapping vulnerabilities, and how these marginalized groups are underrepresented in the disaster cycle and decision-making processes as a result of disaster planning, impact, response, and recovery.

Keywords Marginalization · Disaster · Vulnerable community · Social exclusion · Vulnerability mapping

R. M. Rinaz (✉) · C. S. A. Siriwardana
Department of Civil Engineering, University of Moratuwa, Moratuwa, Sri Lanka
e-mail: rinaz.riyaz123@gmail.com

R. Dissanayake et al. (eds.), *12th International Conference on Structural Engineering and Construction Management*, Lecture Notes in Civil Engineering 266,
https://doi.org/10.1007/978-981-19-2886-4_25

1 Background

Economic losses and damages from disasters totaled more than $300 billion in 2017, with a total of $2.9 trillion between 1998 and 2017 [1]. Sri Lanka is placed 11th in the world in terms of yearly average exposure in relation to its population when it comes to physical vulnerability of the country's people to floods. The most frequently occurring natural hazards in Sri Lanka that affect people are droughts, floods, cyclones, landslides, vector borne epidemics (malaria, dengue, and COVID-19 recently), and coastal erosion [2]. This is clearly a major issue that requires significant global action and focus, especially as the size of these misfortunes is expected to increase over time due to environmental changes and their compounding consequences.

But disasters do not strike everyone evenly. The marginalized communities are the most hit in disasters. We recognize that marginalized groups are frequently overlooked or underrepresented throughout the disaster cycle [3]. Communities that are marginalized are those that are excluded from mainstream social, economic, educational, and/or cultural life. It is a major source of vulnerability, exposing individuals to a wide range of threats, including the possibility of disaster. Marginalization varies depending on the situation, but all marginalized groups have one thing in common: they are frequently pushed to the lower periphery of society and viewed as less significant [4].

Dissanayake (2003) [5] in his finds explains poverty is the primary source of marginalization in Sri Lanka, which is widespread among the rural. Nonetheless, it is clear that poor and oppressed populations have been overlooked as a result of unethical procedures and strategies used in such situations. The following were the main reasons for such exclusion:

- Inability to detect and identify the community's poverty, disadvantaged, and marginalized groups or communities
- Adapting a uniform methodology across potential beneficiary communities regardless of their financial/socioeconomic status
- Lack of opportunity for marginalized communities where the majority of people are poor/marginalized to apply for benefits and the people who are truly in need are overlooked.

Aim

Social exclusion has a strong connection or resemblance to the term disadvantage. Therefore, it can be identified as more relational rather than a quantitative term. Except for the factor of poverty, there has been no assessment of the literature relating to the issue of marginalization faced by vulnerable populations in Sri Lanka [5]. This research presents its findings to bridge the gap of "why numerous disadvantages form the idea of marginalization" by assessing the regions of marginalization encountered by vulnerable communities in disasters. It will also describe how marginalization accelerates as a result of multiple vulnerabilities, as well as how marginalized groups

are underrepresented in disaster preparation, decision-making, impact, response, and recovery.

2 Methodology

2.1 Search Strategy

Systematic Literature Review was performed in two databases "Scopus and Science Direct" using the appropriate specifications for each database. Keywords used were as follows: "marginalization, disaster, vulnerable community, vulnerability mapping and social exclusion"; the complete search strategy for each database is shown in Appendix 1.

Additional documents (gray literature) were sourced by search of Google and relevant web sites.

2.2 Selection of Articles and Documents

For eligibility, the abstracts, titles, and keywords were reviewed. Full copies of the publications that were picked by reviewer in the abstract review were retrieved and evaluated for eligibility. Published studies on disaster risk reduction for marginalized and vulnerable populations from an intersectional viewpoint were the study's inclusion criteria. Studies that were not published in English were eliminated.

Systematic Literature Review exclusion and inclusion criteria play a vital role in identifying the most relevant studies for the analysis. As this study intended to explore the parameters around the concept of marginalization of vulnerable population in disasters and adopting intersection principle to find communities in need during catastrophes, following exclusion criteria were used in the screening process.

- Criteria 1: Studies that do not emphasize disaster risk reduction and marginalization aspects in disasters
- Criteria 2: Studies do not develop a method/framework/model/tool for effective disaster risk reduction of the marginalized population
- Criteria 3: Studies do not cover marginalization of the vulnerable.

3 Results

Figure 1 shows the screening process of the literature carried out. Initially, 1417 articles from Science Direct and 651 articles from Scopus databases have been screened through the aforementioned criteria. After the screening process, 37 articles have been retained for the Systematic Literature Review. (All of these studies which included in the review were published from 2016 to 2021.)

Furthermore, this study employed keyword analysis of the selected articles from the databases to identify the highly researched areas by using VOS viewer software. By creating, visualizing, and exploring maps constructed upon bibliometric data, VOS viewer software provides an analysis of the results in the form of network maps that highlight the connections among the units of analysis using nodes, lines, links, and networks which is shown in Fig. 2.

It is clear that 6 dimensions of marginalization and social exclusion are identified in the context of disaster in the literature review carried out. The identified disadvantages are "poverty, gender, housing condition, age, race, and past experience." It is clearly identified that these disadvantages shape the concept of marginalization,

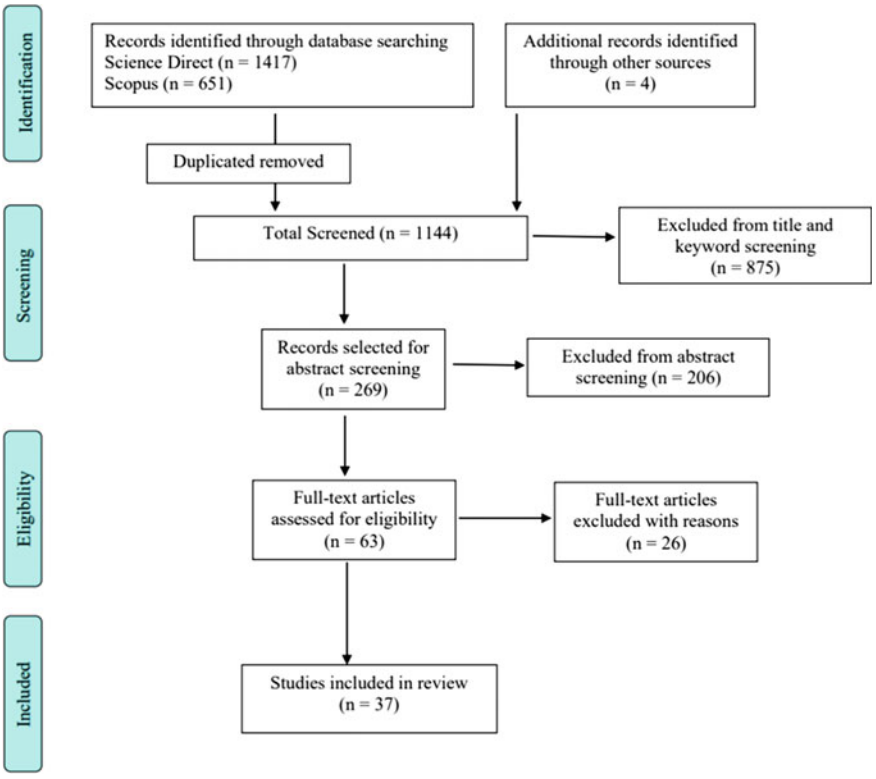

Fig. 1 Prisma flow diagram

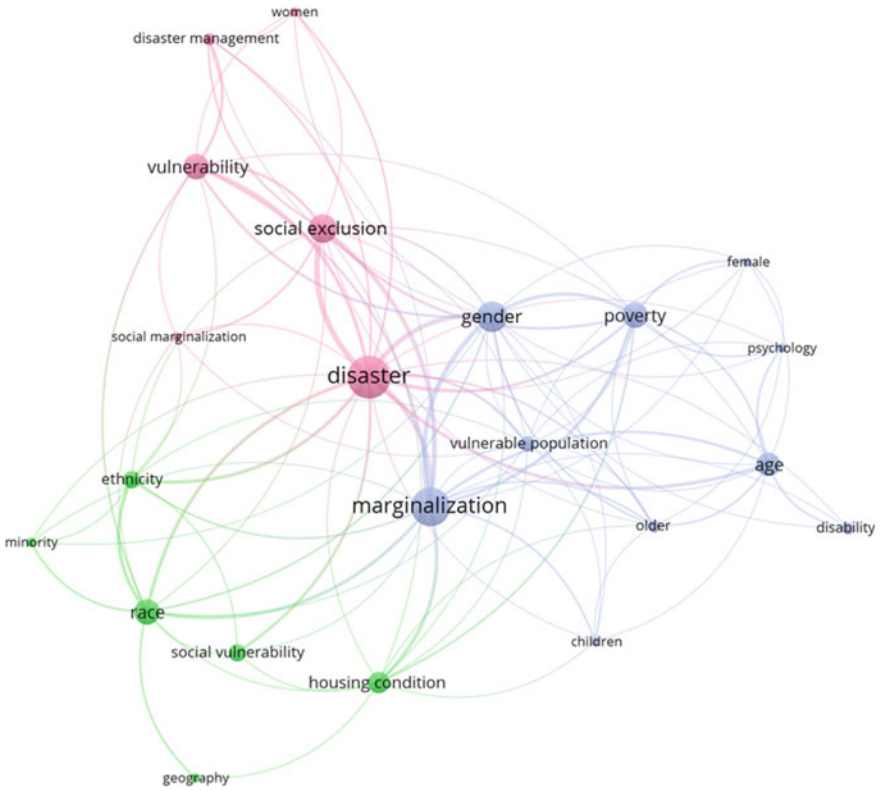

Fig. 2 VOS viewer analysis

and this explains us marginalization of a community increases with the number of overlapping disadvantages which affects the community during pre-disaster event, during catastrophe and post-disaster events. Keywords like minority and ethnicity are considered to be under race. Keywords like psychology and trauma are considered to be past experiences. Keywords like older and children, and disability falls under age.

Table 1 summarizes the main features of the included studies, including the theme of the article, study design or specific disaster contexts considered (if any), and identified indicator/s of marginalization.

4 Discussion

This review revealed that the marginalized population are left behind due to the overlapping of one or more of the main 6 inequalities identified "poverty, race and ethnicity, gender, elderly and disability status (Age), living arrangement, and past

Table 1 Basic information of the selected articles

Article	Theme of the article	Type of event	Indicator of marginalization
1 [6]	Housing Vienna: The socio-spacial effects of inclusionary and exclusionary mechanisms of housing provision	Social programs	Housing condition, poverty
2 [7]	An assessment of livelihood recovery status of earthquake-affected households in Nepal: a study of coping strategies and their effectiveness	Earthquake	Trauma, housing
3 [8]	Housing type matters for pace of recovery: evidence from Hurricane Ike	Hurricane	Housing, trauma
4 [9]	COVID-19 experience among slum dwellers in Nairobi: a double tragedy or useful lesson for public health reforms?	Pandemic	Housing, poverty, psychology
5 [10, 11]	What influences disaster risk perception? Intervention measures, flood, and landslide risk perception of the population living in flood risk areas in Rio de Janeiro state, Brazil	Flood, landslide	Housing, poverty
6 [12]	Perpetuating poverty through exclusion from social programs: lessons from Andhra Pradesh	Social programs	Poverty, spatial segregation
7 [13]	Preferences of vulnerable social groups for ecosystem-based adaptation to flood risk in Central Vietnam	Flood	Poverty, gender
8 [14]	Social exclusion: towards an analytical and operational framework	Social programs	Poverty
9 [15]	Negotiating health amidst COVID-19 lockdown in low-income communities in Aotearoa New Zealand	COVID-19	Age, poverty, housing
10 [16]	Post-traumatic stress due to structural violence after the Fukushima disaster	Disaster	Trauma

(continued)

Table 1 (continued)

Article	Theme of the article	Type of event	Indicator of marginalization
11 [17]	The parental experience of mothers with children who have developmental disabilities: qualitative reflections on marginalization and resilience	Social challenges	Age, gender, trauma
12 [18]	Social marginalization and children's rights: HIV-affected children in the Republic of Trinidad and Tobago	HIV	Age, gender
13 [19]	Planning for inclusion? An assessment of Ontario's emergency preparedness guide for people with disabilities	Disaster	Disability, gender, poverty
14 [20]	How does government discourse make people vulnerable?	Flood, social programs	Age
15 [21]	The virus and the divided city	Virus	Age, poverty
16 [22]	Why social exclusion persists among older people in Australia	Disaster, social programs	Age, gender, poverty
17 [23]	Online education of marginalized children in north Macedonia and Italy during the covid-19 pandemic	COVID-19	Age, poverty, psychology
18 [24]	Pandemic precarity: aging and social engagement	Pandemic	Age, race, gender
19 [25]	Older workers in the time of COVID-19: the senior community service employment program and implications for social work	Pandemic	Age, poverty, gender
20 [26]	Social vulnerability of marginalized people in times of disaster: case of Thai women in Japan Tsunami 2011	Tsunami	Gender, race

(continued)

Table 1 (continued)

Article	Theme of the article	Type of event	Indicator of marginalization
21 [27]	Social work practice: accounting for double injustices experienced by women under the confluence of Covid-19 pandemic and climate change impacts in Nyanga, Zimbabwe	Disaster	Gender, poverty
22 [28]	Segregation, exclusion and LGBT people in disaster impacted areas	Disaster	Gender
23 [29]	Problems and possibilities on the margins: LGBT experiences in the 2011 Queensland floods	Flood	Gender
24 [30]	The blueprint of disaster: COVID-19, the flint water crisis, and unequal ecological impacts	Disaster	Poverty, race, psychology
25 [31]	Marginalized by race and place: a multilevel analysis of occupational sex segregation in post-apartheid South Africa	Social programs	Race, gender, geography
26 [32]	SARS-CoV-2 testing in North Carolina: racial, ethnic, and geographic disparities	COVID-19	Race, geography
27 [33]	Fine-scale assessment of inequities in inland flood vulnerability	Flood	Race and ethnicity
28 [34]	The unequal vulnerability of Kurdish and Azeri minorities in the case of the degradation of Lake Urmia, Iran	Disaster	Race and ethnicity
29 [35]	Indigenous peoples' data during COVID-19: from external to internal	COVID-19	Race and ethnicity
30 [36]	"I hope to hell nothing goes back to the way it was before": COVID-19, marginalization, and native nations	Pandemic	Race and ethnicity

(continued)

Table 1 (continued)

Article	Theme of the article	Type of event	Indicator of marginalization
31 [37]	How COVID-19 may alleviate the multiple marginalization of racialized migrant workers	COVID-19	Race and ethnicity, gender, poverty, health
32 [38]	Marginalized to double marginalized: my mutational intersectionality between the east and the west	Social context	Race and ethnicity, geography, gender
33 [39]	Sex, power, marginalization and HIV amongst young fishermen in Malawi: exploring intersecting inequalities	HIV	Race and ethnicity, age, gender, poverty
34 [40]	An intersectional approach to the understanding of patterns of marginalization among ex-combatants with disabilities in Sri Lanka	Man-made disaster	Disability, gender
35 [41]	Vulnerability assessment of households to flash floods and landslides in the poor upland regions of Vietnam	Flood, landslide	Poverty, housing condition
36 [42]	Marginality, social exclusion, labor force participation and urban poverty: a case study of Lahore, Pakistan	Social programs	Poverty

experiences." Because of that, the most marginalized and vulnerable groups suffer more negative consequences in the face of disaster and emergencies. These marginalized people are left behind in the decision-making processes and left vulnerable during and aftermath of a disaster.

4.1 Before the Disaster

Being on the margins may have an impact on how individuals perceive disaster risks, prepare for disasters, and respond to warnings and evacuation orders. According to research, people of varying socioeconomic statuses may prepare for disasters in different ways [43].

Perception of Disaster Risk

Fothergill and Peek [44] revealed conflicting findings relating to dis aster risk perception in a review of literature on disasters and dangers as experienced by individuals in poverty [43]. They reference studies [45, 46] that show that people with lower incomes perceive more danger and are more concerned about natural and man-made disasters. Given the variety of findings, in another finding it is argued that "a feature such as socioeconomic position should be viewed as a possible contributor to, and predictor of how dangers are seen and interpreted by the community" [47].

Disaster Preparedness

People in poverty, those with low incomes, and those with less education, according to Fothergill and Peek, are less prepared for disasters [44]. The report points out that this finding could be related to the fact that some preparatory steps are expensive and may be out of reach for low-income people (e.g., acquiring earthquake or flood insurance or reinforcing a property for increased earthquake resilience) [44].

According to the theory that disaster preparedness is prohibitively expensive for people from low socioe conomic backgrounds, a World Bank and Global Facility for Disaster Reduction and Recovery (GFDRR) report on the effects of natural disasters around the world found that "poor people, with fewer resources, will in general put less in preventing and mitigating the unfavorable impacts of natural disasters" [48].

A separate set of researchers looked at the preparedness of 1304 persons aged 50 and up. They discovered that those with lower income levels are essentially less prepared for natural disasters [49]. This clearly suggests that, as mentioned in the above paragraphs, more than one type of vulnerability—in this case, older age and lower income, may collaborate to shape how people plan for and experience disasters. The paper highlights the facts that how multiple variables connect in shaping ho w people experience and interpret disasters, beginning in the pre-disa ster stage.

Responses to Warning Communication

According to the literature, those of lower socioeconomic level or those who are marginalized may be unable to respond to government early warnings about disasters in many disaster and emergency scenarios. Poor women, those with lower livelihoods and income, public housing tenants, and women who were homeless, widowed, unemployed, and of low-pay status, according to the Fothergill and Peek report, lacked the money and resources needed to evacuate, and they did not trust the early warnings. As a result, despite receiving early warnings and notifications, they were less prepared to respond than people with greater socioeconomic standing [43].

4.2 Disaster Impact

Findings on how people's social status affects them in the face of disasters show that people with multiple degrees of marginalization are more vulnerable in the face

of disasters and are more likely to suffer more negative and serious consequences, such as property damage, homelessness, and physical and financial impacts. Natural disasters can cause more misfortune for people and groups of lower socioeconomic status than for people and groups of higher socioeconomic status, and, as the World Bank and the Global Facility for Disaster Reduction and Recovery (GFDRR) report points out, natural disasters make it more likely for people to lose their homes, in part due to their financial effects and that people in poverty will remain in poverty [43].

4.3 After the Disaster

As one might imagine, there are disparities in how marginalized and socially excluded individuals experience the post-disaster period compared to the rest of the social groupings. This includes variations in access to disaster help and vital resources according to socioeconomic class, stress and depression, post-traumatic stress and growth, and physical health in the aftermath of a disaster.

Difficulty with Obtaining and Receiving Aid

The research of Fothergill and Peek's presents substantial evidence of difficulties faced by low-income and poor persons interacting with administrative structures to obtain housing and various types of relief or aid in the aftermath of a disaster. The lack of information and knowledge about the systems through which disaster survivors receive assistance, as well as unease with these systems, and issues in getting to and from disaster assistance centers, such as transportation, child care, and work schedules, have all been identified as barriers in studies [43]. The programs are neither designed nor funded to respond as rapidly as disasters generally need, or to be tailored to disaster-related needs, and money transferred to the poor and disenfranchised are typically less than those transferred to the wealthy.

5 Conclusion

Natural or man-made disasters have a severe impact on society's socially disadvantaged communities. It implies that disadvantage among these groups is cumulative in nature as the number of overlapping disadvantages grows. As a result, this susceptible group may be more vulnerable in the event of a catastrophe. This is the strength of our research, which aims to improve understanding of social exclusion among marginalized groups in disasters by analyzing literature from developing countries and developing an inclusive assessment and vulnerability mapping that takes into account the overlapping disadvantages of inclusion in Sri Lanka.

Appendix 1

Appendix 1: Database search.

1. *SCOPUS*

#	Searches	Results
1	TITLE-ABS-KEY (((disaster OR emergency) AND (social exclusion OR social vulnerability mapping OR marginalized population)))	109
2	TITLE-ABS-KEY (((disaster OR emergency) AND (social vulnerability OR Marginalization)))	3928
3	TITLE-ABS-KEY (((disaster OR emergency) AND (vulnerable community OR Marginalization OR social vulnerability) AND (Intersection)))	301
4	TITLE-ABS-KEY (((disaster OR emergency) AND (past experience OR psychology OR trauma) AND (education OR language) AND (Marginalization OR social vulnerability OR social exclusion)))	500
5	TITLE-ABS-KEY (((disaster OR emergency) AND (gender OR age OR disability OR child OR adolescence OR elderly OR aged OR old) AND (Marginalization OR social vulnerability OR social exclusion) AND (housing condition OR shelter OR living arrangements))	26
6	TITLE-ABS-KEY (((disaster OR emergency) AND (poverty OR poor) AND (gender OR male OR female) AND (race OR ethnicity OR minority OR indigenous) AND (Marginalization OR social vulnerability OR social exclusion)))	7

2. *SCIENCE DIRECT*

#	Searches	Results
1	disasters/or disaster planning/	37,506
2	disaster planning/or disaster victim/	4985
3	disaster/or mass disaster/or natural disaster/or relief work/or rescue work/	578
4	natural disasters/or disasters/or emergencies/or emergency relief/	3914
5	floods/or drought/or avalanches/or landslides/or hurricanes/or tornadoes/or typhoons/or earthquakes/or wildfires/	14
6	(disaster OR emergency) AND (social exclusion OR social vulnerability mapping OR marginalized population)	32,235
7	(disaster OR emergency) AND (social vulnerability OR Marginalization)	50,529
8	(disaster OR emergency) AND (vulnerable community OR Marginalization OR social vulnerability) AND (Intersection)	4651
9	(disaster OR emergency) AND (past experience OR psychology OR trauma) AND (Marginalization OR social vulnerability OR social exclusion)	29,238
10	(disaster OR emergency) AND (Marginalization OR social vulnerability OR social exclusion) AND (housing condition OR shelter OR living arrangements)	11,099
11	(disaster) AND (poverty OR poor) AND (gender OR female) AND (race OR ethnicity OR minority)	3704

References

1. Kurniawan (2017) Answering Professor Toshiyuki Tsuchiya's criticism of my three books on Japanese national parks. Keizai Shibayashi 87(1,2):149–200
2. Tissera CH (1997) Natural hazards. In: Somasekeram S (ed) Arjuna's atlas of Sri Lanka. Arjuna Publishers, Colombo, pp 76–78
3. Cordaid (2020) G. (n.d.) Step-by-step guide to inclusive developed by corda id
4. Sevelius JM, Gutierrez-Mock L, Zamudio-Haas S, McCree B, Ngo A, Jackson A, … Gamarel K (2020) Research with Marginalized Communities: Challenges to Continuity During the COVID-19 Pandemic. AIDS and Behavior, 24(7):2009–2012. https://doi.org/10.1007/s10461-020-02920-3
5. Dissanayake A (2003) Inclusion of marginalized groups in rural WATSAN in Sri Lanka
6. Friesenecker M, Kazepov Y (2021) Housing Vienna: The socio-spatial effects of inclusionary and exclusionary mechanisms of housing provision. Social Inclusion, 9(2):77–90
7. Raut NK (2021) An assessment of livelihood recovery status of earthquake-affected households in Nepal: a study of coping strategies and their effectiveness. Prog Disaster Sci 9:100147. https://doi.org/10.1016/j.pdisas.2021.100147
8. Hamideh S, Peacock WG, Van Zandt S (2021) Housing type matters for pace of recovery: evidence from Hurricane Ike. Int J Disaster Risk Reduction 57. https://doi.org/10.1016/j.ijdrr.2021.102149
9. Nyadera IN, Onditi F (2020) COVID-19 experience among slum dwellers in Nairobi: a double tragedy or useful lesson for public health reforms? Int Soc Work 63(6):838–841. https://doi.org/10.1177/0020872820944997
10. Ardaya AB, Evers M, Ribbe L (2017) What influences disaster risk perception? Intervention measures, flood and landslide risk perception of the population living in flood risk areas in Rio de Janeiro state, Brazil. Int J Disaster Risk Reduction 25:227–237
11. Bustillos Ardaya A, Evers M, Ribbe L (2017) What influences disaster risk perception? Intervention measures, flood and landslide risk perception of the population living in flood risk areas in Rio de Janeiro state, Brazil. Int J Disaster Risk Reduction 25(5):227–237. https://doi.org/10.1016/j.ijdrr.2017.09.006
12. Petrikova I (2020) Perpetuating poverty through exclusion from social programmes: lessons from Andhra Pradesh. Oxf Dev Stud 48(1):33–55. https://doi.org/10.1080/13600818.2019.1601173
13. Hagedoorn LC, Bubeck P, Hudson P, Brander LM, Pham M, Lasage R (2021) Preferences of vulnerable social groups for ecosystem-based adaptation to flood risk in Central Vietnam. World Dev 148:105650
14. Bhalla A, Lapeyre F (1997) Social exclusion: towards an analytical and operational framework. Development and change, 28(3), 413-433
15. Elers C, Jayan P, Elers P, Dutta MJ (2021) Negotiating health amidst COVID-19 lockdown in low-income communities in Aotearoa New Zealand. Health Commun 36(1):109–115. https://doi.org/10.1080/10410236.2020.1848082
16. Tsujiuchi T (2021) Post-traumatic stress due to structural violence after the Fukushima disaster. Japan Forum 33(2):161–188. https://doi.org/10.1080/09555803.2018.1552308
17. Stober K, Franzese A (2018) The parental experience of mothers with children who have developmental disabilities: qualitative reflections on marginalization and resiliencey. In: Marginalized mothers, mothering from the margins. Emerald Publishing Limited
18. Jones A (2009) Social marginalization and children's rights: HIV-affected children in the Republic of Trinidad and Tobago. Health Soc Work 34(4):293–300. https://doi.org/10.1093/hsw/34.4.293
19. Pyke C, Wilton R (2020) Planning for inclusion? An assessment of Ontario's emergency preparedness guide for people with disabilities. Int J Disaster Risk Reduction 51:101888. https://doi.org/10.1016/j.ijdrr.2020.101888
20. Tagalo RD (2020) How does government discourse make people vulnerable? Disaster Prev Manag: Int J 29(5):697–710. https://doi.org/10.1108/DPM-07-2020-0225

21. Eckardt F (2020) The virus and the divided city. Leviathan 48(3):470–483
22. Miranti R, Yu P (2015) Why social exclusion persists among older people in Australia. Soc Incl 3(4):112–126
23. Cenedese M, Spirovska I (2021) Online education of marginalized children in North Macedonia and Italy during the COVID-19 pandemic. Dve Domovini 2021(54)
24. Hebblethwaite S, Young L, Martin Rubio T (2021) Pandemic precarity: aging and social engagement. Leis Sci 43(1–2):170–176. https://doi.org/10.1080/01490400.2020.1773998
25. Halvorsen CJ, Yulikova O (2020) Older workers in the time of COVID-19: the senior community service employment program and implications for social work. J Gerontol Soc Work 63(6–7):530–541. https://doi.org/10.1080/01634372.2020.1774832
26. Pongponrat K, Ishii K (2018) Social vulnerability of marginalized people in times of disaster: case of Thai women in Japan Tsunami 2011. Int J Disaster Risk Reduction 27:133–141. https://doi.org/10.1016/j.ijdrr.2017.09.047
27. Nyahunda L, Chibvura S, Tirivangasi HM (2021) Social work practice: accounting for double injustices experienced by women under the confluence of covid-19 pandemic and climate change impacts in Nyanga, Zimbabwe. J Hum Rights Soc Work 6(3):213–224. https://doi.org/10.1007/s41134-021-00170-4
28. Yamashita A, Gomez C, Dombroski K (2017) Segregation, exclusion and LGBT people in disaster impacted areas: experiences from the Higashinihon Dai-Shinsai (Great East-Japan Disaster). Gend Place Cult 24(1):64–71
29. Gorman-Murray A, Morris S, Keppel J, McKinnon S, Dominey-Howes D (2017) Problems and possibilities on the margins: LGBT experiences in the 2011 Queensland floods. Gend Place Cult 24(1):37–51
30. Ezell JM, Griswold D, Chase EC, Carver E (2021) The blueprint of disaster: COVID-19, the flint water crisis, and unequal ecological impacts. Lancet Planet Health 5(5):e309–e315. https://doi.org/10.1016/S2542-5196(21)00076-0
31. Parashar S (2014) Marginalized by race and place: a multilevel analysis of occupational sex segregation in post-apartheid South Africa. Int J Sociol Soc Policy
32. Brandt K, Goel V, Keeler C, Bell GJ, Aiello AE, Corbie-Smith G, Wilson E, Fleischauer A, Emch M, Boyce RM (2021) SARS-CoV-2 testing in North Carolina: Racial, ethnic, and geographic disparities. Health Place 69:102576. https://doi.org/10.1016/j.healthplace.2021.102576
33. Messager ML, Ettinger AK, Murphy-Williams M, Levin PS (2021) Fine-scale assessment of inequities in inland flood vulnerability. Appl Geogr 133(6):102492. https://doi.org/10.1016/j.apgeog.2021.102492
34. Ženko M, Uležić S (2019) The unequal vulnerability of Kurdish and Azeri minorities in the case of the degradation of Lake Urmia, Iran. J Polit Ecol 26(1):167–183. https://doi.org/10.2458/V26I1.22729
35. Carroll SR, Akee R, Chung P, Cormack D, Kukutai T, Lovett R, Suina M, Rowe RK (2021) Indigenous peoples' data during COVID-19: from external to internal. Front Sociol 6:62
36. Foxworth R, Evans LE, Sanchez GR, Ellenwood C, Roybal CM (2021) I hope to hell nothing goes back to the way it was before: Covid-19, marginalization, and native nations. Perspect Polit 1–18 https://doi.org/10.1017/S1537592721001031
37. Isaac M, Elrick J (2021) How COVID-19 may alleviate the multiple marginalization of racialized migrant workers. Ethn Racial Stud 44(5):851–863
38. Abdellatif A (2021) Marginalized to double marginalized: my mutational intersectionality between the East and the West. Gend Work Organ 28:58–65
39. MacPherson EE, Phiri M, Sadalaki J, Nyongopa V, Desmond N, Mwapasa V, Lalloo DG, Seeley J, Theobald S (2020) Sex, power, marginalisation and HIV amongst young fishermen in Malawi: exploring intersecting inequalities. Soc Sci Med 266:113429
40. Meier LD (2020) An intersectional approach to the understanding of patterns of marginalisation among ex-combatants with disabilities in Sri Lanka. Confl Secur Dev 20(4):441–465
41. Pham NTT, Nong D, Sathyan AR, Garschagen M (2020) Vulnerability assessment of households to flash floods and landslides in the poor upland regions of Vietnam. Clim Risk Manag 28:100215

42. Zahra K, Zafar T, Khalid M (2016) Marginality, social exclusion, labour force participation and urban poverty: a case study of Lahore, Pakistan. The Pakistan development review, pp 521–540
43. Johnson K (2017) SAMHSA disaster technical assistance center supplemental research bulletin greater impact: how disasters affect people of low socioeconomic status. Phys Health Health Probl
44. Fothergill A, Peek LA (2004) Poverty and disasters in the United States: a review of recent sociological findings. Nat Hazards 32(1):89–110
45. Flynn J, Slovic P, Mertz CK (1994) Gender, race, and perception of environmental health risks. Risk Anal, 14(6):1101–1108
46. Pilisuk M, Parks SH, Hawkes G (1987) Public perception of technological risk. Soc Sci J, 24(4):403–413
47. Vaughan E (1995) The significance of socioeconomic and ethnic diversity for the risk communication process. Risk Anal 15(2):169–180
48. Hallegatte S, Vogt-Schilb A, Bangalore M, Rozenberg J (2016) Unbreakable: building the resilience of the poor in the face of natural disasters. World Bank Publications
49. Al-rousan TM, Rubenstein LM, Wallace RB (2014) Preparedness for natural disasters among older U.S. adults: A nationwide survey. Am J Public Health, 104(3):506–511. https://doi.org/10.2105/AJPH.2013.301559

Ensuring Biological Hazard Preparedness in Health and Safety of Construction Sector: A Framework for a Code of Practice

Ravindu Jayasekara, Lahiru Kodithuwakku, Chandana Siriwardana, Sudath Samaraweera, and Nimalka Pannila Hetti

Abstract The construction industry is considered one of the most dangerous industries due to its hazardous nature of work. Currently, the health and safety procedures in the construction industry are observed to be low in most parts of the world. The impacts of COVID-19 have extensively revealed the lack of preparedness in health and safety procedures in the industry. Even before COVID-19, dengue outbreaks have posed a significant threat to the industry. In such as a context, this study has aimed at identifying the current practices in the construction industry for enhancing the level of health and safety in construction sites for biological hazards and challenges in implementing those practices. The study has drawn on a focus group discussion considering dengue outbreaks in Sri Lanka as a case in point and a systematic literature review that consists of 21 publications on biological hazards in construction sites. According to the findings, current practices can be identified under four groups namely, hazard elimination, engineering controls, administrative controls, and personal protective equipment (PPE). In implementing these practices, the lack of guidance, inadequate compliance to safety procedures, cost implications, and breakdowns in supply of PPE act as the main challenges. Although some measures are frequently practiced in awake of COVID-19, the long-term run of those measures can pose several consequences. It highlights the need for long-term planning in regard to biological hazard preparedness in construction sites. The paper presents a framework that can be followed in developing a code of practice for biological hazard preparedness of the construction industry. The proposed framework assists policymakers in shaping up the current health and safety procedures into a sustainable stage.

R. Jayasekara · C. Siriwardana (✉)
Department of Civil Engineering, University of Moratuwa, Moratuwa, Sri Lanka
e-mail: chaasi@uom.lk

R. Jayasekara
e-mail: ravindujy@gmail.com

L. Kodithuwakku · S. Samaraweera · N. P. Hetti
National Dengue Control Unit, Ministry of Health, Mawatha, Sri Lanka

R. Dissanayake et al. (eds.), *12th International Conference on Structural Engineering and Construction Management*, Lecture Notes in Civil Engineering 266,
https://doi.org/10.1007/978-981-19-2886-4_26

Keywords Construction industry · Biological hazards · Dengue · COVID-19 · Preparedness

1 Introduction

The construction industry, though a major contributor to the development of countries, is identified as one of the most dangerous industries in the world due to hazardous working conditions inside construction sites. The likelihood of construction workers dying in workplaces is three times higher compared to other industries [1, 2]. According to the International Labour Organization (ILO), approximately one of the six fatal occupational accidents occurs in construction sites globally. Especially, in developing countries, the reported number of construction accidents and deaths associated with them is considerably high [3]. Construction activities are prone to many hazardous outcomes. Working at heights, manual handling of tools and materials, working in confined spaces, and other demolition activities are some of these hazardous activities [4]. With the complexity of construction projects, the risk in these activities has increased significantly [5]. Since the construction industry is highly labor-intensive, the impacts on the health and safety of laborers directly affect productivity, thus poses economic losses finally. Furthermore, exposure to hazardous working conditions adversely affects the socio-economic well-being of workers and their families. Therefore, maintaining health and safety in the construction industry has become challenging.

The impacts of COVID-19 on the construction industry have extensively exposed the existing poor health and safety practices inside construction sites. For instance, limited health and safety monitoring, restricted access to health services, lack of onsite welfare facilities, etc. challenged the effectiveness of measures taken to curtail the spread of the virus within construction sites [6]. In Singapore, negligence of welfare facilities for migrant workers ended up in a major outbreak of COVID-19 [7]. Even before the COVID-19 pandemic, biological outbreaks within construction sites have been problematic. For instance, construction sites are identified as a major catalyst of dengue outbreaks. Ref. [8] have pointed out construction sites as a major reason for rapidly escalating dengue outbreaks in Sri Lanka. Furthermore, in countries such as China and Singapore, dengue outbreaks that originated in construction sites have caused severely spread outbreaks [9, 10]. These impacts of biological hazards emphasized the need for enhancing the preparedness for biological hazards in health and safety practices within the construction industry. However, before COVID-19, a limited number of studies were conducted to investigate and enhance biological hazard preparedness in construction health and safety. COVID-19 became an eyeopener for both academia and practitioners from the industry.

In such as a context, this study aims at identifying the strengths and barriers in enhancing biological hazard preparedness in the construction industry. In this regard, this study addresses two research questions: (1) What are the strategies taken to prevent the impacts of biological outbreaks on construction workers? and (2) What are the barriers in implementing health and safety practices inside construction

sites?. The findings of the study formulate a comprehensive framework that can guide the policymakers and practitioners in building the preparedness of the construction industry to mitigate the impacts of biological hazards on the health and safety of construction workers.

2 Methodology

2.1 Focus Group Discussion

Since dengue outbreaks are closely associated with construction sites in topical countries even before COVID-19, Sri Lanka was selected as a case study to investigate the strategies and challenges in mitigating vector-borne biological outbreaks within construction sites. In this regard, a purposeful sampling approach was used to invite professionals who are related to the construction sector and dengue control to a focus group discussion. The participants of the focus group discussion were selected from National Dengue Control Unit [NDCU], Construction Industry Development Authority, Registrar of Pesticides, Pest Management Association, Sri Lanka, Central Environmental Authority, State Universities, and major contractors in the construction sector. A set of open-ended questions which focuses on reasons for construction sites to become major mosquito breeding places and mitigation strategies for dengue outbreaks associated with construction sites were directed to the participants during the discussion.

2.2 Systematic Literature Review on the Global Context

During this step, a systematic literature review of research publications related to biological hazards in construction sites was conducted following the Preferred Reporting Items for Systematic reviews and Meta-Analysis (PRISMA) guidelines [11]. Research articles published between 2005 and 2021 were extracted from the databases, Scopus, PubMed, and Web of Science. Publications were searched using the combination of keywords: "Construction sites" AND ("Biological hazards" OR "Epidemics" OR "Pandemics"). Peer-reviewed journal articles, book chapters, and conference proceedings that are published only in English were included in the SLR. Furthermore, literature reviews were not included in the SLR.

Two independent reviewers screened the titles and abstracts of the articles for eligibility. Articles that consist of health and safety concerns in construction sites against biological hazards were retained in the review. If an article describes the impacts of biological hazards on the construction industry but does not include any health and safety impacts, that article was excluded from the review. In extracting the data from the selected articles for full-text review, the following areas were used: author(s),

journal, year of publication, type of biological hazards, location, and key findings and limitations.

3 Results

3.1 Dengue Outbreaks Associated with Construction Sites

Sri Lanka is a tropical country located closer to the Bay of Bengal with a population of over 21 million. Since 1960s, Sri Lanka has reported hikes in dengue cases seasonally. These seasonal epidemics of dengue mostly affect areas that receive an annual rainfall of over 2500 mm [12]. According to [13], dengue control activities and hospitalization in Sri Lanka cost around US$3.45 million in the year 2012.

The worst dengue outbreak was experienced in 2017, and the number of dengue-positive cases crossed the 180,000 limit within the year [8, 14]. Recent studies carried out in the country have highlighted construction sites as a major reason for the rapidly increasing number of dengue cases [15]. For instance, a recent assessment done by the Epidemiology Unit of Sri Lanka has revealed potential mosquito breeding places were found in around 70% of construction sites in the country [14].

According to the focus group discussion, three major reasons were identified for the dengue outbreaks associated with construction sites in Sri Lanka. Improper management of water collection areas is one of the major reasons identified during the discussion. Professionals have highlighted that there can be various places in construction sites where water can stagnate easily. For example, uneven slabs, tanks used for curing concrete test cubes, water pools for curing, etc. can easily become breeding places for mosquitos. A limited attention has been paid to these places within construction sites. Furthermore, construction sites discard several items such as construction materials, demolished building parts, and old equipment frequently. However, improper practices followed during discarding these items have created more mosquito breeding places within construction sites. For example, empty containers of paints, polythene packages, etc. are not properly disposed by construction workers. These items easily provide mosquitos with breeding places during rainy seasons.

In addition to the presence of water stagnating places, the lack of monitoring activities has become another major issue. According to the discussion, most of the construction sites do not have a designated officer with the responsibility to inspect, identify, and eliminate mosquito breeding places in construction sites. In most cases, construction authorities have neglected the importance of such activities for vector surveillance within the premises. Since most of the activities which cause water stagnation, such as concrete curing, cannot be stopped, proper monitoring is paramount in stopping those places from turning into mosquito breeding places.

Furthermore, the findings of the focus group discussion have outlined the most suitable mitigation strategies to prevent construction sites from becoming major

breeders of mosquitos. According to the findings, the appointment of trained health and safety officers in vector surveillance plays a key role in dengue prevention practices. Furthermore, the presence of a designated team for regular inspection within construction sites was also identified as an important measure that should be taken at the management level of construction sites. The establishment of a regular reporting system is also paramount as a measure of administrative control to prevent mosquito breeding inside construction premises. In addition to these administrative controls, larvicides can be made available within the site as a biological control measure. In this regard, a sound legal basis is required to work with harmful substances. Since regular inspection and evaluation by both internal and external parties are important, public health inspectors can be authorized to inspect construction sites for possible mosquito breeding places.

3.2 Global Perspective of Biological Hazards in Construction Sites

Figure 1 illustrates the process followed during the SLR for identification, screening, and selection of publications for the review. At the initial stage, 83 articles were identified from the above-mentioned three databases. Thirteen (13) duplicated articles were eliminated initially. Title and abstract screening were performed on 70 articles, and 24 articles were retained for full-text analysis. Finally, 21 articles were included in the data analysis.

3.2.1 Descriptive Analysis of Literature

According to publications included in the systematic literature review, the attention toward biological hazards in construction sites has significantly increased after the occurrence of COVID-19. Out of 21 articles included in the SLR, 15 articles focus on the impacts of COVID-19, while 4 articles were on dengue and 2 articles were on HIV. Figure 2 presents a map created by VOS viewer open-source software based on terms selected from titles and abstracts of selected publications for analysis. In this map, the terms which have been mentioned more than 10 times are included and the size of the nodes is decided based on the number of occurrences. According to the analysis, there are four clusters as shown in Table 1.

It is evident that COVID is the most occurred term in titles and abstracts of the selected publications. Furthermore, the links between the terms ‘COVID’ and ‘construction site,’ ‘COVID’ and ‘measure,’ and ‘construction site’ and ‘community’ are observed stronger.

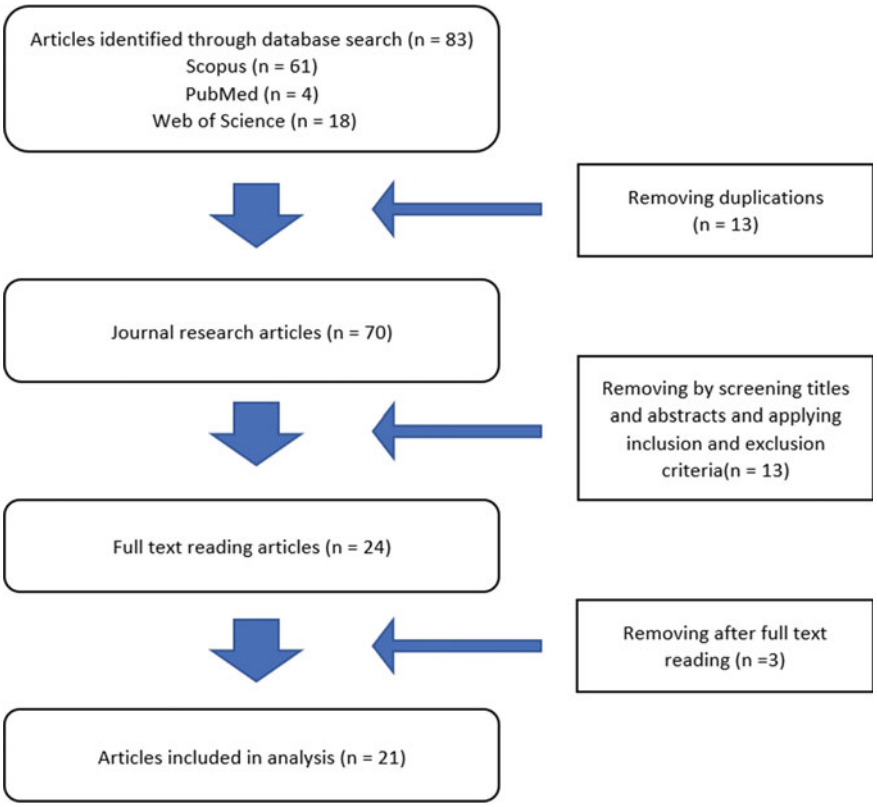

Fig. 1 Process of selecting literature for the review

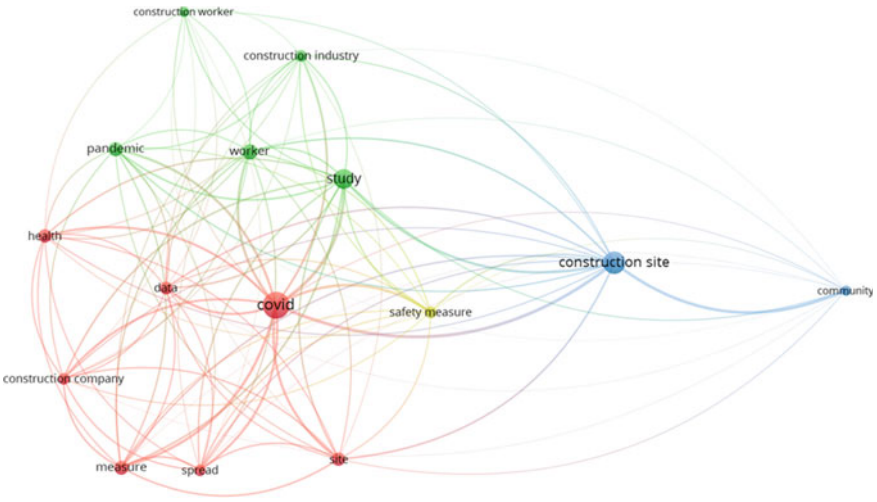

Fig. 2 Network of terms extracted from titles and abstracts

Table 1 Details of identified clusters

Cluster No.	Terms
01	COVID, health, construction company, measure, site, spread, health, data
02	Pandemic, worker, construction industry, construction worker
03	Construction site and community
04	Safety measure

3.2.2 Measures Taken to Prevent the Impacts of Biological Hazards

This section discusses the identified measures against biological hazards within construction sites, during the SLR. The identified measures were categorized into elimination, engineering controls, administrative controls, and personal protective equipment (PPE) [16].

Steps of actions	Practices implemented under each step
Elimination	Activities that are considered under the elimination, focus on removing the exposure to the hazard completely within the construction site. During the COVID-19 pandemic, most of the construction companies have suspended activities that are non-critical and reduced the possibility of the virus entering the site until COVID curves flattened [17]. Furthermore, some companies have moved for work from strategies for the management staff of the construction projects and used techniques such as virtual project meetings, etc. In regard to eliminating the risk of vector-borne diseases, construction authorities have taken measures to minimize the potential mosquito breeding sites within the construction premises [9].
Engineering controls	Engineering controls can be identified as the activities which isolate persons from the hazard by physical or mechanical means. In regard to the risk of COVID-19 in construction sites, authorities have initially taken measures for disinfecting surfaces, objects, and equipment when someone uses them [17]. Furthermore, several measures such as ventilation, outdoor air supply, and air filters were taken to mitigate the risk of spreading the virus within the construction site [18]. In some cases, extra elevators, walking ways, etc. have been established within construction sites [19]. Furthermore, measures have been taken to alter the sitting arrangements inside gathering areas to prevent unnecessary exposure to the virus [20]. When vaccines were introduced, tailored programs and practices were expanded for vaccination among the construction workers [21]. In regard to vector-borne disease outbreaks, construction authorities have looked into hiring pest controlling services to reduce the presence of mosquitoes breeding including fogging and larviciding [22].

(continued)

(continued)

Steps of actions	Practices implemented under each step
Administrative controls	Administrative controls are the changes that have been done in work procedures to prevent biological hazards. Identified administrative controls were categorized under a few sections, named access control, health monitoring, workforce management, personal hygiene, information management, and housekeeping. *Access control* Access to construction sites was controlled through various practices. In some cases, access was limited to a pre-identified set of workers. Furthermore, unauthorized access to construction sites was restricted at the entrance [18, 23]. *Health monitoring* Construction authorities have taken measures to monitor symptoms among all the workers at the site for early case detection. These measures were practiced during both COVID-19 and dengue outbreaks in sites [24–26]. Based on these inspections, workers who fell ill were sent for self-isolation [23]. In addition to these measures, construction authorities have taken measures to monitor the mental health aspects of workers and take necessary actions accordingly [18]. *Workforce management*

(continued)

(continued)

Steps of actions	Practices implemented under each step
	Construction authorities have taken several measures in regard to managing the workforce within the sites to curb the spread of the viruses. Avoiding the clusters of workers is the main objective of these measures [27]. In this regard, daily tasks and activities have been assessed to assess of the risk of exposure to the virus during COVID-19 [18]. Contractors have reduced the number of workers allocated for project activities [27]. In some case a concept named one worker per one work has been introduced [19]. In addition to reducing the likelihood of virus spreading, having a fewer number of workers have minimized the work overlaps and non-productive time [20]. Furthermore, construction workers have been clustered into different groups and practiced the concept of bio-bubble. Within these groups, compliance to health and safety guidelines was monitored frequently during the COVID-19 outbreak [17, 19]. The use of shifted work hours is another strategy used by construction authorities during COVID-19. In relation to shifting work hours, authorities have conducted forward planning of project activities incorporating work sequencing [20]. Findings have highlighted that workforce management practices have immensely contributed to mitigating the virus spread. *Hygiene measures* Enhancing worker hygiene was noticeable in both COVID-19 and dengue outbreaks. For instance, hygiene measures such as handwashing and social distancing were promoted within construction sites [10, 24, 25]. And also, workers were educated on maintaining personal hygiene. In parallel to educating workers on personal hygiene, they were provided with facilities such as sanitizers [28]. *Awareness-raising* Lack of awareness among construction workers was a major reason for their low level of compliance to health and safety procedures. Therefore, during the COVID-19 pandemic, awareness-raising measures were taken to assist workers to understand reasons for worksite closure, physical distancing, and limiting the number of persons in elevators, accommodations, etc. [21]. In addition to the practices established during the COVID-19 pandemic, awareness-raising was conducted among workers for biological hazards such as HIV and dengue as well [29–31]. In regard to awareness-raising, construction authorities have used signboards, infographics, videos, safety meetings, messenger groups, etc. [28]. However, there was the need to constantly remind and re-educate construction workers [20]. *Information management* Monitoring the health of workers constantly is not enough alone. Therefore, construction authorities have practiced effective reporting and record-keeping measures. It has enabled the authorities to keep up with the health status of employees and take necessary actions promptly [27]. *Housekeeping* Housekeeping practices in construction sites can enhance the tidiness within the site. Especially, tidiness is important in battling vector-borne outbreaks [9]. Therefore, frequent monitoring and inspections are needed in keeping the workplace tidy. For instance, having fewer materials within the site makes walkways and working areas clear. Increased space within the workplace assists the practice of social distancing measures to curtail the spread of respiratory viruses. In addition to workplace tidiness, authorities should aim at environmental management within the adjacent communities to construction sites as well [10].
PPE	Personal protective equipment (PPEs) are worn by workers to protect themselves from hazards. In regard to the prevention of COVID-19 risks, wearing face masks and hand gloves/face shields were more frequently observed within construction sites. In addition to those measures, mosquito repellents are used by construction workers to avoid mosquito biting [32].

3.2.3 Barriers in Implementing Health and Safety Measures

During the COVID-19 pandemic, maintaining the health and safety procedures inside construction sites and labor accommodations was one of the major challenges. Specially, adhering to health regulations for reopening construction sites was challenging [33]. After reopening construction sites, respective authorities were supposed to conduct risk assessments both within and outside the sites. However, implementing risk assessment practices have posed financial implications on construction cost [27]. And also, the cost of implementing COVID-19 safety measures has aggravated the issues related to budgets of construction projects [24, 25]. Furthermore, officials have complained that additional planning for reopening construction sites has been time-consuming. Since additional planning is time-consuming and it will increase the time of construction activities, construction projects may take a longer period to be completed [20]. Furthermore, issues have been identified due to the lack of clarity in policies and guidelines published by governments in regard to aspects such as communicating with health officials, information to share, and what guidelines to follow [20, 33].

Furthermore, due to the nature of construction activities, consistently maintaining physical distance has been difficult and challenging [33]. According to construction professionals, practicing social distancing in construction activities can cause a reduction in productivity. And also, sharing tools during construction activities has become challenging while adhering to safety procedures [27]. Lack of compliance among construction workers to COVID-19 guidelines can be identified as another major reason for the difficulties in maintaining social distance within construction sites. Furthermore, construction workers are not adequately aware of COVID-19 and safety measures. And also construction authorities have faced the challenges of educating construction workers on COVID-19 measures. Therefore, officers had to remind the workers more often to adhere to safety guidelines [24, 25, 27, 28].

Attitudes of construction workers have been observed as another challenge during the COVID-19 pandemic. For instance, workers have deliberately supplied wrong information on their symptoms, travel history, etc. [24, 25, 27]. Even before COVID-19, the level of hygiene practices among construction workers was observed considerably low in both working areas and labor accommodations. Furthermore, several issues related to PPE for construction workers also posed challenges to the implementation of safety measures. In most cases, contractors have supplied PPE which are not up to the standards [28]. Furthermore, the number of supplied PPE has been not adequate for all the employees within the sites. In some cases, employers have complained that it is uncomfortable to use PPE while working and it affects their performance [27]. Furthermore, there have been incidents related to the theft of PPE during the pandemic.

4 Discussion

This study has aimed at investigating the impacts and challenges related to the health and safety of employers in preparing and responding to biological hazards inside construction sites by combining findings from the focus group discussion and a systematic literature review on biological hazards in construction sites. The literature review suggests that COVID-19 was an eyeopener for academia, construction professionals, and policymakers to explore biological hazard preparedness in construction sites. It has called for the need for incorporating aspects of biological hazard guidelines into health and safety policies and regulations in the construction sector. In this regard, recommendations made by international institutions such as Occupational Safety and Health Administration (OSHA) and World Health Organization (WHO) are incorporated by the relevant authorities [34, 35].

Illustrating on the guidelines published by national-level authorities, in Sri Lanka, Construction Industry Development Authority recently published a guideline on preparing construction sites for COVID-19 and dengue outbreaks [36]. Even before COVID-19, the National Dengue Control Unit of Sri Lanka in collaboration with one of the leading construction companies in Sri Lanka published a guideline for strengthening construction industry to prevent dengue [37]. National Dengue Control Plan in Sri Lanka also addresses the aspects of dengue prevention in construction sites [38]. In Sri Lanka, several other legal actions have also been carried out in order to mitigate dengue outbreaks associated with construction sites. For instance, Registrar of Pesticides has liberalized four larvicides that can be used for dengue controlling. Elaborating on the global context, the Land Transport Authority (LTA), Singapore, has published a guideline on vector control at sites under the LTA [39].

Recent studies highlight that controlled site access, handling of COVID-19 cases, induction, screening, and social distancing are frequently carried out by a majority of companies [24, 25]. Although social distancing is frequently practiced, the findings of the review highlighted that it could reduce work performance and productivity. Since the long-term reduction in productivity can cause high construction costs, authorities should pay attention to workforce management strategies that can combine the needs of both social distancing and productivity. Furthermore, wearing PPE, sick leaves, sanitization, risk assessment, and clustering of workers are followed rarely by companies [24, 25]. As revealed by findings, the high costs of implementing those measures can be the main reasons for having only a few companies that practiced those measures. Although these measures are not practiced, it is the role of construction professionals to make sure the risk assessment processes are conducted to prepare the construction site for possible health and safety impacts of biological hazards.

During the focus group discussion also, it was identified that risk assessment procedures are paramount in battling the impacts of dengue outbreaks and other vector-borne diseases. For instance, it is necessary to frequently inspect construction sites and adjacent communities for possible mosquito breeding places and assess the risk of impending outbreaks. The preparedness of construction organizations in risk

assessments consists of several steps. For instance, risk assessment plans should be approved before the commencement of work. Furthermore, the required resources for health and safety procedures should be pre-planned. And also, it is the duty of construction officials to ensure the adequate supply of required resources after activities are commenced. The health and safety officers of construction projects should be vested with the responsibility of ensuring the smooth functioning of construction activities without any health and safety issues. Moreover, compliance has become a severe challenge in adhering to health and safety regulations and guidelines. For ensuring compliance at the management level of companies, governments must develop legal policies for the enforcement of safety rules and regulations. At the level of employees, it is required to change the attitudes of employees, educate them on health and safety procedures, and closely monitor compliance.

Considering the above-identified factors, a framework was developed to initiate a code of practice for biological hazard preparedness in construction sites as shown in Table 2.

Table 2 Framework for developing the code of practice

Main element	Content consideration
Risk assessment strategies	Disease surveillance Vulnerability assessments Capacity development
Administrative support	Standard operating procedures (SOPs) Funding Staff Equipment Workforce management
Legislative enactments	Health and safety rules Environmental regulations Policies at the local government level
Education and training	Education on the risk of biological hazards Training on disease prevention practices (social distancing, use of PPE, etc.) Awareness-raising for emergency response Personal hygiene Health promotion and empowerment
Emergency response	Isolation facilities Emergency medical facilities Contingency plans
Review and evaluation	Reporting and feedback systems Periodic reviews Inspections in both site and adjacent community

5 Conclusion

This paper has made an attempt to investigate the current practices for responding to biological hazards inside construction sites and barriers in implementing those practices. The study has drawn on a focus group discussion that considered dengue outbreaks in Sri Lanka as a case in point and a systematic literature review on biological hazard impacts on construction sites. According to the findings, construction industry should pay more attention in regard to ensuring preparedness in health and safety aspects of the construction industry for biological hazards. COVID-19 became a new experience for the practitioners, and although several measures have been implemented, those measures lack durability and stability in the long-term run. Therefore, more attention should be paid to planning the preparedness and response activities for the conditions beyond the present pandemic, COVID-19. Even without the presence of COVID-19, disease outbreaks such as dengue have been a major challenge to the construction industry. Therefore, this paper presents a framework to be used in developing a code of practice for biological hazard preparedness in the construction industry.

Only a holistic view of health and safety aspects inside construction sites is considered during this study. Therefore, in developing the code of practice, there is a need for investigating the main elements of the frameworks deeper to capture specific points under each activity. Since findings have highlighted that short-term strategies can cause losses in the long-term run, it is required to study the long-term impacts of these strategies taken at the present and evaluate their feasibility. Last but not least, the involvement of governing structures of the country is also needed in proceeding with the development of the code of conduct since the possibilities in terms of legal and policy aspects are paramount in implementing these preparedness practices.

References

1. Pinto A, Nunes IL, Ribeiro RA (2011) Occupational risk assessment in construction industry—overview and reflection. Saf Sci
2. Sherratt F, Farrell P, Noble R (2013) UK construction site safety: discourses of enforcement and engagement. Constr Manag Econ 31(6):623–635
3. Durdyev S, Mohamed S, Leang Lay M, Ismail S (2017) Key factors affecting construction safety performance in developing countries: evidence from Cambodia. Constr Econ Build 17(4):48–65
4. Appaih SO (2019) Working conditions and exposure to work related injuries and accidents at Kokompe-Accra Ghana. Ghana J Geogr 11(2):52–76
5. Anfas MM, Indunil LD, Seneviratne P, Abeydeera LHU (2017) Reducing accidents in large construction projects in Sri Lanka. In: The 6th world construction symposium 2017: what's new and what's next in the built environment sustainability agenda? Colombo, Sri Lanka, pp 360–366
6. Chigara B, Moyo T (2021) Factors affecting the delivery of optimum health and safety on construction projects during the covid-19 pandemic in Zimbabwe. J Eng, Des Technol, ahead-of-p (ahead-of-print)

7. Koh D (2020) Migrant workers and COVID-19. Occup Environ Med 77(9):634–636
8. Jayarajah U, Faizer S, De Zoysa IM, Seneviratne SL (2017) A large dengue epidemic affects Sri Lanka In 2017. Int J Progressive Sci Technol (IJPSAT) 6(01):84–86
9. Liang S, Hapuarachchi HC, Rajarethinam J, Koo C, Tang C-S, Chong C-S, Ng L-C, Yap G (2018) Construction sites as an important driver of dengue transmission: implications for disease control. BMC Infect Dis 18(1):382
10. Liu X, Zhang M, Cheng Q, Zhang Y, Ye G, Huang X, Zhao Z, Rui J, Hu Q, Frutos R, Chen T, Song T, Kang M (2021) Dengue fever transmission between a construction site and its surrounding communities in China. Parasit Vectors 14(1):22
11. Moher D, Liberati A, Tetzlaff J, Altman DG (2009) Preferred reporting items for systematic reviews and meta-analyses: the PRISMA statement. BMJ 339
12. Tissera HA, Jayamanne BDW, Raut R, Janaki SMD, Tozan Y, Samaraweera PC, Liyanage P, Ghouse A, Rodrigo C, de Silva AM, Fernando SD (2020) Severe Dengue Epidemic, Sri Lanka, 2017. Emerg Infect Dis 26(4):682–691
13. Thalagala N, Tissera H, Palihawadana P, Amarasinghe A, Ambagahawita A, Wilder-Smith A (2016) Costs of Dengue control activities and hospitalizations in the public health sector during an Epidemic year in Urban Sri Lanka. PLoS Negl Trop Dis 10(2):e0004466
14. Epidemiology Unit (2021) Dengue trends [online]. Available from: http://www.epid.gov.lk/web/index.php?option=com_casesanddeaths&Itemid=448&lang=en [Accessed 25 Mar 2021]
15. Perera UTG, Chandrasekara CMKNK (2018) Spatial dimension of the Dengue Epidemic in relation to age and gender in Kolonnawa Area, Sri Lanka. Sri Lanka J Popul Stud 18(19):55–65
16. NIOSH (2020) Hierarchy of controls|NIOSH|CDC[online]. The national institute for occupational safety and health. Available from: https://www.cdc.gov/niosh/topics/hierarchy/default.html [Accessed 13 Nov 2020]
17. Olanrewaju A, AbdulAziz A, Preece CN, Shobowale K (2021) Evaluation of measures to prevent the spread of COVID-19 on the construction sites. Cleaner Eng Technol 5:100277
18. Bou Hatoum M, Faisal A, Nassereddine H, Sarvari H (2021) Analysis of COVID-19 concerns raised by the construction workforce and development of mitigation practices. Front Built Environ 7:66
19. Iqbal M, Ahmad N, Waqas M, Abrar M (2021) COVID-19 pandemic and construction industry: impacts, emerging construction safety practices, and proposed crisis management. Braz J Oper Prod Manage 18(2):1–17
20. Jones W, Gibb AGF, Chow V (2021) Adapting to COVID-19 on construction sites: what are the lessons for long-term improvements in safety and worker effectiveness? J Eng, Des Technol, ahead-of-p (ahead-of-print)
21. Bushman D, Sekaran J, Jeffery N, Rath C, Ackelsberg J, Weiss D, Wu W, Van Oss K, Johnston K, Huang J, Khatun U, Sheikh T, Sutcliff J, Tsoi B (2021) Coronavirus disease 2019 (COVID-19) outbreaks at 2 construction sites-New York city, October–November 2020. Clin Infect Dis: Official Publ Infect Dis Soc Am 73(Suppl 1):S81–S83
22. Hamidun S, Shafie F, Ishak A, Dom N (2021) Distribution and abundance of Aedes Mosquito breeding sites at construction site workers hostel in Gelang Patah, Johor, Malaysia. Serangga 26(3):57–68
23. Salami BA, Ajayi SO, Oyegoke AS (2021) Coping with the Covid-19 pandemic: an exploration of the strategies adopted by construction firms. J Eng, Des Technol, ahead-of-p (ahead-of-print)
24. Simpeh F, Amoah C (2021) COVID-19 guidelines incorporated in the health and safety management policies of construction firms. J Eng, Des Technol, ahead-of-p (ahead-of-print)
25. Simpeh F, Bamfo-Agyei E, Amoah C (2021) Barriers to the implementation of COVID-19 safety regulations: insight from Ghanaian construction sites. J Eng, Des Technol, ahead-of-p (ahead-of-print)
26. Zhou Y, Zhang Z, Wang B, Ren G, Qi H, Wang X (2020) Construction time, cost and testing data of a prefabricated isolation medical unit for COVID-19. Data Brief 32:106068
27. Kukoyi PO, Simpeh F, Adebowale OJ, Agumba JN (2021) Managing the risk and challenges of COVID-19 on construction sites in Lagos, Nigeria. J Eng, Des Technol, ahead-of-p (ahead-of-print)

28. Amoah C, Simpeh F (2021) Implementation challenges of COVID-19 safety measures at construction sites in South Africa. J Facil Manag 19(01):111–128
29. Bowen P, Govender R, Edwards P, Cattell K (2015) HIV testing of construction workers in the Western Cape, South Africa. AIDS Care 27(9):1150–1155
30. Qu B, Guo H, Sun G, Zuo T, Zhang Y, Li BY (2008) HIV/AIDS knowledge, attitudes, and behaviors of construction workers in China. Int J Biomed Sci: IJBS 4(3):192–195
31. Seet RCS, Ooi EE, Wong HB, Paton NI (2005) An outbreak of primary dengue infection among migrant Chinese workers in Singapore characterized by prominent gastrointestinal symptoms and a high proportion of symptomatic cases. J Clin Virol 33(4):336–340
32. Niroshana N, Siriwardana C, Jayasekara R The impact of COVID-19 on the construction industry and lessons learned: a case of Sri Lanka. Int J Constr Manage 1–18. https://doi.org/10.1080/15623599.2022.2076016
33. Hilary OO, Nor' Aini Y, Ahmad SH (2021) Perceived COVID-19 safety risk and safety behavior on construction sites: role of safety climate and firm size. J Constr Eng Manag 147(11):4021153
34. OSHA (2020) COVID-19—control and prevention—construction work [online]. Occupational safety and health administration. Available from: https://www.osha.gov/coronavirus/control-prevention/construction [Accessed 9 Jan 2021]
35. WHO (2020) Getting your workplace ready for COVID-19 [online]. Available from: https://www.who.int/docs/default-source/coronaviruse/getting-workplace-ready-for-covid-19.pdf [Accessed 21 Nov 2021]
36. CIDA (2020) Health and immunity enhancement guidelines for COVID-19 and dengue [online]. Construction industry development authority. Available from: https://www.cida.gov.lk/newsevents/CIDA COVID and DEGUE guidelines for construction industry version 3(Revised).pdf [Accessed 21 Dec 2020]
37. National Dengue Control Unit (2019a) Strenthening environmental management in construction industry to prevent Dengue
38. National Dengue Control Unit (2019b) National action plan on prevention and control of Dengue 2019–2023, Sri Lanka. Colombo, Sri Lanka: Ministry of Health Nutrition and Medicine Indigenous
39. Land Transport Authority (2019) Vector control at LTA sites. Singapore: Land Transport Authority

Social Network Analysis-Based Approach to Investigate the Network of Risk and Crisis Communication of Government Agencies During Early Stages of COVID-19 in Sri Lanka

K. K. C. L. Kannangara, C. S. A. Siriwardana, and H. A. D. G. S. Jayathilaka

Abstract Effective communication and coordination between government agencies and the general public are important to manage disaster risks and mitigate the risks involved to the public. The main objectives of developing awareness, sending information to the public on time and facilitating swift community responses can be achieved by adopting social media platforms blended with existing communication mechanisms. At present, many government agencies and government officials use social media platforms as one of the leading information dissemination mechanisms. This study was conducted by means of a case study, considering the information dissemination through official Facebook pages maintained by health authorities during the outbreak of the COVID-19 pandemic in Sri Lanka. Primary data were collected through the "Health Promotion Bureau" (HPB) Facebook page, the official page dedicated to sharing health-related information with the community. The social network analysis considered changes in the content at the different stages of the pandemic, languages and the different interfaces used to disseminate information. The number of shares was regarded as active participation, which implies the engagements of followers. Two interaction networks were developed to identify the trends and patterns in information dissemination via social media. Further, this study focussed on the influence of pandemic situations on the HPB page followers' interaction through statistical analysis. Derived interaction networks for different languages showed that posts related to pandemic behaviour and COVID-19 symptoms, etc., have low centrality value. Similarly, the interface interaction network revealed that HPB had used a standard method of reporting particular information like situational updates of COVID-19 in terms of interface. Statistical analysis on the number of shares for different interfaces revealed that the posts with text and image have a higher possibility of sharing by a Facebook user. Quantitative analysis shows that users are sensitive to daily COVID-19 positive cases, although the initial interaction for the HPB's page was reduced. Users tend to share the daily COVID-19 report

K. K. C. L. Kannangara (✉) · C. S. A. Siriwardana · H. A. D. G. S. Jayathilaka
Department of Civil Engineering, University of Moratuwa, Moratuwa, Sri Lanka
e-mail: chamikakannangara@gmail.com

R. Dissanayake et al. (eds.), *12th International Conference on Structural Engineering and Construction Management*, Lecture Notes in Civil Engineering 266,
https://doi.org/10.1007/978-981-19-2886-4_27

posted by the page whenever a cluster was identified, as it leads to an increment in the rate of reporting infected cases.

Keywords Communication · COVID-19 · Social media · Social network analysis

1 Introduction to Disaster Profile of Sri Lanka

A disaster is a significant disruption of the functioning of a community or society at any level due to hazardous events that interfere with exposure, vulnerability and capability, resulting in losses and damages on lives, properties and economic and environmental factors. Sri Lanka has faced several natural and man-made hazardous events and their subsequent disasters, which have made a catastrophic impact on human lives and properties [1, 2]. Floods, landslides, cyclones, droughts, lightning strikes, coastal erosion and epidemics are significant natural hazards that have caused adverse impacts on Sri Lanka [3]. Localised and seasonal floods and associated landslides are the common hazards that have been reported in Sri Lanka. At the same time, droughts, cyclones and tsunamis are other hazards occurring less frequently but causing considerable damage [4]. The highest and most crucial impact has happened in Sri Lanka due to the 2004 Indian Ocean tsunami, which is considered one of the infrequent hazards in Sri Lanka. It shattered the lives of more than one million people and caused much damage to the infrastructure in the coastal belt [5]. Vector-borne epidemics like dengue and influenza have also been reported over the country, and recently, Sri Lanka has been seriously affected by the global pandemic of COVID-19.

1.1 The Early Stage of the Outbreak of COVID-19 in Sri Lanka

COVID-19 is a global pandemic that was declared officially by the World Health Organization (WHO) on 11th March 2020 [6]. Sri Lanka was not severely affected at the early stage of the pandemic due to lockdown and other health measures, controlling caseload and mortality (13 deaths as of October 2020) [7]. In Sri Lanka, first local case was recorded on 11th March 2020. By the end of March 2020, a total of 122 confirmed cases were recorded, with two deaths. By the end of the surveyed period of this study (25th October 2020), a cumulative number of COVID-19 cases were recorded as 7521, with 15 deaths (epid.gov, 2020).

2 Disaster Risk Management and Communication

According to the UNDRR terminology, disaster risk management implements disaster risk reduction policies and techniques to avoid new disaster risk, minimise existing disaster risk and mitigate residual risk while increasing resilience and minimising disaster losses (UNDRR). Communication can be introduced as a key component of disaster risk management because it has a high potential to minimise the damage caused by disasters [8]. Communication improved the perceptions of the community about disaster risk and affected their behaviour in terms of disaster preparedness and disaster response [9].

In the context of Sri Lanka, the leading agency for disaster management is the Disaster Management Centre (DMC). It is mandated to implement and coordinate national and sub-national level disaster risk reduction programmes with the participation of all related stakeholders. Disaster Management Centre (DMC) disseminates disaster risk information to the general community under three levels: national level, provincial/district level and divisional secretariat/village level. Various communication channels such as television, radio, early warning towers, police and military communication systems, SMS alerts and telephone calls are used by the DMC to disseminate disaster risk information to the national and district levels. At the divisional secretariat/village level, DMC has used telephones, police vehicles for announcements, sirens, temple and church bells and messengers [10]. Table 1 provides examples of conventional, contemporary or digital communication channels that can be used for communication in disasters [11–15].

2.1 Social Media for Disaster Communication

Besides the conventional communication modes such as traditional media, communication in disasters has been increasingly taking place via social media due to the timely and interactive communication of user-generated content. Traditional media primarily facilitate one-way information dissemination, while social media creates two-way communication opportunities among organisations, the public and individuals. Traditional media primarily facilitate one-way information dissemination, while social media can create opportunities for two-way communication for users

Table 1 Communication channels

Conventional communication channels	Modern communication channels
Television, radio, newspaper	Social media
Tone alert, radio sirens	Mobile apps
Conversation between two people (by person)	Alert messages
Disseminating warning messages from a vehicle-mounted with a loudspeaker	Internet via Web platforms

because both content creators and consumers in conventional media can disseminate information via social media [16]. Multi-directional communication mechanisms, facility to use different interfaces to share information, the convenience of using social media and other options like safety checks etc. can be identified as major reasons for increasing use of social media for disaster communication [17–21].

2.2 Global Use of Social Media in Disasters

Several kinds of research have been carried out during the past years that illustrate social media's critical role in various disaster situations. Table 2 presents the use of social media in multiple disasters worldwide.

2.3 Infectious Disease Outbreak and Social Media Usage

Social media has been studied in the field of public health research for early detection of epidemic outbreaks as part of the Web surveillance system and to predict infectious disease outbreaks [39]. Most of these studies were conducted after an infectious disease, such as Ebola, H1N1, SARS COV and MERS, occurred in the previous decades. Ref. [40] showed when high-quality epidemic information is available at the early stages of pandemics, social media can make a community more sensitive to external drivers, increasing the public's awareness of infection risk, which is beneficial for epidemic containment. However, studies reveal that these popular and trending topics can become less important with time. It was identified that meeting social media users' expectations through relevant information is the key to survival in the online environment during an epidemic [41, 42]. Further, many studies have investigated the effect of spreading fake news and rumours via social media, highlighting the impact on social and cognitive behaviours of communities such as developing vaccine hesitancy [43, 44]. Furthermore, with the prevailing situation of global pandemic COVID-19, several studies have focussed on using social media platforms by government agencies in different countries. Among these studies, an analysis of Canadian agencies' social media accounts revealed that very few agencies had used videos as an interface to circulate important information via social media [45]. Additionally, government agencies' use of social media has ensured data transparency while enhancing communities' trust within the pandemic [46]. Also, survey results revealed that social media users had about three times more likely to follow the health rules than others [47]. This background highlights both positive and negative impacts of using social media for risk and crisis communication during a pandemic, emphasising the potential opportunity and the measures to minimise fake news circulation via social media.

Table 2 Social media usage in disasters in the global context

Disaster event	Year	Used social media	Country	Reference
Earthquake	2011	Twitter	Japan (Tohoku earthquake)	[22] [23]
	2010	Twitter	Haiti (Haiti earthquake)	[24] [25]
Flood	2010/11	Facebook	Australia (Victoria and Queensland)	[26]
	2015	Facebook WhatsApp	India (Chennai Floods)	[27]
Hurricane	2013	Twitter	Philippine (Typhoon Haiyan)	[21]
	2017	Facebook Twitter	USA (Hurricanes Harvey and Irma)	[28]
Tsunami	2011	Twitter	Japan (Great East Japan Tsunami)	[29] [30]
Volcano Eruption	2010	Twitter Facebook	Indonesia (Mount Merapi Eruption)	[31]
	2017	Twitter Facebook	Iceland (Eyjafjallajökull Volcano Eruption)	[32]
Wildfire	2007	Blogs, Forum, Flickr, Twitter	USA (Southern California Wildfire)	[33]
	2009	Twitter	USA (Oklahoma Fire)	[34]
Droughts	2014	Facebook Twitter YouTube	California–USA	[15]
	2012/13	Twitter	USA (Drought in Nebraska)	[35]
Terrorism	2005	Flickr Photo sharing sites	UK (2007 suicide bomb attack)	[36]
	2008	Twitter Flickr	India (Mumbai Terrorist Attack)	[37]
Violent crises	2010/11	Microblog (Twitter)	USA Johns Hopkins University Hospital shooting	[38]
	2012	Twitter	USA (Seattle Café Shooting)	[37]

2.4 Usage of Social Media for Disaster Communication in Sri Lanka

During the flood in Sri Lanka in May 2016, social media was the main source of communication, and Facebook was the most popular social media platform. Past

studies have been done to identify the gaps in using social media for disaster communication in Sri Lanka. These studies reveal that age and users' experience play an important role in using social media as a disaster communication tool. Further, it highlights the importance of improving the timeliness dissemination of accurate information via social media through technical agencies, which was identified as one of the major demands of Sri Lankan communities [48]. Considering the COVID-19 pandemic situation in Sri Lanka, social media has played a vital role in disseminating the risk information and updates about the COVID-19 pandemic to the general public. Many Facebook pages, Facebook groups and WhatsApp groups have been created to share COVID-19 information by the various stakeholders such as news media, community groups, influencers and researchers. With that, it provides a prospect to assess the role of government agencies authorised in disseminating information to the public. Therefore, this study is aimed to examine the use of social media platforms for risk and crisis communication by government agencies of Sri Lanka during the early stage of the COVID-19 pandemic.

3 Research Methodology

3.1 Data Collection

"Health promotion Bureau" is the official Facebook page dedicated to reporting health-related issues in Sri Lanka, with more than 400,000 followers. Therefore, primary data for the survey was collected from the "Health Promotion Bureau" (HPB) Facebook page. Data collection was limited from December 2019 to October 2020, the early stage of the COVID-19 outbreaks in Sri Lanka. Table 3 summarises the data collection phases of the study with the relevant stage of the pandemic. HPB had shared various contents within the page, and most importantly, the content was varied with the phase of the pandemic. Moreover, the language and interface used to report the content are other key aspects investigated within this study. Further, the interaction of HPB followers was measured in terms of the post share count as sharing option provides users to circulate the content HPB reported. A total of 420 posts were recorded within the surveyed period posted by the HPB page.

Table 3 Data collection duration and pandemic phase

	Data collection period	Phase of the pandemic
1st phase	From December 2019 up to 1st July 2020	First wave
2nd phase	From 1st July up to 3rd October 2020	Intermediate time between the first wave and second wave
3rd phase	From 3rd October up to 25th October 2020	Second wave

Table 4 Data collection

Data type	Purpose
Time	To investigate the content HPB shared during different phases of the pandemic and its effectiveness
Content	Key information that HPB shared with the public and to categorise them into thematic areas to identify the patterns of sharing information
Language	To identify and analyse the effectiveness of language usage while addressing diverse communities in Sri Lanka
Interface	To identify the most effective interface that can be used to share information through Facebook. (i.e. image only, image with text, text only, video only or video with text)

The following table summarised the data collected through the HPB page and its purpose in data analysis (Table 4).

3.2 Social Network Analysis (SNA) and Regression Model

First of all, according to the content that HPB shared within the page, themes were generated through an inductive approach. Under the generated themes, user interactions were statistically organised to identify the trends and effectiveness of using different interfaces in posting COVID-19-related information through the HPB page. Then, a network was derived from visualising different interfaces encountering the language usage of posts reporting identified themes. In order to determine the influence of situational information such as newly infected cases and deaths on the HPB post reach, a correlation analysis was conducted. Since the situational update posts reported on the HPB page contained information regarding daily COVID-19 new cases and cumulative deaths report in Sri Lanka, followers' interaction for these situations' update posts was considered for the analysis. Therefore, a correlation analysis was conducted to identify the linear relationship between the number of shares of daily situation reports posted on the page and the recorded percentage increment of COVID-19 new cases. As a measurement for the relationship, "Pearson's correlation coefficient" was used, which is the best method of measuring the association between variables of interest. It gives information about the magnitude of correlation and the direction of the relationship [49]. Further, a regression model was developed to identify the effect of COVID-19 percentage increment of new cases on the user interaction in terms of percentage increase of shares of the situational update posts.

Table 5 Themes and their definitions

Theme	Definition
Global view and local expert's opinion on COVID-19	The posts describe the WHO's global pandemic notices and local experts' statements regarding the COVID-19 outbreak in Sri Lanka
COVID-19 daily situational information in Sri Lanka	The posts provide daily statistics on new infections, deaths, total infections and discharges
Symptoms of COVID-19	The posts describe health officials' advice on common COVID-19 symptoms
Precautions against COVID-19	The posts recommend maintaining social distance, washing hands, wearing masks and other healthy practices
Government notices and contact information	The posts describe the government's new regulations and protocols for containing the COVID-19 pandemic. It also included authorities' contact information for any health-related queries
Rumour and scam management	The posts were reported to correct the rumour and false news and warn scams and frauds
Post-pandemic behaviour and practices	After Sri Lanka recovered from the first pandemic wave, these posts were published to educate the public about new practices
The risk of the second wave of COVID-19 pandemic	When Sri Lanka was threatened with the 2nd wave of the COVID-19, these posts were reported to educate the public about the risk of the COVID-19 second wave
Other health issues	HPB page had reported articles about other health issues within the surveyed period. (i.e. posts regarding non-communicable diseases)

4 Results

4.1 Themes Generation

The following themes were identified through the content analysis of the HPB posts, and Table 5 summarises the topics and the relevant definition of each theme.

4.2 Social Network Analysis

It was considered to develop a multi-modal network referring to generated themes, used interface and used language as nodes and average shares as edges. However, two separate networks were derived because it is more interpretable with a network of two

modes rather than a network with three modes [50]. Figure 2 represents the language usage network of the HPB page under the generated themes. It is a multi-modal network consisting of 13 nodes and 28 edges. Darker edges show the high values of average shares in the network. Node size represents the betweenness centrality of nodes. Since links are between two modes only, betweenness centrality shows which nodes in mode "theme" are most central in terms of bridging to the other mode "language" in average shares. Sinhala had linked with all themes with higher average shares for each theme which is followed by English and Tamil posts in terms of the link between two modes. Government notices, precautions and situational updates were linked with all the nodes in other modes (Fig. 1 and Table 6).

The user interaction model for the posts reported by the HPB page in the generated themes and post interface consisted of 14 nodes and 31 edges. Figure 3 shows the derived network. The darker edges represent high average shares, and node size correlates to the betweenness centrality of nodes. Most of the content shared in HPB had shared either means of videos or images with text with 17.14 and 17.03 values for betweenness centrality, respectively. Low centrality values denote standard patterns in reporting posts on the HPB page for themes. It can be seen in the themes of the risk

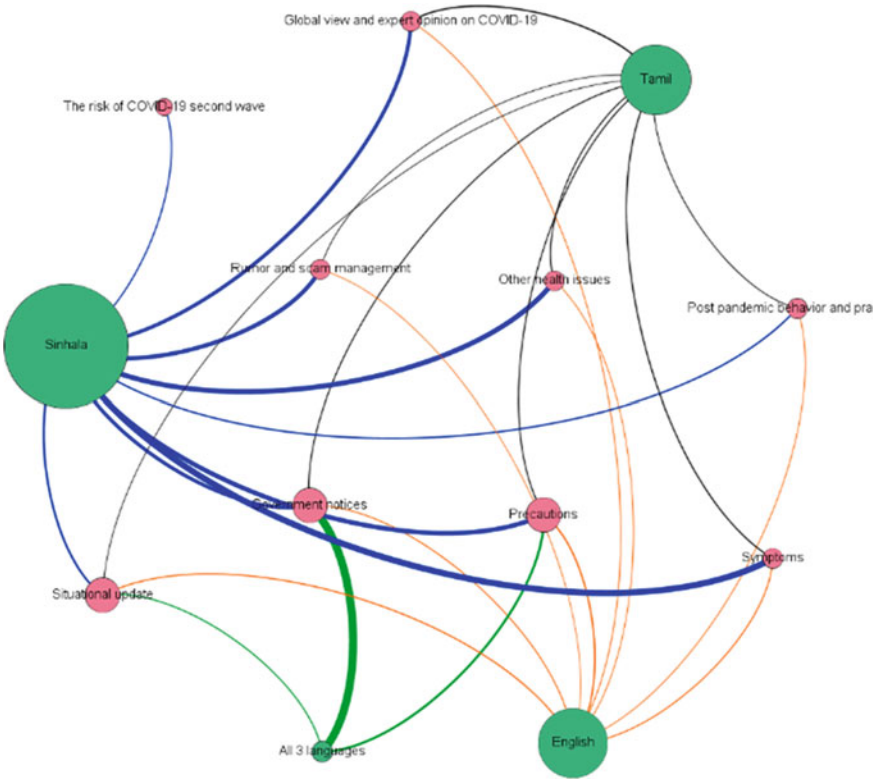

Fig. 1 User interaction network for different languages

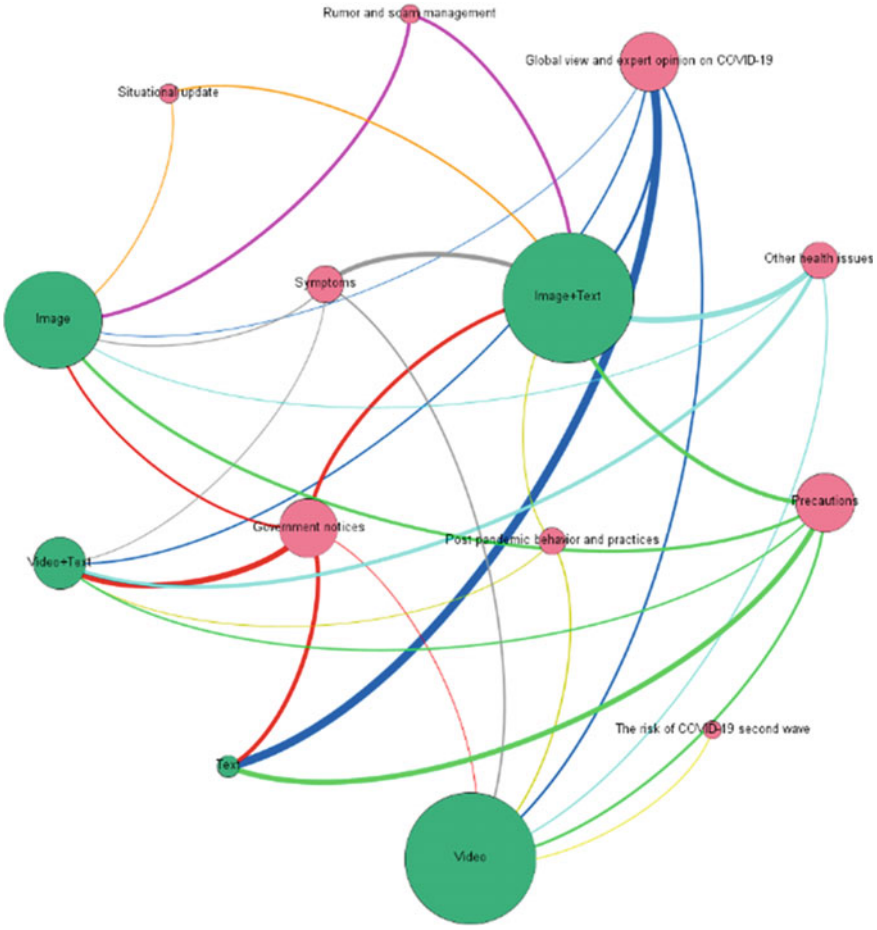

Fig. 2 User interaction network for interfaces

of COVID-19 second wave, rumour and scam management and situational update posts. Table 7 summarises the results of the network analysis.

However, the analysis of the effective interface was conducted irrespective of the themes calculating the average shares for each interface used in HPB posts. Further, the standard deviation of each interface sample was calculated. Table 8 summarises the results obtained from the investigation.

Although the above table suggests that texts will be the ideal way of sharing posts on the HPB page considering the average number of shares for each interface, the calculated sample standard deviation was very high, indicating a controversy in concluding the effective interface. Therefore, a new sample was prepared to refer to posts with shares higher than the mean number of shares of the entire sample (sample mean obtained as 873). Within the new sample formed using the posts having shares

Table 6 SNA results of the language usage network

Id	Label	Mode	Degree	Betweenness centrality
1	Global view and expert opinion on COVID-19	Theme	3	0.625
2	Government notices	Theme	4	3.625
3	Other health issues	Theme	3	0.625
4	Post-pandemic behaviour and practices	Theme	3	0.625
5	Precautions	Theme	4	3.625
6	Rumour and scam management	Theme	3	0.625
7	Situational update	Theme	4	3.625
8	Symptoms	Theme	3	0.625
9	The risk of COVID-19 second wave	Theme	1	0
10	All three languages	Language	3	0.75
11	English	Language	8	10.75
12	Sinhala	Language	9	21.75
13	Tamil	Language	8	10.75

Table 7 SNA results of the user interaction model for interfaces

Id	Label	Mode	Degree	Betweenness centrality
1	Global view and expert opinion on COVID-19	Theme	5	6.18
2	Government notices	Theme	5	6.18
3	Other health issues	Theme	4	2.84
4	Post-pandemic behaviour and practices	Theme	3	1.38
5	Precautions	Theme	5	6.18
6	Rumour and scam management	Theme	2	0.20
7	Situational update	Theme	2	0.20
8	Symptoms	Theme	4	2.84
9	The risk of COVID-19 second wave	Theme	1	0.00
10	Image	Interface	7	12.08
11	Image + Text	Interface	8	17.03
12	Text	Interface	3	0.60
13	Video	Interface	7	17.14
14	Video + Text	Interface	6	5.14

Table 8 Summary of the average number of shares of the posts

Interface	Average shares	Standard deviation of shares	Maximum of shares
Image	470.3	1365.7	11,000
Image + Text	1652.5	2588.2	13,000
Text	3433.3	1281.5	5200
Video	721	1224.1	7800
Video + Text	845.9	1399.4	6500

more than the mean of the original sample, 50% of posts reported using an image with a text, followed by posts reported using only the image (22%), video (18%), video with text (7%) and text (3%), respectively. The investigation on language usage of the HPB page revealed that they intended to address a broader community by reporting posts in Sinhala, Tamil and English, and specially, HPB reported posts using all these three languages. Out of 420 posts in the sample, 43% were reported in all languages, which is followed by 38% in Sinhala, 12% in Tamil and 7% in English. Posts reported in the Sinhala language had average shares of 1742, while it was 405 for the posts reported in all three languages (Sinhala, English, Tamil). However, in terms of interactions, it was noted that average shares were significantly reduced for the posts reported in the Tamil language, which was reported as 190.

4.3 Correlation and Regression Analysis Results

For the quantitative analysis, 179 data points were taken. Pearson's correlation value was obtained as 0.67 between percentage increases of daily COVID-19 new cases and the number of shares of daily situational posts reported by the HPB page. Further, it shows a significant positive relationship with a p-value of 4.7×10^{-5}.

Further, the regression model results indicate that more than 45% of the data sample can be explained by the derived regression model when the average was taken as relative, which can be concluded as a significant model for predicting human behaviours through statistics [51]. Also, the resulting significance value suggests that the regression model is significant that can be concluded; the increasing percentage of the COVID-19 daily new cases in Sri Lanka influenced the number of shares of situational update posts reported in HPB.

5 Conclusion

A Facebook page that is maintained by the authorised government agency can be identified as one of the effective ways for risk communication through social media. As revealed in the analysis, still there is room for improvement in using different languages to reach the diverse communities in Sri Lanka. Therefore, it is important to use different languages regularly to increase the average shares of posts. Also, it can be identified that using a standard method to post certain information like daily situation updates is a good move done by the HPB page. Facebook is a platform where users can share information with others, and it will increase the reach of a particular post. Analysis about the usage of different interfaces shows that a higher number of shares can be achieved by using the image with text as the interface. Correlation analysis and regression model revealed that there is a strong positive relationship between the increasing COVID-19 cases and the number of shares for the daily statistical report posted by the page. Effective communication and coordination between government agencies and the general public are important to manage disasters and mitigate the risks involved with the public. In conclusion, a Facebook page maintained by government officials can be an effective method for risk communication during pandemic situations like COVID-19.

References

1. Wickramasinghe K (2017) Sri Lanka experiences a series of man-made disasters—life online. http://www.life.lk/article/lifestyle/Sri-Lanka-Experiences-A-Series-Of-Man-made-Disasters/45/16950
2. Wijesinghe S (11 June 2016) Salawa—Wisalawa and man made disasters. Colombo telegraph. https://www.colombotelegraph.com/index.php/salawa-wisalawa-man-made-disasters/
3. UNDRR (2019) Disaster risk reduction in Sri LankalUNDRR. https://www.undrr.org/publication/disaster-risk-reduction-sri-lanka
4. ADRC (2019) Asian disaster reduction center (ADRC). https://www.adrc.asia/
5. Arnold M (2006) Natural disaster hotspots case studies. World Bank Publications
6. WHO (2020) WHO director-general's opening remarks at the media briefing on COVID-19—11 March 2020. https://www.who.int/director-general/speeches/detail/who-director-general-s-opening-remarks-at-the-media-briefing-on-covid-19---11-march-2020
7. Arambepola C, Wickramasinghe ND, Jayakody S, Hewage SA, Wijewickrema A, Gunawardena N, Dhanapala S, Prathapan S (2021) Sri Lanka's early success in the containment of COVID-19 through its rapid response: clinical and epidemiological evidence from the initial case series. PLoS ONE 16(7):e0255394. https://doi.org/10.1371/journal.pone.0255394
8. Sjoraida DF, Anwar RK (2018) The effectiveness of risk communications as a disaster risk reduction strategy in Taragong Garut. AIP Conf Proc 1987(1):020041. https://doi.org/10.1063/1.5047326
9. Baudoin M-A, Wolde-Georgis T (2015) Disaster risk reduction efforts in the greater horn of Africa. Int J Disaster Risk Sci 6(1):49–61
10. Bradley DT, McFarland M, Clarke M (2014) The effectiveness of disaster risk communication: a systematic review of intervention studies. PLoS Currents 6. https://doi.org/10.1371/currents.dis.349062e0db1048bb9fc3a3fa67d8a4f8

11. Danaher PJ, Rossiter JR (2011) Comparing perceptions of marketing communication channels. Eur J Mark 45(1/2):6–42. https://doi.org/10.1108/03090561111095586
12. Feldman D, Contreras S, Karlin B, Basolo V, Matthew R, Sanders B, Houston D, Cheung W, Goodrich K, Reyes A, Serrano K, Schubert J, Luke A (2016) Communicating flood risk: looking back and forward at traditional and social media outlets. Int J Disaster Risk Reduction 15:43–51. https://doi.org/10.1016/j.ijdrr.2015.12.004
13. Lindell MK, Perry RW (2012) The protective action decision model: theoretical modifications and additional evidence. Risk Anal 32(4):616–632. https://doi.org/10.1111/j.1539-6924.2011.01647.x
14. Shehara PLAI, Siriwardana CSA, Amaratunga D, Haigh R, Fonseka T (2021) Feasibility of using mobile apps in communication and dissemination process of multi-hazard early warning (MHEW) mechanism in Sri Lankan context. In: Dissanayake R, Mendis P, Weerasekera K, De Silva S, Fernando S (eds) ICSECM 2019. Springer, pp 177–189. https://doi.org/10.1007/978-981-15-7222-7_16
15. Tang Z, Zhang L, Xu F, Vo H (2015) Examining the role of social media in California's drought risk management in 2014. Nat Hazards 79(1):171–193. https://doi.org/10.1007/s11069-015-1835-2
16. Bortree DS, Seltzer T (2009) Dialogic strategies and outcomes: an analysis of environmental advocacy groups' Facebook profiles. Pub Relat Rev 35(3):317–319
17. Freberg K, Saling K, Vidoloff KG, Eosco G (2013) Using value modeling to evaluate social media messages: the case of Hurricane Irene. Pub Relat Rev 39(3):185–192
18. Houston JB, Hawthorne J, Perreault MF, Park EH, Goldstein Hode M, Halliwell MR, Turner McGowen SE, Davis R, Vaid S, McElderry JA, Griffith SA (2015) Social media and disasters: a functional framework for social media use in disaster planning, response, and research. Disasters 39(1):1–22. https://doi.org/10.1111/disa.12092
19. Introducing Safety Check (16 Oct 2014) About Facebook. https://about.fb.com/news/2014/10/introducing-safety-check/
20. Keeping People Safe and Informed About the Coronavirus (5 Oct 2020) About Facebook. https://about.fb.com/news/2020/10/coronavirus/
21. Takahashi B, Tandoc EC, Carmichael C (2015) Communicating on Twitter during a disaster: an analysis of tweets during Typhoon Haiyan in the Philippines. Comput Hum Behav 50:392–398. https://doi.org/10.1016/j.chb.2015.04.020
22. Jung J-Y, Moro M (2014) Multi-level functionality of social media in the aftermath of the Great East Japan Earthquake. Disasters 38(Suppl 2):S123-143. https://doi.org/10.1111/disa.12071
23. Kim T (2014) Observation on copying and pasting behavior during the Tohoku earthquake: retweet pattern changes. Int J Inf Manage 34(4):546–555. https://doi.org/10.1016/j.ijinfomgt.2014.03.001
24. Caragea C, McNeese N, Jaiswal A, Traylor G, Kim HW, Mitra P, Wu D, Tapia AH, Giles L, Jansen BJ, Yen J (1 Jan 2011) Classifying text messages for the haiti earthquake. 8th international conference on information systems for crisis response and management: from early-warning systems to preparedness and training, ISCRAM 2011. 8th International conference on information systems for crisis response and management, ISCRAM 2011. https://sci-hub.ee/https://pennstate.pure.elsevier.com/en/publications/classifying-text-messages-for-the-haiti-earthquake
25. Sarcevic A, Palen L, White J, Starbird K, Bagdouri M, Anderson K (2012) Beacons of hope in decentralised coordination: learning from on-the-ground medical twitterers during the 2010 Haiti earthquake. Proceedings of the ACM 2012 conference on computer supported cooperative work, pp 47–56. https://doi.org/10.1145/2145204.2145217
26. Bird D, Ling M, Haynes K (2012) Flooding Facebook-the use of social media during the Queensland and Victorian floods. Aust J Emerg Manage 27(1):27
27. Bhuvana N, Arul Aram I (2019) Facebook and Whatsapp as disaster management tools during the Chennai (India) floods of 2015. Int J Disaster Risk Reduction 39:101135. https://doi.org/10.1016/j.ijdrr.2019.101135

28. King L (2018) Social media use during natural disasters: an analysis of social media usage during hurricanes Harvey and Irma. International crisis and risk communication conference. https://stars.library.ucf.edu/icrcc/Proceedings/Proceedings/7
29. Ichiguchi T (2011) Robust and usable media for communication in a disaster. https://core.ac.uk/display/236667651?recSetID=
30. Peary BDM, Shaw R, Takeuchi Y (2012) Utilisation of social media in the East Japan earthquake and Tsunami and its effectiveness. J Nat Dis Sci 34(1):3–18. https://doi.org/10.2328/jnds.34.3
31. Nugroho Y (2010) Citizens in action. Documents.Pub. https://documents.pub/document/citizens-in-action-by-yanuar-nugroho.html
32. Nigam S (2010) How social media helped travelers during the iceland volcano eruption. Mashable. https://mashable.com/2010/04/22/social-media-iceland-volcano/
33. Palen L (2008) Online social media in crisis events. https://er.educause.edu/articles/2008/8/online-social-media-in-crisis-events
34. Starbird K, Palen L (2010) Starbird and palen pass it on?: retweeting in mass emergency pass it on?: retweeting in mass emergency
35. Wagler A, Cannon K (2015) Exploring ways social media data inform public issues communication: an analysis of Twitter conversation during the 2012–2013 drought in Nebraska. Faculty publications: agricultural leadership, education and communication department. https://digitalcommons.unl.edu/aglecfacpub/82
36. Press A (8 July 2005) Cell phones capture London blasts. Wired. https://www.wired.com/2005/07/cell-phones-capture-london-blasts/
37. Oh O, Agrawal M, Rao R (2013) Community intelligence and social media services: a rumor theoretic analysis of tweets during social crises. Manage Inf Syst Q 37(2):407–426
38. Heverin T, Zach L (2012) Use of microblogging for collective sense-making during violent crises: a study of three campus shootings. J Am Soc Inform Sci Technol 63(1):34–47. https://doi.org/10.1002/asi.21685
39. Yousefinaghani S, Dara R, Poljak Z, Bernardo TM, Sharif S et al. (2019) The assessment of Twitter's potential for outbreak detection: avian influenza case study. https://doi.org/10.1038/s41598-019-54388-4
40. Du E, Chen E, Liu J, Zheng C (2021) How do social media and individual behaviors affect epidemic transmission and control? Sci Total Environ 761:144114. https://doi.org/10.1016/j.scitotenv.2020.144114
41. Tirkkonen P, Luoma-aho V (2011) Online authority communication during an epidemic: a Finnish example. Pub Relat Rev 37(2):172–174. https://doi.org/10.1016/j.pubrev.2011.01.004
42. Zhu B, Zheng X, Liu H, Li J, Wang P (2020) Analysis of spatiotemporal characteristics of big data on social media sentiment with COVID-19 epidemic topics. Chaos, Solitons Fractals 140:110123. https://doi.org/10.1016/j.chaos.2020.110123
43. Vinck P, Pham Phuong N, Bindu K, Bedford J, Eric J, Nilles MD (2019) Institutional trust and misinformation in the response to the 2018–19 Ebola outbreak in North Kivu, DR Congo: a population-based survey. https://doi.org/10.1016/S1473-3099(19)30063-5
44. Arif N, Ghezzi P, Al-Jefri M, Bizzi IH, Perano GB, GoldmanM, Haq I, Chua K, Mengozzi M, Neunez M, Smith H (2018) Fake news or weak science? visibility and characterization of antivaccine webpages returned by google in different languages and countries. https://www.frontiersin.org/articles/10.3389/fimmu.2018.01215/full
45. Diaz F, Abbasi SJ, Fuller D, Diab E (2021) Canadian transit agencies response to COVID-19: understanding strategies, information accessibility and the use of social media. Transp Res Interdisc Perspect 12:100465. https://doi.org/10.1016/j.trip.2021.100465
46. Mansoor M (2021) Citizens' trust in government as a function of good governance and government agency's provision of quality information on social media during COVID-19. Gov Inf Q 38(4):101597. https://doi.org/10.1016/j.giq.2021.101597
47. Sharif N, Opu RR, Alzahrani KJ, Ahmed SN, Islam S, Mim SS, Khan FB, Zaman F, Dey SK (2021) The positive impact of social media on health behavior towards the COVID-19 pandemic in Bangladesh: a web-based cross-sectional study. Diabetes Metab Syndr 15(5):102206. https://doi.org/10.1016/j.dsx.2021.102206

48. Jayasekara R, Jayathilaka G, Siriwardana C, Amaratunga D, Haigh R, Bandara C, Dissanayake R (2021) Identifying gaps in early warning mechanisms and evacuation procedures for tsunamis in Sri Lanka, with a special focus on the use of social media. Int J Disaster Resilience Built Environ, ahead-of-print. https://doi.org/10.1108/IJDRBE-02-2021-0012
49. Shafer and Zhang (3 April 2014) 10: correlation and regression. Statistics LibreTexts. https://stats.libretexts.org/Bookshelves/Introductory_Statistics/Book%3A_Introductory_Statistics_(Shafer_and_Zhang)/10%3A_Correlation_and_Regression
50. Ghani S, Kwon BC, Lee S, Yi JS, Elmqvist N (2013) Visual analytics for multimodal social network analysis: a design study with social scientists. IEEE Trans Visual Comput Graphics 19:2032–2041. https://doi.org/10.1109/TVCG.2013.223
51. Jim (16 April 2017) How to interpret r-squared in regression analysis. Statistics By Jim. http://statisticsbyjim.com/regression/interpret-r-squared-regression/

Analysing Facebook Practices for Disaster-Related Communication in Sri Lanka: A Case Study of a Facebook Page Dedicated to Disaster-Related Information

H. A. D. G. S. Jayathilaka and C. S. A. Siriwardana

Abstract In the modern world, social media plays a vital role in disaster-related communication. Various community categories responsible for disaster risk management in Sri Lanka have practised social media for disaster-related communication in multiple ways. Out of those community categories, social groups have been identified as the prominent category that used social media for disaster-related communication. The primary objective of this study is to explore the behaviour and community engagement of a Facebook page managed by such a social group named Disaster Info Sri Lanka organised by a research group with an engineering background. Facebook page insight data was explored to measure the community engagement towards the Disaster Info Sri Lanka Facebook page. It was compared with the general attention of the community towards using Internet-based information sources, including social media, to obtain disaster-related information. Moreover, this study adopted social network analysis to interpret the Disaster Info Sri Lanka Facebook page by exploring the posts published through the page. It explores the connections and patterns created by the aggregated interactions on the Facebook page. A similar variation was identified in the engagement of the community towards the Disaster Info Sri Lanka Facebook page and the general concentration of the community towards the Internet-based facilities for disaster-related information. People have more engagement with the information on social media related to specific exciting incidents that caused a stir in society. The shallow attention has been recorded for the daily disaster-related information, such as morning weather updates published through social media. Therefore, more focus should be paid to motivating the community to use social media information sources for daily updates related to disasters. This study will be helpful to improve the effectiveness of information diffusion via Facebook platform by the various parties responsible related to disaster risk management in Sri Lanka.

H. A. D. G. S. Jayathilaka (✉) · C. S. A. Siriwardana
Department of Civil Engineering, University of Moratuwa, Katubedda, Moratuwa, Colombo, Sri Lanka
e-mail: jayathilakahadgs.20@uom.lk

R. Dissanayake et al. (eds.), *12th International Conference on Structural Engineering and Construction Management*, Lecture Notes in Civil Engineering 266,
https://doi.org/10.1007/978-981-19-2886-4_28

Keywords Disasters · Communication · Social network analysis · Social media · Facebook

1 Introduction

Social media has been identified as the prominent and influential communication channel used for disaster-related communication worldwide. Due to the increase of disasters caused by natural and anthropogenic reasons, many researchers have identified that social media is an effective communication channel that can be used for disaster-related communication. Various instances can be identified through the literature review, highlighting the successful utilisation of social media for worldwide disaster-related communication. There, multiple practitioners can be identified who managed social media applications properly for disaster-related information sharing. The study carried out by [1] has identified several social media users who used social media for disaster-related purposes. There, social groups have been recognised as significant social media users who obtained the responsibility to share disaster-related information for the vulnerable communities for various purposes. These users can be referred to as the stakeholders in disaster risk management as they are directly involved in the disaster risk reduction and management practices [2]. Volunteers, researchers, philanthropists, and societies are some social groups actively engaged in social media for disaster-related purposes.

Numerous researchers have examined the strategic use of social media during disasters, using social media data to determine the needs of the disaster-affected and disaster vulnerable communities [3, 4]. Out of them, several studies have been conducted which illustrate the utilisation of social media for disaster-related communication between the affected or vulnerable communities and the responsible authorities and organisations [5, 6]. Several approaches have been followed there to explore the use of social media use during disasters. Some studies have looked into the various social media platforms and messenger apps like Facebook, Twitter, and WhatsApp to investigate the behaviour of those particular applications managed by the different stakeholders [7–10].

The present study mainly focused on exploring the behaviour of a Facebook page dedicated to disaster-related communication handling by a professional social group. Two approaches were followed to conduct this study. Initially, Facebook insight data was taken to explore the performance of the particular Facebook page and compare it with the general community engagement in Sri Lanka towards using Internet-based sources to communicate disaster-related information. Furthermore, social network analysis was applied to understand the characteristics of the disaster-related communication network developed through the Facebook page selected as the case study.

2 The Case: The Facebook Page of Disaster Info Sri Lanka

Facebook has been identified as the most popular social media platform among the community in Sri Lanka ("Digital [11] Re-port", 2020). They have tended to use social media for different purposes. Out of them, the community linked to disaster risk management uses social media to communicate disaster-related information with others [12]. With the emergence of the COVID-19 pandemic in Sri Lanka, the community tended to use Internet-based sources more than ever, including social media, to gain information regarding the COVID-19 pandemic. Therefore, to quench that thirst for knowledge from the people, the Disaster Info Sri Lanka Facebook page was commenced by a professional research team with having an engineering background. Apart from COVID-19-related news, various disaster-related information has been published since the beginning of that Facebook page daily. The primary motive of developing this Facebook page is to provide accurate disaster-related information on time. The interest of the social media community in this Facebook page has grown over time. At the end of October 2021, the page had 5140 likes and 5277 followers, which were high enough reasonable to analyse. The demographic characteristics of the audience who have engaged with the Disaster Info Sri Lanka page were obtained through the page insight data. The community in the age group of 25–34 has engaged more with the Disaster Info Sri Lanka Facebook page than the other communities.

Furthermore, communities in 18–24 and 35–44 age groups have engaged next in the line as second and third, respectively. This engagement is very similar when considering the general attention of the community to use social media for disaster-related communication, as identified from the study carried out by [13]. Overall, most of the online community who engaged with the Disaster Info Sri Lanka represents the younger generation in Sri Lanka. As mentioned earlier, through the Disaster Info Sri Lanka Facebook page, various types of information related to disasters have been published throughout the time. Therefore, to facilitate conducting this study, overall posts publishing was categorised into 13 categories as mentioned below. Each type of post has been denoted with a particular keyword.

i. AI–Awareness Information
ii. MCU–Morning COVID-19 Update
iii. ECU–Evening COVID-19 Update
iv. MWU–Morning Weather Update
v. FCU–Foreign COVID-19 Update
vi. LS–Landslide Information
vii. CL–Cyclone Information
viii. FWL–Flood Water Level
ix. MMD–Man-Made Disasters
x. OWU–Other Weather Update
xi. SUN–Sun Path Moving and Temperature
xii. EQ–Earthquake
xiii. Other–Picture Posts/Memes/Cartoons.

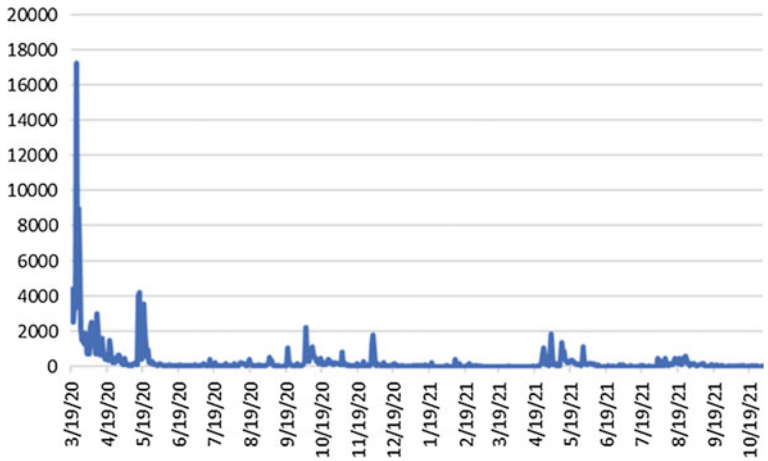

Fig. 1 Daily page engaged users

Facebook insights were explored, which is an analytics dashboard developed to track user behaviour and post-performance on the Facebook business page. In addition, it provides critical metrics like page views and posts reach for paid and organic posts, and this platform also recommends competitor pages to watch and track [14]. Page insight data was obtained for the period of 2020/03/20 to 2021/10/31. Five different metrics were obtained through the page insight data to measure the performance of the Disaster Info Sri Lanka Facebook page with time. Each parameter has a specific definition, as denoted below, which defines how it measures the performance of the Facebook page with time.

2.1 Daily Page Engaged Users

The number of people (Unique Users) who have engaged with Disaster Info Sri Lanka Facebook page by doing any click or creating stories (Fig. 1).

2.2 Daily Total Reach

The number of people who have any content from the Disaster Info Sri Lanka Facebook page or about the page on their screen including posts, check-ins, ads, and social information of people who interact with the page and more (Fig. 2).

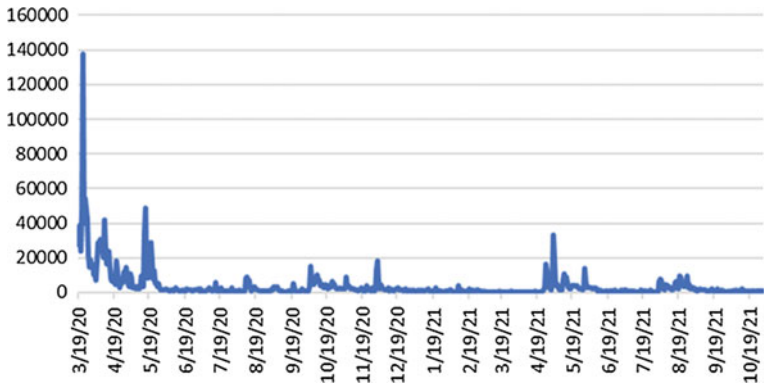

Fig. 2 Daily total reach

2.3 Daily Viral Reach of Page Posts

The number of people who had any Facebook page's posts enters their screen with social information attached. As a form of organic distribution, social information displays when a person's friend interacts with the page or post. This metric includes when someone's friend likes or follows the page, engages with a post, shares a photo of the page, and checks into the page. (Unique Users) (Fig. 3).

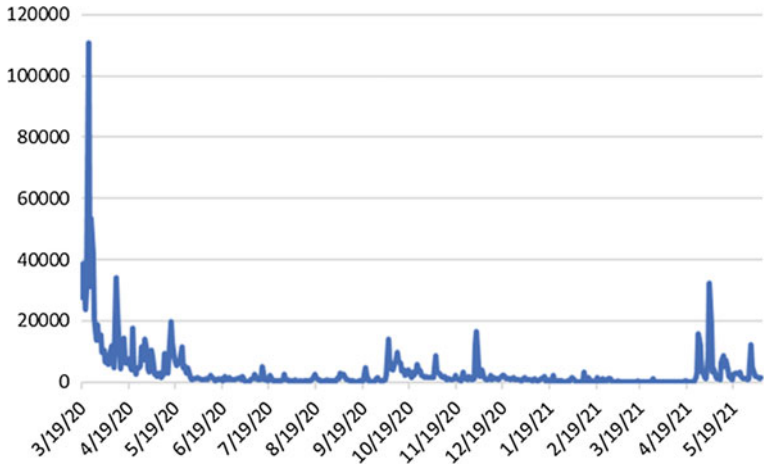

Fig. 3 Daily viral reach of page posts

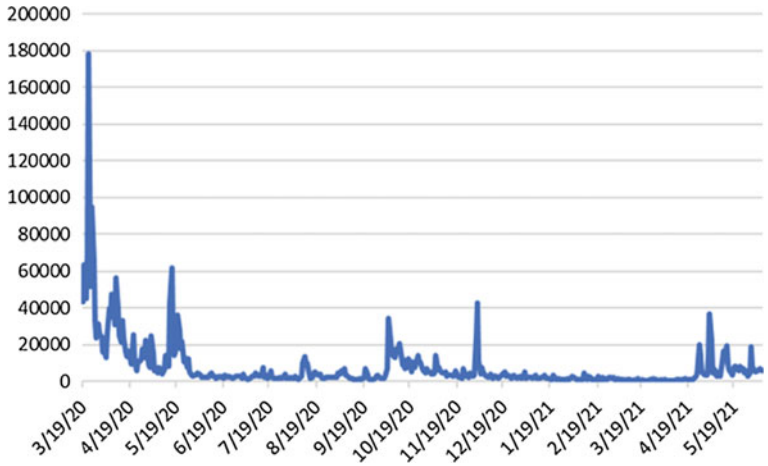

Fig. 4 Daily total impressions of the posts

2.4 Daily Total Impressions of the Posts

The number of times (Total Count) the Disaster Info Sri Lanka Facebook page's content entered a person's screen including, statuses, photos, links, videos, and more (Fig. 4).

2.5 Daily Total Consumers

The number of people (Unique Users) who clicked on any of the Disaster Info Sri Lanka Facebook page's content. This not includes the stories that are created without clicking on-page content (ex, liking the page from the timeline) (Fig. 5).

Similar variation can be seen in every parameter considered. In each graph, high variation can be seen at the beginning, denoted by high community engagement towards the Disaster Info Sri Lanka Facebook page during the first COVID-19 wave in Sri Lanka. This variation can be mainly due to the community's high interest in using Internet-based facilities like social media to gain more information about the coronavirus at the beginning of the outbreak in Sri Lanka. Sharp fallen of the graphs can be seen for the parameters after the first COVID-19 wave in Sri Lanka, which describes that the community interest has decreased with time towards the page. Nevertheless, a slight increment of the variation can be observed at several periods similarly in each graph. This increment seems to suggest that the community interaction towards the Disaster Info Sri Lanka Facebook page has increased during the second and third waves of the COVID-19 pandemic in Sri Lanka. Overall, this highlights the significance of the Disaster Info Sri Lanka Facebook page during the critical periods of Sri Lanka due to the COVID-19 pandemic.

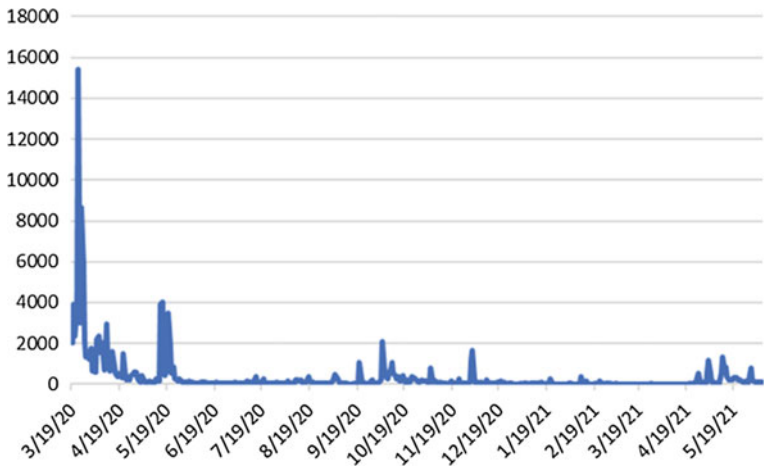

Fig. 5 Daily total consumers

3 Social Network Analysis and Its Application on Disaster-Related Social Media Networks

According to the study carried out by [15], social media are communication technologies that enable social actors to interact through dyadic relationships. Analysing these relationships has become a crucial topic in recent years to make decisions the community network developed through social media. To achieve that, social network analysis was used as the primary analytical tool during the last decade [7]. Social network analysis (SNA) is a sociological strategy to analyse relationships and interactions between social actors to uncover underlying social structures (Wasser-man and Faust, [16]. Social network analysis focused on social relationships through the perspective of network theory, using nodes (individual actors within the network) and edges (unique relationships such as friendship, relatives, organisations, and sexual relationships). These networks are frequently shown in a social network diagram, in which nodes are represented as dots and edges as lines [7]. Several instances emerge that use SNA to visualise, analyse, and understand the communication networks developed through social media applications during disasters worldwide. Different studies with different purposes have been conducted by applying SNA, as presented in Table 1.

Table 1 Different studies conducted worldwide under the application of SNA for disaster-related communication through the social media

Name of the study	Application of SNA	Reference
Social network analysis: characteristics of online social networks after a disaster	Applying social network analysis (SNA) to understand the characteristics of social media networks in Louisiana during emergency responses	[10]
Temporal network analysis of inter-organisational communications on social media during disasters: a study of hurricane harvey in Houston	Analysing communication networks between organisations on social media to characterise the roles of organisations and situational information communication	[17]
Social network analysis of disaster response in 2014 Chiangrai province earthquake	Examining the social network in disaster preparedness for earthquakes at local, provincial, and national levels of Thailand	[18]
Application of social network analysis (SNA) to identify communication network associated with multi-hazard early warning (MHEW) in Sri Lanka	Analysing the behaviour communication network of stakeholders at emergency disaster preparedness and response stages	[19]
Social media data mining: A social network analysis of tweets during the 2010–2011 Australian floods	Using SNA to study interactions between Twitter users during the Australian 2010–2011 floods and to identify influential members of the online communities that emerged during the queensland, NSW, and Victorian floods	[20]
Understanding public interest and needs in health policies through the application of social network analysis on a governmental Facebook fan page	Analysing the interactions between agencies, policies, and the interest of the public using the SNA	[21]

4 Methodology

As the commencing part of this study, a comparison was carried to explore the community engagement towards the Disaster Info Sri Lanka Facebook page with the trend of the general attention of the communities towards the use of the Internet for disaster-related information. Community engagement towards the Disaster Info Sri Lanka page was obtained by considering the Facebook page reach. Facebook page reach denotes the number of people who saw any content from the page or about the page, including posts, stories, and other information from people who interact with the page and more. Reach is different from impressions, which may include multiple views of a particular Facebook page's posts by the same people [14]. To observe the general community engagement towards using Internet-based facilities for disaster-related information, the Google Trends facility was used. Since this study was conducted during the COVID-19 pandemic, the community has tended to use Internet facilities more than previously [22]. Therefore, for comparison with the Facebook page under consideration, Google search-term trend (interest over time)

was considered for the search term of "coronavirus". Through the comparison, the behaviour of the Disaster Info Sri Lanka Facebook page was analysed.

As the second phase of this study, social network analysis method was applied to explore the behaviour of the communication network structure developed through the interaction of the audience towards the Disaster Info Sri Lanka Facebook page. The main focus of SNA is on the relationships in a communication network. It uses a variety of statistical and visual analyses by modelling the particular communication network. Before developing the overall communication network model, nodes and the edges of the model were defined. Since the communication network of this study had to be mapped concerning through the posts published on the Disaster Info Sri Lanka Facebook page, nodes were considered the posts published in the Facebook page, and shared posts of that posts by the community of the Disaster Info Sri Lanka Facebook page. Edges were defined according to the categories of the posts and their connectivity with the shared posts.

In this study, three centrality parameters were considered to analyse the three types of degree centralities. Those centrality parameters are degree centrality, betweenness centrality, and eigenvector centrality. Each parameter describes specific characteristics of the nodes in the communication network. In this study, posts were selected which have been achieved the highest values for each centrality parameter. Several conclusions were made through the top-ranked post considering each centrality parameter in the publishing posts on the Disaster Info Sri Lanka Facebook page.

Required data to conduct this study was collected from Facebook through software called Facepager. It is an application for automated data retrieval on the web [23]. Through the Facepager software, several critical information of the published posts was extracted, such as the description of the post, number of shares, number of reactions, and the number of comments. To facilitate the analysis of this section, each post was numbered as "*Pn*", where "*n*" denotes the post number published on the Facebook page. There was a limitation on data collection due to the privacy policies offered by the social media platforms. Therefore, this study only captured publicly available information supported by the Facepager software. Network visualisation with identified nodes and edges was done using Gephi Open Source Software, generally used for graphical and network analysis of developed models. It helps data analysts intuitively reveal patterns and trends, highlight outliers, and tell stories with their data [24].

5 Results

The first phase of the study is to compare the behaviour of the Disaster Info Sri Lanka Facebook page reach and the general engagement of the community towards the use of Internet-based facilities for disaster-related communication with the time. Two graphs were considered to represent the above two variations. Figure 6 was

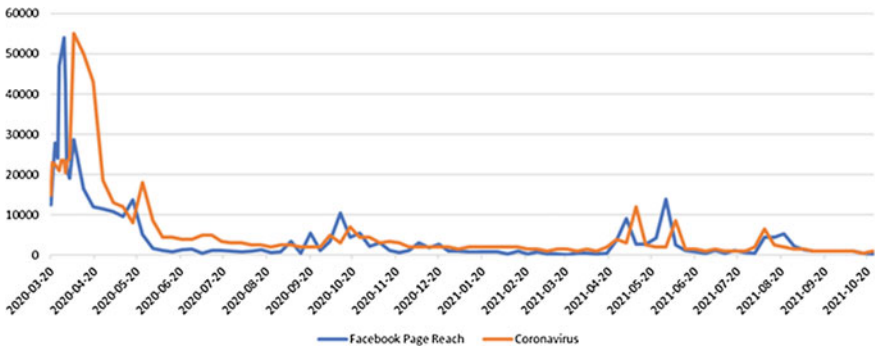

Fig. 6 Variation of the Facebook page reach and the "coronavirus" search term

developed by combining those two graphs into one layer to facilitate the comparison.

For this comparison, the period of 2021/03/20 to 2021/10/31 was considered. The y-axis represents the interest over time, and the x-axis represents the time for both graphs. The graph illustrating the variation of the "coronavirus" search term was scaled up to facilitate the comparison.

Figure 7 presents the visualised behaviour of the Disaster Info Sri Lanka Facebook page by considering the circulation of the post published on the Facebook page. The present developed communication network model consisted of 3061 nodes and 39,836 total edges, with a maximum geodesic distance (diameter) of 4, which defines a maximum of 4 nodes connecting two vertices, averaging 2.40 nodes. Network structure was directed and laid out using the Yifan Hu Proportional layout algorithm.

Three major centrality parameters were obtained through the software for each model node. There, four different posts were illustrated according to the highest value of each parameter. They were recognised as the key centralised posts on the page, as presented in Table 2.

As presented in Table 2, the highest degree centrality and the betweenness centrality have got by the P289 node, which denotes the post number 289 as shown in Fig. 8. A brief description of the P289 node is presented below.

- P289—Post number 289
- P289 type of the post—Awareness information (AI)
- Description of the post—Allegation made by MOH of Kesbewa regarding removal of COVID-19 epidemic restrictions imposed in Piliyandala area (Picture + Text)
- Number of shares—364
- Number of reactions—63
- Number of comments—2.

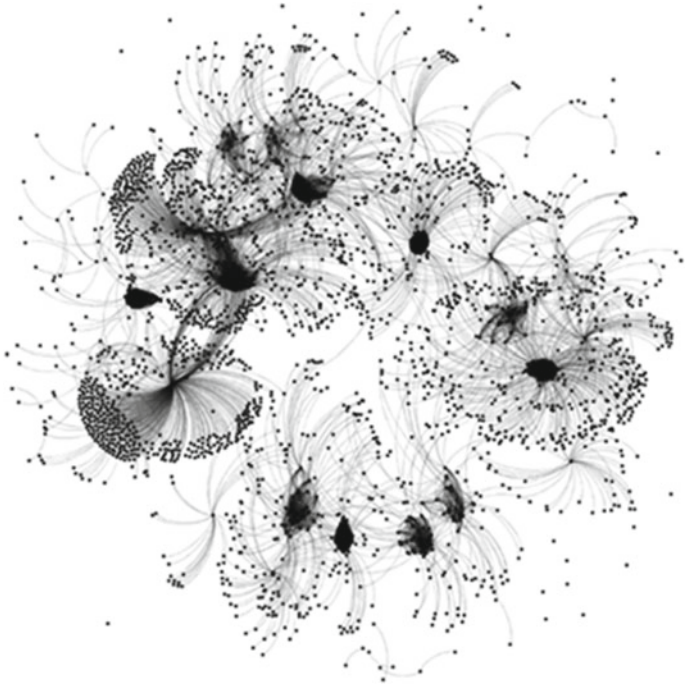

Fig. 7 Visualised network behaviour of the post transmitting of the disaster info Sri Lanka Facebook page

Table 2 Key centralised posts published in the Facebook page

Centrality parameter	Node/post number
Degree centrality	289
Betweenness centrality	289
Eigenvector centrality	18

The highest eigenvector centrality has been achieved by the P18 node, which denotes the post number 18 as shown in Fig. 9. A brief description of post number 18 is presented below.

- P18—Post number 18
- P297 type of the post—Morning weather update
- Description of the post—Weather forecast on 3 June 2021 (Picture + Text)
- Number of shares—3
- Number of reactions—5
- Number of comments—0.

Fig. 8 Post number 289

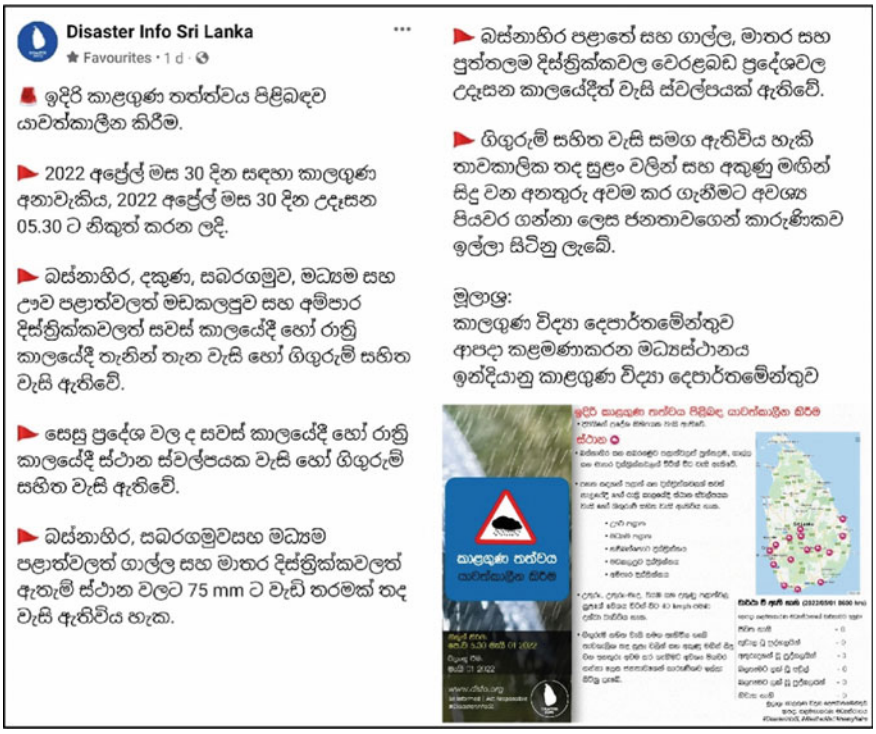

Fig. 9 Post number 18

6 Discussion

As presented in Fig. 6, a similar variation can be observed for both graphs with the time. An interesting observation in both graphs is that the variation of the charts with the time increased during three different periods. When considering those time slots, it can be recognised that those periods had more influence in Sri Lanka due to the first, second, and third of COVID-19 pandemic waves. Approximately, they are from 2020 March to 2020 July, from 2020 October to 2021 January, and from 2021 April to 2021 September for first, second and third waves respectively. Furthermore, both graphs have reached their peak during the first wave of the COVID-19 pandemic. This variation might have occurred since people tended to search for more information about the coronavirus pandemic during the first wave of the coronavirus outbreak, as it was newly experienced for the Sri Lankans.

Degree centrality denotes the number of connections owned by a node or the number of relationship degrees related to a node [25]. Furthermore, it defines the ability of a node (actor) to communicate with other actors in the network directly. Betweenness centrality measures how often a node is located on the shortest path between different nodes in the network [26]. It describes the actors who mediate

more connections in the network, called the network controllers. According to the results, both the highest degree and highest betweenness centrality values have been obtained by post number 289. When considering post number 289, it represents an incident that was talked about in society more during the beginning of the third wave of the COVID-19 pandemic in Sri Lanka. When concerning the representation of post number 289, it has been presented concisely and attractively. It consisted of brief text and a picture. This particular Facebook post has been engaged more with the Disaster Info Sri Lanka Facebook page community. Also, Facebook posts with high betweenness centrality play a vital role in the communication network structure because they act as the gatekeepers of the network structure. Furthermore, they play a critical role in handling the information flow on the Disaster Info Sri Lanka Facebook page with external online communities.

Eigenvector centrality measures a node's importance while considering the extent of its neighbours. It is used to measure a node's influence in the network [27]. Post number 18 has obtained the highest eigenvector centrality value, which belongs to the MWU category, which has been uploaded every morning regarding the weather report updating by the Department of Meteorology, Sri Lanka. Even though the post related to the MWU category has been published daily, the page community has not been engaging more than the other categories as posts related to the MWU category have obtained a low degree of centrality value. Nevertheless, since post number 18 related to the MWU category has achieved the highest eigenvector centrality, it can be concluded that MWU is the most influenced post in the network structure. Eigenvector centrality provides a more sophisticated understanding of centrality. It permits connections to have a variable value, allowing for more advantage from connecting to some nodes than others [28]. Therefore, posts related to these kinds of categories are helpful to keep the consistency of the Facebook page community over time.

7 Conclusion

Ultimately, several takeaways were drawn from the present study to improve the practices of managing a Facebook page dedicated to disaster-related information. The community has engaged more with the Disaster Info Sri Lanka Facebook page during the peak period of the leading waves of the COVID-19 pandemic in Sri Lanka. Furthermore, it can be seen that a sharp fall in community engagement after the first COVID-19 pandemic. Therefore, it can be concluded that there should be necessary actions to keep a consistent community engagement towards the Internet facilities, including the Disaster Info Sri Lanka Facebook page.

Several critical conclusions were made through the considered case study, which is essential to properly understand the social media practices for disaster-related communication in Sri Lanka. Publishing the information related to the incident, which is being discussed in society at a particular time, has more engagement than the other posts. These types of Facebook posts are helpful to have good connectivity

of the different external social media users. Therefore, more attention should be paid not to be missed publishing those kinds of posts. Furthermore, to achieve more engagement towards the post publications on a Facebook page, the content should be brief and attractively presented.

Post published for daily weather updates has not engaged more than other post categories. It was recorded a low usage of social media by the public for daily updates such as day-to-day weather. Therefore, considerable attention should be paid to attracting the online communities to follow social media for the daily weather updates as they are essential in day-to-day life. Also, they are the most influenced posts for the network as they are helpful to keep the consistency of the Facebook page. Overall considering the present research study, it can be wind up that though several things need to be improved, the Disaster Info Sri Lanka Facebook page has successfully disseminated disaster-related information to the public in Sri Lanka.

Acknowledgements We want to show our gratitude to Eng. Ravindu Jayasekara and Eng. Chamika Kannangara, who are currently working as research assistants at the Department of Civil Engineering of the University of Moratuwa, for their immense support in publishing the disaster-related information on the Disaster Info Sri Lanka Facebook page.

References

1. Jayathilaka GS, Siriwardana C, Amaratunga D, Haigh R, Dias N (2021) A conceptual framework for social media use during disasters. In: Amaratunga D, Haigh R, Dias N (eds) Multi-hazard early warning and disaster risks. Springer International Publishing, Cham, pp 659–684. https://doi.org/10.1007/978-3-030-73003-1_44
2. AL-Fazari S, Kasim N (2019) Role of stakeholders in mitigating disaster prevalence: theoretical perspective. MATEC Web Conf. 266:03008. https://doi.org/10.1051/matecconf/201926603008
3. Imran M, Elbassuoni S, Castillo C, Diaz F, Meier P (2013) Extracting information nuggets from disaster-Related messages in social media. In: Iscram
4. Yin J, Lampert A, Cameron M, Robinson B, Power R (2012) Using social media to enhance emergency situation awareness. IEEE Intell Syst 27:52–59. https://doi.org/10.1109/MIS.2012.6
5. Lovari A, Bowen SA (2020) Social media in disaster communication: a case study of strategies, barriers, and ethical implications. J Public Aff 20:e1967. https://doi.org/10.1002/pa.1967
6. Luna S, Pennock MJ (2018) Social media applications and emergency management: a literature review and research agenda. Int J Disaster Risk Reduct 28:565–577. https://doi.org/10.1016/j.ijdrr.2018.01.006
7. Antoniadis I, Serdaris P, Charmantzi A (2014) The application of social networking analysis in marketing: a case study of a product's page in facebook. Proc ICCMI 2014:873–879
8. Bhuvana N, Arul Aram I (2019) Facebook and Whatsapp as disaster management tools during the Chennai (India) floods of 2015. Int J Disaster Risk Reduct 39:101135. https://doi.org/10.1016/j.ijdrr.2019.101135
9. Bird D, Ling M, Haynes K (2012) Flooding Facebook-the use of social media during the queensland and Victorian floods. Aust J Emerg Manag 27:27
10. Kim J, Hastak M (2018) Social network analysis: characteristics of online social networks after a disaster. Int J Inf Manag 38:86–96

11. Digital Outlook 2020 Report (2020) Asia pacific institute digital marketing. https://apidm.lk/digital-outlook-2020-report/ (Accessed 1 July 21)
12. Jayasekara RU, Jayathilaka GS, Siriwardana C, Amaratunga D, Haigh R, Bandara C, Dissanayake R (2021) Identifying gaps in early warning mechanisms and evacuation procedures for tsunamis in Sri Lanka, with a special focus on the use of social media. Int J Disaster Resil Built Environ ahead-of-print. https://doi.org/10.1108/ijdrbe-02-2021-0012
13. Jayathilaka HADGS, Siriwardana CSA, Amaratunga D, Haigh RP, Dias N (2022) Investigating the variables that influence the use of social media for disaster risk communication in Sri Lanka. In: Dissanayake R, Mendis P, Weerasekera K, De Silva S, Fernando S (eds) ICSBE 2020, Lecture notes in civil engineering. Springer, Singapore, pp 259–276. https://doi.org/10.1007/978-981-16-4412-2_19
14. Facebook Business Suite [WWW Document], (2021) https://business.facebook.com/latest/insights/results?asset_id=102432811395151&time_range=%257B%2522end%2522%253A%25222021-10-30%2522%252C%2522start%2522%253A%25222020-12-31%2522%257D (Accessed 11 Feb 21)
15. Peters K, Chen Y, Kaplan AM, Ognibeni B, Pauwels K (2013) Social media metrics—a framework and guidelines for managing social media. J Interact Mark Soc Media Mark 27:281–298. https://doi.org/10.1016/j.intmar.2013.09.007
16. Wasserman S, Faust K (1994) Social network analysis: methods and applications, structural analysis in the social sciences. Cambridge University Press, Cambridge. https://doi.org/10.1017/CBO9780511815478
17. Rajput AA, Li Q, Zhang C, Mostafavi A (2020) Temporal network analysis of inter-organisational communications on social media during disasters: a study of Hurricane Harvey in Houston. Int J Disaster Risk Reduct 46:101622. https://doi.org/10.1016/j.ijdrr.2020.101622
18. Suwanmolee S (2016) Social network analysis of disaster response in 2014 Chiangrai province earthquake. J Soc Res 39:109–145
19. Shehara PLAI, Siriwardana CSA, Amaratunga D, Haigh R, (2019) Application of social network analysis (SNA) to identify communication network associated with multi-hazard early warning (MHEW) in Sri Lanka. In: 2019 Moratuwa engineering research conference (MERCon). Presented at the 2019 Moratuwa engineering research conference (MERCon), pp 141–146. https://doi.org/10.1109/MERCon.2019.8818902
20. Cheong F, Cheong C (2011) Social media data mining: a social network analysis of tweets during the 2010–2011 Australian floods. In: PACIS
21. Huang H-M, Chiu C-J (2020) Understanding public interest and needs in health policies through the application of social network analysis on a governmental Facebook fan page. BMC Public Health 20:1367. https://doi.org/10.1186/s12889-020-09420-y
22. Google's Year in Search [WWW Document] (2020). Google trends. https://trends.google.com/trends/yis/2020/GLOBAL/ (Accessed 11 Feb 21)
23. Jünger J, Keyling T (2021) Strohne/Facepager
24. Bastian M, Heymann S, Jacomy M (2009) Gephi: an open source software for exploring and manipulating networks. Proc Int AAAI Conf Web Soc Media 3:361–362
25. Maharani W, Gozali AA (2014) Degree centrality and eigenvector centrality in Twitter. In: 2014 8th international conference on telecommunication systems services and applications (TSSA). Presented at the 2014 8th international conference on telecommunication systems services and applications (TSSA), pp 1–5. https://doi.org/10.1109/TSSA.2014.7065911
26. Leydesdorff L (2007) Betweenness centrality as an indicator of the interdisciplinarity of scientific journals. J Am Soc Inf Sci Technol 58:1303–1319. https://doi.org/10.1002/asi.20614

27. Golbeck J (2013) Chapter 3—network structure and measures. In: Golbeck J (ed) Analysing the social web. Morgan Kaufmann, Boston, pp 25–44. https://doi.org/10.1016/B978-0-12-405531-5.00003-1
28. Hansen DL, Shneiderman B, Smith MA, Himelboim I (2020) Chapter 3—social network analysis: measuring, mapping, and modeling collections of connections. In: Hansen DL, Shneiderman B, Smith MA, Himelboim I (eds) Analyzing social media networks with NodeXL, 2nd edn. Morgan Kaufmann, pp 31–51. https://doi.org/10.1016/B978-0-12-817756-3.00003-0

A Systematic Review on Different Approaches Used in the Development of Fragility Curves for Buildings

R. A. D. V. Rajapaksha and C. S. A. Siriwardana

Abstract The intensity and the frequency of natural hazards have rapidly increased during past decades due to climate change. Due to reasons such as urbanization, vulnerable communities are being exposed to theses hazardous events, converting them to severe disasters. These disasters have cost millions of lives, affecting billions of people and resulting in trillions of economic losses. However, proper resilience, adaptation and mitigation measures can reduce the impacts of disasters. A cost-effective design of such measures requires knowledge of the hazard and the response of the properties with respect to the losses. The damage model, which is developed by combing hazard curve and fragility curve, is a tool that can be used for the above purpose. Conventional probabilistic hazard analysis can be employed to develop hazard curves. However, authors have followed different approaches to develop fragility curves due to the complexity. This study aims to review the different approaches on the scope of buildings to different disasters, identify their trends, classify the study areas and identify the relationships among the classified areas. A Systematic Literature Review (SLR) has been employed in this study, following the preferred reporting items for systematic reviews. A total of 1597 related records were identified from the Scopus and Web of Science scientific databases. After a structured screening and eligibility criteria, 135 records were selected to include in this study. Results revealed that analytical approaches had been employed in 55% of the selected studies. Also, 63% of the selected studies were based on earthquake-related disasters. Further, it was identified that most of the studies were aimed at reinforced concrete buildings. Furthermore, essential relationships among the classified areas and the future research opportunities in this thematic area were identified and are presented in this paper, which will direct the scholars who are aiming to develop fragility curves for buildings for different types of disasters.

Keywords Fragility curves · Systematic Literature Review · Buildings · Disasters · Natural hazards

R. A. D. V. Rajapaksha (✉) · C. S. A. Siriwardana
Department of Civil Engineering, University of Moratuwa, Moratuwa, Sri Lanka
e-mail: rajapakse.dilum@gmail.com

R. Dissanayake et al. (eds.), *12th International Conference on Structural Engineering and Construction Management*, Lecture Notes in Civil Engineering 266,
https://doi.org/10.1007/978-981-19-2886-4_29

1 Introduction

The impacts of natural hazards continue to adversely affect health, economic and social development worldwide [1]. With the exposure of vulnerable communities to these hazardous events, the number of recorded disasters has shown a sharp increment in the most recent 20 years (2000–2019) than the previous (1980–1999). According to the EM-DAT (Emergency Events Database of the Centre for Research on the Epidemiology of Disasters), 7348 disaster events were recorded in the recent 20 years, claiming approximately 1.23 million lives, 4.03 billion affected people and USD 2.97 trillion of economic loss. Asia suffered the highest number of disaster events (3086 events) in that period, followed by America (1756 events) and Africa (1192 events). Considering the disaster types, the most common disaster during that period was flood-related disasters (3254 events) followed by storms (2043 events) and earthquakes (552 events). The deadliest disaster type was the earthquake, including the severe events such as earthquake and tsunami event that occurred in the Indian Ocean in 2004 and the earthquake event in Haiti in 2010. Storms were responsible for the most economic damage (USD 1.39 trillion), followed by floods (USD 651 billion) and earthquakes (USD 636 billion) [2]. Even though the number of disastrous events has increased by five times, the number of deaths has decreased almost threefold because of the early warning systems and disaster management processes. However, the economic loss due to the disasters kept increasing. The recorded economic loss has increased 7 times from the 1970s to the 2010s [1]. Even though severe hazards occur, disasters can be prevented by enhancing resilience. As the early warning systems have reduced the number of fatalities, proper adaptation and mitigation measures can reduce the economic loss due to the disasters, which is showing a rapid increment.

A cost-effective design of such adaptation, mitigation or disaster risk reduction measures requires the knowledge of a hazard and the likely loss prediction of property in the absence of such measures. A damage model is a tool that can be used in the above-stated purpose and employed in many preceding works in the scope of buildings [3–5]. It can be employed to assess the risk of building, impact estimation after a disaster and assess decision-making regarding emergency planning and disaster risk reduction [6]. A damage model is developed by combining a hazard curve and a fragility curve. A hazard curve represents the probability of exceedance versus the hazard intensity for a particular hazard in a defined area [4]. Conventional probabilistic hazard analysis can be employed to develop a hazard curve [7]. A fragility curve shows the probability of damage of a system over one or more input variables [3]. Authors have used different approaches to develop the fragility curves for building, such as empirical approaches, analytical or mechanical approaches and expert-judgemental approaches due to the complex behaviour [8]. This paper aims to review the different approaches previous authors have followed to develop fragility curves for a building to different disasters, identify their trends, classify the study areas and identify the relationships among the classified areas.

2 Methodology

This section outlines the methodology adopted in this study. A Systematic Literature Review (SLR) has been employed to identify the available literature in the scientific databases, and the steps are briefly discussed. The methodology followed by [9] is used here.

2.1 Research Question

The first step of the SLR is to frame the research question, which defines the scope of the study. Buildings, the development of fragility curves and disasters are selected as the key thematic areas for the study. The following research question has been framed for the study as per the objective.

- What are the used methods for developing fragility curves for buildings for floods, earthquakes, tsunami, landslides, hurricanes, fires and climate change?

2.2 Record Searching Process

The searching process starts with requesting a query from different databases. The Scopus and Web of Science databases were selected for this study. The search query was developed by combining the identified keywords in Table 1 using Boolean operators.

The search query used in this study is given below.

"develop*" AND ("damage model*" OR "damage curve*" OR "fragility curve*" OR "damage assess*") AND "building*" AND ("disaster*" OR "flood*" OR "earthquake*" OR "seismic*" OR "tsunami*" OR "landslide*" OR "hurricane*" OR "tornado*" OR "fire*" OR "climate change").

Table 1 Keywords used in the study

Key term	Keywords
Development of fragility curves/damage models	"Development", "Damage model", "Damage curve", "Fragility curve", "Damage assessment"
Buildings	"Buildings"
Disasters	"Disasters", "Floods", "Earthquake", "Seismic", "Tsunami", "Landslides", "Hurricane", "Tornado", "Fire", "Climate change"

2.3 Record Assessment Criteria

The following inclusion criteria were used to filter out the most recent, reliable articles from the databases.

- Must be a journal article, conference article, review, conference review or book chapter in the discussed databases
- Published between 2015 and 2021 in the English language

The selected records were subjected to a duplicate-filtering process using MS Excel and then the following exclusion criteria (EC) were used to select the most relevant articles for this study.

- EC1—Studies that have not been developed, applied or reviewed one or more damage models or fragility curves
- EC2—Studies that have not been aimed at buildings
- EC3—Studies that have not been developed based on the selected hazard-related disasters

The filtered articles from the above ECs were used to identify the trends and relationships of the different approaches used to develop fragility curves.

2.4 Classification Criteria for Studies

The main objective of this study is to identify the trends and relationships of the different approaches used to develop the fragility curves. The trends and relationships were studied under the following categories.

- Used approach for the development of fragility curve
- Disaster type based on the fragility curve
- Purpose of the study
- Type of building that the fragility curve can be applied
- Based on structural material
- Based on non-structural material
- Based on use
- Other related properties (if any)

Also, the identified relationships among the above-classified areas are discussed in this paper. VOSviewer, a free software tool, was used to identify and present the relationships.

3 Results

This section presents the results of the literature analysis carried out in this study, including the identification, screening, eligibility and inclusion (ISEI) mechanism for sorting out relevant publications, trends of the publications and studies.

3.1 ISEI Mechanism

The search process initially identified 1247 records from Scopus and 1236 records from Web of Science. Firstly, the inclusion criteria were applied, as discussed in Sect. 2.3. The inclusion process concluded the records for 1597 (731 from Scopus and 866 from Web of Science). Secondly, the duplicated records were removed using MS Excel. 1110 unique records were identified. Thirdly, the screening process was followed according to the EC1, EC2 and EC3, and eligible 135 studies were selected to include in this review. The mechanism is described in Fig. 1.

3.2 Trends of Publications

Figure 2 illustrates the research trend of fragility curves based on the selected studies. It can be observed that the number of publications related to the research area has increased from 2015 to 2021. This trend suggests that scholars are more inclined to study fragility curves related to buildings. Figure 3 shows the classification of articles as per the publication type. According to the figure, most of the selected articles are journal articles (70%), and 24% of the selected articles are conference papers. Contribution from book chapters and review papers is a minimum (3% each).

3.3 Different Approaches Used in the Development of Fragility Curves

The development of a fragility curve depends on different factors such as data availability, complexity and computational effort. Also, the accuracy of the prediction can vary with the approach used. Hence, authors have used different approaches to do so. Table 2 summarizes the identified approaches, definitions and references.

Note that most machine learning approaches also use the available data from past events during the process. However, the purpose of the machine learning concept is to make the most accurate predictions, and it distinguishes them from empirical approaches, which aim to capture the relationships between variables. Also, machine learning approaches can handle the multivariable models, which cannot be achieved

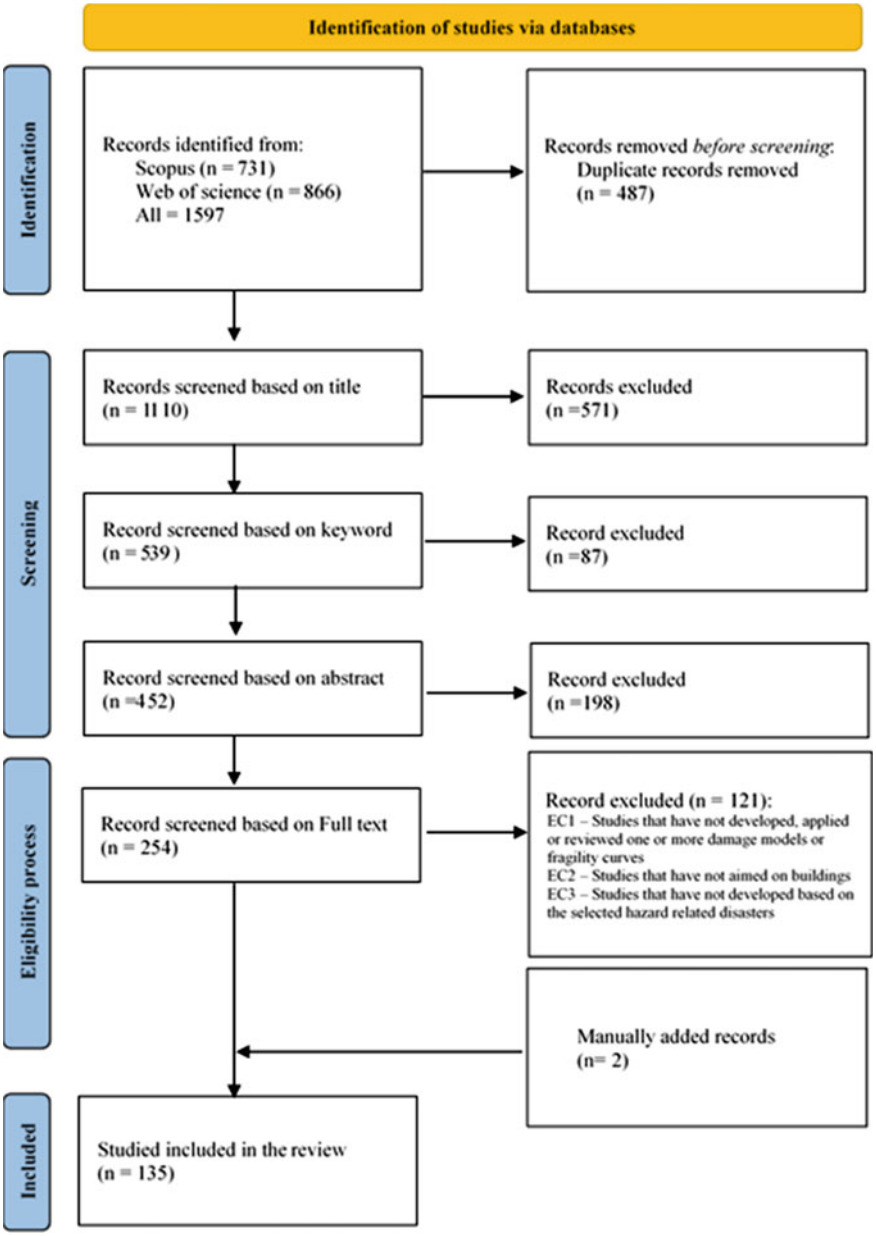

Fig. 1 ISEI mechanism

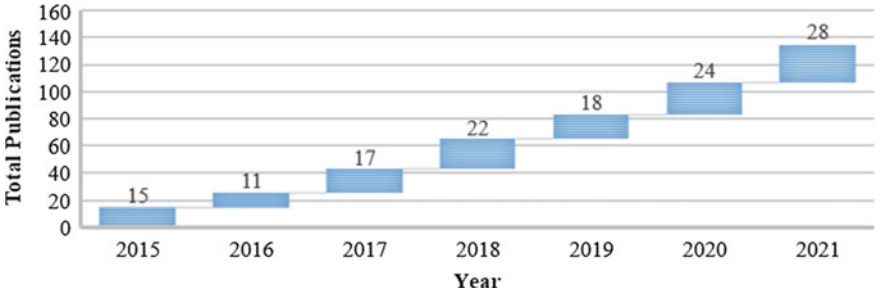

Fig. 2 Research trend of selected studies (2018–2021)

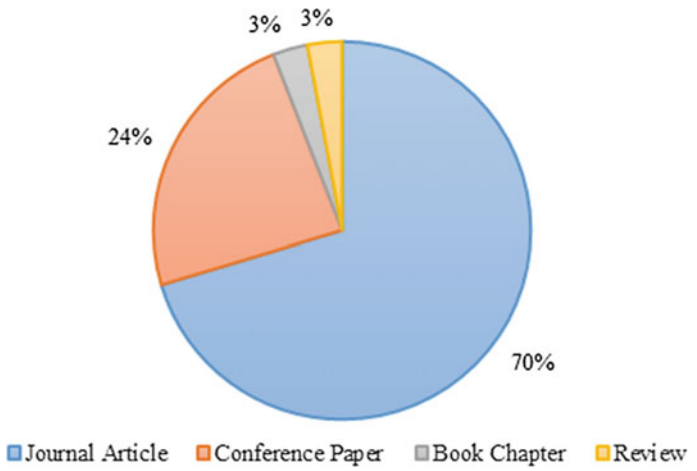

Fig. 3 Classification of articles as per publication type

Table 2 Different approaches used to develop fragility curves

Approach	Definition	References
Expert	Expert-based knowledge has been incorporated to develop the fragility curves	[10–12]
Empirical	Available data from past events have been used to develop the fragility curves	[13, 10, 14, 13–27, 27–38]
Analytical	Results from simulations (ex: finite element simulations), theoretical relationships or mechanical experiments have been used to develop the fragility curves	[39–42, 39–84]
Machine Learning	Machine learning concepts (ex: artificial neural networks) have been incorporated to develop the nonlinear relationships of fragility curves	[85–88]
Hybrid	Two or more above approaches have been combined to develop the fragility curves	[89–102]

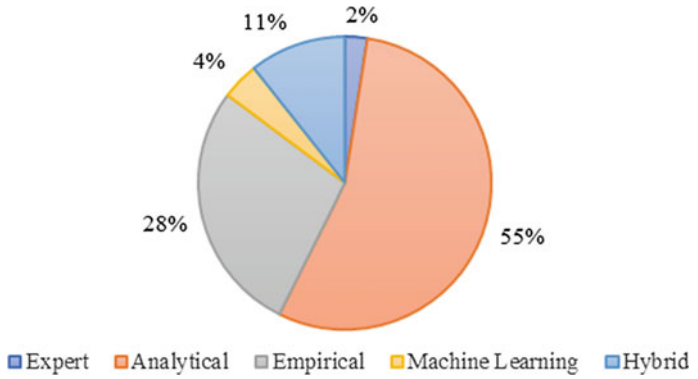

Fig. 4 Approaches used in the development of fragility curves

by the empirical methods [10]. Therefore, some researchers tend to study those approaches separately [103], and the same method is followed here. Different authors have used different combinations under the hybrid approach. The combinations found in this review are expert-analytical, analytical-empirical and expert-empirical.

Figure 4 shows the distribution of the approaches in selected studies. Most authors have used analytical approaches (55%) to develop fragility curves. Empirical approaches are the next most used approach (28%). Eleven per cent of the selected studies have employed the hybrid approaches while the use of other approaches was considerably less.

3.4 Disaster Types that Used to Develop Fragility Curves

Figure 5 illustrates the disaster types used in the fragility curve-related studies. 63% of the studies were based on earthquakes. As identified, the deadliest disaster type is earthquakes, which may be a reason for scholars to focus on earthquakes. Also, many studies have focussed on floods and tsunami (16% and 10%, respectively). However, as the hazard type responsible for the highest economic loss during the recent 20 years, hurricanes (including all the types of strong winds) have not been used for many studies (only 6%).

3.5 Purpose of the Publications

Figure 6 shows the purpose of different studies. 84% of the selected studies were aimed to develop fragility curves, whereas 13% of the studies have used existing fragility curves for the damage prediction. 3% of the studies have reviewed the fragility curves-based studies.

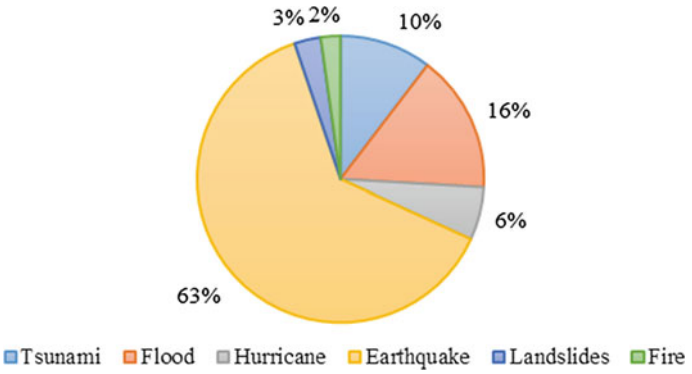

Fig. 5 Studies per disaster type

Fig. 6 Articles based on the purpose

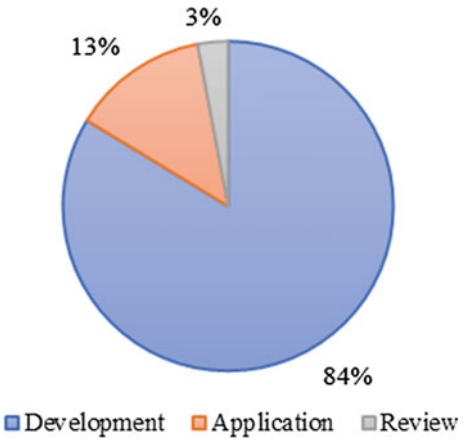

4 Discussion

4.1 Identified Relationships Among the Classified Areas

Figure 7 illustrates the identified relationships among the studies. In the figure, the bubble size represents the co-occurrence, the curved lines represent the interconnection between classified areas, and the thickness of the line represents the strength of the relationship. It can be identified that most of the studies are based on the analytical approaches for earthquakes for reinforced concrete structures. The relationships are separately studied to identify the critical ones. The main disaster types that fragility curves are built around, such as earthquakes, floods and tsunami, are taken as the base points.

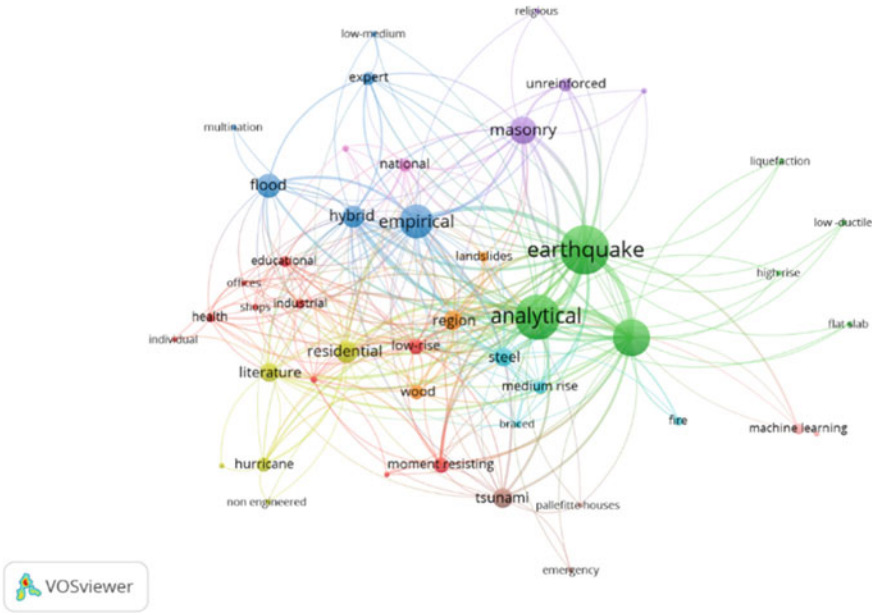

Fig. 7 Relationships among the classified areas

4.2 Relationships Around Earthquakes

Figure 8 shows the relationships around earthquakes. The connection between earthquakes with the analytical approach and reinforced concrete structures shows the strongest relationships. Also, the connection with empirical approaches and masonry structures shows significant strength. Hence, for the development of fragility curves for earthquake-related disasters, analytical and empirical approaches have been used frequently. Also, most studies were aimed at reinforced concrete and masonry structures which fall under the structural material category. Hence, it can be observed that, for earthquake-based studies, structural material is taken as a key variable than the usage of the buildings.

4.3 Relationships Around Floods

Figure 9 shows the relationships around floods. The connection between floods and empirical approaches shows the most substantial relationship. Also, floods and analytical approaches indicate a significant relation. Hence, for the development of fragility curves for flood-related hazards, empirical approaches have been used than analytical approaches. It can be highlighted that the studies are limited to a region, which indicates a limitation of the fragility curves developed for floods. Also, the

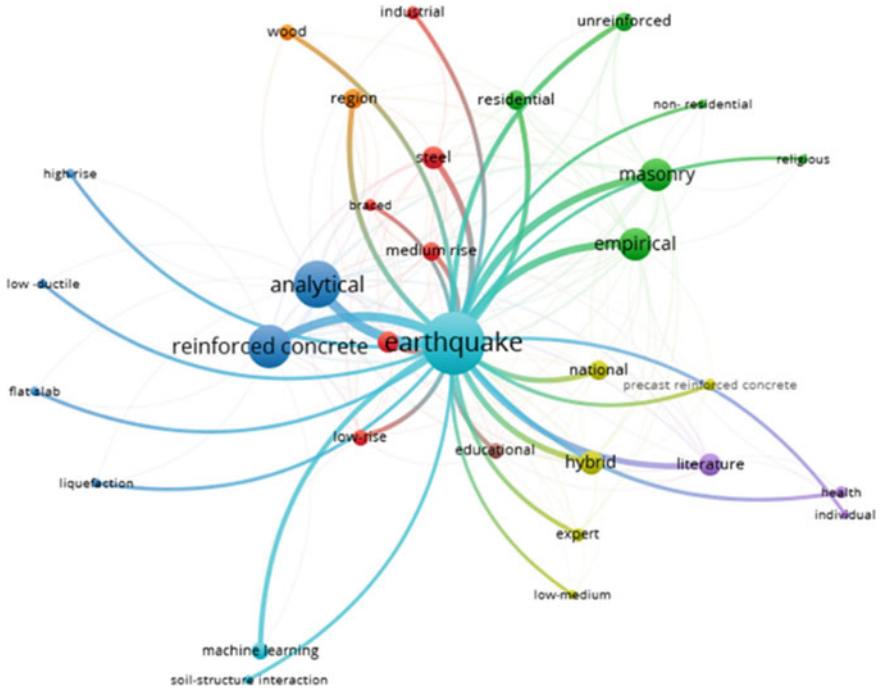

Fig. 8 Relationships around earthquakes

fragility curves are connected with residential, educational and industrial buildings. Therefore, the use of the buildings has been considered as a key variable than the structural material for flood-related fragility curves.

4.4 Relationships Around Tsunami

Figure 10 shows the relationships around tsunami. It shows a strong relationship with analytical approaches, empirical approaches and reinforced concrete structures. Hence, for the development of fragility curves for tsunami, primarily analytical and empirical methods have been employed. The figure shows a strong relationship with reinforced concrete structures and some connections with steel, masonry and wood. It indicates that the structural material is taken as a key variable in studying tsunami-related fragilities.

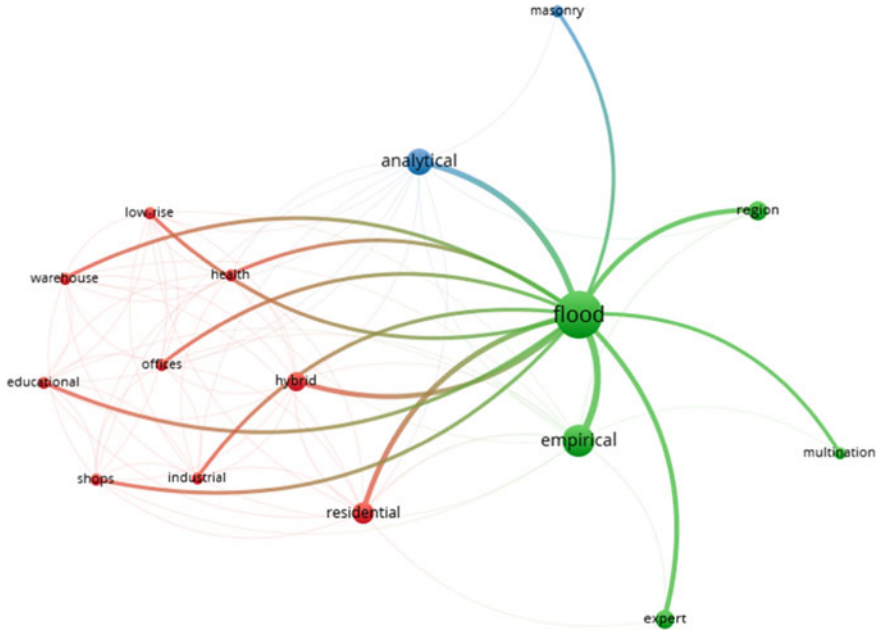

Fig. 9 Relationships around floods

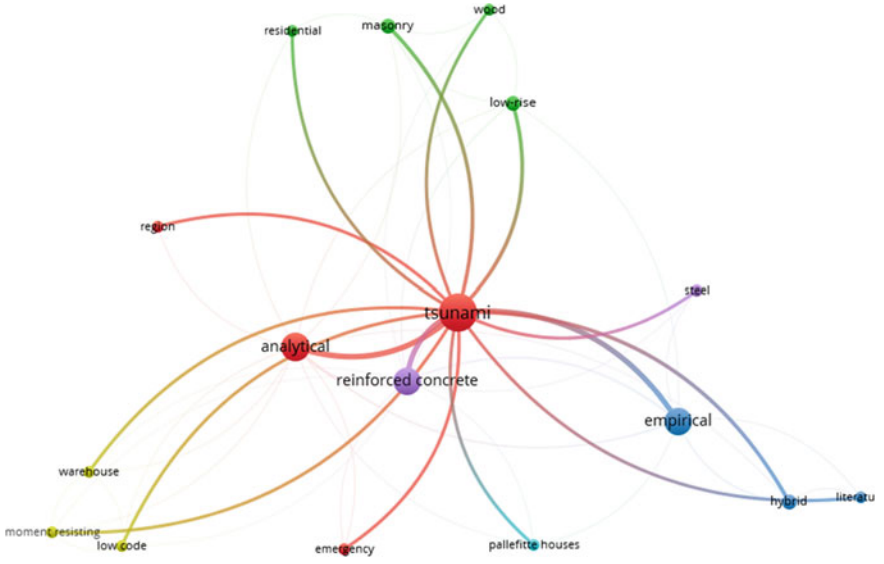

Fig. 10 Relationships around tsunami

4.5 Opportunities for Future Studies

The results showed that more than half of the studies are based on earthquakes. Few studies have focussed on floods, tsunami and hurricanes but studies on landslides and fires are minimal. As identified above, those disasters are among the most common disasters;especially, hurricanes are responsible for the most severe economic damage. Therefore, further studies have to be carried out covering those disaster types. There is a massive opportunity for future studies in those areas.

Analytical and empirical methods are the most common approaches followed by authors to develop fragility curves. Even in the hybrid approaches, only analytical and empirical approaches were shared. However, with the development of technology, machine learning approaches are emerging in almost every study area. But the contribution of machine learning concepts to the development of fragility curves is still minimum. The authors who employed machine learning concepts for the above purpose have claimed a high accuracy of the predictions [86, 87, 104]. Most of the fragility curves are based on only one parameter (peak ground acceleration in earthquakes, flood depth in floods, wave height in tsunami). However, there are other variables that also contribute to the damage. But sometimes they cannot be incorporated due to the limitation of the approaches used in the development of the fragility curve. Using machine learning approaches is a solution for this problem which can handle multivariable. Also, the uncertainties and irregularities related to the study can be addressed in this approach [86, 104]. Therefore, scholars can focus on incorporating machine learning approaches in the development of fragility curves for building in their future studies.

Also, most flood-related studies are based on the empirical approach, and the results highlighted that those studies are limited to the study region. In the study [10], authors have identified that as a drawback of the empirical method. Due to the limitation of the approaches, most fragility curves are limited to a single variable. However, other variables, such as flow velocity, can contribute to the damage. Studies can be aimed to overcome those issues in the future, and machine learning concepts will be a good option for that purpose.

Also, it is identified that structural material is the key variable concerning earthquakes and tsunami. Most of the earthquake-based studies are focussed on reinforced concrete and masonry structures. However, a few studies have focussed on steel structures. The same gap can be identified for the masonry structures in the tsunami-based studies. Therefore, future studies can aim at those aspects as well.

5 Conclusion

This study aimed to perform a systematic literature review covering the studies related to the fragility curves for buildings for different disasters, identify their trends, classify the study areas and identify the relationships among the classified

areas. Over 1500 related records in the Scopus and Web of Science databases, 135 studies have been selected to include in this study through the ISEI mechanism. Different approaches used to develop the fragility curve, disaster types based on the fragility curve and the type of building for which the fragility curve is made are the main categories identified in this study. Results revealed that more than half of the selected studies are based on earthquake-related disasters, and the analytical approach is the most common approach used to develop fragility curves. Also, most of the studies were focussed on reinforced concrete structures during the development of fragility curves. Also, identified relationships were presented, which can direct scholars who are willing to develop fragility curves for buildings. Further, identified research opportunities are also presented in this paper.

References

1. WMO (2021) Atlas of mortality and economic losses from weather, climate and water extremes (1970–2019). World Meteorological Organization
2. CRED and UNDRR (2020) Human cost of disasters, an overview of the last 20 years (2000–2019). Centre for research on the epidemiology of disasters, UN office for disaster risk reduction. https://doi.org/10.18356/79b92774-en
3. Li Y, van de Lindt JW (2012) Loss-based formulation for multiple hazards with application to residential buildings. Eng Struct Elsevier Ltd 38:123–133. https://doi.org/10.1016/j.engstruct.2012.01.006
4. Noshadravan A, Miller TR, Gregory JG (2017) A lifecycle cost analysis of residential buildings including natural hazard risk. J Constr Eng Manag 143(7):04017017. https://doi.org/10.1061/(asce)co.1943-7862.0001286
5. Padgett JE, Dennemann K, Ghosh J (2010) Risk-based seismic life-cycle cost-benefit (LCC-B) analysis for bridge retrofit assessment. Struct Safety. Elsevier Ltd 32(3):165–173. https://doi.org/10.1016/j.strusafe.2009.10.003
6. Maio R, et al (2017) Review of fragility curves for seismic risk assessment of buildings in Europe. 16th world conference on earthquake—WCEE, (March)
7. Nakajima M, Hirata K (2004) Seismic risk evaluation method of structures based on deaggregation of seismic hazard. In: 13th world conference on earthquake engineering, pp. 1–11
8. Rosti A, Rota M, Penna A (2021) Empirical fragility curves for Italian URM buildings. Bull Earthq Eng Springer, Neth 19(8):3057–3076. https://doi.org/10.1007/s10518-020-00845-9
9. Pirbhulal S, Gkioulos V, Katsikas S (2021) A systematic literature review on RAMS analysis for critical infrastructures protection. Int J Crit Infrastruct Prot. Elsevier B.V., 33:100427. https://doi.org/10.1016/j.ijcip.2021.100427
10. Amadio M et al (2019) Testing empirical and synthetic flood damage models: the case of Italy. Nat Hazard 19(3):661–678. https://doi.org/10.5194/nhess-19-661-2019
11. Malgwi MB, Schlögl M, Keiler M (2021) Expert-based versus data-driven flood damage models: a comparative evaluation for data-scarce regions. Int J Disaster Risk Reduction 57(2). https://doi.org/10.1016/j.ijdrr.2021.102148
12. Nofal OM, van de Lindt JW (2020) Minimal building flood fragility and loss function portfolio for resilience analysis at the community level. Water (Switzerland), 12(8). https://doi.org/10.3390/w12082277
13. Afrouz SG et al (2021) Evaluation of seismic vulnerability of hospitals in the Tehran metropolitan area. Buildings 11(2):1–15. https://doi.org/10.3390/buildings11020054

14. Arrighi C, et al (2020) Empirical flash flood vulnerability functions for residential buildings. SN Appl Sci. Springer International Publishing 2(5). https://doi.org/10.1007/s42452-020-2696-1
15. Azizi-Bondarabadi H, et al (2016) Empirical seismic vulnerability analysis for masonry buildings based on school buildings survey in Iran. Bull Earthq Eng. https://doi.org/10.1007/s10518-016-9944-1
16. Biglari M, Formisano A, Hashemi BH (2021) Empirical fragility curves of engineered steel and RC residential buildings after Mw 7.3 2017 Sarpol-e-zahab earthquake. Bull Earthq Eng. Springer Netherlands 19(6):2671–2689. https://doi.org/10.1007/s10518-021-01090-4
17. Buratti N et al (2017) Empirical seismic fragility for the precast RC industrial buildings damaged by the 2012 Emilia (Italy) earthquakes. Earthq Eng Struct Dynam 46(14):2317–2335. https://doi.org/10.1002/eqe.2906
18. Ferlisi S, Nicodemo G, Peduto D (2018) Empirical fragility curves for masonry buildings in slow-moving landslide-affected areas of southern italy. Advan Sci, Technol Innov. Springer Nature, 1825–1828. https://doi.org/10.1007/978-3-319-70548-4_529
19. Foytong P, Ornthammarath T (2020) Empirical seismic fragility functions based on field survey data after the 5 May 2014 Mae Lao (Northern Thailand) earthquake. Int J Disaster Risk Reduction. Elsevier Ltd, 42(May 2014):101344. https://doi.org/10.1016/j.ijdrr.2019.101344
20. Gautam D (2018) Observational fragility functions for residential stone masonry buildings in Nepal. Bull Earthq Eng Springer, Netherlands 16(10):4661–4673. https://doi.org/10.1007/s10518-018-0372-2
21. Gutenson JL et al (2018) Rapid flood damage prediction and forecasting using public domain cadastral and address point data with fuzzy logic algorithms. J Am Water Resour Assoc 54(1):104–123. https://doi.org/10.1111/1752-1688.12556
22. Halder L, Chandra Dutta S, Sharma RP (2020) Damage study and seismic vulnerability assessment of existing masonry buildings in Northeast India. J Build Eng. Elsevier Ltd 29:101190. https://doi.org/10.1016/j.jobe.2020.101190
23. Kim JJ (2018) Development of empirical fragility curves in earthquake engineering considering nonspecific damage information. Adv Civil Eng 2018. https://doi.org/10.1155/2018/6209137
24. Komolafe AA et al (2019) Comparative analyses of flood damage models in three Asian countries: towards a regional flood risk modelling. Environ Syst Decisions Springer, US 39(2):229–246. https://doi.org/10.1007/s10669-018-9716-3
25. Lin SL, Uma SR, King A (2018) Empirical fragility curves for non-residential buildings from the 2010–2011 canterbury earthquake sequence. J Earthq Eng Taylor Francis 22(5):749–777. https://doi.org/10.1080/13632469.2016.1264322
26. Mansouri I, et al (2017) Assessment of seismic vulnerability of steel and RC moment buildings using HAZUS and statistical methodologies. Discrete Dyn Nat Soc 2017. https://doi.org/10.1155/2017/2698932
27. McGrath H, Abo El Ezz A, Nastev M (2019) Probabilistic depth–damage curves for assessment of flood-induced building losses. Nat Hazards. Springer Neth 97(1). https://doi.org/10.1007/s11069-019-03622-3
28. Moya L, et al (2018) Synthetic building damage scenarios using empirical fragility functions: a case study of the 2016 Kumamoto earthquake. Int J Disaster Risk Reduction. Elsevier Ltd, 31(October 2017):76–84. https://doi.org/10.1016/j.ijdrr.2018.04.016
29. Nwe ZZ et al (2018) Development of damage patterns and fragility curves in brick-nogging buildings from the thabeikkyin earthquake, Myanmar, 2012. J Earthq Eng Taylor Francis 22(7):1169–1187. https://doi.org/10.1080/13632469.2016.1277439
30. Paez-Ramirez J et al (2020) A comparative study of empirical and analytical fragility functions for the assessment of tsunami building damage in Tumaco, Colombia. Coastal Eng J. Taylor Francis 62(3):362–372. https://doi.org/10.1080/21664250.2020.1726558
31. Paez-Ramirez J, et al (2021) A comparative analysis of empirical and analytical tsunami fragility functions for buildings in Tumaco, Colombia. IOP Conf Ser: Earth Environm Sci 630(1). https://doi.org/10.1088/1755-1315/630/1/012008

32. Palazzi NC et al (2020) Seismic damage and fragility assessment of ancient masonry churches located in central Chile. Bull Earthq Eng Springer, Neth 18(7):3433–3457. https://doi.org/10.1007/s10518-020-00831-1
33. De Risi R et al (2017) Bayesian tsunami fragility modeling considering input data uncertainty. Stoch Environ Res Risk Assess Springer, Berlin Heidelberg 31(5):1253–1269. https://doi.org/10.1007/s00477-016-1230-x
34. Sadeghi M, Ghafory-Ashtiany M, Pakdel-Lahiji N (2015) Developing seismic vulnerability curves for typical Iranian buildings. Proc Inst Mech Eng, Part O: J Risk Reliab 229(6):627–640. https://doi.org/10.1177/1748006X15596085
35. Scorzini AR, Frank E (2017) Flood damage curves: new insights from the 2010 flood in Veneto, Italy. J Flood Risk Manage 10(3):381–392. https://doi.org/10.1111/jfr3.12163
36. Spence R, Martínez-Cuevas S, Baker H (2021) Fragility estimation for global building classes using analysis of the Cambridge earthquake damage database (CEQID). Bull Earthq Eng Springer, Neth 19(14):5897–5916. https://doi.org/10.1007/s10518-021-01178-x
37. Suppasri A et al (2015) Fragility curves based on data from the 2011 Tohoku-oki Tsunami in Ishinomaki City, with discussion of parameters influencing building damage. Earthq Spectra 31(2):841–868. https://doi.org/10.1193/053013EQS138M
38. Uva G et al (2019) A mechanical approach for estimating regional fragility curves of existing RC buildings stock in Puglia. COMPDYN Proc Nat Tech Univ Athens 1:1664–1676. https://doi.org/10.7712/120119.7027.19153
39. Alwaeli W, et al (2020) Rigorous versus less-demanding fragility relations for RC high-rise buildings. Bull Earthq Eng. Springer Netherlands. https://doi.org/10.1007/s10518-020-00915-y
40. Aránguiz R et al (2018) Development and application of a Tsunami fragility curve of the 2015 Tsunami in Coquimbo, Chile. Nat Hazard 18(8):2143–2160. https://doi.org/10.5194/nhess-18-2143-2018
41. Belliazzi S, et al (2021) Preliminary Tsunami analytical fragility functions proposal for Italian coastal residential masonry buildings. Structures. Elsevier Ltd, (31 Oct 2020):68–79. https://doi.org/10.1016/j.istruc.2021.01.059
42. Borzi B, Faravelli M, Di Meo A (2021) Application of the SP-BELA methodology to RC residential buildings in Italy to produce seismic risk maps for the national risk assessment. Bull Earthq Eng. Springer Netherlands, 19(8):3185–3208. https://doi.org/10.1007/s10518-020-00953-6
43. Cardone D, Perrone G (2015) Damage and loss assessment of pre-70 RC frame buildings with fema p-58: a case study. Improving the seismic performance of existing buildings and other structures 2015—proceedings of the 2nd ATC and SEI conference on improving the seismic performance of existing buildings and other structures. American society of civil engineers (ASCE), pp 363–375. https://doi.org/10.1061/9780784479728.030
44. Chaudhary RK, Roy T, Matsagar V (2020) Member and structural fragility of reinforced concrete structure under fire. J Struct Fire Eng 11(4):409–435. https://doi.org/10.1108/JSFE-02-2019-0015
45. Chen M, et al (2021) Quantitative assessment of physical fragility of buildings to the debris flow on 20 August 2019 in the Cutou gully, Wenchuan, southwestern China. Engineering geology. Elsevier B.V., 293(Oct 2020), p 106319. https://doi.org/10.1016/j.enggeo.2021.106319
46. De-León-Escobedo D, Lazcano G (2021) Probabilistic assessment of damage and losses on buildings under strong winds in Mexico. Eur J Environ Civil Eng. Taylor and Francis 1–16. https://doi.org/10.1080/19648189.2021.1871656
47. Donà M et al (2021) Mechanics-based fragility curves for Italian residential URM buildings. Bull Earthq Eng. Springer, Netherlands 19(8):3099–3127. https://doi.org/10.1007/s10518-020-00928-7
48. Forcellini D (2021) Seismic fragility for a masonry-infilled rc (Mirc) building subjected to liquefaction. Appl Sci (Switzerland) 11(13). https://doi.org/10.3390/app11136117

49. Fotopoulou SD, Pitilakis KD (2021) Towards the vulnerability assessment of low-code RC frame buildings at precarious slopes subjected to rainfall induced landslide hazard. Structures. Elsevier Ltd 34(8):239–261. https://doi.org/10.1016/j.istruc.2021.07.074
50. Del Gaudio C et al (2015) Development and urban-scale application of a simplified method for seismic fragility assessment of RC buildings. Eng Struct Elsevier Ltd 91:40–57. https://doi.org/10.1016/j.engstruct.2015.01.031
51. Gautam D et al (2020) An empirical method for seismic vulnerability assessment of Nepali school buildings. Bull Earthq Eng Springer, Netherlands 18(13):5965–5982. https://doi.org/10.1007/s10518-020-00922-z
52. Gernay T, Elhami Khorasani N, Garlock M (2016) Fire fragility curves for steel buildings in a community context: a methodology. Eng Struct Elsevier Ltd 113:259–276. https://doi.org/10.1016/j.engstruct.2016.01.043
53. Giordano N, et al (2021) Seismic fragility models for typical non-engineered URM residential buildings in Malawi. Structures. Elsevier Ltd, 32(December 2020):2266–2278. https://doi.org/10.1016/j.istruc.2021.03.118
54. Gómez LVD, Kwon OS, Dabirvaziri MR (2015) Seismic fragility of steel moment-resisting frames in Vancouver and Montreal designed in the 1960s, 1980s, and 2010'. NRC Research Press, 42(11):919–929. https://doi.org/10.1139/cjce-2014-0492
55. Halder L et al (2021) Seismic vulnerability assessment of low-rise unreinforced masonry buildings in Northeast India considering variability of material properties. Asian J Civil Eng Springer Int Publishing 22(5):843–863. https://doi.org/10.1007/s42107-021-00350-7
56. Hatzikyriakou A, Lin N (2017) Simulating storm surge waves for structural vulnerability estimation and flood hazard mapping. Nat Hazards Springer, Neth 89(2):939–962. https://doi.org/10.1007/s11069-017-3001-5
57. Jain A, et al (2020) Engineering-based tornado damage assessment: numerical tool for assessing tornado vulnerability of residential structures. Front Built Environ 6(6). https://doi.org/10.3389/fbuil.2020.00089
58. Jeon B, Kim N (2007) Evaluation of comfort limit on bridge vibration. Trans Korean Soc Noise Vib Eng 17(10):923–935. https://doi.org/10.5050/ksnvn.2007.17.10.923
59. Karafagka S, Fotopoulou S, Pitilakis K (2018) Analytical tsunami fragility curves for seaport RC buildings and steel light frame warehouses. Soil Dyn Earthq Eng. Elsevier Ltd, 112(September 2017):118–137. https://doi.org/10.1016/j.soildyn.2018.04.037
60. Karimzadeh S, et al (2017) A study on fragility analyses of masonry buildings in Erzincan (Turkey) utilizing simulated and real ground motion records. Procedia Eng. Elsevier B.V., 199:188–193. https://doi.org/10.1016/j.proeng.2017.09.237
61. Kassem MM et al (2019) Seismic fragility assessment for moment-resisting concrete frame with setback under repeated earthquakes. Asian J Civil Eng. Springer Int Publishing 20(3):465–477. https://doi.org/10.1007/s42107-019-00119-z
62. Kouris LAS, Kappos AJ (2015) Fragility curves and loss estimation for traditional timber-framed masonry buildings in Lefkas, Greece. Comput Methods Appl Sci. Springer Sci Bus Media B.V., 37:199–233. https://doi.org/10.1007/978-3-319-16130-3_8
63. Li Q, Wang C, Zhang H (2016) A probabilistic framework for hurricane damage assessment considering non-stationarity and correlation in hurricane actions. Struct Saf Elsevier Ltd 59:108–117. https://doi.org/10.1016/j.strusafe.2016.01.001
64. Mangkoesoebroto SP, Prayoga MH, Parithusta R (2019) Collapse risks of fail-safe rc frames due to earthquakes: fragility assessments. J Eng Technol Sci Inst Res Community Serv, Institut Teknologi Bandung 51(4):479–500. https://doi.org/10.5614/j.eng.technol.sci.2019.51.4.3
65. McCrum DP, Amato G, Suhail R (2016) Development of seismic fragility functions for a moment resisting reinforced concrete framed structure. Open Constr Build Technol J 10(1):42–51. https://doi.org/10.2174/1874836801610010042
66. Mebarki A, Barroca B (2015) Resilience and vulnerability analysis for restoration after tsunamis and floods: the case of dwellings and industrial plants. Adv Nat Technol Hazards Res Springer, Neth 44:237–258. https://doi.org/10.1007/978-3-319-10202-3_16

67. Medina S, et al (2019) Tsunami analytical fragility curves for the Colombian Pacific coast: a reinforced concrete building example. Eng Struct. Elsevier, 196(October 2018):109309. https://doi.org/10.1016/j.engstruct.2019.109309
68. Megalooikonomou KG, Parolai S, Pittore M (2018) Toward performance-driven seismic risk monitoring for geothermal platforms: development of ad hoc fragility curves. Geoth Energy. Springer Berlin Heidelberg 6(1). https://doi.org/10.1186/s40517-018-0094-3
69. Michel C et al (2018) Deriving fragility functions from bilinearized capacity curves for earthquake scenario modelling using the conditional spectrum. Bull Earthq Eng Springer, Neth 16(10):4639–4660. https://doi.org/10.1007/s10518-018-0371-3
70. Nagashree BK, Ravi Kumar CM, Venkat Reddy D (2016) A parametric study on seismic fragility analysis of RC buildings. Earthq Struct. Techno Press 10(3):629–643. https://doi.org/10.12989/EAS.2016.10.3.629
71. Nazri FM, et al (2017) Seismic fragility curves of industrial buildings by using nonlinear analysis. MATEC web of conferences, p 103. https://doi.org/10.1051/matecconf/201710302017
72. Novelli VI et al (2021) Fragility curves for non-engineered masonry buildings in developing countries derived from real data based on structural surveys and laboratory tests. Soft Comput Springer, Berlin Heidelberg 25(8):6113–6138. https://doi.org/10.1007/s00500-021-05603-w
73. Oubennaceur K et al (2019) Flood risk mapping for direct damage to residential buildings in Quebec, Canada. Int J Disaster Risk Reduction Elsevier Ltd 33:44–54. https://doi.org/10.1016/j.ijdrr.2018.09.007
74. Pan Y, Ventura CE, Tannert T (2020) Damage index fragility assessment of low-rise light-frame wood buildings under long duration subduction earthquakes. Struct Saf. Elsevier 84(May 2019):101940. https://doi.org/10.1016/j.strusafe.2020.101940
75. Peng X, et al (2016) An engineering-based approach to predict Tornado-induced damage. Multi-Hazard Approaches Civil Infrastruct Eng. Springer Int Publishing 311–335. https://doi.org/10.1007/978-3-319-29713-2_15
76. Petrone C, Rossetto T, Goda K (2017) Fragility assessment of a RC structure under tsunami actions via nonlinear static and dynamic analyses. Eng Struct Authors 136:36–53. https://doi.org/10.1016/j.engstruct.2017.01.013
77. Remki M, Kehila F (2018) Facing the challenges in structural engineering. 1st GeoMEast international congress and exhibition, vol 1, pp 42–54. https://doi.org/10.1007/978-3-319-61914-9
78. Rodrigues LG, et al (2021) Application of fragility analysis to timber-framed structures for seismic and robustness assessments. Lecture Notes Civil Eng. Springer Sci Bus Media Deutschland GmbH, 153 LNCE 165–177. https://doi.org/10.1007/978-3-030-73616-3_12
79. Saruddin SNA, Nazri FM (2015) Fragility curves for low- and mid-rise buildings in Malaysia. Procedia Eng. Elsevier B.V., 125:873–878. https://doi.org/10.1016/j.proeng.2015.11.056
80. Sihombing F, Torbol M (2015) Analytical fragility curves of reinforced concrete buildings subject to tsunami waves. Proc 2014 2nd Int Conf Technol, Inf, Manage, Eng Environ, TIME-E 2014 34–39. https://doi.org/10.1109/TIME-E.2014.7011588
81. Torrieri F, Oppio A (2019) The ex-ante evaluation of flood damages for a sustainable risk management. Smart innovation, systems and technologies. Springer International Publishing. https://doi.org/10.1007/978-3-319-92102-0_57
82. Utami AC, Kurniawan R, Fauzan (2021) Analytical fragility curve development of maternity and children's M. Djamil hospital building Padang due to earthquake and tsunami. IOP Conf Ser: Earth Environ Sci 708(1). https://doi.org/10.1088/1755-1315/708/1/012014
83. Zain M et al (2019) Seismic fragility assessment of reinforced concrete high-rise buildings using the uncoupled modal response history analysis (UMRHA). Geotech, Geol Earthq Eng 47:201–218. https://doi.org/10.1007/978-3-319-78187-7_16
84. Zentner I (2017) A general framework for the estimation of analytical fragility functions based on multivariate probability distributions. Struct Saf Elsevier Ltd 64:54–61. https://doi.org/10.1016/j.strusafe.2016.09.003

85. Hait P, Sil A, Choudhury S (2020a) Seismic damage assessment and prediction using artificial neural network of RC building considering irregularities. Taylor Francis 5(1):51–69. https://doi.org/10.1080/24705314.2019.1692167
86. Roeslin S, et al (2020) A machine learning damage prediction model for the 2017 Puebla-Morelos, Mexico, earthquake. Earthq Spectra 36(2_suppl):314–339. https://doi.org/10.1177/8755293020936714
87. Won J, Shin J (2021) Machine learning-based approach for seismic damage prediction method of building structures considering soil-structure interaction. Sustainability (Switzerland) 13(8). https://doi.org/10.3390/su13084334
88. Xiong C, et al (2021) Multiple-input convolutional neural network model for large-scale seismic damage assessment of reinforced concrete frame buildings. Appl Sci. Multi Digit Publishing Inst 11(17):8258. https://doi.org/10.3390/APP11178258
89. Dias P, et al (2018) 'Development of damage functions for flood risk assessment in the city of Colombo (Sri Lanka). Procedia Eng. Elsevier B.V., 212:332–339. https://doi.org/10.1016/j.proeng.2018.01.043
90. Díaz SA, et al (2018) Capacity, damage and fragility models for steel buildings: a probabilistic approach. Bull Earthq Eng. https://doi.org/10.1007/s10518-017-0237-0
91. Fallah Tafti M, Amini Hosseini K, Mansouri B (2020) Generation of new fragility curves for common types of buildings in Iran. Bull Earthq Eng. Springer, Netherlands 18(7):3079–3099. https://doi.org/10.1007/s10518-020-00811-5
92. Frucht E, et al (2021) Tsunami loss assessment based on Hazus approach—the bat galim, Israel, case study. Eng Geol. Elsevier B.V. 289(5):106175. https://doi.org/10.1016/j.enggeo.2021.106175
93. Kamath K, Anil S (2017) Fragility curves for low-rise, mid-rise and high-rise concrete moment resisting frame building for seismic vulnerability assessment. Int J Civil Eng Technol 8(3):510–519
94. Kappos AJ (2016) An overview of the development of the hybrid method for seismic vulnerability assessment of buildings. Struct Infrastruct Eng 12(12):1573–1584. https://doi.org/10.1080/15732479.2016.1151448
95. Lombardi L, De Luca F (2020) Derivation of fragility curves at design stage through linear time-history analysis. Eng Struct. Elsevier 219(6):110900. https://doi.org/10.1016/j.engstruct.2020.110900
96. De Luca F, Verderame GM, Manfredi G (2015) Analytical versus observational fragilities: the case of Pettino (L'Aquila) damage data database. Bull Earthq Eng 13(4):1161–1181. https://doi.org/10.1007/s10518-014-9658-1
97. Mancini M, et al (2017) An integrated model for Ex-ante evaluation of flood damage to residential building. Green Energy Technol 0(9783319496757):157–170. https://doi.org/10.1007/978-3-319-49676-4_12
98. Miluccio G, Parisi F, Cosenza E (2020) Fragility curves for rc framed buildings subjected to earthquake-induced landslide: comparison between 2d and 3d structural models. Proceedings of the international conference on structural dynamic, EURODYN. European association for structural dynamics, vol 2, pp. 3780–3787. https://doi.org/10.47964/1120.9309.20456
99. Rehman K, Cho YS (2016) Building damage assessment using scenario based tsunami numerical analysis and fragility curves. Water (Switzerland) 8(3). https://doi.org/10.3390/w8030109
100. Sandoli A, et al (2021) Fragility curves for Italian URM buildings based on a hybrid method. Bull Earthq Eng. Springer Neth. https://doi.org/10.1007/s10518-021-01155-4

101. Uday Kumar B, Sreekanth GN (2019) A gui framework for the development of fragility curves for a low-rise and medium-rise buildings. Int J Eng Adv Technol 8(5):1146–1152
102. Zeng D, Zhang H, Wang C (2020) Modelling correlated damage of spatially distributed building portfolios under scenario tropical cyclones. Struct Saf. Elsevier B.V., 87. https://doi.org/10.1016/J.STRUSAFE.2020.101978
103. Fan J, et al (2019) Empirical and machine learning models for predicting daily global solar radiation from sunshine duration: a review and case study in China. Renew Sustain Energy Rev. Elsevier Ltd, 100(July 2018):186–212. https://doi.org/10.1016/j.rser.2018.10.018
104. Hait P, Sil A, Choudhury S (2020) Seismic damage assessment and prediction using artificial neural network of RC building considering irregularities. J Struct Integrity Maintenance Taylor Francis 5(1):51–69. https://doi.org/10.1080/24705314.2019.1692167

Development of a Digital Elevation Model Integrating Different Datasets for an Area of Mahaweli Basin, Sri Lanka

P. D. P. O. Peramuna, N. G. P. B. Neluwala, K. K. Wijesundara, P. B. R. Dissanayake, S. De Silva, and S. Venkatesan

Abstract Accurate floodplain inundation estimation remains challenging in hydrodynamic flood modeling studies. Thus, developing a Digital Elevation Model (DEM) featuring all the vital floodplain features is crucial to produce accurate results. In addition, DEM performs a faster representation of topographic data and generates reproducible data useful for future flood modeling studies. However, developing an accurate DEM depends on the factors such as available topographic maps, associated budget requirements, intended accuracy, and purpose of the flood modeling study. Generally, a DEM is derived from various sources such as Light detection and ranging (LiDAR) and Shuttle Radar Topographic Mission (SRTM) in addition to the traditional geographic survey. However, these models and DEM from other sources have their specific advantages and limitations. At times, the data may be available for a part of the required terrain. Thus, this research develops an accurate DEM incorporating all the models from LiDAR, SRTM, and topographical map from Survey Department and measured cross sections from a geographic survey that possessed different accuracy levels, boundaries, and characteristics. The developed terrain map depicts the Upper Mahaweli basin and later will be used for simulation in a dam breach modeling study. Differences and adjustments required for different terrain models were identified in this study. Furthermore, advanced tools in software such as ArcGIS and HEC-RAS (6.0 version) were used in the research as a novel approach. Hence, this study would be beneficial for flood modelers to move toward high-accuracy optimal meshing in flood modeling research generated by such developed DEM, especially in the Sri Lankan context. Furthermore, this study would contribute to understanding strengths and limitations in spatial datasets in Sri Lanka for future research work.

P. D. P. O. Peramuna (✉) · N. G. P. B. Neluwala · K. K. Wijesundara · P. B. R. Dissanayake
Department of Civil Engineering, Faculty of Engineering, University of Peradeniya, Peradeniya, Sri Lanka
e-mail: oshini.peramuna@eng.pdn.ac.lk

P. D. P. O. Peramuna · S. De Silva · S. Venkatesan
School of Engineering, Royal Melbourne Institute of Technology (RMIT) University, Melbourne, Australia

R. Dissanayake et al. (eds.), *12th International Conference on Structural Engineering and Construction Management*, Lecture Notes in Civil Engineering 266,
https://doi.org/10.1007/978-981-19-2886-4_30

Keywords Mosaic · Raster · DEM · LiDAR · SRTM · HEC-RAS

1 Introduction

For almost all flood modeling simulations, Digital Elevation Model (DEM) integrated with Geographic Information System (GIS) plays a major role. In addition, for accurate modeling of the flood propagation, representation of the domain closer to the existing reality is crucial [1]. Currently, the availability of DEMs derived from high-resolution data has partly fueled the use of both high-resolution modeling and 2D modeling [2]. Therefore, a better terrain model with a high horizontal and vertical accuracy will be essential to produce better flood inundation results.

With the advent of modern technology, there are several techniques to obtain accurate topographic data using remote sensing methods other than the traditional geographic surveys. Airborne Light detection and ranging (LiDAR), Shuttle Radar Topographic Mission (SRTM) based on space-borne interferometric synthetic aperture radar (InSAR) [3], and Advanced Space-borne Thermal Emission and Reflection Radiometers (ASTER) based on optical satellite images are the methods to name a few.

Generally, LiDAR uses a focused short wavelength laser beam which has the ability to penetrate vegetation and reduced vulnerability to scatter, resulting higher precision and accuracy [4]. Nevertheless, it is limited to a few number of countries and can be expensive to acquire [3]. Hence, the use of globally available topographic data like ASTER DEM and SRTM becomes a viable alternative with necessary corrections and accuracy assessments due to its lower noise, particularly in the flatter areas which are of concern to flood modelers [5]. The main concern in these data is that their horizontal and vertical accuracies cannot sufficiently address the accurate representation of flood modeling, such as in the case of a dam breach flow. In addition, there are DEM data sources such as NED (National Elevation Dataset) of 1 arc-sec horizontal resolution despite being limited to the USA, Canada, and Mexico and ODP1 of 1 arc-sec horizontal resolution limited for major parts in Europe and Iceland.

In the Sri Lankan context, LiDAR datasets will not be available to most regions of the country. Thus, SRTM is a widely used open-access global DEM that can be freely downloaded from the USGS Earth Explorer Web site [6]. In addition, the topographic maps produced by the Survey Department is also available in 1:50,000 or 1:10,000 scales as stated in the official Web site. DEMs are available for some parts of the country, which are produced from the above topographic maps.

Developing an accurate terrain with the incorporation of different datasets exhibiting different accuracy levels is challenging and rare in Sri Lankan context. This research is focused on developing an accurate terrain for the upper part of the Mahaweli basin in Sri Lanka which will be later used for flood modeling study.

The paper contributes to the literature by describing a successful methodology to develop high-accuracy topography map using both software ArcGIS and HEC-RAS

(version 6.0) in a Sri Lankan context which has not been done according to the best of the author's knowledge. This study incorporates datasets from LiDAR, SRTM, and topographic surveys with different characteristics and extents to generate the DEM. This paper highlights the importance of understanding the projection systems, DEM characteristics, and selection of the datasets based on the spatial requirement and end use. Furthermore, this study would facilitate those who do not necessarily share the same background on the knowledge of both Geographic Information System (GIS) and flood modeling software.

The organization of the paper is as follows. Detailed description of the datasets in the research is followed by the methodology. The results and conclusions are presented in the last two sections.

1.1 Note on Terminology

In this paper, DEM refers to the DEM which represents the fundamental depictions of the three-dimensional shape of the Earth's surface or the elevation in x, y coordinate system [7]. It is an umbrella term that includes both Digital Terrain Model (DTM) which represents a topographic surface excluding trees, buildings, and any other surface objects and Digital Surface Model (DSM) which denotes the topographic surface including surface objects such as structures and vegetation (DSM) [6].

2 Literature Review

2.1 The Use of Datasets in the Sri Lankan Context

Two-dimensional flood modeling studies exhibit high sensitivity to the topographical maps [8]. Therefore, a significant concern is highlighted on the DEM used for the modeling. According to current literature, DEM derived from single sources such as LiDAR, SRTM, ASTER GDEM, HydroSHEDS, and topographic maps has been used for research work in Sri Lanka.

Sri Lanka Survey Department (SLSD) is the national authority for surveying and mapping in Sri Lanka [9]. The availability of the terrain data according to the region with other useful information such as data acquiring data, data collection methodology, scale, and available formats can be obtained from the Web site. In fact, flood modeling studies in Sri Lanka have used DEM developed from 1:10,000 contour maps (contour interval of 5 m) in general [10, 11].

LiDAR is an optical remote sensing technique that uses laser light in the form of a pulsed laser to measure the distance and produce highly accurate x, y, z measurements. The available LiDAR data for Sri Lanka is mainly confined to a small area as shown in SLSD Web site which might be due to the large cost of acquiring data.

However, it has high vertical and horizontal accuracy compared to other terrain maps. Therefore, using DEM derived from LiDAR is an emerging practice in hydrodynamic modeling in Sri Lanka [12].

In Shuttle Radar Topography Mission (SRTM), land elevations are measured using C-band radar interferometry and provide a near-global DEM at one arc-second (1″ approximately 30 m) and three arc-seconds (3″ approximately 90 m) [13]. The SRTM 1 arc-second global dataset was released in phases from 2014 and is available freely, making it the most accurate topographic data available for most of the globe [14]. In the Sri Lankan context, SRTM DEM of resolution of 90 m has been used for flood modeling study [15]. In the study of [16], SRTM of 30 m was shown as the best dataset for delineation in coastal areas.

Recent research has been carried out on comparing the datasets such as LiDAR, SRTM, and ASTER [17] or based only on one type of dataset, either LiDAR or SRTM in flood modeling studies in Sri Lanka. Little research has been done on the development of terrain by the addition or merging of the datasets. In this present study, a detailed description to develop an accurate terrain model is presented. Furthermore, these research findings and methodology will pave the way to do modeling with the available data and would eliminate the necessity for highly accurate good topographical maps throughout the whole area.

2.2 Projection System

SLD99_SriLanka_Grid_1999 and Kandawala_SriLanka_Grid are the coordinate systems generally used by SLSD [18]. The Kandawala_SriLanka_Grid was introduced by the British government ruling Sri Lanka in 1890 and may contain some horizontal errors [19]. The SLD99_SriLanka_Grid_1999 was established using GPS by the SLSD and termed as the national map-grid coordinates. However, both systems are still in practice. Given the improvement of the new system, SLD99_SriLanka_Grid_1999 is recommended to be used [19].

3 Study Area and Datasets

Mahaweli River is the largest and longest river in Sri Lanka which is 335 km long, accounting for 24% of total water resources in the country. It benefits from both southwest and northeast monsoons. The Mahaweli basin is subdivided into the Upper Mahaweli basin and Lower Mahaweli basin. In this study, only a 46 km long stretch of Mahaweli River starting from Kotmale reservoir up to Polgolla Barrage which belongs to Upper Mahaweli basin is considered (Fig. 1).

Different datasets were incorporated in order to develop a DEM, and these datasets had different projection systems, extents, and characteristics even though all were in the same digital format of TIFF (Tagged Image File Format) (Table 1). Figure 2

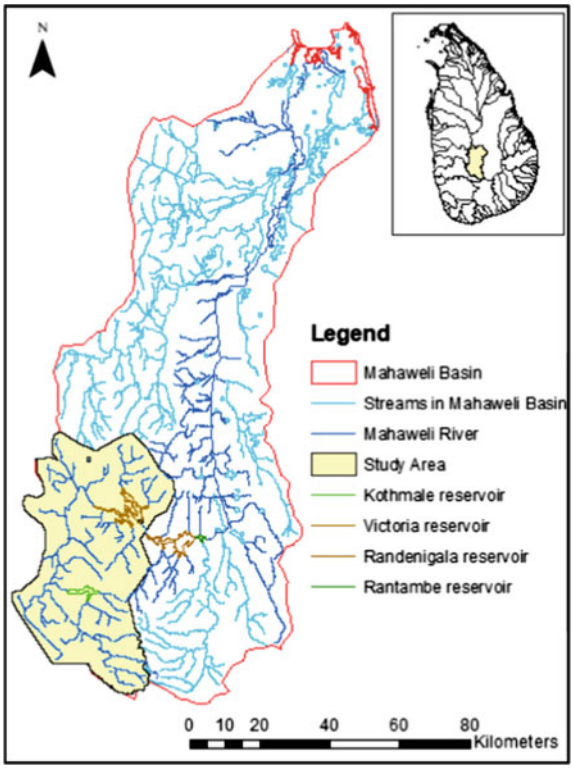

Fig. 1 Study area

Table 1 Characteristics of datasets

Dataset	Source	Projection system	Accuracy	
			Horizontal (m)	Vertical (m)
LiDAR	Sri Lanka survey department	SLD99_SriLanka_Grid_1999	1	1–3
DEM from SRTM 1 Arc-second global	USGS web site	GCS_WGS_1984	30.95	10–15
DEM from topographical maps	Sri Lanka survey department	WGS_1984_Transverse Mercator	5.04	5–10

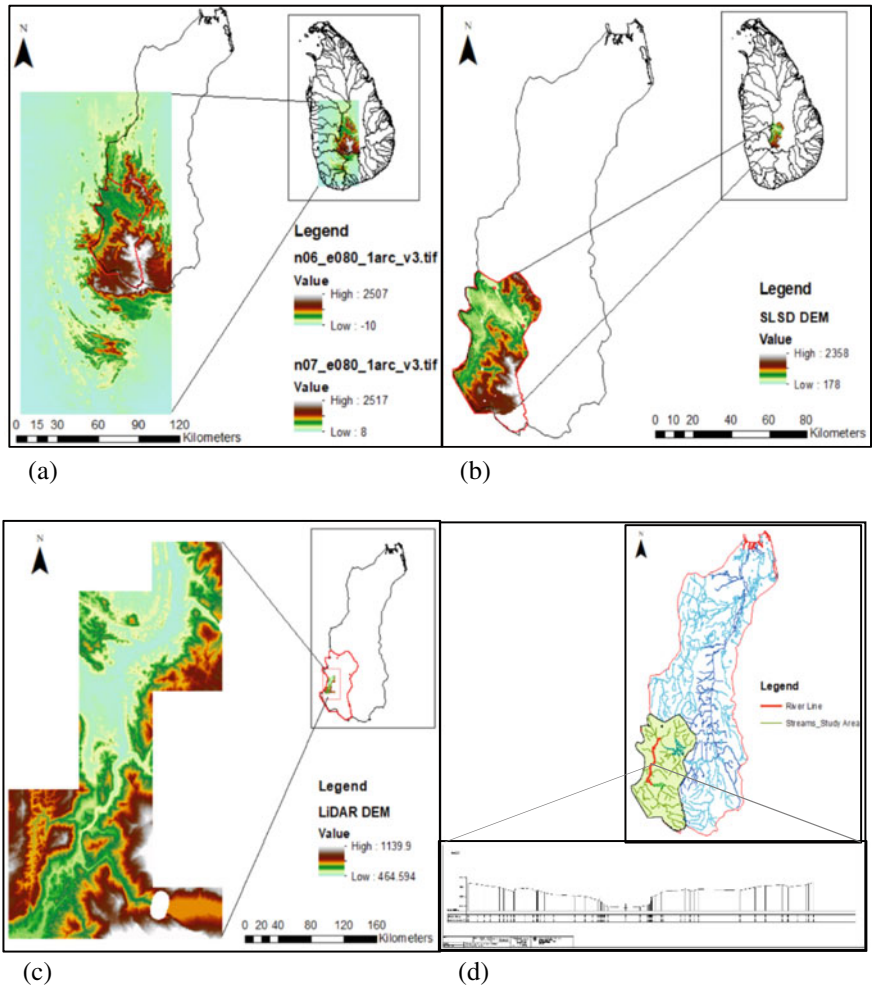

Fig. 2 Datasets used in the study: **a** SRTM DEM; **b** SLSD DEM; **c** LiDAR DEM; and **d** cross section survey

depicts the datasets used in the study area.

River cross section survey (Fig. 2d) has been conducted for the 46 km river profile starting from the spillway end of Kotmale reservoir up to Polgolla Barrage. It depicts the bathymetry of the river along with the terrain features near the banks of the river. The cross sections are of spacing 200 m, and all the data was presented in AutoCAD software. This dataset was used as a reference dataset when determining the elevation of the river bed profile in this study.

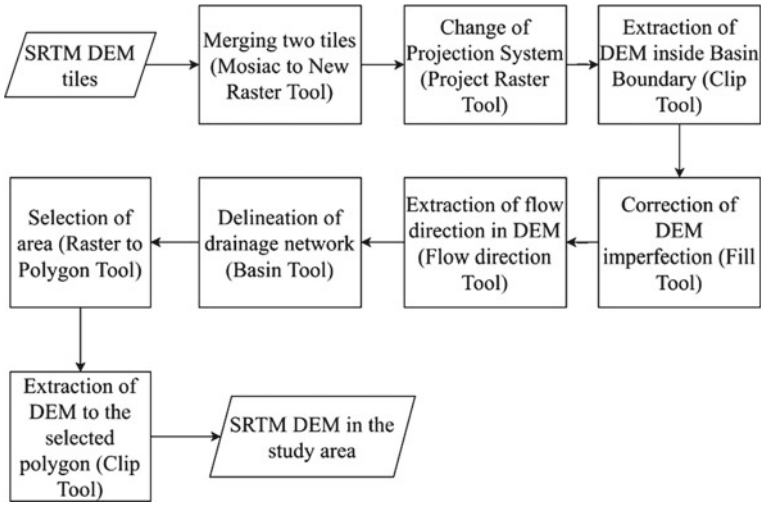

Fig. 3 Flowchart for modification of SRTM DEM

4 Methodology

4.1 Modification of SRTM DEM

SRTM tiles (1 arc-sec) available for the study area of the Mahaweli region are n06_e080_1arc_v3 and n07_e080_1arc_v3 (Fig. 2a) which have a horizontal resolution of 30 m. Generally, the availability of datasets for the study area has to be checked from the USGS Web site after creating an account free of charge following the selection and extraction of dataset.

The methodology used to extract the data in the study area from the SRTM tiles using tools is available in ArcGIS 10.7.1 version which is shown in Fig. 3. In summary, the two SRTM tiles were merged and projected to the SLD99_SriLanka_Grid_1999 system. Next, the raster dataset inside the Mahaweli River basin was extracted following the basin delineation and selecting the appropriate area.

4.2 Modification of SLSD DEM

SLSD DEM purchased from SLSD was of the horizontal resolution of 5 m. However, a shift was identified in SLSD DEM when both LiDAR and SLSD DEMs are overlapped. Figure 4 presents the methodology that is used to identify the shift and rectification of SLSD DEM using both HEC-RAS (6.0 version) and ArcGIS (ESRI) software.

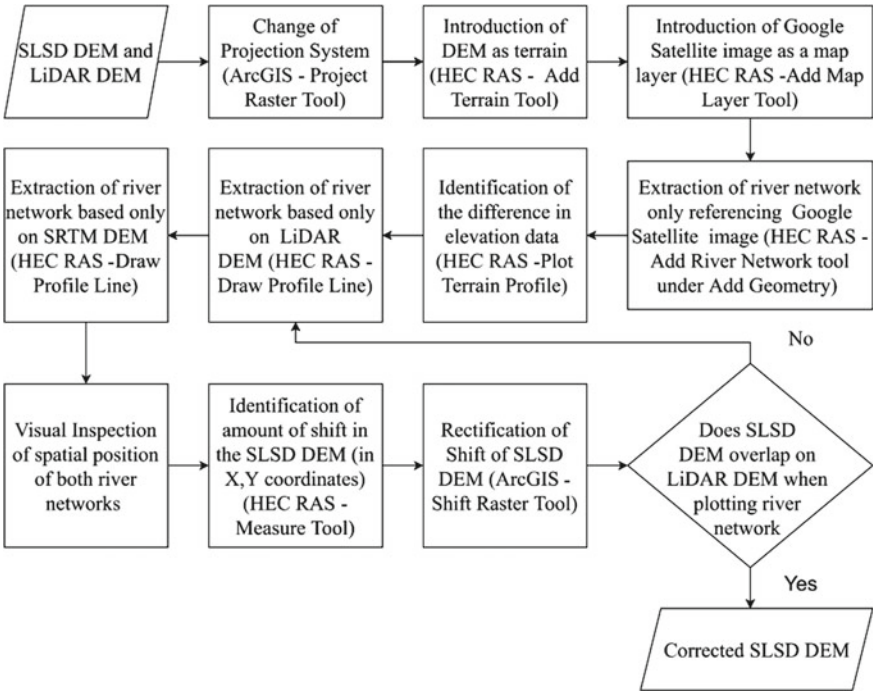

Fig. 4 Flowchart for modification of SLSD DEM

First, SLSD DEM was projected to the SLD99_SriLanka_Grid_1999 system as the common projection system would facilitate the identification of shift when maps overlapped. Then, short river profiles were drawn based on individual DEMs and compared their elevations. Next, the amount of shift was identified by visual inspection, and finally, it was rectified after a trial and error process.

4.3 Development of One Terrain Incorporating All the Datasets

All the modified datasets were used to develop one terrain intended for the dam breach modeling study in Mahaweli basin, Sri Lanka. Figure 5 depicts the methodology used to achieve the task using different tools. It should be noted that all the datasets were not used simultaneously for two reasons, constraints in computational capacity and to prioritize the high-resolution dataset. Thus, LiDAR DEM and SLSD DEM were combined first following the SRTM DEM.

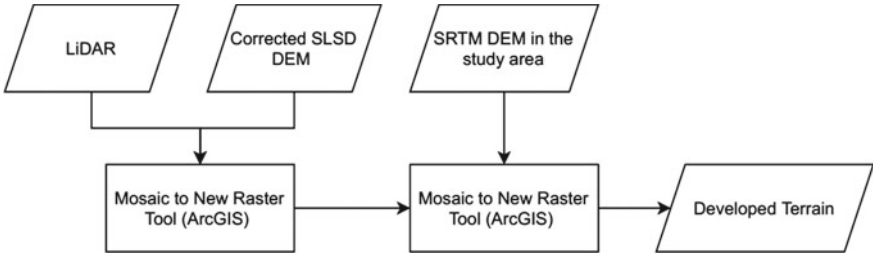

Fig. 5 Flowchart for development of terrain

5 Results and Discussion

5.1 Comparison of Datasets

The terrain was developed in such a way that more focus was given to the 46 km long river profile starting from Kotmale reservoir up to Polgolla Barrage, which will be ultimately used for dam breach modeling of Kotmale reservoir. In this study area, 28 km out of 46 km of the river profile line was covered by LiDAR DEM, which ends up quite close to the Gelioya area starting from the Kotmale reservoir. LiDAR DEM, although was expensive to acquire, showed high accuracy in representing the terrain. As depicted in Fig. 6, out of all the datasets, LiDAR data showed a slight variation in elevation from the cross section survey compared to other datasets. Although not visible clearly in Fig. 6, LiDAR DEM having a spatial resolution of 1–3 m showed more data points resulting in a more accurate representation of the terrain. Therefore, LiDAR DEM was chosen as the reference dataset for that area. Thus, SLD99_SriLanka_Grid_1999 system, the coordinate system of LiDAR DEM was

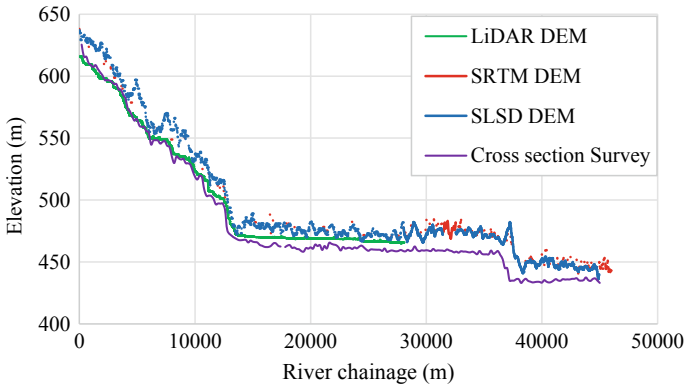

Fig. 6 Comparison of elevation of datasets

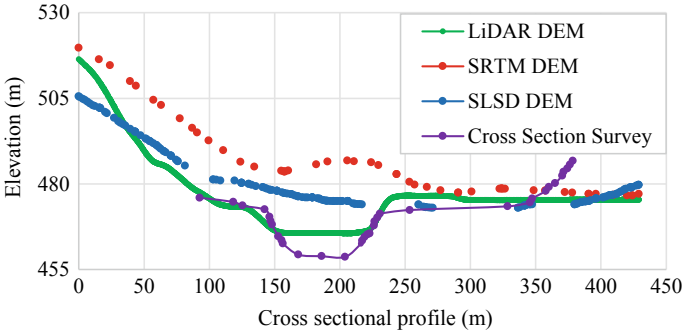

Fig. 7 Comparison of elevation in a cross section at chainage 27,200 m

used as the common projection system for all datasets, which was also recommended in literature.

Generally, in acquiring LiDAR data, receivers detect the reflection of the laser beam that is transmitted toward a target. Technically, the traditional laser system which is used in a topographic LiDAR survey would not penetrate the water column. As a result, sensors will detect the water surface in a water body, not the river bathymetry. This fact is evident from Fig. 7, which shows the change in elevation in a cross section extracted from all the datasets. There is a significant elevation difference inside the river but not in the river valley when comparing the elevation of river bathymetry (orange color) with that of the LiDAR DEM (green color). Therefore, after creating the DEM featuring the floodplain, a separate river bathymetry DEM will be required to propagate floodwaters in a flood modeling study.

As evident from both Figs. 6 and 7, SLSD DEM shows elevations relatively close to LiDAR DEM and cross section survey, compared with SRTM DEM. Thus, SLSD DEM was chosen as the reference dataset at regions where LiDAR data is unavailable. Yet, both LiDAR DEM and SLSD DEM possessed no data regions which represent significant locations in the vicinity of the study area (Fig. 8).

Freely available, SRTM DEM has a spatial resolution of 30 m and covers a larger portion of the Mahaweli basin at little or no cost. As a result, even though the spatial resolution is higher (30 m), it was used to fill the no data value points and retrieve elevation for the upper basin part of the basin.

5.2 Modification of SRTM DEM

The SRTM dataset contributed to the study mainly in three ways. First, this dataset was used to understand the accuracy of elevation with the other datasets as shown in Fig. 3. Second, the SRTM dataset was used to extract elevation for areas where there is no data available. Third, elevation for the upper part of the Mahaweli basin was obtained from SRTM DEM, which SLSD DEM does not represent. Therefore,

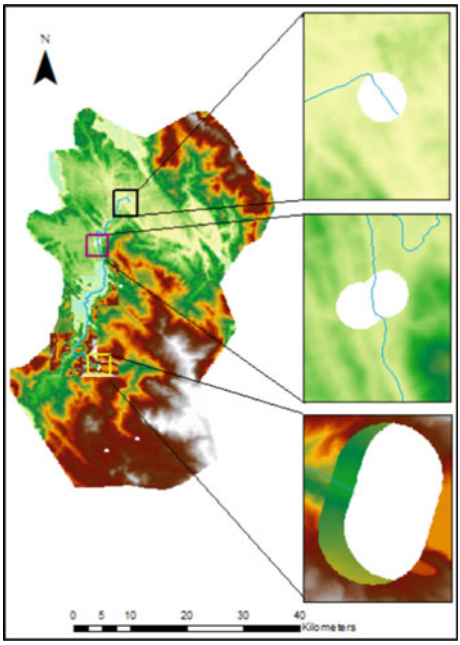

Fig. 8 No data points in both LiDAR DEM and SLSD DEM

SRTM DEM was modified, confining its terrain representation only to the Mahaweli basin, cutting off unnecessary data beyond basin boundary (Fig. 11a).

It should be noted that, tools in HEC-RAS can also be used in order to fill no data values of the SLSD DEM and LiDAR DEM (Fig. 8), in which the approximate elevation can be input to the terrain dataset. In fact, at some places, the no data region spans over 1700 m, and therefore, approximation of elevation for such area is not acceptable.

5.3 Modification of SLSD DEM

Figure 9 denotes a significant elevation difference in the SLSD DEM when river profiles of individual datasets with the same projection system (SLD99_SriLanka_Grid_1999) are overlapped.

When river profiles that were drawn solely based on one dataset (In Fig. 10, the black color river profile line was drawn based on the LiDAR DEM (a) and pink color line drawn based on SRTM DEM (b)) were compared, it showed a slight shift in river profile lines. The shift of the DEM 250 m to positive x-direction and 40 m to positive y-direction was identified in the trial and error process and was rectified such that both SLSD DEM and LiDAR DEM overlap correctly.

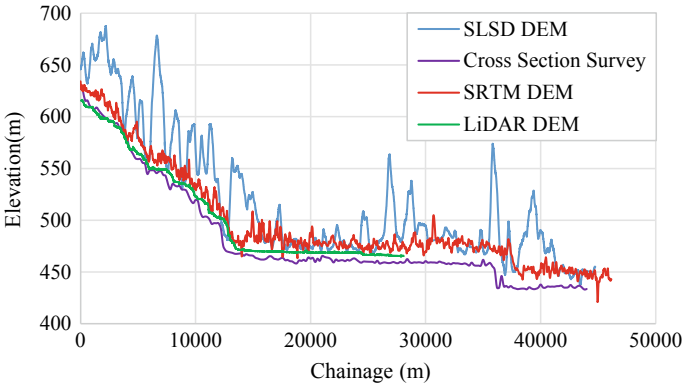

Fig. 9 Elevation of river centreline before rectification of shift

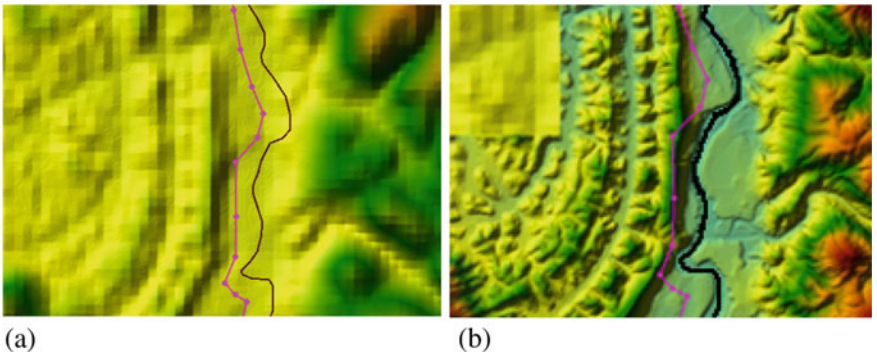

Fig. 10 Discrepancy in river profile lines

5.4 Development of DEM Incorporating All the Datasets

The objective of this research study was to develop a DEM using datasets subjected to various modifications. When generating the terrain, special consideration was paid for the computational capability, which was problematic due to the large computational size of the datasets. The LiDAR dataset has the largest file size, and it has to be handled carefully for the proper functioning of ArcGIS software. The final output of the research is shown in Figs. 11 and 12.

The generated DEM has a cell size of 25 m, and this might represent the whole terrain accurately than using only SRTM or SLSD DEM datasets. However, by specifying the cell size of the DEM, the cell resolution can be altered if necessary. Furthermore, river bathymetry DEM will be introduced to the terrain later.

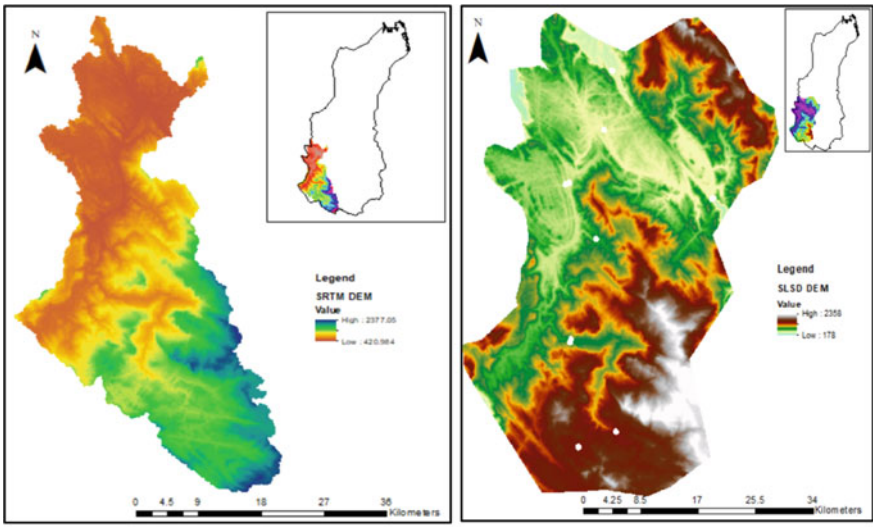

Fig. 11 Modified datasets; **a** SRTM DEM; **b** SLSD DEM

6 Conclusion

From the extensive study of the datasets, a comparison between the characteristic features can be made to select the better dataset for a study. In here, LiDAR dataset represents the existing terrain accurately compared to SRTM DEM and the SLSD DEM. However, it cannot capture the river bathymetry, and therefore, further measures have to be taken to incorporate the river bed topography. In addition to ArcGIS tools for terrain processing, HEC-RAS software is a user-friendly alternative to identify the characteristics of datasets. Furthermore, modifying the SRTM DEM and confining its extents to the study area have reduced the computational power used for overall terrain processing. The results show that an accurate terrain can be developed while also considering the computational capability in the absence of an accurate dataset for the entire study area. On that account, this terrain which is the final output of the study can be used for the flood modeling studies in the upper region of the Mahaweli basin. The methodology discussed in the paper will be helpful for practicing engineers having different types of datasets for flood modeling. For future studies, a comparison between different resolutions of the developed terrain is recommended. Open-source software such as QGIS can also be used to perform the methodology even though ArcGIS software was used in the study.

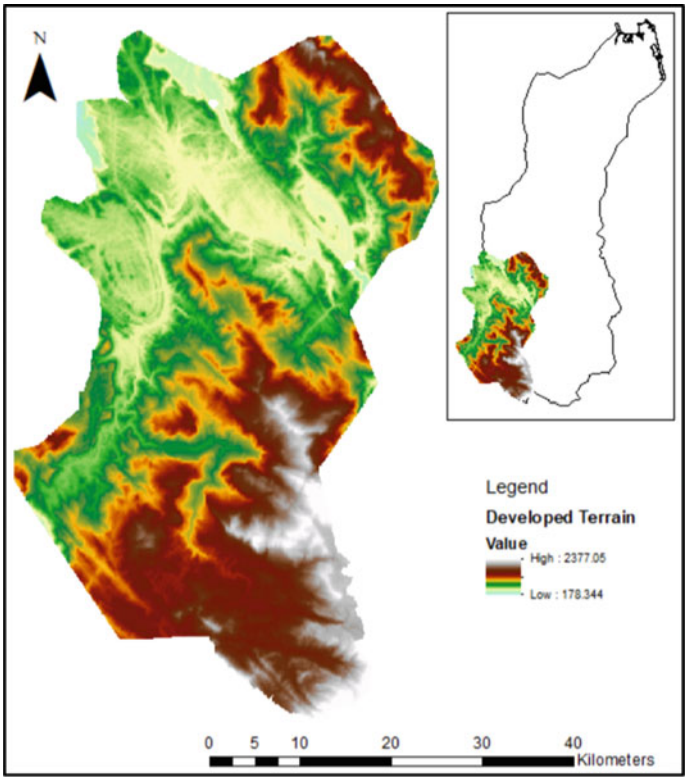

Fig. 12 Developed DEM

Acknowledgements The authors would greatly acknowledge the Department of Civil Engineering of Faculty of Engineering of University of Peradeniya, Sri Lanka, Mahaweli Authority Office, Polgolla and Sri Lanka Survey Department for their assistance and the financial support of RMIT University, Australia with the computational resources funded by Erasmus CCWater Project.

References

1. Abdessamed D, Abderrazak B (2019) Coupling HEC-RAS and HEC-HMS in rainfall–runoff modeling and evaluating floodplain inundation maps in arid environments: case study of Ain Sefra city, Ksour Mountain. SW of Algeria. Environ Earth Sci 78(19). https://doi.org/10.1007/s12665-019-8604-6
2. Bellos V, Papageorgaki I, Kourtis I (2020) Reconstruction of a flash flood event using a 2D hydrodynamic model under spatial and temporal variability of storm. Nat Hazards 101:711–726. https://doi.org/10.1007/s11069-020-03891-3
3. Hawker L, Bates P, Neal J, Rougier J (2018) Perspectives on digital elevation model (DEM) simulation for flood modeling in the absence of a high-accuracy open access global DEM. Front Earth Sci 6(12):1–9. https://doi.org/10.3389/feart.2018.00233

4. Su Y, Guo Q, Ma Q, Li W (2015) SRTM DEM correction in vegetated mountain areas through the integration of spaceborne LiDAR, airborne LiDAR, and optical imagery. Remote Sens 7(9):11202–11225. https://doi.org/10.3390/rs70911202
5. Ali HT (2016) Digital urban terrain characterization for 1D2D hydrodynamic flood modelling in Kigali, Rwanda. University of Twente, Thesis
6. Courty LG, Soriano-Monzalvo JC, Pedrozo-Acuña A (2019) Evaluation of open-access global digital elevation models (W3D30, SRTM, and ASTER) for flood modelling purposes. J Flood Risk Manage 12(S1 October):1–14. https://doi.org/10.1111/jfr3.12550
7. Guth PL, Niekerk AV, Grohmann CH, Muller J, Hawker L, Florinsky IV, Gesch D, Herrera-cruz V, Riazanoff S, López-vázquez C, Carabajal CC, Albinet C, Strobl P (2021) Digital elevation models: terminology and definitions. Remote Sens 13(3581):1–19
8. Yalcin E (2020) Assessing the impact of topography and land cover data resolutions on two-dimensional HEC-RAS hydrodynamic model simulations for urban flood hazard analysis. Nat Hazards 101(3):995–1017. https://doi.org/10.1007/s11069-020-03906-z
9. Survey Department of Sri Lanka. (n.d.) Retrieved October 18, 2021, from https://www.survey.gov.lk/sdweb/home.php?l=h
10. Edirisinghe EAKR, Pussella PGRNI, Vidarshana WDM (2021) GIS based approach for planning the evacuation process during flash floods: case study for gampaha divisional secretariat division, Sri Lanka. J Geospatial Surveying 1(1)
11. Nandalal HK, Ratnayake UR (2011). Flood risk analysis using fuzzy models. J Flood risk Manage, 4(2):128–139.
12. Palamakumbure L, Ratnayake AS, Premasiri HMR (2020) Sea-level inundation and risk assessment along the south and southwest coasts of Sri Lanka. Geoenvironmental Disasters 7(1):1–9
13. Farr TG, Rosen PA, Caro E, Crippen R, Duren R, Hensley S, Kobrick M, Paller M, Rodriguez E, Roth L, Seal D, Shaffer S, Shimada J, Umland J, Werner M, Oskin M, Burbank M, Alsdorf D (2007) The shuttle radar topography mission. Rev Geophys 45(RG2004):1–33. https://doi.org/10.1029/2005RG000183.1
14. EarthExplorer. (n.d.). Retrieved October 17, 2021, from https://earthexplorer.usgs.gov/
15. De Silva MMGT, Weerakoon SB, Herath S, Ratnayake UR, Mahanama S (2012) Flood inundation mapping along the lower reach of kelani river basin under the impact of climatic change. Eng: J Inst Eng Sri Lanka 45(2):23–29. https://doi.org/10.4038/engineer.v45i2.6938
16. Wickramagamage P, Wickramanayake N, Kumarihamy K, Vidanapathirana E (2012) A comparative study of elevation data from different sources for mapping the coastal inlets and their catchment boundaries. J Nat Sci Found Sri Lanka 40(1):55–65
17. Suja ACA, Rajapakse RLHL (2020) Evaluation of topographic data sources for 2D flood modelling: case study of Kelani basin, Sri Lanka. IOP Conf Ser: Earth Environ Sci. https://doi.org/10.1088/1755-1315/612/1/012043
18. Manuranga KP, Abeyratne PGV, Wickramathilake NV (2020) Review on national geodetic control network—Sri Lankan Datum 1999 (SLD_99). In: 13th international research conference of general sir John Kothalawala defence university—built environment and spatial sciences sessions, pp 72–77
19. Abeyratne PGV, Featherstone WE, Tantrigoda DA (2010) On the geodetic datums in Sri Lanka. Surv Rev 42(317):229–239. https://doi.org/10.1179/003962610X12572516251880

Climate Change Impacts on Built Environment: A Systematic Review

Bawantha Rathnayaka, Chandana Siriwardana, Dilanthi Amaratunga, Richard Haigh, and Dilan Robert

Abstract The built environment has to play an essential role in day-to-day activities of the human being because of urbanization and rapid increase of the basic needs of the human. The built environment mainly consists of buildings (residential and commercial) and infrastructures such as water, transportation, electricity, energy, telecommunication, health, and wastewater management. Some infrastructure sectors become critical among these infrastructures as societal well-being fundamentally relies on those infrastructure's reliability. These infrastructure sectors are openly defined as critical infrastructures (CIs). The climate has undergone a dramatic change causing severe natural hazards all over the world. Over the past years, the buildings and CIs have significantly been affected by the disaster and extreme weather conditions. Several scholars have attempted to identify climate change impacts on CIs and buildings in the built environment context. This paper includes a systemic review of the literature available in this area focusing on infrastructures in terms of CIs and buildings in the context of the built environment. This study has drawn on a review of scholarly articles which has been recently published SCOPUS database. This study employed the PRISMA model for the literature screening. Among 6140 records published between 2010 and 2020, 60 articles have been included and reviewed in this study. Then impacts of climate change on CIs, residential buildings, and commercial buildings are identified and summarized. Findings from the study show the importance of identifying impacts of climate change toward sustainable urban policies and regulations toward a more resilient built environment in the future.

Keywords Built environment · Climate change impacts · Systemic risks · Critical infrastructures (CIs) · Buildings

B. Rathnayaka (✉) · C. Siriwardana
Department of Civil Engineering, University of Moratuwa, Moratuwa, Sri Lanka
e-mail: rathnayakarmbs.20@uom.lk

D. Amaratunga · R. Haigh
Global Disaster Resilience Center, University of Huddersfield, Huddersfield, UK

B. Rathnayaka · D. Robert
Department of Civil Engineering, School of Engineering, RMIT University, Melbourne, VIC, Australia

R. Dissanayake et al. (eds.), *12th International Conference on Structural Engineering and Construction Management*, Lecture Notes in Civil Engineering 266,
https://doi.org/10.1007/978-981-19-2886-4_31

1 Introduction

In the past recent years, the climate has undergone a dramatic change. As per the sixth assessment report of the Intergovernmental Panel on Climate Change (IPCC), climate change is unprecedented [35]. It states that human activities contribute unequivocally to global warming and, thereby, climate change [35]. The built environment in different nations has been significantly affected by multiple concurrent climate change-related disasters all over the country [19, 77]. Residential buildings, commercial buildings, and critical infrastructures (CIs) have become principal components of the built environment. The CIs, which are openly defined as primary resources and structures essential to the social and economic well-being and effective functioning of the communities, play a significant role in the built environment by providing crucial day-to-day services to human beings. Due to the systemic nature among the CIs, disruption of the one CI would be highly affected the other CI sectors [20, 27, 46].

On the other hand, climate change has affected different components of the buildings (building envelope, construction material, and indoor environment) [7, 48]. Climate change can change the amount of energy needed for the functioning of heating and cooling equipment. Furthermore, reduced energy consumption for heating and cooling will reduce the greenhouse gas emission and thereby less contribute to climate change [3, 53].

Therefore, identifying climate change impacts on the built environment is vital as it will pave the way toward a climate-resilient and sustainable built environment. Over the past years, numerous studies have been carried out focusing on identifying the climate change impacts on buildings and CIs in the built environment. This paper aims to identify the impacts on the built environment due to changing climatic conditions, focusing on residential buildings, commercial buildings, and CIs.

2 Methodology

This study employed a systematic literature review. Two research questions were developed to identify the significant climate change impacts on the built environment, mainly focusing on CIs and residential and commercial buildings,

a. What are climate change impacts on CIs?
b. What are climate change impacts on energy performance and building materials on residential and commercial buildings?

Afterward, primary keywords for the search mechanisms will be identified for finding research articles. Table 1 illustrates the used keywords in this study. The search terms for this study are developed by combining keywords in Table 1, using Boolean operators.

As presented in Fig. 1, exclusion criteria were used to filter the articles. Articles that discussed climate change impacts on the CIs, residential and commercial buildings published in a journal/conference/book chapter published between 2010 and

Table 1 Key terms used in the study

Key terms	Category
Critical infrastructure, residential buildings, commercial buildings, urban environment, built environment	The articles related to the CIs, residential buildings, and commercial buildings
Energy demand, heating demand, cooling demand, impacts, stresses, building materials	The articles related to the climate change impacts
Climate change, extreme weather events, sea level rise, temperature rise, droughts, extreme precipitation	The article related to climate change evidence and climate change scenarios

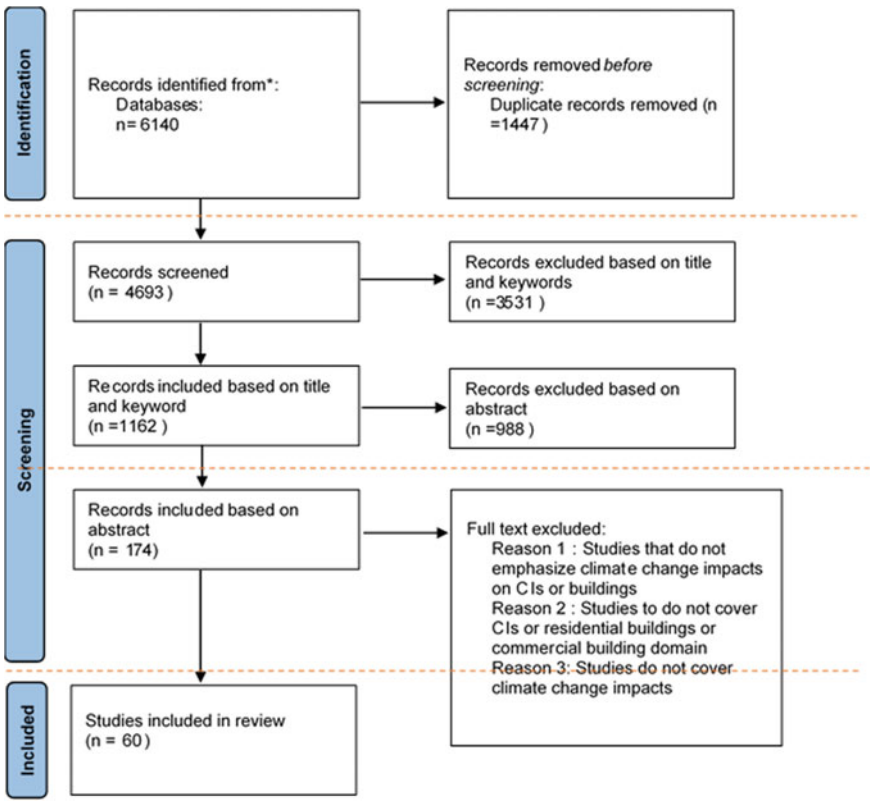

Fig. 1 Literature screening process

May 2021 and indexed in SCOPUS were included in the literature analysis. From 6140 articles, 60 articles were analyzed in this study, as presented in Fig. 1.

3 Climate Change Impacts on the Built Environment

This section summarizes the identified climate change impacts on the built environment. Section 3.1 mainly discusses the identified impacts on CIs, while Sect. 3.2 discusses the impacts on buildings.

3.1 Climate Change Impacts on CIs

This study focuses on identified climate change impacts on five CI categories (i.e., energy and electricity, transportation, wastewater treatment plant, water infrastructure, and telecommunication infrastructure). The selected publications were evaluated in terms of the effects of climate change on CIs, and an overview of the following climate change projections is provided for each of the CI sectors: extreme weather occurrences such as flooding, storms, and hurricanes, sea level rise (SLR); droughts or precipitation declines; and temperature rises.

3.1.1 Electricity and Energy Infrastructure

Over past years researchers investigated the effects of climate change on the electricity and energy sector. Figure 2 illustrates the identified climate change impacts on electricity and energy infrastructure in the literature analysis. According to the literature analysis, the rising temperature is having a detrimental influence on energy and electricity infrastructure [1, 14]. It reduces the efficiency and capacity of the transmission lines, grids generators. Also, more losses will occur in the transformers and substations [1, 18, 24, 37, 51]. In thermal power plants, coal storage may be spontaneously self-ignite due to a rise in temperature [15, 63, 66].

Extreme weather event occurrence, which will have a detrimental impact on energy and electricity infrastructure across all energy sub-sectors, is another significant adverse impact due to climate change [15, 18, 37, 52, 63, 66]. Infrastructure damages, inundations of the facilities and assets, shutting down of the power plant are some key impacts identified in this study associated with extreme weather events [15, 18, 52, 63]. Damages on coastal energy and electricity infrastructure will significantly increase due to the SLR [15, 37]. Furthermore, reduced precipitation level affects the generation capacities of the electric power plants and thereby increases the demand for other alternative energy sources [14, 15, 37, 68]. In addition, more dust can cause damages to the distribution and transmission lines during drought [15, 37, 52].

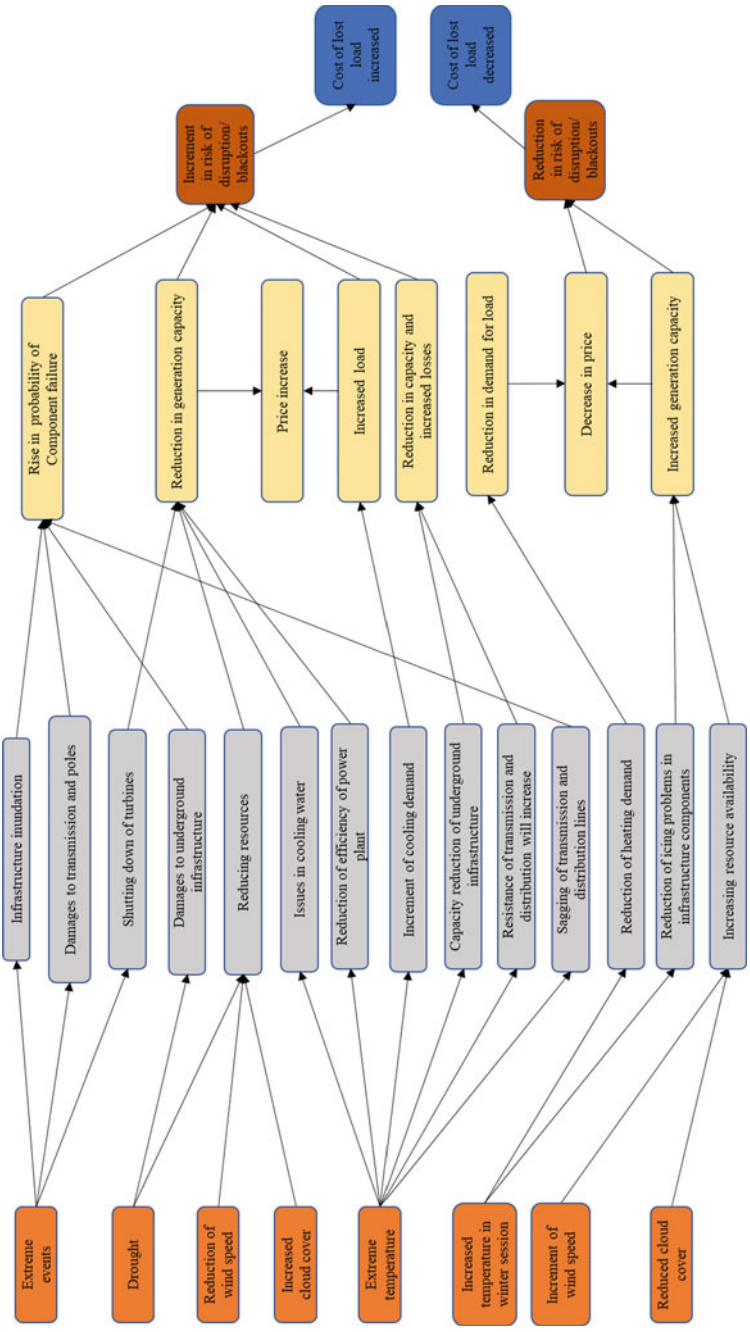

Fig. 2 Climate change impact on electricity infrastructure

3.1.2 Transportation Infrastructure

Table 2 elaborates on the climate change impacts on transportation infrastructure. Extreme weather events, extreme temperatures, and droughts are all hazards that can disrupt transportation networks [10]. These types of occurrences can have a variety of effects on infrastructure, some of which are transient and some of which are long term. For example, high winds can blow debris over roadways, slowing traffic and lowering road capacity in the near term [12, 42]. Extreme temperatures, on the other hand, can create rutting and melting of asphalt, which can lead to long-term problems and the need for maintenance [10, 12, 42, 49, 73].

Table 2 Potential impacts on transportation infrastructure

Climate change	Impacts	References
Extreme precipitation	• Flooded road/tunnels • Reduced visibility leads to accidents and may cause reduced road speed/capacity • Water accumulation on the road • Increased of landslide	[10, 12, 42, 49, 73]
Drought or decrease in precipitation	• Instability of road substructure that will lead to closed or blocked roads and higher maintenance cost	
SLR	• Increased in sea level caused in inundation of road infrastructure and consequences associated with flood	
Extreme events including flooding, storms, hurricanes	• Debris such as trees and branched on the road • Overturned trucks, caravans • Increased noise • Long-term changes to travel patterns and hence increase the demand for new infrastructure to cater to the demand • Flooded roads and tunnels • Evacuation of people from infrastructures at the extreme event • Increased traffic congestion	
Temperature rise	• Melting asphalt and rutting • Roadside fire • Opening/closing problems of steel bridges leading to structural instability	

3.1.3 Water Infrastructure

Table 3 summarizes the potential impacts of climate change on water infrastructure. As can be noted, extreme weather events such as floods, storms, hurricanes, and temperature increase have a more significant impact on water infrastructure [10, 32]. Changes in soil qualities and mobility may have an indirect impact on the functionality of drinking water infrastructure due to climate change. Failures in the construction materials can cause pipe systems to deteriorate [41, 47, 50]. These deterioration processes can be influenced by a variety of climate change-related extreme weather situations. Droughts and high temperatures can cause the soil to dry out and shrink, increasing pipe breakage.

Furthermore, high temperatures often result in increased water demand, raising water pressure and flow velocities near pumping stations. As a result, these

Table 3 Potential impacts on water infrastructure

Climate change	Impacts	References
Extreme precipitation	• Swelling of soils leading to increase pipe loading • Reduced water quality leading to higher capital for purification of water	[10, 32, 41, 47, 50, 68]
Drought or decrease in precipitation	• Consolidation, oxidation of soil, differential settlement • The decreased water level in water resources is affecting water supply services	
SLR	• Salinization of groundwater	
Extreme events (flooding, storms, hurricanes)	• Movement of trees and roots due to extreme wind leading to increase pipe loading • Damages to infrastructures due to debris • Increased turbidity • High concentration of pollutants • Making access to infrastructure facilities for repairing and maintenance work difficult	
Temperature rise	• Thermal expansion of pipes • Increased water demand • Weakening of thermoplastic material leading to reduce pipe strength • Corrosion • Increased evaporation in surface water supplies contributes to water quality degradation due to pollutants concentrations	

impacts can increase the likelihood of water hammer and pipe damage. Higher soil temperatures may alter the temperature of drinking water, lowering its quality [10, 32, 41, 47, 50].

All climate events have the potential to alter the loads or strength of the pipe, resulting in pipe (or joint) failure. For repairs, a small portion of the network will be disconnected from the water supply [32, 41]. The expenditures of repairing both the distribution network and other impacted infrastructure in the area of the burst and the interruption of water supply are among the economic consequences [41, 47, 50].

3.1.4 Wastewater Treatment Plant

As it can be noted from Table 4, high-severity consequences are projected from SLR and precipitation changes [31, 40]. Furthermore, the medium- and low-severity impacts projected from wind and temperature increase [31]. Impacts will range from capacity and service levels to implications on treatment effectiveness and receiving environment water quality. Impacts are predicted to be concentrated in low-lying areas that are vulnerable to coastal and inland floods, but they will also be disseminated throughout the system as a result of higher temperature, groundwater alterations, and changes in user behavior [31].

3.1.5 Telecommunication Infrastructure

The potential climate change impacts have been summarized in Table 5. As noted, extreme weather events and SLR have more significant impacts on the telecommunication infrastructure. Also, as telecommunication infrastructures are highly dependent on the electricity infrastructure, the minor disruption of the electricity infrastructure has a greater impact on the telecommunication infrastructure.

The impacts will exacerbate due to interdependencies with these CI sectors. The minor disruption of the one infrastructure will lead to cascading failure of the entire collapse of the system due to interdependencies within the CI network. Hence, it is crucial to identify these impacts systematically for proactive disaster risk reduction and climate change adaptation.

3.2 Impacts on Buildings

According to recent climate observations, the impacts of climate change appear to be having a growing influence on society. These effects certainly would influence the building construction industry [22, 28]. Several scholars have attempted to estimate the future energy demand of the building [79]. On the other hand, these studies often ignore climate variability and consumer reactions, especially temperature changes [16, 79, 80]. The effect of climate change on buildings is discussed in this section.

Table 4 Potential impacts on wastewater treatment infrastructure

Climate change	Impacts	References
Extreme precipitation	• Increased overflows and increased blockage and breakages in wastewater conveyance and pump stations • Increased inflows to wastewater treatment plants leading to more frequent bypassing • When soils in treatment plants get wet, the performance of the soakage system is harmed • Underground chambers get floated • Damage to the soil structure lowering the performance of soakage • Changes in the soakage field's ecology	[31]
Reduced precipitation levels or droughts	• Corrosion in water conveyance and pump stations owing to increase of concentration of water due to lower flows • With the higher temperature, blockages or siltation limit water utilization in water distribution systems and pump stations • Increase the strength of the influent at the risk of exceeding the toxicity limit • Ecological changes to the soakage field	[31, 43]
SLR	• Pipes get floated as a result of a rise in groundwater level leading to break down • Deterioration of the pipes • Groundwater entrance causes a loss of function and capacities of the plant • Infrastructure destruction due to erosion/inundation • Sludge management is limited by a rising groundwater table • Dewatering problems • Increased pumping heads for outfalls could affect outfalls	[31, 40]
Extreme events (flooding, storms, hurricanes)	• Blockages and breakages due to debris • Flooding has caused a reduction in the pump station's service zone • Damage to infrastructure facilities and accessibility to the site make difficult • Power outages and road closures due to storm • Affects the performance of the soakage	[31]

(continued)

Table 4 (continued)

Climate change	Impacts	References
Temperature rise	• Increase odors • Blockages caused by variations in user behavior during warmer weather • Temperature rise affects the functioning of components of the treatment plant (sludge management systems and oxidation ponds)	[31]

Table 5 Potential impacts on telecommunication infrastructure

Climate change	Impacts	References
Extreme precipitation	• Heavy rains may result in the weakening of telecommunication infrastructures • Subsidence could result from changes in precipitation levels, causing damage to above ground and subsurface infrastructures	[62, 76, 80]
SLR	• The flood can cause to erosion and deterioration of ICT infrastructures	
Extreme events (flooding, storms, hurricanes)	• Debris could damage ICT infrastructures • Lightning strikes can damage transmitters • Increased Internet traffic thereby reducing the accessibility • Carrying capacity for calls has been reduced, lost, or obstructed • The frequency and severity of power outages have an impact on communication equipment • Equipment and supplies in storage can be damaged	
Temperature rise	• Reduce the range of wireless communication • Increased maintenance due to the destruction of the infrastructure	

Impacts on building envelope (primarily triggered by natural hazards due to extreme events), building construction (deterioration of systems of fastening and utility systems such as water supply schemes), properties of construction material, and indoor climate/energy use are the four main categories of potential impacts on buildings that may be experienced throughout their life span [29]. This study focuses on the two major impact categories: (1) impacts on building material and (2) impacts on energy consumption.

Building materials are subjected to severe deterioration due to climate change and associated extreme events [58, 69, 80]. Table 6 indicates durability issues of generic materials due to changing climatic conditions. Also, it can be noted that almost all

Table 6 Durability of the building materials and climate change

Material type	Associated climate changes	Issues in durability	References
Structural concrete	• Temperature • Drying • CO_2	• Reinforcement corrosion	[69]
	• Temperature • Precipitation	• Chemical and salt attack	[39]
Brick and ceramics	• Cycles of freezing and thawing	• Frost damage	[45]
	• Precipitation • Drying	• Shrinkage	[11]
	• Precipitation • Drying	• Salt staining	[8]
Wood	• Temperature • Precipitation	• Biological deterioration	[55]
	• Uneven drying	• Wrapping and structural movement	[26]
Glazing	• Precipitation • Humidity level	• Double-glazing seals failure	[23]
Plastics/polymers	• UV exposure • Temperature	• UV deterioration	[13]
	• Temperature	• Thermal aging	[44]
Steel/metals	• Temperature • Precipitation	• Various corrosion mechanisms	[59]
Stone	• Temperature	• Weathering and erosion	[8]
	• Precipitation	• Acid deposition	[67]
	• Precipitation and drying	• Salt attack	[21]

building materials have a significant impact due to precipitation and temperature changes.

Hence, it is vital to address these issues at the design and construction stages. Building codes and standards provide significant guidance in building design and construction [33, 69, 70, 79, 57].

The energy utilization of the building is another significant consequence of climate change. Currently, concerns about energy use and its environmental effects are growing. The IPCC reports increased public awareness of energy use and its implications for climate change and sparked a lot of interest in learning more about energy use and its relationships with current weather conditions [5, 6]. Previous studies have shown that building energy demand and climate change correlate with each other [3, 16, 79, 33]. A review done by Andric et al. [3] showed the impacts of climate change on building energy demand. Several scholars have illustrated the impact on energy use and energy demand of the buildings in the different regions. A study carried out by Shen [64] observed maximum heat demand decrease around 14.7–48.9% between 2040 and 2069, referring to climate data 1961–1990 in several regions of America

[64]. In addition, Shen [64] observed a 17.4–36.4% increase in cooling demand, leading to a 14–19.5% increase in energy demand of the building [64]. Furthermore, scholars observed a decrease in heating demand and an increase in cooling demand in regions America [4, 34, 36, 72]. In Australia, the findings from the literature imply that 19–81% reduction of heating demand while heating demand increment 39–173% [74]. The selected articles show an increase in the energy demand of buildings in Australia [25, 74]. Ouedraogo et al. [56] have observed during 2030–2049 56% increment in cooling demand in Burkina Faso in Africa, utilizing the climate data during 2010–2029 [56]. European countries will experience a significant reduction of the heating demand, increment in cooling demand, and increment in energy demand [2, 9, 17, 38, 54, 61, 70]. In addition, studies carried out focusing on Asian regions [30, 60, 65, 71, 75, 78, 79] indicate that reduction of heating demand and increase of cooling demand and energy demand.

Also, it should be mentioned that these predictions are highly dependent on the climate data, and modeling techniques [3]. Different scholars have used other modeling techniques for predicting the future demand for heating, cooling, and energy. When calculating the total energy demand, scholars have considered energy demand for whole building services. These studies imply that climate change would result in less energy being used for winter heating and more for summer cooling in terms of global warming. Overall, the cooling and heating demand and other energy utilities of the building energy demand will increase all over the countries [3, 16]. The degree of reduction and increment of the heating and cooling is dependent on the region/climate. Furthermore, it is highly dependent on the local weather conditions and energy efficiency measures [16, 71, 79].

4 Conclusion

Climate change adaptation is a significant challenge posed by communities at present. As a first step toward climate change adaptation, it is crucial to identify the climate change impacts on the built environment. In this study, we have demonstrated the climate change impacts on the built environment in the context of CIs, residential and commercial buildings. This review focuses on five major CI sectors. Furthermore, potential impacts on those five CIs have been discussed and elaborated. As aforementioned, CIs have greater impacts due to the changing climate events, especially climate change-related extreme weather events, SLR, and temperature rises.

Furthermore, these impacts will exacerbate due to interdependencies and dependencies within the system leading to cascading failure of the system. Hence, it is crucial to identify these climate change impacts on CIs to mitigate the systemic risk among CIs effectively. Furthermore, this study provides insights for urban planners, decision-makers, and risk managers to take proactive mitigation measures by identifying potential impacts of climate change on CIs. On the other hand, residential and commercial buildings would have significant implications for climate change. These

impacts can be categorized into impacts on building structures, building construction, building material properties, and indoor climate/energy use. This study focuses on two categories of impacts. The findings from the study have shown that building energy performance will be highly affected by climate change.

Furthermore, it implies that building cooling demand will increase due to the temperature rise in most of the areas. On the other hand, building materials will be subjected to significant deterioration due to climate change stresses. Buildings are typically built to provide occupants with weather protection and achieve a particular internal atmosphere independent of the external weather. The intended purpose of the building envelope is to shield the indoor environment from extreme external climatic conditions. Especially this study focuses on two impact categories, the identification of other impact categories is vital for the effective functioning of the building over its life span.

Hence, the identification of these stresses has paramount importance in the infrastructure design, construction, and maintenance phase. Furthermore, building codes, rules, and regulations should be developed to address these issues, thereby adapting buildings to future climate change scenarios and achieving sustainable development goals.

Acknowledgements The authors wish to acknowledge the "ERASMUS + funded BEACON Project" for the financial assistance provided to conduct this study and all scholars who have contributed to enhancing the research domain's knowledge.

References

1. Abi-Samra NC, Forsten KR, Entriken R (2010) Sample effects of extreme weather on power systems and components, part I: sample effects on distribution systems. In: IEEE PES general meeting. Presented at the IEEE PES general meeting, pp 1–3. https://doi.org/10.1109/PES.2010.5589834
2. Andrić I, Gomes N, Pina A, Ferrão P, Fournier J, Lacarrière B, Le Corre O (2016) Modeling the long-term effect of climate change on building heat demand: case study on a district level. Energy Build 126:77–93. https://doi.org/10.1016/j.enbuild.2016.04.082
3. Andrić I, Koc M, Al-Ghamdi SG (2019) A review of climate change implications for built environment: Impacts, mitigation measures and associated challenges in developed and developing countries. J Clean Prod 211:83–102. https://doi.org/10.1016/j.jclepro.2018.11.128
4. Angeles ME, González JE, Ramírez N (2018) Impacts of climate change on building energy demands in the intra-Americas region. Theor Appl Climatol 133:59–72. https://doi.org/10.1007/s00704-017-2175-9
5. AR4 climate change 2007: impacts, adaptation, and vulnerability—IPCC, n.d. https://www.ipcc.ch/report/ar4/wg2/. Accessed 4.23.21a
6. AR4 climate change 2007: the physical science basis—IPCC, n.d. https://www.ipcc.ch/report/ar4/wg1/. Accessed 4.23.21b
7. Azari R (2014) Integrated energy and environmental life cycle assessment of office building envelopes. Energy Build 82:156–162. https://doi.org/10.1016/j.enbuild.2014.06.041
8. Basu S, Orr SA, Aktas YD (2020) A geological perspective on climate change and building stone deterioration in London: implications for urban stone-built heritage research and management. Atmosphere 11:788. https://doi.org/10.3390/atmos11080788

9. Berger T, Amann C, Formayer H, Korjenic A, Pospischal B, Neururer C, Smutny R (2014) Impacts of climate change upon cooling and heating energy demand of office buildings in Vienna, Austria. Energy Build 80:517–530. https://doi.org/10.1016/j.enbuild.2014.03.084
10. Bollinger LA, Bogmans CWJ, Chappin EJL, Dijkema GPJ, Huibregtse JN, Maas N, Schenk T, Snelder M, van Thienen P, de Wit S, Wols B, Tavasszy LA (2014) Climate adaptation of interconnected infrastructures: a framework for supporting governance. Reg Environ Change 14:919–931. https://doi.org/10.1007/s10113-013-0428-4
11. Brimblecombe P, Bonazza A, Brooks N, Sampedro G, Harris I, Sabbioni C (2011) Impact of climate change on earthen buildings. In: Terra 2008: the 10th international conference on the study and conservation of earthen architectural heritage. Getty Publications, p 278
12. Camp J, Abkowitz M, Hornberger G, Benneyworth L, Banks JC (2013) Climate change and freight-transportation infrastructure: current challenges for adaptation. J Infrastruct Syst 19:363–370. https://doi.org/10.1061/(ASCE)IS.1943-555X.0000151
13. Chaochanchaikul K, Rosarpitak V, Sombatsompop N (2013) Photodegradation profiles of PVC compound and wood/PVC composites under UV weathering. Express Polym Lett
14. Cortekar J, Groth M (2015) Adapting energy infrastructure to climate change—is there a need for government interventions and legal obligations within the German "Energiewende"? In: Energy procedia, 9th international renewable energy storage conference, IRES 2015, vol 73, pp 12–17.https://doi.org/10.1016/j.egypro.2015.07.552
15. Davis M, Clemmer S (2014) Power failure: how climate change puts our electricity at risk—and what we can do 16
16. Ding Y-J, Li C-Y, Wang X, Wang Y, Wang S-X, Chang Y-P, Qin J, Wang S-P, Zhao Q-D, Wang Z-R (2021) An overview of climate change impacts on the society in China. Adv Clim Change Res. https://doi.org/10.1016/j.accre.2021.03.002
17. Dolinar M, Vidrih B, Kajfež-Bogataj L, Medved S (2010) Predicted changes in energy demands for heating and cooling due to climate change. Phys Chem Earth Parts ABC Bio Agro Urban Climatol 35:100–106. https://doi.org/10.1016/j.pce.2010.03.003
18. Dowling P (2013) The impact of climate change on the European energy system. Energy Policy 60:406–417. https://doi.org/10.1016/j.enpol.2013.05.093
19. Eckstein D, Hutfils M-L, Winges M, Germanwatch (2018) Global climate risk index 2019 who suffers most from extreme weather events? Weather-related loss events in 2017 and 1998 to 2017
20. Feng Y, Xiang-Yang L (2018) Improving emergency response to cascading disasters: applying case-based reasoning towards urban critical infrastructure. Int J Disaster Risk Reduct Understand Mitigating Cascad Crises Glob Interconnect Syst 30:244–256. https://doi.org/10.1016/j.ijdrr.2018.04.012
21. Flatt RJ, Caruso F, Sanchez AMA, Scherer GW (2014) Chemo-mechanics of salt damage in stone. Nat Commun 5:1–5
22. Giesekam J, Barrett J, Taylor P, Owen A (2014) The greenhouse gas emissions and mitigation options for materials used in UK construction. Energy Build 78:202–214. https://doi.org/10.1016/j.enbuild.2014.04.035
23. Ginks N, Painter B (2017) Energy retrofit interventions in historic buildings: exploring guidance and attitudes of conservation professionals to slim double glazing in the UK. Energy Build 149:391–399. https://doi.org/10.1016/j.enbuild.2017.05.039
24. Golombek R, Kittelsen SAC, Haddeland I (2012) Climate change: impacts on electricity markets in Western Europe. Clim Change 113:357–370. https://doi.org/10.1007/s10584-011-0348-6
25. Guan L (2012) Energy use, indoor temperature and possible adaptation strategies for air-conditioned office buildings in face of global warming. Build Environ Implications Chang Clim Build 55:8–19. https://doi.org/10.1016/j.buildenv.2011.11.013
26. Haque N (2010) Delamination in timber induced by drying. In: Delamination in wood, wood products and wood-based composites. Springer, pp 197–212
27. Haraguchi M, Kim S (2016) Critical infrastructure interdependence in New York City during Hurricane Sandy. Int J Disaster Resil Built Environ 7:133–143. https://doi.org/10.1108/IJDRBE-03-2015-0015

28. Hertwich EG, Ali S, Ciacci L, Fishman T, Heeren N, Masanet E, Asghari FN, Olivetti E, Pauliuk S, Tu Q, Wolfram P (2019) Material efficiency strategies to reducing greenhouse gas emissions associated with buildings, vehicles, and electronics—a review. Environ Res Lett 14:043004. https://doi.org/10.1088/1748-9326/ab0fe3
29. Hrabovszky-Horváth S, Pálvölgyi T, Csoknyai T, Talamon A (2013) Generalized residential building typology for urban climate change mitigation and adaptation strategies: the case of Hungary. Energy Build 62:475–485. https://doi.org/10.1016/j.enbuild.2013.03.011
30. Huang K-T, Hwang R-L (2016) Future trends of residential building cooling energy and passive adaptation measures to counteract climate change: the case of Taiwan. Appl Energy 184:1230–1240. https://doi.org/10.1016/j.apenergy.2015.11.008
31. Hughes J, Cowper-Heays K, Olesson E, Bell R, Stroombergen A (2021) Impacts and implications of climate change on wastewater systems: a New Zealand perspective. Clim Risk Manage 31:100262. https://doi.org/10.1016/j.crm.2020.100262
32. Hunt A, Watkiss P (2011) Climate change impacts and adaptation in cities: a review of the literature. Clim Change 104:13–49. https://doi.org/10.1007/s10584-010-9975-6
33. Hussain M, Butt AR, Uzma F, Ahmed R, Irshad S, Rehman A, Yousaf B (2020) A comprehensive review of climate change impacts, adaptation, and mitigation on environmental and natural calamities in Pakistan. Environ Monit Assess 192:48. https://doi.org/10.1007/s10661-019-7956-4
34. Invidiata A, Ghisi E (2016) Impact of climate change on heating and cooling energy demand in houses in Brazil. Energy Build 130:20–32. https://doi.org/10.1016/j.enbuild.2016.07.067
35. IPCC (2021) Climate change 2021: the physical science basis (WG1 AR6)
36. Jiang A, Zhu Y, Elsafty A, Tumeo M (2018) Effects of global climate change on building energy consumption and its implications in Florida. Int J Constr Educ Res 14:22–45. https://doi.org/10.1080/15578771.2017.1280104
37. Johnston PC (2012) Climate risk and adaptation in the electric power sector. Asian Development Bank, Mandaluyong City, Metro Manila, Philippines
38. Jylhä K, Jokisalo J, Ruosteenoja K, Pilli-Sihvola K, Kalamees T, Seitola T, Mäkelä HM, Hyvönen R, Laapas M, Drebs A (2015) Energy demand for the heating and cooling of residential houses in Finland in a changing climate. Energy Build 99:104–116. https://doi.org/10.1016/j.enbuild.2015.04.001
39. Kaewunruen S, Wu L, Goto K, Najih YM (2018) Vulnerability of structural concrete to extreme climate variances. Climate 6:40. https://doi.org/10.3390/cli6020040
40. Kirchhoff CJ, Watson PL (2019) Are wastewater systems adapting to climate change? JAWRA J Am Water Resour Assoc 55:869–880. https://doi.org/10.1111/1752-1688.12748
41. Kundzewicz ZW, Krysanova V, Benestad RE, Hov Ø, Piniewski M, Otto IM (2018) Uncertainty in climate change impacts on water resources. Environ Sci Policy 79:1–8. https://doi.org/10.1016/j.envsci.2017.10.008
42. Lambert JH, Wu Y-J, You H, Clarens A, Smith B (2013) Climate change influence on priority setting for transportation infrastructure assets. J Infrastruct Syst 19:36–46. https://doi.org/10.1061/(ASCE)IS.1943-555X.0000094
43. Langeveld JG, Schilperoort RPS, Weijers SR (2013) Climate change and urban wastewater infrastructure: there is more to explore. J Hydrol 476:112–119. https://doi.org/10.1016/j.jhydrol.2012.10.021
44. Leuteritz A, Döring K-D, Lampke T, Kuehnert I (2016) Accelerated ageing of plastic jacket pipes for district heating. Polym Test 51:142–147
45. Lourenço PB, van Hees R, Fernandes F, Lubelli B (2014) Characterization and damage of brick masonry. In: Structural rehabilitation of old buildings. Springer, pp 109–130
46. Mao Q, Li N (2018) Assessment of the impact of interdependencies on the resilience of networked critical infrastructure systems. Nat Hazards 93:315–337. https://doi.org/10.1007/s11069-018-3302-3
47. McNutt M (2013) Climate change impacts. Science 341:435–435. https://doi.org/10.1126/science.1243256

48. Melià P, Ruggieri G, Sabbadini S, Dotelli G (2014) Environmental impacts of natural and conventional building materials: a case study on earth plasters. J Clean Prod 80:179–186. https://doi.org/10.1016/j.jclepro.2014.05.073
49. Meyer MD, Amekudzi A, O'Har JP (2010) Transportation asset management systems and climate change: adaptive systems management approach. Transp Res Rec 2160:12–20. https://doi.org/10.3141/2160-02
50. Miara A, Macknick JE, Vörösmarty CJ, Tidwell VC, Newmark R, Fekete B (2017) Climate and water resource change impacts and adaptation potential for US power supply. Nat Clim Change 7:793–798. https://doi.org/10.1038/nclimate3417
51. Mideksa TK, Kallbekken S (2010) The impact of climate change on the electricity market: a review. Energy Policy Large-Scale Wind Power Electr Markets Regular Pap 38:3579–3585. https://doi.org/10.1016/j.enpol.2010.02.035
52. Mukheibir P (2013) Potential consequences of projected climate change impacts on hydroelectricity generation. Clim Change 121:67–78. https://doi.org/10.1007/s10584-013-0890-5
53. Nejat P, Jomehzadeh F, Taheri MM, Gohari M, Majid AMZ (2015) A global review of energy consumption, CO_2 emissions and policy in the residential sector (with an overview of the top ten CO_2 emitting countries). Renew Sustain Energy Rev 43:843–862.https://doi.org/10.1016/j.rser.2014.11.066
54. Nik VM, Sasic Kalagasidis A (2013) Impact study of the climate change on the energy performance of the building stock in Stockholm considering four climate uncertainties. Build Environ 60:291–304. https://doi.org/10.1016/j.buildenv.2012.11.005
55. Nofal M, Kumaran K (2011) Biological damage function models for durability assessments of wood and wood-based products in building envelopes. Euro J Wood Wood Prod 69:619–631
56. Ouedraogo BI, Levermore GJ, Parkinson JB (2012) Future energy demand for public buildings in the context of climate change for Burkina Faso. Build Environ 49:270–282. https://doi.org/10.1016/j.buildenv.2011.10.003
57. Padilla-Rivera A, Amor B, Blanchet P (2018) Evaluating the link between low carbon reductions strategies and its performance in the context of climate change: a carbon footprint of a wood-frame residential building in Quebec, Canada. Sustainability 10:2715. https://doi.org/10.3390/su10082715
58. Phillipson MC, Emmanuel R, Baker PH (2016) The durability of building materials under a changing climate. WIREs Clim Change 7:590–599. https://doi.org/10.1002/wcc.398
59. Revie RW (2011) Uhlig's corrosion handbook. Wiley
60. Roshan GR, Orosa JA, Nasrabadi T (2012) Simulation of climate change impact on energy consumption in buildings, case study of Iran. In: Energy policy, special section: fuel poverty comes of age: commemorating 21 years of research and policy, vol 49, pp 731–739. https://doi.org/10.1016/j.enpol.2012.07.020
61. Sabunas A, Kanapickas A (2017) Estimation of climate change impact on energy consumption in a residential building in Kaunas, Lithuania, using HEED software. In: Energy procedia, international scientific conference "environmental and climate technologies", CONECT 2017, 10–12 May 2017, Riga, Latvia 128, pp 92–99. https://doi.org/10.1016/j.egypro.2017.09.020
62. Salimi M, Al-Ghamdi SG (2020) Climate change impacts on critical urban infrastructure and urban resiliency strategies for the Middle East. Sustain Cities Soc 54:101948. https://doi.org/10.1016/j.scs.2019.101948
63. Schaeffer R, Szklo AS, Pereira de Lucena AF, Moreira Cesar Borba BS, Pupo Nogueira LP, Fleming FP, Troccoli A, Harrison M, Boulahya MS (2012) Energy sector vulnerability to climate change: a review. Energy 38:1–12.https://doi.org/10.1016/j.energy.2011.11.056
64. Shen P (2017) Impacts of climate change on U.S. building energy use by using downscaled hourly future weather data. Energy Build 134:61–70. https://doi.org/10.1016/j.enbuild.2016.09.028
65. Shibuya T, Croxford B (2016) The effect of climate change on office building energy consumption in Japan. Energy Build 117:149–159. https://doi.org/10.1016/j.enbuild.2016.02.023

66. Sieber J (2013) Impacts of, and adaptation options to, extreme weather events and climate change concerning thermal power plants. Clim Change 121:55–66. https://doi.org/10.1007/s10584-013-0915-0
67. Smith BJ, McCabe S, McAllister D, Adamson C, Viles HA, Curran JM (2011) A commentary on climate change, stone decay dynamics and the 'greening' of natural stone buildings: new perspectives on 'deep wetting.' Environ Earth Sci 63:1691–1700. https://doi.org/10.1007/s12665-010-0766-1
68. Spalding-Fecher R, Chapman A, Yamba F, Walimwipi H, Kling H, Tembo B, Nyambe I, Cuamba B (2016) The vulnerability of hydropower production in the Zambezi River Basin to the impacts of climate change and irrigation development. Mitig Adapt Strateg Glob Change 21:721–742. https://doi.org/10.1007/s11027-014-9619-7
69. Stewart MG, Wang X, Nguyen MN (2011) Climate change impact and risks of concrete infrastructure deterioration. Eng Struct 33:1326–1337. https://doi.org/10.1016/j.engstruct.2011.01.010
70. Waddicor DA, Fuentes E, Sisó L, Salom J, Favre B, Jiménez C, Azar M (2016) Climate change and building ageing impact on building energy performance and mitigation measures application: a case study in Turin, Northern Italy. Build Environ 102:13–25. https://doi.org/10.1016/j.buildenv.2016.03.003
71. Wan KKW, Li DHW, Lam JC (2011) Assessment of climate change impact on building energy use and mitigation measures in subtropical climates. Energy 36:1404–1414. https://doi.org/10.1016/j.energy.2011.01.033
72. Wang L, Liu X, Brown H (2017) Prediction of the impacts of climate change on energy consumption for a medium-size office building with two climate models. Energy Build 157:218–226. https://doi.org/10.1016/j.enbuild.2017.01.007
73. Wang L, Xue X, Zhao Z, Wang Z (2018) The impacts of transportation infrastructure on sustainable development: emerging trends and challenges. Int J Environ Res Public Health 15:1172. https://doi.org/10.3390/ijerph15061172
74. Wang X, Chen D, Ren Z (2010) Assessment of climate change impact on residential building heating and cooling energy requirement in Australia. Build Environ 45:1663–1682. https://doi.org/10.1016/j.buildenv.2010.01.022
75. Wang Y, Lin H, Wang W, Liu Y, Wennersten R, Sun Q (2017) Impacts of climate change on the cooling loads of residential buildings differences between occupants with different age. Energy Proc 142:2677–2682
76. Wilbanks TJ, Fernandez S (2014) Climate change and infrastructure, urban systems, and vulnerabilities: technical report for the US Department of Energy in support of the national climate assessment. Island Press
77. World Economic Forum (2021) The global risk report 2021
78. Xiang C, Tian Z (2013) Impact of climate change on building heating energy consumption in Tianjin. Front Energy 7:518–524. https://doi.org/10.1007/s11708-013-0261-y
79. Yau YH, Hasbi S (2013) A review of climate change impacts on commercial buildings and their technical services in the tropics. Renew Sustain Energy Rev 18:430–441. https://doi.org/10.1016/j.rser.2012.10.035
80. Zimmerman R, Faris C (2010) Infrastructure impacts and adaptation challenges. Ann NY Acad Sci 1196:63–86

New Normal Remote Communication for Collaboration

P. Vaz-Serra, F. Hui, C. Duffield, P. Mendis, and L. Aye

Abstract Remote communication is not new for the architecture, engineering and construction (AEC) industry and academia. Organisations started using what was common, called "conference rooms" with sophisticated technological equipment prepared for "conference calls" when face-to-face meetings were not possible, and the industries culture and work practices were rooted in face-to-face meetings. This was current practice until the beginning of 2020, with the emergence of the global COVID-19 pandemic. The pandemic forced people to have safe distances between them, to be isolated for long periods of time, and several restrictions to travel not being possible to meet face-to-face. This situation rapidly created a new need to find ways to communicate as alternatives to traditional face-to-face meetings, for "conference call rooms" anywhere and accessible at any time by everyone. The extended duration of the pandemic made organisations adapt to that new normal and remarkable new opportunities arose in a new way. This article explores recent situations in academia and industry that can highlight potential guidance towards the new normal in remote communication for learning–teaching and the AEC industry sectors. In conclusion, appropriate use of these electronic processes provides opportunities to significantly

P. Vaz-Serra
Faculty of Architecture, Building and Planning, The University of Melbourne, Melbourne, VIC 3010, Australia

F. Hui · C. Duffield
Engineering Management Group, Department of Infrastructure Engineering, Faculty of Engineering and Information Technology, The University of Melbourne, Melbourne, VIC 3010, Australia

P. Mendis
ARC Centre for Advanced Manufacturing of Prefabricated Housing, The University of Melbourne, Melbourne, VIC 3010, Australia

L. Aye (✉)
Renewable Energy and Energy Efficiency Group, Department of Infrastructure Engineering, Faculty of Engineering and Information Technology, The University of Melbourne, Melbourne, VIC 3010, Australia
e-mail: lua@unimelb.edu.au

R. Dissanayake et al. (eds.), *12th International Conference on Structural Engineering and Construction Management*, Lecture Notes in Civil Engineering 266,
https://doi.org/10.1007/978-981-19-2886-4_32

improve remote communication in future. It is expected that the number of opportunities to develop international relationships and partnerships can be boosted to another level of accessibility.

Keywords Collaboration · Remote communication · Video conferencing · Learning–teaching · Construction management

1 Introduction

New ways to communicate in the construction industry have been introduced in the last two decades. Construction organisations started having conference meeting rooms mainly in their head offices for some international meetings, and mostly, for occasions that were not possible to meet in person. Using these digital tools was mainly for special occasions. That was the current practice until the beginning of 2020. However, because of the COVID-19 pandemic, remote collaboration using digital communications is increasing and becoming more important [20].

With extended lockdowns and periods of travel restrictions, remote communication became essential. "Remote communication is communication between people who are not physically in the same place" [10]. Initially, the switch to remote communication was seen as a temporary way and it was only after almost two years of these "temporary" situations that people started to see potential advantages in using remote communication on a day-to-day basis and not only when face-to-face meetings were not possible. This is beneficial not only for the architecture, engineering and construction (AEC) industry, and international engineering, procurement and construction (IEPC) projects but also in academia, in teaching and learning (student group work) and scientific collaboration (international research).

Remote communication is distinct from face-to-face meetings or activities. It can be conducted asynchronously and synchronously. Asynchronous remote communication has delayed interaction. Texting in short message service (SMS), slack message, email, discussion board, shared document collaboration and project management commentary are examples of asynchronous remote communication. Synchronous communications are real time. Phone calls and video calls are examples of synchronous remote communication. "There is a growing need for effective, face-to-face-like remote communication." [22] However, what works in person may not translate well into remote communication via audio or audiovisual. New forms of miscommunication and misunderstanding are some of the challenges [13]. Students, educators, researchers and managers must understand and practise effective remote communication.

Global competition in construction has increased because of accelerated internationalisation practices such as the formation of multinational teams and international alliances, cross-national outsourcing and bidding [32]. The advances in communication tools and information technologies are the enablers. Because of complexities

and changing needs in the construction industry, the effective and efficient information flow between project team members are essential for success [16]. IEPC projects involve distributed teams around the globe. Real-time remote synchronous communication via online video conference calls, which are the closest substitutes for face-to-face meetings, have been employed. There are several elements of remote synchronous communication to be considered: the video conferencing tool, challenging time zones for scheduling, impersonal interactions, etiquette, digital-meeting fatigue, family and care duties and corporate communication policies [7, 17, 26].

The COVID-19 pandemic created many opportunities for collaboration among scientific communities via remote communication [14]. During the lockdown periods schools, colleges and universities had to adopt remote teaching–learning. It offers copious opportunities for educators and organisations to embrace digitalisation [4]. The aim of this article is to share recent experiences and reflections of the authors for the last two years. The new normal of communicating remotely is effectively changing the way organisations will communicate in future because of the advantages and the familiarity with the tools. The objectives of these reflections, based on case studies, are to demonstrate the effective advantages of new cultural communication adaptation and the opportunity to boost international collaborations with the adoption of a new way to communicate. In this section, the aim and objectives of the work have been described. In the following sections, the methods employed the findings to share, and the concluding discussions are presented.

2 Method

A case study research approach was applied to better understand the issues in a real-life context. Case study as a research method has been recognised in many social sciences studies [34]. It is used extensively in a wide variety of disciplines, particularly in the social sciences [11]. Case studies on remote communications presented in this article include an academic perspective gained from the analysis of student and staff feedback from a Master of Construction Management subject and an Engineering Management subject offered at the authors' university. A reflection of whether industry is also interested in such communication approaches is provided by reflecting on how independent reviews of major projects have been conducted during COVID. Reflections on our experiences with these case studies and beyond enable us to better understand the elements of remote communication for collaboration.

3 Remote Communication and Collaboration

The expression "remote communication" has been introduced in recent years. A document search within article title, abstract, keywords on Scopus abstract and citation database using the keywords "remote" and "communication" identified 43,586

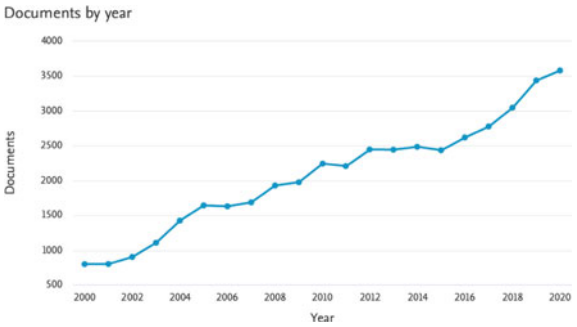

Fig. 1 "Remote" and "communication" 2000–2020 (Scopus)

papers between 2000 and 2020. The papers per year are 2433 in 2015 and 3578 in 2020 (47% growth) (Fig. 1).

When looking at "remote communication" and "construction", 1148 papers were identified in Scopus and the number of papers per year almost doubled from 65 papers in 2015 to 124 papers in 2020, about 91% growth (see Fig. 2a). On the other hand, looking at "remote communication" and "education", the numbers of papers were in average stable from 2008 to 2019 with an average of 150 papers per year to 296 papers, almost double, in 2020 (see Fig. 2b).

Remote communication can be conducted in asynchronous and synchronous ways. The recent world pandemic increased the global demand of web-based tools for synchronous software tools to facilitate a new normal work environment and lifestyle [4]. The authors highlighted the opportunities and the risks that this quick absorption of the digitalisation of communication can have on factors like employee well-being and work-life balance.

Nevertheless, there is consensus between researchers that the digitalisation of communication has enhanced collaboration and overall competitiveness [3, 23, 29]. More advanced and affordable emerging technologies and integrated solutions, to

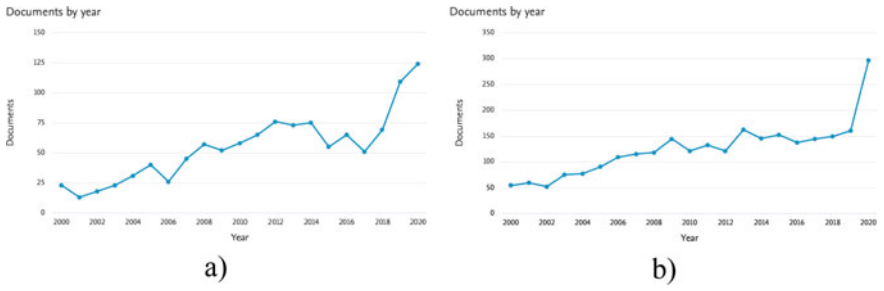

Fig. 2 **a** "Remote" and "communication" and "construction", **b** "remote" and "communication" and "education" 2000–2020 (Scopus)

improve work collaboration and data storage, gave organisations new opportunities to quickly adopt the new normal [6].

4 Case Studies in Remote Communication

There is an expectation that learning involves human interaction in higher education and that this will prepare the students for practical work; the interactions between students and teacher and between students are essential in preparing work ready graduates [8]. Nowadays, this interaction includes the two, synchronous and asynchronous, formats of communication [19]. Research in university teaching methodologies has evolved enormously during the last 20 years. They were integration of technologies with several theories and adjustments on what works and why [18]. The emergence of new technologies opened new opportunities to enhance knowledge sharing, motivation, and student's engagement using combinations of synchronous and asynchronous formats [21].

4.1 A Case Study on the Master of Construction Management Subject

Although, the new technologies presented a challenge to some subjects that were designed to be delivered only face-to-face to suddenly move to remote or blended mode to keep the same sense of belonging [28]. One of the Master of Construction Management subjects at the University of Melbourne (UoM) has more "practical" and less "theoretical" in nature. It was developed to move from traditional passive learning to active project-based learning [9]. The design of the subject included setting learning objectives, activities, and assessments using Bloom's taxonomy of learning [5], social constructivism [12], and project-based learning [30] theories.

Activities and assessment tasks were linked with real cases and strong interaction with external industry experts on real projects. Students are to be physically participating in workshops with the industry, site visits and meetings with professional staff of several organisations [24].

At the beginning of the second semester 2021, Melbourne University classes were planned to be on campus and face-to-face. The agreement with experts and industry partners was to develop the subject face-to-face as planned. During the first week, and before the first class, Melbourne started a sixth lockdown. Two options were possible: to cancel the subject offered or to deliver remotely (i.e. transforming face-to-face classes, tutorials, workshops and industry site visit and meetings to remote communication activities.

The subject that was already designed to be student-oriented needed to quickly change to active learning using online tools and technologies. The initial challenge

was changing student expectations, guest experts and industry partners to a new need, to adapt using remote communication tools.

This began with a meeting with the students enrolled in the subject to propose last-minute changes to the delivery process of the subject. The adoption of a flipped classroom [1] was agreed with student commitment on weekly tasks. The subject coordinator made available the weekly material (reading, pre-recorded videos and relevant website links) for the students on the university collaborative web-based platform. Students agreed to use the available synchronous remote communication tool, Zoom meeting [35] and attend the classes remotely. The students presented their designated topics in online classes, followed by instructor comments and peer reviews.

The next step was to convince experts and construction industry partners to collaborate remotely, exchanging experiences, real projects, and meetings in a completely new way. It required a shift in communication culture, where the ritual of coming to university and interacting face-to-face with students was an important part of the motivation. How would industry partners react? The response from experts and industry was remarkable. After receiving the request, the response was almost instantaneous that the industry, after almost eighteen months in restrictions, was prepared to interact with students remotely. An additional initial challenge was the video conferencing software tool used by the industry for remote communication was Microsoft Teams, but the University adopted Zoom. This barrier was easily overcome by the newer versions of these software tools, which were more user-friendly.

4.2 A Case Study on the Engagement of Student Teams in Engineering Work

In an engineering management capstone subject, students were required to work in teams of four to develop management plans for the construction of a service station, to develop change management plans for an international humanitarian or to prepare a business case for the construction an electric vehicle charging station. The subject has run every semester and since 2020, a total of 47 student teams have collaborated in an online environment and three teams participated in face-to-face type collaboration. The reasons why the teams were not able to participate face-to-face was the extensive travel restrictions and border closures in Australia during 2020–21. Local restrictions were relaxed in April 2021 but were suddenly re-introduced (with travel restrictions of up to 5 km from home) in late July 2021. This has caused many of the groups to opt for online learning right at the start of the semester.

The teams had to develop a team contract at the beginning of the semester, where all team members had to agree on a mode of communication and frequency of communication. An analysis of the team contracts submitted by students showed their preferences. Table 1 gives an analysis of the number of student groups in the subject and the number of groups attempting face-to-face learning.

Table 1 Analysis of team contracts—student team preferences

Semester/Year	Number of student teams	Face-to-face teams	Teams using LMS collaboration tool	Communication tool						File sharing tool						
				Zoom	WhatsApp	WeChat	Canvas (LMS)	Facebook	Not specified	Microsoft Teams	OneDrive	Canvas	Emails	Google Drive	SharePoint	Not specified
1/20	8	0	1	8	4	1	3	4	0	0	0	3	1	7	0	0
2/20	13	0	1	11	7	4	1	0	1	2	0	2	2	8	0	2
1/21	12	3	1	10	3	7	0	0	1	1	1	1	5	8	0	2
2/21	14	0	1	13	5	7	0	2	0	1	6	1	3	6	1	0
Total	47	3	4	42	19	19	4	6	2	4	7	7	11	29	1	4

Observations from the teaching team

Most teams prefer to use the Zoom platform ($n = 42$, Table 1) even though the learning management system (LMS) has its own collaboration tool. The commonly used tool for synchronous communication was having meetings over the Zoom platform. Microsoft Teams was second. Even though the Canvas LMS has a built-in tool, the teams seemed not to want to learn a new platform. Anecdotal evidence points to students not wanting the burden of monitoring another platform and prefer to work with a single communication tool, either WhatsApp or emails. Students prefer to be as flexible as possible and use whatever tools that are convenient to them. One other concern that students highlighted in not using the LMS communication tool was that they might get inundated by notifications, and some of these relatively minor notifications may distract them from reading the important notifications.

The tutorials required the student teams to collaborate during class time. During this time, the tutors assigned to the teams had a good chance to observe how the teams collaborate. Anecdotal evidence from the tutors suggested that almost all the teams work in Zoom breakout rooms with their cameras off. File sharing in Zoom was a common practice as was the use of the chat function to share Weblinks. Most students would only turn on their camera when asked to do so. Only a small percentage would do so when they engaged in a prolonged conversation with the tutor, who was the only person with the camera on. This suggests that perhaps turning the camera on is a sign of willingness to engage. On the other hand, one of the common reasons mentioned for not turning on the cameras was the sufficiency of the bandwidth and its reliability and quality.

As students in teams can be working across different time zones, it is interesting to observe the task allocation and sharing of the completed works. One of the important indicators of how students work is the file sharing arrangement. Students typically work asynchronously across different time zones. It is not uncommon for the tutors to hear that one member of the team is not present and one other member will pass on the message for a piece of work to be completed. These "asynchronous" communication and work arrangements were observed to be commonly used by students in different time zones to overcome time differences. It can be observed that Google Drive seems to be a popular choice even though OneDrive is the official storage media offered to University students. It is also interesting to observe that the use of emails to share files ($n = 11$) was the second most popular option.

Not being able to read body language or know if someone is paying attention meant that tutors had to regularly check to ensure the whole team is engaged by asking questions. It was observed that in all teams, there were usually two or three students who dominated the discussion, and the remaining team members were passive followers. It was difficult to gauge if these team members were as engaged as the students who were interactive. From Table 1, it is observed that even though zoom is the main communication tool ($n = 42$), many teams prefer to complement this with a second tool, such as WhatsApp ($n = 19$) or WeChat ($n = 19$) or instant messaging functions.

4.3 A Case Study on Independent Reviews of Major Projects

It has become best practice that major projects are periodically independently reviewed so that project decisions are improved and risks mitigated [33]. Resourcing independent reviewers for major projects frequently involves accessing experienced personnel from outside the jurisdiction, where the project is being delivered. Without serious engagement with the project team and access to the site, conceptually compromises the integrity of the review.

The advent of COVID restrictions that have limited face-to-face contact has forced this sector of industry to engage in electronic forms of communication. The most common approach has been to implement video meetings (e.g. Microsoft Teams, Zoom and Webex), with industry information sessions often being facilitated via webinar seminars. Many of the construction and building staff are less experienced with computer technology than are university students. Technological difficulties have been overcome by many organisations incorporating a technology specialist into the preparation for important meetings. These technology specialists assist staff in connecting to the meetings and resolve any login or compatibility issues. Once established, the meetings have run smoothly, barring consistent problems with Internet bandwidth when using video links or speaking whilst on mute. Extending use of the technology has been generally limited to the sharing or documents on the screen.

Given the need to observe in independent reviews, some reviews have explored the concept of participating in site visits via shared media on mobile phones linked to the normal meeting platform. To many peoples' surprise, several reviewers have commented on the excellent project visibility provided via linking to dynamic and live site inspection tours. This demonstrates that the new communication approaches progress much further than academic circles, and these approaches are being adopted widely by the building and construction industry, albeit with the assistance of some technical support.

5 Discussion

At the end of the semester, the Master of Construction Management students' experience was very positive. In some cases, the student experience has even increased because some industry experts work from home. Lessons learned from this case study were an in-depth understanding of the advantages of mixed methods and the benefits of using remote communication and digital technologies. It was evident that students and external experts would prefer to return to face-to-face as quickly as possible, but all saw the potential for the flexibility of having the chance to use remote communication in future at all events, when for some reason it was not possible to be face-to-face.

The experience of bringing concepts such as quick questionnaires during classes on weekly topics and flipped rooms using collaborative platforms for sharing teaching

materials will be integrated permanently in the design of the subject. Continuous assessment based on short tasks will be introduced in the redesign of the subject. The flexibility of the remote communication unlocks opportunities to have international experts participate and collaborate on teaching activities during the semester was also highlighted for future improvements as the new normal.

Student project teams learning to be engineering project managers, working on real engineering problems in the classroom, can be taken as a microcosm of the real world of engineering and construction management. When left to their own devices of finding the most efficient way to get tasks executed and projects completed on time, it seems that teams of engineering managers will prefer to use familiar tools like WhatsApp, Zoom or Microsoft Teams rather than something new. Organisations should be mindful of this when dictating the use of platforms, especially when dealing with external stakeholders and organisations.

The state of technology in facilitating communication requires a new protocol where what is considered "acceptable good behaviour" and "impolite behaviour" takes on a new form. In the new world, where remote team members can come from anywhere in the world, it may be considered impolite to not ask for a convenient time to meet. Not meeting in person also takes away the personal touch and rapport building that is also important. It is something that people working online often take for granted. The simple act of turning on the camera during the first few moments of a meeting may be enough to offset some of these difficulties. Situations where team members do not meet in person and visual cues are absent, may be potentially harmful for teamwork as misunderstandings can occur and team members start to view each other's commitments with suspicions.

In the "old" world, where a lot of work was done through synchronous communication, the "new world" work arrangements will necessitate the use of asynchronous communication arrangements, where people can work on tasks in their own time but still contribute to the team goals. This will require the team members to have a higher level of trust in other team members to complete the work assigned to them.

The COVID-19 pandemic accelerated the applications of the remote communication technologies. During the lockdown, the authors have collectively utilised Doodle and Outlook calendar for coordinating and scheduling remote meetings, Zoom, Microsoft Teams, GoToMeeting and WhatsApp for communication and social interaction, OneDrive, SharePoint, PBworks, Basecamp and Google Drive for online editing and file storage. After the COVID-19 crisis, the remote communication technologies will stay in different ways and will be different depending on the nature of the work of each organisation. "Necessity is the mother of invention": the global crisis provoked by the pandemic required various innovative ways of communicating using emerging technologies that were more accessible in a user-friendly environment [25]. The COVID-19 crisis, accelerated the adoption of digital technologies [2, 27]. Organisation members will affect the organising model for digital transformation in the light of the flexibility of communications and knowledge sharing [31]. In the new era of digital communication, people speaking different languages may be able to communicate in real time without human interpreters. At this moment, some video conferencing tools are able to translate into multiple languages simultaneously

with limited accuracy. As pointed out by [15] beyond COVID-19, remote collaboration may equip learning-teaching and research teams with tools and capacities to continue to think together and work apart effectively and productively.

6 Conclusions

Three case studies have been used to examine some elements of remote synchronous communication for collaboration. The following are the conclusions of the findings on these elements. Video conferencing tool: Zoom meetings and Microsoft Teams are the synchronous communication platform of choice because of the familiarity. People do not wish to explore unfamiliar software platform. Schedule a time block: People prefer their own convenient time. We need to be mindful about the scheduling of the meeting time for people with various time zones around the globe. There are some challenges on common ground around politeness and etiquette when using video conferencing.

Contributor Roles Taxonomy (CRediT) authorship contribution statement

P. Vaz-Serra: methodology, formal analysis, investigation, data curation, writing—original draft, visualisation. **F. Hui**: formal analysis, investigation, data curation, writing—original draft, funding acquisition. **C. Duffield**: conceptualisation, writing—review and editing. **P. Mendis**: writing—review and editing. **L. Aye**: validation, resources, writing—original draft, review and editing, project administration.

Acknowledgements The authors would like to thanks Professor Ranjith Dissanayake, Conference Co-Chair, Department of Civil Engineering, University of Peradeniya, Sri Lanka, for the invitation to submit manuscripts. The authors would also like to thank Mr. Shyanaka Rathnayaka Mudiyanselage, Tutor and Ph.D. candidate, Department of Infrastructure Engineering, Faculty of Engineering and Information Technology, The University of Melbourne, for his help in compiling the data for Table 1.

Declaration of Competing Interest The authors declare that they have no known competing financial interests or personal relationships that could have appeared to influence the work reported in this article.

References

1. Abeysekera L, Dawson P (2015) Motivation and cognitive load in the flipped classroom: definition, rationale and a call for research. High Educ Res Dev 34(1):1–14. https://doi.org/10.1080/07294360.2014.934336
2. Agostino D, Arnaboldi M, Lema MD (2021) New development: COVID-19 as an accelerator of digital transformation in public service delivery. Publ Money Manage 41(1):69–72. https://doi.org/10.1080/09540962.2020.1764206

3. Vural A, Ceren VR, Halldórsson Á, Ståhle G, Yaruta M (2020) Can digitalization mitigate barriers to intermodal transport? An exploratory study. Res Transp Bus Manag 37:100525. https://doi.org/10.1016/j.rtbm.2020.100525
4. Amankwah-Amoah J, Khan Z, Wood G, Knight G (2021) COVID-19 and digitalization: the great acceleration. J Bus Res 136:602–611. https://doi.org/10.1016/j.jbusres.2021.08.011
5. Anderson LW, Krathwohl DR (2001) A taxonomy for learning, teaching, and assessing: a revision of bloom's taxonomy of educational objectives. Longman
6. Autio E, Mudambi R, Yoo Y (2021) Digitalization and globalization in a turbulent world: centrifugal and centripetal forces. Glob Strateg J 11(1):3–16. https://doi.org/10.1002/gsj.1396
7. Bahn K, Cohen J, Rodgers YM (2020) A feminist perspective on COVID-19 and the value of care work globally. Gend Work Organ 27(5):695–699. https://doi.org/10.1111/gwao.12459
8. Berge ZL (1999) Interaction in post-secondary web-based learning. Educ Technol 39(1):5–11
9. Biggs J, Tang C (2011) Teaching for quality learning at university. McGraw-Hill Education, UK
10. Buchholz M, Holmgren K, Ferm U (2020) Remote communication for people with disabilities: support persons' views on benefits, challenges, and suggestions for technology development. Technol Disabil 32:69–80. https://doi.org/10.3233/TAD-190254
11. Crowe S, Cresswell K, Robertson A, Huby G, Avery A, Sheikh A (2011) The case study approach. BMC Med Res Methodol 11:100. https://doi.org/10.1186/1471-2288-11-100
12. Detel W (2015) Social constructivism. In: Wright JD (ed) International Encyclopedia of the social & behavioral sciences, 2nd edn. Elsevier, Oxford, pp 228–234
13. Dhawan E, Chamorro-Premuzic T (2018) How to collaborate effectively if your team is remote. Harvard Business Review Digital Article
14. Duek I, Fliss DM (2020) The COVID-19 pandemic—from great challenge to unique opportunity: perspective. Ann Med Surg 59:68–71. https://doi.org/10.1016/j.amsu.2020.08.037
15. Embrett M, Liu RH, Aubrecht K, Koval A, Lai J (2021) Thinking together, working apart: leveraging a community of practice to facilitate productive and meaningful remote collaboration. Int J Health Policy Manag 10(9):528–533. https://doi.org/10.34172/ijhpm.2020.122
16. Fathi MS, Rawai N, Abedi M (2012) Mobile information system for sustainable project management. Paper presented at the 2nd international conference on civil engineering, architecture and building materials (CEABM 2012), Yantai, China, May 25–27
17. Franken E, Bentley T, Shafaei A, Farr-Wharton B, Onnis L, Omari M (2021) Forced flexibility and remote working: opportunities and challenges in the new normal. J Manage Organ:1–19. https://doi.org/10.1017/jmo.2021.40
18. Henderson M, Selwyn N, Aston R (2017) What works and why? Student perceptions of 'useful' digital technology in university teaching and learning. Stud High Educ 42(8):1567–1579. https://doi.org/10.1080/03075079.2015.1007946
19. Hines RA, Pearl CE (2004) Increasing interaction in web-based instruction: using synchronous chats and asynchronous discussions. Rural Spec Educ Q 23(2):33–36. https://doi.org/10.1177/875687050402300206
20. Johnson RJ, Wilson P, Hughes J (2020) Shaping the post-COVID-19 "new normal" with communication and collaboration platforms: state of the art communications for radiology, oncology, MDTs and beyond. BJR Open 2(1):20200038. https://doi.org/10.1259/bjro.20200038
21. Kuepper-Tetzel CE, Nordmann E (2021) Watch party lectures: synchronous delivery of asynchronous material. J Learn Dev Higher Educ. https://doi.org/10.31234/osf.io/ys4jn
22. Li J, Vinayagamoorthy V, Schwartz R, IJsselsteijn W, Shamma DA, Cesar P (2020) Social VR: a new medium for remote communication and collaboration. In: Extended abstracts of the 2020 CHI conference on human factors in computing systems. Association for Computing Machinery, Honolulu, HI, USA, pp 1–8
23. Lupton D (2020) Data mattering and self-tracking: what can personal data do? Continuum 34(1):1–13. https://doi.org/10.1080/10304312.2019.1691149
24. Maloy RW, Edwards SA, Evans A (2014) Wikis, workshops and writing: strategies for flipping a college community engagement course. J Educators Online 11(1):1–23

25. Marion TJ, Fixson SK (2021) The transformation of the innovation process: how digital tools are changing work, collaboration, and organizations in new product development. J Prod Innov Manage 38(1):192–215. https://doi.org/10.1111/jpim.12547
26. Moss VA, Adcock M, Hotan AW, Kobayashi R, Rees GA, Siégel C, Tremblay CD, Trenham CE (2021) Forging a path to a better normal for conferences and collaboration. Nat Astron 5(3):213–216. https://doi.org/10.1038/s41550-021-01325-z
27. Nagel L (2020) The influence of the COVID-19 pandemic on the digital transformation of work. Int J Sociol Soc Policy 40(9/10):861–875. https://doi.org/10.1108/IJSSP-07-2020-0323
28. Peacock S, Cowan J, Irvine L, Williams J (2020) An exploration into the importance of a sense of belonging for online learners. Int Rev Res Open Distrib Learn 21(2):18–35. https://doi.org/10.19173/irrodl.v20i5.4539
29. Ritter T, Pedersen CL (2020) Digitization capability and the digitalization of business models in business-to-business firms: past, present, and future. Ind Mark Manage 86:180–190. https://doi.org/10.1016/j.indmarman.2019.11.019
30. Savery JR (2015) Overview of problem-based learning: definitions and distinctions. Interdiscipl J Probl Based Learn 1(1):9–20. https://doi.org/10.7771/1541-5015.1002
31. Smith P, Beretta M (2021) The Gordian knot of practicing digital transformation: coping with emergent paradoxes in ambidextrous organizing structures. J Prod Innov Manage 38(1):166–191. https://doi.org/10.1111/jpim.12548
32. Soibelman L, Sacks R, Akinci B, Irem Dikmen M, Birgonul T, Eybpoosh M (2011) Preparing civil engineers for international collaboration in construction management. J Profess Issues Eng Educ Pract 137(3):141–150. https://doi.org/10.1061/(ASCE)EI.1943-5541.0000044
33. Xu M, Duffield C, Pelham N, Bradley M (2013) When do mid-project reviews (MPRs) deliver the greatest project benefits? Comparative analysis of Australian review outcomes. J Manage Eng 29(2):140–149. https://doi.org/10.1061/(ASCE)ME.1943-5479.0000126
34. Zainal Z (2007) Case study as a research method. Jurnal kemanusiaan 5(1):1–6
35. Zoom Video Communications Inc. (2021) Simplified video conferencing and messaging across any device. Accessed 9 Oct 2021. https://explore.zoom.us/en/products/meetings/

Advanced Technologies in High-Rise Structures

A Comparison Between Predicted and Actual Thermal Sensation in Non-air-conditioned Residential Buildings in a Tropical Climate: A Case Study

M. A. U. R. Maddumaarachchi, V. M. Jayasooriya, and D. M. Senevirathne

Abstract Maintaining optimal indoor thermal comfort has identified to be a necessity for residential buildings in tropical climates, especially, when there are no countermeasures available such as air-conditioning. Predicted mean vote (PMV) and actual mean vote (AMV) are widely used to determine indoor thermal comfort of buildings in different climatic conditions. PMV predicts the thermal sensation of the occupants considering ambient physical parameters: indoor air temperature, mean radiant temperature, relative humidity, and wind velocity, whereas AMV determines actual thermal sensation of the occupants through standard thermal comfort surveys defined by ANSI/ASHRAE Standard 55. Out of these, predicted mean vote (PMV) is the most popular model in predicting indoor thermal comfort, however, is known to contradict the actual thermal sensation (AMV) of occupants in different intensities for various climatic conditions. Therefore, this study has been carried out to compare the results of predicted and actual values of thermal sensation for a tropical climate using six non-air-conditioned residential buildings located in Gampaha, Sri Lanka. The buildings were selected within an area of 1 km radius to neutralize the effects of microclimatic differences. The data collection was carried out covering four different tropical climatic seasons from the month of July to December 2020 including field measurements and questionnaires ($N = 2200$). Regression analysis and Pearson correlation tests were performed to assess the strength of the relationship between predicted and actual thermal sensations. The results revealed that there is a significant mean difference between AMV and PMV for all four seasons, as + 1.399, + 1.139, + 0.934, and + 0.855, respectively. Furthermore, predicted neutral temperatures recorded for each season were 25.89 °C, 26.39 °C, 26.15 °C, and 26.43 °C, whereas actual neutral temperature recorded for these seasons were 29.58 °C, 28.59 °C, 28.00 °C, and 27.76 °C, respectively. Hence, the results suggest that for a tropical climate, PMV model underpredicts the actual neutral temperature of the occupants.

M. A. U. R. Maddumaarachchi · V. M. Jayasooriya (✉) · D. M. Senevirathne
Department of Forestry and Environmental Science, University of Sri Jayewardenepura, Gamapaha 10250, Sri Lanka
e-mail: varuni.jayasooriya@sjp.ac.lk

R. Dissanayake et al. (eds.), *12th International Conference on Structural Engineering and Construction Management*, Lecture Notes in Civil Engineering 266,
https://doi.org/10.1007/978-981-19-2886-4_33

Keywords Indoor thermal comfort · Residential buildings · Predicted mean vote (PMV) · Actual mean vote (AMV)

1 Introduction

The term thermal comfort can be simply defined as 'the condition of mind that expresses satisfaction with the thermal environment and is assessed by subjective evaluation' (ANSI/ASHRAE Standard 55). The performance of the building occupants is proven to be significantly affected by thermal comfort which includes an inherent psychological component that may affect the occupants' mental well-being and productivity. In addition, poor thermal comfort condition is found to be related to the vast majority of complaints about indoor climate [2]. Current thermal comfort standards in use are based on two basic models of thermal comfort assessment which are predicted mean vote/predicted percentage dissatisfied (PMV/PPD) model and adaptive model [11].

PMV model was proposed by [7] and is based on the heat balance theory of the human body. According to this model, thermal discomfort occurs as a result of the thermal imbalance caused between the occupant and the surrounding environment. PMV index predicts the thermal sensation objectively using four environmental parameters, namely indoor air temperature (T_a), mean radiant temperature (T_{mrt}), relative humidity (RH), and wind velocity (V), alongside two personal parameters of the occupants, namely: metabolic activity level and clothing insulation. Among them, the indoor air temperature has been assumed to be one of the most dominant parameters affecting the thermal sensation of the users [15]. Even though this model is widely adapted by many international thermal comfort standards, its reliability and applicability in real-life scenarios have been often questioned by many researchers, since this model was based on the experiments carried out in climatic chambers with uniform climatic conditions. Reviews indicated discrepancies between the predicted thermal sensation and the actual thermal sensation most of the time [6, 17].

The adaptive model was introduced by [4] with the expectation of minimizing the shortcomings of the PMV/PPD model. Compared to the PMV/PPD model which considers occupants in any building type or any climatic zone as passive recipients of thermal stimuli, adaptive model emphasizes the role of occupants in creating their own thermal comfort through diverse physiological (habituation/expectation and preferences), behavioral (personal, environmental, technological, and cultural), and psychological measures (generic adaptation or acclimatization) [4]. Adaptive measures undertaken by the occupants differ on both climatic and personnel levels. This results in the perception of same thermal environment as different comfort levels by the occupants. According to this model, the actual thermal sensation will be largely dependent upon the respective adaptive measures of the occupants and will be determined with the AMV index. In order to determine the AMV, questionnaire surveys have to be carried out among the occupants, and actual thermal sensation will be indicated on a 7-point thermal sensation scale.

Both these two types of models can execute the calculation of the mean thermal sensation of the occupants in a particular enclosure and can be interpreted on AHSRAE 7-point thermal sensation scale. According to the ASHRAE 7-point thermal sensation scale, the thermal sensation of occupants can vary from cold sensation (− 3) to hot sensation (+ 3). Determining the PMV and AMV values helps to identify the ideal average neutral temperature for occupants. This information is of great importance since it can be referred in designing naturally ventilated buildings, where appropriate passive design strategies can be adapted to maintain the respective average neutral temperature level.

Studies conducted by [5] revealed that the PMV index is better suited for predicting the thermal vote in air-conditioned buildings, while it is not accurate for naturally ventilated buildings. Studies carried out in naturally ventilated buildings in many parts of the world validated this by indicating underpredictions or overpredictions by actual thermal vote (AMV) against the predicted thermal vote (PMV). Evidence also suggests that comfortable temperature is higher than what is predicted most of the times, especially in tropical regions, because of the ability of acclimatization by humans [19]. Therefore, it is evident that AMV is a more suitable index to determine the indoor thermal comfort of the occupants, especially for naturally ventilated/non-air-conditioned buildings in tropical regions. However, PMV is the most popular index in predicting indoor thermal comfort and is widely used all around the world, since it involves fairly a simple method in predicting the neutral temperature of the occupants as it mainly involves measuring ambient environmental parameters.

So far, no studies have been carried out to compare PMV and AMV in Sri Lanka. Therefore, the present study has been carried out as an initiative study, for the comparison of predicted and actual thermal comfort levels and to determine the comfort temperature range based on PMV and AMV indices for the selected area.

2 Materials and Methods

2.1 Study Area and Experimental Set up

For the study, six non-air-conditioned residential houses were selected from Mandawala area in Gampaha district, Sri Lanka. These sites were selected with careful consideration in order to represent the most common house types in the selected area. Since the local climatic conditions may highly influence the thermal comfort conditions and the main objective of the present study is to compare the PMV and AMV values, houses that exhibit similar microclimatic surrounding conditions (within 1 km radius) were chosen to eliminate the impact from different local climatic conditions.

Data collection was carried out under different climatic seasons from July to December 2020. In addition to the three major climatic seasons falling through that period, overhead sun position period was chosen as a separate season, and the selected

Table 1 Instrumentation used for the data collection

Instrument	Measurement parameter	Accuracy
HSETIN temp./RH data logger	Ambient temperature	± 0.6 °C or ± 5%
	Relative humidity	± 3%
Digital anemometer smart sensor AS810	Wind velocity	± 0.1 m/s or ± 5%

seasons were defined as: (1) southwest monsoon season (July–September), (2) overhead sun position season (August 28th–September 7th), (3) second inter-monsoon season (October–November), and (4) northeast monsoon season (December).

For the AMV calculation, an average number of 500 survey responses were collected for each season, and the average PMV for the same time period in which the survey was carried out was also calculated with the measured environmental parameters. Then after, PMV and AMV comparisons were carried out.

2.2 Field Data Collection

Field data collection involved ambient environmental parameter measurement recoding for the PMV calculation. The duration for the data collection for each replicate was selected to be from 10.00 a.m. to 4.00 p.m. since this is a time in which the residents are considered to be the most active and most likely to feel thermal discomfort. The respective parameters were recorded in each 15-min interval. Ambient physical parameters given in Table 1 were measured and recoded during the field data collection.

In addition to the above-mentioned parameters, clothing level and activity level of the occupants which are also needed for the PMV calculation were recorded through the questionnaire survey. The collected field data were used to obtain the PMV through an already developed and tested tool [16] by the Centre for the Built Environment, research center at the University of California, Berkeley.

2.3 Thermal Comfort Survey

A survey was carried out to determine the actual thermal sensation (AMV) of the occupants, and they were requested to demarcate their vote on ASHRAE 7-point thermal sensation scale. For the subjective data collection, the time duration of a single replicate was divided into three sets of 2-h spans as, 10.00 a.m.–12.00 p.m., 12.00 p.m.–2.00 p.m., and 2.00 p.m.–4.00 p.m. The survey was conducted during the

last 15 min of each 2-h span, to determine the thermal comfort level of the occupants at that particular moment.

3 Results

3.1 Comparison of PMV and AMV Values

PMV and AMV for the simultaneous time periods were calculated for the four seasons and were plotted against indoor air temperature for the comparisons. According to the results shown in Fig. 1, it is visible that PMV has overpredicted the actual thermal sensation of the occupants in all the considered seasons. Since the outcome of PMV index is a prediction of the thermal comfort mainly relied upon ambient physical parameters, it can be noticed that there is a strong relationship between PMV and the indoor air temperature. However, the AMV index expressing different degrees of strength with indoor air temperature in different seasons suggests that occupants might have engaged in different adaptive measures to feel better thermal comfort under the respective thermal environment.

Furthermore, it can be identified that the same temperature has been perceived differently by the occupants during different seasons. This also highlights how the occupants' thermal perception has differed due to their different adaptations undertaken during different seasons, depending on the climate and thermal environment to which they are subjected to. Therefore, it can be concluded that the actual thermal sensation of the occupants is an outcome of the combination of meteorological parameters and the adaptive measures of the occupants.

For analysis of PMV and AMV values, Shapiro–Wilk test for normality and Levene's test for homogeneity were carried out, and the results indicated that the datasets are normal and homogenous. Henceforth, parametric t-test was selected for the comparison of PMV and AMV values, and it indicated that there is a significant difference between the values of the two indices in every season ($p < 0.05$). Mean differences obtained for the four seasons were recorded as + 1.399, + 1.139, + 0.934, and + 0.855, respectively.

This led to the need of carrying out further analysis to study the relationship between PMV and AMV. For this, scatter plots were generated for each season and are given in Fig. 2.

Since a linear relationship was observed with the generated scatted plots, Pearson correlation analysis was performed to assess the strength and direction of the relationship among the two variables PMV and AMV and also on the relationship of PMV and AMV against average indoor temperature. Pearson coefficient between PMV and AMV indicated a strong correlation interpreting that PMV and AMV move in the same direction, which also means if one parameter increases, the other parameter also increases and if one parameter decreases the other parameter also decreases.

Fig. 1 Av. indoor air temperature against av. PMV/AMV for the four seasons

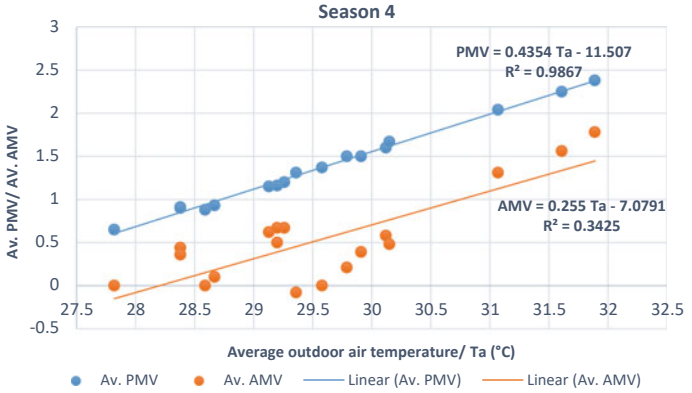

Fig. 1 (continued)

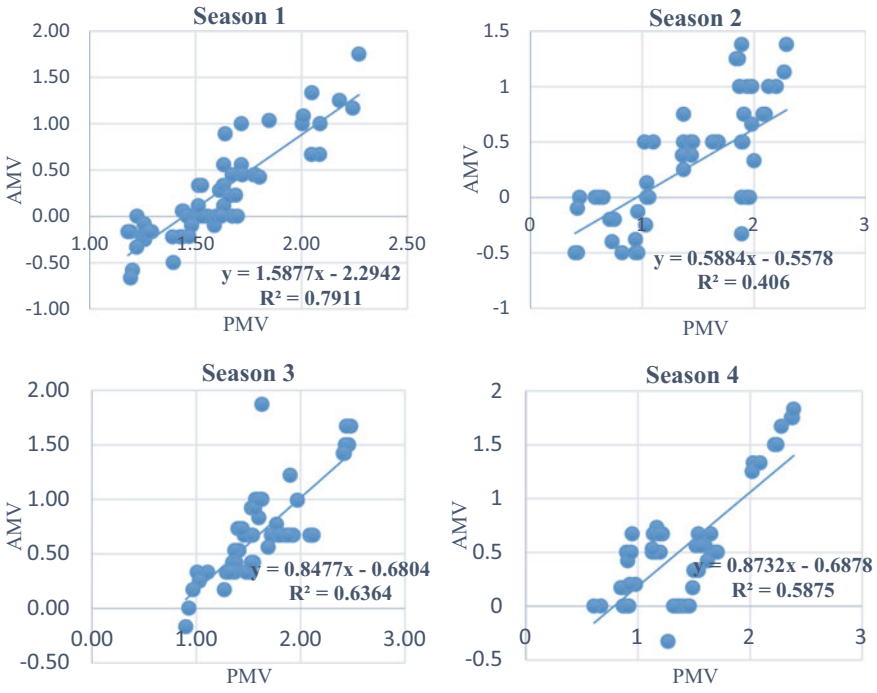

Fig. 2 Scatter plot for PMV and AMV values for the four seasons

Pearson coefficients of PMV and AMV against indoor air temperature also indicated a strong correlation between the two parameters suggesting that indoor air temperature has a strong relationship with the thermal sensation of the occupants, irrespective of the predicted or actual value.

In addition, regression analysis was conducted to find out how one variable affects the other variable. For this, PMV and AMV values were analyzed against indoor air temperature by considering indoor air temperature as the predictor variable. Results indicated that there is a strong causality on PMV by the indoor air temperature. This can also be explained with the underlying basis of the PMV model. Furthermore, it was visible that causality on AMV by indoor air temperature is not as strong and also there is a notable difference of causalities among different seasons as well. These outcomes also provide explanations to indicate that AMV is not only affected by the environmental parameters but by other means as well, which can be identified as occupant adaptive measures.

However, since results from the Pearson correlation indicated a strong correlation between indoor air temperature and AMV and regression analysis indicated a considerable causality by indoor air temperature on AMV, it highlights the importance of maintaining an ideal thermal environment as well, in order to ensure better indoor thermal comfort of the occupants.

3.2 Determination of the Neutral Temperature

ASHRAE 7-point thermal sensation scale indicates that neutral temperature in which the occupants feel the maximum thermal comfort is at the '0' value of the scale, which is PMV = 0. Additionally, ASHRAE 55-2017 [1] defines the neutral temperature range as the 'comfort zone' of the occupants, and it falls within the PMV levels of − 0.5 PMV to + 0.5 PMV.

Accordingly, neutral temperature and neutral temperature range for each season were calculated using the regression equations obtained through average temperature vs. average PMV/AMV graphs and are given in Table 2.

According to Table 2, it is visible that ideal temperature or the 'neutral temperature' differs from season to season along with its 'neutral temperature range'. The most crucial feature here is that during all the seasons, the 'predicted neutral temperature/temperature range' is underpredicted by the PMV model than the actual values.

Table 2 Predicted and actual neutral temperature/temperature range for different seasons

Season	Predicted neutral values		Actual neutral values	
	Predicted neutral temperature (°C)	Predicted neutral temperature range (°C)	Actual neutral temperature (°C)	Actual neutral temperature range (°C)
Season 1	25.89	24.62–27.16	29.58	28.73–30.42
Season 2	26.39	25.26–27.51	28.59	26.92–30.26
Season 3	26.15	24.95–27.35	28.00	26.48–29.52
Season 4	26.43	25.28–27.58	27.76	25.80–29.72

'Actual neutral temperature/temperature range' indicates that the occupants are more tolerant to higher temperatures than what was predicted through the PMV model.

4 Discussion

Several previous researches conducted in the area of thermal comfort have proven that the difference between indoor temperature (T_a) and mean radiant temperature (T_{mrt}) is negligible for indoor environments [18]. Therefore, the present study was carried out based on the said assumption.

The results of the study revealed that there is a mean difference between PMV and AMV for the selected four seasons as + 1.399, + 1.139, + 0.934, and + 0.855, respectively. This indicated that the PMV has overpredicted the actual thermal sensation of the occupants. Similar outcomes have been obtained for the summer period in studies carried out by [20] in Chongqing, China, and [14] in Northeast India. Furthermore, a study conducted by [8] in Ambala, India, also showed a similar trend, where the results of the monsoon period indicated an overprediction of thermal sensation by the PMV.

This difference elaborates on the fact that occupants do not experience thermal sensation completely upon surrounding meteorological parameters, but they can alter their thermal sensation toward their preferred levels through engagement of diverse adaptive measures. These adaptive measures largely vary upon the location, culture, beliefs, available technology, etc., which results in these contrasting thermal perceptions of the occupants for the same thermal environment.

The thermal comfort temperature in almost every moist tropical study is revealed to be higher than that of the ASHRAE Standard, indicating that AHSRAE is not appropriate for moist tropical field studies [12]. In fact, humans are known for their ability of acclimatization, and the occupants who experience wider ranges of temperatures may find comfort under temperatures which are identified to be uncomfortable by the people who experience narrower ranges of temperatures. Furthermore, some studies indicate that people in naturally ventilated buildings have higher tolerance to greater temperatures, and in addition, they adapt to the respective environment through different adaptive measures such as opening/closing of windows/doors, taking on/off of cloths, having a bath, drinking a cold/hot beverage.

Overprediction of the actual thermal sensation by the PMV model revealed that the occupants are tolerant to higher temperatures than the predicted values which ultimately resulted in the underprediction of neutral temperatures. Accordingly, predicted neutral temperatures recorded for the four seasons were 25.89 °C, 26.39 °C, 26.15 °C, and 26.43 °C, while the actual neutral temperatures recorded were 29.58 °C, 28.59 °C, 28.00 °C, and 27.76 °C, respectively, with an average difference of 2.27 °C between the predicted and actual neutral temperatures. Beizaee et al. [3] conducted a study for naturally ventilated houses and offices in Arup, UK, where the neutral temperatures were recorded as 23.4 °C and 23.2 °C, respectively. Study carried out by [10] in Hyderabad, India, and by [9] in humid tropics, Malaysia, identified the

neutral temperatures as 29.23 °C and 30 °C, respectively. Since Malaysia and India also consist of tropical climates similar to the climate in Sri Lanka, near similarities of the neutral temperatures were identified which could be explained as a result of the acclimatization to similarly experienced temperatures. Lu et al. [12] conducted a similar study in Hainan Island, China, which has a tropical climate and recorded the average neutral temperature of the occupants as 26.1 °C. These results reveal how the neutral temperature varies depending upon the adaptations including acclimatization of those respective occupants.

Even though preferred neutral temperature range has been identified for the selected area, further studies will be required to determine the neutral temperature ranges applicable to other climatic regions of the country. For this, researches are needed to be carried out representing different climatic conditions, and the data obtained from such studies could be used to develop a database for the identification of optimum passive design strategies during the designing of residential buildings, to achieve optimum thermal comfort based on the relevant climatic region. It is known that an optimum design with passive designs and strategies can provide low-cost housing offers with acceptable indoor thermal conditions [13].

5 Conclusion

This study assessed the thermal comfort and thermal adaptation of the occupants in non-air-conditioned residential buildings in a tropical wet zone region in Sri Lanka. Results indicated that there is a significant mean difference between the predicted and actual thermal comfort levels of the occupants, indicating the unsuitability of applying the PMV model for non-air-conditioned residential buildings.

It was evident from the results that occupants' thermal comfort is not necessarily consistent with the ambient parameter changes and largely depends upon their adaptive measures as well. This justified the theory behind the adaptive model of thermal comfort, where the actual thermal sensation of the occupants is considered as the outcome of the combination of the thermal environment created due to meteorological parameters and the adaptive measures undertaken by the occupants, which comprises of psychological, physiological, and behavioral components.

The present study provides insights for engineers and architects to consider the aspect of indoor thermal comfort in buildings during the designing and operation phase with respect to the neutral temperature. In this era of climate change, providing indoor thermal comfort to the occupants holds a major importance especially in tropical countries. Therefore, this study will provide better navigation to conduct further studies representing different climatic conditions in Sri Lanka, to determine the respective neutral temperature ranges which can be referred to by the building designers.

References

1. ANSI/ASHRAE Standard 55 (2017) Thermal environmental conditions for human occupancy. American National Standards Institute, American Society of Heating, Refrigerating and Air-Conditioning Engineers, Atlanta, GA, USA
2. Barbhuiya S, Barbhuiya S (2013) Thermal comfort and energy consumption in a UK educational building. Build Environ 68:1–11
3. Beizaee A, Firth S (2011) A comparison of calculated and subjective thermal comfort sensation in home and office environment. In: Proceedings of conference: people and buildings, network for comfort and energy use in buildings, pp 1–6
4. Brager GS, De Dear RJ (1998) Thermal adaptation in the built environment: a literature review. Energy Build 27(1):83–96
5. De Dear RJ, Brager GS (2002) Thermal comfort in naturally ventilated buildings: revisions to ASHRAE standard 55. Energy Build 34(6):549–561
6. Enescu D (2017) A review of thermal comfort models and indicators for indoor environments. Renew Sustain Energy Rev 79:1353–1379
7. Fanger PO (1970) Thermal comfort. Danish Technical Press, Copenhagen
8. Jindal A (2018) Thermal comfort study in naturally ventilated school classrooms in composite climate of India. Build Environ 142:34–46
9. Harimi D, Ming CC, Kumaresan S (2015) A generalized thermal perception approach for indoor thermal comfort assessment in the humid tropics of Malaysia. Energy Build 88:276–287
10. Indraganti M (2010) Adaptive use of natural ventilation for thermal comfort in Indian apartments. Build Environ 45(6):1490–1507
11. Luo M, de Dear R, Ji W, Bin C, Lin B, Ouyang Q, Zhu Y (2016) The dynamics of thermal comfort expectations: the problem, challenge and implication. Build Environ 95:322–329
12. Lu S, Pang B, Qi Y, Fang K (2018) Field study of thermal comfort in non-air-conditioned buildings in a tropical island climate. Appl Ergon 66:89–97
13. Nguyen AT, Reiter S (2014) Passive designs and strategies for low-cost housing using simulation-based optimization and different thermal comfort criteria. J Build Perform Simul 7(1):68–81
14. Singh MK, Mahapatra S, Atreya SK (2011) Adaptive thermal comfort model for different climatic zones of North-East India. Appl Energy 88(7):2420–2428
15. Sui X, Zhang X (2016) Analysis on combinations of indoor thermal microclimate parameters in radiant cooled residential buildings and drawing of new thermal comfort charts. Build Serv Eng Res Technol 37(1):66–84
16. Tartarini F, Schiavon S, Cheung T, Hoyt T (2020) CBE thermal comfort tool: online tool for thermal comfort calculations and visualizations. SoftwareX 12:100563
17. Van Hoof J (2008) Forty years of Fanger's model of thermal comfort: comfort for all? Indoor Air 18(3):182–201
18. Walikewitz N, Jänicke B, Langner M, Meier F, Endlicher W (2015) The difference between the mean radiant temperature and the air temperature within indoor environments: a case study during summer conditions. Build Environ 84:151–161
19. Xi T, Li Q, Mochida A, Meng Q (2012) Study on the outdoor thermal environment and thermal comfort around campus clusters in subtropical urban areas. Build Environ 52:162–170
20. Yao R, Li B, Liu J (2009) A theoretical adaptive model of thermal comfort—adaptive predicted mean vote (aPMV). Build Environ 44(10):2089–2096

A Highly Efficient Numerical Approach Using Fluid–Structure Interaction to Estimate Responses of Super-Tall Structures

K. Wijesooriya, D. Mohotti, and P. L. N. Fernando

Abstract Modern super-tall structures are extremely prone to wind-induced loads especially due to its inherent slenderness and the use of modern strong yet lightweight materials. Numerical methods via the use of computational fluid dynamics (CFD) have gained popularity in wind engineering applications and have been found to be a reliable tool at estimating wind loads. However, fluid–structure interaction (FSI) simulations still pose a challenge due to the complexities involved in the simulation mechanism. Current commercial packages that are available are not capable of providing results within a feasible time frame. Thus, this paper presents an alternate numerical framework to estimate wind-induced structural responses of complex super-tall structures. A novel and efficient one-way uncoupled FSI technique is presented where it is evaluated against a commercial two-way FSI technique and wind tunnel test of a multi-degree of freedom (MDOF) aeroelastic model. It is shown that the novel method is capable of providing higher quality results in terms of structural responses in comparison to the commercially available two-way FSI method. The study shows that using the correct modelling techniques and the novel pressure mapping technique introduced, FSI modelling is feasible and can be used effectively for the design of wind-sensitive structures.

Keywords Wind-sensitive structures · Fluid–structure interaction (FSI) · Vortex-induced vibrations (VIV) · Computational fluid dynamics (CFD) · Structural response

K. Wijesooriya (✉) · D. Mohotti
School of Engineering and Information Technology, The University of New South Wales, Canberra ACT 2600, Australia
e-mail: k.wijesooriya@unsw.edu.au

P. L. N. Fernando
Department of Civil Engineering, University of Moratuwa, Moratuwa, Sri Lanka

R. Dissanayake et al. (eds.), *12th International Conference on Structural Engineering and Construction Management*, Lecture Notes in Civil Engineering 266,
https://doi.org/10.1007/978-981-19-2886-4_34

1 Introduction

Over the last decade, there has been an upsurge on research conducted on computational fluid dynamics (CFD) with emphasis made on tall buildings. New modelling techniques coupled with improved computational capability prompted some of the major developments in this regard [5, 11, 12]. Whilst CFD has proven to be capable of predicting pressure loads, obtaining structural responses requires further high fidelity modelling in the form of fluid–structure interaction (FSI). FSI simulations still present to be a challenge in terms of achieving results within a feasible timeframe. The computational demand required lies within the nature of the simulation where data must be transferred to and from the fluid and structural solvers. Early implementations of FSI can be found in studies presented by Braun and Awruch [1] where alongwind responses were found to be in good agreement but poor crosswind results. Their study also emphasised on extensive computational demands required for the simulations. The method provided by [13] used an alternate approach where better predictions were also made on the crosswind direction. Whilst improvements were made in computational demand in comparison to [1], the overall computation time was still not satisfactory.

To this end, the authors developed a comprehensive numerical framework which comprises an innovative CFD modelling technique and also an uncoupled FSI technique. The FSI technique presents a novel method for mapping wind pressure loads to structural nodal loads via a user-created script. These nodal time history loads were then used in an implicit modal transient analysis where a time history analysis of the structure was performed. This paper presents that numerical framework in a succinct format.

2 The Numerical Framework

2.1 Transient Computation Fluid Dynamics (CFD) Modelling

A transient CFD simulation is an essential prerequisite to determining responses of wind-sensitive structures. The CFD simulation must be capable of replicating atmospheric boundary layer (ABL) flow conditions. This constitutes of wind velocity profile, wind turbulence profile and most importantly the power spectral density (PSD) of the approach flow. In the ABL, the manifestation of wind turbulence is non-uniform and anisotropic and is usually described by velocity power spectrums in the three directions. The Von-Karman spectrum is often used to describe this anisotropic behaviour of wind and is important that this is also correctly replicated in the CFD simulation. Thus, identifying key inflow characteristics is an important requirement in CFD simulation in order to predict reliable pressure loads on super-tall structures.

For this numerical procedure, a scale-resolving turbulence model is essential as Reynolds Averaging Navier–Stokes (RANS) models are incapable of capturing important flow features accurately in complex structures [2]. The Large Eddy Simulation (LES) turbulence model is the most prominent of all scale-resolving models due to its proven capability. However, the computational demand required for LES-type simulation has often been found to be expensive and unfeasible. Hybrid RANS-LES models such as Delayed Detached Eddy Simulation (DDES) have shown to improve simulation time whilst providing scale-resolving features. However, one of the major drawbacks of the DDES model is the use of RANS on wall boundaries which then transitions to LES in regions further away. It was found in the authors previous work [2] that RANS models are not capable of accurately predicting important flow features such as separation especially when separation occurs due to an adverse pressure gradient as found on circular geometries. Thus, the use of LES is paramount in such a simulation. To this end, the authors proposed an Embedded Large Eddy Simulation (ELES) model [10] where LES is used closer to the building vicinity and RANS is used in regions further away. Figure 1 demonstrates two possible methods by which the domain is split and regions of LES and RANS are defined.

The study performed by the authors [10] importantly showed that ELES was capable of providing similar accuracy to that of a full LES model, for the same mesh density and configuration, at half the computational effort required. Also, a comparison of sub-grid scale modelling was performed, and it was recommended that the Wall Adapting Local Eddy-viscosity (WALE) model was most suitable and that DDES-type hybrid RANS models were also undesirable due to reasons explained before.

In LES-type simulations, synthetic turbulence was introduced via the vortex method where a fluctuating vorticity field is used to add perturbation to the input mean velocity profile to generate turbulence [10]. In the ELES domain, the location at which turbulence generates is at the interface. For the case in Fig. 1a, turbulence is generated at interface 2 whilst for Fig. 1b at interface 1. The inflow characteristic tests in CFD are first carried out in an empty domain, measured and then inlet profiles are adjusted if required. This is an iterative process much like in an experimental wind tunnel test. The input of inflow characteristics is defined by turbulent kinetic energy (TKE) and turbulent dissipation rate (TDR) profiles as provided in Eqs. 1 and 2, where U_{avg} is the average velocity, $I_u(y)$ is the turbulence intensity, C_μ is a model constant for the Rkε model, which is equal to 0.09, and L is the integral length scale which is the only parameter obtained from the wind tunnel test and is equal to 0.3 m.

$$\text{TKE} = \alpha\left(U_{\text{avg}} I_u(z)\right)^2 \tag{1}$$

$$\text{TDR} = C_\mu^{3/4} \frac{\text{TKE}^{3/2}}{L} \tag{2}$$

The iterative process mentioned earlier can be carried out by varying α in Eq. (1) which can take a value of either 0.5, 1.0 or 1.5. A complete account to accurately determine α is proposed in the authors' previous work [10].

The mesh plays a significant role, and it is highly recommended that a polyhedral mesh is used. The advantages of the polyhedral cell are the ability to capture complex flow features such as recirculation at lower cell counts in comparison to other types of cells [6]. The mesh structure within the domain needs to be structured with consideration given to regions of interests. As shown in Fig. 2, the ELES setup shows three zones where the mesh is finest at $Z1$ and coarsest at $Z3$ which is furthest away from the region of interest. The building surface mesh must contain inflation layers where the first cell layer thickness must adhere to $y^+ < 1$ criteria [2, 10].

A high-quality CFD simulation with appropriate inflow characteristics, mesh sizing and boundary conditions should result in comparable results to which that are obtained from a wind tunnel experiment. Scale vortices as shown in Fig. 3a show

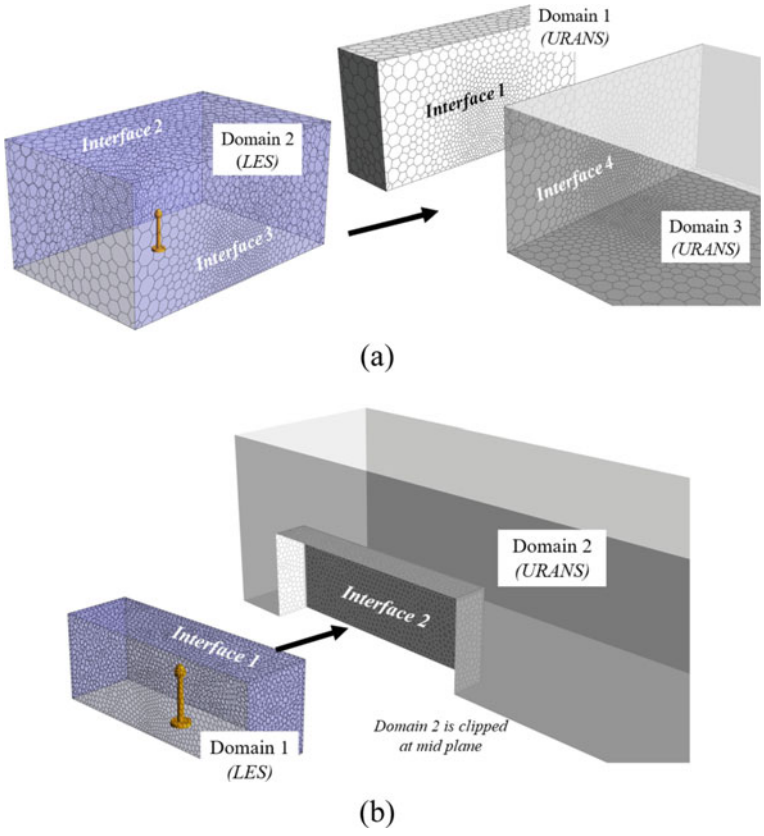

Fig. 1 ELES setup where: **a** domain split into three distinct regions [8] and **b** LES domain confined to box [10]

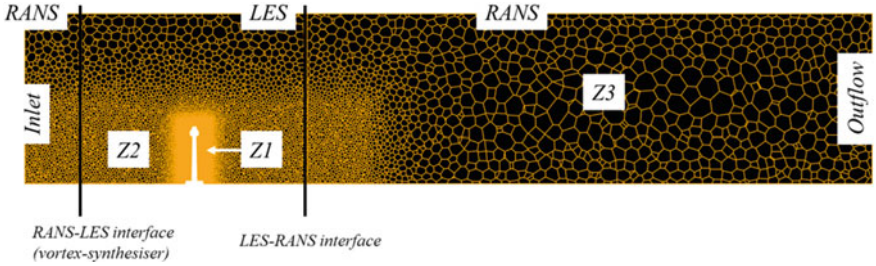

Fig. 2 General polyhedral mesh layout for ELES simulation

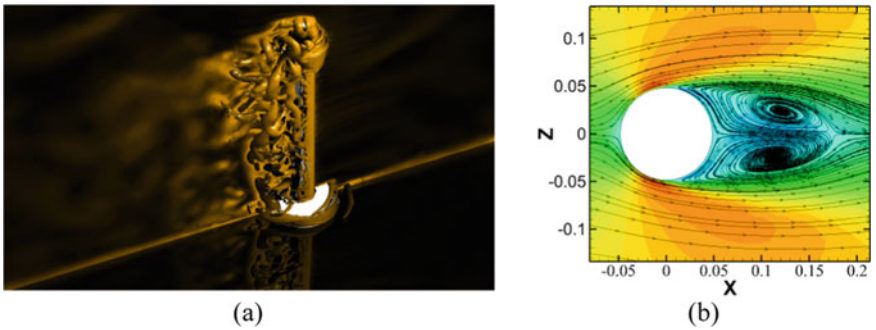

Fig. 3 **a** Q-criterion scale vortices, **b** flow streamline on cross section

the complexity of flow that occurs around the structure where phenomenon such as vortex shedding can be observed at the sides for both small and large turbulent structures. Figure 3b shows the time-averaged flow vectors at a cross section where important features such as recirculation can be observed.

2.2 The Pressure Mapping Algorithm and Transient Modal Analysis

The core of the numerical framework is the pressure mapping technique created by the authors. The CFD simulation which records pressure at fixed locations over a time period is converted to nodal force time histories in the structural domain. This conversion of fluid pressure to time history structural loads is done via a MATLAB script. The mapping of pressure points in a fluid domain to structural domain is done via mathematical procedures where vector calculus is employed. First, the pressure point locations in the fluid domain must be mapped to the appropriate façade locations in the structural domain. It must be noted that façade does not exist in the structural model, and these are pseudo-elements created in MATLAB for the procedure. The

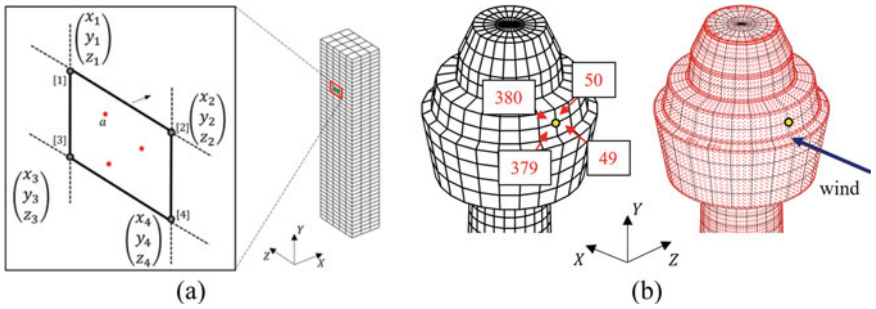

Fig. 4 **a** Pressure mapping visual [8], **b** subject structure example [9]

mapping is done via the following procedure: Fig. 4a shows a Point "a" which is an arbitrary point within the façade where pressure is recorded with coordinates $[x_a, y_a, z_a]$. Two mapping checks are required in order to determine if a point truly lies on the façade. Mapping check 1, inequality check:

$$\begin{aligned}
&\text{if } \min(x_1, x_2, x_3, x_4) \leq x_a \leq \max(x_1, x_2, x_3, x_4)\\
&\text{if } \min(y_1, y_2, y_3, y_4) \leq y_a \leq \max(y_1, y_2, y_3, y_4)\\
&\text{if } \min(z_1, z_2, z_3, z_4) \leq z_a \leq \max(z_1, z_2, z_3, z_4)
\end{aligned}$$

Mapping check 2: check if the point truly lies on the face of the façade. Using vector calculus, the unit normal vector ($\overrightarrow{U_f}$) of a façade can be calculated as follows:

$$\vec{N} = \begin{pmatrix} x_2 - x_1 \\ y_2 - y_1 \\ z_2 - z_1 \end{pmatrix} \times \begin{pmatrix} x_4 - x_1 \\ y_4 - y_1 \\ z_4 - z_1 \end{pmatrix} \tag{3}$$

$$\overrightarrow{U_f} = \frac{\vec{N}}{\sum \text{abs}\left(\vec{N}\right)} \tag{4}$$

where $\overrightarrow{N}$ is a normal vector to the façade and $\overrightarrow{U_f}$ is the normal unit vector of the façade. Assuming that Point 'a' lies on the façade, a direction vector from either of the four vertices of the façade to Point 'a' can also be computed ($\overrightarrow{a_{fd}}$) as follows:

$$\overrightarrow{a_{fd}} = \begin{pmatrix} x_a \\ y_b \\ z_c \end{pmatrix} - \begin{pmatrix} x_4 \\ y_4 \\ z_4 \end{pmatrix} \tag{5}$$

Thus, the dot product of vectors $\overrightarrow{U_f}$ and $\overrightarrow{a_{fd}}$ should equal be to zero if Point 'a' was to truly lie on the façade, as expressed in Eq. (6):

$$\overrightarrow{U_{\mathrm{f}}} \cdot \overrightarrow{a_{fd}} = 0 \tag{6}$$

Figure 4b shows a visual of all pressure points recorded in the fluid domain for the top part of the subject structure. As shown, Node ID:73 (marked in yellow) has contributions of pressure from façade panels as marked in the left diagram. The mathematical procedure for distributing loads is fully explained in [7, 9], and the complete MATLAB script can be found in [4].

3 Case Study

An example of a 406 m tall super-tall structure is used to demonstrate the capability of the uncoupled one-way FSI technique (**1wFSI**) method. It is compared against a multi-degree of freedom (MDOF) aeroelastic model (**Exp**) performed in a boundary layer wind tunnel (BLWT) as shown in Fig. 5. In general practice, tests are performed at the model scale and then translated to the full scale via the use of scaling parameters. This method is also adopted in this study as the experimental wind tunnel tests are conducted at a model scale of 1:300. A similar scale was also used for the numerical models to maintain consistency.

The results of 1wFSI are also compared with a fully coupled two-way FSI simulation (**2wFSI**) undertaken in ANSYS. Finally, an analytical (**TH**) equation of the mean alongwind displacement is also shown for comparison purposes. The analytical model is derived by modelling the structure of constant stiffness (EI) as an Euler–Bernoulli beam as given in Eq. (7), where the complete derivation is provided in [8]. The analytical model is given in a form such that displacement at any location along the structure's height can be identified and for a wind proof that can be described

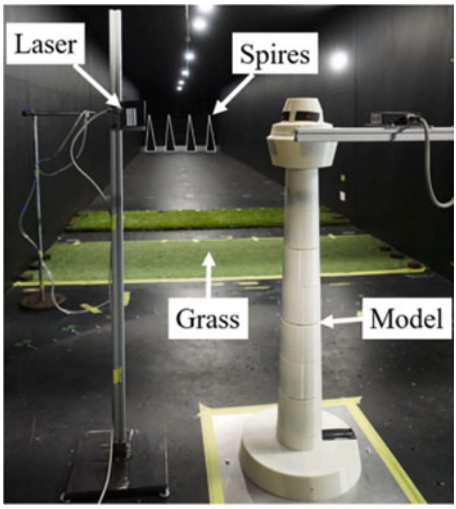

Fig. 5 Wind tunnel [8]

via a power law. The annotations in Eq. (7) are: α an exponent of the wind profile, L the height of the building, y the location at which displacement is calculated and $P = 0.6125 \times C_d A \beta^2 U_{ref}^2$, where A is the projected frontal area, β an exponent of the wind profile, U_{ref} the reference velocity and C_d the drag coefficient of the building. For the maximum and standard deviation quantities, the gust loading factor (GLF) method is used where the mean deflection is multiplied by the GLF as outlined in Ref. [8].

$$x_{mean}(y) = P/EI\left[\frac{y^2}{2}\left(\frac{2\alpha+1}{2\alpha+2}\right)L^{2\alpha+1} + \frac{y^{2\alpha+3}}{(2\alpha+2)(2\alpha+3)} - \frac{(2\alpha+1)y^{2\alpha+3}}{4(\alpha+1)^2(2\alpha+3)} - L^{2\alpha}\frac{y^3}{6}\right] \quad (7)$$

The results presented here are all displacements, where in the alongwind direction, the mean, maximum and standard deviation quantities are compared, whilst in the crosswind direction, the standard deviation quantity is compared as presented in Fig. 6. The results of deflection are compared for reduced velocities (V_r) as shown in Fig. 6. Reduced velocity can be expressed as a function of the structure's first mode of vibration (f_1), reference velocity (U_H) at the apex height (H): $V_r = \frac{U_H}{f_1 H}$. The reduced velocity is a dimensionless unit which is commonly used to describe the behaviour of the structure for different wind speeds. The results at a model scale, therefore, are directly translated to those at the full scale. Table 1 provides a summary of all test comparisons with descriptions.

4 Results and Discussions

Figure 6a displays the alongwind mean result comparisons, and it can be seen that in general, with increasing V_r, the mean deflection measured at the apex increases. In observation to the numerical methods, 1wFSI and 2wFSI, they show comparable results with the experimental outcome where some minor over-predictions are made at higher V_r values. Both theoretical curves (TH) also follow the same trend of increasing in deflection magnitude with V_r. However, it can be observed for $C_d = 1.3$, the deflection is largely over-predicted. For the theoretical curve with $C_d = 0.62$, the mean deflection quantities are comparable to the experimental and numerical model cases. The cause for this over-prediction is the use of a $C_d = 1.3$ which is what the AS/NZS1170.2:2011[3] code recommends to use for circular structures. With the structure's actual $C_d = 0.62$ known, it can be seen that the analytical model can provide closer predictions.

For the maximum and standard deviation alongwind plots (Fig. 6b, c), it can be seen that the 1wFSI is able to predict better results at all V_r values in comparison to 2wFSI. The 1wFSI technique is also able to capture subtle variations of peak values as that observed in the standard deviation plot at $V_r \cong 0.89$. This peak observed for

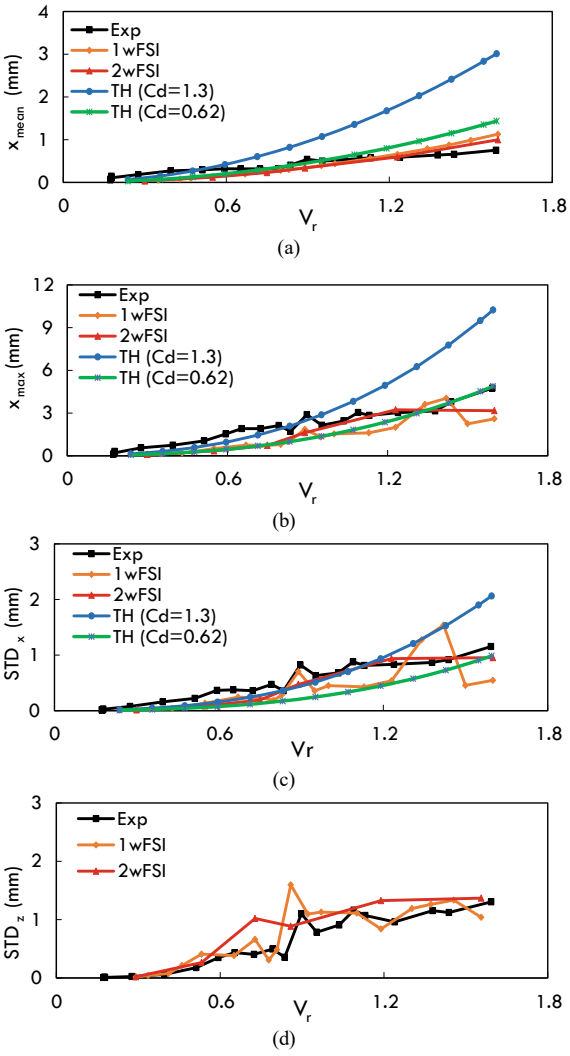

Fig. 6 Displacement for **a** alongwind mean, **b** alongwind maximum, **c** alongwind standard deviation and **d** crosswind standard deviation

experimental and 1wFSI was identified as a vibration induced from the crosswind direction to the alongwind direction, indicating strong aerodynamic coupling. This feature was not captured in 2wFSI albeit being a superior modelling technique in theory. For the theoretical curves, it can be seen that, once again for TH ($C_d = 0.62$) provides closer predictions in comparison to the case where TH ($C_d = 1.30$) for reasons previously explained. These plots were obtained by multiplying the mean curve by a GLF factor calculated and thus would follow a similar curve to that which is observed in the mean deflection plot. Hence, subtle variations such as that recorded in the experimental and numerical (1wFSI) are not observed in these theoretical plots.

Table 1 Test descriptions used for this study

Test	Description
Exp.	Experimental wind tunnel test on a MDOF aeroelastic model
1wFSI	The novel method implemented where an uncoupled one-way FSI technique is utilised via the new pressure mapping technique
2wFSI	Two-way FSI technique used from ANSYS commercial code
TH ($C_d = 1.3$)	The analytical model with a drag coefficient of $C_d = 1.3$ used. The value **1.3** is derived from the AS/NZS 1170.2:2011
TH ($C_d = 0.62$)	The analytical model with a drag coefficient of $C_d = 0.62$ used. The value **0.62** is obtained from the wind tunnel test and also confirmed by the numerical CFD test

In the crosswind direction, it can be seen that 1wFSI is better suited at predictions. Features such as resonant vibration are accurately captured for the 1wFSI at $V_r \cong 0.89$. In comparison, the 2wFSI model shows resonance to occur at a lower V_r and in other regions to deviate from the experimental outcome. The inability for the 2wFSI method to not be able to capture this resonant vibration can be detrimental in design as vortex induce resonance (VIR) can be critical in the design of wind-sensitive super-tall structures. The theoretical models on the other hand cannot be used to predict crosswind response as the mechanism for this is complex and cannot be analytically derived, especially when response occurs due to the phenomenon of vortex shedding.

Overall, it can be said that the 1wI is superior to the 2wFSI simulation. The reason for this is the ability for the 1wFSI to use higher resolution meshes in comparison to the 2wFSI. The computational demand of 2wFSI means that a sacrifice of mesh quality was necessary in order to obtain results within a reasonable time frame. In comparison, the 1wFSI method utilised a high-quality polyhedral mesh where 1.7 million elements were used. For the 2wFSI simulation, a 1.6 million elements mesh was used but as shown in [8] a Hex-Tet mesh had to be opted for two-way FSI to be compatible in ANSYS. As shown in [8], this Hex-Tet mesh is insufficient to predict accurate pressure quantities but had to be selected as computational demand for two-way FSI is much higher. The 1wFSI simulation only took a total of 74 clock hours to run the CFD and structural response simulation for eighteen V_r Values, and in comparison, the 2SI took 4800 clock hours for six V_r values. This shows that for practical applications, the 2wFSI is not feasible to be used for design purposes. Instead, the developed and presented 1wFSI technique by the authors is far more superior and can be used for practical design purposes.

5 Conclusions

This paper presents a numerical framework for an uncoupled one-way FSI method to predict responses of wind-sensitive structures. It was shown that in comparison

to existing commercial codes, the method presented in the paper is to be superior in terms of predictions and computational time. Thus, the adopted method is highly feasible and can be used for the design of wind-sensitive structures of any complex shape and geometry.

References

1. Braun AL, Awruch AM (2009) Aerodynamic and aeroelastic analyses on the CAARC standard tall building model using numerical simulation. Comput Struct 87:564–581
2. Mohotti D, Wijesooriya K, Dias-Da-costa D (2019) Comparison of Reynolds averaging Navier-Stokes (RANS) turbulent models in predicting wind pressure on tall buildings. J Build Eng 21:1–17
3. Standards Australia/New Zealand (2011) Structural design actions, part 2: wind actions, AS/NZS 1170.2:2011(R2016)
4. Wijesooriya K (2021) An uncoupled fluid-structure interaction numerical framework to estimate wind induced loads on super-tall structures. Doctor of Philosophy, The University of Sydney
5. Wijesooriya K, Mohotti D (2017) A validated numerical approach in wind design of super tall buildings. In: 8th international conference on structural engineering and construction management. Sri Lanka
6. Wijesooriya K, Mohotti D (2018) Predicting wind-induced pressure on slender tall structures using steady and unsteady RANS CFD analysis. In: 19th Australasian wind engineering society workshop. AWES (Australasian Wind Engineering Society), Australia
7. Wijesooriya K, Mohotti D, Amin A, Chauhan K (2020) An uncoupled fluid structure interaction method in the assessment of structural responses of tall buildings. Structures 25:448–462
8. Wijesooriya K, Mohotti D, Amin A, Chauhan K (2021) Comparison between an uncoupled one-way and two-way fluid structure interaction simulation on a super-tall slender structure. Eng Struct 229:111636
9. Wijesooriya K, Mohotti D, Amin A, Chauhan K (2021) Wind loads on a super-tall slender structure: a validation of an uncoupled fluid-structure interaction (FSI) analysis. J Build Eng 35:102028
10. Wijesooriya K, Mohotti D, Chauhan K, Dias-Da-costa D (2019) Numerical investigation of scale resolved turbulence models (LES, ELES and DDES) in the assessment of wind effects on supertall structures. J Build Eng 25:100842
11. Xing F, Mohotti D, Chauhan K (2018) Experimental and numerical study on mean pressure distributions around an isolated gable roof building with and without openings. Build Environ 132:30–44
12. Xing F, Mohotti D, Chauhan K (2018) Study on localised wind pressure development in gable roof buildings having different roof pitches with experiments, RANS and LES simulation models. Build Environ 143:240–257
13. Zhang Y, Habashi WG, Khurram RA (2015) Predicting wind-induced vibrations of high-rise buildings using unsteady CFD and modal analysis. J Wind Eng Ind Aerodyn 136:165–179

Challenges in Transport Logistics for Modular Construction: A Case Study

P. A. N. Peiris, F. K. P. Hui, T. Ngo, C. Duffield, and M. G. Garcia

Abstract Construction logistics is one of the essential functions in the modular construction industry due to the high demand for on-time delivery of components. For modular component suppliers, there is minimal flexibility in delivery times as generally, the installation times of modular components are critical to the contractor's construction programme. There are several studies conducted in recent years that articulate novel methodologies in construction logistics scheduling; however, the industry still faces challenges in streamlining the whole supply chain to better cater to potential uncertainties that impact construction logistics. This paper looks at a case study on a modular component supplier in Melbourne, with regarding to the challenges faced and how they have effectively overcome these challenges and provides a framework to mitigate construction logistics related discrepancies in the supply chain. The resilience of these methods in facing unforeseen events such as COVID-19 will also be discussed. The overarching objectives of this paper are to include: (1) bibliographic mapping of related publications; (2) identification of current methods, problems and technologies used in modular construction logistics; and (3) propose best practice guidelines that can be implemented to effectively cater to such uncertainties in construction logistics to minimise the impact on the supply chain. Further, incorporating lean principles for planning construction logistics and transport for the modular construction industry is also in discussion. Finally, the potential future research directions are highlighted to guide the researchers to pursue areas of much importance.

Keywords Modular construction · Logistics planning · Lean principles · Project planning · Transport logistics scheduling

P. A. N. Peiris · F. K. P. Hui (✉) · T. Ngo · C. Duffield · M. G. Garcia
Department of Infrastructure Engineering, The University of Melbourne, Melbourne, VIC, Australia
e-mail: kin.hui@unimelb.edu.au

R. Dissanayake et al. (eds.), *12th International Conference on Structural Engineering and Construction Management*, Lecture Notes in Civil Engineering 266,
https://doi.org/10.1007/978-981-19-2886-4_35

1 Introduction

The timely completion of any construction project depends on reliable materials and parts to the construction site. The coordination between material suppliers and contractors is an important one as it heavily influences the supply and operational decisions [13] such as the decision to construct on-site or to construct modules off-site and move them to site for assembly later. The latter also known as off-site manufacturing, and has the potential to shorten construction time, enhance quality consistency and ease labour shortage problems [4]. Construction sites are usually cramped and offer limited storage space, as illustrated in a case study in Hong Kong by [3]. To avoid bottlenecks due to uncertain site and weather conditions, certain types of construction work have increasingly shifted to off-site production where building components and modules can be made in factories [3, 4]. However, there remains a few constraints that hinder these much-regarded advantages. As brought forward by [7], increased transportation and logistics considerations are within the top five significant constraints the construction industry faces [7].

It is estimated that 10–30% cost savings can be achieved by implementing efficient logistics management practices [13]. Despite the potential savings, appropriate transportation or logistics of the prefabricated components from the off-site plant to the construction site can be a challenge and is crucial to the performance of the prefabricated component supply chain (PCSC) [15]. Logistics planning becomes even more critical in modular construction projects when the site is in the urban area. Due to frequent traffic congestion and crowded environment, the bulkiness and delicacy of modules create additional problems in shipment and site inventory, which in turn can seriously affect the progress of the assembly process [5].

Our paper serves to illustrate the problems faced by modular construction companies in off-site manufacturing of building components and to offer some potential solutions and best practices given the uncertain situation and constraints around disruptions caused by the COVID-19 pandemic. Examples of how construction logistics were managed overseas in similar case studies will be studied and potential improvements the industry can absorb will be discussed.

2 Literature Review

A literature review with bibliographic mapping has been conducted to understand the extent of research undertaken in this space of construction logistics, and it is evident that careful planning construction logistics is essential to the effectiveness of the whole supply chain. From the bibliographic maps created for Scopus and Web of Science, shown in Figs. 1 and 2, construction logistics is tied with costs, economic and social effects, supply chains and the management of overall work processes itself. The bibliographic maps also showed that more recent research articles tend to focus on the topics of supply chain management, system, management and prefabrication.

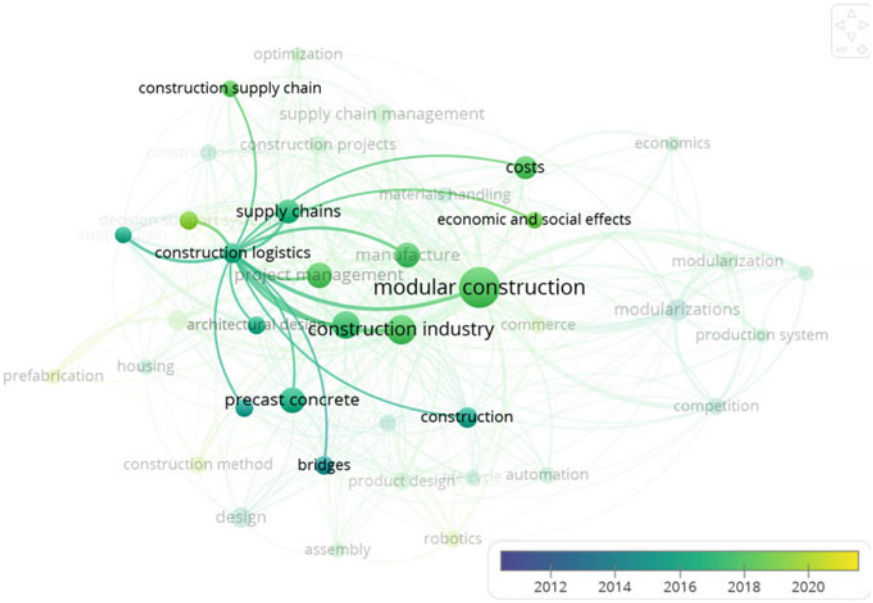

Fig. 1 Bibliographic mapping of Scopus results from VOSviewer

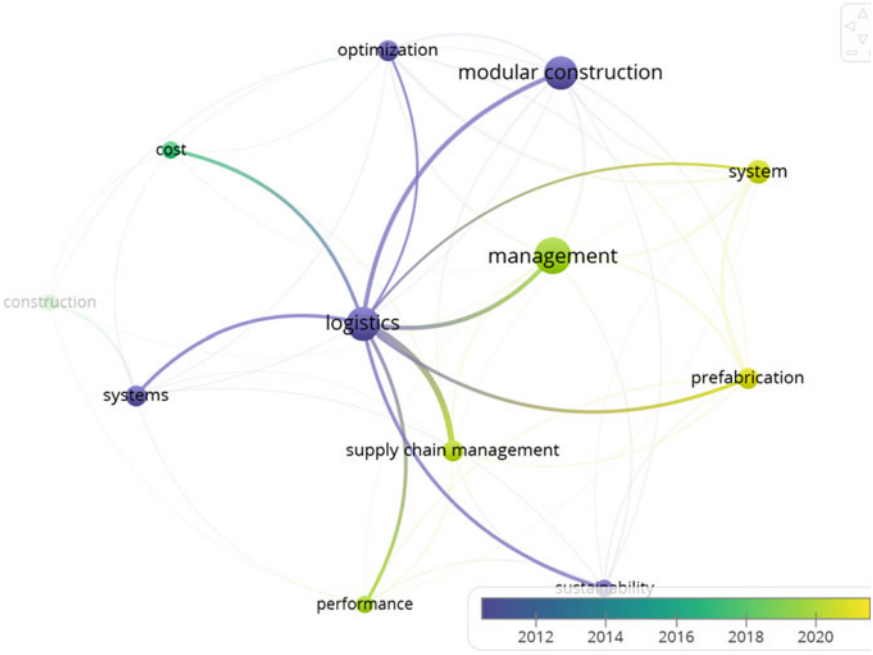

Fig. 2 Bibliographic mapping of Web of Science results from VOSviewer

Source	Search phrase	2011–2021
Scopus	(TITLE-ABS-KEY (construction AND logistics) AND TITLE-ABS-KEY (modular OR precast OR prefab)) AND PUBYEAR > 2010	155
Web of science (WoS)	TOPIC: (construction logistics) AND TOPIC: (modular OR precast OR prefab) timespan: 2011–2021	68

2.1 The Current State of Construction Logistics

The review of recent research articles revealed some of the key challenges in construction logistics and the potential for improvement. In a research on modular construction, [1] examined the effects of 50 key risk factors and found that the most critical factors affecting both cost and schedule of modular projects are (1) shortage of skilled and experienced labourers, (2) late design changes, (3) poor site attributes and logistics, (4) unsuitability of design for modularisation, (5) contractual risks and disputes, (6) lack of adequate collaboration and coordination, (7) challenges related to tolerances and interfaces, and (8) poor construction activity sequencing [1]. Logistics plays an important role in the prefabricated/modular construction industry and depends solely on better sequencing and scheduling the delivery of components considering a vast number of variables like on-site operations, availability of labour, equipment and machinery, inventory holding capabilities, etc. For urban developments, impact of the construction logistics to day-to-day operations in the city should also be considered [8]. Further, the current COVID-19 pandemic has also caused major disruptions to industries worldwide, and the construction industry was hard hit. The critical challenges such as cross-border logistics tracking and intensive module installation monitoring were critical [16]. This illustrate the possibility for construction logistics to be faced with unforeseen events internally or externally and therefore, affecting the modular construction companies and their processes.

The literature searches also revealed that researchers have more questions that need to be answered when implementing new technologies. First, more uncertainties on the PCSC such as component supply delay, inadequate supply, transportation disruption need to be taken into account in addition to supplier change, transportation route and means adjustment, delivery delay and storage requirement change that have been considered [15]. It is noted that additional environmental emissions will increase with the increase of delivery batches. This conflicts with the generated economic performance, since precast construction schedules need to be both responsive to on-site assembly and feasible for transportation—conflict in the construction logistics [9], Venås [14]. Liu et al. [11] found that the concept of transportation time in conventional planning needs careful consideration and showed using modelling that the transportation time on-site is calculated considering the linear distance from the storage position to the tower crane position instead of the specific storage position

to the installation position, is not accurate enough, and the installation time of a component is needed [11].

Therefore, construction efficiency was found to have been significantly improved by implementing smart technologies such as IoT enabled real-time logistics monitoring of module transportation in recent case study of constructing a modular quarantine camp and the Leishenshan hospital in China [2, 16]. However, for majority of the construction companies worldwide, investing in such innovations may not pay-off the scalability of the projects that they undertake. Therefore, a progressive approach to improve the production work flow to minimise the impacts of such changes need to be looked at.

2.2 Use of Lean Principles

The use of lean techniques in improving manufacturing efficiency is quite well-known and successfully applied in the generic manufacturing sector, however, has been slow to be taken up by the construction sector [6]. The Just-in-time (JIT) philosophy is one of the most regarded lean management techniques that can potentially contribute to elimination of wastes caused by overproduction, waiting, transportation, stocks and producing defective products [12]. By incorporating JIT philosophy into the proposed batch delivery scheduling strategy, [9] showed that significantly improved sustainable performance can be obtained, which generates positive effects for both the suppliers and contractors [9]. In addition, Leifgen and Kijajewski [10] proposed a construction logistics model that can schedule deliveries and storage areas as well as logistics related information using lean construction principles. The underlying factor is to have better coordination among all the domain-specific stakeholders [10].

3 Overview of the Case Study

3.1 Background of Case Study

This case study is based on a bathroom pod manufacturer in Melbourne, Australia. Bathroom pod manufacturing process involves several stages until when the pod is ready to be transported as a completed module that is ready to be fitted on-site. Pod construction stages can be identified in ten distinct stages that are; (i) steel frame preparation (base and walls), (ii) pod base preparation, (iii) wall frame installation and cladding, (iv) floor/wall finishes, (v) ceiling preparation and installation, (vi) door, fittings and joinery installation, (vii) plumbing fit-off and pressure test, (viii) finishing works, (ix) Final QA/QC and (x) wrapping and loading. Each of these stages consist of sub-tasks that define the completion of each task. Any change to

the scheduled logistics would impact each of these stages and affect the continuous flow of the tasks being carried out at each and every work station.

3.2 Outbound Logistics Scheduling and Logistics Arrangements

Once the bathroom pods successfully pass the final inspection, they were deep cleaned, wrapped and temporarily stored in the finished goods holding area, which has a limited capacity for bathroom pods. Simultaneously, the company liaise with the client with regarding to the pod quantities and types to be delivered to site, as sometimes one batch of delivery is carried out over a period of days to allow clear planning on-site and cater to any inventory holding limitations. The same information is then passed on to a trusted logistics partner, and the trucks are scheduled as per the agreed plan. Then, the pods are carefully loaded in to the trucks using forklifts and checked for any lose parts before the pods leave the factory (Fig. 3).

3.3 Challenges Faced

The scheduled deliveries are sometimes subjected to last minute changes due to site requirements. The changes might include any of the following: (1) Change in the quantities of modules of each delivery. This might be due to the need to slow down or keep up with the pace of work on-site. (2) Change in the combination of different modules to be delivered (for example: 1 × Type 1 module + 2 × Type 2 module to 2 × Type 1 + 1 × Type 2 module). Again, this might be due to actual on-site requirements. (3) Change of delivery dates. This can mean delays from days up to weeks and potentially cause the factory finished goods inventory to increase.

Apart from the need to keep with the pace of work on-site, there are also external factors on-site that can cause these changes including flooding on-site, asbestos found on-site, COVID-19 effects on labour and shortage of workers or materials. Figure 4 illustrates how the potential change requests result in two key decisions to the factory floor, i.e. the question of sufficient storage of materials, work-in-progress and finished goods if delivery is delayed and the question of resource availability if delivery is pulled forward.

Fig. 3 Bathroom pods ready to be transported to site

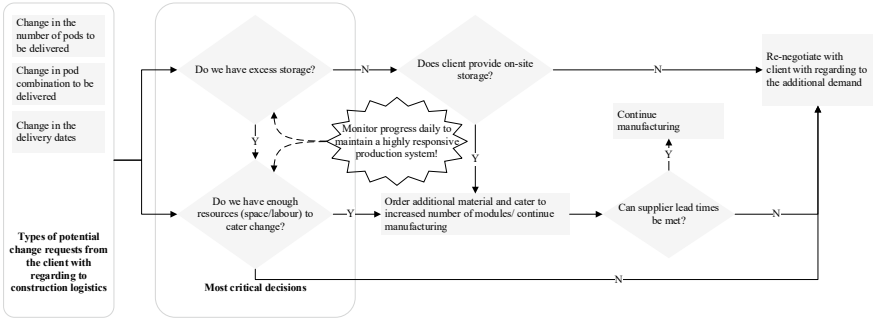

Fig. 4 Types of potential change requests and related decisions

3.4 Impacts to the Production Line

The changes in site requirements and scheduled deliveries have a serious flow on effect on the production line in the factory. The following are some of the impacts that are faced upstream at the factory:

(1) Lack of space for finished goods inventory (stock pile up at the end of the line).
(2) Due to the point above, the pods cannot be moved out from the production line, so that the whole production flow get stagnated.
(3) Due to stagnant production line, materials start to accumulate, procurement orders had to be rescheduled and a lot of time was spent coordinating with the suppliers. This can incur related cost for failing to keep to commitments and changes. (Pods being customised components, not all the material can be used to all the projects that are going on as there are custom components for each pod type and project).
(4) Cost increase for labour, as they can become under-utilised.

For some projects, even with the above impacts for the factory floor, they still need to keep up with the project to maintain a good relationship with the client. Therefore, measures need to be taken to minimise the impact to the production line minimising complications later in the project.

3.5 Best Practice Guidelines

To overcome the logistical challenges described above, the modular construction company was observed to rely on to resolve any issues with the builder or their own supplies mainly using the four key aspects below:

(1) **Contract**. Agree on a minimum time in advance for a modification time-fence, i.e. a last date of notification of change from the client. After that date, delivery will be completed as scheduled, and client will have to store the product on-site or the storage cost will be transferred to client. Before that date, delivery can be modified, and the modular manufacturer will have to take a decision whether to stop manufacturing and resume later or to continue with it, depending on other factors like up-coming projects, cost of stopping manufacturing and duration of that external impact.
(2) **Budget**. Always make an allowance or a special budget risk allocation for uncertainties. Risk management, knowledge of potential risks and a knowledge on pre-mitigation and post-mitigation project cost is important. Researching on competitor pricing and market trends can be useful to make sure, and you still quote a competitive price with the allocation for risks. In addition, agreements can be made on how the losses are going to be absorbed at an unforeseen event.

(3) **Schedule**. Allow some buffer during each delivery and some float during scheduling. This need to be planned based on internal capabilities and capacities. Factory floor need to have the capacity to increase the rate of manufacturing if required and be highly responsive to any such changes that can arise.
(4) **Space**. Planning is essential and contingency planning in case deliveries are rescheduled, e.g. planning for a maximum of number of pods in case a delivery is rescheduled following the terms agreed on the contract. Further, a space for storing the modular components need to be assigned if in case the pods could not be delivered to site as planned. These need to be carefully thought of and planned during the planning stage of the project.
(5) **Lean principles to reduce waste**. The company implemented a series of lean improvement activities such as building standard work into the work procedures which resulted in more consistent quality and less waiting time [12].

In addition to these, the company uses an in-house manufacturing, execution and control system (MECs) to continuously track the progress of the bathroom pods, so if in case of any emergency or uncertainty, the project team can identify and take necessary action to expedite or retard the working pace of the particular pods. Further, continuous tracking of manufacturing progress facilitates a responsive supply chain as the required decisions can be taken more effectively with required data and information.

4 Conclusion

This paper discussed the current problems the modular construction industry faces with regarding to outbound logistics, and some possible measures in dealing with them. However, these are at best "stop-gap" measures and are not the best root cause solutions. It is suggested that the best possible solutions for the modular component supplier lies in having a responsive production system that can respond effectively and swiftly to the trigger from an upstream process. This is a key JIT concept. Having an integrated production system would then allow the scheduler to have a more holistic view for demand planning. Future work and technologies that will help to cater these challenges are incorporating lean and design for manufacturing (DfMa) to the whole supply chain, dynamic scheduling and better collaboration in terms of inbound and outbound logistics.

Acknowledgements The first author would like to acknowledge The University of Melbourne for offering the Melbourne Research Scholarship. This study is sponsored by the Cooperative Research Centres Projects (CRC-P) and the authors would like to acknowledge the support given by Schiavello Group, for the implementations and providing the factory setting. This article was prepared as an industry paper, within the guidelines of the project stated above.

References

1. Abdul Nabi M, El-adaway IH (2021) Understanding the key risks affecting cost and schedule performance of modular construction projects. J Manage Eng 37(4):1–14
2. Chen L-K, Yuan R-P, Ji X-J, Lu X-Y, Xiao J, Tao J-B, Kang X, Li X, He Z-H, Quan S, Jiang L-Z (2021) Modular composite building in urgent emergency engineering projects: a case study of accelerated design and construction of Wuhan Thunder god mountain/Leishenshan hospital to COVID-19 pandemic. Autom Constr 124
3. Fang Y, Ng ST (2019) Genetic algorithm for determining the construction logistics of precast components. Eng Constr Archit Manage 26(10):2289–2306
4. Gibb AGF, Isack F (2003) Re-engineering through pre-assembly: client expectations and drivers. Build Res Inf 31(2):146
5. Hsu PY, Aurisicchio M, Angeloudis P (2019) Optimal logistics planning for modular construction using multistage stochastic programming. City Logist Transp Res Proc 46:245–252
6. Hui KP, Akemi Yokota A, Aye L. Education & training for zero energy and lean manufacturing & construction of housing in Australia. Curtin University
7. Hwang B-G, Shan M, Looi K-Y (2018) Key constraints and mitigation strategies for prefabricated prefinished volumetric construction. J Clean Prod 183:183–193
8. Janné M, Fredriksson A (2021) Construction logistics in urban development projects—learning from, or repeating, past mistakes of city logistics? Int J Logist Manage
9. Kong L, Li H, Luo H, Ding L, Zhang X (2018) Sustainable performance of just-in-time (JIT) management in time-dependent batch delivery scheduling of precast construction. J Clean Prod 193:684–701
10. Leifgen C, Kujajewski S (2018) Integrated digital and model-based construction logistics management based on lean thinking approaches. In: 35th international symposium on automation and robotics in construction and international AEC/FM Hackathon: the future of building things, ISARC 2018, international association for automation and robotics in construction I.A.A.R.C
11. Liu D, Li X, Chen J, Jin R (2020) Real-time optimization of precast concrete component transportation and storage. Hindawi Adv Civ Eng 50(1):1–2
12. Peiris PAN, Hui FKP, Ngo T, Duffield C, Garcia MG (2021) A case study on early stage adoption of lean practices in prefabricated construction industry. ICSECM 2019, Springer, Singapore
13. Said H, El-Rayes K (2014) Automated multi-objective construction logistics optimization system. Autom Constr
14. Venås C, Flyen C, Fufa SM, Janné M, Fredriksson A, Brusselaers N, Mommens K, Macharis C (2020) No or low emissions from construction logistics—just a dream or future reality? World sustainable built environment—beyond 2020, WSBE 2020, IOP Publishing Ltd.
15. Zhang H, Yu L (2020) Dynamic transportation planning for prefabricated component supply chain. Eng Constr Archit Manage
16. Zhiqian Z, Wei P, Zhenjie Z (2021) Fighting Covid-19 through fast delivery of a modular quarantine camp with smart construction. Proc Inst Civ Engineers Civ Eng 174(2):89–96

Readiness of Sri Lankan Construction Industry Towards Implementing Last Planner System in Lean Construction

M. D. L. Priyadarshana, I. W. N. Bandaranayake, and A. K. K. Kulathunga

Abstract The construction industry, where main activities are planning, regulating, designing, constructing, and maintaining buildings and other structures, makes a significant contribution to national economies and employment. Therefore, improving the productivity of the industry would result in significant economic benefits, even though it has proven to be difficult, but the application of lean concepts has shown promising results. The last planner system (LPS), having origins in lean construction practices, is characterised by collaborative planning at the operational level. Other key features include constraint identification and continuous learning which lead to predictable workflows. The global construction industry has increasingly adopted LPS to achieve the cost and time objectives of projects while improving quality and safety. However, in the Sri Lankan construction industry, the application of lean principles is not widespread, an area the study sheds light upon. This study offers practitioners and researchers insights into the state and challenges in the implementation of LPS in Sri Lanka, including suggestions for overcoming those challenges. The study combines interviews, focus group discussions, and a questionnaire survey to show that only certain practices of lean construction have been implemented in the local industry. Even though the professionals in the field are interested in further adoption of lean construction and the LPS concepts, they lack the required knowledge and skills to fully implement it. Resistance to change in organisations and people is also identified as a challenge to this transformation.

Keywords Lean construction · Last planner system · Waste types in construction

M. D. L. Priyadarshana (✉) · I. W. N. Bandaranayake
Department of Engineering Management, Faculty of Engineering, University of Peradeniya, Peradeniya, Sri Lanka
e-mail: mdlakshanmec@gmail.com

A. K. K. Kulathunga
Department of Manufacturing and Industrial Engineering, University of Peradeniya, Peradeniya, Sri Lanka

R. Dissanayake et al. (eds.), *12th International Conference on Structural Engineering and Construction Management*, Lecture Notes in Civil Engineering 266,
https://doi.org/10.1007/978-981-19-2886-4_36

1 Construction Industry Problems

The construction industry is one of the major industries that significantly impact the gross domestic product (GDP) of an economy [21]. Even though it represents a significant financial contribution, studies show this industry is plagued with problems such as low productivity, below-par quality, time overruns, and poor safety, which hinder customer delivered value [22]. Also, the construction industry is found to have a poor health and safety record, producing the highest number of fatal injuries among main industry groups [4], health and safety executive [14]. Furthermore, it produces significant amounts of waste during and at the end of a facility's life. Since traditional construction is based on craft production methods, it is slow and expensive compared to mass and lean production methods used by manufacturing industries.

1.1 Lean Construction (LC)

In the construction industry, the general objective of lean is to make the construction process more efficient by removing waste and non-value generating activities [18]. LC does not replace the critical path method (CPM) or other tools that define the overall work schedule, but it complements them to improve the delivery of short-term assignments. Innovation through lean improvement in construction processes has provided sustainable outcomes in terms of reduced waste, effort, time, and increased productivity [20, 25]. According to [24], the lean approach identifies seven types of waste: overproduction, overstocking, excessive motion, waiting time, transportation, extra-processing, and defects. Lean construction tends to promote the design of products concurrently with the process, maximising firm or professional performance for clients by adopting control measures that ensure the cost and time overruns are minimised, and the desired performance quality is achieved in the life cycle of construction projects [1].

1.2 Last Planner System (LPS)

LPS is a production system that can help produce a predictable workflow. The last planner is the person or group accountable for the production unit at the operational level [5]. The LPS is a socio-technical production planning and control system that helps produce reliable workflow and rapid learning in the planning, design, construction, and commissioning of projects [10]. In lean practices, flow variability is a vital parameter because a delay in completing one work segment can directly affect the process and the progress of the downstream work segment. LPS uses these lean principles to provide improved project control over the flow variability. It identifies that the last planner as the best-positioned person who will adequately understand

the required resources to achieve the planned tasks within the time frame under the downstream work demand. This concept applies to situations with a collaboration between teams and other external parties in a project. LPS directs attention to the workflow, and hence, it improves the project value by reducing costs and time for project completion by enhancing the quality of work, the safety aspects, and productivity [9]. The LPS technique delegates decisions and allows the field crew in direct contact with the tasks to plan and schedule [5]. In a way, the last planners become bound and committed to the work assignments they have planned. Studies show that LPS implementation results in improving project delivery time, labour productivity, safety, and quality [3, 6–8, 11, 12, 13, 17]. The main components of LPS are phase planning, look-ahead planning, constraint analysis, weekly work plan (WWP), percentage plan complete (PPC), and reasons for non-completed task.

1.3 Applications in Lean Principles in Sri Lankan Construction Industry

Studies show that LPS has been used in many construction projects worldwide [2, 15, 16]. Thomassen et al. [23] experienced 65% fewer accidents and up to 70% less absence related to illnesses within a single company using the last planner-managed construction sites in a large Danish contracting firm. However, the use of lean principles is still at preliminary stages in Sri Lanka.

1.4 Objective

This study examines the degree of implementation of lean practices in construction projects and aims to identify the alignment/readiness of the construction industry to implement lean practices and LPS under the local context. Furthermore, the ability to identify certain fundamental lean concepts by the industry professionals is checked during the study.

2 Research Methodology

Both qualitative and quantitative approaches were used in this study to achieve the study objectives. During the initial stages, it was revealed that the respondents' awareness of lean and LPS terminology was limited. This limitation posed significant challenges to the direct measurement of readiness to implement LPS requiring indirect measurement methods. Since LPS implementation involves some of the key characteristics used in the traditional project management practices, the study was

steered towards the implementation challenges of construction projects, emphasising lean aspects and elements of LPS.

Sixteen interviews with construction industry professionals were conducted to obtain deep insights into the elements of lean construction and LPS that are practised in the industry. The interviews were also designed to surface the ability of those professionals to identify the wastes as defined in lean principles, identification of reasons for non-completed tasks, and the organisational, cultural, and other barriers to adopting lean practices. Two focus group discussions were also used to further investigate these aspects. Challenges were discussed under the pre-tender stage, project execution stage, and project orientation stage of the projects.

Subsequently, a questionnaire survey was used to quantify the degree of appreciation and implementation of elements of LPS and lean construction practices among the professionals in the industry. Whereas the interviews were confined to water sector projects, the questionnaire survey was extended to other construction projects as well.

3 Research Findings and Discussion

Results show that professionals tend to recognise idle time waste, process waste, and defects as the three most significant types of wastes. Key findings of LPS implementation show that pull planning, also known as backward planning, analysis of constraints, and investigation of reasons for non-completed tasks are practised to a certain extent in the industry. However, the involvement of last planners remains at a very low level driven by cultural and attitudinal barriers.

3.1 Identification of Construction Waste

Out of the seven types of wastes defined in lean principles, the "idle time waste" was found to be the most common type of waste in the industry which has roots in the project nature, procurement, and logistics. "Process waste" was the most significant waste type identified in the industry since construction projects have many processes to deliver the final product. Attempts to cut down health and safety protocols for short-term gain were found to end up in a large number of injuries and downtime which eventually resulted in massive process waste. Furthermore, the internal operations of private sector companies cause avoidable delays to the entire process, especially in terms of handling finances. A useful insight was provided by a respondent employed in the private sector that "below-par cost estimates for subcontracting" would result in waste as it invariably leads to unsatisfactory completion of proposed work. If the contract awardee proposes an under-par rate to maximise profits or minimise losses, the sub-contractor would be without choice and would proceed with the forced rates which could result in reworks or defective products. "Defects" were

identified as a common type of waste in construction projects. "Inventory waste" was not highlighted as a significant waste type. However, the underutilisation of assets is identified under this category. "Motion and conveyance" are not identified as major waste types, but the reasons for such wastes are elaborated such as improper storage of material, use of under-capacity machinery and tools. Since construction produces a unique product, "overproduction" waste type was not found to have much significance compared to other waste types.

3.2 Implementation of Key Features of LPS

Results show that professionals prefer CPM rather than pull planning in their initial planning. However, both methods are found in projects to a certain extent. In cases where project duration is fixed by the contract, CPM is used to identify the master programme and pull planning is used to generate milestone programmes and monthly programmes. In short-term planning phases such as weekly work plan (WWP), pull planning is used when the deadline of the end product/service is fixed. WWP used in most organisations is based on the period of the entire project. Progress-monitoring intervals are longer when the total duration of the project is above one year. Results show that most frequently project monitoring is done monthly.

Constraint analysis was given higher prominence by all the participants during the planning and execution of tasks since it reveals the most common reasons for non-completed tasks. Finding and analysing reasons for non-completed works were found to be prevalent in current project management systems.

The involvement of the last planners in the planning phase, a key feature of LPS, is minimal in the industry. Reasons include the organisational culture, low recognition given to the last planner, and the reluctance to get the participation of the last planner in the planning phase as organisations to perceive last planners to have low levels of motivation and lower capacity to deal with complexities of the planning phase. In the private sector, a reason for the low involvement of the last planner was given as their tendency to provide planning inputs for their own convenience rather than for achieving the project objectives.

Implementing LPS fully or partially requires substantial awareness building and training, signifying substantial upfront cost burden to an organisation. It was also revealed that the buy-in and the sponsorship of top management are vital to initiate such an innovative approach.

4 Conclusions

Investigation into the participants' ability to recognise the waste types in the construction industry revealed that they were most capable of identifying idle time waste, motion waste, and over-processing waste. Novel insights were elicited regarding the

provision of below-par cost estimates for contractors and sub-contractors leading to poor quality work, resulting in re-work which is a type of waste. Even though conveyance (transportation) waste and wastes due defects seem to be prevalent, over-producing was not recognised as a waste type as it does not play a significant role in construction [19]. Furthermore, design errors including over-design were identified as construction process wastes that are particularly concerning to the construction industry.

Current project management practices such as CPM has certain similarities with the LPS and LC, such as pull planning, WWP, constraint analysis, and examination of reasons for non-completed tasks. Most respondents showed a keen interest in further implementing parts of LPS methodology. However, the involvement of the last planners in WWP, which is a cornerstone of LPS, seems to be the least implemented feature according to the findings. The importance of the last planner involvement and the end-user involvement to the initial planning stage was highlighted by many respondents. However, one of the main obstructions for the last planner involvement is the rigid and inflexible "attitudinal culture" of the organisation.

Successful execution of LPS depends on the participatory approach of the individuals involved in construction, which seems to be lacking in practice. Providing awareness via training to overcome barriers and performing "situational analysis" is recommended to overcome such barriers. Also, it is recommended to build awareness of lean practices during tertiary education. Further explorations through case studies and quantitative studies can help to obtain a broader view of LPS implementation barriers.

Acknowledgements The support extended by the staff of the Post Graduate Programme in Construction Management, the Department of Engineering Management, and the Department of Manufacturing and Industrial Engineering of the Faculty of Engineering of the University of Peradeniya is greatly appreciated.

References

1. Akanbi OA, Oyedolapo O, Steven GJ (2019) Lean principles in construction, sustainable construction technologies. Elsevier Inc.https://doi.org/10.1016/b978-0-12-811749-1.00010-9
2. Alarcon LF, Diethelmand S, Rojo S (2002) Collaborative implementation of lean planning systems in Chilean construction companies. In: 10th annual conference for the international group for lean construction. International Group for Lean Construction, Gramado, Brazil, pp 1–11
3. Alsehaimi A, Tzortzopoulos P, Kosela L (2009) Last planner system: experiences from pilot implementation in the middle east. In: 17th annual conference of the international group for lean construction. International Group for Lean Construction, Taipei, Taiwan, pp 53–66
4. Ashworth A (2010) Cost studies of buildings, 5th edn. Pearson Education Limited, England, UK
5. Ballard G (2000) The last planner system of production control. Ph.D. Diss., Faculty of Engineering, University of Birmingham, U.K.
6. Ballard G, Liu M, Kim YW, Jang JW (2007) Roadmap to lean implementation at the project level. Construction Industry Institute (CII), Austin, TX

7. Ballard G, Hammond J, Nickerson R (2009) Production control principles. In: Proceedings of 17th annual conference of the international. group for lean construction (IGLC-17). International Group of Lean Construction, Taipei, Taiwan
8. Court PF, Pasquire C, Gibb A (2009) A lean and agile construction system as a set of countermeasures to improve health, safety, and productivity in mechanical and electrical construction. Lean Constr J:61–76
9. Ebbs P, Pasquire C (2019) a facilitators' guide to the last planner® system: a repository of facilitation tips for practitioners, Nottingham Trent University
10. Erazo-Rondinel AA, Vila-Comun A, Diaz A (2020) Application of the last planner® system in a sports infrastructure project in Peru. In: Tommelein ID, Daniel E (eds) Proc. 28th annual conference of the international group for lean construction (IGLC28), Berkeley, California, USA. https://doi.org/10.24928/2020/0091 (online at iglc.net)
11. Formoso CT, Moura CB (2009) Evaluation of the impacts of the last planner system on the performance of construction projects. In: Proceedings of 17th annual conference of the int. group for lean construction (IGLC-17). International Group of Lean Construction, Taipei, Taiwan
12. Friblick F, Olsson V, Reslow J (2009) Prospects for implementing last planner in the construction industry. In: Proceedings of 17th annual conference of the international group for lean construction (IGLC-17). International Group of Lean Construction, Taipei, Taiwan
13. Garza JM, Leong MW (2000) Last planner technique: a case study. In: Proceedings of construction congress VI: building together for a better tomorrow in an increasingly complex world. American Society of Civil Engineers, Orlando, FL
14. Health and Safety Executive (HSE) (2013) Construction industry. Available at http://www.hse.gov.uk/statistics/industry/construction/
15. Itri Conte A (2002) Lean construction: from theory to practice. Proceedings IGLC-10, Gramado, p 9
16. Johansen E, Porter G, Greenwood D (2004) Implementing change: UK culture and system change. In: Proceedings of 12th annual conference of the international group for lean construction (IGLC-12). International Group of Lean Construction, Copenhagen, Denmark
17. Khanzode A, Fischer M, Reed D (2008) Benefits and lessons learned of implementing building virtual design and construction (VDC) technologies for coordination of mechanical, electrical, and plumbing (MEP) systems on a large healthcare project. ITcon 13:324–342
18. Koskela L (2000) An exploration towards a production philosophy to construction. Ph.D. Diss., VTT Building Technology, Tampere, Finland
19. Koskela L, Bølviken T, Rooke J (2013) Which are the wastes of construction. In: 21st annual conference of the international group for lean construction, 31st July–2nd August 2013, Fortazela, Brazil
20. Ogunbiyi O (2014) Implementation of the lean approach in sustainable construction: a conceptual framework. Grenfell-Baines School of Architecture, Construction and Environment. University of Central Lancashire, Lancashire, UK
21. Rahman AH, Wang C, Lim IYW (2012) Waste processing framework for non-value-adding activities using lean construction. J Front Constr 1:8–13
22. Senaratne S, Wijesiri D (2008) Lean construction as a strategic option: testing its suitability and acceptability in Sri Lanka. Lean Constr J:34–48
23. Thomassen MA, Sander D, Barnes KA, Nielsen A (2003) Experience and results from implementing lean construction in a large Danish contracting firm. In: Proceedings of 11th annual conference on lean construction, July 22–24, Blacksburg
24. Womack J, Jones D (2003) Lean thinking: banishing waste and create wealth in your corporation. Free Press, New York
25. Wu P, Wang X (2016) A critical review of the factors affecting the success of using lean to achieve green benefits. In: 24th annual conference of the international group for lean construction, Boston, USA, July 20–22, 2016

Life Cycle Assessment for Modular-Constructed Buildings: A Proposed Methodological Framework

J. Jayawardana, A. K. Kulatunga, M. Sandanayake, G. Zhang, and J. A. S. C. Jayasinghe

Abstract Modular construction (MC) is one of the vital members of the off-site construction (OSC) family and identifies as an innovative modern method of construction (MMC). Over the last two decades, several research studies have highlighted the distinctive benefits of MC in contrast to conventional in-situ construction. Particularly in developed economies, a greater inclination towards adopting MC practices is visible. However, there is limited research investigating the environmental sustainability of MC, especially in developing countries such as Sri Lanka. Even the available literature, the majority only addresses limited phases of the life cycle of the buildings. Furthermore, selecting the system boundary and collecting reliable and comprehensive process data are some of the inherent difficulties in the environmental assessment processes, explaining the lack of research in this domain. Moreover, the lack of country-specific life cycle data is a significant barrier the developing regions face when conducting environmental performance research of MC. Notably, a systematic methodological framework for assessing the environmental sustainability of modular construction through a life cycle perspective still lacks in the relevant literature. Hence, this paper proposed a methodological framework through a life cycle perspective for assessing the environmental sustainability of MC projects by employing the so-called life cycle assessment (LCA) methodology. The application of the proposed framework will attempt to validate through a pilot case study. The proposed framework offers a systematic method for future studies on investigating the environmental performance of modular constructed facilities using an LCA approach.

J. Jayawardana (✉) · A. K. Kulatunga · J. A. S. C. Jayasinghe
Faculty of Engineering, University of Peradeniya, Peradeniya 20400, Sri Lanka
e-mail: s3884217@student.rmit.edu.au

J. Jayawardana · G. Zhang
School of Engineering, RMIT University, Melbourne, VIC 3001, Australia

M. Sandanayake
College of Engineering and Science, Victoria University, Melbourne, VIC 3011, Australia

R. Dissanayake et al. (eds.), *12th International Conference on Structural Engineering and Construction Management*, Lecture Notes in Civil Engineering 266,
https://doi.org/10.1007/978-981-19-2886-4_37

Keywords Environmental sustainability · Life cycle assessment (LCA) · Methodological framework · Modular construction (MC) · Off-site construction (OSC)

1 Introduction

Building construction is one of the industrial sectors that contributes largely to the adverse impacts caused on the global environment. It is identified that 40–50% of global CO_2 emissions and 30–40% of world energy consumption resulted from the building industry [1]. Growing pressure to adhere to environmental standards and sustainable development goals (SDGs) influences building construction shifting towards adopting emerging and innovative technologies in their construction. OSC is an innovative MMC that is increasingly recognised as a viable alternative for traditional in-situ construction of buildings. MC is one of the most efficient OSC methods that have the potential to provide benefits in the triple bottom line (environmental, economic, and social) of sustainability [2]. It is vital to evaluate the environmental performance of modular buildings over the life cycle, to clearly outline the potential environmental savings of MC compared to the conventional construction. LCA is a widely identified environmental assessment methodology that has been applied in investigating the environmental impacts of buildings across all life cycle phases [3].

Developed economies have conducted considerable research in benchmarking the environmental performance of modular construction, whereas developing countries lag behind them significantly. Lack of process data and support from the government are some of the major barriers developing economies face in conducting environmental assessments. Developing countries such as Sri Lanka need to conduct systematic LCAs on MMC, such as modular construction, to increase the uptake rate and compare the environmental performance of these construction technologies. However, a systematic methodological framework for assessing the environmental sustainability of modular construction through a life cycle perspective still lacks in the relevant literature. Therefore, this study has identified the necessity for a decision-based methodological framework for environmental assessment studies related to MC. Thus, this study aims to propose an LCA decision-based methodological framework for investigating the environmental sustainability of modular building projects.

2 Life Cycle Approach in Environmental Sustainability Evaluation

2.1 Life Cycle Assessment

The life cycle assessment is a valuable tool that evaluates the environmental performance throughout the sequence of activities carried out in manufacturing a product or performing a service. Resources extraction and consumption (including energy), variety of emissions to air, water, and soil are quantified throughout the life cycle stages of the product or service. Subsequently, their potential contribution to environmental impact categories is assessed [4]. In the ISO 14040 series, two main ISO standards support the execution of an LCA, namely ISO 14040:2006 and ISO 14044:2006. ISO 14040:2006 describes the four main stages of LCA as follows.

2.1.1 Goal and Scope Definition

Defining the goal, intended application, reasons for carrying out the study, the intended audience should be clearly defined. Scope states what is included in the study and the key parameters of the study. The scope should include the product system, elementary flow, unit processes, system boundary, functional unit, data quality requirements, type and format of the report, and assumptions.

2.1.2 Life Cycle Inventory Analysis Phase (LCI Phase)

Collection and quantification of the input and output data of a product system relative to the defined scope of this study. Three LCA methods are generally used in compiling an LCI, namely process-based LCA, input–output (I-O)-based LCA, and hybrid-based LCA. Process-based LCA uses specific data of a process, product in a chosen project/factory location. Thus, this method can produce more accurate and product-specific results, which explains why process LCA was the frequently used method by LCA practitioners. However, the demand for a large amount of data to cover all life cycle phases is challenging considering the high labour and time-intensive requirements [5]. Nonetheless, it is commonly accepted that if data availability, quality, and accuracy are adequate, process LCA is still the most accurate method for environmental assessment [6].

I-O LCA method uses sectoral financial transactions describing complex inter-industry relationships within a national economy [7]. I-O analysis successfully addresses typical issues such as system boundary incompleteness and data reliability. However, this method still has its own limitations, such as aggregation level decides the accuracy and is not suitable if the purpose is to conduct a detailed LCA study targeting industry-specific products [8]. Thus, this method is more appealing for national, sector-level general LCAs. Hybrid LCA methods have been developed

to attempt to combine the merits of process and I-O LCA. Process-based hybrid LCA only uses I-O data for the elements of the model upstream to the process data. Whereas in I/O-based hybrid LCA, the I/O model targets upstream, downstream processes, and also horizontal truncation [9]. In simple terms, the I-O hybrid method uses available process data firstly, and I-O model data will fill all the remaining gaps.

Life cycle impact assessment phase (LCIA) aimed to evaluate the significance of potential environmental impacts based on the LCI flow results. The fourth phase namely "Interpretation" is a systematic technique to identify, quantify, check, and evaluate information from the results of the LCI and the LCIA.

2.2 Modular Construction

OSC is an industrialized construction technology that manufactures complete or semi-completed prefabricated building components in an off-site manufacturing facility, subsequently transports, erects, and assembles these components on the final construction site [10, 11]. Based on the level of prefabrication, OSC methods can be categorised into five classes as: component level (1D single element), 2D panelised system, 3D volumetric system, hybrid system, and unitized whole buildings [12]. Panelised and volumetric construction, interchangeably called modular construction. And it is the most efficient technology of OSC in building construction [13]. Modular construction offers a range of benefits from reduced construction times [14] and costs [15] to improved productivity [16] and environmental savings such as reduced carbon emissions [8].

2.3 LCA of Modular Construction

LCA methodology has been applied in the construction industry for more than twenty years. One significant feature of LCA in the construction sector is the possibility of carrying out a systematic and comprehensive environmental assessment to evaluate and optimize the construction processes [17]. Table 1 presents a set of significant environmental assessment studies of modular buildings using LCA methodology. This summary table has listed some key aspects such as country/region of study, LCA type adopted, scope assessed of the selected research studies. The process-based LCA was the most often used method to assess the environmental sustainability of MC.

The building life cycle has several main process stages: raw material production, construction, operation, and end of life. In the case of MC, the construction phase can be separated into off-site and on-site construction. The past literature has given enough evidence that the operation phase of a building has the highest environmental impacts, especially in terms of carbon emissions and energy consumption [2, 5, 8]. Nevertheless, these impacts stretched over the long-life span of a building. Thus, in

Table 1 LCA studies of modular buildings

Research study	Country/region	LCA type	Scope	Modular building application	Software/method	Database
[18]	UK	Process-based LCA	Cradle-to-site	Two-storey residential buildings	SimaPro	U.S. life cycle inventory
[5]	Australia	I/O-based hybrid LCA	Whole life cycle	Multi-storey residential buildings	TRNSYS	SimaPro Australian database
[19]	Italy	Process-based LCA	Cradle-to-cradle	Single-storey building	EnergyPlus	Meteonorm
[20]	Canada	Process-based LCA	Cradle-to-gate	Single-family residential buildings	Athena impact estimator for buildings	Athena LCI database
[21]	Hong Kong	Process-based LCA	Cradle-to-grave	30-storey public residential building	Based on PAS 2050	SimaPro
[3]	Australia	Process-based LCA	Cradle-to-cradle	Prototyped two-storey building	SimaPro	Ecoinvent
[22]	China	Process-based LCA	Cradle-to-cradle	Single-level residential buildings	SimaPro	Ecoinvent
[23]	Malaysia	Process-based LCA	Cradle-to-grave	Single-family residential building	SimaPro	Malaysia life cycle inventory database

respective to impact reduction potential per unit time, the possibility of improving the process in the construction phase and in the raw material production stage is higher than the operation phase [8]. These considerations validate the importance of evaluating the environmental impacts of the construction phase of modular buildings.

When considering the LCA studies carried out in evaluating the environmental sustainability of MC in the two major economy categories in the world, it has been seen that major focus was given to the carbon emissions and energy analysis in terms of investigated performance indicators. Under the carbon emissions category, embodied carbon emissions, CO_2 emissions, and GHG emissions were the most explored indicators of the buildings. Furthermore, in the energy analysis cluster, embodied energy and operational energy received the prominent focus. Acidification potential and eutrophication potential were also assessed notably in the environmental sustainability of MC literature. Moreover, SimaPro is the most used software in the LCA modelling process.

Literature survey revealed that developed economies had conducted considerable research in benchmarking the environmental performance of modular construction with traditional construction practices over the last two decades. Comparatively, developing countries lag behind in terms of the adoption of MC and investigating the environmental impacts of MC. However, emerging industrial economies such as China and Malaysia have conducted systematic LCAs of the environmental sustainability of MC. Conversely, other developing countries such as Sri Lanka, India, and Iran did not conduct published LCA studies to evaluate the environmental performance of MC. Lack of country-specific life cycle data and lack of support from the government in creating policies, regulations, and incentives are some of the major barriers these economies face. Furthermore, defining the scope and system boundary and collecting reliable and comprehensive process data are some of the inherent difficulties in the LCA methodology explaining the lack of research in this domain, particularly in developing economies.

Notably, a decision-based methodological framework for assessing the environmental sustainability of modular construction using LCA methodology still lacks in the relevant literature. A current requirement is a methodological guide to choose the scope, LCA method, and data collection methods considering the critical factors affecting them aggregated in a single framework. Moreover, insights on interpretation strategies that can be adopted to derive more reliable and comprehensive results would greatly help LCA practitioners with less exposure to them. Hence, this paper proposed a decision-based methodological framework through a life cycle perspective for assessing the environmental sustainability of MC projects by employing the LCA methodology. The proposed framework offers a systematic method for future studies investigating the environmental performance of modular constructed facilities using an LCA approach.

3 Proposed Methodological Framework

The developed methodological framework shown in Fig. 1 is based on the ISO 14040:2006 LCA framework. An explanation for the four phases of LCA is given in Sect. 2. A literature review is carried out to identify and understand the different aspects of LCA methodology, focusing on aggregating these ideas and concepts in one decision-based methodological framework. Subsequently, the framework was developed incorporating the methodological steps, findings, learnings, and gaps derived from the literature review.

3.1 Phase 01: Goal and Scope

Firstly, the LCA practitioner has to identify the study purpose and objectives, and scope. Three main factors were identified that affect the scope elements and the selection of the LCA method (see Sect. 2), namely study purpose and objectives (Factor 1—F1), data availability (Factor 2—F2), and data requirements (Factor 3—F3). LCA focus can be identified under F1, where it can be mainly categorised as specific case study-based LCA and general LCA (national/sector level). Therefore, depending on the LCA focus, F2 and F3, the LCA method can be decided. If the focus is to conduct a general LCA to evaluate the environmental performance at a sector/national level, then I/O-based LCA method can be employed. This method does not require specific process/product data; aggregated level data is adequate. Else LCA focus is to carry out a process/product-specific environmental assessment, then LCA users can choose between process-based LCA and hybrid LCA depending on the data availability and data requirements (specificity and accuracy). If F2 is high and F3 high or low, process-based LCA is more suitable to derive demanded results. Else if both F2 and F3 are low, process-based hybrid LCA is adequate to facilitate the demanded completeness. Else F2 low but F3 high, then the practitioner can employ I/O-based hybrid LCA, the most comprehensive LCA method described in Sect. 2.

System boundary selection of the LCA is one of the crucial steps in this methodology. Decisions on the inclusion and exclusion of the processes affect the accuracy and the reliability of the final results. More importantly, in comparative LCA studies, it is vital to keep the system boundary consistency to effective comparison [7]. Ultimately, depending on the F1, F2, and F3, LCA users can select the system boundary of the study. Environmental impacts assessed in the LCA can be decided based on F1, F2, and F3. Building application solely depends on the F1. LCIA can be performed using LCA modelling software such as SimaPro, GaBi, Athena, and BEES, or manual quantitative models can be employed in place of software. The selection of the LCIA method also depends highly on F1 and other factors such as availability of software resources and competency of handling this software.

Identifying the unit of analysis (UoA) is crucial to plan the data collection process and to achieve effective and reliable comparisons. The decision on selecting the UoA

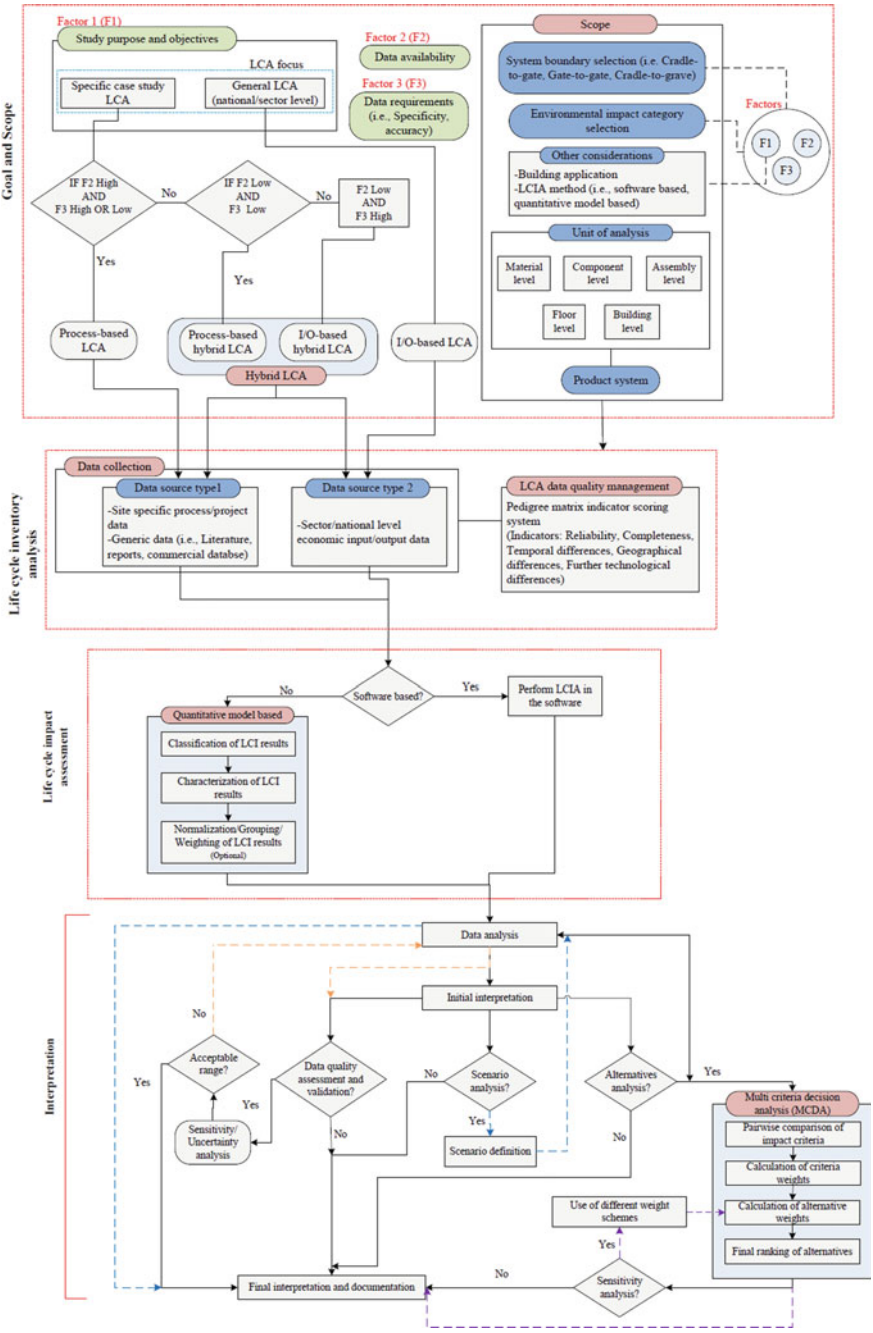

Fig. 1 Proposed LCA decision-based methodological framework

will depend on F1 and F2. MC LCA practitioners can select one or more UoAs (see Fig. 1) considering the F1 and F2. Moreover, defining the functional unit (FU) of the analysis is critical, considering that the whole data flow will depend on it. FU should be defined to relate all inputs and outputs with results. FU is imperative in comparative analyses of products. In building construction-related LCAs, typically, FU has defined as related to the floor area of the buildings (gross floor area and unit floor area). It is essential to differentiate the concept of UoA and FU when conducting MC-related LCAs.

3.2 Phase 02: Life Cycle Inventory (LCI) Analysis

Data collection is the most challenging and tedious activity of an LCA study. Depending on the LCA type, the data collection sources can be decided. For process-based LCA, data source type 1 can be employed. I/O-based LCA can be conducted only using data source type 2. However, for hybrid-based LCAs, these two types of data source types will be needed. Data reliability and transparency are imperative to validate and to keep the demanded quality of LCA studies. Pedigree matrix commonly used by ecoinvent databases can be used to manage the data quality.

3.3 Phase 03: Life Cycle Impact Assessment (LCIA)

As mentioned in the study scope, LCA practitioner can choose between software or manual quantitative-based method considering the relevant deciding factors. In the classification stage, inventory parameters are sorted and assigned to specific impact categories. Subsequently, category indicators (quantifiable representation of impact categories) can be defined. Then, using a selected characterization model, LCI flows are characterized into common equivalence units (i.e. $kgCO_2eq$). Moreover, depending on the study objectives, results can be normalized, grouped, and weighted.

3.4 Phase 04: Interpretation

The final stage of the proposed methodological framework is the interpretation of the findings. LCA user has different options in the interpretation stage after the initial interpretation of data. Data quality assessment and validation are imperative to check the data's reliability and accuracy. Additionally, this will consolidate the quality of the LCA study. Sensitivity analysis and uncertainty analysis are the common methods applied in this validation step. Sensitivity analysis examines the contributions of the inputs to the total uncertainty in the outputs of the model by only changing one

variable at a time [24]. Uncertainty analysis checks the uncertainty of the model outputs given a set of inputs, where each input has some uncertainty [25].

Scenario analysis defines a set of scenarios (hypothetical) that are possible or desired to achieve in future. In simple terms, scenario analysis assesses the effect of changing all the input variables simultaneously [26]. Thus, this kind of interpretation approach helps decision-makers in the MC industry to identify possible solutions to existing problems and plan for negative impacts in future. Alternative analysis focuses on comparing product alternatives based on the calculated environmental impacts. In the current context, this approach supports finding the best-performing construction method from a set of alternatives. LCA studies have shown an increasing trend to assess more than one environmental indicator in the last decade. Therefore, when LCA studies evaluate more than one impact and require a comparison with alternatives, weighting schemes can be applied to calculate the relative importance of the environmental indicators.

4 Research Methodology

The methodology section will be elaborated based on the proposed methodological framework.

4.1 Study Goal, Objectives, and Scope

The study's main purpose is to promote the MMC and sustainable construction methods in the Sri Lankan construction industry. The main objective is to evaluate the environmental performance (GHG emissions) of a conventional building and prefabricated building (hypothetical building) using the LCA methodology. Process-based LCA will be carried out considering the purpose of the study, data availability (medium), and data requirements (low).

The system boundary of the study is set as cradle-to-gate. The selected boundary covers material production, material transportation, and prefabricated component transportation, and construction (off-site/on-site) stages. The unit of analysis is the material level, and the functional unit is set as the construction floor area (CFA), which is 1749.36 m^2. The conventional building (CB) is located in Sri Lanka, and the prefabricated building (HPB) is a hypothetical building extrapolated using the prefabrication rates from the study [27] for the comparison. It was assumed that the two buildings comprised similar building characteristics and stakeholders (project management, suppliers, and contractors) when creating the hypothetical building.

Table 2 Material and resource consumption of CB and HPB

Building material	In CB (tonne)	In HPB (tonne)	
		Off-site	On-site
Concrete	1223.40	133.35	1080.63
Reinforcement steel	47.94	7.09	44.31
Brick	85.66	–	72.78
Cement	235.64	–	208.14
Sand	554.98	–	490.21
Paint	54.65	–	54.65
Tiles	14.44	–	14.44
Coarse aggregates	379.68	–	335.37
Resource			
Electricity use (kWh)	8785.84	436.66	8229.70
Diesel use (L)	939.79	40.60	813.67

4.2 Inventory Analysis

Bill of quantities (BOQs) and the drawings of the selected case study conventional building were the primary methods for the data collection. Moreover, relevant literature, relevant reports from Sri Lankan and internationally authorized organizations, and ecoinvent 3.0 were used as secondary sources. Material quantities, electricity usage and fuel (diesel) usage were the main inputs collected, as shown in Table 2. To calculate the electricity and diesel consumption, the energy density values for the construction activities were determined from the Sri Lankan [28], and South Asian countries [29, 30] published literature. Distances were calculated based on the route maps and supplier locations. The hypothetical prefabricated off-site factory was mapped 20 km away from the construction site.

4.3 Impact Assessment

The impact assessment was carried out in SimaPro 8.3 (Ph.D. version). IPCC 2013 GWP 100a characterization method was employed to quantify the GHG emissions of the construction methods. Emission factors of the building materials were acquired from a similar case study conducted in Sri Lanka and relevant existing literature [28, 31]. Moreover, carbon emission factors for resources were taken from the Sri Lanka Sustainable Energy Authority website [32].

5 Pilot Case Study

Basic information on the CB and HPB is presented in Table 3. Specific details of the case study building will not be disclosed considering the commercial limitations. Foundation and roof system of the two buildings were assumed as similar.

5.1 Results and Discussion

The total GHG emission of the CB is 466.01 tCO_2, whereas PHB is 461.41. In this context, PHB slightly performs better than the CB in terms of GHG emissions (see Fig. 2). The raw material production stage is the hotspot of both CB and PHB. This life cycle stage accounts for more than 90% of the GHG emissions.

Table 3 Basic details of CB and HPB

Specification	CB	HPB
Location	Sri Lanka	Sri Lanka
Number of floors	4	4
CFA (m^2)	1749.36	1749.36
Prefabricated rate	0%	10.5% (by volume)
Structure: column, beam, slabs	Reinforced concrete, in-situ	Reinforced concrete, in-situ
Structure: staircase, corridor, slabs	Reinforced concrete, in-situ	Reinforced concrete, off-site prefabricated
External wall	Brick masonry	Brick masonry, off-site prefabricated facades
Internal wall	Brick masonry	Brick masonry
Finishes	Ceramic tiles, cement rendering, and plastering, painting	Ceramic tiles, cement rendering, and plastering, painting

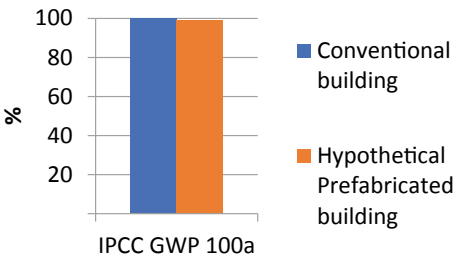

Fig. 2 Total GHG emission comparison of CB and HPB

6 Conclusions, Limitations, and Future Suggestions

The main focus of the study was to introduce an LCA decision-based methodological framework to LCA practitioners in OSC and MC industry with less methodological guidance. This research conducted a pilot case study to demonstrate the proposed methodological framework. HPB was extrapolated using conversion ratios from an example case study in China [27]. Thus, this is a rough estimation of the GHG emissions of the HPB. The conclusion should be derived with care considering the hypothetical nature of the comparison between CB and HPB. Moreover, particularly in selecting a LCA method, it is not that straightforward as shown in the proposed framework, however, practitioner can use the logic presented and seek more guidance in making the decision.

Future, research can focus on conducting comparative analyses with actual prefabricated buildings. Moreover, research can extend their assessments into other vital environmental impacts such as acidification potential, eutrophication potential, ozone depletion potential, and human toxicity potential. Furthermore, scenario analyses can be conducted to check the effect of the level of prefabrication, transportation distances, and alternative greener material options on the total GHG emission values.

Acknowledgements The authors would like to express their sincere gratitude to Dr. C. S. Bandara for the support given in acquiring valuable information needed for this research study.

References

1. Abd Rashid AF, Yusoff S (2015) A review of life cycle assessment method for building industry. Renew Sustain Energy Rev 45:244–248
2. Kamali M, Hewage K (2016) Life cycle performance of modular buildings: a critical review. Renew Sustain Energy Rev 62:1171–1183
3. Minunno R, O'Grady T, Morrison GM, Gruner RL (2020) Exploring environmental benefits of reuse and recycle practices: a circular economy case study of a modular building. Resour Conserv Recycl 160:104855
4. Sonnemann G, Vigon B (2011) Global guidance principles for life cycle assessment (LCA) databases: a basis for greener processes and products
5. Aye L, Ngo T, Crawford RH, Gammampila R, Mendis P (2012) Life cycle greenhouse gas emissions and energy analysis of prefabricated reusable building modules. Energy Build 47:159–168
6. Sandanayake M, Zhang G, Setunge S (2014) Life-cycle assessment for construction processes in building construction: a proposed conceptual framework. In: Proceedings of the 3rd world construction symposium 2014: sustainability and development in built environment, 20–22 June 2014, Colombo, Sri Lanka, 2014. Ceylon Institute of Builders (CIOB), pp 344–355
7. Suh S, Lenzen M, Treloar GJ, Hondo H, Horvath A, Huppes G, Jolliet O, Klann U, Krewitt W, Moriguchi Y (2004) System boundary selection in life-cycle inventories using hybrid approaches. Environ Sci Technol 38:657–664
8. Du Q, Bao T, Li Y, Huang Y, Shao L (2019) Impact of prefabrication technology on the cradle-to-site CO_2 emissions of residential buildings. Clean Technol Environ Policy 21:1499–1514

9. Crawford RH (2008) Validation of a hybrid life-cycle inventory analysis method. J Environ Manage 88:496–506
10. Hu X, Chong H-Y, Wang X (2019) Sustainability perceptions of off-site manufacturing stakeholders in Australia. J Clean Prod 227:346–354
11. Jin R, Hong J, Zuo J (2020) Environmental performance of off-site constructed facilities: a critical review. Energy Build 207:109567
12. Boafo FE, Kim J-H, Kim J-T (2016) Performance of modular prefabricated architecture: case study-based review and future pathways. Sustainability 8:558
13. Thai H-T, Ngo T, Uy B (2020) A review on modular construction for high-rise buildings. Structures. Elsevier, pp 1265–1290
14. Nam S, Yoon J, Kim K, Choi B (2020) Optimization of prefabricated components in housing modular construction. Sustainability 12:10269
15. Hammad AW, Akbarnezhad A, Wu P, Wang X, Haddad A (2019) Building information modelling-based framework to contrast conventional and modular construction methods through selected sustainability factors. J Clean Prod 228:1264–1281
16. Jeong J, Hong T, Ji C, Kim J, Lee M, Jeong K, Lee S (2017) An integrated evaluation of productivity, cost and CO_2 emission between prefabricated and conventional columns. J Clean Prod 142:2393–2406
17. Alhumayani H, Gomaa M, Soebarto V, Jabi W (2020) Environmental assessment of large-scale 3D printing in construction: a comparative study between cob and concrete. J Clean Prod 270:122463
18. Monahan J, Powell JC (2011) An embodied carbon and energy analysis of modern methods of construction in housing: a case study using a lifecycle assessment framework. Energy Build 43:179–188
19. Tumminia G, Guarino F, Longo S, Ferraro M, Cellura M, Antonucci V (2018) Life cycle energy performances and environmental impacts of a prefabricated building module. Renew Sustain Energy Rev 92:272–283
20. Kamali M, Hewage K, Sadiq R (2019) Conventional versus modular construction methods: a comparative cradle-to-gate LCA for residential buildings. Energy Build 204:109479
21. Teng Y, Pan W (2019) Systematic embodied carbon assessment and reduction of prefabricated high-rise public residential buildings in Hong Kong. J Clean Prod 238:117791
22. Satola D, Kristiansen AB, Houlihan-Wiberg A, Gustavsen A, Ma T, Wang R (2020) Comparative life cycle assessment of various energy efficiency designs of a container-based housing unit in China: a case study. Build Environ 186:107358
23. Balasbaneh AT, Ramli MZ (2020) A comparative life cycle assessment (LCA) of concrete and steel-prefabricated prefinished volumetric construction structures in Malaysia. Environ Sci Pollut Res 27:43186–43201
24. Saltelli A (2002) Sensitivity analysis for importance assessment. Risk Anal 22:579–590
25. Renschler P (2013) What is the difference between sensitivity analysis and uncertainty analysis? [online]. Quora. Available https://www.quora.com/What-is-the-difference-between-sensitivity-analysis-and-uncertainty-analysis. Accessed Oct 20 2021
26. CFI Education. Scenario analysis vs sensitivity analysis
27. Mao C, Shen Q, Shen L, Tang L (2013) Comparative study of greenhouse gas emissions between off-site prefabrication and conventional construction methods: two case studies of residential projects. Energy Build 66:165–176
28. Kumanayake R, Luo H (2018) Life cycle carbon emission assessment of a multi-purpose university building: a case study of Sri Lanka. Front Eng Manage 5:381–393
29. Devi P, Palaniappan S (2014) A case study on life cycle energy use of residential building in Southern India. Energy Build 80:247–259
30. Sim J, Sim J, Park C (2016) The air emission assessment of a South Korean apartment building's life cycle, along with environmental impact. Build Environ 95:104–115
31. Latawiec R, Woyciechowski P, Kowalski KJ (2018) Sustainable concrete performance—CO_2-emission. Environments 5:27
32. Sri Lanka Sustainable Energy Authority. Carbon footprint

Innovative Building Materials and Concrete Technology

Pre-treated Coir Fibres Reinforced Biocomposite Structures for Green Wall Cultivations

K. R. Jayasingha, K. H. G. P. Tharanga, D. G. J. P. Dayarathne, M. M. I. Ahamed, T. N. Fernando, and A. P. Pallewatta

Abstract Coir fibres are one of the widely available lignocellulose materials in Sri Lanka. The use of pre-treated coir fibre as reinforcement material in a biocomposite exhibits additional characteristics such as resistance to water absorption, low thermal conductivity, low density and higher elongation at the breaking point. The present study aims to prepare biocomposite structures for green wall cultivations using alkaline hydrogen peroxide pre-treated coir fibres as a reinforcement material. It is also expected to find an innovative way to develop environmental-friendly green fences and wall panels along with a suitable structure to minimize the drawbacks of existing green walls such as wash-off plant nutrients during irrigation and damages due to the cultivation of crops on walls. Four different composite mixtures were prepared with varying pre-treated coir fibre weights of 0, 20 g, 40 g and 80 g to 1.5 kg of a homogenous mixture, which was prepared by mixing earth soil, cement, cow dung ash and goat dung ash in the ratio of 6:1:1.5:1, respectively, with an addition of 7 L of water. Then, 36 blocks (100 mm × 100 mm × 100 mm) were prepared by replicating each composite mixture three times to measure compressive strength and the percentage (%) of water absorption over the intervals of 7, 14 and 21 days after curing. In addition, making use of the growing performance of the surface of the prepared structures (wall panels and blocks) from the best composite mixture was evaluated by planting the selected crops such as *Hedera helix, Rhoeo spathacea* and *Soleirolia* species. The results indicated that fibre added biocomposite blocks show porous structure, satisfactory compressive strength that varied between 2.5 and 4.0 N/mm^2 and 2–8% of water absorption after 21 days of curing. Also, growth parameters of selected crops indicate that the coir fibre reinforced sustainable wall panels are suitable for establishing vertical growing green structures.

K. R. Jayasingha · K. H. G. P. Tharanga · D. G. J. P. Dayarathne · M. M. I. Ahamed · A. P. Pallewatta
Faculty of Computing and Technology, University of Kelaniya, Colombo, Sri Lanka

T. N. Fernando (✉)
National Engineering Research and Development Centre of Sri Lanka, Ja-Ela, Sri Lanka
e-mail: nilanthifernando45@yahoo.com

A. P. Pallewatta
Gampaha Wickramarachchi University of Indigenous Medicine, Yakkala, Sri Lanka

R. Dissanayake et al. (eds.), *12th International Conference on Structural Engineering and Construction Management*, Lecture Notes in Civil Engineering 266,
https://doi.org/10.1007/978-981-19-2886-4_38

Keywords Alkaline hydrogen peroxide pre-treatment · Biocomposite · Coir fibre · Green wall

1 Introduction

Sustainability is the new trend in today's world to overcome the causes that occur due to widespread environmental disruption. Thus, modern building constructions tend to minimize the negative impacts of conventional practices by replacing and experimenting with sustainable materials. For this, several numbers of materials such as soil, drain sludge waste, residual coal waste rocks as well as natural waste materials such as cow dung and goat dung could be identified as eco-friendly materials and could be used to cast biocomposite structures. Recently, many researchers are exploring various innovative approaches to develop different types of sustainable designs using different kinds of plant residue fibres as reinforcement materials that were identified as waste or low-cost materials widely available in Sri Lanka such as cornhusks, coir, paddy straw and bagasse [1]. Out of all the ubiquitous agro-plant residues in Sri Lanka, coir fibres could be considered as a highly suitable material for this need. According to Sri Lankan Export Development Board (EDB) records [2], around 12% of the agricultural sector is counted for coconut (*Cocos nucifera*) cultivation and produces about 2500–3000 million coconuts per year. In 2014, it was reported that the production of coconut fibre in Sri Lanka was around 150,400 tonnes [2], which was practically about 90% of the world's coir production. 33–35% of the coconut fruit consists of the husk and remains 70% as the pith and 30% as fibres. This fibre content is a major by-product of coconut processing, where a significant amount of coir fibres are removed while consuming coconut nuts. Therefore, bulk amounts of coir fibres are being produced as a waste at domestic level in Sri Lanka. Recent studies show that coir fibres could be used for the development of green composites as a reinforcement material, which helps to strengthen the composites [3]. The surface of raw coir fibres consists of cellulose, lignin, hemicellulose, pectin, fats and waxes, resins, ash, moisture and other constituents. In Sri Lanka, coconut coir dust averagely contains 329 g/kg cellulose, 56 g/kg hemicellulose and 476 g/kg lignin in dry weight [2] and raw fibres consist of 21–40% cellulose, 15–47% lignin and 12–27% hemicellulose in weight [4]. However, [5] indicate that the raw lignocellulose fibres (agro-plant residues) cannot be used as reinforcement fibres in composite materials without pre-treating, as the pre-treated surface is needed for the reacting of fibre surface forming a bridge of chemical bonds between the fibres and the matrix during reinforcing.

Fernando et al. [1] have used an effective, simple and low-cost pre-treatment with alkaline hydrogen peroxide (AHP) for the preparation of pre-treated fibres from available agro plant residues. Moreover, AHP pre-treatment is considered an environment-friendly pre-treatment that can be conducted under normal atmospheric conditions where all the waste could be easily recycled, does not emit any hazardous

materials to the environment and is an effective method of extracting a bulk amount of pre-treated fibres in a short time at an industrial level.

The present study focuses on the preparation of a sustainable composite mixture to develop green wall panels to overcome the identified issues in the exiting green walls. Recently, different types of greening walls, green facades and fences have been designed for integration in modern gardens, especially in the urban cityscapes [6]. Different types of materials such as coir fibre, bamboo, jute fibre and felt mats have been used for the development of growing composite for such green wall cultivations. However, plants seemingly growing out of the wall could offer a huge impact in any space or add a fantastic backdrop for the rest of the garden; nevertheless, these green walls carry momentous drawbacks as follows

- High Cost: green walls are very luxury items which normally cost $900–$1500 per square metre [7].
- Complex maintenance: green walls are very labour intensive to maintain and sometimes difficult to water and to replace the dead plants. When different types of trays, planting tiles and flexible bags are used for living walls cultivations, there are some disadvantages such as complex implementation, high insulation cost and limited space for root development.
- Instability of the material: some green wall materials could be damaged to the cultivated wall and that could affect the growth of mould.

Therefore, the present research also attention on developing sustainable vertical growing structures is to create greener environments, thoroughly addressing the mentioned drawbacks seen in the recent green walls by reinforcing of soil, cement, cow dung and goat dung ashes with pre-treated coir residues.

2 Materials and Methodology

2.1 Location

The experiment was conducted at the National Engineering Research and Development Centre of Sri Lanka.

2.2 Preparation of Materials

Earth soil, Ordinary Portland Cement (OPC), cow dung ash, goat dung ash, pre-treated coir fibres and water were used as the main raw materials in the experiment. The earth soil samples were collected from the Anuradhapura (Anuradhapura District, North Central Province, Sri Lanka). It has a reddish colour, and the soil type is red-brown laterites, which has 90% clay. Then, the collected soil sample was

Fig. 1 **a** Raw coir fibre with coconut husk, **b** coir fibres during alkaline hydrogen peroxide pre-treatment

spread on the floor and solar-dried. Finally, it was sieved using a sieve (mesh size 4.00 mm/No: 5). Cow dung and goat dung ashes were prepared first, by spreading the collected dung on the floor and solar-dried. Then, the solar-dried samples were burnt in a sustainable furnace (low emit greenhouse gases to the surrounding environment) that was fabricated and designed by NERD Centre to be introduced for making bakery products in domestically. Prepared ash samples were left for a few hours to bring down to atmospheric temperature. Finally, ash samples were sieved using a sieve (mesh size 3.36 mm/No: 6).

2.3 Pre-treating of Coir Fibres Using AHP Pre-treatment

Pre-treatment solution was prepared by mixing 10 ml of 5 mol/L NaOH and 0.75 ml of 34% H_2O_2 to 1 g of dried raw coir fibres as described by [1]. The percentage of cellulose in the pre-treated fibres was measured using chlorination method and the confirmation of the pre-treated fibres was done using a Fourier transform infrared spectroscopy (FTIR) as described in [1]. In addition, morphological characteristics of raw and pre-treated fibres were identified using a scanning electron microscopy (SEM). A universal testing machine was used to measure the tensile load of raw and pre-treated fibres (Fig. 1).

2.4 Preparation of Composite Mixtures

The homogenous mixture was prepared by mixing soil, cement, cow dung ash and goat dung ash in the ratio of 6:1:1.5:1, respectively. The compositions of used materials were found from particular preliminary studies. Subsequently, 7 L of water was added to the mixture. Four (04) soil blocks were prepared using four composite mixtures, which were prepared by mixing the pre-treated coir fibre ratio of 0, 20, 40 and 80g with 1.5 kg of prepared homogenous mixture. The prepared composite mixtures were named as follows.

- $T1$ (treatment1)—Control mixture/(soil + cement + cow dung ash + goat dung ash) Moist (M)
- $T2$—(soil + cement + cow dung ash + goat dung ash) (M) + (pre-treated coir fibres 20 g)
- $T3$—(soil + cement + cow dung ash + goat dung ash) (M) + (pre-treated coir fibres 40 g)
- $T4$—(soil + cement + cow dung ash + goat dung ash) (M) + (pre-treated coir fibres 80 g)

2.5 Preparation Composite Blocks for the Testing

Thirty-six (36) eco-blocks (100 mm × 100 mm × 100 mm) were prepared using four treatments and replicating each treatment three times (03) to test the compressive strength at intervals of 7 days, 14 days and 21 days after curing. Additionally, average percentages of water absorption were tested after 21 days to identify the best composite mixture for the preparation of vertical growing structures.

2.5.1 Testing of Compressive Strength

The compressive strength of prepared blocks in each treatment during the intervals of 7, 14 and 21 days after the curing was measured using a universal testing machine.

2.5.2 Determination of Water Absorption Percentage

The prepared soil blocks were immersed in a water tank for 24 h to calculate the weight difference, which was then expressed as a percentage of water absorbed by the developed blocks as Eq. (1).

$$\text{Moisture Content} = \frac{(\text{Wet Weight} - \text{Dry Weight})}{\text{Dry Weight}} \times 100\% \tag{1}$$

2.6 Evaluation of Growth Performance of Selected Crops

Using data from test results, composite mixture was selected for the best compressive strength and water absorption percentage of the finished composite blocks. Then, using the best composite mixture, slip form wall panels were prepared as described in Fig. 2a–d. Subsequently, the lightweight growing mixture was prepared by mixing pre-treated coir fibres and composted cow dung to fill the internal holes in the prepared

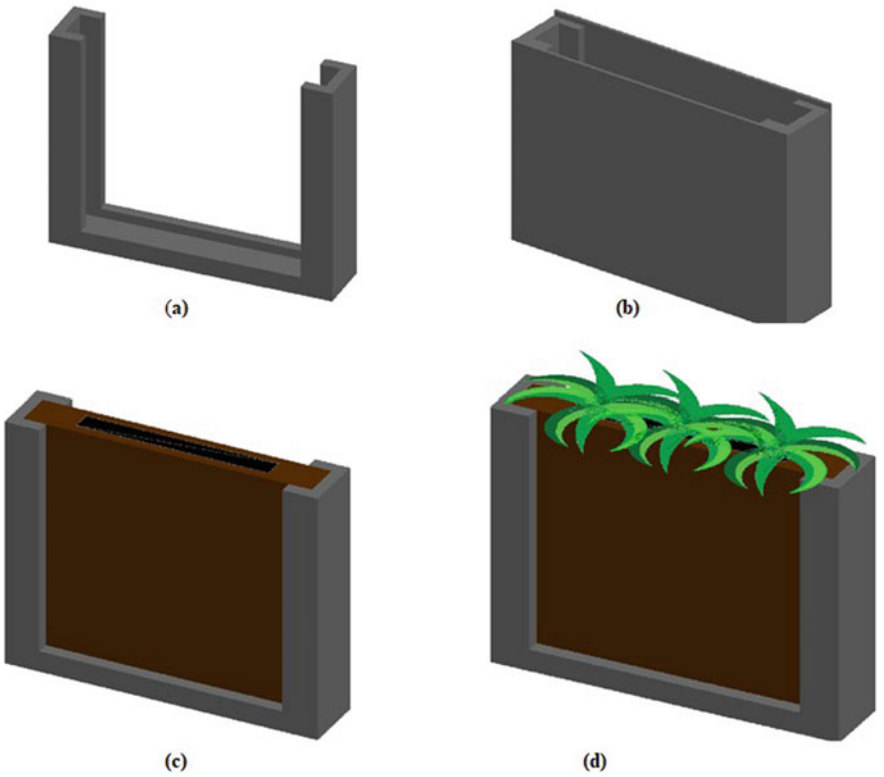

Fig. 2 Method of preparation of slip form composite panel **a** iron frame, **b** iron mould, **c** moulded slip form panel, **d** prepared slip form growing structures (the size of the panel − 30 cm height × 40 cm width × 5 cm thickness)

panels. Use of pre-treated fibres as the growing mixture has more advantages than use of coir dust. The reason is that the coir dust, which is more than 6 months old is required to be prepared as growth media and this growth medium can easily wash off.

However, pre-treated coir fibre has high strength and mould proof characteristics. Also, fibre network helps to increase porosity and helps proper growth of roots by avoiding degradation of the structure during irrigation. Finally, the selected crops of *Hedera helix, Rhoeo spathacea* and *Soleirolia* species were allowed to grow on the surface of the prepared panels. Additionally, growth performance and the degradation characteristics on the wall surface were observed during the period of growth.

2.7 Data Analysis

Microsoft Excel (version 16) was used to determine the average of measured data and to plot.

3 Results and Discussions

3.1 Characteristics of Pre-Treated Sample

The pre-treated coir fibres show yellowish colour prior to being neutralized and turn into a whitish to light yellow after neutralization (Fig. 3). Further, pre-treated fibres had rough and thin surface due to removal of surface impurities comparison with raw coir fibres. The raw coir fibres have an outer surface layer with waxy, gummy, lignin, hemicellulose, pectin and other impurities. Hence, raw coir fibres do have not to roughen the surface and show hydrophilic behaviour due to the availability of hydroxyl groups [8]. It leads to swell the fibre in the matrix and bonding strength decreases due to the swelling of the coir fibre.

The average tensile load value was 0.097 kN and 0.124 kN, respectively, in raw and pre-treated coir fibres. This is evident that the increase of the tensile strength value in pre-treated fibres comparison with raw coir fibres. Thus, [5] mentioned that the pre-treated surface needed for the reacting of fibre surface forming a bridge of chemical bonds between the fibres and matrix during reinforcing. Also, SEM images of raw and pre-treated coir fibres (Fig. 4a, b) indicate the impurities in the raw coir fibres have been removed and one type of bundle of fibres was observed on the surface. The

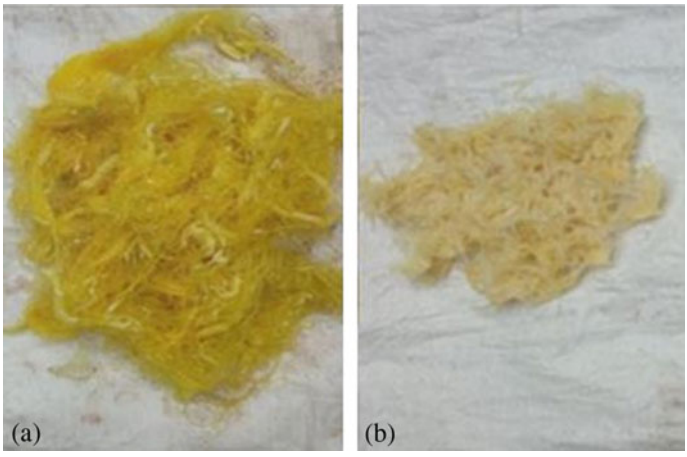

Fig. 3 Coir fibres **a** pre-treated alkaline coir sample, **b** pre-treated neutralized coir sample

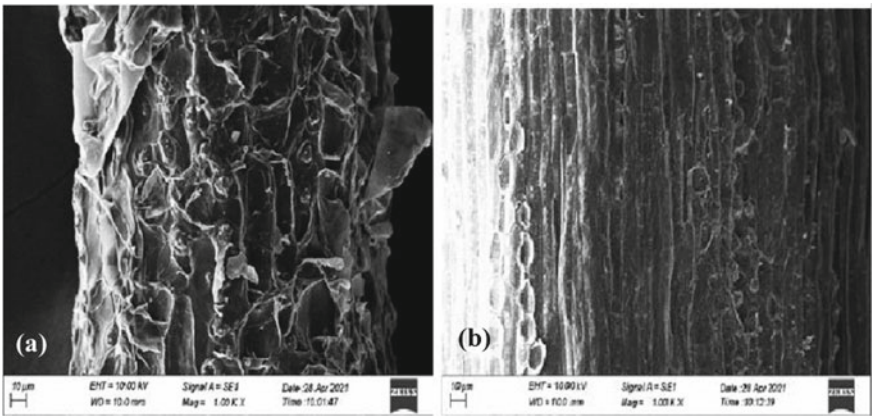

Fig. 4 SEM results **a** raw coir fibres, **b** pre-treated coir fibres

FTIR results proved that this bundle of fibres was cellulose after comparison of the wavenumbers as shown in Fig. 5 with the finding of [1]. Chamath et al. [9] mentioned that untreated coir fibre contains high amounts of hemicellulose, pectin and lignin. These compounds contain ester and aldehyde. Therefore, C=O stretching at 1731 cm^{-1} in the raw coir fibres and reduced after the pre-treatment. Also, the intensity of 1235–1600 cm^{-1} increased due to the removal of pectin, wax, gummy substances and hemicellulose from the raw coir fibres. Further, the peak at 1024 cm^{-1} shows the

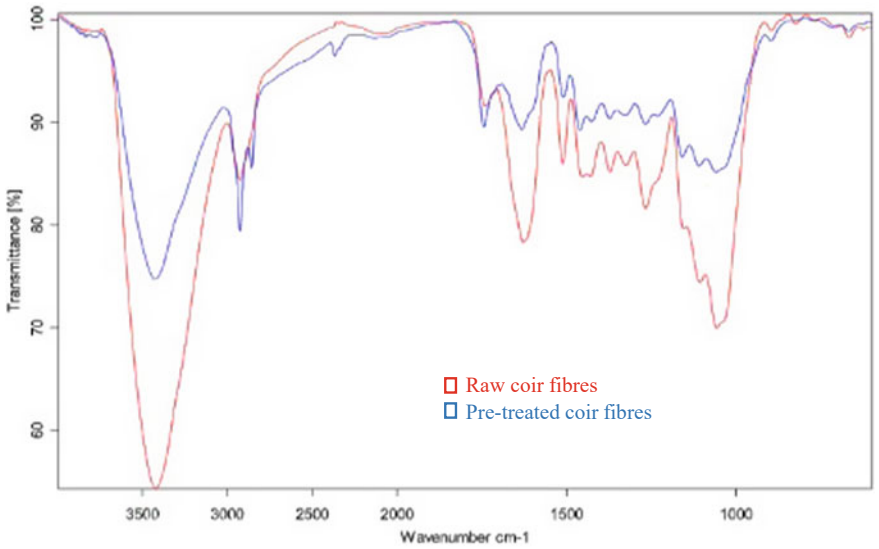

Fig. 5 FTIR results of the raw and pre-treated coir fibres

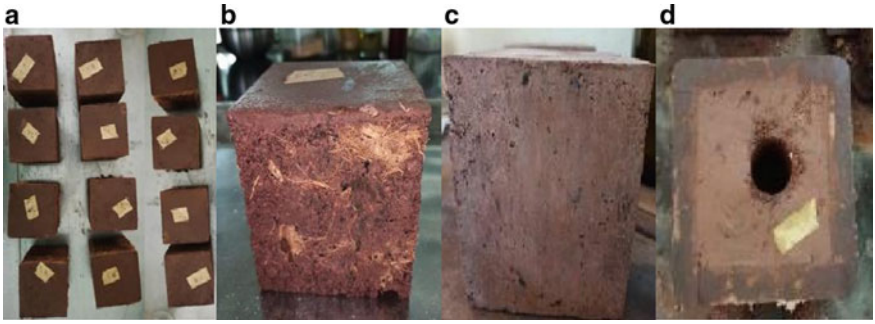

Fig. 6 Visual observations **a** prepared composite blocks, **b** side view of fibre added block, **c** side view of a control block, **d** prepared composite block with hollow space

C–O–C stretching of the cellulose. Similar results were observed in the comparisons of wavenumbers and intensity of the raw and pre-treated coir fibres in Fig. 5.

3.2 Characteristics of Developed Composite Blocks

The developed blocks had a dark brown colour (Fig. 6a), where the fibre added blocks ($T2$, $T3$ and $T4$) show porous structure on the external surface (Fig. 6b) compared with the control sample ($T1$) in Fig. 6c. Thus, the porous structure of the external surface is varied as $T4 > T3 > T2$, respectively. The added fibre amount may be affected to increase the porosity of the developed blocks, and the porous structure is helpful for the penetration of plant roots, which is good for the preparation of growing structures. Further, coir fibres are mainly used as reinforcement material to increase the strength of the structure as well as to increase the porosity. Also, it helps to retain the moisture of the structure since the mixture of soil and cement do not perform as a growing platform itself. Further, soil and cement particles bond tightly to each other in the control block ($T1$) and do not show porousness in the blocks.

The percentage of water absorption rates of prepared soil blocks were plotted as shown in Fig. 7. The water absorption rate of all block samples varied between 2 and 8% and $T4$ samples showed the highest absorption rate due to their high fibre amount compared with other sample blocks. The result of the water absorption rate indicated that the fibre amount may be affected to increase the porous structure of the blocks and that due to the increased water absorption rate.

Figure 8 shows the results of the compressive strength of cast composite blocks after the curing of 7, 14 and 21 days. The compressive strength values were higher in all blocks after the curing period of 21 days and lower after the curing period of 7 days. For the increment of the compressive strength after the curing of 21 days rather than 7 days moisture absorption may be a reason. Also, the block strength reduces as the increasing of pre-treated coir fibres and a clear indication that further introduction

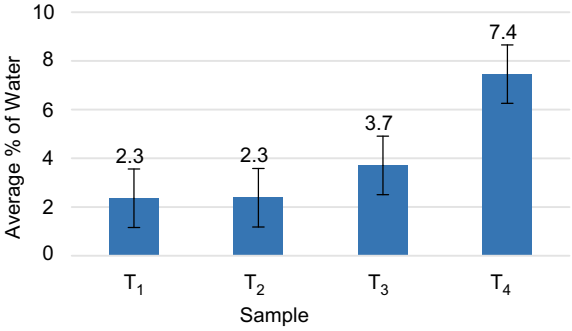

Fig. 7 Variation of percentage of average water absorption

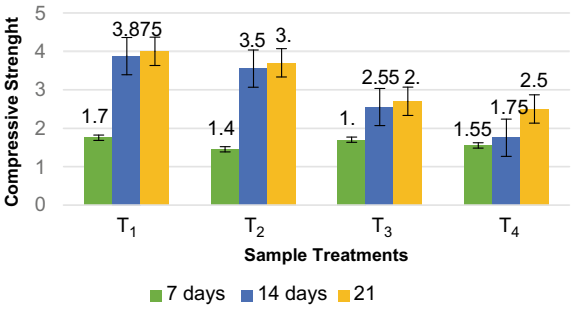

Fig. 8 Variation of compressive strength (N/mm^2)

of coir fibre beyond 20 g per block affects the strength properties of the specimen negatively according to Fig. 8. Thus, the compressive strength of blocks in each curing period, highest value recorded at 21 days of the blocks without the pre-treated coir fibres (control block) while the lowest value recorded at after 7 days curing in the highest pre-treated coir fibre added blocks ($T4$ block). Kumar et al. [10] observed that the 5% cow dung ash (CDA) could add in cement as a partial replacement to cement. Thus, a more detailed study is essential to find the compressive strength at longer ages. During hydration, the calcium hydroxide (Ca(OH)2) produced reacts with the silica from CDA over time to form the more stable calcium silicate hydrates (CaH_2O_4Si), which could be responsible for the appreciable strength gain. Several researchers reported that pozzolanic materials incorporation into cement reduces the $Ca(OH)_2$ formation (which promotes micro-cracking) and enhances the formation of CaH_2O_4Si, which promote later strength gain. Hence, an increase in strength could be possible to observe at the later curing ages (i.e. 60 and 90 days) than at the early curing periods of 7 and 28 days. The results of the present study show that the strength of the casted blocks increases when the curing period is increased from 7 to 21 days. Further, [10] has used 5% to 16% of cow dung ash by weight as cement replacement, where it is used as partial replacement materials in concrete mixtures to reduce carbon footprint [11]. However, in the present study a high amount of cow dung and goat dung ash 1:1.5 has been used to prepare a homogeneous mixture with cement and earth soil ratios of 1:6, respectively, to develop blocks and wall panels

for green wall cultivations. In addition, added amounts of cow dung ash and goat dung ash as partial replacement materials for the cement could increase sustainable properties of the growing composite. Furthermore, [12] have developed bricks by adding clay, cement and cow dung for use in low-cost buildings. Also, the developed bricks have compressive strengths between 1.5 and 4.5 N/mm^2 after 14 day curing. When compared, the compressive strength of growing composite in the present study falls within the value shown in result of [12].

As the visual observation of developed wall panel structure and the surface of the structure, Fig. 9a shows panels allow penetration and holds the plant roots of selected crops on the front surface. Figure 9b shows the structure, after 6 months and shows high growing performance on the surface of the panel without surface cracks. The pre-treated coir fibres were used to avoid wash off the growth medium of the developed vertical growing panels and highly porous surface helps penetration of plant roots. Further, Fig. 9c, d indicates growing performances of *H. helix* and *Rhoeo spathacea,* respectively. Especially, the plant height of *H. helix* (English Ivy) shows an increase of 80% after six months of cultivation. Normally, the growth of English Ivy plants requires a low warm condition and the results of the growing performance of English Ivy indicated that the suitably low warm environment may be created

Fig. 9 Developed primarily vertical wall panel structures **a** initial establishment, **b–d** 6 months after the establishment of wall panels

from the use of cow dung ash, goat dung ash, soil and cement, which is good for reducing warming of the environment. The reason that the developed structures could be shifted easily is that they are soil-based, highly porous and cultivation mixture retains on the pores when the environmental temperature increases. Therefore, the developed structures are good for tropical climates.

4 Conclusion

Four different composite mixtures ($T1$–$T4$) were prepared with varying amounts of pre-treated coir fibre with earth soil, cement, cow dung ash and goat dung ash. Subsequently, 36 blocks (100 mm × 100 mm × 100 mm) were prepared by using each composite mixture three times to measure compressive strength and the percentage (%) of water absorption over the intervals of 7, 14 and 21 days after curing. Observations show that the strength of the blocks increased as $T2 > T3 > T4$. As the $T1$ (control sample) does not show a porous structure, it is not suitable for cultivation purposes. Thus, $T2$, $T3$ and $T4$ are suitable ratios for the cultivation purposes and the results of the present study show that $T2$ could be identified as the best mixture ratio with low cost, sufficient strength and satisfactory level of growing performance for the panel among the developed biocomposite mixtures. Coir fibres were mainly used to increase the bonding of the used materials as the reinforcement to avoid the surface cracking of the structure, to increase the porosity and cow and goat dung ashes were used as partial replacement material as the mixture of soil and cement itself do not perform as a growing platform. The observations show that the prepared structures were sustained without cracks on the surfaces in the duration of 6 months after establishment. Moreover, positive growing performance of the English Ivy plant could be used as an effective approach to address the matter of global warming.

5 Recommendations

A homogenous mixture prepared by mixing all the ingredients is needed before use in the development of composite mixtures. In addition, eco-vertical growing structures could be developed in areas where high amounts of laterite are available in hilly areas in Sri Lanka for growing vegetables. Further, establishing of green fences using the prepared composite mixture as durable eco-fences are better than less durable fences made of wood and weaved palm fronds. Also, they help reduce visual pollution of the environment and help create a green environment. In addition, an automatic aquaponics irrigation system could be designed as shown in Fig. 10 automating the irrigation system for applying water and fertilizers without any external watering and fertilizing input.

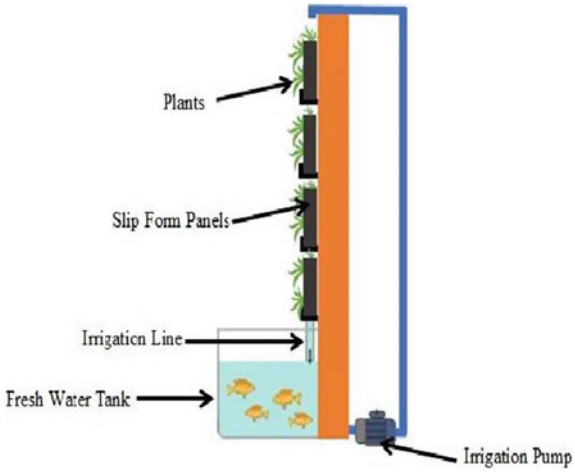

Fig. 10 Proposed automatic aquaponics irrigation system for fertilizing and watering

References

1. Fernando TN, Aruggoda AGB, Ariadurai SA, Disanayaka CK, Kulathunge S (2015) Evaluation of alkaline peroxide pretreatment for extraction of cellulose from selected plant biomasses. J Eng Technol Open Univ Sri Lanka 3:1–10
2. EDB Sri Lanka (2017) Coconut and coconut based products from Sri Lanka [WWW Document]. https://www.srilankabusiness.com/coconut/. Accessed 9/30/21
3. Jayavani S, Deka H, Varghese TO, Nayak SK (2015) Recent development and future trends in coir fiber reinforced green polymer composites: review and evaluation [online]. https://www.researchgate.net/publication/276852739_Recent_development_and_future_trends_in_coir_fiber_reinforced_green_polymer_composites_Review_and_evaluation. Available at https://doi.org/10.1002/pc.23529. Accessed 8 Dec 2021
4. Savastano H, Fiorelli J, Santos S (2017) Sustainable and nonconventional construction materials using inorganic bonded fiber composites, 1st edn. Wood head Publishing
5. Ashori A, Ornelas M, Sheshmani S, Cordeiro N (2012) Influence of mild alkaline treatment on the cellulosic surfaces active sites. Carbohydr Polym 88:1293–1298. https://doi.org/10.1016/j.car-bpol.2012.02.008
6. Peng K-H, Lin H-Y (2015) A Study on the types of vertical greening applying to urban existing buildings in Taiwan [online]. Available at http://www.avestia.com/NewTech2015_Proceedings/files/papers/ICEPR214.pdf. Accessed 8 Dec 2021
7. Perini K, Ottelé M, Fraaij ALA, Haas EM, Raiteri R (2011) Vertical greening systems and the effect on air flow and temperature on the building envelope. Build Environ 46(11):2287–2294
8. Hao LC, Sapuan SM, Hassan MR, Sheltami RM (2018) Natural fiber reinforced vinyl polymer composites. Nat Fibre Reinf Vinyl Ester Vinyl Polym Compos:27–70. https://doi.org/10.1016/B978-0-08-102160-6.00002-0
9. Chamath LG, Srimal LKL, Sewvandi GA (2020) Effect of alkaline concentration on the surface properties of coir fibres. In: Proceeding of the national engineering research symposium (NERS, 2020), pp 7–12
10. Kumar PT, Reddy RH, Bhagavanulu D (2015) A study on the replacement of cement in concrete by using cow dung ash. Int J Sci Eng Appl Sci 1:314–327
11. Tank YR, Thaker G (2018) A review on strength assessment of green concrete using different admixtures. Int J Tech Innov Mod Eng Sci 4:79–83
12. Katale D, Kamara VS, Adedeji AA (2013) Significant of use of clay soil mixed with cow dung to produced bricks for low cost buildings. J Res Inf Civ Eng 1:10

Improving Impact Resistance of Plain-Woven Ultra-High Molecular Weight Polyethylene Fabrics

D. Weerasinghe, S. Breen, H. Wang, D. Mohotti, P. J. Hazell, and J. P. Escobedo-Diaz

Abstract Several commercial spray coatings were used on ultra-high molecular weight polyethylene (UHMWPE) plain-woven fabrics, and yarn pull-out tests were carried out. Spray materials consisted of various polymers and adhesives. Samples were prepared with single- and double-coated surfaces. On average, 23.5% of additional areal density was introduced by the coatings. Yarn pull-out force significantly increased upon coating the fabric samples. For the rubber-coated sample, the peak pull-out force was increased by approximately 98 times that of the neat counterpart. Three samples which exhibited the highest pull-out load per unit of areal density were subjected to high-velocity gas gun testing using a 12-mm (7.05 g) steel ball projectile. Impact velocities ranged from 140 to 230 m/s. Each sample consisted of four plies of coated and neat fabrics. Rubber-coated samples showed the highest specific energy absorption. Changes in failure mechanism due to coating were observed. While the neat fabric targets were perforated purely by a wedge-through mechanism, the coated samples were perforated by a combination of wedge-through mechanism and yarn failure. Energy absorption was higher in the coated samples than in the neat counterparts. The method proposed herein is a viable alternative to other existing techniques such as shear thickening fluid impregnation due to less complexity and relatively lower areal density increase. This study showcases the potential of using plain-woven fabrics in impact resistant applications.

Keywords Woven fabric · UHMWPE · High-velocity projectile impact · Coating · Yarn pull-out

D. Weerasinghe
School of Civil Engineering, Faculty of Engineering and IT, The University of Sydney, Darlington, NSW 2006, Australia

S. Breen · H. Wang · D. Mohotti (✉) · P. J. Hazell · J. P. Escobedo-Diaz
School of Engineering and Information Technology, The University of New South Wales, Canberra ACT 2600, Australia
e-mail: d.mohotti@unsw.edu.au

R. Dissanayake et al. (eds.), *12th International Conference on Structural Engineering and Construction Management*, Lecture Notes in Civil Engineering 266,
https://doi.org/10.1007/978-981-19-2886-4_39

1 Introduction

Even though aramid fibres such as Kevlar® and Twaron® are commonly used in soft armour systems currently, UHMWPE fibres such as Dyneema® and Spectra® possess more desirable properties. Lower density, higher tensile modulus and resistance to chemical and physical degradation are some properties that UHMWPE possess in comparison to aforementioned aramids [10]. The density of UHMWPE is approximately 0.97 g/cm^3 [4] while for aramids such as Kevlar®, it is 1.44 g/cm^3 [2]. The moduli of UHMWPE fibres are also higher than those of aramids in general. Consequently, the elastic wave propagation speed through UHMWPE is higher compared to aramids, which facilitates more efficient energy dissipation upon ballistic impact [3]. Owing to the notably lesser density in comparison to aramids, the potential of using UHMWPE for lightweight applications is highlighted. Higher tensile strengths and longitudinal moduli [9] are also obvious advantages as far as ballistic impact applications are concerned.

However, UHMWPE fabrics are not commonly used in impact resistance-related applications in plain weave construction due to their inherently poor frictional properties. Recent findings of [14] reported that plain-woven UHMWPE Spectra fabrics subjected to ballistic impact using a 7.05-g spherical ball projectile were perforated purely due to the wedge-through or windowing effect. UHMWPE yarns simply slipped over the projectile surface, creating a window for the projectile to perforate the target without any yarn failure.

However, if inter-yarn frictional properties of plain-woven UHMWPE fabrics can be improved, there is potential to transform the failure mechanism from a wedge-through dominant perforation to a yarn failure dominant perforation. A potential improvement in inter-yarn friction in UHMWPE fabrics is likely to utilise the extremely high strengths of its constituent yarns, thereby leading to higher energy absorption compared to a neat fabric without any surface modification.

Shear thickening fluid (STF) impregnation of fabrics has been utilised as a means of impact resistance improvement of woven fabrics for over two decades [15]. However, STF impregnation of fabrics has numerous shortcomings, including, but not limited to, the complexity and overall cost of processing, high areal density increase due to impregnation and instability to external conditions such as temperature and weathering [7, 15]. Consequently, the concurrent trend in emerging research efforts focuses on more stable and lightweight polymeric and adhesive coatings [1, 5–7]. Kim et al. [7] reported that the energy absorption of a Heracron aramid fabric was increased by 90% with an adhesive coating with only 15% of additional areal density. Ignatova et al. [5] also reported a 90% increase in the ballistic limit velocity of Twaron CT709 aramid fabrics with a polyvinyl alcohol coating introducing an additional weight of only 6%. Despite the increasing interest in performance increment in aramid fabrics such as Kevlar® and Twaron® using thin coatings, there is currently little attention being paid on UHMWPE fabrics such as Spectra® and Dyneema®. This constitutes the premise for the present work. Using thin coatings of various materials, impact resistance of UHMWPE fabrics could be improved. In the

Table 1 Properties of the UHMWPE Spectra® fabric used

Property	Value
Bulk density (g/cm^3)	0.97
Tensile modulus (GPa)	97–113
Tensile strength (MPa)	2900–3300
Tensile elongation (%)	2.9–3.5
Specific modulus (GPa/(g/cm^3))	100–116
Specific strength (MPa/(g/cm^3))	2990–3400
Cross sectional area (mm^2)	0.074
Fibres per yarn	120

present work, UHMWPE Spectra® plain-woven fabrics were coated using different materials and yarn pull-out tests were conducted to assess the inter-yarn frictional improvement. Subsequently, single-stage gas gun tests were carried out on neat and selected coated targets containing four plies.

2 Materials and Methods

2.1 UHMWPE Plain-Woven Fabrics

UHMWPE Spectra® plain-woven fabrics sourced from JPS Composite Materials (Anderson SC) were used in the present work. Properties of the used fabric are summarised in Table 1.

2.2 Coating Materials

The rubber-based coating used in this study was Flex Seal®. Flex Seal® is also considered a multipurpose adhesive with a density of 1.09 g/mL and is thermally stable in temperatures ranging from − 28 to 60 °C [11].

Polyurethane conformal coating (PUC): The polyurethane material used within this study was a clear amber modified polyurethane coating. PUC is characterised as a good dielectric material; this is regularly used to design electronic circuitry protections. PUC has a density of 0.87 g/mL and an operating temperature range of 16–130 °C. When applied in thin layers, the product takes approximately 45 mins to dry and 24 h to fully cure.

SikaBond® SprayFix is a polyvinyl acetate multipurpose adhesive product. This adhesive has a density of 1.04 g/mL and a maximum operating temperature of 50 °C. The recommended dry time is 4 mins, and cure time is 24 h.

2.3 Sample Preparation

Two flat frames of inner dimensions 250 mm × 150 mm were used to sandwich the fabric plies prior to spray coating the surface. After the materials were sprayed onto the fabric surfaces, excess material on the surfaces was removed by a sweeping action.

2.4 Yarn Pull-Out Testing

Yarn pull-out tests were conducted on a Shimadzu AG-X universal testing machine (UTM). Specimen dimensions and other specifications of the test are similar to those reported by [7].

2.5 Gas Gun Testing

Single-stage gas gun tests were performed on 4-ply targets of both neat and coated targets. The experimental set-up is described in detail in the authors' previous work [14]. Impact velocities as well as residual velocities were also measured using image analysis of high-speed video data (Phantom Cine Viewer software) and recorded using a Phantom v710 high-speed camera operating at 20,000 fps.

3 Results and Discussion

3.1 Yarn Pull-Out Testing

The yarn pull-out force of the neat/uncoated fabric samples did not register a readable pull-out force output. The maximum pull-out force was 0.32 N on average. However, the Flexseal-, polyurethane- (PU) and SikaBond-coated samples exhibited average peak pull-out forces of 31.0 N, 22.8 N and 17.3 N, respectively. When the peak pull-out load of the neat fabric is considered as 0.32 N on average, the pull-out forces increased by as much as 98 times, 71 times and 54 times for the Flexseal-, polyurethane- (PU) and SikaBond-coated samples, respectively. The pull-out force versus pull-out displacement plots of different coated fabric samples are shown in Fig. 1.

The results indicate that all three coating types are highly effective in improving the inter-yarn frictional properties. In Fig. 1, it can also be observed that the shape of the pull-out force versus displacement plots displays a sharp peak followed by a steep drop in the pull-out force, to nearly zero. The gradient of the plot post-peak is nearly

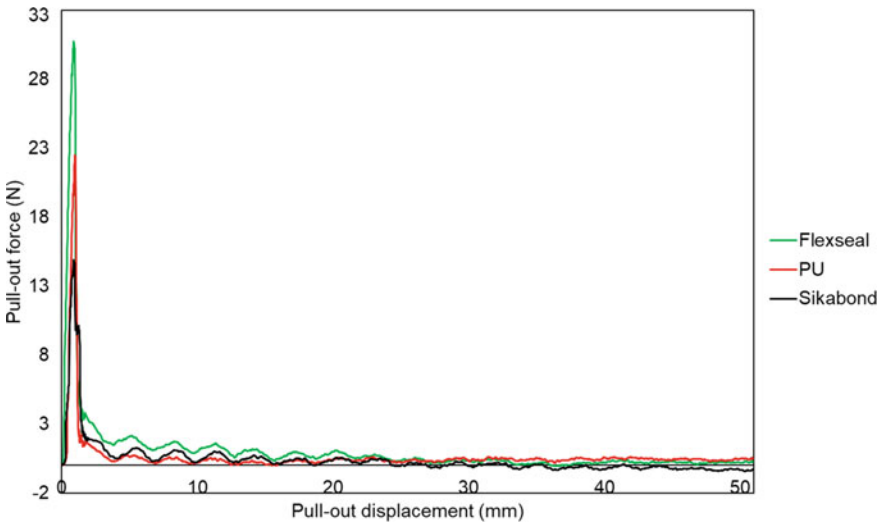

Fig. 1 Yarn pull-out force versus pull-out displacement plots of different coated fabric samples

zero. This indicates that the static coefficient of friction was increased by the coatings. However, the dynamic coefficient of friction was comparatively much lower. This differs from the previous research on coated aramid fabrics such as Twaron® and Kevlar®, where the initial peak in the pull-out force was followed by a gradient close to 45° [5, 7]. This could be due to the differences in the coating materials used in the studies. Moreover, UHMWPEs have inherently low frictional properties as well as low surface energies [8]. Therefore, it is likely that the coating materials did not bond to the UHMWPE fibres/yarns as they would to an aramid fibre/yarn surface, thereby compromising the dynamic frictional behaviour. Kim et al. [7] reported that the inter-yarn friction was improved due to the formation of polymeric anchors on fibre surfaces due to polymeric adhesive fracture which caused yarn translation difficult. Therefore, poor adhesion of UHMWPE surfaces could minimise this effect, thereby leading to poor dynamic frictional coefficient. However, the static frictional coefficient is highly improved since the coating may act as a bond, initially holding the orthogonal yarns together.

3.2 Residual Velocity Distribution and Specific Energy Absorption Behaviour

Residual velocity versus impact velocity distribution of uncoated and coated targets is shown in Fig. 2.

It can be observed that the uncoated UHMWPE targets exhibited the highest residual velocities. All the coated targets exhibited lower residual velocities than the

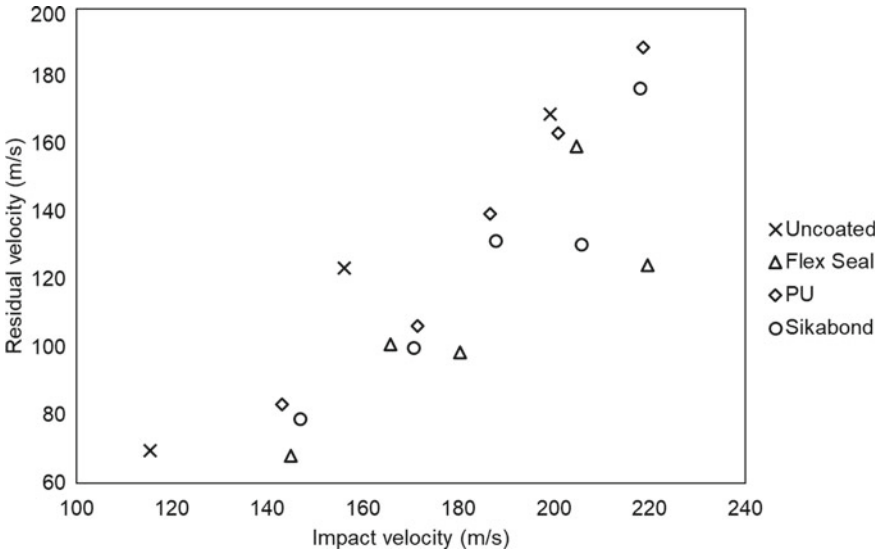

Fig. 2 Residual velocity versus impact velocity plots of uncoated and coated targets

neat counterpart. High residual velocities indicate low energy absorption by a target since the absorbed energy is considered to be the difference between the initial and residual kinetic energies of the projectile. Therefore, this indicates that the coating of UHMWPE fabrics increased the energy absorption of the fabrics, regardless of the coating material. Since the areal density introduced to the targets by coating is also important in applications such as armour, specific energy absorption (SEA) is also studied. Specific energy absorbed versus impact velocity plots of uncoated and coated targets are shown in Fig. 3.

It can be observed that the SEA of the rubber (Flexseal)-coated samples is higher than all the other samples. Compared to the neat sample, SEA of the rubber-coated sample increased with increasing impact velocities. Interestingly, polyurethane-coated targets showed a decreasing trend of SEA versus impact velocity for impact velocities above ~ 171 m/s. SikaBond-coated targets also showed an increasing trend with the exception of projectile impact at the highest impact velocity (218 m/s). All the coated samples generally increased the energy absorption capacity of the UHMWPE fabrics, even after the additional weight increment was considered in the calculations.

3.3 Failure Mechanism

[13] reported that the failure mechanism of plain-woven UHMWPE fabrics is purely wedging-through, without any yarn failure. This is shown in Fig. 4. Yarn/fibre failure

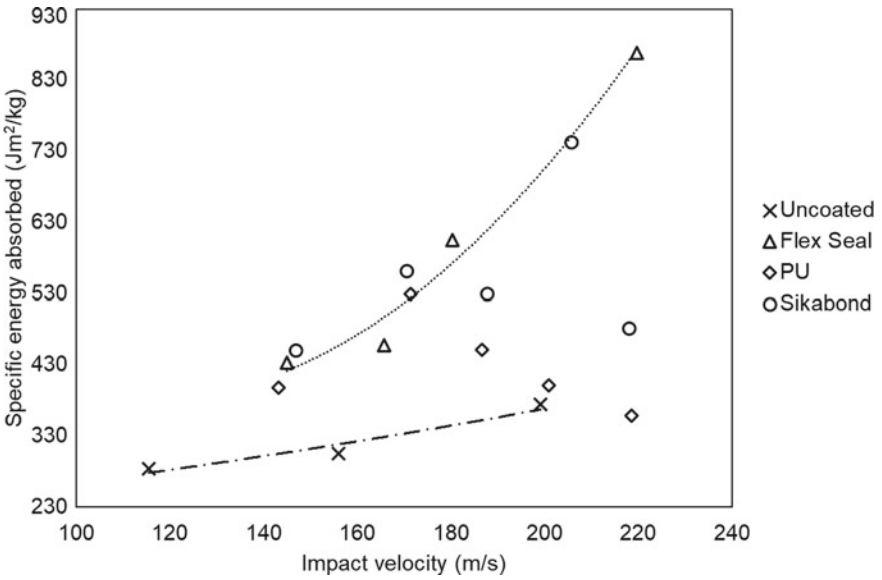

Fig. 3 Specific energy absorbed versus impact velocity plots of uncoated and coated targets

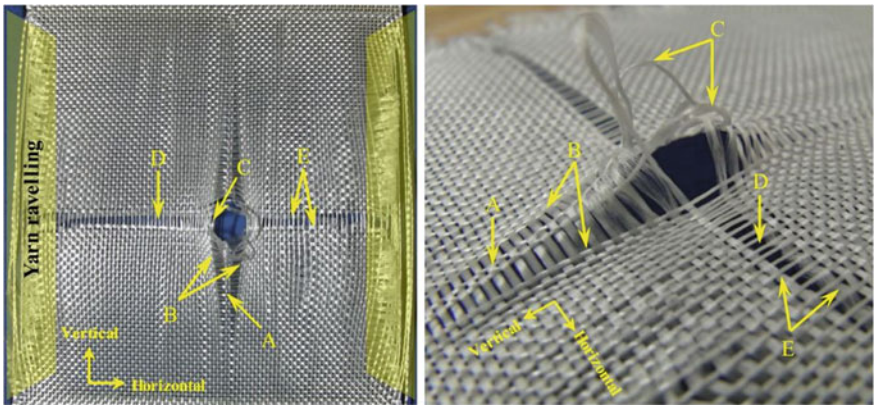

Fig. 4 Failure behaviour of a 1-ply uncoated target [13]

occurs due to inter-molecular chain slippage at low velocities (strain rates) and by molecular chain scission at high velocities (strain rates) [12]. Consequently, yarn/fibre failure is one of the most prominent modes of energy absorption by a fabric target. As a result, when a fabric target is perforated purely by the wedge-through mechanism, significantly lesser energy is absorbed by the target, compared to a target which fails through a combination of wedge-through effect and yarn failure.

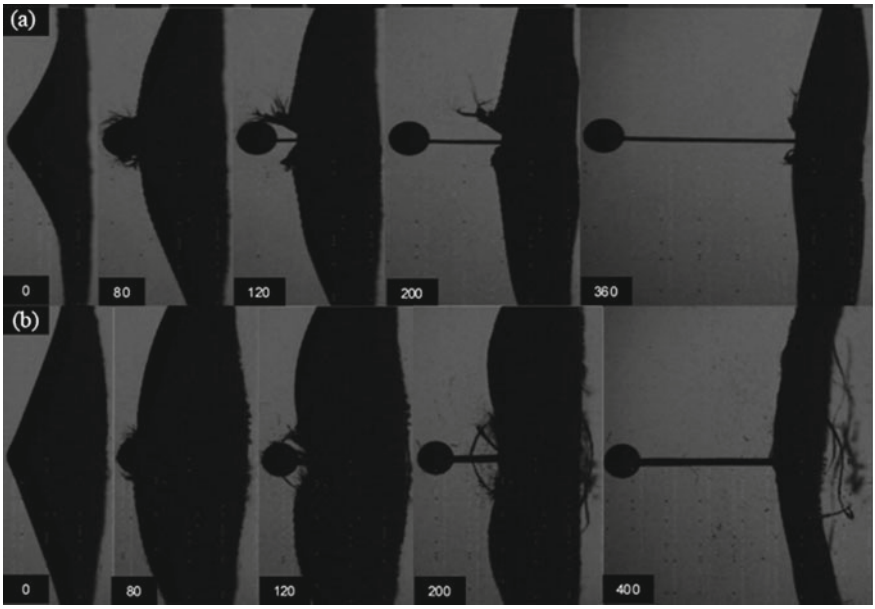

Fig. 5 High-speed camera sequential captures of projectile impacts on rubber-coated fabrics at **a** 205 m/s and **b** 220 m/s velocities

Figure 5 shows high-speed camera sequential captures of projectile impacts on rubber-coated fabrics at 205 and 220 m/s impact velocities.

It can be observed that some yarns fail during target perforation. This is further evident from the post-impact target observation, shown in Figs. 6 and 7.

A close-up view of the rubber-coated target strike face subjected to impact at 220 m/s shown in Fig. 7 where it is shown that the clamped vertical yarns failed during perforation. Similarly, yarn failure was observed in all coated targets in contrast to the neat targets. Consequently, coated targets absorbed higher impact energies than the neat counterparts. The failure mechanism changed from a pure wedge-through perforation to a combination of wedge-through effect and yarn failure due to coating application. This suggests that the high strengths of UHMWPE yarns were more effectively used in the coated targets as opposed to neat targets where the projectile slipped across the target.

In this study, a limited number of coatings and their effects were discussed. In addition to the factors considered herein, the effects on performance from other factors such as number of coatings, ambient temperature and fatigue have not been considered. Finally, the increase of stiffness of the system due to coatings has also not been considered.

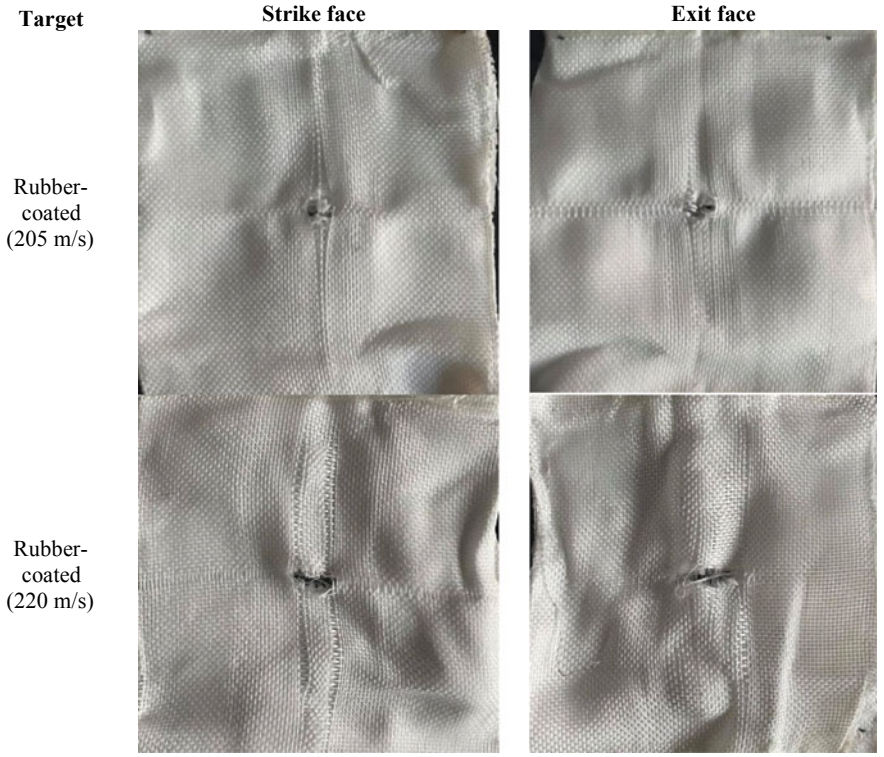

Fig. 6 Post-impact target strike face and exit face of rubber-coated samples

Fig. 7 A close-up view of the rubber-coated target strike face subjected to impact at 220 m/s

4 Conclusion

Based on the results from the present work, the following conclusions can be drawn.

- Peak pull-out load was significantly increased by coating application, thereby indicating inter-yarn friction improvement and higher impact resistance. Particularly, the peak pull-out load of rubber-coated fabrics was increased by 9800%.
- All coated fabrics exhibited higher energy absorption upon projectile impact than the neat counterparts. The rubber-coated sample exhibited an 84% increase in specific energy absorption compared to the neat counterpart.
- Failure mechanism changed from a purely wedge-through mechanism perforation to a combination of yarn failure and wedge-through perforation due to the application of the coating.

References

1. Asemani SS, Liaghat G, Ahmadi H, Anani Y, Khodadadi A, Charandabi SC (2021) The experimental and numerical analysis of the ballistic performance of elastomer matrix Kevlar composites. Polym Testing 102:107311. https://doi.org/10.1016/j.polymertesting.2021.107311
2. DuPont (2020) Kevlar aramid fiber. In: Kevlar Aramid Fiber® technical guide. https://doi.org/10.1016/0261-3069(93)90147-n
3. Hazell PJ (2016) Armour: materials, theory, and design
4. Honeywell (2008) Product information sheet honeywell spectra® 2000 fiber the ultimate high-strength, light-weight performer. http://www51.honeywell.com/sm/afc/common/documents/PP_AFC_Honeywell_spectra_fiber_2000_Product_information_sheet.pdf
5. Ignatova AV, Kudryavtsev OA, Zhikharev MV (2020) Influence of surface polymer coating on ballistic impact response of multi-layered fabric composites: Experimental and numerical study. Int J Impact Eng 144:103654. https://doi.org/10.1016/j.ijimpeng.2020.103654
6. Khodadadi A, Liaghat G, Ahmadi H, Bahramian AR, Razmkhah O (2019) Impact response of Kevlar/rubber composite. Compos Sci Technol 184:107880. https://doi.org/10.1016/j.compscitech.2019.107880
7. Kim YH, Sathish Kumar SK, Park Y, Kwon H, Kim CG (2020) High-velocity impact onto a high-frictional fabric treated with adhesive spray coating and shear thickening fluid impregnation. Compos B Eng 185:107742. https://doi.org/10.1016/j.compositesb.2020.107742
8. Oosterom R, Ahmed TJ, Poulis JA, Bersee HEN (2006) Adhesion performance of UHMWPE after different surface modification techniques. Med Eng Phys 28(4):323–330. https://doi.org/10.1016/j.medengphy.2005.07.009
9. Ramakrishna S, Huang Z-M (2016) Biocomposites. In: Reference module in materials science and materials engineering, Apr 2015. https://doi.org/10.1016/B978-0-12-803581-8.00965-6
10. Sanborn B, DiLeonardi AM, Weerasooriya T (2015) Tensile properties of Dyneema SK76 single fibers at multiple loading rates using a direct gripping method. J Dyn Behav Mater 1(1):4–14. https://doi.org/10.1007/s40870-014-0001-3
11. Swift Reponse LLC (2021) Flex seal products. https://flexsealproducts.com/pages/faqs#spray
12. Tan VBC, Zeng XS, Shim VPW (2008) Characterization and constitutive modeling of aramid fibers at high strain rates. Int J Impact Eng 35(11):1303–1313. https://doi.org/10.1016/j.ijimpeng.2007.07.010

13. Wang H, Hazell PJ, Shankar K, Morozov EV, Escobedo JP, Wang C (2017) Effects of fabric folding and thickness on the impact behaviour of multi-ply UHMWPE woven fabrics. J Mater Sci 52(24):13977–13991. https://doi.org/10.1007/s10853-017-1482-y
14. Wang H, Weerasinghe D, Mohotti D, Hazell PJ, Shim VPW, Shankar K, Morozov EV (2021) On the impact response of UHMWPE woven fabrics: experiments and simulations. Int J Mech Sci 204:106574. https://doi.org/10.1016/j.ijmecsci.2021.106574
15. Weerasinghe D, Mohotti D, Anderson J (2019) Incorporation of shear thickening fluid effects into computational modelling of woven fabrics subjected to impact loading: a review. Int J Protect Struct. https://doi.org/10.1177/2041419619889071

Investigation of Mechanical Properties of Borax-Treated *Bambusa vulgaris* (Sri Lankan Bamboo)

R. Vipushnan, M. T. R. Jayasinghe, S. L. Platt, and H. D. Hidallana-Gamage

Abstract Bamboo has become increasingly popular as a sustainable construction material due to its low embodied energy and low carbon footprint in recent times. Bamboo is a strong, lightweight, fast-growing woody grass belonging to the sub family *Bambusoideae* of the family *Poaceae* (*Gramineae*), it has a variety of uses, and its use in construction is long established as a structural material in many regions. Bamboo can also be utilized in culinary and decorative areas as well as a substitute for wood in many industries. Despite these attributes, bamboo is limited in its application due to its limited durability. The application of Borax as preservation treatment for full culm *Bambusa vulgaris* (Sri Lankan Yellow bamboo) was investigated. Comparative average strength values in compression, shear, tension and flat ring flexure are presented for treated and untreated sections obtained from the top and bottom of each culm. Comparison across all four tests showed that mechanical properties can be affected in short term due to preservation treatment since the 7-day immersion needed with Borax may affect the fibres.

Keywords *Bambusa vulgaris* · Embodied energy · Borax treatment · Compressive strength · Shear strength · Flat ring flexure · Tensile strength

1 Introduction

The construction industry has been turning towards the usage of sustainable construction materials in order to minimize the environmental footprint of development. Bamboo, a woody grass belonging to the sub family *Bambusoideae* of the family *Poaceae* (*Gramineae*), is one sustainable construction material with high potential for varied uses.

R. Vipushnan (✉) · M. T. R. Jayasinghe · H. D. Hidallana-Gamage
Department of Civil Engineering, University of Moratuwa, Moratuwa, Sri Lanka
e-mail: rvipushnan@gmail.com

S. L. Platt
Department of Architecture and Civil Engineering, University of Bath, Bath, UK

R. Dissanayake et al. (eds.), *12th International Conference on Structural Engineering and Construction Management*, Lecture Notes in Civil Engineering 266,
https://doi.org/10.1007/978-981-19-2886-4_40

The use of bamboo in construction is long established and still used extensively as a structural material in many regions [1]. Bamboo can also be utilized in culinary and decorative areas. Bamboo is becoming popular as an excellent substitute for wood in paper industries, domestic commodities, cottage industries, board industry and charcoal industries [2]. Laminated bamboo hybrid could be used as an alternative to wood-based composites for furniture manufacturing [3].

Bamboo is strong but lightweight and is therefore an extremely versatile building material. Bamboo forest biomass stores a large quantity of carbon with nearly half of the total biomass being carbon. It has great potential in removing heavy metal ions as a biological absorbent. Bamboo has high potential in carbon sequestration, controlling soil erosion, land rehabilitation and water conservation [4]. The increasing need for sustainable building construction and the use of natural local materials have made bamboo a popular material. Bamboo is a strong, lightweight, fast-growing material which also has a very low embodied energy [5].

The durability of bamboo limits its application and therefore needs to be treated to ensure its long-term usage. Untreated bamboo has a lower lifetime if in contact with the atmosphere and soil. Good detailed design such as keeping the culms away from the ground and under cover will help to increase its lifespan [6]. Stone foundations separating bamboo from the soil and large overhangs on roofs are a common detailing design practice. Traditional methods of bamboo treatment such as white washing and smoking are not expensive although long-term durability is still not ensured by them [7]. Heat treatment at 180 °C and cooling in sunflower oil are expected to improve the compressive strength and durability of bamboo [8]. Mercerization treatment does not reduce the mechanical performance of bamboo fibres which are to be used as reinforcement in green polymeric composites [9]. When specifying bamboo, it is important to ensure that it comes from a sustainable source and is harvested, procured and visually graded by a reputable and experienced organization [5]. It is also possible to undertake bamboo plantations in large scale so that sustainable harvesting practices can be implemented.

In order to address the durability issues, many preservation methods are available. However, the treatment with Borax stands clear as a more environmentally friendly approach. Since the bamboo varieties grown differ widely from country to country, it is useful to have studies carried out on country specific varieties. In this context, this study has concentrated on one of the commonly available varieties in Sri Lanka, *Bambusa vulgaris*, or Sri Lankan yellow bamboo.

The main objective of this detailed study is to determine the short-term effects of commonly adopted type of Borax treatment on the mechanical properties of *B. vulgaris.*

In order to achieve the above objective, the following methodology is adopted:

1. The commonly used method of Borax-based preservation method lasting about 7 days of immersion is adopted for treatment for typical samples.
2. The sample with and without treatment have been tested for important mechanical properties, and the results have been compared to determine the effects.

2 Preservation Treatment with Borax

Preservation treatment ensures the durability of harvested bamboo by removing the nourishment that attracts insects and other pests that feed on bamboo [10]. Treatment of harvested bamboo could be broadly categorized into two types, oil- and water-based. Oil-based chemicals penetrate quicker and deeper than water but the ingredients are usually more expensive and may cause adverse health effects. The second type, water-based chemicals, is produced by dissolving Borax, boron, copper or chrome containing salts in water. Among these, Borax treatment is considered most eco-friendly and most commonly used in the treatment of fresh bamboo poles [11].

Fattah [12] found that bamboo betung without bark which underwent Borax preservation treatment showed a maximum tensile strength of 170.6 N/mm^2 for 24 h immersion duration and mentions that tensile strength begins to reduce once immersion duration increases beyond 24 h. The effectiveness of the preservation treatment process increases with the duration of immersion in the preservation treatment chemical in case of wood. However, extended immersion will lead to a lower strength than the untreated wood before immersion. This is because the cells become more tenuous and finally unravel when the wood is immersed for a longer term [13]. The above phenomenon could be expected in the case of bamboo as well, since the main constituent components of both bamboo and wood are almost same [12]. Tensile strength of bamboo decreases with increasing water content [14]. Conversely, Gauss [15] found that both 7- and 10-day immersions did not adversely affect the mechanical strengths when treated with disodium octaborate tetrahydrate (DOT) or chromated copper borate (CCB). Handana [16] states that 30% to 50% Borax in the preservative solution is sufficient to provide significant increase in strength for compressive strength, tensile strength and bending strength of bamboo specimen.

Selection of the suitable treatment technique depends on the size of bamboo, time allowed and labour availability.

Horizontal dip diffusion is a method suitable for industrial treatment plants where large numbers of poles are to be treated at once. In this method, the poles are drilled thorough both ends and immersed into tanks filled with the Borax solution. The suggested curing period for cold water solution is 1 week, and for hot water solutions, the curing period reduces to 3 days.

Vertical sap diffusion is a smaller scale treatment method. The bamboo poles are kept vertically by forming a tripod among themselves or by placing slightly inclined along a tree. In this method, the poles are drilled at only one end and filled with Borax solution.

Treatment in trough is a method which is suitable for short bamboo. The bamboo strips are immersed in a trough which is filled with Borax solution and heated from below. Heating 2–3 h at 70 °C is enough to treat the strips.

Boucherie method can be done within one day of cutting the bamboo. The cut bamboo is placed in a bucket filled with Borax solution with leaves and shoots

intact so that the transpiration pulls the solution upwards. However, this may not be adequate for industrial usage.

Under modified Boucherie method, the pressure enabling the diffusion of the treatment solution is created artificially using pumps. Treated poles are stored without direct exposure to atmosphere under a roof without placing directly on soil. If necessary, the treated poles must be bleached for aesthetic appearance.

3 Experimental Methodology

A total of 58 culms were tested, out of which 29 were classified as bottom culms and the rest were classified as top culms. Among them, 8 culms were selected to undergo treatment, namely 4 bottom culms and 4 top culms. This investigation considers the bottoms and tops to be representative of their respective groups. All culm sections were marked for identification as well as mapping out each node and internode, as seen in Fig. 1. Culms that underwent treatment were cut in half for treatment, thereby providing four groups *bottom–bottom* (BB), *bottom–top* (BT), *top–bottom* (TB) and *top–top* (TT) sections. For example, if a sample is taken from the lower part of a bottom culm, it is identified as bottom–bottom. Samples from culms which did not undergo treatment were also classified into the above four groups according to their positions.

3.1 Preservation Treatment of Poles

The horizontal dip diffusion method was selected for this investigation due to laboratory space and tank size limitations. The 16 Sri Lankan Yellow bamboo culm

Fig. 1 Samples being marked on a pole prior to cutting

sections were perforated at their nodes with rebar to permit the preservation solution to penetrate the inner layers of the culm.

Borax treatment was selected as it is considered relatively eco-friendly and least toxic compared to other preservation treatment methods. Some of the guidelines indicate that the use of 5% Borax solution can bring about good results with respect to durability [11]. Hence, a total of 120 L of 5% Borax solution was prepared which comprised of the following:

- Borax powder (Borax Decahydrate) 2.5 kg per 100 L of solution
- Boric acid 2.5 kg per 100 L of solution.

The culms were immersed in the treatment solution for 7 days. Concrete cubes were placed on top of culms to prevent them floating up. Replacement of sap in bamboo fibres with Borax solution was apparent due to the solution turning dark at the end of treatment period as seen in Figs. 2 and 3. All culm sections were dried directly under the sun for 4 h immediately at the end of the treatment. Then onwards, they were allowed to dry indoors for a period of 4 weeks till testing.

Fig. 2 Preservation treatment of poles (day 1)

Fig. 3 Preservation treatment of poles (day 7)

Table 1 Distribution of samples relative to their position

	Bottom	Middle		Top	
Tests	Bottom–bottom	Bottom–top	Top–bottom	Top–top	Total tests
Compressive strength	29	28	29	29	115
Shear strength	29	28	29	29	115
Flat ring flexure	29	28	29	29	115
Tensile strength	29	29	29	29	116
Total tests	116	113	116	116	461

Fig. 4 A set of samples ready for testing

3.2 Preparation of Samples

Test samples were prepared in accordance with ISO 22157:2019. In order to obtain representative values for this particular species of bamboo (*B. vulgaris*), samples were obtained from *bottom* and *top* of culm sections for each test. Hence, a total of 8 samples were tested from each culm. The full distribution of the samples relative to their location is provided in Table 1. A set of cut samples prepared for testing is shown in Fig. 4.

3.3 Testing

Tests were conducted to determine four different mechanical properties that would be important when it is used as a structural material. The tested parameters are as follows.

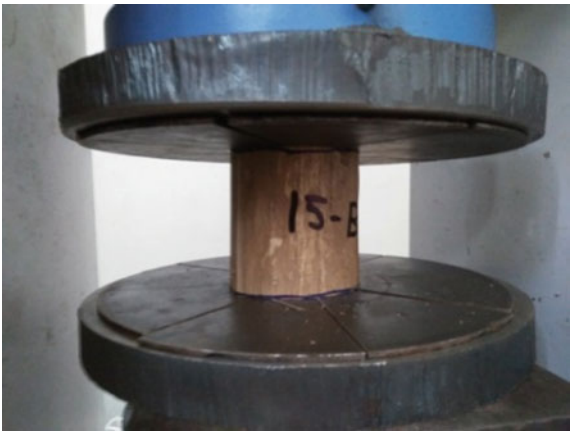

Fig. 5 Compressive strength testing with standard compression machine

3.3.1 Compressive Strength Testing

Compressive strength was tested using the ADR Touch 2000 standard compression machine. Test samples were prepared according to ISO 22157:2019. Compressive strength was calculated using average cross-sectional area of the samples according ISO 22157:2019 [17]. Rate of loading of 0.2 kN/s was maintained for compressive strength testing (Fig. 5).

3.3.2 Shear Strength Testing

Shear strength was tested using the ADR Touch 2000 standard compression machine. Test samples were prepared according to ISO 22157:2019. Shear strength was calculated using average area of shearing planes of the samples according ISO 22157:2019 [17] (Fig. 6).

3.3.3 Flat Ring Flexure Testing

Transverse tensile strength represented by modulus of rupture was evaluated via the four-point flat ring flexure test. Flat ring flexure was carried out using the ADR Touch 2000 standard compression machine as seen in Fig. 7. Flat ring flexure (FRF) test samples were prepared with height of 0.2D–0.3D based on the work of Virgo [18] on the test as shown in Fig. 8. All samples were tested for four-point bending. Bending strength and modulus of rupture were calculated using the equations developed for the four-point bending flat ring flexure test.

Fig. 6 Shear strength testing with standard compression machine

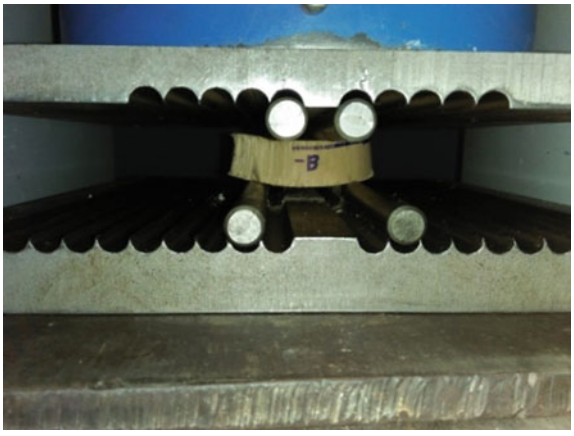

Fig. 7 Flat ring flexure testing with standard compression machine

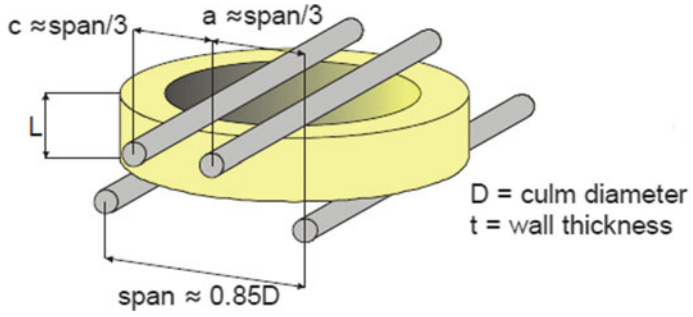

Fig. 8 Four-point bending flat ring flexure test geometry [18]

Fig. 9 Tensile testing with Hounsfield Tensometer

3.3.4 Tensile Testing

Tensile testing was carried out using the Hounsfield Tensometer. Test samples were prepared in accordance with ISO 22157:2019. Tensile strength of the samples was calculated using the average cross-sectional area of the respective samples according to ISO 22157:2019 [17] (Fig. 9).

4 Results

Test results from bottom–bottom samples have been considered to be representative of bottom of culms. Strength values representative of the middle of culms has been considered the combination of values from bottom–top samples and top–bottom samples. The top–top values have been considered to be representative of the top part of culms. The treated samples are identified as “T” and non-treated as “NT” in the below tables.

4.1 Compressive Strength

Treated poles showed slightly lower compressive strength values compared to untreated poles. Table 2 provides a summary of the average compressive strength results in N/mm^2 with the coefficient of variation (CoV = standard deviation divided by the mean value).

The results indicate that the treatment of samples could marginally affect the compressive strength. There could be two reasons for this. Both treated and untreated samples had the average moisture content within the preferred limit of 12–19% [5]. However, the average moisture content of the treated samples was 1.1% higher than the untreated samples. This higher moisture content at the time of testing could be one reason. The other is that for the Borax-based treatment, bamboo samples have been immersed in the solution for 7 days. This also could have some effect on the fibres and hence could lead to a lower strength.

Table 2 Summary of observed average compressive strengths and respective coefficient of variations

Bottom–bottom			**Bottom–top**		**Top–bottom**		**Top–top**	
T		***NT***	***T***	***NT***	***T***	***NT***	***T***	***NT***
N/mm^2	38.3	38.3	39.0	38.6	39.3	43.9	45.9	47.0
CoV	0.48	0.25	0.54	0.26	0.35	0.22	0.30	0.21
Bottom			**Middle**				**Top**	
T		***NT***	***T***		***NT***		***T***	***NT***
N/mm^2	38.3	38.3	39.1		41.3		45.9	47.0
CoV	0.48	0.25	0.42		0.25		0.3	0.21
Overall average								
Treated (T)					***Not Treated (NT)***			
N/mm^2	40.6				42.0			
CoV	0.38				0.25			

4.2 Shear Strength

Most of the treated pole samples showed lower shear strength values compared to untreated poles as seen in Table 3. The difference in average moisture content between treated and untreated shear strength test samples was 1.7%.

4.3 Flat Ring Flexure

It could be observed from Table 4 that treated poles showed significantly lower bending strength values compared to untreated poles. Modulus of rupture also showed a pattern similar to bending strength (Table 5). Flat ring flexure samples that underwent treatment averaged 1.0% higher in moisture content compared to untreated test samples. Hence, this significant reduction may not be due to slightly higher moisture content in the treated samples. As can be seen, keeping the samples immersed in the Borax solution for nearly one week has affected the bending strength and modulus of rupture to a greater extent than the compressive and shear strengths.

4.4 Tensile Strength

Values displayed in Table 6 summarize the observed tensile strengths for both treated and untreated samples. Tensile strength test samples showed a relatively small difference of 0.6% in average moisture content between treated and untreated samples. This could be due to the samples prepared for the test having a higher surface area

Table 3 Summary of observed average shear strengths and respective coefficient of variations

Bottom–bottom			**Bottom–top**		**Top–bottom**		**Top–top**	
T		***NT***	***T***	***NT***	***T***	***NT***	***T***	***NT***
N/mm^2	6.6	7.8	7.6	7.9	6.4	9.8	9.7	9.4
CoV	0.50	0.29	0.46	0.22	0.29	0.28	0.33	0.25
Bottom			**Middle**				**Top**	
T		***NT***	***T***		***NT***		***T***	***NT***
N/mm^2	6.6	7.8	7.0		8.9		9.7	9.4
CoV	0.50	0.29	0.38		0.28		0.33	0.25
Overall average								
Treated (T)					***Not Treated (NT)***			
N/mm^2	7.6				8.7			
CoV	0.40				0.28			

to volume ratio. Hence, the drop in strength could be due to fibres being affected by the treatment process.

On the basis of all these results, it can be stated that the prolonged immersion time of 7 days when Borax treatment is carried out at normal temperatures could have some effect on the mechanical properties of the samples. Since bamboo will be used for its applications immediately after the treatment, determination of the effect on mechanical properties will be important. Despite giving lower values, Borax treatment can still be considered positively since with the treatment, the deterioration of bamboo will be arrested to a great deal, and with the drying of bamboo with time, it is expected that the use of short term-based mechanical properties would be a conservative approach.

5 Conclusions

In order to improve the long-term durability of bamboo, it is necessary to undertake appropriate treatment. When more environmentally friendly Borax treatment is used for preservation, it is shown with a detailed experimental programme that the important mechanical properties can be affected to a variable degree. It is shown that the bending strength, modulus of rupture in four-point bending flat ring flexure and the tensile strength properties can be affected to a greater extent. The moisture content of the treated samples can be slightly higher than the untreated samples. However, it is argued that this significant drop in properties could not be due to this slightly higher moisture content, but could be due to fibres being affected due to prolonged immersion that is needed for the Borax treatment carried out under atmospheric temperatures.

Table 4 Summary of observed average bending strengths as determined from the FRF test and respective coefficient of variations

Bottom–bottom			**Bottom–top**		**Top–bottom**		**Top–top**	
T		***NT***	***T***	***NT***	***T***	***NT***	***T***	***NT***
N/mm^2	48.2	60.0	40.3	68.2	49.8	76.2	36.8	70.4
CoV	0.24	0.37	0.12	0.30	0.31	0.40	0.38	0.35
Bottom			**Middle**				**Top**	
T		***NT***	***T***		***NT***		***T***	***NT***
N/mm^2	48.2	60.0	44.4		72.4		36.8	70.4
CoV	0.24	0.37	0.24		0.36		0.38	0.35
Overall average								
Treated (T)					***Not Treated (NT)***			
N/mm^2	43.4				68.8			
CoV	0.27				0.37			

Table 5 Summary of observed average modulus of rupture values as determined from the FRF test and respective coefficient of variations

Bottom–bottom			**Bottom–top**		**Top–bottom**		**Top–top**	
T		***NT***	***T***	***NT***	***T***	***NT***	***T***	***NT***
N/mm^2	12.0	15.0	10.1	17.1	12.4	19.1	9.2	17.6
CoV	0.25	0.37	0.12	0.30	0.31	0.41	0.39	0.36
Bottom			**Middle**				**Top**	
T		***NT***	***T***		***NT***		***T***	***NT***
N/mm^2	12.0	15.0	11.1		18.1		9.2	17.6
CoV	0.25	0.37	0.24		0.37		0.39	0.36
Overall average								
Treated (T)					***Not Treated (NT)***			
N/mm^2	10.8				17.2			
CoV	0.27				0.37			

Table 6 Summary of observed average tensile strengths and respective coefficient of variations

Bottom–bottom			**Bottom–top**		**Top–bottom**		**Top–top**	
T		***NT***	***T***	***NT***	***T***	***NT***	***T***	***NT***
N/mm^2	84.3	86.9	82.2	100.7	94.7	113.9	110.2	132.0
CoV	0.46	0.30	0.53	0.24	0.29	0.31	0.32	0.40
Bottom			**Middle**				**Top**	
T		***NT***	***T***		***NT***		***T***	***NT***
N/mm^2	84.3	86.9	88.4		107.3		110.2	132.0
CoV	0.46	0.30	0.39		0.29		0.32	0.40
Overall average								
Treated (T)					***Not Treated (NT)***			
N/mm^2	92.8				108.4			
CoV	0.38				0.37			

In practice, treated bamboo could be used shortly after the treatment. Therefore, it is useful to assess the effect of preservation treatment and to use the mechanical properties of bamboo after treatment for applications. Since the treated bamboo is expected to retain the strength over a longer period due to improved durability, the reduction in strength due to treatment methods undertaken can still be taken positively. Hence, the properties established with this detailed experimental study will be of significant use for applications involving the commonly available variety in Sri Lanka, *B. vulgaris*.

Acknowledgements The authors wish to thank the Head and other academic staff of the Department of Civil Engineering, University of Moratuwa for their support and valuable comments towards

the research work. We also wish to appreciate the support of the staff of Structural testing laboratory, Mechanics of materials laboratory and Machine workshop of the Department of Civil Engineering and the Die and mould centre of the Department of Mechanical Engineering of University of Moratuwa. Authors also thank Industrial Development Board, Katubedda for the opportunity to participate in the bamboo preservation workshop organized.

References

1. Mera F, Xu C (2014) Plantation management and bamboo resource economics in China. Cienc Tecn 7(1):1–12
2. Lobovikov M, Paudel S, Piazza M, Ren H, Wu J (2007) World bamboo resources. Food and Adriculture Organization of the United Nations, Rome
3. Suhaily S, Islam M, Asniza M, Rizal S, Khalil H (2020) Physical, mechanical and morphological properties of laminated bamboo hybrid composite: a potential raw material for furniture manufacturing. Materials Research Express
4. Yasin I, Priyanto A (2018) Analysis of bamboo mechanical properties as construction eco-friendly materials to minimizing global warming effect. In: IOP conference series: materials science and engineering. IOP Publishing
5. Kaminski S, Lawrence A, Trujillo D, Feltham I, López L (2016) Structural use of bamboo: part 3: design values. Structural Engineer
6. Janssen J (1995) Building with bamboo, a handbook, 2nd edn. Intermediate Technology Publications, London, UK
7. Davies C, Walker P (2008) Bamboo connections. Department of Architecture and Civil Engineering
8. Bui Q, Grillet A, Tran H (2017) A bamboo treatment procedure: effects on the durability and mechanical performance. Sustainability
9. Costa M, Melo S, Santos J, Araújoa E, Cunha G, Deus E, Schmittb N (2017) Influence of physical and chemical treatments on the mechanical properties of bamboo fibers. In: 3rd international conference on natural fibers: advanced materials for a greener world, ICNF2017, 21–23 June 2017, Braga, Portugal. Procedia Engineering, Braga, pp 457–464
10. United Nations Industrial Development Organization (2012) Bamboo training manual 1: bamboo harvesting and preservation. United Nations Industrial Development Organization
11. Stamm J, Tesfaye M, Girma H (2014) Construction manual with bamboo. African Bamboo, Addis Ababa
12. Fattah AR, Prinindya KN, Ardhyananta H (2014) The effect of chemical substance and immersion time to tensile strength of bamboo betung (dendrocalamus asper) as chemical preservation treatment. IPTEK J Proc Ser 1:119–124. eISSN: 2354-6026
13. Suranto Y (2002) Pengawetan Kayu Bahan dan Metode. Penerbit Kanisius, Yogyakarta
14. Janssen J (1980) The mechanical properties of bamboo used in construction. In: Proceeding of workshop held in Singapore. Singapore
15. Gauss C, Harries K, Kadivar M, Akinbade Y, Savastano H (2020) Quality assessment and mechanical characterization of preservative-treated Moso bamboo (*P. edulis*). Euro J Wood Wood Products:257–270
16. Handana M, Surbakti B, Karolina R (2020) The effect of borax solution as preservative to the mechanical properties of bamboo. Int J Sustain Constr Eng Technol:79–88

17. ISO (2019) ISO 22157: 2019 Bamboo structures—determination of physical and mechanical properties of bamboo culms—test methods. International Standards Organisation, Switzerland
18. Virgo J, Garcia J, Moran R, Harries K, Platt S (2018) Flat ring flexure test for full-culm bamboo. In: Non-conventional materials and technologies. Materials Research Forum LLC, pp 349–358

Production of Bricks Using Spent Diatomaceous Earth Used in Brewing Industry

Rumesh Nanayakkara and Chamila Gunathilaka

Abstract In breweries, diatomaceous earth (DE) is used as a filter material. Spent diatomaceous earth (SDE), as an industrial waste, is mainly generated once this DE pores are filled with impurities generated from brewing industries. After the final filtering process, this spent DE is disposed into dumping areas leads to environmental pollution. Therefore, as a remedy for that problem, SDE can be adulterate with clay to produce bricks. Mixing clay with SDE leads to an increase in the quality of the bricks. Also, the incorporation of SDE for brick production can reduce the adverse effects on the environment by reducing the quantity of clay excavated and discharged SDE. This study was conducted to analyze the suitability of using SDE as a secondary raw material for brick production. The chemical characteristics of SDE were analyzed using both XRF and TGA tests. Bricks containing 0, 5, 10, and 15 wt% of SDE were sun-dried and fired at 950 °C for 6 h with suitable temperature ramp. The obtained results reveal that compressive and bending strengths were increased with increasing the SDE weight percentage. Highest compressive strength (4.78 MPa) and bending strength (0.57 MPa) were recorded for the sample prepared with 15 wt% of SDE. Furthermore, the addition of SDE is worth as no significant differences in physical properties are observed. To produce SDE incorporated bricks on a large scale, further research and development by considering, the technical, economic, and environmental aspects of SDE are recommended.

Keywords Spent diatomaceous earth · Clay · Bricks · Compressive strength · Firing temperature

R. Nanayakkara · C. Gunathilaka
Department of Chemical and Process Engineering, Faculty of Engineering, University of Peradeniya, Peradeniya 20400, Sri Lanka

C. Gunathilaka (✉)
Department of Nano Science Technology, Faculty of Technology, WUSL, Kuliyapitiya 60200, Sri Lanka
e-mail: chamila@wyb.ac.lk; chamilag@pdn.ac.lk

R. Dissanayake et al. (eds.), *12th International Conference on Structural Engineering and Construction Management*, Lecture Notes in Civil Engineering 266,
https://doi.org/10.1007/978-981-19-2886-4_41

1 Introduction

Globally, the generation of waste materials and by-products from the industries has become a major problem to the environment and society. Therefore, the scientific communities are doing some research to reduce the generation of those products or to reuse or recycle the generated wastes. Also, the government and respective authorities have been implemented several regulations behind the discharging of wastes to protect the environment and society. Therefore, all industries try to reduce their waste generation or reuse those waste for other purposes [1]. In breweries, spent diatomaceous earth is generated as a waste, and they are looking for an ecofriendly way to manage them.

Diatomaceous earth is obtained from deposits that were formed by sedimentation of the fossilized skeletons of unicellular marine algae called diatoms that are having siliceous skeletons associated with clay minerals and quartz [2, 3]. Among the several reserves of diatomites, the world's largest reserves are located in the USA and China. World production of DE in 2013 was 2.3 MT, where the USA accounting for 33%, China for 18%, Denmark for 14%, and Peru for 5.3%. Small amounts of diatomaceous earth are obtained in other 25 countries [3]. As diatomaceous earth which is known as Kieselguhr is a non-metallic, soft, friable, fine-grained, and silicious sedimentary rock, it can be used as a filter medium to separate very fine particles. Diatomaceous earth is suitable for filtering water, juice, wine, spirits, syrups, and gelatin [2].

Diatom structure is quite complex as it contains lots of fine pores and channels which help the material to maintain a low specific weight, low heat conduction, high specific surface area, and high absorption capacity [2]. Diatomaceous earth is useful for insulations as it contains silica-rich small particles with a highly porous structure. The organic waste mixed with SDE can help to reduce the fuel consumption during the firing process and to decrease the weight of the brick by increasing the porosity inside the brick. Also, SDE contains silica aluminate ($SiO_2.Al_2O_3$) which changes into different crystal and glass phases during the firing of bricks. That contributes by reducing the firing temperature required to complete the firing process of bricks by acting as fluxes [1]. Therefore, SDE can be used to make lightweight calcium silicate bricks with good thermal insulating properties [4]. There are records found on the usage of diatoms in the construction of ancient Egyptian buildings, mixed with mud, sand, and water [2].

As mentioned above, spent diatomaceous earth is mainly generated as waste from the brewing industry because the brewery industries globally produce 189.05 billion liters of beer annually [5]. In the general process of brewing, initially, rice and malted barley, which are used as raw materials, are grounded and then transferred for the mashing. Then wort, the aqueous form, separated from the grains and solids called bagasse using lauter tun. Subsequently, the wort is boiled with hops and other ingredients. Before the fermentation, clarified wort is cooled to the temperature where the yeast can be added and aerated. After the fermentation, solid particles are separated by centrifuge and filtered using diatomaceous earth, also known as Kieselguhr is used for further filtrations [4]. Many types of research have been conducted about utilizing

spent diatomaceous earth. Some of them are focused on using spent diatomaceous earth (SDE) for brick production.

Kieselguhr, generated as waste in breweries, is currently deposited in landfills due to the production of large quantities and the lack of any alternatives to reuse or to make a value-added product. SDE should safely deposit into landfills because of its toxicity after use. Though the SDE can be used as animal feed, because of its high cellulose and hemicellulose content, it can only be fed to ruminants. One of the possibilities for the disposal of diatomite earth is to use them to increase the porosity in brick [6].

Disposing SDE into landfills is not economically viable for the industry and has several negative effects on the environment including land degradation, inland water pollution, loss of agricultural lands, deforestation, air pollution, and loss of biodiversity [2]. Using spent diatomaceous earth to produce bricks has several benefits such as reducing the waste disposal costs and conserving the environment. Also, the high water content in SDE saves the amount of water required for the brick production process. Instead of using the typical synthetic pore-forming material (expanded polystyrene), which has regulatory limits on effluent gaseous emission, this by-product offers a practical and affordable option to reduce the bulk density of ceramic bricks [2]. Therefore, if we can minimize the usage of clay for brick production by replacing some percentage of clay with an alternative material such as SDE, the environmental impact can be reduced to a considerable level.

It was found from the literature that the SDE can be directly applied in the agricultural lands as a soil conditioner, uses as a raw material in the construction industry (concrete and brick production), as an ingredient in composting, or as a raw material for biofilter production. A preliminary study reveals that removing water from SDE is beneficial in ease storage and reduction of the odor problem. However, this process can be costly expensive to the brewing industry. Thus, DE regeneration for the brewing industry is unlikely to be a viable option in the current situation. Recycling SDE directly into the agricultural, construction, and brick production industries seems feasible, environmentally friendly, and economically viable. Replacing the type of filter and filter aids used are unlikely to be worth it in economic aspects. In the current study, considering various factors including time, energy, resources, and total cost, etc., the production of bricks using waste DE, SDE, (as it is and dry form) is identified as the most convenient, viable option. In this paper, physical property changes of bricks with the addition of SDE, the suitability of reusing SDE as a silica precursor with brick production, physical properties, and chemical components in SDE have been studied.

Fig. 1 Diatomaceous earth [7]

2 Experimental Analysis

2.1 Preparation of the Samples

The SDE was provided by one of the local breweries. It was kept in a container for few hours to sediment. Then it was sundried for three days to remove the remaining moisture content. Clay was collected from a clay pit located in Chilaw (Sri Lanka). Collected clay was mixed with 0%, 5%, 10%, and 15% of dried spent diatomaceous earth (SDE) until the mixture became homogenized. Bricks were prepared as steps shown in Fig. 2.

To measure the moisture content of clay and SDE-wet form, initial sample weight was measured before drying. Then the samples were heated in an oven at 70 °C until their weight remains constant. Subsequently, the weight of the dried samples was measured. Moisture content was calculated by subtracting the weights of the initial samples and dried samples. By considering those results, an adequate amount of water was added to SDE—clay mixture to eliminate defects in the molding step and to ensure adequate plasticity. With no diatomaceous earth, four bricks were made using selected clay. Those bricks were taken as reference bricks and the same properties were measured and compared with different percentages of SDE-clay bricks. The dimensions of the mold were taken as 220 mm × 105 mm × 65 mm which is given by Sri Lankan standards. Bricks that were made previously were dried for two weeks under sunlight. Then dried samples were fired at a rate of 10 °C/min up to 950 °C for 6 h in a muffle kiln (muffle furnace). Then the samples were cooled to room temperature by natural convection inside the muffle kiln.

2.2 Characterization of the Raw Materials and Bricks

Microstructure of SDE was obtained using Hitachi SU6600 Field Emission Scanning Microscope. For the scanning electron microscope (SEM) imaging, sample was mounted onto the sample stub using carbon tapes and images were taken after gold sputter coating for 15 s. In the SDTQ600 thermogravimetric analyzer, moisture

content in SDE was calculated. During the thermogravimetric analysis (TGA), the temperature was varied from ambient to 1000 with the heating rate of 10 °C/min. High purity nitrogen was used as the purge gas. Chemical compositions of SDE were evaluated using X-Ray Fluorescence (XRF) analysis using HORIBA Scientific XGT—5200 X-ray Analytical Microscope. Six different spots per sample were analyzed to obtain chemical compositions. X-ray guide tube (XGT) diameter was set to 100 μm, and X-ray tube voltage was maintained at 50 kV. Also, processing time was set to P4 and live time was set to 300 s.

Compressive strength was determined by applying an incremental load onto the center of the load-bearing surface of a brick until fracture. Average of both load-bearing surfaces were taken to get the area of force applied. Compressive strength was calculated by dividing applied force at brick's fractural point by the average area of load-bearing surfaces, expressed in MPa. Bending strength was determined by a three-point bending strength test with a 5 kN load cell 100 mm as the distance between the points of support and the displacement rate of 10 mm/min.

3 Results and Discussion

3.1 Characterization of SDE (Wet and Dry Foam)

Characterization of wet and dry forms of SDE is mandatory to design proper composition of SDE that should be mixed with soil samples. So TGA, XRF, SEM coupled with energy-dispersive X-ray (EDX) have been carried out.

Thermogravimetric (TG) and differential TG analysis was performed for dry and wet foam SDE. This study was done to calculate the water percentage of both samples which will be needed to estimate the amount of water that should be added to mix the selected soil with different percentages of SDE. It was also found that SDE-wet foam contains 89.32% of water while 28.87% of water remains in the dry foam of SDE. The residue remaining in SDE wet and dry foam are respectively, 4.45% and 65.29% (see Fig. 3 left and right panels).

Scanning electron microscope (SEM) images are taken to analyze to the porous structure of SDE in wet and dry forms. It was obvious to observe the porous nature of both forms (Fig. 4).

EDX was carried out to identify the elemental composition of the dry form of the SDE. As compared to XRF results, EDX analysis provided the composition of elements including low molecular weight elements at three different locations which were to take SEM images of the sample. Results obtained from three locations are summarized in Table 1.

The elemental composition of C, O, Si, and Fe content of the SDE is shown in Table 1. The content of carbon is 61.1% which indicated the amount of organic matter. So, SDE could be act as a fuel during the firing process to fulfill the heating

(a) SDE Drying

(d) Drying

(b) Mixing SDE with Clay

(e) Firing of Bricks

(c) Molding

(f) Fired Bricks

Fig. 2 Brick casting process

requirements. Since the SDE does not contain sulfur, it does not produce SO_2, during the firing.

As seen in Table 2, SiO_2 (95.43%) is the predominant oxide in SDE and Al_2O_3 (aluminum oxide) (2.53%) as second constituent. Fluxing oxides (K_2O) and auxiliary fluxing oxides ($CaO + Fe_2O_3$) [1] are contained in SDE. Firing temperature can be decreased due to those oxides. According to chemical composition, the SDE was suitable as a secondary raw material for brick production.

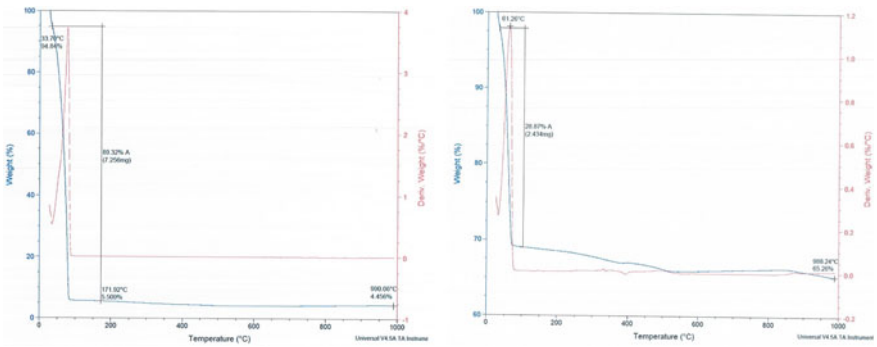

Fig. 3 TGA and DTG studies of wet (left panel) and dry (right panel) foams of SDE

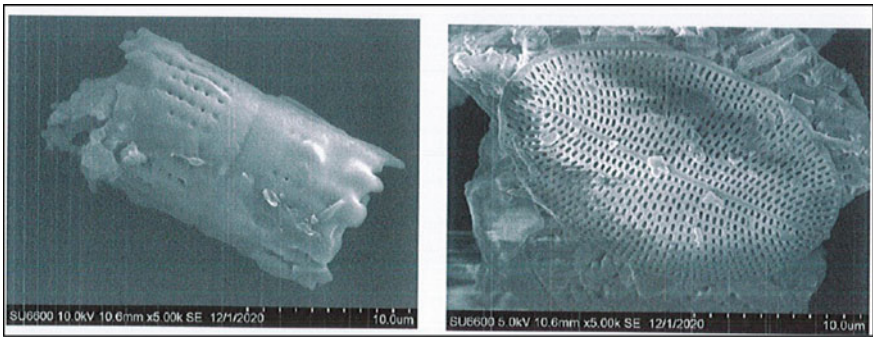

Fig. 4 SEM image of SDE before adsorption

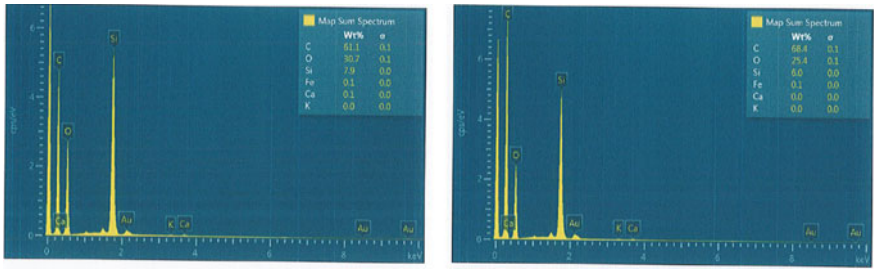

Fig. 5 Energy-dispersive X-ray (EDX) spectrum of SDE dry form

3.2 Chemical Reactions Occurred and Changed of the Composition of Bricks During the Firing

Several processes occur during the firing bricks such as loss of water (surface and chemically combined), mineral decomposition, carbon burnout, quartz inversion,

Table 1 Elemental composition of dry form of the SDE

Element	Site no. 1 (wt%)	Site no. 2 (wt%)
C	61.1	68.4
O	30.7	25.4
Si	7.9	6.0
Fe	0.1	0.1
Ca	0.1	0.0
K	0.0	0.0

Table 2 XRF analysis of SDE (wet form) and oxide composition

Oxide	Mass %
Al_2O_3	2.53
SiO_2	95.43
SO_3	0.28
K_2O	0.25
CaO	0.47
TiO_2	0.13
MnO_2	0.01
Fe_2O_3	1.17
ZnO	0.01

and vitrification. When the firing starts, initially, loosely attached water evaporates around 100 °C [8]. Between 200 and 500 °C, the weight loss can be attributed to the combustion of organic matter of the clay [1]. When the temperature rises further, chemically combined water removes, which is called dehydroxylation occurs in different stages. From 400 to 700 °C, kaolin dehydroxylation occurs by the reaction, $Al_2O_3.2SiO_2.2H_2O$ $Al_2O_3.2SiO_2 + 2H_2O$. Dehydroxylation in montmorillonite contains two steps. The first step is larger compared to the second step, and it occurs from 600 to 800 °C. The second step occurs from 850 to 925 °C. Its reaction is $Al_2O_3.4SiO_2.H_2O$ $Al_2O_3.4SiO_2 + H_2O$. Muscovite mica which can be found as a mineral in clay dehydroxylates close to 700 °C. Some clay types contain additional minerals like pyrite (FeS_2) and limestone ($CaCO_3$). The red color of the bricks was caused by the oxidized iron which is given by the two-stage decomposition of pyrite. First reaction, $FeS_2 + O_2 \rightarrow FeS + SO_2$ occurs at 380 °C and the second reaction, $4FeS + 7\ O_2 \rightarrow 2Fe_2O_3 + 4SO_2$ occurs around 412 °C [8].

Also, $CaCO_3$ decomposes at 800 °C into CaO (lime) and CO_2 [1] which helps to increase the porosity of the brick [9]. With the presence of water, CaO is converted into $Ca(OH)_2$. Finally, it converted to calcium carbonate in the presence of atmospheric carbon dioxide. As a result of these reactions, volume increases and causes the formation of fissures which is called lime blowing [10] which causes further increasing the porosity. Lime and periclase (MgO) which are decomposition products of dolomite transform into portlandite and brucite ($Mg(OH)_2$) in the presence

of water contribute to increasing the porosity of brick. The latter in the presence of carbon dioxide may then become hydromagnesite ($Mg_5(CO_3)_4(OH)_2{\cdot}4H_2O$) [11].

4 Technological Properties of Waste-Clay Mixtures

During the preparation of the SDE-clay mixture, it was difficult to obtain a homogenous mixture when SDE was at its slurry form. Therefore, SDE was sundried before mixing with clay and there is no additional cost involved with the preparation of SDE to the clay since drying of SDE done by natural heat.

When the moisture content is high in the brick, swelling and bloating happen during the firing process which is caused by the expansion of entrapped water. By preventing that situation during the drying process excess moisture remove gradually at a low temperature [12]. But bricks were shrunken after both drying and firing processes in a significant amount due to the loss of mechanically and physically bound water. As seen in Table 3, all three dimensions were reduced concerning the initial mold size. Therefore, when producing bricks, those reductions should be considered in order to have standard dimensions to the final bricks.

According to the properties measure in the Material Laboratory Department of Civil Engineering, University of Peradeniya, the compressive strength of bricks was increased when the SDE percentage was increasing. According to Table 3, incorporating 5% of SDE into the bricks displays 2.75 MPa which increased to 4.73 MPa for 15% incorporation of SDE. This confirmed that the dry form of spent diatomaceous earth has a substantial effect to increase the compressive strength of the bricks prepared with SDE. As mentioned in [1], formation of open porosity results to decrease the compressive strength due to the acting of concentrated stresses on the microscopic defects and irregular shaped pores. However, incorporating higher SDE wt% has been improved the mechanical properties of the bricks. This could be due to the effect of melting capacity (acting as silica precursor) of the SDE which is greater than the effect of the porosity formation in the bricks with the incorporation of SDE. Compressive strength is the most relevant mechanical index for building material. Table 4 shows the minimum Sri Lankan Standardization values of compressive

Table 3 Variation of compressive and bending strength of brick with SDE incorporation percentage

Clay type	SDE % (Wet form)	Length (mm)	Width (mm)	Height (mm)	Breaking load (KN)	Compressive strength (MPa)	Flexural (bending) strength (MPa)
1	0	207	103	57	46	2.20	0.41
	5	208	103	57	56	2.75	0.32
	10	206	104	55	56	2.77	0.42
	15	207	104	58	97	4.73	0.55

Table 4 Bricks' compressive strength according to SLS 39:1978 [13]

Characteristic	Type 1	Type 2	
Characteristic compressive strength average not less than (N/mm^2)	10	Grade I	Grade II
		4.8	2.8

strengths for commercial bricks. According to Table 4, the minimum compressive strength for type 2, grade II is 2.8 MPa. Therefore, the brick which has 15% SDE incorporation satisfied the minimum requirement for the type 2, grade II brick. Thus, by incorporating a high percentage of SDE into the clay mixture, it is possible to produce SDE-containing bricks to reach that expectation and applications.

The bending strength of bricks is important when walls have to resist lateral loads such as wind and earth pressure. Bending strength of a brick especially important for loaded or slightly loaded flexurally stressed components such as cellar walls beneath patios, veneer, non-loading, and freestanding walls [14]. Though the incorporation of SDE on bending strength has no significant effect, the highest bending strength of 0.55 MPa has been recorded with 15% SDE; thus, the reference bricks' bending strength is 0.41 MPa. Therefore, the incorporation of SDE has a positive effect on the bending strength of a brick.

No significant changes were observed during the mixing, drying, and firing stages of SDE incorporated bricks. After the firing stage, all bricks had identical colors. There were no observable bloating, cracking, wrinkles, or pyroplastic defects on the fired bricks. There is no black core observed at the broken cross sections of specimens. Not appearing of black core confirms that the major gaseous compounds were completely released and the organic matter present in the SDE was completely burnt [15]. During the storing time, SDE emanated a strong odor due to the decomposition of the organic matter content of the spent diatomaceous earth. Also, that odor is emitted during the mixing and drying. This odor generation can be reduced by introducing odor inhibitors [16].

5 Future Expectations

Since both compressive strength and bending strength had a positive effect with increasing SDE weight percentages, this study can be further extended with higher SDE incorporations as 20, 25, 30, and 35%. Also, chemical composition of clay has a significant effect on final brick properties. Therefore, specimens can be made with different clay types that are collected from different locations in the country. Prior to the mixing, chemical composition of each clay type is expected to be analyzed. Effect of chemical composition of clay can be analyzed by comparing compositions of the bricks before and after firing. As mentioned in literatures, mechanical parameters of bricks are significantly change with the firing temperature. Therefore, experiment can be done for different firing temperatures. In construction industry, they are looking for

several parameters of a brick such as compressive strength, bending strength, tensile strength, and water absorption capacity. Identifying variation those parameters with firing temperature, clay composition and SDE incorporation percentage will help to understand optimum condition to be maintained during both firing and drying, to prepare bricks with required characteristics. By doing XRF and SEM imaging for bricks before and after firing, changes of microstructure and bond formations can be identified.

6 Conclusion

The utilization of SDE as a silica carrier and pore-forming agent for brick production was evaluated in this study. Since SDE consists of high silica content (95.43%), it was a good alternative raw material for mixing with clay to produce bricks. SDE has been incorporated with clay in different percentages as 0, 5, 10, and 15%wt and fired at 950 °C. The mixing percentage of SDE has no significant impact on the physical properties of the brick. But with increasing SDE percentage has a significant effect on the mechanical properties of bricks. Mainly higher SDE percentage has a positive effect on the compressive strength of a brick. Also, bending strength was increased with increasing SDE incorporation percentage but the effect was relatively lower compared to the compressive strength. Maximum compressive strength of 4.73 MPa and bending strength of 0.55 MPa were obtained when the waste incorporated percentage was 15 wt% which was higher than the reference brick. The reuse of spent diatomaceous earth in bricks does not affect the inert classification of these construction products which is contributed to sustainable construction. Also, it is sustainable waste elimination when compared with landfill deposition. Although much research has been conducted, the commercial production of bricks from spent diatomaceous earth is still limited. The possible reasons are related to the methods for producing bricks from SDE, the potential contamination from the SDE, the absence of relevant standards, and the slow acceptance of SDE-based bricks by industry and the public. We suggest that research should be extended for different temperatures, higher SDE incorporation percentages, and different clay types. In this way, they should be used to evaluate more objectively the use of SDE as the secondary raw material for the brick production.

Acknowledgements The authors specially thank Dr. Eshantha Salgaduo, Lion Brewery (Ceylon) PLC, Biyagama, Sri Lanka, for providing raw materials—spent diatomaceous earth, and financial supporting to conduct experiment and characterization/measurements of materials. Furthermore, the authors are grateful to the support given by Sri Lanka Institute of Nanotechnology (Pvt) Ltd, Department of Engineering Services—Central Province Council and Mr. Gihan at Central Environmental Testing and Consultancy (Pvt) Ltd.

References

1. Cotes-Palomino M, Martínez-García C, Eliche D, Pérez- L (2015) Production of ceramic material using wastes from brewing industry. Key Eng Mater 663:94–104
2. Ferraz E, Coroado J, Silva J, Gomes C, Rocha F (2011) Manufacture of ceramic bricks using recycled brewing spent Kieselguhr. Mater Manuf Processes 26(10):1319–1329
3. Galán-Arboledas R, Cotes-Palomino M, Bueno S, Martínez-García C (2017) Evaluation of spent diatomite incorporation in clay-based materials for lightweight bricks processing. Constr Build Mater 144:327–337
4. Mateo S, Cuevas M, La Rubia M, Eliche D (2016) Preliminary study of the use of spent diatomaceous earth from the brewing industry in clay matrix bricks. Adv Appl Ceram 116(2):77–84
5. Kirinholdings (2021) Available at https://www.kirinholdings.co.jp/english/news/2020/index.html. Accessed 9 June 2021
6. Russ W, Mörtel H, Meyer- R (2005) Application of spent grains to increase porosity in bricks. Constr Build Mater 19(2):117–126
7. Wikipedia Contributors (2019) Diatomaceous earth. [online] Wikipedia. Available at: https://en.wikipedia.org/wiki/Diatomaceous_earth. Accessed 10 June 2021
8. Karaman S, Gunal H, Ersahin S (2006) Assesment of clay bricks compressive strength using quantitative values of colour components. Constr Build Mater 20(5):348–354
9. Elert K, Cultrone G, Navarro C, Pardo E (2003) Durability of bricks used in the conservation of historic buildings—influence of composition and microstructure. J Cult Herit 4(2):91–99
10. Laird RT, Worcester M (1956) The inhibiting of lime blowing. Trans Br Ceram Soc 55:545–563
11. Cultrone G, Rodriguez-Navarro C, Sebastian E, Cazalla O, De La Torre M (2001) Carbonate and silicate phase reactions during ceramic firing. Eur J Mineral 13(3):621–634
12. Sedat K, Sabit E, Hikmet G (2006) Firing temperature and firing time influence on mechanical and physical properties of clay bricks. J Sci Ind Res 65:153–159
13. Yasarathne U, Thalgaspitiya T, Karunasinghe T, Athapattu B (2018) Annual sessions of IESL. [online], pp 167–174
14. Schubertl P (1994) Tensile and flexural strength of masonry-influences, test methods, test results. Stress 50(2)
15. Toledo R, Dossantos D, Fariajr R, Carrio J, Auler L, Vargas H (2004) Gas release during clay firing and evolution of ceramic properties. Appl Clay Sci 27(3–4):151–157
16. Pimraksa K, Chindaprasirt P (2009) Lightweight bricks made of diatomaceous earth, lime and gypsum. Ceram Int 35(1):471–478

Evaluate the Feasibility for Making of Non-load Bearing Blocks Using Plastic Waste as Partial Replacement for Fine Aggregate

S. Srisaisoruban, S. Jamesbager, M. Kajalakshi, and M. S. T. Priyadarshana

Abstract Solid waste disposal can contribute to the problem of environmental degradation. Most of the waste material is plastic-based because nature is not susceptible to plastic degradation. Numerous studies have been conducted to overcome the issue of the reuse of plastic waste in various fields such as civil engineering and construction. In this study, rejected polythene packaging covers from the manufacturing industry were used for partially replacing the sand in cement-sand non-load bearing block production. The high-density polyethylene (HDPE) and low-density polyethylene (LDPE) raw plastic waste used in this study were obtained from a packaging factory "Cleanpoly Packaging Pvt. Ltd, Kegalle," and they were obtained in the fine particle size form from the "GREEN EARTH Waste Management Technologies Pvt Ltd, Negombo." About 1:6 cement-sand mix design and 0.45 water-cement ratio were maintained with partial replacement of recycled plastic waste instead of sand in the percentages 15%, 20%, 25%, 30%, and 35%, respectively, for the sandcrete block production. All specimens were included for testing and for determining the compressive strength, split tensile strength, and water absorption at the 7th and 28th days. The density of the specimens was also measured. The findings show that specimens with 15% recycled plastic waste partial replacement at 28 days of age curing show the highest compressive strength and highest tensile strength which are 3.39 N/mm^2 and 0.38 N/mm^2 compared to the controlled specimen 2.8 N/mm^2 and 0.28 N/mm^2, respectively.

Keywords Recycled plastic waste (RPW) · Sandcrete · Compressive strength

1 Introduction

Plastic plays a vital role in the current era. These wastes are non-biodegradable and cause environmental pollution and hygiene problems. Toxic plastic is found to be nearly 5% of municipal solid waste (MSW). Large-scale efforts are required for

S. Srisaisoruban · S. Jamesbager · M. Kajalakshi (✉) · M. S. T. Priyadarshana
Department of Civil Engineering, Open University of Srilanka, Colombo, Sri Lanka
e-mail: mkaja206@gmail.com

R. Dissanayake et al. (eds.), *12th International Conference on Structural Engineering and Construction Management*, Lecture Notes in Civil Engineering 266,
https://doi.org/10.1007/978-981-19-2886-4_42

reducing the disposal of plastic waste in an environment, and the global consumption of the aggregate is very high due to the extensive use of concrete. The demand for the aggregate is quite high in developing cities owing to infrastructural growth. Plastic waste disposal is managed by considering the impacts of technological factors, environmental factors, regulatory factors, economic factors, and social factors. As time goes on, technology becomes more sophisticated to the point where it can process plastic waste optimally. Regulations stipulated by the government such as legislation related to policies in managing waste will be a limitation in implementing a plastic waste management system. The application of plastic waste recycling processes can improve the industry's economy indirectly. Therefore, this can be a consideration for the industry in implementing a plastic waste management system. There is an issue currently prevailing in the Cleanpoly Packaging Pvt. Ltd, and they are looking for a solution in disposing of the waste polymers effectively. Hence, the recycled plastic materials are used in the formation of blocks as a partial replacement for fine aggregate in the project. Nowadays, disposal of plastic wastes in an eco-friendly manner is a major problem. Sand is one of the constituents used in the production of concrete has become very expensive and also becoming scarce due to the depletion of rock and the rapid development of massive structures in the construction industry of Sri Lanka. Over-extraction of the aggregate has led to environmental concerns, the diminishing of sand deposits, and an increase in the price of cement blocks. In the mass production of sandcrete blocks, partial replacement of plastic waste in the non-load bearing blocks will be more effective to cope with the sand scarcity and as well as environmental degradation.

2 Methodology

Methodology includes selection of materials, manufacturing of sandcrete blocks with recycled plastic waste, and laboratory experiments.

2.1 Materials

Recycled plastic waste: Raw plastic wastes were obtained from "Cleanpoly Packaging Pvt. Ltd, Kegalle," since they are looking for a solution in disposing of the waste polymers effectively. Then, they were recycled and obtained in the fine particle size form in the "GREEN EARTH Waste Management Technologies Pvt. Ltd, Negombo" (Figs. 1 and 2; Table 1).

Cement: Cement is one of the binding materials in this project. Ordinary Portland cement (OPC) conforming to Sri Lankan standard code SLS 107 was used in the study.

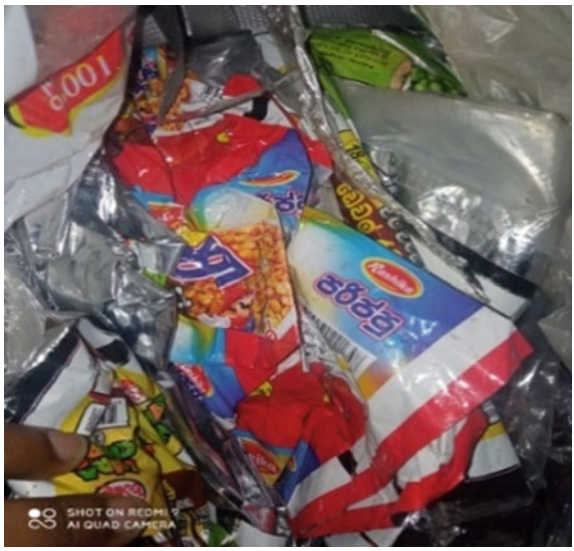

Fig. 1 Raw plastic waste in the form of bags

Fig. 2 Recycled plastic waste in the form of fine aggregate

Table 1 Raw materials of ingredients and density

Raw materials	Density (kg/m^3)
Cement	1440
Sand	1669
Water	1000
Recycled plastic waste	695

Sand: River sand was used as the fine aggregate, and sieve tests were done before adding into the mixture. The clean, sharp river sand which is free from clay, loam, dirt, and organic or chemical matter was used in this study.

Water: Water is an important ingredient of sandcrete as it actually participates in the chemical reaction with cement. Water not only makes bonds between all particles of sandcrete blocks but also helps to make bonds stronger through curing.

2.2 Test Specimens and Testing

The specimen for the compressive strength test was also used to determine the block density. It will be weighed to determine the weight of the block before specimens was placed for compression test (Table 2).

A water absorption test was carried out to determine the water absorption property of recycled plastic waste partially added cement-sand blocks. Three samples of each mix proportion cement-sand blocks were used for the absorption test. First, the samples were kept in an oven at a temperature of 100 °C (Fig. 6) for 24 h, and the dry weight of the blocks was measured. Then, the similar blocks were immersed entirely in a water basin for 24 h. Then, the wet weight of blocks was measured. Water absorption was calculated in the percentage of the ratio of the reduction in weight to the dry weight of the block. Water absorption of individual blocks was determined, and the average value was calculated.

The compressive strength was carried out on 150 mm cubes in accordance with BS 1881-116, and the tensile strength of sandcrete block specimen was determined by using a cylindrical specimen consists 150 mm diameter and 300 mm height.

The curing process is recognized as the most essential part of the exercise because the strength achieved by the blocks depends upon the curing of the blocks. There is a gain of compressive strength with the continuation of the curing process. Curing was commenced after twenty-four hours of block manufacturing and continuously done until the testing day. Blocks were cured by placing them into the water basin in the fully immersed position (Figs. 3, 4, 5, 6, 7, and 8).

Table 2 Mix design of sandcrete blocks

	Cement	Sand	Recycled plastic waste
Mix proportion-1	1	5.1 (85%)	0.9 (15%)
Mix proportion-2	1	4.8 (80%)	1.2 (20%)
Mix proportion-3	1	4.5 (75%)	1.5 (25%)
Mix proportion-4	1	4.2 (70%)	1.8 (30%)
Mix proportion-5	1	3.9 (65%)	2.1 (35%)

Fig. 3 Specimens manufactured for testing compressive and tensile strength

Fig. 4 Specimens placed at water basin for curing

Fig. 5 Testing for split tensile strength

3 Results and Discussions

3.1 Density

A block with good workability will facilitate the production of a high-density block. These factors illustrate the existence of differences in density that occurs between all the samples tested. Raw materials and the manufacturing process influence the density of cement blocks. The density of the manufactured specimen is affected by the mechanical properties of cement blocks containing HDPE and LDPE. The results of the average density of the sandcrete blocks after 7 days and 28 days are displayed in Table 3 and Fig. 9.

From the graph of the results obtained, they ranged from about 1535.407 kg/m^3 to 1922.764 kg/m^3 depending on the proportion of sand in the mix and the age of curing. And 15% recycled plastic waste added cement blocks specimen recorded the highest average density at 7 days of curing and 28 days of curing with the value of 1922.764 kg/m^3, 1672.495 kg/m^3, respectively. The lowest density was recorded for a block with 35% recycled plastic waste for 7 day at 1762.07 kg/m^3, while the same percentage block specimen also recorded the lowest density at 28 days at 1535.407 kg/m^3.

Fig. 6 Blocks in oven

3.2 Water Absorption

Water absorption of a unit block is related to porosity. High water absorption of a block will cause swelling of the soil particles in the blocks and it will cause a decrease in strength. Average water absorption for sandcrete block specimen produced is indicated in Table 4 and Fig. 10.

The water absorption of sandcrete block varies between 4.73 and 9.97%. The recommended maximum value of water absorption for a sandcrete block is 15%. Specimen with 30% recycled plastic waste instead of sand showed the lowest water absorption reading at the age of 28 days curing which is 4.73%. Meanwhile, 15% recycled plastic waste added block recorded the highest value at the age of 28 days of curing at 9.97%. Water is the agent of chemical reactions in cement to bind all the raw materials in the mixing of a block. Hence, it can be concluded from the results attained that the mixing proportion of raw materials in a block have a huge impact on deviating the percentage rate of water absorption in the block.

Fig. 7 Measuring weight

Fig. 8 Keep the cubes to rest for drying surface water

Table 3 Results of density of blocks

Recycled plastic replacement instead of sand (%)	Average hardened density (kg/m^3)	
	At 7th day	At 28th day
0	1936	1654.222
15	1922.764	1672.495
20	1896.791	1686.913
25	1863.801	1640.098
30	1832	1666.268
35	1762.07	1535.407

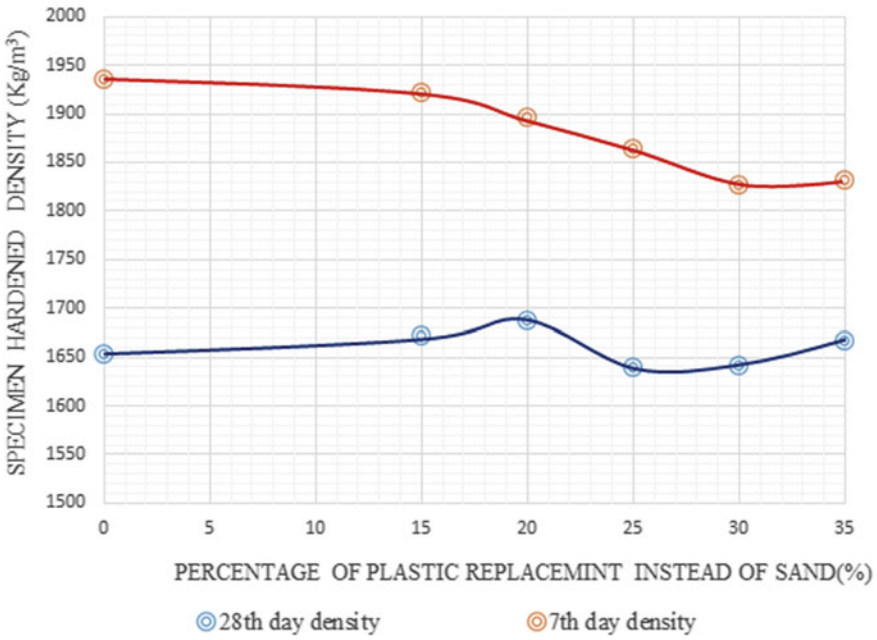

Fig. 9 Variation of average density with the percentage of RWP (as partial replacement for sand)

Table 4 Results of water absorption test of blocks

Recycled plastic replacement instead of sand (%)	Average water absorption at 28th day
0	8.13
15	9.97
20	7.77
25	5.83
30	4.73
35	5.50

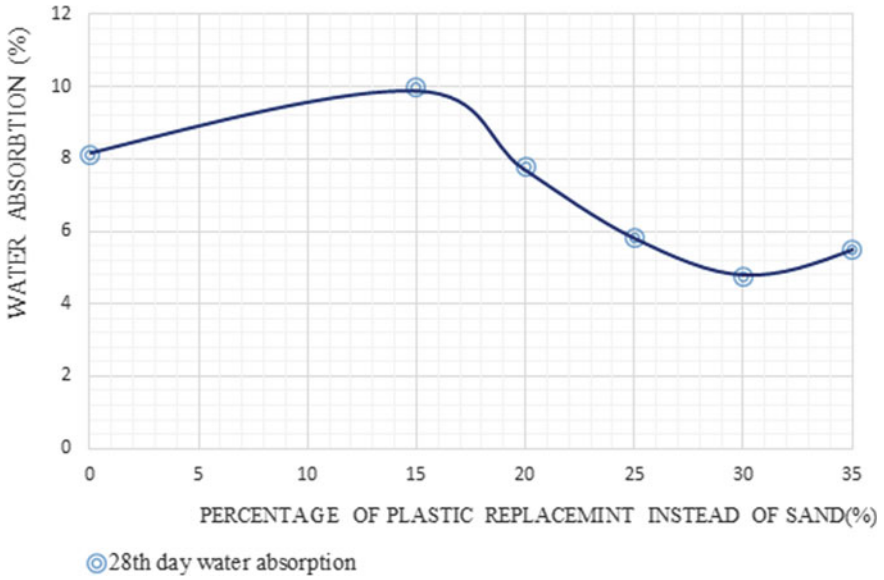

Fig. 10 Variation of average water absorption with the percentage of RWP (as partial replacement for sand)

3.3 Compressive Strength

The compressive strength is a vital aspect in assessing the load-bearing capacity of a block. It is determined by using the compressive strength testing machine. The strength characteristics of recycled plastic waste added cement-sand blocks were compared with the minimum standard compressive strength value of cement-sand blocks at 28 days. It is known as 2.8 N/mm^2 as per BS6073: Part 2: 1981.

Figure 11 shows the reading of the compressive strength of the RPW added sandcrete blocks. The recycled plastic waste was used as a partial replacement for sand with a constant amount of cement. The average 28 day compressive strength of samples (5%, 10%, 15%, 20%, and 25% of RPW) satisfied the minimum standard compressive strength value of cement-sand block at 28 days (2.8 N/mm^2). The average compressive strength of sandcrete blocks ranged from 2.6 N/mm^2 to 3.39 N/mm^2.

Based on the results obtained, the compressive strength at 28 days of age showed an increase of compressive strength with the increase of RPW up to 25%. Beyond RPW 25%, the compressive strength of the block decreased as shown in Fig. 11. These results can also be sustained by the results from the compressive strength test, where the specimen with the lowest RPW replacement which is 15%, recorded the highest compressive strength; therefore, it also can be observed that with lowest RPW replacement resulted in the highest water absorption of the block at the age of 28 days curing. And the specimen consists of the mix proportion with 35% RPW replacement

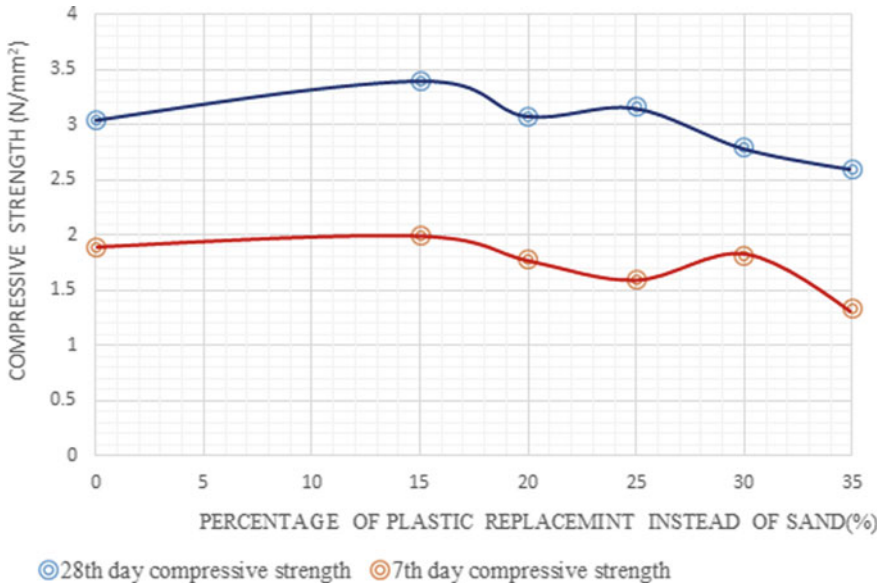

Fig. 11 Variation of average compressive strength with the percentage of RPW (as partial replacement for sand)

recorded the lower compressive strength which had the highest replacement of RPW (Table 5).

However, for RPW-based blocks, the material cost for RPW was less than the material cost for sand. It is the cost-effective method with the rapid increase in the price of sand since there is no expenditure involved in collecting RPW. And the material cost will be less than conventional sandcrete blocks.

Table 5 Results of compressive strength test of blocks

Recycled plastic replacement instead of sand (%)	Average compressive strength (N/mm^2)	
	At 7th day	At 28th day
0	1.89	3.04
15	1.99	3.39
20	1.78	3.07
25	1.59	3.16
30	1.82	2.79
35	1.33	2.6

3.4 Tensile Strength

The tensile strength at 28 days of age of curing ranged from 0.24 to 0.38 N/mm^2. The peak value of 0.38 N/mm^2 was obtained for the specimen which contains 15% RPW as a partial replacement for sand. These values are found to be less than the compressive strength of sandcrete specimens which ranged from 2.6 to 3.39 N/mm^2 (Fig. 12; Table 6).

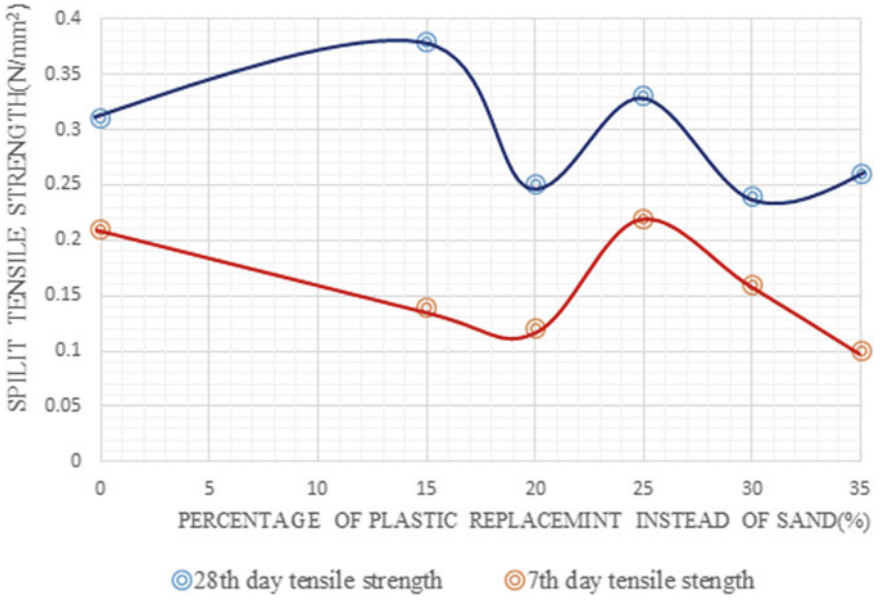

Fig. 12 Variation of average tensile strength with the percentage of RWP (as partial replacement for sand)

Table 6 Results of tensile strength test of blocks

Recycled plastic replacement instead of sand (%)	Average tensile strength (N/mm^2)	
	At 7th day	At 28th day
0	0.21	0.31
15	0.14	0.38
20	0.12	0.25
25	0.22	0.33
30	0.16	0.24
35	0.1	0.26

4 Conclusions and Recommendations

Plastics are non-biodegradable material that comprises a source of hazard to the environment and society in numerous emerging countries when they are disposed in a random manner and haphazardly after they have been used. Polyethylene plastic wastes were recycled and used as partial replacement of fine aggregate for producing building blocks. Sandcrete (sand and Portland cement) blocks are universally used in building construction in several developing countries.

Some conclusions can be made from the results above presented as follows:

(1) Five different mix proportions of cement-sand blocks with 15%, 20%, 25%, 30%, and 35% RPW replacement (plastic-to-sand) were used to investigate the tensile strength, compressive strength, hardened density, and water absorption. The optimum mix proportion is turned out to be the 1:6 (25% RPW replacement) mix which provided the higher strength in tension, compression, and lower water absorption. Hence, mix proportion-3 can be suggested as the optimum design mix.
(2) This study also shows that RPW can be used as sand replacement in block production, where the utilization of RPW can reduce the waste dump at the landfill.
(3) The percentage of RPW used in the production of cement blocks affects the percentage of water absorption. From the results of experimental work that have been carried out, the percentage of water absorption decreases with the increasing percentage of RPW replacement in the production of the concrete blocks.

In order to enhance the research of using RPW in a cement block, there are numerous recommendations that are suggested to be investigated. The recommendation includes:

a. Percentage of RPW replacement that can be varied to get more range of data.
b. Study the effect of different mix design ratios can also be considered.
c. Other kinds of testing can be conducted, for example, impact resistance testing, wetting expansion test, and drying shrinkage test.
d. A feasible solution to be found to cope with the huge environmental problem arising due to the micro-plastic generation problem during the demolition of the structure after its serviceability period.

References

1. British Standard 6073-Part2 (1981) Precast concrete masonry units. Method for Specifying Precast Masonry Units. s.l.:s.n.
2. BS 3921 (1985) Specification for clay bricks. British Standards Institution, Londan
3. Kankama CK, Ansa-Asarea K, Meisuh BK, Sasahc J (2018) Study of recycled polyethylene plastic waste as binder in building block for greener construction

4. Keralli AG (2001) Durability of compressed and stabilised building block. Ph.D. thesis, University of Warwick
5. Ali N, Yusup NF, Khalid FS, Shahidan S, Abdullah SR (2018) The effect of water cement ratio on cement brick containing high density polyethylene(HDPE) as sand replacement
6. Pushpakumara BHJ, Subashi De Silva GHMJ (2012) Characteristics of masonry blocks manufactured with rice husk ash (RHA) and lime

Assessment of Concrete Durability by Surface Resistivity and Initial Surface Absorption

N. H. I. C. Fonseka and S. M. A. Nanayakkara

Abstract Performance-based durability design has gained considerable attention in the construction industry for the service life-based designs of new constructions. Currently, prescriptive-type specifications are used in durability design to meet the service life requirements which prescribe the constituent materials with limiting values of the concrete mix proportion and cover to reinforcement under a given exposure condition. In this context, performance requirements are assumed to be satisfied during the life span of the structure. Prescriptive specifications are valid within a selected range of the cement composition and exposure conditions of concrete, and therefore, these descriptive requirements are often not applicable in the rapidly changing concrete industry. Contrarily, in the case of performance-based durability design approach, there is more flexibility in selection and proportioning of constituent material in producing concrete to satisfy a particular exposure condition. In order to change from prescriptive specifications to performance-based design for durability of concrete, it is essential to find relevant durability indicators with appropriate test methods to evaluate those indicators. In this research, the main focus was given to evaluate two durability-related tests which are commonly used in the construction industry such as surface resistivity test and initial surface absorption test (ISAT) for concrete with the addition of fly ash as a supplementary cementitious material as a partial replacement of Ordinary Portland cement. Experimental investigations were carried out by varying the fly ash percentage, water-to-cement (w/c) ratio and curing condition. It was found that initial surface absorption and surface resistivity are having higher sensitivity toward the variation of factors affecting durability such as w/c ratio, fly ash content and curing condition and can be used as reliable concrete durability indicators.

Keywords Concrete durability · ISAT · Surface resistivity · Fly ash · W/C ratio · Curing condition

N. H. I. C. Fonseka (✉) · S. M. A. Nanayakkara
Department of Civil Engineering, University of Moratuwa, Moratuwa, Sri Lanka
e-mail: isurfonseka@gmail.com

R. Dissanayake et al. (eds.), *12th International Conference on Structural Engineering and Construction Management*, Lecture Notes in Civil Engineering 266,
https://doi.org/10.1007/978-981-19-2886-4_43

1 Introduction

Recently, durability and service life prediction have increasingly gained importance in the construction industry for the existing concrete structures and service life-based design of new constructions. This is mainly due to unsatisfactory durability performance of many reinforced concrete structures built in the recent past [4].

Figure 1 shows the performance of a structure over the time. In case "a", the durability is in accordance with the design service life, and hence, no preventive or corrective maintenance is required. In case "b", within the design service life period, corrective maintenance is needed to restore the performance on an acceptable level above the critical limit. Therefore, this has been foreseen during the design stage, the costs for remedial actions are a part of the foreseen exploitation costs. If not foreseen, we call it damage [5].

Therefore, evaluating the performance requirements on concrete durability is a very important scenario even though it is difficult to assess.

Usual durability design methods are based on prescribed limiting values in specifications for selected mix design parameters and deal with durability of concrete entirely based on prescriptive specification. In the case of performance-based design approach, there is more flexibility in selection and proportioning of constituent material in producing concrete to satisfy a particular exposure condition. However, further development of performance-based specifications has been hindered by the lack of reliable, consistent and standardized test procedures for evaluating concrete durability [17].

In the British standards [7], for instance, the concrete grade, maximum w/c ratio, minimum cement content and cover to reinforcement are the factors considered in specifying concrete under a given exposure condition to achieve the durability of

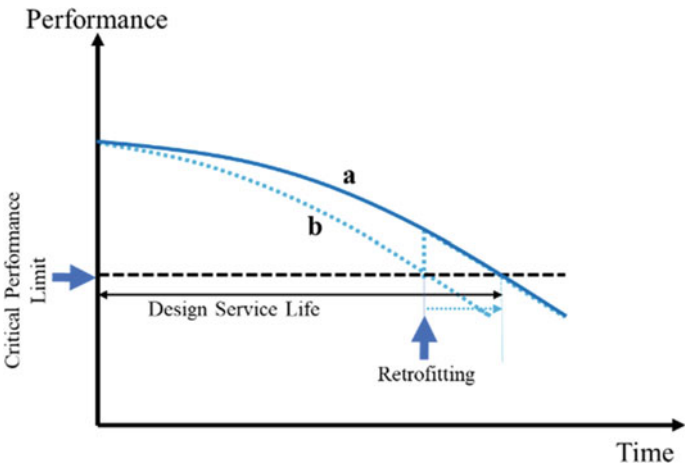

Fig. 1 Performance of a structure over the time [5]

the concrete structure. There is strong believe that higher the concrete strength, better the resistance to deterioration mechanisms. Under normal circumstances, to achieve a higher strength, it is necessary to lower the water-to-cement (w/c) ratio, which results in a lower permeability and diffusivity. In fact, the strength or concrete grade requirement is a prescriptive requirement which is related to the performance requirement. For concretes having same strength but different concrete compositions can have considerable difference in resistance to various deterioration mechanisms because of their different microstructure, chemical composition and covercrete properties. Factors such as cement type, supplementary cementitious materials, curing and exposure conditions appear to be as important as w/c ratio. In order to change from prescriptive specifications to performance-based design for durability of concrete, it is essential to find relevant durability indicators with appropriate test methods to evaluate those indicators.

Rate of water ingress into the hardened concrete is a key parameter when determining the concrete durability because of the reinforcement corrosion significantly depends on the water content inside the concrete. Furthermore, surface resistivity of concrete can be used as an indicator to determine the rate of corrosion of embedded steel in reinforced concrete. Therefore, in the present research, the main focus was given to evaluate two durability-related tests which are commonly used in the construction industry, i.e., surface resistivity test and initial surface absorption test (ISAT), for concrete with fly ash as a partial replacement of Ordinary Portland cement (OPC).

In this research, the surface resistivity and initial surface absorption of concrete at 56 days were investigated with respect to w/c ratio (0.3, 0.5 and 0.7), fly ash percentage (0, 15 and 35%) and curing condition (with and without initial curing for 7 days). Furthermore, strength development of concrete with respect to w/c, fly ash content and curing condition was also investigated by measuring compressive strength at 1, 7, 28 and 56 days.

2 Methodology

2.1 Constituent Materials

Ordinary Portland cement conforming to SLS 107 [20] and fly ash from Norochcholai power plant for partial replacement of OPC (15 and 35% by weight of OPC) were used in this experimental investigation. Chemical composition of fly ash is shown in Table 1.

Each of these cement and cement combinations were used to prepare concrete with w/c ratios of 0.7, 0.5 and 0.3 to obtain a wide range of durability performance.

A widely used chemical admixture in the local construction industry was chosen to produce the required workability of concrete. Concrete mixtures with w/c ratio of 0.7 were prepared without using chemical admixtures, while concrete with w/c ratios

Table 1 Chemical composition of fly ash

Oxides	Percentage (% by mass)
SiO_2	46.89
Al_2O_3	33.07
Fe_2O_3	3.28
MgO	1.56
CaO	7.56
TiO_2	1.79
Na_2O	0.23

of 0.5 and 0.3 was prepared with a Polycarboxylate (PCE)-based high-performance superplasticizer.

River sand with particles finer than 4.75 mm and having water absorption of 0.7% was used as the fine aggregate, while aggregates with the maximum aggregate size of 20 mm and having water absorption of 0.6% were used as coarse aggregates. For mixing concrete and curing purposes of concrete specimens, potable water was used.

2.2 Experimental Plan

In the experimental investigation, nine different concrete mixtures were prepared with three cement combinations and three different w/c ratios.

For each mix, fifteen 150 mm × 150 mm × 150 mm cubes and two 150 mm (diameter) × 300 mm (height) cylinders were cast. Vibrating table was used for the compaction of concrete specimens. All specimens were demolded after 24 h and then cured as described in Table 2.

One set of samples from each concrete mix was subjected to 7 days of water curing by immersing in water at temperature of 27 °C ± 2 °C and air curing for remaining days before testing (C). Another set of samples from the same concrete mix was subjected to air curing at the ambient temperature (AC). Temperature and relative humidity variation during the period were recoded.

Each mix was identified by cementitious materials in the mix, e.g., "OPC" means 100% of Ordinary Portland cement and "OPC + 35FA" means 65% of Ordinary Portland cement with 35% of fly ash by weight.

2.3 Mix Proportions

The mix proportions chosen for this study are given in Table 3. All the concrete mixes were designed to maintain a slump in the range of 175–200 mm.

Table 2 Summary of the concrete mixtures

Cement type	w/c ratio	Curing condition
OPC	0.7	C
		AC
	0.5	C
		AC
	0.3	C
		AC
OPC + 15 fly ash	0.7	C
		AC
	0.5	C
		AC
	0.3	C
		AC
OPC + 35 fly ash	0.7	C
		AC
	0.5	C
		AC
	0.3	C
		AC

"C" denotes for the 7 days water curing, and "AC" denotes for air curing in ambient temperature

Table 3 Concrete mix proportions (per $1m^3$)

Mix	Mix-1	Mix-2	Mix-3
W/C ratio	0.7	0.5	0.3
Cement (kg)	321	360	516
Fine aggregate (kg)	771	777	668
Coarse aggregate (kg)	1022	1073	1090
Water (kg)	225	180	155
Admixture (l)	Nil	3.6	5.16

3 Test Methods

3.1 Testing Fundamentals

The movement of aggressive fluids, ions and gases through concrete is very important because of their interactions with concrete components and the pore water, and therefore, it can directly change the integrity of concrete which leads to deterioration [12]. The movement of those aggressive substances may be driven by one or a

combination of four main transport mechanisms: absorption, diffusion, permeability and adsorption as explained below.

- Absorption—one of the main fluid transport mechanisms, which takes place in concrete due to capillary suction to fill the available voids in concrete.
- Diffusion—the mechanism of penetrating a gas or ion into the concrete under the influence of a molar concentration gradient.
- Permeability—the resistance of concrete to the penetration of a liquid or gas under the influence of a pressure gradient.
- Adsorption—the mechanism of molecules adhering to the internal surface of concrete pores. It can happen as a result of chemical bonding or physical adhesion forces.

The first three of above transport mechanisms are collectively named as permeation properties such as absorption, diffusion and permeability [11].

Several permeation tests with in situ application are available to measure individual permeation properties of concrete. These tests can provide necessary information about the reaction of the pore system to harmful substances. Moreover, the deviation in concrete durability arising from several important parameters such as constituent materials, w/c ratios, curing conditions, exposure classes, covercrete (i.e., cover to reinforcement) properties and workmanship can be measured using permeation tests, which give a single parameter assessment of concrete quality [14].

In this experimental investigation, two tests which can be easily carried out, i.e., initial surface absorption test (ISAT) and surface resistivity test, were selected to assess the durability of concrete. These two durability test methods are commonly used for field evaluations due to its rapidness, simplicity, being portable and low cost to conduct the test. Apart from these two durability test methods, compressive strength measurements were also taken to assess the mechanical properties of the concrete mixes.

Test samples were prepared to test the compressive strength and durability indicators as per the relevant standard methods given below.

- Compressive strength—BS EN12390-3:2009 [8]
- ISAT—BS 1881–208:1996 [10]
- Surface resistivity by Wenner four-probe method-ACI 222R [6].

3.2 Compressive Strength

Compressive strength tests were conducted on concrete specimens having dimensions of 150 mm × 150 mm × 150 mm after 1 day, 7 days, 28 days and 56 days of casting. Three cubes were tested at each of these time periods as per BS EN12390-3:2009.

3.3 Initial Surface Absorption Test (ISAT)

The ISAT is an experiment that measures the absorptivity of concrete at near-surface layers. Near-surface layers, which are generally having poorest quality, thus provide the worst-case scenario for concrete durability.

ISAT was conducted using 150 mm × 150 mm × 150 mm air dried cubes at the 56 days of casting. Concrete samples were allowed to remain in the laboratory for a period of 48 h at the ambient temperature before testing. Temperature and relative humidity variation during the period were recoded, and it varied between 27 °C and 33 °C and 61–75%, respectively.

The test apparatus consists of an acrylic cap which is attached to the concrete surface and clamped with a rubber O-ring to make it watertight. As per the standard, this cap should be connected to a reservoir having a head of 180 mm–200 mm at one opening. A calibrated horizontal capillary tube is also connected to the cap at the other opening as shown in Fig. 2.

Water is allowed to penetrate the concrete surface from the reservoir through the cap. Initially, water flows to fill the cap after opening the inlet tap and then flows into the horizontal capillary tube through the outlet tube. The tap should be closed after 10 min, and the rate of water suction by the concrete can be observed by following the meniscus retract in the capillary tube. This measurement, i.e., at 10 min was obtained as the initial surface absorption of concrete specimen. The absorption values at 30 min and 1 h from the start of the test were also determined by following the same procedure. After taking each measurement, the inlet tap was opened, and the reservoir was topped up with water to maintain the water head at 200 mm.

Assembly of typical ISAT apparatus is illustrated in Fig. 2.

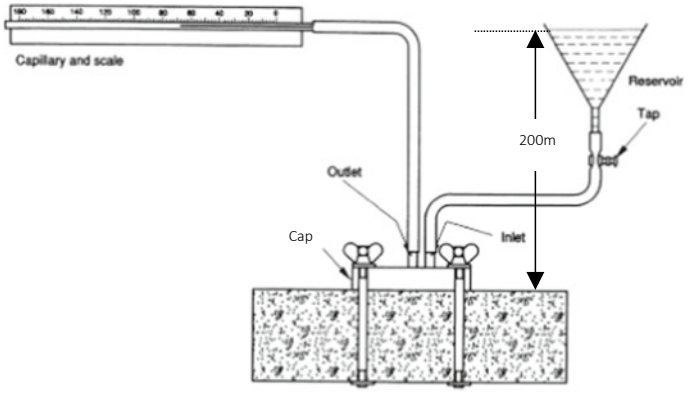

Fig. 2 Assembly of typical ISAT apparatus [10]

3.4 Surface Resistivity Test

The rate of corrosion of embedded reinforcing steel in concrete is influenced by the concrete's resistivity, which is a function of electrolyte and moisture content. As a result, it is sometimes necessary to check the moisture content and resistivity of concrete. However, determining these parameters is not a common practice, and no standard test methods are currently available. Limiting values for surface resistivity measurements taken from the four-point Wenner probe meter are described in Table 4 referring to corroding reinforcing steel embedded in concrete [6].

In the recent past, surface resistivity measuring techniques in concrete have gained considerable attention to evaluate durability of concrete structures as a non-destructive test. American Society for Testing and Materials (ASTM)—C1760 has been standardized the surface resistivity test in 2012 to measure the bulk resistivity of concrete [2] while American Association of State Highway and Transportation Officials (AASHTO)—TP 95 standardizing a method to quantify the surface resistivity of concrete in 2011 [1]. However, there is a gap that still exists between the construction practice and current knowledge.

In the present study, surface resistivity was measured using a commercially available four-point Wenner probe surface resistivity meter having a probe spacing of 50 mm. This is a simple, quick and non-expensive test which can be used to evaluate concrete durability. A current with nominal voltage limit of 25 V (peak-peak) is applied to the two outer probes, and the potential difference is measured between the two inner probes (see Fig. 3). The current flow is carried by ions in the pore liquid [19].

The calculated resistivity depends on the spacing of the probes, and the resistivity is calculated by the following Eq. (1).

$$\text{Resistivity} = \frac{2\pi a V}{I} \tag{1}$$

where

a—probe spacing (cm), V—voltage difference (V), I—current (A).

Two 150 mm dia. × 300 mm cylindrical specimens were used to measure surface resistivity. The resistivity or conductivity of concrete will be affected by change in the degree of saturation of concrete as it would vary the water content in the pore structure. A consistent curing method is recommended to ensure the test specimens

Table 4 Relationship between concrete resistivity and corrosion rate [6]

Resistivity, kΩcm	Corrosion rate
>20	Low
10–20	Low to moderate
5–10	High
<5	Very high

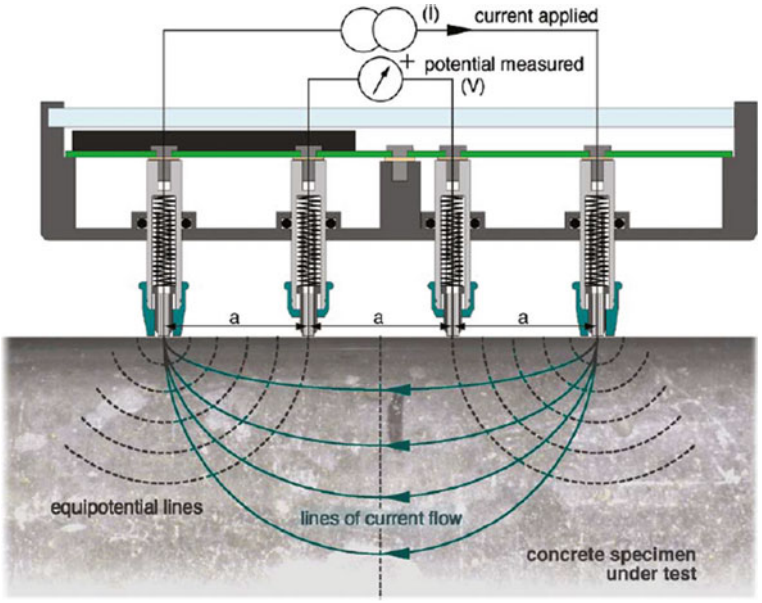

Fig. 3 Measurement principle of four-point Wenner probe surface resistivity meter [19]

are in saturated surface dry (SSD) condition at the time of testing to make reliable and repeatable surface resistivity measurements. Therefore, all cylindrical specimens were fully immersed in water for 24 h prior to the resistivity measurements. Concrete specimens were removed from water, and excess surface moisture was wiped off.

For each specimen, surface resistivity testing was performed on four different positions of the cylindrical surface at 0°, 90°, 180° and 270° angles with respect to the axis of cylindrical sample. To get a good indication of concrete resistivity, average of eight measurements was taken.

4 Results and Discussion

4.1 Compressive Strength Test Results

Compressive strength results are given in Table 5 for different concrete mixes.

Table 5 Compressive strength results with time

Cement type	w/c ratio	Compressive strength (MPa)							
		1 day		7 days		28 days		56 days	
		C	AC	C	AC	C	AC	C	AC
OPC	0.7	8.7	8.5	21.5	20.9	29.6	26.9	32.7	31.0
	0.5	19.2	18.7	45.5	43.7	58.4	53.6	61.7	58.1
	0.3	40.5	39.2	74.3	70.9	95.2	94.3	97.9	97.2
OPC + 15FA	0.7	8.2	7.2	19.1	18.9	26.2	23.7	33.2	28.2
	0.5	13.6	12.2	33.4	32.5	40.8	39.9	51.4	50.2
	0.3	34.8	34.4	60.5	55.7	78.9	70.0	82.8	72.3
OPC + 35FA	0.7	6.1	5.6	14.5	11.8	23.4	18.9	25.7	24.5
	0.5	3.0	2.6	30.0	24.1	34.1	33.3	53.8	47.3
	0.3	3.2	3.1	49.8	41.4	54.4	51.4	70.8	60.4

4.1.1 Strength Gaining Pattern of Concrete Mixes with Curing Condition

The following Fig. 4 shows the strength gaining patterns of different concrete mixes under both curing conditions.

Concrete with OPC only did not show a significant impact on the strength with respect to curing condition (i.e., 7-day water curing and air curing), while concrete

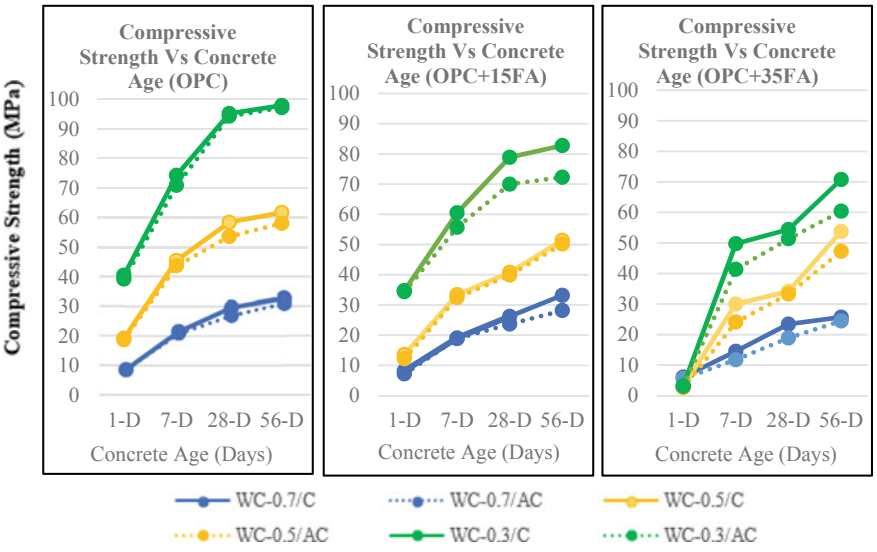

Fig. 4 Strength gaining patterns of different concrete mixes with curing condition

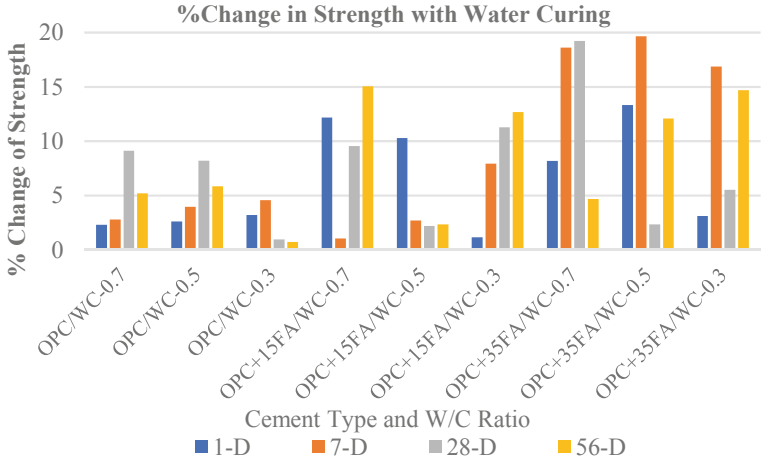

Fig. 5 % change in strength with water curing

with fly ash-OPC cement combination showed a significant impact on strength especially with respect to low w/c ratio. Fly ash-OPC cement combination showed a significant strength gain especially with concrete mixes having low w/c ratios beyond 28 days. However, OPC concrete did not show a considerable strength gain beyond 28 days for all w/c ratios.

The percentage change in compressive strength between air-cured and 7 days water-cured samples is presented in Fig. 5.

The rate of the pozzolanic reaction is slower than the rate of cement hydration at the ambient temperature. As a result of it, fly ash concrete mixes often have lower early age strengths. If the full benefits of fly ash concrete are to be realized, it must be properly cured. It is generally recommended that the concrete with high levels of fly ash replacement should be water cured for at least 7 days [21]. The amount of fly ash used in the concrete should be limited if adequate curing cannot be provided in construction practice. Due to those reasons, with increasing fly ash content, a considerable reduction in compressive strength can be observed between air-cured samples and 7 days water-cured samples.

One of the primary benefits of fly ash is its reaction with available $Ca(OH)_2$, which is product of hydration of C_3S and C_2S, which resulted in pozzolanic reaction of fly ash to produce additional calcium silicate hydrate (C–S–H). The additional binder allows fly ash concrete to continue gaining strength over time. Since the pozzolanic reaction is slow at early age, as the fly ash content increases, the early age strength decreases. However, long-term strength development is improved when fly ash content is increased as so long as sufficient curing is provided.

4.2 Initial Surface Absorption Test Results

ISAT results are given in Table 6. It can be seen that the ISAT values increase with the increase of w/c ratio, reflecting surface layer porosity of concrete.

4.2.1 Effect of w/c Ratio and Fly Ash Content on Initial Surface Absorption of Concrete

Figures 6 and 7 show the initial surface absorption variation with time at 56 days of water-cured and air-cured concrete samples for three different concrete mixes having w/c ratios of 0.7, 0.5 and 0.3.

Following observations can be made with respect to the ISAT values by analyzing results shown in Figs. 6 and 7.

- ISAT values decreased with reducing w/c ratio
- ISAT values decreased as the percentage of fly ash increases.

As expected, the above graphs show that the ISAT values decreased with reducing w/c ratio for both curing conditions. The w/c ratio influences the durability properties

Table 6 ISAT values

Cement type	w/c ratio	Curing condition	ISAT value at 56 days [ml/(m^2 s)]		
			10 min	30 min	1 hour
OPC	0.7	C	1.940	1.020	0.770
		AC	2.320	1.280	1.000
	0.5	C	0.480	0.250	0.105
		AC	1.800	0.950	0.730
	0.3	C	0.280	0.150	0.100
		AC	1.720	0.900	0.580
OPC + 15FA	0.7	C	1.100	0.600	0.340
		AC	2.000	1.000	0.730
	0.5	C	0.320	0.180	0.070
		AC	1.020	0.630	0.440
	0.3	C	0.200	0.100	0.048
		AC	0.870	0.450	0.220
OPC + 35FA	0.7	C	0.600	0.380	0.170
		AC	1.840	0.870	0.520
	0.5	C	0.260	0.110	0.020
		AC	0.450	0.220	0.150
	0.3	C	0.090	0.045	0.000
		AC	0.400	0.150	0.105

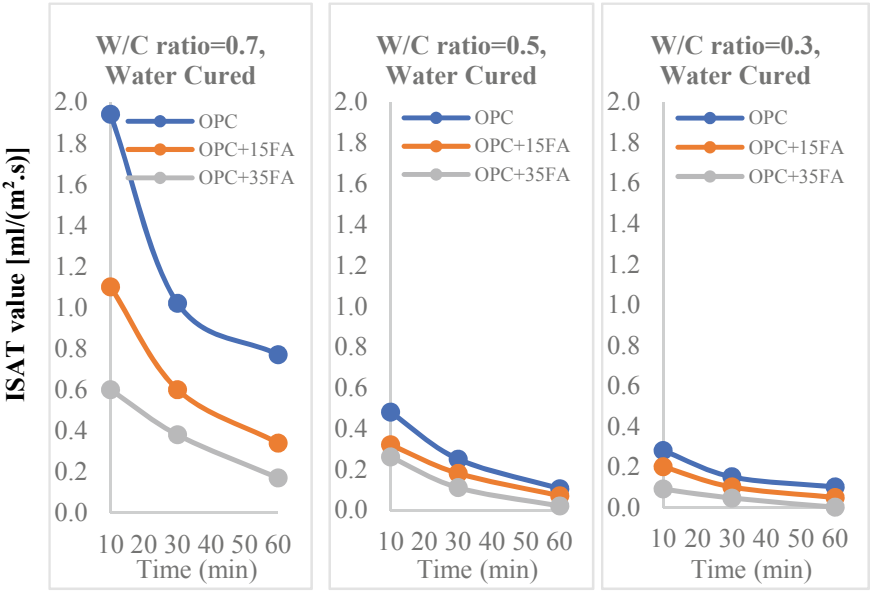

Fig. 6 Initial surface absorption of 7 days water-cured concrete samples for different w/c ratios (0.7, 0.5 and 0.3) with time

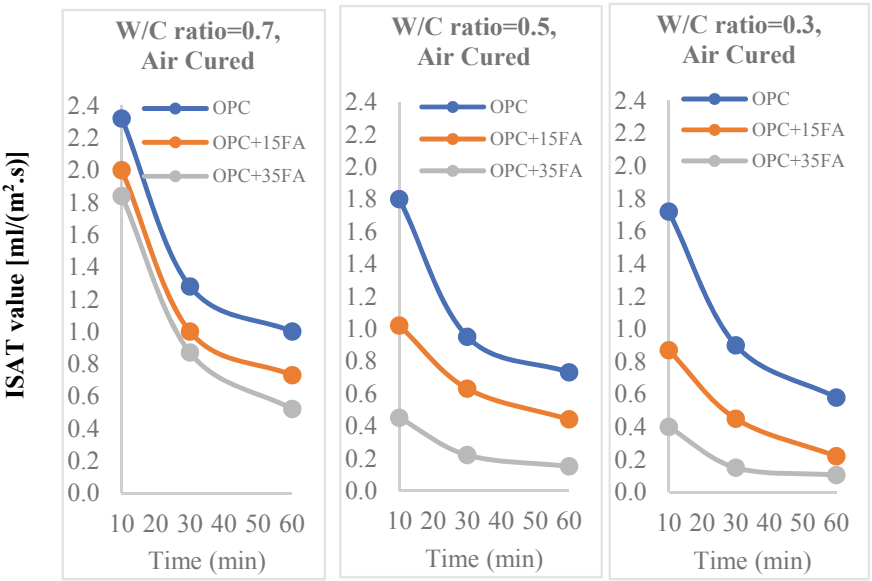

Fig. 7 Initial surface absorption of air-cured concrete samples for different w/c ratios (0.7, 0.5 and 0.3) with time

of concrete in a significant way. In general, capillary pores in concrete depend on the w/c ratio. Lowering the w/c ratio makes a poor pore interconnectivity hydrated cement paste in concrete. Therefore, decreasing w/c ratio would lead to reduction in concrete porosity and, hence, lower permeability and lower initial surface absorption at the zone of immediately behind the surface [13]. Hence, lower w/c ratios lead to higher concrete durability.

It can be seen that there was a reduction in ISAT values for concrete with higher fly ash percentages, compared to normal OPC concrete mix (see Figs. 8 and 9). This

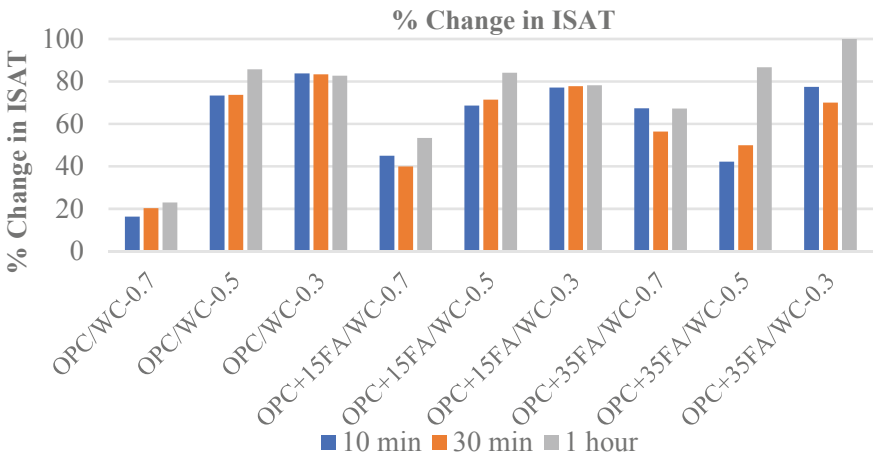

Fig. 8 % change in ISAT with water curing

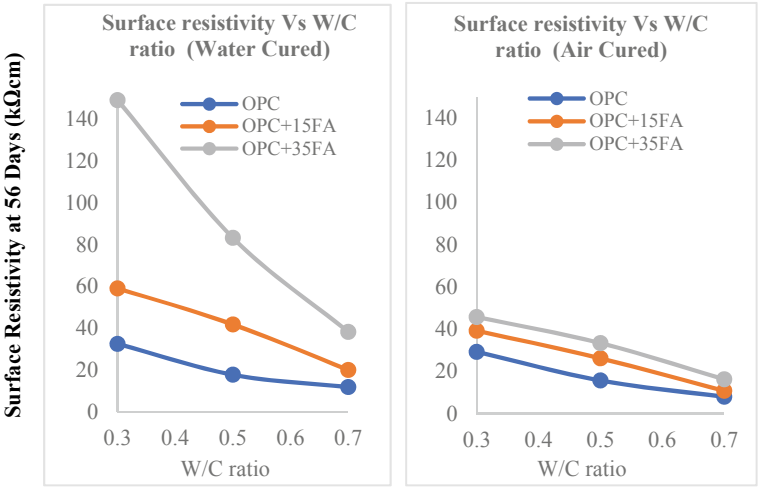

Fig. 9 Effect of w/c ratio and fly ash content on surface resistivity of concrete

effect is significant for air-cured specimens with low w/c. This behavior may be due to enhanced microstructure due to pozzolanic activity [9, 16]. The decrease in w/c ratio combined with the additional fly ash creates a denser product with reduced porosity, thus decreasing the permeability of concrete. Therefore, the durability of concrete structures and resistance to various forms of deterioration will enhance as a result of it.

4.2.2 Effect of Curing Condition on the Initial Surface Absorption

Figure 8 shows the effect of curing condition on the ISAT values for the different concrete mixes. Percentage increment of ISAT values between air-cured and 7 days water-cured concrete samples with respect to air-cured samples was graphically presented in this Fig. 8.

It can be noted that all concrete mixes showed a significant positive impact on ISAT values with water curing. ISAT values were reduced drastically due to water curing, and hence, a considerable durability enhancement is evident with adequate curing.

With the water curing, connectivity of the capillary pores in the hydrated cement paste becomes segmented [18] which causes in reduction of permeability of concrete. Therefore, it will give lower initial surface absorption results. Blended cements take more time to complete their reaction process with the latent chemical reactions which cause to develop additional calcium–silicate–hydrate gels (C–S–H) in the pore structure [9]. Thus, as observed in this study, adequate curing enhances the performance of concrete due to reduction of surface absorption with fly ash as a supplementary cementitious material.

4.3 Surface Resistivity Test Results

Surface resistivity values of cylindrical concrete specimens measured by Wenner four-probe method are given in Table 7.

4.3.1 Effect of w/c Ratio and Fly Ash Content on Surface Resistivity of Concrete

Figure 9 shows effect of w/c ratio and fly ash content on the surface resistivity of concrete.

According to the test results, concrete with low w/c ratio gives higher surface resistivity than those with high w/c ratio for both curing conditions. This is because of the number of interconnected pores decreases as the w/c ratio decreases [15].

The fly ash content has a substantial influence on the concrete resistivity according to the test results. There is significant increase in surface resistivity of water-cured

Table 7 Surface resistivity at 56 days (kΩcm)

Cement type	w/c ratio	Surface resistivity at 56 days (kΩcm)	
		C	AC
OPC	0.7	11.80	7.90
	0.5	17.70	15.60
	0.3	32.50	29.20
OPC + 15FA	0.7	20.00	10.70
	0.5	41.80	26.10
	0.3	59.00	39.20
OPC + 35FA	0.7	38.20	16.20
	0.5	83.20	33.30
	0.3	149.10	45.70

concrete specimens with higher fly ash content and low w/c (see Fig. 9). When OPC was replaced with 35% by fly ash, surface resistivity was increased four times more than that of OPC concrete for water-cured concrete samples having a w/c ratio of 0.3. This is because of pozzolanic reaction of fly ash, and fly ash causes lower ionic concentration and finer pore size distribution, which resulting in higher surface resistivity than OPC concrete [22].

4.3.2 Effect of Curing Conditions on Surface Resistivity of Concrete

Curing condition also affects the surface resistivity of concrete. According to the test results shown in Table 7, water curing increases the resistivity of concrete than air curing.

Figure 10 shows the effect of curing condition on the surface resistivity for different concrete mixes. Percentage increment of surface resistivity between air-cured and 7 days water-cured concrete samples with respect to water-cured samples was graphically presented.

According to Fig. 10,

- Surface resistivity is having a higher sensitivity to the curing condition of the concrete specimens with fly ash.
- There is no significant effect of curing condition on surface resistivity for OPC concrete with low w/c ratio.

Two key components that influence this variation in surface resistivity are the degree of hydration of the cementitious material and the degree of saturation of the specimen [3]. The samples that were continuously immersed in water for 7 days can be subjected to a higher degree of hydration in the surface layer of the concrete samples than the air-cured samples at the same age. Furthermore, with the water curing, connectivity of the capillary pores in the hydrated cement paste becomes

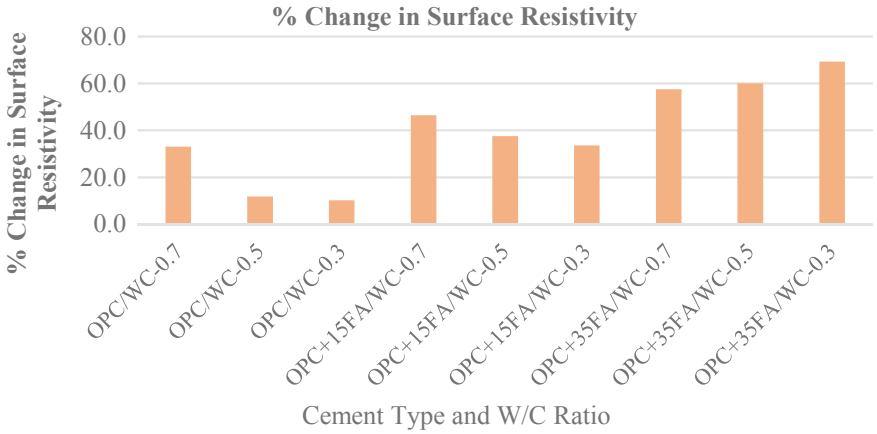

Fig. 10 % change in surface resistivity with water curing

segmented which causes in reduction of permeability of concrete [18]. Hence, it will affect the current flow through the saturated pores in the concrete, and surface resistivity will be increased as a result of it. It is also important to note that differences in resistivity can develop as a result of sample moisture conditions, and therefore, wetting the specimens 24 h prior to the surface resistivity measurements is recommended.

5 Conclusions

Based on the experimental results reported above, the following conclusions can be drawn:

- In the case of concrete with fly ash, adequate curing is an essential requirement to achieve the required gain in both strength and durability.
- ISAT values decreased with decrease in w/c ratio for both air-cured and water-cured concrete specimens.
- There was a reduction in ISAT values for concrete with higher fly ash percentages, compared to normal OPC concrete mix.
- All concrete mixes showed a significant positive impact on ISAT values with water curing, and ISAT values were reduced drastically under water curing.
- Surface resistivity of concrete increased with addition of fly ash as a partial replacement of OPC.
- Both initial surface absorption and surface resistivity are having higher sensitivity toward the variation of factors affecting durability such as w/c, fly ash content and curing. Therefore, those two properties, i.e., initial surface absorption and surface resistivity can be used as reliable concrete durability indicators.

References

1. AASHTO (2011) AASHTO TP 95—standard method of test for surface resistivity indication of concrete's ability to resist chloride ion penetration | Engineering360. American Association of State Highway and Transportation Officials (AASHTO TP)
2. ASTM (2012) ASTM C1760—12:standard test method for bulk electrical conductivity of hardened concrete. ASTM International
3. Azarsa P, Gupta R (2017) Electrical resistivity of concrete for durability evaluation: a review. In: Advances in materials science and engineering
4. Beushausen and Luco (2016) Performance-based specifications and control of concrete durability. RILEM TC 230-PSC State-of-the-Art report
5. Bijen J (2002) Performance based durability design. In: Challenges of concrete construction: Volume 5, Sustainable Concrete Construction, pp 605–616
6. British Standards (1996) (2001) Protection of metals in concrete against corrosion. ACI Committee 222, ACI 222R-1
7. British Standards Institution (1997) Bs 8110–1:1997. British Standard Institution London 1:168
8. British Standards Institution B (2009) Testing hardened concrete. Part 3, Compressive strength of test specimens. BSI Standards Publication, BSEN 12390, p BSEN 12390
9. Brooks (2002) Advanced concrete technology. Pearson Education (Singapore) Pte. Ltd, Indian Branch, Second Indian Reprint
10. BS 1881-208 (1996) Recommendations for the determination of the initial surface absorption of concrete. In: British standard, pp 1–14
11. Dhir R et al (1994) Predicting concrete durability from its absorption. In: Durability of concrete, pp 1177–1194
12. Dhir RK et al (1988) Near-surface characteristics of concrete: assessment and development of in situ test methods. Mag Concr Res 40(145):234–244
13. Hago AW et al (2007) Compressive strength and surface absorption of high strength silica fume concrete under different curing conditions. J Eng Res 4(1):17–22
14. Holmes N, Basheer L (2009) Performance-based testing methodology for concrete durability
15. Hornbostel K, Larsen CK, Geiker MR (2013) Relationship between concrete resistivity and corrosion rate—a literature review. Cement Concr Compos 39:60–72
16. McCarthy MJ, Dhir RK (2005) Development of high volume fly ash cements for use in concrete construction. Fuel 84(11):1423–1432
17. Nanukuttan S, Yang K, Basheer J (2017) Methods of assessing the durability and service life of concrete structures
18. Olufemi FS (2016) Absorption characteristics of cement combination concrete containing portland cement, fly ash, and metakaolin. Civ Eng Dimension 18(1):46–56
19. Resipod (2016) Technical specification-the world's most accurate concrete surface resistivity meter-resipod. Proceq SA
20. Standards S (2008) SLS 107—2015 specification for ordinary portland cement | Cement | Concrete. Sri Lanka Standards Institute
21. Thomas MDA (2007) Optimizing the use of fly ash in concrete. Portland Cement Association, p 24
22. Whiting D et al (1993) Synthesis of current and projected concrete highway technology

Investigation of Properties of Ultra-High-Performance Concrete and Development of UHPC Waffle Deck Panels for Pedestrian Bridges

R. M. W. Perera, T. S. Dinushika, M. S. Swarnamali, T. Priyadarshana, and K. P. Arandara

Abstract As a developing country, Sri Lanka is in the requirement of constructing bridges and high-rise structures under infrastructure development projects based on the country's need or on behalf of structurally unstable old structures. Therefore, new technologies are useful to improve the construction efficiency while using precast items which can achieve the required performance with improved durability. Accordingly, the full depth ultra-high-performance concrete (UHPC) waffle panels (3 m long, 2 m wide, and 0.2 m thick) are introduced as a possible alternative to the construction industry. The usage of UHPC is highly limited in Sri Lanka, and UHPC waffle deck panels are not available in Sri Lanka as a precast item for bridge construction. Then this study is focusing on the development of UHPC waffle deck panels using locally available materials. Accordingly, a number of trials were performed to find out a suitable mix proportion for UHPC with compressive strength $\geq$150 MPa at 28 days. Therefore, cubes (75 mm $\times$ 75 mm $\times$ 75 mm) were cast based on different mix designs and specimens were tested for compressive strength at 01, 07, 28, and 56 days. Then other properties of the selected UHPC mixture were investigated through testing flexural strength, tensile strength, water absorption, porosity, thermal expansion, and drying shrinkage after completion of 28 days for cast specimens. Finally, a representative sample of the waffle deck panel was tested for panel service test and ultimate load test. As per the properties of UHPC and load test results of designed waffle deck panel, this development is recommended for pedestrian and light vehicle bridges.

Keyword Ultra-high-performance concrete (UHPC)

R. M. W. Perera (✉) · T. S. Dinushika · M. S. Swarnamali · T. Priyadarshana · K. P. Arandara
Department of Civil Engineering, Faculty of Engineering Technology, The Open University of Sri Lanka, Nawala, Nugegoda, Sri Lanka
e-mail: ravindraperera.200@gmail.com

R. Dissanayake et al. (eds.), *12th International Conference on Structural Engineering and Construction Management*, Lecture Notes in Civil Engineering 266,
https://doi.org/10.1007/978-981-19-2886-4_44

1 Introduction

Ultra-high-performance concrete (UHPC) is an advanced cementitious composite with high strength and excellent durability. The use of UHPC is a practical solution for the improvement of the sustainability of structures and other infrastructure components [1].

An UHPC is a new class of concrete that has been developed in recent decades for its exceptional strength and durability characteristics with improved particle packing characteristics which led to low porosity, high durability, and self-compatibility [3] UHPC was first developed in the early 1980s and since then has been used for applications which need exceptional strength and durability, such as nuclear power plants, thin-profile bridges, structural beams, and seawall anchor plates [4].

UHPC formulations often consist of a combination of Portland cement, fine aggregate (less than 2mm), silica fume, high-range water-reducing admixture (HRWR), fibers (usually steel), and water [4]. Workability of UHPC places limits on optimizing the packing density. With a better/higher packing density, the pores between the particles are getting smaller, making the water hard to lubricate the particles. In addition, with the large number of ultrafine particles, the surface areas to be wetted increase significantly [8].

Ultra-high-performance concrete (UHPC) has been recently used in the construction industry due to many advantages in terms of mechanical properties and durability. Following are some advantages:

- High early and compressive strength ranging up to 120 and 200 MPa
- High modulus of elasticity
- Low diffusion and permeability with low maximum aggregate size
- Abrasion resistance
- Resistance to chemical attack
- Low segregation
- High resistance to impact loads [9].

Water is the key ingredient used to start the cement hydration process. However, it is also the culprit for the majority of today's early degradation of normal concrete. High content of water in fresh mixture creates higher porosity in the hardened concrete structure resulting in early degradation of the concrete. It also decreases the pH value which leads to the corrosion of the steel reinforcement. However, use of high W/C ratio improves the workability of fresh mixture, and it remains the major problem for all cast-in-situ concrete applications. In contrast, UHPC works with a very low water to binder ratio, as low as 0.16. As this low ratio does not allow the binder to be fully wetted, a high-range water-reducing agent (HRWR) must be used. This HRWR or superplasticizer (SP) supports the wetting of the blend of cement, supplementary cementitious materials and sand creating a flowable, low viscosity system when mixed in a high shear mixer. As HRWR or SP is typically added to the UHPC system during the wet mixing process, these admixtures can be easily

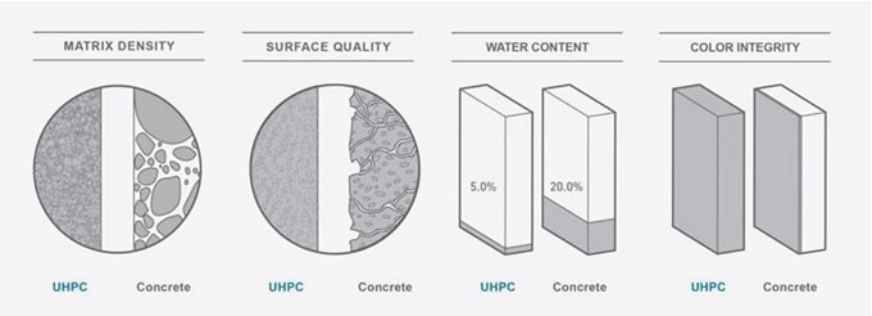

Fig. 1 Attributes of normal concrete versus UHPC

adjusted to optimize the desired slump of the UHPC system or adjust it to changes in temperature or humidity [4] (Fig. 1).

In addition, manipulating the viscosity of the UHPC makes it easier to manage its pot life and allows for transportation in concrete mixer trucks. UHPC can be mainly used for two applications: architectural and structural.

This study was carried out to achieve the following objectives.

- To identify a suitable mix proportion (above 150 MPa) of ultra-high performance concrete.
- To determine properties of ultra-high-performance concrete.
- To identify the properties of high-performance concrete waffle deck panels focusing on practical application.

2 Methodology

2.1 Material Used

Cement, fine aggregate, silica fumes, steel fiber, water-reducing admixture, fly ash, and water are used throughout the experiments to prepare ultra-high-performance concrete.

Ordinary Portland cement (42.5R) is used for the trial mixers. Fine aggregate with particle size less than 2mm is used for the UHPC mixtures.

Steel fibers (RC 65/35 Length-35 mm Diameter-0.65 mm Tensile Strength-1000 MPa) are used as the reinforcement and superplasticizing admixture is used to improve the workability of mixture at low water/binder ratios while focusing on high early strength.

3 Mix Design Method Used

The referred chart is mentioned below (Fig. 2).

- Specimens were tested for 13 numbers of trial mixers.
- In first four mixtures (TM 1, 2, 3, 4) admixture dosage was changed while keeping other components as constant. Next two mixtures (TM 5, 6) cement quantity was increased while keeping other factors as constant and in TM 6 steel fiber content was reduced.
- In TM 7, go back to the beginning trial mix and change water/cement ratio to 0.27.
- In TM 8,9,10 increase cement dosage to 1100 kg, reduce silica fumes dosage and cement replace by use in fly ash while keeping others constant. TM 8-Fly ash content 0%, TM 9 fly ash content 5%, TM 10-fly ash content 10%.
- Replace total silica fume quantity with the use of another cementations material in TM 11 & 12.
- In TM 13, finer adjustment was done by increasing fine aggregate quantity than TM 8.
- From TM 7 to TM13, heat curing was done during first 3 days. Maintain the temperature of 60'c in water bath.

A size of 75 mm × 75 mm × 75mm specimens was cast and tested for compressive strength. In trail mix, 1 to 6, 9 cubes were cast to test compressive strength at 1, 7, and 28 days. In trail mix, 7 to 13, 12 cubes were cast to test compressive strengths at 1, 7, 28, and 56 days.

Based on compressive strength test results (above 150 MPa), suitable mix proportions were selected. Then cylindrical and prismatic specimens were cast to determine tensile strength and flexural strength, respectively, as per selected mixtures (Figs. 3, 4, and 5; Table 1).

Typical composition of UHPC

Material	lb/yd^3	kg/m^3	Percentage by Weight
Portland Cement	1,200	712	28.5
Fine Sand	1,720	1,020	40.8
Silica Fume	390	231	9.3
Ground Quartz	355	211	8.4
HRWR	51.8	30.7	1.2
Accelerator	50.5	30.0	1.2
Steel Fibers	263	156	6.2
Water	184	109	4.4

Fig. 2 Typical composition of UHPC [8]

Fig. 3 Mixing of UHPC

Fig. 4 UHPC slump flow test

Fig. 5 Casting UHPC cubes

3.1 Laboratory Tests

(a) Compressive strength test

UHPC cube samples (75 mm × 75 mm × 75 mm) were tested for compressive strength at 28 day and 56 day according to the test method described in SLS 1144. During the test, specimen was subjected to compression load through lower bearing block of the testing equipment due to its upward movement while keeping the upper bearing block in a fixed position (Fig. 6).

(b) Flexural strength test

Three-point bending test was performed as per the method described in BS 1881-part 121 standard to estimate flexural strength of UHPC. 40 mm × 40 mm × 200 mm size concrete prisms were cast according to the selected mixtures which achieved the highest compressive strength at 28 day and 56 day (Figs. 7 and 8).

(c) Tensile strength test

Cylindrical specimens with 100 mm diameter and 200 mm length were cast for tensile strength test of UHPC with the use of selected mixtures and test was performed as per BS 1881-part 121 standard (Figs. 9 and 10).

(d) Water Absorption test

Water absorption was measured for 100 mm × 100 mm × 100 mm cube samples as per BS 1881 part 122 standard. Water absorption test results are expressed as percentage mass increment of the specimen due to its immersion in water bath (Figs. 11 and 12).

Table 1 Trial mixes summary

Mix no.	Materials per meter cube (kg/m^3)									
	Cement	Fine sand	Silica fume	ä 2000	CPS1	Fly ash	Admixture (Glenium- Sky-8562)	Steel fiber	Water	W/C
TM-01	712	1020	231	0	0	211	45	100	206	0.29
TM-02	712	1020	231	0	0	211	60	100	150	0.21
TM-03	712	1020	231	0	0	211	75	100	166	0.30
TM-04	712	1020	231	0	0	211	85	100	164	0.23
TM-05	800	946	231	0	0	211	100	100	160	0.20
TM-06	900	862	231	0	0	211	100	0.14	180	0.20
TM-07	712	1020	231	0	0	211	62	78	192	0.27
TM-08	1100	920	150	0	0	0	70	78	156	0.14
TM-09	1045	920	150	0	0	55	70	78	149	0.14
TM-10	990	920	150	0	0	110	70	78	158	0.16
TM-11	1100	920	0	99	0	100	70	78	176	0.16
TM-12	1100	920	0	0	100	100	70	78	176	0.16
TM-13	1100	1000	150	0	0	0	70	78	158	0.14

Fig. 6 UHPC compressive strength test

Fig. 7 Casting of the prisms

Fig. 8 Flexural strength test of UHPC

Fig. 9 Cylinder cubes casting of UHPC

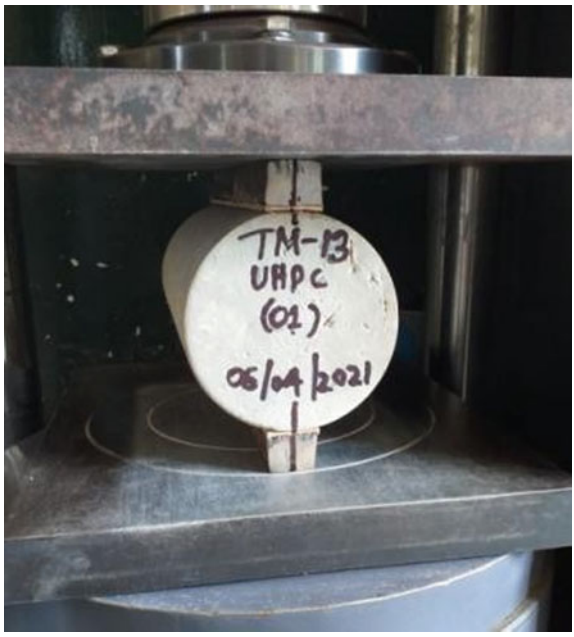

Fig. 10 Tensile strength test of UHPC

Fig. 11 Sample immersed in water-for water absorption test

(e) Thermal expansion test

This test covers the measurement of linear shrinkage during setting and hardening. The linear shrinkage measured its length change which occurs after initial hardening of the specimen size 25 mm × 25 mm × 280 mm and four numbers of specimens were tested from mixture (Figs. 13 and 14).

Fig. 12 Sample in the oven-for water absorption test

Fig. 13 Sample prepared for thermal expansion test

(f) Drying shrinkage test

This test was done for determining the effect of aggregates on the drying shrinkage of concrete. Followed standard is BS EN 1367-4:2008.

The aggregate under test is mixed with cement and water and cast into prisms of specified dimensions. The prisms are subjected to wetting and drying (at 110 ± 5 °C) cycles, and length change was determined in the dried specimens. The excess drying shrinkage of the concrete is attributed to the aggregate and is expressed as the average change in length of the prisms, as a percentage of their final dry lengths.

Three numbers of specimens (200 mm × 50 mm × 50 mm) were tested for drying shrinkage by inserting 8 mm stainless steel balls to the center points of two ends (50 mm × 50 mm) of each specimen (Figs. 15 and 16).

(g) Permeability test

Since UHPC has relatively low porous structure, constant pressure head (5 bar) was applied to the specimen's (150 mm × 150 mm × 150mm cube) surface

Fig. 14 Expansion measure of UHPC

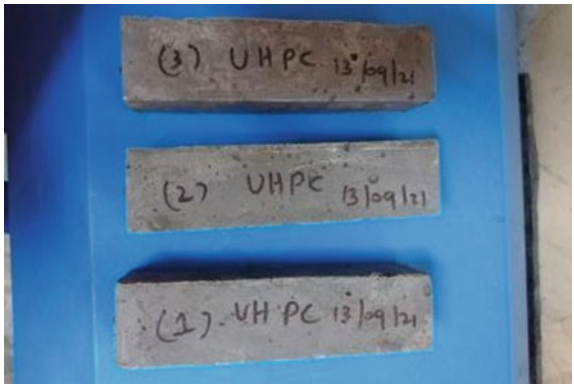

Fig. 15 Sample prepared for drying shrinkage test

Fig. 16 Drying shrinkage test

to determine the depth of water penetration. Three numbers of specimens were tested according to the BSEN 206-1 standard. In a concrete structure, permeability is important to identify the corrosion possibility of reinforcement bars (Fig. 17).

Fig. 17 Permeability test

4 Result and Discussion

4.1 Compressive Strength

According to the compressive strength test results indicated in Table 2, TM 13 mixture was selected for further tests considering its higher compressive strength value.

Compressive strength variation of different mixtures is graphically presented in Figs. 18 and 19.

Table 2 Results of the trial mixers

Mix no.	Slump flow (mm)	Strength (N/mm^2)			
		1 day	7 day	28 day	56 day
TM-01	190	35.5	68.3	82.6	–
TM-02	195	41.0	85.5	97.8	–
TM-03	205	28.0	47.8	63.4	–
TM-04	200	40.5	85.5	107.8	–
TM-05	195	41.5	65.8	84.4	–
TM-06	205	39.5	84.4	103.5	–
TM-07	215	42.0	93.6	116.8	125.1
TM-08	205	57.2	132.6	160.4	164.5
TM-09	230	56.0	110.5	131.1	138.2
TM-10	210	47.3	102.5	125.5	130.6
TM-11	225	55.6	120.5	140.4	143.7
TM-12	260	46.8	81.0	105.1	109.4
TM-13	205	68.9	135.8	165.2	168.4

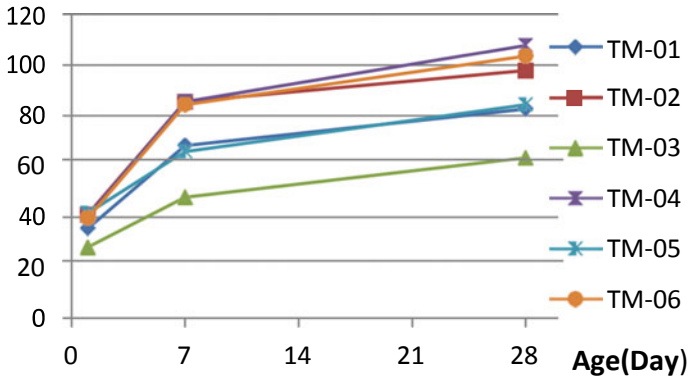

Fig. 18 TM 01–TM 06 strength variation in 28 days

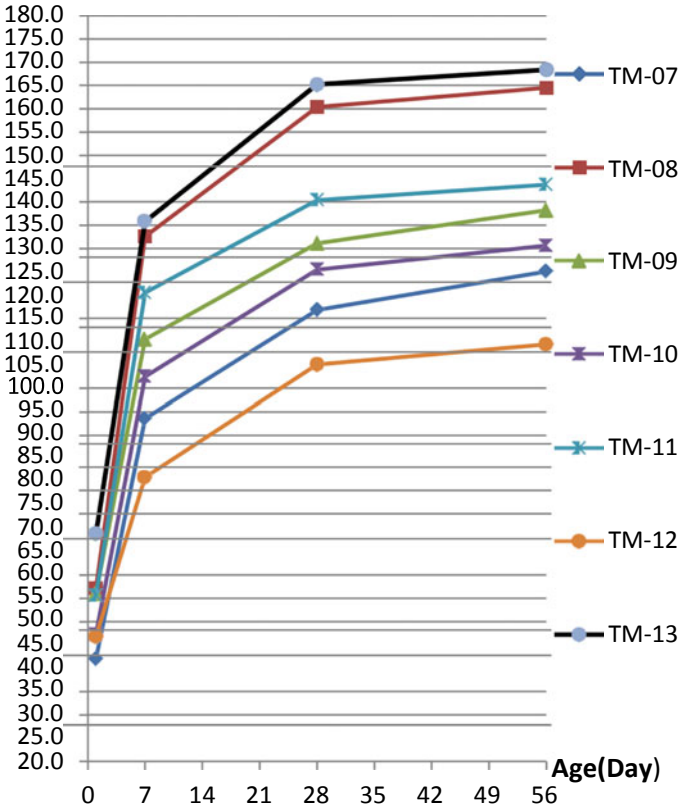

Fig. 19 TM 07–TM 13Strength variation in 56 days

4.2 Flexural Strength

Flexural strength of TM 13 mixture was estimated as 20.5 MPa and 22.8 MPa at 28 days and 56 days, respectively. Flexural strength value of UHPC lies in the range of 15–50 MPa. Accordingly, flexural strength of TM 13 mixture is at satisfactory level.

4.3 Tensile Strength

Tensile strength was measured as 13.1 MPa and 13.9 MPa at 28 days and 56 days, respectively for the specimens cast using TM 13 mixture tensile strength of UHPC is in the range of 6–10 MPa. Based on test results, selected mixture gives higher tensile strength comparative to normal UHPC mixtures.

4.4 Water Absorption

Water absorption of selected mixture was estimated 1.33%.

4.5 Thermal Expansion

Average linear coefficient of thermal expansion was estimated as 1.46×10^{-6} °C for selected mixture.

4.6 Shrinkage

Average drying shrinkage was measured as 0.253% for the selected mixture.

4.7 Permeability

Maximum water penetration depth was measured as 17 mm which is comparatively low value due to the presence of less number of interconnected pores in the hardened concrete structure (Figs. 20, 21, and 22).

Fig. 20 UHPC waffle deck panel

Fig. 21 UDL test of panel

Fig. 22 Concentration load test of panel

Table 3 UDL test results

Load (KN)	Deflection (mm)
0	0
2.56	0
5.32	0.02
7.98	0.1
10.64	0.15
15.62	0.29
20.28	0.41
25.26	0.55
30.25	0.67
35.24	0.8
40.23	0.91

4.8 Loading Test

Test was done until UDL to 40.23 KN. At that load deflection is 0.91 mm at the panel center without any crack.

Loading test was done according to the BS EN-1991.2.2003 (Table 3, Fig. 23, and Table 4).

Ultimate concentration load is 76.1 KN. At this load, hairline crack appeared.

5 Conclusion and Recommendations

- Compare the trial mix 01 to 13, trial mix 13 achieved high compressive strength above160 MPa.
- In that mix other engineering properties are also within the acceptable limit of UHPC. Flexural strength is 5 times higher and tensile strength is 3 times higher than the normal concrete.
- Water absorption, permeability, thermal expansion, and drying shrinkage are lower than the conventional concrete.
- UHPC waffle deck panel has higher surface finishes than comparing the other concrete element.
- Loading test of deck panel also satisfy the requirement of pedestrian bridge according to the BS EN 1991.2.2003.
- Required limit to uniform distributed load (UDL) for pedestrian bridge is 5.0kN/m2. The loading test is achieved 22.6 KN/m2, and it is mostly higher than the required limit
- UHPC concrete cost is very high, and it is over LKR 100,000.00 per 1m3. Initial cost of UHPC bridge is higher than normal concrete bridge. But according to

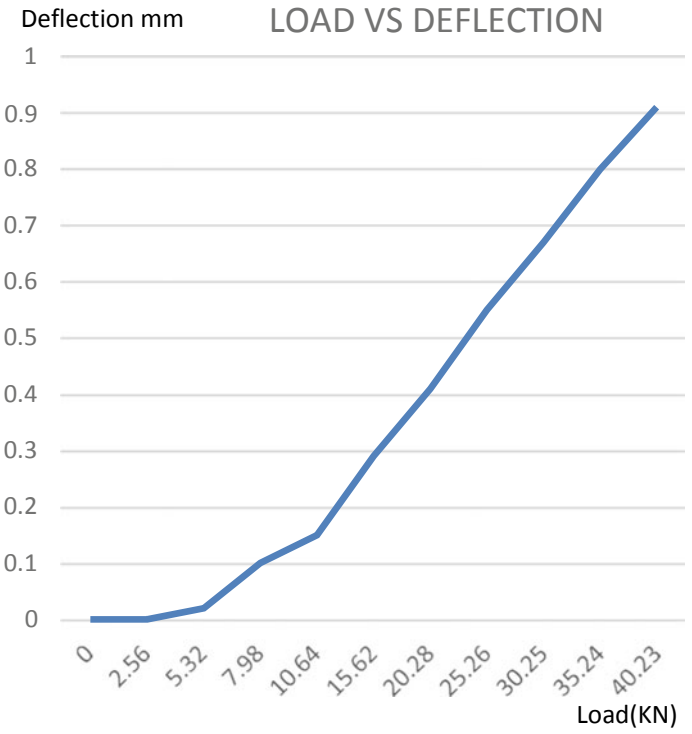

Fig. 23 Graph of load versus deflection for uniform distributed load test

Table 4 Concentration load test results

Load (KN)	Deflection (mm)
0	0
4.7	0.10
9.5	0.23
14.2	0.33
19.0	0.42
23.7	0.54
28.5	0.82
37.0	1.19
47.5	1.52
57.0	2.03
66.6	2.45
76.1	3.16

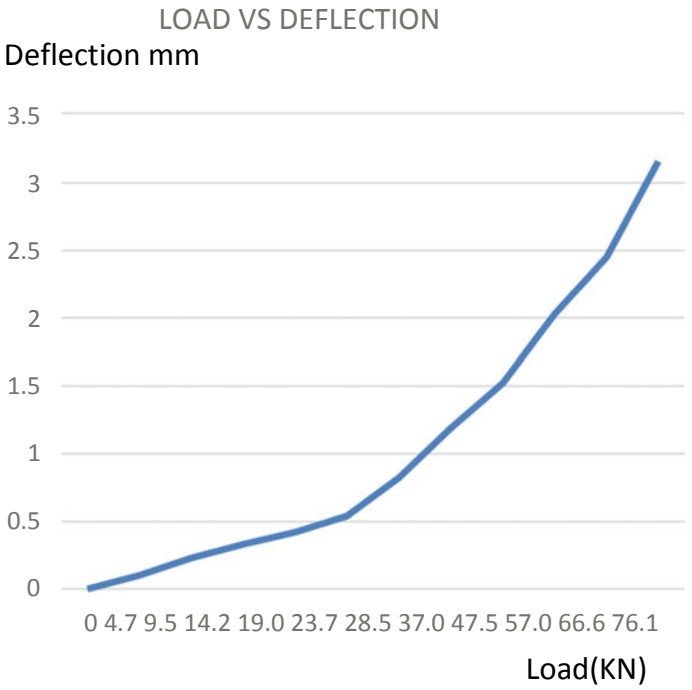

Fig. 24 Graph of load versus deflection for concentrating load

UHPC properties can be reduced element thickness and reinforcement. Also, UHPC is high durable than conventional concrete (minimum 100 years).

- According to this results, we can suggest for UHPC waffle deck panel to pedestrian and light vehicle bridges.
- Our UHPC waffle deck panel can be suggested (Figs. 25, 26, and 27).

Fig. 25 Picture of foot bridge casted over the road

Fig. 26 Picture of foot bridge casted over the small cannel

Fig. 27 Picture of pedestrian bridge casted in the rural area

Acknowledgements We would like to acknowledge Dr. Thushara Priyadarshana, senior lecturer of the Department of Civil Engineering of the Open University of Sri Lanka, our project supervisor, for his patient guidance, enthusiastic encouragement, and useful critiques of this project work and also to our research assistant, Engineer K. P. Arandara, who is a postgraduate researcher. For his guidance, comments and support made it possible for us to work on the topic which is of great interest.

Thanks to the project engineer and technical and laboratory staff of research lab of International Construction Consortium precast research laboratory, Piliyandala, for their help in offering us the resources in running this project from the beginning.

References

1. Azmee NM, Shafiq N (2018) Ultra high performance concrete: from fundamental to applications. Universiti Teknologi PETRONAS, Department of Civil and Environmental Engineering, Perak, Malaysia
2. ceENTEK (2020) UHPC blog. [Online] Available at: https://ceentek.com/uhpc-blog/f/how-is-uhpc-different-from-normal-concrete. Accessed 19 Oct 2020
3. PCA (2018) Ultra high performance concrete. [Online]. Available at: https://www.cement.org/learn/concrete-technology/concrete-design-production/ultra-high-performance-concrete. Accessed 20 July 2018
4. Priyadarshana T, Dissanayake R (2020) NRC PPP in NRC PPP in R&D: development and applications of ultra high-performance concrete in Sri Lanka, Colombo: s.n.
5. Priyadarshana T, Ranjith D (2020) Development and applications of ultra high-performance concrete in Sri Lanka. Issue 07.12.2020, p 14
6. Q Green Techcon pvt. ltd. (2018) Normal concrete vs high-strength concrete properties and differences. [Online] Available at: https://qgreentech.com/normal-concrete-vs-high-strength-concrete/. Accessed 12 Oct 2018
7. RDC (2018) RDC website UHPC for people: The Rdc's Blog. [Online] Available at: https://rdconcrete.com/uhpc-for-people/. Accessed 24 June 2018
8. Russell HG, Graybeal BA (2013) Ultra-high performance concrete: a state-of-the-art report for the bridge community. s.n., Georgetown Pike
9. UHPC Solutions (2018) UHPC Solutions North America. [Online] Available at: https://www.uhpcsolutions.com/blog/what-is-ultra-high-performing-concrete. Accessed 12 May 2018

Development of Blended Fly Ash-Rice Husk Ash–Based Alkali-Activated Bricks: A Sustainable Alternative to Portland Cement Brick

Sarah Fernando, Chamila Gunasekara, David W. Law, M. C. M. Nasvi, Sujeeva Setunge, and Ranjith Dissanayake

Abstract In order to reduce the impact arising from the higher energy requirement for fired bricks and to reduce the GHG emission from the use of Portland cement (PC) in PC-based bricks, researchers have focussed on alternative materials for brick production. Alkali-activated concrete bricks manufactured using waste by-products are one of the potential alternatives to replace the fired bricks and PC bricks. In this study, 20% replacement of PC with rice husk ash (RHA) was undertaken to evaluate the mechanical performance of blended low calcium fly ash-RHA–based brick (20RHA). The results are compared with PC bricks with similar binder content. The mechanical properties were assessed up to 90 days for both mixes in order to provide a holistic view of the performance of blended fly ash-RHA alkali-activated bricks. Blended fly ash-RHA alkali-activated bricks showed improved mechanical properties in terms of tensile strength and modulus of rupture compared to PC bricks, i.e. early age (7 day) compressive strength, tensile strength and modulus of rupture for all ages up to 90 days. The 20RHA brick showed a compressive strength growth rate of 4% between 7 and 28 days as compared to 13.8% for 100PC bricks. The bonding between blended fly ash-RHA alkali-activated paste and aggregate enhanced the tensile strength properties of the 20RHA bricks. It is concluded that the 20RHA brick is feasible for use as load-bearing bricks in construction industry based on the reported strength properties.

Keywords Alkali-activated bricks · Fly ash · Mechanical properties · Portland cement bricks · Rice husk ash

S. Fernando (✉) · C. Gunasekara · D. W. Law · S. Setunge
Civil & Infrastructure, School of Engineering, RMIT University, Melbourne, VIC 3001, Australia
e-mail: s3765050@student.rmit.edu.au

S. Fernando · M. C. M. Nasvi · R. Dissanayake
Department of Civil Engineering, Faculty of Engineering, University of Peradeniya, Peradeniya 20400, Sri Lanka

R. Dissanayake et al. (eds.), *12th International Conference on Structural Engineering and Construction Management*, Lecture Notes in Civil Engineering 266,
https://doi.org/10.1007/978-981-19-2886-4_45

1 Introduction

Bricks are one of the most common and longest-lasting manufactured building materials and have been used over a long period of time. Asia and China are responsible for over two-thirds of global annual brick production, approximately 87% of the 1500 billion clay bricks produced annually [1]. Concrete is the material commonly used to produce traditional Portland Cement (PC) bricks. The PC production is responsible for about 5–8% global CO_2 emissions accounting for around 2.2 billion tonnes of CO_2 emission per year [2]. In more recent times, the development of alternative brick is considered as an ecofriendly solution to reuse waste by-products [i.e. fly ash and rice husk ash (RHA)] in alkali-activated binders in order to avoid the environmental impact associated with traditional PC bricks. Furthermore, natural resources can be conserved by avoiding the consumption of natural resources for brick manufacturing by the construction industry. Apart from saving natural resources and reducing wastes, strength and durability properties of alkali-activated bricks have also improved with the utilization of such wastes [3].

Fly ash is an industrial aluminosilicate by-product which is obtained from coal combustion in coal power plants. RHA, an agricultural residue, is obtained from combustion of rice husk in either rice mills or electricity-generated power plants. Previous studies have shown [3, 4] the use of RHA with low calcium fly ash to produce alkali-activated bricks. [3] reported the effect of replacing unground RHA as fine aggregates in the manufacturing of alkali-activated bricks. The results demonstrated that the bricks with up to 30% of the sand volume replaced by RHA performed well at a curing temperature of around 35 °C and a relative humidity of around 50% conforming to the Vietnamese standards for solid construction bricks. Huynh et al. [4] investigated the mechanical–microstructural properties and thermal conductivity bricks that contained different percentages of sodium-hydroxide-activated residual RHA and low calcium fly ash. The study concluded that 10% replacement of RHA brick samples provided the maximum compressive and flexural strength values, and these were 3.5 and 2.7% above the corresponding compressive strength and flexural strengths of the 100% fly ash bricks without RHA.

The present study investigates the RHA as a replacement (20% by weight) for low calcium fly ash alkali-activated bricks. Strength properties (i.e. compressive strength and tensile strength) were evaluated up to 90-day period, and the performances were compared with PC bricks having similar binder content. Results were explained by using microstructural analysis of both alkali-activated and PC bricks.

2 Material and Method

2.1 Materials Used

Low calcium class F fly ash and RHA were used as the source of aluminosilicate to produce alkali-activated bricks. Low calcium Fly ash was obtained from Lakvijaya coal power plant, Puttalam, Sri Lanka. The RHA was obtained from local rice mills in Sri Lanka and was ground into fine particles and sieved to achieve particles 75 microns and below. General-purpose cement was used as PC in accordance with [5]. The chemical composition, mineralogical composition and physical properties of raw materials are summarized in Table 1. The chemical composition and mineralogical composition and of fly ash, RHA and PC were determined by X-ray fluorescence (XRF) analysis and X-ray Diffraction (XRD) analysis.

For alkali-activated concrete mix, a combination of sodium hydroxide (NaOH with 15 M) and sodium silicate solution (Na_2SiO_3 with $SiO_2 = 14.7$, $Na_2O = 29.4\%$, $H_2O = 55.9\%$ by mass) was used as the alkaline binder. Natural river sand (uncrushed) in oven dried condition (with a specific gravity of 2.5 and fineness modulus of 2.75) and 10 mm crushed aggregate (with a specific gravity of 2.6 and water absorption of 0.76%) in saturated surface dry condition were used as fine and coarse aggregate in both mixes.

Table 1 Chemical composition of low calcium fly ash, RHA and PC

Component		Fly ash	RHA	PC
Chemical composition (%)	SiO_2	45.10	91.55	17.34
	Al_2O_3	33.22	0.42	4.00
	[a]$SiO_2 + Al_2O_3$	78.33	91.97	21.34
	Fe_2O_3	3.33	0.47	3.36
	CaO	9.26	1.25	69.32
	P_2O_5	1.30	1.43	0.78
	TiO_2	2.08	0.04	0.28
	MgO	2.27	1.28	1.68
	K_2O	0.74	2.87	0.54
	SO_3	0.56	0.21	2.43
	MnO	0.06	0.23	0.07
	Na_2O	1.07	0.00	0.00
Specific gravity		2.12	1.95	3.15
Amorphous Content (%)		55.8	53.1	18.2

[a] Total aluminosilicate content

2.2 Mix Design

The mix design was developed based on the activator modulus (AM), 1.375 (i.e. AM is the mass ratio of SiO_2 to Na_2O in an alkaline activator) for blended alkali-activated mortar, which has been already optimized for 100% fly ash alkali-activated binders [6]. The replacement level of RHA was optimized initially with the RHA replacement level of 10%, 20% and 30% for alkali-activated mortar by maintaining similar binder content with 100% fly ash mortar (473 kg/m^3). The average 28-day compressive strength was obtained for blended fly ash-RHA alkali-activated mortar for RHA replacement level of 10%, 20% and 30% as 29.7 MPa and 21.1 MPa and 10.4 MPa, respectively. The standard concrete building brick criteria was selected based on ASTM C55 (2017). This corresponds to a concrete building brick (225 mm × 110 mm × 75 mm) intended for interior and exterior use in constructing structural masonry. A considerably higher characteristic compressive strength than the recommended brick strength (17.2 MPa) was observed for the 10% RHA replacement mix, while 30% replacement of RHA showed significantly lower compressive strength than standard brick strength-based ASTM C55-17 (2017). Hence, 20% replacement level of RHA was selected for the brick mix design development by considering the recommended strength value for concrete building bricks of 17.2 MPa (equivalent to 19.8 MPa for 100 mm × 100 mm × 100 mm cube) and optimizing the level of RHA replacement. The water to solid ratio (w/s) is fixed to 0.37. The Na_2O dosage (i.e. mass ratio of Na_2O content in alkaline activator to fly ash) was maintained at a fixed value of 15% based on the previous study [7]. Mix design for 20% RHA replacement (denoted as 20RHA hereafter) was optimized by reducing binder content to develop equivalent strength and similar binder content for brick mix design with 100PC.

The mix design for 100PC concrete brick was developed according to the ACI 211 standards (2002). Target 28 day strength was selected as 15 MPa for 100PC concrete when developing the mix design in order to maintain similar strength with 20RHA concrete while maintaining similar binder content for both mixes. The mix proportions for each mix are summarized in Table 2.

2.3 Brick Production

Brick mixes were prepared using 100-L capacity mechanical mixer. First, dry materials (fly ash, RHA, PC, coarse and fine aggregate) are mixed for 4 min. Then, liquid materials (water, NaOH and Na_2SiO_3) are added to the dry mix and mixed for another 8 min until the mix was well combined. Immediately after mixing, the concrete mixture was poured into moulds and compacted using a vibration table to remove air bubbles. All 20RHA samples were maintained at room temperature for one day and then cured in a dry oven for 24 h at 80 °C temperature. After that, samples were demoulded and kept under ambient conditions until being tested. All 100PC

Table 2 Mix design for 20RHA and 100PC concrete (kg/m^3)

Material		20RHA	100PC [8]
Fly ash		221	–
RHA		55	–
PC		–	276
Aggregate	Fine	1051	1154
	Coarse	709	778
Water		5	194
NaOH		43	–
Na_2SiO_3		195	–
[a]w/s or bw/c		a0.37	b0.7

[a] w/s = (sum of water contained in the sodium silicate, sodium hydroxide and added water)/ (sum of the mass of source material (fly ash and RHA) and the solids contained in the alkaline activator solution), [b]w/c = water/cement

Fig. 1 Casted (**a**) 20RHA brick and (**b**) 100PC brick

brick specimens were demoulded 1 day after casting and then cured in a water tank at 23 °C until being tested. The cast 20RHA and 100PC brick are shown in Fig. 1.

2.4 Testing

The brick samples were manufactured and tested according to the minimum requirements of testing in compliance with the relevant Australian/New Zealand Standard (AS/NZS 4456) [9]. All strength properties were tested at 7, 28 and 90 days of age. The slump tests were conducted in accordance with AS1012.3.1 (2014) [10]. The compressive strength of concrete specimens (100 mm × 100 mm × 100 mm) was determined in accordance with AS/NZS4456.4 (2003) [11] with a loading rate of 9 MPa/min. The dry density of brick specimens (225 mm × 110 mm × 75 mm) was determined according to AS/NZS4456.8 (2003) [12]. The lateral mod ulus of rupture (MoR) is determined with a loading rate of 6 kN/min using the test specimens (300 mm × 75 mm × 75 mm) based on the AS/NZS4456.15 (2003) [13]. Indirect splitting strength (tensile strength) is determined using the MTS testing machine according to AS/NZS4456.18 (2003) [14]. The 20RHA and 100PC brick images are shown in Fig. 1.

3 Results

Density and workability

The density variation of 20RHA and 100PC concrete bricks up to 90 days is illustrated in Fig. 2. The dry density of the 20RHA increased from 2183.7 to 2189.5 kg/m^3 and 100PC from 2203.5 to 2222.8 kg/m^3. The 20RHA brick exhibited lower density (0.7–1% reduction) when compared to 100PC. A higher increment is noted at early age for 20RHA, 7–28 days, when compared with 100PC bricks. However, from 28 to 90 days, a higher incremental ratio is observed for 100PC (by 0.65%) when compared to 20RHA bricks (by 0.24%). When considering the workability, 20RHA had a slump of 305 mm, while 100PC exhibited a collapsed slump of 100 mm.

Compressive strength

Figure 3 illustrates the compressive strength development of 20RHA and 100PC brick samples up to 90 days. The compressive strength of all brick samples increased with the testing age. Compressive strength increased from 16.6 to 20.3 MPa for 20RHA, while 100PC showed an increment of 15.0–20.1 MPa between 7 and 90 days. Both bricks obtained similar compressive strength for 28 and 90 days. It was noted that the 20RHA mix obtained almost 82% of its ultimate strength in the first 7 days, while

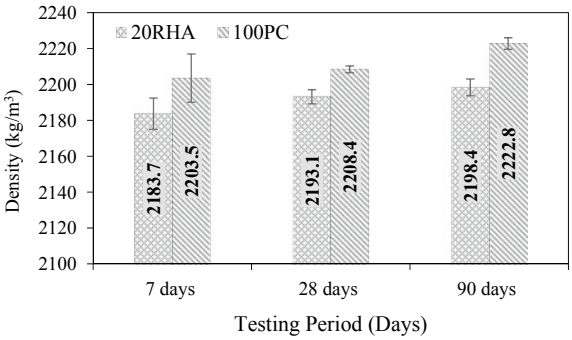

Fig. 2 Density development of 20RHA and 100PC bricks

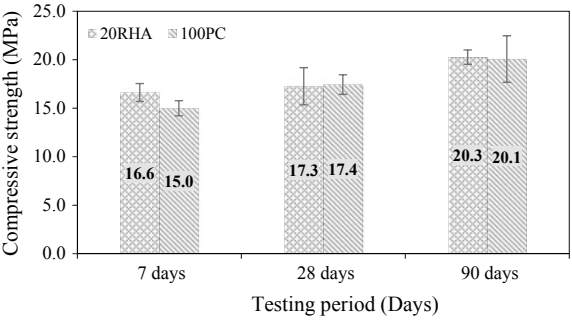

Fig. 3 Compressive strength development of 20RHA brick and 100PC brick up to 90 days

100PC brick gained approximately 75% of the strength gain at 7 days. The enhanced early age (7 day) strength gain observed for 20RHA brick is attributed to elevated temperature curing [15]. It is noteworthy that the lower growth rate of compressive strength (4%) between 7 and 28 days is observed for 20RHA when compared to 100PC brick (14%). However, from 28 to 90 days, both bricks showed an approximately 13–14% of strength gain in compressive strength. The compressive strength value recommended for concrete building brick (intended for interior and exterior use in constructing structural masonry) is 17.2 MPa brick strength (equivalent to 19.8 MPa for 100 mm × 100 mm × 100 mm cube strength) based on ASTM C55-17 (2017) [16]. Hence, 28 day strength results of the 20RHA bricks do not satisfy the strength requirement according to ASTM C55-17 (2017) [16]. However, the compressive strength value recommended for load-bearing solid concrete bricks (intended for load-bearing application in constructing structural masonry) is 13.8 MPa brick strength (equivalent to 15.9 MPa for 100 mm × 100 mm × 100 mm cube strength) according to the [17] for concrete brick production. Therefore, this satisfies the requirement of the 28-day brick strength as reported in Fig. 3; thus, the 20RHA mix can be used for structural masonry purposes utilizing as load-bearing bricks.

Tensile Strength

Figure 4 shows the variation of tensile strength (indirect splitting strength) of the 20RHA and 100PC bricks with time. Tensile strength increased from 3.2 to 3.7 MPa for 20RHA, while 100PC showed an increment variation from 3.1 to 3.6 MPa between 7 and 90 days. Overall, a slight increase in tensile strength is observed for 20RHA for all ages when compared with 100PC bricks.

Modulus of Rupture (MoR)

Figure 5 illustrates the MoR variation of the 20RHA and 100PC bricks. 100PC has the lowest MoR for all ages (ranged from 3.1 to 3.4 MPa), while 20RHA has the highest MoR, which ranges between 4.0 MPa and 4.8 MPa. Overall, a higher incremental ratio is observed for 20RHA from 7 to 90 days, approximately 19% (by 0.8 MPa) MoR. However, a slightly lower incremental ratio (12.4%) is observed from 7 to 90 days for 100PC bricks when compared to 20RHA. The reported lateral MoR is

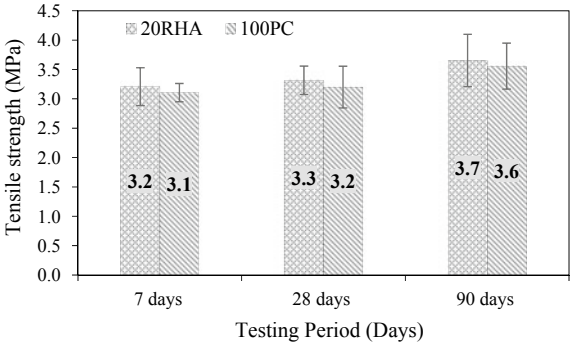

Fig. 4 Variation of tensile strength of 20RHA brick and 100PC brick up to 90 days

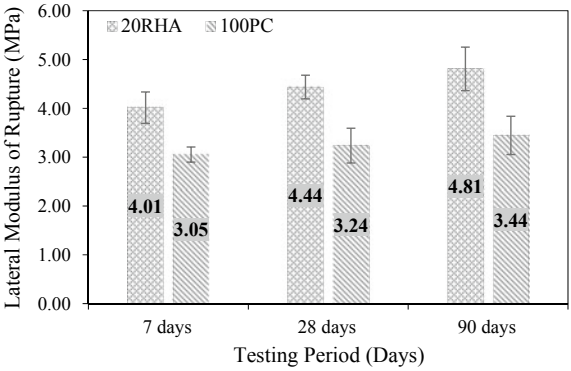

Fig. 5 Variation of lateral MoR of 20RHA brick and 100PC brick up to 90 days

in excess for all ages for both concrete as per the default value of 0.8 MPa stated in AS 3700.

4 Discussion

Alkali activation consists of several processes that take place in transforming a solid aluminosilicate source into a synthetic alkali aluminosilicate, i.e. Dissolution, Speciation Equilibrium, Gelation, Reorganization and Polymerization and Hardening [18]. Alkali-activated binders differ substantially from PC binders, mainly due to the different reaction mechanisms involved.

The 100PC showed a considerably higher collapsed slump due to the higher water/cement ratio. Although 20RHA showed a lower water/binder ratio than 100PC, the high flowability in 20RHA is due to the combined effect arise from the spherical shape of the fly ash particles (Fig. 5) and the lubricating nature of sodium silicate solution.

The blending of 20% RHA negatively contributed to the workability of 20RHA bricks. The irregular shaped, multilayered and microporous surface (Fig. 6) leads to attraction of more water molecules towards RHA particles. This is attributed as one of the reasons for the lower flow observed than the values reported in the literature [19] (i.e. 350 mm to 735 mm) for fly ash alkali-activated concrete. Furthermore, the higher unburnt carbon content (~6%) in RHA performs as an inert particulate and absorbs the available water and activator solution. The lower density of the 20RHA is due to the specific gravity of both fly ash and RHA, which is much lower than that of cement. This observation is consistent with the findings of the other researchers [20].

Generally, PC binders depend on the presence of calcium-silicate hydrate for matrix formation and strength, whereas alkali-activated binders utilize the polycondensation of silica and alumina precursors (fly ash and RHA) and a high alkali content

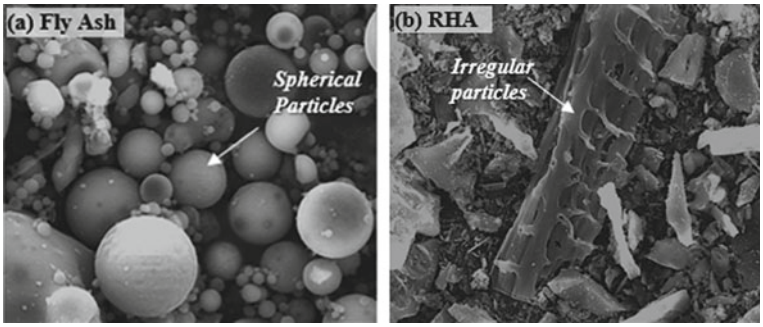

Fig. 6 SEM images of precursor material **a** fly ash and **b** RHA

to attain structural strength [21]. The primary binding phase in low calcium fly ash-based alkali-activated bricks (20RHA) is an alkali aluminosilicate hydrate (N–A–S–H) gel with composites, while calcium-silicate hydrate (C–S–H) is the principal binding phase in 100PC bricks [22]. The reason for the increment of all mechanical properties (including compressive strength, tensile strength and lateral MoR) over time for 20RHA is attributed to ongoing alkali activation and the continuous cement hydration reactions in 100PC bricks.

The 20RHA brick had higher tensile strength and MoR than 100PC bricks. The greater bond strength at the interface of the 20RHA alkali-activated binder and the aggregates make the fracture plane pass more through the aggregates than through the interface [23]. For 20RHA bricks, this resulted in a denser interfacial transition zone (ITZ) between aggregates and alkali-activated gel matrix as compared to that with PC matrix, Fig. 7. Past studies have reported that the ITZ in alkali-activated concrete is considered to be stronger than that in PC concrete [23]. The stronger ITZ contributed to the higher splitting tensile strength and bond strength (MoR) of the 20RHA bricks.

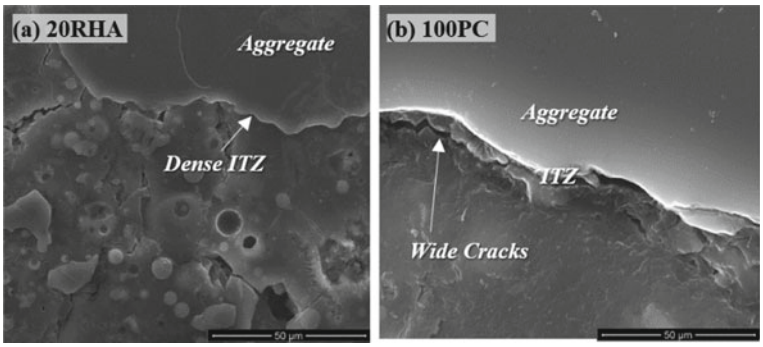

Fig. 7 SEM images of ITZ of **a** 20RHA and **b** 100PC brick

5 Conclusions

The present study investigated the strength performances of blended low calcium fly ash-Rice husk ash (RHA) alkali-activated bricks (20RHA) up to 90-day period and compared the results with Portland cement-based brick (100PC). The following conclusions are drawn based on the findings of this research:

- The 20RHA showed a compressive strength growth rate of 4% between 7 and 28 days as compared to 13.8% for 100PC bricks, with both achieving similar 28 day compressive strength (approximately 17 MPa).
- The strength data indicates that 20RHA bricks can be used for structural masonry purposes as load-bearing bricks.
- The blended fly ash-RHA leads to an increase in tensile strength properties, i.e. early age (7 day) tensile strength and modulus of rupture for all ages up to 90 days.
- Lower workability and lower density in the 20RHA compared to 100PC are due to the higher unburnt carbon content and lower specific gravity of fly ash and RHA.
- A stronger interfacial transition zone (ITZ) contributed to the higher splitting tensile strength and bond strength of the 20RHA bricks.

Acknowledgements Scholarship provided by the School of Engineering, RMIT University, Australia, Faculty of Engineering, University of Peradeniya, Sri Lanka, and Tokyo Cement Lanka PLC to the first author is gratefully acknowledged.

References

1. Weyant C, Athalye V, Ragavan S, Rajarathnam U, Lalchandani D, Maithel S, Baum E, Bond TC (2014) Emissions from South Asian brick production. Environ Sci Technol 48:6477–6483
2. Fernando KSDM, Nasvi MCM, Gunasekara MCM, Law DW, Setunge S, Dissanayake PBR (2021) Systematic review on alkali-activated binders blended with rice husk ash. J Mater Civ Eng 33:04021229
3. Hwang C-L, Huynh T-P (2015) Investigation into the use of unground rice husk ash to produce eco-friendly construction bricks. Constr Build Mater 93:335–341
4. Huynh T-P, Hwang C-L, Lin K-L, Ngo S-H (2018) Effect of residual rice husk ash on mechanical-microstructural properties and thermal conductivity of sodium-hydroxide-activated bricks. Environ Prog Sustainable Energy 37:1647–1656
5. AS 3972 (2010) General purpose and blended cements. Standards Association of Australia, Sydney
6. Fernando KSDM, Nasvi MCM, Gunasekara MCM, Law DW, Setunge S, Dissanayake PBR (2019) Mix optimization of geopolymer mortar produced with low calcium fly ash in Sri Lanka. In: 10th International conference on structural engineering and construction management (ICSECM*),* Kandy, Sri Lanka
7. Adam A (2009) Strength and durability properties of alkali activated slag and fly ash-based geopolymer concrete. Ph.D. thesis. RMIT University
8. ACI 211 (2002) Standard practice for selecting proportions for normal, heavyweight and mass concrete ACI: 211.1-91. American concrete Institute

9. AS 1012.3.1 (2014) Methods of testing concrete determination of properties related to the consistency of concrete—slump test. Standards Australia, Sydney
10. AS/NZS 4455.1 (2008) Masonry units, pavers, flags and segmental retaining wall units-Masonry units. Australian/New Zealand Standards
11. AS/NZS 4456.4 (2003) Masonry units, segmental pavers and flags—Methods of test Determining compressive strength of masonry units. Standards Australia
12. AS/NZS 4456.8 (2003) Masonry units and segmental pavers and flags—Methods of test—determining moisture content, dry density and ambient density. Standards Australia
13. AS/NZS 4456.15 (2003) Masonry units and segmental pavers and flags—methods of test—determining lateral modulus of rupture. Standards Australia
14. AS/NZS 4456.18 (2003) Masonry units and segmental pavers and flags—Methods of test—determining tensile strength of masonry units and segmental pavers. Standards Australia
15. Bakharev T (2005) Geopolymeric materials prepared using Class F fly ash and elevated temperature curing. Cem Concr Res 35(6):1224–1232
16. ASTM C55-17 (2017) Standard specification for concrete building brick. West Conshohocken, PA, ASTM International
17. ASTM C90 (2016) Standard specification for loadbearing concrete masonry units. ASTM International
18. Duxson P, Fernández-Jiménez A, Provis JL, Lukey GC, Palomo A, Van Deventer JS (2007) Geopolymer technology: the current state of the art. J Mater Sci 42:2917–2933
19. Gunasekara C, Setunge S, Law DW (2017) Long-term mechanical properties of different fly ash geopolymers. ACI Struct J 114
20. Ling IH, Teo DCL (2011) Properties of EPS RHA lightweight concrete bricks under different curing conditions. Constr Build Mater 25:3648–3655
21. Khale D, Chaudhary R (2007) Mechanism of geopolymerization and factors influencing its development: a review. J Mater Sci 42:729–746
22. Richardson IG (2008) The calcium silicate hydrates. Cement Concrete Res 38:137–158
23. Sarker PK, Haque R, Ramgolam KV (2013) Fracture behaviour of heat cured fly ash based geopolymer concrete. Mater Des 44:580–586

Sustainable Construction and Resource Efficiency

Modeling Building Envelop with Vertical Green Living Walls as an Urban Heat Island (UHI) Mitigation Strategy

T. A. N. T. Perera, G. Y. Jayasinghe, R. U. Halwatura, and H. T. Rupasinghe

Abstract Outdoor thermal comfort simulation has been modeled by ENVI-met 4.4.5 to explore the applicability of selected tropical plant species (*Axonopus fissifoliu*) under three different tropical conditions in Sri Lanka. The selected study locations were Colombo Sethsiripaya administrative complex, Matara urban council building, and Kandy urban council building. Different thermal performances of selected three plants out of nine plant species (*Desmodium triflorum, Roheo spathacea, Centella asiatica, Axonopus fissifoliu, Axonopus compressus, Elusine indica, Dieffenbachiae* spp*, Tectaria* spp*, and Bigonia* spp) have been investigated for 16 weeks. Thermal performances were assessed by comparing temperatures at (a) 20 cm distance in front of the green wall, (b) substrate surface of the green wall modules, and (c) inside the green wall compared to (d) adjacent bare wall (control). Because of its high LAI, *Axonopus fissifoliu* had the largest coverage on the living wall (LAI = 3.20). As a result, the influence of *Axanopus fissifoliu* on temperature reduction was investigated by modeling a selected building in an urban microclimatic context in Sri Lanka. *Axonopus fissifoliu* demonstrated the highest temperature decrease (5.06 °C) when compared to other species because it covers a large extent of the wall. The simulation study of the green walls created with *Axonopus fissifoliu* signified a possible maximum temperature reduction of 2.07 °C, 3.29 °C, and 2.03 °C in Colombo Sethsiripaya administrative complex, Matara urban council building, and Kandy urban council building, respectively. Therefore, installing vertical greening utilizing *Axonopus fissifoliu* can significantly improve the cooling effect in urban cities due to their optimal LAI values and thermal performances.

T. A. N. T. Perera · G. Y. Jayasinghe (✉)
Department of Agricultural Engineering, Faculty of Agriculture, University of Ruhuna, Mapalana, Kamburupitiya, Sri Lanka
e-mail: jayasinghe@ageng.ruh.ac.lk

R. U. Halwatura · H. T. Rupasinghe
Department of Civil Engineering, Faculty of Engineering, University of Moratuwa, Moratuwa, Sri Lanka

T. A. N. T. Perera
Department of Export Agriculture, Faculty of Animal Science & Export Agriculture, Uva Wellassa University, Badulla, 90000, Sri Lanka

R. Dissanayake et al. (eds.), *12th International Conference on Structural Engineering and Construction Management*, Lecture Notes in Civil Engineering 266,
https://doi.org/10.1007/978-981-19-2886-4_46

Keywords ENVI-met · Plant thermal performances · Tropical plants · Microclimate

1 Introduction

Green living walls provide significant social, environmental, and economic benefits such as significantly reducing the urban heat island (UHI) effect, reducing energy-related carbon dioxide emissions (over air conditioners), boosting citizens' well-being and productivity (aesthetic and noise control), and providing habitat for organisms. By incorporating greenery into urban settings, metropolitan environments will become more pleasant, cooler, and inconspicuous [1]. The selection of plant species for a living wall is influenced by various factors, including gardening structures, microclimatic conditions, sunlight exposure, and aesthetic values. Plant species that can be utilized for living walls vary depending on the microclimatic conditions (i.e., sun exposure, wind exposure, and height) around the building [2].

European researchers have explored living wall systems, and information regarding their positive benefits and emerging trends are available [3]. However, researches in tropical climates, particularly in Sri Lanka, have been limited. As a result, the current study was carried out to: (a) analyze the thermal and growth performance of tropical *Axonopus fissifoliu* on vertical living wall panels; and (b) visualize the feasibility of ENVI-met software with selected plant type in different climatic regions with selected plant. As a preliminary study, the feasibility of mitigating UHI was assessed using computer simulation and the adaptive usage of ENVI-met, a numerical simulation model software (LEONARDO). One of the most used dynamic simulation tools for microclimate modeling is the ENVI-met model. ENVI-met analyzes microclimate and air quality in cities, and its physical principles are based on fluid mechanics and thermodynamics [4].

2 Materials and Methodology

2.1 Plant Selection and Thermal Performance Study

The plant species were chosen based on a prior study done by Perera et al. [4]. Thermal performance of *Axonopus fissifoliu, Axonopus compressus*, and *Elusine indica* was investigated. In the research site, selected living wall panels were attached to a wall with a 10 cm air gap. The chosen wall faced west and therefore immediately exposed to sun radiation. Using a data logger type Graphtec-midi GL820, the (a) interior wall temperature, (b) ambient air temperature (20 cm above canopy level), and (c) substrate surface temperature were measured during the experimental period for both the vegetated and bare wall (control) during the day on a clear day. Measurements

were obtained every 10 min for 48 h at 1.5 m from the ground level, which is the sensible height of a person.

2.2 Simulation Study

The effect of *Axanopus fissifoliu* on temperature reduction in vertical living walls was investigated by simulating a selected building in several urban microclimatic contexts in Sri Lanka. The Colombo Sethsiripaya administrative complex (A_0), Matara urban council building (B_0), and Kandy urban council building (C_0) were chosen to symbolize distinct agro-climatic zones in the country. Furthermore, these places are densely inhabited during the day.

The 3D model of selected buildings with designed living walls utilizing *Axanopus fissifoliu* was created using ENVI-met version 4.4.5. Herath et al. [5] demonstrated that ENVI-met software may be used to simulate microclimates in tropical climates. As a result, preliminary validation of the ENVI-met was performed to assess the feasibility of using *Axanopus fissifoliu* by modeling the building on the Department of the Civil Engineering Department, University of Moratuwa, Sri Lanka (6.7969 °N, 79.9018 °E). In the software, a new database for *Axanopus fissifoliu* and the studied living wall system was built (Table 1).

Temperature changes were recorded by placing two temperature sensors 1.5 m above the ground. Temperature data were gathered in 10 min intervals for 48 h on the hottest day of the research period. All of the instances were simulated in ENVI-met program in 60 × 60 × 30 grid size with five nested grids. A plant database was created using the selected plant for all instances, with the details in Table 1 that are acceptable

Table 1 Created database for new living wall system

LAI	0.44
Leaf angle distribution	0.7
Plant thickness (m)	0.2
Substrate layer 1	Cocopeat
Substrate layer 1 thickness (m)	0.038
Emissivity substrate layer 1	0.85
Albedo substrate layer 1	0.7
Water coefficient of substrate layer 1 or plant	0.5
Substrate layer 2	Wooden panel
Substrate layer 2 thickness (m)	0.02
Emissivity substrate layer 1	0.95
Albedo substrate layer 1	0.9
Water coefficient of substrate layer 1 or plant	0.5
Air gap between wall and living wall (m)	0.15

for tropical climates. For further discussion, the simulation was performed for 24 h on a hot, humid day, taking into account day and night time thermal performances.

To represent existing microclimatic conditions in the selected sites, the Sethsiripaya administrative complex, Colombo (A_1), Matara urban council building (B_1), and Kandy urban council building (C_1) were modeled.

Additionally, selected locations were modeled with vertical living walls (A_2, B_2, and C_2) to compare temperature reduction with current circumstances (Fig. 1). Table 2 summarizes the meteorological input data utilized in the research. The Colombo meteorological department provided hourly climatic data.

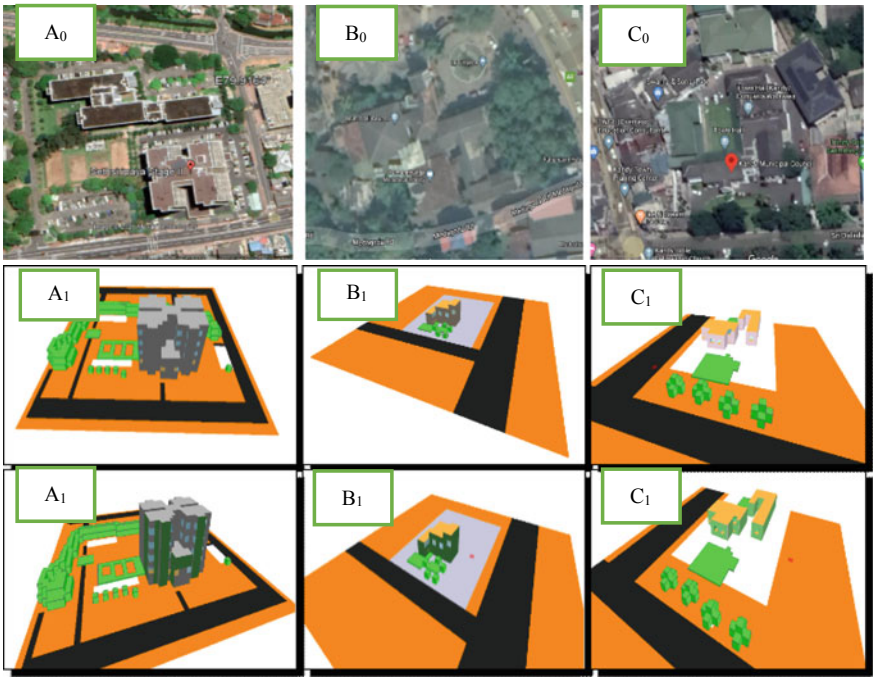

Fig. 1 Selected study sites (A_0) Sethsiripaya administrative complex (Colombo), (B_0) Matara urban council building, (C_0) Kandy urban council building. Existing building model of A_1) Sethsiripaya administrative complex B_1) Matara urban council (C_1) Kandy urban council. Building model with *Axanopus fissifoliu* vertical living wall (A_2) Sethsiripaya administrative complex (B_2) Matara urban council building (C_2) Kandy urban council

Table 2 Meteorological input data for the model

Condition	Colombo	Matara	Kandy
Simulating duration (h)	24	24	24
Start time (h)	1900	1900	1900
Wind speed (m/s)	2.2	5	0.2
Wind direction	270°	270°	270°
RH in 2 m (%)	75	75	75
Specific humidity at model top	9	9	9
Roughness length at the measuring site	0.1	0.1	0.1
Initial temperature (°C)	28	28	28

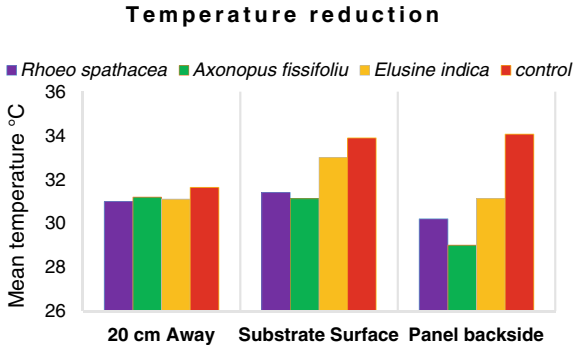

Fig. 2 Temperature reduction of each species

3 Results and Discussion

3.1 Plant Selection and Thermal Performance Study

According to Fig. 2, different plant species showed varying temperature which decreases behind the panels. The average temperature difference between the exterior and surface of the green facades, according to [6], was 2.4 °C. The *Axonopus fissifoliu* had the greatest temperature gradient across the wall of the three species studied.

3.2 Simulation Study

Outdoor thermal environmental variations were simulated by integrating a living wall with *Axanopus fissifoliu* to the building envelope. Three-dimensional models of selected government administrative buildings in Colombo, Matara, and Kandy were built, both with and without living walls. Previous research has validated ENVI-met

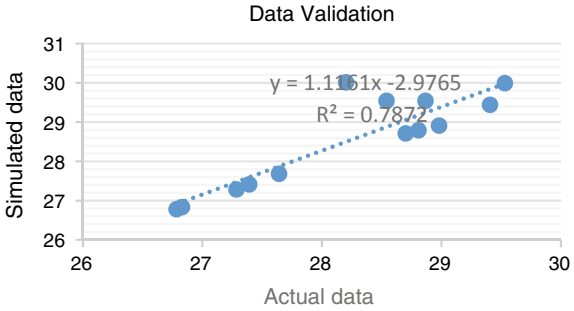

Fig. 3 Regression plot for data validation

software for tropical climate [7] and subtropical climate [8]. The above investigations had R^2 values of 0.96 and 0.69, respectively. In Sri Lanka, [5] found 0.78, 0.80, and 0.91 R^2 values for asphalt, cement, and grass at 1.5 m above ground. The coefficient of determination (R^2) between the simulated temperature values from the software and the actual observed data in this investigation was 0.78 (Fig. 3). Because R^2 in this simulation model is close to 1, it may be used in microclimatic simulations with *Axanopus fissifoliu* living walls.

Sethsiripaya administrative complex (Colombo-A_0) current building modeling results in an average temperature ranging from 26.98 to 33.71 °C, with the greatest temperature recorded at 11.00 h. The highest temperature reduction after enclosing the building with vertical living wall was 2.07 °C. The average temperature with the living wall ranged from 26.96 to 31.99 °C, with the maximum temperature reaching 31.99 °C at 11.00 h (Fig. 4a).

Matara municipal council, existing building modeling results in an average temperature ranging from 26.61 to 31.91 °C, with the maximum temperature reaching 31.91 °C at 11.00 a.m. The average temperature range with the living wall was 26.16–30.53 °C, with highest temperatures of 30.53 °C at 13.00 h (Fig. 4b). However, the highest temperature drop was recorded at 10.00 h as 3.29 °C.

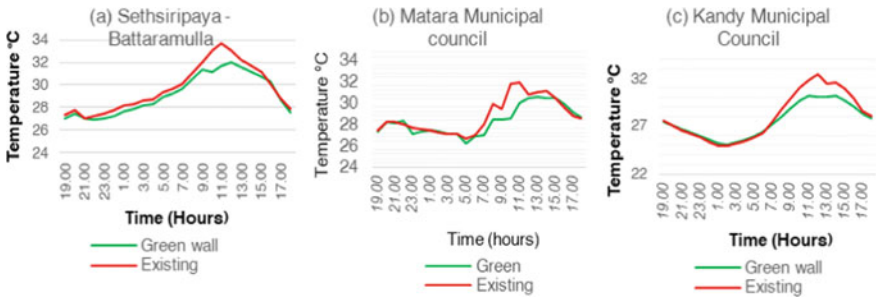

Fig. 4 Temperature variations in each locations with the time **a** Sethsiripaya, **b** Matara urban council, **c** Kandy urban council

Kandy municipal council building was built mostly with concrete walls and terracotta roofs. Temperatures vary from 24.85 to 32.37 °C in the current building condition and from 25.04 to 30.06 °C in the living wall condition. At 12.00 h, the maximum temperature drop caused by the *Axanopus fissifoliu* living wall was 2.03 °C (Fig. 4c). The Kandy municipal council building's pavements and floor have been adorned with decorative concrete blocks. It might be the cause of the high temperatures that surround the structure, despite the fact that there was acceptable greenery. Impermeable surfaces prevent cooling from occurring through evapotranspiration and water infiltration [9].

The albedo of building materials, pavements, and roads can be affected by high temperatures in the proximity of these structures. Concrete was used to make all of the building walls as well as the terracotta roofing and concrete slabs. The usage of asphalt roads, concrete, and bricks with high albedo absorbs solar energy and re-emits it into the environment, causing temperature to rise [10]. Takkanon and Chantarangul [11] found that non-shaded asphalt surfaces exhibited a significant temperature differential ranging from 39.00 to 49.70 °C. Bangkok's temperature has fallen by 3.80 °C due to the greenery. Numerous earlier research proposed various materials for surfaces with low albedo values ranging from 0.41 to 0.77 [9]. The majority of the building's walls are made up of glass windows. It causes lengthy solar waves to be blocked and reflected back into the surroundings. As a result, the building becomes extremely hot, necessitating the installation of additional air conditioners. There was less greenery around the structures. Photosynthesis helps to cool the atmosphere by absorbing solar energy and CO_2 and then releasing water vapor into the surroundings. As a result, decreased vegetation may result in a reduced cooling effect [12].

4 Conclusion

Based on the findings of this study, it is possible to conclude that covering the walls with vegetation can reduce the maximum temperature of the wall surface. Heat fluctuations of up to 5.06 °C were measured in the living walls. *Axonopus fissifolius* had the greatest temperature decrease, followed by *Roheo spathacea* and *Elusine indica.* Maximum temperature reductions from using *Axonopus fissifolius* plants in vertical living walls in tropical climates range from 2.03 to 3.29 °C. Temperature reductions in the Sethsiripaya administrative complex (Colombo), Matara urban council building, and Kandy urban council building were 2.07 °C, 3.29 °C, and 2.03 °C, respectively. Further studies on a broader range of plant species, substrate preparations, and irrigation management are mandatory to assess for long-term usage in green infrastructure for Sri Lanka. It is necessary to determine the sustainability of living wall plants and media in a tropical context, both with and without supplementary irrigation.

References

1. Perkins M, Joyce D (2012) Living wall and green roof plants for Australia. RIRDC-Available at: https://rirdc.infoservices.com.au/items/11-175
2. Pérez G, Coma J, Sol S, Cabeza LF (2017) Green facade for energy savings in buildings: the influence of leaf area index and facade orientation on the shadow effect. Appl Energy 187:424–437. https://doi.org/10.1016/j.apenergy.2016.11.055.32 Elsevier Ltd
3. Malys L, Marjorie M, Christian I (2014) A hydrothermal model to assess the impact of living walls on urban microclimate and building energy consumption. Build Environ 73:187–197. https://doi.org/10.1016/j.buildenv.2013.12.012
4. Perera TANT, Jayasinghe GY, Halwatura RU, Rupasinghe HT (2021) Modelling of vertical greenery system with selected tropical plants in urban context to appraise plant thermal performance. Ecol Indicators 128:107816. https://doi.org/10.1016/j.ecolind.2021.107816. ISSN 1470-160X
5. Herath HMPIK, Halwatura RU, Jayasinghe GY (2017) 'Evaluation of green infrastructure effects on tropical Sri Lankan urban context as an urban heat island adaptation strategy. Urban For Urban Greening 29(November):212–222. https://doi.org/10.1016/j.ufug.2017.11.013.93 Elsevier
6. Widiastuti R, Prianto E, Budi WS (2016) Performance evaluation of vertical gardens. Int J Arch Eng Const 5:13–20
7. Ghaffarianhoseini A, Berardi U (2015) Thermal performance characteristics of unshaded courtyards in hot and humid climates. Build Environ 87:154–168
8. Gusson CS, Duarte DHS (2016) Effects of built density and urban morphology on urban microclimate—calibration of the model ENVI-met V4 for the subtropical Sao Paulo, Brazil. Procedia Eng 169:2–10. https://doi.org/10.1016/j.proeng.2016.10.001
9. Sailor DJ (2006) Mitigation of urban heat islands-recent progress and future prospects. Paper presented at the Paper presented on American meteorological society 6th symposium on the urban environment and forum on managing our physical and natural resources
10. Huttner S, Bruse M, Dostal P (2008) Using envi-met to simulate the impact of global warming on the microclimate in Central European Cities. In: 5th Japanese-German meeting on urban climatology, pp 307–312
11. Takkanon P, Chantarangul P (2019) Effects of urban geometry and green area on thermal condition of urban street canyons in Bangkok. Arch Sci Rev 62(1):35–46. https://doi.org/10.1080/00038628.2018.1534724. Taylor and Francis Ltd.
12. Palomar T, Silva M, Vilarigues M (2019) Impact of solar radiation and environmental temperature on Art Nouveau glass windows. Herit Sci 7:82. https://doi.org/10.1186/s40494-019-0325-3

Role of Compatibilization of Phthalic Acid in Cassava Starch/Poly Vinyl Alcohol Thin Films

O. H. P. Gunawardene, S. M. Amaraweera, W. M. D. B. Wannikayaka, N. M. L. Fernando, C. A. Gunathilake, W. A. Manamperi, A. K. Kulatunga, and A. Manipura

Abstract Owing to rapid industrialization and urban development across the globe, the usage of non-degradable petroleum-based plastic materials has been drastically increased leading to accumulation of inert plastic waste which takes billions of years to naturally degrade. Therefore, this work focuses on producing and evaluating "green" multifunctional film materials based on a mixed eco-friendly thermoplastic starch (TPS)/polyvinyl alcohol (PVA) matrix compatibilized with phthalic acid. In this study, the blend films of gelatinized TPS/PVA thin films were prepared by means of solution casting. Fourier transform infrared spectroscopy (FTIR) was used to evaluate the structure of the films while the dynamic mechanical analysis (DMA) and thermogravimetric analyzer (TGA) were used to examine the thermal behavior. The tensile, water absorption, and the biodegradability tests were carried out according to ASTM-D-882-02, ASTM-D-570-98, and aerobic compost environment test, respectively. Compatibilized blends exhibited enhanced thermal stability and homogeneity forming new hydrogen bonds in the presence of phthalic acid while possessing a dense molecular network. Moreover, the biodegradation was slowed by the incorporation of phthalic acid while the least water absorption capacity was demonstrated by the TPS/PVA (40/60 % w/w) blend compatibilized with 5 wt% phthalic acid (T4P6-5) valuing 43.8%, and 55.2% at 2 h and 24 h, respectively. Besides, improved mechanical properties could be obtained by T4P6-5 blended film

O. H. P. Gunawardene · W. M. D. B. Wannikayaka · C. A. Gunathilake (✉) · A. Manipura
Department of Chemical and Process Engineering, Faculty of Engineering, University of Peradeniya, Peradeniya, Sri Lanka
e-mail: chamila@wyb.ac.lk; chamilag@pdn.ac.lk

S. M. Amaraweera · N. M. L. Fernando · A. K. Kulatunga
Department of Manufacturing and Industrial Engineering, Faculty of Engineering, University of Peradeniya, Peradeniya, Sri Lanka

C. A. Gunathilake
Department of Nano Science Technology, Faculty of Technology, Wayamba University of Sri Lanka, Kuliyapitiya, Sri Lanka

W. A. Manamperi
Materials Engineering Department, California Polytechnic State University, San Luis Obispo, USA

R. Dissanayake et al. (eds.), *12th International Conference on Structural Engineering and Construction Management*, Lecture Notes in Civil Engineering 266,
https://doi.org/10.1007/978-981-19-2886-4_47

valuing 30.2 MPa and 221.6% for tensile strength and elongation at break, respectively. Therefore, enhanced mechanical and thermal properties, lower water absorption, non-toxicity, and low cost make the compatibilized cassava starch/PVA films beneficial for potential food packaging applications.

Keywords Biodegradable thin films · Cassava starch/PVA blends · Compatibilization · Mechanical properties · Phthalic acid

1 Introduction

Due to the rapid industrialization and urban development across the globe, the usage of petroleum-based inert plastics has been drastically increased [21, 28, 67] in daily life, the biomedical field, agriculture, and in the food industry [27, 47] owing to their low cost, lightweight [17], strength-to-weight ratio, easy processability, durability [1, 17, 42] improved barrier properties, and heat stability [26]. However, the tremendous increase in the usage and production of petroleum-based plastic materials has resulted in the generation of huge amounts of plastic waste on the land sites [28, 48] since they take 100–450 years to naturally degrade [12, 22, 44, 45]. Apart from the above, it is a well-known fact that non-degradable polymers are derived from petroleum and its allied components [67]. Consequently, the depletion of petroleum resources can occur since the natural resources take millions of years to form and are finite in quantity [2].

Despite the fact that, at present, numerous ways of managing polymeric wastes are introduced, including incineration, recycling, and energy recovery systems, incineration in landfilling sites may lead to the release of heat and unacceptable emissions of harmful compounds, such as greenhouse gases and volatile compounds, into the atmosphere [49, 64] while the recycling process is rarely used due to the consumption of a considerable amount of thermal energy, complexity of design, and relatively high cost, which reduces the process sustainability [18, 26]. Nevertheless, plastic waste cannot be recycled forever. Thus, waste plastics are eventually destined to be burnt or buried in landfilling sites [26]. Therefore, disposal problems, strong regulations, criteria for a cleaner and safer environment [11, 45], as well as the global shortage of petroleum resources have driven the development of biodegradable and renewable materials [22, 50].

Generally, single-use plastic materials used in food packaging applications, personal care products, agricultural purposes, and fishing equipment which are not collected after use are released directly into the environment [40]. Therefore, it is conclusive that recycling is not practicable and economical for single-use plastics [3]. At present, due to the depletion of petroleum resources and environmental concerns, the development of environmentally friendly alternatives to meet the ever-increasing demand for plastics materials which are known as "green materials" [65] has become of vital importance. Therefore, many approaches are currently underway to utilize

biodegradable polymers as alternatives for non-biodegradable polymers, minimizing the environmental issues and other commercial issues as mentioned previously [59].

Interestingly, starch, as a packaging material, has attracted much attention both in academia and industry [8, 15] owing to its high production from annually renewable resources [58, 61], biodegradability [61], low cost, easy handling [47], and the capability of dissolving in water [34]. Among different botanical origins of starch production, cassava is considered to be one of the major tuber crops which is grown in more than 80 countries due to its easy growing nature and at the expense of minimum labor and fertilization as well as comparatively higher yield [20].

Despite starch's inherent superior properties, native starch cannot be utilized in practical applications due to its ever-increasing brittleness with time in the absence of a suitable plasticizer, poor processability, poor nature in storage stability, as well as poor mechanical and thermal properties [3, 13, 33]. Though starch is plasticized to obtain thermoplastic starch (TPS) in order to overcome the disadvantageous properties of native starch, TPS alone also cannot be used as a substitute for petroleum-based inert plastic materials due to its poor mechanical and thermal properties, water sensitivity, deterioration of mechanical properties during the exposure to humid environments, poor barrier properties, and plasticizer migration [3, 7, 25, 44, 68]. On the contrary, packaging films composed of entirely of starch, however, lack the strength and rigidity to withstand the stresses to which many packaging materials are subjected. Hence, the logical solution is to incorporate starch into a film with a stronger support base [28] in terms of widening its range of applications [47]. Therefore, the blending of TPS with synthetic biodegradable polymers has become an attractive pathway to overcome the major drawbacks associated with TPS while achieving specific requirements of a particular application [3].

Interestingly, in recent, the blending of TPS and polyvinyl alcohol (PVA) has captured a greater attention since, starch lowers the cost, improves gas barrier properties, and enhances the biodegradation rate while PVA is capable of improving excellent mechanical, thermal, and water resistance properties of the film materials [22, 26, 30, 39, 47]. PVA is one of the few synthetic polymers which is produced via hydrolysis of polyvinyl acetate [39], a non-petroleum route [30]. Moreover, PVA is a water-soluble polymer [39] which possesses distinct characteristics including chemical resistance [11], non-toxicity [6, 68], easy processability [27], higher thermal stability [36], biocompatibility [44], better mechanical [6, 11, 12, 44], and barrier properties [22]. Since 1980s, starch/PVA blends have been underway to examine primarily for preparing films by means of solution casting [39, 60], since PVA is easily degraded during the melt processing [56].

Even though the combined properties of starch/PVA make them as popular biodegradable blends, mechanical and water barrier properties are still poorer than those of some synthetic petroleum-based polymeric materials [27, 47]. Furthermore, from cost and practicality point of view, it is preferable that the blend contains as much as starch as possible. However, the properties of the blends deteriorated as the starch content in the blend films increased owing to poor compatibility between starch and PVA leading to phase separation during blend preparation [22].

Therefore, many techniques are currently underway to improve the compatibility between PVA and starch such as addition of nanoparticles, plasticizers, plasma treatment, cross-linking agents, acid modification [60], fillers [35], and compatibilizers [21]. Several studies have previously investigated the effective compatibilization of starch/PVA blend films. Jose et al. [31] reported that the fall in tensile strength, elastic modulus, and elongation at break can be overcome by incorporating carbon nanotubes into corn starch/PVA blend films. Besides, Widiarto [62] showed the effective improvement of mechanical properties in sago starch/PVA/glycerol blend films in the presence of Borax as the cross-linking agent. Jayasekara et al. [28] displayed a reduction of the hydrophilic nature of starch/PVA blends via surface modification by chitosan. On the contrary, Park et al. [45] studied the gradual increase of tensile strength, elongation at break and degree of swelling of corn starch/PVA blend films with the increased addition of citric acid. Aswathy et al. [6] achieved enhanced water barrier properties, UV barrier properties, and mechanical properties by incorporating ZnO nanoparticles into starch/PVA biodegradable films. Apart from the above, Khan et al. [34] cured sago starch/PVA blends using UV radiation to obtain better physical properties. In contrast, an improved compatibilization between potato starch and PVA was obtained while improving mechanical properties in the presence of $CaCl_2$ as a plasticizer [30]. Furthermore, enhanced mechanical properties, reduced water absorption capacity, and water solubility in corn starch/PVA/glycerol films were observed in the presence of succinic acid as the compatibilizing agent [26, 66]. Moreover, Kochkina and Butikova [35] noted an improvement in both tensile strength and water vapor transmittance in maize starch/PVA composite films by the addition of TiO_2 particles. However, the increased addition of silica as a filler material has reported a deterioration in essential properties such as tensile strength, elongation at break, water resistance in sago starch/PVA blends [26]. Also, it was revealed that an enhancement of mechanical properties and water resistance could be obtained by incorporating nano-SiO_2 in corn starch/PVA blend films [57]. Furthermore, a twofold increase in modulus and a significant improvement in both tensile strength and stiffness depending on the storage conditions were obtained in starch/PVA blend prepared via simultaneous cross-linking and cellulose nano-fiber addition [44].

In this study, we report the effect of phthalic acid in cassava starch/PVA/glycerol thin films on mechanical properties, biodegradability, water uptake, and thermal stability. Herein, the thin films were prepared via solution casting while the cassava starch used during the film preparation was extracted in the laboratory. To the best of our knowledge, this is the first attempt to use phthalic acid as a cross-linking agent while acting as a compatibilizer in TPS/PVA blend films which are capable of replacing petroleum-based inert plastic packaging materials.

2 Materials and Methods

2.1 Materials

PVA (Molecular weight; 27,000) for the study was purchased from Inner Mongolia Shuangxin Environment-friendly Material Co., Ltd. Glycerol (not less than 99.0%) and Phthalic acid (97%) were of analytical grade were purchased from Sigma Aldrich Co., St. Louis, MO, USA and Sisco Research Laboratories Pvt. Ltd., respectively. All the reagents were used without any further purification. Native cassava starch extracted using a wet method was used for thin film preparation.

2.2 Extraction of Cassava Starch

Extraction of cassava starch was performed according to the wet method described by Benesi et al. [9]. Initially, cassava roots were peeled, washed, and disintegrated into cubes of 1 cm × 1 cm × 1 cm. Afterward, the obtained cassava cubes were pulverized in a high-speed blender for 5 min. Next, the resulted pulp was suspended in water such that the mixture contained pulp: water volume fraction at 1:10 and stirred for 5 min. Subsequently, the pulp was filtered using a double-fold cotton cloth, and the filtrate was maintained at rest for 2 h for the settlement of starch granules. Then, the top liquid was discarded. After that, water was added to the sediment, and the mixture was vigorously stirred for 5 min. Finally, the extracted cassava starch was dried at 65 °C for 3 h. After the extraction process, the yield was evaluated and it was around 20.21 ± (0.01)%. The extracted—dried cassava starch was passed through a 100-mesh sieve before using for further experiments.

The moisture, protein, fat, ash, and the fiber contents of the extracted cassava starch were determined using the Association of Official Analytical Chemists (AOAC) 920.36, 984.13, 948.22, 923.03 (2000), and AOAC 962.09 (2005) standards, respectively [4, 5], while the amylose and amylopectin content in extracted cassava starch was determined by the blue value method described by Stawski [55]. The gelatinization temperature was measured using the differential scanning calorimetry (DSC, 131-Evo, Setaram Instrumentation, Caluire, France). The moisture content of the extracted cassava starch was approximately 12 ± (0.01)%, whereas the gelatinization temperature of starch was 43.27 °C. The composition of the dry cassava starch used for the thin film preparation is depicted in Table 1. All the analyses were carried out in triplicate.

Table 1 Composition of the extracted cassava starch using the wet method

Components	Percentage (%)
Protein	0.66 ± (0.00)
Fat	0.19 ± (0.00)
Ash	0.23 ± (0.00)
Crude fiber	0.10 ± (0.01)
Amylose	21.04 ± (0.01)
Amylopectin	76.69 ± (0.00)
Other elements	1.09 ± (0.00)

2.3 Preparation of Thin Films

2.3.1 Preparation of Film Forming Dispersion

Biodegradable thin films were obtained by means of solution casting procedure after the preparation of film forming dispersions according to the method described by Cano et al. [12], along with some modifications.

PVA (5% w/w) was dispersed in an aqueous solution at 85 °C for 1 h while being stirred at 600 rpm for the preparation of neat PVA thin films.

For the preparation of thermoplastic starch film, cassava starch (5% w/w) and glycerol (cassava starch: glycerol weight ratio was maintained at 1: 0.25, on the basis of previous study [62]) were dispersed in an aqueous solution at 85 °C for 30 min under vigorous stirring at 600 rpm to induce starch gelatinization.

TPS/PVA film forming dispersions were obtained as follows. Initially, the pre-calculated amounts (compositions of thin films are depicted in Table 2) of cassava starch and glycerol were dissolved in distilled water and stirred at 600 rpm at 85 °C

Table 2 Composition and the thickness of cassava starch-based biodegradable thin films (w.r.t.: with respect to)

Sample code	TPS % w.r.t total polymer weight	PVA % w.r.t total polymer weight	Phthalic acid % w.r.t TPS share	Thickness (mm)
T	100	0	0	0.14 ± (0.03)
P	0	100	0	0.10 ± (0.02)
T4P6-0	40	60	0	0.23 ± (0.05)
T4P6-1	40	60	1	0.22 ± (0.03)
T4P6-2	40	60	2	0.22 ± (0.02)
T4P6-5	40	60	5	0.18 ± (0.04)
T6P4-0	60	40	0	0.25 ± (0.03)
T6P4-1	60	40	1	0.23 ± (0.04)
T6P4-2	60	40	2	0.22 ± (0.02)
T6P4-5	60	40	5	0.19 ± (0.04)

for 30 min. The respective amount of PVA was dispersed in another aqueous solution while being stirred at 600 rpm at 85 °C for 15 min. Afterward, the PVA solution and gelatinized TPS solution were mixed together such that the total polymer weight ratio in the mixture was maintained at 5% w/w. Subsequently, the dispersion was rapidly stirred at 85 °C for another 1 h at 600 rpm to form a homogeneous gel-like solution. The TPS/PVA weight ratios were maintained at 40/60, and 60/40, respectively.

For the preparation of TPS/PVA compatibilized blends, phthalic acid was incorporated at 1, 2, and 5 wt%, w.r.t TPS share. Initially, the pre-calculated amounts of cassava starch and glycerol were dissolved in distilled water and stirred at 600 rpm at 85 °C for 30 min. The respective amount of PVA was dispersed in another aqueous solution while being stirred at 600 rpm at 85 °C for 15 min. Next, the PVA solution and gelatinized TPS solution were mixed together such that the total polymer weight ratio in the mixture was maintained at 5% w/w. Subsequently, the dispersion was rapidly stirred at 85 °C for another 30 min at 600 rpm. Afterward, the respective amount of phthalic acid was incorporated and the mixture was allowed to homogenize at 85 °C for another 1 h at 600 rpm.

2.3.2 Film Formation

From the above-described film forming dispersions, dried thin films were obtained by means of solution casting method. Freshly obtained hot dispersions were poured into petri dishes (12 cm diameter) in the right amount to provide a surface solid density at 88.41 gm^{-2}. Afterward, these petri dishes were left under room temperature for 6 h to allow bubbles to dissipate. Subsequently, the petri dishes were dried at 65 °C for five hours. Next, the petri dishes were conditioned in a desiccator for 24 h and finally, peeled off the casting surface.

2.4 Characterization of the Prepared Thin Films

2.4.1 Fourier Transforms Infrared Spectroscopy (FTIR)

FTIR spectra of prepared thin films were obtained using FTIR Spectrum two (PerkinElmer, USA) equipped with ATR reflectance cell. Spectra were collected in the wave number range of 400–4000 cm^{-1}. For each sample, 4 scans were taken at a resolution of 4 cm^{-1}. FTIR spectra were analyzed using the Origin software.

2.4.2 Thermogravimetric Analysis (TGA)

The thermal weight loss (TG), and its derivative (DTG), of the thin film samples, native cassava starch powder, and PVA crystals were obtained using a TGA 4000 (PerkinElmer, USA) under the nitrogen atmosphere. To this end, approximately

10 mg of each sample was placed in platinum pans of 100 μl with a heating rate of 15 °C/min while maintaining the temperature range from 50 to 700 °C [39]. The maximum degradation temperature, difference in temperature at maximum degradation, residue mass at 600 °C were calculated using the TRIOS software (4.4.0 version, PerkinElmer, USA).

2.4.3 Dynamic Mechanical Analysis (DMA)

Dynamic mechanical analysis (DMA) was carried out using the DMA Q8000 (TA Instruments, New caste, DE, USA) in tension mode at a frequency of 1 Hz. A standard heating rate of 5 °C min^{-1} over a temperature range of −60 to 80 °C was used.

2.5 Evaluation of Physical Properties

2.5.1 Film Thickness

The thickness values of the prepared thin films were measured at twelve random positions using a manual Thickness Gauge (Te Clock Dial, SM—528) to the nearest 0.01 mm.

2.5.2 Mechanical Test

The mechanical test was conducted according to ASTM-D 882-02 to investigate the tensile strength and percentage elongation at break. The tensile strength test was performed using the Intron 3365 Universal Testing machine (Instron Ltd, Buckinghamshire) with crosshead speed fixed at 25 mm/min. All the specimens were prepared according to the dimensions provided by the standard. The specimens were cut from the thin films (five different samples from one film) bearing 30 × 110 cm^2 dimensions. For each test, five samples were analyzed. During the stretching, the tensile strength (MPa) and elongation at break were recorded. The mechanical properties were calculated as the average of five measurements.

2.5.3 Water Absorption Test

The percentage water absorption of the prepared thin films was measured according to ASTM-D570-98. Initially, all the samples were conditioned at 50 °C for 24 h and weighed (M_o) before being tested. Afterward, the samples were soaked in distilled water. After 2 h, all the samples were removed from distilled water, blotted with a cloth, and immediately weighed (M_1). Next, those samples were soaked in water

for another 22 h and weighed (M_2). The experiments were carried out in triplicates. The percentage water absorption capacities of the thin films were calculated as demonstrated in Eqs. (1) and (2).

$$\text{Water absorption } (\%) \text{ at } 2\,\text{h} = \frac{M_1 - M_0}{M_0} \times 100 \tag{1}$$

$$\text{Water absorption } (\%) \text{ at } 2\,\text{h} = \frac{M_2 - M_0}{M_0} \times 100 \tag{2}$$

2.5.4 Biodegradability Test

The degradation behavior of prepared thin films was investigated according to the aerobic compost environment test described by Seligra et al. [51]. The compost soil used as the compost medium consists of 13.87% of total C and 1.07% of total N, respectively. Initially, the test specimens were cut into square pieces of 2.0 cm × 2.0 cm. Afterward, the samples were buried inside the soil medium at a depth of 3 cm at 25 °C. Water was sprayed to maintain the moisture content of the compost environment. The remaining weight of the thin film over the degradation period was measured according to the given Eq. (3).

$$\text{Remaining amount of weight } (\%) = \frac{W_1}{W_0} \times 100 \tag{3}$$

where W_0 and W_1 are the weights of thin films before and after the test, respectively. The reported results represent the average of three replicates for each sample.

3 Results and Discussion

3.1 General Properties of the Thin Films

During drying of the thin films, all the films were not allowed to be completely dried in order to maintain flexible and not brittle. According to visual inspection, the air–contact surface was slightly rougher compared to that of the glass contact surface of the solution cast films as previously reported by Jayasekara et al. [28]. The neat PVA thin films were completely transparent and the flexibility was comparatively higher. Moreover, the neat PVA films were easily peeled off from the petri dishes as mentioned by Awasthy et al. [6]. Despite the fact that neat PVA films were completely transparent, the neat TPS films were somehow opaque. Besides, the addition of starch to PVA reduced the transparency to some extent as noted by, Jayasekara et al. [6], Widiarto [28] and Awasthy et al. [62].

3.2 *Molecular Interactions of Thin Films*

Surface characterization plays a vital role in determining the interactions between the components and the structure after incorporation of phthalic acid. Figure 1 demonstrates the FTIR spectra of PVA crystals, cassava starch powder, pure TPS/PVA thin films, and TPS/PVA films compatibilized with phthalic acid. According to the peak assignment, it is evidenced that, the FTIR spectra of PVA crystals exhibit absorbance bands related to C=O group and C–O–C group vibrations and this indication is due to the residual acetate group remaining after manufacturing of PVA via hydrolysis of polyvinyl acetate or oxidation [6, 10]. On the contrary, this implies that PVA is partially hydrolyzed.

IR spectra of pure TPS/PVA show all specific bands of cassava starch, PVA, and glycerol along with some variations. Besides, compatibilized TPS/PVA thin films exhibit characteristic peaks associated with cassava starch, PVA, glycerol, and phthalic acid [10, 23, 32]. However, the characteristic absorption bands related to phthalic acid could be identified at lower wave numbers. This behavior could be ascribed to the comparatively lower concentration of phthalic acid in blend films compared to that of other components while the bands associated with phthalic acid could have been dominated by the characteristic absorbance bands associated with starch, PVA, and glycerol [23, 32].

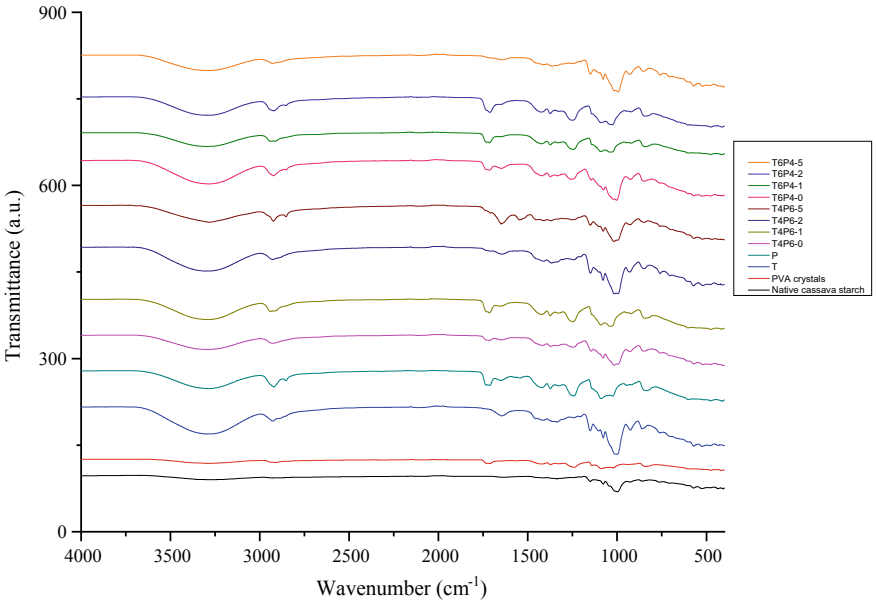

Fig. 1 FTIR-ATR spectrum of PVA crystals, native cassava starch powder, pure TPS/PVA thin films, and TPS/PVA films compatibilized with phthalic acid

Given the spectral changes (peak shifting) w.r.t. the addition of each components, distinct chemical; interactions (hydrogen bonds) were observed. The intensity of hydrogen bonds can be diagnosed through the analysis of FTIR spectra of cassava starch-based thin films [53]. The indication of the formation of hydrogen bonds within the species can be found at the range of 2700–3700 cm^{-1} [47]. Usually, the vibration of absorption within this range is greatly influenced by the intensity and the number of hydrogen bonds [30]. The formation of hydrogen bonds weakens the stretching frequency of O–H bond causing band elongation and leading to a lower O–H stretching vibration frequency and thin phenomenon is known as "red shift" [24]. It can be noted that, cassava starch-based films exhibited a decrease in the frequency associated with O–H group stretching after the addition of phthalic acid compared to that of their respective non-compatibilized films. The peak absorbance frequency of hydroxyl groups shifted from 3293 cm^{-1} of non-compatibilized TPS/PVA (40/60) to 3291, 3288, and 3280 cm^{-1} with the phthalic acid content increased from 1, 2, and 5 wt%, respectively. Moreover, the same observation was exhibited by TPS/PVA (60/40) films. This indicated that phthalic acid could form strong interactions while forming new hydrogen bonds with starch, PVA, and glycerol molecules, and these interactions were enhanced with the content of phthalic acid. Similar observations were reported by Jiang et al. [30] for potato starch/PVA thin films compatibilized with $CaCl_2$.

3.3 Effect of Phthalic Acid on Thermal Stability

The influence of phthalic acid on the thermal stability of the thin films was evaluated by thermogravimetric analysis. Herein, the loss of mass due to volatilization of degradation products was monitored as a function of temperature. The thermal stability of a polymeric material depends on the interactions between the macromolecules present in the blends and the characteristics of the sample [30]. Table 3 enumerates the temperature difference at maximum degradation (ΔT), temperature at maximum degradation (T_{peak}), and the residue mass at 600 °C.

The difference in temperature (ΔT) at the maximum degradation at a particular derivative TG provides an evidence for the blend homogeneity and the reduction in ΔT may be attributed to the increase in blend homogeneity [54]. As can be evidenced from Table 3, the ΔT gradually decreases with the increased addition of phthalic acid compared to that of their respective non-compatibilized blend. This behavior can be ascribed to the increase in blend homogeneity due to the compatibilization of TPS/PVA thin films in the presence of phthalic acid.

In contrast, during pyrolysis in an inert gas atmosphere, char formation was observed for all samples. At 600 °C, the ash concentration for neat PVA is approximately 5.13% (see Table 3) of the original weights, which is comparatively lower than TPS/PVA blend films (5.5–12.5%). Moreover, the amount of char formed increased along with the increment of starch content. Similar observations were reported by

Table 3 Variation of ΔT, T_{peak}, residual mass at 600 °C, degree of relative crystallinity (X_c), glass transition temperature (T_g), and melting temperatures (T_m) of the samples

Sample	ΔT (°C)	T_{peak} (°C)	Residual mass at 600 °C (%)	T_g (°C)
Starch powder	122.31	317.8	8.82	–
PVA crystals	368.79	398.7	4.43	–
T	239.15	327.5	9.47	−4.28
P	335.62	343.1	5.73	31.4
T4P6-0	323.04	327.9	5.57	10.77
T4P6-1	315.98	330.8	6.49	–
T4P6-2	298.35	334.1	7.17	–
T4P6-5	297.81	336.8	10.70	15.17
T6P4-0	314.18	315.5	10.88	–
T6P4-1	312.59	319.8	11.15	–
T6P4-2	311.61	322.9	12.51	–
T6P4-5	300.38	325.9	12.83	–

Yoon et al. [67] and Luo et al. [39], and such behavior might be due to the chemical structure of starch which is capable of forming a thermal resistance layer by possessing a high degree of residual carbon at higher temperatures [37]. Besides, the char formation increased with the increased addition of phthalic acid.

Apart from the above observations, native starch showed a typical main decomposition step with a maximum degradation rate centered at around 317.8 °C (see Table 3) as previously reported by Cano et al. [12]. However, pure PVA exhibits a higher thermal stability compared to that of native cassava starch. As concerning starch, a slight increase in thermal stability can be noted for compatibilized blends compared to that of their pure blend films, as evidenced by the shifting of T_{peak} toward elevated temperatures as depicted in Table 3. On the contrary, T_{peak} shifts to higher temperatures, as a consequence of a strongly packed complex network [43]. This T_{peak} shifting can be further explained by the inter-component hydrogen bonds between starch, PVA, glycerol, and phthalic acid. At a higher loading of phthalic acid, both the thermal stability and char residue increased along with an increase in blend homogeneity. These results are in accordance with mechanical properties.

According to Fig. 2, TG profiles of both native cassava starch and pure TPS thin films demonstrate two distinct weight loss regions in the temperature range of 50–170 and 200–500 °C. The former event represents a weight loss of physically absorbed water in native starch sample while the weight loss of both water and glycerol is exhibited by TPS film [39]. For both samples, the latter event is attributed to the thermal decomposition of starch. However, both PVA crystals and neat PVA thin films exhibit three distinct weight loss regions ranging from 50–150, 200–440, and 450–550 °C. The first thermal event in PVA crystals can be attributed to the loss of water while the evaporation of both water and glycerol is taken place in neat PVA film. The second thermal event involves the dehydration of the hydroxyl groups and the

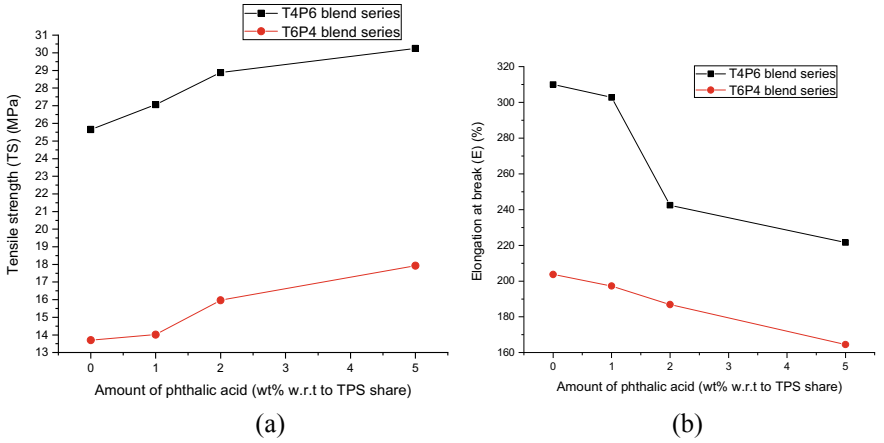

Fig. 2 Mechanical properties of TPS/PVA blended thin films w.r.t phthalic acid amount **a** Tensile strength, **b** Elongation at break

final decomposition step is attributed to the formation of volatile organic compounds which subsequently produced conjugated unsaturated polyene structures. Previous studies have also proved the two-step decomposition mechanism of PVA [12, 19, 30].

Apart from the above, both T4P6-0 and T6P4-0 blend films exhibit five distinct weight loss regions in the temperature range of 50–140 °C, 150–230 °C, 250–350 °C, 360–430 °C, and 430–550 °C. The first thermal event is attributed to the evaporation of weekly physiosorbed water and the second weight loss region is due to evaporation of remaining volatiles.

The third weight loss region is due to the decomposition of starch according to the previously reported data [12]. The last two thermal events can be ascribed to the PVA thermodegradation, the main degradation stage followed by a final decomposition of the previously formed compounds as deduced by Cano et al. [12] and Frone et al. [19]. Previous studies have also reported that the polymer separation in TPS/PVA blend films and the independent degradation of each polymer [12] as observed in the present study. This behavior might be due to the poor compatibility between both starch and PVA. However, for all the compatibilized blends of both TPS/PVA weight ratios, three distinct weight loss regions can be observed in the temperature range 50–170 °C, 240–400 °C, and 420–550 °C except for T6P4-5 blend film which exhibits only two distinct weight loss regions ranging from 50–150 °C, and 200–480 °C as shown in Fig. 2. For the compatibilized films except for T6P4-5, the initial weight loss is due to the loss of volatiles (water and glycerol) and the seconds thermal event is the main degradation zone of dehydration of hydroxyl groups and the subsequent formation of low molecular weight unsaturated and aliphatic carbon species of both starch and PVA as previously noted by Luo et al. [39]. Besides, the third weight loss can be attributed to the degradation of byproducts generated by PVA during the thermal process. In contrast, for T6P4-5 blend film, the first thermal event is due

to the evaporation of physically absorbed water and glycerol in the film while the second weight loss region is attributed to the main degradation of both starch and PVA. However, the disappearance of second PVA degradation step is observed at the highest concentration of phthalic acid in T6P4-5 thin film. This suggests that, though phthalic acid has interacted to a different extent with starch and PVA fractions in the blend, in both cases, the bonds in the film network were notably affected by the presence of phthalic acid in the system.

3.4 Variation of Film Thickness

In spite of maintaining the same solid surface density during casting process, some differences in film thicknesses were observed. According to Awasthy et al. [6], the thickness of the films varies with the chemical composition, molecular organization, and interactions among the macromolecules. Among the various thin films, the least thickness was exhibited by neat PVA film as depicted in Table 2. Besides, the blend films showed thickness values in the range of 0.18–0.25 mm, higher compared to that of both neat PVA and TPS thin films. The thickness values obtained for the films in this study are in agreement with the previously reported values by Awasthy et al. [6] and Cano et al. [11]. As shown in Table 2, it is evident that, with the increase of starch content in non-compatibilized blends, the thickness increased. This behavior can be ascribed to the less tightly packed chains in the blend matrix which gives rise to more open network as the starch content increased. However, in compatibilized blends, phthalic acid seems to provoke greater chain aggregation due to more intense interaction forces by forming new hydrogen bonds between the macromolecules, leading to greater film compactness while reducing film thickness values as confirmed by FTIR.

3.5 Effect of Phthalic Acid on Mechanical Properties

The determination of mechanical properties is of vital importance in practical point of view, since, polymeric materials such as films are subjected to various stresses during usage. The mechanical behavior of prepared films was analyzed in terms of tensile strength (TS) and elongation at break (Ɛ%) [11]. TS represents the resistance to elongation at break, whereas Ɛ% is a measure of the capacity of the films for stretching. The calculated mean values of TS and elongation at break of starch-based thin films are demonstrated in Fig. 2a, b, respectively, as a function of compatibilizer amount.

Poor mechanical properties were exhibited by neat TPS film indicating a maximum tensile strength and elongation at break valuing 3.82 MPa and 6.52%, respectively while performing a typical mechanical behavior of a brittle material. Similar observations were reported by Cano et al. [11], Magalhaes and Andrade [41]

and Jiang et al. [30]. Such observation can be attributed to the strong inter-chain interactions of starch polymer through via hydrogen bonding which increases the cohesion forces of the matrix, thus making it difficult for the chains to shift during tensile test [11]. On the contrary, the highest resistance toward break was exhibited by neat PVA film demonstrating a TS of 54.67 MPa and Ɛ% of 447.53%.

According to Fig. 2, it is indicative that, incorporation of starch into PVA caused a fall in tensile properties to a large extent as previously reported by Jose et al. [31], Guohua et al. [21], Aswathy et al. [6], Khan et al. [34], Parvin et al. [46] and Shi et al. [52] and such behavior can be attributed to increase crystallization of the blended thin films. However, it is evident that, with the addition of phthalic acid, a notable increase in TS can be observed for compatibilized blends while demonstrating a decrease in Ɛ% compared to that of their respective TPS/PVA non-compatibilized blend. The increment of TS can be ascribed to improved interfacial adhesion between both cassava starch and PVA macromolecules in the presence of phthalic acid by cross-linking via hydrogen bonds.

Moreover, the cross-linking among the polymers may cause in the formation of three-dimensional network structure causing restricted mobility of molecules as in accordance with Parvin et al. [46]. Besides, the reduction of Ɛ% with the increased addition of phthalic acid might be due to the enhanced interactions between starch and PVA which prevent the facile sliding of polymer chains and thereby decreased the Ɛ% as previously noted by Panaitescu et al. [44]. These results suggest that, a small amount of phthalic acid is sufficient for a remarkable increase in maximum tensile strength. Furthermore, according to results of mechanical properties illustrated in Fig. 2, it is evident that, one can increase the starch content in the blend film for the purpose of cost reduction without sacrificing tensile properties of the material.

3.6 Water Uptake

One of the major drawbacks associated with starch-based materials is its water sensitivity which causes poor in storage stability [13]. Therefore, improvement in reducing water sensitivity and enhanced water resistance of cassava starch-based thin films is of paramount importance. Nevertheless, water absorption capacity acts as an important property, especially for biodegradable materials. Figure 3 demonstrates the water absorption capacities of the thin film samples at 2 and 24 h. As can be seen from Figure 3, the lowest water absorption capacity was exhibited by neat PVA film (39.78% and 46.67% at 2 h and 24 h, respectively) while the incorporation of starch in PVA caused an increase in water uptake and these results are in conformity with the previous studies conducted by Jose et al. [31] and Guohua et al. [21]. This behavior can be ascribed to the comparatively higher hydroxyl group density of starch molecules than that of PVA molecules causing greater hydrophilicity of starch than that of PVA as noted by Shi et al. [52].

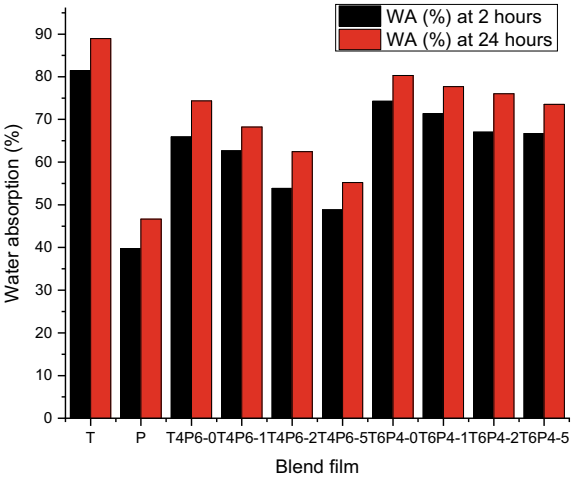

Fig. 3 Water absorption (WA) (%) of TPS/PVA blended thin films

Furthermore, the results revealed that the water absorption of compatibilized films was lower compared to that of their respective non-compatibilized blends. Interestingly, according to the data depicted in Fig. 3, it is evidenced that the water absorption capacity gradually decreases with the increased addition of phthalic acid. The least water uptake rate was exhibited by T4P6-5 thin film valuing 48.82% and 55.21% at 2 h and 24 h, respectively. Similar results were previously reported by Yoon et al. [66] and Yun et al. [69] where a reduction in water absorption capacity was observed in TPS/PVA blends in the presence of succinic acid. It is a well-known fact that the biopolymers are susceptible to environmental relative humidity Popescu et al. [47]. Therefore, it can be revealed that the hydroxyl groups of starch, PVA, and glycerol are involved in the formation of hydrogen bonds in the presence of phthalic acid in between them. Consequently, the number of free hydroxyl groups is decreased while reducing the probability of the formation of hydrogen bonds between the polymers and the water molecules in the environment. Moreover, the decrease in water uptake in thin films supports the proposal about cross-linking of the components in the blend via hydrogen bonding as demonstrated in Fig. 3.

3.7 The Effect of Phthalic Acid on Dynamic Mechanical Properties of Starch/PVA Films

Dynamic mechanical analysis (DMA) is considered to be an intricate way of determining the interactions between different components at molecular level as the dynamic mechanical properties of polymers can sensitively represent their molecular motion, which has a close relationship with the chain structure of polymers [29, 30]. The DMA studies were carried out only for four selected samples, namely neat

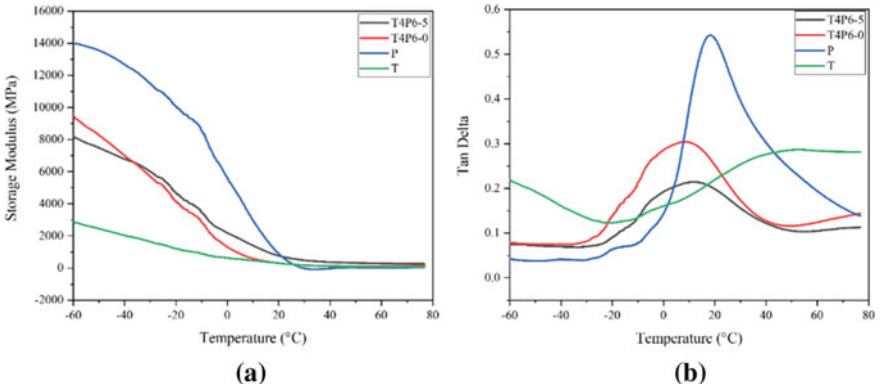

Fig. 4 Plots of **a** storage modulus (G'), and **b** tan δ versus temperature of T, P, T4P6-0, and T4P6-5 films

cassava starch film, neat PVA film, T4P6-0 film, and T4P6-5 film since T4P6-5 film demonstrated the highest value for tensile strength and the lowest value for water absorptivity. Figure 4 demonstrates the plots of storage modulus (G') and tan δ versus temperature for the aforementioned film samples.

According to the literature, G' is a symbol of mechanical strength and a measurement of the stiffness (rigidity) of the material [29, 30]. It can be seen from Fig. 4a that G' of all the film samples gradually decreased with the increase of temperature. This indicates that the mechanical strength gradually decreased with the increasing temperature. Moreover, it is evidenced from Fig. 4a that the G' increased at elevated temperature above −20 °C in the compatibilized blend compared to that of the pure starch/PVA film. This behavior can be attributed to the incorporation of phthalic acid between starch and PVA molecules which helped to restore a larger amount of elastic energy during dynamic loading at elevated temperatures. This increment of G' with the addition of phthalic acid to starch/PVA films meant that the film became harder compared to con-compatibilized film at higher temperatures.

Tan δ is a damping term defined as the ratio of energy dissipated as heat to the maximum energy stored in the material, whereas it is an index of the material viscoelasticity. Apart from the above, the size of the tan δ peak is believed as a reflection of the volume fraction of the material undergoing transition [29, 30]. On the contrary, in DMA studies, the position of tan δ peak is often taken as the glass transition temperature (T_g) of a polymeric material [30]. As can be seen from Fig. 4b, both T4P6-0 and T4P6-5 films demonstrate only single peak position of tan δ indicating only single glass transition temperature. Only single glass transition also indicated that the starch and PVA are compatible as previously reported by Jiang et al. [30]. Interestingly, the position of the tan δ slightly increased with the addition of phthalic acid (see Table 3). This behavior can be ascribed to the cross-linking that occurred via hydrogen bonding could result in decreased chain mobility in the film matrix. The increase of T_g suggests that the compatibilized starch/PVA film was resistance to higher temperatures than the pure starch/PVA film material. Similar

observations were also reported by Detuangchan et al. [16] for the cross-linked rice starch films. Furthermore, for compatibilized film sample, the peak size of the tan δ decreased and this behavior might be due to the reduction in amorphous fraction in starch/PVA films after compatibilized with phthalic acid.

3.8 Degradation Behavior of Thin Films

Compared to petroleum-based polymeric materials, biodegradable polymers are capable of decomposing in the environmental conditioned under the action of natural microorganisms [52]. The test carried out to evaluate the biodegradability of the prepared thin films is an outdoor experiment which provides a realistic environment where soil, humidity, temperature and type and the amount of microorganisms change with season [21]. All the test specimens consisted of the same shape and size to avoid the effects of the shape of the film on its degradation rate. The films were degraded via surface absorption of moisture and microorganisms such as fungi and bacteria as reported by Guohua et al. [21].

Figure 5 depicts the remaining weight of the films as a function of degradation time. According to Fig. 5, it can be observed that, during the first two weeks, the weight of all the test specimens slightly increased due to the water absorption by the films owing to the hydrophilic nature of the samples as previously observed by Magalhaes et al. [41] and Parvin et al. [46]. For all the films except for neat PVA film, the weight loss after the first two weeks was mainly caused by the gradually breaking down of starch molecules in the presence in the presence of Glycosidases and Amylases which are responsible for the cleavage of glycosidic bonds and starch hydrolyzing as reported by Cano et al. [12] and Shi et al. [52]. On the contrary, the starch film degraded rapidly in the initial 4 weeks and a complete degradation was achieved after 16 weeks. Similar observations were noted by Magalhaes et al.

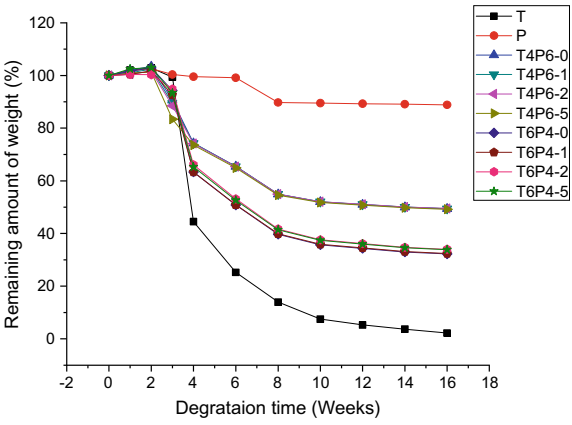

Fig. 5 Variation of remaining weight (%) of prepared thin films w.r.t degradation time period

[41]. However, the neat PVA film exhibited a higher resistance against degradation due to the vinyl polymer in which the backbones are joined by the C–C linkages as previously reported by Chiellini et al. [14] and Guohua et al. [21].

Besides, TPS/PVA blend films performed an intermediate degradation profile between that exhibited by the neat PVA and TPS films. In contrast, the highest values of weight loss were recorded for the films containing a higher amount of cassava starch in the blend films (T6P4-0, T6P4-1, T6P4-2, and T6P4-5). This suggests that the weight loss of the starch-based films is highly influenced by the compositions of the mixture while the weight loss increased as the starch content increased. These findings are in agreement with the previously published data by Shi et al. [52], Parvin et al. [46], and Cano et al. [12]. Together with the literature, it can be proposed that a two-stage degradation has taken place in aerobic compost environment test, (i) swelling of the samples and the growth of microorganisms due to diffusion of water into film samples, and (ii) weight loss and the disruption of the film samples via enzymatic degradation.

Apart from the above, a slow degradation at the end of the degradation time period can be noted. Interestingly, it is evidenced that the degradation rate is somehow hindered in the presence of phthalic acid and such behavior can be attributed to the enhanced interactions within the components in the film samples, and thus, cross-linking via hydrogen bonds results in slow rate of film deterioration in soil.

3.9 Comparison with Other Studies

Several studies have been previously reported to investigate the effect on mechanical properties, thermal stability, degradation behavior, and water uptake of starch/PVA blends in the presence of different compatibilizers. Table 4 presents a comparison of the properties of the present study with different starch/PVA thin films reported in the literature. Interestingly, the cassava starch/PVA (40/60) thin film compatibilized with 5 wt% phthalic acid w.r.t TPS share exhibited comparatively better properties; see Table 4.

3.10 Modeling of Preferred Interactions

In this section, a conceptual model was developed for the preferred interactions in the blend films. The findings of FTIR led to discover that phthalic acid was cross-linked via hydrogen bonding between PVA, cassava starch, and glycerol. Moreover, by identifying the characteristic peaks of PVA crystals, it was evidenced that PVA has been partially hydrolyzed during manufacturing process. The chemical structures of cassava starch, partially hydrolyzed PVA, glycerol, phthalic acid, and the possible structure of cross-linked system via hydrogen bonds are illustrated in Fig. 6.

Table 4 Comparison of the present study with previous experiment data of compatibilized starch/PVA thin films

Composition of the thin film	TS (MPa)	Ɛ (%)	T_m (°C)	WA after 24 h (%)	t (mm)	RM at 600 °C (%)	Weight loss (%) during degradation	References
Potato starch: PVA at 3:5 v/v with STMP, boric acid and limonene 0.1 mg each	4.51	11.39	–	–	–	–	–	[38]
Tapioca starch: PVA at 1:1 w/w with 2 g of glycerol and 2 g of glutaraldehyde	5	80	–	65	–	–	–	[26]
Corn starch: PVA at 3:7 with 2 wt% carbon nanotubes	8.09	33.7				10.10	–	[31]
Sago starch (4 g), PVA (4 g), Glycerol (3 g), Glutaraldehyde (2 g) with 2 wt% of Silica	13	150	–	100	–	–	~92.5% after 60 days	[27]
1.2 g of PVA, 0.27 of starch with 0.624 ml nutmeg oil and 1.25 ml of ZnO nanoparticles	27.22	12.19	–	60	0.2	–	–	[6]
Sago starch (2.5 g), PVA (2.5 g), Glycerol (1 ml), and Borax (0.4 g)	27.3	234	–	–	–	–	~60% after 63 days	[62]
TPS:PVA blend ratio with 4:6 containing 5 wt% phthalic acid	30.25	221.57		55.21	0.18	10.7	33.86% after 120 days	Present study
Pea starch:PVA:Glycerol:$AgNO_3$ (1:0.5:0.25:0.16) weight basis	30.7	33.4	–	–	–	21.21	–	[12]
Maize starch:PVA:TiO_2 (1:1:0.05)	31.3	89.1	200.2	–	–	–	–	[35]
Corn starch: PVA at 1:1 w/w with 40% nano-sized poly(methyl methacrylate-co-acrylamide) particles	86.7	6.5	–	–	–	–	~50% after 160 days	[67]

Note: TS; Maximum tensile strength, Ɛ; Percentage elongation at break, T_m; Melting temperature, X_c; Degree of crystallinity, *t;* Film thickness, and RM; Residual mass, L

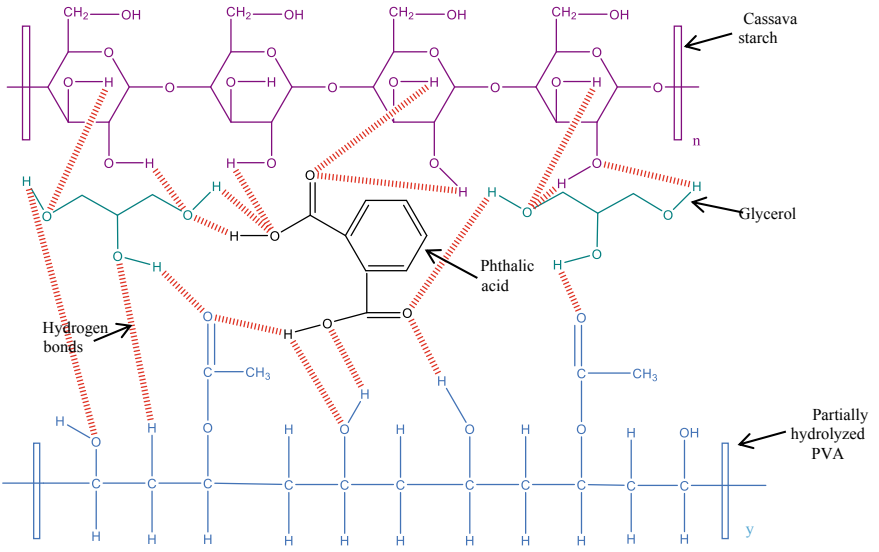

Fig. 6 Possible structure of cross-linked system via hydrogen bonds in compatibilized blend films

According to FTIR data, hydrogen bonding interactions among cassava starch and PVA is favorable, and especially the blends of T4P6-5 and T6P4-5 possess the highest strengths of interactions.

It is a well-known fact that the highly polar hydroxyl groups in both PVA and starch macromolecules could easily form intermolecular and intramolecular hydrogen bonds. One of the basic principles of additives is that they are capable of forming interactions among cassava starch and PVA molecules in the replacement of intermolecular and intramolecular hydrogen bondings [30]. According to preferential interactions among the molecules in compatibilized TPS/PVA blends with phthalic acid (see Fig. 5e), hydrogen bonding interactions between functional groups (O–H or –C–O– or carbonyl group) cassava starch, PVA, glycerol, and phthalic acid might have taken place.

During the preparation of film forming dispersions at an elevated temperature (85 °C), the cassava starch granules swell and collapse eventually. As a result, the number of free hydroxyl groups within the system increases while enhancing the interactions between PVA and gelatinized starch [39]. Apart from the above, with the increased addition of phthalic acid, the interaction intensity is dramatically enhanced compared to that of their respective non-compatibilized thin films. Therefore, these increased interactions among cassava starch and PVA macromolecules can be ascribed to the newly formed high-intensity hydrogen bonds between cassava starch, PVA, glycerol, and phthalic acid. As a result, the interactions in T4P6-5 and T6P4-5 thin films are relatively higher compared to that of their corresponding compatibilized blends with lower phthalic acid concentrations as in conformity with

the enhanced mechanical properties, reduced water absorption capacities, higher thermal stability, and increased homogeneity.

Based on the preferred model, it is evident that the presence of phthalic acid has significant positive impacts on properties in TPS/PVA thin films.

4 Conclusion

In this study, starch/PVA biodegradable films possessing enhanced thermal stability, mechanical properties, and water resistivity were successfully prepared using cassava starch, PVA, glycerol as the plasticizer, and phthalic acid as the compatibilizing agent. With the increased addition of phthalic acid, increased homogeneity of the blend films was attained. The conceptual model of increased hydrogen bonding interactions between starch and PVA in the presence of phthalic acid could be used to explain the resulted structural and thermal behaviors. However, though the biodegradation was somehow slowed down, the effect was not significant. The results in this study have effectively demonstrated that phthalic acid can be used as a successful compatibilizer for starch/PVA blends. Moreover, it can also be expected that phthalic acid could act as a compatibilizer for other biodegradable polymers such as cellulose and polyacrylic acid that contain a lot of hydroxyl groups. Cassava starch-based thin films with 5 wt% phthalic acid exhibited high strength and percentage elongation at break (30.25 MPa & 221.57%, respectively) close to that of polyolefins and can be seen as a low cost "green" substitute for packaging applications. Besides, prepared packaging material can be a solution of problems due to solid waste accumulation as well as to meet the demand of global requirement.

Acknowledgements The authors sincerely acknowledge the encouragement and guidance provided by all the members of the academic and non-academic staff members of the Department of Chemical and Process Engineering, University of Peradeniya, University of Peradeniya. The authors would also like to acknowledge the support from Ms. W.M.W.K. Weerasekara from the Department of Chemical & Process Engineering, Faculty of Engineering, University of Peradeniya.The authors wish to express their sincere appreciation to Accelerating Higher Education Expansion and Development (AHEAD) for the financial assistance (AHEAD/RA3/DOR/65).

References

1. Abdulkadir HK, Jaya H, Noriman NZ, Dahham OS, Mazelan AH, Latip NA, Aini AK (2018) The effects of phthalic anhydride on R-HDPE/Eva/Cff composites: tensile and physical properties. In: International conference on materials engineering and science, p 454
2. Abioye OP, Abioye AA, Afolalu SA, Ongbali SO (2018) A review of biodegradable plastics in Nigeria. Int J Mech Eng Tech 9:1172–1185
3. Ahmed J, Tiwari BK, Iman SH, Rao MA (2012) Starch-based polymeric materials and nanocomposites. In: Chemistry, processing, and applications. CRC Press, p 13. 978-1-4398-5177-3

4. Association of Official Analytical Chemists (AOAC) (2000) Methods 920.36 (Moisture), 984.13 (Protein), 948.22(Lipid and Oil) and 923.03 (Ash of Flour), 17th edn; AOAC (2000) Official methods of analysis. The Association of Official Analytical Chemists, Gaithersburg, MD, USA
5. Association of Official Analytical Chemists (AOAC) (2005) Method 962.09 (Crude Fibber), 18th edn; AOAC (2005) Official method of analysis. Association of Officiating Analytical Chemists, Washington, DC, USA
6. Aswathy J, Heera KV, Sumi TS, Joseph M, Mathew S, Praveen G, Nair IC, Radhakrishnan EK (2019) Starch-PVA composite films with ZnO-nanoparticles and phytochemicals as intelligent pH sensing wraps for food packaging applications. Int J Biol Macromol 136:395–403
7. Ayadi F, Mamzad S, Portella C, Dole P (2013) Synthesis of bis(pyrrolidone-4-carboxylic acid)-based polyamides derived from renewable itaconic acid—application as a compatibilizer in biopolymer blends. Soc Polym Sci 45:766–774
8. BeMiller J, Whistler R (2009) Starch: chemical and technology, 3rd edn. Academic Press
9. Benesi IR, Labuschagne MT, Dixon AG, Mahungu NM (2004) Stability of native starch quality parameters, starch extraction and root dry matter of cassava genotypes in different environments. J Sci Food Agric 84:1381–1388
10. Blout ER, Karplus R (1947) The infrared spectrum of polyvinyl alcohol. Notes 70:862–864
11. Cano A, Chafer M, Chiralt A, Gonzalez-Martinez C (2015) Physical and microstructural properties of biodegradable films based on pea starch and PVA. J Food Eng
12. Cano A, Chafer M, Chiralt A, Gonzalez-Martinez C (2016) Development and characterization of active films based on starch-PVA, containing silver nanoparticles. J Food Packag Shelf Life 10:16–24
13. Chen L, Zhang Z, Zhuang X, Chen X, Jing X (2010) Compatibilizng effect of starch-grafted-Poly(L-lactide) on the Poly(ξ-caprolactone)/starch composites. J Appl Polym Sci 117:2724–2731
14. Chiellini E, Cinelli P, Chiellini F, Imam SH (2004) Environmentally degradable bio-based polymeric blends and composites. Macromol Biosci 4:218–231
15. Demirgoz D, Elvirs C, Mano JF, Cunha AM, Piskin E, Reis RL (2000) Chemical modification of starch based biodegradable polymeric blends: effects on water uptake, degradation behavior and mechanical properties. Polym Degrad Stab 70:161–170
16. Detduangchan N, Sridach W, Wittaya T (2014) Enhancement of the properties of biodegradable rice starch films by using chemical crosslinking agents. Int Food Res J 21(3):1255–1235
17. Doppalapudi S, Jain A, Khan W, Domb AJ (2014) Biodegradable polymers—an overview. J Polym Adv Technol 25:427–435
18. Dwivedi P, Mishara PK, Mondal MK, Srivastava N (2009) Non-biodegradable polymeric waste pyrolysis for energy recovery. J Heliyon 5
19. Frone AN, Panaitescu DM, Donescu D, Spataru CI, Radovici C, Trusca R (2011) Preparation and characterization of PVA composites with cellulose nanofibers obtained by ultrasonication. Bio Resour 6:487–512
20. Grace M (1997) Cassava processing. FAO plant production and protection series; no 3. Food and Agriculture Organization of the U. N., Rome, Italy
21. Guohua Z, Ya L, Cuilan F, Min Z, Caiqiong Z, Zangdao C (2006) Water resistance, mechanical properties and biodegradability of methylated-cornstarch/poly (vinyl alcohol) blend film. J Polym Degrad Stab 91(703):711
22. Gupta VK, Priya B, Pathania D, Singh AS (2014) Synthesis, characterization and antibacterial activity of biodegradable starch/PVAA composite films reinforced with cellulose fibre. Carbohydr Polym
23. Hase Y, Devanzo CU, Kawai K, Sala O (1975) The vibrational spectra of phthalic anhydride. J Mol Struct 30:37–44
24. He Y, Zhu B, Inoue Y (2004) Hydrogen bonds in polymer blends. Prog Polym Sci 29:1021–1051
25. Huneault MH, Li H (2007) Morphology and properties of compatibilized polylactide/thermoplastic starch blends. J Polym 48:270–280

26. Ismail H, Zaaba NF (2011) Effect of additives on properties of polyvinyl alcohol (PVA)/tapioca starch biodegradable films. J Polym-Plast Technol Eng 49:37–41
27. Ismail H, Zaaba NF (2014) The mechanical properties, water resistance and degradation behavior of silica-filled sago starch/PVA plastic films. J Elastometer Plast 46:96–109
28. Jayasekara R, Harding I, Bowater I, Christie GBY, Lonergan GT (2004) Preparation, surface modification and characterisation of solution cast starch PVA blended films. J Polym Test 23:17–27
29. Jiang X, Dai H, Zhang X (2015) Effect of magnesium chloride hexahydrate on thermal and mechanical properties of starch/PVA films. Plast, Rubber Compos 44(8):299–305
30. Jiang X, Jiang T, Gan L, Zhang X, Dai H, Zhang X (2012) The plasticizing mechanism and effect of calcium chloride on starch/poly (vinyl alcohol) films. Carbohyd Polym 90:1677–1684
31. Jose J, De SK, Almadeed MA, Dakua JB, Sreekumar PA, Sougrat R, Al-Harthi MA (2014) Compatibilizing role of carbon nanotubes in poly(vinyl alchohol)/starch blend. Starch/Starke 67:147–153
32. Juchnovski I, Veltcheva E, Kolev K (2006) Infrared spectra of phthalic anhydride and Its ^{18}O substituted derivative. Spectrosc Lett 26(1):17–30
33. Kalambur S, Rizvi SSH (2006) An overview of starch-based plastic blends from reactive extrusion. J Plastic Films Sheeting 22:39–59
34. Khan MA, Bhattacharya SK, Kader MA, Baihari K (2006) Preparation and characterization of ultra violet (UV) radiation cured bio-degradable films of sage starch/PVA blend. Carbohyd Polym 63:500–506
35. Kochkina N, Butikova OA (2019) Effect of fibrous TiO_2 filler on the structural, mechanical, barrier and optical characteristics of biodegradable maize starch/PVA composite films. Int J Biol Macromol 139:431–439
36. Krimm S, Liang CY, Sutherland GBBM (1956) Infrared spectra of high polymers. V. Polyvinyl alcohol. J Polym Sci 22:227–247
37. Liu X, Yu L, Xie F, Li M, Chen L, Li X (2010) Kinetics and mechanism of thermal decomposition of cornstarches with different amylose/amylopectin ratios. Starch/Stärke 62:39–146
38. Liu B, Xu H, Zhao H, Wei L, Zhao L, Li Y (2016) Preparation and characterization of intelligent starch/PVA films for simultaneous colorimetric indication and antimicrobial activity for food packaging applications. Carbohydr Polym
39. Luo X, Li J, Lin X (2012) Effect of gelatinization and additives on morphology and thermal behavior of corn starch/PVA blend films. Carbohyd Polym 90:1595–1600
40. Ma P, Xu P, Chen M, Dong W, Cai X, Schmit P, Spolstra AB, Lemistic PJ (2014) Structure-properties relationship of reactively compatibilized PHB/EVA/starch blends. J Carbohydr Polym 108:299–306
41. Magalhaes NF, Dahmouche K, Lopes GK, Andrade CT (2013) Using an organically-modified montmorillonite to compatibilize a biodegradable blend. J Appl Clay Sci 72:1–8
42. Manimekalai TK, Sivakumar N, Periyasamy S (2015) Real-world mixed plastics waste into activated carbon and its performance in adsorption of basic dye from textile effluent. J Nanomater Biostruct 10:985–1001
43. Ortega-Toro R, Santagata G, Gomezd'Ayala G, Cerruti P, Talens OP, Chiralt MA, Malinconico M (2016) Enhancement of interfacial adhesion between starch and grafted poly(*epsilon*-caprolactone). Carbohyd Polym 147:16–27
44. Panaitescu F, Frone AN, Ghuvrea M, Chiulan I (2015) Influence of storage conditions on starch/PVA films containing cellulose nanofibers. J Ind Crops Prod 70:170–177
45. Park H, Cough S, Yun Y, Yoon S (2005) Properties of starch/PVA blend films containing citric acid as additive. J Polym Environ 13:375–382
46. Parvin I, Ralman MA, Islam JMM, Khan MA, Saadat AHM (2010) Preparation and characterization of starch/PVA blend for biodegradable packaging material. Adv Mater Res 12–125:351–354
47. Poescu M, Dogavu B, Goanta M, Timpu D (2018) Structural and morphological evaluation of CNC reinforced PVA/Starch biodegradable films. Biomac

48. Pour ZS, Makvandi P, Ghaemy M (2015) Performance properties and antibacterial activity of crosslinked films of quaternary ammonium modified starch and poly(vinyl alcohol). Int J Biol Macromol 80:596–604
49. Saha B, Ghoshal A (2005) Thermal degradation kinetics of poly(ethylene terephthalate) from waste soft drinks bottles. Chem Eng J 111:39–43
50. Sailaja RN, Deepthi MV (2010) Mechanical and thermal properties of compatibilized composites of polyethylene and esterified lignin. J Mater Des 31:4369–4379
51. Seligra PG, Jaramillo CM, Fama L, Goyanes S (2015) Biodegradable and non-biodegradable eco-films based on starch-glycerol with citric acid as crosslinking agent. Carbohydr Polym
52. Shi R, Zhu A, Chen D, Jian X, Xu X, Zhang L, Tian W (2009) *In Vitro* degradation of starch/PVA Films and biocompatibility evaluation. J Appl Polym Sci 115:346–357
53. Sin LT, Rahman WAWA, Rahmat AR, Samad AA (2010) Computational modeling and experimental infrared spectroscopy of hydrogen bonding interactions in polyvinyl alcohol-starch bends. Polymer 51:1206–1211
54. Sreekumar PA, Al-Harthi MA, De SK (2012) Effect of glycerol on thermal and mechanical properties of polyvinyl alcohol/ starch blends. J Appl Polym Sci 123:135–142
55. Stawski D (2008) New determination method of amylose content in potato starch. Food Chem 110:777–781
56. Tang XZ, Alavi S (2011) Recent advances in starch, polyvinyl alcohol based polymer blends, nanocomposites and their biodegradability. Carbohyd Polym 85:7–16
57. Tang S, Zou P, Xiong H, Tang H (2008) Effect of nano-SiO_2 on the performance of starch/polyvinyl alcohol blend films. Carbohyd Polym 72:521–526
58. Utrilla-Coello RG, Hernández-Jaimes C, Carrillo-Navas H, González F, Rodríguez E, Bello-Perez LA, Vernon-Carter EJ, Alvarez-Ramirez J (2014) Acid hydrolysis of native corn starch: morphology, crystallinity, rheological and thermal properties. Carbohyd Polym 103:596–602
59. Velde KV, Kiekens P (2002) Biopolymers: overview of several properties and consequences on their applications. J Polym Tests 21:433–442
60. Wang W, Diao E, Zhang H, Dai Y, Huo H, Dong H (2015) Effect of co-plasticization of acetyl tributyl citrate and glycerol on the properties of starch/PVA films. J Appl Polym Sci 42544:1–9
61. Waterschoot J, Gomand SV, Fierens E, Delcour JA (2014) Production, structure, physiochemical and functional properties of maize, cassava, wheat, potato and rice starches. J Starch/Strake 66:1–16
62. Widiarto S (2005) Effect of Borax on mechanical properties and biodegradability of sago starch-poly(vinyl alchohol) blend films. J Sains Tek 11:151–157
63. Xie G, Shang X, Liu R, Hu J, Liao S (2011) Synthesis and characterization of a novel amino modified starch and its adsorption properties for Cd (II) ions from aqueous solution. Carbohyd Polym 84:430–438
64. Yasuhara A, Katami T, Okuda T, Shibamoto T (2002) Role of inorganic chlorides in formation of PCDDs, PCDFs, and coplanar PCBs from combustion of plastics, newspaper, and pulp in an incinerator. Environ Sci Technol 36:3924–3927
65. Yin Q, Chen F, Zhang H, Liu C (2015) Fabrication and characterization of thermoplastic starch/poly (butylene succinate) blends with maleated poly (butylene succinate) as the compatibilizer. Plast, Rubber Compos 44(9):362–367
66. Yoon S, Chough S, Park H (2005) Effects of additives with different functional groups on the physical properties of starch/PVA blend film. J Appl Polym Sci 100:3733–3740
67. Yoon S, Park M, Byun H (2012) Mechanical and water barrier properties of starch/PVA composite films by adding nano-sized poly(methyl methacrylate-co-acrylamide) particles. Carbohyd Polym 87:676–686
68. Yun YH, Kim ES, Shim WG, Yoon SD (2018) Physical properties of mungbean starch/PVA bionanocomposites added nano-ZnS particles and its photocatalytic activity. J Ind Eng Chem 68:57–68
69. Yun Y, Na Y, Yoon S (2006) Mechanical properties with the functional groups of additives for starch/PVA blend film. J Polym Environ 14(1):71–77

Adaptation of Scrum and Web-Based Integrated Techniques to Construction Sector of Sri Lanka

P. Ashokkumar, I. V. H. Wiratunga, and A. K. Kulatunga

Abstract Sri Lankan contractors are facing competition from foreign construction companies. Due to the very liberal policies of the government, many foreign contractors find ways to enter this very lucrative market. However, in competitive bidding, local construction companies find it very difficult to control some cost and time parameters due to macro-economic factors. VUCA factors are considered in this paper. Hence, to prevent the cost and time overruns, it is needed to enhance the efficiency of internal practices with agile techniques to counter the effects of the VUCA world. Although, many applications are used in the construction industry to improve performance, an integrated web-based project management interface plays a significant role in the construction industry. The main aim of the research paper is to study agile practices (mainly scrum) with developed integrated web-based interfaces could help project managers of local construction companies to optimize the results of triple constraints and decision-making in the local contractor companies. The primary outcome of the research is identifying relationships of cash flows and inter-company operational factors with project performances and, through those factors, enhancing project performances in Sri Lankan construction industry. In this case study, the real-time project performances of a leading construction company in Sri Lanka are studied.

Keywords VUCA—volatility, uncertainty, complexity and ambiguity · Scrum framework · Web-based integrated project management · Agile techniques · Team collaboration

P. Ashokkumar (✉) · I. V. H. Wiratunga · A. K. Kulatunga
Department of Manufacturing and Industrial Engineering, University of Peradeniya, Peradeniya, Sri Lanka
e-mail: apkumar789@gmail.com

I. V. H. Wiratunga
e-mail: ivhw2006@gmail.com

A. K. Kulatunga
e-mail: aselakk@eng.pdn.ac.lk

R. Dissanayake et al. (eds.), *12th International Conference on Structural Engineering and Construction Management*, Lecture Notes in Civil Engineering 266,
https://doi.org/10.1007/978-981-19-2886-4_48

1 Introduction

After three decades of civil war, the opening of the Sri Lankan construction industry in the late 2010s revolutionized the Sri Lankan GDP. After agriculture, manufacturing, and services, the stream now ranks fourth in the GDP sector [1]. The situation in war-torn areas increased the demand for construction projects. Because of Sri Lanka's strategic location 2 in the Indian Ocean, many foreign investors are interested in investing in the local construction industry. Due to the modified regulations by the government to attract foreign investment on foreign contractors, local contractors face more difficulties in competitive bidding. In the e-paper article, Eng. Col. N Wijeratna [2] states the statistical data in 2018 found that the foreign contractors, especially Chinese, had won the bids 30% cheaper than the lowest local tenderer. Further, he states that 95 Chinese companies are undertaking work, whereas there are only about 70 local construction companies out of 2000 local construction companies in CIDA grades C2 and above. Further, he states that although some supporting regulations already generated for local contractors are still challenging to implement due to several practical reasons. In the current situation, Sri Lankan local contractors use traditional project management practices while foreign contractors use agile project management practices/hybrid practices. Local construction industries project handling and project management practices are slightly lagging behind foreign contractor project management practices, so if local contractor's companies need to be successful in the bidding, it is necessary to adapt to the next level from the current situation. Because many Sri Lankan contractor companies use traditional project management, they face less project control (cost overruns and schedule overruns), client payments issues (customer satisfaction), and less client involvement in the system, so client decision-making is delayed, resulting in delayed job idling. In local internal operations, documentation works are done on much manual paperwork, using email for data communication and separated into departmentalized functionality with different application platforms such as SAP, MS project, document management system, costing software without the integrity or less collaboration among cross-functional teams. Further, they do not know what happens on the project in real time. In this case study, a leading contractor organization has been chosen and identified some of the issues they face in successful project delivery by direct observation. Scrum practices with web-based project management interface techniques are applied to a real-time project. The study's main aim is to demonstrate whether or not this new practice is adaptable to the Sri Lankan construction industry in controlling cost overruns, contractor investment, and schedule delays.

The objective of this research is agile technology (scrum) is used in project management handling with the stakeholder (client and others) collaboration into the project on time basis through that reducing the reworks and wastages, as well as through the customer collaboration increasing the customer satisfaction, thus increasing the receiving of the payments on time and reducing local contractor investment. Another objective of this research is to increase the transparency in information sharing and accessibility among whole cross-functional teams as a centric

data source by replacing paper works into adapting web-based operational practice into a data feeding facility and enhancing the project monitoring (real time) and excellent decision-making with inter cross-functional team collaboration through the integration of all project information into a shared web-based developed system.

This paper is structured as follows: the next section is on literature done on agile and traditional project management, and the third section discusses the methodology of how the scrum and web-based integrated project management system is used. The fourth section discusses the data collection method and analysis of how adaptation of operation processes into the web-based system improvise the speed of the processes (i.e., material delivery to the site) as well as through the scrum-based practice how long time taken to the payments (interim payment approved certificates) received/how much reworks reduced, the achievement of work done against time and analysis on how much reworks reduced/ how much human hours reduced on the projects as well as how it is adopted some of the VUCA factors. In the fifth section, results are concluded into how the scrum and web-based integrated interface helps for successful project performance. In the following few sections, limitations of this study and recommendations are discussed for proper implementation, and future research areas are discussed.

2 Literature Review

Project Management Institute (PMI) defines the project management methodology as a set of methods, techniques, procedures, rules, templates, and best practices used on a project [3] (Refer Fig. 1). Similarly, researcher Charvat [4] defines project management methodology as a collection of guidelines and principles that can be tailored and applied to a particular situation, where procedures can be as simple as a task list or as complex as a defined approach the project with defined tools and techniques.

The most extensive definition of the project management methodology is given by Cockburn [5], who defines it as any principle project management team relies on to deliver project results successfully. In the practical environment, a suitable project management methodology will guide the project manager through a controlled, managed, and visible set of activities to achieve project results and

Fig. 1 Project management process [3]

successful delivery in triple constraints. Wysocki illustrated in 2014 that in traditional project management, initiation, planning, executing, monitoring and controlling, and closing are done linearly and incrementally (Refer Fig. 2). In agile project management, these are done more iteratively adaptively (Refer Fig. 3). Based on these process models, Wysocki defines five different project management lifecycle (PMLC) process models. Linear, incremental, iterative, adaptive, and Extreme/Emertxe process models are used. The degree of solution and goal ambiguity influences the choice of the PMLC model. Linear and incremental PMLC falls under traditional project management (TPM). They have a low amount of solution ambiguity and a clear project goal. APM encompasses iterative and adaptive PMLC. They have a significant amount of uncertainty about the answer, but the project goal remains clear. Extreme and Emertxe PMLC are examples of extreme project management. The project purpose is unclear, and there is a significant level of solution uncertainty in Extreme PMCL. In reverse, Emertxe PMLC is extreme. The solution uncertainty is low in this case, but the project purpose is ambiguous [6] (Fig. 4).

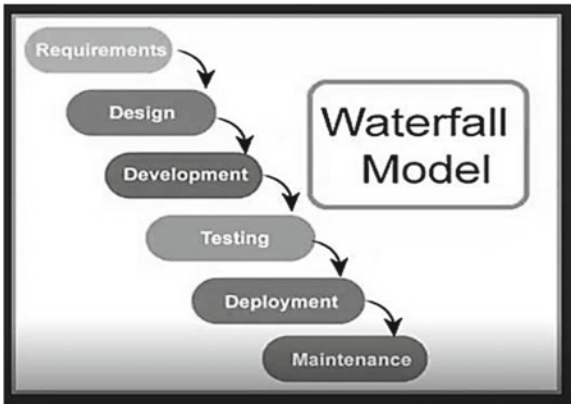

Fig. 2 Traditional project management method

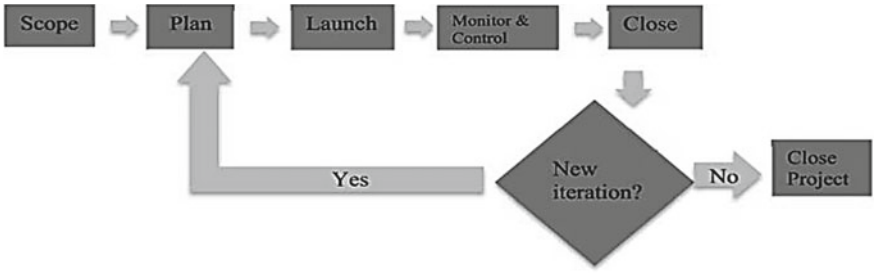

Fig. 3 Iterative PMLC model by Wysocki (agile project management method)

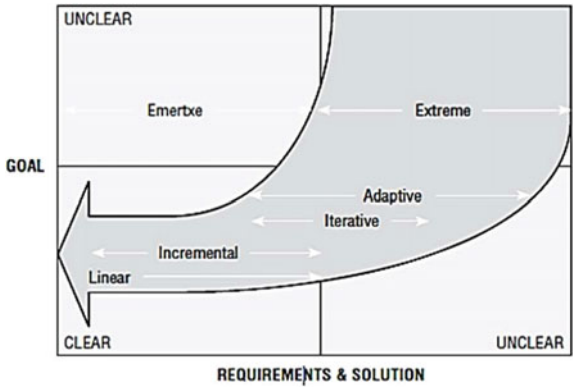

Fig. 4 Iterative PMLC model graphical representation by Wysocki

Due to the complexity of the operations, many of the construction and manufacturing entities following traditional methods may affect the high cost. In some instances, it is difficult to change. Dvir and Shenhar [7] mentioning that even though the traditional approach to project management emphasizes robustness as one of its advantages, prescribing that project managers apply the same methods and techniques to all projects uniformly, he mentioned one of the crucial disadvantages of such an approach. Today, an increasing number of authors stress that "one size does not fit all." The next major disadvantage in traditional project management is the assumption that the project is isolated from its environmental causes. The next major disadvantage in traditional project management is the assumption that the project is detached from its ecological reasons. Simon Collyer [8] and Olsson [9] state another disadvantage of traditional project management: Changes in the initial plan are inevitable due to adjustments to unpredictable and dynamic changes in the project environment or within the project itself. Also, it is sometimes tough to create a complete project plan at the outset of the project due to the inability to clearly define project goals [7]. Williams [10] summarizes those main reasons for the inappropriateness of the traditional approach to the majority of today's projects are structural complexity, uncertainty in goal definition, and project time constraints. This volatility, uncertainty, complexity, and ambiguity environmental factors (VUCA) make the traditional project management method weaker and need to evoke a new project management methodology. Different types of agile approaches, such as scrum, Agi-lean (agile plus lean), Kanban, and Scrumban (Scrum and Kanban), have already been used by the software and manufacturing sectors to combat the negative consequences of the VUCA world. Many researchers began debating the implementation of agile concepts in the construction industry in the mid-1990s. Already there are many studies carried out worldwide, some of the research on agile practices and some of them received successful adaptation in agile project management techniques. Pollock et al. [11] state that the UK joined with the industry to form the agile construction initiative to foster the adoption of lean and agile methods in construction projects.

2.1 Research Gap

Sri Lankan local contractors show that construction projects have continued to underperform, the question of construction methods remains open to inquiry. In particular, it is instructive to understand whether agile methods hold advantages over traditional methods, what benefits they yield, and whether their practice requires establishing any supporting mechanisms. The relative agile project management research done on Sri Lankan construction industry is scarce. That reason motivates us to carry out case study-based research on agile practices (especially on scrum-based interface) using an Internet-based interface to enhance the integration sector project management.

3 Methodology and Case Study

This case study has been carried out on a leading construction firm located in Colombo. Initial issues have been observed by the researcher for particular time intervals and listed out the internal issues, and validated through a survey among the employees. The identified key issues are mapped as in Fig. 5. The mapping clearly shows how these issues will be solved by whether it is from either scrum or the web-based integrated platform itself.

3.1 Scrum Methodology

On observation, the researcher found that employees in the organization lacked knowledge and skills on agile methodology. Developing their knowledge and skills, seminar sessions had been carried out by interrelating existing (traditional project management) practices with scrum (Refer Table 1).

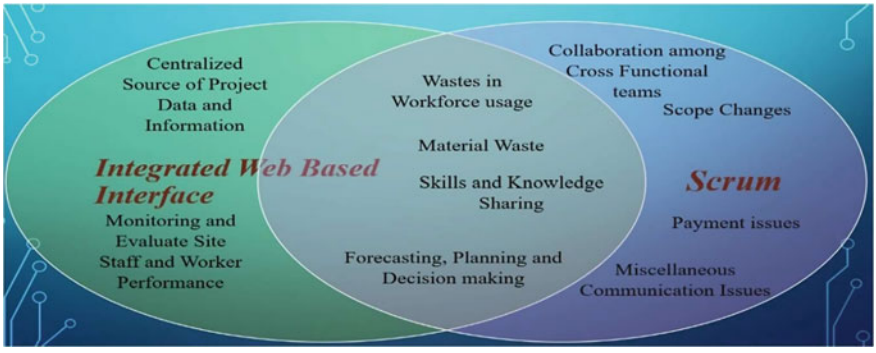

Fig. 5 Mapping of issues observed in internal practices

Table 1 Similarities in traditional and scrum method

Feature	Current practice (traditional method)	Scrum framework
Role	Client/top management of company (CEO/GM)	Product owner
	Engineering manager (projects)/ project manager	Scrum master
	Cross-functional team responsible peoples (design, planning, implementing responsible people and other representatives of supporting services)	Scrum team
Meetings	The client and contractor team discuss the tasks to implement and the time duration period to complete the selected tasks	Sprint planning meeting
	Contractor's project manager discussion with the project implementing team regarding the project progress and tasks to complete to his subordinates in regular intervals by solving the raising issues on specific time intervals	Daily scrum meeting
	Client and contractor team jointly inspect the works completed on-site and accepting or what are the rectifications that need to be done on the relevant tasks for specific time interval works	Sprint review meeting
	The Contractor's project manager conveys the rectifications has to be carried out for completed element to his subordinate elements /tasks to complete	Scrum retrospective meeting
	Client and contractor together discussing to prioritize activities due to the client/contractor need	Backlog refine meeting
Artifacts	Construction prioritization list	Product backlog
	Elements/tasks to complete	Sprint backlog
	BOQ task to meet	Sprint task
	Catch up on the delay /project crashing decision-making tool	Sprint burnt down chart

For better understanding, the scrum model is developed concerning the traditional approach (Fig. 6).

3.2 Web-Based Integrated Interface

The developed integrated web-based system was developed to use in both agile and traditional project management methodologies; in the developed web-based integrated interface, there are many associated sub-platforms such as document management platform, the progress monitoring platform (daily basis), cost monitoring platform (cash inflows and cash outflows), project data/project portfolio management platform, inventory tracking platform, order tracking platform, and scheduling platform, HR resource management platform, and other supporting platforms. These features help to gather whole departmentalized works into a single standard table.

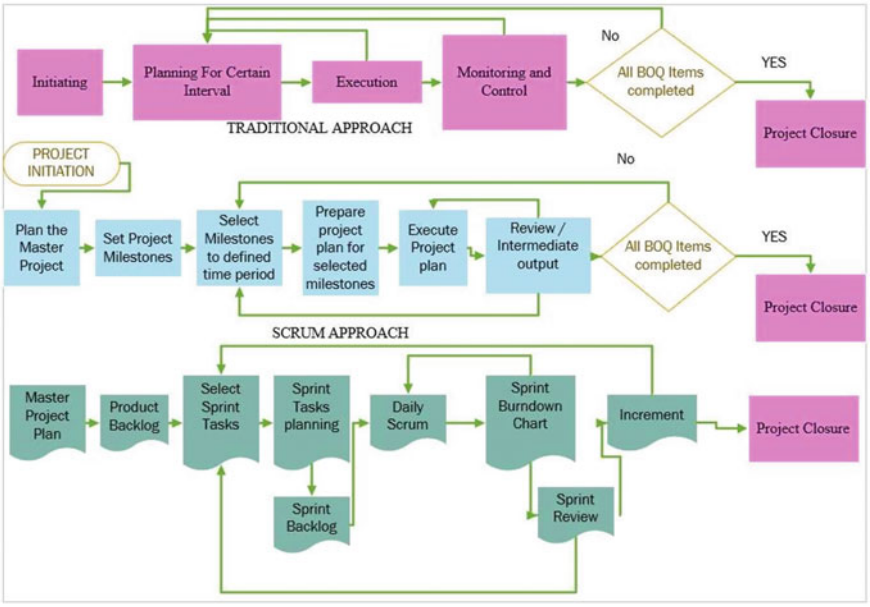

Fig. 6 Interrelate the components in the project flow

Thus, it enhances the cross-functional teams' collaboration by data sharing (data transparency) and eases the inter cross-functional team operations. Further, the developed platform auto-generates the wanted project-related reports within the needed time interval from anywhere at any time on up-to-date. Thus, one of the significant attributes of less documentation in an agile environment is automatically satisfied, and most of the human hours are saved. Further procurement is also integrated into the system; thus, it helps to create the actual tender bid estimation that is more accurate because the latest material and labor rates are updated. To justify that the web-based integrated system speeds up the process and efficiently delivers material to the site has been taken as an example for detailed study (Fig. 7).

In the traditional method of operation, the material ordering process is shown in Fig. 8, employees handled the material ordering forms in hard copies, and too many approvals were undergoing. Complete signatures are needed to process the orders other than emergency material orders. A single project manager in the organization must handle one or more projects depending on the situation, so the project manager is frequently unavailable at the head office or a specific site at the time of material ordering processing. Thus, the material ordering process was getting delayed. In the newly developed interface, all steps are web-based developed; necessary training was provided to the employees in the organization. A couple of projects with similar types of construction projects (heavy steel construction) were chosen to analyze the performance of the new practice. One project was managed using the traditional approach already in use in the organization, while the other was controlled using the

Fig. 7 Developed integrated web-based interface

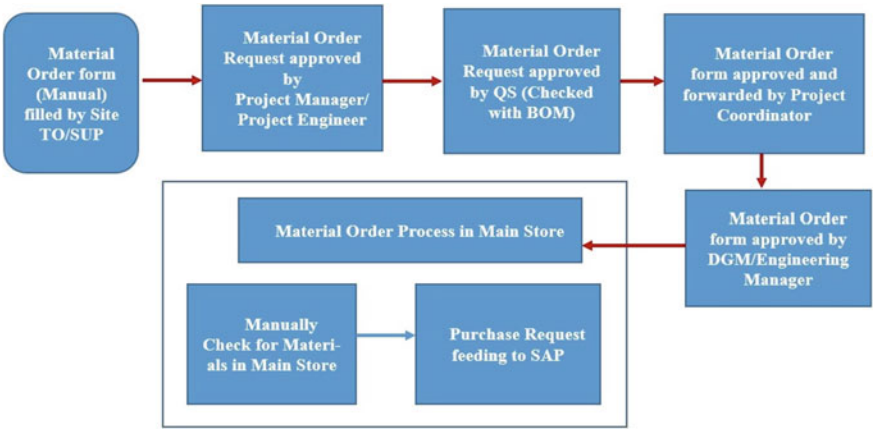

Fig. 8 Material order processing up to receiving the main store (traditional method)

new method. The new methodology was used for the petroleum fuel tank project, while the traditional system was used for the Gantry project. The results are compared at the end of the project, and conclusions are drawn based on the findings.

4 Data Collection and Data Analysis

Initial data collection has been carried out by directly observed by the researcher in the working environment of his workplace and according to the observation issues in

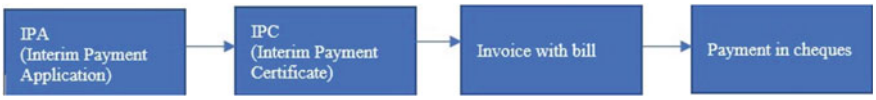

Fig. 9 Procedure of payments between contractor & client

internal practices identified. The Gantry project (traditional style) data are collected from manual hardcopies from various departments, and the fuel tank (project) relevant information is directly collected from scrum artifacts the developed web-based integrated interface.

4.1 Data Analysis on Operational Factors

4.1.1 Data Analysis on Client Satisfaction and Client Collaboration/Reworks

To measure client satisfaction and client collaboration, measurement of the time taken for payment receiving procedure (especially duration taken from IPA to IPC, which includes rework days and client approved) is shown in Fig. 9.

There are significant differences in the days to get IPA certified in the gantry and tank project graphs. Through the discussion with the client and contractor, the IPA could be certified within 2–3 days if there are no reworks. So in the Gantry project, there are more reworks done than the tank project. Since the tank project is managed in scrum methodology, the client participation was on time basis so that reviews of activities were done, so no massive reworks occurred. In the Gantry project, the review processes occurred after the IPA submission; thus, the defects were accumulated, and more reworks occurred. So agile practice helps increase the client collaboration in discussions, reviewing on time, and increasing the satisfaction rate to both client and contractor (Fig. 10).

4.1.2 Data Analysis on Material Receiving at the Site (Operational Processes Functionality)

Figure 11 clearly illustrates the relationship between delay in material receiving at site and days conceded in material order processing. When comparing tank project and Gantry project, it is clearly described that the modified new approach has significantly sped up the processing speed. Thus, the total delay is reduced to less than one or two days in the tank project. While in the Gantry project, it is clearly understood how the issues in material order processing impact delay in material receiving in construction site and direct impact on project delays.

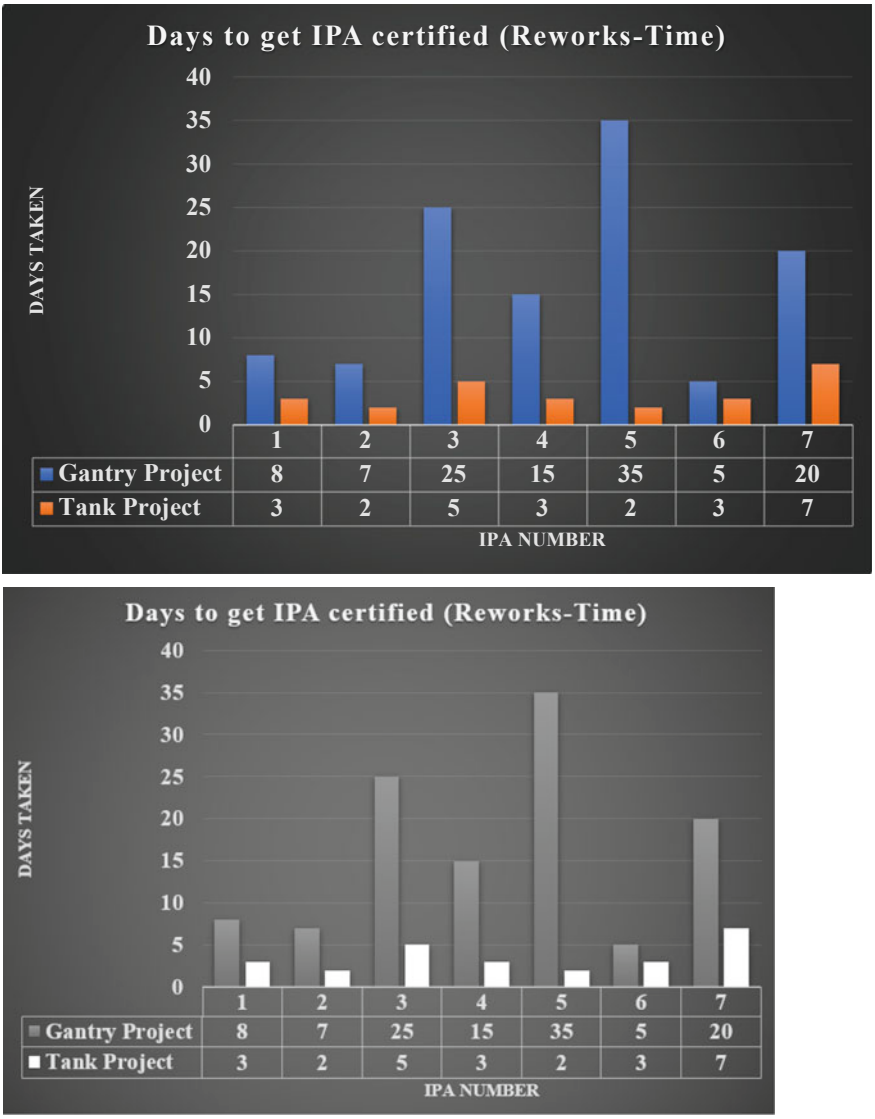

Fig. 10 Days to get IPA certified (reworks) from client

4.1.3 Handling of VUCA Factor in the New Methodology

From the user stories, the client also has the requirement to complete the tank project on time as planned since it affects their sales target, so there are a couple of activities

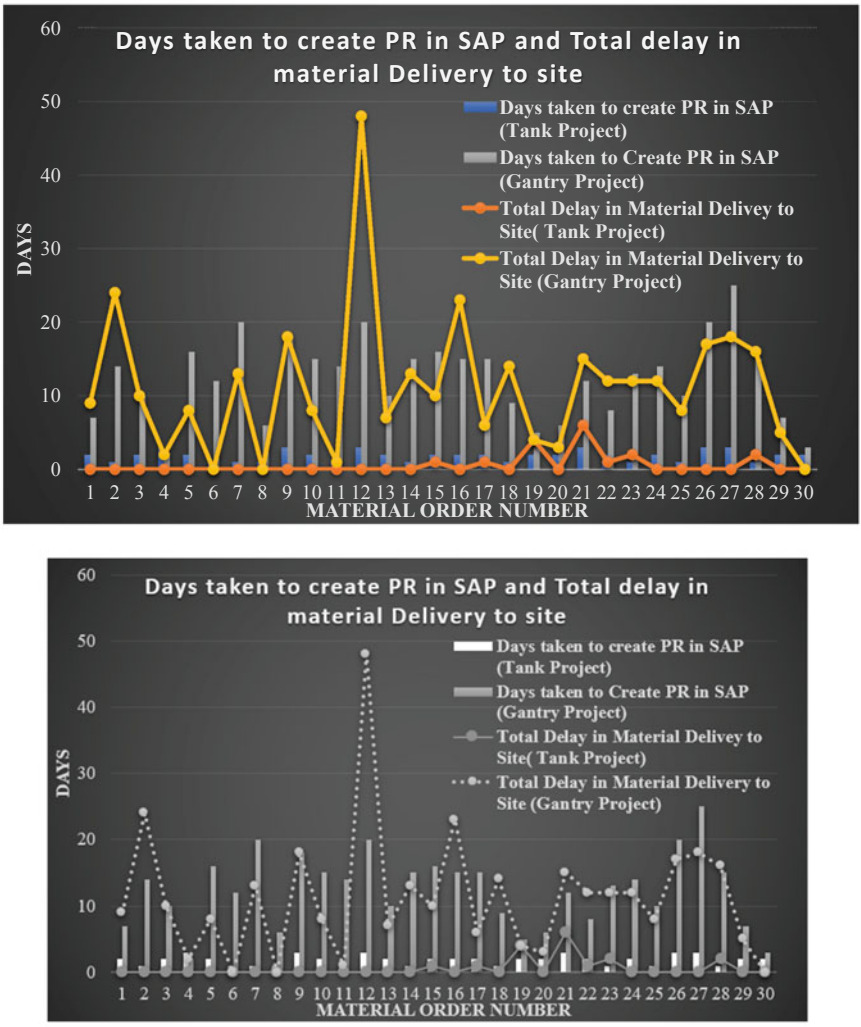

Fig. 11 Relationship with days spend to create PR in SAP and total delay when material received at site

affected due to VUCA factors such as weather (raining) and uncertainty of work-related subcontractor issues on client side are managed with reduction of progress idling (Table 2).

Table 2 VUCA factors managed in new approach

Activity	VUCA factor	Solution	How managed
Sand blasting and painting	Raining due to low pressure	The contractor has the facility to do shot blasting and painting in the acceptable technical environment	Shot blasting is allowed by the client while the payment is made in 5% contingencies
Access way to the tank (client scope in the main contract)	Uncertainty of subcontractor (client side)	Activity added to main contractor's scope	Main contractor agreed to do the work on the amount that offered to subcontractor, and separate work order issued asap
Cannot perform hot works during oil bunkering	Uncertainty of ship arrival	With a duration of 1 week time interval of bunkering, it is informed to contractor, and to plan to do other works in sprint planning meetings/in daily scrum meetings in advance	
Supply and installation of seals to tank	COVID-19 pandemic	No solutions found Island wide curfew imposed (uncontrollable) [Refer Tank project work done graph (March 2020–June 2020)]	

4.2 Data Analysis on Overall Project Performance

In Fig. 12, it is clearly showing that corrective actions/review the project performances from time to time and quick decision-making with the new approach is almost successful in the project on time rather than the whole island lockdown in the country. When analyzing the cash flow in Fig. 13, cash inflows are more satisfactory than the traditional approach due to the developed relationship with the client and involving the client in the process. Figure 14 shows the summary of the project performances with the planned quantities at the tender stage.

5 Conclusion

In this analysis, the material delivery has been taken as a representation of any project execution operation factors that affect project performance such as staff and worker allocation, fleet management or skills of the workforce, customer relationship, or any of the operations so that the same conclusions can be interpreted to other processes also. For example, when changing the material flow with reworks, the relationship of cash flow and rework flow with successful project delivery is the same. According to the case study, the generated graphs clearly show how delays in material flow (material delivered to site) affect project performances and how work done affects cash inflow for the project. So as described in Fig. 13, the entire thing generates a strong cyclic relationship in Sri Lankan local construction industry. Thus

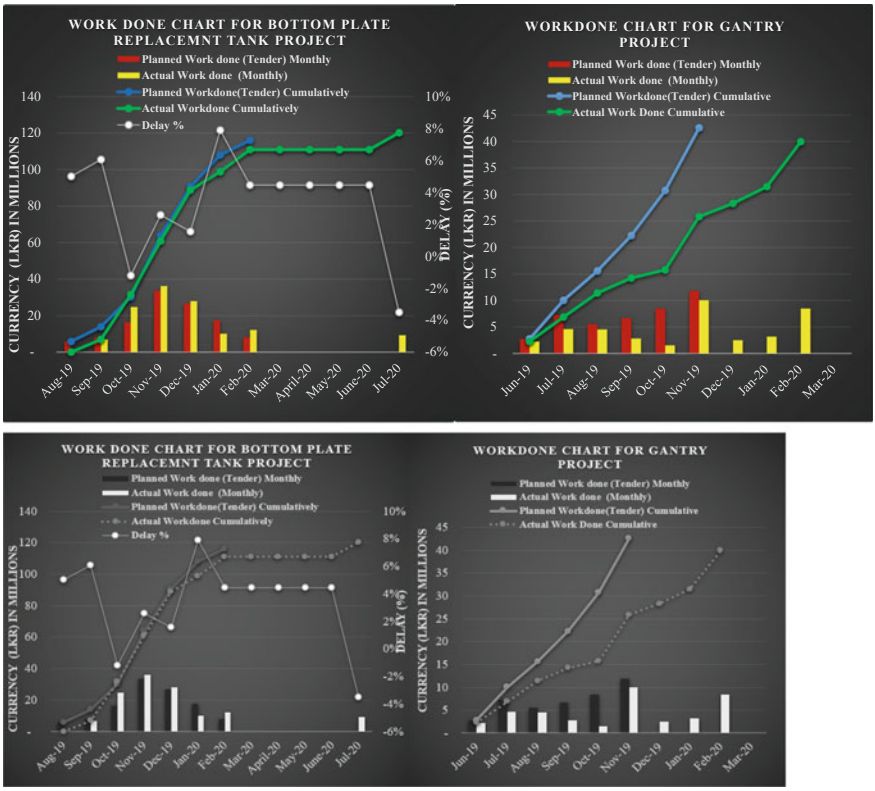

Fig. 12 Planned work done versus actual work done

for successful project delivery, it needs to charge the whole thing under control; if one fails, then it affects the entire system, as shown in Fig. 15. For successful project delivery in project completion, a web-based integrated project management interface helps the process run faster and enhances speed and quality, increasing the data transparency and accessibility, presenting real-time progress and forecasts, so the project is in control. At the same time, scrum practices increased the collaboration with the client and the cross-functional team within the local contractor company. Further, clients taking part in scrum meetings on an ongoing basis helps the whole team in which discovery, questioning, learning, and adjusting during the project are routine, acceptable, and systematically enhancing the outcomes. Moreover, client review is an add-on to the system so that each sprint review on prioritizing works, site situation on next sprint, and the waste on reworks can reduce.

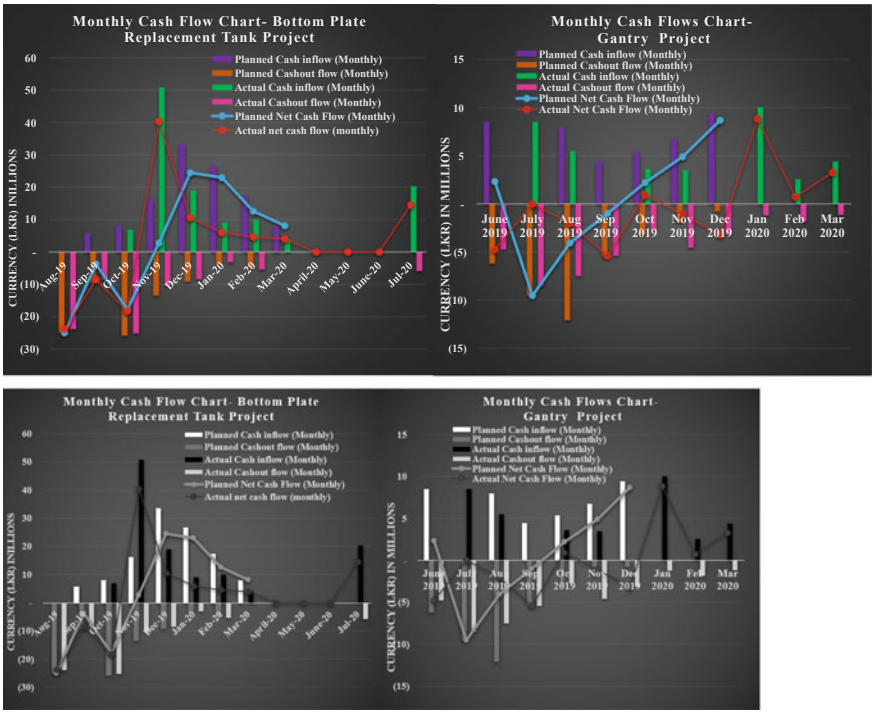

Fig. 13 Monthly cash flows

6 Recommendations of the Research

The most efficient way of educating the people in agile and lean project management concepts is a seminar on comparative analysis with the traditional framework. Top management is highly needed to support initiating in any companies later on with the maturity lead role provided by the project manager. Client support is a requirement, so research does not recommend initiating the approach with a new client. Assign a separate team to admin the web-based integrated project management system. Data transparency, even though agile project management recommends data transparency the higher authorized person (project manager/top management) can control confidential information. Most of the earlier issues can be solvable in Sri Lankan context. So that this proposed solution is increasing the project performances rather than traditional ways.

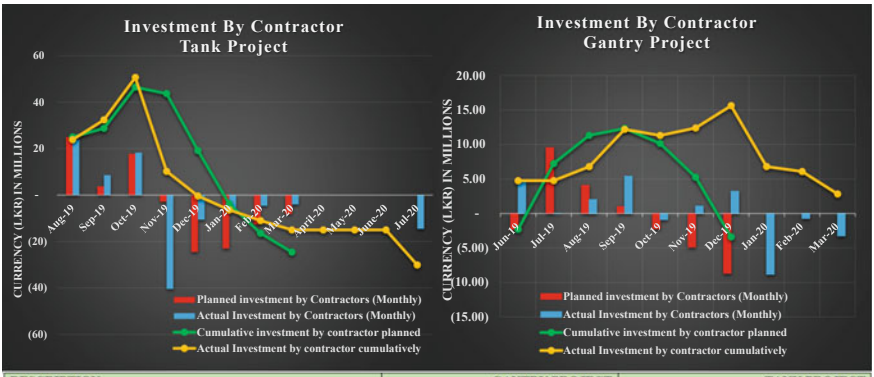

DESCRIPTION	GANTRY PROJECT	TANK PROJECT
Planned Contractor Investment	LKR 12,335,561.00	LKR 46,462,033.00
Planned Profit	LKR 3,405,281.00	LKR 24,589,948.00
Planned Rate of Return	28%	53%
Actual Contractor Investment	LKR 15,622,664 (▲26.64%)	LKR 50,622,199(▲8.95%)
Actual Profit	LKR (2,829,115.00) (▼183.1%)	LKR 30,124,216.00(▲22.51%)
Actual Rate of Return	-18% (▼46%)	60% (▲7%)

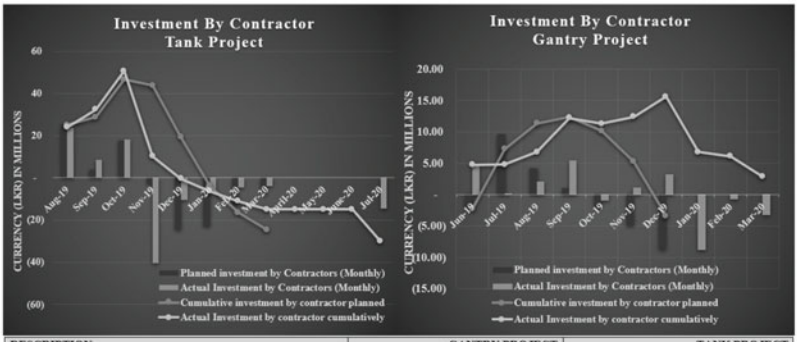

DESCRIPTION	GANTRY PROJECT	TANK PROJECT
Planned Contractor Investment	LKR 12,335,561.00	LKR 46,462,033.00
Planned Profit	LKR 3,405,281.00	LKR 24,589,948.00
Planned Rate of Return	28%	53%
Actual Contractor Investment	LKR 15,622,664 (▲26.64%)	LKR 50,622,199(▲8.95%)
Actual Profit	LKR (2,829,115.00) (▼183.1%)	LKR 30,124,216.00(▲22.51%)
Actual Rate of Return	-18% (▼46%)	60% (▲7%)

Fig. 14 Monthly investment graph and performance table

7 Limitations

Because of data privacy, the rates and project values are highly confidential, and all values are ethically updated (proportionally). Due to the COVID-19 reason, it is impossible to carry out most projects due to lockdown's external laws and restrictions in a distinctive manner. This study compared project performance with the old technique and recommended methods.

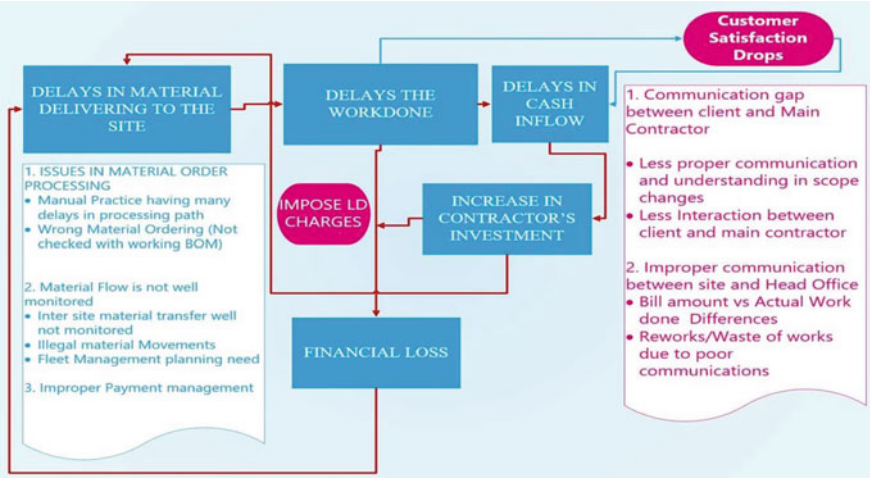

Fig. 15 Relationship cash flow and material flow with successful project delivery

8 Future Research Areas

Integrate IoT-based things into the project management systems for monitoring sites in real time, including safety and hazard management in Sri Lanka and develop agile project management methodologies in the Government projects in Sri Lanka.

References

1. Department of Census and Statistics (2020) Sri Lanka GDP from construction. Department of Census and Statistics, Sri Lanka. Retrieved 20 Apr 2021, from Trading Economics: https://tradingeconomics.com/sri-lanka/gdp-from-construction
2. Nissanka N, Wijeratne T (2019) Construction industry in a crisis. Retrieved from Daily FT E-NewsPaper: https://www.ft.lk/opinion/Construction-industry-in-a-crisis/14-674025
3. A Guide To The Project Management Body of Knowledge (PMBOK), 5th ed (2013). PMI (Project Management Institute)
4. Charvat (2003) Project management methodologies: selecting, implementing, and supporting methodologies and processes for projects. Wiley & Sons, Inc., Hoboken, NJ
5. Cockburn (2003) People and methodologies in software development. Doctoral Dissertation, University of Oslo, Oslo, Norway
6. Wysocki (2014) Effective project management: traditional, agile, extreme. Wiley, Indianapolis, Indiana
7. Dvir D, Shenhar AJ (2007) Reinventing project management: the diamond approach to successful growth and innovation. Harvard Business Press, Boston
8. Collyer S, Warren C, Hemsley B, Stevens C (2010) Project planning styles in dynamic environments. PMI Res Educ Conf 41(4):108–121

9. Olsson NOE (2006) Management of flexibility in projects. Int J Project Manage 24:66–74
10. Williams T (2005) Assessing and moving on from the dominant project management. IEEE Trans Eng Manage, pp 497–508
11. Pollock AM, Price D, Player S (2007) An examination of the UK treasury's evidence base for cost and time overrun data in UK value-for-money policy and appraisal. Public Money Manage 27(2):127–134

An Integrated Approach for Municipal Buried Infrastructure Asset Management

H. T. K. G. Jayawickrama, S. V. Gurupatham, P. Perera, and C. S. A. Siriwardana

Abstract Ageing municipal infrastructure and a growing population lead to efficient municipal asset management practices. The conventional asset management practices consume extensive time and cost for planning and management activities in local municipalities due to the lack of integration among different assets and their respective asset management activities. This leads to inefficient infrastructure-related management decisions and planning inefficiencies in the long run. Novel and smart approaches are appreciated to integrate and modernize conventional decision-making practices that are related to municipal asset management. The objective of this study is to acquire municipal asset life cycle information and to develop an asset management database for municipal buried infrastructure for the Colombo municipality. A sample road network will be used to develop this database, and a concept will be proposed to integrate parallel activities of different assets to reduce the cost and time of the municipality. Expert interviews and literature data will be used to develop the aforementioned database and identify the relationship of different asset management practices. This proposed concept and the database will be later used to develop a computer-aided asset management platform for local municipalities.

Keywords Municipal infrastructure planning · Long-term decision-making · Asset management

1 Introduction

Integrated municipal infrastructure asset management is a very timely topic to be discussed in the Sri Lankan context as most of our assets are ageing and require attention to maintain the required level of service. Municipal infrastructure assets

H. T. K. G. Jayawickrama · S. V. Gurupatham · P. Perera (✉) · C. S. A. Siriwardana
Department of Civil Engineering, Faculty of Engineering, University of Moratuwa, Moratuwa, Sri Lanka
e-mail: piyaruwanh@uom.lk

C. S. A. Siriwardana
e-mail: chassi@uom.lk

R. Dissanayake et al. (eds.), *12th International Conference on Structural Engineering and Construction Management*, Lecture Notes in Civil Engineering 266,
https://doi.org/10.1007/978-981-19-2886-4_49

can be identified as the assets which are maintained and protected to output their intended level of service, performances and conditions by the asset management processes [2]. Asset management is defined as an integrated activity to realize value from the system of assets [13]. In this paper, the data collection and development of the BIM-based municipal infrastructure asset database which focused on sewer networks and road networks in local municipalities will be elaborated.

Municipal asset management in the Sri Lankan context has not been considerably discussed in the past literature. There are very few papers on various aspects of Sri Lankan municipalities, but not specifically regarding integrated infrastructure asset management. Regarding the global context also, most researches have focused on asset management approaches considering different municipal assets separately. Many municipalities have established pavement management systems, anyway, integrated approaches to managing all the municipal assets such as road, sewer, and water have been implemented only by very few [1]. However, an integrated approach for asset management using Building Information Modelling (BIM) was very rare in the past literature.

With the rapid population growth and urbanization in Sri Lanka, the demand for municipal services has been drastically increased [11]. Hence, the amount of municipal assets also has been increased rapidly. However, in proportion to the growth in demand and the infrastructures, maintenance, and repair processes have not been improved. Because of those problems such as poor level of service (LOS), high cost and time for maintenance activities, and in the end, huge inefficiencies in asset management have occurred.

One of the major issues identified was the lack of a proper database for municipal infrastructures such as sewer, road and water networks in local municipalities to make informed decisions on preventive asset maintenance. This has been emphasized as the main problem in Sri Lanka as a developing country with a large asset inventory (*Strategic Municipal Asset)* [18] and also confirmed with municipal expert interviews that were conducted with several municipal engineers. To address the above issue, a sample database was created using municipal experts' data for a sample asset using the BIM platform. The developed asset database consists of a sewer network and road network with all the functional and characteristic features of those assets. Implementing such a database in local municipalities will optimize the decision-making process since it addresses one of the burning issues with them. Also, managers, engineers, technical officers who involve in these maintenance interventions, and in the end, the ordinary people who get the service will be benefited through this approach. At the same time, this database can be effectively used to develop an integrated decision-making framework to make informed decisions on municipal assets. Municipalities would be able to save a considerable amount of money in the long term by integrating different asset management activities and would be able to reduce asset downtime by doing preventive maintenance using the database. This paper covers the literature findings and findings of the expert interviews, methodology for the database development, results of the case study and a brief discussion on the way that database can be used in integrating the asset management process.

2 Literature Review

As mentioned in the Introduction, a limited number of researches regarding Sri Lankan asset management practices can be observed. From the available limited number of papers, it was proven that because of the lack of information and data, high demand, and the lack of funds, the Sri Lankan municipalities are struggling to maintain or renew the current municipal assets [12].

When considering the global context, countries have started using BIM to develop their municipal asset databases and automated asset management approaches already. Countries such as the USA, UK and Australia have adopted BIM for their projects in design, planning and construction stages for a long time, and BIM has been well-established in those developed countries [5]. However, with a case study in the UK, [14] have highlighted that BIM-based infrastructure management is now overtaking the traditional asset management practices [14]. According to Koulutusohjelma et al. [10] with the development of BIM databases for infrastructures, more transparent and automated workflows can be implemented with the integration among various asset types [10]. BIM can be used as a resource to share information about the asset between stakeholders and can form the basis of decision-making during the asset's lifecycle [6]. The other main importance of using BIM is the data can be accessed and analysed irrespective of the software and the user interaction. By using BIM in operation and maintenance phases, data redundancy, data re-entry, data loss, and translation errors can be eliminated [9]. At the same time, [9] highlighted that mobile devices are being introduced widely in the world to access these BIM databases irrespective of the time and location of access [9].

Unfortunately, according to the latest research done by Sinenko et al. [17], the percentage of adoption in BIM among developing countries is still unsatisfactory [17]. Anyway, the Sri Lankan situation is worse than in several other Asian countries [17]. In Sri Lanka, many sectors in the construction industry are still lacking in BIM application even for planning, designing, and construction stages of their infrastructure projects anyway, having said that it is a buzzword for Sri Lanka [8]. This paper will open the paths to implementing BIM in municipalities to maintain their asset systems.

Asset management is defined as the creation, acquisition, maintenance, operation, renewal, rehabilitation and disposal of assets [14]. To implement those tasks with data-driven decisions, BIM will help since it can be identified as a tool for generating, storing, managing, exchanging and sharing asset information in an interoperable and reusable manner [14]. Regarding municipal assets, it is specifically mentioned that 3D models are essential to deal with underground assets such as pipe networks [7]. Conventional 2D data representations are very poor to describe the location and directions about such layered assets.

With a BIM-based 3D database for sewer and road networks, benefits such as a more realistic and illustrative database, easiness of understanding, the capability of viewing a large amount of data at once, integration of planning and construction with

maintenance, easy file management for drawings and more transparency in decision-making and implementation can be obtained [15]. Koulutusohjelma et al. [10] had mentioned another importance of using such a 3D BIM database which all the parties who are permitted can comment with relevant to the assets [10].

During the literature survey, it was proven that institutions have to face many challenges when adopting BIM. Doumbouya et al. [4] pointed out top management support, subjective norm, compatibility and computer self-efficacy as key points that affect adopting BIM in an institution [4]. In some researches, it is clear that the attitudes of people are the main challenge to overcome to implement BIM-based approaches [19]. According to his surveys, he has highlighted that 40% of the respondents from the USA and 20% from the UK think that investment in training for BIM is less efficient [19]. At the same time, establishing government policies that support to use of BIM-based systems has been driven the USA and UK to cement BIM use in their infrastructure projects [17].

Regarding the Sri Lankan context, [12] it has been specifically mentioned that lack of engineering professionals, insufficient English literacy among municipal engineering management, and poor information technology knowledge are several challenges in Sri Lankan municipalities [12]. These can be identified as challenges to the BIM adoption process in local municipalities.

Since it was hard to acquire information on the asset management practices in Sri Lankan municipalities specifically from research papers, several interviews were conducted with a group of municipal engineers in the drainage division of a local municipality. According to those municipal engineers who have experience of approximately 10 years in the sewer sector, the sewer network data in the local municipalities are stored in GIS files and road network data are stored in AutoCAD format. Hence, decision-making has to be done by manually navigating through different types of data sources [3]. These are considered as old technologies which are in 2D maps consisting of lines and points [7]. Even though there are maps for sewer networks, many significant data such as materials of manholes, the depth of the manholes, buried depth of the pipelines, previous maintenance records for each asset separately, and underlying soil strata are not included in the database. After further discussion with the engineers, it was clear that some orders to the on-site labourers are given based on the data in their memory, and experience not based on proper data. While observing the maintenance process there, it was identified that on-site engineers or technical officers ask for information related to underground pipe locations from head-office engineers over the phone.

Taking the above-mentioned weaknesses into account, proper software to develop the new database was selected referring to the available literature. ESRI City Engine, Bentley Map and Autodesk InfraWorks 360 are some commercial software that is used to develop 3D city models. Among the available software, InfraWorks 360 was the best software suited for modelling the 3D model of the sewer network and the road network in the real city environment [10]. Mainly all other software is designed for planning, designing and construction phases.

3 Methodology

The methodology performed in this research has been compressed as in Fig. 1.

Phase 1: Literature Review and Data Collection

At the initial stage of this research, a comprehensive literature review was done to identify the implementations of asset management frameworks along with the asset databases developed. It was clear that the majority of such researches had been done in the American region and European region. However, in the past literature, it has been emphasized that having a shared asset database within the organization is highly important to get the intended results of asset management practices. By using the BIM platform that highlighted issue with sharing data can be easily overcome.

Phase 2: Assets and parameter identification

After having an understanding of the existing municipal asset databases developed recently in other countries, the municipal infrastructure assets and the various parameters of them to be included in this database were studied. The expert interviews were conducted to aware of the different municipal assets and the related parameters that exist currently in the system. Two chartered municipal engineers who have experience in the drainage sector for more than 10 years, a technical officer and, a tax officer in a municipal council in the Western province were incorporated for these data-gathering purposes. In the sewer network, assets such as sewer mains, gravity sewer lines, sewer force mains, manholes, sewer valves and pumping stations were identified. According to the current asset data in local municipalities, a limited number of parameters have been included in the system for each asset. As an example, for gravity sewer lines, a few major parameters such as diameter, pipe material, upstream and downstream elevations, the length of the pipe segment, and year of laid have been included in the existing asset database. However, in other asset databases developed in other countries recently, these parameters have been identified in social, environmental, economic and operational aspects [16]. As included in that database, parameters such as pipe buried depth, underlying soil strata, road type, traffic volume data and critical

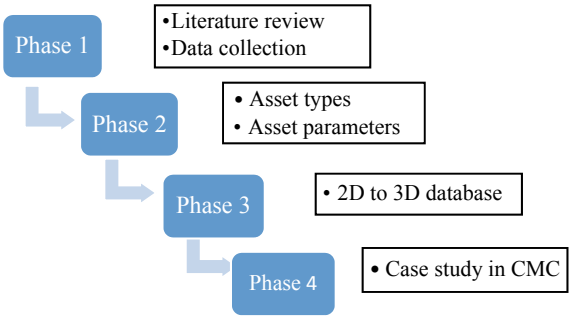

Fig. 1 Methodology diagram

consumers of that particular asset (hospitals), past maintenance activity data are not included in the current asset database in Sri Lankan municipalities.

Phase 3: Developing the asset database

With this understanding of the different assets and those parameters, the database development was started. For this, asset inventory was first established according to the GIS data files in the local municipalities. To develop the database, the software used was InfraWorks 360. The ArcGIS files and the AutoCAD drawings of the assets were acquired from the drainage division of a local municipal council. Next, using the Model Builder platform in the InfraWorks software, a 3D model of the city was created. After that sewer network was modelled manually after changing the coordinate system to the local coordinate system which is Kandawala coordinate system. Under that the road surface, underlying gravity sewer line, sewer force mains and manholes were 3D modelled. The available data with the assets were included as attributes and new parameters had to be defined to insert data such as maintenance activities. In InfraWorks, new parameters or custom properties for assets can be introduced using a JSON file. Using that file, InfraWorks identifies what new parameters are to be inserted in the property palette under different categories according to the user requirement. This 3D BIM model of the road along with the sewer infrastructure, itself is the asset database developed. It consists of all the characteristics and functional data regarding every component of the system.

Phase 4: Application to a case study

The above-mentioned database development methodology was used to develop a BIM-based 3D asset database for a 1.3 km road segment in R.A. De Mal Mawatha, Bauddhaloka Mawatha and Galle Road which is under the CMC. Using existing GIS data and AutoCAD drawings, the roads and sewer infrastructure were modelled using InfraWorks 360 platform. Those data were gathered from a municipal council in the Western province. Further discussions with the engineers helped to get a clear understanding of the current asset database and the implementation of intervention activities. Using the GIS data, gravity sewer lines, sewer force mains, manholes were modelled with their exact geo locations, according to the Kandawala coordinate system. Road network data too were inserted into the model. The available data such as pipe ID, pipe diameter, pipe material, laid year, starting and endpoint elevations were embedded in the properties' palette for every asset. In this BIM-based database, those mentioned attributes were embedded for every element. Also, the long-term future preventive maintenance interventions and cost of those maintenances for each asset were included after introducing new parameters for those interventions. And the frequency of implementing those interventions was included along with every component. Now this 3D BIM model is a data-rich database for the municipal asset managers which will help them to implement their repair and other maintenances with more informed decisions. After that, this database was uploaded to the BIM 360 cloud-based platform and allowed one of the municipal engineers to navigate through it.

4 Results and Discussion

The BIM-based asset database developed using InfraWorks 360 platform was shared with an experienced chartered engineer in the drainage division of a local municipal council. After allowing him to use this asset database as a trial, it was proven that existing issues with the current database can be overcome. As emphasized in the literature also, a more realistic view of the road and sewer infrastructure, the ability to view a large set of data at once, easiness to understand the orientation of those underground assets, are several highlighted points that came from the interviewed engineer as well.

As shown in Figs. 2 and 3, that engineer clearly stated that rather than using these 2D maps for sewer infrastructure which are made up of lines, this newly developed 3D model is understandable.

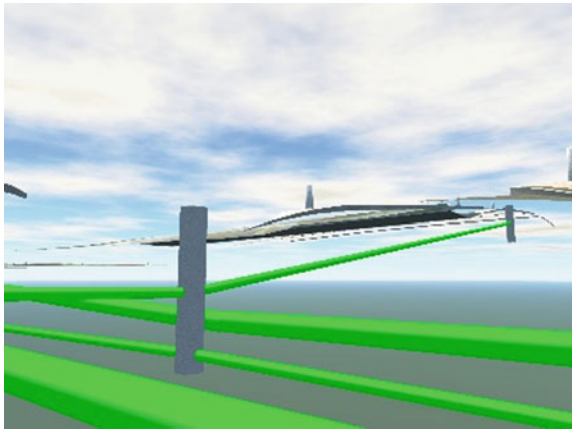

Fig. 2 A snapshot from InfraWorks database

Fig. 3 A snapshot from GIS database

Since this database need not essentially be stored in a local hard disk of a computer, the limitations with accessing data can vanish. Having this database in BIM 360, the engineers can access the data irrespective of the time and location he is at. With the development of the BIM 360 mobile application, it is easier to access data, add comments under any asset or intervention and also reply to those comments conveniently. Regarding that point, the municipal engineer emphasized that for a pandemic situation like COVID-19, such a database is timely and very much helpful to manage infrastructures remotely and smoothly with informed decisions.

The other main significant factor, he pointed out was that the transparency of the decisions based on this new database. Each officer who is in this decision-making process accesses the same updated data without any changes. This leads the tender processes and approving them more reliable and transparent.

This discussion with the engineer ended up after giving some attention to the cost of this software. Of course, to develop this database, any municipal council has to purchase the InfraWorks 360 from Autodesk. Also, the licence has to be renewed annually. At the same time, they have to pay for the BIM 360 cloud account to upload the database and use it confidentially only among the allowed engineers. These figures sum up to a high cost. However, cost and time saving by decision-making with this data-rich model will earn that money in the long run.

This newly developed BIM database will be used in future to establish an integrated asset management framework for Sri Lankan municipalities. The data included in this 3D model will be further checked and improved with more literature findings. It was noted that it would be better to have a methodology to model these assets in InfraWorks automatically rather than doing it manually. Carrying out it manually for large areas consumes a lot of time and energy.

To develop the schedule of asset interventions, the data from this InfraWorks model will be exported out and arranged in an optimum way in such a way that the cost and time for those interventions to be minimized. This multi-criterion decision-making approach is to be used. With having such a framework for the local municipalities, the long-term cost and the time for the interventions will be considerably reduced.

5 Conclusion

According to the initial expert interviews and discussions carried out while developing this database with engineers in the local municipal councils, it is evident that Sri Lankan municipalities are in essential need of such an asset database. Moreover, having such a centralized BIM-based asset database will enhance their efficiencies in municipal infrastructure asset management practices while reducing their cost considerably in the long run.

References

1. Abu-Samra S, Ahmed M, Amador L (2020) Asset management framework for integrated municipal infrastructure. J Infrastruct Syst 26(4):04020039. https://doi.org/10.1061/(asce)is.1943-555x.0000580
2. Amadi-Echendu JE, Brown K, Willett R, Mathew J, Springer © (2010) Definitions, concepts and scope of engineering asset management
3. Bakry I, Elsawah H, Moselhi O (n.d.) Multi-tiered database schema for integrated municipal asset management
4. Doumbouya L, Gao G, Guan C (2016) Adoption of the building information modeling (BIM) for construction project effectiveness: the review of BIM benefits. Am J Civ Eng Arch 4(3):74–79. https://doi.org/10.12691/ajcea-4-3-1
5. Ghaffarianhoseini A, Tookey J, Ghaffarianhoseini A, Naismith N, Azhar S, Efimova O, Raahemifar K (2017) Building information modelling (BIM) uptake: clear benefits, understanding its implementation, risks and challenges. In: Renewable and sustainable energy reviews, vol 75. Elsevier Ltd., pp 1046–1053. https://doi.org/10.1016/j.rser.2016.11.083
6. Heaton J, Parlikad AK, Schooling J (2019) A building information modelling approach to the alignment of organisational objectives to asset information requirements. Autom Constr 104:14–26. https://doi.org/10.1016/j.autcon.2019.03.022
7. Hu Z, Guo J, Zhang X (2020) Three-dimensional (3D) parametric modeling and organization for web-based visualization of city-scale pipe network. ISPRS Int J Geo-Inf 9(11). https://doi.org/10.3390/ijgi9110623
8. Jayasena HS, Weddikkara C (2012) Global challenges in construction industry. In: World construction conference 2012, pp 28–30
9. Jazayeri I (2012) Trends in 3D land information collection and management
10. Koulutusohjelma, Pääaine, Koodi (2016) Semantic 3D modelling for infrastructure asset management
11. Malalgoda C, Amaratunga D, Haigh R (2013) Empowering local governments to make a disaster resilient built environment within Sri Lankan Cities. In: Cities
12. Mohan V (2015) Future skill needs in municipal engineering in Sri Lanka. Proc Inst Civ Eng Municipal Engineer 165(4):239–246. https://doi.org/10.1680/MUEN.11.00025
13. Moodley K (2014) Editorial—Is ISO 55000:2014 the new dawn in asset management? Infrastructure Asset Manage 1(2):21–22. https://doi.org/10.1680/iasma.14.00019
14. Munir M, Kiviniemi A, Jones SW (2019) Business value of integrated BIM-based asset management. Eng Constr Archit Manag 26(6):1171–1191. https://doi.org/10.1108/ECAM-03-2018-0105
15. Onungwa I, Olugu-Uduma N, Shelden DR (2021) Cloud BIM technology as a means of collaboration and project integration in smart cities. SAGE Open 11(3). https://doi.org/10.1177/21582440211033250
16. Shahata K, Zayed T (2010) Integrated decision-support framework for municipal infrastructure asset
17. Sinenko S, Hanitsch P, Aliev S, Volovik M (2020) The implementation of BIM in construction projects. In: E3S web of conferences, p 164. https://doi.org/10.1051/e3sconf/202016408002
18. Strategic municipal asset management (2000)
19. Yan H, Damian P (2008) Benefits and barriers of building information modelling

Thermal Assessment of Terrace Houses Constructed with Light Weight Eps-Based Panels

R. Kathiravelu, N. Athukorala, and M. T. R. Jayasinghe

Abstract Terrace houses are used in many countries as a solution for the scarcity of land due to the ability to complete houses with smaller footprint and hence generally tend to reduce the cost incurred. However, there are drawbacks in the terrace houses in tropical climatic conditions due to restrictions on providing thermal comfort. Newly introduced expanded polystyrene (EPS)-based lightweight concrete wall panel has less self-weight and less thermal conductivity and absorbs less heat to minimize thermal effect. This detailed study was carried to assess the applicability of EPS-based lightweight concrete wall panels as the wall material of terrace houses with proper passive design in order to enhance the indoor thermal comfort. Three storey terrace houses have been developed to comply with the locally adopted building regulations. These houses have been assessed with the aid of computer simulations carried out using the DesignBuilder software using the climatic data pertaining to different climates. Comparative studies were conducted to determine the thermal behaviour of the terrace house by modifying various factors in six ways, such as materials, thickness, climatic condition, orientation of house cluster, floors and courtyard formations. As an outcome of these detailed studies, a set of ideas and rules were developed for improvement in internal temperature of terrace houses.

Keywords Terrace house · Thermal comfort · Tropical climate conditions · EPS lightweight load-bearing wall panels · Thermal conductivity

1 Introduction

There has been a rapid increase in the world's human population in recent decades [13]. Sri Lanka also recorded higher population growth rate which results environmental pollution and exploitation of natural resources. As well as the demand for land has increased due to the migration to the cities in search of facilities. As a solution to this, terrace houses are recommended in many countries to use the land

R. Kathiravelu (✉) · N. Athukorala · M. T. R. Jayasinghe
Department of Civil Engineering, University of Moratuwa, Moratuwa, Sri Lanka
e-mail: kathiravelur.21@uom.lk

R. Dissanayake et al. (eds.), *12th International Conference on Structural Engineering and Construction Management*, Lecture Notes in Civil Engineering 266,
https://doi.org/10.1007/978-981-19-2886-4_50

effectively. Anyhow, the main drawback of the terrace houses is poor ventilation due to the fewer windows. As a result, unnecessary energy consumption is realized by mechanical cooling to make living spaces comfortable for occupants [9]. In order to find a solution, nowadays insulated walls like expanded polystyrene-based concrete panels are commonly recommended to reduce above effects and to provide comfortable temperature.

The main challenges of the present construction industry are the shortage of affordable buildings and the higher cost of building materials. Therefore, there is a need to reuse the resources and welcome new materials which can be used at present without compromising sustainable utility. The temperature of terrace house can be reduced as much as possible by using a suitable wall material and passive concepts. This research tends to find the effect of temperature performance of terrace house made out of EPS wall panel as a possible substitute for conventional houses and solutions of the problems of energy demands.

1.1 Expanded Polystyrene-Based Lightweight Concrete Wall Panels

EPS is a plastic foam insulation material produced from solid beads of polystyrene, which is a waste product in large amount from packaging in various industries. This is not a decomposable material in nature and causes environmental problems [8]. The use of expanded polystyrene beads as aggregates has shown benefits such as reduced sand use and reduced waste in the environment [3]. EPS is a lightweight, spherical-shaped material that contains 2% polystyrene and approximately 98% air [1]. Thus, these beads can be easily combined with any other materials to produce lightweight concrete composite panels for applications such as thermal and acoustic insulation [7]. Here, the dead weight by the structural elements is considerably reduced [8]. There will be a reduction in the strength of the concrete because EPS has almost zero strength, although it has achieved strengths above the minimum required for structural concrete [4]. EPS wall panels are interlocked by using their tongue and groove arrangement, and it gives further rigidity [5]. Therefore, houses can be constructed without using a concrete frame and lightweight concrete panels can bear all vertical and lateral loads acting on the structure [14].

Therewith, the implementation of thermal insulation solutions in buildings can greatly contribute to reducing their environmental impact [12] (Figs. 1 and 2).

1.2 Thermal Performance and Thermal Comfort

Sri Lanka is a tropical country with hot and humid mixed climates and have no significant difference between summer and winter seasons. The days are usually hot,

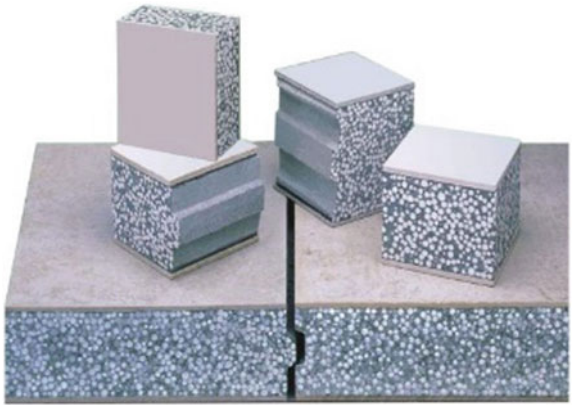

Fig. 1 EPS-based wall panels

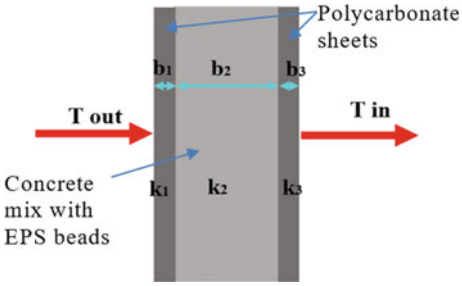

Fig. 2 Cross section of EPS-based panel

but the nights are cold. It will be an issue for urban areas without air conditioning. Thermal comfort is affected by micro climatic conditions and human expectations. Air temperature, radiant temperature, humidity and wind speed variables must be taken into account in the design of the building. Herewith, the personal adaptability (level of activity, clothing), biological (age, sex) of the occupant and environmental expectations (open-closed window) also affect thermal comfort [2].

Today, the thermal insulation of walls has become one of the key elements of the zero-energy house which means energy consumption per year is nearly negligible [15]. Therefore, it is wise to aim to reduce heat gain on the building envelope by following proper passive technique and insulated walls. This research focuses on the design of a terrace house with zero-energy power, and the temperature performance in the absence of cooling methods by using simulation software. It is hoped that the results obtained from the simulation will provide useful information on the energy saving techniques (Figs. 3, 4, 5 and 6).

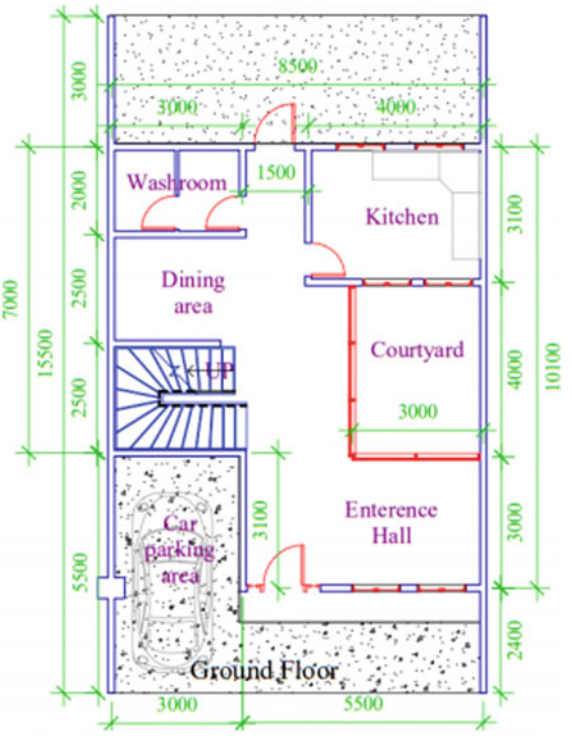

Fig. 3 Ground floor house layout

2 Objectives

The main objectives of this research were to assess the effectiveness of EPS-based concrete wall panel in warm humid tropical climatic conditions and to develop a set of ideas and rules for improvement in internal temperature of terrace house.

3 Methodology

The knowledge on structural behaviour of EPS-based lightweight panels have been used to develop a medium-sized three-storey terrace house. The proposed house complying with the usually adopted building regulations pertaining to tropical climatic regions has been assessed for simulation. DesignBuilder computer simulation software is used to simulate the model which is a user-friendly version of Energy-Plus tools for checking buildings energy, carbon, lighting and comfort performance.

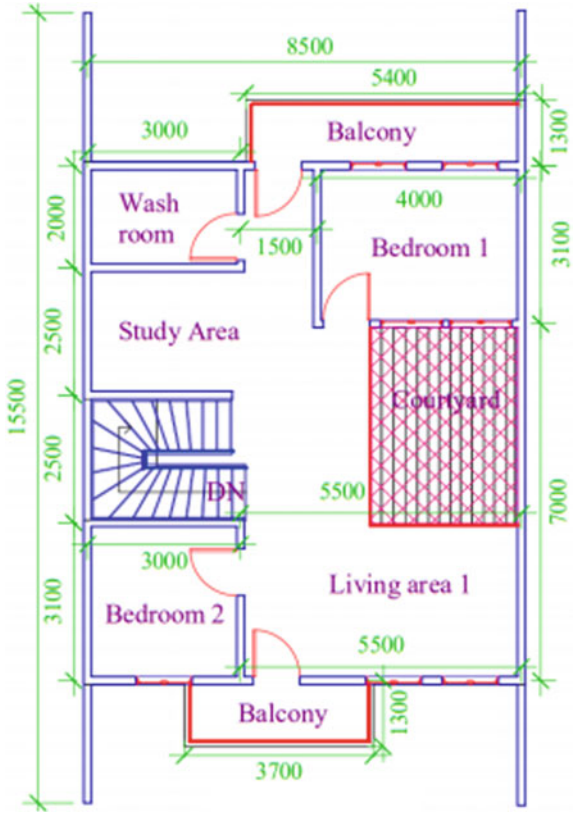

Fig. 4 1st floor house layout

The parameters required were identified and prepared from ASHRAE 55 for Design-Builder software. Since thermal performance is very complicated, there is a need to be investigated widely. Therefore, different simulations were done by changing the wall and house parameters, and subsequently, six comparative studies were conducted to develop terrace housing rules. Selected parameters were wall material, wall thickness, outdoor climatic condition, orientation of house cluster, floors levels and courtyard formations. Each simulation was conducted in the absence of cooling for the same house to find desirable features. The iterative calibration approach is employed in this study for validation. The model accuracy is inspected with respect to the benchmarks defined in ASHRAE Guidelines (Fig. 7).

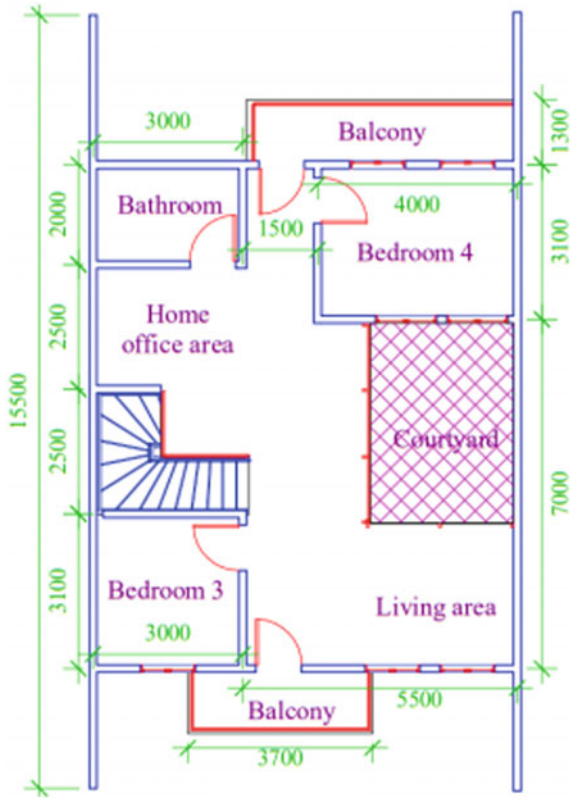

Fig. 5 2nd Floor house layout

Fig. 6 3D view of terrace houses

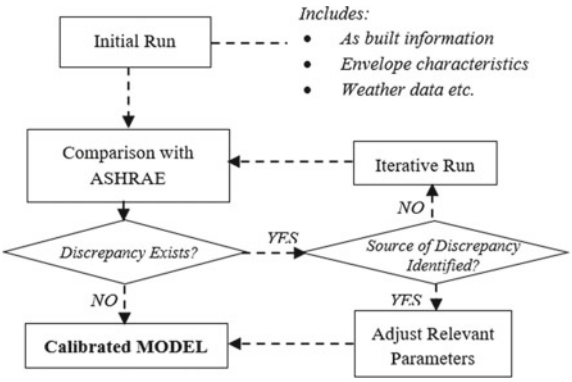

Fig. 7 The iterative calibration process

4 Results and Discussion

4.1 Temperature Variation by Changing the Wall Materials

Heat gain in the wall increases the indoor temperature. This study examines the characteristics of heat transfer in various wall materials. Thermal properties of wall materials from literature survey [11] were included in model.

The model was simulated, and the average temperature of middle terrace house for each material was obtained. The graph below gives the average indoor temperature for a year of each wall material in the same outdoor condition (Table 1; Chart 1).

When the values of all the materials are observed, all are within the range of 28 °C. Since there is no significant difference, graphs varying with the hours for the selected three days were again observed.

EPS wall panel maintains a low temperature when the temperature is high during the day and vice versa at night. The same tendency is shown by other elements with the value of thermal conductivity. However, to maintain a consistent temperature throughout the day, EPS-based wall panel is performing better than other wall materials (Chart 2).

Table 1 Thermal properties of material used

The thermal properties of the materials			
	Conductivity	Specific heat	Density
Unit	W/mK	J/kgK	kg/m^3
Concrete	1.63	1000	2300
EPS-based concrete	0.2417	1200	750
Brick	0.84	900	1800
Cement sand block	1.26	1000	1200
Cement sand earth block	0.8	900	200

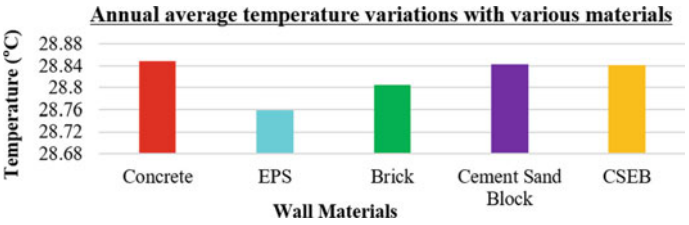

Chart 1 Annual average indoor temperature for each wall material

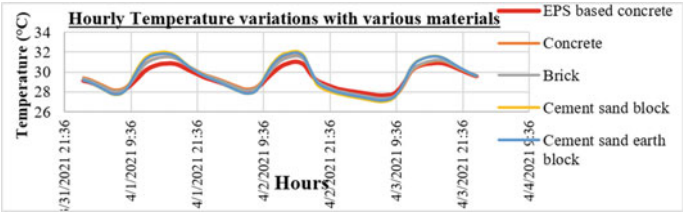

Chart 2 Hourly indoor temperature for each wall material

4.2 Comparison of Temperature Change When EPS-Based Wall Panel Thickness Varies

Choosing suitable thickness of wall can reduce consuming heating or cooling energy significantly. Because, the thickness of the wall influence thermal properties of wall (Eg: Thermal resistance). EPS-based wall panel has three layers with polycarbonate sheets on both sides as shown in the figure. Usually, there is no thickness change in polycarbonate board. There will be thicknesses change only in the concrete EPS mixture at the middle.

Climate data were collected for each distinct tropical zones such as Anuradhapura, Nuwara Eliya and Colombo for this comparison. The model was simulated by changing the thicknesses for each climatic data. Selected thickness of EPS-based wall panel for simulation which is available in the industry today.

I. 75 mm (0.075 m)
II. 100 mm (0.100 m)
III. 150 mm (0.150 m).

The chart below shows the temperature variation with thickness for a randomly taken day. The gradient of the line with was observed (Chart 3).

The resultant direction of heat flow varies with outdoor conditions. This leads uncomfortable indoor environment. In Colombo and Anuradhapura, with the increment of wall thickness, indoor temperature can be minimized. It works in opposite way in case of Nuwara Eliya. This shows the insulation behaviour of wall.

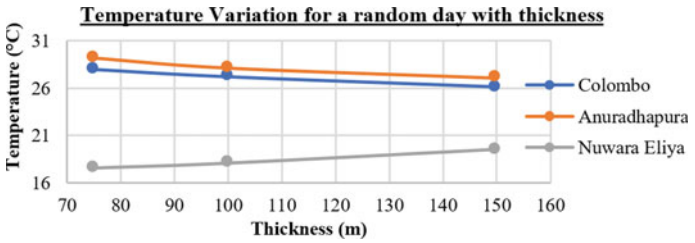

Chart 3 Indoor temperature variation for a random day

Table 2 Thermal resistivity calculation

	Thickness (b) (mm)			Resistance (R)
	b_1	b_2	b_3	m^2 K/W
Case I	5	75	5	0.3557
Case II	5	100	5	0.4592
Case III	5	150	5	0.6660

$$R = \frac{b_1}{k_1} + \frac{b_2}{k_2} + \frac{b_3}{k_3} \quad (\mathrm{m}^2\,\mathrm{K/W}) \tag{1}$$

R—Thermal resistance—(m^2 K /W).
b—Thickness of layer—(m)
k—Thermal conductivity—(W/mK).
Conductivity: k_1-0.2200, k_2-0.2417, k_3-0.2200 (Table 2).

When the thermal resistance increases, it reduces heat gain (in case of warmer outdoor climate) or heat loss (in case of cooler outdoor climate). Hence, the thicky wall can be used to withstand a comfortable temperature. But it may increase construction costs and reduces the usable space of the building. Therefore, need to pay attention to these two factors and select the optimal thickness will be the best solution.

4.3 Comparison of Temperature Variations Between District of Sri Lanka

This comparative analysis was conducted to observe the suitability of EPS-based wall. Climate data includes available districts on EnergyPlus: Anuradhapura, Batticaloa, Nuwara Eliya, Katunayake, Ratmalana, Hambantota, Kankesanthurai, Puttalam and Trincomalee.

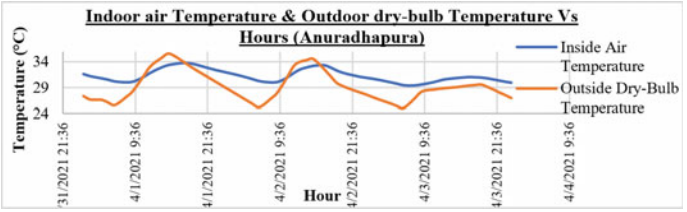

Chart 4 Indoor air T and outdoor dry-bulb temperature versus hour

4.3.1 Influence of Indoor Temperature on Outdoor Temperature When Using EPS-Based Wall Panel

It is generally observed that the change in outdoor temperature cause indoor temperature change. Therefore, before examining the relationship between districts, it is necessary to find out how the outside and inside temperature varies. Anuradhapura was taken as an example, and graph was drawn for random 3 days (Chart 4).

Inside temperatures were approximately 3–4 °C less than outside temperature in day time. As well as at night, it prevents temperature loss. The characteristic feature of EPS-based concrete is that it maintains the same range of room temperature despite the temperature differences during the day.

4.3.2 Indoor Temperature Difference Between Districts When Using EPS-Based Wall Panel

Although Sri Lanka is generally considered a tropical country, it has a climate variability and wide range of climates. So, choosing a wall material that is suitable for all districts is a challenge. The graph of temperature versus time was drawn for all districts. Most districts except Nuwara Eliya have almost the same temperature range (Chart 5).

This shows the uniform climate distribution across the country of Sri Lanka.

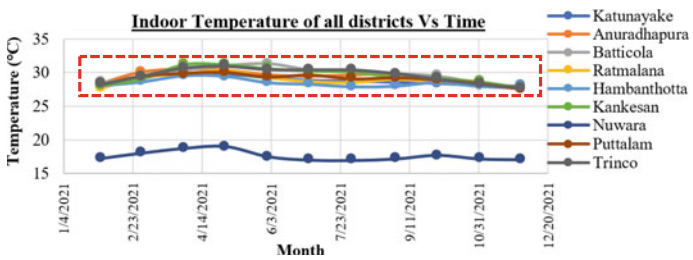

Chart 5 Indoor temperature of all districts versus time

Table 3 Average of daily indoor temperature of all district from simulation

Average of daily temperatures in each district (°C)			
	Min Temp	Max Temp	Ave Temp
Anuradhapura	26.1	33.4	30.2
Batticaloa	26.9	33.4	30.8
Katunayake	26.9	33.81	29.94
Ratmalana	26.94	32.9	30
Hambantota	25.8	32.1	29.7
Kankesanthurai	26	34.6	30.7
Nuwara Eliya	18.8	24.3	21.3
Puttalam	26.6	32.7	30
Trincomalee	22.6	33.9	30.6

From Table 3, it is clear that even without mechanical cooling EPS-based concrete walls can give suitable indoor temperature ranges for all the districts including tropical uplands.

4.3.3 Diurnal Temperature Variation Throughout the year

The variation in the temperature reached from the maximum temperature of the day to the cold of the night is called the diurnal temperature difference [10]. If the difference is too large, occupants of the house can feel discomfort and this can lead to total body heat imbalance (Chart 6).

The graph was drawn for temperature variation of each hour in a day for hotter months (March–May). The air temperature difference within the day and night should not exceed 5 °C to prevent discomfort [6]. But diurnal temperature observed is 3–4 °C which is within comfortable temperature range for human.

Therefore, EPS-based panels are suitable for all districts in every manner to achieve comfortable indoor temperatures.

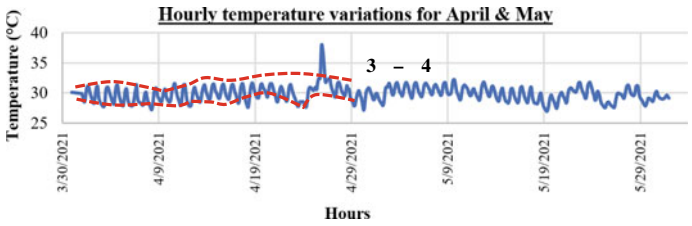

Chart 6 Temp variation along the day of Colombo-Katunayake

4.4 *Analysing the Indoor Temperature Variation During the Change of Directions of the Terrace House*

Orientation and position have an impact on buildings' overall thermal performance and helps occupants to achieve thermal comfort without using any cooling or heating facilities (Fig. 8).

The three houses were drawn up in DesignBuilder software, and the direction of the houses was rotated by 45°. The model simulated for each position. The average temperature for the whole year was found for all three houses, and the radar graph was drawn as shown in Fig. 9. The indoor temperatures of the houses facing West and East are higher than the North and South. In addition, the obtained graph shows that the building in the middle (Building 2) has a lower temperature than end houses. Because, generally intermediate walls of middle houses are not exposed to sun. Therefore, the application of terrace houses significantly reduces the overall temperature. Facing to the north and south can be used to maximize the effect.

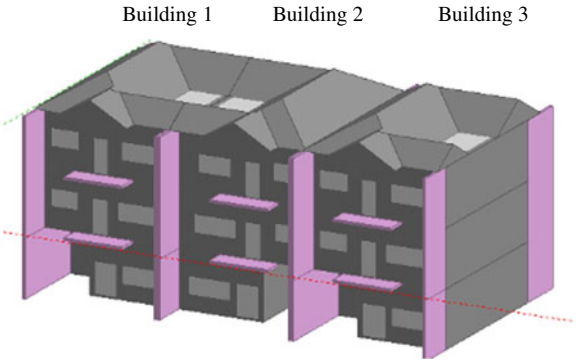

Fig. 8 Three house model in DesignBuilder software

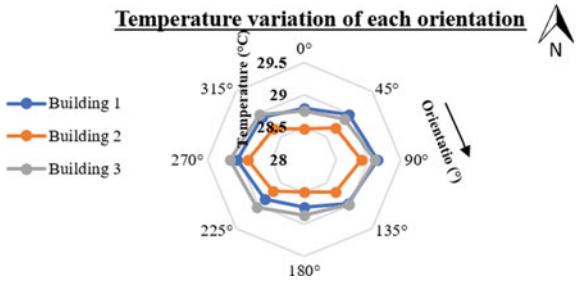

Fig. 9 Average indoor temperature for each direction

4.5 *Analysing the Temperature Variation Based on Number of Floors and House Rows*

The number of floors was limited up to 3 storeys in EPS-based concrete. Multi-storey building provides good natural light and ventilation. In addition, top floors act as a shade and influences the temperature of the floors below. Therefore, exploring the effect of number of storeys of the terrace house is essential in this research. The average temperatures of each floor for three houses were obtained as below (Table 4).

The smallest temperature was selected, and the percentage at which other temperatures varied was calculated. Bubble diagram was drawn to indicate each floors' temperature percentages for visual comparison. The thickness of the bubble indicates temperature variation percentage from ground floor of middle house (Fig. 10).

It was observed that the temperature on the second floor was higher and the ground floor was lower. Top floors resist heat penetration of lower floors, and the middle houses is protected from direct sunlight. Therefore, concept of multi-storey houses can considerably reduce the temperature effects in terrace houses than one-storey houses.

Table 4 Average indoor temperature variation depending on location and levels of terrace houses

	Average temperatures (°C)		
	Building 1	Building 2	Building3
2F	31.5	30.5	31.0
1F	31.4	30.2	30.6
GF	30.9	**29.7**	30.2
Minimum temperature, °C			**29.7**

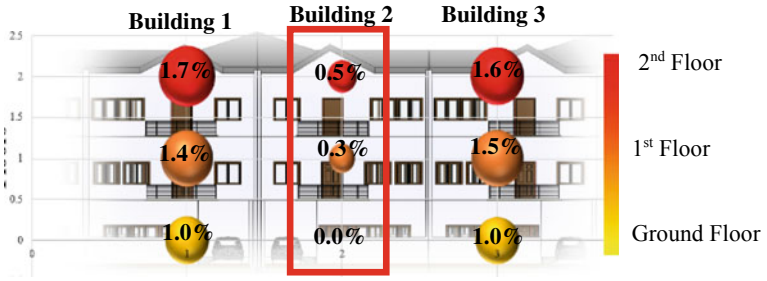

Fig. 10 Bubble diagram of temperature percentage

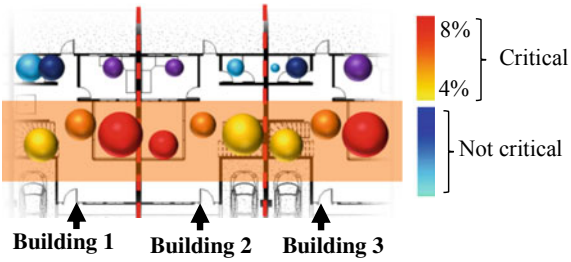

Fig. 11 Bubble diagram of each room temp in ground floor

4.6 Contribution of Courtyards to Indoor Temperatures in Terrace

Courtyards allows more ventilation and natural light, thus reducing the energy needed for lighting. But the temperature can rise due to the intensity of solar radiation and undesirable during the summer season. In this study, the effect of heat gain in courtyard was examined.

4.6.1 Exploring the Temperature Difference for Each Zone

The temperature variations are not same in all rooms. To find out the temperature relationship in each zone, the temperature variation percentage from lower was calculated as previous study. The bubble diagram of all three houses on ground floor is shown below (Fig. 11).

When comparing to the dimensions of the bubble, higher temperatures were observed in courtyard (Red) and living room (orange). Though courtyard allows more ventilation, also the solar radiation enters into house and increase the living room temperature. Terrace houses usually do not let in natural light as they have fewer windows. Therefore, avoiding courtyard is not the best solution to reduce indoor temperature. Therefore, in the following areas the corresponding solutions were explored selectively.

4.6.2 Exploring Temperature Change with the Types of Courtyards

In order to find out the solution, same model was modified with the following.

I. Without courtyard
II. Small courtyard (2 m × 2 m)
III. Large courtyard (4 m × 3 m)
IV. Courtyard covered with sheets (Polycarbonate sheet).

The graphs give the average temperature of the courtyard. The temperature is lower when the courtyard is absent, and it increases with the size of the yard. The

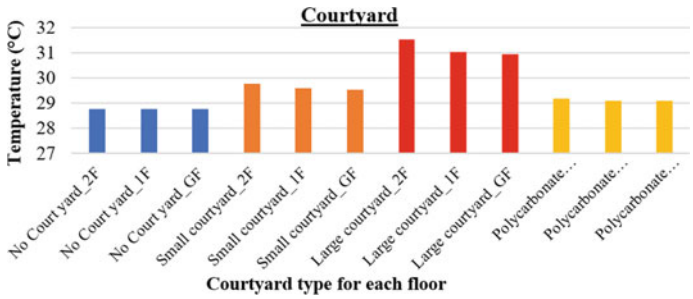

Chart 7 Annual average temp variation of courtyard with the size of courtyard

temperature can be minimized by reducing the size of the yard as much as possible. Thus, in cases where the size of the courtyards cannot be reduced, the yard can be covered using transparent plastic-based materials such as polycarbonate will be a best solution (Chart 7).

5 Conclusion

It is well known that terrace houses are widely used all over the world. However, the main obstacle for using it in Sri Lanka is its hot climate. In this study, the use of EPS-based concrete and the set of ideas recommended to minimize effect. Identified main factors that influence on the indoor environmental temperature are summarized below.

(1) The use of EPS-based concrete panel is able to resist heat transfer from outer wall surface to inner surface due to its lower thermal conductivity and can maintain the indoor temperature ranging between 28 and 29 °C which is lower than other conventional wall materials.

(2) As a manifestation of the nature of thermal insulation, with the increase of thickness of the material layers thermal resistance of the wall increase, i.e. in hot climates, it minimizes heat gain, and in cool climates, it minimizes heat loss. Therefore, it is wise to choose thicker wall to get comfortable temperature. However, it is necessary to go for optimum by considering the cost.

(3) It is possible to maintain indoor temperature of just 3–5 °C lesser than the outside temperature by using EPS-based walls. This is relatively high compared to ordinary materials. This wall is suitable for all selected districts including Nuwara Eliya. In addition, the indoor temperature change in a day is only about 3–4 °C from morning to night. This value is sufficient to give comfort to human.

(4) Houses of West and East faces get higher indoor temperature compared to the houses faced on the North and South sides, and it can be recommending

for terrace houses. Moreover, middle houses have the less indoor temperature significantly than other two, because of the less wall exposure area to sun.

(5) The lower floors' indoor temperature percentage can be reduced to 2–5% than 2nd floor, because the above floors are more exposed to the sun and it act as shading for lower floors. Therefore, for terrace houses, choosing multi-storey houses is highly recommended than one-storey houses.

(6) Although the courtyards allow more ventilation and light, courtyards allows more solar radiations. From these comparative studies, it is recommended that the size of the courtyard should be reduced to minimize the house temperature. In cases where such reduction is not possible, plastic-based materials such as polycarbonate can be used to cover the courtyard.

6 Recommendations

This study deals with determination of suitability of EPS-based panel on terrace houses and explore the factors that are essential for house thermal performance. The study concludes the use of EPS panel as a wall material reduces the indoor temperature. Its use has proven to be optimal for the whole of Sri Lanka. Moreover, this wall material brought about a significant reduction in temperature change compared to other materials. Also, of the 75, 100 and 150 mm sizes available on the market, 150 mm is better than the others to get better thermal comfort.

Apart from the choice of wall material, changes in the design and orientation of the terrace house cause a large influence on temperature. In order to prove it, the study was carried out by changing the directions of the house. It has been revealed that North and South facing terrace houses are blocking solar radiation through windows. Also, as far as terrace houses are concerned, the houses at the end get higher temperature. Therefore, higher number of houses in a row can reduce the average temperature as much as possible. In addition, the temperature can be reduced as much as possible by reducing the size of the courtyard, or by using transparent plastic materials like polycarbonate.

Therefore, from the above-detailed study it is proved that by using EPS-based lightweight concrete and introducing the appropriate design and passive concepts, terrace houses can be made suitable for Sri Lanka.

Acknowledgements Author wishes to express sincere thanks to the staff of the Department of Civil Engineering, University of Moratuwa, for the support and guidance provided towards this research.

References

1. Aciu C, Manea DL, Molnar LM, Jumate E (2015) Recycling of polystyrene waste in the composition of ecological mortars. Procedia Technol 19:498
2. Auliciems A, Szokolay SV (1997) Thermal comfort—PLEA Notes No. 3. The University of Queensland, Australia
3. Coppola B et al (2016) Investigation on the use of foamed plastic waste as natural aggregates replacement in lightweight mortar. Compos B Eng 99:75–83
4. Dissanayake DMKW, Jayasinghe C, Jayasinghe MTR (2017) A comparative embodied energy analysis of a house with recycled expanded polystyrene (EPS) based foam concrete wall panels. Energy Build 135:85–94
5. Fernando P, Jayasinghe M, Jayasinghe C (2017) Structural feasibility of expanded polystyrene (EPS) based lightweight concrete sandwich panels. Constr Build Mater 139:45–51
6. Guowen S (2011) Improving comfort in clothing. Woodhead Publishing Limited.
7. Kan A, Demirboğa R (2007) Effect of cement and EPS beads ratios on compressive strength and density of lightweight concrete. Indian J Eng Mater Sci 14:158–162
8. Kan A, Demirboğa R (2012) Thermal conductivity and shrinkage properties of modified waste polystyrene aggregate concrete. Constr Build Mater 35:730–734
9. Koenigsberger, Ingersoll (1978) Manual of tropical housing and building, part 1,climatic design. Longman Group, LTD., London and New York
10. Qu M (2014) Analysis of diurnal air temperature range change in the continental United States. Weather Clim Extreme 4:86–95
11. Mohammad D, Al-Homoud S (2005) Performance characteristics and practical applications of common building thermal insulation materials. Build Environ 40:353–366
12. Spirinckx C (2014) Exploratory study with regard to Ecodesign of thermal insulation in buildings, pp tasks 0, 1 and 7
13. UNFPA (2011) United Nations population fund. [Online] Available at: http://www.unfpa.org/publications/state-world-population-2011
14. Vishnu P, Thilakarathna PSM, Mendis P, Jayasinghe MTR (2017) The feasibility of using lightweight eps-based panels for staircases of apartments. In: 8th International conference on structural engineering and construction management, ICSECM-114
15. Wang L, Gwilliams J, Jones P (2009) Case study of zero energy house design in UK. Energy Build, pp 1215–1222

Key Procurement Selection Factors for Sri Lankan Private-Sector Commercial Building Projects

H. A. L. V. Silva and U. Kulatunga

Abstract Procurement is the complete process of distributing responsibilities among stakeholders, organizations as well as all those contributing towards the clients' satisfaction. The procurement method plays a major role in the construction industry. The application of the wrong procurement method could cause an unnecessary increment in the total cost for the client, disrupting outlined project schedules and creating undesirable situations for the client. Thus, selection of the most suitable procurement method is important for the success of any construction project. Selection of a procurement system usually takes long time due to consideration of numerous factors. However, analysing key procurement factors is helpful for clients who have limited time to finish the project. Hence, this research focuses on finding the most suitable procurement selection factors for private-sector commercial building projects in Sri Lanka. A comprehensive literature review was carried out to acquire the knowledge on existing procurement methods and procurement selection factors. Thereafter, the study incorporated expert interviews to identify, analyse, and validate the key procurement selection factors. Purposive sampling was selected as the sampling technique, and 13 experts were interviewed through online. The main four procurement systems were identified as traditional, integrated, management oriented, and collaborative procurement systems. Each procurement method has different characteristics which make them different from one another. The selection of a procurement method is different due to various procurement selection factors which vary from project to project. These factors include speed, cost, quality, risk allocation, responsibility, accountability, price certainty, and market competition for the project, regulatory environment, public accountability, culture, government policy, disputes and arbitration, availability of experience contractor, policy or objective of organization, technology, and many more. Within the context of Sri Lanka, speed, nature, scope, and complexity, price certainty, and risk and responsibility were revealed as the most important procurement selection factors. Moreover, these procurement selection factors were identified as key factors internationally.

H. A. L. V. Silva · U. Kulatunga (✉)
University of Moratuwa Sri Lanka, Moratuwa, Sri Lanka
e-mail: ukulatunga@uom.lk

R. Dissanayake et al. (eds.), *12th International Conference on Structural Engineering and Construction Management*, Lecture Notes in Civil Engineering 266,
https://doi.org/10.1007/978-981-19-2886-4_51

Keywords Procurement · Procurement selection factors · Private sector · Commercial building

1 Introduction

The construction industry is a lucrative industry of work worldwide which is very sensitive to uncertainties and risks in the global market [35]. The complexity of the construction industry has increased with the improvements of technology [34] and has become more complex [25] impacting the world economy by contributing more than 6% of the world GDP [62]. Though the percentage of the contribution appears small, the impact due to this contribution varies on the delivery of efficient and successful construction projects [2].

Researchers have identified application of a proper procurement system as a major improvement area in the construction industry [44, 56, 65] To promote project success and construction cost estimation, procurement is a critical influencing factor as it defines the overall structure of authorities and responsibilities [10]. Therefore, the selection and application of a suitable procurement system are important for the successful completion of a construction project [11].

Lahdenperä [31] has classified procurement systems broadly into four main categories as separated, integrated, collaborative (discretionary), and management oriented. These procurement systems include various procurement methods such as design and build, turnkey, package deal, design and construct, partnering, joint venture, construction management and management contracting [6, 20, 36].

As construction projects vary significantly from each other, the selection measures for the project procurement also vary from client to client. This also depends on each person's needs and requirements as per the project [11]. Therefore, it is understood that a single procurement system cannot be suitable for every project [54]. Ogunasanmi [39, 49, 53] has stipulated that different factors assist clients to select the finest procurement method to undertake the work. According to [33] and Bhutto et al. [5], procurement selection factors can be categorized as internal (project characteristics, client's characteristics, and client's requirements) and external factors (globalization, market competition, natural causes, regulatory environment, and information technology). It is essential to consider these procurement selection factors because they effect the project performance [39] project failure and client's dissatisfaction [46].

Within the context of Sri Lanka, there are number of studies carried out on procurement selection [43]. However, these studies were not focused on identifying the key factors that influence the procurement selection in Sri Lanka. Therefore, this study has been carried out to fill this gap by investigating the main procurement selection factors within the Sri Lankan context.

The procurement selection factors differ from the client sector it holds, which is either public sector or private due to the inherent differences between them [12]. Since the government sector projects mostly bound on transparency, accountability [22, 29,

64], public opinions and prefer using the same procurement system [29]. In Sri Lanka, the public sector has to follow the National Procurement Agency's (NPA) guidelines when selecting the appropriate procurement route. Therefore, factors affecting the procurement selection in the private-sector projects were considered as the focus of this study.

2 Procurement Systems

2.1 Procurement Systems Available in the World

The world is more concerned about delivering the best output from projects to their clients [3]. Moreover, [17] have derived that effective procurement methods consist of a high impact for a project to succeed. However, most of the projects tend to select the traditional method in procurement, but there are many innovative and fast-tracking procurement methods used in the worldwide construction industry [40].

There are several procurement systems available in the world. Jaafar and Naruddin [22] have divided procurement systems mainly into two categories as traditional and alternative (non-traditional) procurement systems, whereas [52] have categorized procurement systems as conventional and non-conventional delivery approaches. Further, [31] in his research has divided these systems as separated, integrated, management oriented, and collaborative procurement systems.

Liu et al. [33] have described the reason for calling the traditional procurement system as traditional based on its existence in the world for such a long period of time, and it has been the only option available for many years for the most employers of the construction industry. In a separated or traditional procurement arrangement system, both contractors and designers work separately, and responsibility is only levying on the work of them [20]. Integrated procurement system combines the responsibilities of design and construction of a project by contracting out all these duties to one contractor which is also called as sequential or a linear contracting system [50]. Design and build, package deal, turnkey, and develop and construct procurement methods come under the integrated procurement system.

The design and build procurement method does not separately undertake design and construction activities, and a single contractor is in charge [63]. Since the design and construction are on one party, many designs-related problems may arise in the design and build procurement method [37]. In package deals procurement method often utilizes a modular structure to enhance the ability of changing the size of the building later, and the contractor provides an 'off-the-shelf building' [4]. The viewpoint of turnkey procurement method applies a single responsibility in a project's design, building, assigning, and handing over and would be one of the effective project procurement methods in addressing the adversarial working practices and fragmentation [1]. The application of turnkey procurement method is getting common for similar projects, while the usage of design and build procurement method has

been selected by the public-sector client for educational and administration type of projects [22]. Develop and construct procurement method is a variation and is one that is similar to the design and build procurement method, except in develop and construct procurement method, as a baseline document, the employer issues a concept design for the advancement of the design [63].

While the traditional procurement system is based on impermeable and rigid boundaries among design and construction, collaborative systems have been developed in the last decade which makes room for project procedures to improve based on trust, communication, transparency, and commitment [18]. Therefore, collaborative procurement systems offer significant advantages over the traditional procurement method [30]. Partnering and joint ventures can be categorized under collaborative procurement systems.

In order to achieve specific objectives of a business, project partnering is utilized between two or more organizations together [24, 26]. Than non-partnering projects, partnering helps to satisfy clients by achieving technical performance and controlling costs [19]. A partnership, an enterprise established by two or more firms, an organization, or a corporation is described as a joint venture [24]. This is important in projects as it creates the best opportunity to merge unique capabilities and resources involving companies [42].

In management-oriented procurement method, an organization is carrying out the management of the project working with the consultants and designer to create the design and manage the physical activities which are done by the contractors [32]. Construction management and management construction procurement methods are subcategories of management-oriented procurement systems.

Construction management procurement method is used when the clients are required to work directly with specialized trade contractors [58]. Moreover, construction management is more suitable for employers placing a high priority on the project's buildability [36]. Management construction is a procurement method where a main contractor called as the management contractor is appointed by the client. His duty is to manage and coordinate individual subcontractor's work packages [40]. Management construction procurement method is much flexible since it permits development of design and the performance of the works to move concurrently [58].

In Sri Lanka due to the existing accountability and transparency within the traditional procurement system, it is what is generally used in the country. Secondly, the integrated procurement system is used [23]. Although, in a country, public procurement is higher than private procurement [9], Sri Lankan public procurement is mainly focused on objectives of stakeholders, whereas in the private sector, optimum benefit to the owner through least cost and accepted quality is considered [16].

The construction industry has constantly been criticized due to harmful disputes and conflicts in the relationship among parties which generally happens due to the selection of the wrong construction procedures [59]. Therefore, main procurement selection factors should be identified by the users before selecting a procurement method.

2.2 Procurement Selection Factors

Several studies done previously identified that many factors affect the selection of a particular procurement method in construction [39]. Thus, different researchers have identified different factors affecting the selection of procurement systems which are identified under Table 1.

Several factors affecting the selection of a procurement method for a particular project were discovered by different authors as shown in Table 1. These factors can be mainly divided as internal and external factors. The internal factors are client requirements, procurement policy, project characteristics, project location, finance,

Table 1 Different authors identifying factors influencing on the selection of a procurement system

Factors influencing the selection of procurement system	Authors
Risk allocation of the project, client's technical capability, responsibility, client's willingness to control over design and to be involved, and responsibility	[28]
Disputes, scope definition, flexibility, project type, project complexity, and the project scale	[27]
Client's involvement, clear risk allocation, user familiarity, ease of application, quality performance, cost certainty, deliver on schedule, reduction of cost or enhance performance of cost, collaboration among project participants, and differentiation and specialization among participants	[8]
Building information modelling (BIM), value management, constructability, lean construction, supply chain, technology development, value management, sustainability, and e-procurement	[57]
Nature of the client, nature of the project, risk avoidance, availability of information, technical complexity of the project, consultancy service offered, flexibility to entertain change for clients' requirements, complexity of design, high degree of control, financial arrangement, cheapest cost, minimization of design time, minimization of construction time, quality assurance, project completion at estimated time, and estimated cost	[4]
Client experience, financial capability of client, project size, project's time constraints, degree of project complexity, and price competition	[11]
Client's financial ability, material availability, time, requirement of client for value for money, market competitiveness, risk allocation, quality level, regulatory impact, flexibility to change design during pre and post-construction stage, project size, political constraints, responsibility, political constraints, price competition, complexity, client's trust in other parties, project site location, disputes and arbitration, certainty of cost and time, client's willingness to actively involved, experienced contractor availability, project type, and client's experience	[41]
Time-related factors, cost-related factors, quality-related factors, external environment, project characteristics, and general needs	[39]
Price certainty, price competition, flexibility for changes, familiarity, accountability, and quality of work	[47]
Market condition, economic condition and the fiscal policy, technology, sociocultural suitability, and regulatory environment	[48]

time, quality, and complexity of project, the external factors (environmental factors) are socio-economic considerations, capital cost, legal, political, technology, and competition [32, 45], and a visual representation is included in Fig. 1.

As shown in Fig. 1, internal factors include the client's requirements, characteristics and project characteristics while external factors include external environment-related factors which influence in deciding a procurement path. Therefore, the selection of a procurement method is influenced by internal and external procurement selection factors.

The identified factors were categorized as internal and external factors and included in Table 2.

In Table 2, internal factors were further subdivided into client's requirements, client's characteristics, and project characteristics. The client's requirements and

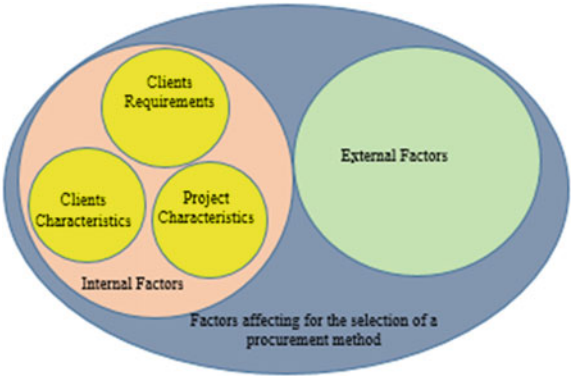

Fig. 1 Classification of factors affecting the procurement selection

Table 2 Types of internal and external factors

Internal factors			External factors
Client's requirements	Client's characteristics	Project characteristics	
Speed Quality of the work Clarity of the scope Flexibility for changes Accountability Price competition Price certainty Time certainty Risk management Familiarity Time availability and predictability Degree of complexity Responsibility	Type of client Client's involvement in the project Knowledge of the strategy Experience and intuition of the decision-maker Dissatisfaction with earlier method used	Time constraints Project cost and method of funding Project type Project size Project complexity Payment modality of the project Degree of flexibility Financial capability of the client In-house technical capability of the client	Market competition for the project Regulatory environment Public accountability Culture Government policy Disputes and arbitration Availability of experience contractor Policy or objective of organization Technology

Adopted from: [4, 8, 21, 28, 41, 57]

client's characteristics may differ from client to client as people are different in nature [11]. Moreover, the construction industry is unique in nature [38]. Therefore, project characteristics differ from project to project. In the external environment of a project, different criteria should be considered before selecting a procurement method [46]. Hence, the selection of a procurement depends on client's requirements, client's characteristics, project characteristics, and external procurement selection factors.

3 Research Methodology

Research approaches can be divided as qualitative, quantitative, and mixed [15]. Qualitative research approach was followed to collect data for the study. Within the qualitative research stance, expert interviews were selected as the data collection technique. Dada [14] and Sohu [60] have presented through their studies three main types of interviews, namely structured, semi-structured, and unstructured. Semi-structured interviews were conducted to collect the required information as more open-ended questions were required to ask from the interviewees.

Expert interviews were carried out through Zoom meetings, with the use of the phone and a previously prepared Google form. The prepared Google form was emailed to the interviewee to be familiarized with it to give a holistic answer. At the end of the expert interviews, the objectives were achieved through finalizing main four procurement selection factors for private-sector building projects in Sri Lanka.

Interviews were piloted with two experts to finalize the interview guideline, and thereafter expert interview was conducted with thirteen (13) industry professionals in quantity surveying profession practising as Chartered Quantity Surveyors (QSs). Table 3 illustrates the profile of the respective interviewees.

As per Table 3, all the experts were those with a significant industry experience specifically on procurement practices. Importantly, QSs were preferred since QSs perform the primary task of procurement in a consultant organization. Therefore, the expert interview was done with the Chartered QSs with a prolonged experience within the construction industry, specifically related to procurement were considered to have the required capacity to make a judgement on the factors affecting the procurement selection. Moreover, the experts were to incorporate their perspective across the procurement methods and procuring process, via their extensive knowledge and experience in procurement selection.

4 Findings and Analysis of Expert Interviews

The 'Expert Interview Guideline' consisted of three (03) sections developed under the advice of two experts in the field (PI02 and PI03). During the pilot interviews, both PI02 and PI03 suggested limiting the study to one size of building projects from

Table 3 Profile of expert interviewees

Code	Designation	Experience	
		No. of years	Key experience
PI.01	Ch. QS	10	Procurement, building project construction
PI.02 (Piloted)	Ch. QS	20	Procurement, building, and civil project construction
PI.03 (Piloted)	Ch. QS	20	Procurement, building, and civil project construction
PI.04	Ch. QS	12	Procurement, building project construction
PI.05	Ch. QS	14	Procurement, building, and civil project construction
PI.06	Ch. QS	27	Procurement, building, and civil project construction
PI.07	Ch. QS	28	Procurement, building, and civil project construction
PI.08	Ch. QS	25	Procurement, building, and civil project construction
PI.09	Ch. QS	20	Procurement, building, and civil project construction
PI.10	Ch. QS	22	Procurement, building, and civil project construction
PL11	Ch. QS	25	Procurement, building, and civil project construction
PL12	Ch. QS	21	Procurement, building, and civil project construction
PL13	Ch. QS	10	Procurement, building project construction

above 12 storey, below four storey, or any other. Their idea was that size of the building affects the building's speed, nature, scope, and complexity. Therefore, the study was limited to below four-storey building projects. To reduce the difficulty of answering and selecting the procurement selection factors, PI02 and PI03 proposed to select only internal procurement selection factors since external procurement selection factors are considered after taking into account the internal procurement selection factors. They further argued that more weight is given for the internal procurement selection factors in a procurement selection process. For the speed factor, PI03 commented to use durations in National Procurement Agency's (NPA) guideline of Sri Lanka as a basis to define the speed as the durations included in NPA guideline are the normal durations required to procure a project. PI02 and PI03 suggested to select only traditional, design and build, collaborative, and management-oriented procurement system for the study as they are the main procurement methods used in Sri Lanka. Moreover, they mentioned although turnkey projects are also used in Sri Lanka, for below four-storey building projects, application of turnkey projects is less.

Table 4 Procurement selection factors

Procurement selection factor	Code
Speed	F01
Quality of the work	F02
Clarity of the scope	F03
Accountability	F04
Degree of complexity	F05
Price certainty	F06
Time certainty	F07
Risk management	F08
Responsibility	F09
Project cost	F10
Project size	F11
Degree of flexibility	F12

The finalized interview guideline of the study focused progressively on the factors which influence on the selection of a procurement method. The factors included in Sect. 2 were finalized, and similar factors were removed from the list which were identified through the literature review to minimize the difficulty of answering the guideline.

According to the literature findings, Table 4 contains the factors which influence the selection of a procurement system. Interviewees were asked to give their opinions on these factors considering private-sector commercially valued below four-storey building projects in Sri Lanka based on the client's perspective. Further, they were asked to select the most considered four procurement selection factors among them.

Based on the opinions provided by the expert interviewees, collected data can be summarized as in Table 5.

PI01 revealed that speed has a direct and high impact on procurement selection, as slow speed of construction may increase the cost in the long run and market loss can happen due to that. Further, all other interviewees also agreed that speed has a main impact on the procurement selection. PI04 stated that speed is especially needed in private-sector projects.

The opinion of all interviewees turned out to be that the quality of the work is not an essential factor since any client needs their project to be done with the best way whether it is luxury, standard, or average. PI03 mentioned that although workmanship quality can be ignored, design intent and design quality cannot be ignored since it impacts on the procurement selection.

PI01 agreed that clarity of scope has a high impact on the procurement selection. However, PI02 mentioned that the impact of clarity of scope on procurement selection is low compared to other factors. Further, PI05 mentioned that it impacts on cost, time, and quality of the project which are the main considerable factors when selecting a procurement method.

Table 5 Analysis of the expert interviewees' answers on procurement selection factors

Code of interviewee	Code of selected factors												Opinions of interviewees
	F01	F02	F03	F04	F05	F06	F07	F08	F09	F10	F11	F12	
PI.01	✓		✓		✓	✓		✓	✓		✓	✓	Merge F08 and F09; F11 is related to F05
PI.02	✓			√	✓	✓		✓	✓		✓	✓	Merge F08 and F09; F11 is related to F05; other factors business compatibility, contract type, project finance modality, nature, scope, and complexity
PI.03	✓				✓	✓		✓				✓	Merge F08 and F09; F10 and F11 is related to F05; F12 is related to payment method
PI.04	✓			✓	✓	✓	✓	✓		✓		✓	Merge F08 and F09; F11 is related to F05
PI.05	✓		✓		✓	✓		✓				✓	Time, cost, and quality are the main considerations
PI.06	✓		✓	✓	✓	✓		✓				✓	Merge F08 and F09; F11 is related to F05
PI.07	✓				✓	✓		✓				✓	Merge F08 and F09; F11 is related to F05
PI.08	✓				✓	✓		✓				✓	Merge F08 and F09; F11 is related to F05
PI.09	✓				✓	✓		✓				✓	Merge F08 and F09; F11 is related to F05
PI.10	✓				✓	✓		✓				✓	Merge F08 and F09; F11 is related to F05
PL11	✓				✓	✓		✓				✓	Merge F08 and F09; F11 is related to F05
PL12	✓				✓	✓		✓				✓	Merge F08 and F09; F11 is related to F05
PL13	✓				✓	✓		✓				✓	Merge F08 and F09; F11 is related to F05; Other factors buildability and constructability

As per PI01, PI03, and PI05, accountability can be ignored as the focus of the study is on the private sector. The interviewees' opinion was, even though accountability has an impact on procurement selection, the impact which is low compared with other procurement selection factors. However, PI02 mentioned that accountability is a main procurement selection factor. Overall, majority of interviewees suggested accountability is not needed to be considered within the study context as a procurement selection factor. All the interviewees agreed that the degree of complexity is a main procurement selection factor in a private-sector commercial building project. Also, participants were suggested to combine complexity and project size together since both are related together from the client's perspective.

Price certainty as a main procurement selection factor was considered by all the interviewees, and majority of expert interviewees commented that time certainty can be ignored since speed of the project is considered and the time certainty has less impact compared to other factors. Risk management and responsibility were asked to combine by most of the interviewees since they have similar requirements. Project size was asked to combine with complexity by expert interviewee PI01 and PI02.

PI02 suggested combining nature, complexity, and scope together and applying it as a single factor. All other interviewees accepted this particular combination. Most of the interviewees mentioned that the project cost has less impact on the procurement selection and the degree of flexibility is related to the payment method. Thus, only few interviewees agreed on accepting the degree of flexibility as a procurement selection factor. Other than these factors, PI02 suggested to include business compatibility (to sell or rent) for the enhanced model output. PI13 mentioned that buildability and constructability are also essential in procurement selection.

Based on the expert interviewees' opinion and suggestions, speed was selected as a main procurement selection factor, and the scope and complexity were combined as nature, scope, and complexity. Price certainty was selected as the third important procurement selection factor, and as the final factor, risk and responsibility factor was selected. Here 'risk and responsibility' factor is considered from the client's perspective. The 'nature, scope, and complexity' of a project and risk and responsibility of a client were combined based on the recommendations of the expert interviewees and later clarified with other expert interviewees. It was assumed that the design intent is anyhow essential in a particular project, and therefore, quality of the project and accountability was ignored.

5 Discussion

As discussed above, there are different procurement selection factors affecting the selection of a procurement system in Sri Lanka. These factors can be categorized as internal factors and external factors. To analyse procurement selection factors, procurement methods used in private-sector commercial buildings were considered. Based on the expert interview carried out, four key procurement selection factors were identified.

The key factors identified from the data analysis are speed, nature, scope, and complexity, price certainty, and risk and responsibility. The selected procurement selection factors were identified as the suitable procurement selection factors by many international researchers [4, 21, 41] and Sri Lankan researchers [46, 55]. Speed can be described as the time taken for the completion of a construction project. Speed of a construction project can be high, medium, and low. The complexity of construction projects (combination of nature, scope, and complexity) is also identified as another important procurement selection factor from the context of Sri Lanka. Clarity of scope and allocation of responsibility is taken as main procurement selection factors in Malaysia by [13]. Moreover, [4] have found technical complexity of a project, complexity of design, and nature of the project are main factors in selection of a procurement method. Thus, according to the Sri Lankan context as proposed by the interviewees, combining these factors under the term complexity is justifiable.

According to Wood and Gidado [61], measuring complexity at the early stage of the construction project provides great benefits to manage the project successfully and decrease the risk associated with the project. Similar to the findings of this study, from the global context also, the importance of risk as a procurement selection factor has been highlighted by [7]. Based on the findings of [51], under project complexity, it is associated with managerial perspective, operative, and technological perspective which are considered. Therefore, nature, scope, and complexity factor covers part of risk and responsibility factor in a project. For both clients and contractors, cost certainty and time certainty are major concerns in construction projects as they have dire impact on resources [63]. Further, [53] have identified price certainty as the major concerned procurement selection factor in Malaysia and degree of complexity and time constraints of project are other main factors. Time certainty is considered under speed factor, and as the next key procurement selection factor, price certainty was selected within the context of Sri Lanka.

6 Conclusion

The selection of a procurement method is difficult due to various procurement selection factors which vary from project to project. Therefore, the focus of this study was to identify the procurement selection factors related to private-sector construction projects in Sri Lanka. The study was limited to private sector below four-storey commercial building projects.

Expert interviews were conducted among 13 interviewers to find the most considered four procurement selection factors and concluded as ‘speed’, ‘nature, scope, and complexity’, ‘price certainty’, and ‘risk and responsibility’. These key procurement selection factors are finalized for private-sector commercial building projects in Sri Lanka. Although there are many types of building projects and infrastructure projects in Sri Lanka, as the procurement selection differs with the project type, commercial buildings were considered for the analysis. At last, these key procurement selection factors could be considered by private-sector clients who have limited time to analyse

the procurement systems. Even if these factors are for commercial buildings, since these factors are mainly considered in any type of construction project, it can be used as a start point for other private-sector clients.

Acknowledgements Authors would like to acknowledge technical assistance given by Lakshmi Siriwardane for the preparation of the paper.

References

1. Adnan H, Rosman MR (2018) Risk management in Turnkey projects in Malaysia. WSEAS Trans Bus Econ 15:35–43
2. Ahmed S, El-Sayegh S (2020) Critical review of the evolution of project delivery methods in the construction industry. Buildings 11:11. https://doi.org/10.3390/buildings11010011
3. Alzahrani JI, Emsley MW (2013) The impact of contractors' attributes on construction project success: a post construction evaluation. Int J Project Manage 31:313–322. https://doi.org/10.1016/j.ijproman.2012.06.006
4. Babatunde S, Opawole A, Ujaddughe I (2010) An appraisal of project procurement methods in the Nigerian construction industry. Civil Eng Dim 12(1):1–7. https://doi.org/10.9744/ced.12.1.1-7
5. Bhutto IH, Memon NA, Khoso AR, Leghari MA, Khahro SH (2019) Factors affecting selection of procurement method in public sector construction projects 9
6. Bolpagni M (2013) The implementation of BIM within the public procurement. A model-based approach for the construction industry, vol 242. http://www.vtt.fi/inf/pdf/technology/2013/T130.pdf
7. Chaurasia A, Jadhav K, Kamble S, Hindlekar P (2021) Analysis of risk in construction industry, vols 1, 6. http://www.viva-technology.org/New/IJRI/2021/190.html
8. Dada MO (2012) Predictors of procurement selection: an investigation of traditional and integrated methods in Nigeria, vol 15. http://eprints.usm.my/42124/1/Art_5_jcdc17-1.pdf
9. Dim NU, Ezeabasili ACC (2015) Strategic supply chain framework as an effective approach to procurement of public construction projects in Nigeria. Int J Manage Sustain 4:163–172. https://doi.org/10.18488/journal.11/2015.4.7/11.7.163.172
10. Ekung S, Lashinde A, Adu E (2021) Critical risks to construction cost estimation. J Eng Project Prod Manage 11:19–29. https://doi.org/10.2478/jeppm-2021-0003
11. El Sawalhi NI, El Agha O (2017) Multi-attribute utility theory for selecting an appropriate procurement method in the construction projects. JCDC 22:75–96. https://doi.org/10.21315/jcdc2017.22.1.5
12. Eriksson PE (2008) Procurement effects on coopetition in client-contractor relationships. J Constr Eng Manage 134:103–111. https://doi.org/10.1061/(ASCE)0733-9364(2008)134:2(103)
13. Ghadamsi A, Braimah N (2010) The influence of procurement methods on project performance: a conceptual framework. Montreal, Canada, Birmingham City University, UK, pp 860–871. http://nrl.northumbria.ac.uk/38620/2/CIB%20MCRP2012%20conference%20proceedings%20Volume%202.pdf#page=359
14. Gill P, Stewart K, Treasure E, Chadwick B (2008) Methods of data collection in qualitative research: interviews and focus groups. Br Dent J 204:291–295. https://doi.org/10.1038/bdj.2008.192
15. Grover V (2015) An overview. Research Gate. Golden Research Thoughts 4. https://www.researchgate.net/publication/273352276_RESEARCH_APPROACH_AN_OVERVIEW. Accessed on 30 Sept 2021

16. Gunawardhane KAP, Karunasena G (2015) Conceptual framework for sustainable public procurement process in construction industry. Sri Lanka 12. Available at: https://www.researchgate.net/profile/Gayani-Karunasena/publication/324493815_Conceptual_Framework_to_the_Sustainable_Public_Procurement_Process_in_Construction_Industry/links/5ad0250d0f7e9b18965cd9aa/Conceptual-Framework-to-the-Sustainable-Public-Procurement-Process-in-Construction-Industry.pdf. Accessed 30 Sept 2021
17. Gunduz M, Yahya A (2018) Analysis of project success factors in construction industry. Technol Econ Devel Econ 24(1):67–80. Available at: http://journals.vgtu.lt/index.php/TEDE/article/view/89. Accessed on 30 Sept 2021
18. Gustavsson T, Gohary H (2012) Boundary action in construction projects: new collaborative project practices. Int J Manag Proj Bus 5(3):364–376. https://doi.org/10.1108/17538371211235272
19. Hasanzadeh S, Hosseinalipour M, Hafezi M (2014) Collaborative procurement in construction projects performance measures, case study: partnering in Iranian construction industry. Procedia Soc Behav Sci 119:811–818. https://doi.org/10.1016/j.sbspro.2014.03.091
20. Heenkenda HMNSB, Chandanie H (2012) Minimizing conflicts in building construction through proper procurement arrangements. In: Proceedings of international conference on business management. Available at: https://journals.sjp.ac.lk/index.php/icbm/article/view/1681. Accessed on 30 Sept 2021
21. Iqbal SCR, Holschemacher K, Ali A, Tamosaitiene J (2015) Risk management in construction projects. Technol Econ Devel Econ 21(1):65–78. https://doi.org/10.3846/20294913.2014.994582
22. Jaafar M, Nuruddin AR (2012) The development of public and private construction procurement systems in the Malaysian construction industry. N. R. 11. Available at: http://ajba.um.edu.my/index.php/jdbe/article/view/5327. Accessed on 30 Sept 2021
23. Joseph AL, Jayasena HS (2008) Impediments to the development of design and Build procurement system in Sri Lanka. Available at: https://www.irb.fraunhofer.de/CIBlibrary/search-quick-result-list.jsp?A&idSuche=CIB%2BDC11512. Accessed on 30 Sept 2021
24. Kale VV, Patil SS, Hiravennavar AR, Kamane SK (2013) Joint venture in construction industry. IOSR J Mech Civil Eng 60–65. https://www.iosrjournals.org/iosr-jmce.html. Accessed on 29 Sept 2021
25. Kent DC, Becerik-Gerber B (2010) Understanding construction industry experience and attitudes toward integrated project delivery. J Constr Eng Manage 136:815–825. https://doi.org/10.1061/(ASCE)CO.1943-7862.0000188
26. Lahdenperä P (2012) Making sense of the multi-party contractual arrangements of project partnering, project alliancing and integrated project delivery. Constr Manag Econ 30:57–79. https://doi.org/10.1080/01446193.2011.648947
27. Liu B, Huo T, Liang Y, Sun Y, Hu X (2016) Key factors of project characteristics affecting project delivery system decision making in the Chinese construction industry: case study using Chinese data based on rough set theory. J Prof Issues Eng Educ Pract 142:05016003. https://doi.org/10.1061/(ASCE)EI.1943-5541.0000278
28. Liu B, Huo T, Shen Q, Yang Z, Meng J, Xue B (2015) Which owner characteristics are key factors affecting project delivery system decision making? empirical analysis based on the rough set theory. J Manage Eng 31:05014018. https://doi.org/10.1061/(ASCE)ME.1943-5479.0000298
29. Love PED, Edwards DJ, Irani Z, Sharif A (2012) Participatory action research approach to public sector procurement selection. J Constr Eng Manage 138:311–322. https://doi.org/10.1061/(ASCE)CO.1943-7862.0000440
30. Manley K, Chen L (2016) The impact of client characteristics on the time and cost performance of collaborative infrastructure projects. Eng Constr Archit Manag 23:511–532. https://doi.org/10.1108/ECAM-06-2015-0084
31. Masterman JWE (2003) An introduction to building procurement systems. Google Books. Available at: https://books.google.lk/books/about/An_Introduction_to_Building_Procurement.html?id=ov2CAgAAQBAJ&source=kp_book_description&redir_esc=y. Accessed on 30 Sept 2021

32. Mathonsi M (2012) Factors influencing the selection of procurement systems ... researchgate. Available at: https://www.researchgate.net/publication/272687841_Factors_influencing_the_selection_of_procurement_systems_in_the_South_African_construction_industry. Accessed on 29 Sept 2021
33. Mathonsi M, Thwala W (2012) Factors influencing the selection of procurement systems in the South African construction industry. African J Bus Manage 6(10):3583–3594. Available at: https://academicjournals.org/article/article1380872244_Mathonsi%20and%20Thwala.pdf. Accessed on 29 Sept 2021
34. Molavi J, Barral DL (2016) A construction procurement method to achieve sustainability in modular construction. Procedia Eng 145:1362–1369. https://doi.org/10.1016/j.proeng.2016.04.201
35. Murtazova K, Aliyev S (2021) Current state and development prospects of the construction industry. Nexo Revista Científica 34:916–925. https://doi.org/10.5377/nexo.v34i02.11619
36. Naoum S, Egbu C (2015) Critical review of procurement method research in construction journals. Procedia Econ Finan 21:6–13. https://doi.org/10.1016/S2212-5671(15)00144-6
37. Nieto-Morote A, Ruz-Vila F (2011) A fuzzy approach to construction project risk assessment. Int J Project Manage 29:220–231. https://doi.org/10.1016/j.ijproman.2010.02.002
38. Ofori G (2015) Nature of the construction industry, its needs and its development: a review of four decades of research 20(2). http://eprints.usm.my/41472/1/JCDC_20(2)_2015-Art._7(115-135).pdf. Accessed on 29 Sept 2021
39. Ogunsanmi O (2013) Effects of procurement related factors on construction project performance in Nigeria. Ethiopian J Environ Stud Manage 6(2):215–222. https://doi.org/10.4314/ejesm.v6i2.12
40. Oladinrin OT, Olatunji SO, Hamza BT (2013) Effect of selected procurement systems on building project performance in Nigeria 4:15
41. Onosakponome OF, Rani NSA, Shaikh JM (2011) Cost benefit analysis of procurement systems and the performance of construction projects in east Malaysia. IMBR 2:181–192. https://doi.org/10.22610/imbr.v2i5.897
42. Ozorhon B, Arditi D, Dikmen I, Birgonul MT (2010) Performance of international joint ventures in construction. J Manage Eng 26:209–222. https://doi.org/10.1061/(ASCE)ME.1943-5479.0000022
43. Perera GPPS, Tennakoon TMMP, Kulatunga U, Jayasena HS, Wijewickrama MKCS (2020) Selecting suitable procurement system for steel building construction. BEPAM. https://doi.org/10.1108/BEPAM-03-2020-0056
44. Preece CN, Chong H-Y (2014) Improving construction procurement systems using. researchgate. Available at: https://www.researchgate.net/publication/268872793_Improving_Construction_Procurement_Systems_using_Organizational_Strategies. Accessed on 30 Sept 2021
45. Rajeh MA, Tookey J, Rotimi J (2014) Procurement selection model: development of a conceptual model based on transaction costs. AJCEB-Conf Ser 2:56. https://doi.org/10.5130/ajceb-cs.v2i2.3889
46. Rameezdeen R, Jayasena E (2013) Comparing the procurement selection parameters of private and public sector clients. Int J Construct Project Manage 5(2):171–184. Available at: http://ndl.ethernet.edu.et/bitstream/123456789/3928/1/Construction%20Project%20Management%20Research%20Compendium-Nova%20Science%20Pub%20Inc%20%282014%29.pdf#page=165. Accessed on 30 Sept 2021
47. Ratnasabapathy S, Rameezdeen R, Gamage I (2006) Macro level factors affecting the construction procurement selection: a multi criteria model. s.l., s.n., pp 581–591. Available at: https://www.researchgate.net/profile/Shiyamini-Ratnasabapathy/publication/338385073_MACRO_LEVEL_FACTORS_AFFECTING_THE_CONSTRUCTION_PROCUREMENT_SELECTION_A_MULTI_CRITERIA_MODEL/links/5e104bd0299bf10bc38f3a2c/MACRO-LEVEL-FACTORS-AFFECTING-THE-CONSTRUCTION-PROCUREMENT-SELECTION-A-MULTI-CRITERIA-MODEL.pdf. Accessed on 30 Sept 2021
48. Ratnasabapathy S, Rameezdeen R, Lebbe N (2008) Exploratory study of external environmental factors influencing the procurement selection in construction. Heritance Kandalama,

Sri Lanka, School of the Built Environment, University of Salford, UK, pp 1576–1586. Available at: http://usir.salford.ac.uk/9822/1/101_Elvitigalage_Dona_NG_et_al_Women%E2%80%99s_career_advancement_and_training_%26_development_in_construction_industry_Bear_2008.pdf#page=1601. Accessed on 30 Sept 2021

49. Sackey S, Kim B-S (2018) Development of an expert system tool for the selection of procurement system in large-scale construction projects (ESCONPROCS). KSCE J Civil Eng 22(11). https://doi.org/10.1007/s12205-018-0439-2
50. Sadek K, El-Bastawissi I, Raslan R (2018) The adopted procurement systems in the construction processes of the informal settlements in Beirut, vol 13. https://discovery.ucl.ac.uk/id/eprint/10064915/
51. San Cristóbal JR, Carral L, Diaz E, Fraguela JA, Iglesias G (2018) Complexity and project management: a general overview. Complexity 2018:1–10. https://doi.org/10.1155/2018/4891286
52. Sarhan S, Pasquire C, King A, Manu E (2018) Institutional waste within the UK construction procurement context: a conceptual framework. Eng Project Org J 8. http://irep.ntu.ac.uk/id/eprint/32796/
53. Shan YZ, Kah KS, Chim BL (2019) Factors affecting the selection of the procurement methods for construction projects in Malaysia. INTI J 11. http://eprints.intimal.edu.my/1283/1/vol.2019_011.pdf
54. Sha K (2011) Vertical governance of construction projects: an information cost perspective. Constr Manag Econ 29:1137–1147. https://doi.org/10.1080/01446193.2011.637939
55. Shiyamini R, Rameezdeen R, Amaratunga D (2005) Macro analysis of construction procurement trends in Sri Lanka, vol 14. Available at: http://citeseerx.ist.psu.edu/viewdoc/download?doi=10.1.1.392.4269&rep=rep1&type=pdf. Accessed on 30 Sept 2021
56. Shu Hui W, Othman R, Hj Omar N, Abdul Rahman R, Husna Haron N (2011) Procurement issues in Malaysia. Intl Jnl Publ Sec Manage 24:567–593. https://doi.org/10.1108/09513551111163666
57. Suresh Tiwari ST, Chan SW, Mubarak MF (2018) Critical analysis of procurement techniques in construction management sectors. IOP Conf Ser Mater Sci Eng 342:012100. https://doi.org/10.1088/1757-899X/342/1/012100
58. Sundar SB (2018) Efficacy of procurement management in construction projects and property. Int J Market Technol. Available at: http://www.indianjournals.com/ijor.aspx?target=ijor%3Aijmt&volume=3&issue=7&article=003. Accessed on 29 Sept 2021
59. Vennstrom A, Eriksson PE (2010) Client perceived barriers to change of the construction process. Constr Innov 10(2):126–137. https://doi.org/10.1108/14714171011037156
60. Walliman N (2018) Research methods, the basics, 2nd edn. Oxon: Routledge. Available at: https://www.routledge.com/Research-Methods-The-Basics-2nd-edition/Walliman/p/book/9781138693999. Accessed on 29 Sept 2021
61. Wood H, Gidado K (2008) Project complexity in construction. Dublin, Ireland, RICS Foundation UK
62. World Economic Forum (2018) Future scenarios implications industry report 2018. Available at: https://www3.weforum.org/docs/Future_Scenarios_Implications_Industry_report_2018.pdf. Accessed on 29 Sept 2021
63. Xia B, Chen Q, Xu Y, Li M, Jin X (2015) Design-build contractor selection for public sustainable buildings. J Manage Eng 31:04014070. https://doi.org/10.1061/(ASCE)ME.1943-5479.0000295
64. Yang J, Shen GQ, Drew DS, Ho M (2010) Critical success factors for stakeholder management: construction practitioners' perspectives. J Constr Eng Manage 136:778–786. https://doi.org/10.1061/(ASCE)CO.1943-7862.0000180
65. Yeow J, Edler J (2012) Innovation procurement as projects. J Publ Procure 12:472–504. https://doi.org/10.1108/JOPP-12-04-2012-B002

External Stakeholder Management in the Sri Lankan Construction Industry

H. G. A. R. Randeniya, K. M. P. Wickramasuriya, and P. B. G. Dissanayake

Abstract External stakeholders are a major source of uncertainty in construction projects. Therefore, management of project stakeholders is an important task to be carried out during a construction project. Successful construction project management can be carried out only when the responsible project managers take into account the influence of the project's stakeholders towards the project during all stages of the project. The aim of this research was to identify and assess the role of stakeholders in construction projects in the Sri Lankan construction industry. Data were collected from two major representative projects, namely the Southern Expressway Project carried out by RDA and a Project carried out by National Water Supply and Drainage Board of Sri Lanka. The top three factors affecting the stakeholder management process in construction projects were ranked based on their Relative Importance Index were identifying external stakeholders (RII = 88.00%), communication and engaging with the external stakeholders properly and frequently (RII = 84.00%), and understanding the area of external stakeholders' interests (RII = 83.20%). The findings of the study show that the stakeholder priority according to their influence index which is ranked from the highest to lowest influence on the construction industry placed the Road Development Authority at the first position followed by Survey Department and Central Environmental Authority. The attributes of stakeholders are assessed by considering seven major considerations: Attitude, Vested Interest, Power, Proximity, Legitimacy, Urgency and Knowledge. The data that have been gathered under these attributes were transferred into a Probability of Impact Matrix to distribute the stakeholders into categories based on their engagement level. The stakeholders who are directly and actively participating for the ongoing project (both government and non-government) and stakeholders who are responsible for administration and funding are recognized as key players while the stakeholders representing minority communities and associations should be kept satisfied with the project.

Keywords Classification · Prioritization · Stakeholders · Management

H. G. A. R. Randeniya (✉) · K. M. P. Wickramasuriya · P. B. G. Dissanayake
University of Peradeniya, Peradeniya, Sri Lanka
e-mail: E15298@pdn.ac.lk

R. Dissanayake et al. (eds.), *12th International Conference on Structural Engineering and Construction Management*, Lecture Notes in Civil Engineering 266,
https://doi.org/10.1007/978-981-19-2886-4_52

1 Introduction

Management of external stakeholders is an important task to be carried out during a construction project as they are a major source of uncertainty. There are four objectives in this study: to identify and rank the most common factors affecting the stakeholder management process in construction project; to identify external stakeholders and assess the stakeholder attributes within Sri Lankan construction Industry; to identify the stakeholders' engagement level based on their influence; and to suggest solutions to minimize negative influence of external stake holders in the Sri Lankan construction Industry. External stakeholders are secondary stakeholders who are affected by the construction project either positively or negatively. The basic problem associated with external stakeholders is that if a facility is to be built some external stakeholder will be negatively affected by that facility or by the implementation of the construction project progress. Therefore, the challenge is how to face negative impacts.

1.1 External Stakeholder Management

The basic problem is that if a facility is to be built some external stakeholder will be negatively affected by that facility or by the implementation of the construction project progress. The issue is how to face these negative impacts? The challenge of the project is then to plan and implement the project in a manner that fulfils as many external stakeholders' needs and concerns as possible without compromising the purpose of the project in the Sri Lankan construction industry.

1.2 Construction Industry of Sri Lanka

As a developing country, the construction industry is one of the most important industries in Sri Lanka. Sri Lanka's construction industry has been a major contributor to the country's rapid economic development over the past six years. However, the construction industry always faces problems and challenges in the developing countries, because the earth's resources are under critical situation due to increase in population and economic expansion. One of them is to face negative influence of external stakeholders in the Sri Lankan construction industry.

1.3 Objectives

- To identify and rank the most common factors affecting the stakeholder management process in construction project.
- To identify external stakeholders and assess the stakeholder attributes within Sri Lankan construction Industry.
- To identify the stakeholders' engagement level based on their influence.
- To suggest solutions to minimize negative influence of external stakeholders in the Sri Lankan construction Industry.

2 Methodology

Non-probability sampling techniques were used in this study where target population involves in large-scale Southern Highway Project by RDA and Project by National Water Supply and Drainage Board (NWSDB) ($N = 50$). A structured questionnaire was used in here, and data are collected in a general manner from sample of the population. The general manner makes way to perform statistical analysis of the data by using SPSS statistical software and Microsoft Office Excel. The survey was carried out between the months of February and March (2021).

2.1 Relative Importance Index (RII)

The contribution of each of the factors regarding the effectiveness in managing the external stakeholders was examined by use of Relative Importance Index (RII).

$$RII = \frac{\sum W}{AN} \tag{1}$$

where,

$W =$ Weightage given to each factor

$A =$ Highest weight in Likert scale (i.e. 5 in this case)

$N =$ The total number of respondents.

2.2 Prioritizing Stakeholders

Olander [13] adapt this approach to determine whom the most important stakeholder in the construction project.

$$\text{Impactlevel} = \text{Power} + \text{Proximity} + \text{Legitimacy} + \text{Urgency} + \text{Knowledge} \quad (2)$$

$$\text{Impactindex} = \sqrt{(\text{vestedinterest} * \text{impactlevel})} * 25 \quad (3)$$

$$\text{Influenceindex} = \text{Impactindex} * \text{Attitude} \quad (4)$$

2.3 Classification of the Stakeholder

The classification of construction stakeholder is based on the impact/probability matrix approach which is adapted from [13].

$$\text{Probabilityofimpact} = \text{Vestedinterest} \quad (5)$$

3 Results and Discussion

3.1 Respondents' Profile

Table 1 shows the percentage involvements of the institutions, job titles and years of experience.

Table 1 Respondents' profile

General information	Percentage
Institution	
RDA—Southern Highway	42%
NWSDB	58%
Job title for respondent	
Project Engineer	68%
Engineer Assistant	32%
Years of experience	
Less than 5 years	4%
5—less than 10 years	34%
10—less than 15 years	22%
More than 15 years	38%

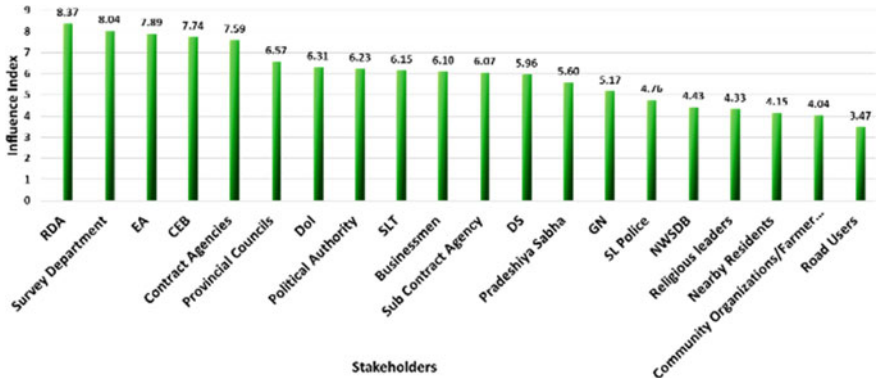

Fig. 1 Summary of stakeholder influence index

3.2 Ranking the Factors Affecting the Stakeholder Management Process

When considering the sixteen identified factors affecting for stakeholder management, 'identifying external stakeholders' with RII (88.00%) was ranked in the top of the factors that affect stakeholder management process and 'Evaluate the stakeholder power' with RII (66.40%) was ranked in the last position.

3.3 Stakeholder Assessment

3.3.1 Stakeholder Prioritization

As can be seen in Fig. 1, the RDA and Survey Department ranked on top; meaning that these stakeholders are likely having the most influence and should therefore receive the project manager's most attention. Community representatives are thought to impact poorly on construction projects. However, they were to highlight a particular issue with a decision, it is likely that serious consideration would be given to refining the decision made as they are highly associated end-users.

3.3.2 Classification of the Stakeholders and Assessing the Engagement Level

Figure 2 shows the classification of stakeholder ranks based on their level of impact upon vested interest. The community representatives which ranked lowest are included in keep informed group (Involve engagement) and rest of the stakeholders

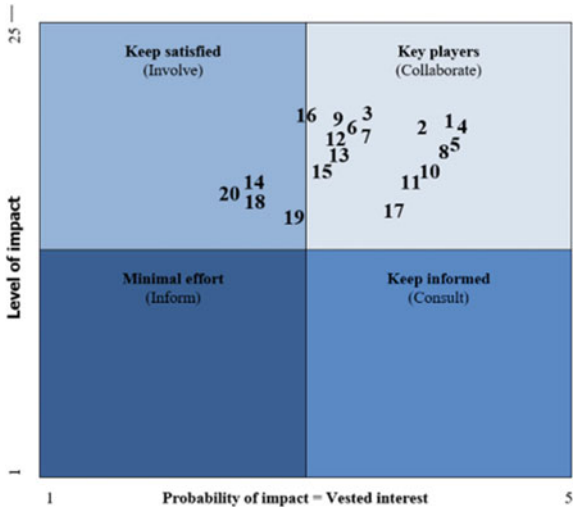

Fig. 2 Probability impact matrix

are considered as key players (Collaborative engagement). Key stakeholders (collaborators) have a high probability of impact and level of impact to project success. As long as the interests of involved group are achieved, they are remained satisfied and retain passive.

4 Conclusions

Based on the above results, the following suggestions are deduced to minimize negative influence of external stakeholders in the Sri Lankan construction Industry; recruit a project manager based on his competencies to lead the management; provide training on communication and negotiation with stakeholders; work closely with the 'key players'; should not neglect the effect of 'involved' stakeholders; and adopt the stakeholder assessment strategies within projects.

Acknowledgements Authors are grateful to the project engineer, Mr. Sudath Silva, and other project engineers and engineering assistants in Road Development Authority (Southern Highway constructions, Sri Lanka) and engineering assistant, Mr. Thilakasiri, and other project engineers and engineering assistants in National Water Supply and Drainage Board for their great support with gathering the data.

References

1. Aaltonen K (2010) Stakeholder management in international project, pp 72–86
2. Atkin B, Skitmore M (2008) Stakeholder management in construction. Construction Manage Econ 26(6):549–552
3. Bothen N, Brantas E, Stening CJ (2010) Who matters? External stakeholder analysis in projects, pp 1–52
4. Carroll AB, Buchholtz AK (2006) BUSINESS & SOCIETY: ethics and stakeholder management, 6th ed, s.l.:s.n
5. Chinyio E, Olomolaiye P (2009) Construction stakeholder management. Wiley
6. Driscoll C, Starik M (2004) The primordial stakeholder: advancing the conceptual consideration of stakeholder status for the natural environment. Bus Ethics 79(1):55–73
7. Hammad S (2013) Investigating the stakeholder management in construction projects in, Degree of Master of Science in Civil Engineering—Construction Management: Nabil El Sawalhi
8. Karlsen JT (2002) Project stakeholder management. Eng Manage 14(4):19–24
9. Larsen G, Harty C (2009) Analysis of external syakeholder influence. In: Proceedings 5th Nordic conference on construction economics and organisation, 1 ed. Reykjavik, Iceland, pp 89–98
10. Mitchell RK, Agle BR, Wood DJ (1997) Toward a theory of stackholder identification and salience: defining the principle of who and what really counts. Acad Manag Rev 22(4):853–887
11. Naguyen THD, Chileshe N, Rameezdeen R (2018) External stakeholder strategic actions in construction projects: a Vietnamese study. Constr Manag Econ 36(8):443–458
12. Olander S (2006) Conctruction management and economics. Stakeholder impact analysis in construction project management, pp 227–287
13. Olander S (2007) Stakeholder impact analysis in construction project management. Constr Manag Econ 25(3):227–287
14. Olander S, Landin A (2008) A comparative study of factors affecting the external stakeholder management process. Constr Manag Econ 26(6):553–561
15. Oppong GD, Chan AP (2017) Managing the expectations of external stakeholders in construction projects. Eng Construct Arch 24(5)
16. Perera KK, Sumanarathna N, Senaviratne I (2016) Stakeholder management of the impact of design changes on the time, cost, and quality targets of building projects in Sri Lanka. s.l., s.n.
17. Phillips R (2003) Stakeholder theory and organizational ethics. s.l.:Berrett-Koehler
18. Suchman MC (1995) Managing legitimacy: strategic and institutional approaches. Acad Manag Rev 20(3):571–610
19. Walker DH, Bourne LM, Rowlinson S (2008) Stakeholder and the supply chain. In: A cross industry project management oerspective
20. Yang J, Shen GQ, Drew DS, Chan AP (2009) Exploring critical success factors for stakeholder management in construction. Civil Eng Manage 15(4):337–348

Evaluation of Risk in Water Supply Projects by Relative Importance Index Method

A. W. K. Arif and C. K. Pathirana

Abstract Water supply projects face higher risk due to their nature of complexity, involvement of different engineering disciplines, involvement of different parties, etc. Project risk increases when the project scope gets bigger. All such risks cause negative impacts to project success. Many of large projects implemented by National Water Supply and Drainage Board (NWSDB) in Sri Lanka are 'Plant and Design-Build' projects. Thus, aim of the study is to evaluate the project risk in-order to take pro-active risk response measures at the project formulation stage. Fifty (50) risk factors were identified and they were categorized into five (5) groups. A questionnaire survey was done by randomly selected professionals representing both contractors and client who are engaged in water supply projects. Two dimensional Likert scale was adopted in this study to improve the precision of responses, where respondents were allowed to select weightage for both likelihood and impact level for each risk factor from five point Likert scale. Importance level of each risk factor was quantified by Related Importance Index (RII) analysis method and they were ranked accordingly. Responses of Project experts consist of project directors, contract specialists (arbitrators and adjudicators) were collected to validate the results. Results of both survey and experts' responses revealed that 'Unavailability of funds on time, delayed contract bill payment, financial failure of the client' as the most important risk factor having RII value of 0.7629 and 0.8067, respectively. Overall project risk evaluated based on the average of RII values, in survey and validated experts' responses possessed values of 0.5119 and 0.5168, respectively, showing medium level of importance. Agreement between each respondent group was checked by Spearman's correlation analysis showed positive agreement, which further validates the findings. Results of this study clearly indicate that the Plant and Design-Build water supply projects implemented by NWSDB have a medium level of risk, thus it requires workable risk response measures at the project formulation stage and

A. W. K. Arif (✉)
National Water Supply & Drainage Board, Kandy, Sri Lanka
e-mail: eng.ariff@gmail.com

C. K. Pathirana
Faculty of Engineering, Univeristy of Peradeniya, Peradeniya, Sri Lanka

R. Dissanayake et al. (eds.), *12th International Conference on Structural Engineering and Construction Management*, Lecture Notes in Civil Engineering 266,
https://doi.org/10.1007/978-981-19-2886-4_53

throughout the project life cycle, while paying more attention to the most significant risk factors identified in this study.

Keywords Plant and design-build · Water supply projects · Project risk · Relative importance index · Risk factors · Likelihood and impact level

1 Introduction

National Water Supply and Drainage Board (NWSDB) implements many large scale water supply projects every year island-wide in Sri Lanka. Many of those projects are implemented as 'Plant and Design-Build' contract, under the international federation of consulting engineers (FIDIC) Yellow Book guidelines with foreign or local bank loan funds. Most of these projects are large or medium large scale projects. Hence, cost of these projects is billions in Sri Lankan Rupees. There are many challenges in completing those projects with desired level of success due to the risks involved which lead to cost overrun, time overrun, quality issues, and in many occasions expected performance level does not reach, such as quality issues, cost overrun, sustainability issues in completed projects, opportunity losses to NWSDB due to project delay, disputes, arguments, litigation, dissatisfaction to the employer and the contract parties. Therefore, Plant and Design-Build projects implemented by NWSDB with foreign and local funds were taken for this study.

Project success is depending on foreseeing the project risk and measures taken to mitigate or minimize such risks, while, some risk cannot be avoided and in such a situation necessary cost and time contingency shall be allocated. Figure 1 illustrates contingency allocation procedure in project cost estimation.

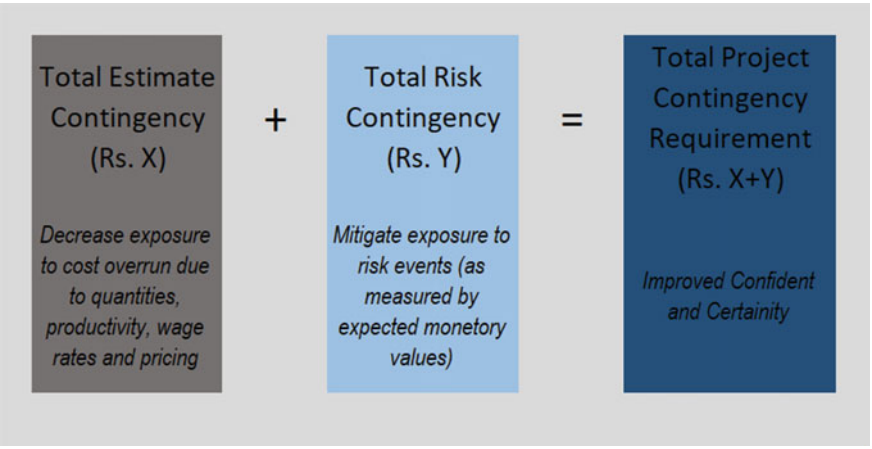

Fig. 1 Contingency allocation procedure in project cost estimation [1]

Project risk has two primary components for a given event, namely, likelihood of occurrence and impact (consequence) of the event occurring. Risk management aims at identifying sources of risk and uncertainties, determining the impact of risk, and developing appropriate risk management response.

Hence, it is clear that identifying project risk factors and their impact level a key role toward project success. Client and the contractor shall carefully identify the project risk factors and quantify their importance level. Which will help to take precautionary measures to minimize the risk and to determine a reliable cost and/or time contingency at the project formulation stage to make projects success. Thus, there is a requirement to identify the relative importance level of risk factors through evaluation of likelihood and impact level of those risk factors, thereby to determine the overall project risk level.

2 Aim of the Study

Aim of the study is to evaluate the project risk in-order to take pro-active risk response measures at the project formulation stage. To achieve the above aim, following objectives are to be fulfilled:

i. Identify the risk factors in Plant and Design-Build water supply projects
ii. Categorize the risk factors into groups
iii. Quantify relative importance level of each risk factor and rank them by RII method
iv. Evaluate the importance level of overall project risk.

3 Literature Review

'Risk' is defined as the potential for complications and problems with respect to the completion of a project and the achievement of a project goal [2]. It is an uncertain future event or condition with an occurrence rate of greater than 0% but less than 100%, which has an effect on at least one of a project's objectives (i.e., scope, schedule, cost, or quality, etc.). In addition, the impact or consequences of this future event must be unexpected or unplanned. It is well accepted that risk can be effectively managed to mitigate its' adverse impacts on project objectives, even if it is inevitable in all project undertakings [3].

Contribution of this study to the existing literature is, this study specifically considered two-dimensional Likert scale, where impact level is also has been considered in addition to likelihood of the event, where previous studies had considered likelihood only for questionnaire survey. Thus, outcome of the results will be more precise than one-dimensional Likert scale responses. Accordingly, equation for RII calculation is modified to get the collective output of both likelihood and impact level of the risk concerned. Further, agreement between the respondents was checked by Spearman's

correlation analysis, in addition to the validation of the results by experts' responses, Hence, dependability of the study output is higher.

4 Methodology

A total number of fifty (50) risk factors in five (5) groups of risk factors in Plant and Design-Build water supply projects were identified through detailed literature review and secondary data of ongoing and completed projects. These fifty (50) risk factors were categorized into five groups as follows;

(1) Project Related Risk Factors (PRF)—7 factors
(2) NWSDB's/Engineers Contract Management Related Risk Factors (EMR)—10 factors
(3) Contractor's Designs Related Risk Factors (CDR)—6 factors
(4) Contractor Construction and Contract Management Related Risk Factors (CMR)—17 factors
(5) External Related Risk Factors (EXR)—10 factors.

A questionnaire was developed to evaluate the risk factors considering likelihood and impact level of the risk factors. A two-dimensional five point Likert Scale was adopted for likelihood and impact level as shown in the Tables 1 and 2.

The questionnaires were distributed to randomly selected sample of contractors, and client's staff who are engaged in Plant and Design-Build water supply projects. Sampling method used in this study was convenience and snowball sampling. Sample elements were identified from Plant and Design-Build water supply project staff. 45 completed responses out of 60 randomly selected samples were received. Respondents were consisting of 6 contract specialists, 13 Project Directors, 7 Project Managers/Chief Engineers, a quantity surveyor and a chief accountant, and 17 project/site engineers who were engaged in designs, contract management and quality assurance of Plant and Design-Build water supply projects.

Table 1 A five point Likert scale for likelihood

Likelihood				
1:Very low likelihood	2: Low likelihood	3: Medium likelihood	4: High likelihood	5: Very high likelihood

Table 2 A five point Likert scale for impact level

Impact level				
1: Very low impact	2: Low impact	3: Medium impact	4: High impact	5: Very high impact

Spearman's correlation analysis was done to check the agreement between the respondents. Relative Importance Index (RII) method was used to quantify the relative importance levels of each risk factor. RII results were presented with ranks of respective risk factors, in which most significance 10 risk factors were discussed. Importance level of overall project risk was quantified by averaging the RII values. The results were validated using the experts' responses (Project Directors, Contract Specialists) by repeating the previous steps.

5 Data Analysis and Results

5.1 Data Analysis by RII Method

Kometa [4] used the RII method to determine the relative importance of risk factors. The same method was adopted with modified equation to suit the study. The five point Likert scale ranged from 1 (very low important) to 5 (very high important) for likelihood and impact level was separately adopted, so that the highest weight range expands to 25 (5×5) and weighing ranges for responding made separately for likelihood and impact level. Though, previous literatures discussed this requirement and its importance, no study was found which used this method. This method improves the preciseness of results compared to single Likert scale responses, and transformed to Relative Importance Indices (RII) for each factor by using the Eq. (1) as shown:

$$\text{RII} = \frac{\sum Pi\,Qi}{A * N} \tag{1}$$

where P is the weightage given to each factor by the respondents as likelihood (ranging from 1 to 5), and Q is the weightage given to each factor by the respondents as impact level (ranging from 1 to 5) A is the highest weight (i.e., $5 \times 5 = 25$ in this case), and N is the total number of respondents. The RII value had a range from 0 to 1 (0 not inclusive), higher the value of RII, more important is the risk factor. The RII was used to rank (R) the different risk factors, these rankings made it possible to cross compare the relative importance of the factors as perceived by the respondents (i.e., expert groups). Each individual RII value perceived by all respondents was used to assess the general and rankings to find picture of the overall project risk.

It shall be emphasized that two-dimensional Likert scale method for identification of risk factors importance level was introduced for this study; i.e., first the respondents select likelihood of occurrence of the specific risk factor from 1 to 5. Then respondents are allowed to select the impact level by selecting 1 to 5 for the same risk factor was used. So that errors which may cause by selecting only one scale for the importance level of a risk factor is avoided, by identifying their likelihood and impact level.

RII values of each risk factors were quantified by the Eq. (1). based on the questionnaire survey. Accordingly, top 3 importance risk factors in each risk group are

Table 3 Top three most significant risk factors in each risk group

Risk group	Most significant factors of the group (Top 3)
Project related factors (PRF)	1. Failures in establishment of project scope and cost at contract formulation stage 2. Contract document error or vagueness (scope, specification and conditions of contract, etc.) 3. Contractual disputes and litigation
NWSDB's project management related factors (EMR)	1. Lack of warnings and follow up contractors on timely completion of contract 2. Decision delay on change orders and variation approval delay 3. Delay in possession of site/right of way/site access
Contractors' design related factors (CDR)	1. Delay in design finalization (delay in design and approval at construction start) 2. Design errors/incomplete designs 3. Failure to procure materials complying to contract specifications (poor quality materials/incompatible materials)
Contractors' construction and project management related factors (CMR)	1. Contractor's financial failure 2. Contractor's/sub contractor's lower bid rate 3. Unreliable and frequent change of sub-contractors
External related factors (EXR)	1. Unavailability of funds on time, delayed contract bill payment and financial failure 2. Lengthy procedure and delay of statutory clearance (permits/approval-customs, road, borrow pits, blasting, dumping, transport, etc.) 3. Unforeseen site conditions

listed in Table 3, and top 10 most significant risk factors out of all fifty risk factors are listed in Table 4.

Responses of project experts consist of 13 project directors, 6 contract specialists (arbitrators and adjudicators) were used to validate the results. Results of both survey and experts' responses validation, revealed that 'Unavailability of funds on time, delayed contract bill payment, financial failure' was identified as the most significant risk factor with a distinct RII value of 0.7629 and 0.8067, respectively, showing very high importance. And top nine factors identified in the questionnaire survey results were within the top ten list of expert responses. Nine out of ten risk factors identified were within the top ten most significant risk factors. From the above top ten most significant risk factors, it was revealed that 'NWSDB's project management related risk factors' group contributed for the most number of top ten significant risk factors.

Based on the average of RII values, overall project risk in both survey and validated experts' responses possessed values of 0.5119 and 0.5168, respectively, showing a medium level of importance. Also, the agreement between each respondent group was checked by Spearman's correlation analysis showed positive agreement between respondent groups, which further validated the results.

Table 4 Top 10 most significant risk factors

Risk factor	Risk group	RII value	Rank
Unavailability of funds on time, delayed contract bill payment and financial failure	EXR	0.7629	1
Lack of warnings and follow up contractors on timely completion of projects	EMR	0.6229	2
Decision delay on change orders and variation approval delay	EMR	0.6086	3
Contractor's financial failure	CMR	0.5962	4
Lengthy procedure and delay of statutory clearance (permits/approval-customs, road, borrow pits, blasting, dumping, transport, etc.)	EXR	0.5876	5
Incapability and lower commitment of Client's project management staff	EMR	0.5790	6
Delay in possession of site/right of way/site access	EMR	0.5762	7
Failures in establishment of project scope and cost at contract formulation stage	PRF	0.5743	8
Unavailability of as built drawings of existing utilities	EMR	0.5629	9
Bureaucracy/hierarchy/favoritism/negative attitudes/Corruption	EMR	0.5562	10

5.2 Analysis of Agreement Between Each Respondent's Groups by Spearman Correlation Coefficient Analysis

A nonparametric (distribution-free) rank statistic developed by Spearman in 1904, as a measure of the strength of the associations between two variables [5]. The Spearman correlation coefficient can be used to give an R-estimate, and is a measure of monotone association that is used when the distribution of the data make Pearson's correlation coefficient undesirable or misleading. The Spearman rank correlation coefficient equation Eq. (2) as shown;

$$r_s = 1 - \frac{6\sum D^2}{n\left(n^2 - 1\right)} \tag{2}$$

where r_s denotes Spearman's correlation coefficient, D is difference between a pair of scores, n is the number of pairs of ranks.

Agreements between responded groups were determined by the Spearman's correlation analysis (correlation values lies between -1 and $+1$) and values obtained were

- Contractors versus NWSDB: $r_s = +0.37912$
- Contract specialist versus NWSDB: $r_s = +0.7058$
- Contractors versus Contract Specialists: $r_s = +0.5857$.

All the above three groups show positive relationships. Therefore, all respondents' groups have positive agreement on the response of risk.

6 Conclusion and Recommendation

There were four objectives in this study, fifty (50) risk factors were identified from Plant and Design-Build Water Supply Projects and categorized into five groups based on the controllability of the risk by the stakeholders. Two-dimensional Likert scale responses were obtained from the respondents of the survey. RII analysis were done to quantify the relative importance and ranked all fifty risk factors.

Results of both survey and experts' responses validation, revealed that 'Unavailability of funds on time, delayed contract bill payment, financial failure' was identified as the most significant risk factor with a distinct RII value of 0.7629 and 0.8067, respectively, showing very high importance. Based on the average of RII values, overall project risk in both survey and validated experts' responses possessed values of 0.5119 and 0.5168, respectively, showing a medium level of importance. Also, the agreement between each respondent group was checked by Spearman's correlation analysis showed positive agreement between respondent groups, which further validated the results.

This study clearly indicates that the Plant and Design-Build water supply projects implemented by NWSDB has a medium level of risk, thus it requires workable risk response measures at the project formulation stage and throughout the project life cycle, while paying more attention to the most significant risk factors identified in this study. Particularly, it can make aware the decision makers on the significant levels of identified risk factors and make mutually agreed solution, such as policy and process improvement; thereby project value chain could be improvement. Also, it will be useful to forecast the cost and/or time contingency allocation requirements to manage the important project risks of future similar projects.

Acknowledgements Our sincere thanks go to head of the Department of Civil Engineering, supervisors of this study, lecturers and all other members in the staff of the University of Peradeniya, for their immense guidance to pursue this research. We acknowledge, General Manager, Additional General Manager (WSP), Project Director (GMWSP) of National Water Supply and Drainage Board for funding and granting permission for the study. Also our thanks extend to all Project Directors, contract experts and all the professionals and fellow colleagues who assisted by responding for the questionnaire survey for this study.

References

1. Moreci K (2012) Contingency—are you covered? Brit Columbia. Newtown Square, PA, s.n.
2. Rezakhani P (2012) A review of fuzzy risk. Fuzzy risk analysis, decision support

3. Chia S (2006) Risk assessment framework for project management. In: IEEE international engineering management conference
4. Kometa ST (1994) Attributes of UK construction clients influencing project consultants' performance. Construct Manage Econ
5. Lehmann EL, D'Abrera HJM (1998) Nonparametrics: statistical methods based on ranks. In: Nonparametrics: statistical methods based on ranks. s.l.: Upper Saddle River N.J.: Prentice Hall
6. Akinsola A (1996) Neural networks, model for predicting building projects' contingency allowance. s.l., Sheffield Hallam University., s.l.: s.n.

Application of GIS to Detect Vulnerability of Water Distribution System

H. A. N. S. Kadurugamuwa, G. W. A. S. Dilthara, and H. K. Nandalal

Abstract The water distribution industry is facing challenges of water leakages in drinking water distribution networks. Mainly high pressure and the deterioration of ageing pipes and fittings cause the increase of the leak, and the consuming water and the number of bursts in the network. This study based on hydraulic and geospatial information system model has been suggested to estimate the probability of leaking for each pipe segment in the selected water distribution network. In this model, the likelihood of leaking is illustrated using pressure, age, length, diameter and slope of the pipe. The system is implemented with GIS tools, WaterGEMS, Google Earth Pro and Minitab software. Google Earth Pro is used to design the pipe network. The hydraulic model creates with WaterGEMS is integrated with ArcGIS. Minitab is used in elaborating the linear regression model, which is proposed to gain the leakage probability. The formed methodology is applied in identifying vulnerability ranges that have been identified for the pipe segments in the water distribution network. For the adducting results, a Geographic Information System (GIS) is used. Using the capabilities of this GIS model, the colour coded map represents the vulnerability ranges of the areas. The gained results can be used in detecting the most leakage areas and control pipeline leakage in the water distribution network. This methodology is developed to provide maximum protection against water leaks in the selected region.

Keywords Geographic information system (GIS) · WaterGEMS · Google earth pro · Minitab

1 Introduction

Water not only gives us life; it is the origin of life. The development and survival of life and civilization are centred around water. Man's need for water consumption has increased with his standard of living. Therefore, when considering settlements,

H. A. N. S. Kadurugamuwa (✉) · G. W. A. S. Dilthara · H. K. Nandalal
Department of Civil Engineering, Faculty of Engineering, University of Peradeniya, Peradeniya, Sri Lanka
e-mail: nawoda_kadurugamuwa@eng.pdn.ac.lk

R. Dissanayake et al. (eds.), *12th International Conference on Structural Engineering and Construction Management*, Lecture Notes in Civil Engineering 266,
https://doi.org/10.1007/978-981-19-2886-4_54

the existing water distribution system is a crucial requirement in the modern world. Due to water and revenue losses, the water industry worldwide is facing demanding consequences. So, it has become a requirement to improve the efficiency of water distribution systems by reducing these losses [1].

According to the World Bank study, water distribution systems is lost about 48 billion m^3 of water. It has cost water utilities nearly US$14 billion per year around the world (Liemberger, R. and Marin, P et al. 2006). In Sri Lanka, where the National Water Supply and Drainage Board maintains most of the urban schemes, Non-Revenue Water (NRW), being 33% on average, is reasonable amongst South Asian countries. Major expenditures on municipalities and state governments have been imposed, especially in urban environments, due to the repair and replacement of ageing water pipes. So, there is a gradual increase in the necessity to more actively occupy in the monitoring and managing such water distribution networks. According to Puust et al [2], as presented by companies that maintain water distribution networks, it is an economic issue and an environmental, sustainability, and possibly a health and safety issue. Colombo and Karney [3] reported that due to low-pressure conditions, water leakage may affect water quality due to contamination into water distribution networks.

This study focused on developing a system for detecting and controlling pipeline leakage in drinking water distribution. At first, an integrated GIS and hydraulic model is produced. This model can be able to combine spatial data with hydraulic and quality parameters of the network. A multilinear regression model is then developed, consisting of different criteria such as the probability of leakages, pressure, length, diameter, age of pipe, and elevation to be used in a pipe rehabilitation and replacement programme by decision-makers. The model is applied in the subsection of the Kandy Municipal Council water distribution network. Finally, the study aims at the graphical representation of the risk in a visual GIS-based interface that assists users to evaluate the degree of risk. Vulnerability ranges are colour coded and continually updated as the system processes time-related data.

2 Literature Review

If water escapes from the pipe network by means other than through a controlled action that can be interpreted as a general definition for leakage [2]. For the operation of water distribution, many parameters will be affected. Many pipes' bursts and accidents are occurring in a water network due to the influence of these parameters.

Intending to develop or improve predictive planning models, researchers have considered many factors that affect the deterioration of water pipes. As Wang et al. [4] emphasized, the factors contributing to pipe deterioration can be classified as dynamic or static. The factors that do not change over time are interpreted as static factors. Pipe diameter or pipe material can be considered as static factors. In contrast, pipe age, water pressure, temperature, water contents of the surrounding soil, and previous pipe breaks are examples of time-dependent factors called dynamic factors. Due to the

interaction of static and dynamic factors, internal and external deterioration of pipes occurs [5]. System pressure is the primary factor affecting the leakage. If the pressure is high, the leak flow is more prominent. According to Zyoud [6], controlling pressure is not a solution because it increases the side effects such as leakage, busting and, to some extent to water hammering [2], Walski and Pelliccia [7], Kettler and Goutler [8], and O'Day [9] also have presented factors affecting the leakage. Studies conducted previously also identified several environmental factors that affect the deterioration of water mains, such as soil conditions, frost and traffic loading, and quality of external underground water [10]. Other factors, such as rehabilitation methods, water quality, and break history, were critical for water pipes deterioration [11]. Incorporating these parameters, most studies in the literature present a relationship between failure rates and time of failure and some of them propose a methodology to optimize the replacement time of pipes.

Evaluating leakage probability is an efficient way to detect, rehabilitate, and maintain the pipeline system [12], has introduced a physica l probabilistic failure model for PVC-U pipes. This model uses fracture mechanics to forecast slow crack growth from inherent defects in the pipe wall. From the Monte Carlo Stimulation, the failure rate versus age curves was derived. Assumption deliberated was that all pipe segments along a pipeline have the same probability of failure. The expected failure rate (predicted failures per unit pipe length/time period) can be predictable through this model.

$$E[N(t)] = nh(t) \tag{1}$$

$E[N(t)]$	the expected number of failures
n	the number of segments in the pipeline
$H(t)$	a measure of the probability of imminent failure at time t
t	the pipeline at time.

Shamir and Howard [13] introduced a method for determining the optimal time to replace a pipe. To carry out the study, they studied break data. These data had been used to estimate how the number of breaks in the existing pipe is going to change over time. In this analysis, the number of breaks that would happen in a replacement length of pipe has to be assessed. Here, pipe break data were plotted against time, and regression was used to develop an equation that gives the number of breaks (per year per 1000 ft) as a function of time. After further analysing, [13] had extended this exponential regression equation further. They have incorporated additional parameters. Their study was based on observations made by the US Army Corps of Engineers in Binghamton, NY. Clark et al. [14] improved Shamir and Howard [13] model further to transform it into a two-phase model. They used the Eq. 2.

$$NY = x_1 + x_2 D + x_3 P + x_4 I + x_5 RES + x6LH + x7T \tag{2}$$

NY = the number of years from installation to the first repair.

x_i = regression parameters.

D = diameter of the pipe.

P = absolute pressure within a pipe;

I = percentage of pipe underlain by industrial development.

RES = percentage of pipe underlain by residential development.

LH = length of pipe in highly corrosive soil;

T = pipe type (1 = metallic, 0 = reinforced concrete).

They observed a pause between the year of installation of the pipe and the first break. So suggested the above model forecast the time elapsed to the first break.

Tabesh et al. [15], presented two types of linear and nonlinear regression for analysis of break rates to show the importance of renovation scheme. For linear regression, the Eq. 3 is used.

$$y = \beta 0 + \beta 1x \tag{3}$$

and nonlinear regression is determined as:

$$y = cd\,x \tag{4}$$

$c = 10\beta 0$ and $d = 10\beta 1$.

Tabesh et al. [15] all the burst records were assembled and examined. Analysing the assembled data, areas with the highest burst records were marked and highlighted on the map using the GIS model records. Also, this GIS model can recognize the position of the valves required to be isolated for rupture repair. According to a decision aid GIS-based risk assessment, [16] studied the risk of vulnerability and pipe failure in distribution networks in Miami, Florida. In their research, [11] used a strategy model to find the number of annual failures in the water networks of three cities. Rasooli et al. [17], Patel and Katiyar [18], Vairavamoorthy et al. [19] interpreted GIS as a powerful tool to analyse pipe networks and introduced it as the best application to manage, manipulate and maintain geospatial data and to develop and sustain asset management for today's water utilities worldwide. Rasooli and Kang [17] reported that GIS is comprehensive and multifunctional computer-based software being used in water transmission and distribution systems in a modern and systematic water supply. To manage water systems, researchers have used a combined GIS and hydraulic model. According to Rossman et al. [20], the employment of the EPANET software is capable because of its availability, popularity, and capability to be linked with GIS models. Rasooli and Kang [17] presented a method to design and balance Water Distribution networks based on loops hydraulically as well as using GIS methodology with the contribution of EPANET. In this research, they

have analysed water flows in each pipe. They performed the iterations process on loops to make the algebraic summation of head loss around any closed loop zero, in case the outline of pipe flows must be equal to the flow amount entering or leaving the system through each node. Stimulation was done by using EPANET and GIS for the water distribution network. They have examined and replicated hydraulics parameters for the targeted area in Kabul city.

Researchers were used different parameters according to their methodology to find leakages in water distribution systems. Then they have developed various models to find the degree of risk of failure. According to them, the spatial analyses in ArcMap allowed visualization of the vulnerable areas, identification of the regions with different levels of vulnerabilities, and quantification of the potential impacts.

3 Methodology

The methodology was developed to detect and control pipeline leakage in drinking water distribution using the hydraulic and geospatial information systems model. The proposed hydraulic and geospatial information system model approach narrows down leaks to specific pipe segments of the water distribution system. The summary of the methodology is shown in Fig. 1.

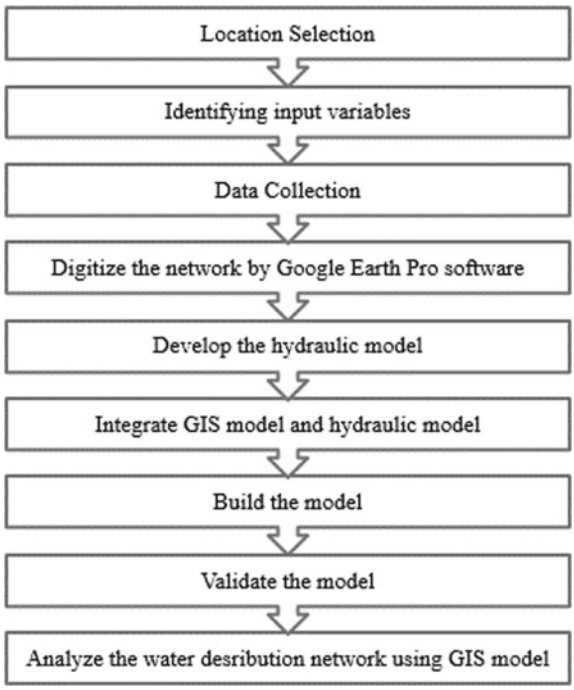

Fig. 1 Summary of the methodology

3.1 Location Selection

The water resource of Kandy Municipal Council water distribution network is Dunumadalawa reservoir and Roseneath reservoir. The intake of the Roseneath reservoir is selected as the subjective area of the study. Roseneath reservoir supplies water to the regions including Thottipallama (Ginihiriya), Rajapihilla, Kamhillwatta, Dalukgolla, Keerthi Sri Jajasingha Mawatha. The daily intake of the Roseneath reservoir is 370 m^3. The water distribution network that is used as a case study in the project is an isolated medium size network which supplies water to Rajapihilla and Kamhillwatta. The location of the study area is shown in Fig. 2. The number of houses, temples, and hotels in these areas are shown in Table 1.

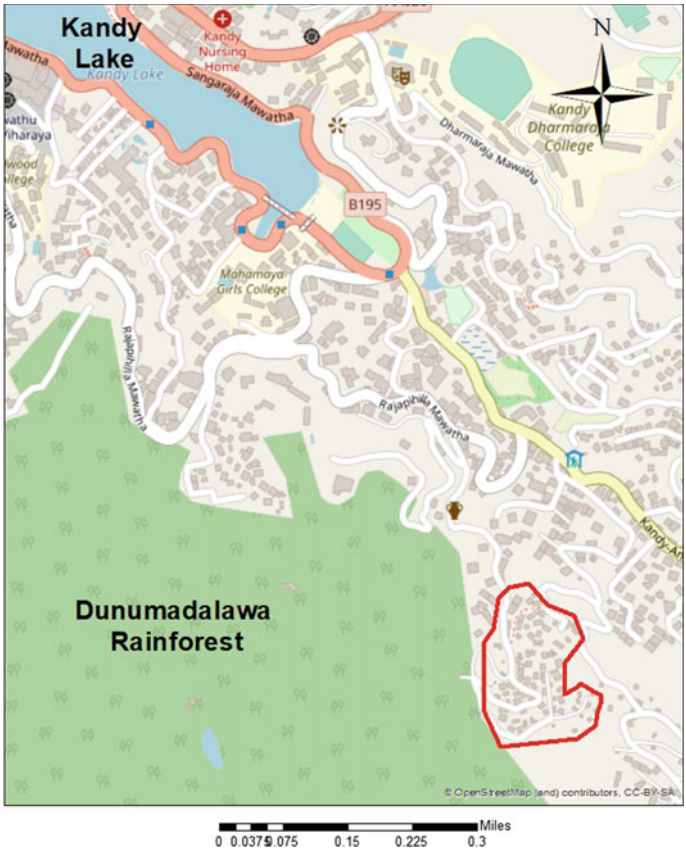

Fig. 2 Study area

Table 1 Service area and number of houses/hotels/temples

Service area	Number of houses/hotels/temples
Kamhillwatta	48
Rajapihilla	11

3.2 Input Data

There are many factors and incidents which are adversely affecting the vulnerability of a pipe network. This research mainly focuses on pipe length, pipe diameter, pressure, age of the pipe, and slope of the pipe.

3.3 Methodology

Kandy Municipal Council has not modelled the selected water distribution network in any electronic format. As the preliminary step, the GPS coordinates of the nodes of the pipe network was measured from the CT Droid mobile application during the site visit. CT Droid Sri Lanka 3.0.0 application is designed for Sri Lanka to perform coordinate transformation to project Geographic coordinates to Cartesian coordinates that suit Sri Lanka. It supports both KANDAWALA EPSG:4244 and SLD99 EPSG:5233 datums. Collected GPS coordinates were exported to Google Earth Pro. Considering these coordinates, the pipe network was drawn as in Fig. 3.

The drawn water distribution network was imported to WaterGEMS as a base map. In the WaterGEMS, the pipe network was hydraulically modelled. The relevant

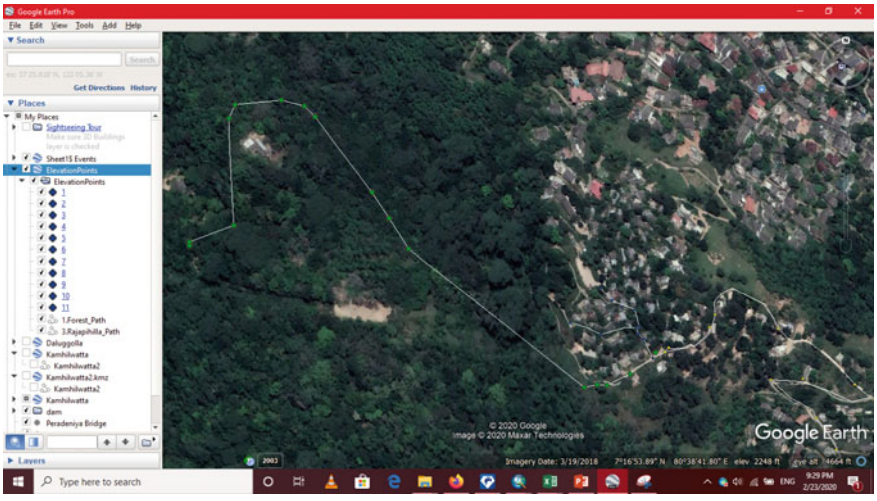

Fig. 3 Representation of pipe network using Google Earth Pro

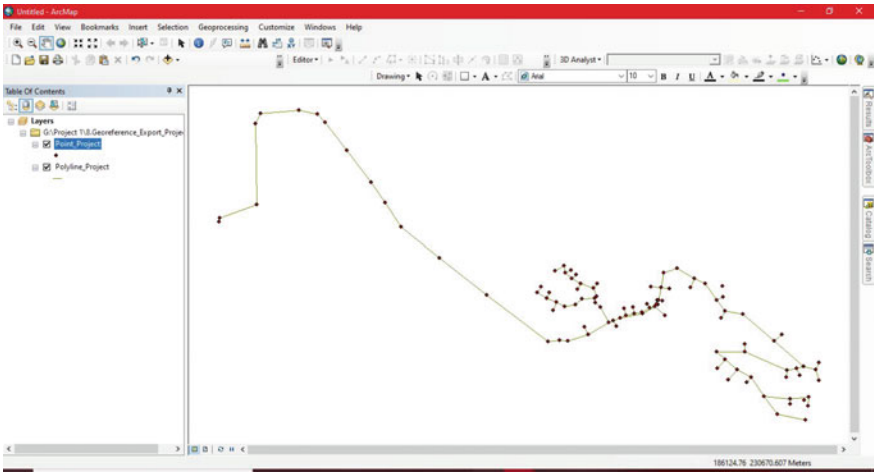

Fig. 4 Pipe network in GIS interface

properties such as diameter, material, demand and Hazen-Williams coefficient for the pipe network were intercalated to the hydraulic model.

This hydraulic model was integrated with ArcGIS. Then, the pipe network was modelled using the Geospatial Information System (GIS) in the ArcGIS 10.6 version. The water network was georeferenced using the "add control points" tool. The coordinate system was defined to WGS1984 using the "Define Projection" tool. Afterwards, the network was projected from WGS1984 to Kandawala Sri Lanka grid using the "project" tool in the "Projection and Transformation" tool, as shown in Fig. 4.

Then the Digital Elevation Model (DEM) was created as shown in Fig. 5.

Required data such as average slope, nodal elevation and length of the pipe was obtained using the attribute table. In the hydraulic model, the obtained above data was inserted. Then the model was computed to get the pressure distribution. In the next step, using the relevant data obtained, the equation was executed. For this, MiniTAB Software was used. Afterwards, the validation part was carried out.

In this research, it is mainly focused on the probability of leakages in pipe segments of selected area and effect of external factors to the vulnerability of pipes and it is considered that the topography of a certain area would make a huge influence in this case. Depending on the factors that we considered, the probability of leakage being the pipe network vulnerable varies. The probability of Leakage (N) would be developed on those factors.

$$N = \beta + \beta_1 l + \beta_2 d + \beta_3 p + \beta_4 a + \beta_5 s \tag{5}$$

N = Probability of leaking

l = Length of the pipe

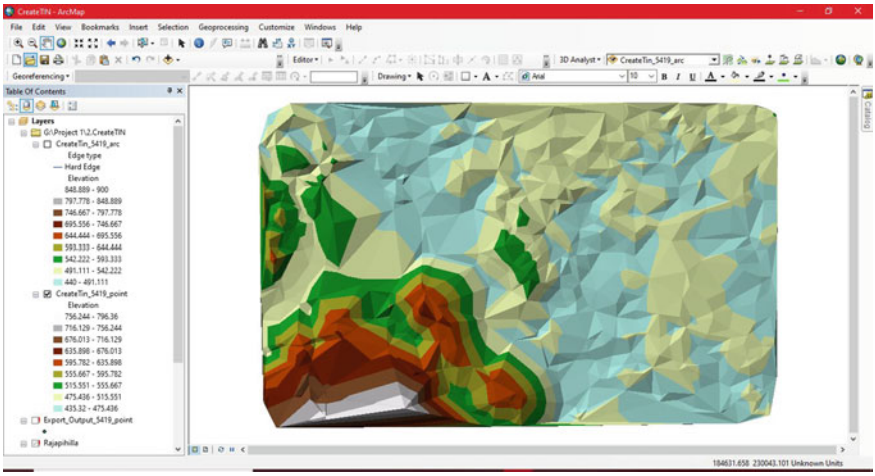

Fig. 5 Digital Elevation Model (DEM)

d = Diameter of the pipe

p = Pressure

a = Age of the pipe

s = Slope of the pipe.

4 Results and Discussion

Leakage records collected from the Kandy Municipal Council was used to calibrate and validate these models. In the calibration process, the highest number of leakages on a segment of a pipe per year is considered as the probability of a hundred per cent. Then the leakage probability of the other segments of pipes is compared concerning that value. By using the Minitab software, the equation was obtained as follows.

$$N = 0.877 - 0.576d + 0.000008p + 0.1525l + 0.01468s \quad (6)$$

Linear regression is a linear approach to modelling the relationship between a scalar response and one more variable. In this modelling length of the pipe, the diameter of the pipe, pressure and the slope of the pipe are variables.

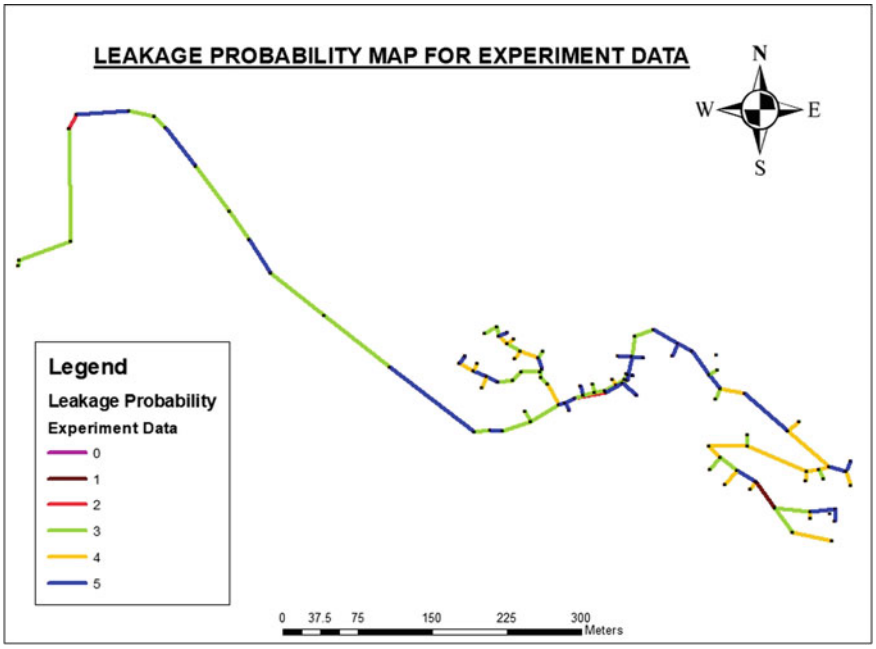

Fig. 6 Leakage probability map for experiment data

4.1 Risk Map for Leakage Probability

All the pipes with burst records can be easily identified, marked and emphasized on the map using the GIS model. For the replacement programme, this map is the key tool to identify the vulnerable area with the highest burst records for the replacement programme. The risk map generated for the KMC case study area is shown in Fig. 6. This figure elaborates that most of the water pipes have a medium or low risk. However, a small number of pipes have a high risk of leakage probability. Then the results obtained for the regression model has been validated with actual field data. The R-squared value for this model is 0.68. It is a little bit low. But it shows a positive correlation between actual data and results obtained for the regression model. For further clarification, leakage probability map for actual data (Fig. 7) and experimental data depicted by GIS-based tools. Then the validation was carried out in a more precise manner.

5 Conclusion

Leakage vulnerability levels are shown in the selected area, considering the risk map for leakage probability. The map for leakage detection is an easy and effective

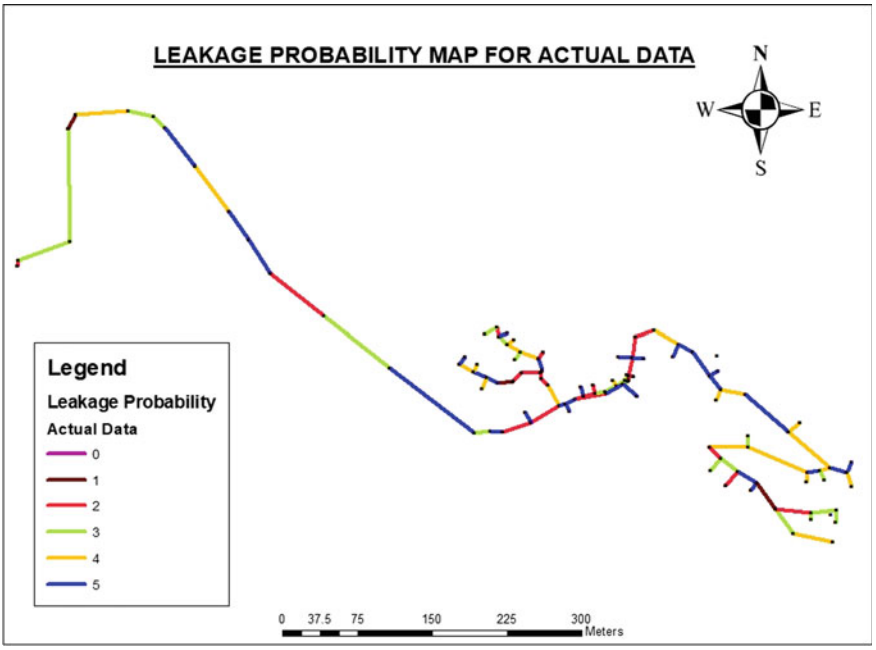

Fig. 7 Leakage probability map for actual data

method to detect and control pipeline leakages. Under this research, the importance of measuring the probability of pipe leakage is highlighted and represents a methodology to analyse and evaluate the vulnerability numerically. From the results of this methodology, it can be identified the places where the worst consequences for the functioning of the water distribution network may occur. It has also been focused on tools for planners and engineers in designing the critical location of the pipe network.

References

1. Mutikanga HE, Sharma SK, Vairavamoorthy K (2013) Methods and tools for managing losses in water distribution systems. J Water Resour Plan Manag 139(2):166–174
2. Puust R, Kapelan Z, Savic DA, Koppel T (2010) A review of methods for leakage management in pipe networks. Urban Water J 7(1):25–45
3. Colombo AF, Karney BW (2002) Energy and costs of leaky pipes: toward comprehensive picture. J Water Resour Plan Manag 128(6):441–450
4. Wang Y, Zayed T, Moselhi O (2009) Prediction models for annual break rates of water mains. J Perform Constr Facil 23(1):47–54
5. Al-Aghbar A (2005) Automated selected trenchless technology for the rehabilitation of water mains. MS thesis, Dept. of Building, Civil, and Environmental Engineering, Concordia Univ.
6. Zyoud SHAR (2003) Hydraulic performance of palestinian water distribution systems (Jenin Water Supply Network as a Case Study) (Doctoral dissertation)

7. Walski TM, Pelliccia A (1982) Economic analysis of water main breaks. J Am Water Works Ass 74(3):140–147
8. Kettler AJ, Goulter IC (1985) An analysis of pipe breakage in urban water distribution networks. Can J Civ Eng 12(2):286–293
9. O'Day DK (1982) Organizing and analyzing leak and break data for making main replacement decisions. J Am Water Works Ass 74(11):588–594
10. Rajani B, Zhan C (1996) On the estimation of frost loads. Can Geotech J 33(4):629–641
11. Pelletier G, Mailhot A, Villeneuve JP (2003) Modeling water pipe breaks—three case studies. J Water Resour Plan Manag 129(2):115–123
12. Davis P, Burn S, Moglia M, Gould S (2007) A physical probabilistic model to predict failure rates in buried PVC pipelines. Reliab Eng Syst Saf 92(9):1258–1266
13. Shamir U, Howard CD (1979) An analytic approach to scheduling pipe replacement. J Am Water Works Ass 71(5):248–258
14. Clark Robert M., Stafford Cheryl L., Goodrich James A. (1982) Water Distribution Systems: A Spatial and Cost Evaluation. Journal of the Water Resources Planning and Management Division 108(3):243–256. https://doi.org/10.1061/JWRDDC.0000257
15. Tabesh M, Delavar MR, Delkhah A (2010) Use of geospatial information system-based tool for renovation and rehabilitation of water distribution systems. Int J Environ Sci Technol 7(1):47–58
16. Inanloo B, Tansel B, Shams K, Jin X, Gan A (2016) A decision aid GIS-based risk assessment and vulnerability analysis approach for transportation and pipeline networks. Saf Sci 84:57–66
17. Rasooli A, Kang D (2016) Designing of hydraulically balanced water distribution network based on GIS and EPANET. Int J Adv Comput Sci Appl 7(2):118–125
18. Patel A, Katiyar SK (2013) Prediction of water demand in water distribution system using geospatial techniques. Eur Int J Sci Technol 2(10):121–133
19. Vairavamoorthy K, Yan J, Galgale HM, Gorantiwar SD (2007) IRA-WDS: a GIS-based risk analysis tool for water distribution systems. Environ Model Softw 22(7):951–965
20. Rossman LA (2000) Water supply and water resources division. National Risk Management Research Laboratory. Epanet 2 User's Manual. Technical report United States Environmental Protection Agency

Embodied Energy and Lifecycle Assessment of EPS based Light-weight Panel Apartments in Tropical Uplands

R. Shiveswarran, N. Athukorala, and M. T. R. Jayasinghe

Abstract The buildings demand a great amount of energy in their life cycle right from the extraction of raw materials to demolition stage. Hence, it is prudent to optimizing the energy embodied in the construction materials and needed to operate the building. The waste-based building materials will have very little embodied energy associate with and that is the energy needed for converting from the waste stage to the building material stage. One such material that is considered as a waste material is Expanded Polystyrene (EPS) used as a packaging material. Embodied energy calculations were done according to Inventory of Carbon and Energy (ICE) data base and other relevant literature. The thermal performance of properly planned three-storey apartment building has been assessed using Design Builder software to determine the energy associated with the operational phase to ensure adequate thermal comfort indoors. In Sri Lanka, Tropical uplands have low outdoor temperature distribution when compared to other climatic zones such as wet and dry lowland climates that can be ranked as warm humid. The energy (electricity) required for heating and lighting was obtained from Design Builder energy simulations. The passive techniques to minimize the heating energy demand such as: selecting the desirable orientation of the building, window-to-wall ratio, etc. have been analysed. With the data on embodied energy and the operational energy, a complete life cycle assessment which is a process-based, is carried out according to the ISO 14044:2006 standards using the OneClick LCA tool. A comparative study was undertaken to prove the suitability of EPS lightweight panels for Tropical Upland Climate when compared with the other conventional construction materials such as bricks and concrete blocks. EPS panel apartment contributes about 20% energy savings in Embodied Energy: about 30% energy (electricity) savings in its Operational phase and about 40–50% environmental impact reduction when compared with conventional building materials.

Keywords Embodied energy · Life cycle assessment · EPS panels · Tropical upland

R. Shiveswarran (✉) · N. Athukorala · M. T. R. Jayasinghe
Department of Civil Engineering, University of Moratuwa, Moratuwa, Sri Lanka
e-mail: shiveswarranr.22@uom.lk

R. Dissanayake et al. (eds.), *12th International Conference on Structural Engineering and Construction Management*, Lecture Notes in Civil Engineering 266,
https://doi.org/10.1007/978-981-19-2886-4_55

1 Introduction

The construction industry is one of the largest and fast-growing industries which consume a lot of energy and resources [8]. Due to the possibilities of energy crisis, construction industry must reduce the consumption of high energy as embodied energy and in its life cycle. Sri Lanka is developing in the socio-economic field; more housing apartments are needed for the urban settlements of working community. But the resources are in shortage stage. Therefore, an energy efficient construction material is needed. Expanded Polystyrene (EPS) is becoming a substantial and supplementary material for the construction of wall panels. EPS bead is a very low-density material that contains 98% air and only the rest is polystyrene [1]. The use of EPS as aggregates showed benefits such as reduction in the usage of sand, less self-weight and reduction of waste [4].

Expanded Polystyrene (EPS) that is used as a packaging material when transporting finished products that needs special protection from shock and for insulation purposes [20]. EPS is not decomposable in nature, and it causes environmental problems [19]. Once recycled to produce beads by crushing the large used pieces of such packaging material, it would have very little embodied energy; it is only due to the energy needed for crushing operation. One application of such lightweight concrete is in panels formed by sandwiching the lightweight concrete between cement fibre sheets of 5 mm thickness (Fig. 1).

One of the key advantages of lightweight panels produced this way is the lower thermal conductivity. The presence of randomly dispersed EPS beads will offer a significant resistance to thermal conductivity. The actual thermal conductivity will depend on the density of lightweight concrete as equal to about 0.4 W/mK for a density of about 1400 kg/m^3. This can further drop to about 0.27 W/mK when the density is about 700 kg/m^3 [10]. Previous studies have shown that lightweight concrete panels can be used as loadbearing walls of apartments up to three floors when the lower floor wall thickness can be maintained at 150 mm with the top floor walls supporting the roof slab is of 100 mm thickness [11]. Sustainable Development

Fig. 1 EPS foam concrete panel

Goals (SDG) created by United Nations Org., especially SDG 12 has indicators like sustainable development involves minimizing the usage of natural resources and generation of waste and pollutants [29]. The outcomes of the research would target the SDG 12 in the whole life cycle phases of the buildings.

2 Objectives

The main objective of this research is to determine the overall life cycle energy performance and impact assessment of the EPS-based lightweight panel apartments for the tropical upland climate of Sri Lanka through a comparative study with the buildings constructed with conventional materials to determine the total energy savings in their life cycle and to determine the passive techniques suitable for EPS panel apartments in Tropical uplands.

3 Methodology

The following methodology was adopted in this research study:

1. A plan of a three-storey apartment building with some passive features to build with EPS panels was developed
2. The embodied energy of EPS-based lightweight panel apartment has been assessed and compared with conventional building materials like bricks and concrete blocks
3. The operational phase energy requirement for EPS panels apartment was derived from Design Builder software and compared
4. The Lifecycle Assessment (LCA) was conducted using the data from Embodied Energy, Operational Energy, and Impact Assessment from OneClick LCA tool.

4 Planning of a Three-Storey Apartment Building for Analysis

For the study and analysis, a three-storey apartment plan was developed, and the 3-D view is shown in the Fig. 2.

The apartment building developed for this study has rubble foundation; Ground floor with 100 mm cast concrete and tile finishes; Floor slabs made of National Engineering Research and Development Centre (NERDC) slab system consists of 50 mm thick in-situ cast concrete topping retained on trapezoidal pre-stressed beams in 600 mm intervals [24]; Walls made of 150 mm panels at ground floor and 1st-floor level and 100 mm panels at the 2nd-floor level; Roofs with NERD slab system and each 50 mm thick EPS panel pieces and screed concrete; Staircase with EPS

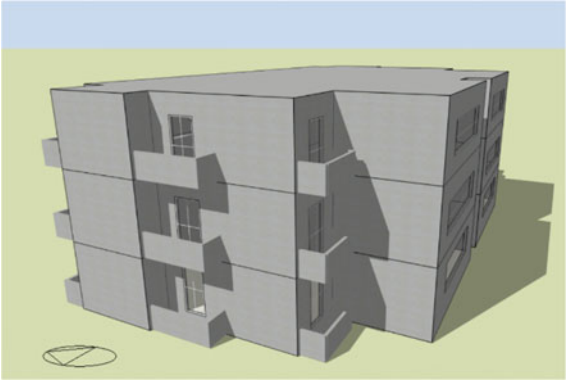

Fig. 2 3-D rendered view of the apartment using design builder

panels [30]; Windows of double glazed and doors made of timber. This three-storey apartment consist of two double-bedroom and two triple-bedroom houses at each floor level. Total floor area is 1251 m^2.

Overhanging balconies are provided for all bedrooms, in the direction parallel to the longer axis of the building which act as shading for below floors. The orientation of the longer axis suitable for tropical uplands is analysed in this research below. Similar apartments with changes in the wall materials as Bricks and concrete blocks; typical concrete floor and staircases are developed for comparative study.

5 Embodied Energy

The energy needed to extract, refine, process, transport and fabricate is called as embodied energy [8]. Since the EPS panels are lightweight, the embodied energy associated with the transport and fixing would be reduced. The coefficients of embodied energy (EE) of building materials are obtained from the inventory of carbon and energy (ICE) database drawn by the University Of Bath, England [12]. The calculation was carried out analytically, multiplying the weight of the materials with the respective coefficients of EE. Some alterations are done to EE co-efficient according to Sri Lankan context. EE of cement is taken as 4.9 MJ/kg [21]; 25.8 MJ/kg for glass; 144 MJ/kg for paint; 106 MJ/kg for PVC are taken from Indian context [6].

Energy consumption of vehicles used for transport in the units of MJ/tonne/km are obtained [7]. The embodied energy associated with the production of 100% recycled EPS panels manufactured by EPCI Homes (pvt) ltd in Ekala, of thickness 100 mm is 313 MJ/m^2 and 150 mm thick panel is 398 MJ/m^2 [9]. The total embodied energy calculated to the system boundary of cradle to gate to the apartment building construction at Nuwara Eliya (A city with Tropical upland climate in Sri Lanka) is shown in Table 1.

Table 1 Total embodied energy of each apartment

Materials	Apartment constructed with EPS panels (MJ)	Apartment constructed with concrete blocks (MJ)	Apartment constructed with burnt bricks (MJ)
Cement	1,369,196	1,341,145	1,278,513
Sand	124,598	398,650	254,678
Coarse aggregate and rubble	96,428	180,399	180,399
Bricks	85,641	85,641	1,001,742
EPS (recycled)	77	0	0
Steel	256,426	1,191,340	732,490
Ceramic tile	486,980	486,980	486,980
Tile adhesives	423,902	423,902	423,902
Paint	250,458	250,458	250,458
Putty	9,448	9,448	9,448
Timber	34,900	28,982	28,982
Copper	18,741	18,741	18,741
PVC	74.562	74.562	74.562
Cement fibre sheet	492,652	0	0
Plywood	49,371	88,612	88,612
Total embodied energy	3,628,893	4,504,373	4,755,020
Embodied energy per unit area (GJ/m^2)	2.90	3.60	3.80

From the results, apartment constructed with 100% recycled EPS panel shows significant reduction in Embodied Energy (2.90 GJ m^2). Apartment constructed with EPS wall panel requires less amount sand which is very beneficial because excessive river sand mining has resulted in many environmental problems [22], less plywood as they require minimal formwork. Due to the nature of lightweight of EPS panels, it requires less steel for pre-stressed beams (less dead weight) and hence, the energy associated with the construction, labour requirements also can be minimized to great extent, and it enhances local manufacture of building materials, thus reduce transportation energy. These EPS panels can be recycled again and make it possible to overcome the, from cradle to grave, approach to materials and to aim for a more sustainable approach called from cradle to cradle [25].

6 Operational Energy

The energy required to maintain thermal comfort inside the building and lighting purposes which is associated with the operational phase was obtained from the building energy simulation software "Design Builder", which comprises the calculation core Energy Plus, tool for building energy performance assessment [5].

6.1 Weather Data

The climatic data used in this simulation is based on the weather data of Nuwara Eliya, Sri Lanka, generated by the Solar and Wind Energy Resource Assessment (SWERA) Programme for the Energy Plus software [27]. Nuwara Eliya (1880 m above MSL) lies in the Tropical Upland climatic zone. The profile of hourly outdoor dry bulb temperature variation in every month is shown in Fig. 3.

The maximum temperature of 20.6 °C occurs at 12:00 h of April whilst minimum value of 10.8 °C occurs at 06:00 h of January every year. The maximum value of Direct Solar radiation is 717 Wh/m^2 in March whilst lower values in June and July. The hourly statistics of other parameters like relative humidity, wind speed, wind direction, diffuse solar radiation and undisturbed ground temperature are also included in the Energy Plus Weather file (Standard EPW data file format) and fetched to the simulation.

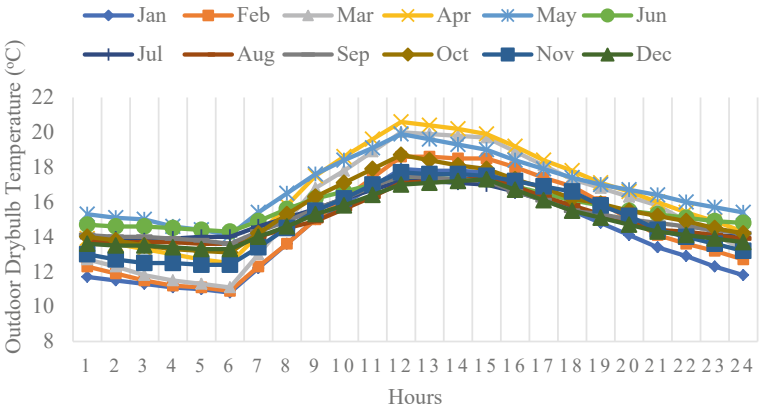

Fig. 3 Hourly average variation of outdoor dry bulb temperature of Nuwara Eliya

Table 2 Thermal properties of building materials

Material	Conductivity (W/mK)	Density (kg/m^3)	Specific heat (J/kgK)
EPS foam concrete	0.035	25	1400
Brickwork	0.840	1800	800
Cement blocks	1.200	1200	900
Cement fibre sheet	0.400	1500	1050
Plastering	0.500	1300	1000

6.2 Thermal Comfort

The mean annual temperature of Nuwara Eliya is 16.9 °C and hence the neutrality temperature is calculated as 22.8 °C. By the psychrometric chart analysis, the heating set point temperature of the building is designed as 20 °C.

6.3 Constructional Properties

The thermal conductivity values of the building materials in different case studies, used for the simulation are given in Table 2 [17]. The U-values (W/m^2 K) of the walls, roofs, slabs, and partitions for each case studies are calculated by the Design Builder software and checked with the standards [26]. Infiltration rate for airtightness of the building is taken as 0.4 ACH by considering medium air tightness [2].

6.4 Internal Gains and Openings

LED lights with normalized power density of 2.5 W/m^2 of target illuminance 100 lx is provided with the lighting schedule of 18:00–23:00 h daily. Occupancy density is calculated as 0.5 people/m^2 by considering average of 6 people in 3-bedroom house of floor area 119.5 m^2. Occupancy schedule is set to weekdays as from 06:00 to 09:00 and from 16:00 to 23:00. The clothing levels of occupants is chosen as 0.5 and metabolic rate as 0.8 for general household activities. Internal gains due to electrical and electronic appliances, kitchen works are assumed as 1.5 W/m^2.

Windows are provided with double clear glazing with 6 mm air gap with the U-value of 2.708 W/m^2 K [15]. Windows are scheduled to close during night and open from 11:00 to 17:00 h to get solar radiation and natural ventilation of 1.5 ach [18] inside the building to maintain adequate indoor air quality.

6.5 HVAC

Since the apartment is located in an upland climate of very cold weather, it is obviously having a heating demand throughout the year. Therefore, Unitary Heat Pump is provided with heating system seasonal COP as 2.0 for heating schedule of 20:00–07:00 h. The heating set point temperature is set to 20 °C.

6.6 Simulation and Results

At first, the building was analysed for free running provided with natural ventilation. The monthly operative temperature (Indoor) along with the outdoor dry bulb temperature is shown in Fig. 4. There is about 2–3 °C temperature rise observed in the EPS panel apartment. But when considering the minimum indoor temperature for every month from the hourly simulations as shown in Fig. 5, there are months from June to January having indoor temperature less than 20 °C (heating set point temperature) (about 349 h out of 8760 h in a year) for EPS panel apartments. It requires heating during nights of the colder months. Therefore, heating unit is provided for further analysis.

Energy required for heating with different orientations (Fig. 6) of the longer axis of the building towards North–South or East–West was derived as shown in Fig. 7.

Buildings with a "rectangular form" can orient their longer axes towards North–South direction. Greater the walls and windows in East and West, greater is the heat gain of the building in tropical uplands. The excess solar radiation through windows in West can be minimized overhanging balconies. When the window-to-wall ratio (WWR) is increased to 30%, there can be seen a significant reduction in Energy for heating as shown in Fig. 8, as more amount of solar gain through windows keep the indoor comfort.

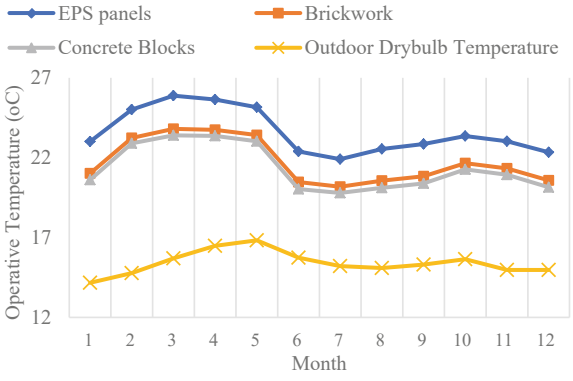

Fig. 4 Monthly average operative temperature

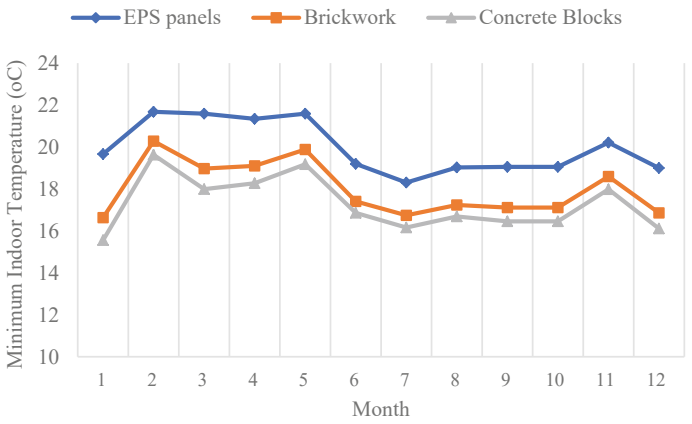

Fig. 5 Minimum indoor temperature (monthly)

Fig. 6 Different orientations of longer axis of the apartment building with Sun path diagram

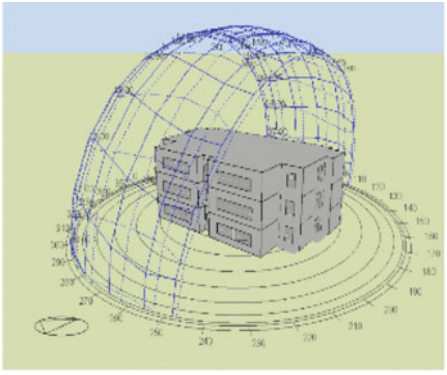

(a) North-South

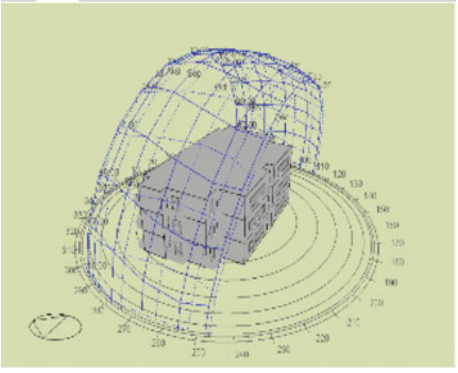

(b)east - West

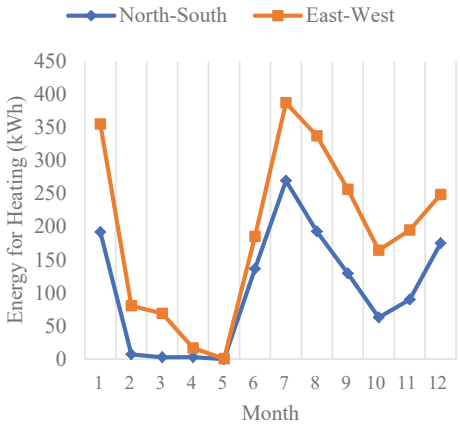

Fig. 7 Variation of energy for heating with orientation

Fig. 8 Variation of energy for heating with window-to-wall ratio

The energy required for heating the building constructed with EPS panels is about 1/5 of concrete blocks apartments and 1/4 of Brick apartments in every month in a year (Fig. 9). This shows that a huge amount of energy can be saved for heating the EPS panel apartments.

The designed capacity of heating units for steady-state heat loss to achieve the thermal comfort, at floor levels (Fig. 10) and houses in a floor (Fig. 11) are shown.

It can be observed that the house at the 1st floor level (middle floor) facing the direction East have low heating capacity since less heat loss through ceilings and floor (confined floor). The EPS panel apartments can run without heating during the months from February to May. Other passive features like use of darker colours

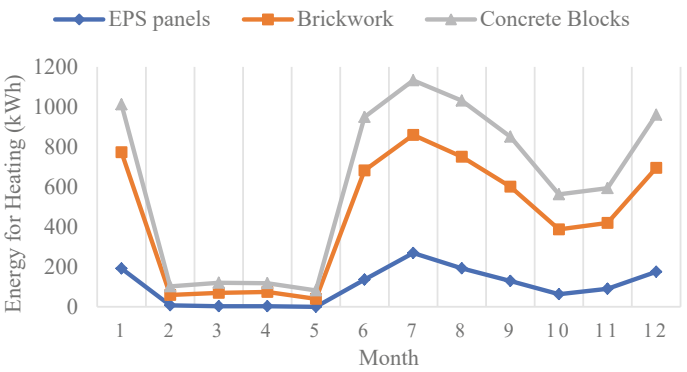

Fig. 9 Variation of annual energy for heating with wall materials

Fig. 10 Design heating capacity at different floor levels

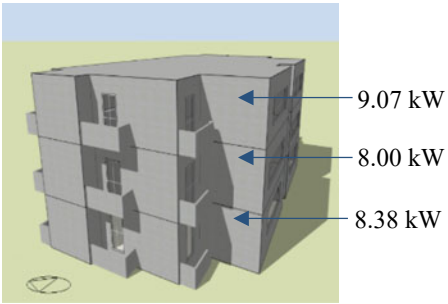

Fig. 11 Design heating capacity of houses at 1st floor level

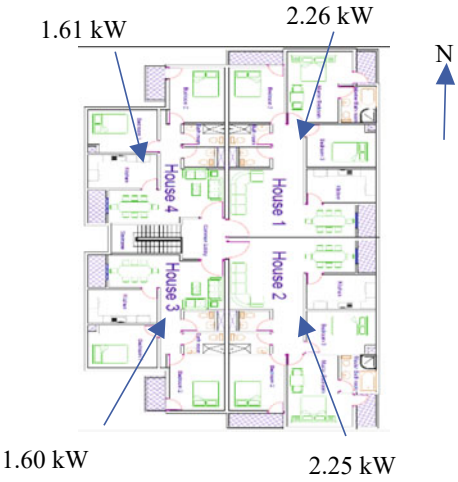

for the walls and roof enhance the absorption of solar radiation. Thus, increase the operative temperature and reduces heating energy [18].

7 Lifecycle Assessment (LCA)

In the case of residential construction, the total life cycle energy consumption is made up of two components: Embodied energy and operational energy [13]. The apartment buildings' lifespan is considered 50 years for LCA in general [23]. Operational energy by electricity is calculated by adding energy for heating, lighting, and other common equipment for nominal household for three types of apartments obtained from Design Builder analysis.

Operational energy contributed by electricity is shown in Table 3. But operational energy associated with a residential building of Sri Lanka includes energy for cooking like; kerosene, firewood, L.P. gas, etc. [28] which are not included in this research.

The procedure of Life Cycle Assessment of the EPS panel apartments follows the ISO 14044:2006 standards. OneClick LCA tool developed by Bionava Ltd which is compliant with EN 15,978 standards is used for the LCA. It is followed by Environmental Product Declarations (EPDs) based on ISO 14044 standards which are related with environmental performance of building materials. The framework for the LCA is as follows: [16].

7.1 Goal and Scope Definition

The Goal of the LCA is determining the energy performance and environmental impacts of EPS-based lightweight panel apartments in tropical uplands when compared with conventional building materials in Sri Lanka. The assessment would be in functional unit of m^2. The system boundaries are defined according to EN 15,978, and the stages selected for the analysis are indicated in Fig. 12.

Table 3 Operational energy calculation

Wall material	EPS panel apartments	Bricks	Concrete blocks
Annual electricity requirement (kWh)	9776	13,727	15,873
Operational energy by electricity per area for 50 years lifespan (GJ/m^2)	1.41	1.98	2.28

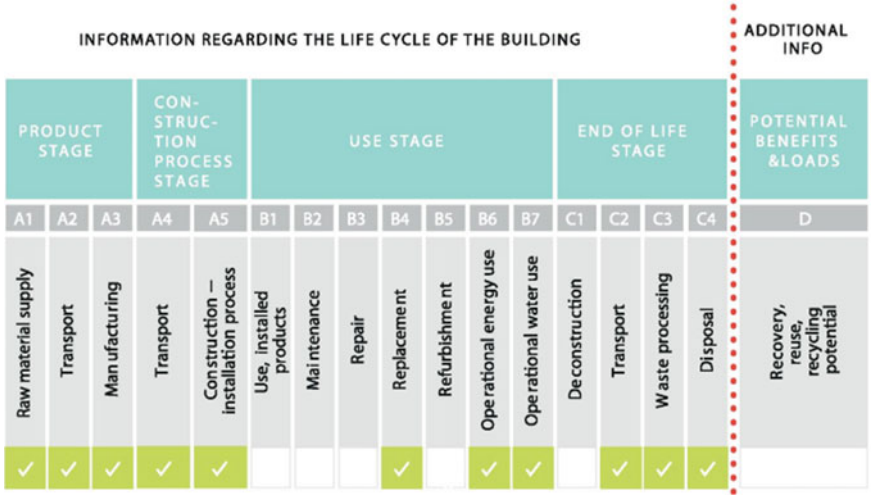

Fig. 12 Life cycle stages according to EN 15,978 standard [14]

7.2 Life Cycle Inventory (LCI) Analysis

According to ISO 14040, the inventory analysis of the buildings involves data collection and validation of raw materials, processes, energy consumption of the building. Embodied energy covered life cycle stages A1–A4 in this research. Operational energy covered stage B6. OneClick LCA used the data extracted from the Design Builder model and mapped with the EPD databases of Sri Lanka and missed inventories are mapped to Indian database in the tool and validated using existing literature.

7.3 Life Cycle Impact Assessment (LCIA)

LCIA is conducted using One Click LCA tool using Mid-point method [3] for the EN-15978 Impact categories for the selected life cycle stages. The LCIA result summary for the EPS panel apartments in Nuwara Eliya during 50 years' service life is shown in Table 4. The comparison of the LCIA results of EPS apartments with conventional materials is shown in Fig. 13.

Table 4 Results of LCIA for EPS apartments

Impact category	Unit	Results
Global warming potential (GWP) (greenhouse gases)	$kgCO_2eq$	481,830
Acidification potential (AP)	$kgSO_2eq$	2437
Eutrophication potential (EP)	$kgPO_4eq$	437
Ozone depletion potential (ODP)	$kgCFC_{11}eq$	0.03
Formation of ozone of lower atmosphere (POCP)	kgC_2H_4eq	235

Fig. 13 Comparison of life cycle impact assessment with conventional building materials

Table 5 Summary of the findings in this research

Wall material	EPS panel	Brick	Concrete blocks
Embodied energy per area (GJ/m^2)	2.90	3.80	3.60
Operational energy by electricity per area for 50 years lifespan (GJ/m^2)	1.41	1.98	2.28
Embodied carbon ($kgCO_2e)/m^2$	386	747	806

7.4 Interpretation of Results

The summary of the findings of whole LCA of this research is shown in the Table 5. The very common category GWP (changes in temperatures caused by Green House gas emission) indicates that EPS panel apartments affects the nature only by 35% of GHG emission by conventional building materials.

8 Conclusions

EPS-based lightweight panel apartment constructed in Nuwara Eliya (Tropical upland climate) is expected to perform very well in its all-life cycle stages. This contributes about 20% energy savings in embodied energy (Cradle to gate); about

30% energy (electricity) savings in its operational phase and about 40–50% environmental impact reduction. The adoption of EPS panels in the apartment construction in Sri Lanka paves the path for sustainable construction towards reaching SDG and for green certifications from reputed organizations.

References

1. Aciu C, Manea D, Molnar LM, Jumate E (2015) Recycling of polystyrene waste in the composition of ecological mortars. Procedia Technol 19:498–505
2. ASHRAE (2018) Standard 90.2-2018, Energy efficient design of low-rise residential buildings
3. Bare et al (2000) Midpoints versus endpoints: the sacrifices and benefits. Brighton: State-of-the-Art: LCIA. Retrieved from pre-sustainability.com
4. Coppola (2016) Investigation on the use of foamed plastic waste as natural aggregates replacement in lightweight mortar. Compos B Eng 99:75–83
5. Design Builder (2019) Design builder SBEM v6.1.8 manual
6. Devi PL, Palaniappan S (2014) A case study on life cycle energy use of residential building in Southern India. Energy Build 80:247–259
7. Dissanayake DMKW, Jayasinghe C, Jayasinghe MTR (2017) A comparative embodied energy analysis of a house with recycled expanded polystyrene (EPS) based foam concrete wall panels. Energy Build 135:85–94
8. Dixit MK, Fernandez JL, Lavy S (2010) Identification of parameters for embodied energy measurement. Energy Build 42:1237–2128
9. Eric TB, Jayasinghe MTR (2018) Embodied energy and carbon footprint of apartment buildings with lightweight load bearing panels. Unpublished thesis submitted for B.Sc. degree at University of Moratuwa
10. Ganesan S, Mydin M, Yunos M, Nawi M (2015) Thermal properties of foamed concrete with various densities and additives at ambient temperature. Appl Mech Mater 747:230–233
11. Gunawardana SGW, Eric TB, Jayasinghe MTR (2019) Three-storied apartment buildings constructed using lightweight eps concrete panels for tropical climatic regions. ICCEA, p 24
12. Hammond G, Jones CI (2008) Embodied carbon: the concealed impact of residential construction. Green Energy Technol 31:367–384
13. Haynes R (2010) Embodied energy calculations within life cycle analysis of residential buildings
14. Hoxha et al (2021) Influence of technical and electrical equipment in life cycle assessments of buildings: case of a laboratory and research building. Int J Life Cycle Assess 26:852–863
15. ISO 10292 (1994) Glass in building—calculation of steady-state U values (thermal transmittance) of multiple glazing. ISO
16. ISO (2006) ISO 14040:2006 environmental management—life cycle assessment—principles and framework
17. Jayasinghe C (2015) Thermal performance of composite walls made out of recycled building waste and stabilized rammed earth. In: NBRO research symbosium 2015—resilient built environment. NBRO
18. Jayasinghe MTR, Priyanwada AKM (2002) Thermally comfortable passive houses for tropical uplands. Energy Sustain Devel 45–54
19. Kan A, Demirboga R (2009) A novel material for lightweight concrete production. Cement Concr Compos 31(7):489–495
20. Kaya A, Kar F (2016) Properties of concrete containing waste expanded polystyrene and natural resin. Construct Build Mat Elsevier Ltd 105:572–578
21. Namal DDA (2003) Analysis of energy embodied in cement produced in Sri Lanka. Thesis, University of Moratuwa, M.Sc

22. Pereira K, Ratnayake R (2013) Curbing illegal sand mining in Sri Lanka. Water Integrity Network
23. Rashid AAF, Yusoff S (2015) A review of life cycle assessment method for building industry. Renew Sustain Energy Rev 45:224–248
24. Sanjaya BGV, Srilal WMS, Perera WWPK, Sooriyaarachchi HP, Appuhamy JMRS (2015) Investigation on improvement of low cost NERD slab system. In: 6th international conference on structural engineering and construction management
25. Sicignano E, Ruocco GD, Melella R (2019) Mitigation strategies for reduction of embodied energy and carbon, in the construction systems of contemporary quality architecture. Sustainability
26. Sri Lanka Sustainable Energy Authority (2020) Energy efficient building code of Sri Lanka. Sri Lanka sustainable energy authority
27. SWERA (2011) Retrieved from https://openei.org/wiki/Solar_and_Wind_Energy_Resource_Assessment_(SWERA)
28. Udawattha C, Halwatura R (2016) The embodied energy and life cycle costing: a case study on basic dwellings in Sri Lanka. Research Paper submitted for M.Sc dissertation to University of Moratuwa
29. UNEP (2015) Retrieved from https://www.un.org/sustainabledevelopment/
30. Vishnu P, Thilakarathna P, Mendis P, Jayasinghe MTR (2017) The feasibility of using lightweight EPS based panels for staircases of apartments. In: 8th international conference on structural engineering and construction management. Kandy

Sustainable Water Consumption in Building Industry: A Review Focusing on Building Water Footprint

Bhagya Nallaperuma, Zih-Ee Lin, Jithya Wijesinghe, Amila Abeynayaka, Safa Rachid, and Selim Karkour

Abstract Sustainable water consumption has become a primary concern of the building industry. The water footprinting assesses the freshwater use and associated effects on local and global freshwater resources plus ecosystems therein. This review elaborates two extensively adopted water footprinting approaches, Water Footprint Network (WFN) and ISO 14046 Life Cycle Assessment (LCA), discussing their methodologies and perspectives of analyses with special regard to the building industry. An appraisal of water footprints of common building materials is presented in this study with glimpses of the hotspots of freshwater consumption along their supply chains. Further, it advances its water footprints appraisal into the use phase/case study level referring to the real-world applications of the building industry. The importance of comprehensive water footprint analysis covering the complete life cycle of buildings, the inclusion of allied environmental impacts into analyses, influence of building type/structural design/site-specific variables were highlighted under this discussion in support of the dependable judgment of freshwater appropriation performances. Ultimately, the review dedicated a segment to set a futuristic view

B. Nallaperuma · Z.-E. Lin · J. Wijesinghe · A. Abeynayaka · S. Rachid · S. Karkour
Beyond Borders of Life Cycle Assessment (2BLCA), Shinjuku-ku, Tokyo 169-0075, Japan

B. Nallaperuma (✉) · J. Wijesinghe
Department of Indigenous Medical Resources, Faculty of Indigenous Health Sciences and Technology, Gampaha Wickramarachchi University of Indigenous Medicine, Kandy Road, Yakkala, 11870, Sri Lanka
e-mail: bhagya@gwu.ac.lk

Z.-E. Lin
Graduate Institute of Environmental Engineering, National Taiwan University, Taipei 10617, Taiwan

S. Rachid
Mining Environment and Circular Economy, Mohammed VI Polytechnic University (UM6P), Lot 660—Hay Moulay Rachid, 43150 Ben Guerir, Morocco

A. Abeynayaka
Institute for Global Environmental Strategies (IGES), 2108-11 Kamiyamaguchi, Hayama, Kanagawa, 240-0115, Japan

R. Dissanayake et al. (eds.), *12th International Conference on Structural Engineering and Construction Management*, Lecture Notes in Civil Engineering 266,
https://doi.org/10.1007/978-981-19-2886-4_56

into the matter featuring sustainable freshwater consumption, economic and developmental interests, challenges faced by the industry, prioritization and compromise of freshwater uses of the building industry.

Keywords Water footprint · Building industry · Water footprint network · Life cycle assessment · Building materials · Sustainable water consumption

1 Introduction

Freshwater sustains the life on earth and reinforces the course of civilization accompanying agriculture, industrial processes, urban development and almost all human-induced activities [27]. Sustainable management of freshwater resources stands to satisfy the changing demands placed on water resources, at present and on into the future without system degradation [14]. The water footprint (WF) is a concept developed within the water resources research community by way of an assessment tool of sustainability of freshwater appropriation [9].

Water footprinting appraises freshwater use and its related effects from the consumption of goods and services [9, 20]. The assessment of water consumption is of paramount importance as freshwater resources are currently under greater pressure worldwide. Climate change, speeded-up industrialization, extensive urbanization, population growth and associated higher standards of lifestyle dynamics are aggravating the crisis of freshwater resources [2]. During the twentieth century, the growth of global water consumption was twice as the population growth and at this juncture, many of the comprehensive policy agendas focused on increasing the limited availability of freshwater to meet ever-growing and competing demands [28].

The constructions sector, especially the building industry's contribution to the total freshwater withdrawal is sizable as per the accounts documented. The World Bank [25] reports that around 19% of total water is withdrawn by the industrial sector in which the construction industry is among the top water consumers [7]. Abd El-Hameed et al. [1] report that the built environment globally consumes 20% of water and the green buildings can possibly reduce usage by almost 40%. Along the value chains, the water consumption profiles of different materials vary greatly during raw material extraction, processing, manufacturing, transportation and construction. Besides, both direct and indirect water uses have to be accounted for along their supply chains to explore the critical points of water efficiency's interests [17]. As the building construction is supported by complex supply chains involving many a manufacturing sector, comprehensive quantification of water footprints is difficult and intricate [5, 18]. Therefore, the need for metric(s) with methodical protocols to quantify the volumetric water use and/or potential environmental impacts related to the water use was of prime importance, and the international consensus for such metric(s) was well appreciated in facilitation of comparative analyses of water consumption performance assessments of products or processes in the sphere of building industry.

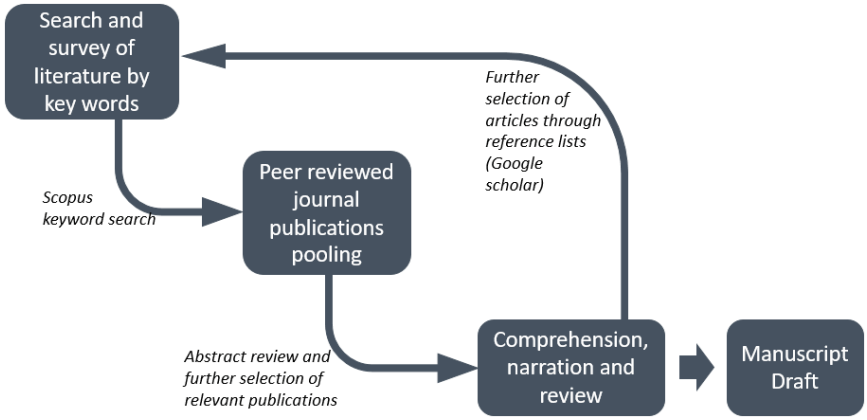

Fig. 1 The iterative operationalization of developing this review study

This review bids to present a landscape analysis of water footprinting discussing the developments and salient points with regard to sustainable freshwater consumption in the building industry. The literature was surveyed in Google Scholar by the keywords and the resourceful articles were pooled perusing the abstracts of the search results. Thereby, twenty-nine articles were selected as the primary reservoir of information for this review. This process was iterated as the narration of the review develops. Figure 1 illustrates the operationalization of this work.

2 Water Footprint Analysis in the Building Industry

At the outset, it is worth briefly review the two widely applied water footprinting approaches proposed by two different communities, the Water Footprint Network (WFN) and the Life Cycle Assessment (LCA). Both these methods are broadly similar standing for the computation of freshwater use and its impact. The WFN considers water footprinting as a volumetric approach (total volume of freshwater used by an individual/community/business activity), focusing on water productivity. It views freshwater as a limited global resource, and the environmental relevance of both consumptive (green and blue waters) and degradative (gray water) freshwater uses are accounted referring to the sustainability limits, environmental needs, efficiency of use and equitability of global freshwater resources [9]. Berger and Finkbeiner [4] define this approach as a volumetric water footprinting method since it determines the freshwater appropriation on an inventory level.

On the other hand, the LCA quantifies potential environmental impacts related to a particular freshwater appropriation going beyond the primary reporting of the volumetric water use [20]. The LCA approach extends the freshwater use assessment to the consequences resulting from water consumption (impact-based water

footprinting) through weighting and characterization pertinent to the case of interest. Moving beyond the volumetric water use accounting (inventory level/LCI—life cycle inventorying), the LCA approach works on life cycle impact assessment (LCIA) based on freshwater scarcity/water quality/vulnerability of ecosystems/sensitivity of the population to human health damages [4]. This integration of freshwater use into life cycle assessments by the LCA community has formulated the international standard on water footprinting in ISO 14046.

Although the WFN and LCA approach manifest differences in their terminologies and communications, they share common fundamental principles in freshwater accounting. Both approaches intend for water efficiency, water productivity and environmental well-being giving complementary inputs to the system improvements. Further, both methods account for volumetric water use following the life cycle approach with nearly similar steps. Still, in contrast to the WFN's viewpoint (freshwater is deemed as a limited global resource), the LCIA of LCA approach adopts a damage-oriented analysis of local freshwater use [20]. Having all in mind, the WFN and LCA approaches should be regarded not as competing water footprinting tools, but as complementary methods. Thus, the approach/es should be fittingly adapted for the intended purpose.

The establishment of a transparent and replicable approach to quantify freshwater use in building industry entirely depends on the quality of available data. The embodied water demand of a particular product/process of the building industry is the overall freshwater need of manufacture/delivery covering both direct and indirect water uses. Though the direct water component of a product/process is straightforwardly assessed, the indirect water accounting is a hard task as it involves the freshwater use of all the processes along the upstream supply chain in which the main product moved through utilizing resources and raw materials [1]. The supply chain dispersion of the building industry moves across the national borders. Even though it observes variations of international building WFs among different countries, the supply chains of the building industry is highly dispersed going beyond country borders [21]. Therefore, the higher degree of sector disaggregation and the availability of corresponding fine resolution data throughout the supply chain nexuses become key determinants over the dependable quantification of water use in the building industry.

The process boundary of the water footprint analysis is another principal aspect in the evaluation of the material, technology and structural design alternatives in the field of the building industry. For instance, the water use performance of a building construction should be appraised referring to its practical applications of durability, water footprints of maintenance, repair, demolition/treatment/disposal (end-of-life), post-construction use phase water footprints, water footprints of material transportations, water footprints of compatible and complementary materials (e.g., stainless steel/glass fiber reinforcements for concretes with seawater and/or marine aggregates), gray water footprints related to effluents [2, 8, 23]. Thus, the establishment of comprehensive reasoning for a particular water-efficient alternative will only be rationalized by cradle-to-grave water footprint analyses. Moreover, the case-specific interests have to be duly inventoried and the associated water footprints should be

well accounted for to secure the interpretational accuracy of individual case analyses. The case-specific water footprints of raw material extraction and processing, sources of energy used, mode of labor employed, soil characteristics of the construction site (influencing the load resisting structures of buildings), technologies adopted in different unit operations should be carefully surveyed throughout the supply chain network [1, 5, 11].

3 Appraisal of Water Footprints at the Construction Materials Level

In this section, a review on appraising water footprints of common building materials is presented based on the published work. A water footprint analysis of blue and gray waters for most common types of steel, cement and glass has been reported by [8] adopting a combined approach of LCA and WFN, and their findings are shown in Fig. 2.

Among the materials studied, steel records the top WF values with leading figures in both blue and gray WF components. In a cradle-to-grave LCA analysis of Ultra-High-Performance Concrete (UHPC) in comparison to Conventional Concrete (CC), [23] also have reiterated the predominance of steel's WF. The alloyed steel leaves the highest WF with a predominant blue WF for energy used. This is attributed to the relatively large electricity demand for ferronickel melting in the alloying process [8]. Further, the substantial gray WF values of steels and Portland cement are caused by the heavy metal (Cd, Hg, Cu) laden effluents of their manufacturing processes. Specifically, Cd is the critical pollutant responsible for the gray WFs of alloyed steel, unalloyed steel and Portland cement. These WF estimations at the material level are supported by a study [3] that has reported embodied water volume of building

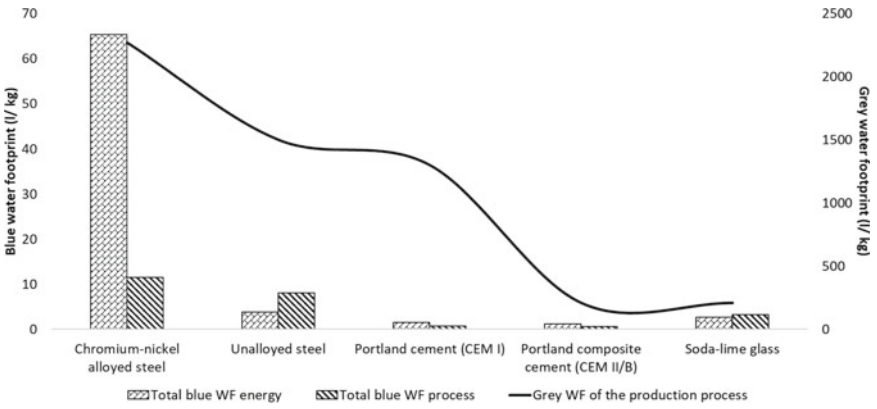

Fig. 2 Blue and gray WFs of common building materials pertaining to the direct production process, energy inputs of the production process and pollutant effluent of wastewaters [8]

materials per unit floor area basis. Those estimations are comparable to the data presented above recording values for steel, cement and bricks as 25, 0.5 and 0.1 kl/m^2, respectively. Moreover, [3] has assessed both water use during the construction phase and embodied water use of building materials as 2 and 25.6 kl/m^2, respectively. This assessment stands with the study of [11] as they have recorded the extents of direct water consumption of on-site constructions and indirect water consumption of off-site processes (energy use, material production, transportation, food, water use for equipment and machinery, etc.) as 2.26% and 97.74%, respectively. Therefore, it can be deduced that the building industry exerts comparatively less pressure on local freshwater resources while its greatest impact is on national water resources or beyond (Fig. 3). This matter would be very much insightful in the determination of the water footprinting approach for case studies. To be specific, for the off-site freshwater use quantifications of the building industry, the WFN approach can be generally recommended whereas LCA water footprinting fits most for the on-site operations of building constructions.

In [8], the total blue WF of the process represents the direct blue water use by the material excluding water use for transportation. The blue WF of energy is a sizable predictor of the water use performance of each material as it ranges from 32 to 85% of the total blue WFs. Thus, the WF of the energy source of material manufacturing becomes a critical determinant of the overall blue WF of construction materials. The WFs of energy sources corresponding to this study have been tabulated below

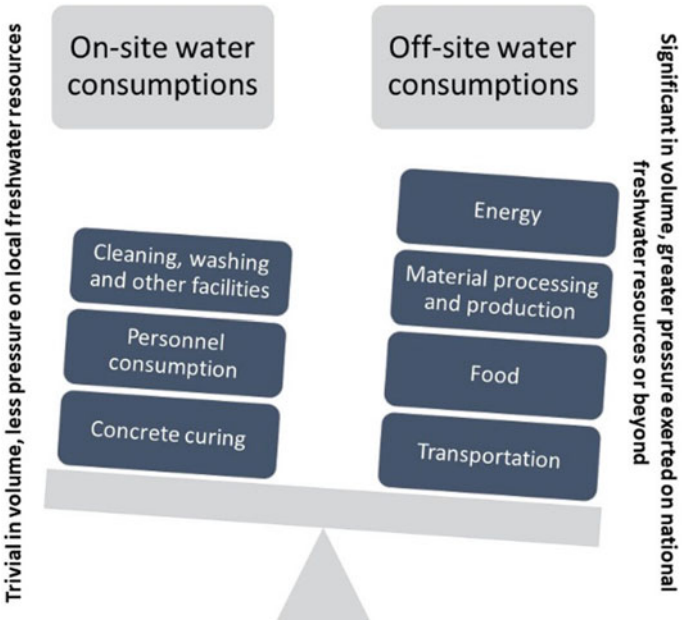

Fig. 3 On-site and off-site water consumptions of building industry and their relative pressure exerted on freshwater resources

Table 1 Ranges and median values of blue WFs of energy sources reported by [8]

Energy source	Blue WF range (l/GJ)	Blue WF median value (l/GJ)
Diesel	28–376	80
Light fuel oil	19–259	55
Heavy fuel oil	10–133	28
Natural gas	0.6–18	2.2
Coal	6.6–228	15–39
Hard coal cokes	42–321	52–82
Electricity	4241	

(Table 1), and the relative variation of blue WF ranges implies the significance of the choice of energy source over the total blue WF of the material. This claim is further supported by [11] as they have weighted >50% of the total WF of building construction to its material use in which >50% of WF is of the energy used for manufacturing and processing.

If the energy sources of building material manufacturing and processing can be inclined toward alternatives with lower WFs (solar/wind/geothermal energy) it can be improved the water use performances of most of the common building materials. At the same time, the industry should seek new technologies to relieve higher WFs spotting critical points of freshwater efficiencies along its supply chains: reusing and recycling of materials, effluent treatment before discharge, encouraged rain and stormwater use in material manufacturing and processing, replacement of freshwater with seawater where workable (cooling activities), improved concrete curing technologies with lower WFs, promotion of local purchases of building materials to minimize the WF of transportation, etc.

4 Appraisal of WFs at Use Phase/Case Study Level

Moving forward from the WF analysis at the construction materials level, a review of water footprinting at the case study level is presented here based upon available literature. The study of the complete life cycle of buildings includes not only extraction and processing of raw materials, production, transport and on-site construction activities. It extends to the analysis of use, reuse and maintenance, recycling, and final disposal phases as well [15, 16]. Thus, environmental performances of a building construction should be comprehensively appraised through a systematic methodology (LCA based on ISO 14040 and ISO 14044) to produce inputs for well-judged sustainability assessments of natural resources [1, 23].

The importance of the inclusive analysis of building construction is exhibited in a WF assessment of Ultra-High-Performance Concrete (UHPC) in comparison to Conventional Concrete (CC) done by [23]. At the level of the materials, UHPC shows nearly three times higher WFs compared to CC for both ready-mix and precast

concretes (from raw material production to construction site) (Fig. 4). Nevertheless, the UHPC design (a bridge design) compared to its corresponding CC design had a WF around 30% lower (Fig. 5). Further, as UHPC is superior to CC in compressive and tensile strengths, it is anticipated that the UHPC's end-of-life (EoL) phase would leave a relatively higher WF (especially of demolition) compared to the CC. Besides, the WF analyses should reach out to emerging sustainability-oriented applications in the sphere of building construction. For instance, in urban mining as a key approach of circular economy, the materials flow reverse bringing in new dimensions of process boundaries (e.g., concrete manufacturing from recycled aggregates in EoL-to-gate boundaries) [19].

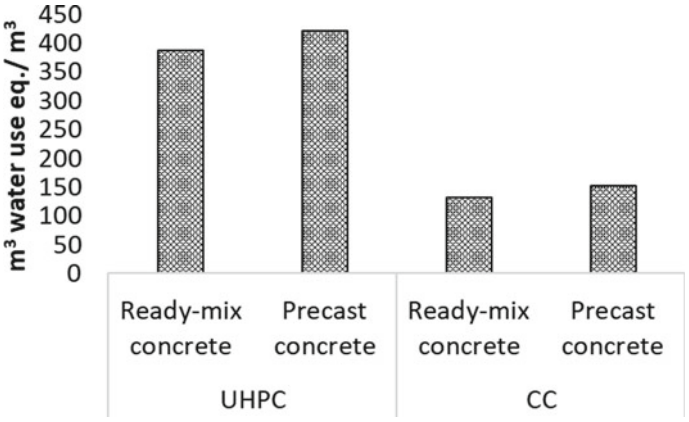

Fig. 4 Water footprints of ultra-high-performance concrete (UHPC) in comparison to conventional concrete (CC) [23]

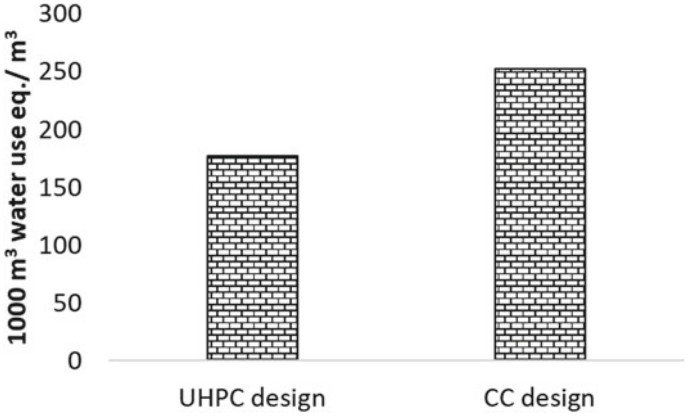

Fig. 5 Water footprints of two bridge designs of ultra-high-performance concrete (UHPC) and conventional concrete (CC) [23]

From the perspective of overall environmental impact, the WFs of building constructions should be appraised in tandem with other environmental footprints entailed (carbon footprint, energy footprint, material footprint, ecological footprint). These environmental footprints do not always follow congruous patterns mutually. As per [21], no collinearity of WF with energy and carbon footprints was observed in environmental footprints associated with the construction sector of India, Italy, South Africa, and the UK. Further, in an environmental assessment of recycled concrete, the material footprint had a clear improvement though the water use remained without a significant saving [19]. This claim was confirmed in a cradle-to-gate assessment of environmental footprints for different design alternatives of building elements using recycled aggregates for concrete production [22]. Still, a contrasting finding was documented in the environmental assessment of UHPC compared to CC where all the footprints of carbon, material and water for UHPC recorded comparatively higher figures at the construction materials level [23]. At the same time, all the three footprints of UHPC had comparatively lower values than CC at the case study level (for a bridge design case study) of the same study. To cut short, it can be observed case-wise discrepancies of the way WF is left with other environmental footprints. Therefore, drawing recommendations for the practical applications of building construction becomes a multi-faceted phenomenon extending beyond materials level and case study level assessments of mere WF analyses.

Viewing the case study level from a different perspective, [5] carried out quantification of WFs of buildings in China considering the variable of building type. Its results divulge how the scale of heavy structural designs that directly depend on water-intensive steel and cement consumptions be predictors of their embodied WFs. Thereby, the public buildings preceded residential buildings in WFs while the urban residential buildings having 55–130% greater WFs in comparison to the rural residential buildings. Figure 6 shows the factual evidence of water withdrawals (surface and groundwater withdrawals) and water consumptions (permanent water withdrawals as no longer available for any other use) for the thirteen building subsectors studied under that analysis. Moreover, [11] assessed the effects of structural parameters of residential buildings on the WFs. The work declared WF mitigation recommendations by way of: concrete structures over steel structures, short structures over tall structures, composite slabs over steel deck and compute precast slabs, and building sites with dense soils over building sites with soft soils.

5 Challenges and Futuristic View

Even amidst the global pandemic, the developing economies, especially in Asian and African regions are in a healthy economic revival in terms of their Gross Domestic Product (GDP) growth rates [24]. Around one-third of the top twenty-five developing economies suffers with either lack of basic access to water for the majority of

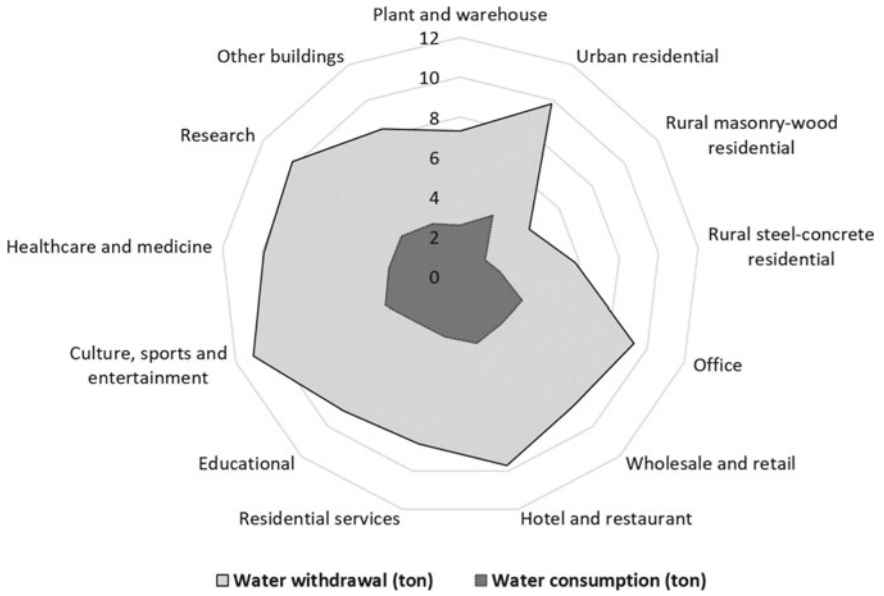

Fig. 6 Water withdrawal and water consumption values estimated per 1 m^2 of building area in China [5]

their populations (Eritrea, Ethiopia, Uganda) or higher baseline water stress (Turkmenistan, Syria, Egypt, San Marino, China) [10, 29]. These countries undergo intensive infrastructure development projects that probably exert substantial impacts on the national freshwater resources. This crisis gets compounded with the outward-bound virtual waters related to the building industry in these developing economies. For instance, having a swelling building industry China is one of the countries with the most deficient per capita water resources of which the spatial distribution is highly uneven [13]. Further, China extensively exports virtual waters via building materials and other inputs of the construction sector putting extra pressure on local freshwater resources [21]. Thus, alleviation of this crisis through mindful freshwater appropriations is a crying need that ought to be placed top in sustainable management practices. Along with the collective effort toward Sustainable Development Goals (SDGs) intended to be achieved by 2030 and mid-century climate goals, the building industry's role is decisive due to its significant contribution to the global environmental burden. Therefore, to overcome the challenges posed by irreconcilable demands of environmental, economic and social interests all the stakeholders of water handling (industry, academia, regulators and general public) have to seek water-efficient alternatives.

With special regard to the local context of Sri Lanka, a set of potential challenges can be anticipated in gearing water-efficient alternatives in the building industry. In the Sri Lankan construction sector, there are few inherent drawbacks that may pose challenges to the aspiring transition of sustainable water management. Low level of

new technological development and transfer, poor documentation and communication, reluctance in using innovative building materials and disadvantaged industry-oriented research and developments reported by [6] may probably loom by way of potential challenges.

These challenges are to be tackled in a participatory approach with all the key stakeholders of the industry through information, communication and education. At the same time, sustainable water management should be integrated into the water governance by the national government to regulate freshwater appropriations of the industry [26]. However, the industry demand for freshwater is to be compromised with other priorities of freshwater uses (e.g., freshwater demand for agriculture to assure national food security) [12]. Ultimately, the industry well-being should be secured under the developing economy of Sri Lanka through economic analysis of water-efficient alternatives (life cycle costing of water-efficient materials/technologies).

References

1. Abd El-Hameed AK, Mansour YM, Faggal AA (2017) Benchmarking water efficiency of architectural finishing materials based on a "cradle-to-gate" approach. J Build Eng 14:73–80
2. Arosio V, Arrigoni A, Dotelli G (2019) Reducing water footprint of building sector: concrete with seawater and marine aggregates. IOP Conf Ser Earth Environ Sci 323:012127
3. Bardhan S (2011) Assessment of water resource consumption in building construction in India. Ecosyst Sustain Devel VIII 144:93–102
4. Berger M, Finkbeiner M (2013) Methodological challenges in volumetric and impact-oriented water footprints. J Ind Ecol 17(1):79–89
5. Chang Y, Huang Z, Ries RJ, Masanet E (2016) The embodied air pollutant emissions and water footprints of buildings in China: a quantification using disaggregated input–output life cycle inventory model. J Clean Prod 113:274–284
6. De Silva N, Rajakaruna R, Bandara K (2008) Challenges faced by the construction industry in Sri Lanka: perspective of clients and contractors. Build Resilience 158
7. FAO (2021) AQUASTAT—FAO's global information system on water and agriculture. Available at: http://www.fao.org/aquastat/en/. Accessed on 7 Sept 2021
8. Gerbens-Leenes P, Hoekstra A, Bosman R (2018) The blue and grey water footprint of construction materials: steel, cement and glass. Water Res Ind 19:1–12
9. Hoekstra AY (2016) A critique on the water-scarcity weighted water footprint in LCA. Ecol Ind 66:564–573
10. Hofste RW, Reig P, Schleifer L (2019) 17 countries, home to one-quarter of the world's population, face extremely high water stress
11. Hosseinian SM, Ghahari SM (2021) The relationship between structural parameters and water footprint of residential buildings. J Clean Prod 279
12. IWMI (2021) IWMI in Sri Lanka :: IWMI. Available at: https://www.iwmi.cgiar.org/about/where-we-work/asia/south-asia-region/sri-lanka/. Accessed on 7 Sept 2021
13. Liu S, Zhang F, Li K, Wang K, Shang B, Li D (2020) Analysis on research status of water footprint of ceramic tile (board). IOP Conf Ser Earth Environ Sci 526:012220
14. Loucks DP (2000) Sustainable water resources management. Water Int 25(1):3–10
15. Mannan M, Al-Ghamdi SG (2020) Environmental impact of water-use in buildings: latest developments from a life-cycle assessment perspective. J Environ Manage 261:110198

16. Marrero M, Wojtasiewicz M, Martínez-Rocamora A, Solís-Guzmán J, Alba-Rodríguez MD (2020) BIM-LCA integration for the environmental impact assessment of the urbanization process. Sustainability 12(10):4196
17. Matarazzo A, Gambera V, Suriano E, Conti MC (2017) Water footprint applied to construction sector. Environ Eng Manage J (EEMJ) 16(8)
18. Meng J, Chen G, Shao L, Li J, Tang H, Hayat T, Alsaedi A, Alsaadi F (2014) Virtual water accounting for building: case study for E-town, Beijing. J Clean Prod 68:7–15
19. Mostert C, Sameer H, Glanz D, Bringezu S (2020) Urban mining for sustainable cities: environmental assessment of recycled concrete. In: IOP conference series: earth and environmental science
20. Pfister S, Boulay A-M, Berger M, Hadjikakou M, Motoshita M, Hess T, Ridoutt B, Weinzettel J, Scherer L, Döll P (2017) Understanding the LCA and ISO water footprint: a response to Hoekstra (2016) A critique on the water-scarcity weighted water footprint in LCA. Ecol Ind 72:352–359
21. Pomponi F, Stephan A (2021) Water, energy, and carbon dioxide footprints of the construction sector: a case study on developed and developing economies. Water Res 194:116935
22. Sameer H, Mostert C, Bringezu S (2020) Product Resource and climate footprint analysis during architectural design in BIM. In: IOP conference series: earth and environmental science
23. Sameer H, Weber V, Mostert C, Bringezu S, Fehling E, Wetzel A (2019) Environmental assessment of ultra-high-performance concrete using carbon, material, and water footprint. Materials 12(6):851
24. The World Bank (2021) GDP growth (annual %)|Data. Available at: https://data.worldbank.org/indicator/NY.GDP.MKTP.KD.ZG. Accessed on 7 Sept 2021
25. The World Bank (2017) Annual freshwater withdrawals industry (% of total freshwater withdrawel)-Sri Lanka. Available at https://data.worldbank.org/indicator/ER.H2O.FWIN.ZS?locations=LK. Accessed on 7 Sept 2021
26. UNDP (2021) What is water governance? Water governance facility—water governance facility. Available at: https://www.watergovernance.org/governance/what-is-water-governance/. Accessed on 7 Sept 2021
27. Vollmer D, Regan HM, Andelman SJ (2016) Assessing the sustainability of freshwater systems: a critical review of composite indicators. Ambio 45(7):765–780
28. World Economic Forum (2021) On the Agenda/Water|World Economic Forum. Available at: https://www.weforum.org/agenda/archive/water. Accessed on 7 Sept 2021
29. World Vision (2020) 10 worst countries for access to clean water|World Vision. Available at: https://www.worldvision.org/clean-water-news-stories/10-worst-countries-access-clean-water. Accessed on 7 Sept 2021